RADIO WAVE PROPAGATION

CONSOLIDATED SUMMARY TECHNICAL REPORT
OF THE

COMMITTEE ON PROPAGATION
OF THE

NATIONAL DEFENSE RESEARCH COMMITTEE

CHAS. R. BURROWS, *Chairman*
STEPHEN S. ATTWOOD, *Editor*

PUBLISHERS' NOTE

The consolidation of the three volumes of the Summary Technical Report of the Committee on Propagation of the National Defense Research Committee was undertaken because the limited edition of the Report published by the Summary Reports Group of the Columbia University Division of War Research and distributed by the War and Navy Departments restricted the availability of this material after declassification The manuscript and illustrations for the three volumes were prepared for publication by the Summary Reports Group of the Columbia Division of War Research.

This volume contains all the scientific information and report of experiments contained in the three separate volumes and omits only that part relating to the administrative activities of the Committee, its origin and organization, with a description of the needs of the armed forces which called it into being.

THE PUBLISHERS

December 1948

FOREWORD

The success of the propagation program was the result of the wholehearted cooperation of many individuals in the various organizations concerned, not only in this country but in England, Canada, New Zealand, and Australia. The magnitude of the research work accomplished was possible only because of the willingness of the workers in many organizations to undertake their parts of the overall program. In fact, the entire program of the Committee on Propagation was carried out without the necessity of the Committee exercising directive authority over any project.

Dr. Hubert Hopkins of the National Physical Laboratory in England and Mr. Donald E. Kerr of the Radiation Laboratory at the Massachusetts Institute of Technology, who were working on this phase of the war effort when the Propagation Committee was formed, were instrumental in giving a good start to its activities. The largest single group working for the Committee was under Mr. Kerr.

The existence of a common program for the United Nations in radio-wave propagation resulted from the splendid cooperation given the Propagation Mission to England by Sir Edward Appleton and his Ultra Short Wave Panel. Later, through the cooperation of Canadian engineers and scientists, Dr. W. R. Mc-Kinley of the National Research Council of Canada and Dr. Andrew Thomson of the Air Services Meteorological Division, Department of Transport, Toronto, Canada, undertook to carry on a part of the program originally assigned to the United States. The program was further rounded out by the willingness of the New Zealand Government to undertake an experiment for which their situation was particularly favorable. Dr. F. E. S. Alexander of New Zealand and Dr. Paul A. Anderson of the State College of Washington initiated this work. Needless to say, the labor of the Committee on Propagation could hardly have been effective without the cooperation of the Army and Navy. Maj. Gen. H. M. McClelland personally established Army co-

operation, and Lt. Comdr. Ralph A. Krause and Capt. Lloyd Berkner were similarly helpful in organizing Navy liaison and help.

Officers and scientific workers of the U. S. Navy Radio and Sound Laboratory at San Diego, California, altered their program on propagation to fit in with the overall program of the Committee. Capt. David R. Hull, Bureau of Ships, understanding the importance of the technical problems, paved the way for effective cooperation by this laboratory.

Dr. Ralph Bown, Radio and Television Research Director, Bell Telephone Laboratories, integrated the research programs undertaken by Bell Telephone Laboratories for the Committee on Propagation. This joint research program included meteorological measurements on Bell Telephone Laboratories property by meteorologists of the Army Air Forces working with Col. D. N. Yates, Director, and Lt. Col. Harry Wexler of the Weather Wing, Army Air Forces. The accomplishments of the Committee on Propagation are a good example of the effectiveness of cooperation—all parts were essential and none more than the rest.

I want to thank Dr. Karl T. Compton, President of Massachusetts Institute of Technology, who was always willing to discuss problems of the Committee and who helped me to solve many of the more difficult ones, and also, Prof. S. S. Attwood, University of Michigan, whose continual counsel throughout my term of office was in no small way responsible for the success of our activity.

Credit is also due Bell Telephone Laboratories, which made my services available to the Government and paid my salary from August 1943 to September 1945, and to Cornell University, which has allowed me time off with pay to complete the work of the Committee on Propagation since September 1945.

CHAS. R. BURROWS
Chairman, Committee on Propagation

FOREWORD TO CONSOLIDATED EDITION

SCIENTISTS and engineers in the field of radio wave propagation are indebted to the Academic Press for making available to them this condensed volume of the entire report of the Committee on Propagation of NDRC which otherwise would only be available in the two hundred and fifty copies of the three-volume report printed for the government. This volume contains material of great value to present and future studies of the problems encountered in the propagation of radio waves not otherwise available to the public.

The results of the work of the Comimttee will eliminate repetitive steps in many instances, and will serve as fundamental data in the approach to future investigations. Furthermore, the text of Volume 3, complemented by the contents of Volumes 1 and 2, may be easily adapted to classroom use.

The declassification of the Summary Technical Report makes it possible to publish this consolidated edition of the three volumes. It will, in my opinion, fill a need for the greater distribution of information essential to further developments in the field of radio wave propagation.

CHAS. R. BURROWS, *Director,*
School of Electrical Engineering,
Cornell University, Ithaca, New York

October 15, 1948

PREFACE*

In this series of three volumes, which is part of the Summary Technical Report of NDRC, the Committee on Propagation is presenting a record of its activities and technical developments. The material presented, concerning as it does the propagation of radio waves through the troposphere, is of permanent value both in war and in peace.

[In Volume 1, Part I] gives a critical overall view of the technical developments in the study of tropospheric propagation. Outlined is the general theory of both standard and nonstandard propagation together with descriptions and results of transmission experiments carried out in widely separated parts of the earth and designed to test the theory. Included also is a résumé of the meteorological factors affecting propagation of waves and their attenuation in the atmosphere.

One of the important contributions of the NDRC Committee on Propagation of permanent value is the publication of the technical papers presented at the several Conferences on Propagation. The first Conference was held at the Radiation Laboratory at Massachusetts Institute of Technology in July 1943 prior to the formation of the Committee on Propagation. Those sponsored by the Committee were the second, third, and fourth Conferences held, respectively, in New York, February 1944; in Washington, November 1944; and in Washington, May 1945.

The bulk of the material published is taken from the Columbia University reports and from the papers presented at the third and fourth Conferences; the remainder comes from the second Conference. By careful selection it has been possible to avoid excessive repetition; and yet on continuing projects, such as transmission studies, it is possible to follow their development over a considerable period of time.

Some of the material has been published in Volume 1 of this series — that dealing with the theoretical aspects of propagation, both standard and nonstandard. In [Part I of Volume 2] the subject considered is meteorology: first theory, then equipment, and finally the development of forecasting techniques in which the ultimate goal is the ability to predict radio performance from meteorological measurements made considerably earlier.

[In Part II of Volume 2 a chapter] on reflection coefficients presents a certain amount of new material which, however, tends to confirm previous views and further substantiates formulas already available. [In a chapter] on dielectric constant, absorption, and scattering, the reader will find a considerable volume of new material. With decreasing wavelength the

absorption by the components of the atmosphere becomes increasingly important while the problems of absorption and scattering, as related to wavelength and water droplet size, bear importantly on the ability to track clouds and storms by radar.

[In a chapter] on echoes and targets, the reader will find an interesting treatment of some of the more unusual problems concerning the radar behavior of targets. Volume 2 closes with a consideration of an angle-of-arrival experiment.

The material presented [in Volume 3] was prepared by the Columbia University Wave Propagation Group at the request of the Committee on Propagation of the National Defense Research Committee. The International Radio Propagation Conference, meeting at Washington in May 1944, recommended that a book be prepared dealing with problems of radio wave propagation in the standard atmosphere at frequencies above 30 megacycles. The importance of these higher frequencies is apparent when it is recalled that most radars operate in this range and that an increasing number of communication circuits are being equipped for operation above this frequency.

A certain amount of evidence from operational theaters indicates that lack of familiarity with the underlying theory of propagation and calculations based thereon not infrequently has resulted in ineffective installation and operation of radar and communication sets. This is ascribable, in part at least, to the lack of publications which give a clear picture of the problems of propagation or show how the important factors may be evaluated.

A considerable volume of basic material on propagation had appeared in technical journals before World War II, and during the war a great quantity of classified material has come from laboratories and operational theaters, illustrating new applications of old principles, giving valuable information on propagation problems as well as on characteristics of radar and communication sets, antennas, targets, siting problems, etc. But this information has not been coordinated under one cover for practical use by signal personnel in the field. The Columbia University Wave Propagation Group was asked to undertake this task, and it is hoped that this book will, in some measure, answer the need.

Our effort, then, has been to provide a book designed for men with college training in radio, physics, or electrical engineering, which states the basic laws of propagation, that is, shows how the characteristics of the earth and the atmosphere control the propagation of radio waves; gives the fundamental properties of the basic types of antenna

---

*The Editor's Prefaces to the three volumes of the Summary Technical Report of the Committee on Propagation have been consolidated and abridged for reprinting as the Preface to the present volume.

v

systems, particularly their directivity and gain;
gives the reflecting properties of targets such as
airplanes for use in detection by radar; teaches the
reader how to calculate field strength or obtain the
coverage diagrams given a particular set, power, and
site; gives the fundamental information required in
the above calculations for application to the radar
and communication sets used in operational theaters;
and provides illustrative material and sample calcu-
lations which show how the laws of propagation
may advantageously be used in the location and
operation of radar systems, communication sets, and
countermeasure equipment designed to deceive the
enemy and to prevent jamming of equipment by
enemy action or by mutual interaction of our own sets.

The reader [will find in the Appendix] a summariz-
ing review of six transmission experiments carried
out in widely separated geographical locations;
namely, Massachusetts Bay, San Diego, Arizona,
Antigua, West Indies, and Great Britain. The basic
objectives here have been to learn the facts concern-
ing transmission, and, as far as possible, to correlate
them with the transmission theory given in Volume 1
and with the meteorological factors presented in
Volume 2.

One of the main functions of the NDRC Com-
mittee on Propagation was to bring about a rapid
exchange of information between the laboratories
and Service units working on the subject, and make
the results available to all workers technically con-
cerned with the military application of radar and
other short wave radio equipment. To fulfill this
function the Columbia University Propagation
Group operating under contract with the Committee
periodically published a comprehensive bibliography
on propagation, beginning in the spring of 1944.
Its fifth and last edition, issued in August 1945, is
included [in the General Bibliography]. [This]
General Bibliography lists reports on tropospheric
propagation issued by numerous Service and civilian
organizations and is a rather exhaustive accumula-
tion of the efforts made during the war in this field by
Great Britain, Canada, New Zealand, Australia, and
the United States. With a few exceptions, original
reports listed in the Bibliography have been micro-
filmed. A few, such as summary reports issued by
the Columbia University Wave Propagation Group
and the compiled Propagation Reports, are included
in the present series.

STEPHEN S. ATTWOOD
Editor

CONTENTS

Volume I

TECHNICAL SURVEY

Volume II

RADIO WAVE PROPAGATION EXPERIMENTS

Volume III

THE PROPAGATION OF RADIO WAVES THROUGH THE STANDARD ATMOSPHERE

TECHNICAL SURVEY

VOLUME I

Chapter 1

STANDARD PROPAGATION

INTRODUCTION

B Y STANDARD PROPAGATION is meant radio wave propagation through an atmosphere free from irregular stratifications, particularly of vertical distributions of water vapor and temperature. With irregular stratification the propagation is said to be nonstandard and will be treated extensively in the later chapters.

In this chapter the fundamental general relations between transmitted and received power is first reviewed; then the main factors influencing the transmission of electromagnetic waves such as refraction, diffraction, and dielectric properties of the ground are surveyed; and finally the computation of the field at the receiver for various heights of transmitter and receiver above a homogeneous smooth earth of given electromagnetic properties is very briefly discussed. The last subject divides naturally into the determination of the field above the line of sight and the determination of the field below the line of sight in the earth's shadow.

The text of the present chapter largely follows the book, issued by the Columbia University Wave Propagation Group [CUDWR WPG] under the title *Propagation of Radio Waves through the Standard Atmosphere*

POWER TRANSMISSION

Certain relations occur so frequently in wave propagation problems that it is convenient to summarize them here before entering into a description of the characteristic features of short wave propagation. Some of these are mere definitions; some are consequences of electromagnetic theory.

It is convenient to use, as a standard antenna, one which has a length which is small compared to the wavelength, designated as "doublet." Such doublets may be used for both the transmitting and receiving antennas. In the latter case it is assumed that the load resistance is matched to the output resistance of the antenna. In free space, optimum transmission is achieved when the two doublets are parallel to each other and perpendicular to the line connecting their centers. If their distance apart, d, is large compared to the wavelength, the ratio of power transmitted to maximum useful power received is found from electromagnetic theory to be

$$\frac{P_2}{P_1} = \left(\frac{3\lambda}{8\pi d}\right)^2, \tag{1}$$

where λ and d are measured in the same units. Here P_2 is the power delivered to a matched load at the output terminal of the receiver and P_1 the power fed to the transmitting antenna.

The gain G of any directive antenna is the ratio of the power transmitted by a doublet to the power transmitted by the antenna in question, to produce the same response in a distant receiver, when both transmitting antennas are adjusted for maximum transfer of power. The gain of a receiving antenna is similarly the ratio of the power delivered to the transmitting antenna when a doublet receiving antenna is used to the power delivered to the transmitting antenna to produce the same response when the antenna in question is used at the receiver.

Two methods of expressing antenna gain are in common use: the one just indicated where the gain is measured as the ratio of the power in the optimum direction relative to that of a doublet, and the other where the gain is that relative to a hypothetical isotropic radiator which is one assumed to radiate the same power density in all directions. Simple geometrical considerations show that the gain of a doublet over that of an isotropic radiator is 3/2 so that the gains expressed in the former system are converted into the latter system by multiplying them by 3/2. In the equations below, the gain is expressed relative to the doublet.

If transmission takes place, not in free space, but over a conducting ground, in a refracting atmosphere, etc., the power ratio will be expressed as

$$\frac{P_2}{P_1} = G_1 G_2 \left(\frac{3\lambda}{8\pi d}\right)^2 A_r^2, \tag{2}$$

1

FIGURE 1. Nomogram for free space transmission between parallel doublets.

to a matched load is

$$P_2 = \frac{E^2}{120\pi} \cdot \frac{3\lambda^2}{8\pi} G_2 . \tag{4}$$

The combination of equations (3) and (4) gives again the general transmission formula (2).

The lower limit of possible receiver sensitivity is set by the thermal noise in the receiving system. At ordinary temperatures the thermal noise power in watts is very approximately

$$P_{\text{noise}} = 4 \cdot 10^{-15} \Delta f, \tag{5}$$

where Δf is the radio-frequency bandwidth of the receiver in megacycles.

The minimum power P_{min} required for intelligible reception being usually in excess of the thermal noise power, it is customary to use the ratio $P_{\text{min}}/P_{\text{noise}}$ expressed in decibels as a measure of the receiver sensitivity Ten times the logarithm of this ratio (to the base 10) is the sensitivity of the receiver in decibels above thermal noise.

As may be seen from this brief outline, the problem of transmission in free space is a very simple one from the engineering viewpoint. There are certain questions regarding noise limit, receiver sensitivity, and matching of the load which constitute refinements of the above procedure. They are of interest primarily for those concerned with receiver design; apart from these the problem of power transmission may be considered solved by these formulas. The most important and difficult part of ultra short wave propagation then becomes the quantitative determination of the path factor A, as a function of the geometry of the transmission path, electromagnetic properties of the ground, refractive properties of the atmosphere, etc

OPTICAL PROPERTIES OF THE EARTH'S SURFACE AND ATMOSPHERE

REFLECTION COEFFICIENTS

In dealing with standard propagation it is usually assumed that the ground has electromagnetic properties which are constant over the length of the transmission path. Deviations from this idealized behavior are treated below as diffraction phenomena.

The electromagnetic properties of the ground are completely described by its complex dielectric constant,

$$\epsilon_c = \epsilon_r - j\epsilon_i = \epsilon_r - j60\sigma\lambda, \tag{6}$$

where ϵ_r is the relative dielectric constant, σ the conductivity in mhos per meter, and λ the wavelength in meters. In general, and especially in the microwave region, ϵ_r and ϵ_i are themselves functions of the frequency. Figure 2 shows the variation of the real and imaginary parts of the complex dielectric constant of sea water at 17 C for ultra-high frequencies according to the best available experimental data.

where $G_1 G_2$ are the antenna gains of the transmitting and receiving systems, respectively, and A, is the "path factor." The nomogram, Figure 1, gives this relation for $G_1 = G_2 = A$, $= 1$. Often the electric field at the position of the receiver is desired. It is given by

$$E = \frac{3\sqrt{5}}{d} \sqrt{P_1 G_1} A_p, \tag{3}$$

where E is in volts per meter, P_1 in watts. If E is known, the power delivered by the receiving antenna
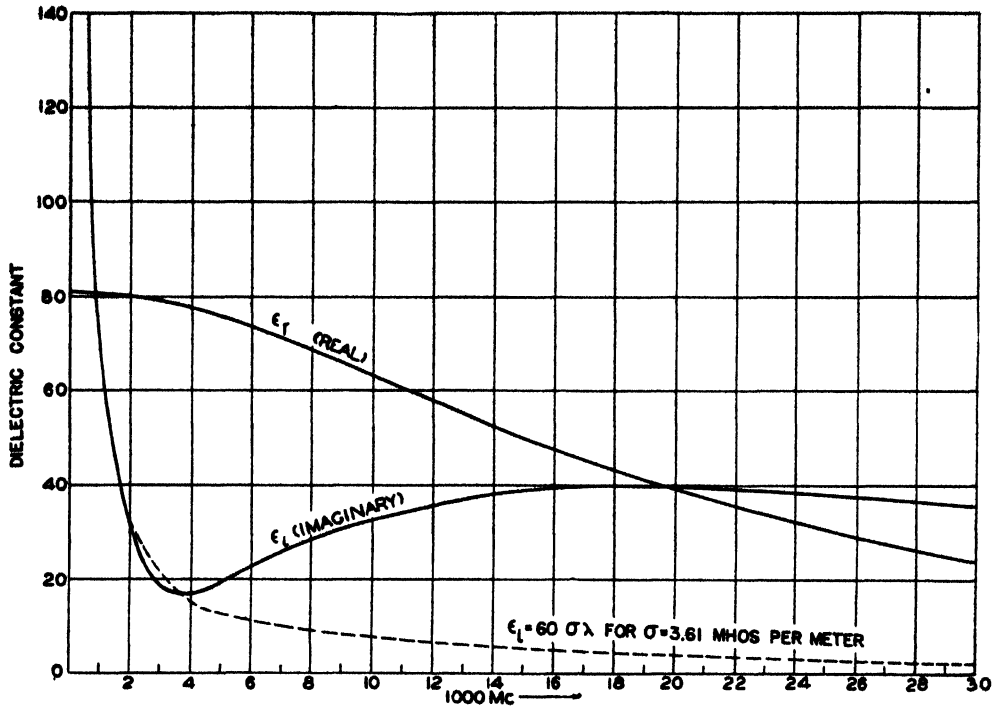
FIGURE 2. Dielectric constant of sea water at 17 C.

The reflection coefficient is given by Fresnel's formulas. Let ψ indicate the angle between the incident ray and the horizontal reflecting surface. Then, for horizontal polarization

$$R = \rho e^{-i\phi} = \frac{\sin \psi - \sqrt{\epsilon_c - \cos^2 \psi}}{\sin \psi + \sqrt{\epsilon_c - \cos^2 \psi}}, \quad (7)$$

and for vertical polarization

$$R = \rho e^{-i\phi} = \frac{\epsilon_c \sin \psi - \sqrt{\epsilon_c - \cos^2 \psi}}{\epsilon_c \sin \psi + \sqrt{\epsilon_c - \cos^2 \psi}}, \quad (8)$$

where ρ designates the magnitude of the reflection coefficient, and ϕ the phase lag of the reflected ray at reflection. Figure 3 illustrates the amplitude of the reflection coefficient for sea water as a function of the angle ψ for several frequencies. Figure 4 shows the corresponding phase lag at reflection.
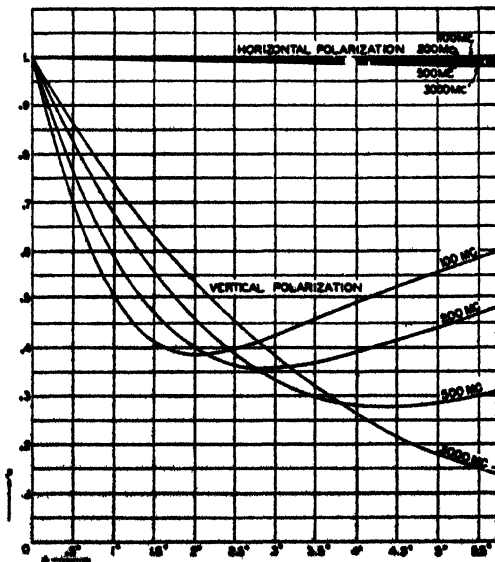
FIGURE 3. Amplitude, ρ, of the reflection coefficient versus reflection angle, ψ, from $\psi = 0$ to $\psi = 5.5°$ for sea water.
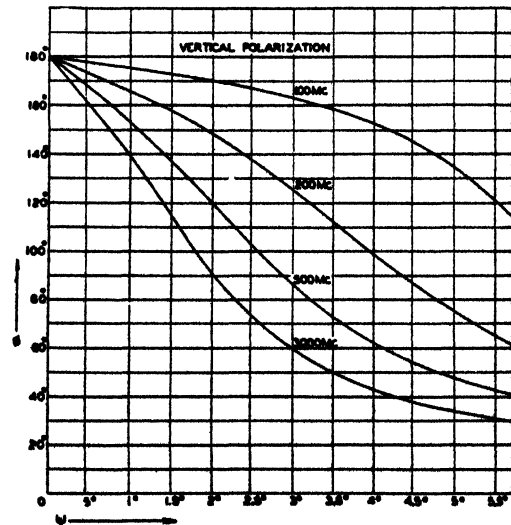
FIGURE 4. Phase lag, ϕ, of the reflection coefficient versus reflection angle, ψ, from $\psi = 0$ to $\psi = 5.5°$ for sea water.

From the practical viewpoint the following summary may give an overall picture of the more outstanding features of ground and sea reflection.

For *horizontal* polarization over the sea the reflection coefficient may be taken as unity and the phase shift as 180 degrees for frequencies up to and including the centimeter range, for practically all angles of reflection. Over land there is a slight decrease of the amplitude of the reflection coefficient with increasing angle; for instance, for a frequency of 200 mc, at an angle of 15 degrees the reflection coefficient has decreased to 0.9 or slightly more for moist soil and to 0.8 or slightly more for dry soil. These statements apply when the ground or sea surface is reasonably smooth. In order to decide whether a surface is smooth or rough, Rayleigh's criterion, explained below, is usually applied. When the surface is rough or wavy, irregular scattering predominates and reduces the intensity to a small part of the value attained with a smooth surface.

For *vertical* polarization the curve of the magnitude of the reflection coefficient versus the angle goes through a minimum (see Figure 2). When the imaginary term of the complex dielectric constant is negligible so that the ground behaves like a pure dielectric material, the reflection coefficient goes to zero at a certain angle (Brewster angle). Ordinary soil nearly fulfills this condition. For instance, at a frequency of 200 mc the Brewster angle occurs at about 12 degrees with moist soil and at about 21 degrees with dry soil.

For the ocean surface, and vertical polarization, the imaginary part of the dielectric constant cannot be neglected, and the reflection coefficient as a function of the angle does not vanish at any angle but goes through a minimum, the pseudo-Brewster angle. The actual variation of amplitude and phase lag is represented in Figures 2 and 3 for the small angles of reflection which are most important in practice.

When the ground is rough the reflection coefficient for both types of polarization is reduced to a very small value. For 10-cm waves and still more for shorter ones, most types of land are rough. A reflection coefficient of 0.2 may be taken as representative for an average ground covered with vegetation. A slightly ruffled sea is a fairly good reflector for 10-cm waves but appears somewhat rough at shorter wavelengths.

STANDARD REFRACTION

Numerous experiments have resulted in the following formula for the refractive index of moist air:

$$(n - 1) \cdot 10^6 = \frac{79}{T} \left(p - e + \frac{4{,}800e}{T} \right) \quad (9)$$

where n = the index of refraction,
    p = the barometric pressure in millibars
        (1 mm mercury = 1.3332 mb),

    e = partial pressure of water vapor in millibars,
    T = absolute temperature.

The mixing ratio, s, which is practically equal to specific humidity, is connected with e by the relation

$$e = 0.00161 ps . \quad (10)$$

A recent analysis[278] has shown, moreover, that this expression for refractive index must, on theoretical grounds, be substantially independent of frequency down to the shortest waves employed in microwave engineering.

In an average atmosphere temperature, pressure, and water vapor density decrease with height, and, in the lowest few kilometers where most of the short and microwave propagation takes place, it may be assumed to a good approximation that the decrease of refractive index with height is linear though the rate of decrease is somewhat dependent on the climate. In middle latitudes it is given by

$$\frac{dn}{dh} = -0.039 \cdot 10^{-6} \text{ per meter} . \quad (11)$$

Refraction at the boundary of two media is familiar from optics and is expressed by Snell's law:

$$n_1 \cos \alpha_1 = n_2 \cos \alpha_2 , \quad (12)$$

where n_1 and n_2 are the refractive indices of the two media and α_1 and α_2 the angle between the boundary and the direction of the ray in the first and second media respectively. In the atmosphere the refractive index is a continuous function of height, and the sudden change of direction at a boundary is then replaced by a *curvature* of the rays. Equation (12) can be written

$$n \cos \alpha = n_0 \cos \alpha_0 , \quad (13)$$

where n and α are now continuous functions of the height and the subscript 0 designates a reference level.

The above formulas refer to a plane earth. If the earth's curvature is taken into account so that the planes relative to which the angle α is measured are replaced by spheres about the earth's center, formula (13) must be modified; and the mathematical analysis shows[442] that it is replaced by

$$nr \cos \alpha = n_0 r_0 \cos \alpha_0 \quad (14)$$

where r is the distance from the center of the earth to the level considered.

If now we set $r = r_0 (1 + h/r_0)$ where $h = r - r_0$ and h/r_0 is a small quantity and, furthermore, if we note that with a linear gradient of n

$$n = n_0 + \frac{dn}{dh} h \quad (15)$$

we obtain on substituting into (14) and neglecting small quantities of the second order

$$\left[1 + \left(\frac{1}{r_0} + \frac{dn}{dh} \right) h \right] \cos \alpha = \cos \alpha_0 . \quad (16)$$

It results from this equation that a linear gradient of refractive index has the same effect on refraction as the curvature of the earth, $1/r_0$. By introducing an effective earth's radius it is possible to eliminate the refraction term entirely and to treat the atmosphere as if it were homogeneous. This device was first introduced by Schelleng, Burrows, and Ferrell,[24] and has since been generally accepted. Some German writers have introduced a quadratic function to represent the variation of refractive index with height in the atmosphere,[443] the coefficients of the quadratic terms being characteristic of the air mass or type of atmosphere involved. This has the advantage of permitting a close fit with observed refractive index curves up to heights of 6 to 8 km. It seems, however, that the advantage of the greater analytical simplicity of the linear refractive index curves far outweighs the increased accuracy of the quadratic form, and the latter has therefore not found acceptance in this country and Great Britain.

It is customary to designate the effective, or modified earth radius by ka where k is a numerical constant and a replaces r_0 used above and represents the mean radius of the earth. Hence

$$\frac{1}{a} + \frac{dn}{dh} = \frac{1}{ka}, \qquad (17)$$

and by comparison with equation (11) it follows that

$$k = \frac{4}{3} \qquad (18)$$

since $dn/dh = -0.039 \cdot 10^{-6} = -1/4a$. The earth's radius $a = 6.37 \cdot 10^6$ meters.

In view of this result coverage diagrams of radar and radio communication sets are commonly drawn with a $4/3$ earth's radius. In such a diagram the rays, which are curved in a "true" geometric representation, appear as straight lines.

The value $k = 4/3$ does not, of course, represent a universal law. It is merely an expression of the fact that the rate of decrease of the refractive index with height has, in the middle geographical latitudes, a certain average value. In arctic climates k as a rule is somewhat smaller, lying between $4/3$ and $4/4$, while in tropical climates k is somewhat larger, between $4/3$ and $3/2$. In temperate and tropical climates, the main factor determining the magnitude of k is the humidity gradient in the lower atmosphere. In Figure 5 is shown a nomogram from which the appropriate value of $1/k$ can be read directly as function of the gradient of *relative* humidity and air temperature. The table has been computed under the assumption that the temperature gradient has the "standard" value of -0.65 C per 100 m, but the value of k is relatively insensitive to variations in the temperature gradient

Usually the value of $k = 4/3$ is referred to as the standard case, but this term is also used to designate more generally an atmosphere with a linear refractive index distribution where k might differ somewhat from $4/3$. Experience shows that the atmospheric conditions under which the refractive index is a linear function of height are quite common, but this is only one case out of several that may, and do, arise in the atmosphere. A full appreciation of the

(RH)	-30C	-25C	-20C	-15C	-10C	-5C	0C	+5C	+10C	+15C	+20C	+25C	+30C	+35C	+40C
10%	.009	.012	.017	.027	.039	.055	.078	.090	.118	.151	.194	.240	.301	.371	.455
20%	.008	.011	.015	.024	.034	.049	.069	.080	.105	.134	.172	.214	.267	.329	.405
30%	.007	.009	.014	.021	.030	.043	.060	.070	.092	.118	.151	.187	.234	.288	.354
40%	.006	.008	.012	.018	.026	.037	.052	.060	.079	.101	.129	.161	.200	.247	.304
50%	.005	.007	.010	.015	.021	.031	.043	.050	.066	.084	.108	.134	.167	.206	.253
60%	.004	.005	.008	.012	.017	.024	.034	.040	.052	.067	.080	.107	.134	.165	.202
70%	.003	.004	.006	.009	.013	.018	.026	.030	.039	.050	.065	.080	.100	.123	.152
80%	.002	.003	.004	.006	.009	.012	.017	.020	.026	.034	.043	.065	.067	.082	.101
90%	.001	.001	.002	.003	.004	.006	.009	.010	.013	.017	.021	.027	.033	.041	.051

FIGURE 5. Graph: $1/k$ versus RH gradient and temperature for 100 per cent RH at ground. Add correction tabulated to obtain $1/k$ for RH at ground $\neq 100\%$.

limitations of the concept of standard refraction requires some knowledge of the phenomena of non-standard propagation which will be dealt with extensively in later chapters.
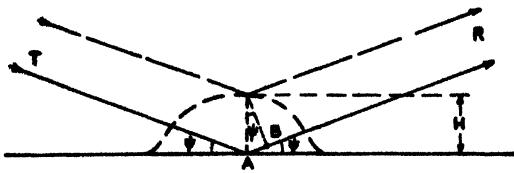
FIGURE 6. Geometry for Rayleigh's criterion for rough ground.

ROUGHNESS OF THE GROUND

In order to estimate how closely the ground approximates the condition of an ideal reflecting surface, a rule is required that gives results sufficiently accurate to be used in radio and radar practice. The subject has not been very thoroughly explored, but Rayleigh's criterion for roughness, originally developed for optical purposes, has been applied with good success. Since it seems to be the only criterion of its kind and since it is often necessary to decide whether the terrain in front of a given radio or radar site is reflecting, it deserves some detailed consideration.

The principle of Rayleigh's criterion is illustrated in Figure 6. The roughness is assumed to be produced by a large number of elevations in the reflecting plane of average height H. One such "hump" is shown in the figure together with two rays one of which is assumed to be reflected from the ground surface and one from the top of the "hump." The difference in phase between the two rays is $2H\psi(2\pi/\lambda)$. The criterion now requires that the surface be considered as rough when this phase difference exceeds $\pi/4$ radians. This gives for the critical value of H, when ψ is in degrees, λ in meters,

$$H = \frac{\lambda}{16\psi} \tag{19}$$

If n is the "lobe variable," that is, a quantity equal to $1 \; 3 \cdots (2n - 1), \cdots$ at the first, second, nth interference maximum of the direct and ground-reflected rays, namely,

$$n = \frac{4h_1\psi}{\lambda}, \tag{20}$$

where h_1 is the height of the transmitter above the ground, the criterion can be written in the form

$$H = \frac{h_1}{4n}. \tag{21}$$

Although admittedly rough, the criterion indicates the order of magnitude of the angle above which specular reflection will be greatly reduced in favor of diffuse scattering of the type which, in ordinary

optics, is produced by a dull, white surface. It is reasonably safe to assume that for angles exceeding the critical angle the amount of specular reflection will be reduced to a small fraction, perhaps to the order of one-fifth, of the value of the reflection under ideal conditions.

DIFFRACTION BY TERRAIN

A number of the influences of the earth's surface upon wave propagation have the common characteristic that they represent deviations of the actual earth from the idealized model of a smooth sphere endowed with homogeneous electrical constants. Diffraction by the earth's average curvature is not included among the effects considered here since it is dealt with extensively in Volume 3.

There are two main classes of phenomena that fall under the general heading of diffraction. One is the diffraction by obstacles, such as hills, trees or houses, and the other is the diffraction by the structure of an otherwise fairly level ground, in particular, roughness and horizontal variations of dielectric constant.

The diffraction by hills and similar obstacles of the terrain is commonly treated theoretically by means of the Fresnel-Kirchhoff diffraction theory as found in textbooks on optics. The only problem which is sufficiently simple to admit of a direct application to
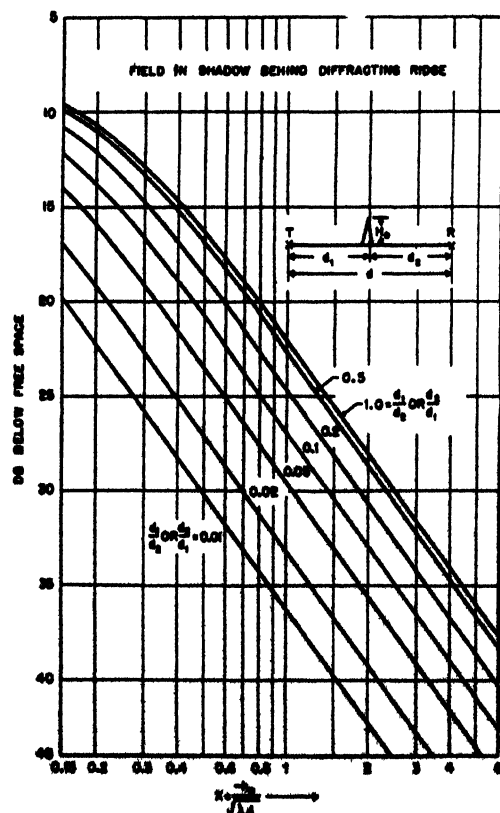
FIGURE 7. Field in shadow behind a diffracting ridge.

short wave transmission is that of diffraction by a straight edge. It is not necessary that the edge be perpendicular to the line connecting the transmitter and receiver but for, the validity of the theory it is necessary to suppose that the distances from the diffracting obstacle to the transmitter and receiver are large compared to the height of the obstacle, which means that the angles of diffraction are small. Figure 7 shows a nomogram from which the field strength in the shadow of a diffracting edge can be read in decibels below that of free space. The geometrical significance of the quantities used is illustrated on the figure.

Such experiments as have been made show a general agreement with theory, but it is difficult in practice to realize conditions of transmission that approach ideal ones, to which the Fresnel-Kirchhoff theory refers. When appropriate values are taken for the reflection coefficient of the ground and the four components of the resulting field are added vectorially, good agreement has been found between experiment and theory for selected terrain. (See Chapter 11 of this volume.) Sometimes the terrain conditions are often so complicated that they do not readily lend themselves to idealization by simple geometrical· models. For these reasons the Fresnel-Kirchhoff diffraction theory has been of only limited value in short wave radio propagation.

A case which quite often can be described adequately by an idealized model is that of a sudden change of the dielectric properties of the ground, as at a coast line.[340-346] If the land is rough while the sea surface produces full specular reflection, the coast line can be considered as a diffracting straight edge with respect to the image antenna, rays of which represent the field reflected by the sea surface. The straight edge serves to cut off that part of the radiation from the image that would represent reflection from the land area. The geometrical conditions are shown schematically in Figure 8. For·the details of
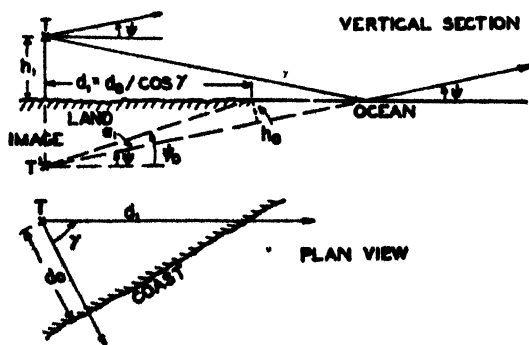
FIGURE 8. Diffraction by a coast line.

the analytical treatment the reader is referred to the comprehensive report on standard propagation contained in Volume 3 of the Summary Technical Report of the Committee on Propagation. The distor-

tion of the coverage diagram of a radar set caused by this type of diffraction is often quite large and becomes important operationally at frequencies of 100 to 200 mc. This is illustrated here by a computed coverage diagram shown in Figure 9. If diffraction is
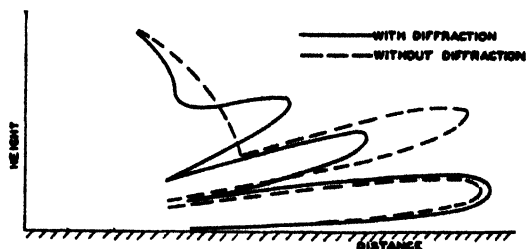
FIGURE 9. Coverage diagram for coast line diffraction (relative field strength). (Heights exaggerated 3.5 to 1.)

not taken into account the coverage pattern shows a constant amplitude through higher angular elevations reached only by the direct rays since the ground reflection is negligible. At lower angular elevations rays reflected from the sea add to the direct rays, and the "lobe" type of pattern appears. It is clear that if the diffraction effect were neglected very serious errors of the estimated coverage would result.

Similar methods can be used to treat diffraction caused by cliffs, edges of wooded areas, lakes, etc., but these cases are not so often of importance in radar practice.

THE ELECTROMAGNETIC FIELD

FIELD STRENGTH DISTRIBUTION

If a transmitter is erected over a plane, ideally reflecting earth, the well-known lobe pattern results
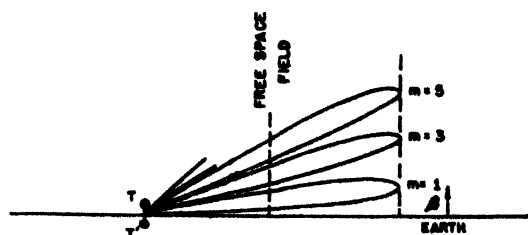
FIGURE 10. Typical coverage diagram (lobes) over plane earth.

(Figure 10), the curves being ones of constant field strength. The field is given by

$$E = E_0 \cdot 2 \sin \left(\frac{2\pi h_1 h_2}{\lambda d} \right) \qquad (22)$$

where h_1 and h_2 are the transmitter and receiver heights, and d the distance from transmitter to receiver. The maxima and minima occur at the positions in space where

$$h_1 h_2 = \frac{n}{4} \lambda d \tag{23}$$

with $n = 1, 3, 5 \cdots$ for the maxima,

$n = 0, 2, 4 \cdots$ for the minima.

If $h_2 \gg h_1$, the angle of elevation is $\psi = h_2/d$ and the formula for the maxima and minima can be written

$$\psi = \frac{n\lambda}{4h_1} \tag{24}$$

If the earth curvature is taken into account the pattern remains essentially the same above the line of sight, but a number of corrections enter which change somewhat the position and strength of the lobes. The problem is primarily one of geometry, taking into account the modification of the direction, phase, and intensity of the reflected ray caused by the earth's curvature. It can be solved by suitable numerical and graphical methods such as are given in Volume 3 where the details are extensively treated. It may suffice here to enumerate the main modifying factors.

If a tangent to the earth is drawn at the point of reflection (Figure 11), the distances h'_1 and h'_2 of transmitter and receiver from this line are the equiv-

FIGURE 11. Geometry over spherical earth.

alent heights in terms of which the problem is a plane-earth problem for that particular ray. They are smaller than the heights above the ground h_1 and h_2, but clearly they are functions of the angle of elevation. Thus a set of implicit equations has to be solved for each angle of elevation giving h'_1 and h'_2 as functions of h_1, h_2, and d, whereupon the interference between the direct and reflected rays is computed as in the case of a plane earth.

In addition to the modification of direction and phase at reflection, there is also a change in intensity of the reflected ray caused by the fact that the reflecting surface is curved. This modification is taken into account by the *divergence factor*, a purely geometrical quantity which is part of the reflection coefficient, reducing the intensity of the reflected ray.

The behavior of the field below the line of sight requires a more powerful line of attack. The line of sight itself is given by a tangent to the earth's surface

passing through the transmitter. The distance from the transmitter to the horizon, when a modified earth's radius ka is used is

$$d_T = \sqrt{2kah_1} \tag{25}$$

When $k = \frac{4}{3}$, h_1 is in meters and d_T in kilometers, this becomes

$$d_T = 4.12 \sqrt{h_1}. \tag{26}$$

The diffraction region actually extends at least from the lower surface of the first lobe downward to the earth's surface. In the diffraction region well below the line of sight, the field strength decreases very rapidly and very nearly exponentially with the distance.

Figure 12 shows a typical example for the ground

FIGURE 12 Field strength versus distance for fixed height, vertical polarization.

constants indicated. The ordinate is the ratio of field strength to the free space field; the transmitter and receiver heights are fixed and d is plotted as abscissa. Above the line of sight the typical lobe pattern is exhibited. The decrease of the field in the diffraction region is the more rapid the shorter the wavelength. In the centimeter band this decrease is so rapid that for most practical purposes the field is nonexistent near the ground at distances exceeding the horizon distance by more than a few kilometers. Figure 13 shows a similar diagram for fixed distance and variable receiver height.

MODES

The description of the electromagnetic field above the line of sight is adequately given by means of rays and their phases as used in optics. This method obviously breaks down in the diffraction region into which the rays do not penetrate. For this region a solution of the wave equation is required. Many distinguished mathematicians have contributed varying techniques for solving the wave equation. The theory in its present form as applied to short and microwave propagation has been worked out by van der Pol and Bremmer[20] for vertical polarization

and Marian C. Gray for horizontal polarization.

The results of the theory may be summarized as follows. The electromagnetic field can be represented as an infinite series of the form

$$E = E_0 \sqrt{d} \sum_m c_m e - \zeta_m d \ U_m(h_1) \ U_m(h_2) \quad (27)$$

·where E_0 is the free space field and c_m and ζ_m are complex constants depending upon the wavelength and the electromagnetic ground constants. h_1 and h_2 are again the heights of the transmitter and receiver above the ground, d is the distance between the two; U_m are the height-gain functions, and e is the base of natural logarithms. The formula is symmetrical with respect to the interchange of transmitter and receiver, in agreement with the principle of reciprocity.

Each of the terms which compose the sum (27) is called a *mode*. The coefficients ζ_m are complex constants with their real parts positive. They represent therefore an exponential decrease of the field strength with distance. The real part of ζ_m is *the attenuation factor* of the mth mode expressed in nepers per unit distance. The height-gain functions U_m are found to increase with height above the ground. The increase is first slow but eventually becomes exponential and remains that way for large heights.

The real part of ζ_m, the attenuation factor, increases with increasing mode number; hence, if the receiver is far enough from the transmitter, all modes except the first one become very small and the sum in equation (27) reduces to its first term which can be computed without much difficulty.
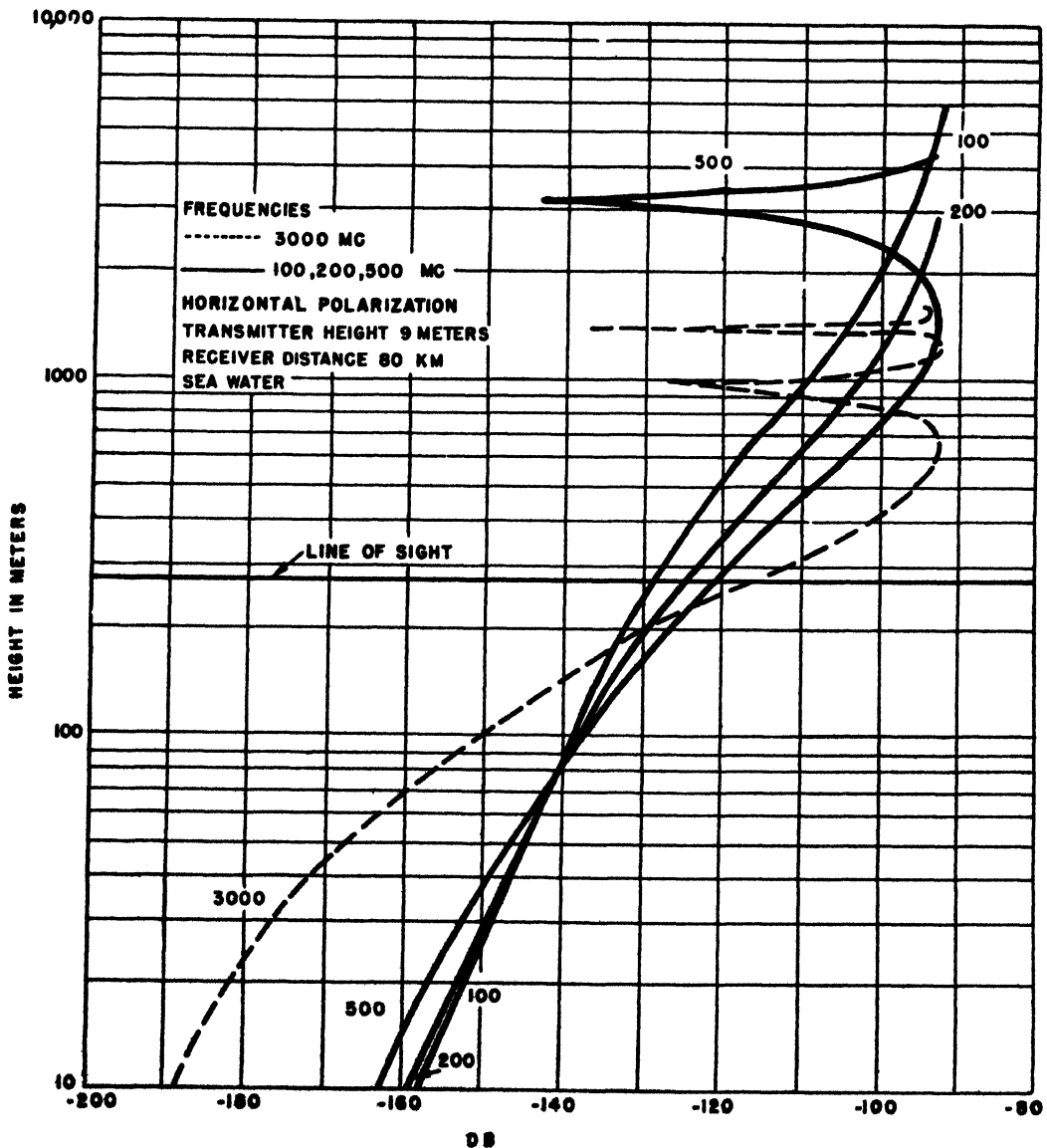
FIGURE 13. Field strength versus height of receiver for fixed distance relative to radiation field at one meter from transmitter.

This applies when the heights h_1 and h_2 are fairly small. The height-gain functions increase with height the more rapidly the higher their order, and as one approaches the line of sight the number of modes that contribute to the field strength becomes large. It is true that the series (27) converges everywhere, but above the line of sight the number of terms required for a good approximation is so large that the expression is useless for numerical work. Here the methods of ray optics become applicable. It is usually found that, at a given distance d, the field in the lower part of the diffraction zone can be computed by using one or a few terms of the series (27). At large heights above the line of sight the field is determined by the methods of ray optics, and the two curves can be joined with a good degree of accuracy by graphical means on a decibel diagram. This has been done in Figures 12 and 13.

The series (27), though simple in external appearance, still proves extremely difficult to evaluate. Burrows and Gray,[18] however, have simplified the mechanics of evaluation to such a degree that numerical data can be obtained by means of a small number of graphs. The detailed procedures employed in computing field strength and contour diagrams by the method of modes are summarized and collected in Volume 3.

ELEMENTARY THEORY OF NONSTANDARD PROPAGATION

HISTORICAL

DURING 1941 AND 1942, short and microwave radar sets became available in England and were installed along the Channel and North Sea coast. Very soon it was found that at certain times these sets were able to pick up targets such as ships and fixed echoes from the French coast which were well below the line of sight and which under the conditions of standard propagation would have given entirely negligible responses. A relationship with the weather soon became apparent. In 1942, enough had become known to establish most of the correlations between excessive ranges and meteorological conditions which have remained fundamental and which are based on the picture of refraction in the lower atmosphere that is now generally accepted.

Later on similar effects with radar sets were discovered all over the world. An example in point is in the Mediterranean where nonstandard propagation, during certain seasons, is the rule rather than the exception. These conditions will be discussed in more detail in the chapter on radiometeorology. The most extraordinary ranges, perhaps, were found in the Indian Ocean where radar sets operating at frequencies of 200 mc were found on occasion to record fixed echoes from as far away as 1,500 miles. The mechanism of this phenomenon is not yet fully understood.

In the Pacific theater extended ranges have also been observed; but, on account of the vast territory covered, the technical difficulty of all operations, and the inadequacy of meteorological coverage, it is difficult to evaluate the results systematically. Up to the present, reports on the conditions responsible for nonstandard propagation have been received from many parts of the world which vary widely in their characteristic features and dependence upon season, weather time of day, properties of the ground, etc. It is possible to lay down certain general rules, but on the whole the phenomena are exceedingly complex.

During 1943 and 1944, a number of systematic experiments on nonstandard propagation were carried out by the British and American Services and affiliated organizations. Most of these were one-way transmission experiments that have a number of advantages over radar experiments, but some of the latter also were undertaken. Extensive transmission experiments were conducted by the British in the Irish Sea and the Americans in Massachusetts Bay, the State of Washington, southern California, and Arizona, and in the West Indian Ocean.

These experiments will be described in the next chapter. Because of the nature of the subject, it will be profitable to discuss the theory before the experiments and to give, in this chapter, an outline of our present conceptions of the theory of nonstandard propagation.

REFRACTIVE INDEX

Nonstandard propagation takes place whenever the rate of variation of the refractive index in the lower atmosphere deviates considerably from the "standard" linear slope defined by equation (11), Chapter 1. The variation might consist either in a deviation from linearity, which is the most common case, or in a linear slope in the lowest layers that is widely different from the value assumed for the standard. The refractive index is a function of temperature, pressure, and the partial pressure of water vapor, given by equation (9), Chapter 1 The dependence of the refractive index on pressure leads to a regular decrease with height, but the change of barometric pressure with the weather produces only an insignificant effect on the gradient. The variations of refractive index in the lower atmosphere owe their existence to stratifications in which the temperature and moisture changes rapidly with height.

In order to express refraction in quantitative terms Snell's law for a curved earth is used as given by equation (14), Chapter 1:

$$nr \cos \alpha = n_0 r_0 \cos \alpha_0 . \qquad (1)$$

Now let

$$n = 1 + (n - 1) \text{ with } n - 1 \ll 1$$

$$r = a \left(1 + \frac{h}{a}\right) \text{ with } \frac{h}{a} \ll 1 \qquad (2)$$

$$\cos \alpha = \left(1 - \frac{1}{2}\alpha^2\right) \text{ with } \alpha \ll 1$$

where a is the earth's radius. Similar expressions are valid for the quantities having the subscript 0. Multiplying out and neglecting quantities that are small of the second order, one obtains

$$n - n_0 + \frac{1}{a}(h - h_0) = \frac{1}{2}(\alpha^2 - \alpha_0^2) . \qquad (3)$$

It has become customary to introduce the modified refractive index M by

$$n + \frac{h}{a} = 1 + M \cdot 10^{-6}, \qquad (4)$$

whereupon Snell's law assumes the form

$$(M - M_0) \cdot 10^{-6} = \frac{1}{2}(\alpha^2 - \alpha_0^2) . \qquad (5)$$

This equation indicates how the angle α between a ray and the horizontal changes as a function of M which, in turn, is a function of the height, both explicitly by equation (4) and implicitly because n is a function of the height in a stratified atmosphere

TYPES OF M CURVES

An M curve is a diagram in which M as abscissa is plotted against the height h as ordinate. Extensive experience has led to a classification of M curves which is shown in Figure 1. The six types exhibited

STANDARD   TRANSITIONAL   SUBSTANDARD

SIMPLE SURFACE TRAPPING   ELEVATED S SHAPE   GROUND-BASED S SHAPE
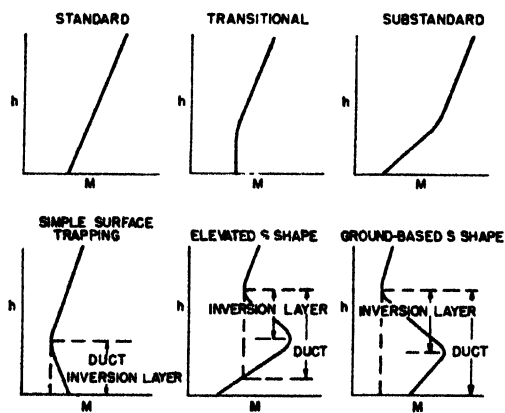
FIGURE 1   Types of M curves

comprise all cases that are of practical interest M curves of a more involved structure are rare. In all cases it is assumed in accord with experience that at sufficiently high elevations the M curves become linear and have, or nearly have, the standard slope.

The height at which these variations in refractive index occur may vary from a few feet to several hundred or even a few thousand feet though they are likely to be found at very low elevations in cold climates and at higher elevations in warm climates. The meteorological conditions which yield these curves will be dealt with extensively in Chapter 5, and few indications may suffice here. Ordinarily, on going aloft the temperature decreases at a slow and fairly steady rate. When, instead, the temperature *increases* with increasing height, a phenomenon known to meteorologists as a temperature inversion, equation (9), Chapter 1, shows that n decreases with increasing height. This does not necessarily imply that M decreases with height since, by equation (4), M contains the term h/a, which increases with height. If, however, the variation of temperature is sufficiently great, a decrease or inversion of M results. Such an inversion produces a *duct*, a term which refers essentially to certain meteorological phenomena and whose exact significance is explained below. A variation of humidity over the layer has

an effect essentially analogous to, but distinctly more pronounced than, the effect of temperature. In this case M increases with height with a decreasing moisture content and vice versa. Variations of humidity are common in the lower atmosphere, and they constitute the main cause of refractive index variations, with temperature variations frequently a contributing factor.

The six cases shown in Figure 1 are as follows: the standard case which needs no further comment; the transitional case where the moisture or temperature variation is not great enough to produce a true inversion of the M curve but merely results in a nearly constant value of M in the lowest strata; the substandard case in which M increases more rapidly with height than in the standard case; and three cases of ducts The simple ground-based duct or surface trapping, consists in an M inversion immediately adjacent to the ground or sea. There are two types of elevated M inversions distinguished by the position of the *minimum* value of M aloft. If this minimum is larger than the value of M at the ground so that the vertical projection from the minimum intersects the M curve, it is considered a true elevated, S-shaped duct. If this minimum is less than the value of M at the ground it is an elevated M inversion but a ground-based duct.

In dealing with these M curves it is universally assumed that the stratification is the same over the whole length of the transmission path. This is a severe restriction, but it has proved indispensable up to date in order to make the problem susceptible to mathematical treatment, and it is reasonably often fulfilled in practice.

RAY TRACING

In order to understand the mechanism of transmission of radiant energy in a duct the course of rays issuing from the transmitter is traced according to equation (5). Note that for the small angles with the horizontal at which these phenomena occur,

$$\alpha = \frac{dh}{dx}, \qquad (6)$$

where x designates the horizontal distance. Hence from equation (5)

$$x = \int \frac{dh}{\alpha} = \int dh [\alpha_0{}^2 + 2(M - M_0) \cdot 10^{-6}]^{-\frac{1}{2}}. \quad (7)$$

Since M is a given function of height, equation (7) gives in integral form the relation between distance and height, where α_0 is the angle with the horizontal of the ray emitted by transmitter and M_0 is the value of M at the transmitter height.

Practicable graphical methods of ray tracing have been developed and used extensively to compute actual coverage diagrams.[44,45,46,71,76,81,93,99] Three schematic pictures of ray tracing, showing the main
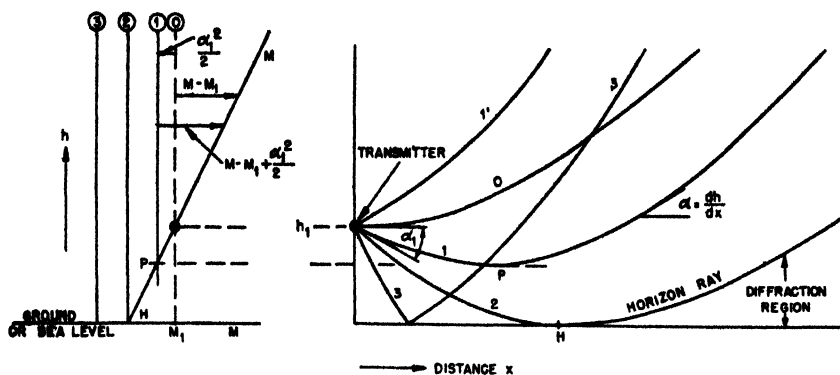
FIGURE 2 Rays in the standard atmosphere
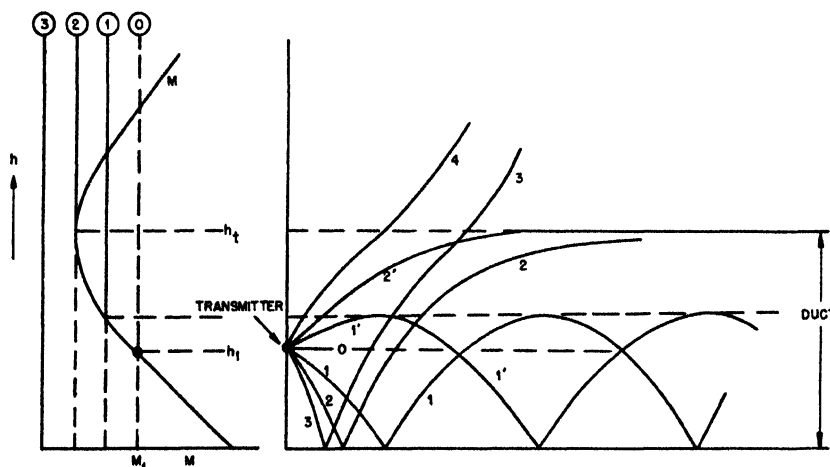
FIGURE 3. Rays with a ground-based duct
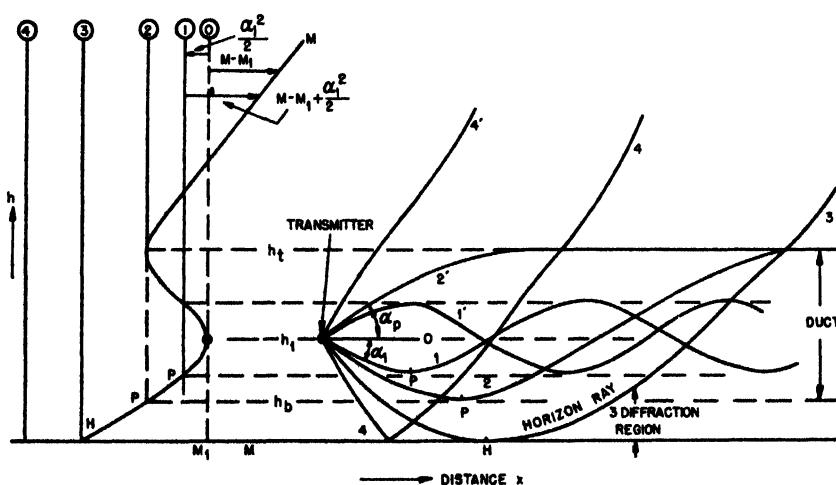
FIGURE 4. Rays with an elevated duct.

phenomena of interest, are presented in Figures 2, 3, and 4. These figures are plane earth diagrams in which the ordinary downward curvature of the earth has been eliminated and replaced by an additional upward curvature of the rays. On the left-hand side of each diagram the M curve is plotted. By equation

(5) we have

$$\alpha = 0 ,$$

if

$$M = M_0 - \tfrac{1}{2} \alpha_0^2 \cdot 10^6 . \tag{8}$$

The vertical lines drawn on the M curve diagram are the values of $M_0 - \tfrac{1}{2} \alpha_0^2 \cdot 10^6$ for the rays

selected. Wherever this line intersects the M curve the corresponding rays become horizontal and thereafter reverse the sign of dh/dx. In the case of Figure 3 these reversals combine with reflections from the ground to make a family of rays oscillate between an upper limit, different for each ray, and the ground. The limiting angle of emergence beyond which re-

FIGURE 5. Calculated coverage diagram.

versal no longer occurs is designated by (2 or 2') in Figures 3 and 4. The duct is the vertical interval cut out by the intersection of the vertical line designated by 2 with the M curve or with the ground. The terms *trapping*, *superrefraction*, or *guided propagation* are often employed to describe these phenomena.

A word might be said here about the substandard

case which, although much less frequent than the duct, is of operational significance. It is readily seen that in this case the rays undergo a strong upward curvature in the layer in which there is a substandard slope of the M curve. As a result of this the apparent horizon distance is reduced, and the ranges of radar and radio equipment for targets or receivers near the ground are greatly diminished. M curves of the substandard type occur often when fog is present but are not uniquely correlated with fog.

In order to compute coverage diagrams on this basis it is necessary to know the phases associated with the rays so as to determine their mutual interference. If this is done by an appropriate graphical or numerical method, contours of *constant field strength* can be drawn. Figure 5 shows, typical coverage diagrams computed in this way,[14] corresponding to a value of $h_1/\lambda = 20$. The lines separating the "detection zones" from the "blind zones" indicate ranges at which a medium bomber would just become visible to the particular radar to which these diagrams apply. Diagram 1 shows the undistorted lobe diagram for standard refraction while diagrams 2, 3, 4, 5 show the coverage diagram for various types of ground-based and elevated ducts.

In Figure 6 is shown the variation of field strength with height for various distances for the M curve shown on the left-hand side of the figure.[73] The transmitter is at a height of 60 m.

In all diagrams shown in this section the vertical scale is vastly exaggerated as compared to the horizontal scale. It may readily be shown that when the representation is such that the earth is curved, the contours of constant height can be represented by parabolas in the approximation where the true vertical elevations are small compared to the horizontal distances involved.

GENERAL CHARACTERISTICS OF DUCTS

It is evident that the number of types of M curves that one can construct a priori is almost unlimited. In practice both the types actually occurring and their variability within each type of classification are severely limited by meteorological conditions.

M, as defined by equation (4), is the sum of two parts, the true refractive part $(n - 1)$ and the earth curvature part h/a. At higher elevations the absolute moisture in the atmosphere decreases, and irregular variations of temperature become more and more exceptional so that eventually, at a relatively great height, any M curve approaches the standard curve. An additional limitation comes from the fact that both the temperature and moisture variations in any one climate are subject to definite limitations. An extreme moisture change occurs when there is a boundary separating a nearly or fully saturated

FIGURE 6. Variation of field strength with height for various distances.

warm air mass from a very dry cool air mass. Temperature inversions involving differences of more than 10 to 15° C are quite exceptional. As a consequence of this both the actual height of the M inversion as well as the difference ΔM between the maximum of M at the bottom and the minimum at the top of the M inversion are limited. The height of the M inversion layer may be only a few feet if it is close to the ground or sea surface. It frequently is of the order of 50 to 100 ft or even larger. Under particularly favorable conditions in warm climates, elevated M inversions may have heights of several thousand feet. The duct itself can be appreciably thicker than the M inversion layer, as may be seen from the structure of the last two M curves in Figure 1.

Again, the decrease ΔM over the height of the inversion is limited for the same reasons. For low ducts values of the order of $\Delta M = 5$ to 10 are common. Somewhat larger values will sometimes occur. The maximum value observed is about $\Delta M = 40$ in high-level inversions at San Diego which originate in the singular climatic conditions found there.

An important consideration for the detailed mathematical treatment of duct propagation is the shape of the knees of the M curve. This, again, depends on the physical nature of the atmospheric stratification. Very often the inflections are so sharp that a succession of two or three straight lines furnishes an excellent approximation. These are known as bilinear and trilinear ducts and are of very common occurrence, especially with elevated ducts and a large class of ground-based ducts. On the other hand, there are also ground-based ducts in which the corners are extremely well rounded.

It follows from the restrictions on the numerical values of M that there are severe limitations on the angle α for which duct effects can occur. Thus $\Delta M =$ 10 represents a change of one part in 10^5 in the re-

fractive index. Now from equation (5), we have by differentiation

$$\Delta M \cdot 10^6 = \alpha \Delta \alpha . \qquad (9)$$

For a complete reversal of a ray we must have $\Delta \alpha \backsim \alpha$, and then α is proportional to the square root of ΔM. In the above case, where $\Delta M = 10$, we find that α is of the order of $3 \cdot 10^{-3}$, or about 10 minutes of arc.

Carrying considerations of this type into a little more detail it is found that the major effects of nonstandard refraction occur only for rays which emerge from the transmitter at an angle of less than $\frac{1}{2}$ degree. For angles between $\frac{1}{2}$ and $1\frac{1}{2}$ degrees the refractive effects produced by the typical nonstandard M curves consist merely in minor modifications of the standard coverage pattern, while for angles above $1\frac{1}{2}$ degrees the refractive effects are negligible.

SURVEY OF WAVEGUIDE THEORY

The ray tracing method presented on pages 12-14 is only a rather rough approximation to the true solution of the wave equation. It neglects diffraction, which on closer investigation is found to be very important. In order to visualize this, the waveguide analogue was introduced at an early stage of the development. Consider a two-dimensional waveguide consisting, for instance, of two parallel plane sheets of copper of infinite extent. The propagation of an electromagnetic wave in such a guide is somewhat analogous to that in a duct. The reversal of the vertical component of the rays by refraction in the duct corresponds to the reflection by the walls in the case of a metallic waveguide. It is well known that wave propagation under these conditions can be described by the methods of geometrical optics

only to a very rough approximation. Soon after the discovery of ducts the accurate theoretical treatment of duct propagation was initiated in England. [67,70,71, 73,88,94] The general result of these investigations may be summarized as follows. For an atmosphere of arbitrary stratification the field can be formally expressed by the series development, equation (27) of Chapter 1. The constants appearing therein and the height-gain functions involved are, however, different from the standard case and depend on the particular M curve involved. The solution, therefore, consists again of a superposition of "modes" which decay exponentially with distance from the transmitter. The height-gain functions do not, in general, increase with altitude all the way up from the ground. In the case of a duct the height-gain functions of the lowest modes have a pronounced maximum in the duct, similar to the curves for the overall field strength shown in Figure 6. This maximum becomes flatter and eventually disappears entirely for the height-gain functions of the higher modes.

It is useful to supplement the rather complex mathematical development into modes, represented by equation (27) of Chapter 1, by a simpler type of analysis which connects it with the ray picture. For the sake of simplicity let the phenomena be two-dimensional, confined to the horizontal x direction and the vertical z direction. If the wavelength is small enough compared to the dimensions of the duct, the electromagnetic field at some distance from the transmitter may, in any sufficiently small volume element, be represented by a plane wave whose wave front is perpendicular to the direction of the rays. Such a plane wave may be written as

$$E = E_0 e^{j\omega t} e^{-j(kx+lz)} . \tag{10}$$

Confining ourselves for the moment to the case of the plane earth, it is found from electromagnetic theory that

$$k^2 + l^2 = \left(\frac{2\pi n}{\lambda}\right)^2 , \tag{11}$$

where n is the refractive index in the volume element considered, and λ is the free space wavelength. Since k and l are proportional to the directional cosines between the direction of the ray and the x and z axes, we may put

$$k = \frac{2\pi n}{\lambda} \cos \alpha , \qquad l = \frac{2\pi n}{\lambda} \sin \alpha \tag{12}$$

where α is the angle between the ray, or the normal to the wave, and the horizontal.

The further mathematical analysis shows that, for a horizontally stratified medium where n is a function of z only, we have $k =$ constant. In view of equation (12) this gives us $n \cos \alpha =$ constant, which is just Snell's law for a plane earth, as enunciated before.

The ray picture, being a rough approximation, gives an electromagnetic field in some regions and none in others. In the rigorous solution of the wave equation there is some electromagnetic field strength everywhere. Consider in particular the region just above a duct. There are regions of "shadow" above the duct caused by the fact that some of the rays are bent downward in the duct. Clearly, at the point of reversal of a ray, $\alpha = 0$ and hence $l = 0$. If we proceed farther upward in a duct n decreases, and it follows from equation (11) that if n decreases sufficiently l must eventually become imaginary. Instead of a wave component in the z direction we then have an electromagnetic field which decreases exponentially as we go upwards. In the top layer of a duct, the decay takes place very gradually because the change in refractive index is extremely slow. Eventually, however, n must begin to increase again as we go still farther upwards from the duct and there comes a height where l is again real and an ordinary wave is again possible. This behavior might be likened to that of a metal foil so thin as to be partly transparent for the waves considered. The duct thus may be likened to a waveguide bounded on one side by a solid reflector, the ground, and on the other by a semi-transparent reflector. The mathematical theory of ducts has therefore often been designated as *leaky waveguide* theory.

A closer study of the height-gain functions which appear in the mode formula, equation (27) of Chapter 1, shows that in the presence of a duct the leakage across the upper boundary of the latter is the more pronounced the higher the order of the mode, and that for sufficiently high modes there is almost no confinement of the electromagnetic field within the region of the duct. In consequence of this fact the exponential damping with *horizontal* distance, which is characteristic of each mode, is more pronounced for the higher modes, because for these modes the electromagnetic energy rapidly "leaks away" from the duct. At large distances from the transmitter the field in and near the duct is therefore described by the lowest mode alone. This depends, of course, partially on the relative strength of excitation as well as on the attenuation of the various modes.

Another aspect of the wave theory of ducts which is of great practical importance is the cutoff effect. It is well known that any ordinary metallic waveguide has a cutoff frequency below which the guide cannot transmit an electromagnetic wave. The mathematical treatment of the duct shows that there is a similar lower limit of frequency for transmission through a duct, but, because of the "leakage" phenomenon, it is found that there is no sharply defined cutoff frequency but a gradual decrease of the duct's ability to confine radiation within itself with decreasing frequency. Figure 7 is a graph giving representative values for what may be taken

as the cutoff frequency of a duct as a function of its height in feet and ΔM, the decrease of M in the inversion layer. These values are the result of a somewhat crude approximation and should not be taken to indicate more than the order of magnitude of the frequency at which this effect occurs.
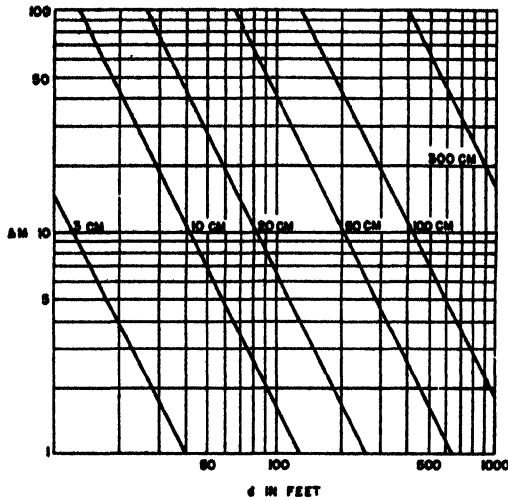
FIGURE 7. Maximum wavelength trapped in a simple surface duct. Duct width d in feet. ΔM is total decrease of M in duct. $\lambda_{max} = 2.5 d \sqrt{\Delta M \ 10^{-6}}$.

REFLECTION FROM ELEVATED LAYERS

Reflection from elevated layers has so far been observed systematically only under the rather special meteorological conditions at San Diego, but it probably occurs elsewhere, though with a lesser degree of regularity. It appears when there is a strong elevated M inversion. Such an M curve is very nearly equivalent to a true discontinuity of refractive index, and the effect on a wave traversing such a region is similar to that of a boundary between two media, the more nearly so, the larger the M-inversion gradient. If there is a true discontinuity, an incident wave is split up into a reflected and a transmitted wave. If the discontinuity is replaced by an M inversion layer, the reflected wave still persists but becomes weaker the less steep the inversion. The distinction between this phenomenon and the apparent reflection in the duct where the rays become horizontal before turning downward is usually fairly clear-cut. The true reflection described here occurs primarily in waves which are so long as to be below the cutoff.

There exists a case of gradual transition between two media with different refractive indices for which the wave equation can be integrated.[444, 445]

This can be applied qualitatively to the case,[77, 91] in so far as earth's curvature can be neglected. Figure 8 shows the calculated ratio in decibels of
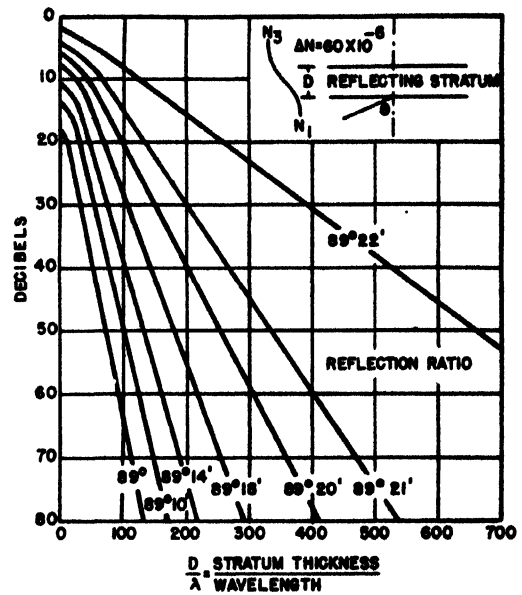
FIGURE 8. Calculated reflection ratio in decibels.

reflected to incident wave for various angles of incidence plotted against the ratio of thickness of the transition layer to wavelength as abscissa.

The verification of this theoretical concept in the San Diego experiments will be discussed in the next chapter.

METEOROLOGICAL MEASUREMENTS

INTRODUCTION

THE DIRECT MEASUREMENT of the refractive index of air is carried out in the laboratory under closely controlled conditions. The variations of the refractive index in the atmosphere which are of paramount importance for propagation problems are determined indirectly by measurements of the temperature and humidity. From the values of these latter the refractive index is computed by equation (9) of Chapter 1. There has been no reason, so far, to doubt the reliability of this procedure, and speculative assumptions of the failure of this relation which have been brought forward at times during the war have not been accepted.

This chapter describes measuring equipment that was especially developed during 1943 to 1945 to study refractive index variations. Following this description is a collection of actual M curves which have been measured in different parts of the world.

TEMPERATURE AND HUMIDITY ELEMENTS

The value of the refractive index n, or of M as defined by equation (4), Chapter 2, is sensitive to relatively small changes in temperature and especially in humidity. Both accuracy and speed in determination of M are required. Speed is especially necessary because a considerable number of points generally are needed to determine the shape of an M curve. Electrical methods have been used almost exclusively for these measurements, though an ordinary psychrometer will do in the absence of more specialized equipment.

There is no particular difficulty in measuring the temperature with suitable accuracy, such as ± 0.2 C. The electric resistance element used in the Bureau of Standards radiosonde is well suited to the purpose and is commercially available. More recently thermistors have been used. At stationary installations in England ordinary nickel or platinum resistance thermometers have been installed, primarily for recording purposes.

Humidity may be measured either directly, or indirectly by measuring the wet bulb temperature. Hair hygrometers are unsuitable because of their large time lag. For the direct measurement of humidity electrolytic resistance elements, such as are standard in the U. S. Weather Bureau radiosonde, are used. The active agent in this type of element is an aqueous solution of lithium chloride which is

deposited as a film on a small cylinder. The resistance of the solution is highly sensitive to changes in relative humidity of the surrounding air. In England a variant of this principle has been employed where the lithium chloride solution is absorbed in a cotton cloth.

In the indirect method of measuring humidity a thermistor of cylindrical form is surrounded by a moist wick which, with proper aeration, indicates the wet bulb temperature. To insure insulation the element is covered with several coats of insulating lacquer before the wick is attached.

The main problem in all these devices is that of time lag. When mobile carriers such as captive balloons, kites, airplanes, or ships are employed, it is in general necessary to obtain an individual reading within less than a minute, and the response of the measuring elements to the temperature and humidity of the ambient medium must be reasonably close within the time available.

The time lag constant is the time required to attain the fraction $1 - (1/e) = 0.63$ of the total change, if the temperature (or humidity) is changed suddenly. For the temperature elements the time lag constant is several seconds in an air stream with a velocity of 2 to 5 m per sec. The lag depends somewhat on the position of the element relative to the air stream and is a maximum when the element is perpendicular to the stream. The lag constant of the same element, used as wet bulb indicator with wick applied, is only slightly larger than that of the dry element. The lag constant of the Bureau of Standards humidity element has been measured in several laboratories, and there seems to be some controversy as to its exact value, the results varying from a few seconds to about 45 sec,[238] the latter in an air stream of 2 to 5 m per sec.[238]

THE WIRED SONDE

Temperature and humidity elements of the type described are combined in a lightweight assembly which can be moved rapidly through the lower atmosphere. Such equipment, when first built in England, used dry and wet thermopiles,[237] and soon thereafter the same method was adopted by the State College of Washington,[238,239,240] and, with slight modification, by the Navy Radio and Sound Laboratory [NRSL] at San Diego.[241-244] This design uses a combination of a resistance temperature element and an electrolytic humidity element. The instrument developed by the Radiation Laboratory

of the Massacnusetts Institute of Technology uses dry and wet resistance elements.[229]

The physical assembly consists of bakelite tubing, in which the two elements are mounted perpendicular to the axis. The tube is surrounded by a radiation shield of aluminum foil. Wet and dry bulb instruments need artificial aeration in calm air which is provided by a small electric fan. Among the instruments containing electrolytic humidity strips only the late model of NRSL incorporates artificial aeration. Other instruments of this type, when used in calm weather with a captive balloon, are aerated by giving the cable a few jerks of several feet amplitude.

In both captive balloon and kite equipment only the measuring elements are carried aloft with fine wires in the cable to connect with the rest of the circuit. The assembly that is carried aloft is therefore quite light, weighing only about a pound in the case of nonaerated instruments and 3 to 4 pounds for aerated ones.

Figure 1 shows a wiring diagram for the Washington State College sonde. The diagram is largely self-explanatory. The switches S_1 S_2 S_3 are contained in the pile-up of a single relay and are actuated by a miniature worm-geared motor as shown. They reverse the current through the elements in order to avoid polarization, while at the same time maintaining constant polarity at the meters. The period of reversal is 0.5 sec and the 1,000-μf condensers in parallel with the meters serve to smooth the interrupted current.

Figure 2 shows a schematic wiring diagram for the dry and wet bulb resistance elements of the Radiation Laboratory instrument. The resistance of the thermal element X controls the bias of one triode of the double triode 6SN7 which acts as a vacuum tube voltmeter to compare the resistance of the thermal element with a standard resistance. A 1-ma recording meter is placed between the two plates. In operation the dry and wet elements are switched into the

FIGURE 2. Circuit diagram for electronic amplifier for measuring temperature. (Radiation Laboratory, MIT.)

circuit alternately. Calibration of the amplifier is obtained by switching a series of precision resistors in steps of 1,000 ohms into the circuit in place of the thermal element. The stability of this voltmeter is such that with a change in line voltage between 95 and 120 v there is no observable change of the meter at any given deflection.

REFRACTIVE INDEX MEASUREMENTS

The methods which have been used to make refractive index measurements in the lower atmosphere are the following:

1. Stationary installations on towers, usually with automatic recording on the ground. Aerated wet and dry bulb instruments are installed at several heights giving a continuous survey of the M curve between the ground and the top of the tower.

2. Installations similar to (1), on shipboard, with the meters or recording equipment in the ship's cabin. In order to explore the humidity distribution in the lowest layers adjacent to the sea surface, the instruments have been mounted at the end of a beam that pivots about a horizontal axis fastened to the side of the ship. This device has been used extensively in the Irish Sea experiments. Artificial aeration of shipborne installations is not usually necessary because in calm weather the necessary velocity of the air is provided by the motion of the ship.

3. Airborne installations. The unit is mounted at a convenient place on the outside of the plane where it is not affected by motor exhaust or propeller slip stream, with the meters or recorders in the ship's cabin. Comparatively slow-flying planes have been used for such measurements, not only in order to minimize the dynamic temperature correction, but also because in a fast-flying plane too long a column of air will be sampled during the period of relaxation of the instrument. In airplane measurements it is

FIGURE 1. Circuit diagram for State College of Washington wired sonde.

necessary to keep track of the altitude of the plane by means of a carefully calibrated altimeter.

4. Captive balloons and kites. In these devices only the measuring unit is carried aloft, the indicating or recording meters remaining at the ground. Three wires are required when the instrument is nonaerated and two additional ones when an aeration motor is provided. The wires are of thin insulated copper, stranded together into a cable, although more recently aluminum wires have been tried because of their greater mechanical strength.[233] The fine wires of the cable are wound in a high-pitch spiral around a strength member consisting of fishline and then glued to the latter. Considerable effort has been spent on the development of these cables which constitute the most critical part of the balloon sonde equipment.

Captive balloons are used in calm weather and in winds not exceeding about 4 m per sec. For higher wind velocities the balloons become difficult to manipulate, and a kite is then used to carry the measuring unit aloft from the ground or even from shipboard. Small barrage balloons have a greater lift than ordinary weather balloons and can be used in the same winds as kites because of their streamline shape. They are, however, less mobile and require more hydrogen than the smaller balloons.

The cable for the balloon or kite is wound on a drum, and connection with the stationary meters is made by means of slip rings. The height of the balloon or kite is determined by the length of cable paid out together with a rough measurement of the angle of the cable.

Captive balloons reach heights of several hundred feet without difficulty and even heights of 1,000 to 2,000 ft are not infrequent

OTHER METEOROLOGICAL INSTRUMENTS

It is hardly necessary to say that measurements of atmospheric temperature and humidity are possible and have been made, with instruments of a
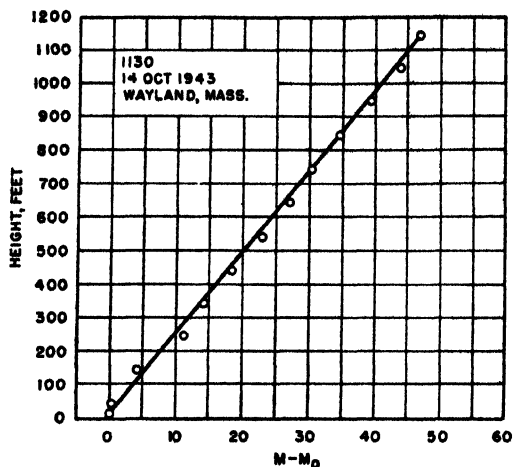
FIGURE 3. Representative standard M curve (36 M units per 1,000 ft)

more conventional type In the early stages of our knowledge of nonstandard propagation, surveys were made by means of an ordinary psychrometer held out of the window of a slowly cruising plane and aerated by the slip stream. The British installations commonly use multijunction dry and wet thermopiles which have the advantage of not requiring elaborate calibration. In connection with captive balloons this type of equipment is somewhat clumsy in that the cold junctions have to be carried aloft in a Dewar flask

It should be noted here that the ordinary noncaptive radiosonde as used in the routine meteorological observations of the U. S. Weather Bureau and of the Armed Services is not suitable for radio-meteorological purposes. The reason is that these sondes are designed to give representative data only at definite and fairly large vertical intervals, 100 ft or more. These are too widely spaced to yield a representative M curve, as the characteristic features of the latter are usually concentrated in the lowest strata of the atmosphere.

Wind measurements are of importance in connection with propagation problems, for reasons which will be given in detail in the chapter on weather
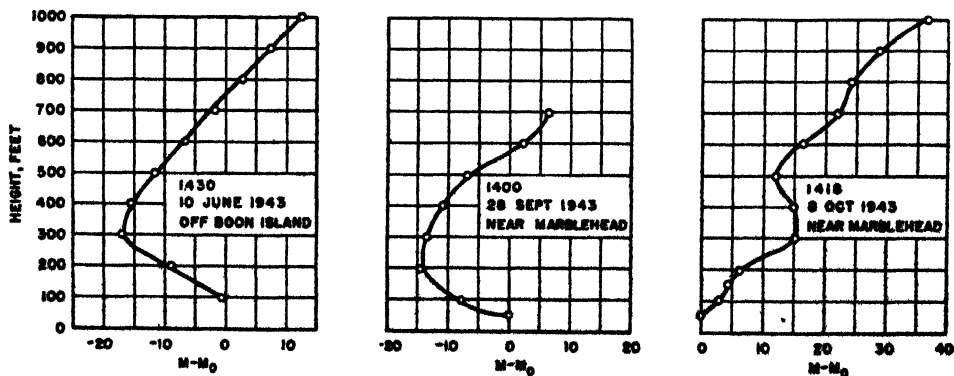
FIGURE 4. Representative nonstandard M curves from the Massachusetts coast.
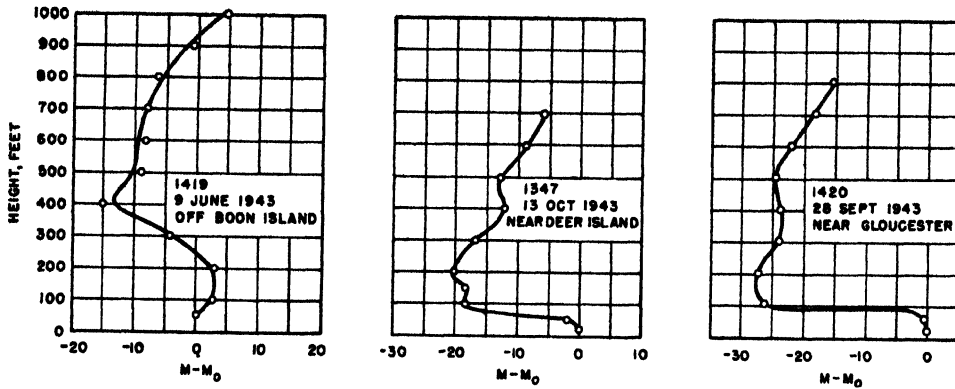
FIGURE 5. M curves from the Massachusetts coast showing strong ducts

forecasting. They are particularly significant at coasts when off-shore winds or land and sea breezes are present. Sensitive and carefully calibrated anemometers with ordinary wind vanes prove adequate for measurements of this type. Special equipment such as supersensitive anemometers, developed for particular purposes such as chemical warfare problems, are not usually needed because the large area covered by radio transmission paths or radars renders too detailed measurements useless.

REPRESENTATIVE OBSERVED
M CURVES

A small catalogue of M curves that have been actually measured in various parts of the world by means of the equipment described previously concludes this chapter. Most of the curves presented were taken over the ocean merely because the majority of experimental measurements have been made there. Experience indicates that there is not
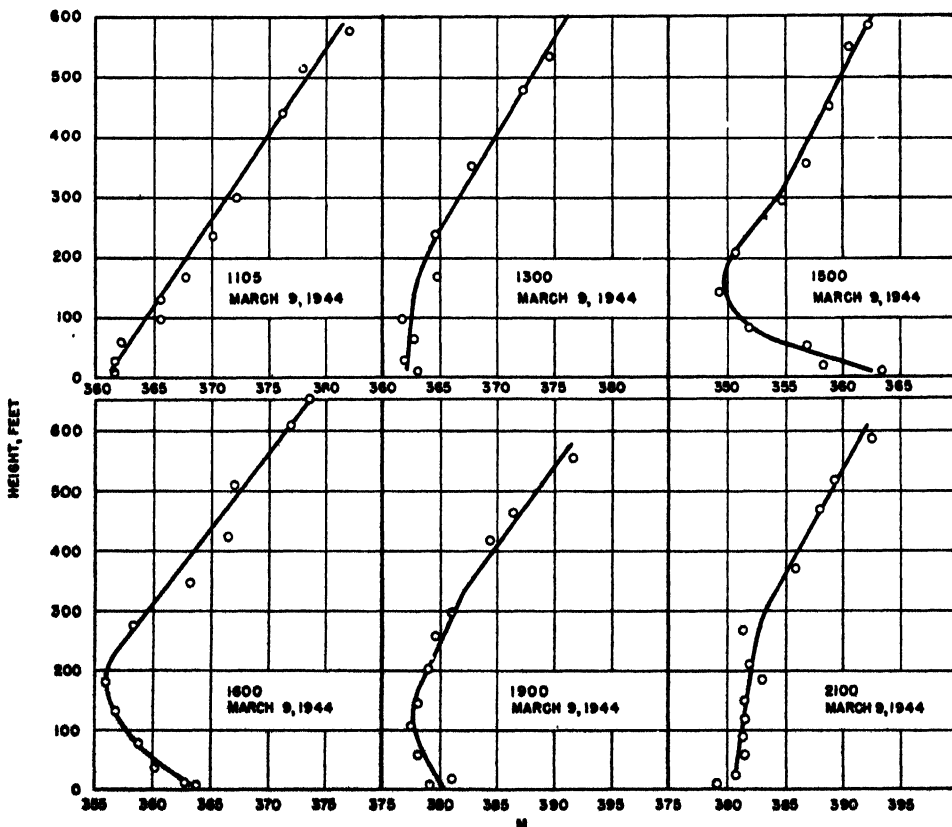
FIGURE 6. M curves from Taboga Island near Balboa, Canal Zone.
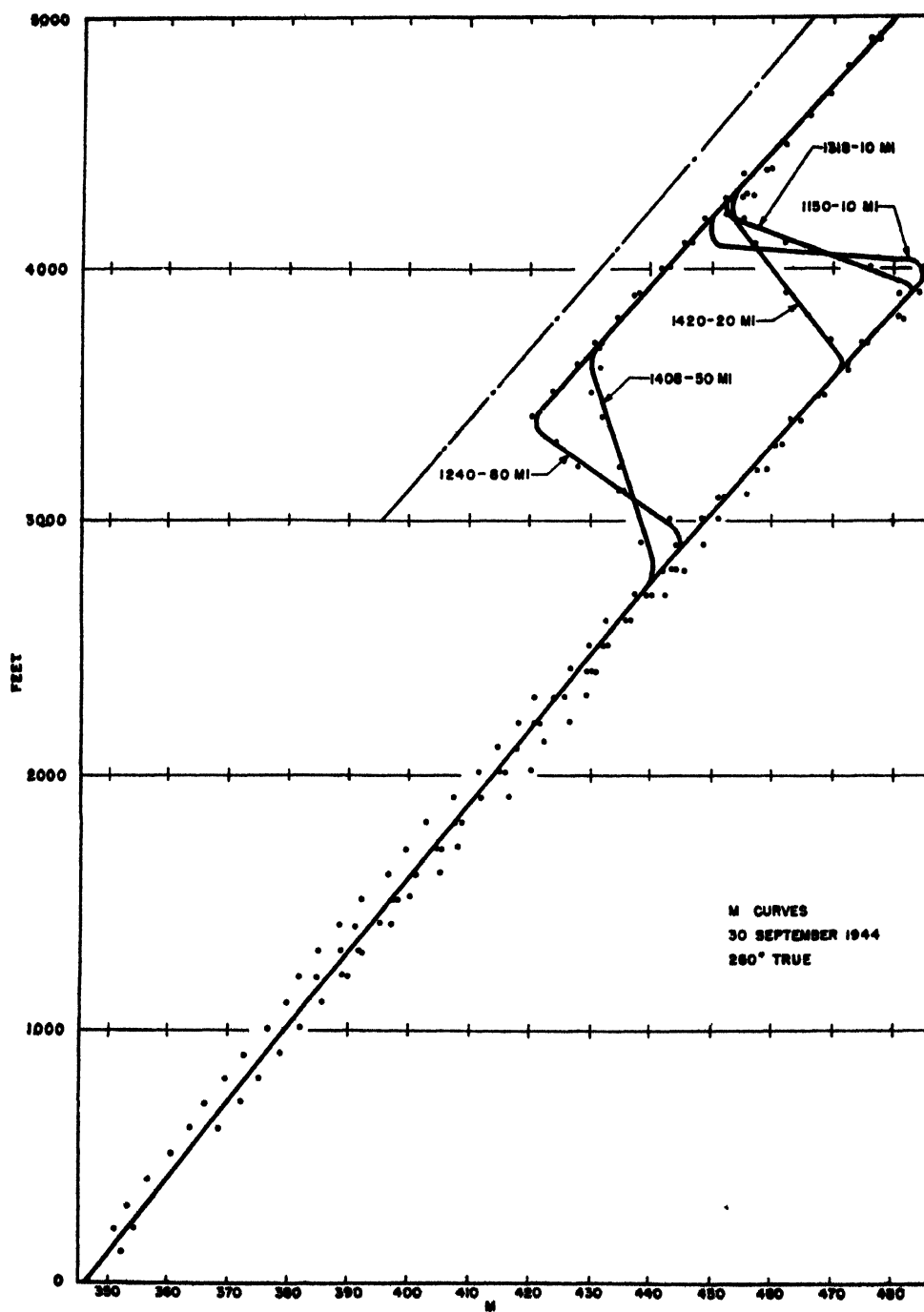
FIGURE 7. *M* curves from a flight west of San Diego.
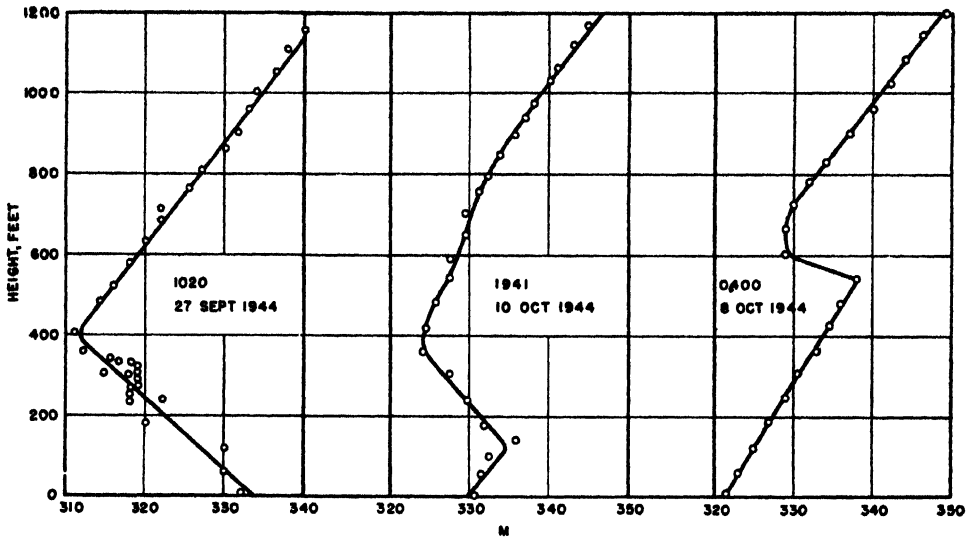
FIGURE 8. M curves from New Zealand, east coast near Cook Strait.

much difference in the types of M curves over land and over sea except that standard propagation conditions will in general be much more common over land for reasons that will appear in Chapter 5. In all these graphs the actually measured points are entered so that the reader may gain an idea of the degree of accuracy obtained with this equipment.

Figure 3 shows a standard curve as measured at the coast of Massachusetts. The linearity of the refractive index in this case is not an accident but is the result of the definite physical condition of thorough turbulent mixing in the lower atmosphere, as will be explained in more detail in Chapter 5. Since this is a fairly frequent condition, standard curves are actually quite common, and in them the measured points cluster well around a straight line as shown in Figure 3.

Figures 4 and 5 show a set of nonstandard curves selected from a large series of measurements taken on the Massachusetts coast in the summer and fall of 1943.[210] Here the M curves are quite irregular, perhaps more so than is common at other locations. These curves show various types of ducts, some of them rather weak, others with a decrease of M as
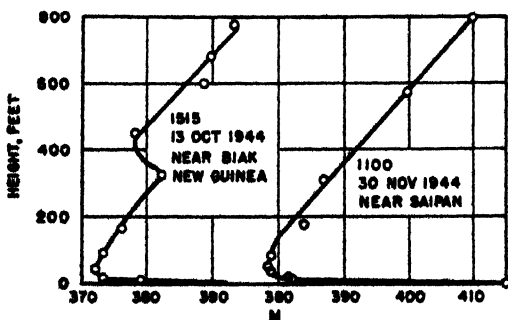
FIGURE 9. M curves from the New Guinea area.
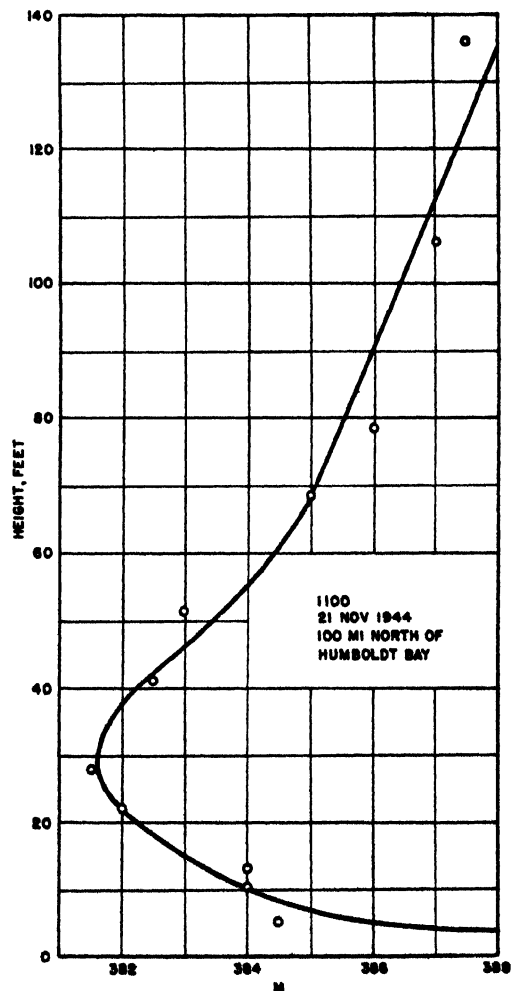
FIGURE 10. Detailed M curve taken over the ocean near New Guinea.
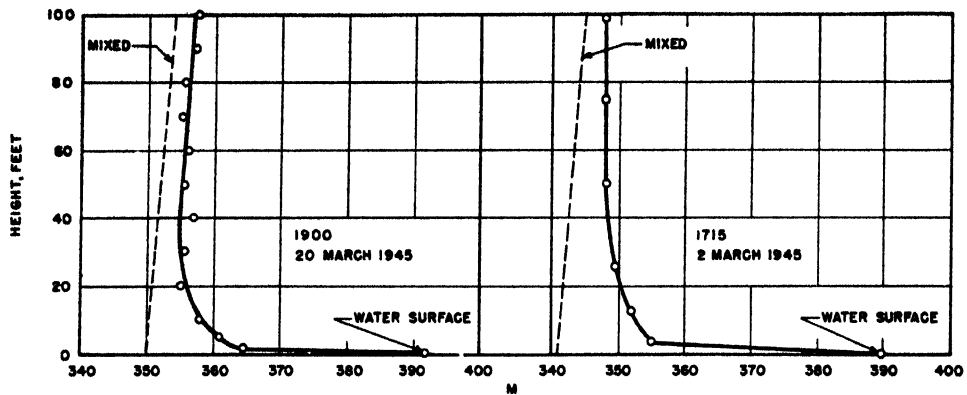
FIGURE 11 M curves over the ocean at Antigua, British West Indies.

much as 20 units or even more.

The curves of Figure 6 were taken at Taboga Island, some 15 miles south of Balboa, at the eastern entrance to the Panama Canal. They show various familiar types of ducts; two of the curves represent transitional cases where the M curve is steeper than standard but does not bend backward.

Figure 7 illustrates the typical elevated duct found in the San Diego region. Both below and above the inversion region the M curve is standard. The various curves shown were measured at several distances on a flight from San Diego outward.

Figure 8 is a set of M curves that were measured on the east coast of New Zealand, at a point some 100 miles south of Cook Strait.[123] These curves

provide good examples of the type of M curves that consist of several very nearly linear sections.

Figure 9 shows two soundings from the tropical Western Pacific. The curve at the left was taken at Biak Island, New Guinea, and is remarkable for the presence of two ducts, a ground-based and an elevated one. The curve at the right was taken at Saipan.

Figure 10, taken near New Guinea, shows in more detail the structure of the low maritime duct which in this case is only about 30 ft high.[125] This type of duct has been studied carefully in the transmission experiments at Antigua in the West Indies which are reported in Chapter 4. Two typical soundings taken near Antigua are reproduced in Figure 11.[124]

TRANSMISSION EXPERIMENTS

BRITISH EXPERIMENTS

IN THE DEVELOPMENT of short and microwave communication and radar, the British were first to make systematic transmission experiments on a large scale. A number of such experiments were carried out at wavelengths below 50 cm, beginning about 1936 with some transmission paths over land, some over sea; and experiments in the 10-cm band were undertaken in the early years of the war. These experiments will not be reported individually because the earlier results are reproduced and verified in the later and more elaborate trials. Instead, attention will be confined to two major experiments, one over the sea and one over land.[9,10]

THE IRISH SEA EXPERIMENT

This transmission experiment represents a cooperative enterprise undertaken jointly by the Radio Division of the National Physical Laboratory, the Telecommunications Research Establishment, Signal Research and Development Establishment, The Ministry of Supply, The Naval Meteorological Service, The Meteorological Office, and the General Electric Company, Ltd. One-way transmission with stationary apparatus was carried on in the winter of 1943 to 1944 and continued in operation until the end of the war.

Practically all the transmission is over the sea at wavelengths of about 9, 6, and 3 cm. At each frequency the transmitted signal consists of square pulses, with equal on-off periods and a repetition frequency of 1,000. The 1,000 cycle component of the modulation is rectified in the receivers to operate the recording milliammeters, and provision is made for monitoring the transmitter power and the sensitivity of the receivers in terms of a suitable standard. Parabolic mirrors 48 in. in diameter are used for all transmitters and receivers and are permanently mounted inside the station buildings behind large canvas-covered "windows."

There are two transmission paths, 57 and 200 miles in length, which run roughly from south to north, but diverge from each other by about 17 degrees and have the transmitting station in common at the southern tip in South Wales. There are transmitting stations A and B at 540 and 90 ft above sea level respectively. The receivers, C and D, for the short path are in North Wales at two heights, and E and F, for the long path, in Scotland at two heights. In units of the geometrical horizon distance the

lengths of the various transmission paths are as follows.

$\dfrac{AC}{0.89}$	$\dfrac{BC}{1.21}$	$\dfrac{AD}{1.40}$	$\dfrac{BD}{2.40}$	$\dfrac{AE}{3.82}$	$\dfrac{AF}{4.92}$	$\dfrac{BE}{5.63}$	$\dfrac{BF}{8\,45}$

It has not been found possible to utilize all these paths at the same time, because the amount of records accumulated proved too great for evaluation, but selected runs at various frequencies and for several paths have been made.

There is an elaborate setup for measuring meteorological conditions simultaneously with the intensity of the transmitted signal. A weather station is located at each of the three terminals, but the main meteorological program is carried out from ships which ply along the transmission paths. The Admiralty has detailed three ships for the sole purpose of making these measurements so that the transmission path is continuously covered by at least one ship on duty. The ships are provided with elaborate meteorological equipment of the type described in Chapter 3.

RESULTS

The following is a qualitative summary of some of the results obtained thus far.

1. There is general agreement between signal variations over the two paths, though the short period variations often differ.

2. Signals are obtained over the long path only when the signal strength over the short path BD is high. But if the latter condition is fulfilled, the former does not always follow.

3. There is a marked diurnal variation when the general signal level is low or moderate with strong signals in the late afternoon or evening and a minimum between 6 a.m. and 9 a.m.

4. There is evidence of an appreciable seasonal variation with high level for a greater fraction of the time in summer than in winter or spring.

5. Low level occurs commonly, but not always in conditions of fog or low visibility.

6. Low signal level is usually observed at the passage of warm fronts and high level at the passage of cold fronts.

7. Generally speaking, high signal level tends to occur in periods of anticyclonic weather.

A typical record of signal strength for 9-cm waves, representing hourly mean values for a month, is shown in Figure 1. These records are from two links of the short path, both nonoptical. Important meteorological phenomena, especially passage of
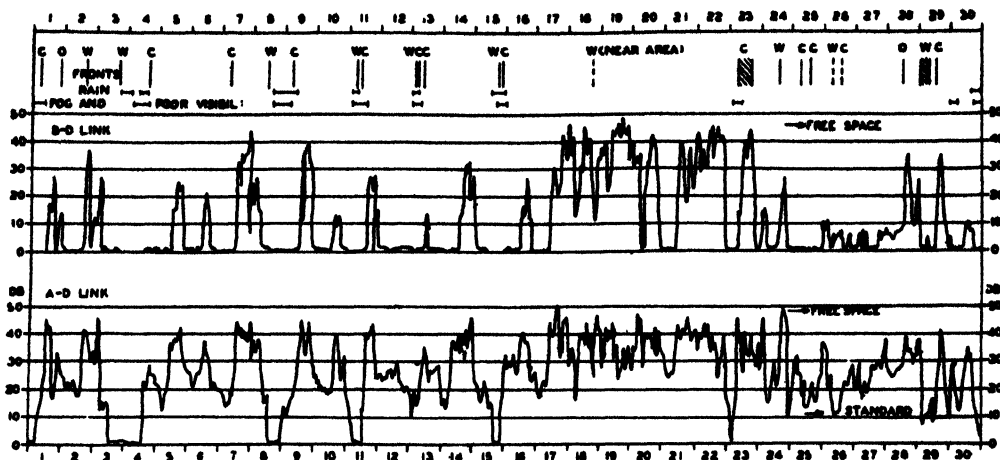
FIGURE 1. Signal strength in decibels above 1 μv receiver input. S band hourly means, June 1944. (Irish Sea experiment.)
(C = cold front, W = warm front, O = occluded front)

fronts, are shown at the top of the diagram. W indicates warm, C cold, O occluded. Note in particular the standard and the free space level indicated on the lower record and the free space level on the upper. The standard level for the latter would be about 33 db below the zero line. This record, which is by no means exceptional, gives a fair idea of how vastly the signal exceeds the magnitude calculated for standard conditions. At the same time it shows the highly irregular character of these phenomena and the difficulty of correlating them in a simple way with the weather or other conditions.

OVERLAND PATH

An experimental overland path 38 miles has long been operated in the neighborhood of London between the Admiralty Signal Establishment at Whitwell Hatch and the General Electric Laboratories at Wembley. The wavelength is in the 10-cm band, and transmission, monitoring, frequency control, and recording are fully automatic. The path is optical except for some houses and trees near the receiver

FIGURE 2. Whitwell Hatch-Wembley path, March 1944. S band hourly mean intensities in decibels above 1 μv receiver input.

which introduce a diffraction loss estimated at 30 db. As is generally the case with paths that are optical or nearly so, the fluctuations of received intensity are far less than in the case of long nonoptical paths. Figure 2 shows a record for one month in 1944. The large diurnal fluctuations in amplitude with maxima above normal in the early morning hours occur in the beginning of the month and at several occasions later, especially from the 21st to the 26th. These are related to weather conditions with clear skies, as will be explained in Chapter 4.

The work undertaken in England on experimental transmission paths of various types is quite extensive, and the preceding description hardly gives an idea of the variety of experiments made and results obtained. Most of the experiments are of a smaller size than the ones described here.

EXPERIMENTS AT THE EASTERN COAST OF THE U. S.

In the early years of the war a transmission experiment was undertaken by RCA Communications, Inc., between New York and two points on Long Island.[131,155] The short path of 42 miles was optical, but the long path of 70 miles was nonoptical, the receiver being about 400 ft below the transmitter's line of sight calculated on a $\frac{4}{3}$ earth's radius basis. Transmission was carried out on 45, 475, and 2,800 mc. The results show what has been confirmed by later experiments, that the amplitude of fluctuations is larger the higher the frequency. On the optical path the range of fluctuations of the 45-mc signal averages only ±3 db, whereas over the same path the 475-mc and 2,800-mc signals exhibited fluctuations which were in excess of 40 db, so far as they could be measured. As was to be expected, the 2,800-mc signal fluctuated more than the 475-mc one. Over the nonoptical path all three signals show
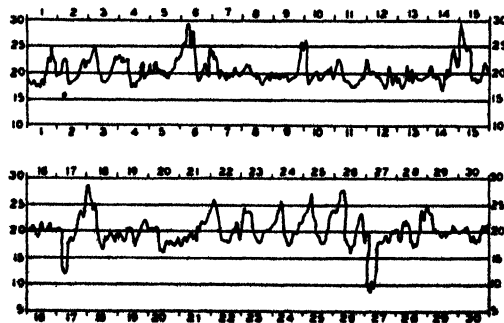
very wide fluctuations of intensity, the rate and amount again increasing with the frequency.

In the course of these experiments a certain amount of meteorological study was carried out and forecasting of propagation conditions was done on a tentative basis. The general results again fore-shadowed the more complete data obtained by later studies, and a description of the details will be omitted here.

Similar experiments were carried out simultaneously by the Bell Telephone Laboratories [BTL] on optical paths near New York City. The wavelengths employed were 10, 6, and 3 cm.[165,174] Here we find clearly established the different signal or fading types that are described in detail below.

A very extensive program of transmission measurements was carried out by the Radiation Laboratory of Massachusetts Institute of Technology [MIT]. The meteorological records were made in cooperation with the U. S. Army Air Forces. The first measurements were made in 1942, and experiments on a very large scale were carried out in 1944.[3,10,12,163,183] Two optical transmission paths were operated in 1943, a 22-mile path over the sea and a 45-mile path over land. A 10-cm continuous signal was used, and the strength was monitored by means of thermistors. The antennas were dipoles with 30-in. parabolic reflectors. The received signal was automatically recorded on meters having a range of 60 db. The signals received were correlated with meteorological observations, the results of which will be given below.

In the spring of 1944 a new over-water transmission path was installed which was operated simultaneously with the 22-mile one. This path was nonoptical, 41 miles long, and crossed Massachusetts Bay from the southern tip of Cape Ann to the northern tip of Cape Cod near Provincetown. Transmission over this path was carried on with 256-cm waves, 10-cm S band, 3-cm X band, and 1.25-cm K band. The 256-cm equipment used Yagi antennas and operated with continuous waves. The microwave transmitters used pulses with a repetition frequency of 700 c and used parabolic reflectors as antennas.

The transmitter for the short path was about 120 ft above mean sea level, and the transmitters for the long path were at a similar height. The two receivers were about 136 and 30 ft above mean sea level. The transmitter power was monitored and continuously recorded during the experiments while the receivers had automatic frequency control with apparatus which searches for the signal if it is lost. The automatic gain control of the receivers was arranged to give a spread of the signal over 70 to 80 db. The receivers were directly calibrated by means of signal generators and a very close check was kept on their performance throughout. The rectified output of all receivers was fed directly into recording milliammeters.

Coincident with the operation of these transmission paths there was a very extensive meteorological program determining sea and air temperatures and atmospheric humidities by means of fixed installations, captive balloons, ships, and airplanes. The distribution of the refractive index along the transmission path was thus known in considerable detail during practically the whole course of the experiments. Concurrently with these measurements, a program of forecasting the transmission conditions was carried out.

RESULTS

The results obtained on the various transmission paths on the east coast of the United States are rather closely similar to each other, and the graphs presented here may be taken as being characteristic of all of them.

Figure 3 shows the signal types observed at the microwave frequencies, S band and X band. The first type is well above the standard level with high signal on the average. It has roller fades with periods of from 2 min to an hour or so which may go down to the minimum detectable level. These periods are generally shorter at any time on the X than on the S band. When this type of signal was present on the S band, it was almost invariably present on the X band and on both the short and long paths. It always occurred simultaneously on the high and low receivers at any frequency.

The second type is high and steady at anywhere from 5 to 30 db above the standard, generally higher on the X than on the S band. Most of the time this type occurred simultaneously on both bands, but there were some occasions when the S-band signal was of the high and steady type while the X one was of the first type, high with roller fades.

The third type of signal is about standard and fairly steady which may be a limiting case of the high and steady variety. It does not necessarily occur on both frequencies and on both high and low receivers at the same time.

The fourth type is standard on the average, with scintillations of more than 10 db. The reason for the difference between this and the preceding type has not yet been established. The scintillations may occur on either the S or X band while at the same time the other signal is steady.

The fifth type, known as "blackout," is far below standard and shows strong scintillations. In general it occurs simultaneously on both frequencies, both paths, and on both high and low receivers.

Figure 4 shows a similar set of signal types as observed with 256-cm waves. These are distinct from those observed at the microwave frequencies not only in appearance but also in times of occurrence. In general no relation has been found to exist between the signal type at this frequency and that observed simultaneously on S or X band, although on rare occasions such a relation is indicated; the
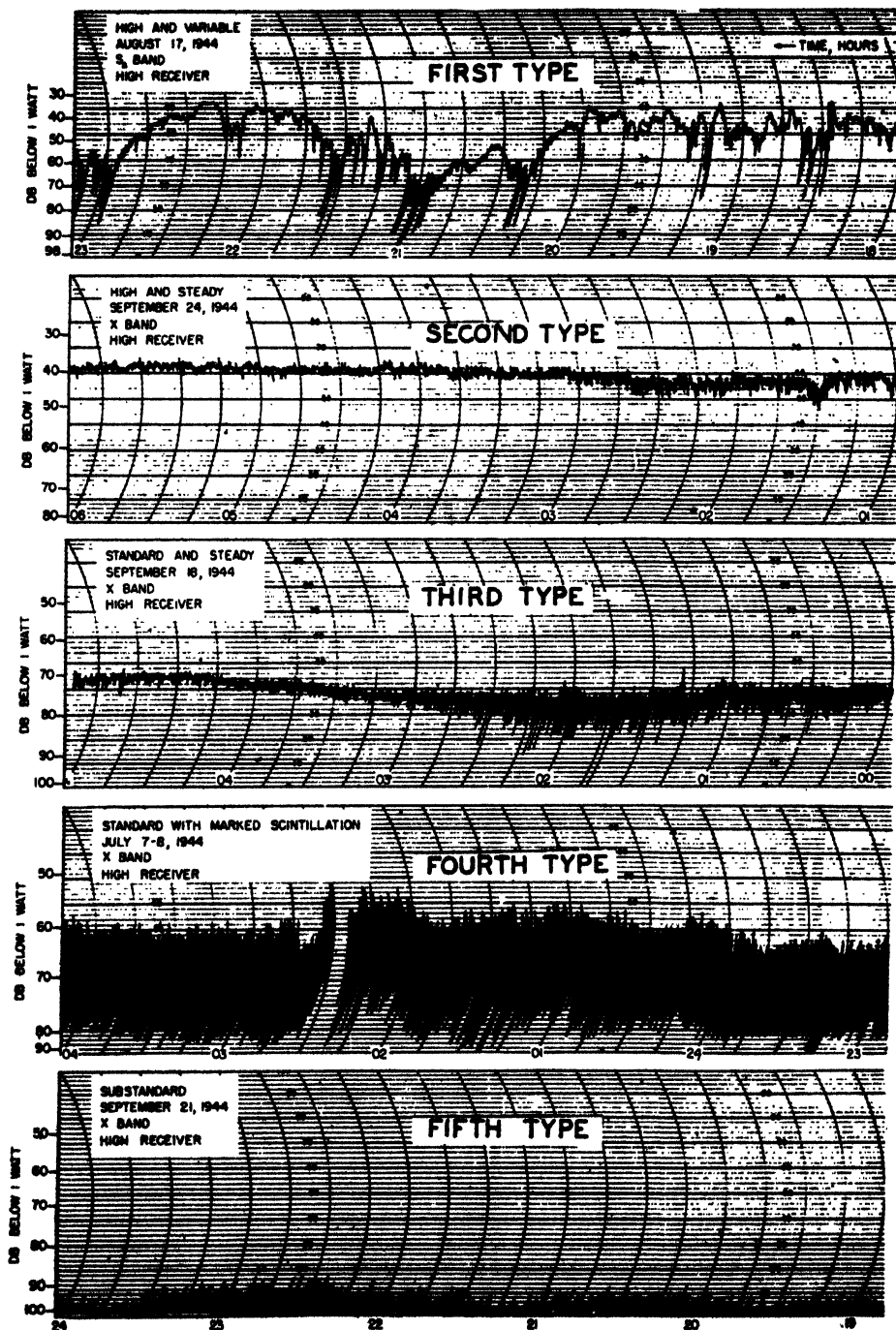
FIGURE 3. Microwave signal types S_A and X band, Massachusetts Bay.

type may remain constant on one frequency and change on the other. Steady signal is most frequent at 256 cm, but the other types shown also occur fairly often. Variations of 30 to 40 db overall take place, and the variations may be fast or slow.

A statistical study of the frequency of occurrence of various signals reveals some rather interesting features. Table 1 shows the frequency of occurrence

of above standard, standard, and below standard types on the S and X bands during three typical weeks in the summer of 1944. In these statistics the range of the standard signal was taken as ±5 db for the S band and ±10 db for the X band. The behavior of the K-band signal is quite similar to that of the other two.

As the season progressed into the fall, standard
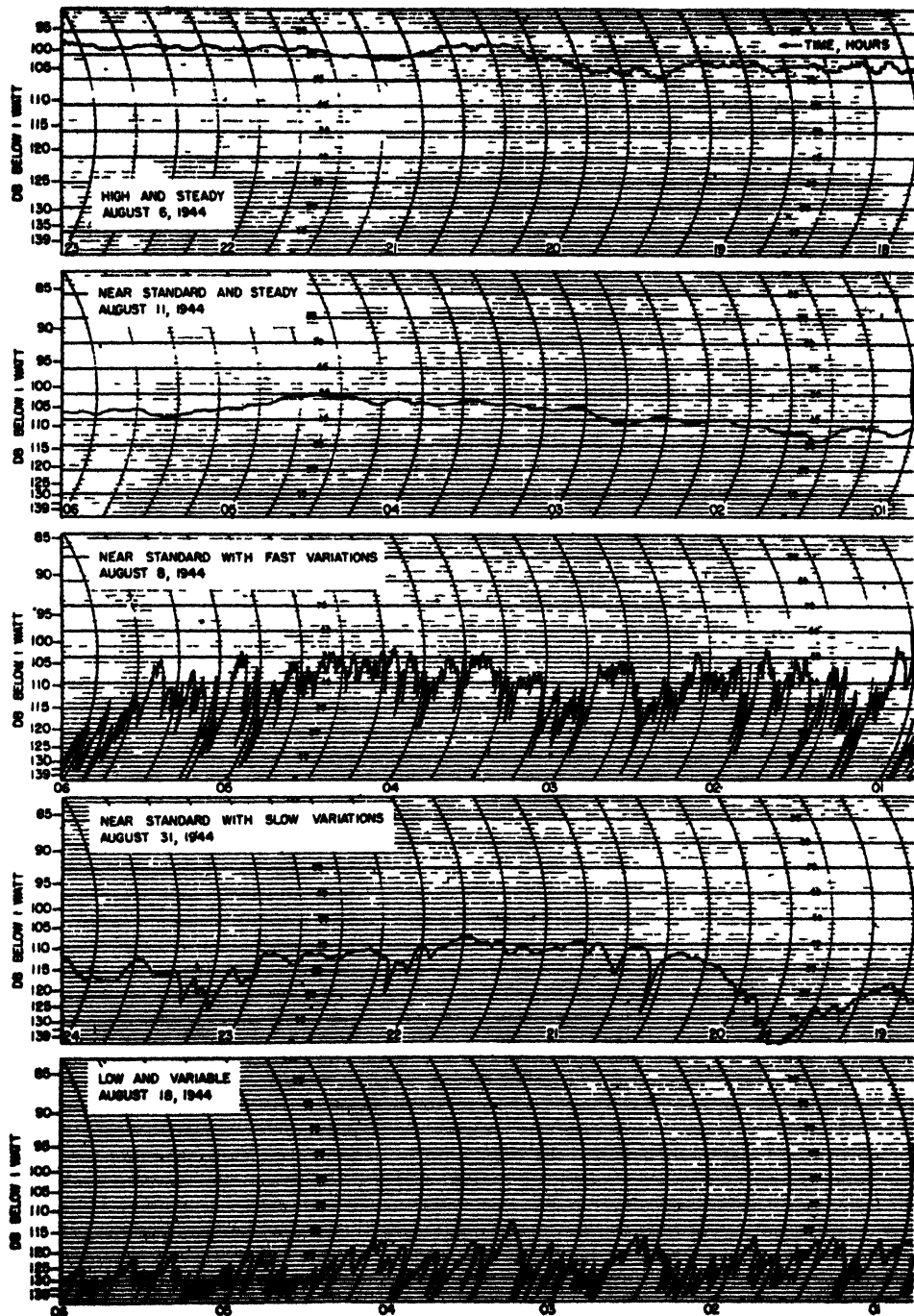
FIGURE 4. Signal types at 256 cm (117 mc per sec), Massachusetts Bay.

signal became more common and substandard signal less frequent especially in the S band. This is shown in Table 2.

These statistical results are characteristic of the over-water path near a coast used in the experiments of the Radiation Laboratory; and, while the signal types shown in Figures 3 and 4 are about the same in overland paths, the relative frequency of incidence

tor the various types is quite different. This frequency depends not only on the location of the path but, also as shown above, on the season. A more detailed analysis shows that it also depends on the particular weather situation, which may prevail for periods of several days or longer.

It has been mentioned before that the signal patterns on the S and X bands and those on the

TABLE 1. S and X bands, July and August.

Date	Per cent of time above standard	Per cent of time below standard	Per cent of time standard
July 10-16	63	36	1
Aug. 21-27	97	3	0
Aug. 28-Sept. 3	80	15	5

TABLE 2. S and X bands, September and October.

Date		Per cent of time above standard	Per cent of time below standard	Per cent of time standard
Sept. 25-Oct. 1	S	58	15	27
	X	80	10	10
Oct. 16-22	S	76	2	22
	X	92	0	8

high and low receivers are closely parallel. Figures 5 and 6 show these correlations graphically; the first is between the S and X bands and the second is between the high and the low S-band receivers. In contradistinction there is practically no correlation between
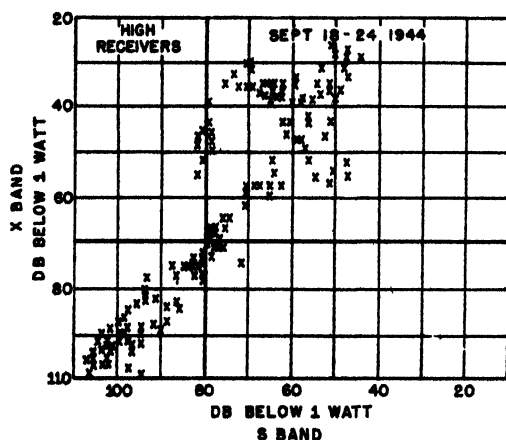
FIGURE 5. Correlation between S- and X-band signal strengths, Massachusetts Bay.
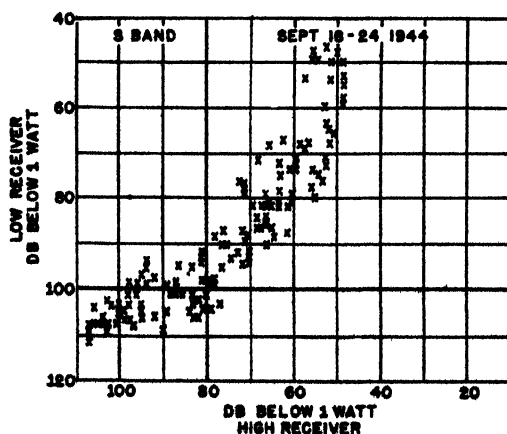
FIGURE 6. Correlation between signal strengths at high and low receivers, Massachusetts Bay.
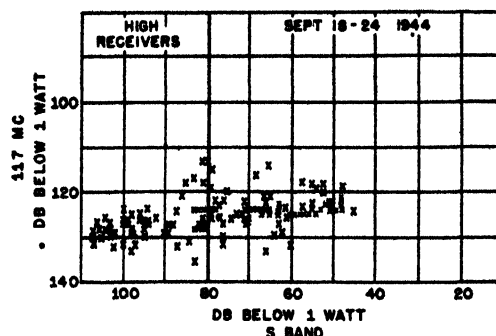
FIGURE 7. Correlation between 117-mc and S-band signal strengths, Massachusetts Bay.

the S-band and 117-mc signal levels, as Figure 7 indicates.

It is hardly necessary to state that the high signal levels occur when the meteorological measurements show the presence of a duct and the substandard signals occur when the M curve is of the substandard type. It will not be possible, in this summary report, to enter into the detailed relationship between signal strength and M distribution. In a general way the experimental results confirm the electromagnetic theory in so far as it has been worked out at present.

Another aspect of the short wave transmission that has been studied in these experiments is the relationship between radio and radar transmission. Since radar involves two-way transmission, its path factor, as defined in the beginning of Chapter 1, is the square of the path factor for one-way transmission. Therefore the change with distance in the received-field strength is more rapid with radar than with the one-way radio.

In order to study this relationship, two small mobile radar sets on the S and X bands were set up near the transmitter of the long path, at Provincetown. Echoes from natural targets along the coast of the mainland were studied in connection with the soundings and correlated with the one-way transmission measurements. In Figure 8 is shown a correlation between the signal strength of the X-band radar and the signal strength of the high X-band receiver of the long transmission path. The radar target is near the one-way receiver so that both paths are practically coincident. When the radar signal was below the limit of sensitivity, it is indicated on the graph by this limit so that the lower points of the diagram really have little physical significance. If a straight line is drawn, averaging the variation of the higher points, its slope is roughly 2:1 as should be expected.

Figure 9 shows a correlation between the one-way signal strength on the S band and the maximum range of fixed echoes detected by the S-band radar along the coast. It is interesting to note that superstandard radar ranges do not appear until the one-way signal has reached a certain, rather larger value.

The one-way signal does not seem to be able to increase much beyond this value, whereas the range of detectable radar targets rises with extreme rapidity.
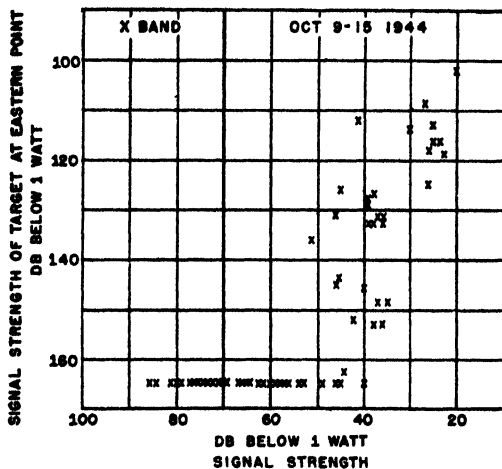
FIGURE 8. Correlation between one-way and radar signal strengths over the same path. X band, Massachusetts Bay.

EXPERIMENTS IN NORTHWESTERN UNITED STATES AND CANADA

STATE COLLEGE OF WASHINGTON PROJECT

During 1943, a series of transmission experiments were carried out by a group of workers from the State College of Washington under the auspices of Division 14, NDRC.[184, 137, 164, 228] The first series of tests were made in the neighborhood of Spokane over 14- and 52-mile optical paths and over a 112-mile nonoptical path. Later in the same year a transmission path 20 miles long with receivers both below and above the optical horizon was installed on the east side of Flathead Lake, Montana.

Among the tests carried out by this group was an experimental telephone communication on 10-cm waves which gave excellent results. The earlier experiments demonstrated the necessity of having detailed data on the refractive index variation in low levels and thus led to the development of the State College of Washington wired balloon sonde, described in the preceding chapter and of basic importance for further propagation work. The first model of the sonde was used systematically in connection with the Flathead Lake transmission path.

The location of these experiments has a climate of a continental type, there being several mountain ranges between these spots and the Pacific coast. The air is comparatively dry, and the structure of the lowest strata is subject to the large variations of temperature and of stability typical of continental conditions.

The general results of these tests are similar in many respects to those found at the east coast of
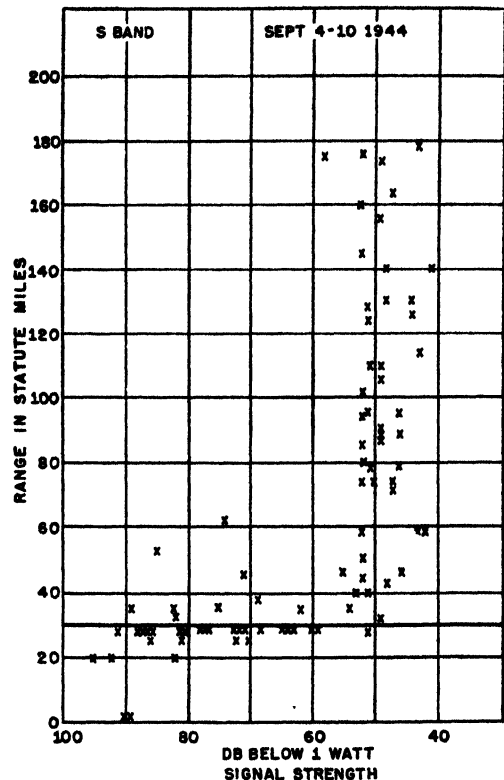
FIGURE 9. Correlation between maximum radar ranges and one-way signal strength. X band, Massachusetts Bay.

the United States. The signal types are analogous, but the times and frequencies of occurrence are often quite different. In the Flathead Lake experiments, where strong ducts were often present, signal level variations of 50 db were observed for the optical path, 55 db for the nonoptical paths. The correlation between the observed M curves and the received signal strength was extremely close, high signal levels being observed when the measured M curves showed the presence of a duct; and standard signal levels, when the M curve was of the standard type. Similar observations were later made many times over in other experiments such as those at Massachusetts Bay, already described.

Figure 10 shows typical signal records in form of hourly maxima and minima over a three-day period for the 20-mile path on Flathead Lake. Though the path itself is entirely over water, the over-water trajectory of the air is limited by the dimensions of the lake. Both receiving stations are below the line of sight, the upper by .91 ft, the lower by 132 ft. There is, in this graph, a rather clearcut distinction between periods of standard propagation with a comparatively limited margin of variability of the signal, and periods of superrefraction accompanied by very deep fades. This behavior is found in most propagation experiments but is perhaps rarely as
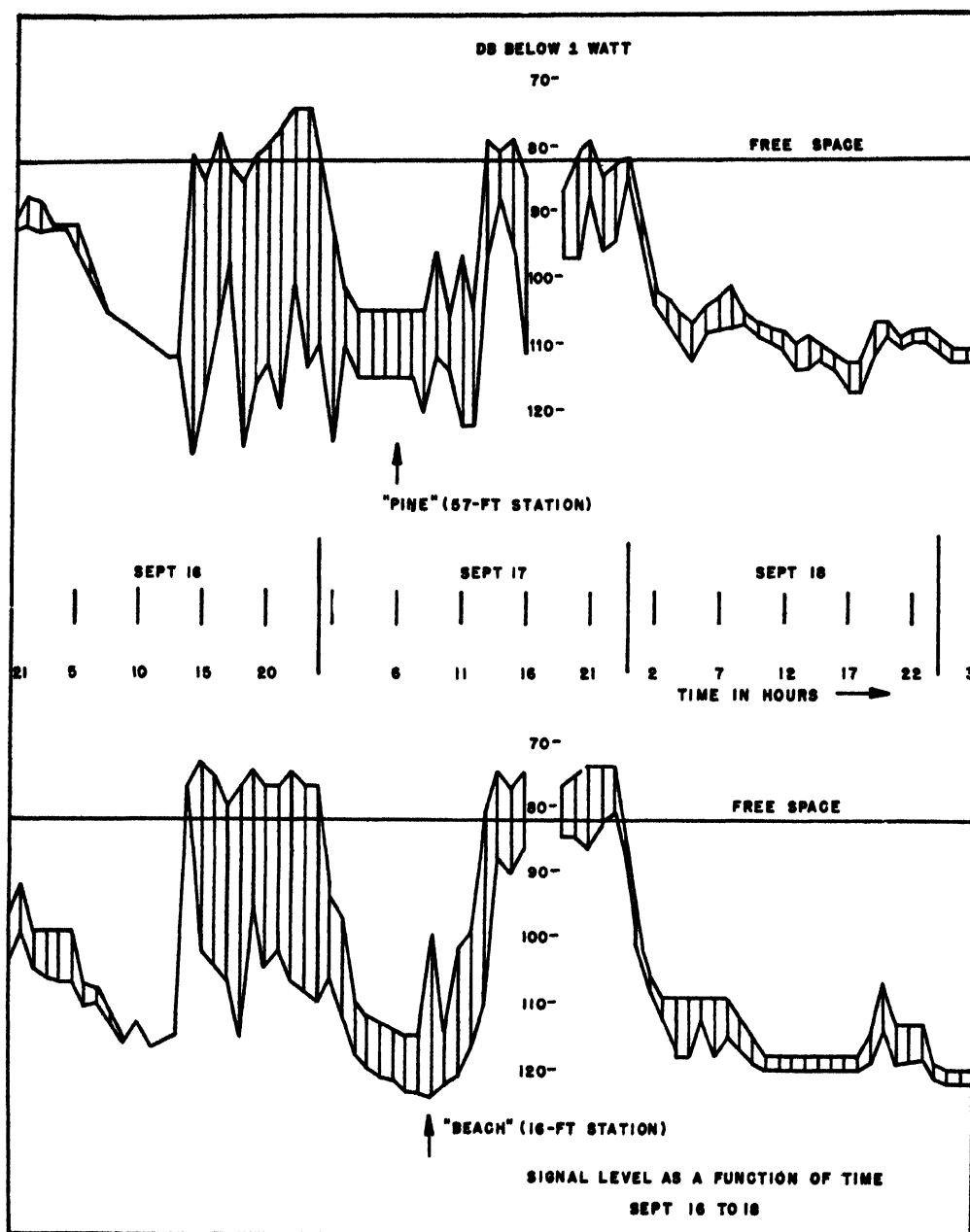
FIGURE 10. Variation of signal strength over 3 days. Two receivers on S band, Flathead Lake, Montana.

well marked as in this graph. Another feature of interest is the fact that the maximum signal level is fairly close to the free space level. This has been found to hold approximately in a number of other propagation experiments where, in the presence of a duct, the maximum received level seems to occur not far from the theoretical free space signal level. No explanation for this behavior has been given, and it may be purely accidental.

Figure 11 presents, for part of the same period as shown in Figure 10, the value of k as a function of

time at a point on the transmission path. Here k is a measure of the slope of the M curve in the lowest strata. Combining equation (17), Chapter 1, and equation (4), Chapter 2, we have $1/ka = dM/dh \cdot 10^{-6}$. Thus when k is negative a duct is present. It will be seen that the incidence of negative values of k correlates well with high signal strength in Figure 10.

CANADIAN EXPERIMENTS

The Canadian transmission experiments are being undertaken by the Tropospheric Subcommittee of
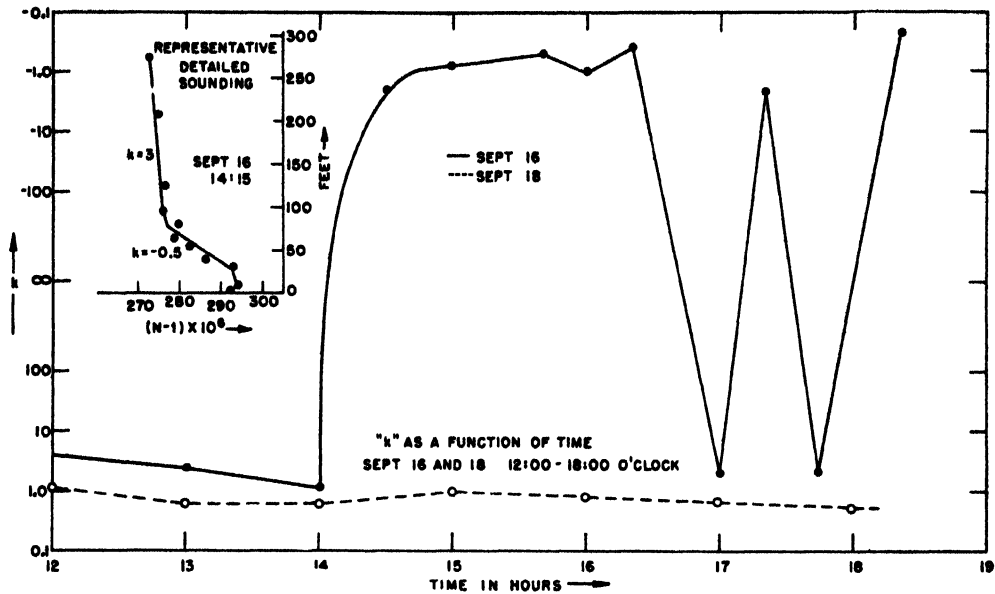
FIGURE 11. Values of k as a measure of M or N gradient for part of period shown in Figure 10.

the Canadian Wave Propagation Committee. They were started in the last year of the war and are still under way at the writing of the present report. These tests promise to throw light upon certain aspects of the propagation problem that are difficult to investigate elsewhere. The equipment is located on the prairies of western Canada. The transmission path is over terrain that is as near perfectly level

as can be found. The ground is covered with short grass and is without trees or houses. The region forms part of a large flat area in which the atmosphere can be expected to be much more homogeneous than in more densely populated regions. Extensive meteorological measurement by means of stationary installations, captive balloons, and airplanes are being carried out simultaneously with the transmission
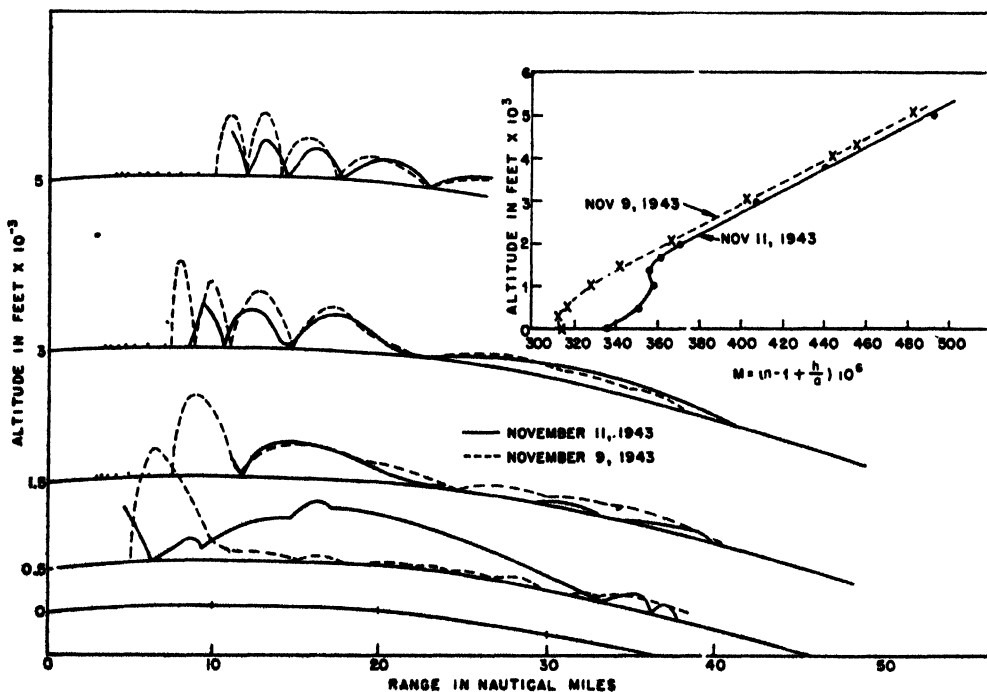
FIGURE 12 Signal strength at several elevations as function of distance. (Near San Diego.)

experiments. The path is 27 miles long with receivers mounted on a tower at several altitudes. The transmitters operate on the S and X bands and are pulsed. In addition, radar measurements are being undertaken by means of corner reflectors that are spaced at regular intervals along a path 45 miles long. It may be expected that valuable results will soon be received on the completion of these experiments.

EXPERIMENTS IN
THE SOUTHWESTERN UNITED STATES

The Navy Radio and Sound Laboratory at San Diego has performed a considerable number of propagation experiments which have substantially aided our understanding of the phenomena of guided propagation. Moreover the meteorological conditions

During the winter of 1942 to 1943, a series of measurements were made on the intensities of artificial fixed echoes of a 700-mc radar located near San Diego,[125,126] and these were compared with measured temperature and humidity gradients in the lower atmosphere. A pronounced correlation between excessive echo ranges and nonstandard M gradients at once appeared. The quantitative aspects of these correlations will not be discussed here since they are very similar to others of this type already reported.

Another set of observations where the receiver was located in a plane is shown in Figure 12.[3] The receiving antenna was a Yagi, mounted in the nose of the plane, records being made when the plane was flying over the ocean toward the transmitter which was a 500-mc radar. Figure 12 represents the results of flights at various altitudes on two different days, the maxima of the signal strength curves corres-
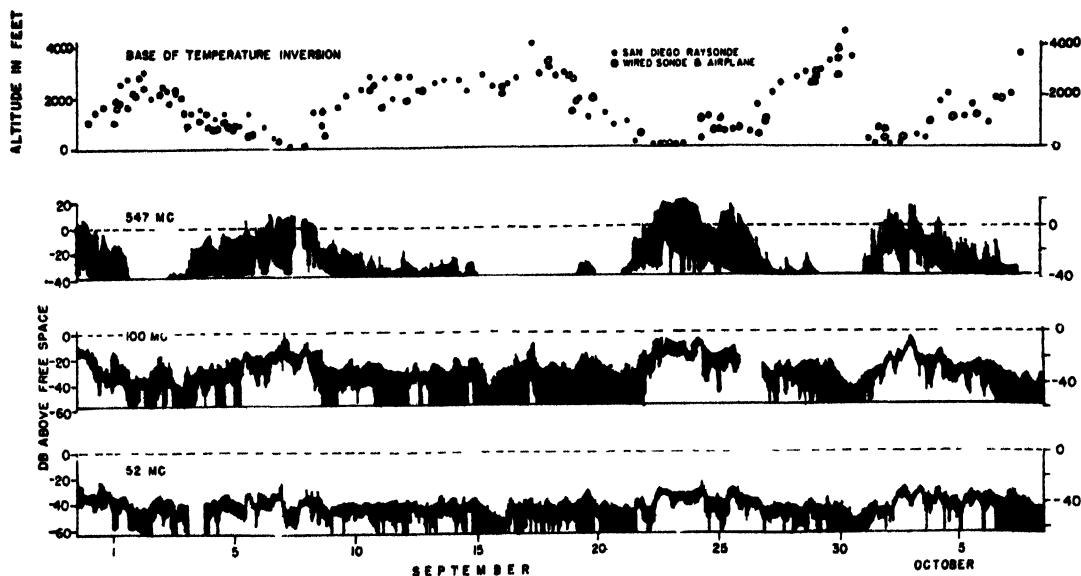
FIGURE 13   Signal strength over 80-mile path, San Diego to San Pedro, correlated with height of temperature inversion

found in this part of the United States are rather unique; and, while they are not, perhaps, reproduced at many other places of the earth, they are so clear-cut and regular as to facilitate greatly experimental investigations and their interpretations.

The meteorological conditions at San Diego during most of the year are characterized by the presence of a high-pressure area and high-level subsidence. In more concrete terms, there is a surface stratum of comparatively cool and moist air on top of which there is a layer of very dry, warm air. The transition between the two strata is as sharp as can be found anywhere, and the transitional layer is often no more than a few hundred feet thick. The height of the transition layer above the ground is usually between 1,000 and 3,000 ft and sometimes as much as 4,000 ft.

ponding to the "lobes" of the transmitter pattern. On one of these days a duct was present as shown in the inset where M is plotted against height. The dot-and-dash straight line in this diagram represents the condition dh/dM = constant. The most conspicuous feature of Figure 12 is the difference between the signal distribution in the absence and presence of a duct at 500 ft, the lowest level measured, whereas the intensities agree fairly well at the higher levels. This behavior is in full agreement with the general predictions of propagation theory. Nevertheless, the detailed interpretation led to a slightly different result from that expected, as was brought out by subsequent experimental investigations.

In 1944 a one-way transmission path was operated between San Pedro and San Diego, an over-water

path[10,15a] 80 miles long with both terminals at an elevation of 100 ft, which were thus well below the optical horizon. Three fairly low frequencies, 52, 100, and 547 mc, were used. Figure 13 shows a field strength diagram of bihourly means for a period of about six weeks in the early fall of 1944. At the top of these diagrams is shown the height of the base of the temperature inversion, which is a quantitative measure of the height of the elevated duct. In order to compare these data with the results of duct theory, Figure 14 shows the number of lowest modes, trapped in the elevated duct, plotted against the signal strength. For each point indicated, the number of trapped modes is calculated by simple waveguide theory from the measured M curves while the field strength is that simultaneously measured on the transmission path. For the lowest frequency, 52 mc, the duct is always beyond cutoff and no trapping should occur; nevertheless, the field strength record shows considerable fluctuation.

As seen from Figure 14 there is no correlation between the field strength and the number of modes
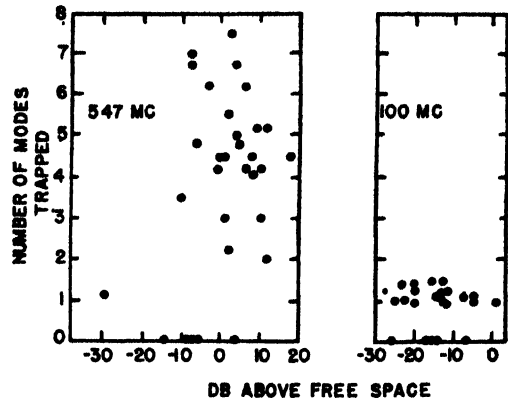
FIGURE 14 Computed number of modes trapped versus observed field strength, San Diego Bay

that, theoretically, are transmitted by the duct. On the other hand, there is a very pronounced inverse correlation between the height of the inversion layer and the strength of the received signal This is just what should be expected on the basis of *reflection*, as
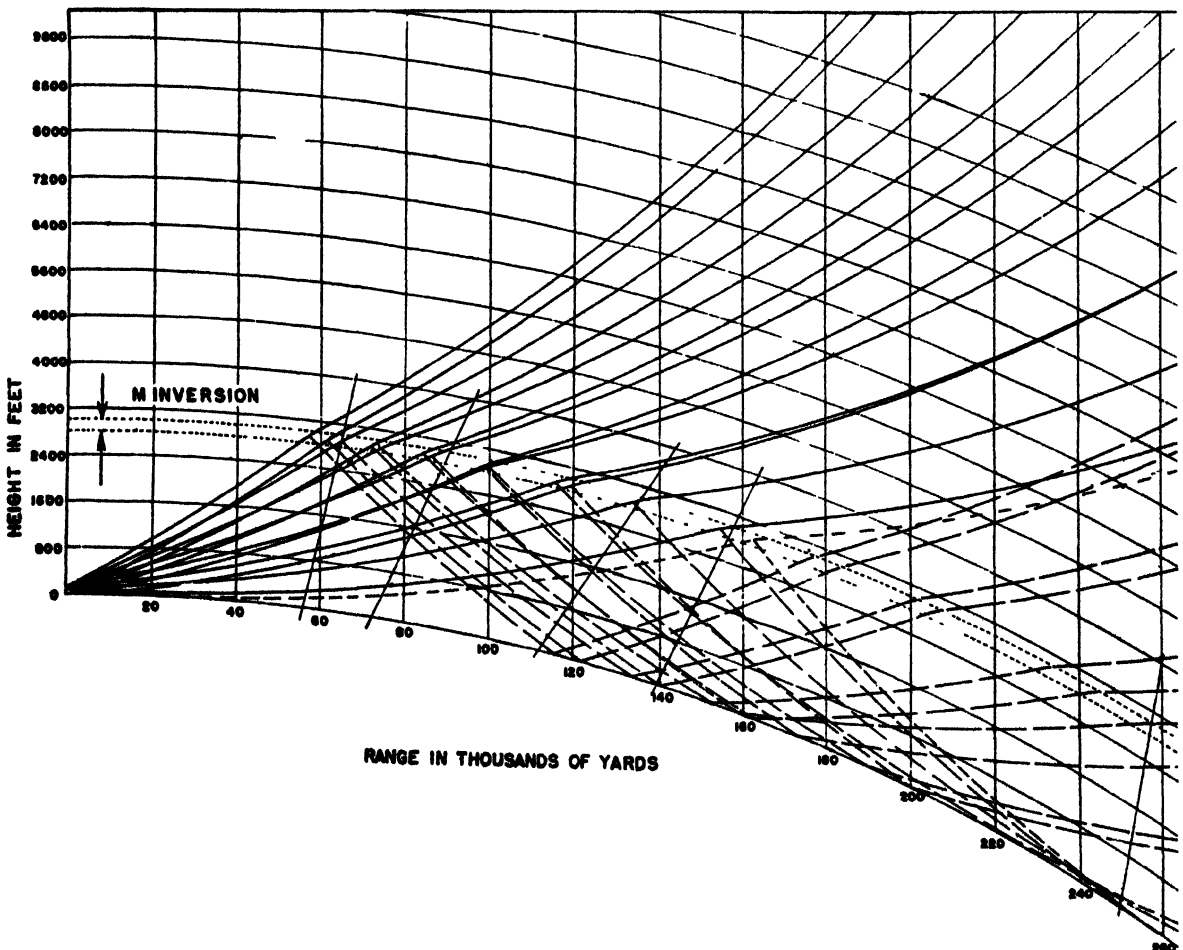
FIGURE 15. Ray tracing diagram including rays reflected from elevated inversion layer, San Diego Bay. M changes by 50 units through the inversion.

distinguished from ray bending, from the elevated layer of M inversion. The principle of this reflection phenomenon has previously been outlined at the end of Chapter 2, on page 17. Further study shows that the rate of change of the field intensity and its variation with frequency are just of the magnitude required by the theory. Figure 15 shows a ray-tracing diagram on which the paths of the reflected rays are indicated. Summarizing the results of this experiment, it may be said that the phenomenon of reflection from an elevated layer has been well established qualitatively and, in some respects, quantitatively The meteorological conditions at San Diego are rather singular, and so far such reflection occurring in a systematic fashion has not been described elsewhere though indications of similar effects have occasionally been reported.

Another transmission experiment was made by the Navy Radio and Sound Laboratory in the Arizona desert in December 1944.[188] The path was nonoptical, 47 miles long, and the frequency used was 3,200 mc. The desert air is extremely dry so that the contribution of water vapor to the refractive index is small and the change in M owing to changes in humidity with height is nearly negligible. During the clear nights a pronounced temperature inversion develops from radiative cooling of the ground, a ground-based duct thus being formed. The received field strength varied in close correlation with the formation and disappearance of the duct, with a pronounced diurnal period. The overall results of this experiment are again in excellent qualitative agreement with the predictions of the duct theory. At the same time the experiment also furnished an opportunity for studying the development over land of low temperature inversions which are valuable for radiometeorological forecasting.

EXPERIMENTS AT ANTIGUA

Operational experience in the Pacific Ocean led to the conclusion that low ducts are very common over the ocean surface in subtropical and tropical climates. In order to study these ducts, an experiment was undertaken by the Naval Research Laboratory in the spring of 1945.[194] The island of Antigua, one of the Leeward Islands of the Lesser Antilles in the British West Indies, was chosen as the site. The prevailing winds there are northeasterly and the air has an over-water trajectory of several thousand miles before arriving at the island and is therefore considered characteristic of large portions of the central Atlantic and Pacific oceans. There is almost no diurnal and only a limited seasonal variation in the air at the lowest levels.

Equipment for the transmission experiments was comprised of S-band and X-band sets provided by the Radiation Laboratory, MIT. The transmitters with parabolic antennae were mounted on a ship at heights of 16 and 46 ft. There were two parabolas for each height and each frequency, one set pointing to the stern and one to the bow, so that measurements could be made on both the outward and inward runs of the vessel. Receivers were located at heights of 14, 24, 54, and 94 ft on a tower at the edge of the water. Monitoring and automatic recording were similar to those used in the transmission experiments previously described. Records were obtained while the ship was traveling away from the receiving station and again on its return. Signals could usually be detected up to 190 miles for some combination of transmitter and receiver heights. Direction finding equipment was used for keeping the ship on its course, and fading of the signal caused by the ship's being off course could be readily detected and rectified.

An extensive program for measuring low-level M curves paralleled the transmission measurements. Since the weather conditions at Antigua are quite steady there is little variation in these curves, as shown by two typical ones illustrated in Figure 11 of Chapter 3. The low-level duct indicated by these graphs has been found present at all times in this location.

Typical field strength records for the S band and the X band are shown in Figures 16 and 17, respectively, the most outstanding feature being the variation of field strength with antenna heights. For the S-band transmission, the field strength increases slightly with increasing antenna height but not nearly so fast as it would under standard conditions. For the X band, on the other hand, the field strength, as a rule, is increased by lowering the antennas. This behavior can be explained on the basis of the mode theory of duct propagation as outlined in Chapter 2 For the shorter wavelength X band, we have genuine trapping, so that the field strength is greatest when the transmitter or receiver or both are in the duct. In terms of the height-gain functions of equation (27), Chapter 1, it appears that these functions of the lowest mode or modes have a pronounced maximum in the duct and decrease rapidly above it. For S-band transmission there is a transition between the complete cutoff, indicated by a highly simplified wave-guide theory, and complete trapping. This intermediate effect is caused by some leakage of this wave train from the duct and the retention by the duct of a portion of its wave-guiding properties. The height-gain functions, while still much larger in the duct than in the case of standard propagation, no longer have distinct maxima but show a gradual increase with height from the ground. This case is particularly interesting because it clearly exemplifies the possible variety of conditions intermediate between trapping, as described by the ray tracing of geometrical optics, and the diffraction around the earth's surface characteristic of standard propagation.

Figure 16 shows two regions with distinctly
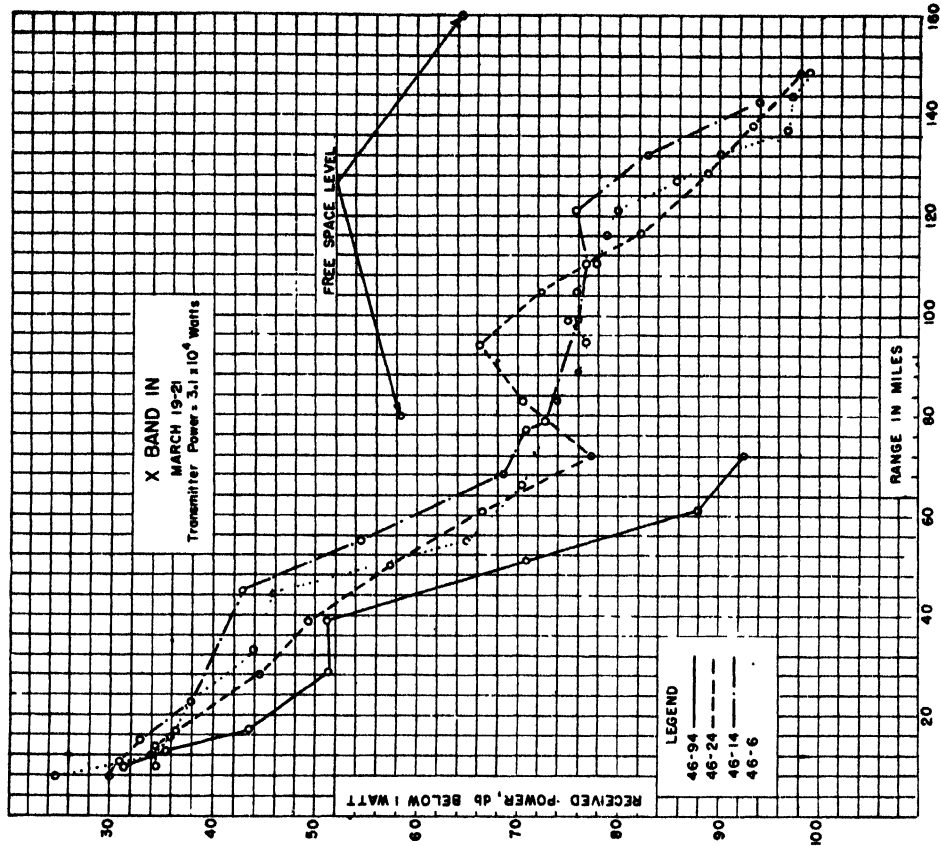
FIGURE 17. Signal strength as function of range. X band, Antigua experiments.
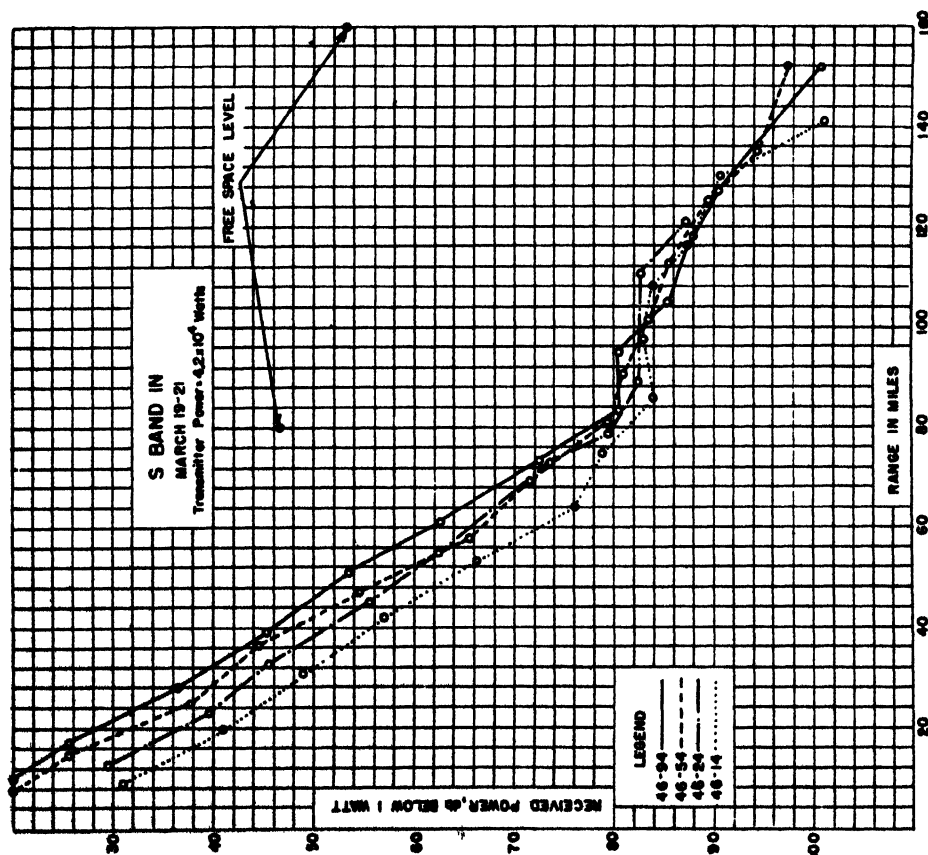
FIGURE 16. Signal strength as function of range. S band, Antigua experiments.

37

different slopes in the curves of power versus distance. This probably indicates that two different modes predominate in these two regions. The pattern shown in Figure 16 can occur if for some distance near the ground the height-gain function of the second mode is greater than that of the first mode. The second mode, however, is attenuated more rapidly with distance than the first. At moderate distances from the transmitter the second mode prevails, but at greater distances it will become smaller than that of the first which decreases less rapidly with distance.

Finally Figure 18 shows a set of curves for attenuation versus distance of the target for an X-band radar on Antigua. Again it is evident that, on the whole, the lowest elevation of the radar gives the largest signal strength.
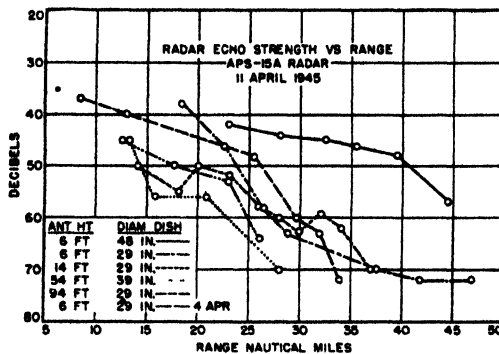
FIGURE 18. Radar echo strength as function of range. X band, Antigua experiments. Target is a PC boat.

ANGLE-OF-ARRIVAL MEASUREMENTS

Because the effects of nonstandard propagation are most pronounced at great distances from the transmitter, they are most important for early warning radar and communication work. These effects were investigated earlier than the question of the deviation of the angle of arrival from that prevailing in a standard atmosphere. This deviation, though small, may nonetheless be significant for fire control radars operating in the microwave band. The angle of arrival may vary by several minutes of arc because of ducts, and this effect was first studied systematically by BTL in 1944.[10,183]

Figure 19 is a schematic view of the receiving antenna used for such measurements. This antenna is a section of a parabolic cylinder arranged so that its beam, at the center of swing, is directed toward the transmitter, this being the angle at which waves arrive on a day with standard propagation. The antenna measures the vertical angle of arrival and a duplicate antenna rotates about a vertical axis and measures the horizontal angle. The antennas are periodically swung through an angle which is set to include the largest variations of the angle of
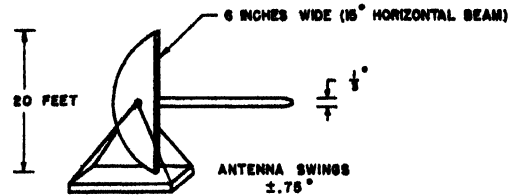
FIGURE 19. Sharp-beamed antenna for angle-of-arrival measurements.

arrival. Figure 20 shows a typical record of received field strength versus time for a periodic swing, the upper record representing the presence of a direct ray only, and the lower indicating both a direct and a ground-reflected ray.

Observations near New York during the summer of 1944 were made on two optical paths 24 and 12.6 miles long with a common receiving antenna. These measurements are estimated to be accurate to 0.04 degree, and they indicate that the greatest variation of the horizontal angle of arrival is 0.10 degree. Fluctuations within this magnitude, however, are quite common. The maximum in the vertical angle for the long path was 0.46 degree above the standard for the direct ray and 0.17 degree below the standard for the reflected ray. No correlation between departures from the standard of the direct ray and the ground-reflected ray has been observed. When the direct ray was 0 46 degree above the standard, it was apparently being trapped and no reflected ray was observed. The greatest spread observed between the direct and reflected rays was 0.75 degree, as compared to a standard of 0.35 degree. The variation of vertical angle over the short path was less than over the long one, the greatest change in angle being an increase of 0.28 degree over the standard for the direct ray while that of the ground-reflected ray was too small to be observed.

For early warning radars where the target is perhaps 75 to 100 miles away, the difference in bending of the rays between standard atmospheres of moderate and warm climates becomes appreciable. In this case differences in estimated height vary by as much as 2,000 ft, if the target height is determined by the first signal in the lowest standard lobe.
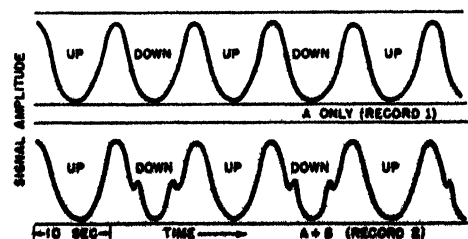
FIGURE 20. Typical record of angle-of-arrival measurements. Top, direct ray only. Bottom, direct and ground-reflected ray.

Chapter 5

GENERAL METEOROLOGY AND FORECASTING

INTRODUCTION

IN CHAPTER 1, equation (9) was given for the refractive index as

$$(n - 1) \cdot 10^6 = \frac{79}{T} \left(p - e + \frac{4{,}800e}{T} \right) \quad (1)$$

On adding to this the term $(h/a)10^6$ the "modified refractive index M" of equation (4), Chapter 2 is obtained, namely

$$M = \left(n - 1 + \frac{h}{a} \right) \cdot 10^6 \quad (2)$$

When the temperature increases with height, other things being constant, $n - 1$ decreases with height and when this decrease is strong enough it will outweigh the increase of M caused by the term h/a. Similarly, a decrease of moisture with height will produce a decrease of $n - 1$ which, if strong enough, will again produce a negative slope of the M curve. In Chapter 3 we have dealt with these changes purely from the observational viewpoint. Now the origin of these variations owing to the physics and dynamics of the lower atmosphere will be considered. A knowledge of general meteorological conditions may enable a trained weather forecaster to predict, from weather maps and other pertinent data relating to the structure of the lower atmosphere, the presence of ducts and other meteorological factors affecting transmission.

The first attempts at radio forecasting were made as early as 1943 by the British Meteorological Office in conjunction with the services operating the radar sets along the North Sea and Channel Coast. While the correlation between forecasts and observed results was imperfect, results were promising enough to encourage further studies. Since then, the forecasting technique in the British home waters has been developed to a considerable degree of effectiveness. Studies regarding the relationship between the dynamics of the lower atmosphere and radio wave propagation have been initiated by the interested Services in various parts of the British Empire, particularly in Australia where a number of interesting correlations have been discovered. In the United States the problem was first systematically attacked by the propagation group of the Massachusetts Institute of Technology Radiation Laboratory [MIT-RL], and at about the same time by the Army Air Forces Tactical School in Florida. The latter established a training course for radio meteorological forecasters, a number of whom participated in offensive operations in the Pacific at Leyte and later.

In connection with the transmission experiment across Massachusetts Bay, which was described in Chapter 4, a forecasting unit was established cooperatively by MIT-RL, the AAF, and the U. S. Weather Bureau at Boston. Regular forecasts were made and checked by both meteorological and radio observations. The pertinent information required for radio meteorological forecasting was assembled by a number of agencies in England[244] and in this country. The most extensive American texts on the subject have been issued by Headquarters, Weather Division, AAF,[245] and by the Columbia University Wave Propagation Group.[157] The latter report, *Tropospheric Propagation and Radiometeorology* is published in Volume 2 .

ATMOSPHERIC STRATIFICATION

From the meteorological viewpoint it is convenient to distinguish three factors which tend to affect the temperature and moisture distribution in the lower part of the atmosphere. These factors are known to meteorologists as (1) advection, (2) nocturnal cooling (over land) and (3) subsidence.

Advection is a term that designates the horizontal displacement of an air mass of specific properties over an underlying surface which tends to modify the structure of the mass. Thus one speaks of the advection of dry polar air over a warm water surface. Advection is not the modification of air mass properties but merely a preliminary to such modification.

Advection changes the physical characteristics of the lower strata of the atmosphere through transfer of heat or moisture between the air and the underlying ground or sea surface. The operating factor in this exchange is turbulence, and a brief review of its effects in the atmosphere will be given.

Nocturnal cooling over land is caused by a loss of heat from the ground by infrared radiation. The cooling thus effected is communicated to the lower strata of the atmosphere by means of turbulence. Nocturnal cooling occurs to an appreciable degree only if the sky is clear. Any layer of clouds will exert a "blanketing" effect which reduces the cooling of the ground to a small fraction of that for clear nights.

Subsidence is a meteorological term for the slow vertical sinking of air over a very large area. It is usually found in regions where barometric highs are located. By a dynamic process, too complicated to be described here, subsidence often produces a temperature inversion, the air in a subsiding stratum being, as a rule, very dry. Subsidence is usually strongest in

a layer somewhat elevated from the ground, and when the dry subsiding mass overlies a moist stratum near the ground, a sharp moisture gradient is created which is favorable for the formation of the duct. The elevated ducts at San Diego are of this type.

Convection occurs whenever the vertical temperature gradient exceeds in absolute value the critical gradient of about −1 C per 100 m. It is usually the result of the heating of the ground by the sun's rays, and over land on a hot summer day it may extend to great heights in the atmosphere. Since convection mixes the air thoroughly, it establishes small and constant moisture gradients throughout the lower atmosphere, resulting in a very nearly linear *M* curve. Consequently standard conditions of propagation prevail on summer days over land from late morning until late afternoon, this being the time when convection is most likely to be present. Often this applies also to summer days with a light overcast.

Frictional turbulence occurs normally in the lowest 1,000 m of the atmosphere even when convection is absent. It is caused by the wind, requires at least light winds, and is fully developed with moderate or strong winds over land. Since turbulence is caused by the roughness of the ground it is less well developed over the sea surface. It can safely be assumed that over land with moderate or strong winds standard propagation conditions prevail because of the regularizing action of turbulence.

Temperature inversions occur when the temperature of the sea or land surface is appreciably lower than that of the air. The temperature transition from the ground to the free air takes the form shown in Figure 1. The heat and moisture transfer caused by turbulence in a temperature inversion is less simple than that in a frictional layer. The turbulent processes in inversion regions are highly complex and, as yet, are not very well explored. It is known, however, that the intensity of the vertical transfer of heat and moisture is much less than the rate of transfer with frictional turbulence and decreases with the vertical increase of temperature. In a steep inversion the rate of transfer may be many times less than in a frictional layer. This tends to produce a vertical stabilization of the air layers in the inversion region. As soon, therefore, as a temperature inversion has begun to form, the rapid mixing in the lowest layers, usually effected by frictional turbulence, stops and is replaced by a much more gradual diffusion.

Assuming that the rate of diffusion has become so slow that the transfer of moisture over a height of a few hundred feet takes many hours or, perhaps, a day or two, when the air in the inversion is dry to begin with and flows over the sea or moist land there will be established, in such an air mass, a steep moisture lapse, since the water vapor that has been taken up by the air near the ground will only gradually diffuse into the dry air aloft. Conditions are then favorable for the formation of an evaporation duct,

in addition to whatever tendency toward duct formation may be caused by the temperature inversion itself.
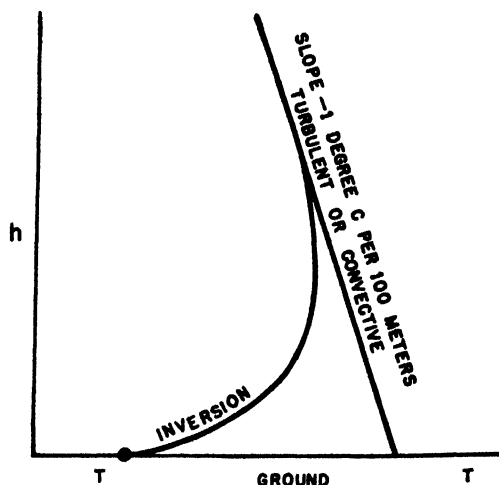
FIGURE 1 Air temperature versus height for a temperature inversion.

CONDITIONS OVER LAND

Because of the considerable variation of the ground temperature by cooling at night and heating during the day, there is to be found over land an alternation of convection during the day and conditions of a temperature inversion during the night. There is some phase shift in that the atmospheric conditions lag about three to four hours behind the sun. The amount of nocturnal cooling caused by infrared radiation of the ground is very nearly independent of its constitution. It is, however, strongly reduced by the presence of clouds which in turn radiate toward the ground, canceling part of the cooling effect. High moisture content in the lower atmosphere acts partly in the same way and somewhat reduces the heat lost by the ground. With a full overcast, nocturnal cooling is negligible and normally no temperature inversion will be formed.

In temperate climates temperature inversions alone can produce only weak ducts because the effect of temperature upon the refractive index is relatively small. In the fairly common case, however, where the inversion is accompanied by sufficient moisture gradient, a strong duct will result. This occurs when the air is dry enough to allow evaporation into it from the ground. In warmer climates where the transition between night and day is rapid, evaporation may set in early in the morning before the nocturnal inversion has been completely destroyed by the action of the sun. A strong duct will then be formed for a short period.

Fog. Contrary to what might perhaps be expected, the formation of fog results generally in a decrease of

increase with height through the fog layer. In this event propagation will be standard, or ducts may even form occasionally within the fog layer.

COASTAL AND MARITIME CONDITIONS

Advection is of prime importance near a coast where the wind may blow the air from land to sea or vice versa. The former case, which is the more important in practice, will be considered. A temperature inversion is formed, if the air from above a warmer land surface flows out over a cooler ocean surface. Over the land the air will usually have attained a state of convective equilibrium with correspondingly slow variations of temperature and humidity with height. When this air comes in contact with the cold water surface a temperature inversion is formed which increases gradually as the air
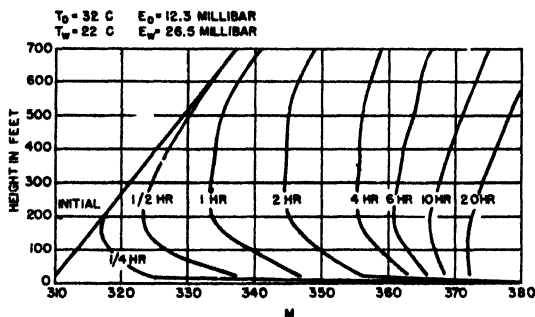
FIGURE 2. Successive M curves resulting from modification of warm dry air over cool moist surface. Zero time corresponds to the coastline; 1/4 hr, 1/2 hr, etc. refer to the time the air has been over water.

proceeds over the water. Thus the inversion is the more pronounced, the greater the distance from the shore. Eventually, however, at very large distances, refractive index. For instance, when fog forms by nocturnal cooling of the ground, the total amount of water in the air remains substantially unchanged, although part of the water changes from the gaseous to the liquid state. It is found that water suspended in the air in the form of drops contributes less to the refractive index than the equivalent amount of vapor. The formation of fog, therefore, reduces the effective contribution of the water vapor to the refractive index. If there is a temperature inversion in the fog layer, the vapor pressure required for saturation increases with height, and a substandard M curve usually results.

With a substandard M curve the electromagnetic field near the earth surface is diminished instead of increased, a case opposite to that of superrefraction. In practice this weakening of the field not uncommonly leads to a more or less complete radio blackout.

Fog, however, does not always produce a substandard M curve although that is usually the case. In certain less frequent types of fog, the temperature and saturation vapor pressure may be constant or

equilibrium between the air and the water surface will again be reached.

The temperature inversion formed during this process would in itself give rise to only a comparatively weak duct. When, however, the air is dry, evaporation from the sea surface takes place simultaneously with heat transfer, and a fairly strong negative humidity gradient is established in the lowest layers. This combination of temperature inversion and moisture gradient is very favorable for the formation of a pronounced duct off shore.

The progressive formation of an advection duct, created by the mechanism just outlined, is shown schematically in Figure 2. The successive M curves correspond to a series of time intervals measured from the passage of the air over the shore line. The increase of the duct toward the maximum and the subsequent flattening of the M curve as the air approaches a new state of equilibrium is clearly seen from the figure.

Duct formation in such a case depends on two quantities: (1) the excess of the unmodified air temperature above the water temperature, and (2) the humidity deficit, that is, the difference between the saturation vapor pressure corresponding to the water temperature and the actual water vapor pressure in the unmodified air. The problem can be treated by means of the mathematical theory of diffusion in a turbulent medium, and a considerable amount of effort has been spent in investigating this type of advective duct. Extensive mathematical work has been carried out in England[200] based primarily on the large body of data on atmospheric diffusion gathered in connection with chemical warfare problems.[197] In the United States such ducts have been studied very extensively in connection with the propagation experiments in Massachusetts Bay where conditions are favorable for their formation.[201,204]

Another phenomenon often responsible for ducts in coastal regions is the land and sea breeze. This type of wind is of thermal origin and is produced by temperature differences between land and sea. During the day, when the land gets warmer than the sea, the air over the land rises and that over the sea descends, thus causing a circulation in which the air in the lowest layers flows from sea to land. This is the sea breeze. Vice versa, during the night the land becomes colder than the sea, and circulation is in the reverse direction, creating the land breeze. As a rule this type of phenomenon is extremely shallow, and the winds do not extend above a few hundred feet at the most. A sea breeze modifies the advective conditions described above in various ways, and extremely strong ducts have occasionally been observed under sea breeze conditions. The land and sea breezes are of a strictly local nature and in some cases will extend only a few miles to land or sea from the shore. Nevertheless this region may be

an important part of the radiation trajectory of coastal radars. These breezes develop only under fairly calm conditions; they are wiped out by a moderate or strong wind.

The advective ducts of the types described here are by their very nature of only limited horizontal extent. The horizontal variation of refractive index presents a problem that till now has not been systematically studied from either the experimental or the theoretical angle.

A particular type of duct has been discovered in purely maritime air, that is, air which has had an extremely long sea trajectory and thus should have reached an approximately steady state of diffusion relative to the underlying sea surface. The Antigua experiments described in the preceding chapter reveal the existence of a type of low duct which seems to be characteristic of maritime air. It appears probable that similar ducts are permanent in the oceanic regions of many parts of the earth. The relative humidity of the air at Antigua was found to be 60 to 80 per cent, indicating that a continuous upward diffusion of moisture must take place, since the air immediately adjacent to the water surface is always practically saturated. On the other hand, there is little difference between the air and sea temperatures in this case, the ocean being about 25 C while the air temperature varies between 23 and 26 C. The ducts are therefore caused solely by the variation of water vapor in the lowest layers and are much lower than the advective ducts described before, their height rarely exceeding 40 ft. Typical M curves have been shown in Chapter 3, and, for the particular effects caused by the low height of these ducts, we refer to the discussion of the experimental results.

The diurnal change of ocean temperature is insignificant, except in extremely shallow water, and therefore, at some distance from the coast, propagation conditions do not show any appreciable diurnal variation.

DYNAMIC EFFECTS

The physical processes in the lower strata of the atmosphere which determine the formation of ducts are to a considerable extent controlled by the large-scale dynamics of the atmosphere. It is therefore often possible to make at least a qualitative forecast of propagation conditions on the basis of a knowledge of the synoptic weather situation. An example in point is the diurnal variation over land in clear weather from standard conditions during the day to duct conditions in the latter part of the night and the early morning hours.

Conditions in a barometric low pressure area generally favor standard propagation. Winds are usually strong or at least moderate resulting in a well-mixed layer of frictional turbulence. Local thermal stratifications are destroyed, and abnormal moisture gradients will not develop because of the intense turbulent mixing. The sky is frequently overcast in the low pressure area and nocturnal cooling therefore is often negligible.

On the other hand, meteorological conditions in a high pressure area are frequently favorable for the formation of ducts. The sky is commonly clear, thus giving rise to pronounced nocturnal cooling of the ground and to the attendant formation of a temperature inversion in the lowest layers. This, again, often gives rise, by evaporation, to steep moisture gradients within the inversion layer resulting in the formation of ducts in the manner already described. Winds in high pressure areas are often slight, or a calm prevails, resulting in a formation of local thermal stratifications and of land and sea breezes.

One of the prime phenomena conducive to non-standard propagation conditions in a barometric high is subsidence, already described. Subsidence is closely connected to high pressure areas on the weather map and is always found in such areas, but it is not always intense enough to produce an inversion. The typical pattern of air flow in a baro-
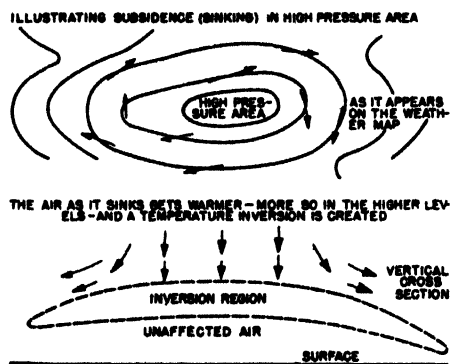
FIGURE 3. Schematic diagram illustrating subsidence in a region of high barometric pressure.

metric high is shown in Figure 3 in both horizontal projection and vertical cross section.

The air in the lower parts of a region of subsidence is very dry because it has descended from a high level in the atmosphere where the temperature is low and hence the saturation vapor pressure is small. If such air is located over a surface capable of evaporation such as the ocean, a steep moisture gradient may be established at some level above the ground. This is the most common mechanism for the formation of elevated ducts. Quite often subsidence combines with some or the other effects mentioned earlier enhancing their tendency toward the formation of the duct. The elevated ducts found in the San Diego region are perhaps the most outstanding example of this type of dynamically induced stratification.

The effect of fronts in the atmosphere upon propa-

cation does not seem to be very pronounced. This is probably due to the fact that in a front the transition between warm and cold air is comparatively gradual extending over a height of perhaps 1 km. In the English propagation experiments some effects of fronts have indicated slightly substandard conditions with warm fronts and slightly superstandard conditions with cold fronts. Often, however, the effect of fronts upon radio propagation is negligible. This, of course, refers only to the frontal region itself and not to the change in air mass and attendant propagation conditions connected with the passage of a front.

WORLD SURVEY

It clearly appears from the preceding sections that climate has a fundamental influence on the nature of propagation conditions. A systematic attack on the problem of the occurrence of ducts over the ocean has been made in England on a world-wide scale.[250] Monthly maps based on estimates drawn from general low-level weather data, giving regions of the most frequent occurrence of superrefraction and substandard refraction, were issued. However, these need much further checking by actual observations. The propagation features of some important parts of the world where some knowledge has been accumulated is outlined briefly below.

Atlantic Coast of the United States. Along the northern part of this coast superrefraction is common in summer, while in the Florida region the seasonal trend is reversed, a maximum occurring in the winter season.

Western Europe. On the eastern side of the Atlantic, around the British Isles and in the North Sea, there is a pronounced maximum in the summer months. Conditions in the Irish Sea, the Channel, and East Anglia have been studied by observing the appearance or nonappearance of fixed echoes. Additional data based on one-way communication confirmed the radar investigations.

Mediterranean Region. The campaign in this region provided good opportunities for the study of local propagation conditions. The seasonal variation is very marked, with superrefraction more or less the rule in summer, while conditions are approximately standard in the winter. An illuminating example is provided by observations from Malta, where the island of Pantelleria was visible 90 per cent of the time during the summer months, although it lies beyond the normal radar range.

Superrefraction in the Central Mediterranean area is caused by the flow of warm, dry air from the south (sirocco) which moves across the ocean, thus providing an excellent opportunity for the formation of ducts. In the winter, however, the climate in the Central Mediterranean is more or less a reflection of Atlantic conditions and hence is not favorable for duct formation.

The Arabian Sea. Observations covering a considerable period are available from stations in India, the inlet to the Persian Gulf, and the Gulf of Aden. The dominating meteorological factor in this region is the southwest monsoon which blows from early June to mid-September and covers the whole Arabian Sea with moist equatorial air up to considerable heights. Where this meteorological situation is fully developed, no occurrence of superrefraction is to be expected. In accordance with this expectation, all the stations along the west side of the Deccan report normal conditions during the southwest monsoon season. During the dry season, on the other hand, conditions are very different. Superrefraction then is the rule rather than the exception, and on some occasions very long ranges, up to 1,500 miles (Oman, Somaliland), have been observed with fixed echoes on 200-mc radar, based near Bombay.

When the southwest monsoon sets in early in June, superrefraction disappears on the Indian side of the Arabian Sea. However, along the western coasts conditions favoring superrefraction may still linger. This has been reported from the Gulf of Aden and the Strait of Hormuz, both of which lie on the outskirts of the main region dominated by the monsoon. The Strait of Hormuz is particularly interesting as the monsoon there has to contest against the "shamal" from the north. The Strait itself falls at the boundary between the two wind systems, forming a front, with the dry and warm shamal on top, and the colder, humid monsoon underneath. As a consequence, conditions are favorable for the formation of an extensive radio duct, which is of great importance for radar operation in the Strait.

The Bay of Bengal. Such reports as are available from this region indicate that the seasonal trend is the same as in the Arabian Sea, with normal conditions occurring during the season of the southwest monsoon, while superrefraction is found during the dry season. It appears, however, that superrefraction is much less pronounced than on the northwest side of the peninsula.

The Pacific Ocean. This region appears to be the one where, up to the present, least precise knowledge is available. There seems, however, to be definite evidence for the frequent occurrence of superrefraction at some locations, e.g., Guadalcanal, the east coast of Australia, around New Guinea, and on Saipan. Along the Pacific coast of the United States, observations indicate frequent occurrence of superrefraction, but no statement as to its seasonal trend seems to be available. The same holds good for the region near Australia.

In the tropics there is a very strong and persistent seasonal temperature inversion, the so-called trade wind inversion. It has no doubt a very profound influence on the operation of radar and short wave communication equipment in the Pacific theater.

RADAR FORECASTING

The forecasting of propagation conditions for early warning radars is of great operational significance because ranges for airplane as well as ship targets often vary by as much as a factor of 2 or more depending on the weather conditions. Forecasting is based on the general meteorological principles presented above which can be organized into a system of standard procedures for the prediction of propagation in a given area.[244,253,255] It is usually quite difficult to make a quantitative forecast of such parameters as duct height, but this has been tried with a fair degree of success.

A radio forecast is made by first taking the general synoptic weather situation as presented on a weather map and including such upper air data as may be available. Usually one forecast cannot be applied to more than a limited area of specific local conditions; fortunately such a forecast is in general adequate for the area covered by one or a few radar sets. The formation of ducts depends principally on the temperature difference between the air and the ground or sea surface and on the humidity of the air. Data on sea temperature, which is usually fairly constant, are collected while over land it is necessary to obtain data on the diurnal variation of the soil temperature.

Wind velocities may be gathered from the weather map, and the trajectory of the air previous to and during the forecast period can then be determined. If the relative humidity of the air is known, it is possible from the theories at hand to draw estimated curves of the temperature and moisture variation in the lowest layers. From these an estimated M curve is obtained. The success of this method depends to a large degree upon the familiarity of the forecaster with local conditions.

The forecasting of advective ducts over the ocean is the main problem in which radio forecasting requires other tools than those used for ordinary weather forecasting; but most other problems are closely similar to those presented by conventional practice, among which are the forecasting of subsidence from upper air meteorological data, the forecasting of nocturnal temperature inversions in dry climates, and the forecasting of standard propagation conditions.

In order to facilitate weather forecasting in the Pacific, where data have been very scanty during the war, a system has been worked out whereby localities in the Pacific area are compared to those of closely similar climatic and meteorological character in the Atlantic. A rough estimate of propagation conditions to be expected may be derived therefrom.[25,215]

SCATTERING AND ABSORPTION OF MICROWAVES

T HE OBJECT of the present chapter is to summarize the status of absorption and scattering of microwaves by different solid obstacles, by liquid water or ice particles floating or falling in the atmosphere like those present in clouds, fog, rain, hail, and snow. The absorption of microwaves by the atmospheric gases as well as the aforementioned meteorological elements will also be summarized here.

The following grouping of the material included suggests itself naturally: absorption and radar cross section; targets (planes, ships); absorption and scattering by rain, hail, snow, clouds, and fog; and absorption by the atmospheric gases, oxygen, and water vapor.

ABSORPTION AND RADAR CROSS SECTION

Any object irradiated by electromagnetic waves will in general remove energy from the incident beam both by absorption and by scattering. The absorbed energy is transformed into heat in the body, while the scattered energy appears in the form of radiation propagated generally in every direction around the scatterer as the source.

Let us call P_a the power removed from the beam through the internal absorption of the object. Its absorption cross section is defined by

$$A = \frac{P_a}{W_i}, \qquad (1)$$

where W_i is the power density in the incident beam, that is, the power passing a unit cross-sectional area.

Similarly, if P_s is the total power removed from the beam through scattering in every direction, then the scattering cross section associated with this object is

$$S = \frac{P_s}{W_i}. \qquad (2)$$

The value of S gives information about the total scattered energy, but this is not directly useful in radar work because one is interested only in that fraction of the total scattered power which travels in the direction of the receiver. One wants then a parameter involving the scattered power per unit area W_r at the radar receiver instead of the total. If the target is an isotropic scatterer,

$$W_r = \frac{P_s}{4\pi d^2}, \qquad (3)$$

d being the distance from the target to the receiver.

The scattering cross section can thus be written as

$$S = 4\pi d^2 \frac{W_r}{W_i}. \qquad (4)$$

For targets other than isotropic scatterers, however, this procedure fails since one cannot say that the power per unit area at the radar is $P_i/4\pi d^2$. Nevertheless, it is useful to define a parameter,

$$\sigma = 4\pi d^2 \frac{W_r}{W_i}, \qquad (5)$$

which is called the radar cross section in analogy with the scattering cross section S of an isotropic scatterer. This cross section σ may be thought of as the scattering cross section which the target in question would have if it scattered as much energy in all directions as it actually does scatter in the direction of the radar receiver. For an isotropic scatterer $\sigma = S$, but in general it does not.

TABLE 1. Radar cross sections.

Targets	Condition	Radar cross section
Conducting sphere, radius a	$\lambda << a$	πa^2
	$\lambda >> a$	$\dfrac{144\pi^5 a^6}{\lambda^4}$
Metallic plate, area S	All dimensions $>> \lambda$	$\dfrac{4\pi S^2}{\lambda^2}$
Cylinder, diameter $= d$ length $= l$	Axis of cylinder parallel to electric field, $\lambda << d, \lambda << l$	$\dfrac{\pi d l^2}{\lambda}$
Matched load dipole	Oriented parallel to the incident electric field	$\dfrac{9\lambda^2}{16\pi}$
Shorted dipole	Oriented parallel to the incident electric field	$\dfrac{9\lambda^2}{4\pi}$
Corner reflector		$\dfrac{4\pi S^2}{\lambda^2}$ $S =$ cross section of triply reflected beam
Triangular corner reflector	$L =$ length of reflector's edge. $\theta =$ angle between direction of incidence and axis of symmetry of reflector	$\dfrac{4\pi L^4}{3\lambda^3}(1-0.0076\,\theta^2)$
Square corner reflector		$\dfrac{12\pi L^4}{\lambda^3}(1-0.0274\,\theta)$

It can be shown[a] that the ratio of the received power P_2 to the output power P_1 is given by

$$\frac{P_2}{P_1} = G_1 G_2 \frac{\sigma}{4\pi d^2} \left(\frac{3\lambda}{8\pi d}\right)^2 A_p^4 . \qquad (6)$$

The gains G_1, G_2 and path factor A_p are defined in Volume 3, Chapter 2, and λ is the wavelength of the radiation used. (See also Volume 3, Chapter 9.) This formula can be used for the determination of σ. Or if σ is known, it may serve to calculate the possible range. (It may be noted here that sometimes σA_p^4 is called radar cross section.) Also, a characteristic length L, sometimes called the scattering coefficient, is occasionally defined in relation to σ by

$$\sigma = 4\pi L^2 . \qquad (7)$$

For simple targets σ may be calculated. Table 1 contains a few calculated radar cross sections.

AIRCRAFT TARGETS

Diagrams showing the dependence of σ on the orientation of the aircraft indicate very large and irregular fluctuations. The radar cross section can change by 100 to 1 with a change of aspect of only a few degrees. These varying values of the radar cross section are dependent on wavelength, polarization, details of plane design, etc. Reflection patterns such as shown in Figure 1 have been measured in the laboratory for a few simplified models. Actually an observer would see only the time average of the
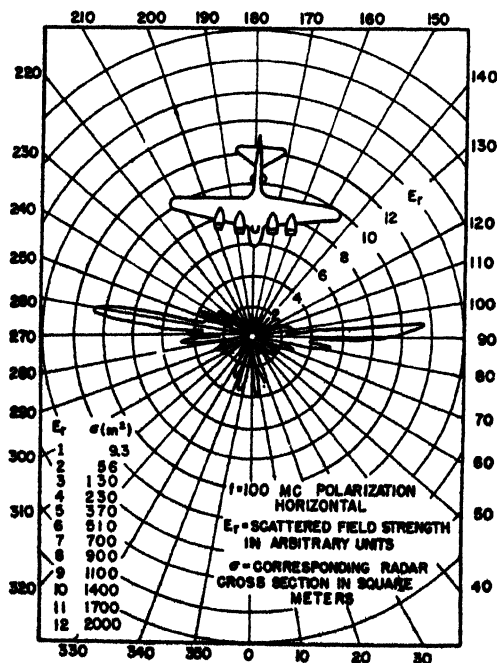
Figure 1. Aspect diagram of a B-17E at 5 degrees above horizon.

[a] See Volume 3 .

radar cross section of a plane, and it is only this average value which is of operational importance.

Table 2 gives measured values of σ for various aircraft. These are the values to be used in equation (6). As far as is known, these empirical cross sections

TABLE 2. Airplane radar cross sections.

Airplane	σ, sq m	σ, sq ft
SNC	3.9	42
SNJ	5.0	54
OS-2U	9.5	100
Taylorcraft	9.5	100
CESSNA	9.5	100
O-47	10	110
AT-11	11	120
SWB	13	140
15-D (Curtiss Wright)	23	250
J2F	25	260
JRF	30	320
PBY	31	340
B-18	36	380
B-17	45	480
B-29	67	710

are independent of wavelength. This result may be interpreted to mean that a plane in motion behaves more or less like a collection of good reflecting surfaces oriented at random. It is worth noting in this connection that the radar cross section of a circular plate of radius a, whose normal is at an angle θ with the direction of incidence, is

$$\sigma = \pi a^2 \left[\cot \theta \times J_1 \left(\frac{4\pi a}{\lambda} \sin \theta\right)\right]^2 , \qquad (8)$$

where J_1 is the first order Bessel function of the first kind. The maximum of σ occurs for $\theta = 0$, when equation (8) reduces to

$$\sigma = \frac{4\pi^2 a^4}{\lambda^2} \qquad (9)$$

This sharp maximum of σ at $\theta = 0$ is the phenomenon of specular reflection. The average value of σ over all values of θ turns out to be

$$\sigma_{ave} = \frac{1}{2}\pi a^2 . \qquad (10)$$

This result is independent of wavelength and suggests that a large number of specularly reflecting surfaces oriented at random will have a cross section independent of λ, or that a few surfaces of rapidly changing orientation may have this property. The lack of dependence of wavelength of aircraft radar cross sections might be understood on the basis of these results.

SHIP TARGETS

A ship being a collection of both complicated and flat surfaces, a rigorous computation of the radar cross section of any given ship of known design is not feasible. Nevertheless, the Naval Research Laboratory workers have been able to give a good account of these problems.[374,376,385,393,417,421]

The path factor in the formula (6) raised to the

fourth power is

$$A_p^4 = 6\left[1 - \frac{\sin \delta_0}{3\delta_0}(4 - \cos \delta_0)\right], \quad (11)$$

where

$$\delta_0 = \frac{4\pi h_1 H}{\lambda d},$$

h_1 = antenna height,

H = height of ship above water including superstructure.

The above result follows by integrating the received power over the height H, assuming perfect reflection from sea.

It is seen in equation (11) that whether $\delta_0 < \pi$, the region called the "far zone," or $\delta_0 > \pi$, the "near zone" (short ranges), materially affects the qualitative behavior of the factor A_p^4. In the latter region

$$A_p^4 \cong 6.$$

The radar cross section of a ship which does not exhibit marked specular reflection is given roughly by

$$\sigma = \alpha \frac{B^2 H}{\lambda}, \quad (12)$$

where α = dimensionless constant dependent on ship design,

B = the breadth of the aspect under observation,

H = height of ship above water including superstructure.

The approximate values of α to be used are indicated in Table 3.

TABLE 3. Ship targets.

Type of ship	α	Remarks
Battleship	0.1	
Cruiser	0.1	
Aircraft carrier	0.05	Except at direct broadside aspect
Submarine	0.01	

In Tables 4 to 7, values of σ computed from equation (12) are called theoretical values. Experimental values are computed from observations made by the Naval Research Laboratory workers with each quantity the mean of several observations. The 200-mc experimental result is unexpectedly low while the values at the higher frequencies are a little higher than would be anticipated. This points to the existence of some specular reflection for this ship, which would not be surprising in view of its great size. Considering the uncertainty in the experimental values, the agreement with the theoretical results is not unsatisfactory and bears out the assumed dependence on wavelength.

The aircraft carrier shows pronounced specular reflection at the direct broadside aspect, particularly at the higher frequencies. These values of σ are typical of the ship for aspects other than direct broadside.

In Table 8, the same ship is analyzed at direct

TABLE 4. Radar cross section of a battleship (BB-63), broadside aspect. $\alpha = 0.1$, $B = 270$ m, $H = 24$ m.

f(mc)	σ (exp), sq m	σ (theory), sq m
200	0.12 $\times 10^5$	1.9 $\times 10^5$
700	10.2 $\times 10^5$	6.8 $\times 10^5$
970	15. $\times 10^5$	9.4 $\times 10^5$
3,060	110. $\times 10^5$	30. $\times 10^5$

TABLE 5. Radar cross section of a cruiser (CL-87), broadside aspect. $\alpha = 0.1$, $B = 180$ m, $H = 24$ m.

f(mc)	σ (exp), sq m	σ(theory), sq m
100	2.45 $\times 10^4$	2.6 $\times 10^4$
200	5.06 $\times 10^4$	5.2 $\times 10^4$
700	7.79 $\times 10^4$	18.1 $\times 10^4$
970	28.4 $\times 10^4$	25.1 $\times 10^4$
3,060	102.2 $\times 10^4$	79.3 $\times 10^4$

TABLE 6. Radar cross section of submarine (SS-171), broadside aspect. $\alpha = 0.01$, $B = 83$ m, $H = 7.6$ m.

f(mc)	σ(exp), sq m	σ(theory), sq m
200	30 $\times 10^2$	3.5 $\times 10^2$
700	18.7 $\times 10^2$	12.2 $\times 10^2$
3,060	71.4 $\times 10^2$	53.4 $\times 10^2$

TABLE 7. Radar cross section of aircraft carrier (CV-36), near broadside aspect. $\alpha = 0.05$, $B = 250$ m, $H = 46$ m.

f(mc)	σ(exp), sq m	σ(theory), sq m
200	0.22 $\times 10^5$	0.96 $\times 10^5$
700	2.6 $\times 10^5$	3.4 $\times 10^5$
970	6.3 $\times 10^5$	4.6 $\times 10^5$
3,060	11.3 $\times 10^5$	14.4 $\times 10^5$

TABLE 8. Radar cross section of aircraft carrier (CV-36), direct broadside aspect.

f(mc)	σ(exp), sq m	$\lambda^2 \sigma$(exp)
200	0 055 $\times 10^7$	1.2 $\times 10^6$
700	1.0 $\times 10^7$	1.8 $\times 10^6$
970	5.0 $\times 10^7$	4.8 $\times 10^6$
3,060	7.1 $\times 10^7$	7.1 $\times 10^6$

broadside. No theoretical calculation of σ has been attempted because of a lack of sufficient data from other ships of this type. The column $\lambda^2 \sigma$ is near enough to a constant to indicate the existence of specular reflection. Since the hull at broadside can be considered as a flat surface, specular reflection is to be expected under normal incidence with a radar cross section proportional to $1/\lambda^2$ as indicated by equation (9).

In view of the complicated reflecting properties of targets of operational interest, it may be said that the experimental results can be considered as being in fair agreement with theoretical predictions.

ABSORPTION AND SCATTERING BY CLOUDS, FOG, RAIN, HAIL, AND SNOW

The theory of the scattering and absorption of microwaves by a collection of spherical particles of known concentration, size, distribution, and given

dielectric properties was completely worked out before systematic experimental work was done on these phenomena.[258, 277, 279] The electromagnetic theory predicts that the total scattering cross section of a sphere of given electrical properties is

$$S = \frac{\lambda^2}{2\pi} \sum_{n=1}^{\infty} (2n + 1) (|a_n|^2 + |b_n|^2) \text{ cm}^2 , \quad (13)$$

where λ is the wavelength in centimeters of the incident radiation in air and a_n and b_n are the so-called scattering amplitudes associated with the magnetic and electric $2n$-poles induced in the sphere by the incident electromagnetic field. Similarly the absorption cross section of a sphere defined as the ratio of the total power removed from the incident beam both by "internal absorption" (heating) and by scattering is

$$A = \frac{\lambda^2}{2\pi} (-\text{Re}) \sum_{n=1}^{\infty} (2n + 1) (a_n + b_n) \text{ cm}^2 . \quad (14)$$

Here Re means "Real part of . . . ." The complex scattering amplitudes depend on the dielectric constants of the sphere, its diameter, and the wavelength of the incident radiation. The observations which are available seem to indicate that a collection of spherical particles with random distribution scatter microwaves incoherently, although under certain circumstances, existing for very short time intervals, they may scatter coherently.[419] On the assumption of incoherent scattering, given a collection of spherical particles of diameters $D_1, D_2, \cdots, D_k, \cdots$, D_n, whose number per unit volume or cc is $n_1, n_2, \cdots$, $n_k, \cdots, n_n$, the scattering cross section of such a collection per unit volume or the absorption coefficient due to scattering is

$$\alpha_s = 4.343 \times 10^5 \sum_{i=1}^{n} n_i S_i \text{ db/km} , \quad (15)$$

where S_i is the scattering cross section of one drop of diameter D_i centimeters, and the summation extends over all possible drops present in the collection. Similarly, the "absorption coefficient" or "attenuation" associated with the absorption cross section A_i (sphere of diameter D_i) defined by equation (14) is

$$\alpha_a = 4.343 \times 10^5 \sum_{i=1}^{n} n_i A_i \text{ db/km} . \quad (16)$$

RAIN AND HAIL ABSORPTION

In order to compute the theoretical absorption coefficient of a rain or thunderhead (heavy storm cloud) one has to know the raindrop size distribution, since the computation of the cross sections for one spherical drop is straightforward provided its dielectric properties are known. The greatest uncertainties in the theoretical predictions of scattering or absorption by rain are due to the relatively limited knowl-

edge of drop size distributions in rains of different rates of fall. There is no evidence that a rain with a known rate of fall has a unique drop size distribution though the latest studies on this problem seem to indicate that a certain most probable drop size distribution can be attached to a rain of given rate of fall.[446] Results of this study are included in Table 9. On the basis of these results the absorption cross

TABLE 9. Drop size distribution.

p, mm/hr D, cm	Percentage of total volume							
	0.25	1.25	2.5	12.5	25	50	100	150
0.05	28.0	10.9	7.3	2.6	1.7	1.2	1.0	1.0
0.10	50.1	37.1	27.8	11.5	7.6	5.4	4.6	4.1
0.15	18.2	31.3	32.8	24.5	18.4	12.5	8.8	7.6
0.20	3.0	13.5	19.0	25.4	23.9	19.9	13.9	11.7
0.25	0.7	4.9	7.9	17.3	19.9	20.9	17.1	13.9
0.30		1.5	3.3	10.1	12.8	15.6	18.4	17.7
0.35		0.6	1.1	4.3	8.2	10.9	15.0	16.1
0.40		0.2	0.6	2.3	3.5	6.7	9.0	11.9
0.45			0.2	1.2	2.1	3.3	5.8	7.7
0.50				0.6	1.1	1.8	3.0	3.6
0.55				0.2	0.5	1.1	1.7	2.2
0.60					0.3	0.5	1.0	1.2
0.65						0.2	0.7	1.0
0.70								0.3

section of raindrops of different size has been computed for use in Table 10. This table gives the decibel attenuation per kilometer in rains of different rates of fall and for radiation of wavelengths between 0.3 and 10 cm. In Table 11, similar to Table 10, another set of results is contained for rains of measured drop size distributions. This table is extended to include radiations of wavelengths up to 100 cm. It seems equally interesting to give a graphical representation of those results. Figure 2 corresponds to Table 10 and Figure 3 to Table 11. All these data refer to raindrops at 18 C.

Since the scattering coefficients a_n and b_n depend on the temperature, because of its effect on the
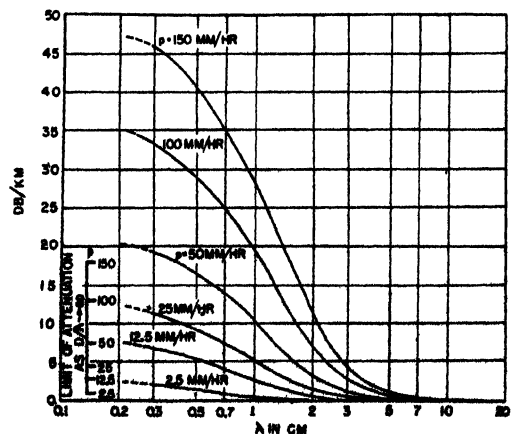
FIGURE 2. Graphical presentation of data given in Table 10.

TABLE 10. Attenuation in decibels per kilometer for different rates of precipitation of rain. Temperature 18 C, λ in cm.[177]

p, mm/hr	Attenuation, db/km.								
	λ = 0.3	λ = 0.4	λ = 0.5	λ = 0.6	λ = 1.0	λ = 1.25	λ = 3.0	λ = 3.2	λ = 10
0.25	0.305	0.230	0.160	0.106	0.037	0.0215	0.00224	0.0019	0.0000997
1.25	1.15	0.929	0.720	0.549	0.228	0.136	0.0161	0.0117	0.000416
2.5	1.98	1.66	1.34	1.08	0.492	0.298	0.0388	0.0317	0.000785
12.5	6.72	6.04	5.36	4.72	2.73	1.77	0.285	0.238	0.00364
25	11.3	10.4	9.49	8.59	5.47	3.72	0.656	0.555	0.00728
50	19.2	17.9	16.6	15.3	10.7	7.67	1.46	1.26	0.0149
100	33.3	31.1	29.0	27.0	20.0	15.3	3.24	2.80	0.0311
150	46.0	43.7	40.5	37.9	28.8	22.8	4.97	4.39	0.0481

TABLE 11. Attenuation in rains of known drop size distribution and rate of fall (decibels per kilometer).

mm/hr	Wavelength λ, cm											Distribution
	1.25		3		5		8		10		15	
2.46	1.93	10^{-1}	4.92	10^{-2}	4.24	10^{-3}	1.23	10^{-3}	7.34	10^{-4}	2.80 10^{-4}	A
4.0	3.18	10^{-1}	8.63	10^{-2}	7.11	10^{-3}	2.04	10^{-3}	1.19	10^{-3}	4.69 10^{-4}	C
6.0	6.15	10^{-1}	1.92	10^{-1}	1.25	10^{-2}	3.02	10^{-3}	1.67	10^{-3}	5.84 10^{-4}	D
15.2	2.12		6.13	10^{-1}	5.91	10^{-2}	1.17	10^{-2}	5.68	10^{-3}	1.69 10^{-3}	E
18.7	2.37		8.01	10^{-1}	5.13	10^{-2}	1.10	10^{-2}	6.46	10^{-3}	1.85 10^{-3}	F
22.6	2.40		7.28	10^{-1}	5.29	10^{-2}	1.21	10^{-2}	6.96	10^{-3}	2.27 10^{-3}	G
34.3	4.51		1.28		1.12	10^{-1}	2.32	10^{-2}	1.17	10^{-2}	3.64 10^{-3}	H
43.1	6.17		1.64		1.65	10^{-1}	3.33	10^{-2}	1.62	10^{-2}	4.96 10^{-3}	I

mm/hr	Wavelength λ, cm										Distribution
	20		30		50		75		100		
2.46	1.52	10^{-4}	6.49	10^{-5}	2.33	10^{-5}	1.03	10^{-5}	5.85	10^{-6}	A
4.0	2.53	10^{-4}	1.08	10^{-4}	3.88	10^{-5}	1.72	10^{-5}	9.75	10^{-6}	C
6.0	3.02	10^{-4}	1.25	10^{-4}	4.34	10^{-5}	1.93	10^{-5}	1.09	10^{-5}	D
15.2	7.85	10^{-4}	2.95	10^{-4}	9.23	10^{-5}	4.15	10^{-5}	2.35	10^{-5}	E
18.7	9.09	10^{-4}	3.60	10^{-4}	1.20	10^{-4}	5.36	10^{-5}	3.03	10^{-5}	F
22.6	1.17	10^{-3}	4.81	10^{-4}	1.66	10^{-4}	7.41	10^{-5}	4.19	10^{-5}	G
34.3	1.75	10^{-3}	6.83	10^{-4}	2.24	10^{-4}	9.95	10^{-5}	5.63	10^{-5}	H
43.1	2.29	10^{-3}	8.71	10^{-4}	2.78	10^{-4}	1.23	10^{-4}	6.98	10^{-5}	I

dielectric properties of water, it seems important to evaluate the attenuation of rains whose drops are at temperatures different from those included in the preceding tables. Table 12 contains the necessary data relative to the changes of attenuation with temperature and is to be used primarily in connection with Table 10.

TABLE 12

Rate of precipitation, mm/hr	λ, cm	Correction factor θ (T)				
		T = 0 C	T = 10 C	T = 18 C	T = 30 C	T = 40 C
0.25	0.5	0.85	0.95	1.0	1.02	0.99
	1.25	0.95	1.0	1.0	0.90	0.81
	3.2	1.21	1.10	1.0	0.79	0.55
	10.0	2.01	1.40	1.0	0.70	0.59
2.5	0.5	0.87	0.95	1.0	1.03	1.01
	1.25	0.85	0.99	1.0	0.92	0.80
	3.2	0.82	1.01	1.0	0.82	0.64
	10.0	2.02	1.40	1.0	0.70	0.59
12.5	0.5	0.90	0.96	1.0	1.02	1.00
	1.25	0.83	0.96	1.0	0.93	0.81
	3.2	0.64	0.88	1.0	0.90	0.70
	10.0	2.03	1.40	1.0	0.70	0.59
50	0.5	0.94	0.98	1.0	1.01	1.00
	1.25	0.84	0.95	1.0	0.95	0.83
	3.2	0.62	0.87	1.0	0.99	0.81
	10.0	2.01	1.40	1.0	0.70	0.58
150	0.5	0.96	0.98	1.0	1.01	1.00
	1.25	0.86	0.96	1.0	0.97	0.87
	3.2	0.86	0.88	1.0	1.03	0.89
	10.0	2.00	1.40	1.0	0.70	0.58
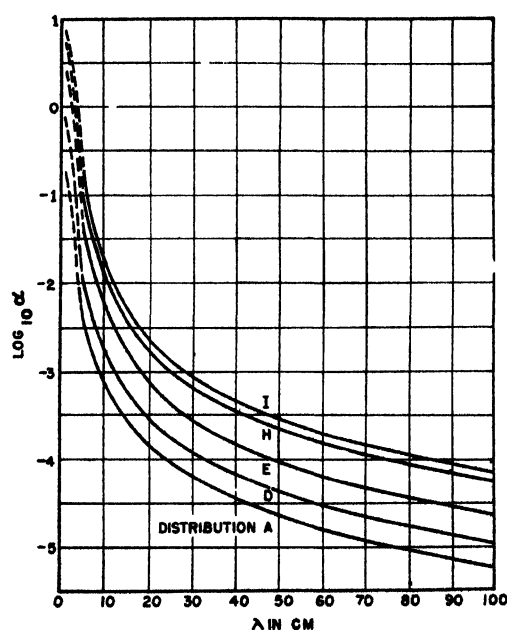
FIGURE 3. Attenuation in rains of known drop-size distribution as a function of the wavelength λ in centimeters. The ordinate scale gives $\log_{10} \alpha$, where the attenuation constant α is expressed in decibels per kilometer. The letters on the curves refer to the drop size distributions given in Table 11.

It will suffice to mention here that, for waves larger than about 3 cm, the attenuation produced by hail of the same water precipitation rate as a rain will be but a few per cent of the rain attenuation. At shorter waves, in the millimeter region, hail attenuation may become larger than that of rain. Similarly the attenuation of snow should be considerably less than rain; however, Canadian reports indicate approximately the same value for the same water content.

As mentioned above, the whole theory of attenuation is based on equation (14). The formulas giving the amplitudes a_n and b_n are too complicated to be reproduced here. Their numerical evaluation for spherical drops of given size and temperature is quite laborious except for small values of the parameter $\pi D/\lambda$. They involve Bessel and Hankel functions of half-integer order of the parameter $\pi D/\lambda$.

A series of experimental results are given in Table 13. These results are to be regarded as maximum attenuation values.

If these results are compared with those of Table 10 and Figure 2 one sees that, in view of the uncertainty in the temperature of the raindrops and their size distribution, the agreement between theoretical

TABLE 13. Experimental values of the maximum attenuation per unit precipitation rate.

λ, cm	(α/p) db per km/mm per hr	References
0.62	0.37	269
0.96	0.15	256
1.069	0.2	262
1.25	0.19	176
	0.09–0.40	276
	0.63	281
3.2	0.032–0.042	261

and observed values is, on the whole, satisfactory. It will be seen that the results reported on K-band rain attenuation in Hawaii by the U. S. Navy Radio and Sound Laboratory workers[261] are higher than those observed by other workers on the same wavelength. The orographic character of these Hawaiian rains which were made up of drops falling about 300 m instead of ordinary rains falling 1,500 to 2,000 m may be one of the reasons for this divergent result.

CLOUDS AND FOG

Observations indicate that fair weather clouds and fog are composed of droplets whose diameters do not seem to exceed 0.02 cm. Under these conditions the attenuation formula takes on a remarkably simple form since it becomes independent of the drop size distribution. The attenuation formula in this limit of very small values of the parameter $\pi D/\lambda$ is

$$\alpha_{ab} = \frac{4.092 \, mc_1}{\lambda} \text{ db/km} , \qquad (17)$$

where m is the mass of liquid water per cubic meter, λ is the wavelength of the radiation in centimeters, and

$$c_1 = \frac{6\epsilon_1}{(\epsilon_r + 2)^2 + \epsilon_i^2} , \qquad (18)$$

where ϵ_r and ϵ_i are the real and imaginary parts of the dielectric constant of water at the temperature in question and for radiation of wavelength λ. Figure 4 represents the attenuation in clouds and fog in the range 0.2 to 10 cm. This graph corresponds to a
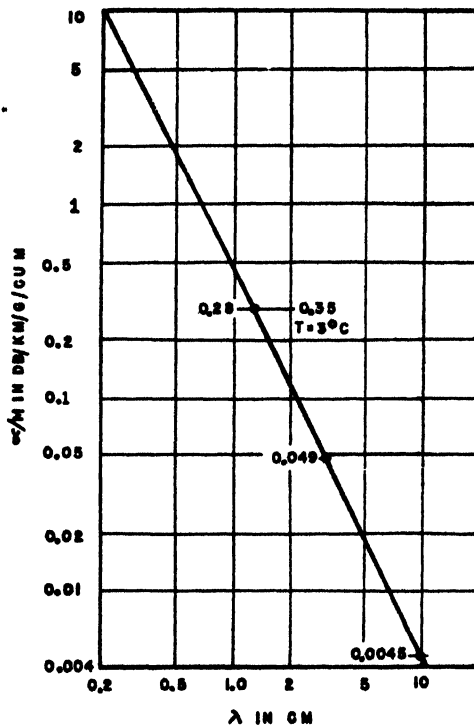
FIGURE 4. Attenuation factor in liquid clouds and fogs. $T = 18$ C.

liquid water concentration of 1 g per cu m, which is undoubtedly rather high. Actually, the observations indicate that the liquid water concentrations in clouds and fog rarely exceed 0.6 g per cu m.

To this may be added the Table 14 for attenuation by ice clouds. In ice clouds m will rarely exceed 0.5 and will often be less than 0.1 g per cu m.

TABLE 14. Attenuation in decibels per kilometer for ice crystal clouds.

Shape of crystals	$T = -40$ C	$T = 0$ C
Spherules	0.00044 m/λ	0.0035 m/λ
Needles	0.00062 m/λ	0.0050 m/λ
Disks	0.00067 m/λ	0.0070 m/λ

SCATTERING (ECHO)

If we denote by $\sigma(\pi)$ the back-scattering cross section per unit solid angle of a spherical water drop

and if there is a distribution $n_1, n_2, \cdots, n_k, \cdots, n_s$ drops per cubic meter, the cloud or rain cross section for scattering is

$$S(\pi) = \sum n_i \sigma_i(\pi) \Delta V \qquad (19)$$

where ΔV is the scattering volume of the cloud, on the assumption of incoherent scattering on account of the random character of the drop distribution. The summation includes all the drop groups. The rain front is usually wider than the irradiated area so that the radar beam intersects it. Under these conditions, taking ΔV approximately as a spherical shell of thickness Δd, at a distance d from the radar set, and denoting by 2θ the half-power beam width of the radar beam, one gets

$$\Delta V = 2\pi d^2 (1 - \cos \theta) \Delta d . \qquad (20)$$

The rain echo cross section is then

$$S(\pi) = 2\pi d^2 (1 - \cos \theta)\left(\Delta d \sum_i n_i \sigma_i(\pi)\right) \qquad (21)$$

Remembering that $\sigma_i(\pi)$ or $S(\pi)$ is precisely the cross section per unit solid angle in the direction of the radar set, one gets instead of equation (6) for the ratio of received to transmitted power

$$\frac{P_2}{P_1} = \frac{G_1 G_2}{4} \left(\frac{3\lambda}{8d}\right)^2 \theta^2 \left(\Delta d \sum_i n_i \sigma_i(\pi)\right) \qquad (22)$$

for small angles θ which must be given in radians.

TABLE 15. Fraction of incident power scattered backward by a layer of 1 km of rain in different types of rain.
(Decibels)

Drop size distri-bution*	p, mm/hr	Wavelength in centimeters							
		3	5	8	10	15	20	30	50
A	2.46	−45	−54	−61	−65	−72	−77	−84	−93
D	6.0	−38	−46	−54	−58	−65	−69	−76	−85
E	15.2	−32	−37	−45	−48	−55	−61	−68	−77
H	34.3	−29	−35	−42	−46	−53	−58	−65	−74
I	43.1	−27	−33	−40	−44	−51	−56	−63	−71

*See Table 11 for drop size distributions

The quantity $[\Delta d \Sigma_i n_i \sigma_i(\pi)]$ or its value in decibels for known drop size distributions has been tabulated in Table 15. With this table and the known characteristics of a radar set the ratio P_1/P_2 can be computed at once. In the table Δd is taken as 1 km. Since the maximum thickness Δd cannot exceed the pulse length, the values found in the table can be adapted immediately to any pulse length l by adding to it ($10 \log_{10} l$), l being expressed in kilometers. Using equation (22) for particular radar sets it is found that the theoretically computed echo powers from rains agree well with the observed values, if the uncertainties of the meteorological knowledge of the echoing elements, which are mostly rains and storm clouds, is kept in mind. As expected, the echoing

power of snow is very much less than that of rain. The systematic observations on S band by the Canadian group[402,422] and on X band by Bent[424] clearly indicate that precipitation either in the form of rain or snow is necessary to produce an echo on the scope of the radar set.

ABSORPTION BY THE ATMOSPHERIC GASES

It was predicted that oxygen and water vapor will absorb electromagnetic waves in the microwave range.[259,275] In particular, oxygen was predicted as having a resonance band around 5 mm and one line at 2.5 mm, while the water vapor absorption is caused mainly by a single rotational line of relatively small strength around 1 cm. Experiments have confirmed both these absorption effects.[272,273] In Figure 5, the individual oxygen and water vapor attenuation curves have been plotted in the 0.2- to 10-cm wavelength range. Any change in the water vapor content from the one adopted for this graph (7.5 g per cu m or 6.5 g per kg of air) or the total pressure can be taken into account in computing the combined
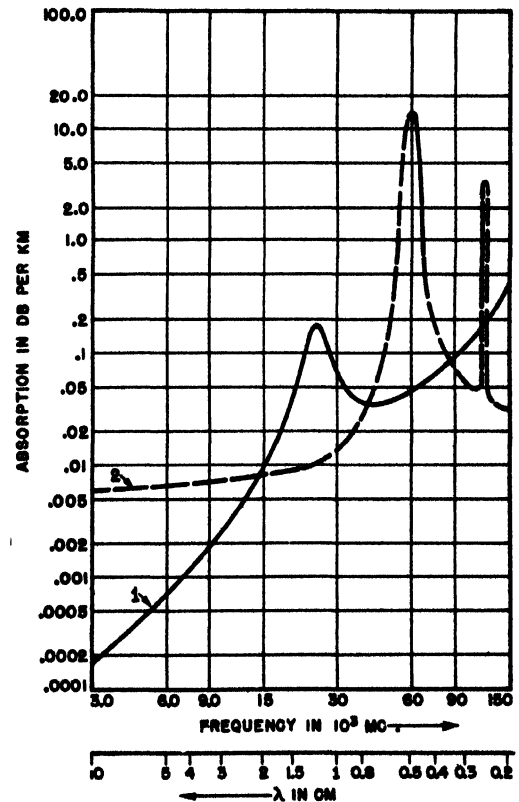
FIGURE 5. (1) Absorption due to water vapor in an atmosphere at 76-cm pressure containing 1 per cent water molecules, or 7.5 g per cu m. The water resonance line is assumed to be at 24,000 mc, and its half width at half maximum (line breadth) is 3,000 mc. (2) Absorption due to oxygen in an atmosphere at 76-cm pressure whose resonance band at 60.10³ mc is supposed to have a line breadth of 600 mc.

oxygen and water vapor attenuations, since these are proportional to the partial pressures of oxygen and water vapor. For practical purposes the effect of temperature variations can be neglected.

In Figure 6, curve 1, is plotted the total attenuation of oxygen plus water vapor in an atmosphere at 76-cm pressure, with the same water vapor content as the curve of Figure 5. Curves 2, 3, and 4 are additional rain attenuation curves computed for a moderate rain of rainfall 6 mm per hr, a heavy rain of 22 mm per hr and an excessive rain of 43 mm per hr, which is of cloudburst proportions. In any rain the result of total attenuation is the sum of the oxygen, water vapor, and liquid drop attenuation.

It is thus seen that for waves of 3 cm or shorter the rain attenuation may become prohibitive, whereas the gaseous attenuation loses its·practical importance at waves longer than about 2 cm. In this connection it is to ·be noted that for millimeter waves the rain attenuation begins to level off at waves of a few millimeters, as Table 10 indicates, and would actually decrease at waves shorter than 1 mm. However in this range, the water vapor absorption due to the strong water lines situated at much shorter waves becomes more and more intense, and communication or radar on these bands is almost totally excluded. It is worth noting in this connection that using radiation which is strongly absorbed might, in certain cases, be of great operational interest. In the˙oxygen band, for example, short-range communication could be achieved without any likely interference by the enemy.

Electromagnetic theory thus gives a satisfactory picture of the absorption and scattering phenomena of microwaves both by floating or falling water
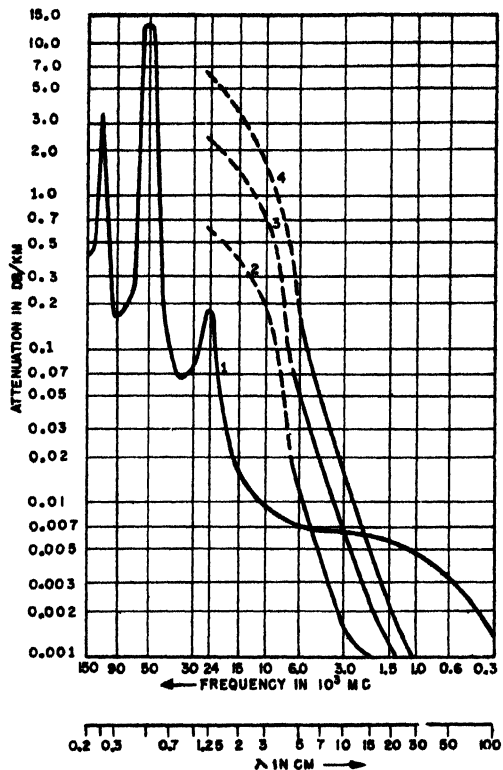
FIGURE 6. Atmospheric one-way attenuation. (1) Oxygen and water vapor (total for $p = 76$ cm Hg, $T = 20$ C, water vapor. $= 7.5$ g per cu m). (Van Vleck.) (2) Moderate rain (6 mm per hr) of known drop size distribution. (3) Heavy rain (22 mm per hr). (4) Rain of cloudburst proportion (43 mm per hr).

drops, or their equivalent in hail and snow, and by the oxygen and water vapor of the atmosphere.

PART II

CONFERENCE REPORTS ON STANDARD PROPAGATION

Chapter 7

A GRAPHICAL METHOD FOR THE DETERMINATION OF STANDARD COVERAGE CHARTS*

THE POWER DENSITY at distance S from a transmitter of unit power depends upon h_1 and h_2, the heights of the transmitting and receiving antennae, and upon λ, the wavelength of the radiation For the high frequencies under discussion, we assume the earth to be a perfectly conducting sphere, of effective radius r, equal to ⅚ that of the earth. We are to take into account the so-called divergence factor D resulting from the earth's curvature.

Even with the simplifying assumptions above, one cannot express the power as a simple function of S, h_1, h_2, and λ in a single equation. Accordingly, most workers on this problem have introduced various arbitrary parameters, as intermediate steps. Differences in procedure lie primarily in the choice of parameters. Whether a method is simple or difficult depends upon the character of the parameters. Certain procedures suggested are satisfactory for determining the number of decibels by which the signal is below the adopted standard of 1 μw per square meter, designated here by A; but if we are given A, h_1, and f and then are asked to compute h_2 as a function of S, as for a coverage diagram, some of the methods become very unwieldy. The present method works satisfactorily for either case.
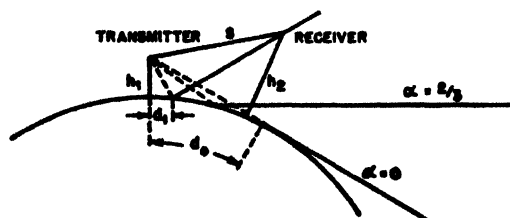
FIGURE 1. Geometry for determination of standard coverage.

In selecting a parameter we have been guided by the following conditions. The number of parameters should be kept to a minimum; the remaining variables h_1, h_2, and S should appear in the final equations, if possible. Also it should be unnecessary to interchange transmitter and receiver according to

the condition that h_2 is or is not greater than h_1

The arbitrary parameter α is defined as follows. Let d_1 be the distance from the transmitter to the point at which the ray is reflected and d_0 the distance to the point where a ray is tangent. Then

$$a_1^2 = d_0^2(1 - \alpha) = 2h_1 r(1 - \alpha) \qquad (1)$$

α, therefore, is constant along a reflected ray; $\alpha = 0$ corresponds to the continuation of the tangent ray; $\alpha = \frac{2}{3}$ corresponds to a reflected ray perpendicular to the mast of the transmitting antenna; $\alpha = 1$ is the vertical ray. Thus

$$0 \leq \alpha \leq 1 ,$$

with $\alpha > \frac{2}{3}$ over a large portion of the range of interest for the frequencies involved.

Equation (1) leads to the following relationship

$$S^2 + \frac{(-2 + 3\alpha)}{(1 - \alpha)^{\frac{3}{2}}} S \sqrt{2rh_1} + 2rh_1 \cdot (1 - 2\alpha)$$
$$- 2rh_2 = 0 , \qquad (2)$$

an irreducible cubic in α. It is this fact that makes the problem mathematically difficult and makes impossible the explicit elimination of α.

Additional equations are

$$D^2 = \frac{\alpha}{4 - 3\alpha - 4\sqrt{2_1 h_1} \ S^{-1}(1 - \alpha)^{\frac{1}{2}}} \cong \frac{\alpha}{4 - 3\alpha} , \qquad (3)$$

an approximation holding well over the region of interest since $\alpha > \frac{2}{3}$. The phase difference ϕ, resulting from the difference in optical path between the reflected and direct rays, is

$$\phi = \frac{4\pi h_1^2 \alpha^2}{\lambda} \left[\frac{1}{\sqrt{2rh_1(1 - \alpha)}} - \frac{1}{S} \right] , \qquad (4)$$

and for the transmitted power

$$10^{-A/10} = \frac{10^6}{\pi} \frac{1}{S^2} \left[\frac{(1 - D)^2}{4} + D \sin^2 \frac{\phi}{2} \right] . \qquad (5)$$

Here we have four equations. If h_1, λ, and A are specified, there remain five unknowns: D, ϕ, α, h_2, and S. Thus we should be able theoretically to elimi-

nate all but h_2 and S, defining our coverage diagram.

We may substitute the approximate value for D into equation (5) and also use equation (4) to eliminate S from the equation

$$10^{-A/20} = \frac{10^3}{\pi}\left[\frac{1}{\sqrt{2rh_1\,(1-\alpha)}} - \frac{\lambda\Phi}{4\pi h_1^2\alpha^2}\right] \times$$

$$\left\{\frac{\left[1 - \left(\frac{\alpha}{4-3\alpha}\right)^{\frac{1}{2}}\right]^2}{4}\left[\frac{\alpha}{(4-3\alpha)}\right]^{\frac{1}{2}} \sin^2\Phi\right\}^{\frac{1}{2}}. \quad (6)$$

We may now set

$$\Phi = \left(n - \frac{1}{2}\right)\pi\ ;\quad n = 1, 2, 3, \cdots \quad (7a)$$

which correspond to the maxima of the lobes. We may alternatively take

$$\Phi = n\pi\ , \quad (7b)$$

corresponding to lobe minima or, more generally

$$\Phi = (n + b)\,\pi \quad (7c)$$

to represent any specific position on the lobe.

With A, h_1, $\lambda\Phi$, and α as variables, we may throw equation (6) into the form of a nomogram, from which we determine α, first for the lobe tips, second for the minima, and third for as many intermediate points as are necessary.

With the α's so determined, proceed to equation (4), also in nomographic form, to get S. Finally, use equation (2), to determine h_2. This equation can also be thrown into nomographic form if we set

$$\frac{S^2}{2r} - h_2 = h'_2 \quad (8)$$

where h'_2 is measured vertically from the line tangent to the base of the transmitter.

Another somewhat simpler type of coverage diagram is possible. If we take

$$10^{-A^*/10} = \frac{10^6}{4\pi S^2} \quad (9)$$

as defining the intensity for a transmitter in free space, we get for the ratio of the two

$$10^{-(A-A^*)/10} = 10^{B/10} = \left[1 - \left(\frac{\alpha}{4-3\alpha}\right)^{\frac{1}{2}}\right]^2 +$$

$$4\left(\frac{\alpha}{4-3\alpha}\right)^{\frac{1}{2}} \sin^2\frac{\Phi}{2}, \quad (10)$$

where B is the number of decibels by which the actual field exceeds the free space value. Coverage diagrams of this type consist of lines radiating from the transmitter, rather than contours. For nonstandard propagation the drawings have some complications, but the procedures are clear. This method has the additional advantage of fitting in with the theory used for surface targets, for which it is simpler to use free space intensities and lump the field strength integrated over the target area as an "effective" target area in a uniform field.

NOMOGRAPHIC SOLUTIONS FOR THE STANDARD CASE*

THE EQUATIONS GIVEN in the preceding chapter have now been thrown into nomographic form. When these nomograms are employed a rapid method for constructing coverage diagrams results.

Let h_1 denote the height of the transmitter in feet, f_{mc} be the frequency in megacycles, n be an integer (1, 2, 3, $\cdots$) specifying the number of the lobe, $b(0 \leqq b < 1)$ a "phase" factor specifying the position on the lobe, and r the radius of the earth. Introduce the quantity B defined as follows.

$$B = \frac{150 \, (n - b) \, \sqrt{2N} \, (3.281)^{!}}{h_1^! f_{mc}}$$

$$= 3.676 \times \frac{10^6 \, (n - b)}{h_1^! f_{mc}} , \qquad (1)$$

where we have taken $r = 8.50 \times 10^6$ m, as the approximate ⅔ earth value. We have to decide on the interval for b. By taking $b = 0$, ⅙, ⅓, ½, ⅔, ⅚, we actually obtain seven points on each lobe, which should be sufficient for the purpose of drawing a coverage diagram. Hence, $n - b = 0$, ⅙, ⅓, ½, ⅔, ⅚, 1, 7/6, $\cdots$, etc., spaced at intervals of ⅙.

Equation (1) is represented in the nomogram of Figure 1. We are given h_1 and f_{mc}, the height and frequency of the transmitter. Connect the appropriate values on the scales by a straight line and mark the point of intersection on the central vertical line.

Define a quantity k by the equation

$$n - b = \frac{k}{6} ,$$

so that $k = 3$ corresponds to the maximum of the first lobe, $k = 6$ to the minimum, $k = 9$ to the next maximum, $k = 12$ to the minimum, etc. $k = 15, 21$, and 27 correspond to the third, fourth, and fifth maxima, respectively. Other values of k determine intermediate points on the lobe.

Now draw a straight line from $k = 1$ through the point previously determined on the central vertical line until it intersects the left-hand axis of B. Read off B or $1/B$, whichever is given. Repeat the process for $k = 2, 3, \cdots$, etc., until a value of B is obtained that exceeds 10; in other words, continue until the straight line runs off the lower edge of the left-hand scale.

There will be cases, however, usually involving large values of h_1 or f_{mc}, where B will still be small ($1/B$ large) even for $k = 27$. When this condition

exists, the lobes tend to be so closely spaced that the individual maxima are difficult to define and even more difficult to draw on a coverage chart. For such conditions an alternative procedure is recommended, which will be given later.

If no difficulty is encountered, however, enter the values of B or $1/B$ (designate the latter with an asterisk) in a table such as Table 1.

TABLE 1

f_{mc} = Frequency in mc
h_1 = Height of antenna in ft

k =	B^*	n	b
1		1	⅙
2		1	⅓
3		1	½ max.
4		1	⅔
5		1	⅚
6		2	0 min.
7		2	⅙
8		2	⅓
9		2	½ max.
10		2	⅔
11		2	⅚
12		3	0 min.
15		3	½ max.
21		4	½ max.
27		5	½ max.

*Put an asterisk after an entry if the value read off is equal to $1/B$. The corresponding values of n and b are entered in columns 3 and 4 of the form sheet

It should be noted that equation (1) is easy to solve, and the operator familiar with mathematical procedures may prefer to use direct calculation, by slide rule or logarithm tables, as much more accurate. In general, however, the nomogram values are sufficiently accurate for the work.

Next, for the five or six assumed values of decibels for which contours are desired, we solve a subsidiary equation for Y by means of a nomogram (not reproduced here). We note that

$$Y = db + 60 - 10 \log (2\pi r h_1) ,$$

and slide-rule calculation is extremely convenient. For each of the selected values of b, we have prepared a nomogram connecting Y, B, and α. Although there are six adopted values of b, the expressions for $b = $ ⅙, ⅓, ⅔, ⅚ coincide, so that four charts suffice. A representative sample of these charts, for $b = 0$, is given in Figures 2 and 3. Connect each value of Y, for which a contour is desired, with the value of B on the appropriate chart, according to the value of b (or k). Read off the corresponding value of α.

Having determined α for a given point on the coverage chart, we now calculate S from the nomo-
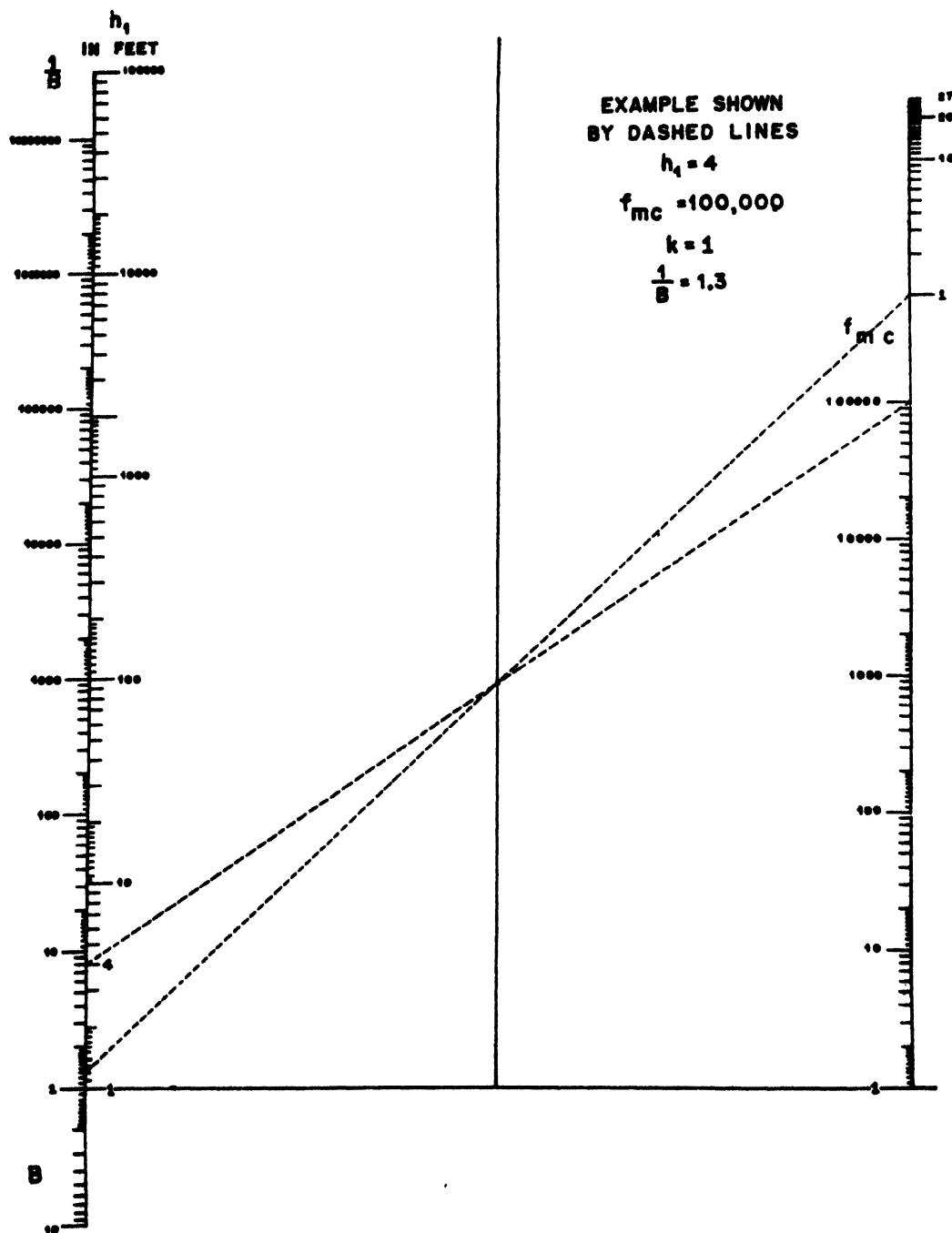
FIGURE 1

gram in Figure 4, with α, db, and S as variables. For S measured in units of 1,000 yd, we have

$$10^{-db/20} = \frac{10^3}{\sqrt{\pi}}\left(\frac{1}{914\,S}\right)$$

$$\left\{\frac{\left[1-\left(\frac{\alpha}{4-3\alpha}\right)^{\frac{1}{2}}\right]^2}{4}+\left(\frac{\alpha}{4-3\alpha}\right)^{\frac{1}{2}}\sin^2\pi b\right\}^{\frac{1}{2}}$$

A typical example for the selected values of b is shown, as before.

Finally, we must calculate h_2. For heights we have

$$H = h_2 + (1-\alpha)h_1 = \frac{(3.281)(914)^2}{2r}S^2$$

$$+ \frac{(3.281)^2(914)(150)(n-b)}{h_1\,f_{mc}}\frac{(-2+3\alpha)}{\alpha^2}S \ . \quad (2)$$

b = 0

EXAMPLE SHOWN BY DASHED LINE
B = 0.112
Y = 12.2
$\alpha_1 = 0.465$, $\alpha_2 = 0.910$
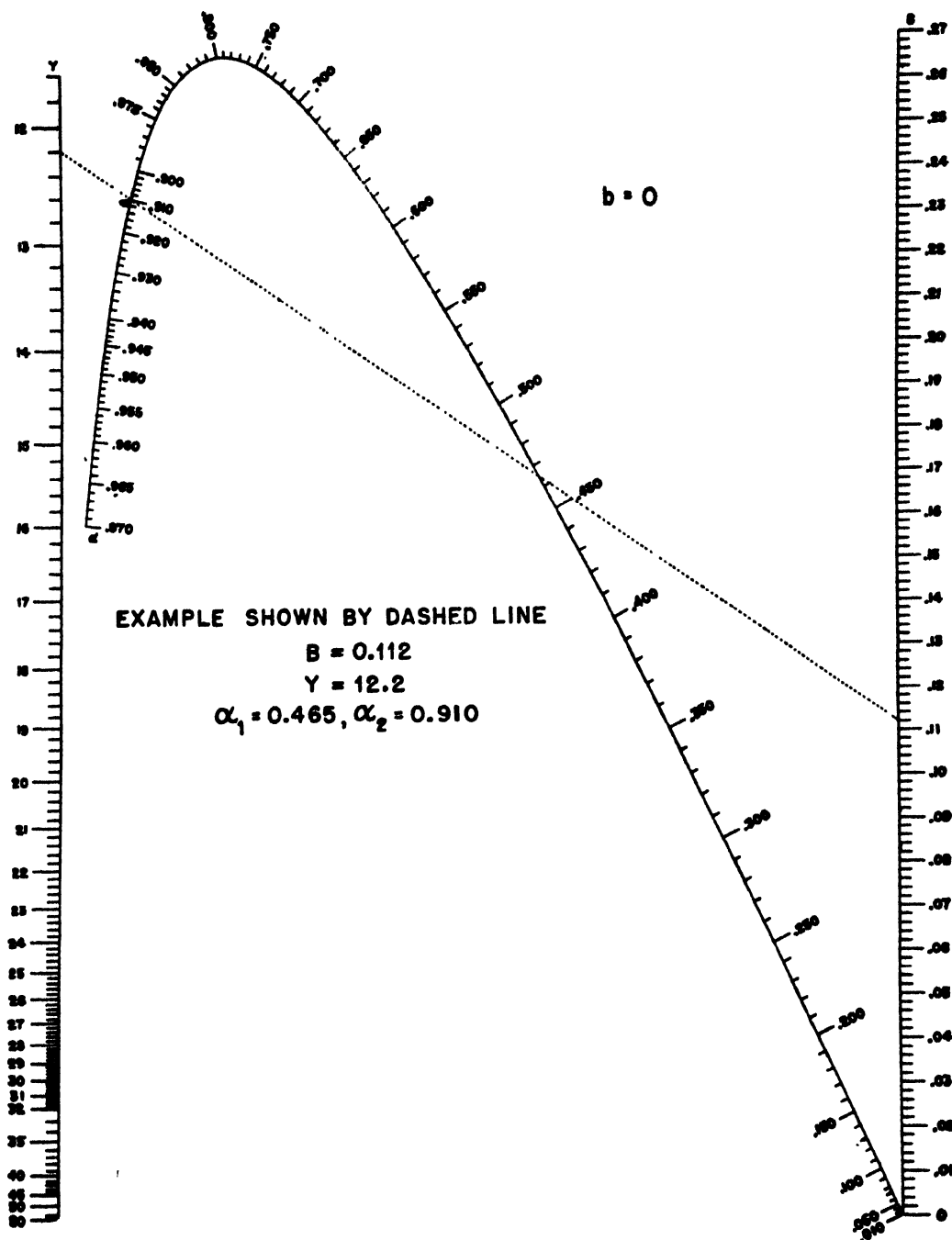
FIGURE 2

This equation, unfortunately, has too many variables for nomographic solution in a single step. We first define a quantity C, such that

$$C = \frac{(3.281)^2\,(914)\,(150)\,(n - b)}{h_1 f_{mo}}\,\frac{(-2 + 3\alpha)}{\alpha^2}.$$

Obtain the simple product $h_1 f_{mo}$, which is a characteristic of the set. Then use the nomogram of Figure

5 to obtain the values of C for the selected ranges of k and α. Then we can determine H from the nomogram of Figure 6, for each value of S and C. Finally, from a nomogram (not shown here), representing the equation

$$h_2 = H - (1 - \alpha)h_1$$

we determine h_2. Actually, for much of the range, $\alpha \sim 1$ and $h_2 \sim H$.

b = 0

EXAMPLE SHOWN BY DASHED LINE

B = 0.112

Y = 12.2

$\alpha_1 = 0.47, \alpha_2 = 0.91$
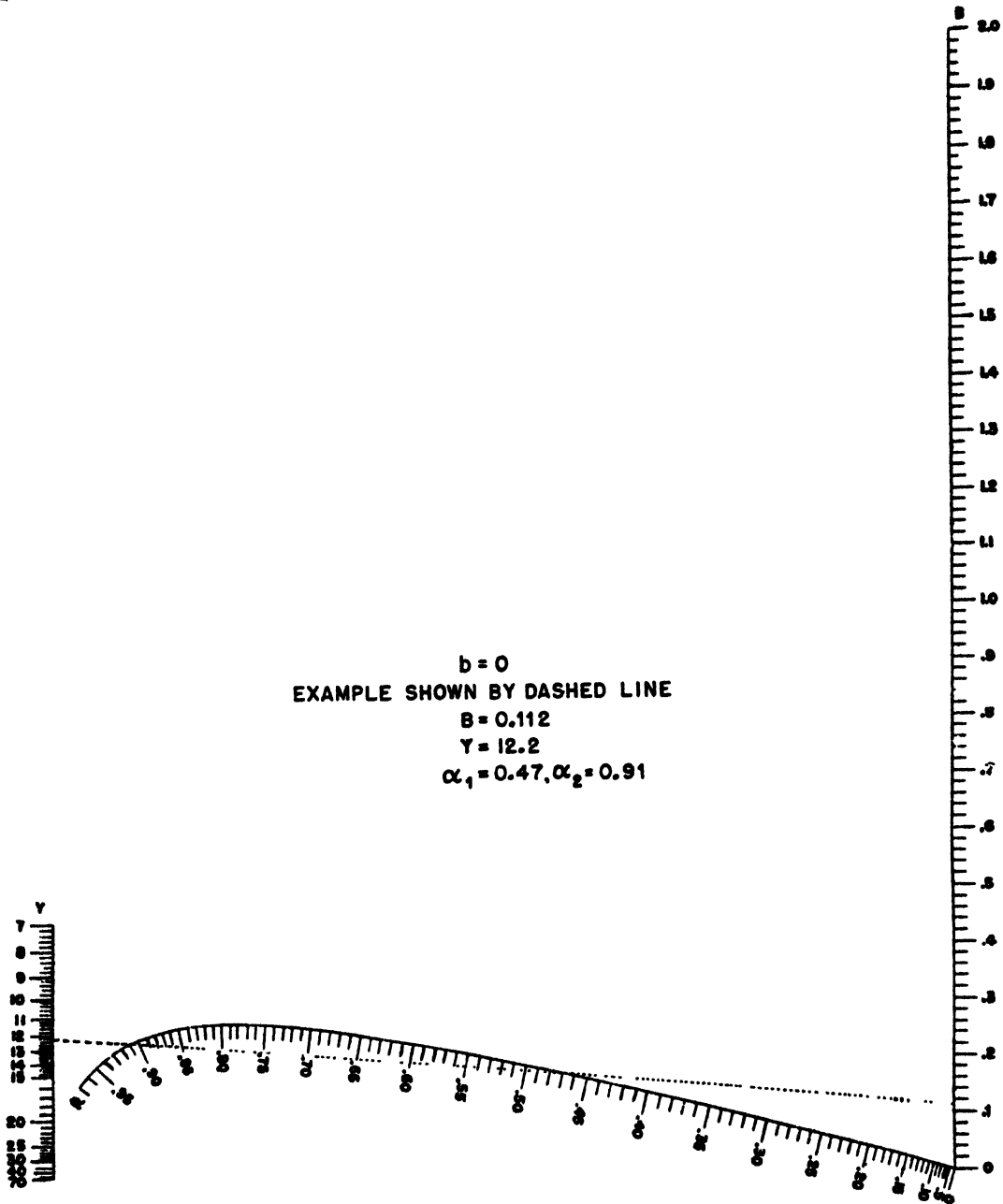
FIGURE 3

For the upper lobes considerable simplification is possible. We may omit all the steps involving calculation of α. We determine the various B's as before. Then, as long as $B \gg 1$ we employ the equation

$$10^{-db/10} = \frac{10^6}{\pi} \left(\frac{1}{914S}\right)^2 \times$$

$$\left[\frac{1}{B^4} + \left(1 - \frac{1}{B^2}\right) \sin^2 \pi b\right]$$

This equation gives S directly for each decibel value

and assumed value of b. The nomogram for this problem appears in Figure 7. We then obtain H from equation (2), with α set equal to unity.

$$H = \frac{(3.281)(914)^2}{2r} S^2$$

$$+ \frac{(3.281)^2(914)(150)}{C'} S . \qquad (3)$$

In equation (3) we have written C' instead of C. For much of the range, wherever B is very large,

EXAMPLE SHOWN BY DASHED LINE
b = 0
α = .3
DB = 57
S = 150
Ṡ IN THOUSANDS OF YARDS
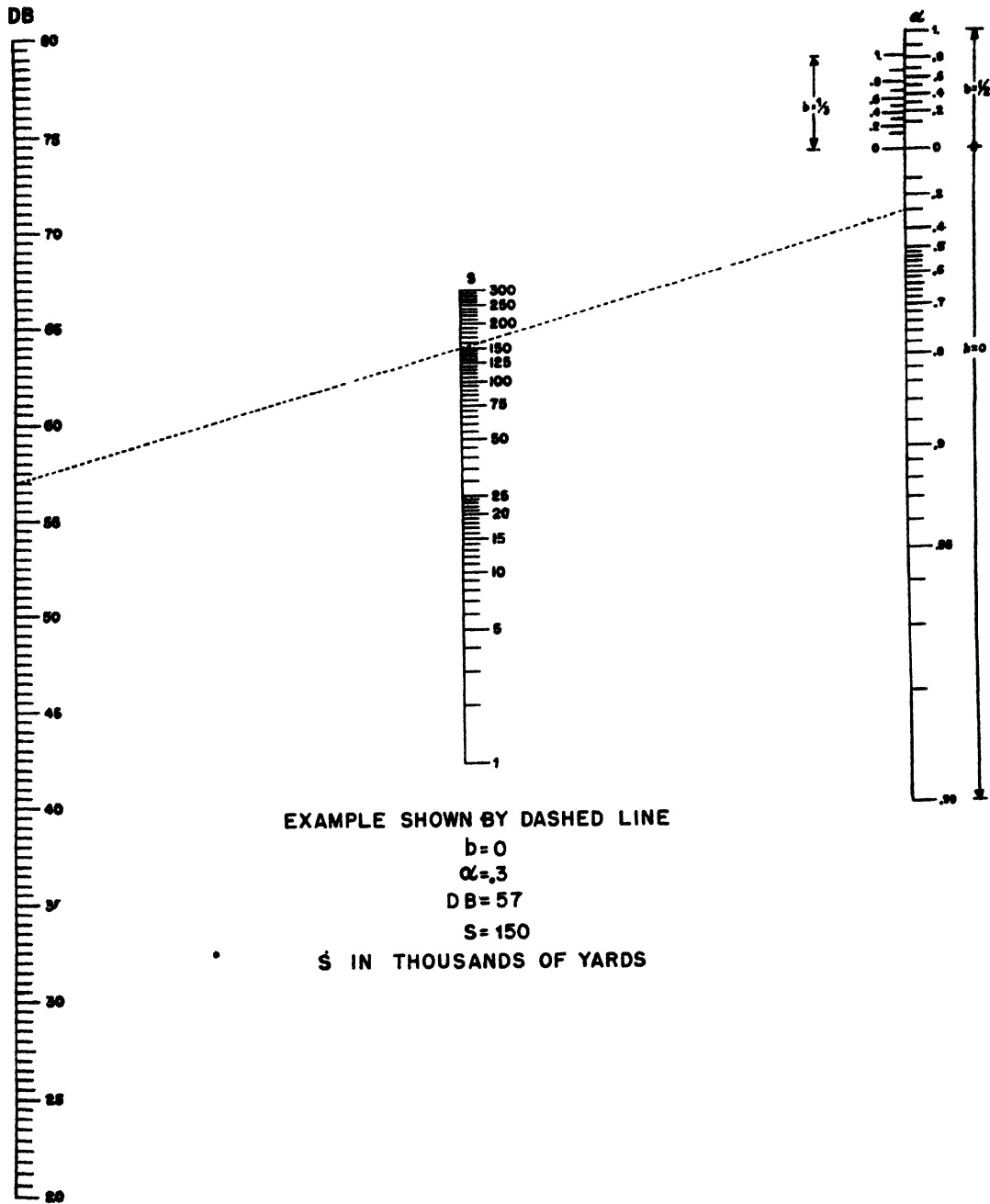
FIGURE 4

we may take $C' \sim C$. If greater accuracy is desired, we may compute C' directly by the equation

$$C' = \frac{(3.281)^2 \,(914)\,(150)\,k}{6\,f_{mc}\,h_1}\left(1 - \frac{1}{B^2}\right).$$

It is interesting to note that equation (3), apart from the correction factor $(1 - 1/B^2)$, which merely serves to improve the accuracy of the result, is familiar to many in the construction of so-called "fade charts." These diagrams depict merely the lobe minima (and sometimes also the maxima). If

we set $b = 0$ we get the former, and if we take $b = \frac{1}{2}$ we determine the latter.

The total number of lobes N is approximately

$$N = \frac{2h_1}{\lambda} = \frac{h_1 f_{mc}}{(150)\,(3.281)} = 2.03 \times 10^{-3} h_1 f_{mc}$$

for h_1 in feet. These will be distributed over an angle of 90 degrees. Hence $\bar{A}$, the average angle per lobe, is

$$\bar{A} = \frac{90°}{N} = \frac{4°43 \times 10^4}{f_{mc}\,h_1}.$$

EXAMPLE SHOWN BY DASHED LINES

$k = 3$

$\alpha = 0.48$

$h_1 f_{mc} = 100,000$

$C = 18$

NOTE: WHEN $\alpha < 2/3$, C IS NEGATIVE

WHEN $\alpha > 2/3$, C IS POSITIVE

h_1 IN FEET, f_{mc} IN MEGACYCLES
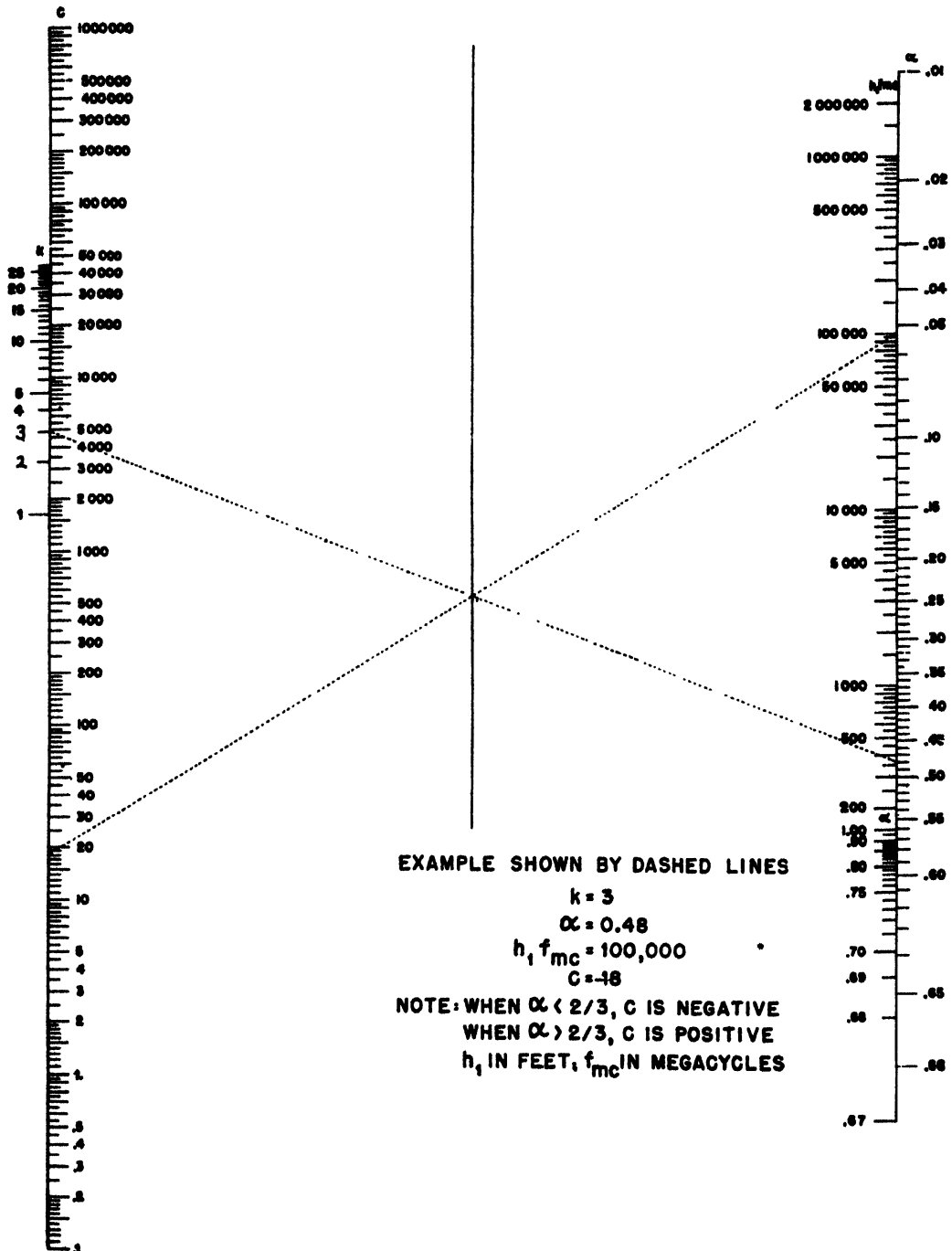
FIGURE 5

Near the horizon, however, the angle per lobe A_0 is somewhat smaller, to wit:

$$A_0 = \frac{360°}{\pi N} = \frac{5°64 \times 10^4}{f_{mc} h_1}.$$

When $A_0 < 0°.1$, the lower lobes are so closely packed that the drawing of a coverage diagram becomes almost impossible. For such cases one should determine, for a given decibel value, the lower edge of the lowest lobe. Then, with the aid of the nomograms for $b = \frac{1}{2}$, calculate merely the positions of maxima of the other lobes.

A work sheet for coverage diagram calculations is shown in Table 2. As an illustrative example we have selected the case in which

$$h_1 = 100 \text{ ft}, f_{mc} = 3,000 \text{ mc}, db = 46 .$$

EXAMPLE SHOWN BY DASHED LINE
S = 220
C = + 10
H = 10,000
H IN FEET
S IN THOUSANDS OF YARDS
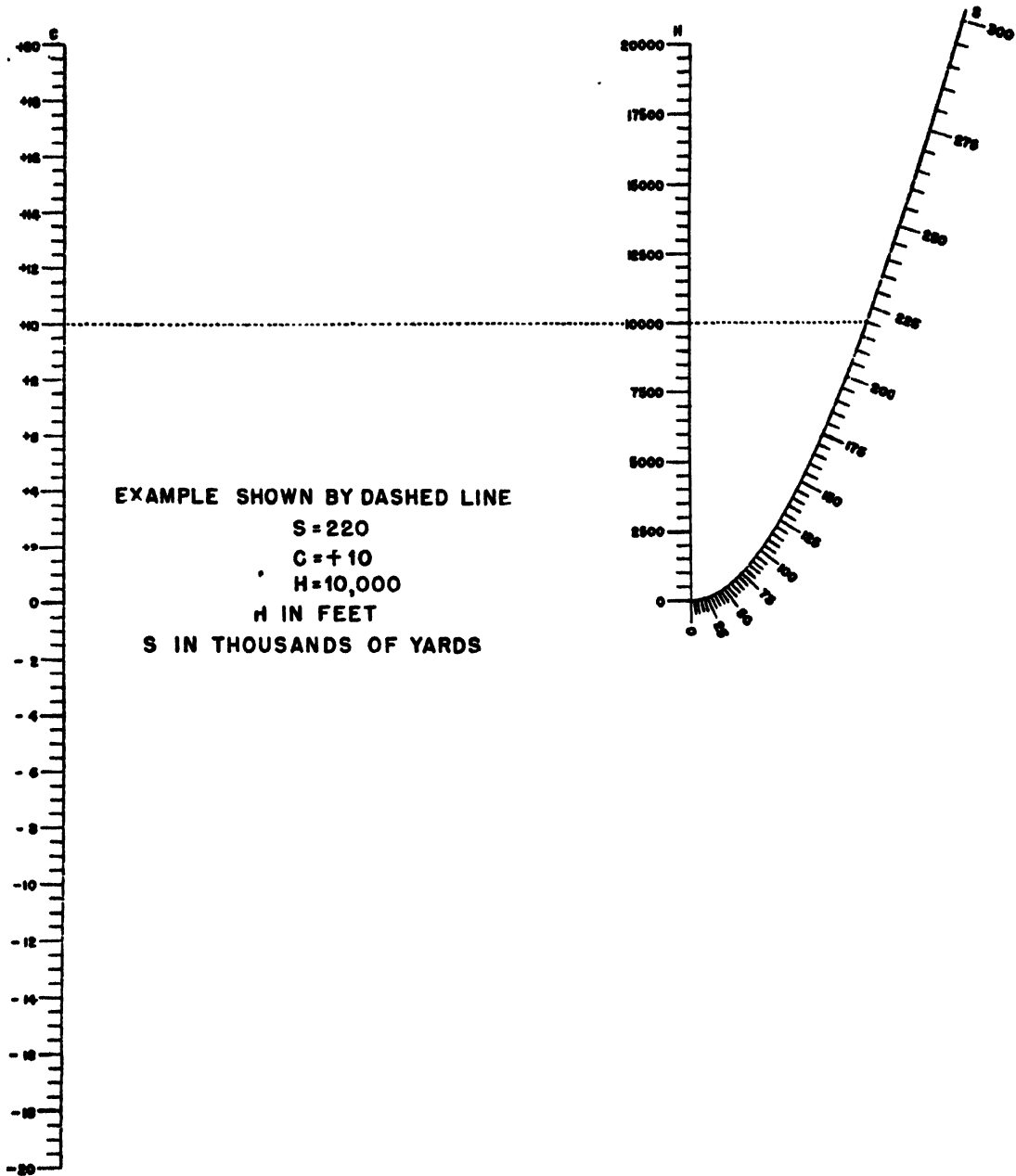
FIGURE 6

Here db stands for the number of decibels that the power density is *below* standard, where we have assumed a power of 1 w for the transmitter. The symbol db is defined differently by the MIT group. The correspondence is:

$$db \longleftrightarrow - [db_{MIT} + 49] .$$

The value of λ, which depends only on db and h_1, was obtained from the nomogram of Figure 4 and equals 13.9. The product $h_1 f_{mc}$ is, of course, 300,000. The rest of the table was filled out by the methods just described.

The lobes corresponding to this data were also computed by the MIT method and are shown plotted in dotted lines in Figure 8. In general, these lobes agree completely with our own. In the cases where there is some slight variance, we have also drawn our lobes in heavy lines. Note that the MIT db of 95 corresponds to our db of 46. The nomograms presented herein correspond to a reflection coefficient of −1. For any other value they would have to be redrawn.

FIGURE 7

EXAMPLES SHOWN BY DASHED LINES
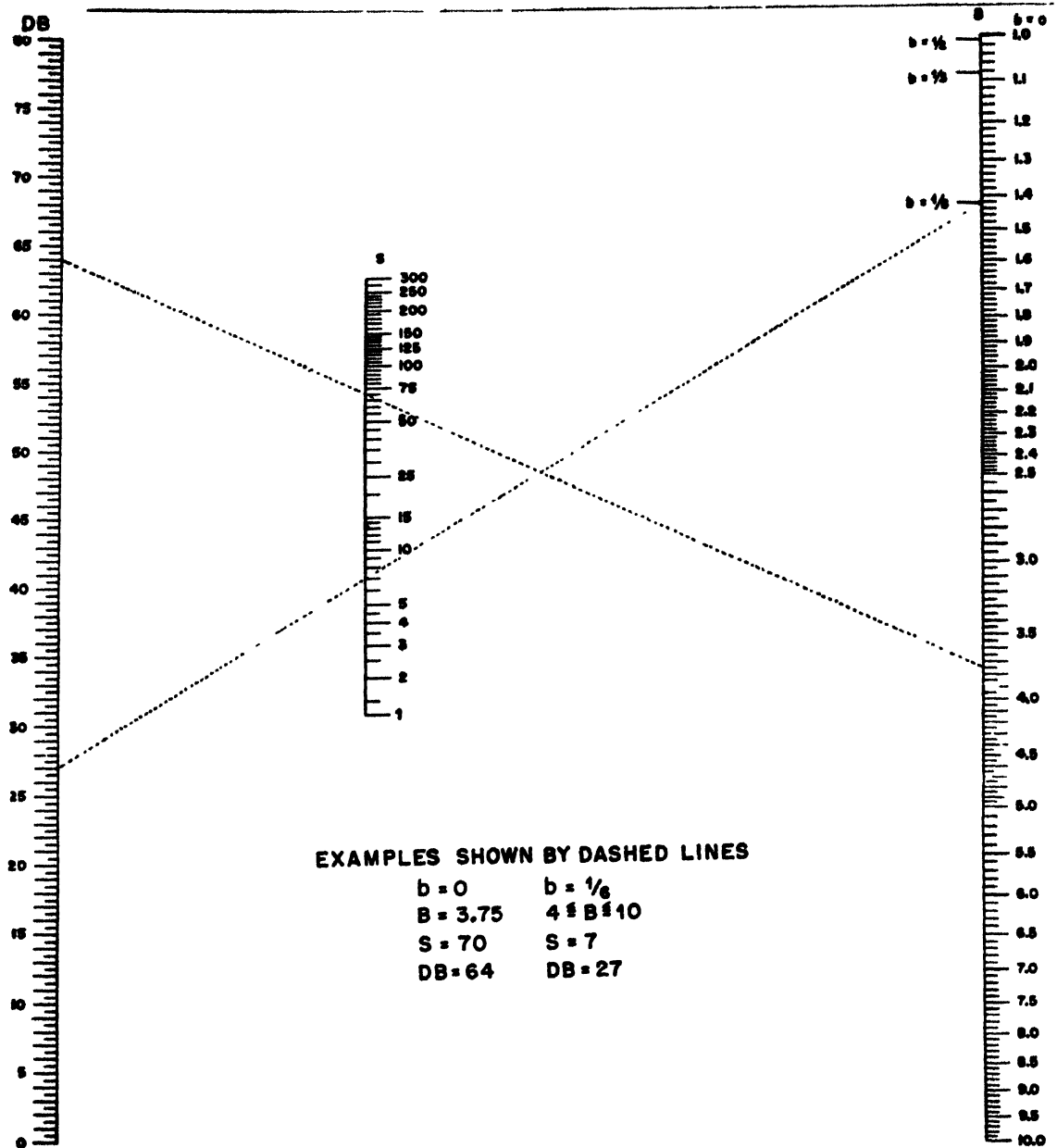
b = 0	b = 1/8
B = 3.75	4 ≤ B ≤ 10
S = 70	S = 7
DB = 64	DB = 27

TABLE 2. Work sheet for coverage diagram calculations. db = 46 (MIT − 95 db), f_{mc} = 3,000 , $h_1 f_{mc}$ = 300,000
Y = 13.9 h_1 = 100 ft

k	B	n	b	α	S	C	H	h_2
1	0.21	1	⅛	0.478	53.5	−2.15	350	300
2	0.42	1	⅛	0.581	82.5	−1.29	950	908
3	0.63	1	⅛	0.655	93.0	− .20	1,350	1,316
4	0.84	1	⅛	0.72	85.0	1.07	1,250	1,222
5	1.02	1	⅛	0.778	82.5	2.45	600	568
6	1.22	2	0					
7	1.35	2	⅛	0.828	56.0	4.10	750	733
8	1.55	2	⅛	0.835	94.0	4.70	1,850	1,834
9	1.85	2	⅛	0.863	109.0	5.70	2,550	2,536
10	1.95	2	⅛	0.873	98.0	6.60	2,200	2,187
11	2.1	2	⅛	0.893	57.0	7.80	950	939
12	2.3	3	0					
15	2.9	3	⅛	0.928	114.0	10.80	3,300	3,292
21	3.9	4	⅛	0.951	118.0	15.40	4,100	4,095
27	5.3	5	⅛		119.0	23.5	5,100	5,100
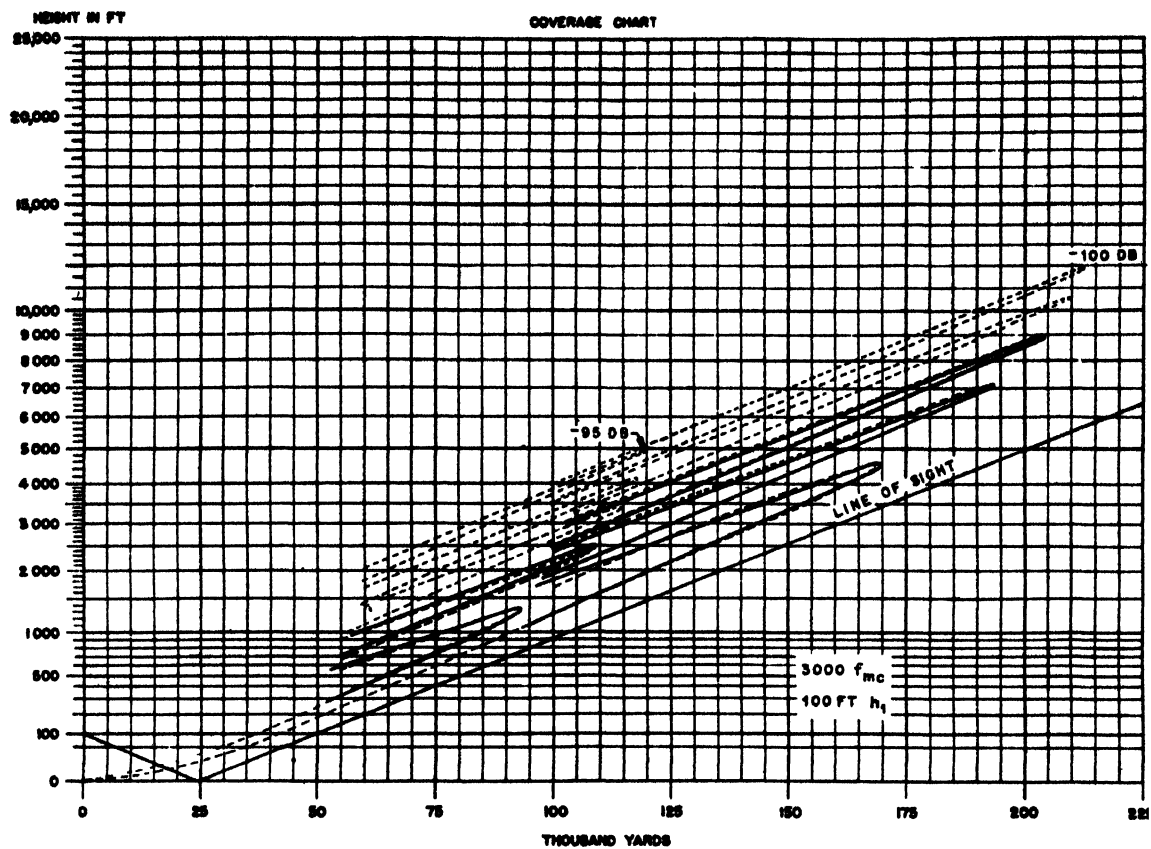
FIGURE 8

Chapter 9

THEORETICAL ANALYSIS OF ERRORS IN RADAR DUE TO ATMOSPHERIC REFRACTION[a]

PURPOSE

THIS REPORT is a theoretical evaluation of errors in altitude, azimuth, and range caused by atmospheric refraction. These errors are compared with the error tolerance specified in military characteristics for fire control radar equipment. Regional climatological data are utilized to determine probable refractive index gradients used in the determination of the error. Errors in heightfinding resulting from ducts are also treated. An Evans Signal Laboratory [ESL] report now under preparation discusses errors which may occur during specific meteorological situations and which may exceed the errors indicated in this report.

PROCEDURE

The variation of the index of refraction perpendicular to the path of a radio wave results in a curvature of the ray toward the higher index. The curvature of the ray is approximately equal to the rate of decrease of the index of refraction with altitude. Errors due to atmospheric refraction will therefore depend on the rate of decrease of the index of refraction perpendicular to the ray path and to the range. A simplified equation for the error in azimuth and altitude is derived below and is utilized in this report. This method has been found to check to within a thousandth of a degree with more accurate methods[b] of ray tracing.[c]

The rate of decrease of the index of refraction in a standard atmosphere is 12×10^{-6} unit per 1,000 ft up to 4,000 ft above mean sea level. This corresponds to a curvature of the path of the ray approximately one fourth the curvature of the earth. The standard atmosphere represents average conditions in temperate zones. In tropical air such as exists in equatorial regions and southeast Asia and southeast United States in summer, the average rate of decrease of the index of refraction is approximately 18×10^{-6} unit per 1,000 ft up to 6,000 ft corresponding to a curvature of the ray ⅜ that of the earth. Over trade wind regions of the ocean (latitude 10° to 30°) dry

subsiding air exists over a moist tropical layer. The rate of decrease of the index of refraction in these regions is approximately 24×10^{-6} unit per 1,000 ft corresponding to a curvature of the ray one-half that of the earth. Within layers of atmosphere designated as "ducts" the curvature of the ray may exceed the earth's curvature and may result in a trapping of the ray within the duct. Errors due to atmospheric conditions in each of the above atmospheres are analyzed. In Table 1 are tabulated values of the index of refraction at selected levels for the standard atmosphere, tropical atmosphere, and tropical dry atmosphere as utilized in this report.

TABLE 1. Values of the index of refraction for selected levels in different air masses.[*]

$(n - 1) 10^6$; n = index of refraction.

Elevation above mean sea level (feet)	Standard atmosphere	Tropical atmosphere	Tropical air dry air above
0	324	394	348
2,000	300	358	300
4,000	276	322	260
6,000	255	286	242
8,000	236	255	227
10,000	219	234	216
15,000	191	195	179
20,000	151	159	146
30,000	105	107	105

[*]Aerological data for Miami and San Diego for July 1943 were utilized to compute the indices of refraction for the tropical atmosphere and the tropical atmosphere with dry air above, respectively.

APPLICATION TO GROUND RADAR EQUIPMENTS

GUNLAYING (ANTIAIRCRAFT) RADAR

Military characteristics for gunlaying radar call for a tolerance of 50-yd error in a range of 29,000 yd and an angle of 1.5 mils in azimuth and elevation. Initial angles of sight are between 10° and 90°.

RESULTS

In a standard atmosphere, errors in angle of elevation for a range of 29,000 yd and an initial angle of sight 10° are 0.5 mil. A maximum error is obtained at 0.9 mil. For an initial angle of sight of 20° the maximum error is about 0.6 mil as compared to an error in a standard atmosphere of 0.4 mil. Errors in azimuth and range are negligible..

EARLY WARNING HEIGHTFINDING RADAR

Military characteristics call for the following tolerances in heightfinding radars.

---

[a]By Raymond Wexler, Signal Corps Ground Signal Agency.

[b]Errors in angle of altitude due to a duct with a standard atmosphere above the duct have been computed by members of Group 42 of the Radiation Laboratory. Values computed by the method outlined below under Derivation of Formulas have been found to agree with their results.

[c]For a more detailed analysis of ray tracing methods, see reference 75.

Set	Freq. Band	Accuracy Required
AN/CPS-4	S	1,000 ft in absolute altitude and 500 ft in relative altitude at 45 miles range, preferably 90 miles.
AN/CPS-6	S	1,000 ft in absolute altitude and 500 ft in relative altitude at 75 miles range, preferably 100 miles.
AN/TPS-10	X	1,500 ft in absolute altitude and 500 ft in relative altitude at 50 miles range.

Thus with the ⅚ earth radius correction the error remains under 1,000 ft at 75 miles. However, these atmospheric conditions represent normal conditions so that in specific meteorological situations the error may exceed 1,000 ft in 75 miles especially in the trade wind regions.

Since the maximum error occurs at a true angle of 0°, these errors in absolute altitude for a range of 75 miles are tabulated for true angles of 0° to 3°.
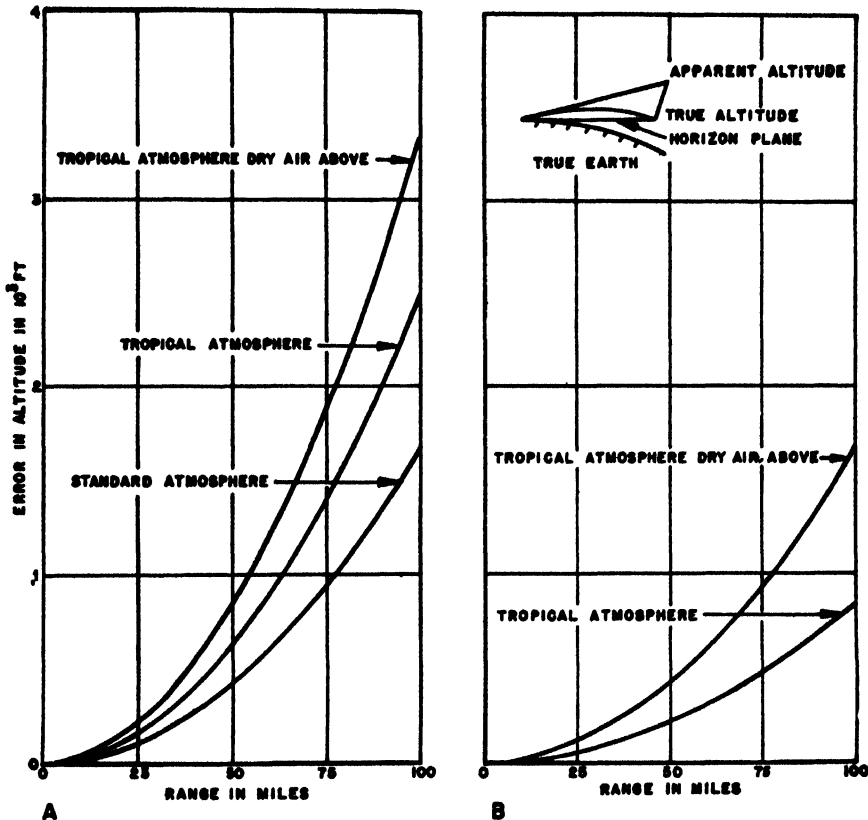
FIGURE 1. Maximum errors in absolute altitude due to atmospheric refraction. A. True earth radius. B. 4/3 earth radius. Target assumed to be at true angle of zero degrees.

ABSOLUTE ALTITUDE

Figure 1A indicates the errors in absolute altitude for different air masses on the assumption that the target is at a true angle of zero degrees. Thus at a range of 75 miles the error in elevation is 940 ft in

TABLE 2. Errors in absolute altitude for early warning heightfinding. Range 75 miles.

True angle	Angle of sight (degrees) Standard	Tropical	Errors in altitude (feet) Standard	Tropical
0	0.14	0.20	941	1,412
1	1.12	1.17	823	1,332
2	2.10	2.14	705	970
3	3.09	3.12	626	845

a standard atmosphere and 1,880 ft in a tropical atmosphere with dry air above. Figure 1B depicts the errors on the assumption that the standard atmosphere correction (⅚ earth radius) is applied.
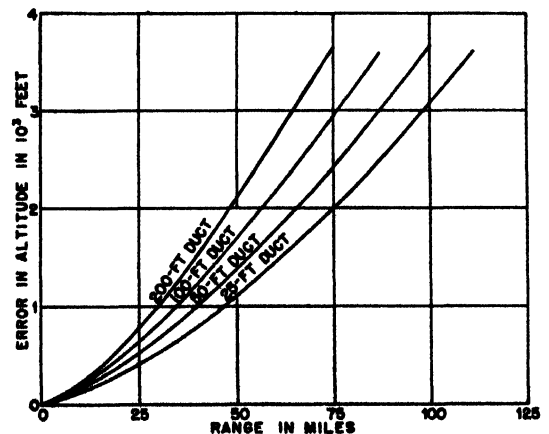
FIGURE 2. Maximum errors in absolute altitude due to surface ducts with standard atmosphere above.

Ducts in the lower layer of the atmosphere will cause errors to exceed those specified by military characteristics. For a duct depth of 25 ft and 1-unit decrease in the modified index of refraction, errors in absolute altitude may exceed 1,000 ft within ranges of 50 miles. A 200-ft duct, in which the modified index of refraction decreases 10 units, may cause an error of more than 2,000 ft in 50 miles range. Figure 2 depicts errors in absolute altitude for ducts of various depths on the assumption that the ray just escapes the top of the duct into a standard atmosphere above. The rate of decrease of the modified index of refraction in the duct is 1 unit per 20 ft (corresponding to a curvature of the ray about twice that of the earth).

RELATIVE ALTITUDE

For example, let us assume that five aircraft are located at altitudes of 3,000, 8,000, 13,000, 23,000, and 33,000 ft above mean sea level. Suppose that these planes are detected by radar at ranges of 50, 75, and 100 miles. Errors in relative altitude occur because of differential refraction at high and low levels. Even in a standard atmosphere errors in relative altitude arise since the rate of decrease of the index of refraction near sea level is 12×10^{-6} unit per 1,000 ft, while at 15,000 ft it is only 6×10^{-6} unit per 1,000 ft. In a tropical atmosphere with dry air aloft the errors are likely to be considerably greater since the rate of decrease of the index of refraction with height is greater.

TABLE 3. Errors in altitude relative to lowest plane located at 3,000 ft above mean sea level.

Separation of planes (feet)	Standard atmosphere (feet)	Tropical atmosphere (feet)	Tropical dry (feet)
Range 50 miles			
5,000	35	24	317
10,000	73	107	380
20,000	131	243	514
30,000	171	306	572
Range 75 miles			
5,000	78	54	713
10,000	164	242	924
20,000	287	539	1,158
30,000	389	693	1,290
Range 100 miles			
5,000	139	97	1,270
10,000	376	431	1,644
20,000	527	960	2,061
30,000	673	1,237	2,296

Thus in a tropical atmosphere with dry air aloft such as exists in the trade wind areas over the ocean errors of some 500 ft relative altitude for planes separated by 20,000 ft would occur in a range of 50 miles. For 100-mile range, errors can be as much as 2,000 ft. Even in a standard atmosphere errors are more than 500 ft for ranges of 100 miles for the higher level planes.

AZIMUTH AND RANGE

Errors in azimuth are negligible for all meteorological conditions except possibly for propagation parallel to a sea coast or sharp cold front (see paragraph below). Errors in range are likewise negligible for all possible meteorological conditions.

SURFACE SURVEILLANCE RADAR

Military characteristics for sets AN/MPG-1 and AN/FPG-2 specify errors up to 0.05° in azimuth at 28,000 yd and 50,000 yd respectively. Range error toleration is 20 yd in 50,000 yd.

RANGE

Errors in range due to vertical refraction within a duct are approximately of the order of 1 yd in 50,000 yd. The error in range corresponding to an azimuth error of 0.05° is estimated at less than 0.2 yd in 50,000 yd.

AZIMUTH

Errors in azimuth arise from horizontal variations in the index of refraction in the atmosphere. Generally these variations are of insufficient magnitude to cause such errors to be appreciable. In order to obtain an error of 0.05° in 50,000 yd it can be shown that a change in the index of refraction of 1.5×10^{-6} unit in 44 yd perpendicular to the path of propagation is required. This corresponds to an increase of 1C temperature and a decrease of 0.1 mb in vapor pressure. Such changes within 44 yd may occur in propagation parallel to a sea coast or to a sharp cold front, or in isolated regions such as between forest and meadow, valley and plain, or land and water surfaces. Except in the vicinity of a cold front or sea coast it is unlikely that such horizontal gradients of the index of refraction exist along the entire path of the ray.

CONCLUSIONS

1. For gunlaying (antiaircraft) radar, the maximum error in angle of elevation at 29,000-yd range is 0.9 mil, as compared to a military tolerance of 1.5 mil.

2. In early warning heightfinding radar, errors of 1,000 ft absolute altitude at 75 miles range may be exceeded even with the application of a standard atmosphere (⅘ earth radius) correction. Because of ducts, errors may be as much as 2,000 ft at 50 miles. Errors in relative altitude may likewise exceed 500 ft in 75 miles.

3. Errors in azimuth may exceed 0.05° in 50,000 yd in propagation parallel to a sea coast or a cold

front. Errors of this magnitude will, however, be rare.

4. Errors in range are negligible for all possible meteorological situations.

DERIVATON OF FORMULAS

Let the origin of the coordinate system be the point where a ray is initially tangent to a line of constant index of refraction n_0, and let the Y axis coincide with this line. Since the ray curves toward higher index of refraction n, according to Snell's law:

$$n \cos \beta = n_0 , \qquad (1)$$

where β is the angle the ray makes with the line n. Then from trigonometric relations:

$$\tan \beta = \frac{dX}{dY} = \frac{\sqrt{n^2 - n_0^2}}{n_0}$$

$$= \frac{\sqrt{n - n_0}\,\sqrt{n + n_0}}{n_0} . \qquad (2)$$

Since n and n_0 are extremely close to unity no appreciable error will result if we assume that $n + n_0 = 2$, hence

$$\frac{dX}{dY} = \frac{\sqrt{2}}{n_0} \sqrt{n - n_0} .$$

Assuming a linear variation of the index of refraction in the X direction, $n = n_0 + \omega X$, and

$$Y = \frac{n_0}{\sqrt{2\omega}} \int_0^X \frac{dX}{\sqrt{X}} = n_0 \frac{\sqrt{2X}}{\sqrt{\omega}} , \qquad (3)$$

$$Y^2 = \frac{2 n_0^2 X}{\omega} .$$

Equation (3) indicates that the ray follows a parabolic path. Let us convert into polar coordinates by the transformation $X = r \sin \phi$ and $Y = r \cos \phi$, where r is the actual range. Then the equation of the path becomes

$$r = \frac{2 n_0^2}{\omega} \tan \phi \sec \phi . \qquad (4)$$

Since in actual practice, ϕ is extremely small and n_0 is extremely close to unity, equation (4) can be written as

$$\tan \phi = \frac{\omega r}{2} . \qquad (5)$$

Here ω represents the rate of change of the index of refraction perpendicular to the ray, and ϕ is the error. If the ray were initially at an angle α to the line of equal index of refraction, then the rate of change of the index of refraction perpendicular to the ray would be $\omega \cos \alpha$. Hence, more generally, the equation for the path of a ray at a mean angle α to the lines of index of refraction can be written as

$$\tan \phi = \frac{\omega r}{2} \cos \alpha . \qquad (6)$$

Equation (6) has been utilized to compute errors in azimuth and angle of elevation.

DIFFRACTION OF RADIO WAVES OVER HILLS[*]

EXPERIENCE HAS SHOWN that frequencies in the VHF (very high frequency) range and higher are propagated over hills and behind obstacles more easily than has been commonly expected. Hills or other obstacles in the transmission path cast shadows which may make a radio system unworkable when either antenna is located close to the obstacle, but recent experiments, notably the work of Jansky and Bailey,[384] have shown that hills and mountains can cause constructive interference as well as destructive interference. In other words, *with proper antenna siting, the field intensity beyond the line of sight may be higher than is expected for the same distance over plane earth. This improvement in field intensity may be 5 to 10 db or more.*

One attempt to develop a theory for radio transmission over hills is based on the computed field intensity over the solid triangle shown in Figure 1.
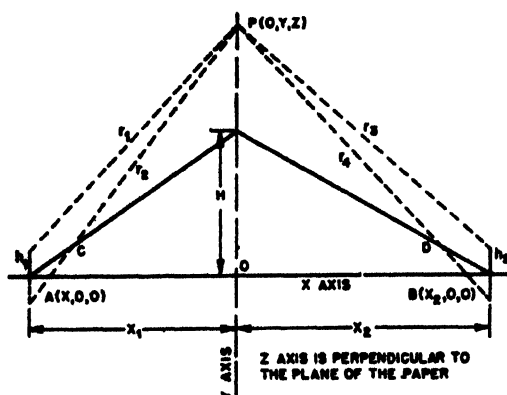
FIGURE 1. Analysis of field intensity over a solid triangle.

It was reasoned that a good approximation to the field over any profile might be obtained from a knowledge of (1) the field over a perfectly smooth earth, (2) the field over the solid triangle that encloses the actual profile, and (3) the field over a knife edge equal in height to the highest point in the profile. The theory of propagation over a perfectly smooth earth is well known; it is the basis of all the published theoretical curves on radio propagation. The corresponding expressions for the field intensity over a solid triangle and over a knife edge are indicated in a paper by Schelleng, Burrows, and Ferrell,[447] but some effort is needed to place these expressions in a convenient form for computation.

The method of obtaining an expression for the field over a solid triangle is indicated in Figure 1,

and the same analysis applies to each of the ideal profiles shown in Figure 2. The field intensity at any
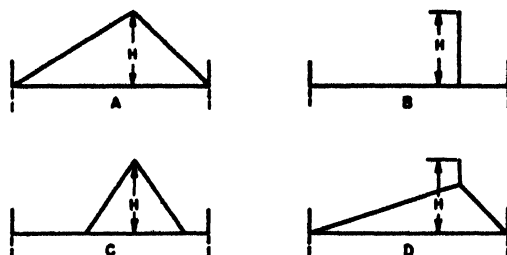
FIGURE 2. Analysis of field intensity over various triangular profiles.

point P in the vertical plane through the apex of the triangle is assumed to be the sum of a direct ray and a ray reflected from the ground which is equivalent to a ray from an image antenna. In a similar manner the field at point P is propagated to the receiving antenna by means of a direct ray and a ground reflected ray. By integrating over the plane above the apex of the triangle (that is, from $y = H$ to $y = \infty$ and from $z = -\infty$ to $z = \infty$) an expression for the total received field is obtained. The complete expression is not as complicated as the expression for propagation over a smooth sphere, but two simple approximations will be sufficient for the present discussion. When the height of the hill $H = 0$ and when the ground reflection coefficient is -1, the complete expression reduces, as it should, to the well-known formula for VHF propagation over plane earth.

$$E = 2E_0 \sin \frac{2\pi h_1 h_2}{\lambda (x_1 + x_2)}. \qquad (1)$$

When the height of the triangle H is greater than three to five times the average height of the antennas
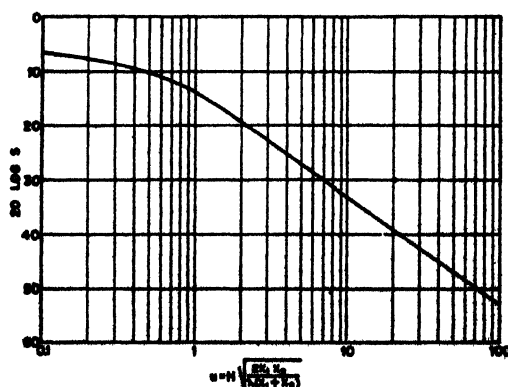
FIGURE 3. Shadow-loss factor S.

and when the reflection coefficient is -1, the complete expression reduces to

$$E = 4E_0 S \sin \frac{2\pi H h_1}{\lambda x_1} \sin \frac{2\pi H h_2}{\lambda x_2} . \quad (2)$$

The factor S is the shadow loss shown in Figure 3 as a function of

$$u = H \sqrt{\frac{2x_1 x_2}{\lambda (x_1 + x_2)}} .$$

The other symbols in the above expressions have the following meanings:

E = field intensity in microvolts per meter,

E_0 = free space field intensity in microvolts per meter

$$= \frac{3 \sqrt{5P} \times 10^6}{x_1 + x_2} ,$$

P = radiated power in watts,

λ = wavelength in meters,

H = height of the obstruction in meters,

h_1, h_2 = antenna heights in meters,

x_1, x_2 = distances as shown in Figure 1 in meters.

The approximate expression given in equation (2) indicates that the field intensity for points well beyond the line of sight may be greater than the field over a plane earth which is given in equation (1). The sine terms in equation (2) indicate interference patterns beyond the line of sight which seem to offer an explanation for the experimental fact that behind hills raising the antenna may cause a loss, or lowering the antenna may result in a gain, in signal intensity.

A comparison between theory and experiment is shown in Figure 4. These data, which were taken from the previously mentioned NDRC report prepared by Jansky and Bailey, show measured values at 116 mc for horizontally polarized waves propagated over the profile shown in the bottom of the
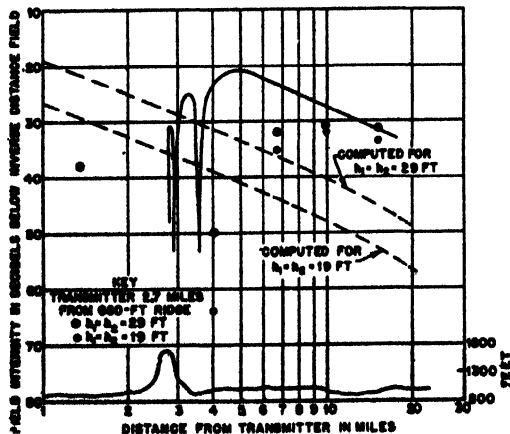
drawing. The open circles show the field intensity in decibels below the free space value when both antennas are 29 ft in height, and the dots give similar data for 19-ft antennas. The two dashed lines running from upper left to lower right are the computed values for smooth earth for 29-ft and 19-ft antennas, respectively. The solid line with the interference fringes is obtained from equation (2) for the case of 29-ft antennas. The correlation between theory and experiment is not complete, but at least the theory may be a step in the right direction. Similar theoretical and experimental results are obtained with vertical polarization.

Thus far the only type of profile considered has been one with a single prominent hill, and it is natural to ask what happens over profiles containing several hills. There are less experimental data available on this point than for propagation over a single hill, and consequently the remainder of this discussion is more speculative than the preceding part.

An ideal profile consisting of two hills of equal height is shown in Figure 5. The complete mathematical solution for this case is difficult, but an approximation can be obtained in the following manner. The field at any point P midway between the two hills can be obtained by means of the expression for the diffraction over a single hill. The field at this point is then propagated over the second hill to the receiver. The total received field is obtained by mechanical integration, that is, by adding the effect (magnitude and phase) of many evenly spaced points in the vertical plane midway between the two hills. The net result is that the total received field is represented more closely by the path ACB than by the path $ADEB$. The energy received over any given
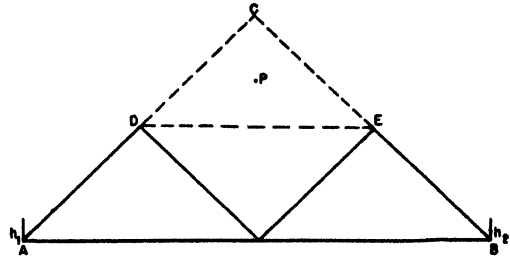
FIGURE 5. Field intensity computation for a profile of two hills by a solid triangle.

path such as path $ADEB$ decreases rapidly as the number of diffractions in that path increases. However, for any profile there is always at least one path between transmitter and receiver such as path ACB that requires no more than one diffraction, and the field intensity over this path is usually controlling. In other words, the profile consisting of two hills can be approximated for computation purposes by a solid triangle which is formed by a line from the base of the transmitting antenna to the base of the receiving antenna and lines from the base of

FIGURE 4. Theoretical and experimental results in measuring field intensity of horizontally polarized waves. Frequency 116 mc.

each antenna tangent to the hill that blocks the line of sight. By the same reasoning it appears that a profile which includes any number of hills can be represented approximately by the circumscribing triangle.

The principal assumptions that are basic to this method of treating radio propagation over hills and other obstructions are as follows: (1) the height of antennas is greater than about one-half wavelength, (2) the size of obstructions is large compared with the wavelength, and (3) the distance between antennas is large compared with either the antenna height or the size of the obstructions. These assumptions limit the application of this theory to wavelengths shorter than a few meters

The principal differences between the diffraction over an irregular earth and the diffraction over a smooth sphere is illustrated in Figure 6 for transmission of S-band waves over sea water. The dashed line shows the field intensity versus distance over a perfectly smooth earth. The solid line shows diffraction over a solid triangle which represents what is expected when the sea is rough, that is, when the height of the water waves is large compared with the S-band radio waves. It will be noted that there is little difference between the two methods for

distances less than about twice the optical range, but at greater distances the solid triangle theory indicates that some energy will be received at appropriate distances.

These views on the transmission of meter and centimeter radio waves over multiple obstacles are speculative. There is little experimental evidence to support them, but also there appears to be even less experimental evidence to contradict them.
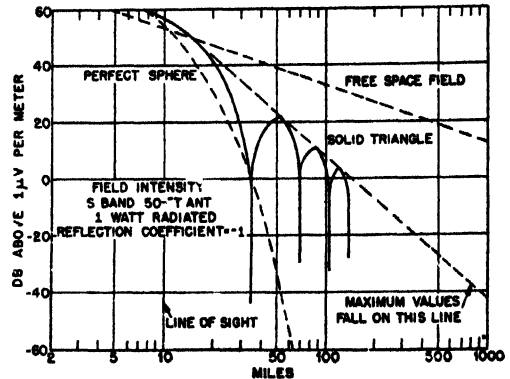
FIGURE 6 Comparison of diffraction over irregular earth and over a smooth sphere for S-band waves over sea water.

SITING AND COVERAGE OF GROUND RADARS[*]

INTRODUCTION

THIS IS A GENERAL discussion of the effects of terrain on the operation of ground radar systems. Written to supplement a Signal Corps publication *Radar Performance Testing*, it is intended to provide a practical, engineering type of solution of siting problems. The principal emphasis is on early warning and other very high frequency [VHF] systems although application may be made to microwave and other types of radio equipment.

The objective has been to enable field personnel to compute coverage and other characteristics of a given site and radar and reduce the number of test flights required to a minimum. Thus the terrain factors may be evaluated, and a definite, numerical description of the capabilities of a site may be stated.

Since it is not possible to anticipate all problems that may arise in the field, sufficient theory has been included to cover a fairly wide scope. In most cases several types of solutions are provided so that the accuracy and detail required may be related to the labor involved. A number of fully worked examples are included with a discussion of significant features. The drawings are made to scale and to fit practical situations.

RADAR SYSTEMS

Types of Ground Radar

Tactical requirements and intensive technical development have led to the introduction of numerous types of ground radar equipment. The characteristics and descriptions of these units are given in several Service publications.

Ground radars may be divided into two classes: (1) those which utilize ground reflection; (2) those which use only the direct ray. Sets which are sited so that ground reflection influences their performance usually have stringent siting requirements and the coverage is dependent on the site. This report is concerned chiefly with this type of radar. Equipment that uses only direct rays is relatively free from site restrictions, and the terrain has little effect on the coverage.

Radar Systems—Tactical Aspects

In most cases radar stations are operated in groups for the defense of a region of considerable extent. The several stations are assigned sectors in which searches are conducted for designated targets, and these, when located, are reported to a central agency for tactical disposition. Technical operation of such groups requires close study of the topography of the region so that available equipment and personnel may be used to the best advantage. In this way adjacent stations may support each other in the event of outage due to maintenance or enemy activity, and other factors may be taken into account, such as jamming, atmospheric effects, and permanent echoes.

The nature of the region to be protected and the type of application for which the radar equipment is to be employed are controlling factors determining the number, location, and kind of sets which must be used. Thus, harbors, islands, and inland mountainous regions present problems with widely differing operational characteristics. Early warning [CHL], fighter control [GCI], gunlaying (coast defense), gunlaying (antiaircraft), and searchlight control radars all have different siting requirements. This report deals mainly with the first three types of equipment listed above, but the methods have general application to other problems such as the siting of direction finding sets [DF].

The early warning radar usually has the mission of reporting and identifying enemy aircraft (at say 20,000 ft) 45 minutes before they can reach the vital defense area. This is based on the time required to alert the area and to give the defense aircraft time to take off and make their attack. Other missions may be assigned, such as detection of ships or observation of friendly aircraft for purposes of control and air-sea rescue. Using the moderate plane speed of 240 miles per hour it is apparent that the early warning radar must have a range of 180 miles if located near the defense area. Sometimes suitable outlying sites, such as islands, are available, and the coverage may be extended accordingly. The disadvantages of outlying sites presented by communication and supply difficulties, exposure to enemy attack, etc., should be carefully considered. More often, however, the success of the warning system depends on effective long-range operation of radars located relatively close to the defense area. The early warning stations give periodic reports of the grid position of an aircraft and its response to interrogation signals.

The GCI radar is used to direct from the ground

---

[*]By Capt. E. J. Emmerling, detailed by Signal Corps to the Columbia University Wave Propagation Group.

the operation of friendly fighters against enemy aircraft. It has a range of about 50 miles and is capable of handling a large volume of traffic. In addition to the grid position and identification of the target it also determines the height. Surrounding the defense area is a region whose width depends on the time required to make an interception on an incoming enemy plane. The siting objective of the GCI stations is the continuous and effective coverage of the interception region. Close coordination is maintained between early warning and fighter stations, and the coverage deficiencies of one station are counteracted by favorable characteristics of the other stations.

The coast defense gunlaying radar is concerned primarily with accurate location of ships. It has a range up to 100,000 yd and must be sited fairly high and within a few miles of the coast defense guns which it directs. This radar supplies accurate data on the azimuth and range of the target.

The antiaircraft gunlaying radar is used primarily for directing the guns. Long-range search features are usually provided so that they may function also as early warning radars, at least to a limited extent. They are sited near the guns which are located to meet artillery requirements. These units provide a continuous flow of data to the gun director giving the azimuth, elevation, and range with great accuracy.

The searchlight control radar is a short-range high angle set which is located near the light it directs. It furnishes the azimuth, angular elevation, and altitude of the target.

Radar Siting—Technical Aspects

In the past some elaborate air warning systems have been set up without a competent analysis of terrain effects. This resulted in a waste of time and money and in failure to adequately provide urgently needed radar screens. This failure was caused in many cases by the use of prepared coverage diagrams, furnished with the equipment, which were computed for idealized sites. In mountainous regions where only limited reflection areas occur and where the sites are very much higher than those used in laboratory tests, such diagrams are likely to be very misleading. A result of this experience is an unfortunate tendency to explain variations from expected coverage by resort to various abstruse speculations, with weather not infrequently bearing the brunt of the odium.

It is the purpose of this report to provide an engineering type of solution for the bulk of the problems that arise in siting and in field computation of coverage. A more accurate analysis, with increased attention to detail, probably is not warranted at this time in view of the relatively rough measurements which now are made in the field of radar.

The common early warning radar uses horizontal polarization and operates in the VHF band. It must be sited from several hundred to several thousand feet high in order to obtain sufficiently low angles for the range and low coverage desired. Suitable sites of the required height may be far inland so that an important part of the reflecting surface may be rough land or sloping flat areas. Such features and also cliff edges, ridges, hills or other obstacles, nearby towers and structures will, in general, produce a marked effect on the coverage pattern.

The GCI radar uses horizontal polarization, operates in the VHF band and should be sited on a large, flat area. The determination of the height of an airplane is accomplished by comparing signals from two antennas of different heights. If reasonable accuracy is to be attained the lobe structure in the vertical plane must be known with considerable precision. Best results are obtained by using a site of the extent and flatness prescribed in the instruction manual. In practice it may be necessary to operate on rough ground or limited areas. The question may then arise concerning the benefit that will be obtained by grading the surrounding areas, or how much forest or vegetation should be removed for acceptable operation.

Similar problems arise in siting DF stations. Large errors may be introduced by reflection from sloping land or other terrain features.

The effects described above, involving reflection from limited areas or rough land or passage of waves past an edge, may all be treated as problems of diffraction, for which solutions are well known or may be readily computed. This subject is unfamiliar to most Service personnel; but a working knowledge of the methods of computation may be obtained by anyone who has the usual engineering education. Since it is not possible to anticipate all problems which may arise in the field, a fairly comprehensive discussion of diffraction has been included in this report so that even in the absence of other references the majority of problems may be treated.

Other important considerations such as orientation, visibility, permanent echoes, interference, and test methods are discussed. There have been many ingenious developments in these subjects in different theaters, and where available they have been included in this report. Only standard atmosphere propagation has been considered. Those who are interested in nonstandard propagation should refer to the articles on this subject published in this series.

TOPOGRAPHY OF SITING

Introduction

The performance of equipment which utilizes radio propagation depends upon the character of the intervening land or sea and in particular upon the local

terrain at the terminals of the propagation path. Siting refers to the general problem of selecting and utilizing available locations for the best operation of the equipment involved. With some types of equipment the effects of local conditions are minor, and with other types the requirements are most exacting. In many cases practical and tactical considerations will compel the use of unfavorable locations. Performance may then be considerably below that obtained in the laboratory or under ideal conditions, and familiar characteristics may be drastically modified.

Field personnel are frequently called upon to predict or explain abnormal operation, to devise methods of improving poor performance, and to make modifications to fit local requirements. This discussion will be limited to general principles, and reference is made to the instructions furnished with the individual equipment for specific details.

Elements of a communication or radar network should ordinarily be viewed as parts of a system and not as isolated, self-sufficient units. From this point of view a site that gives outstanding results would not be satisfactory if it did not help achieve the mission of the *system*. This interrelation between various parts of a system, which may extend over hundreds of miles, raises numerous problems of orientation, visibility, and coverage.

Maps and Surveys

Where available, topographic maps of a scale on 1 or 2 miles to the inch and contour intervals of not more than 100 ft, preferably 20 ft, should be secured. Hydrographic charts are valuable in coastal areas. If there are no reliable maps, aerial photographs may be used to a limited extent.

Due consideration should be given to the suitability of the map projection for the purposes for which it is to be used. The grid system used for reporting should be based on the Lambert polyconic projection, and not on the Mercator projection. Otherwise important errors in azimuth may occur. This is especially true at high latitudes. If in coordinating with other services, such as the Navy, it is required to use the Mercator projection, the transfer from the Lambert projection may be made with a transparent overlay of one grid system on the other.

A transit and a stadia rod are most useful for orientation, surveys, profiles, etc. Compasses, clinometers, and other surveying instruments should be provided. In the absence of some of this equipment much may be done with improvised devices made with plumb bobs and protractors. Rough surveys may be made with only a sketching board and by pacing off distances. Navigation instruments may be used for approximate determination of position. Engineer and artillery publications describe orientation methods in detail. Close attention should be

given to the grid system used for reporting nets so that all stations are accurately located. Grid errors may be minimized by making all charts from a master copy.

Profiles

The height of the center of the antenna should be determined to within a few per cent. The reference level is the main reflecting surface, which is normally the sea. Heights given on maps should be checked against available bench marks and the terrain. Barometers or airplane altimeters are useful for height determinations, but their readings should be corrected for temperature.

Where the reflection surface is part or all land, a profile is usually necessary for estimation of the effective antenna height and the reflection characteristics of the terrain. Profiles should be prepared of several representative azimuths in the operating sector. The accuracy required decreases with the distance from the transmitter. In most cases sufficient detail is not available on maps so that a personal inspection of the terrain should be made to become familiar with the nature of the soil and the degree of roughness. Special attention should be given to ridges, flat areas, bodies of water, distance to the shore, hills to the rear, obstacles in the operating area and at the boundaries. A knowledge of the antenna pattern in both the vertical and horizontal planes is necessary for judging what parts of the terrain should be more closely examined.

Orientation

Where long distances and directive beams are involved fairly accurate orientation is required. This is especially true of the narrow beam, precision type radars. Of the many ways of determining the direction of north, one of the most convenient is observation of the azimuth of the sun. Care must be taken when using compasses because of local attractions or inadequate information of the declinations. Star observations are capable of good accuracy, but where Polaris is not visible they require the same procedure as solar shots. Caution must be used in aligning on permanent echoes because nonstandard refraction may bring in confusing distant echoes, or side lobes may give false echoes. In general several methods should be used in order to obtain independent checks. When an accurate orientation has been obtained reference marks should be provided so that the azimuth may be readily checked.

Solar azimuths, correct to the nearest quarter of a degree, may be determined from the date, time to the nearest minute, and the latitude and longitude to the nearest degree. Two methods will be given for obtaining the azimuth of the sun: (1) by calculation, (2) from tables. A third method gives true

south only.

The azimuth of the sun may be calculated from the formula:

$$\tan \beta = - \frac{\sin HA}{\cos \Phi \tan \delta - \sin \Phi \cos HA} \ . \quad (1)$$

β = bearing of the sun.

The bearing is east or west of south when $\Phi-\delta$ is positive. The bearing is east or west of north when $\Phi-\delta$ is negative. The bearing is east in the morning (β will be negative), and west in the afternoon (β will be positive).

HA = hour angle of the sun.

During the morning hours when the hour angle is greater than 12 hours, its value should be subtracted from 24 hours for use in the formula.

Φ = latitude of the place of observation.

δ = declination of the sun at the time of observation.

The signs of Φ and δ are important and each is positive when north of the equator and negative when south.

The hour angle HA is the local apparent time [LAT] minus 12 hours. To convert the observed time into LAT the civil time at Greenwich [GCT] must be found and combined with the equation of time to correct for the apparent irregular motion of the sun. This gives Greenwich Apparent Time [GAT] which is converted to LAT by allowing for the longitude. The equation of time and the declination of the sun are plotted in Figure 1 for 1945. The annual change is small, and these curves may be used for radar ·work without regard to the year. Standard time meridians are every 15° east or west of

Greenwich, each zone corresponding to 1 hour. Care should be used to take daylight saving, or other changes from standard, into account correctly.

Example 1. It is desired to compute the azimuth of the sun.

Given: Date   March 16.
          Time   1345 hours PWT
          Latitude   40° North
          Longitude   118° West

Solution:

The hour angle will be determined first:

Observed time PWT	13^h	45^m
Zone difference	+ 7^h	
Greenwich civil time	20^h	45^m
Equation of time (Figure 1)		− 9^m
Greenwich apparent time	20^h	36^m
Longitude difference for 118° W	− 7^h	52^m
Local apparent time	12^h	44^m
LAT − 12 ·· HA	− 12^h	
Hour angle of sun	+ 0^h	44^m
HA in arc (4^m = 1°)		+ 11°
Latitude Φ		+ 40°
Declination of sun δ (Figure 1)		− 2°

Substituting in equation (1):

$$\tan \overset{\circ}{\beta} = - \frac{\sin 11°}{\cos 40° \tan (-2°) - \sin 40° \cos 11°}$$

$$= - \frac{0.19}{0.766 \times (-0.0349) - 0.643 \times 0.982}$$

$$= 0.29 \ ,$$
$$\beta = 16°10' .$$

Since $\Phi - \delta$ is positive, β is the bearing from the south. The bearing is west of south since β is positive (p.m.). The azimuth of the sun is

$$180° + 16°10' = 196°10' .$$

A quicker solution may be obtained from a book
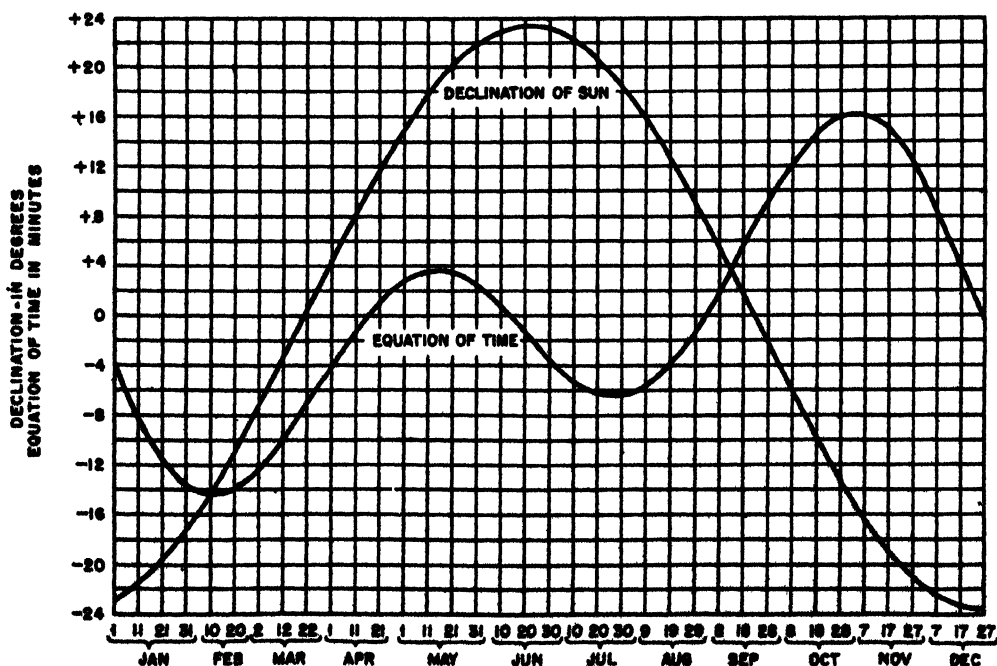
Figure 1. Sun data from nautical almanac, 1945.

Azimuths of the Sun, H. O. 71, published by the U. S. Navy, Hydrographic Office. The equation of time may be obtained from a current copy of *The American Nautical Almanac*, United States Naval Observatory, Washington, D. C.

This method will be illustrated by the data from Example 1. The LAT is obtained as before. Between September 23 and March 21 the sun is in south declination and since the latitude in this case is north, the second part of the book labeled "Declination Contrary Name to Latitude" is used. For latitude 40° an interpolation is made between 12:40 and 12:50 obtaining 164°. The table is marked "the angular departure of the sun west of north" for readings in the afternoon, and the tabular value is therefore subtracted from 360°, giving 196° as the azimuth of the sun. It is usually more convenient to plot a curve of azimuth against time for the hours during which it is expected that the observation will be made. Such a curve may be used for several days without much error.

A method that is less convenient but requires no calculation is the equal altitude method. This consists in measuring the horizontal angles between the sun and a mark, when the sun is at the same altitude on both sides of the meridian of the observer. The bisector of the horizontal angle between the two equal altitude positions of the sun during the observations is very close to true south, and the azimuth of the mark may be determined.

A horizontal radiation pattern should be obtained to determine whether the electrical and mechanical axes of the antenna coincide and to discover any abnormalities in the main or secondary lobes. Defective patterns should be corrected by appropriate maintenance.

Visibility Problems

It is frequently necessary to estimate the effect on rays of intervening obstacles or the curvature of the earth, or to compute the distance to the horizon, or the amount a ray would have to be diffracted to clear an intervening hill. The methods described here enable one to solve such problems quickly and simply.

DISTANCE TO THE HORIZON

The distance d of the horizon on a spherical earth as seen by an observer at elevation h is given by the well-known formula:

$$d = \sqrt{\frac{3h}{2}} \quad \text{or} \quad h = \frac{2}{3}d^2, \qquad (2)$$

with d in statute miles and h in feet. This expression makes no allowance for refraction and is commonly used in visual work.

In radio propagation work the refraction of the standard atmosphere is sufficient to increase the distance of the "radio horizon" to

$$d = \sqrt{2h} \quad \text{or} \quad h = \frac{1}{2}d^2, \qquad (3)$$

where d is expressed in statute miles and h in feet. This corresponds to the use of an effective radius of the earth equal to ka where k is $\frac{4}{3}$ and a is 3,960 miles. This value of k will be used throughout this report. If it is desired to use other values of k, equation (3) may be written as

$$d = \sqrt{\frac{3kh}{2}} \quad \text{or} \quad h = \frac{2d^2}{3k}.$$

Points at heights h_1 and h_2 which are separated by the sea or smooth earth are visible from each other if the distance between them is less than

$$d_L = \sqrt{2h_1} + \sqrt{2h_2}. \qquad (4)$$

DIP AND RISE

Over land, visibility is determined by the profile of the path involved. Elevations obtained from map contours may be plotted on a profile so as to take the effective earth curvature into account, and visibility can then be determined by graphical means. However, construction of such profiles on a curved datum line is tedious, and it is easier to compute

FIGURE 2. Relations between various heights on earth's surface. Dip and rise.

the earth curvature and the visibility directly from the map by methods given below.

In Figure 2 is shown the relations between various heights on the earth's surface. In considering the reference line (sea level) flat as on a map or ordinary profile diagram, use is made of the line H_1TH_2T' instead of the curve H_1HH_2H'. This will be compensated for by using a fictitious ray path P_1PP_2P' instead of the line P_1QP_2Q'. The deviation of this fictitious path from P_1QP_2Q' at P is $QP = HT$ and is called the dip. The deviation at P' is $Q'P' = H'T'$ and is called the rise.

In the figure on the left the triangles HH_2T and H_1KT are similar and

$$\frac{TH_2}{TK} = \frac{HT}{H_1T},$$

or approximately (right-hand figure)

$$HT \times 2ka = d_1d_2.$$

Therefore the dip,

$$QP = \frac{5,280 \times d_1d_2 \times 3}{2 \times 3,960 \times 4} = \frac{d_1d_2}{2}. \tag{5}$$

Similarly for the rise

$$Q'P' = \frac{d_1'd_2'}{2}.$$

The application of these formulas will be shown by a number of examples.

Example 2. Intervening Obstructions — Graphical Solution. In Figure 3 is shown a profile as may be

FIGURE 3. Intervening obstruction of radiation between two points.

obtained from a topographical map. It is desired to ascertain whether P_2 will receive radiation from P_1 without being obstructed by the intervening hill P.

Owing to the curvature of the earth the line marked "datum level" is actually curved instead of being straight as shown. To compensate for this distortion the line of sight of the radar is taken as the parabola P_1XP_2 (shown dashed) instead of the straight line P_1QP_2. If X lies above the top of the intervening hill P, the ray is not obstructed. The distance QX is from equation (5).

$$QX = \frac{d_1d_2}{2} = \frac{20 \times 30}{2} = 300 \text{ ft}.$$

Scaling this distance down from Q, it will be found that X lies above P and there is no obstruction to the radiation.

It will be noted that QX is a maximum midway between P_1 and P_2.

$$QX_{max} = \frac{1}{8}\left(d_1 + d_2\right)^2. \tag{6}$$

Where there are several obstructions to be considered the work may be speeded by drawing a line S_1S_2 (Figure 4) parallel to P_1P_2 at a vertical distance

FIGURE 4. Several obstructions of radiation between two points.

below it equal to the maximum dip. Then intervening hills which do not rise above S_1S_2 will not have to be considered, and those that do cut the line may be checked for obstruction by equation (5) as before.

Example 3. Remote Shielding—Graphical Solution. It is frequently desired to know from a position as P_1 what degree of shielding will be obtained from a given profile. In Figure 5 the rise $Q'X'$ is computed

FIGURE 5. Remote shielding obtainable from a given profile.

by equation (5). Since P' lies below X' it is shielded from P_1 and the minimum height of radiation is indicated by the dotted lines

$$Q'X' = \frac{d_1'd_2'}{2} = \frac{90 \times 80}{2} = 3,600 \text{ ft}.$$

Example 4. Visibility Determined by Computation. In many case it is not necessary to construct profiles, as visibility may be determined by a simple computation. The critical height, h_c, which an intervening hill must equal or exceed to obstruct the line of sight, may be computed from Figure 4. Let the height of the line P_1P_2 at d_1 be h'. Then

$$\frac{h_1 - h'}{d_1} = \frac{h' - h_2}{d_2},$$

or

$$h' = \frac{h_1d_2 + h_2d_1}{d_1 + d_2}.$$

But the height h' exceeds h_c by the dip $(d_1d_2)/2$; therefore

$$h_c = \frac{h_1d_2 + h_2d_1}{d_1 + d_2} - \frac{d_1d_2}{2}. \tag{7}$$

For the values given in Figure 4 the critical height at d_1 is

$$h_c = \frac{3,000 \times 35 + 1,500 \times 15}{15 + 35} - \frac{15 \times 35}{2}$$

$$= 2,287.5 \text{ ft} .$$

Since the hill P is 2,300 ft high it will interfere with radiation to P_2.

Example 5. Remote Shielding—Computation. An important problem is illustrated in Figure 5. A transmitter is located at P_1, and it is desired to know if the nearby hill P_2 shields the distant mountainous island. The height of the line P_1Q' at a distance of d_1' from P_1 is denoted by h' and may be obtained from the relation:

$$\frac{h_2 - h'}{d_2'} = \frac{h_1 - h'}{d_1'} ,$$

giving

$$h' = \frac{d_1'h_2 - d_2'h_1}{d_1' - d_2'} .$$

For this case the rise $Q'X'$ due to earth curvature must be added to give the elevation X' of the line of sight. The height of the lowest ray is therefore

$$h = \frac{d_1'h_2 - d_2'h_1}{d_1' - d_2'} + \frac{d_1'd_2'}{2} . \quad (8)$$

For the values given in Figure 5

$$h = \frac{90 \times 2,200 - 80 \times 2,400}{90 - 80} + \frac{90 \times 80}{2}$$

$$= 4,200 \text{ ft} .$$

It is apparent that the hill P' is shielded from P_1 by the nearby hill P_2 except by diffraction.
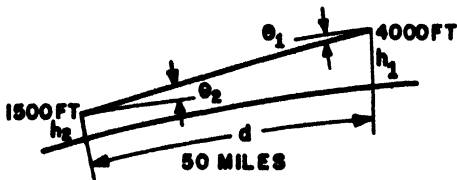
FIGURE 6. Vertical angle computation.

Example 6. Vertical Angles. The slope of the line of sight at the near end (Figure 6) is given by

$$\theta_1 = \frac{h_2 - h_1}{5,280d} - \frac{d}{10,560} . \quad (9)$$

θ_1 is in radians and is measured from the horizontal at h_1. The angle with respect to the horizontal at the far end is given by

$$\theta_2 = \frac{h_1 - h_2}{5,280d} - \frac{d}{10,560} .$$

Thus for the values shown

$$\theta_1 = \frac{1,500 - 4,000}{5,280 \times 50} - \frac{50}{10,560} = -0.0142 \text{ radian} ,$$

and

$$\theta_2 = 0.00474 \text{ radian} .$$

Example 7. Angle of Diffraction. One of the principal problems in connection with intervening obstacles is the computation of the angle of diffraction. In Figure 7 the angle of diffraction is θ_d. The line P_1P is the geometrical shadow line; h_c is the height of the
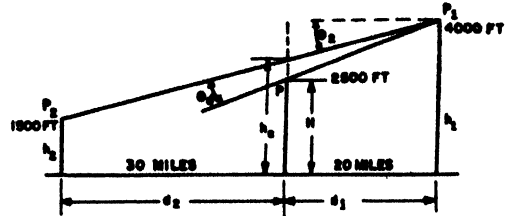
FIGURE 7. Angle of diffraction computation.

direct line P_1P_2 at the distance d_1 and is given by equation (7).

$$\theta_d = \frac{h_c - H}{5,280d_1} . \quad (10)$$

For the values shown in Figure 7

$$h_c = \frac{4,000 \times 30 + 1,500 \times 20}{20 + 30} - \frac{20 \times 30}{2}$$

$$= 2,700 \text{ ft} ,$$

$$\theta_d = \frac{2,700 - 2,500}{5,280 \times 20} = 0.00189 \text{ radian} .$$

P_2 is therefore in the illuminated region. Had h_2 been 100 ft instead of 1,500 ft, h_c would be 2,140 ft and

$$\theta_d = \frac{2,140 - 2,500}{5,280 \times 20} = -0.00341 \text{ radian} ,$$

and P_2 would then have been in the shadow region.

DIFFRACTION OF RADIO WAVES

Introduction

Whenever interference effects are important, the reflecting surface must be examined to determine to what extent the assumption of an ideal plane or spherical surface with uniform values for the ground constants is valid. This uniformity holds when the reflecting surface is the sea; but it is often not true over land areas, and especially at the coastline. More important deviations from the ideal case are roughness of the reflecting surface, such as waves on the sea, or irregularities of the land, such as hilly or broken terrain. This frequently causes diffuse reflection and virtual elimination of useful reinforcement of the direct ray. To deal with these practical terrain problems the methods of physical optics are employed.

Wave Propagation

For most purposes the antenna may be considered as a point source of radiation. Near the antenna the wavefront (the locus of points of constant transit time) is spherical, but at great distances it is practically plane. According to Huyghens' principle each point of a wavefront may be considered as a source emitting wavelets whose envelope at a given time is the new wavefront. In Figure 8A, O is the source
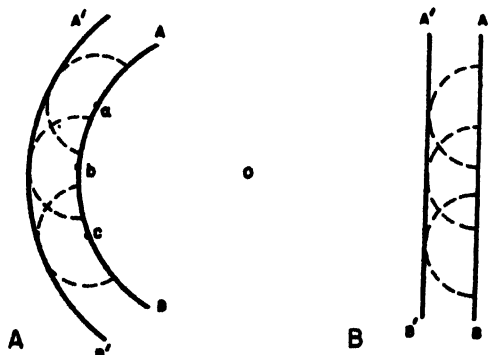
FIGURE 8. Radiation wavefronts. A. Spherical wavefront. B. Plane wavefront.

of radiation, and AB a portion of the spherical wavefront. From centers a, b, and c, secondary waves spread out as shown by the dotted lines and are enveloped in the new front A'B'. A similar construction is made in Figure 8B for a plane wavefront.

Another example showing how waves are reflected from a plane surface is given in Figure 9. A wavefront AB is descending in an oblique direction on the
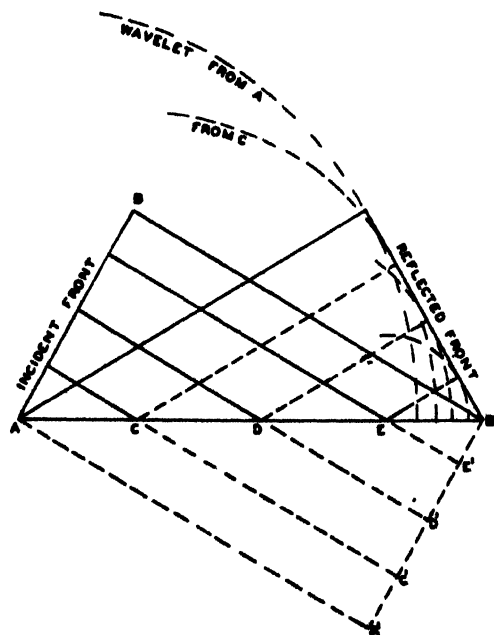
FIGURE 9. Reflection of waves from a plane surface. Huyghens' construction.

reflecting surface AB' Points ACDEB' are struck successively and in turn become centers of new wavelets. In the time required for B to reach B' the wavelet from A spreads to a radius AA', the distance it would have traveled if there were no reflector. Other wavelets have lesser radii which, in spreading, form a new wavefront. This is the reflected wavefront, and its angle with the reflecting surface is the same as that of the incident wavefront.

The secondary wavelet from a point on a spherical wavefront (AB in Figure 10) does not produce the same effect in all directions. The field strength in a direction ac varies in proportion to $(1 + \cos \theta)$. The field strength drops from a value 2 in the forward direction to 1 along the line xy and to zero in the backward direction $(\theta = 180°)$. While in Figure 8A an envelope of secondary wavelets can also be drawn to the right of AB so as to produce a convergent wave traveling back to zero, it can be shown that this backwave does not exist. Only waves in the forward direction should be considered.
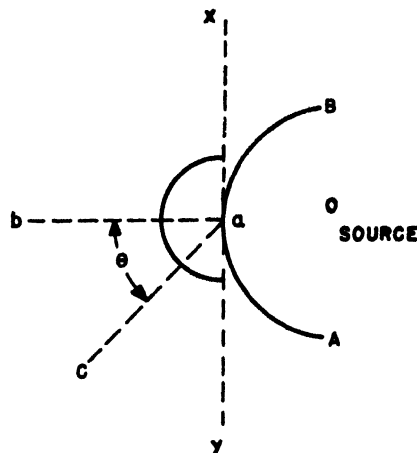
FIGURE 10. The secondary wavelet.

Fresnel Zones

In Figure 11, BC denotes a plane wavefront moving from a distant source on the right toward a point P to the left. It is desired to know the effect at P of the secondary wavelets emanating from the wavefront. A straight line is drawn from the distant source to point P cutting the wavefront at C. In the wavefront with C as a center are drawn circles such that the first is a half wavelength further from P than C is, the second is 2 half wavelengths, etc., so that the secondary disturbance from any circle will reach P half a wavelength ahead of those from the circle enclosing it.

If $PC = b$, the radius r_1 of the first zone may be obtained from

$$\left(b + \frac{\lambda}{2}\right)^2 - b^2 = r_1^2 .$$
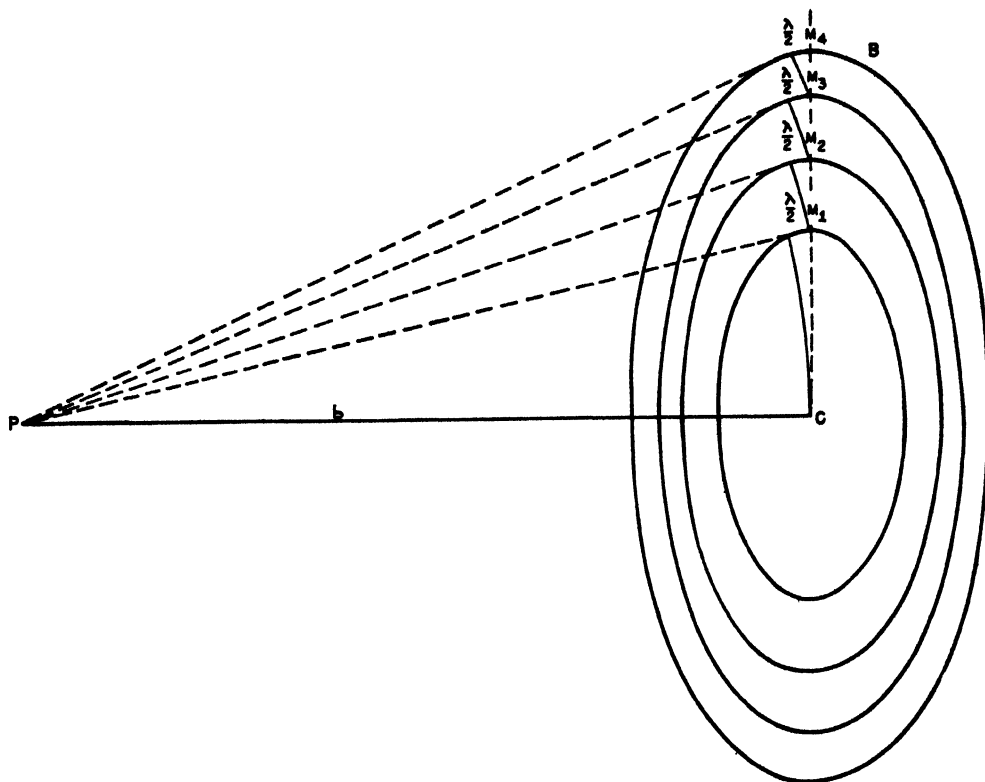
FIGURE 11 Fresnel zones

Neglecting $\lambda^2/4$, the radius $r_1 = \sqrt{b\lambda}$ and the radii, $r_2 = \sqrt{2b\lambda}$, $r_3 = \sqrt{3b\lambda}$, etc., and in general

$$r_m = \sqrt{mb\lambda} . \tag{11}$$

The corresponding areas are approximately $\pi b\lambda$, $2\pi b\lambda$, $3\pi b\lambda$, and $m\pi b\lambda$. The area of the central zone is $\pi b\lambda$, and each succeeding ring or zone is slightly greater.

The effect which one of the zones produces at P is proportional to its area and inversely proportional to its distance from P. These factors compensate as the radius increases, so that the successive zones may be regarded as producing equal and opposite effects at the point P. The zones become less effective further from the center owing to the increased obliquity, since the effect at P is proportional to $1 + \cos\theta$ (see Figure 10). The resultant effect may be represented by a series of terms of alternate sign which decrease slowly at first and then more rapidly, eventually becoming zero, thus:

$$S = m_1 - m_2 + m_3, \text{ etc.,}$$

$$= \frac{1}{2}m_1 + \left(\frac{1}{2}m_1 - m_2 + \frac{1}{2}m_3\right)$$

$$+ \left(\frac{1}{2}m_3 - m_4 + \frac{1}{2}m_5\right) + \cdots \frac{1}{2}m_n .$$

It can be shown that all terms except the first cancel so that

$$S = \frac{1}{2}m_1 . \tag{12}$$

The resultant effect of the entire wavefront is equal to one-half of that due to the central zone.

The secondary wavelets from the central zone unite into a disturbance whose phase is midway between the center and the rim. This may be shown by dividing the first zone into rings such that the effect of each ring at the point P is equal in amplitude, and the phases range over half a complete period. The electric vectors corresponding to these subdivisions may be combined to obtain the resultant phase as in Figure 12. The vector for the central area of the first zone is AB with succeeding surrounding rings represented by BC, CD, etc. These vectors fall along the perimeter of a half circle, as a consequence of which the resultant amplitude is $2/\pi$ times the sum of the amplitudes of the individual vectors. The vectors for the second zone are shown dotted.

In Figure 13 is shown the first six half-wave zones and the phases relative to the center of the first zone are indicated. A set of alternate black and white zones as shown at the top is known as a zone plate.

If a screen is provided which has an aperture of the same diameter as the first zone, it will be found
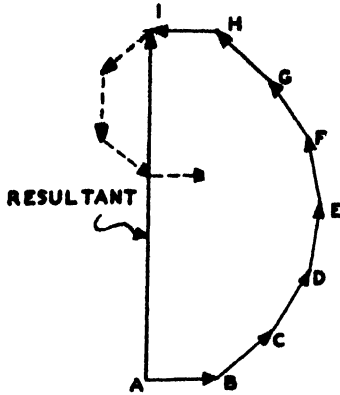
FIGURE 12. Phase of a zone

that the electric intensity of the wave at the point P is doubled ($m_1 = 2S$) and the power intensity is four times as great as for the unobstructed wave. If the aperture is increased to include the second zone, the intensity at P will be reduced nearly to zero. The disturbances from the second zone are out of phase with those of the first zone and equal in magnitude and therefore cause cancellation.
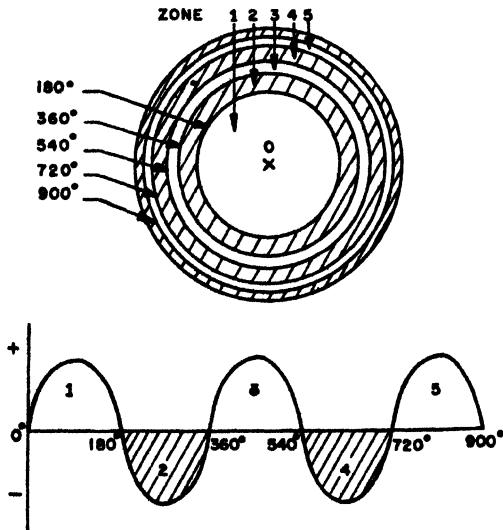
FIGURE 13. Polarity of zones.

Reflection from Rough Surfaces—Rayleigh's Criterion

A rough surface may destroy all phase relations between the elements on the wavefront. The secondary wavelets start from the elevated portions of the surface first, since these portions are struck first by the incident wave, and the lower portions send out secondary disturbances at various other times in random phase. It is impossible to arrange any zone system on such a surface for there are all possible

phase differences irregularly distributed over the reflected wavefront and each point on the surface acts as an independent source radiating in all directions.

In Figure 14 is shown a plane surface xy with incident rays SB and SA falling on a raised portion and a crevice respectively and being reflected to P. The path difference is $SA + AP - (SB + BP)$. Since BP and AP are practically parallel, the path difference may be taken as $BA - BK$.

$$BA = \frac{H}{\sin \Psi},$$

$$BK = BA \cdot \cos 2\Psi.$$
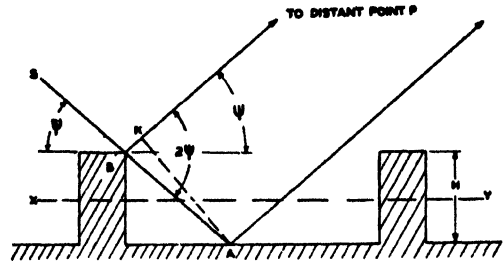
FIGURE 14. Reflection from rough surface.

The path difference

$$\Delta = \frac{H}{\sin \Psi} (1 - \cos 2\Psi)$$

$$= 2H \sin \Psi. \tag{13}$$

The corresponding difference in phase is

$$\Phi = \frac{2\pi\Delta}{\lambda} = \frac{4\pi H}{\lambda} \sin \Psi. \tag{14}$$

Since the path difference increases as the grazing angle increases, the diffusion is greatest when the rays are perpendicular. When the angle is small, near zero, regular reflection may be obtained. It was suggested by Rayleigh to take as an upper limit for the grazing angle, giving regular reflection, the value corresponding to a phase difference of $\pi/4$. By equation (14) this angle is given by

$$\frac{\pi}{4} = \frac{4\pi H}{\lambda} \sin \Psi,$$

or

$$\sin \Psi = \frac{\lambda}{16H}. \tag{15}$$

For a given wavelength and lobe angle the terrain at the reflection point may be examined to determine the limiting height of the roughness for regular reflections. Equation (15) may also be given in a more convenient form using the approximation $\sin \Psi = \Psi$ radians for small values of Ψ:

$$H = \frac{3,520}{f\Psi}, \tag{16}$$

with H in feet, f in mc, and Ψ in degrees. Thus for 100 mc regular reflection may be obtained over ridges as high as 35 ft for a grazing angle of 1°, but for 3,000 mc° the roughness could not exceed 1 ft in height at this angle.

Diffraction at Obstacles

The preceding considerations of Fresnel zones in a wavefront will now be applied to the problem of radio wave diffraction past hills, ridges, or nearby objects. These obstacles will be treated as though they were straight edges, narrow screens, or rectangular slits.

In Figure 15 is shown a distant source of radiation
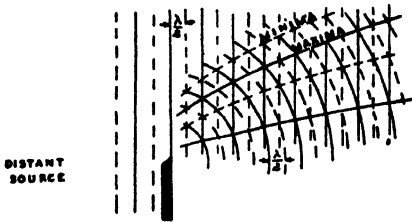
FIGURE 15. Interference of waves at an edge.

and a diffracting edge. The illuminated edge is considered to send out secondary cylindrical wavelets which interfere with the plane waves which are not shielded by the edge. The dotted and solid lines are spaced a half wavelength apart. In the unshaded region the intersection of two dotted or two solid lines indicates reinforcement and the intersection of a dotted and a solid line indicates cancellation. The loci of maxima and minima are parabolas along which the relative intensities are practically constant. In the shadow region, where only the wavelets from the edge are propagated, the relative
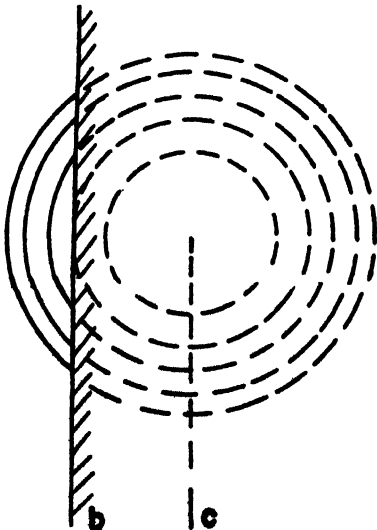
FIGURE 16. Fresnel zones in the shadow region.
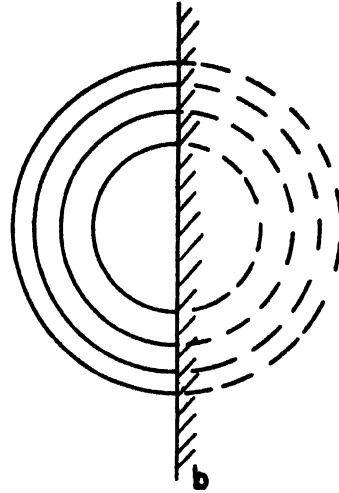
FIGURE 17. Fresnel zones on the shadow line.

intensity falls off continuously as the angle of diffraction is increased, since the angle θ (see Figure 10) approaches 90°.

In Figure 16 is shown the zone system obtained because of a diffracting edge with the source of radiation at a distance behind the paper and with the edge viewed from a screen on which diffraction fringes are formed. The observer is within the shadow region a distance bc, and the zone system is largely obscured as indicated by the dotted lines. The radiation received at c comes from the exposed zones, and its intensity is equal to a series of the form $m_1 - m_2 + m_3 \cdots$, etc., where m_1 is the electric intensity due to the exposed portion of the first uncovered zone, etc. The sum of this series is a fraction of m_1 since the outer zones tend to cancel As c is moved to the right, that is, further into the shadow, m_1 will decrease very rapidly without passing through maxima and minima.

In Figure 17 the observer is at the geometrical edge of the shadow. Only one-half of the wave is
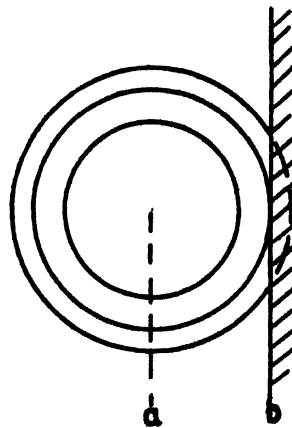
FIGURE 18. Fresnel zones in the illuminated region.

effective and the electric intensity is reduced to one-half, considering the unobstructed wave as unity. Outside the edge, Figure 18, at a distance ab the electric intensity is that due to the half of the wave, plus such portions of the zones between a and b that are uncovered. If an even number of zones is uncovered there is approximately a minimum of radiation received at the line a, that is, the half wave plus the effect of the two zones, $\frac{1}{2} + m_1 - m_2$, for the case shown. If a were moved to the right so that slightly less than one zone were uncovered there would be a maximum, $\frac{1}{2} + m_1$, in which case m_1 is greater than one-half owing to the partial screening of the other zones, which, if allowed to operate, would reduce the effect due to the right-hand half of the central zone. For this reason the fringes formed outside the shadow may exceed the electric intensity of the unobstructed wave. As a is moved to the left, more zones are uncovered, and the maxima and minima are spaced approximately according to the radii of the zones; that is, the distances are proportional to the square roots of 1, 2, 3, etc.

Fresnel Integrals

The preceding discussion is approximate and provides a qualitative picture of diffraction phenomena. The problem will now be formulated quantitatively by the method of Fresnel. Since the applications in view all have to do with diffraction by straight edges, slits, etc., the theoretical approach will be limited to diffraction of cylindrical waves by long edges parallel to the axis of the cylinder. The diffraction images of the source will then be bright bands also parallel to this axis, and the whole problem may be reduced to the consideration of rays in a plane perpendicular to the axis. The fact that in the applications to be discussed later the illumination is due to a point source rather than a line source is probably of little importance provided the distance from the source to the diffracting edge is sufficiently large.

In Figure 19 is shown a cylindrical wavefront AB with its axis at the line source S' (say an illuminated narrow slit). The secondary wavelets from the various line elements ds of the wavefront arrive at P with different phases, having traveled different distances MP. It is desired to find the resultant field strength MP due to wavelets from any given finite part of the front.

Let the electric field strength at a point in the wavefront be given by the expression

$$E = E_0 \sin 2\pi f t , \qquad (17)$$

where t is the time, f the frequency, and E_0 the amplitude of E. The phase has been adjusted so as to make $E = 0$ when $t = 0$.
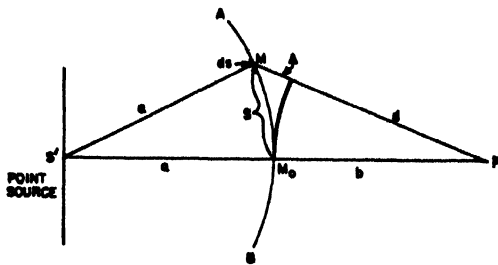
FIGURE 19. Effect at point P of wavefront AB.

Consider next the secondary wavelets spreading from the front in the direction of P. The field intensity at P due to the secondary wavelet emanating from the line element ds at the point M (see Figure 19) is proportional to $ds E_0$ and is inversely proportional to the square root of the distance $MP = d$ (since this is a cylindrical wave). Further, the field intensity must show a phase retardation corresponding to the distance d, that is $2\pi d/\lambda$. Hence the field strength of the wavelet at P is given by an expression of the form

$$dE = kE_0 \, ds \sin \left(2\pi f t - \frac{2\pi d}{\lambda}\right), \qquad (18)$$

where k is a factor of proportionality which depends to some degree on the angle MPM_0 and the distance d, but which will be considered constant here, as the dependence of the phase on d is of much greater importance. To obtain the intensity due to wavelets emanating from a finite part of the front, equation (18) must be integrated over the corresponding region of s. For this purpose we need a relation between d and s. This is obtained by applying the cosine law to the triangle MSP, which gives at once

$$d^2 = (a + b)^2 + a^2 - 2a(a + b)\cos\frac{s}{a}, \quad (19)$$

or after a simple reduction, using the identity

$$\cos\left(s/a\right) = 1 - 2\sin^2\frac{s}{2a}$$

then

$$d^2 = b^2 + 4a(a + b)\sin^2\frac{s}{2a}. \qquad (20)$$

For the present purpose it is sufficient to consider the case when angle s/a is so small that powers of s/a above the square may be neglected in comparison with unity. This means that

$$d = \sqrt{b^2 + 4a(a + b)\sin^2\frac{s}{2a}} \sim b$$

$$+ 2a\frac{(a + b)}{b}\sin^2\frac{s}{2a} \sim b + \frac{(a + b)}{2ab} \cdot s^2, \quad (21)$$

or again, on writing

$$\sqrt{\frac{(a + b)}{2\lambda ab}}\, s = \frac{1}{2}\, v , \qquad (22)$$

the phase lag $2\pi d/\lambda$ assumes the form

$$\frac{2\pi d}{\lambda} = \frac{2\pi b}{\lambda} + \frac{\pi}{2} v^2 . \qquad (23)$$

Using equations (22) and (23), expanding the sine expression of equation (18), it follows that

$$dE = k\sqrt{\frac{ab\lambda}{2(a+b)}}\, E_0\left[\cos\left(\frac{\pi}{2}v^2\right) \cdot \sin 2\pi\left(ft - \frac{b}{\lambda}\right)\right.$$
$$\left. - \sin\left(\frac{\pi}{2}v^2\right) \cdot \cos 2\pi\left(ft - \frac{b}{\lambda}\right)\right] dv . \qquad (24)$$

This expression may now be integrated over a certain region of the wavefront, say from $v = v_0$ to $v = v$, corresponding to $s = s_0$ to $s = s$, giving the following expression for the electric field strength at P:

$$E = k\sqrt{\frac{ab\lambda}{2(a+b)}}\, E_0\left[f(v,v_0) \sin 2\pi\left(ft - \frac{b}{\lambda}\right)\right.$$
$$\left. - g(v,v_0) \cos 2\pi\left(ft - \frac{b}{\lambda}\right)\right] \qquad (25)$$

where

$$f(v,v_0) = \int_{v_0}^{v} \cos\left(\frac{\pi}{2}v^2\right) dv , \qquad (26)$$

and

$$g(v,v_0) = \int_{v_0}^{v} \sin\left(\frac{\pi}{2}v^2\right) dv . \qquad (27)$$

Equation (25) may be brought into a more convenient form by writing

$$\tan \theta = \frac{g(v,v_0)}{f(v,v_0)} , \qquad (28)$$

and

$$R = \sqrt{f^2(v,v_0) + g^2(v,v_0)} \qquad (29)$$

It then follows that equation (26) assumes the form

$$E = k\sqrt{\frac{ab\lambda}{2(a+b)}}\, E_0 R \sin\left[2\pi\left(ft - \frac{b}{\lambda}\right) - \theta\right]. \qquad (30)$$

For tabulation purposes the quantities $f(v,v_0)$ and $g(v,v_0)$ are replaced by the Fresnel integrals, defined by:

$$C(v) = \int_0^v \cos\left(\frac{\pi}{2}v^2\right) dv \qquad (31)$$

and

$$S(v) = \int_0^v \sin\left(\frac{\pi}{2}v^2\right) dv \qquad (32)$$

Evidently

$$f(v,v_0) = C(v) - C(v_0) , \qquad (33)$$

and

$$g(v,v_0) = S(v) - S(v_0) . \qquad (34)$$

In the sequel the arguments will be omitted wherever it can be done without causing misunderstandings, and the above symbols will be written simply as f, g, C, and S.

The Cornu Spiral

In Figure 20 the two Fresnel integrals are plotted against each other, S being the ordinate and C the abscissa, for different values of v. The resulting curve is known as Cornu's spiral. The upper positive branch (C and S positive) corresponds to points on the wavefront above the line. $S'P$ in Figure 19, and the lower or negative branch corresponds to the wavefront below the line $S'P$.

By their definition f and g signify the coordinate differences between any two given points on the Cornu spiral, and it follows that R, as defined by equation (29), represents the corresponding distance between these points.

Differentiating equations (31) and (32) for C and S, squaring and adding, it follows that

$$(dC)^2 + (dS)^2 = (dv)^2 , \qquad (35)$$

so that dv is the line element of the spiral, and v measures length along the curve from the origin.

In order to see more in detail how the Cornu spiral is built up of contributions from different zones we may suppose the half-wave zones on the wavefront to be divided into equal areas and the contributions of these areas to the field strength vectorially combined to obtain the resultant effect as in Figure 22. Then as smaller areas are used and more zones are summed up the vector diagram becomes in the limit the Cornu spiral. This is shown in greater detail in Figures 21 and 22. Here the first half-period zone of Figure 21 is divided into nine parts and the resultant is AB (Figure 22). The second half-period gives a resultant BC. The sum of the first two half-periods is AC. The sum of all

TABLE 1. Fresnel integrals.

v	C	S	v	C	S
0.00	0.0000	0.0000	2.50	0.4574	0.6192
0.10	0.0999	0.0005	2.60	0.3889	0.5500
0.20	0.1999	0.0042	2.70	0.3926	0.4529
0.30	0.2994	0.0141	2.80	0.4675	0.3915
0.40	0.3975	0.0334	2.90	0.5624	0.4102
0.50	0.4923	0.0647	3.00	0.6057	0.4963
0.60	0.5811	0.1105	3.10	0.5616	0.5818
0.70	0.6597	0.1721	3.20	0.4663	0.5933
0.80	0.7230	0.2493	3.30	0.4057	0.5193
0.90	0.7648	0.3398	3.40	0.4385	0.4297
1.00	0.7799	0.4383	3.50	0.5326	0.4153
1.10	0.7648	0.5365	3.60	0.5880	0.4923
1.20	0.7154	0.6234	3.70	0.5419	0.5750
1.30	0.6386	0.6863	3.80	0.4481	0.5656
1.40	0.5431	0.7135	3.90	0.4223	0.4752
1.50	0.4453	0.6975	4.00	0.4984	0.4205
1.60	0.3655	0.6389	4.10	0.5737	0.4758
1.70	0.3238	0.5492	4.20	0.5417	0.5632
1.80	0.3337	0.4509	4.30	0.4494	0.5540
1.90	0.3945	0.3734	4.40	0.4383	0.4623
2.00	0.4883	0.3434	4.50	0.5258	0.4342
2.10	0.5814	0.3743	4.60	0.5672	0.5162
2.20	0.6362	0.4556	4.70	0.4914	0.5669
2.30	0.6266	0.5531	4.80	0.4338	0.4968
2.40	0.5550	0.6197	4.90	0.5002	0.4351
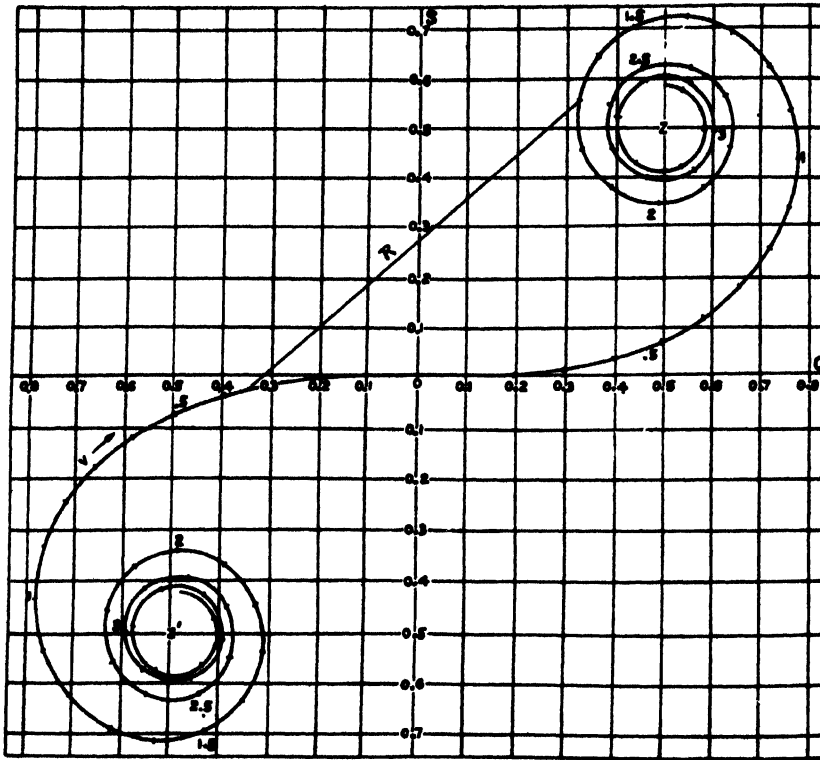
FIGURE 20. Cornu spiral.

half-periods is AZ, which is thus the resultant effect at P of the upper half of the wavefront. A similar result is obtained for the lower half.

It may be remarked that the superiority of the dimensionless variable v over s shows itself in the fact that one Cornu spiral suffices for all situations of the diffracting edge, while the use of s would have necessitated the construction of a special spiral for each specific set of values, a, b, and λ. In Figure 20 the values $v = 1$ and $v = 2$ are marked and correspond to path differences $\Delta = \lambda/4$ and $\Delta = \lambda$, respectively.

Equation (30) shows that the electric field strength in the diffraction region which is due to a certain section of the wavefront is proportional to the corresponding value of R. Hence, it follows that the power per unit area is proportional to R^2. Let W denote peak power per unit area at the point P for a certain arbitrary value of R. Then

$$W = K \cdot R^2 , \qquad (36)$$

where K is a certain constant. When the whole wave is acting, the integration limits extend from $v = -\infty$ to $v = +\infty$, that is, along the full length of the Cornu spiral. The coordinate difference between the foci of the spiral being $(1,1)$ (see Figure 20) it follows that their distance is $R = \sqrt{2}$, so that the corresponding peak power per unit area W_0 is, by equation (36), $W_0 = 2K$ which defines K as $\frac{1}{2}W_0$.

Hence it follows that equation (36) may also be written as

$$\frac{W}{W_0} = \frac{1}{2} R^2 . \qquad (37)$$

Straight Edge Diffraction

Using Cornu's spiral the diffraction pattern due to a straight edge may be obtained. In Figure 23 is shown a diffracting edge at M_0. At P the upper half of the wave is effective, and on Figure 22 the amplitude is AZ of length $1/\sqrt{2}$. The square of this is one-half, which by equation (37) is multiplied by $\frac{1}{2}$ to get $\frac{1}{4}$ for the power intensity at the edge of the shadow. The electric field intensity is $\frac{1}{2}$.

Consider next a point such as P' at a distance x above P (see Figure 23). To be specific, the point
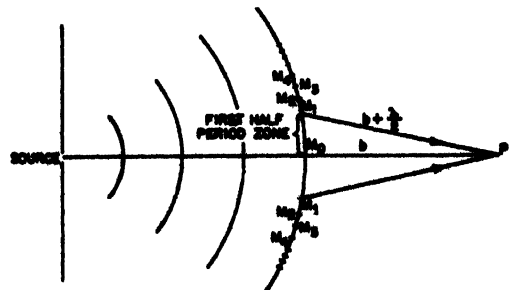
FIGURE 21. Division of wavefront into half-period zones.
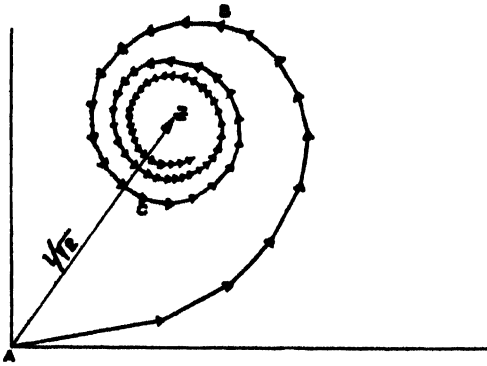
FIGURE 22. Vector sum of subzone contributions.

FIGURE 23. Diffraction at shadow line.

amplitude vector moves to the left along the spiral while its head is fixed at Z.

The amplitude goes through a maximum at b', a

P' is chosen in the direction of SM_1 of Figure 23, where M_1 is the upper edge of the first half-wavelength zone. The illumination at the point P' is, firstly, due to all wavelets emanating from the half wavefront above $P'S$. In addition, there is the contribution from the lower half of the wavefront extending from M_1 to M_0. The situation is, in fact, the same as if P' were brought down to P and the diffracting edge were lowered from M_0 to M'_1 (see Figure 24). The resultant amplitude R is represented on Figure 25 by ZB. Starting at the point P at the edge of the shadow (Figure 23) where the amplitude is AZ, if the point is moved upward, the tail of the

FIGURE 24. Diffraction in illuminated region.
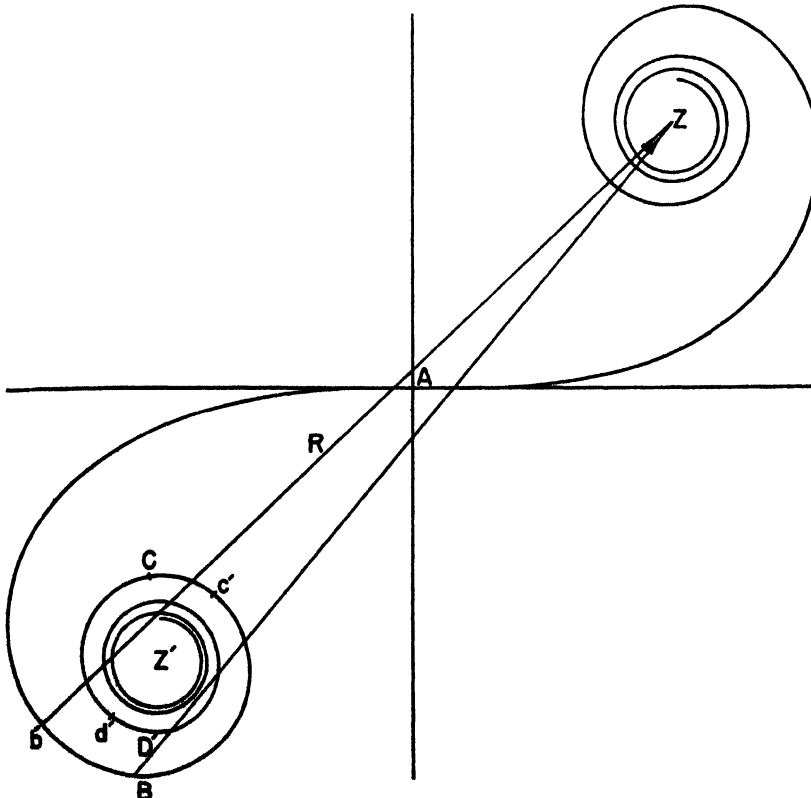
FIGURE 25. Method of using the Cornu spiral.

minimum at c', etc., approaching a value ZZ' for the unobstructed wave. Moving in the other direction, into the shadow, the vector moves to the right from A, decreasing steadily to zero.

The power intensity versus v is plotted in Figure 26, and the points B, C, D, etc., corresponding to those in Figure 25 represent the exposure of 1, 2, 3, etc., half-period zones below M_0. The maxima and minima occur a little before these points are reached. This curve may be plotted from the table of Fresnel integrals with the equations

$$f = 0.5 + C ,$$
$$g = 0.5 + S , \qquad (38)$$
$$z^2 = \frac{1}{2}(f^2 + g^2) ,$$

where z^2 is the relative power intensity compared to the unobstructed wave. The relative electric intensity is

$$z = \sqrt{\frac{f^2 + g^2}{2}} . \qquad (39)$$
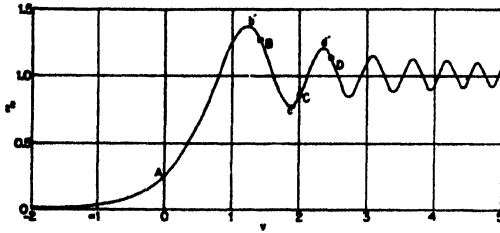
FIGURE 26. Relative power intensity—straight edge diffraction.

Equation (39) is plotted in Figure 27. The portion of the curve for $-v$ has been drawn to the right and is to be used with the right-hand ordinate.
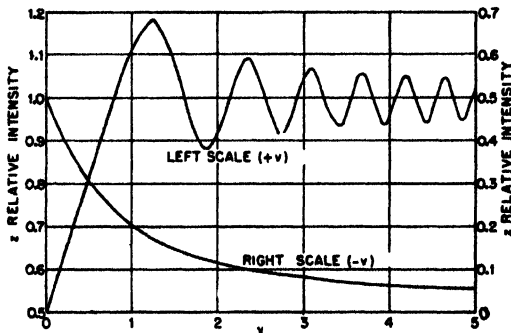
FIGURE 27. Relative electric intensity—straight edge diffraction.

The phase lag ζ due to diffraction may be determined from the angular position of the vector R in Figure 25. In the illuminated region the phase lag oscillates about the reference value, $Z'Z$, and is given by

$$\frac{\pi}{4} - \tan^{-1} \frac{g}{f} .$$

At the shadow line the relative value is the same as $Z'Z$. In the shadow region the phase lag varies continuously along a parabolic curve and is given by
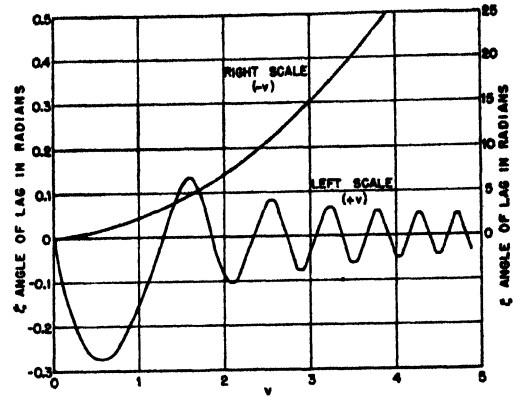
FIGURE 28. Phase lag—straight edge diffraction.

$$\pi \frac{v^2}{2} + \frac{\pi}{4} .$$

The phase lag relative to that of the shadow line is plotted in Figure 28. The portion of the curve for $-v$ is drawn to the right, and its ordinate, on the right, has a different scale from that used with the $+v$ portion of the curve.

Location of Maxima and Minima

When the source is close to the diffracting edge, the positions of the maxima and minima in the illuminated region may be determined by the following analysis. The effect of the wave RM (Figure 29) at P' may be considered to be due to the upper half of the wave (above R), which is unaffected by the edge, and the lower half of the wave (below R), which is partly shielded by the edge. If RM contains an even number of half-period elements the intensity at P' is a minimum. If the number of half-period elements is odd the intensity is a maximum. That is

$$MF' - RP' = \frac{n\lambda}{2} , \qquad (40)$$

where n is an integer with values 1, 3, 5, etc., for maxima and 2, 4, 6, etc., for minima. The difference $MP' - RP'$ is a constant, and the locus of the point P' is a hyperbola having M and S for loci.
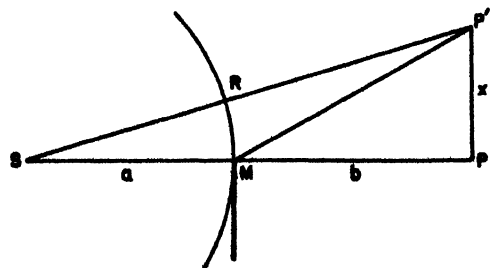
FIGURE 29. Path differences at a straight edge.

That is,

$$SP' - MP' = SR - (MP' - RP'), \quad (41)$$

and SR is constant; therefore, the difference of the distances of P' from the fixed points S and M is constant. P' describes a hyperbola, but its curvature is so small that it almost coincides with its asymptotes.

The distance x to a maximum or minimum may be computed as follows

$$SP' = (a + b)\left[1 + \frac{x^2}{(a + b)^2}\right]^{\frac{1}{2}}.$$

Since x is small compared to $a + b$

$$SP' = a + b + \frac{x^2}{2(a + b)}$$

also

$$MP' = b + \frac{x^2}{2b}.$$

Therefore from equations (40) and (41):

$$MP' - RP' = \frac{x^2}{2}\left(\frac{1}{b} - \frac{1}{a + b}\right) = \frac{n\lambda}{2}; \quad (42)$$

hence

$$x = \sqrt{\frac{b(a + b)n\lambda}{a}}, \quad (43)$$

where n is odd for maxima and even for minima.
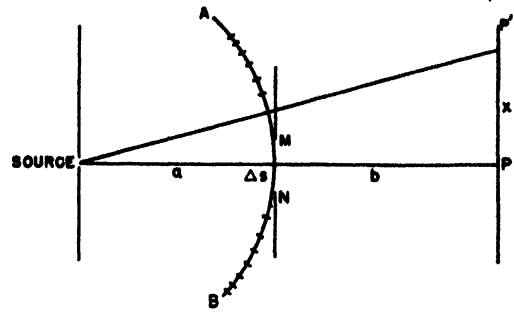
FIGURE 30. Rectangular slit.

The Rectangular Slit

A problem similar to the straight edge is the rectangular slit (see Figure 30). Cornu's spiral will be used to determine the field intensity along the plane PP'. With the slit in the central position, the only radiation at the plane is due to the wavefront in the interval $\Delta s = MN$. Equation (31) is used to determine what length Δv corresponds to Δs. The resultant field strength at P is given by the chord of the spiral which has a length Δv. Since the point of observation P is centrally located, this chord will be centered on the spiral. Thus, if $\Delta v = 0.5$ the chord (see Figure 20) will extend from approximately
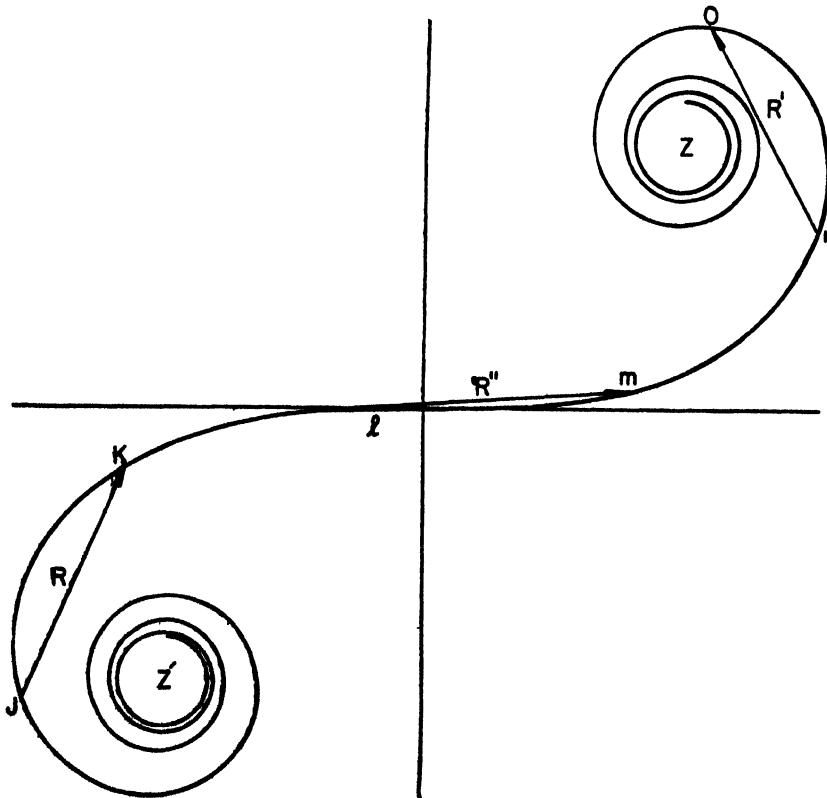
FIGURE 31. The Cornu spiral applied to obstacles and slits.

$C = -0.25$ to $C = +0.25$. The resultant $R \cong 0.5$ substituted in equation (37) gives a power intensity of $\frac{1}{4}$ relative to the unobstructed wave and a field strength of 0.353.

The field intensity at P' is due to the same length Δv but taken over a different portion of the spiral. For this purpose, it is desired to use distances along the plane PP', x, instead of s (Figure 30).

$$x = \frac{a + b}{a} s = v \sqrt{\frac{b\lambda (a + b)}{2a}}. \quad (44)$$

Thus the portion of the spiral nO in Figure 31 from $v = 0.9$ to $v = 1.4$ has an average value of $v = 1.15$ which multiplied by the radical term of equation (44) gives x. The chord connecting these points is 0.43, and the relative power intensity is 0.092. This same result may be computed from the table of Fresnel integrals by obtaining the values of ΔC and ΔS for $v = 0.9$ and $v = 1.4$. The sum of the squares of ΔC and ΔS is R^2. Typical patterns for slits of several widths are shown in Figure 32. It will be noted that there is little radiation outside the slit.

Diffraction by a Narrow Obstacle

The effect of a narrow object with parallel sides may be determined with the Cornu spiral. In the case of the slit only a fixed length slid along the spiral is effective, the remainder being shielded by the edges of the slit. With an obstacle, however, a fixed length slid along the spiral represents the ineffective portion. If the obstacle is of such size that it covers an interval $\Delta v = 0.5$ on the spiral, Figure 31, the segment Δv may be located as JK. The radiation at the point considered will be due to the two parts of the spiral Z' to J and K to Z. The resultant amplitude is obtained by adding the two vectors $Z'J$ and KZ. The sum is R for a point
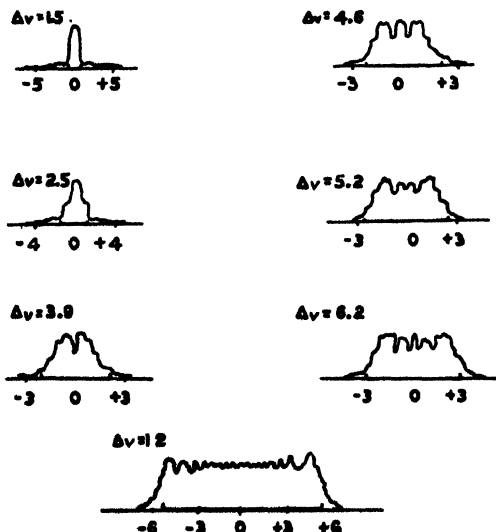
FIGURE 32. Diffraction patterns of slits.
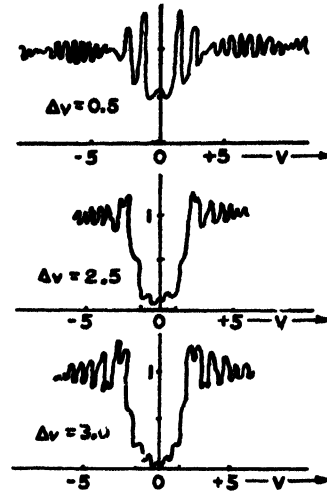
FIGURE 33. Diffraction of narrow obstacles.

midway between J and K. The head of the vector is always in the direction Z along the spiral. Typical patterns for narrow obstacles are shown in Figure 33.

Multiple Slits and Obstacles

Slits or obstacles with parallel sides may be treated by means of the Cornu spiral and the resultant sum of the vectors obtained. Thus, with two slits of a width such that $\Delta v = 0.5$ and spaced so that $\Delta v = 0.5$ may be located on the spiral as JK and lm in Figure 31. The total R is the vector sum of R and R''. The field strength pattern is then obtained by sliding the two lengths along the spiral holding their spacing fixed.

In similar fashion two narrow obstacles would cause two absent sections such as JK and lm and three open sections $Z'J$, Kl, and mZ. The three vectors, obtained by joining these three latter pairs of points, are combined to give the resultant amplitude R.

Limitations of Fresnel's Theory

Neither Huyghens' principle nor Fresnel's theory, on which the above treatment is based, is rigorous, and their limitations must be kept in mind when making applications to radio and radar problems.

In the development of the theory no mention was made of the effect of the shape and composition of the edge. Actually within a region of about one wavelength around the edge the wavefront is affected by the presence of the edge. In Figure 34 the region of the edge disturbance is DE, and first half period of the wave front is DF. The first half turn of the Cornu spiral is due to DF. The position of F depends on the point considered. When DE is an appreciable part of DF, the simple Fresnel theory should not be depended upon. This occurs when the
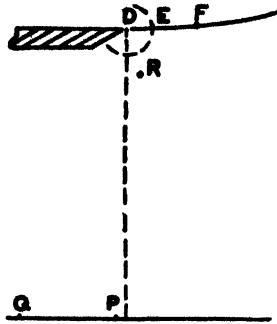
FIGURE 34. Edge effects.

field point is at Q, lying at a large angle of diffraction, or at R, close to the edge.

Near the diffracting edge, a certain amount of reflection occurs, especially near R. This reflection is divergent and decreases rapidly in intensity as one recedes from the edge. When the edge is blunt or has a large radius of curvature, the amount reflected is increased and the field is affected over a greater distance. Since the angle is near grazing, the nature of the reflecting surface is not important. If Fresnel's theory is applied to spheres and cylinders, the results may be only approximate.

When the edge and the electric vector are parallel, the theory gives good results. When the electric vector is perpendicular to the edge, the field strength in the shadow region may be several times larger than that obtained with the electric vector parallel, and the theory should then be used only for small angles of diffraction.

Other discrepancies are due to ignoring the obliquity factor and the effect of the inclination of the wavelets with respect to each other. The theory does not give the correct phase angle for the diffracted wave.

The same objections may be raised for apertures and obstacles whose dimensions are of the order of a wavelength.

It should be noted that

1. *Fresnel's theory is valid* when the wavelength is small compared to the dimensions of the diffracting object (as in optics).

2. *Fresnel's theory should not be used:*
   a. For large angles of diffraction.
   b. Close to the diffracting edge.
   c. For apertures or obstacles of the order of a wavelength.
   d. When the diffracting edge is not parallel to the direction of polarization of the wave.

In spite of these shortcomings the theory is useful because it provides simple solutions for the majority of the diffraction problems encountered in the field, and, considering the difficult nature of the general problem, it is still the most manageable treatment that has been developed.

PERMANENT ECHOES

Introduction

Permanent echoes are due to reflection from terrain features such as mountains, islands, or even smooth surfaces near the antenna (ground clutter). Nearby hills and surfaces produce strong echoes which obscure the indicator and widen the main pulse so that the minimum range of detection is increased. More important are the distant hills, especially those in the operating sector which obscure areas of tactical importance. Permanent echoes are a prime consideration in siting, as many otherwise excellent sites are rendered worthless by excessive fixed echoes. A careful analysis of the terrain will enable an approximate prediction of such echoes. In this section is presented a systematic method of preparing permanent echo predictions so that the suitability of sites may be determined *without* actual field tests.

Several factors combine to make permanent echoes more troublesome than might be expected on first thought.

1. Hills and land surfaces are so much greater in extent than the target which the equipment is designed to detect, that strong echoes may be obtained from distances where an ordinary target would give an echo far below normal detection levels.

2. The low elevation of the land surfaces places them in regions most subject to nonstandard propagation effects where extreme ranges and large responses are frequently obtained.

3. Side lobes of the horizontal pattern of the antenna cause permanent echoes to appear at several other azimuths in addition to that of the main lobe. Although the signal intensity of the side lobes is much reduced, the echoes may still be strong enough to obscure targets.

4. Strong permanent echoes causing considerable trouble may be obtained from distant mountains in the rear as a result of back radiation. Again, the weakness of the radiation and distance of the mountains are often compensated for by the large extent of the reflecting surface.

5. Antennas with wide beams cause permanent echoes to be much wider than the object that produces them.

6. Diffraction over intervening ridges is often sufficient to nullify their screening action so that objects behind the ridge are visible.

Permanent Echo Diagrams

The permanent echoes associated with a radar station may be plotted on a chart and their extent, location, and strength represented. Permanent echo diagrams should be prepared for each unit of a radar system using a standard procedure for the taking and presentation of data. These diagrams are very

useful for:

1. Indicating blind areas in a station's coverage.
2. Assigning the operating area of a station.
3. Checking the range and azimuth accuracy.
4. Checking the transmitter output and receiver sensitivity.
5. Estimating nonstandard propagation.
6. Planning test flights.

While methods used in different theaters vary as to detail, the typical permanent echo diagram is prepared about as follows. The equipment should be in normal operating condition: that is, the transmitter output and receiver sensitivity should be as recommended by the instruction manual; the range and azimuth calibrations should be accurate; and the weather conditions that affect propagation should be average. The receiver gain should be set to some standard level, usually maximum, or to some definite noise height. The value of the data taken will depend to a considerable extent on the skill and judgment

of the operator. The station would normally be taken out of operation for about an hour while data are taken, although it is possible to take observations during normal scanning by stopping momentarily. Where antenna switching is provided, the low-angle, long-distance beam should receive the most attention although the other combinations should be checked also.

If the beam is highly directive and can be changed in elevation, a low angle such as would be used for distant search should be used for recording permanent echoes. In some situations several elevations should be used. On *plan position indicator* [PPI] scopes it may be more convenient to photograph the screen if proper equipment is available. Care should be taken not to confuse storm and fog echoes with permanent echoes on microwave sets.

A more detailed procedure is required where A-scope presentation is used. After the initial adjustments have been made the next step is to decide on
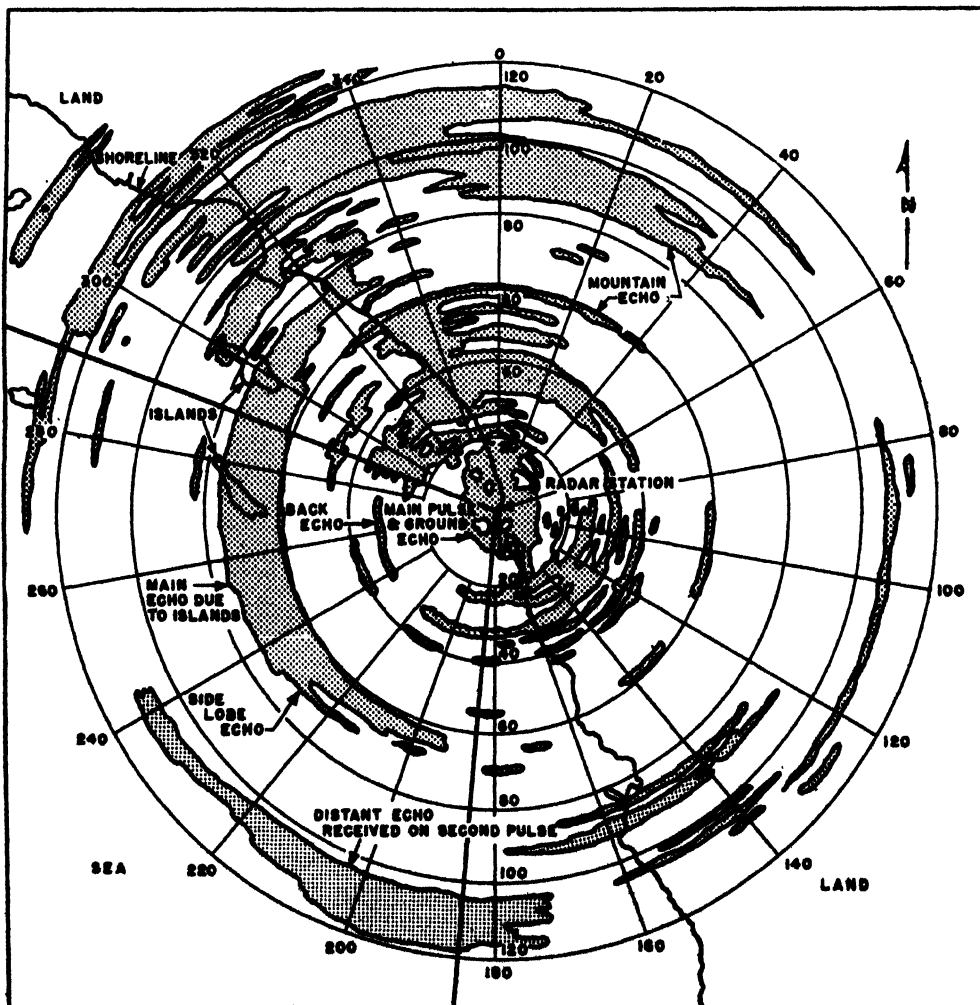
FIGURE 35. Permanent echo diagram.

the intervals in azimuth at which readings are to be made. The definition of the echoes will depend in part upon the beam width so that the narrow beam radars should be checked at closer azimuth intervals. Readings may be taken at intervals of 10° or 5° or even less depending upon the detail desired; in general an interval of about a fourth of the beam angle is sufficient. Permanent echo readings should be taken through 360° regardless of the sweep sector used, so that back and side echoes may be investigated also.

At each azimuth the range of all permanent echoes is recorded from zero out to the extreme range. The width of the main pulse and local ground echoes should be noted as well. Echoes one mile or less in width are recorded by a single reading at the center of the echo. Wider echoes are recorded by two readings, one at the left of the echo where the trace leaves the baseline and a second at the right where the trace returns. Adjacent echoes less than 1 mile apart are recorded as a single echo. Where the separation is greater, care should be taken not to lump echoes together.

For most purposes variations in amplitude may be disregarded. Amplitude is, however, sometimes recorded for a few azimuths of special interest such as those used for test flights or in tactically important regions.

To plot the data an overlay of a regional aeronautical map or other chart with a scale of 1 to 1,000,000 may be made showing some of the significant features as coastlines, islands, and cities. On this should be drawn radial azimuth lines every 10 degrees and range circles every 10 miles. The data are then marked on the chart as short lines, and these lines are connected as indicated by inspection. The enclosed areas may then be shaded lightly. If it is desired to represent amplitudes, a few equal amplitude contours may be shown within an echo area. More detail may be shown by plotting amplitude versus range on a rectangular graph for each azimuth.

The completed permanent echo diagram should be compared with a topographical map to check the degree of shielding obtained and the range and azimuth accuracy of the equipment and back and side lobe radiation effects. Care must be exercised in identifying the cause of an echo, as distant echoes may come in on the second or third sweep on the scope after the main pulse.

In Figure 35 is shown a permanent echo diagram which was selected for purposes of illustration rather than as an example of a good site. A few miles from the coast is an extensive range of mountains which are poorly shielded to the north. The large echo at 200° is due to a mountainous island 260 miles away.

Use of Permanent Echoes in Testing

Permanent echoes are useful for tuning the equipment, estimating the output and sensitivity, and checking the range and azimuth accuracy. While such observations may be used as an overall test of performance, care should be used in selecting the test echo and in interpreting the indications.

Careful tests have shown that, even though equipment performance is closely controlled, the strength of permanent echoes varies over a considerable range. It is noted further that indications from aircraft also vary, but there is little correlation with the changes in permanent echoes. Other tests show that, as the performance of the set is reduced, the maximum range for small targets is reduced at a much faster rate than for large targets. Thus a reduction of receiver sensitivity may cause weak echoes to disappear entirely without a noticeable effect on strong permanent echoes.

Permanent echoes vary for the following reasons:

1. Atmospheric changes affect both the direct and reflected rays. This may be due to a change in the amount of refraction from standard or in the degree of trapping. Under some conditions marked absorption may occur. The changes may occur slowly or fluctuate erratically, being most marked in connection with microwaves.

2. If the reflecting surface is the ocean, variation of the reflected ray may occur if the tide changes or the roughness of the surface becomes excessive.

3. Frequency variations will affect the echo from complex reflectors such as rugged terrain. Peaks which are separated in distance such that the returns from a single pulse overlap are said to be frequency sensitive. In the overlap portion the echo strength will depend upon the relative phase of the two returns. Thus if the pulse width is 10 μsec the wave train will be about 2 miles long. If there are peaks at 10 miles and 10¼ miles their echoes will appear as follows on an A scope:

10 to 10½ miles	near peak echo only
10½ to 12 miles	combined echo of both peaks
12 to 12½ miles	far peak echo only

The combined portion of the echo may have a height from zero to twice that of the individual echoes and usually fluctuates rapidly as the frequency drifts. A change of a half wavelength in the separation of the peaks will change the combined echo from maximum to minimum. This means that a frequency stability of the order of one part in a million is required for a steady combined echo.

Permanent echoes used for testing should therefore be (1) nearby but distinct from ground clutter and other echoes, (2) separated from the transmitter by rough nonreflecting land, (3) a single distinct target such as a steel tower, (4) weak in response, that is, comparable to that of a distant aircraft.

The range of echoes which come in on the second or third pulse may be estimated by adding one or

two times the length of the range scale to the observed range plus an allowance for the return trace time, usually several miles. To determine by test which sweep an echo is associated with, the pulse repetition rate should be changed, and the shift in range of the echo observed. Thus if the range scale is 200 miles long and the pulse rate is reduced 10 per cent, then a target at 250 miles which had been appearing at 48 miles would shift to an indicated range of 23 miles and could thus be distinguished from a 48-mile target that would shift to 43.2 miles.

Frequency-sensitive permanent echoes are not suitable for checking range accuracy. The frequency changes from maximum to minimum return are usually too small to be detected on a frequency meter, so that frequency-sensitive echoes are recognized chiefly by their unsteady appearance.

Azimuths may be determined to best accuracy by "beam splitting." This consists in turning the antenna slightly to one side of the maximum until the signal decreases to a predetermined level. The antenna is then turned past the maximum until the same level is reached and the two azimuths are averaged. When checking azimuth accuracy the possibility of horizontal diffraction due to a nearby hill should be considered.

Shielding

The principal device for control of fixed echoes is shielding. This means that the antenna is to be sited in such a way that distant hills are screened by a local obstruction. A local echo at say 3 miles, is combined with the main pulse or ground return, and the distant echo is weakened or eliminated entirely. In operating regions the loss of coverage may be more serious than the permanent echo, so shielding should be used with caution.

Rear areas which are not scanned should be well shielded so that back and side echoes do not interfere with targets in important tactical regions. Operation over such shielded sectors would be limited to high targets.

Construction of artificial shields made of poultry netting has been suggested in some cases, where the back radiation and side lobes were relatively strong. The very large size of such structures ordinarily renders them impractical. Most of the antennas using parabolas have a small back radiation, and permanent echo problems are much simpler.

In special cases it may be desirable to eliminate a particular echo from some obstacle without using shielding. This may be done by constructing a target of sheet metal on the side of the obstacle, spaced so that the target echo and obstacle echo are about 180° out of phase. This requires accurate alignment of the target (so that it is normal to the radiation to within 5° or less) and close control of the frequency.

It is also necessary that the area be adjusted so that the response of the target and obstacle are equal.

Prediction of Permanent Echoes

Permanent echoes may be determined by several methods:

1. Tests with the radar at the site.
2. Profile method.
3. Radar planning device [RPD].
4. Supersonic method.

The feasibility of moving the radar to the site to determine the permanent echoes is dependent on portability, accessibility, etc. Echoes obtained with one type of equipment may be very different from those from another type of radar with different directivity, frequency, and range.

The profile method, which will be described in detail below, involves a study of topographical maps and plotting the echoes according to their visibility and the amount of diffraction. A fairly difficult site may be handled in perhaps 8 man-hours. This method is adapted to long-range, low-frequency radars where diffraction and side and back lobe radiation are important. On microwave equipment fixed echo prediction is simpler and the profile method may be worked out in a few hours.

The RPD technique requires construction of a relief model of the terrain considered. A small light source is used to simulate the radar and the echoes are plotted as a result of a study of the areas illuminated. This method is adapted for short ranges and microwaves where the diffraction and side and back lobe radiation are small. Construction of a fairly difficult model may take a crew of men several days to a week, as a model should be accurate. Once completed, all possible sites or aspects from a plane or ship may be readily examined. Models of enemy areas may be used to predict the coverage of possible enemy sites, and evasive action may be planned. The RPD is well suited for training and briefing of air personnel. Kits are provided containing the light source, supports, etc. Darkroom facilities are required, and special processing of films is used to secure more realistic pictures.

The supersonic method requires a model made of sand, glass beads, etc., to be used under water. Such models are much easier to construct than the RPD type. Supersonic gear is used to send out pulses which are reflected like radar pulses and the echo is picked up and presented on a PPI scope. Photos may be taken of the scope picture, and the method may also be used for training and briefing. Special equipment is required, but the models may be made easily and the presentation is obtained direct on the PPI scope without further processing. This method is well adapted for training, as flight, changes in altitude, etc., may be simulated readily by movement

of the sonar head.

In general the profile method should be used on long waves or on microwaves where only a few sites are being considered. It is well adapted for the estimation of nonstandard atmospheric effects. For air- or ship-borne radar the RPD or supersonic methods are convenient because of the large number of aspects involved. It may be noted that the latter two methods should not be considered more exact than the profile method, as the principle of similitude does not apply unless all elements including the wavelength are changed in proportion. The principal difficulty is to secure a source which has the same radiation characteristics as the antenna system.

Prediction by Profile Method

The profile method will be described in detail. The discussion will refer chiefly to VHF radars in a mountainous terrain, but the methods have general application. The principal requirements are topographic maps of the surrounding area with a scale of 1 or 2 miles to the inch and a contour interval of 20 ft, although intervals up to 100 ft may be used. Maps with a scale of about 20 miles to the inch are needed for checking distant echoes. Regional aeronautical maps, with a scale of about 1 inch to 16 miles and 1,000-ft contours, are suitable as the height of prominent peaks is indicated.

From the maps, profiles are prepared for various azimuths about the radar station. The first mile or so should be plotted accurately, and at greater distances the critical points such as hills and breaks should receive the most attention. A convenient scale is 2 miles to the inch for range and 500 ft to the inch for elevation. The distances to which the profile should be plotted is a matter of judgment, but it should be extended to perhaps 20 miles, or further if there is doubt.

On each profile is drawn the tangent line from the center of the antenna to the point on the profile which determines the shielding, as in Figure 36.
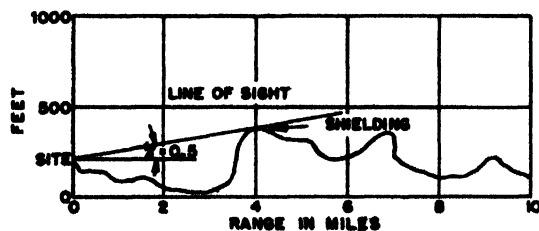
FIGURE 36. Typical profile. (Note: γ in degrees).

This is the line-of-sight curve; it is drawn for each azimuth, and the vertical angle γ is marked on the profile. If the angle is below the horizontal it is negative, and caution must be used on high sites not to exceed the limiting shielding angle of the radar horizon. This is given by the expression

$$\gamma = -0.0108 \sqrt{2h_1}, \qquad (45)$$

where γ is the angle between the effective horizon and the horizontal at the antenna in degrees and h_1 is the height of the center of the antenna in feet.

The line of sight is actually curved, as explained in the section on visibility problems, but for ranges up to 10 miles the error in using a straight line is small. For longer distances the dip QX as computed from equation (5) should be considered. More convenient for this purpose are the curves of the line of sight for various angles which are calculated from Figure 37. Standard refraction is taken into account by use of $\frac{4}{3} a$ instead of a for the earth's radius,

$$\frac{4}{3} a = 1.33 \times 3,960 = 5,280,$$

$$h_2 - h_1 = 5,280d \tan \gamma + \frac{d^2}{2}, \qquad (46)$$

with h_1 and h_2 in feet and d in miles. Above 10°, or where the shielding is distant, equation (8) should be used.
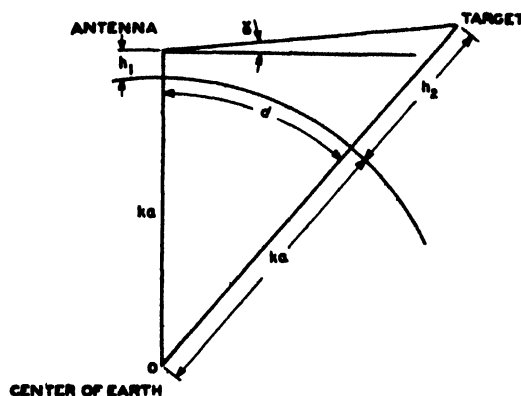
FIGURE 37. Line-of-sight geometry.

These curves are plotted in Figures 38 and 39, and their use is illustrated in Figure 36. The center of the antenna is at 200-ft elevation, and the height of the shielding ridge 4 miles away is 400 ft. For a 200-ft rise in 4 miles the angle is found from Figure 38 to be 0.5 degree. This curve can then be used to determine the height of the shielded region at other ranges. Thus the range at which the shielded region is 4,000 ft high for the case considered is found from Figure 39 by using $h_2 - h_1 = 4,000 - 200 = 3,800$ ft for height and the ½-degree curve, giving 53 miles.

It is desirable to be able to estimate diffraction effects in a simple fashion suited to the approximate nature of this kind of work. As shown in Section 15.4.8 the field intensity varies in a rather complicated manner with the diffracting angle θ_d and the distance of the shield d_1 [Figure 7 and equation (10)]. In Figure 40 is plotted the relative field intensity compared to that obtained without a shield for
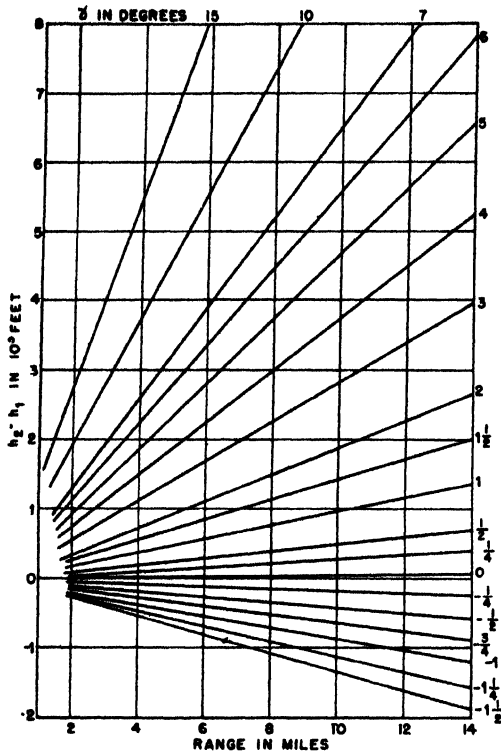
FIGURE 38. Line-of-sight curves.
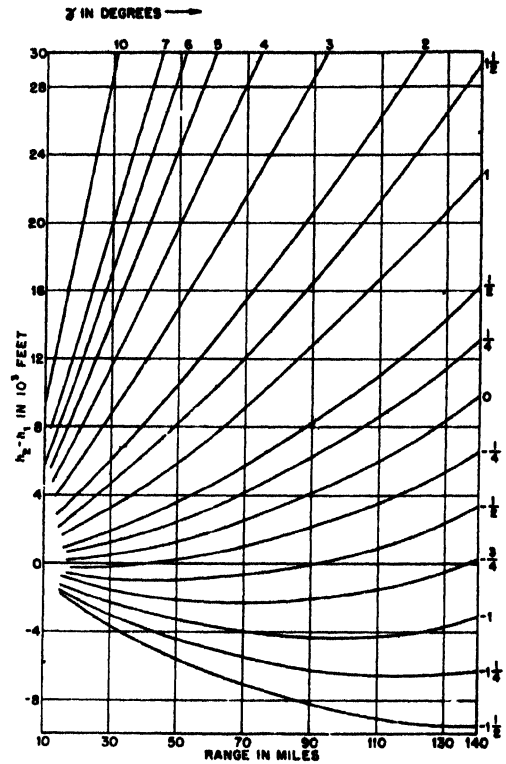
FIGURE 39. Line-of-sight curves.

shields at several distances. This graph is intended for 200 mc but may be used on other frequencies by changing d_1 in proportion to the change in λ. It enables one to make an estimate of the effectiveness of a shield. Thus if a shield is 1 mile away it may be neglected for values of θ_d in excess of $+3°$. Likewise

objects below $-3°$ in the shadow region would give weak echoes in most cases. For intermediate angles the relative intensity may be read from the curve. For shields closer than 0.1 mile the methods discussed on pages 84 - 86 should be employed.

Figure 15 shows that the relative intensity of a
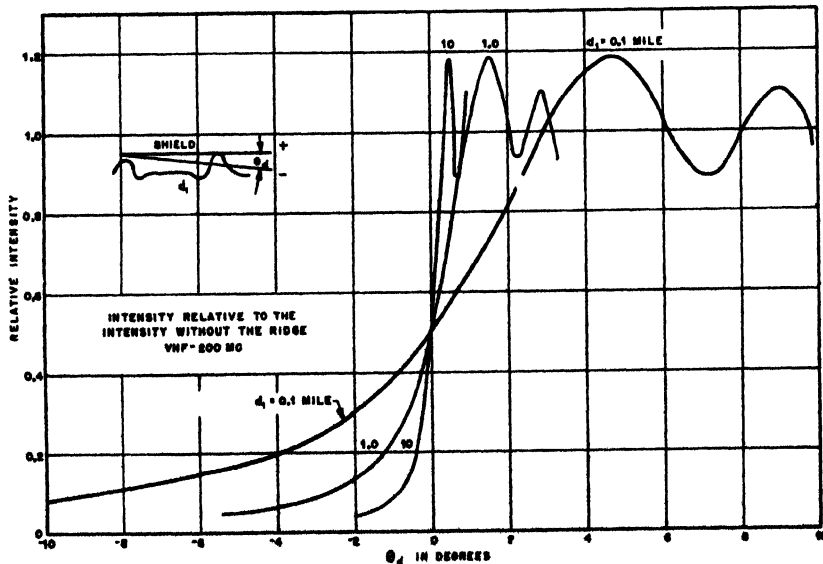
FIGURE 40. Diffraction over a ridge. (200 mc) (For other frequencies change d_1 in proportion to the change in wavelength.)

diffracted wave is virtually constant for a given angle when the distance from the edge is large. Equation (22) may then be written in the form

$$v = \frac{\theta_d}{\sqrt{\dfrac{\lambda}{2d_1}}} \qquad (47)$$

where θ_d is in radians (1 radian = 57.3°) measured from the geometrical shadow line (Figure 7) and d_1 is in the same units as λ. This equation is approximate, and the error is of the order of a/b.

Where the shield consists of several ridges close together, an equivalent shield is used instead of successive shields. The height and distance of the equivalent shield is found by constructing a triangle between the radar and the reflecting object which encloses the shielding ridges. The apex of this triangle is then treated as though it were the diffracting edge. In Figure 41 H and d_1 are the quantities to be used in equations (10) and (47).

The general procedure to be followed in preparing
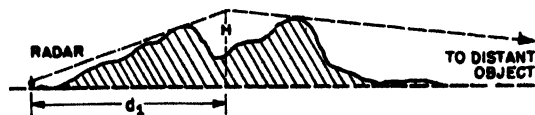
FIGURE 41. The equivalent shield.

a prediction of permanent echoes will now be outlined. By examining a topographical sheet the azimuths are determined at which profiles should be prepared. This will normally be about every 10 degrees. Where the shielding is obviously good the interval may be 20 degrees, but where the terrain is questionable such as a region of low hills the profiles should be taken at 5-degree intervals. The profiles are prepared and the angle of the line of sight determined as described above.

The next step is to make an overlay of a map of scale 1 to 1,000,000. The principal features as coastline, towns, and rivers are sketched in to aid in reading the completed chart. On this is drawn a polar coordinate system with azimuths marked every 10 degrees and range circles every 10 miles out to the full range of the indicator.

On the overlay are now drawn the coverage contour lines. These lines represent the limits of the heights of the shielded regions. Targets or mountains below these coverage contours will not be visible except by diffraction, and targets above the contours are in line of sight and receive direct radiation. For each azimuth and the corresponding angle of sight (Figure 36) the ranges are plotted for various contour heights as 1,000, 5,000, 10,000, and 15,000 feet. Where these coverage contour lines are close together the shielding is good but the coverage is poor; where the lines are widely separated, the

shielding is weak, and toward the sea there is no shielding except by the horizon.

With the coverage contour diagram superimposed on a map, the peaks exposed to radiation may be noted. The extent of the echoes due to these peaks depends on the horizontal radiation pattern and pulse width. The horizontal beam width is only a very rough measure of the width of an echo, and some other angle usually between the half-power points and the nulls will determine the echo width. The angle may be estimated by considering the range and size of the peak. The extension of the echo in range will be at least as great as the pulse width in miles, which as it appears on the indicator is about 0.1 mile per μsec. Actual echoes are usually much wider than this, as all of the exposed hill sends back an echo.

The echoes are then sketched in, based on inspection of the profiles. The plotter's judgment is a very important factor, but the following rules may be used as a guide.

1. Shade in a circle for the main pulse several miles wide, depending on the pulse width and local return.

2. Consider each profile in turn and for each peak or hillside in front of the shielding plot an echo on the main and all sidelobes.

3. A series of sharp hills within the shielding region should be plotted as a single echo rather than a number of echoes.

4. The inner edge of an echo should be at the same range as the hill, and its extension depends on the slope of the hill and the pulse width, which may be several miles with some sets.

5. In case of doubt plot the echo.

6. Peaks beyond the shield may be in the diffraction region and the relative intensity of the radiation at these peaks will then be obtained from Figure 40 as described above.

7. If the mountain is large enough to intercept several lobes, the interference effects may be ignored. The echo strength may be estimated roughly as proportional to the cross-sectional area of the mountain, the relative intensity of the radiation from Figure 40, and the inverse square of the distance. For side and back lobes an additional factor is required.

8. The 1 to 1,000,000 scale map should be carefully checked to make sure that no peaks are missed in between the azimuth considered or at extreme ranges.

In the above method much is left to the judgment of the plotter but it will be found that with experience a reasonably good estimate of permanent echoes may be made from a map.

Example 8. Profile Method. A detailed example of a difficult site will be worked out, and comparison will be made with the actual recorded echoes. The site selected is that of Figure 35. The characteristics of the SCR-270B radar are given in Table 2.

TABLE 2. Type SCR-270B. Characteristics of antenna pattern.

	Horizontal pol.	Vertical pol.
Half-power beam angle	26°	6.5°
First null angle	40°	14°
Secondary lobe angle	45°	.....
Secondary null angle	90°	....
Secondary lobe angle	5%	....
Back radiation	4%	....

Other characteristics of this set are as follows:

Pulse width	30 μsec = 3 miles
Nominal range	150 miles
Sweep sector	185° to 290°
Elevation: center of antenna	387 ft

From these data may be calculated the relative echo strengths of mountains at various distances and the relative side and back echoes. A reference value of 1.0 is taken for the main echo from a typical mountain 100 miles distant, and the relative intensity from Figure 40 is taken equal to 1.0. It is estimated that all echoes whose strength compared to the reference value is over 0.25 will be strong enough to obscure targets. Thus the back echo of a mountain 10 miles away in a diffraction region where the relative strength is 0.5 would have an echo value of $(100/10)^2 \times 0.5 \times 0.04 = 2.0$ and should be plotted since it exceeds 0.25.

A table may be constructed for the main, side, and back lobes (M, S, B) for various distances and degrees of diffraction to show which echoes should be plotted. Table 3 is such a table, corresponding to a reference strength equal to 0.25. This table will apply only for the conditions of this example.

In Figure 42 is shown a topographical map of the
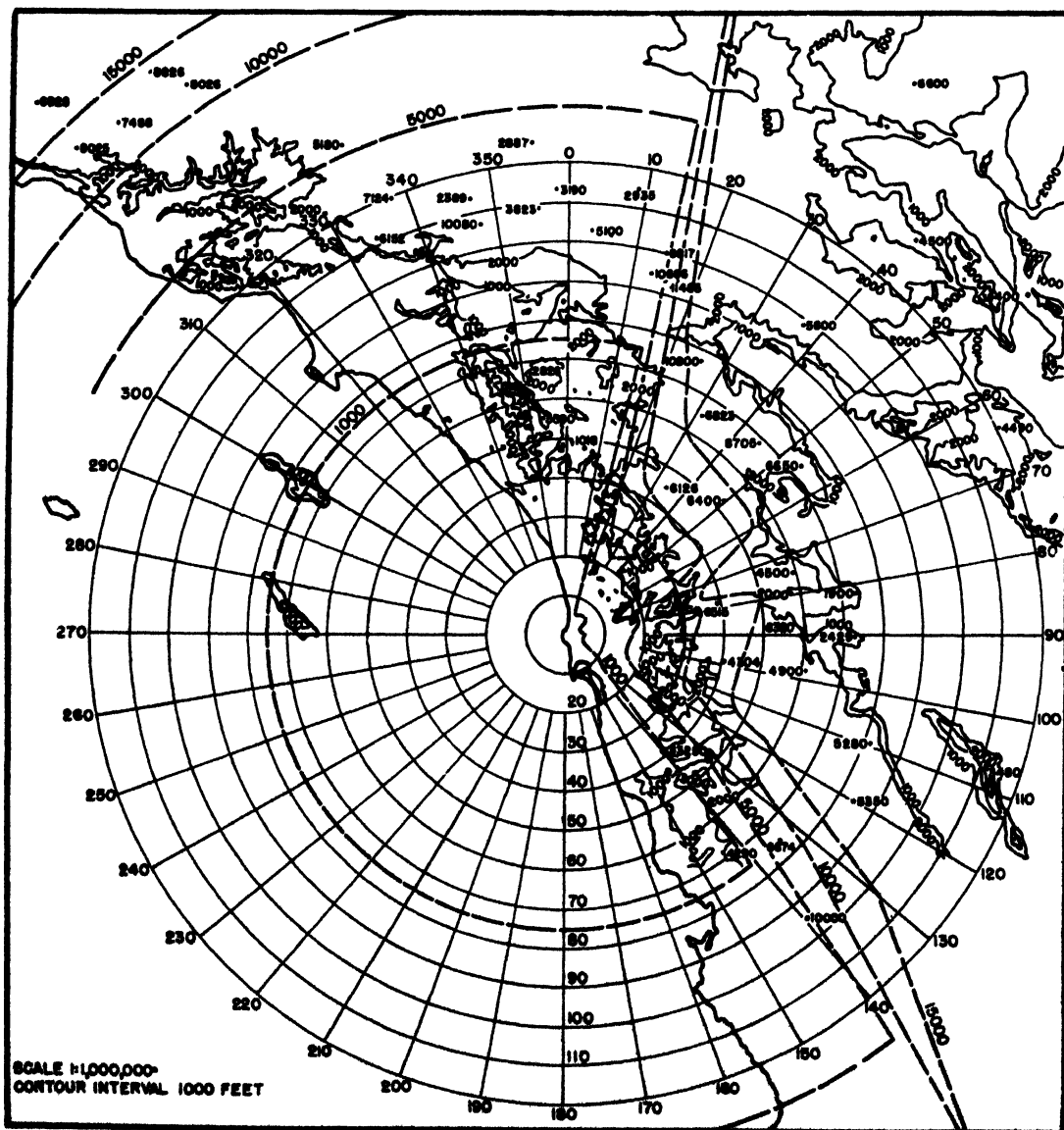
FIGURE 42. Topographical map for Example 8.

TABLE 3. Prediction of permanent echoes.*

Distance in miles	Relative intensities from Figure 40.						
	1.18	1.00	0.75	0.50	0.25	0.10	0.03
1	MSB	MSB	MSB	MSB	MSB	MSB	MSB
10	MSB	MSB	MSB	MSB	MSB	MSB	M
20	MSB	MSB	MSB	MSB	MSB	M	M
50	M	M	M	M	M	M	..
100	M	M	M	M	M	..	..
200	M	M	..	..	..	..	..

*This table will apply only for the conditions of Example 8.

area. Contours are drawn for the first few thousand feet, and prominent peaks are indicated. From topographical sheets of a 20-ft interval and a scale of 2 in. to the mile the profiles of Figures 43 and 44 are obtained. From the center of the antenna to the "effective" shielding, the line of sight has been drawn and the angle of the line of sight noted. In some cases, as at 20 degrees (Figure 43) a near sharp ridge is not considered an effective shield because of the large diffraction around such obstacles. The map is inspected between the azimuths used and the horizontal limit of shielding of a ridge noted. Thus the shielding ridge on 120 degrees (Figure 44) is found
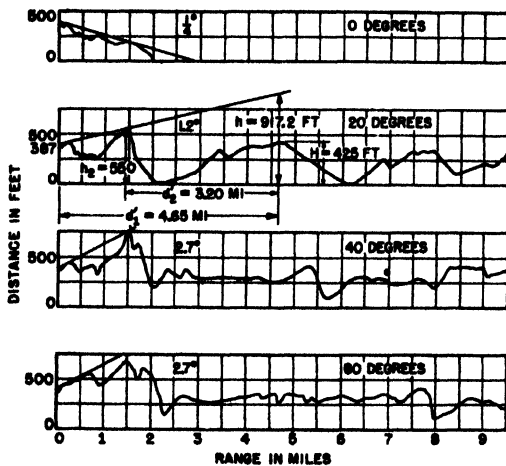
FIGURE 43. Profiles for Example 8.

to drop off at 138 degrees. From the curves of Figures 38 and 39 are read the ranges for $h_2 - h_1 =$ 1,000, 5,000, 10,000, and 15,000 ft for the line-of-sight angles at various azimuths. These points are plotted on Figure 42; they are connected by heavy dashed lines and are the coverage contours.

In Figure 45 are plotted the predicted echoes. It will be noted that the shielding to the east is very good and most of the mountains are not visible. To the north the numerous mountains are unshielded and give rise to many echoes which extend into the search sector to the west. The islands are inherently bad and cannot be shielded without drastic loss of coverage. In some cases, as along azimuth 345°, ridges which cause large echoes shield more distant ridges. The broken terrain in this region is taken to
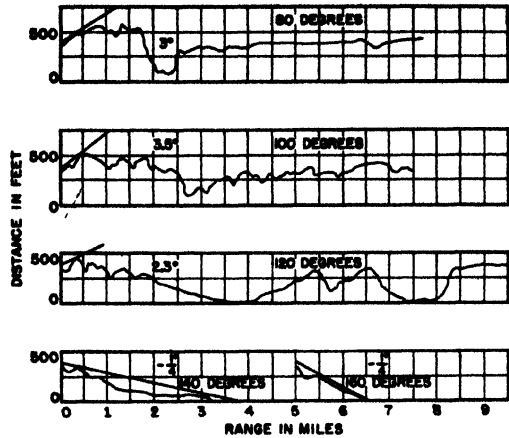
FIGURE 44. Profiles for Example 8.

give one large echo rather than a number of small echoes. In most cases the simple rules for plotting echoes may be applied directly.

Where diffraction is involved the procedure should be more detailed. In Figure 43 azimuth 20° will be examined to determine the visibility of the hill at 4.65 miles. The following data are obtained from the profile.

$$h_1 = 387 \text{ ft}; d'_1 - d'_2 = 1.45 \text{ miles}$$
$$h_2 = 550 \text{ ft}; d'_2 = 3.20 \text{ miles}$$
$$H = 425 \text{ ft}; d'_1 = 4.65 \text{ miles}$$

From equation (8):

$$h = \frac{4.65 \times 550 - 3.20 \times 387}{4.65 - 3.20} + \frac{4.65 \times 3.20}{2}$$
$$= 917.2 \text{ ft}.$$

From equation (10):

$$\theta_d = \frac{425 - 917.2}{5,280 \times 4.65} \times 57.3 = -1.15°.$$

From Figure 40 the intensity is found to be 15 per cent. At the very short range of this hill a strong echo would be expected at this intensity, and all lobes would be plotted.

At 138.5° azimuth and 160 miles is a 10,000-ft mountain (not shown in any figure). The data for this case are:

$$h_1 = 387 \text{ ft}; d'_1 - d'_2 = 0.27 \text{ miles}$$
$$h_2 = 380 \text{ ft}; d'_2 = 160 \text{ miles approximately}$$
$$H = 10,000 \text{ ft}; d'_1 = 160 \text{ miles approximately}$$

$$h = \frac{160 \times 380 - 160 \times 387}{0.27} + \frac{160 \times 160}{2}$$
$$= 16,950 \text{ ft}.$$

$$\theta_d = \frac{10,000 - 16.950}{5,280 \times 160} \times 57.3 = -0.472°.$$

From Figure 40 the relative intensity is 43 per cent. A main lobe echo is plotted on the second sweep
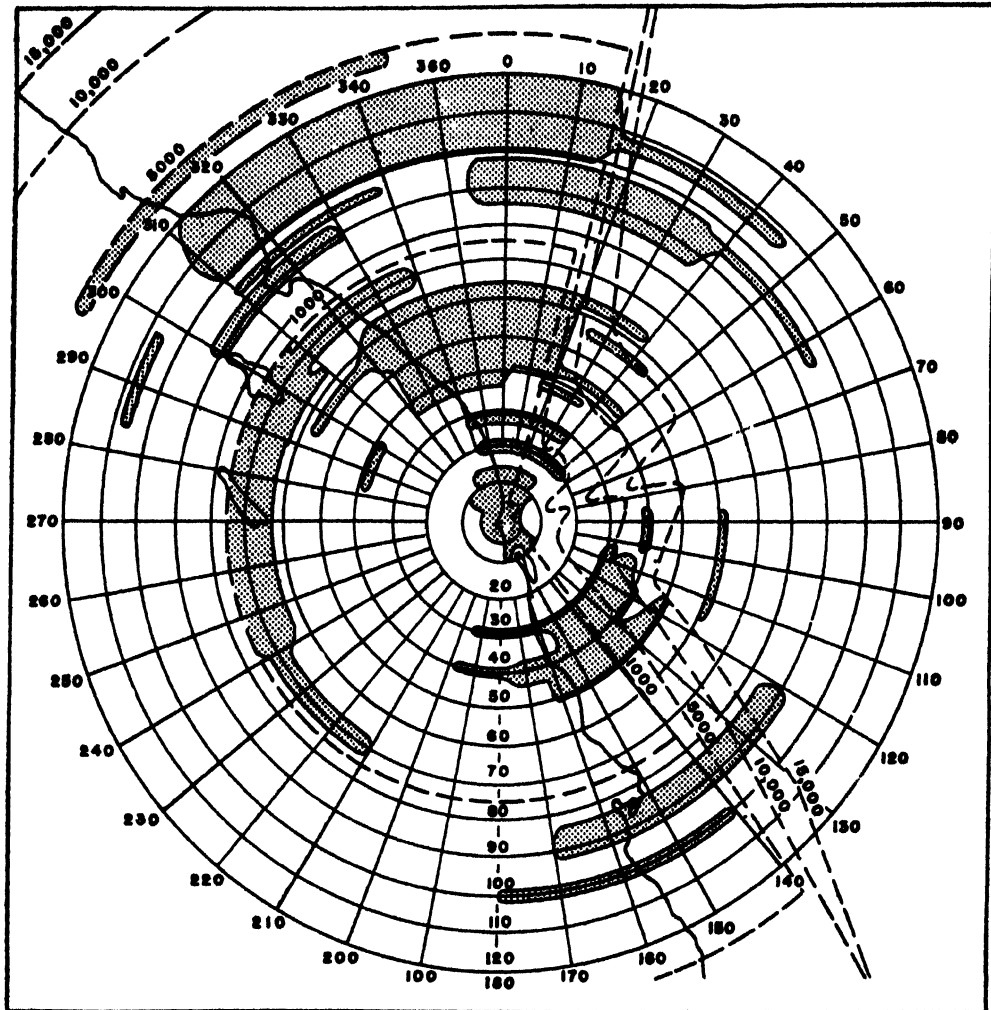
FIGURE 45. Predicted permanent echoes. (Example 8.)

at 10 miles since the first sweep is only 150 miles.

In Figure 35 is shown a large echo at 110 miles from 175 to 242 degrees. This is received only when there is trapping, and the size of this echo indicates the unusual weather conditions at the time the data were taken. This echo is due to a mountainous island 260 miles away and about 5,000 ft high. There is no shielding except from the curvature of the earth. The relative intensity compared to the free space intensity computed from the formulas for the diffractive region (not given here) is 0.5 per cent. This echo would not ordinarily be plotted in spite of the large area of the mountain side.

In correlating the predicted and actual fixed echo diagrams, Figures 45 and 35 respectively, it will be noted that the degree of success achieved depends on the effort expended. Numerous small echoes were not predicted, but these are unimportant from an operating standpoint. "Permanent" echoes vary over wide limits with changes in weather conditions and

efficiency of the equipment so that only a fair agreement should be expected in their predictions.

Microwave Permanent Echoes

With microwave equipment a simple analysis of the terrain is generally sufficient. The beam may be treated virtually as a searchlight, as the back radiation and diffraction effects are small. Trapping is likely to be severe and in some regions it is the controlling factor. Sea or land clutters are important and the extent of such echoes may be estimated from equation (16).

Microwave sets because of their narrow beamwidth, high resolution, and PPI presentation are well adapted to navigational uses. Coastlines may be readily identified, and ships near land may accurately determine their position. Over land it is frequently difficult to correlate a PPI picture with a map. In many cases it may be very desirable to be able to locate terrain features accurately.

The presence of some distinctive echo is of great assistance in orientation of the picture, but scope distortions and the nature of the echoes cause much confusion. It is therefore desirable to be able to correct the distortions and to be able to prepare a radar map which shows the terrain features likely to contribute to the observed pattern.

The PPI distortions are due to the beamwidth, range marker errors, and nonlinear sweep. The width of the beam causes objects to appear wider than they are, as discussed in preceding sections. The range marker errors may be determined by calibration with a precision-type calibrator. By preparing a cardboard scale to line up with the range pips the correct ranges of echoes may be obtained. Because the sweep usually takes about 15 μsec to attain a steady speed the pattern is displaced inward with respect to the map. This may be compensated in part by adjusting the centering control so that at least one of the range markers is moved out radially to its true range. The pattern will then show a central hole, and the first half mile will be displaced from its true position, but the pattern as a whole will be more accurate.

For construction of the radar map it is desirable to have topographic sheets of a scale of 1 to 20,000 which show modern structures. Aerial photographs are also useful. Map matching is done by adjusting the sweep length and centering controls with major changes in scale made photographically. To eliminate detail of little interest it is desirable to ink in only those contours which correspond to equal increments of radar range based on the curved surface of the earth. That is, the retraced contour intervals should form a sequence of squared numbers (1, 4, 9, 16, 25 $\cdots n^2$), for example, 20, 80, 180, 320, and 500 ft. The amount of distortion to introduce into the radar map is obtained from the range correction scale and the shift of the PPI center. For each azimuth considered the map is shifted to compensate for the centering error, and the corrected range scale is used to lay off distance.

THE CALCULATION OF VERTICAL COVERAGE

Introduction

The computation of vertical coverage diagrams in the optical region consists essentially of adding two vectors, the contributions of the direct and reflected waves, which have been modified by earth curvature, antenna directivity, etc. The actual computation of the contours of constant field strength tends to be laborious because of the implicit nature of the parameters. The problem may be formulated in a rigorous, general manner, but the solution is likely to be unwieldy.

For field purposes where high accuracy is not required, a method of computing vertical lobe patterns is desired that is direct, does not require excessive calculations, provides a simple physical interpretation of terrain effects, and is flexible. The methods presented here are designed to meet these requirements, and the computer may readily accommodate the labor of calculations to the required accuracy and the complexity of the problem.

The path difference of the direct and reflected rays, the distance of the reflection point, and the vertical angle are functions of each other, while the reflection coefficient, the divergence factor, and other factors depend on the vertical angle. It is therefore desirable to examine the problem in a general way to determine what simplifications may be introduced.

With microwaves the reflecting surface must be quite smooth to be effective. Thus by equation (16) for the S band and an angle of 1 degree the roughness must be less than 15 in. if the reflection is to be of much assistance. The rolling character of sea waves makes a substantial variation in signal strength so that the reliable range is only slightly greater than that of the direct wave alone. Also highly directive antennas are commonly used with microwave radars. These factors reduce the magnitude of the interference effects. The fineness of the structure of a microwave pattern and the relatively weak reflection effects commonly encountered therefore render it a useful approximation to deal with the direct wave pattern only for most purposes.

Fire control and searchlight radars normally operate at high angles so that they also are mainly concerned with the direct wave. The GCI and other low-sited radars have their reflection areas within a mile of the antenna so that earth curvature may be ignored, which means a considerable simplification. The case which requires the most careful consideration is early warning, VHF, high-sited radar which is dependent on the reflected wave for much of its performance. A careful analysis of all factors involved is therefore usually required. Prepared diagrams for various heights and wavelengths must be considered carefully before being used, as local terrain features may radically alter the lobe pattern.

The accuracy and detail desired and the type of site influence the amount of calculation involved. With a low-sited VHF radar only a few lobes are formed so that the shape and location of the lobes is of interest. With a high-sited VHF radar the lobes are numerous and the gaps are small so that there is little likelihood of losing a target in a null area or of being able to associate an echo with a particular lobe. In this case the envelope of the lobes is of particular interest.

The high-power microwave radars are best suited for vital areas with high traffic density. However, for most purposes the basic long-range, early warning radars used by the ground forces operate in the VHF band. They are normally sited high, that is several hundred feet and up, in order to secure low lobe
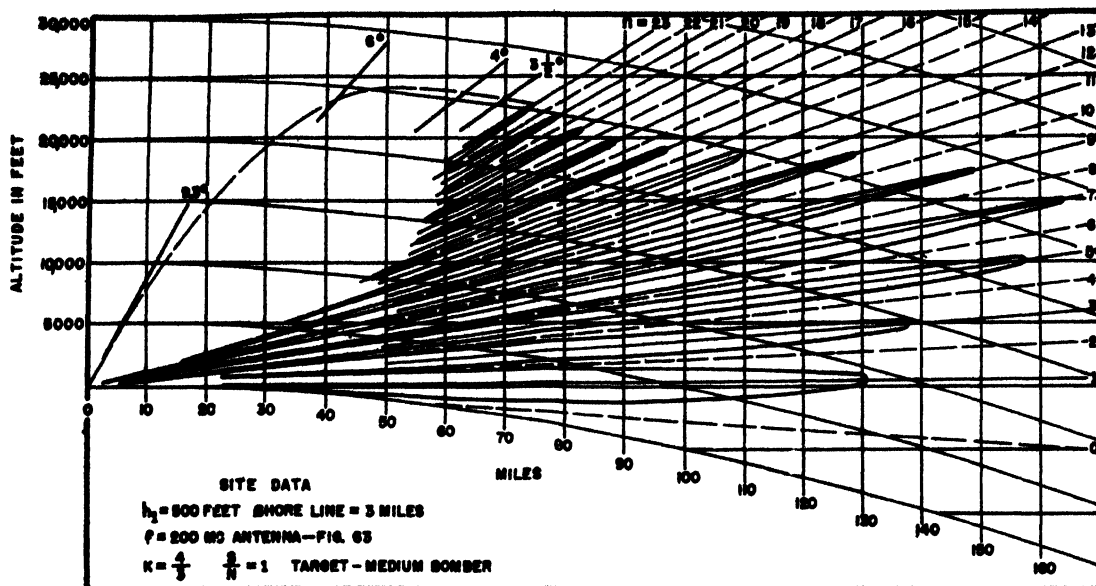
FIGURE 46. Vertical lobe diagram.

angles and numerous lobes. The need for good rein-
forcement and tactical considerations lead to the
use of the sea as a reflecting surface where feasible.
The general high-sited radar problem will be ana-
lyzed in detail, and the use of approximate, simplified
methods of calculation will be described where
applicable.

The Vertical Coverage Diagram

The object of test flights and field intensity
calculations is the construction of the vertical cover-
age diagram. A typical diagram for a long-range,
early warning, VHF radar is shown in Figure 46.
The contours or lobes on this diagram represent the
locus of all points in space along a particular azimuth
where an incoming plane of standard type, usually
a twin engine medium bomber, will produce a mini-
mum detectable signal. A minimum detectable signal
is ordinarily taken to be one that has a signal-to-noise
ratio of unity. This may also be expressed in other
terms such as field intensity or voltage at the
receiver terminals. For other types of planes, or a
number of planes, or different aspects of the same
plane, the lobe pattern has a different size.

It will be noted that the vertical scale is nearly
10 times as great as the horizontal scale, causing a
marked distortion in angles and crowding of angles
above 10 degrees. The lines of constant altitude are
parabolas, owing to the curvature of the earth. Their
shape is given by the equation

$$y = h - \frac{d^2 \cdot 5,280}{2ka}. \qquad (48)$$

Here $y =$ the ordinate measured from the horizontal
line through zero;

$h =$ the height of the curve at zero range, in
feet;

$d =$ distance along the earth in miles;

$a =$ radius of the earth in miles;

$ka =$ equivalent earth radius.
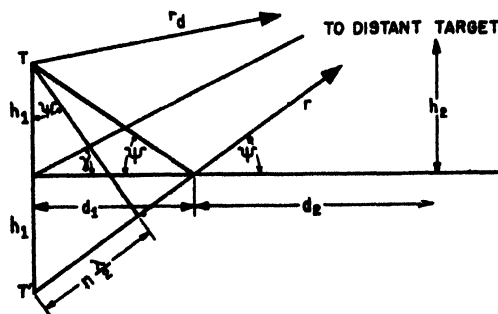
FIGURE 47. Flat earth ray diagram.

For standard conditions k is taken as $\frac{4}{3}$. At 40°
latitude the radius of the earth is 3,960 miles. Sub-
stituting in equation (48) gives the convenient
relation:

$$y = h - \frac{d^2}{2}, \qquad (49)$$

with y and h in feet, and d in miles.

Thus in Figure 46 a medium bomber coming in
at 5,000 ft would first be detected at 108 miles, the
signal would increase in strength, reaching a maxi-
mum around 96 miles, and then decrease and be lost
at 84 miles. In the null region between 84 and 77
miles there would be no detection. Similar regions
of detection and nulls would be encountered as the
plane came in closer. The nulls do not come into
the origin when the direct and reflected rays are

unequal. This gap filling is secured at the price of shorter lobes. Above 3 degrees the lobes cannot be distinguished from the nulls.

Only lobes due to the main free space lobe of the antenna pattern are ordinarily plotted, as targets higher than about 10 degrees are of little interest to an early warning radar. Because most detection occurs at angles under 2 or 3 degrees, no distinction will be made between slant range and horizontal range.

The calculation of the coverage diagram will be approached in successive steps. The first step will consist of calculation of the angular position of the lobe maxima and minima. This will be done in three different degrees of approximation corresponding to different situations encountered in practice. The next step is the calculation of the length and shape of the lobes themselves, which is given in a later section.

Flat Earth Lobe Angle Calculations

When the reflection point is so close that earth curvature may be ignored, the rays may be drawn as in Figure 47. The transmitter T has the center of the antenna at height h_1 above the horizontal reflecting surface. The antenna is assumed to have horizontal polarization; that is, the dipoles are parallel to the reflecting plane and perpendicular to the direct ray r_d. The target height is h_2. Both h_1 and h_2 are several wavelengths or more, and r_d is so large that the field at the target falls off as $1/r_d$. The image of the antenna is at T' at a distance h_1 below the reflector. The length of the ray from T' is r.

The coefficient of reflection is ρ, and the phase lag at reflection is ϕ. The electric field strength due to the combined direct and reflected waves ($r_d \sim r$) may be written as

$$E = \frac{E_1}{r} \sqrt{1 + \rho^2 + 2\rho \cos(\phi + \delta)} \, . \quad (50)$$

where $\delta = 2\pi \dfrac{\Delta}{\lambda}$ = phase lag due to the path difference,

$\Delta = r - r_d$ = path difference of the direct and reflected rays,

E_1 = the field strength at unit distance.

For horizontal polarization and small angles ρ is unity and ϕ is 180 degrees and equation (50) reduces to

$$E = \frac{2E_1}{r} \sin \frac{1}{2}\delta \, ,$$

$$= \frac{2E_1}{r} \sin \frac{\pi\Delta}{\lambda} \, . \quad (51)$$

In the construction of a vertical coverage diagram it is important to be able to draw the lines of constant path difference. Of special interest are the lines of

maxima in the center of the lobes and the lines of minima or nulls. These lines correspond to

$$\Delta = r - r_d = \text{constant} \, . \quad (52)$$

For the case of a flat earth these lines are by definition confocal hyperbolae with T and T' as foci and Δ as the major axis. This is shown in Figure 48 for a target at short range. In a typical case β will be
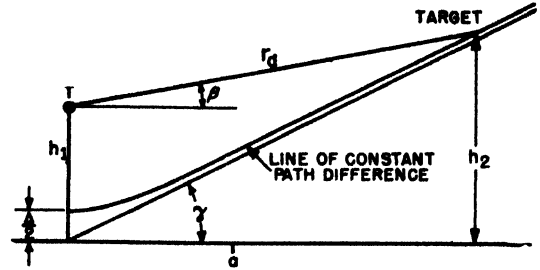
FIGURE 48. Constant path difference hyperbola.

positive and approximately equal to γ. From geometry

$$r_d = \frac{4h_1^2 - \Delta^2}{2\Delta - 4h_1 \sin \beta} \, . \quad (53)$$

When r_d is very large compared with h_1 the angle γ is equal to β, and the denominator of equation (53) is practically zero, giving

$$\sin \gamma \cong \frac{\Delta}{2h_1} \, . \quad (54)$$

Using equation (51) with the $(\pi\Delta)/\lambda = \pi/2$, the lobe maxima are given by

$$\Delta = n\frac{\lambda}{2} \, , \quad (55)$$

where $n = 1, 3, 5 \cdots$. Minima are given by values of $n = 0, 2, 4, 6, \cdots$.

Substituting in equation (54)

$$\sin \gamma = \frac{n\lambda}{4h_1} \, , \quad (56)$$

or to a sufficient approximation

$$\gamma = \frac{n\lambda}{4h_1} \, . \quad (57)$$

Here γ = the angle of elevation of the target referred to the horizontal at the ground below the antenna, in radians;

n = number of half-wavelengths · difference between the direct and indirect paths. $n = 1, 3, 5$, etc., for maxima of lobe number 1, 2, 3, $\cdots$ $(n + 1)/2$ counting from the reflector up. $n = 0, 2, 4, 6$, etc., for minima of null numbers 1, 2, 3, 4, $\cdots$ $(n + 2)/2$;

h_1 = the height of the center of the antenna above the reflector;

λ = wavelength;

with h_1 and λ in the same units.

From Figure 47 it follows that d_1, the distance to the reflection point, is given by

$$d_1 = \frac{h_1}{\tan \Psi},$$

or taking $\tan \Psi = \sin \Psi = \gamma$ (which may be done provided d_1 is small enough compared to d_2 and large compared to h_1) and substituting in equation (57),

$$d_1 = \frac{4h_1^2}{n\lambda}. \tag{58}$$

Here d_1, h_1, and λ must be expressed in the same units·

For high sites and distant targets the angle γ becomes smaller, and the approximation involved in equations (57) and (58) requiring d_1 to be small compared to d_2 becomes worse. In Table 4 are listed the minimum values that $n\lambda$ may have for an error of 1 per cent or less in equation (57) at different antenna heights. Also is given the minimum value

TABLE 4   One per cent error in γ.

h_1, ft	Minimum γ°	Minimum $n\lambda$, ft
400	1.5	43
200	1.1	15
100	0.8	6
50	0.6	2
15	0.3	0.3

of γ corresponding to $n\lambda$. Thus equation (57) when used on a 100-ft site at 100 mc ($\lambda = 9.84$ ft) will give values which are in error by less than 1 per cent for all lobes and for angles above 0.8 degree. If the 100-ft site operated at 1,000 mc ($\lambda = 0.98$ ft) the minimum value of n would be 6 corresponding to the fourth null. The error in γ is always positive and increases rapidly with antenna height, and at a height of 1,000 ft and a frequency of 100 mc the formula is incorrect for all angles of interest. At distances such that the earth curvature drop is comparable to h_1, equation (57) does not even give the correct order of magnitude for γ.

Examples 9 and 10. Flat Earth Lobe Angle Computations. Lobe angles for two cases will be computed, Example 9, a 200-mc set at 15 ft and Example 10, a 500-mc set at 50 ft.

	Example 9	*Example 10*
$\lambda = \frac{300}{200} \times 3.28 = 4.92$ ft		$\lambda = 1.97$ ft

For $n = 1$ (first lobe)

$\gamma = \frac{1 \times 4.92}{4 \times 15} \times 57.3 = 4.7°$ $\gamma = 0.564°$

$d_1 = \frac{4 \times (15)^2}{1 \times 4.92} = 183$ ft $d_1 = 5{,}080$ ft

In practice some of the lobes listed for Example 9 may be absent because of nulls in the antenna pattern. The angle listed for the first lobe of Example 10 is slightly over 1 per cent too large.

TABLE 5.   Lobe angle and distance to reflection point.

n	Example 9		Example 10	
	γ, degrees	d_1, ft	γ, degrees	d_1, ft
1 (lobe 1)	4.7	183.0	0.56	5080
2 (null 2)	9.4	91.5	1.13	2540
3 (lobe 2)	14.1	61.0	1.69	1693
4 (null 3)	18.8	45.7	2.26	1270
5 (lobe 3)	23.5	36.6	2.82	1016

Lobe Angles Corrected
for Standard Earth Curvature

Equation (57) may be modified to include the effect of earth curvature approximately and to give the lobe angles for the majority of sites with acceptable accuracy.

For antennas several hundred or more feet high, d_1 as given by equation (58) may be large enough so that the earth curvature drop is appreciable. In Figure 49 is shown a transmitter of height h_1 above the horizontal plane GH. The radius of the standard earth is ka. At D, the center of the reflection area for the lobe considered, is drawn a tangent plane CDE, which intersects h_1 at a distance h'_1 below the center of the antenna and which will be considered the equivalent antenna height. This then is the part of h_1 which determines the angle γ' which the lobe center line CL makes with the tangent plane CDE. Subtracting from γ' the angle θ which
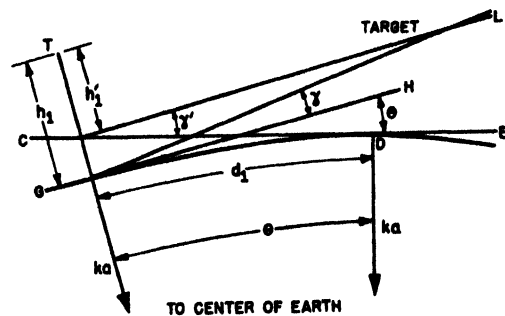
FIGURE 49. Lobe angles corrected for earth curvature.

the tangent plane CDE makes with the horizontal at the base of the antenna GH, the lobe angle γ referred to the horizontal at the antenna is obtained. From equation (49) it follows that

$$h_1' = h_1 - \frac{d_1^2}{2}. \tag{59}$$

Here h_1' and h_1 are expressed in feet, d_1 in miles, and k is assumed to be ⅘.

This height h_1' is the portion of h_1 that is effective in connection with the plane CDE and when substituted in equation (57) gives the angle γ'.

$$\gamma' = \frac{n\lambda}{4h_1'} = \frac{n\lambda}{4\left(h_1 - \frac{d_1^2}{2}\right)}. \tag{60}$$

Since the earth's radius ka is perpendicular to GH and CDE, the tangent angle is θ. It is always negative:

$$\theta = -\frac{d_1}{ka} = -\frac{d_1}{5,280}, \qquad (61)$$

$$\gamma = \gamma' + \theta = -\frac{n\lambda}{4\left(h_1 - \frac{d_1{}^2}{2}\right)} - \frac{d_1}{5,280}. \qquad (62)$$

n is an odd integer for lobe maxima and an even integer for lobe minima, $-h_1$ in feet, d_1 in miles.

The value of d_1 to substitute in equation (62) must also satisfy equation (58). A convenient method of solving these equations is to plot a curve of equation (59) and also of equation (58) in the form

$$n = \frac{4(h_1')^2}{5,280 d_1 \lambda}. \qquad (63)$$

Corresponding values of h_1' and d_1 for the desired value of n are then substituted in equation (62).

While equation (62) is subject to the same sort of limitation as equation (57), it will be noted that in the region of greatest interest, that is, small angles, h_1' is itself small, and this tends to compensate the error. The modifications introduced permit the use of the simple plane earth formulas, since for a particular angle the tangent plane is taken as the reflection surface.

The angle γ given by equation (62) is the transformed angle to be used in constructing the vertical coverage diagram based on a modified earth radius of $ka = 5,280$ miles. If the true angle is desired, the true earth radius $a = 3,960$ miles must be used in equation (62) instead of 5,280 miles.
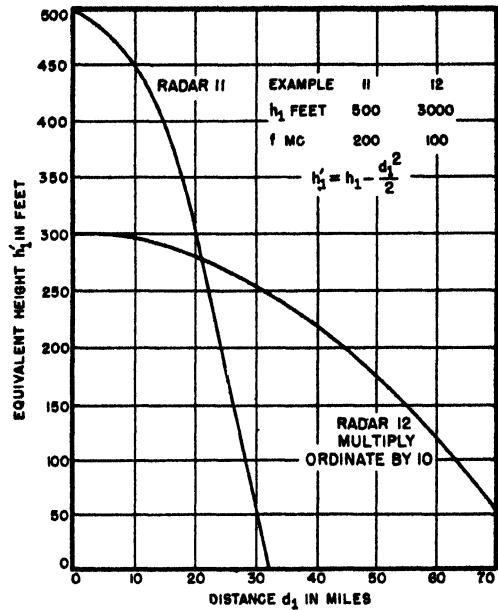
FIGURE 50. Equivalent height graph.

Examples 11 and 12. Lobe Angles Corrected for Earth Curvature. Lobe angles will be computed by this method for two radar sites.

Example 11	*Example 12*
$h_1 = 500$ ft	$h_1 = 3,000$ ft
$f = 200$ mc	$f = 100$ mc

From equation (59)

$$h_1' = 500 - \frac{d_1{}^2}{2} \qquad\qquad h_1' = 3,000 - \frac{d_1{}^2}{2}$$

TABLE 6. Lobe angles for radar. (Example 11.)

From Figures 50 and 51.			Equation (60) $\gamma' = 1.23\,\dfrac{n}{h_1'}$	Equation (61) $\theta = -\dfrac{d_1}{5,280}$	Equation (62) $\gamma = \gamma' + \theta$		Equation (57) $\gamma = \dfrac{n}{4h_1}$
n	h_1'	d_1	radians	radians	radians	degrees	radians
0	0	31.6	0	−.005983	−.005983	−0°20′22″	0
1	341.5	17.8	.003602	−.003372	+.000230	+0° 0′47″	.00246
2	414.0	13.1	.005943	−.002481	.003462	0°11′54″	.00492
3	448.0	10.2	.008238	−.001932	.006306	0°21′39″	.00739
4	464.6	8.4	.010592	−.001591	.009001	0°30′56″	.00985
5	475.5	7.0	.01294	−.001326	.01161	0°39′54″	.0123
6	481.4	6.1	.01532	−.001155	.01417	0°48′43″	.0148
7	486.0	5.3	.01772	−.001004	.01672	0°57′29″	.0172
8	489.0	4.7	.02011	−.000890	.01922	1° 6′ 4″	.0197
9	491.6	4.1	.02252	−.000776	.02174	1°14′45″	.0221
10	493.2	3.7	.02493	−.000701	.02423	1°23′19″	.0246
11	494.6	3.3	.02734	−.000625	.02672	1°31′55″	.0271
12	495.5	3.0	.02978	−.000568	.02921	1°40′26″	.0295
13	496.1	2.8	.03222	−.000530	.03169	1°48′58″	.0320
14	496.6	2.6	.03468	−.000492	.03419	1°57′33″	.0345
15	497.1	2.4	.03720	−.000454	.03675	2° 6′23″	.0369
16	497.4	2.3	.03955	−.000436	.03911	2°14′30″	.0394
17	497.6	2.2	.0420	−.000417	.0416	2°23′ 2″	.0418
18	497.8	2.1	.0445	−.000398	.0441	2°31′44″	.0444
19	498.0	2.0	.0469	−.000379	.0465	2°39′54″	.0468
20	498.2	1.9	.0494	−.000360	.0490	2°48′30″	.0492
21	498.4	1.8	.0518	−.000341	.0515	2°57′ 8″	.0517
22	498.6	1.7	.0542	−.000322	.0539	3° 5′22″	.0541
23	498.8	1.6	.0567	−.000303	.0564	3°14′ 0″	.0567

TABLE 7.   Lobe angles for radar. (Example 12.)

From Figures 50 and 51			Equation (60) $\gamma' = 2.46 \dfrac{n}{h_1'}$	Equation (61) $\theta = -\dfrac{d_1}{5,280}$	Equation (62) $\gamma = \gamma' + \theta$		Equation (57) $\gamma = \dfrac{n}{4h_1}$
n	h_1'	d_1	radians	radians	radians	degrees	radians
0	0	77.4	0	−.01466	−.01466	−0°50'24"	0
1	930	64.3	.002645	−.01218	−.00954	−0°32'49"	.00082
2	1245	59.2	.003952	− 01121	−.00726	−0°25' 0"	.00164
3	1458	55.5	.005063	−.01051	−.00545	−0°18'44"	.00246
4	1638	52.2	.006007	−.00989	−.00388	−0°13'20"	.00328
5	1788	49.2	.006880	−.00932	−.00244	−0° 8'22"	.00410
6	1910	46.7	.007730	−.00885	−.00112	−0° 3'52"	.00492
7	2013	44.4	.008550	−.00841	+.00014	+0° 0'29"	.00574
8	2108	42.4	.009335	−.00803	.00130	0° 4'28"	.00656
9	2195	40.6	.01018	−.00769	.00249	.0° 8'33"	.00738
10	2246	38.8	.01095	−.00735	.00360	0°12'22"	.00820
11	2308	37.2	.01173	.00705	.00468	0° 16' 6"	.00902
12	2359	35.8	.01251	−.00678	.00573	0° 19'41"	.00984
13	2408	34.4	.01328	−.00651	.00677	0°23'16"	.01066
14	2452	33.1	.01404	−.00627	.00777	0°26'44"	.01148
15	2488	32.0	.01484	−.00606	.00878	0°30'10"	.01230
16	2525	30.8	.01558	−.00583	.00975	0°33'31"	.01312
17	2559	29.7	.01635	−.00562	.01073	0°36'50"	.01394
18	2588	28.7	.01712	−.00544	.01168	0°40' 8"	.01476
19	2623	27.8	.01782	−.00526	.01256	0°43'10"	.01558
20	2638	26.9	.01866	−.00509	.01357	0°46'40"	.01640
21	2662	26.0	.01940	−.00492	.01448	0°49'48"	.01722
22	2685	25.1	.02030	−.00475	.01555	0°53'26"	.01804
23	2702	24.4	.02093	−.00462	.01631	0°56' 4"	.01860

Reading values of h_1' and d_1 from Figure 50 and substituting in the above equations, curves of n and d_1 are plotted in Figure 51. From these two curves may be read the values of h_1' and d_1 corresponding to integral values of n. The calculation of γ' and θ from equations (60) and (61) are conveniently performed by arranging columns as shown in Tables 6 and 7.

For purposes of comparison with equation (62) the last column gives values of γ computed by means of equation (57). In Table 6 the error in the figures computed from equation (57) is seen to be consider-

ably below $n = 10$; for higher values of n the two formulas tend to show fair agreement. In Table 7 the disagreement is marked even at $n = 23$ indicating that equation (57) is unsuitable for high sites.

The lobe angles are shown in Figures 52 and 53. The lines of constant altitude over the modified earth are plotted from equation (49). The lobe angles are constructed by drawing radial lines from the center of the antenna, while the height in feet at a given distance is obtained by multiplying γ (in radians) by 5,280 times this distance in miles. The lines have not been drawn close in because of the crowding and because they actually start near the origin rather than at the center of the antenna.

The error in the position of the center lines of the lobes near the antenna is a limitation on this method; but this occurs in a region which, because of gap filling, has no nulls and is therefore of little concern. Another difficulty is that the lower lobes are actually curved instead of straight; but as long as the site is not too high, say under 100 ft (100 mc), the curvature is small and unimportant. In general the method of equation (62) gives reasonably correct lobe angles for most high sites and with a moderate amount of computation. This is the first step in the preparation of the coverage diagram. Later sections will discuss construction of lobes about these center lines.

These equations are plotted in Figure 50. From equation (63):

FIGURE 51. Reflection area graph.

$$n = \frac{4(h_1')^2}{5,280 \times 4.92 \times d_1}, \quad n = 0.000077 \frac{(h_1')^2}{d_1}.$$
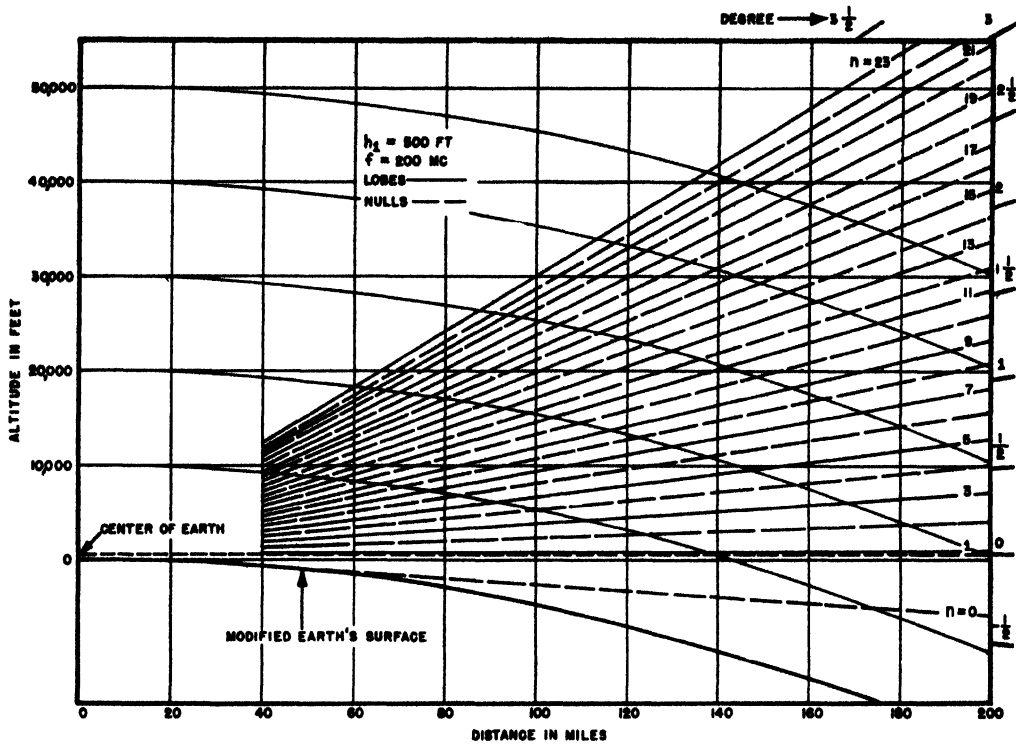
FIGURE 52. Lobe angles for Example 11

The General Lobe Angle Formula

For very high sites (over 1,000 ft) and frequencies over 200 mc. it is desirable to have a more accurate expression for the locus of constant path difference than is afforded by straight lines. This is of especial interest in the first few lobes as these determine the low coverage which is of great tactical importance.
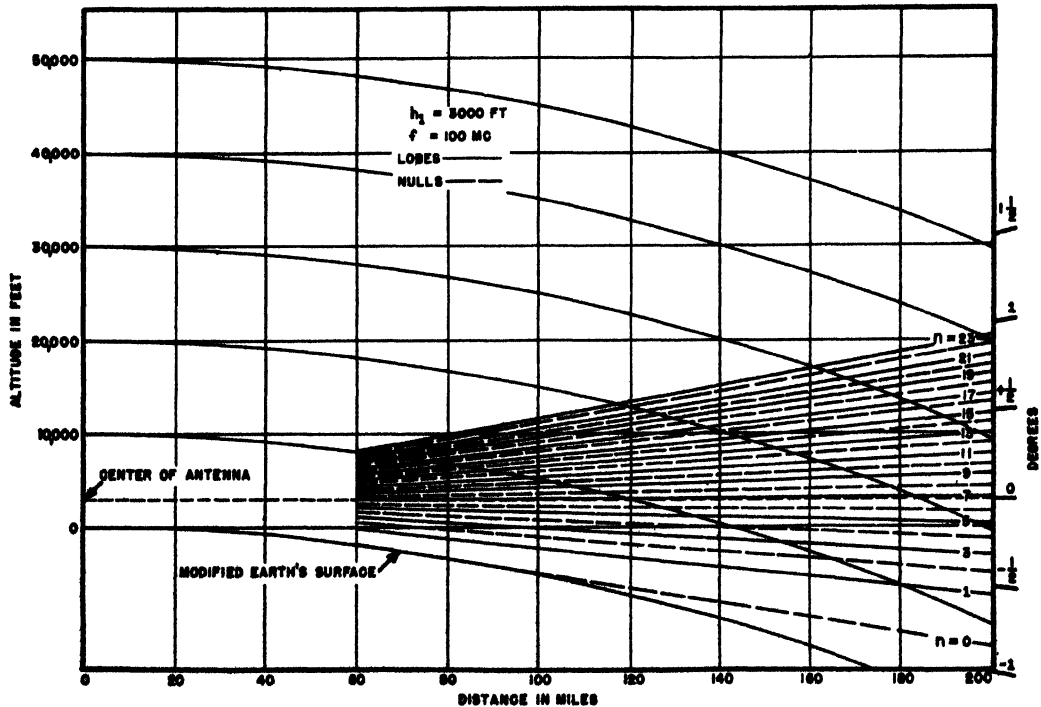
FIGURE 53. Lobe angles for Example 12.

The method described here overcomes the limitations of equation (62) and may be used for the highest sites.

In Figure 54 is shown the antenna above a curved reflecting surface whose radius is taken as $\frac{4}{3}$ of the earth's radius to allow for atmospheric refraction. The tangent plane CE makes an angle θ with the horizontal at the antenna, and θ is given by $-(d_1/ka)$ as shown in Figure 49.

h_1 = height of the center of the antenna above the earth's surface, in feet.

h_1' = equivalent height of the antenna, in feet — equation (59).

r_d = distance from the antenna to the target, in miles.

A = distance from the antenna to the reflection point, in miles.

B = distance from the reflection point to the target, in miles.

Δ = path difference, $A + B - r_d$, in miles.

λ = wavelength, in feet.

θ = angle between the tangent plane CE and the horizontal at the antenna, in radians. This angle is always negative.

ka = radius of the modified earth, 5,280 miles.

Ψ_d = angle between the direct ray r_d and the horizontal plane CE, in radians.

Ψ = angle between the reflected ray A or B and the horizontal plane CE, in radians.

n = number of half-wavelengths path difference.

In the triangle ABr_d (cosine law)
$$r_d = \sqrt{A^2 + B^2 + 2AB \cos 2\Psi} . \qquad (64)$$
From the definition of path difference:
$$\Delta = A + B - r_d = \frac{n\lambda}{2 \times 5,280} , \qquad (65)$$
$$A + B - \Delta = \sqrt{A^2 + B^2 + 2AB \cos 2\Psi} ;$$
squaring and dropping terms that cancel out gives
$$2AB - 2AB \cos 2\Psi - 2B\Delta = 2A\Delta - \Delta^2 ,$$

or solving with respect to B,
$$B = \frac{A\Delta - \frac{1}{2}\Delta^2}{A(1 - \cos 2\Psi) - \Delta} . \qquad (66)$$
Substituting
$$\Delta = \frac{n\lambda}{2 \times 5,280} ,$$
into equation (66) gives
$$B = \frac{\frac{n\lambda}{10,560}A - \frac{1}{2}\left(\frac{n\lambda}{10,560}\right)^2}{A(1 - \cos 2\Psi) - \frac{n\lambda}{10,560}} . \qquad (67)$$

Several approximations will be introduced to simplify equation (67):

A will be taken to equal d_1 since Ψ is of the order of 3° or less.

From Figure 54 it follows that $\sin \Psi = h_1'/5,280A$, or for small angles, $\Psi \doteq h_1'/5,280A$.

Substituting for h_1' [equation (59)] it follows that
$$\Psi = \frac{h_1 - \frac{1}{2}d_1^2}{5,280d_1} . \qquad (68)$$

Using the approximation
$$\cos 2\Psi = 1 - 2\Psi^2 ,$$
and neglecting $\frac{1}{2}(n\lambda/10,560)$ compared to A, equation (67) becomes
$$B = \frac{\frac{n\lambda}{10,560}d_1}{2d_1\Psi^2 - \frac{n\lambda}{10,560}} . \qquad (69)$$

From the law of sines
$$\frac{\sin 2\Psi}{r_d} = \frac{\sin (\Psi + \Psi_d)}{B} = \frac{\sin (\Psi - \Psi_d)}{A} ,$$
$$\sin (\Psi + \Psi_d) = \frac{B \sin 2\Psi}{r_d} .$$
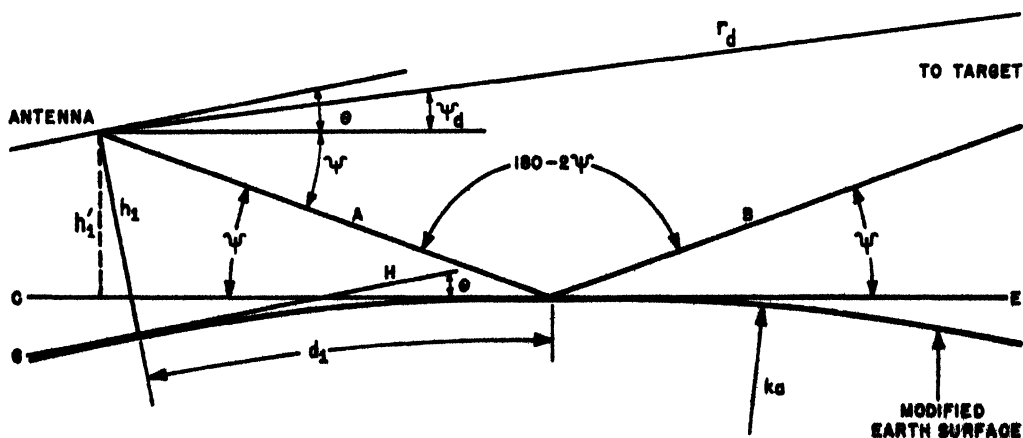
FIGURE 54. Reflection point geometry.

When Ψ and Ψ_d are small

$$\Psi + \Psi_d = \frac{B}{r_d} 2\Psi ,$$

and

$$\Psi - \Psi_d = \frac{A}{r_d} 2\Psi ,$$

and hence by subtraction

$$\Psi_d = \frac{B - A}{r_d} \Psi .$$

Since Ψ is a small quantity r_d may be taken to equal $A + B$, and $A = d_1$, that is

$$\Psi_d = \frac{B - d_1}{B + d_1} \Psi . \tag{70}$$

This is the angle of the target with respect to the tangent plane CE as seen from the antenna. The angle desired however is γ, which is measured with respect to the horizontal at the antenna, GH. As shown in Figure 54

$$\gamma = \Psi_d + \theta .$$

From equation (61)

$$\theta = \frac{d_1}{5,280} .$$

The line of minimum path difference ($\Delta = 0$) is along the earth's surface from the transmitter to the horizon, and beyond it is along the line of sight tangential to the horizon since the direct and indirect waves are equal in that case. Maximum path difference occurs directly below the antenna and is equal to $2h_1$. Since the path difference is also $n\lambda/2$, the maximum value of n is $4h_1/\lambda$. In practice the vertical directivity of the antenna limits n to a much smaller value.

Consider a wave which is reflected from directly under the antenna, and let h_0 denote the height above the reflector at which the path difference is $n\lambda/2$. Then

$$h_1 + h_0 - (h_1 - h_0) = \frac{n\lambda}{2} ,$$

or

$$h_0 = \frac{n\lambda}{4} . \tag{71}$$

Thus if λ is 10 ft the center of the first lobe will be 2.5 ft high at zero range. For most purposes the lobes and nulls may therefore be considered to start at the origin.

To use this method it is best to arrange the calculations in a tabular form. Points along the lobe center are selected by using various values of d_1 for the value of n desired. Next Ψ is obtained from equation (68) and substituted in equation (69), and B and Ψ are substituted in equation (70) yielding Ψ_d, which is combined with θ to obtain γ. The curve of constant path difference is then plotted from γ and r_d, which are now known.

Example 13. The General Lobe Angle Formula. To illustrate this method a radar 3,000 ft high and operating at 100 mc will be used. A trial value of 60 miles is arbitrarily selected for d_1 and substituted in equation (68), giving

$$\Psi = \frac{3,000 - \frac{1}{2} \times (60)^2}{5,280 \times 60} = 0.003788 \text{ radian} .$$

In equation (69) using $n = 1$ and $\lambda = 9.84$ ft,

$$B = \frac{\dfrac{1 \times 9.84}{10,560} \times 60}{2 \times 60(0.003788)^2 - \dfrac{1 \times 9.84}{10,560}} = 70.85 \text{ miles} .$$

$$\Psi_d = \frac{70.85 - 60}{70.85 + 60} \times 0.003788 = 0.000314 \text{ radian} .$$

$$\theta = -\frac{60}{5,280} = -0.01136 \text{ radian} .$$

$$\gamma = 0.000314 - 0.01136 = -0.01105 \text{ radian} .$$

$$r_d = 60 + 70.85 = 130.85 \text{ miles} .$$

Laying out the angle γ from the antenna and marking off the distance r_d gives one point on the curve of constant path difference. Enough other points are computed to enable one to draw a smooth curve. The computations may be arranged as shown

TABLE 8. General lobe angle formula. (Example 13.)

d_1, miles	Ψ, radians	B, miles	Ψ_d, radians	$-\theta$, radians	$-\gamma$, radians	r_d, miles
$(n = 1)$ 65	.002800	696.0	.0023220	.0123105	.00999	761.0
62	.003290	141.2	.0012810	.0117450	.01046	203.2
60	.003788	70.85	.0003140	.0113636	.01105	130.85
58	.004300	44.60	−.0005618	.0109850	.01155	102.60
55	.005118	26.32	−.0018050	.0104166	.01222	81.32
50	.006628	13.45	−.0038380	.0094698	.01331	63.45
30	.016090	1.91	−.0141600	.0056820	.01984	31.91
$(n = 2)$ 60	.003788	..	..	.0113636	..	..
58	.004300	386.0	.0031770	.0109850	.007808	440.0
56	.004840	137.5	.0020390	.0106060	.008567	193.5
55	.005118	101.0	.0015090	.0104166	.008908	156.0
58	.005700	62.6	.0004733	.0100381	.009565	115.6
50	.006628	36.78	−.0010115	.0094698	.010480	86.78
30	.016090	4.09	−.0122300	.0056820	.017910	34.09
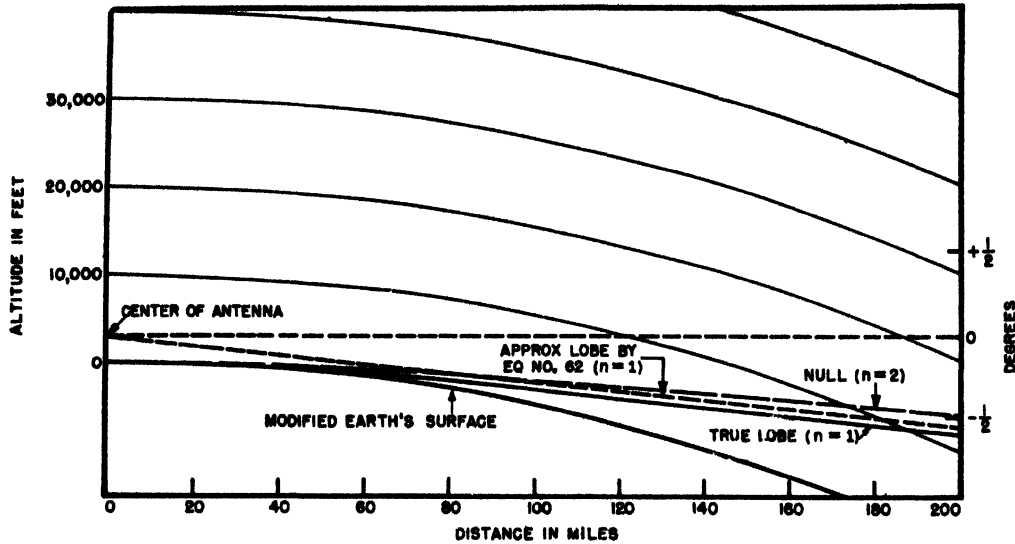
FIGURE 55. Lobe and null lines. (Example 13.).

in Table 8. The values selected for d_1 should be small enough so that the denominator of equation (69) is positive.

These two curves are plotted in Figure 55. For comparison is shown the first lobe as computed from equation (62), and it can be seen that this equation may lead to appreciable error in estimating low coverage. For most·purposes it will suffice to calculate lobes higher than the first one or two by means of equation (62).

The Calculation of Lobes

Three methods of computing lobe angles were given corresponding to low, medium, and high sites, in order to relate the labor of the computations to the complexity of the problem. A similar procedure will be followed in the calculation of the lobe shapes.

The lobe diagram represents the locus of all points along a particular azimuth of a definite field intensity, usually the threshold of detection. If the site has horizontal symmetry throughout its sector of operation one diagram will suffice. Usually several diagrams are required, and it is common practice to prepare a diagram for the central azimuth of the sector and for 10 degrees inside of each limit of scan.

Low Site Lobes

The electric field intensity at the target is the resultant of the direct and reflected waves which have the same amplitude and a phase angle which varies continually as the lobe angle γ is increased. For a perfect reflector and horizontal polarization the phase lag is equal to $+\pi + (2\pi/\lambda) \times (n\lambda/2)$ which adds up to $n\pi + \pi$. Odd integral values of n give lobe maxima, and intermediate values give other points on the lobes.

The sum of the two vectors practically parallel and of equal magnitude, E_1/d, is

$$E = \frac{2E_1}{d} \cos\left[(n + 1)\frac{\pi}{2}\right]. \qquad (72)$$

where E_1 is the electric intensity (microvolts per meter) in the equatorial plane 1 mile from the antenna in free space, that is, without a reflecting surface. E is the electric intensity at the point considered in microvolts per meter. d is the distance to the point, in miles. n is a number related to the angle of elevation. It is an odd integer for lobe maximums and an even integer for nulls. For a given antenna and radar the electric intensity E will produce at the input of the receiver a voltage,

$$V_2 = \frac{k_1 E_1}{d} \sin(90°n), \qquad (73)$$

where k_1 is a proportionality factor for the voltage applied to the receiver input. If V_2 is set equal to the minimum operating voltage of the receiver equation (73) becomes

$$d = \frac{k_1 E_1}{V_{min}} \sin(90°n) .$$

The term $k_1 E_1 / V_{min}$ is usually obtained from test flights on the particular radar or on radars of the same type. The usual form is

$$d = d_{max} \sin(90°n) , \qquad (74)$$

where d_{max} stands for $k_1 E_1 / V_{min}$ and is a measure of the performance of the radar set.

The lobes will be polar sinusoids and the minima will go to zero only when the amplitude of the direct and indirect waves are equal. These conditions will not obtain if the vertical directivity of the antenna affects the rays unequally, if the reflected wave suffers imperfect reflection or divergence, or the atmosphere or terrain has unequal effects on the
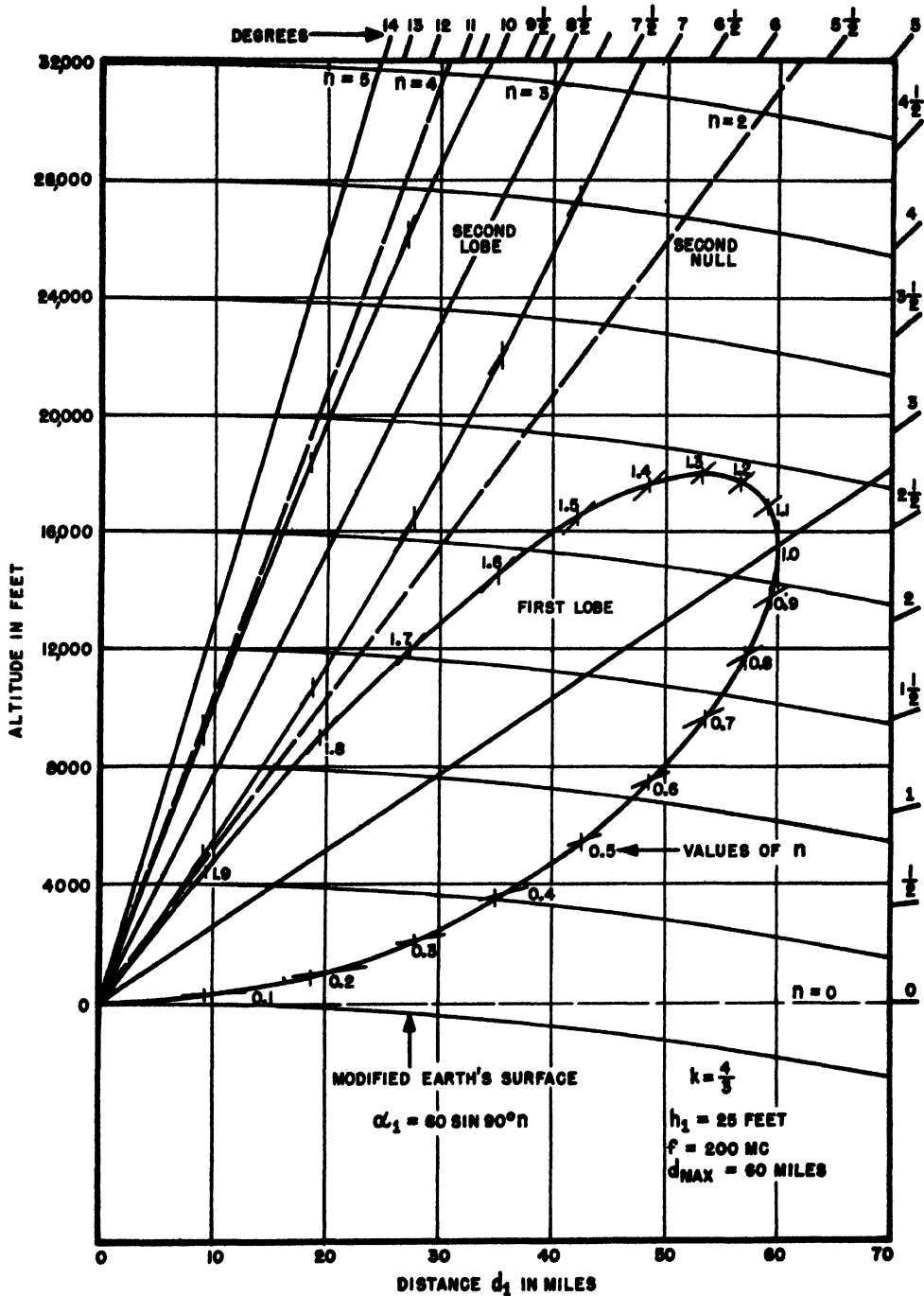
FIGURE 56. Low site lobes. (Example 14)

two waves. Low sites are generally free from the above effects and equation (74) may be used with acceptable accuracy.

Example 14. Low Site Lobes. A radar operating on 200 mc is 25 ft high and has a maximum range of 60 miles. The lobes occur at 2.82°, 8.46°, and 14.1° and the nulls at 0°, 5.64°, 11.28°. The method of

plotting a lobe is shown in Figure 56. n may be divided into as many parts as desired, and the corresponding range for each obtained from equation (74). Thus at $n = 0.7$ the angle is

$$\frac{0.7 \times 4\ 92}{4 \times 25} = 0.0344 \text{ radian} ,$$

$$d = 60 \sin (90° \times 0.7) = 53.46 \text{ miles.}$$

A line is drawn at this angle, and a point is marked off at a range of 53.46 miles.

Lobe Diagrams of Medium Height Sites

In dealing with radars at medium heights, say from 100 to 1,000 ft, a more involved treatment is required, owing to earth curvature effects. The procedure followed in this section is to compute a value of d_{max} for each lobe from which a sinusoid is constructed at the angle of the lobe. The envelope of the lobes is considered to be of principal interest, the lobe shape being of secondary importance.

The strength of a wave is measured in miles, that is, the distance at which the standard target must be to give a standard signal response such as a signal-to-noise ratio of one. The distances corresponding to the direct and reflected waves are added to get lobe maxima and subtracted to get minima. The direct and reflected waves will therefore be computed separately. The phase shift due to reflection will be taken as 180°, and the phase shift due to other causes than path difference will be considered negligible. This assumption greatly simplifies calculations and is a good approximation for small angles and horizontal polarization. For vertical polarization, especially in the VHF band, it is a poor approximation.

The direct wave is affected only by the modified antenna pattern. The reflected wave is affected by:
1. Shoreline diffraction.
2. The modified antenna pattern.
3. Earth curvature.
4. Coefficient of reflection.
5. Divergence.

Terrain effects such as reflection areas of limited extent, the shoreline, cliff edges, and obstacles involve diffraction. A simple, flexible method for solving such problems will be developed in the next section.

Shoreline Diffraction

Unfortunately sites of sufficient height are frequently some distance inland, and a considerable portion of the reflection surface is on land. The poor reflecting qualities of land, especially when rough, cause the high angle lobes due to nearby reflection to be reduced as much as 50 per cent in length. This is a common cause of poor high coverage so often experienced in field installations and the inability to detect high-level bombing attacks except at perhaps 10-mile ranges. In this section will be developed a method of computing the vertical coverage pattern for the typical high site with part land and part sea reflecting surfaces.

In most cases the profile of the land between the transmitter and the shore will be found to be too rough for coherent reflection, as may be determined from equation (16). If substantial regular areas or obstacles occur between the antenna and the shore line they should be treated as described in the section on the modified antenna pattern on page 115.

Sea Reflection
with Diffuse Land Reflection

The problem treated in this section will be that shown in Figure 57. The land in the foreground is so rough as to cause only diffuse reflection, and no regular areas exist which will affect the vertical pattern below 15°.

The diffuse reflection from the land area has a random phase relation, and the field intensity in a particular direction is relatively small. The effect of the land reflection on the interference pattern is therefore neglected. This is equivalent to termination of the reflecting surface at the shore line.

In order to describe diffraction at a shore line a system of Fresnel zones for each lobe is considered to be formed on the sea with the reflection point of the lobe as their center. The zones will be ellipses because of the inclination of the rays. The influence of the shore line will be determined by the number of zones which are not interfered with by the shore.

Thus a low angle lobe which has its central Fresnel zone far out to sea would be virtually unaffected by the limited reflection area, as numerous zones are

FIGURE 57. Fresnel zones on land and sea areas.

FIGURE 58. Shore line diffraction.

formed on the sea. This is indicated by A in Figure 57, which represents the reflected wave. At B, a higher angle lobe, there are only two zones intact, and the reflected wave is weak. Had only one zone been complete, the reflected wave would have been stronger than A. At C only portions of outer zones are formed on the sea, and the reflected wave is negligible.

The effect of the reflecting surface may be represented by an image antenna located in the earth under the radar antenna at a depth h_1 below the surface as in Figure 58. The nonreflecting land surface then acts precisely as a straight diffracting edge for the image antenna and indirect ray. A general formula will be developed which gives the situation of any Fresnel zone of any lobe for a given radar station. From this formula and the distance to the shoreline it may be determined for each lobe which zone is intercepted by the shore. In the graph in Figure 58 is plotted the relative intensity of the reflected ray as a function of m, the number of the zone touching the shore. In the illuminated region at large angles, as A, the relative intensity is close to unity. Approaching the shore it oscillates about unity, reaching a maximum of 1.18. In the shadow region, the intensity drops to low values. Thus, knowing m, the effect of shoreline diffraction on the reflected ray may be obtained. The derivation will be developed for a plane reflecting surface, since, as it has been explained on page 102, for lobe angles

corrected for standard earth curvature, the effect of earth curvature may be taken into account by using h_1' [equation (59)] instead of h_1. In most cases d_1 will be small and h_1 may be used with little error.

General Formula
for the Reflection Area

In Figure 59 is shown an image antenna T'' sending radiation through a plane of indefinite extent. In

FIGURE 59. Fresnel zones on the reflecting surface.

order to simplify the calculations it will be assumed that the distance from the reflection point to the target is large, so that the rays from the Fresnel zones may be considered parallel. With regard to

the transmitter distance, however, no such approximation will be made.

h_1 = depth of the image antenna below the reflecting surface, in feet.

Ψ = angle of the lobe considered with reference to the tangent plane at the reflection point, in radians.

m = number of the Fresnel zone.

m = 0 for the center of the first zone.

m = +1 for the far edge of the first zone.

m = −1 for the near edge of the first zone.

m = +2 or −2 for the edge between the second and third zones.

n = lobe number. For a given radar station n is related to the angle Ψ by the equation $n = (4h_1/\lambda) \sin \Psi$.

λ = wavelength in feet.

d_n = distance from the transmitter to the near edge for the Fresnel zone and lobe considered, in feet.

d_f = distance from the transmitter to the far edge for the Fresnel zone and lobe considered, in feet.

d_1 = distance from the transmitter to the center of the first Fresnel zone for a particular lobe, in feet.

In Figure 59 is shown the first Fresnel zone for an angle Ψ with a corresponding value of n. Ray 2 passes through the center of the first zone and rays 1 and 3 pass through the near and far edges respectively. Because of the great distance of the target the rays 1, 2, and 3 are parallel.

For the first zone the path difference between 1 and 2 is $\lambda/2$. For zone m the path difference is $m\lambda/2$ (where m = 1, 2, 3, etc.). Since the points d_1 and d_n are not equidistant from the target, the distance $x_1 \cos \Psi$ must be subtracted from ray 2 to compensate for the increased path length of ray 1 above the plane.

$$\frac{m\lambda}{2} = l_1 - \left(\frac{h_1}{\sin \Psi} - x_1 \cos \Psi\right).$$

In the right triangle

$$l_1^2 = x_1^2 \sin^2 \Psi + \left(\frac{h_1}{\sin \Psi} - x_1 \cos \Psi\right)^2.$$

Eliminating l_1 from these equations and solving for x_1

$$x_1 = \frac{-m\lambda \cos \Psi + \sqrt{m^2\lambda^2 + 4m\lambda h_1 \sin \Psi}}{2 \sin^2 \Psi}. \quad (75)$$

For the far point of the zone

$$\frac{m\lambda}{2} = l_2 - \left(\frac{h_1}{\sin \Psi} + x_2 \cos \Psi\right),$$

also

$$l_2^2 = x_2^2 \sin^2 \Psi + \left(\frac{h_1}{\sin \Psi} + x_2 \cos \Psi\right)^2.$$

By a similar process of elimination of l_2 and solving for x_2:

$$x_2 = \frac{m\lambda \cos \Psi + \sqrt{m^2\lambda^2 + 4m\lambda h_1 \sin \Psi}}{2 \sin^2 \Psi}. \quad (76)$$

For the near point of the zone

$$d_n = \frac{h_1}{\tan \Psi} - \frac{-m\lambda \cos \Psi + \sqrt{m^2\lambda^2 + 4m\lambda h_1 \sin \Psi}}{2 \sin^2 \Psi}.$$

Since $\sin \Psi = n\lambda/4h_1$ and Ψ is small, $\cos \Psi$ may be taken as unity with the following error:

up to $2\frac{1}{2}°$ less than 0.1 per cent,
up to $10°$ less than 1.5 per cent,
up to $15°$ less than 4.5 per cent,

$$d_n = \left(\frac{1}{2n} + \frac{m}{n^2} - \frac{\sqrt{m^2 + mn}}{n^2}\right)\frac{8h_1^2}{\lambda}.$$

For the far point

$$d_f = \left(\frac{1}{2n} + \frac{m}{n^2} + \frac{\sqrt{m^2 + mn}}{n^2}\right)\frac{8h_1^2}{\lambda}.$$

These equations may be combined:

$$d = \left(\frac{1}{2n} + \frac{m}{n^2} \pm \frac{\sqrt{m^2 + mn}}{n^2}\right)\frac{8h_1^2}{\lambda}, \quad (77)$$

where the plus sign gives the far point and the minus sign gives the near point. The reflection point is obtained by using $m = 0$ and equation (77) reduces to:

$$d_1 = \frac{4h_1^2}{n\lambda} \quad (78)$$

Thus to obtain the range of the near edge of the first Fresnel zone for the first lobe, substitute $n = 1$, $m = 1$ and use the minus sign in equation (77):

$$d_n = 0.688 \frac{h_1^2}{\lambda}. \quad (79)$$

The far edge of this zone is obtained by using the plus sign

$$d_f = 23.3 \frac{h_1^2}{\lambda}. \quad (80)$$

Equation (77) is in the form

$$d = T \frac{h_1^2}{\lambda}, \quad (81)$$

where

$$T = 8\left(\frac{1}{2n} + \frac{m}{n^2} \pm \frac{\sqrt{m^2 + mn}}{n^2}\right), \quad (82)$$

or

$$T_1 = \frac{d_1 \lambda}{h_1^2}. \quad (83)$$

If d_1 is taken as the distance of the shoreline, T_1 may be considered as a characteristic site or terrain factor at a particular azimuth and combined with

the height and wavelength to obtain the range of any zone of any lobe.

In order to read the relative intensity and phase lag of the reflected wave from the diffraction graphs, Figure 27 and Figure 28 respectively, it is necessary to have m expressed in terms of v. In Figure 19 the path difference is by definition of m

$$\Delta = m\frac{\lambda}{2}. \qquad (84)$$

Equation (23), with $\Delta = d - b$, yields

$$\Delta = \frac{\lambda v^2}{4},$$

hence

$$m = \frac{v^2}{2}. \qquad (85)$$

It is also desirable to have an expression for v in terms of n and T. This is obtained by substituting $v^2/2$ for m in equation (82) and solving

$$v = \sqrt{\frac{Tn^2}{8} - n + \frac{2}{T}} \qquad (86)$$

The width of the zones, that is, along a chord at d_1 parallel to the minor axis of the elliptical rings,
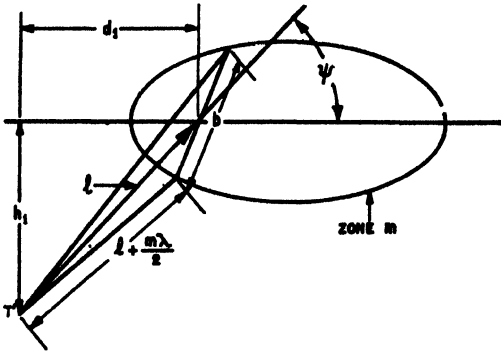
FIGURE 60. Width of Fresnel zones.

may be obtained from Figure 60. Zone m is shown with a chord length b. The distance from the image antenna to the intersection of the chord and ring m is $l + m\lambda/2$. From this may be written

$$\left(l + \frac{m\lambda}{2}\right)^2 = l^2 + \left(\frac{b}{2}\right)^2. \qquad (87)$$

Neglecting $m^2\lambda^2/4$ since it is small compared to the other terms,

$$l^2 + m\lambda l = l^2 + \left(\frac{b}{2}\right)^2,$$

$$b = \sqrt{4m\lambda l},$$

$$l = \frac{d_1}{\cos \Psi} = d_1 = \frac{4h_1^2}{n\lambda},$$

from equation (78), since Ψ is small.

Where earth curvature effects are appreciable the effective height, from equation (59), should be used.

$$b = 4h_1'\sqrt{\frac{m}{n}}. \qquad (88)$$

To apply this method the distance of the shoreline, d_1, is substituted in equation (81), and the equation is solved for T_1, the terrain factor. This quantity is a constant for a particular azimuth and is substituted in equation (86) along with the values of n desired and solved for v. The values of m corresponding to these values of v are the numbers of the zones which intersect the shoreline for each value of n. These values of v are entered in Figures 27 and 28 to obtain the intensity and phase lag relative to that which would be obtained if the rough land were replaced by the sea.

Example 15. Shoreline Diffraction. A radar station is assumed to have the same height and frequency as in Example 11. The shoreline distance is 3 miles, and the intervening land is occupied by a large city. $h_1 = 500$ ft; $f = 200$ mc; $d_1 = 15,840$ ft. At this distance the effect of earth curvature is less than 1 per cent and may be neglected. The greatest angle at which waves are reflected from the sea is given by

$$\frac{500}{15,840} \times 57.3 = 1.81°.$$

In equation (16) the maximum height of roughness for regular reflection is

$$H = \frac{3,520}{200 \times 1.81} = 9.7 \text{ ft}.$$

The land is evidently a diffuse reflector. From equation (83)

$$T_1 = \frac{d_1\lambda}{(h_1')^2} = \frac{15,840 \times 4.92}{(500 - 4.5)^2} = 0.317.$$

Substituting in equation (86) for $n = 2$

$$v = \sqrt{\frac{0.317 \times 4}{8} - 2 + \frac{2}{0.317}} = 2.11,$$

$$m = \frac{v^2}{2} = 2.23.$$

That is, somewhat more than two zones are completely formed on the sea. In order to determine which sign to use in reading Figure 27 it is only necessary to know whether the main reflection point d_1 for this lobe falls on the land or the sea corresponding to shadow or illuminated regions. A more general procedure is to solve equation (63) using the shoreline distance for d_1:

$$n = \frac{4 \times (500 - 4.5)^2}{15,840 \times 4.92} = 12.6.$$

For all values of n less than 12.6, d_1 will be on the sea and equation (84) applies to the near edge, and the minus sign is used in equation (82) corresponding to $+v$ in Figure 27. For n greater than 12.6 the

plus sign is used in equation (82) and $-v$ in Figure 27. Thus, for $n = 2$ and $v = +2.11$, is read in Figure 27 the relative intensity $z = 0.980$ and in Figure 28 the phase lag, $\zeta = -0.103$ radians. Other values are listed in Table 9.

TABLE 9. Shoreline diffraction. (Example 15.)

n	v	Sign	z	ζ	n	v	Sign	z	ζ
0	2.51	+	1.036	+0.080	12	0.14	+	0.582	−0.130
1	2.31	+	1.083	−0.015	13	0.089	−	0.459	+0.2
2	2.11	+	0.980	−0.103	14	0.28	−	0.377	+0.5
3	1.91	+	0.884	−0.038	15	0.49	−	0.308	+0.9
4	1.71	+	0.938	+0.100	16	0.68	−	0.261	+1.4
5	1.51	+	1.082	+0.120	17	0.87	−	0.223	+1.9
6	1.32	+	1.170	+0.030	18	1.08	−	0.192	+2.6
7	1.12	+	1.156	−0.085	19	1.27	−	0.170	+3.3
8	0.92	+	1.073	−0.181	20	1.48	−	0.150	+4.2
9	0.72	+	0.953	−0.255	21	1.67	−	0.135	+5.2
10	0.52	+	0.825	−0.273	22	1.88	−	0.121	+6.4
11	0.32	+	0.696	−0.224	23	2.07	−	0.111	+7.6

The width of the second zone may be computed from equation (88). The effective height for $n = 2$ is obtained from Figures 50 and 51 and is 414 ft.

$$b = 4 \times 414 \sqrt{\frac{2}{2}} = 1,656 \text{ ft} .$$

The Modified Antenna Pattern

The vertical directivity of the antenna is modified by the local terrain. Unless the ground under the antenna is an extension of the reflection plane the modification of the free space directivity characteristics should be taken into consideration in the calculation of radar coverage.

The vertical pattern of the antenna in the absence of a reflecting surface is referred to as the free space pattern, f_A. This is usually given in the instruction manual for the set. If this pattern is not available or if the antenna has been modified, the vertical directivity may be computed by methods given in the next section. Local terrain effects are treated in some detail as they are in many cases a controlling factor. The resultant effect of the local terrain and free space pattern is called the modified antenna pattern, $f(\gamma)$. It does not include the effect of the main reflecting surface.

Antenna Patterns

To obtain f_A, the relative amplitude of the radiation from the antenna, as a function of the vertical angle γ it is only necessary to take into account the path differences of the elements of the array. The absolute field intensity and time phase will not be considered. In Figure 61 is shown an array of four horizontal half-wave dipoles spaced a half wavelength apart. The radiation from A in the direction γ may be taken as proportional to $\cos \omega t$. The path difference of radiation from B is $\lambda/2 \cdot \sin \gamma$. The corre-
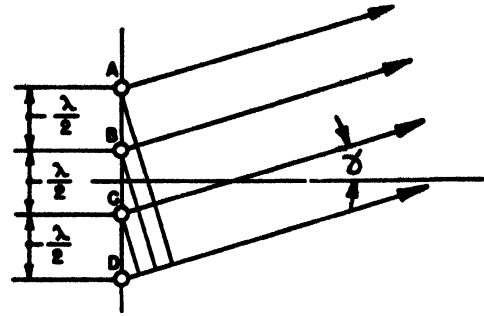
FIGURE 61. The four-element array.

sponding phase difference is

$$-\frac{2\pi}{\lambda} \times \frac{\lambda}{2} \sin \gamma = -\pi \sin \gamma .$$

For C and D the phase is $-2\pi \sin \gamma$ and $-3\pi \sin \gamma$ respectively. The total field intensity pattern is

$$f_A = \cos \omega t + \cos (\omega t - \pi \sin \gamma)$$
$$+ \cos (\omega t - 2\pi \sin \gamma) + \cos (\omega t - 3\pi \sin \gamma) ,$$

grouping

$$[\cos \omega t + \cos (\omega t - 3\pi \sin \gamma)]$$
$$+ [\cos (\omega t - \pi \sin \gamma) + \cos (\omega t - 2\pi \sin \gamma)] . \quad (89)$$

From the identity

$$\cos A + \cos B = 2 \cos \tfrac{1}{2} (A + B) \cos \tfrac{1}{2} (A - B)$$

equation (89) may be written

$$f_A = 2 \cos \left(\omega t - \frac{3\pi}{2} \sin \gamma \right) \cos \left(\frac{3\pi}{2} \sin \gamma \right)$$
$$+ 2 \cos \left(\omega t - \frac{3\pi}{2} \sin \gamma \right) \cos \left(\frac{\pi}{2} \sin \gamma \right) ,$$

$$f_A = 2 \cos \left(\omega t - \frac{3\pi}{2} \sin \gamma \right) \cdot$$

$$\left[\cos \left(\frac{3\pi}{2} \sin \gamma \right) + \cos \cdot \left(\frac{\pi}{2} \sin \gamma \right) \right] ,$$

$$f_A = 4 \cos \left(\omega t - \frac{3\pi}{2} \sin \gamma \right) \cos (\pi \sin \gamma) \cdot$$

$$\cos \left(\frac{\pi}{2} \sin \gamma \right) .$$

Since only the rms value of this equation is significant, the terms containing ωt may be dropped, and the result for the four-element array is

$$f_A = \cos (\pi \sin \gamma) \cos \left(\frac{\pi}{2} \sin \gamma \right) . \quad (90)$$

It is easily verified that this is a special case of the general expression for an N element array spaced at intervals of $n\lambda$ and excited in phase (not derived here)

$$f_A = \frac{\sin (Nn \pi \sin \gamma)}{N \sin (n \pi \sin \gamma)} . \quad (91)$$

The effect of a reflecting screen may be computed by treating it as though it were $\lambda/4$ from the dipole

as in Figure 62. In practice the spacing may be
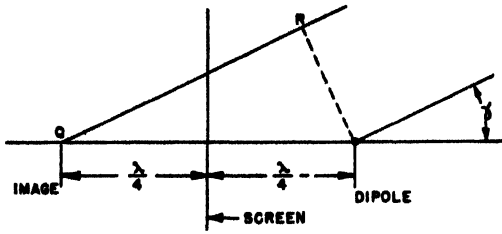
FIGURE 62. The reflecting screen.

FIGURE 63. Vertical pattern of a typical antenna. (Example 16.)

more nearly $\lambda/8$ but for γ less than 30° the method given here is satisfactory and avoids a complicated analysis. The path difference QR is $(\lambda/2)\cos\gamma$, and the phase difference is $\pi\cos\gamma$. Then

$$f_A = \cos\omega t - \cos(\omega t - \pi\cos\gamma). \quad (92)$$

From the relation

$$\cos A - \cos B = -2\sin\tfrac{1}{2}(A+B)\sin\tfrac{1}{2}(A-B),$$

it follows that equation (92) may be written in the form

$$f_A = -2\sin\left(\omega t - \frac{\pi}{2}\cos\gamma\right)\sin\left(\frac{\pi}{2}\cos\gamma\right).$$

Dealing only with the rms value,

$$f_A = \sin\left(\frac{\pi}{2}\cos\gamma\right). \quad (93)$$

For small angles this factor is usually unimportant. Factors are given in Table 10 for some typical arrays with horizontal radiators in a vertical column and a reflector screen.

Example 16. Vertical Pattern of an Antenna. Using the eight element array in Table 10, the relative intensity at angle of 5° from the horizontal is computed as follows.

$$\begin{aligned}
f_A &= \cos(90\sin 5°)\cos(180\sin 5°)\\
&\quad \cos(540\sin 5°)\sin(90\cos 5°),\\
&= \cos 7°51' \times \cos 15°41'\\
&\quad \times \cos 47°4' \times \sin 89°39',\\
&= 0.9906 \times 0.9628 \times 0.6809 \times 0.9999,\\
&= 0.65.
\end{aligned}$$

The main vertical lobe is plotted in Figure 63. The first null is at 9°36' and the half-power beam width

is 4.53°. It will be noted that the effect of the reflector screen may be neglected for small angles.

The pattern from a parabola is closely dependent on the feed system which controls the uniformity of illumination. To reduce side lobes it is common practice to taper the illumination toward the edge of the dish. This is accompanied by a broadening of the beam and a loss of gain. The half-power beam width for uniform illumination is $59\lambda/D$ degrees, where D is the diameter of the aperture. The first side lobe is then about 2 per cent of the maximum. A typical dish with a tapered feed would have a half-power band width of $68.8\lambda/D$ degrees. This reduces the first side lobe to 0.5 per cent. Some designs are further modified by deforming the dish, off-center feeds, etc., so that the patterns may not be easily computed. Such patterns are best obtained experimentally and are usually given in the manual for the equipment.

Local Terrain Effects

The vertical pattern of the antenna may be modified by reflection from local flat areas or by diffraction over hills or other obstacles. To take these effects into account, factors are computed from the diffraction equations which are used to modify the direct and reflected ray patterns.

A detailed method of calculating $f(\gamma)$ cannot be given because of the great variety of sites encountered. However, the following discussion of the

TABLE 10. Antenna pattern factors.

Array with screen	Vertical pattern f_A
Two radiators spaced $\dfrac{\lambda}{2}$	$\cos\left(\dfrac{\pi}{2}\sin\gamma\right)\sin\left(\dfrac{\pi}{2}\cos\gamma\right)$
Four radiators spaced $\dfrac{\lambda}{2}$	$\cos\left(\dfrac{\pi}{2}\sin\gamma\right)\cos(\pi\sin\gamma)\sin\left(\dfrac{\pi}{2}\cos\gamma\right)$
Two sets of four radiators each	$\cos\left(\dfrac{\pi}{2}\sin\gamma\right)\cos(\pi\sin\gamma)\times$
(Vertical spacing between centers of sets is 3λ.)	$\cos(3\pi\sin\gamma)\sin\left(\dfrac{\pi}{2}\cos\gamma\right)$

effects of particular terrain features will suggest methods of combining them to analyze a particular site.

A large, flat land area will in general produce lobes and nulls at angles given by equation (57) with an envelope twice as large as the free space pattern. If the land area is not level, the lobe pattern will be tilted by the angle of the land. However, the problem is essentially a matter of diffraction since the land is of limited extent. Equation (16) should be used to determine whether the area is sufficiently flat to act as a regular reflector.

If the land is flat from the antenna out to a distance d_1 the relative intensity of the reflected ray is ½ when $d_1 = h_1 \times \cot \gamma$. This assumes the land beyond d_1 to be nonreflecting and that the distant boundary acts as a diffracting edge. As d_1 increases further, the relative intensity increases to about 1.18 and then decreases again and oscillates about unity in gradually decreasing swings. This is accompanied by a variation of phase.

Several typical terrain problems will be solved in detail to illustrate the methods.

Example 17. Limited Reflecting Area. A 200-mc radar, Figure 64, with an antenna as described in
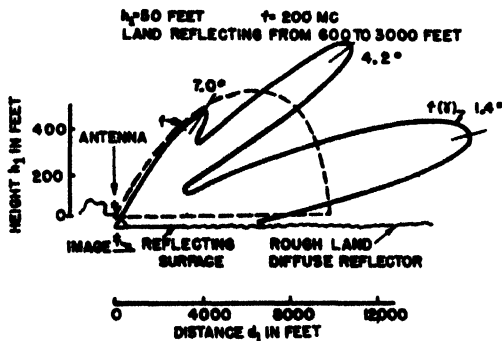
FIGURE 64. Lobes from a limited reflecting area.

Example 16, is 50 ft above a smooth reflecting surface (a lake) which extends from 600 to 3,000 ft. From 0 to 600 ft and from 3,000 ft on is rough land. The shore line diffraction method will be used to determine the effect of the reflection from the limited area upon the antenna pattern f_A. The vertical pattern is plotted from Figure 63 and shown dotted. To obtain the pattern for the reflected wave the shore at 600 ft is taken as a diffracting edge, and the relative intensity computed as a function of γ as though the surface from 600 ft on were a perfect reflector. This is then repeated using the shore at 3,000 ft. The difference between these two functions is then the effect of the area between 600 and 3,000 ft. From equation (83) for $n = 1$

$$T_{600} = \frac{600 \times 4.92}{1 \times (50)^2} = 1.18; \quad T_{3,000} = 5.9 \; ;$$

$$v_{600} = \sqrt{\frac{1.18}{8} \times 1} - 1 + \frac{2}{1.18} = 0.918 \; ;$$

$$v_{3,000} = 0.279 \; .$$

From equation (78)

$$n_{600} = \frac{4 \times (50)^2}{600 \times 4.92} = 3.39 \; ; \quad n_{3,000} = 0.678 \; .$$

From Figure 27, using the plus sign for v_{600} and the minus sign for $v_{3,000}$, is obtained the relative intensity

$$z_{600} = 1.073; \quad z_{3,000} = 0.375.$$

The reflection factor for $n = 1$ is given by

$$z = 1.073 - 0.375 = 0.698.$$

From equation (57)

$$\gamma = \frac{1 \times 4.92}{4 \times 50} = 0.0246 \text{ radian} = 1 41°$$

Other values are given in Table 11.

TABLE 11. Limited reflecting area. (Example 17.)

n	γ	v_{600}	$v_{3,000}$	z_{600}	$z_{3,000}$	z	f_T	$f(\gamma)$
0	0	+1.30	+0.583	1.177	0 870	0.307	0.693	0.693
0.1	0.14	+1.26	+0.498	1.181	0.810	0.371	0.658	0.658
0.4	0.56	+1.15	+0.241	1.164	0.645	0.519	0.973	0.973
0.5	0.70	+1.11	+0.155	1.153	0.592	0.561	1.147	1.147
0.6	0.85	+1.071	+0.077	1.142	0.544	0.598	1 314	1.314
1.0	1.41	+0.918	−0.279	1.073	0.375	0.698	1.700	1.650
1.5	2.11	+0.727	−0.707	0.960	0.257	0.703	1.223	1.137
2.0	2.82	+0.535	−1.136	0 838	0.186	0 652	0.349	0.314
3.0	4.23	+0.155	−1.995	0.592	0.116	0.476	1 475	1.090
4.0	5.64	−0.237	−2.853	0.393	0.082	0.311	0.689	0.386
5.0	7.05	−0.619	−3.710	0.277	0 067	0 210	1.210	0.436

The values of z multiplied by f_A from Figure 63 are plotted in Figure 65 as the reflected pattern. The
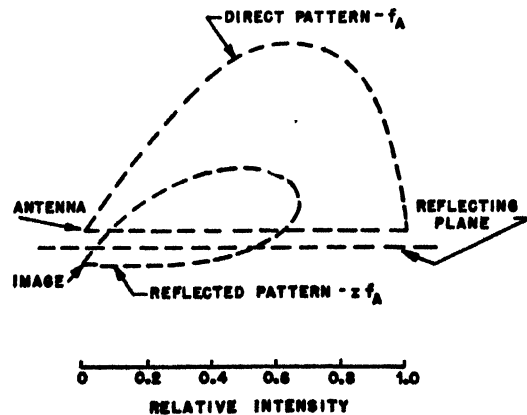
FIGURE 65. Components of the modified antenna for a limited reflecting area.

resultant of the two vectors, f_A and zf_A, in terms of n is given by the cosine law:

$$f_T = \sqrt{1 + z^2 - 2z \cos (n\pi)} \; . \qquad (94)$$

Thus for $n = 0.1$

$$f_T = \sqrt{1 + (0.371)^2 - 2 \times 0.371 \cos (0.1\pi)} = 0.658$$

The product of f_T and f_A is the modified antenna factor $f(\gamma)$. This is plotted in Figure 64. With a larger reflecting surface, the length of lobes would approach twice the value of f_A. Figures 64 and 65 were drawn for purposes of illustration and would not ordinarily be required.

Example 18. Cliff Edge Diffraction. A 200-mc radar, Figure 66, with an antenna as described in Example
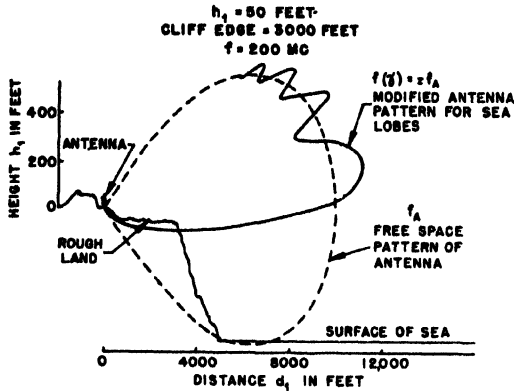
FIGURE 66. Cliff edge diffraction. (Example 18.)

16, is 50 ft above a rough land surface, the top of a cliff whose edge is 3,000 ft away.

The geometrical shadow line makes an angle with the horizontal of

$$\tan^{-1}\left(-\frac{50}{3,000}\right) = -0.955°.$$

At this angle, the relative intensity, $z = 0.5$. Other values of z may be read from Figure 27 after converting the angle of diffraction to v by means of equation (47).

$$v = \frac{\theta_d°}{\sqrt{\dfrac{4.92}{2 \times 3,000}} \times 57.3} = 0.61\ \theta_d°.$$

At 0.377° in the shadow region $v = -0.377 \times 0.61 = -0.23$. From Figure 27, z is 0.4. This angle, referred to the horizontal at the antenna, is

$$\gamma = \Phi - 0.955 = -1.332°.$$

Some other values are:

$\gamma°$	z
+3.535	0.917
+1.060	1.18
−0.955	0.50
−8.335	0.05

The modified antenna pattern $f(\gamma)$ is the product of z and f_A and is plotted in Figure 66. This pattern gives the factors for both the direct and reflected waves for the sea lobes.

Example 19. Land Reflection and Diffraction. This site is similar to that of Example 18 except that the cliff top is smooth. This is shown in Figure 67.
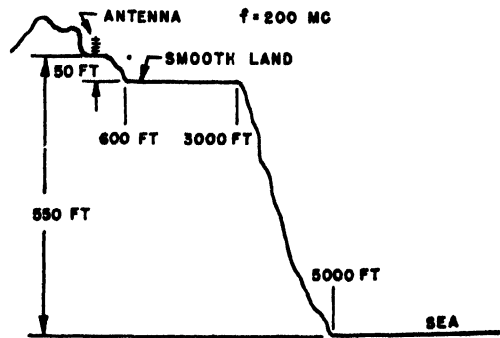
FIGURE 67. Land reflection and diffraction. (Example 19.)
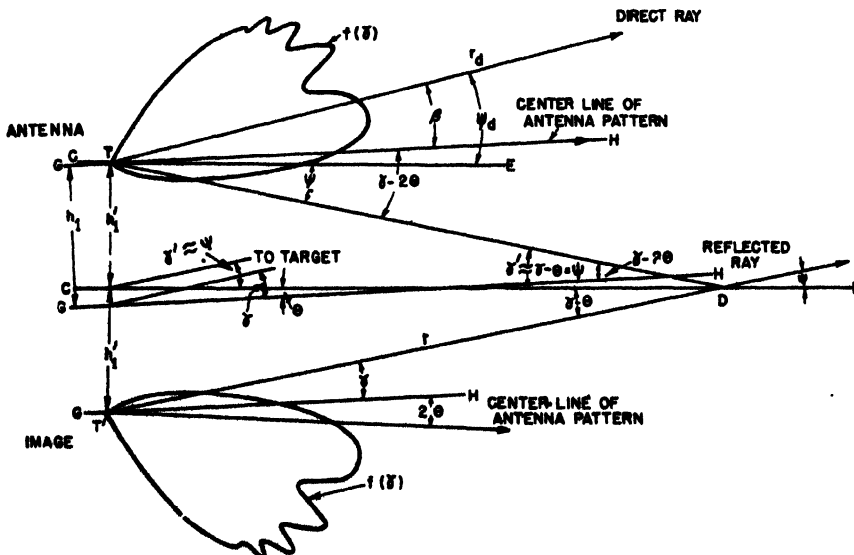
FIGURE 68. Earth curvature effect on direct and image patterns. Note: GH horizontal at the antenna; CE horizontal at the reflection point $\theta = \dfrac{d_1}{ka}$

The smooth land causes land lobes to be formed as in Example 17 which furnish high angle coverage. The sea lobes are computed using the method of Example 18 for the direct and reflected rays. If the cliff top were tilted down, the land lobes would be tilted by the angle of the land. Speculation about complex sites yields many unusual patterns, but in practice the results are usually disappointing. Complex sites seldom have horizontal symmetry, and gaps in the coverage pattern may be expected. Attempts to reinforce the pattern in a particular direction by siting back from the cliff edge generally cause poor coverage at other angles. Best all-round CHL operation results from siting on cliff edges and exclusive use of the sea as a reflector.

Earth Curvature Effect on Lobe Lengths

The effect of earth curvature on lobe angles was described on pages 102-104. The angles to be used with the modified antenna pattern of the image antenna are affected by earth curvature, and therefore the strength of the reflected wave is also affected. In Figure 68 is shown a radar antenna at height h_1 above the earth's surface, with the center line of the antenna pattern parallel to GH, the horizontal at the base of the antenna. Because of diffraction at a cliff edge the modified antenna pattern $f(\gamma)$ is unsymmetrical as in Example 18. The lines GH are parallel to the horizontal at the antenna. The line CE is horizontal at the reflection point and makes an angle θ with GH. The target is at an angle γ with respect to GH. The incident and reflected rays make the

angle $\gamma - \theta$ with CE. It will be noted that the direct ray makes the angle $\gamma \approx \beta$ with the centerline of the antenna pattern, and the reflected ray makes the angle $\gamma - 2\theta$.

Coefficient of Reflection

The coefficient of reflection of the reflecting surface is in general complex. That is, both the magnitude and phase of the reflected wave are affected. The reflection coefficient varies with the conductivity and dielectric constant of the reflector and with the frequency, polarization, and angle of incidence. Careful consideration should be given to the roughness of the surface, and a substantial reduction in the coefficient should be made when the height of roughness is comparable to that computed from equation (16). In general the reflection obtained with microwaves is of minor importance.

The magnitude and phase angle of the reflection coefficient are plotted as functions of the angle of reflection, Ψ in Figures 69 and 70. Curves are given for horizontal and vertical polarization and for the extreme conditions of sea water and dry soil. For dry soil the reflection coefficient is not sensitive to frequency changes, and the 100-mc curve may also be used for 3,000 mc.

For most purposes the reflection coefficient for horizontal polarization may be taken as unity, and the phase angle as 180°. The use of these values simplifies computations.

The coefficients of reflection and phase angle for vertical polarization vary rapidly with frequency
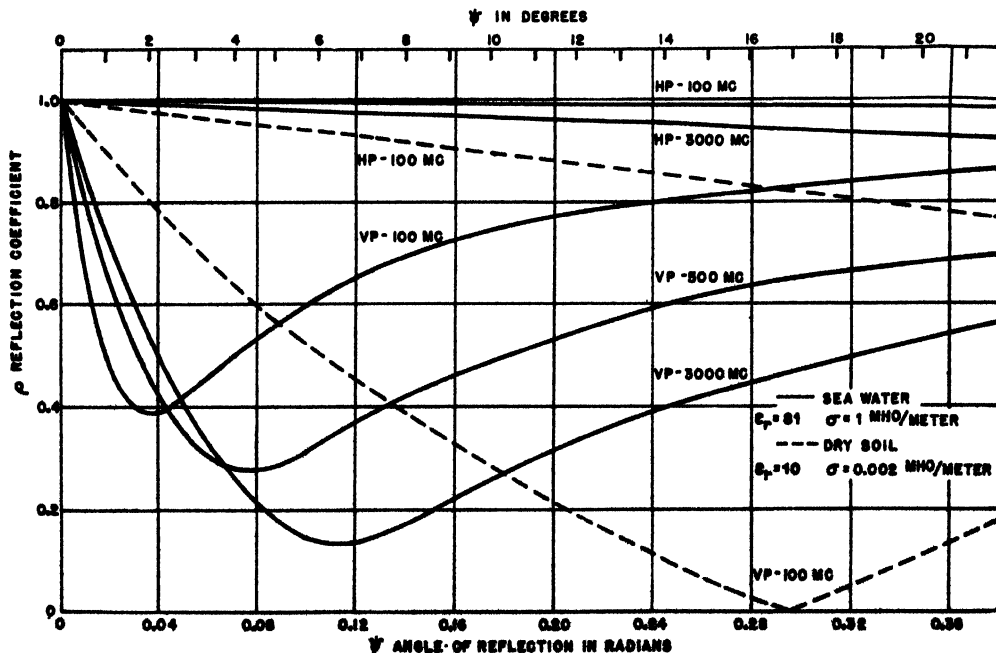
FIGURE 69. Reflecting coefficient curves.
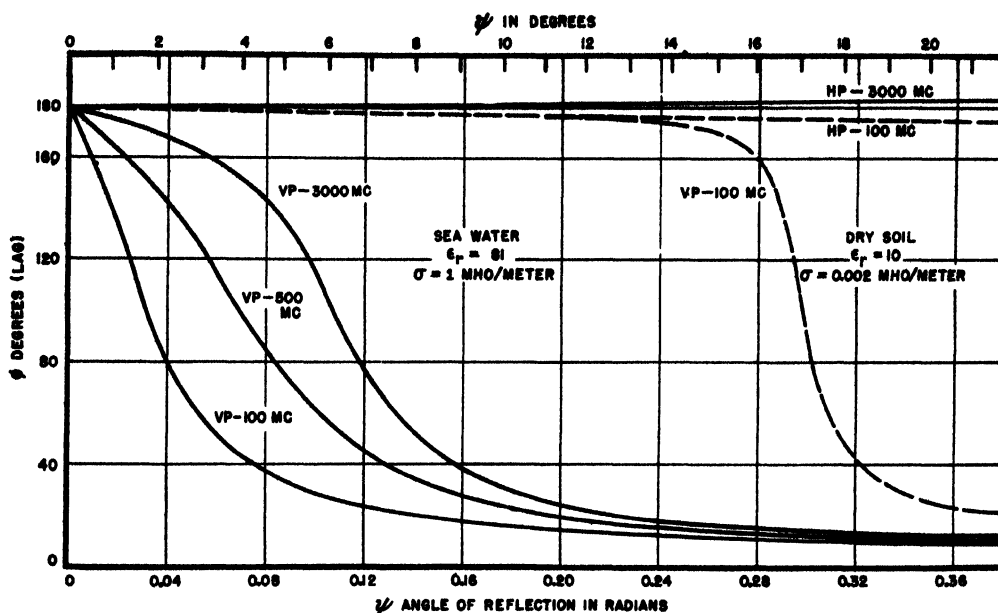
FIGURE 70. Phase of reflection coefficient curves. Note: Solid curve represents seawater. Dotted curve represents dry soil.

and angle of reflection for sea water and more gradually for dry land. The minimum point of the curves in Figure 69 is known as the pseudo-Brewster angle corresponding to a similar angle in optics.

TABLE 12. Terrain reflection characteristics.

Type of terrain	ϵ_r	σ, mhos per meter
Fresh water	81	10^{-3}
Sea water	81	1
Rich soil	20	3×10^{-2}
Heavy clay	13	4×10^{-3}
Rocky soil	14	2×10^{-3}
Sandy dry soil	10	2×10^{-3}
City—industrial area	5	10^{-4}

Cases not covered by Figures 69 and 70 may be computed from the following equations.

Vertical Polarization:

$$\rho \exp(-j\phi) = \frac{\epsilon_c \sin\Psi - \sqrt{\epsilon_c - \cos^2\Psi}}{\epsilon_c \sin\Psi + \sqrt{\epsilon_c - \cos^2\Psi}}, \quad (95)$$

Horizontal Polarization:

$$\rho \exp(-j\phi) = -\frac{\sqrt{\epsilon_c - \cos^2\Psi} - \sin\Psi}{\sqrt{\epsilon_c - \cos^2\Psi} + \sin\Psi}, \quad (96)$$

where Ψ = the angle of reflection measured from the horizontal;

$\epsilon_c = \epsilon_r - j60\sigma\lambda$;

ϵ_r = dielectric constant of the reflector relative to air;

σ = conductivity of the reflector, mhos per meter;

λ = wavelength, in meters;

ϕ = phase angle, lagging.

Some typical ground constants are given in Table 12.

Divergence

The reflected wave is scattered somewhat by being reflected from the spherical surface of the earth instead of a plane surface, and this reduction of field strength is taken into account by the divergence factor. This is dependent on geometrical considerations and may be expressed as follows (for $\gamma' < 3°$):

$$D = \frac{1}{\sqrt{1 + \frac{n\lambda}{2(5,280)^2 (\gamma')^2}}}, \quad (97)$$

where n is the lobe number,

λ is the wavelength, in feet,

γ' is the reflection angle, in radians, obtained from equation 60.

A convenient chart for obtaining D is given in Figure 71. The parameters are γ' in radians and $n\lambda$, with λ expressed in feet.

As γ' approaches zero, n also approaches zero, and the equation is indeterminate. At the point of tangency of the line of sight and the earth, D is 0.5773. At low angles the field is modified by diffraction around the curved earth. The lower limit of the angle γ' for which the optical treatment is valid is usually given by

$$\gamma' > \sqrt[3]{\frac{\lambda}{2\pi ka}} > 0.00382 \sqrt[3]{\lambda}, \quad (98)$$
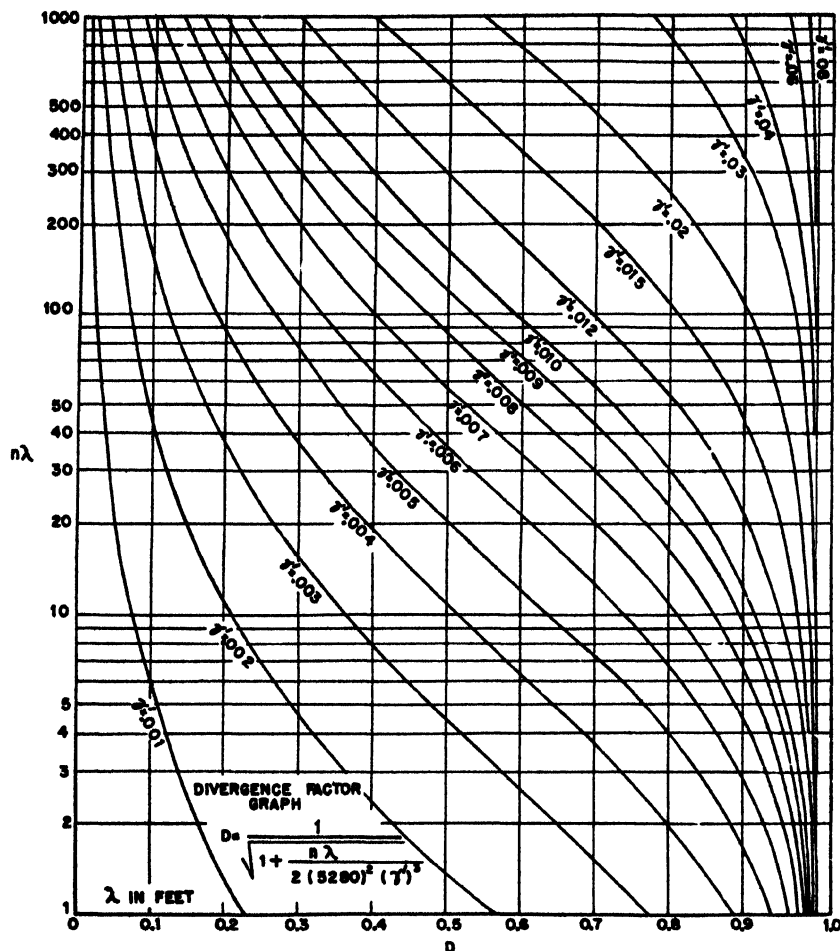
FIGURE 71   Divergence factor graph.

where k is $\%$ and λ is in feet.

For angles below this limit the theory for diffraction of radio waves around the earth is required for a rigorous solution. *However, in practice it is found that angles as low as the first maximum ($n = 1$) may be treated by the ray theory with little error.*

Applying equation (98) to Example 11

$$\gamma' > 0.00382 \quad \sqrt[3]{4.92} = 0.0065 \text{ radian.}$$

In Table 6 this corresponds to $n = 2.25$. However using $n = 1$ and $\gamma' = 0.0036$ the divergence factor D is found from Figure 71 to be 0.58. For angles below $\gamma' = 0.0036$ it is necessary to estimate D. Experience indicates that a fair minimum value to select for D is 0.5773. For angles much below the first maximum, the optical treatment gives values of field strength which are too low because it neglects diffraction. This may be compensated in part by using values of D between 0.5773 and 1.0.

Lobe Lengths

The contributions of the direct and reflected waves may now be added to obtain the length of the lobes.

$$L = [f(\gamma) \pm f(\gamma - 2\theta) \, z\rho D] d_0 \qquad (99)$$

where L is the distance to the end of the lobes or the nulls, in miles. d_0 is the maximum range (in miles) at which a given response (usually the minimum detectable signal) would be obtained if the antenna were in free space. If the lobe diagram were plotted for some signal level above the minimum detectable, d_0 and L would be correspondingly smaller.

Example 20. Lobes for a Medium Height Radar. A 200-mc radar using horizontal polarization has an antenna composed of two groups of dipoles spaced three wavelengths between centers, each group having four dipoles spaced $\lambda/2$, as in Example 16. The antenna is 500 ft high and 3 miles inland as in Examples 11 and 15. It is desired to compute the vertical coverage pattern.

From previous tests on this type of equipment it is known that the maximum range that would be obtained in free space d_0 is 80 miles. Since the polarization is horizontal, ρ will be taken as unity.

Precision is not required for most of this kind of work, and it will suffice to compute values for equation (99) at each integral value of n and to consider the values for odd n's (with the plus sign) as the average of the lobe. The lobe shape will be taken as sinusoidal and the range at the nulls obtained by using even values of n and the minus sign; $f(\gamma)$ and $f(\gamma - 2\theta)$ are obtained from Figure 63, by using values of γ and $\gamma - 2\theta$ from Example 11 corresponding to integral values of n. The values of z are obtained from Example 15. The computations are shown in Table 13. Had cliff edge diffraction been involved $f(\gamma)$ and $f(\gamma - 2\theta)$ would be read from curves as in Example 18 with marked effects on the pattern.

The lobes are plotted in Figure 46 using equation (74) and the value of L for odd numbered n's. For intermediate values of n the factors are:

Fractional value of n	$\sin(90° \, n)$
0.33	0.500
0.50	0.707
0.70	0.891

Using these three points above and below the lobe line and the maximum and minimum values from Table 13 the lobes may be plotted quickly as explained in Example 14.

TABLE 13. Lobes for a medium-height radar. (Example 20.)

n	$f(\gamma)$	$f(\gamma - 2\theta)$	z	D	$f(\gamma - 2\theta) \times \rho z D$	$f(\gamma) \pm f(\gamma - 2\theta)\rho z D$	L
0	0.999	0.999	1.036	0.577	−0.597	0.402	32.2
1	1.000	0.998	1.083	0.580	+0.627	1.627	130.2
2	0.999	0.997	0.980	0.735	−0.718	0.281	22.5
3	0.999	0.994	0.884	0.823	+0.723	1.722	137.8
4	0.997	0.992	0.938	0.890	−0.828	0.169	13.5
5	0.992	0.989	1.082	0.912	+0.976	1.968	157.4
6	0.989	0.987	1.170	0.933	−1.077	0.088	7.0
7	0.985	0.981	1.156	0.942	+1.068	2.053	164.3
8	0.980	0.978	1.073	0.959	−1.006	0.026	2.1
9	0.975	0.972	0.953	0.963	+0.892	1.867	149.4
10	0.970	0.967	0.825	0.968	−0.772	0.198	15.8
11	0.963	0.961	0.696	0.973	+0.651	1.614	129.1
12	0.958	0.952	0.582	0.979	−0.542	0.416	33.3
13	0.950	0.947	0.459	0.981	+0.426	1.376	110.0
14	0.941	0.939	0.377	0.984	−0.348	0.593	47.4
15	0.932	0.929	0.308	0.987	+0.282	1.214	97.2
16	0.923	0.920	0.261	0.989	−0.237	0.686	54.9
17	0.913	0.910	0.223	0.991	+0.201	1.114	89.1
18	0.903	0.900	0.192	0.992	−0.171	0.732	58.6
19	0.893	0.890	0.170	0.992	+0.150	1.043	83.5
20	0.881	0.879	0.150	0.992	−0.131	0.750	60.0
21	0.871	0.869	0.135	0.992	+0.116	0.987	79.0
22	0.857	0.853	0.121	0.992	−0.102	0.755	60.4
23	0.844	0.841	0.111	0.992	+0.093	0.937	75.0

The General Lobe Formula

The assumption of a sinusoidal lobe shape and the neglect of the phase of reflection and diffraction in the preceding section may in some cases lead to considerable error, especially when the direct and reflected waves are very different in strength. In

general a more accurate method is required for sites over 1,000 ft in height, where vertical polarization is used or where it is desired to know the lobe shape in detail. The method given in this section provides a general solution of the coverage problem in the optical region (except along the bottom of the first lobe).

The development of the lobe formula will be reviewed, and equation (99) will be given in a somewhat different form. The expression for the electric vector due to the direct wave is

$$E_d = \frac{E_1}{r_d} f(\gamma) \exp\left(-j2\pi\frac{r_d}{\lambda}\right). \quad (100)$$

For the reflected wave

$$E_r = \frac{E_1}{r} f(\gamma - 2\theta) R \exp\left(-j2\pi\frac{r}{\lambda}\right), \quad (101)$$

where E_d = electric field intensity at the target due to the direct wave, microvolts per meter;

     E_r = electric field intensity at the target due to the reflected wave, microvolts per meter;

     E_1 = electric field intensity at 1 mile in the equatorial plane of the antenna, microvolts per meter;

     $f(\gamma)$ = modified antenna factor for the direct wave (page 114);

   $f(\gamma - 2\theta)$ = modified antenna factor for the reflected wave (page 118);

     R = a complex factor for the reflected wave given by

$$R = D\rho z \{\exp[-j(\phi + \zeta)]\} ; \quad (102)$$

where D = divergence factor (page 119);

  $\rho \exp(-j\phi)$ = complex reflection factor (page 118);

  $z \exp(-j\zeta)$ = complex diffraction factor (pages 111-114).

The net field at the target is

$$E_T = E_d + E_r ,$$

$$\left| E_T \right| = \frac{E_1}{d} \left| f(\gamma) + f(\gamma - 2\theta) \right.$$

$$\left. D\rho z \{\exp[-j(\phi + \zeta + \delta)]\} \right| , \quad (103)$$

considering only the absolute value of E_T and taking $r = r_d = d$ except where the path difference is involved. The path difference phase shift is

$$\delta = \frac{2\pi}{\lambda}(r - r_d) . \quad (104)$$

Equation (103) may for convenience be written

$$| E_{r'} | = \frac{E_1}{d} A . \quad (105)$$

The target is assumed to have a complicated form and to be changing its aspect constantly. The

reflected energy is considered to be of random phase and magnitude. The magnitude of the reradiated field (microvolts per meter at a distance of 1 mile from the target) is found by using a coefficient of reradiation, ρ_T, which varies with the target and aspect.

The received field intensity is by the reciprocity theorem:

$$| E | = \frac{\rho_T | E_T |}{d} A .$$ (106)

Substituting from equation (105)

$$| E | = \frac{\rho_T E_1}{d^2} A^2 .$$

For a particular coverage contour, such as the threshold of detection, usually taken as a signal-to-noise ratio of unity, a minimum received field intensity $| E_N |$ may be assumed. This is related to receiver noise voltages, antenna gain, and other factors of design. Using $| E_N |$ for $| E |$ and solving for d

$$d = \sqrt{\frac{\rho_T | E_1 |}{| E_N |}} A = d_0 A .$$ (107)

Because of the way in which E_1 and ρ_T are defined, d_0, the maximum free space range, has the dimensions of length (in miles). It depends on the design of the transmitter and receiver and on the target. A may be considered a coverage factor which depends

on γ and terrain effects.

Because of the implicit character of the parameters of A in equation (103), a general solution of A as a function of γ is not feasible. However, examination of typical problems discloses that the range of variation of some of the factors is limited, and a method of successive approximations may be readily applied. In most cases ϕ and ζ will vary slowly (about $\frac{1}{30}$ as fast) compared to δ below 2° or 3°. At higher angles the rate of change may be faster, but contribution of the reflected wave at these angles is likely to be unimportant.

The method described here consists in computing the lobe angles, diffraction, and divergence as though the only phase shift involved was that due to path difference as given on pages 102-104, 111-114, 119. The phase shifts from the apparent lobe angles thus computed are then determined. The diffraction phase shift is ζ, and the reflection phase shift is

$$\phi' = \phi - 180°,$$ (108)

where ϕ is obtained from Figure 70. If horizontal polarization is used ϕ may be taken as 180°, and ϕ' is then zero. With curves of the phase shift $\phi' + \zeta$ and the product $f(\gamma - 2\theta)D\rho z$ plotted against γ the apparent lobe angles and lengths computed above may be corrected to obtain the actual values. The details of this method will be given in the example below.
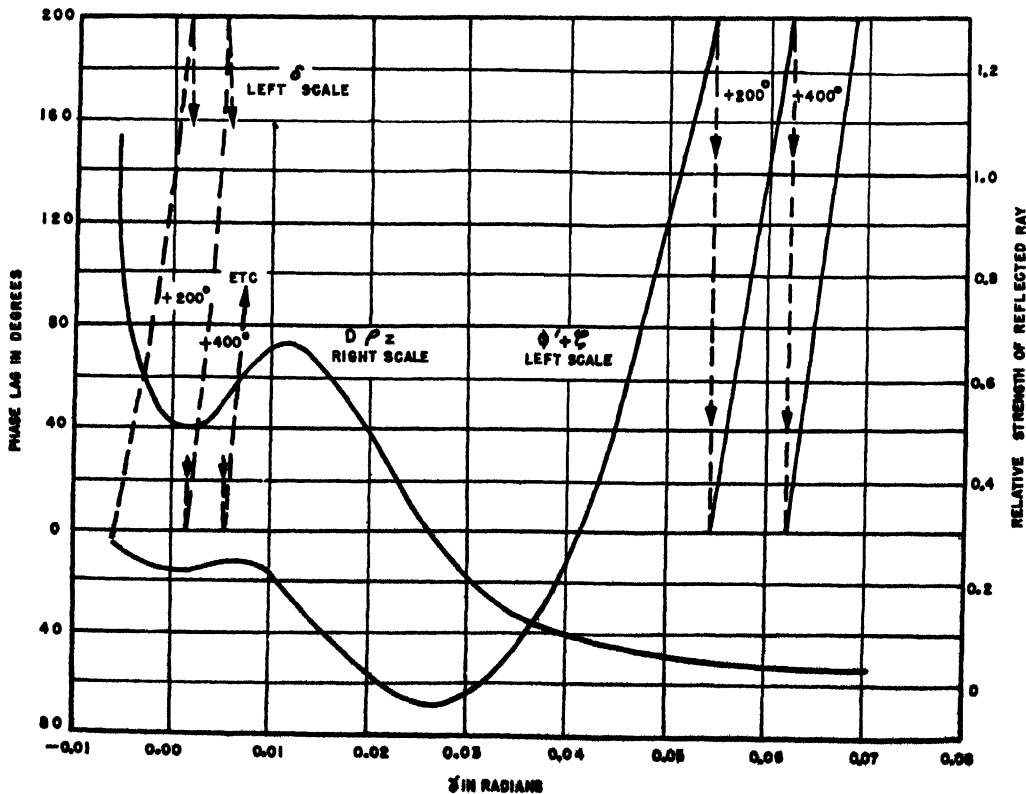
FIGURE 72. Relative magnitude and phase of the reflected ray.

Example 21. The General Lobe Formula. An interrogator equipment is used with the radar of Example 20. It operates on 160 mc; the height of the antenna above the sea is 500 ft; and the distance to the shore is 15,840 ft. The intervening land is too rough for coherent reflection. The antenna consists of two vertical radiating elements and parasitic reflectors. The radiators are approximately a half wavelength long and spaced a half wavelength apart. The maximum distance at which reliable interrogation may be obtained in the absence of a reflecting surface has been found to be 110 miles for this particular equipment. It is desired to construct for this site the vertical coverage diagram of the interrogator system.

The vertical pattern of a vertical half-wave dipole is given by

$$f_A = \frac{\cos\left(\dfrac{\pi}{2}\sin\gamma\right)}{\cos\gamma}$$

Since this factor is over 0.98 for angles up to 10 degrees, $f(\gamma)$ and $f(\gamma - 2\theta)$ will be taken as unity. The lobe angles are then computed neglecting ϕ and ζ, as in Example 11. Diffraction and divergence are computed as in Example 15 and as on page 119. The results of these calculations are listed in Table 14.

The values of ρ and ϕ depend on γ' and are read from Figures 69 and 70. Using equation (108), ϕ' is obtained and added to ζ. The sum $\phi' + \zeta$ is the net phase shift of the reflected wave from the values used in computing the lobe angles and is plotted against γ in Figure 72. For purposes of comparison δ has also been plotted, but this curve is not required otherwise. The product $D\rho z$ is the relative strength of the reflected ray and is plotted in Figure 72.

The points on the coverage diagram are obtained in polar form from equation (107).

$$d = 110\sqrt{1 + (D\rho z)^2 - 2D\rho z\, \cos\,(\overline{\phi' + \zeta + \delta})}\ .$$

The vector representing the reflected wave is shifted in the lagging direction by $\phi' + \zeta$ degrees when this sum is positive, and in the leading direction when the sum is negative. The effect of this phase shift on the point on the lobe being considered may be determined by inspection of Figure 72.

Thus, to determine the first maximum point the following procedure may be used. At $n = 1$ the angle γ is 0 0011 radian and $\phi' + \zeta$ is -14.8 degrees. This means that for the cosine term to be -1 the path difference must be increased until δ is 194.8 degrees. The angle γ_d at which this value of δ occurs is found by interpolating between 0 00110 and 0.00492 since δ changes from 180° to 360° in this interval. This angle is then 0.00141 radian. Had the angle $\phi' + \zeta$ changed appreciably from 0.00110 to 0 00141 the interpolation would be repeated using the new value of $\phi' + \zeta$. In most cases the new value of $\phi' + \zeta$ may be estimated from the curve, and the first approximation will be close enough.

At 0 00141 radian $D\rho z$ is 0.501 Substituting this value:

$$d = 110\sqrt{1 + (0\,501)^2 - 2 \times 0\,501 \times (-1)}$$
$$= 165.0 \text{ miles},$$

which is laid off on the coverage diagram at an angle of 0 00141 radian. As many other points as required to sketch the diagram may be computed in a similar fashion. For an intermediate point it is convenient to use the net angle equal to 90° since the equation then reduces to

$$d = 110\sqrt{1 + (D\rho z)^2}\ .$$

The angles of the lobes have been listed in Table 14 under γ_d and the lobe lengths under d.
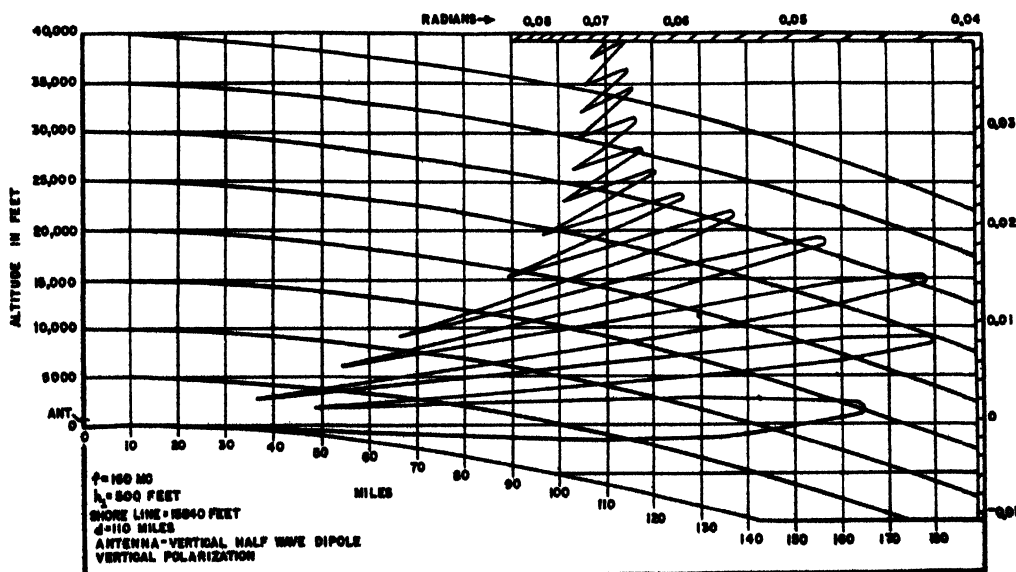
Figure 73. Coverage diagram for Example 21.

TABLE 14. The general lobe formula. (Example 21.)

n	γ' radians	γ radians	z	$\zeta°$	D	γ_4 radians	d
0	0	−.00600	1.061	− 2.86	1.000	−.00589	0
1	.00421	+.00110	0.920	− 5.27	0.640	+.00141	165.0
2	.00712	.00492	0.897	+ 3.04	0.792	.00527	48.5
3	.01000	.00835	1.039	+ 7.56	0.862	.00858	180.5
4	.01295	.01163	1.158	+ 2.75	0.908	.01206	36.3
5	.01595	.01485	1.158	− 5.04	0.938	.01557	178.5
6	.01897	.01802	1.067	− 10.88	0.955	.01894	52.7
7	.02200	.02119	0.930	− 15.00	0.963	.02225	155.6
8	.02500	.02428	0.779	− 15.00	0.969	.02544	66.5
9	.02810	.02744	0.648	− 11.00	0.973	.02860	137.0
10	.03110	.03051	0.500	0.00	0.982	.03161	89.1
11	.03420	.03365	0.408	+ 17.18	0.984	.03453	126.4
12	.03720	.03669	0.332	+ 43.0	0.987	.03731	96.6
13	.04050	.04005	0.267	+ 74.4	0.991	.04024	120.6
14	.04330	.04288	0.222	+108.9	0.991	.04253	100.7
15	.04640	.04600	0.190	+154.6	0.992	.04493	117.7
16	.04950	.04912	0.165	+206.2	0.993	.04894	103.0
17	.05250	.05216	0.143	+263.3	0.993	.05010	116.5
18	.05560	.05528	0.129	+326.2	0.994	.05264	104.0
19	.05870	.05840	0.114	+412.3	0.995	.05479	115.6
20	.06170	.06142	0.104	+492.6	0.997	.05694	104.5
21	.06480	.06454	0.094	+590.0	0.998	.05909	114.6
22	.06780	.06755	0.089	+687.0	0.998	.06127	105.6
23	.07090	.07067	0.081	+813.0	0.998	.06436	114.2

The vertical coverage diagram is shown in Figure 73. The lobe maxima and minima and the 90-degree points have been sufficient for sketching the lobes except on the first lobe where a few additional points have been computed. When the net angle is 60 degrees, the field strength at the bottom of the first lobe is equal to the free space field. At ranges shorter than this the reflected wave opposes the direct wave. Directly under the antenna the contour passes near the surface so that the waves are very nearly in opposition. Because of the variation in $D\rho z$ with γ the maxima will not occur exactly when the cosine is unity, but this effect is generally negligible.

CALIBRATION AND TESTING

One should not infer from the foregoing that a reliable coverage diagram can be obtained by calculation alone. Under field conditions it is necessary to make test flights and other checks before equipment can be depended upon to meet a calculated performance. On the other hand it is seldom possible or desirable to obtain a satisfactory coverage diagram from tests alone. Best results are attained when tests and analysis supplement each other.

Test flights are arduous, expensive in personnel and materials, and time consuming. In most theaters a number of agencies become involved, and careful planning and organization are required to achieve a useful result. For these reasons the amount of test flying should be held to a minimum by intensive analysis and equipment tests before and after the test flights.

Equipment Tests

It is difficult to overemphasize the importance of proper equipment maintenance. An unfortunate tendency of inexperienced personnel is to maintain on an emergency basis, rather than as a matter of systematic routine. In most cases the need is for a careful check of all elements and restoration to as-good-as-new condition, rather than a brilliant intuitive process known as "trouble shooting." One survey of a large number of systems disclosed an average reduction from optimum performance of 13.5 db. This corresponds to a maximum range of 50 per cent of normal. Careful tests have shown the use of "standard targets" to be very misleading in many cases. Large changes in the maximum ranges of small targets were found without appreciable changes in the strength of the permanent echoes used for checking purposes.

Full use of test instruments available should be made in checking the equipment. Orientation should be completed and the accuracy of range and azimuth indicators checked. Tuning and modifications should be done before the test flights are made, unless the tests indicate poor performance. A great handicap in this work is the lack of absolute measures of power output, but much may be done with echo boxes and field intensity meters.

Signal Measurements

Several methods are used for recording signal strengths, and these determine the type of receiver calibration required. Estimation of signal-to-noise ratios by means of scales on the face of the scope requires some means of specifying the gain setting. The means used, such as height of noise, position of gain dial, and so forth, should be calibrated with a signal generator so that there is an assurance of adequate sensitivity and a way of checking the measurements. The saturation line on the scope is assigned a height of 10, and the signal and noise heights are read in proportion. Ratios in excess of 10 are usually read as 10+. This method requires considerable skill on the operator's part and is limited in scope. In Figure 74 is shown a calibration curve on a typical "square law" receiver. In the circle is represented a signal on an A scope which would commonly be read as a signal-to-noise [S/N] ratio of 8. Actually the ratio of receiver inputs corresponding to the signal and noise heights is 8.5/3.25 or 2.6.

A considerable improvement over the above method may be obtained as follows. An index line is drawn on the face of the A scope about an inch from the baseline. To measure a signal it is brought to the index line by adjustment of the gain control, and the gain control voltage is recorded. The gain voltage required to bring the noise to the index line is also noted occasionally during the test. A calibration curve is made using a pip signal generator or a modulated signal generator connected to the receiver input. The gain voltage required to bring the signal to the index line is measured for various inputs. Gain voltage readings on the test target and noise are converted by means of the curve to equivalent
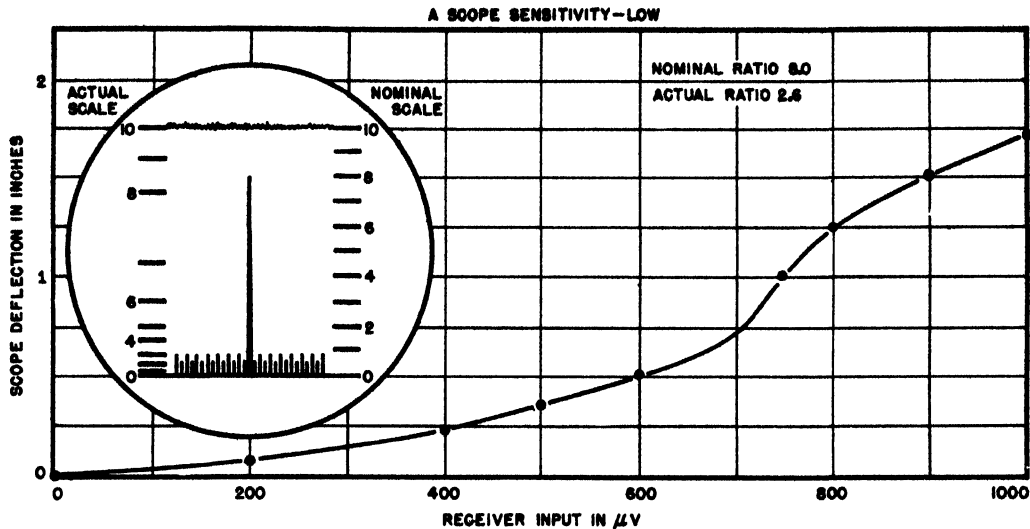
FIGURE 74. Typical receiver characteristics.

input voltages. Test data may be conveniently plotted as decibels above noise after this conversion. It should be noted that the calibration depends upon the type and percentage of modulation.

A third method involves calibration of the gain control dial by comparison of permanent echoes. Three lines are drawn on the scope face such as ½, 1, and 1½ in. from the baseline. The position of the gain dial with the noise at ½ in. is marked 0 db. A permanent echo is selected which comes to the 1-in. line at this setting. The gain dial is then turned to bring this echo to the ½-in. mark, and this position of the dial is marked 6 db. Another echo is then selected which is 1 in. high, and it is brought down to ½ in. by further adjustment of the gain dial. This position is marked 12 db. In this manner the gain dial may be calibrated over the full range of adjustment. It may be necessary to change the series resistor on the gain potentiometer to spread the working part of the scale over a sufficiently wide angle. A common difficulty with this method is lack of suitable permanent echoes (see page 92).

A fourth method is suitable for microwave gear where search is conducted with a PPI scope. As the beam sweeps past the target a hit or miss is recorded. If desired, additional note may be made such as miss, very weak, weak, or hit. In analyzing the data the percentage of hits in an arbitrary period of 30 sec is

plotted against range, counting very weak signals or stronger as a hit, as in Figure 75. The data may be scattered, but it is not difficult to decide the range at which the percentage of hits is 50 per cent. This is taken as the maximum range. At lower altitudes a lobe structure may be detected, indicating ground reflection.

Conduct of Test Flights

The test planes should have two or more engines. Slow-speed, high-ceiling, long-range planes are most desirable. They should be equipped with navigational aids such as radio compass, DF system, and loran, and full complement of communication sets, transponders, and altimeters. For positive identification in regions of high traffic density, a distinctive IFF (identification friend or foe) response is essential. Mark II transponders may be readily modified in the VHF band to give a double pulse by shifting the condenser rotors.

Tests are conducted by flying out from the station and returning at a specified altitude to a range estimated to be about 10 per cent beyond the maximum of the lobes. Suitable altitudes are from 5,000 to 20,000 ft. Little is learned from tests below 1,000 ft since nonstandard propagation effects are most pronounced in this region.

Data should be taken by specially trained operators as considerable judgment is required. Where feasible, flights over sea should pass near landmarks, etc., to check navigation. Other radars and agencies should be employed to assist the test plane in holding its course. The permanent echoes should be noted during the test and compared with average conditions so that an estimate of nonstandard propagation may be made. Similar checks should be made at other nearby radars.
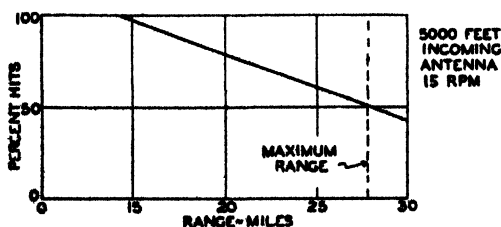
FIGURE 75. Test flight data for PPI scope.

Analysis of Test Data
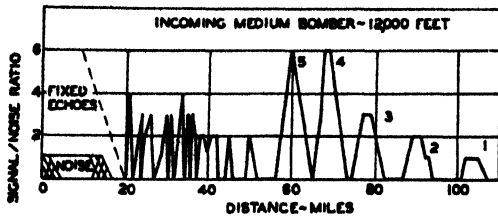
FIGURE 76. Typical signal-to-noise test data.

In Figure 76 is shown a signal-to-noise graph for a station similar to Example 20. The noise is set at a relative height of 1, and the signals are read in proportion as the plane comes in. The weak signals at medium ranges are due to shore line diffraction. The peaks correspond to lobe maxima and ranges at S/N = 1 to the locations of the lobe contour at 12,000 ft. The receiver in this case is of the "linear" type, and the lobe maxima may be obtained by extrapolation. Along a line of constant path difference such as the maxima of the lobes the signal-to-noise ratio varies as the inverse square of distance. Thus the fourth lobe has a peak S/N ratio of 6 at 68.5 miles, and the lobe length is $L = 68.5 \sqrt{6} = 167.5$ miles.

In practice the length computed in this manner would be compared to those obtained from tests at other altitudes. Notes made during the test and other factors would be considered and the data weighted accordingly. For example, at 90 miles the S/N ratio is 2 and the percentage error is probably greater than on the reading at 68.5 miles. The location of points on the lobe cannot be read with accuracy from Figure 76 at S/N = 1 since this is threshold data which

may be in considerable error.

To determine the maximum free space range F, the lengths of the lobes obtained from the test data may be listed along with the site factors from equation (99) or equation (107). A value of F is then selected which will most nearly fit the test data. Variations in performance of the equipment affects the lobe lengths in proportion. Variations from the standard atmosphere assumed will shift the position of the lobes, particularly at low altitudes.

Where better accuracy is desired or the receiver is nonlinear, the calibrated receiver method is required. Such data are recorded as gain voltage, range, and time. For each gain voltage, the equivalent receiver input voltage is read from a calibration curve such as Figure 74. The equivalent value of the noise voltage of this set is 30 μv. Dividing the equivalent receiver signal voltages by 30 gives the S/N ratio which is plotted against range in Figure 77. The lobes are identified by reference to a lobe angle diagram. The extrapolated lobe lengths may be listed as follows:

Height, feet	Length of lobes, miles			
	1	2	3	4
20,000	...	243	196	235
10,000	159	212	169	162
5,000	156	216	163	158

The 20,000-ft data were taken last and indicate the effect of certain equipment adjustments. The ability to maintain this performance is one of the questions to be considered in arriving at a weighted average value of lobe lengths. Comparison of these lobe lengths with the computed lobe factors will indicate a fair value to be used for the free space maximum range.
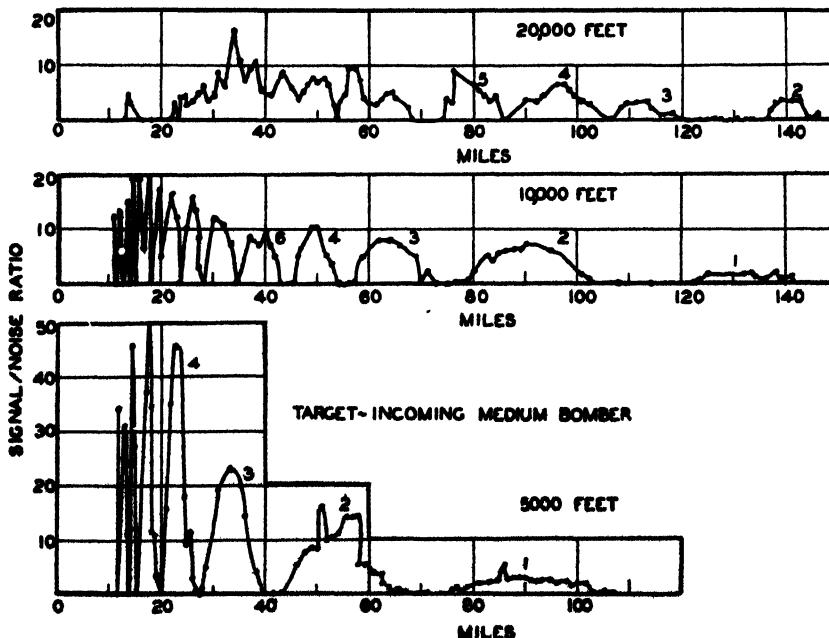
FIGURE 77. Test flight data from a calibrated receiver.

VARIATIONS IN RADAR COVERAGE

VARIATIONS IN COVERAGE of radio and radar equipment are caused by atmospheric factors which influence propagation of very short radio waves.

The rapid and accurate evaluation of radar signals is dependent to a great extent upon our knowledge and understanding of the effects produced by the variable conditions of the lower atmosphere.

Evaluation of radar signals influenced by weather introduces problems of identification, actual range determination with second or third sweeps, and radar coverage characteristics, each having a direct bearing on the tactical situation.

Enemy ships far beyond the horizon have been located by radar and sunk by radar-controlled gunfire. United States warships in the Pacific, in several instances, have picked up targets by radar at ranges four to five times those obtained under standard conditions.

Army coastal radars have tracked convoys on some occasions to 20 or 30 miles beyond normal radar ranges. The same radars, a few hours later, may have failed entirely to pick up targets clearly visible to the eye.

Allied forces are employing radar and VHF (very high frequency) equipment with steadily increasing effectiveness. But we are forced to revise and improve our early conceptions of the capabilities and limitations of these useful instruments of World War II. Serious errors and false evaluation of radar presentation may result if we do not take into consideration the effects of weather and atmosphere on radar ranges and VHF coverage.

Complete reports of the variability of radar coverage show that certain weather and atmospheric conditions prevailing along the transmission path may greatly modify the normal range characteristics of radar and VHF radio. The operator, at certain times, can "see" targets or hear messages far beyond the horizon, sometimes at unbelievable distances. At other times he is unable to contact, by radar or VHF, aircraft or surface craft well within the normal range limit.

These effects of a *nonstandard* atmosphere might leave doubt in our minds as to the effectiveness of radar and the usefulness of VHF radio. But we should adopt the reverse view. We can, by understanding and allowing for these phenomena, make a useful instrument more effective—the weather will work *for*, *instead of against*, radar and microwave equipment.

Unusual ranges are caused by *bending* or refraction of the radio waves by the atmosphere. A most important special case of refraction is the concentration of the wave energy in ducts within the atmosphere. This *bending* and *duct formation* is a direct result of the meteorological factors involved—factors of weather and atmosphere—peculiar, in many cases, to the locality and the season. Such factors are discussed later.

BENDING

The VHF or radar operator usually assumes that short waves and microwaves, at frequencies above about 30 mc, travel along the line of sight from the transmitter to the receiver and, in the case of radar, to and from the target. Experience has shown that this assumption, nearly true in many instances, may lead to serious errors or false evaluation if applied to radar operation and microwave communication.

Radio waves are bent from a straight line path as a result of refraction by the lower atmosphere. This bending, or refraction, is generally recognized as a property of light. It is equally a property of radio waves. The underlying principles are exactly the same in both cases.

The quantity that determines refraction is called the index of refraction. Refraction occurs whenever there is a change of index of refraction, as at the boundary of two substances. In the interior of a material of constant refractive index, the rays travel in a straight line. The change in angle at the boundary is the larger, the greater the difference in refractive index from one material to the next.

Radio waves are refracted or bent in the atmosphere because the index of refraction of the atmosphere changes with height. The properties of the atmosphere which determine the refractive index and which change with height are temperature, pressure, and moisture content. These changes from one level to another are very small compared with that from water to air, and the resulting refraction itself is small. Nevertheless this refraction is of great importance in radar operations and radio communications above 30 mc.

If the atmosphere were composed of a number of successive layers each having a different index of refraction, a wave passing across the successive boundaries of the layers would be abruptly deflected at each surface. The atmosphere does not consist of such distinct layers. Instead, the change in its physical properties and its index of refraction is gradual, continuous. There is, then, no sudden change in direction of the waves; the change in direction becomes gradual and continuous. In other words, a bending of the waves occurs as they pass through the atmosphere. Radio waves passing through the
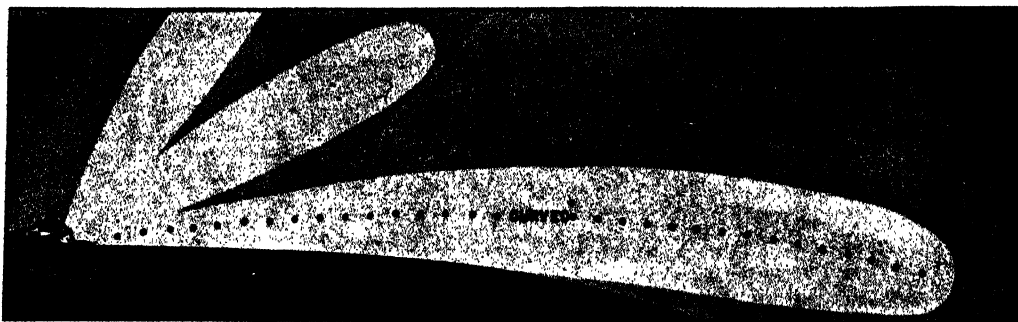
FIGURE 1. Actual pattern showing radar coverage for standard propagation.
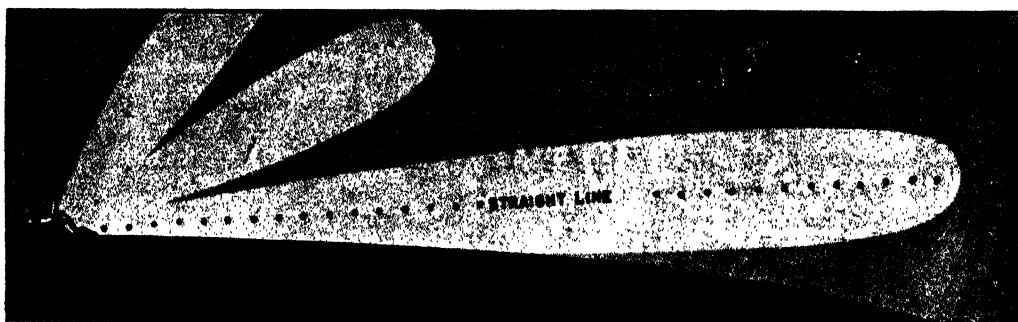
FIGURE 2. Modified presentation of the information shown in Figure 1.

lower atmosphere are usually bent *downwards*.

As can be seen from the illustration of the actual pattern (Figure 1), the bending of the waves, or rays, by the atmosphere permits one to see farther than he would otherwise. In the figure the vertical dimensions have been strongly exaggerated so that the earth's curvature becomes clearly visible. Under average weather conditions the horizon distance is increased by about 15 per cent, but at an elevation near the first lobe the increase in range is much less than this amount. This is the case of standard refraction, or *standard propagation*.

It is rather inconvenient to draw curved rays in radar coverage and calibration diagrams. This can be avoided by assuming that the earth's radius is ⅚ the actual radius. Then in the diagrams the rays appear as straight lines when the propagation is of the standard type. This method often is adopted in radar calibration practice, with coverage diagrams drawn or printed to the ⅚ value of the earth's radius (see Figure 2). This corrects for the effect of normal bending in the atmosphere. The radar operator merely plots the position of his target on such a diagram and assumes that the radiation travels along a straight line between the radar and the target. In this way he takes into account the effects of standard refraction while doing his work.

Wave propagation deviating from standard occurs under special weather conditions. The most important type is called "guided propagation," "trapping," or "superrefraction"—formerly referred to as anomalous propagation. The main feature of this

type of propagation is an excessive bending of the rays due to refraction. This bending occurs principally in the lower layers of the atmosphere and mainly in the lowest few hundred feet. In certain regions, notably in warmer climates, excessive bending is observed as high as 5,000 ft. The amount of bending in regions above this height is almost always that of the standard atmosphere.

As a consequence of the excessive bending in the lower layers the coverage pattern of a radar set is deformed, as illustrated in Figure 3. The fact that
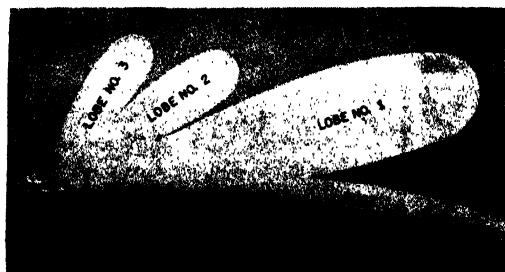
FIGURE 3. Radar lobe pattern in nonstandard atmosphere. A duct has been formed on the surface of the ocean and a ship is detected. Lobe No. 1 is bent downward more than normal, but the other lobes remain substantially unchanged by the duct.

atmospheric influences are effective only in the lower layers does not imply that the echo strength from a target will be affected only as it lies in these layers, though the effects will be strongest there. It merely means that excessive bending is suffered by the rays only while passing through the lower layers. How-

ever, the deformation of the coverage pattern itself will in general extend to a greater height.

Two factors are operative in producing a rapid change of refractive index with height: variation of moisture with height and variation of temperature with height. Excessive refraction occurs when there is a rapid decrease of moisture with height ("moisture lapse") and, to a lesser degree, when there is a rapid increase of temperature with height ("temperature inversion"). The most pronounced cases of excessive refraction occur when both these conditions prevail at the same time. These conditions will be discussed later from the meteorological viewpoint.

Since the atmosphere is a very tenuous substance, the amount of refraction, that is, the amount of angular deflection of the rays, is very small and in no case exceeds a fraction of a degree. How then can these small effects influence radar operations? The answer is that they do not influence operations unless the angle between the ray itself and the horizontal is very small. If radar is used for fire control, search-light control, or fighter intercept control, the targets are usually at medium or short ranges, and the angle between the line of sight and the horizontal is usually larger than one to two degrees. Refraction has practically no effect on such an application of radar.

However, the same equipment may be used for long-range search and then the story is different. With early warning radar the target may be an airplane 50 or 100 miles away, and it may fly at an elevation of only a few thousand feet. In this case the angle of elevation of the target above the horizontal, as seen from the radar, is only a fraction of a degree. This applies still more to seaborne targets. The atmospheric effects then become operationally important. It should always be kept in mind that only low-angle search is affected by meteorological conditions.

As a rule, the operational characteristics of a radar for angles of elevation of the target exceeding 1 degree may be calculated on the assumption of a standard atmosphere, with confidence that all non-standard meteorological effects are negligible.

GUIDED PROPAGATION

It is obvious that excessive bending of the rays in the lower layers of the atmosphere must distort radar coverage patterns. One case of special importance is illustrated in Figure 4. Four rays, out of many, are shown which leave the transmitter at different angles with the horizontal.

Ray 1 is bent so much that after some distance it returns to the ground; there it is reflected and then the same course is repeated again. In this way the ray may be reflected a number of times in succession, remaining always in the lowest layer. This super-refraction "traps" the rays in a "duct" and results in guided propagation of the radar waves. Trapping does not occur under standard atmospheric condi-
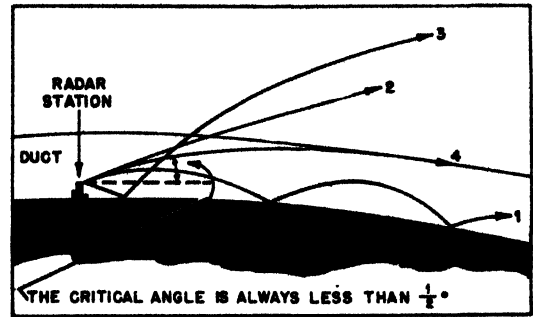
FIGURE 4. Wave paths illustrated as rays in ground-based duct.

tions. A ray, under standard conditions, may be reflected by the earth's surface only once before it escapes into space.

Ray 2 is also bent in the lowest layer but not enough to keep it from escaping into the upper atmosphere whence it does not return to earth.

Ray 3 is similar to 2 except that it undergoes one reflection by the ground before it escapes into the upper atmosphere.

Ray 4 separates the two types of rays illustrated by rays 1 and 2. This ray becomes horizontal when it reaches the top of the trapping layer or duct and from there on travels along at the same height. All rays are divided into two groups: those that leave the transmitter at an angle with the horizontal less than the critical angle and are trapped, and those that leave the transmitter at a larger angle and proceed into the upper atmosphere.

The critical angle is always small, practically never larger than ½ degree. Its magnitude may be taken as a measure of the intensity of guided propagation, that is, of the amount of radiant energy trapped within the duct. Rays that leave the transmitter at a somewhat larger angle up to about twice the critical angle are sufficiently deflected while passing through the lowest layers to distort that part of the radar coverage pattern lying just above the duct. Rays leaving the transmitter at a still larger angle are not appreciably affected.

The ground-based duct or trapping layer guides the wave along the earth's surface in much the same way that hollow metal tubes guide microwaves. Within the duct there is less decrease of signal strength with distance than there is above the duct. Radar ranges on surface craft and low-flying aircraft located within a duct, similar to the one illustrated in Figure 5, are increased—sometimes to two, three, or four times the normal ranges. Ground echoes would be increased at the same time and might, in some cases, obscure partly, or even entirely, the echoes from incoming aircraft.

When the radar is located within the duct, ranges on aircraft flying above the duct will be decreased only slightly, if at all. Often there may be a slight

FIGURE 5. Rays in an elevated duct. In this, another common form of duct, the amount of bending may be approximately normal both below and above the duct The rays oscillate between the upper and lower boundaries; maximum ranges in or near the duct may be even greater than with a ground-based duct

increase in effective ranges. If the angle of elevatior of the aircraft is greater than 1 degree, the effects become inappreciable and failure to detect the target cannot be attributed to excessive refraction.

If the duct does not include the radar within its boundaries, as, for example, when a duct forms below a high-sited radar, the effective ranges on surface craft may be either increased or decreased. Similar reasoning may be applied in the case of airborne VHF radio communication. Usually there is no very pronounced effect upon the signal strength when VHF communication is carried on between two aircraft, both flying above the duct.

Interference between the direct rays and the rays reflected from the ground—resulting in the well-known lobe pattern of the coverage diagram—has not been mentioned. Under standard conditions the position of the lobes depends only on the wavelength used and the height of the radar above the ground. When a duct is present the lowest part of the coverage diagram may be strongly distorted.

Coverage depends upon a variety of factors of which the most important are these: height of the top and base of the duct, amount of refraction in the duct, position of the transmitter relative to the duct, frequency (or wavelength) of the radar equipment, and height of the transmitter above ground.

A coverage diagram for standard conditions is shown in Figure 6, diagram 1, with height strongly exaggerated. Only the lowest three lobes are shown, and the higher lobes appear compressed as compared to the lowest lobe. In diagrams 2, 3, 4, 5 the lower part of the same diagram is drawn as it appears under various conditions of guided propagation. The bottom part of the "standard" main lobe is shown by a broken line. The lines which separate the "blind zones" from the "detection zones" represent the range at which a medium bomber would just become visible to this particular radar set.

The diagrams clearly indicate the great extension of ranges in the duct and also the moderate change in ranges—sometimes an extension, sometimes a reduction—above the duct. Another feature of some
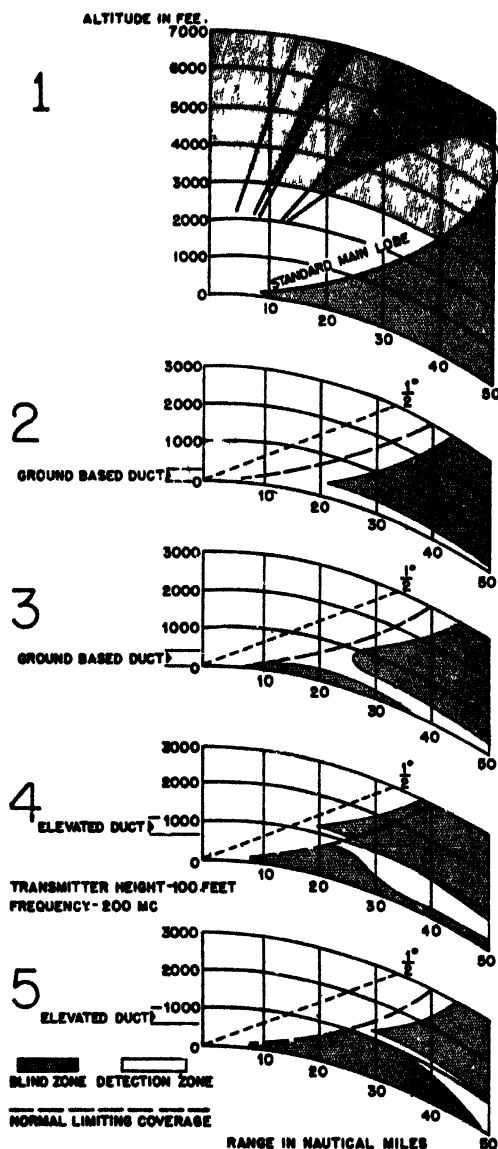
FIGURE 6. Standard and nonstandard coverage diagrams

of these diagrams is the appearance of "skip-ranges" A plane flying at an altitude of 500 ft, for instance, would be detected early under the conditions shown in diagrams 4 and 5. As the plane approaches, the echo will disappear from the scope and reappear only at a range less than 20 miles. Similar conditions will prevail for ground clutter. In diagram 3 there would be ground clutter close in and also from beyond 33 miles but not from the space between. For conditions shown in diagram 5, there would be echoes from very remote ground targets but not from targets at intermediate ranges.

A change in echo strength from day to day is not necessarily caused by the weather but might simply be caused by a variation in performance of the set. Cases have occurred where there was extensive trap-

ping, but because of lowered set performance there was no corresponding increase in fixed echo strength. The set then will appear to be in good operating condition, and the operator will be deceived about ranges of detection for craft flying above the duct. Equipment for checking set performance is not usually available in the field. The change in intensity of nearby fixed echoes may be, in some cases, a measure of set performance, but in the absence of more elaborate checks this method can be misleading and should not be relied upon entirely.

Failure of detection of targets is not necessarily due to weather influences. Electrical failure of the set or inadequate adjustment may be the difficulty and may be far more troublesome to identify than meteorological effects which should not be used as a "scapegoat" to .be indiscriminately blamed for poor coverage.

METEOROLOGICAL FACTORS

The atmosphere is responsible for bending and duct formation. To understand the "why" of nonstandard ranges of radar and radio with respect to the weather, it is necessary to consider the meteorological factors involved.

The strong refraction which results in guided propagation is caused by a rapid decrease of index of refraction with height within certain layers. The decrease depends upon distribution of moisture and temperature in the atmosphere, particularly in the lowest few hundred or thousand feet. Normally the temperature decreases with height in the atmosphere (at a rate of about 2°C per 1,000 ft), and the moisture decreases gradually with height. Under these conditions the propagation is of the standard type.

Temperature may sometimes increase with height for a few hundred or thousand feet above ground and then, at greater heights, begin to decrease again. The vertical increase of temperature is called a temperature inversion. Sometimes a layer of moist air is found near the ground, and the air overlying it is very dry. There is then a rapid decrease of moisture over a short vertical distance: in other words there
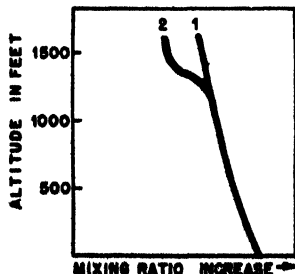
FIGURE 7. Moisture variation aloft. 1. Moisture distribution with height in standard moist atmosphere. 2. Example of sharp moisture lapse (dry air overlying moist air) conducive to guided propagation. Mixing ratio is amount of moisture in a unit weight of dry air expressed as grams of water per kilogram of dry air.

is a pronounced moisture lapse (see Figure 7). A moderate or strong moisture lapse almost always will produce trapping, but a temperature inversion (except at low temperatures) will lead to trapping only if the moisture distribution is favorable. A combination of both effects within the same layer usually will produce trapping.

The meteorological conditions to be found over sea and over land are quite different and must be considered separately.

OVER SEA

When warm, dry air flows over colder water, a temperature inversion will be established, and there will be evaporation into the lowest layers of the air, thus creating conditions of pronounced trapping. This weather condition is one of the most common causes of guided propagation. An example in point is the Mediterranean, which to the south, east, and west is surrounded by dry land masses producing a flow of dry, warm air over the water when the winds
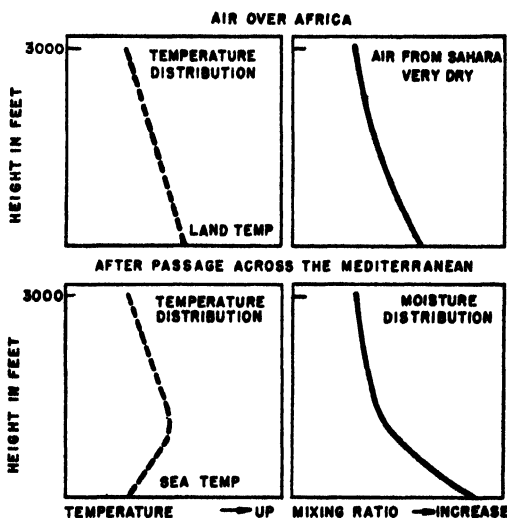
FIGURE 8. Modification of air from Sahara Desert in passing over the Mediterranean.

blow from these directions (see Figure 8). Similar conditions are often caused by westerly winds.blowing from land to sea across the eastern boundary of a continent. Land and sea breezes may influence radar operation along a coast line. The wind direction at a coast is often an important factor in determining propagation conditions and should be closely watched. Whenever unusual propagation is observed by coastal radar stations, a record of prevailing winds at the time is very helpful in determination of future expected performance.

OVER LAND

Temperature inversions are produced mainly by nocturnal or night cooling of the ground (see Figure 9). Trapping may occur when the moisture distribu-
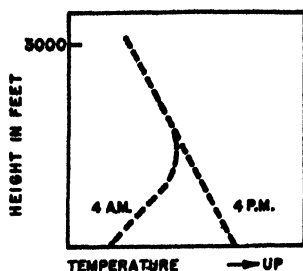
FIGURE 9 Formation of temperature inversion over land due to nocturnal cooling.

tion in the lowest layers is such as to reinforce or at least not to counteract the effect of the temperature distribution, that is, when the moisture decreases not too slowly with height. Nocturnal cooling is greatest with clear skies and is quite small under an overcast. Hence guided propagation over land occurs at night almost exclusively with clear skies. This type of temperature inversion is strictly confined to land areas. It does not occur over the ocean because the sea temperature does not show appreciable daily variations. Temperature inversions caused by nocturnal cooling are most pronounced over dry land (desert) but will occur almost anywhere over land with a clear sky and a not too humid atmosphere.

SUBSIDENCE

Another weather phenomenon favorable to trapping is subsidence. By subsidence is meant the slow downward motion, combined with horizontal spreading, of air above the lowest layers of the atmosphere. This process, which most frequently occurs in the area of barometric high, will produce temperature inversions; the subsiding air moreover becomes relatively much drier than the unaffected air below. In general the subsidence inversion is quite high (e.g., above 4,000 to 5,000 ft). In the light of present knowledge it appears that high subsidence inversions do not generally affect guided propagation when the sets are situated at low altitudes. It appears, however, that such subsidence inversions might materially affect communications or airborne radar search aloft. Lower subsidence inversions (1,000 to 2,500 ft) along the southwestern coast of the United States are known to produce stable duct layers affecting radar coverage at low angles.

TURBULENCE OF THE AIR

This has a distinct normalizing effect in that it tends to smooth out the temperature and moisture variations which are conducive to guided propagation. Moderate to strong winds produce a turbulent layer extending normally to a height of about 4,000 ft. The air is well mixed within this layer, and consequently the standard type of refraction prevails. Regions of a barometric low are characterized by strong to moderate winds and pronounced turbu-

lence in the lower layers. In addition low pressure areas usually have overcast skies. Hence a barometric low will as a rule lead to propagation of the standard type.

FREQUENCY OF OCCURRENCE

It is extremely difficult to estimate in general terms the frequency of occurrence of guided propagation, since statistical data are almost nonexistent at present except for very limited regions in Europe such as the North Sea. In the central Mediterranean during the summer months of 1943, ducts have been observed on 9 days out of 10. Frequent trapping has also been observed in some parts of the Pacific. At other times and places guided propagation might be an unusual occurrence, especially if the barometric pressure is generally low and the winds strong. It seems advisable to consult a weather officer with regard to any given locality.

MEASUREMENTS

In order to determine weather's influence upon radar in a quantitative way, the variation of refractive index with height must be determined. This requires accurate knowledge of the temperature and moisture distribution in the lowest few hundred or thousand feet of the atmosphere. The ordinary radiosonde is not well adapted to measurements of this type because the measured points on an ascent are usually spaced several hundred feet apart. Among the methods which have been developed for this purpose during the past two years, the one most generally adopted uses a captive balloon (or kite) which carries aloft electrical temperature and moisture—measuring elements. These are connected to a meter on the ground by means of thin wires attached to the cable holding the balloon. This device permits measurements at intervals as closely spaced as desired. A psychrometer held out of the window of a slowly flying plane has been used with good success in the absence of more elaborate equipment.

CLOUD ECHOES IN RADAR

Cloud echoes (more precisely, precipitation echoes) are observed frequently on radar scopes. At times they have caused confusion by blotting out other targets. Their similarity, upon certain occasions, to actual targets have caused some difficulty in the interpretation of the signals.

These echoes are caused by a reflection of the radar pulse from the raindrops in the clouds (or in rain storms). The amount of reflection increases very rapidly with frequency. Cloud echoes are quite exceptional below about 1,000 mc. In microwave radar they first appeared as a nuisance, but more recently they have been put to practical use. In tropical climates they are very helpful for aerial navigation.

Cloud echoes may be distinguished from other echoes by their fuzzy and diffuse appearance. Not all clouds show up on a scope with equal strength. The strength of the echo seems to depend primarily on the size of the water drops within the cloud or rain storm. Ordinary clouds such as form an even overcast (stratus clouds) are not usually visible on the scopes; the droplets that compose these clouds are so small that they reflect very little energy. Violent showers give intense echoes on the scopes. Storm echoes can be seen much farther than normal land targets, even under standard conditions, because of their great spread in the vertical direction.

In discussing cloud reflections it must be clearly understood that there is no physical relation between cloud echoes and refraction; the mechanics of duct formation is not related to clouds, and with respect to the bending of radio waves a cloud is merely another airborne target.

SUMMARY OF BASIC FACTS CONCERNING PROPAGATION AT RADAR FREQUENCIES

1. Standard propagation results in a slight downward bending of the rays throughout the atmosphere, leading to an increase of the horizon distance compared to the geometrical value. It is taken into account operationally by using coverage diagrams with a ⁴⁄₃ earth's radius; on a diagram modified in this way the rays appear as straight lines.

2. Guided propagation occurs almost exclusively in the lowest 2,000 ft above the ground and usually is confined to the lowest few hundred feet (except in warm climates).

3. Effects of nonstandard propagation are negligible when the angle of elevation of the target is over 1 degree. Failure of detection at such angles must be attributed to other causes.

4. Of the meteorological conditions conducive to guided propagation or trapping, the most outstanding are:

    a. Over sea: flow of warm, dry air over colder water producing temperature inversions and evaporation into the lowest layers.

    b. Over land: nocturnal cooling of the ground with clear skies and calm air or light winds (if moisture distribution is favorable).

    c. Over both sea and land: low-level subsidence.

5. Conditions in a barometric high, including calm and clear skies and especially low-level subsidence, favor trapping especially during the night (but do not necessarily produce it). Conditions in a barometric low, including strong winds, intense turbulence in the lowest layers, and overcast skies are conducive to standard propagation.

6. When the transmitter is within the duct, radar range is increased for surface targets (ships) and aircraft flying in the duct. At the same time there is an increase in fixed echo strength and consequently in ground clutter on the scopes. This may be accompanied by a change in the range of detection for craft flying above the duct.

7. When the transmitter is outside the duct, the range may be either increased or decreased from its standard value.

8. Superrefraction resulting in guided propagation or trapping is produced:

    a. By a pronounced decrease of moisture with height (moisture lapse), or

    b. By a pronounced increase in temperature with height (temperature inversion), and

    c. Particularly, by a combination of both of the above conditions.

Chapter 13

TROPOSPHERIC PROPAGATION AND RADIO METEOROLOGY*

FUNDAMENTALS OF PROPAGATION

Significance of Propagation Problems

THE CENTRAL PROBLEM of short and microwave propagation (at frequencies greater than 40 to 60 mc) is the determination of accurate coverage patterns for a given transmitter. These patterns are usually calculated from electromagnetic theory and then may be checked by experiment. For communication work the check is simple, namely, the establishment of satisfactory communication. In the case of radar it is necessary to calibrate by time-consuming airplane flights.

Experience has shown that actual coverage is not constant in time but suffers large variations which are caused by the changeable refraction of the atmosphere. The variations in weather conditions that influence the refraction often are irregular and very rapid, and it is technically impossible to test all these conditions. Coverage diagrams, therefore, must be based on the physical principles of wave propagation, assuming that the characteristics of the atmosphere remain constant for reasonable periods. These principles are outlined here.

At the present stage of technical development it is not always permissible to ascribe an observed variation in coverage to changing atmospheric conditions. Variations in transmitter output or receiver sensitivity are always likely to be present to a degree sufficient to influence results considerably. In practice it is often extremely difficult to tell these causes apart. In fact, investigations carried out with operational radar-equipment make it probable that an increase in surface coverage due to favorable conditions of refraction frequently passes unnoticed because of poor set performance. The coverage appears normal, while the set in reality is operating considerably below peak efficiency.

A knowledge and understanding of the effects of weather upon propagation therefore will also be of help in checking set performance in the absence of suitable electrical equipment for measuring output and sensitivity. In dealing with coverage problems

*By Columbia University Wave Propagation Group.

this double aspect of propagation phenomena should always be kept in mind. By a suitable analysis of the various factors determining coverage, and by an intelligent understanding of their interplay, the responsible officer may achieve a better control of the operational performance of his equipment.

In tactical operations and in planning, a knowledge of the nonvariable factors affecting propagation, such as dielectric constant and conductivity of the ground or sea, contours of the terrain, vegetation, etc., is equally important. Many problems concerning these factors cannot be considered in this manual

Factors Influencing Propagation

This volume is confined to the propagation of waves within the troposphere and hence is not concerned with ionospheric propagation, which is responsible for the long distance transmission of short waves (high frequency band). The higher the frequency above 30 mc, the less frequently radio waves are returned to the earth by the ionosphere. Consequently very short radio waves are confined to the troposphere, and the treatment given here does not need to be supplemented by a study of the ionosphere. Propagation in the lower atmosphere is called "tropospheric propagation" (see Figure 1).
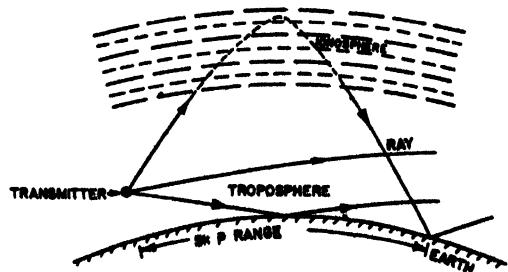
FIGURE 1. Tropospheric versus ionospheric propagation.

The main factors influencing the shape of a coverage diagram under these circumstances are: (1) reflection by the ground, (2) diffraction by the ground contour, (3) refraction by the atmosphere, and (4) guided propagation by superrefraction in the lower

134

atmosphere. The present chapter deals mainly with refraction phenomena, but reflection and diffraction will be briefly considered.

Refraction is influenced by the physical state of the atmosphere, in which the distributions of the temperature, pressure, and humidity are the most important elements. With refraction, rays are bent, and the electromagnetic energy flows along the curved ray paths. A situation frequently realized in practice is that in which the curvature of the rays is independent of height above ground. This is known as *standard refraction*. The term standard propagation is used to designate propagation under conditions where the refraction is of the standard type.

During the war years the increased number of observations, which resulted from the world-wide use of radar, showed that, under certain weather conditions, radio field strengths may depart markedly from the values ∙expected with standard refraction. These deviations are now known to be attributable to a stratification of the atmosphere which is predominantly horizontal and is produced by vertical variations in water-vapor content and temperature. Since these quantities control the index of refraction, and therefore the curvature of the rays, it follows that this curvature varies with the elevation above ground.

Any stratification of the atmosphere tends to produce a distribution of the radiated energy different from that which occurs in the standard atmosphere. Of particular importance is a type of stratification which results in a duct being formed in the atmosphere. In this event, a portion of the wave energy may be∙guided horizontally along the duct and may be effectively "trapped" within the duct's upper and lower boundaries. This is known as "guided" propagation. The radiation energy may then travel to distances far beyond the geometrical horizon, producing unusually long ranges for short wave receivers or radar targets. The phenomenon which tends to constrain the wave energy to follow the duct is∙called "superrefraction." When this occurs, the rays in passing through the inversion layer in the upper part of the duct are bent downward with a curvature which exceeds that of the curvature of the earth. The regions covered by the inversion layer and the duct are illustrated in Figures 15, 20, 22, and 23. The distribution of moisture and temperature in the atmosphere, responsible for the formation of ducts, is discussed on page 152.

As the stratification of the lower atmosphere that produces superrefraction is part of the weather, the prevailing meteorological conditions become of importance for problems of propagation and coverage. Meteorology as related to wave propagation is treated in the discussion on pages 152-154.

Reflection from the Ground.

A coverage diagram is a curve, or a set of curves, of constant field strength in a vertical or horizontal plane. The horizontal coverage diagram is determined chiefly by the antenna∙pattern itself. In the vertical plane, however, the diagram depends primarily upon the interference between the radiation coming directly from the transmitter and that which is reflected from the ground or sea surface. This effect produces the lobe structure of the vertical coverage diagram. At the lobe maxima the two rays reinforce each other, while they cancel each other out, more or less, at the lobe minima.

The propagation problem in its full generality leads to mathematical formulas of forbidding complexity. In order to understand the processes at work it is necessary to proceed in steps and gradually add refinements to the basic features of the problem.

Consider first the field radiated from an antenna which is remote from the earth. This free space field decreases in strength in inverse proportion to the distance, R_1, from the transmitter and varies with the angular position in accordance with the shape of the radiation pattern of the transmitting antenna. Let this free space field strength at any point at distance R_1 be designated by E_0.
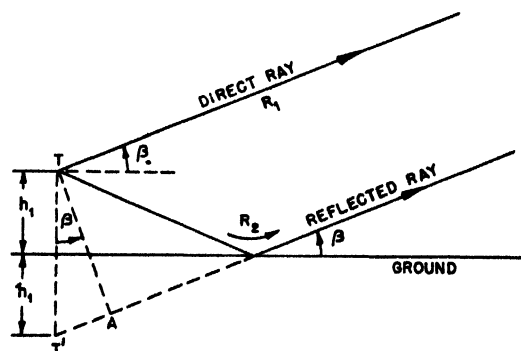
FIGURE 2. Interference of direct and reflected rays.

If, instead, the transmitter is placed near the ground, as at T in Figure 2, the field at any point in space is produced partly by the direct wave (giving the free space field E_0) and partly by the wave which is reflected from the ground. The resultant field is given by the vector sum of the two component fields.

The magnitude of the field strength of the *reflected* beam depends upon:

1. The antenna radiation pattern, which gives the relative strength of the radiation field for different directions.

2. The attenuation, proportional to $1/R_2$, resulting from the length of path R_2 of the reflected wave.

3. The attenuation due to increased divergence of nearly parallel rays reflected from the curved earth. This is taken into account by the use of a divergence factor, D, which depends on range and heights of transmitter and receiver.

4. The magnitude, ρ, that the coefficient of reflec-

tion of the ground would have if the ground were plane. The reflection surface for a spherical surface, F, is then equal to ρD.

5. Irregularities of the earth's surface which affect the reflection coefficient.

If E_0 is the magnitude of the direct wave and F is the magnitude of the reflection coefficient, then the field strength of the reflected ray is FE_0.

The phase difference between the direct and reflected fields is given by an angle δ which is the sum of:

1. The phase difference, Ψ, resulting from the difference in path length, $R_2 - R_1$;

2. The phase difference, ϕ, suffered by the reflected wave upon reflection from the ground.

The amplitude of the resultant field for a nondirective antenna is then given by GE_0, where

$$G = \sqrt{1 + F^2 + 2F \cos \delta} \qquad (1)$$

is the earth gain factor which is illustrated in Figure 3
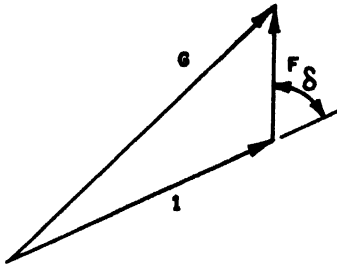
FIGURE 3. Phase addition of direct and reflected rays

A curve drawn to represent the contour of constant field strength $E = GE_0$ as a function of the range R_1 and the angle of elevation β gives the vertical coverage diagram for that particular field strength. Calculation of these diagrams usually requires a considerable amount of detailed and laborious work.

Consider the simple case of the vertical coverage diagram of a horizontal dipole antenna located above a plane earth in a homogeneous atmosphere. If the plane of Figure 2 is perpendicular to the dipole axis, the radiation pattern of the antenna is a circle of unit radius. The ratio, F_2, of the magnitude of the reflected wave to that of the incident wave is given by the magnitude, ρ, of the reflection coefficient. For propagation to distances that are great compared with the antenna elevation, the path lengths R_2 and R_1 are not greatly different, and the attenuation due to path length is approximately the same for both direct and reflected waves. For this set of conditions the resultant field is $E = GE_0$, and equation (1) reduces to

$$G = \sqrt{1 + \rho^2 + 2\rho \cos \delta} \cdot \qquad (2)$$

In this form G is the plane earth gain factor and a plot of the curves $E = GE_0 = $ constant as a function of range and angle of elevation gives the coverage dia-

gram. It depends only upon the magnitude of the reflection coefficient, the phase changes related to reflection and to the difference in path length $R_2 - R_1$.

Since radar requires two-way transmission the received field strength is proportional to G^2/R^2_1. Other modifying factors must, however, be introduced if the antenna and the target have directional radiative properties

Both the magnitude of the reflection coefficient $+F$ and the phase angle ϕ by which the reflected wave lags behind the incident wave are functions of the frequency, the polarization of the radiation, the angle of grazing with the surface, the conductivity, dielectric constant, and roughness of the ground or sea surface. Figure 4 illustrates the variation of $F(=\rho)$ and ϕ for reflection from a smooth plane sea surface for frequencies of 100 to 3,000 mc, for both types of polarization, at different grazing angles. It may be noted that for horizontal polarization ρ is approximately unity and ϕ nearly 180°, irrespective of the frequency and the magnitude of the grazing angle. This is the simplest situation to be encountered and most nearly approximates the idealized case of a perfect reflector with horizontal polarization. For this case ρ is exactly unity, and ϕ is exactly 180°.

For vertical polarization over the sea or either type of polarization over ground, both ρ and ϕ depart widely from unity and 180°, respectively. Variations in these quantities greatly complicate the calculation of coverage diagrams.

The reflection coefficient of microwaves is usually found to be small over land. This is essentially due to irregularities of the land surface. When these irregularities are sufficiently small, reflection from land is found to be considerable.

Since the receiver, or target, is usually located at a distance from the transmitter which is large in comparison to the height above the ground, the direct and reflected rays are very nearly parallel, making an angle β with the horizontal (Figure 2). The reflected ray may be supposed to issue from an image transmitter T', which is as far below the ground as the true transmitter is above it. The path difference between the direct and reflected rays is equal to the distance $T'A$. By the figure this is equal to $2h_1 \sin \beta$, where h_1 is transmitter height. For small values of β this is practically equal to $2h_1\beta$ if β is measured in radians. The corresponding phase shift due to path difference is equal to

$$\Psi = 2h_1\beta \frac{2\pi}{\lambda} .$$

At the point of reflection the phase of a ray changes discontinuously by the amount ϕ, which is the phase angle of the reflection coefficient. For horizontal polarization, to again take the simplest case, the phase shift ϕ at reflection is practically 180°, or π radians. (For vertical polarization, see Figure 4, ϕ is more complicated.) Adding the phase change Ψ, corresponding to difference in path length, gives the
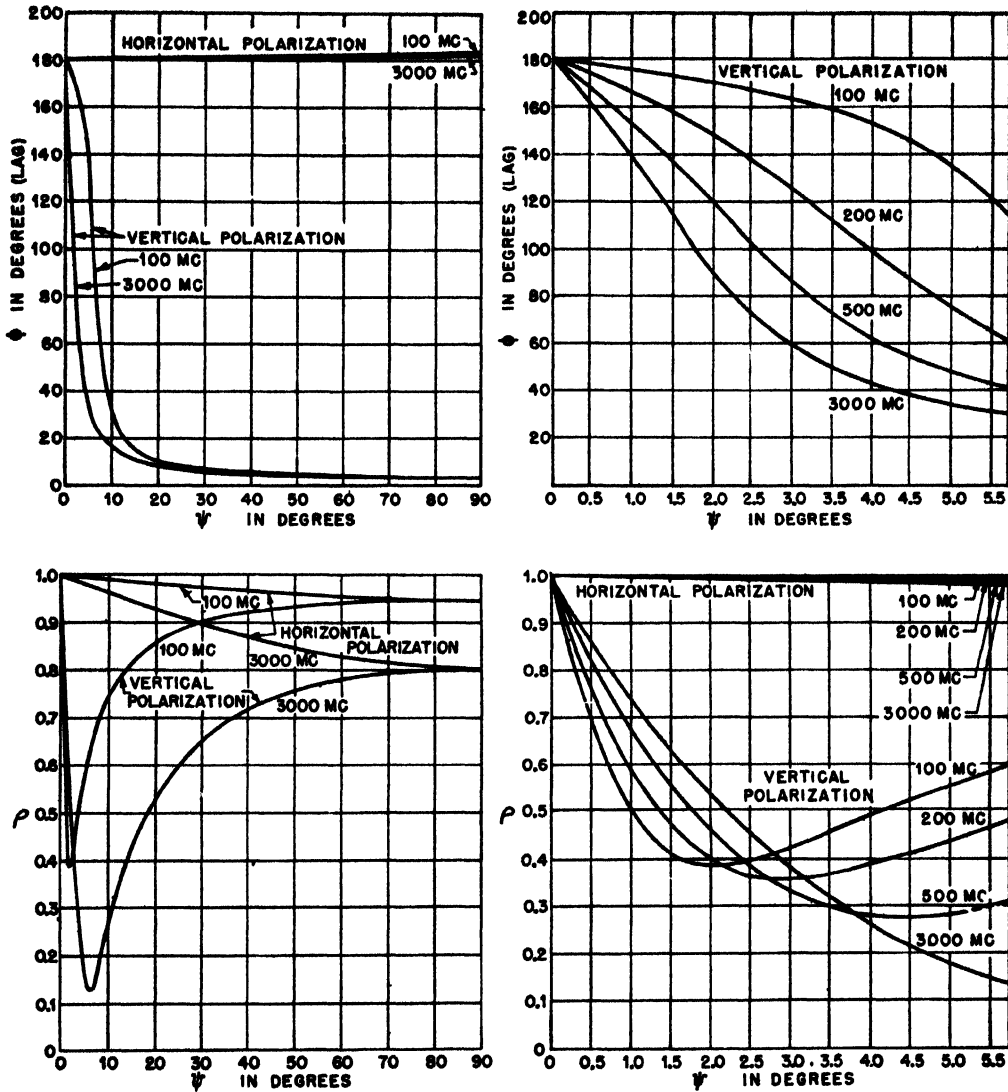
FIGURE 4. Phase and magnitude of reflection coefficient for sea water.

complete phase change δ in the form

$$\Psi + \phi = 2h_1\beta\frac{2\pi}{\lambda} + \pi \text{ (for horizontal polarization)}.(3)$$

Maximum values of the earth gain factor G occur when δ is an integral multiple of 2π, minimum values, for odd integral values of π. The corresponding values of the angle of elevation β are given by

$$\beta = \frac{\lambda}{4h_1} m \quad \begin{cases} m = 1, 3, 5, \cdots & \text{(maxima)} \\ m = 0, 2, 4, \cdots & \text{(minima)} \end{cases}$$

(for horizontal polarization.)

If the reflection coefficient F of the surface is assumed to be unity (see Figure 4) the plane earth gain factor G, from equation (2), reduces to

$$G = 2 \cos\left(\frac{\delta}{2}\right),$$

which fluctuates between the limits of 2 and zero.

The coverage diagram drawn for propagation over a perfectly conducting plane on horizontal polarization is illustrated in Figure 5. As an example, consider
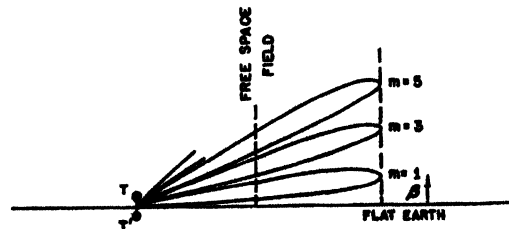
FIGURE 5. Simplified coverage diagram.

$f = 200$ mc, $\lambda = 1.5$ m, $h_1 = 30.5$ m. The values of β for the first three lobe maxima are 0.68°, 1.37°, and 2.05°, and the maximum ranges are twice the free

space values. The angles at which the minima occur lie half way between. The scale of vertical distances is greatly exaggerated compared with the horizontal scale. Coverage diagrams for the same frequency and transmitter height, but taking account of the earth's curvature, are shown in Figure 24.

Coverage diagrams for more complicated situations must take into account, in addition to the factors already mentioned, the curvature of the earth, the refraction of the atmosphere, and diffraction into the region below the line of sight.
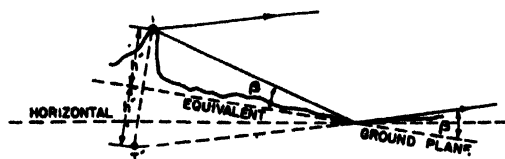
FIGURE 6. Use of equivalent ground plane

When the ground is sloping, the above construction may be modified as indicated in Figure 6. For any specified lobe, determine approximately the part of the ground where reflection takes place. Draw a tangent to the ground in this region and determine the perpendicular projection of the antenna site or this plane ("equivalent ground"). Use the equivalent height thus determined in equation (3), and let the angle β refer to the plane of the equivalent ground. This procedure is also required when the transmitter and receiver or target are of comparable height so that the reflection point is not near the transmitter.

When the transmitter is set up near a coast, the lobe pattern over the ocean will undergo periodic variations caused by the tides. Since, in equation (3), β is multiplied by h_1, it follows that the lobes will be low at high tide and high at low tide. This phenomenon may become very important for heightfinding sets.

A more complicated case occurs if ground reflection is not complete. Then ρ is less than unity, and ϕ differs from $180°$. In this event the lobes have max-
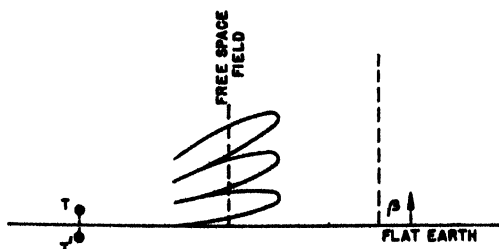
FIGURE 7. Coverage diagram for incomplete reflection.

ima which are less than twice the free space field and minima which never reach zero. The angular positions of the lobes are changed somewhat, but the most noticeable change is found on the lower side of the first lobe. It is likely to lie at a lower elevation and reaches the ground at some distance from the

transmitter (compare Figures 5 and 7).

Refraction—Snell's Law

The bending of rays in the atmosphere depends upon the refractive index n which is a function of the temperature, pressure, and moisture content of the air. The manner in which these quantities control the index of refraction is explained on pages 142-143. To a first approximation, assuming horizontal stratification of the atmosphere, the index may be considered to be a function only of height above the ground. The corresponding case, familiar in optics, is that of two media, such as water and air, with different refractive indices n_1 and n_2 (Figure 8A). If α_1 and α_2 are the angles between the rays and the plane of the boundary, Snell's law of refraction states that

$$n_1 \cos \alpha_1 = n_2 \cos \alpha_2 .$$

In the atmosphere the refractive index changes continuously with height. The simplest case, often
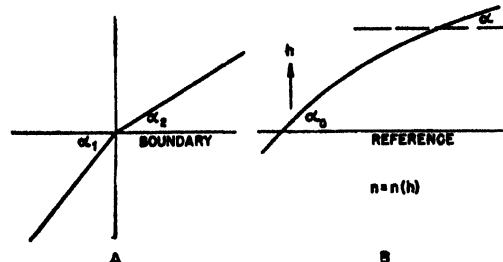
FIGURE 8. A. Refraction at a sharp boundary. B. Refraction through a layer with variable n.

encountered in practice, is that of a refractive index which decreases linearly with height. This is known as standard refraction. Snell's law applies here also, since the atmosphere may be divided up into an infinity of parallel boundaries, the change of refractive index from one boundary to the next being infinitesimally small. Instead of a sudden change of direction there is then a gradual change or bending of the rays (Figure 8B). Snell's law may then be stated generally as

$$n \cos \alpha = n_0 \cos \alpha_0 ,$$

where now n and α are continuous functions of height and the zero subscript on the right-hand side refers to any fixed reference level. The curvature of the refracted rays is downwards or upwards according to whether the refractive index decreases or increases with height.

Refraction over a Curved Earth

In reality the surfaces of constant refractive index are not planes but are concentric spheres about the earth's center. In this case Snell's law assumes a

slightly different form. Instead of using angles referred to the plane surfaces it is now necessary to refer the angles to horizontal planes tangent to spheres about the center of the earth (see Figure 9). The new form, as given on page 165, is

$$nr \cos \alpha = a n_0 \cos \alpha_0 , \qquad (4)$$

where r and a are values of the radius vector from the center of the earth to a point in the atmosphere and
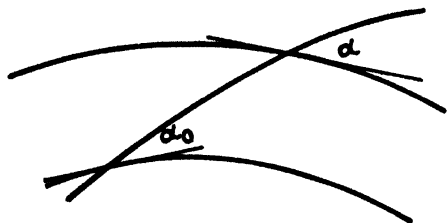
FIGURE 9. Refraction through a curved layer.

to the earth's surface, respectively. α now stands for the angle formed by the ray with a plane normal to the radius vector. α_0 and n_0 are the values of α and n at the ground surface.

If h is the height above the ground surface, so that $r = h + a$, the above equation may also be written in the form

$$n \left(1 + \frac{h}{a} \right) \cos \alpha = n_0 \cos \alpha_0 . \qquad (5)$$

h/a is a very small quantity, and n differs from unity by only a few parts in 10,000. Under these conditions $n(1 + h/a)$ may be replaced by $n + h/a$ with negligible error. The quantity $n + h/a$ is called the modified refractive index, or the modified index for short Equation (5) then assumes the form

$$\left(n + \frac{h}{a} \right) \cos \alpha = n_0 \cos \alpha_0 . \qquad (6)$$

As a result of general agreement it is customary to use, instead of $n + h/a$, the symbol M defined as follows:

$$M = \left(n + \frac{h}{a} - 1 \right) 10^6 . \qquad (7)$$

At the surface of the ground M reduces to

$$M_0 = (n_0 - 1) \, 10^6. \qquad (8)$$

Hence M is the excess of the modified refractive index above unity, measured in units of one millionth. This unit is called an M unit [MU]. Values of M for the atmosphere lie in the range of 200 to 500. Customarily M is referred to simply as the modified index of refraction.

Using the numerical value for the radius of the earth, 6.37×10^6 m (21×10^6 ft), the rate of increase of M with height, owing to the term h/a, is $(1/a) \, 10^6$, which is equal to 0.157 MU per meter (0.048 MU per foot). As the result of a large number of experiments, carried out chiefly in the northern temperate lati-

tudes, the rate of decrease with height of the refractive index has been found, on the average, to be

$$\frac{dn}{dh} \, 10^6 = - \frac{1}{4} \frac{1}{a} \, 10^6$$
$$= -0.039 \text{ MU per meter} . \qquad (9)$$

This is the rate of decrease assumed for the standard atmosphere.

It will be noticed that the average rate of decrease of n with height is one quarter of the rate of increase of the term h/a which results from the curvature of the earth. The fact that these quantities are of comparable magnitude is of great importance, as will be seen later.

Consequently the vertical gradient of M for the standard atmosphere is

$$\frac{dM}{dh} = \left(\frac{dn}{dh} + \frac{1}{a} \right) 10^6$$
$$= \left(\frac{3}{4} \frac{1}{a} \right) 10^6 = \frac{1}{\left(\frac{4}{3} a \right)} 10^6, \qquad (10)$$

which has the value 0.118 MU per meter (0.036 MU per ft). The value of M at any height, relative to the surface value M_0, for the standard atmosphere, is equal to

$$M - M_0 = 0.118 \, h; \quad h \text{ in meters},$$
$$M - M_0 = 0.036 \, h; \quad h \text{ in feet}. \qquad (11)$$

Equivalent Earth Radius— Flat Earth Diagram

An important conclusion may be drawn from equation (11). As will be shown on pages 146-147, dn/dh is the negative of the curvature of a ray in the atmosphere, and $1/a$ is the curvature of the earth. The algebraic sum of these two quantities (their numerical difference) is the curvature of the ray relative to that of the earth. The net result is this: if the earth is replaced by an equivalent earth with an enlarged radius equal to $4a/3$ the rays may be drawn as straight lines. To state the result in another way: using the equivalent earth with radius equal to $4a/3$ corresponds to replacing the actual atmosphere, in which the index n decreases with height, by a homogeneous atmosphere with an equivalent index n' which is independent of height (see Figures 10, 11, 13, 14, and 15). This transformation of coordinates greatly facilitates the calculation and interpretation of coverage diagrams for the standard atmosphere.

More generally, if the rate of change of n with height differs from the value $-(1/4) \, (1/a) \, 10^6$ MU per meter given above, which may be true in certain parts of the world, the equivalent earth radius departs from the value $4a/3$. In general the equivalent earth radius is designated by ka. For a steeper drop of refractive index with height, k increases and becomes infinite when the curvature of the ray is just equal to the curvature of the earth.

In the general case, when k is not equal to $\frac{4}{3}$, equation (11) must be modified to the form:

$$M - M_0 = \frac{h}{ka} 10^6,$$

$$= 0.157 \frac{h}{k} ; \quad h \text{ in meters},$$

$$= 0.048 \frac{h}{k} ; \quad h \text{ in feet}, \quad (12)$$

to account for a linear moisture gradient corresponding to a different value of k.

Since the change of the earth's radius takes care of the variation of refractive index and substitutes a homogeneous atmosphere for the actual atmosphere, it follows that in a diagram in which the earth is given a radius ka, the radiation propagates along
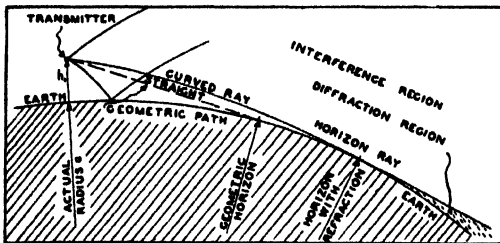
FIGURE 10. Ray curvature over earth of radius a in an actual atmosphere.

straight lines. The difference is illustrated in Figures 10 and 11. In Figure 10, which shows the true geometrical conditions, the radio horizon appears extended as compared to the geometrical horizon, be-

cause of the curvature of the rays. In Figure 11 the rays have been straightened out, but a line that was straight in Figure 10 appears curved in Figure 11.

The value of $\frac{4}{3}$ for k is a good average for the atmosphere in the middle latitudes. For particular
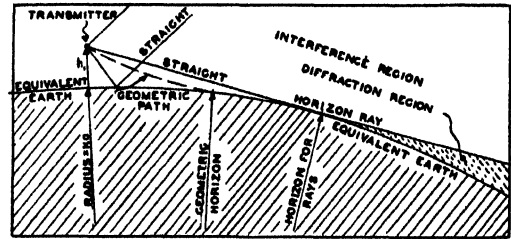
FIGURE 11. Rays in a homogeneous atmosphere. Equivalent radius ka.

atmospheric conditions the value of k may be considerably different. The moisture content of the atmosphere is small at the low temperatures of the arctic regions and increases considerably with the higher temperatures of the tropics. However, the value of k depends more particularly on the manner in which the moisture content varies with height above the surface of the earth, and to a lesser extent on the distribution of temperature with height. Figure 12 has therefore been constructed to show the dependence of k on the gradient of relative humidity, measured in per cent per 100 m, for a series of surface temperatures varying between $T_0 = -30$ C and $T_0 = +40$ C. It has been found convenient to plot $1/k$ rather than k itself. The lines drawn correspond to the assumption of saturation humidity at the

(RH)	-30C	-25C	-20C	-15C	-10C	-5C	0C	+5C	+10C	+15C	+20C	+25C	+30C	+35C	+40C
10%	.009	.012	.017	.027	.039	.055	.078	.090	.118	.151	.194	.240	.301	.371	.455
20%	.008	.011	.015	.024	.034	.049	.069	.080	.105	.134	.172	.214	.267	.329	.405
30%	.007	.009	.014	.021	.030	.043	.060	.070	.092	.118	.151	.187	.234	.288	.354
40%	.006	.008	.012	.018	.026	.037	.052	.060	.079	.101	.129	.161	.200	.247	.304
50%	.005	.007	.010	.015	.021	.031	.043	.050	.066	.084	.108	.134	.167	.206	.253
60%	.004	.005	.008	.012	.017	.024	.034	.040	.052	.067	.080	.107	.134	.165	.202
70%	.003	.004	.006	.009	.013	.018	.026	.030	.039	.050	.065	.080	.100	.123	.152
80%	.002	.003	.004	.006	.009	.012	.017	.020	.026	.034	.043	.065	.067	.082	.101
90%	.001	.001	.002	.003	.004	.006	.009	.010	.013	.017	.021	.027	.033	.041	.051

FIGURE 12. Graph: $1/k$ versus RH gradient and temperature for 100 per cent RH at ground.

ground; if the humidity at the ground is less than 100 per cent the correction read from the auxiliary table is added to the value of $1/k$ obtained from the graph. The standard temperature gradient of -0.65 C per 100 m is assumed for all the curves.

The curves of Figure 12 indicate that as the temperature increases, smaller and smaller values of relative humidity gradients are required to produce changes in k of considerable magnitude. This should be of greater importance in the tropics where the moisture content is relatively high.

Changing k from its standard value of $\%$ has an important influence on the strength of the field at any point in space. Though it is not easy to state the result in general terms for any position, it is possible to evaluate the change in field strength near the surface (below 60 m altitude for 600 mc and somewhat higher for lower frequencies) and well within the diffraction region, for moderate changes in k. Here the decibel attenuation below that for the free space field is decreased approximately in the ratio $k^{\frac{2}{3}}$. If, for instance, k changes from $\%$ to 8, the original decibel attenuation is to be divided by 3.3. To state the matter another way, the range at which a given field strength is found will be increased approximately in the ratio $k^{\frac{2}{3}}$. This has an important bearing on the problem of propagation for communication purposes in this region.

It has been shown above that a linear variation of refractive index can be converted into a change of earth's curvature. The reverse process is equally feasible: to eliminate the earth's curvature by using a modified refractive index curve. This is a general procedure which involves no assumption about the variation of refractive index with height. From the equations in this section, it is seen that the effects of the earth's curvature are equivalent to those of a refractive index increasing linearly with height at the rate of $1/a$. Hence one effectively flattens the earth, thus eliminating the curvature effect, by adding to the refractive index the term h/a. In other words, the angles between a ray and the horizontal over a curved earth are the same as the angles between a ray and the horizontal over a flat earth when the refractive index n has been replaced by $n + h/a$. In practice, the quantity M defined by equation (7) is used. If M increases steadily with height, which is the case for the standard atmosphere, the rays appear curved upwards on a flat earth diagram, which is illustrated in Figure 13.

Summarizing, it is seen that three types of graphi-

TRUE EARTH
RADIUS a

EQUIVALENT EARTH
RADIUS $k a$

FLAT EARTH
$k = \infty$

FIGURE 14. Shape of lobes as affected by method of representation.

cal representations of a coverage diagram may be used. (These are illustrated in Figure 14 for the lowest lobe.)

1. The true geometrical representation. With standard refractive conditions the lobes appear bent downwards. Refractive index n decreases with height.

2. The equivalent earth radius representation. Earth's radius changed to ka (normally $k=\%$). For standard refractive conditions the lobes appear straight. Equivalent refractive index n' is independent of height since the equivalent atmosphere is homogeneous.

3. The flat earth representation. The earth's surface and other surfaces of constant height have been flattened out. For standard refractive conditions the lobes appear bent upwards. Excess modified index M increases with height.

The quantities n, n', and M for these three cases are illustrated in the left-hand series of diagrams in Figure 15.

The Horizon—Diffraction

From simple geometrical considerations it can be shown that two points at elevations h_1 and h_2 are within sight of each other when their distance is less than the horizon distance d_h (Figure 16) given by

$$d_h = \sqrt{2kah_1} + \sqrt{2kah_2}, \qquad (13)$$

FIGURE 13. Rays in a plane earth diagram.
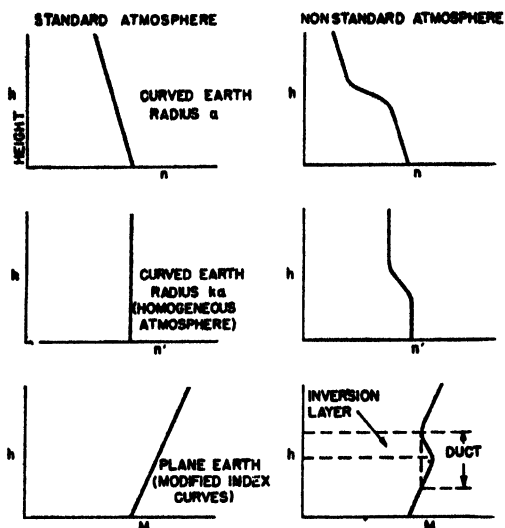
FIGURE 15 Types of index curves.

where d_h, a, and h are all expressed in the same units.

For the particular value of $k = \frac{4}{3}$,

$$d_h = \sqrt{17h_1} + \sqrt{17h_2}, \tag{14}$$

where d_h is measured in kilometers and h is in meters; and

$$d_h = \sqrt{2h_1} + \sqrt{2h_2}, \tag{15}$$

where d_h is given in statute miles and h in feet.
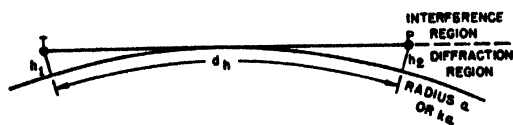
FIGURE 16. Horizon distance.
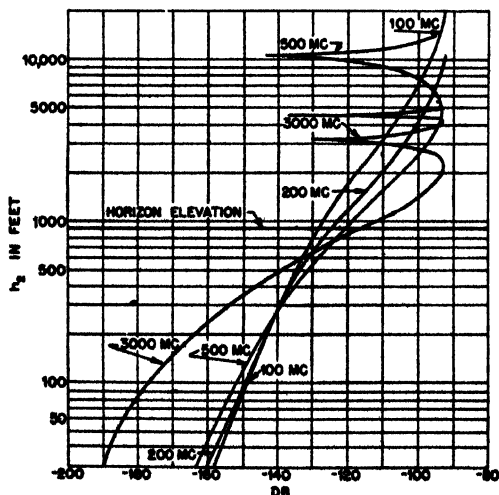
FIGURE 17. Diffraction and interference fields at height h_2. Field strength at 50 statute miles over sea water in db relative to field at 1 m from transmitter. Horizontal polarization. Transmitter height 30 feet.

The field strength at different elevations h_2 (Figure 16) for a given range varies in the manner illustrated in Figure 17. The field is given in decibels; relative to the intensity at 1 m from the transmitter, for a range of 50 miles over sea water for frequencies of 100, 200, 500, and 3,000 mc. The horizon elevation for this point is 888 ft. Above point P in Figure 16, is the interference region where, with increasing height, the field strength first increases rapidly and then oscillates between maxima and minima determined by the lobe patterns of the coverage diagrams.

Below point P, the field strength declines rapidly with decreasing height to a minimum at ground level; the rate of decrease is larger for the higher frequencies. Neither the direct nor the reflected rays can penetrate into this region, which therefore, receives radiation entirely by diffraction of the energy around the earth's curvature.

Radar targets are rarely visible when they are in the diffraction region. This is certainly true for airplane targets. Very large targets, such as warships or islands, are occasionally visible in this region; but more often the detection of targets is caused by superrefraction. For communication work, on the other hand, the diffraction region is of importance, especially at the longer wavelengths.

ATMOSPHERIC STRATIFICATION AND REFRACTION

Origin of Refractive Index Variations

The variation with height of the index of refraction n controls the curvature of rays in the atmosphere. The value of n exceeds unity by only a few hundred parts in a million and may be computed from the following formula:

$$(n - 1) \, 10^6 = \frac{79p}{T} - \frac{11e}{T} + \frac{3.8 \times 10^5 e}{T^2} \tag{16}$$

in which n = index of refraction at height h above ground;

p = barometric pressure of the atmosphere in millibars at height h. (1 mm Hg pressure = 1.334 mb);

e = partial pressure of the water vapor in millibars (order of 1 per cent of p);

T = absolute temperature (°C + 273) at height h.

In equation (16) the term $11e/T$ is very small in comparison with the other terms and may, without serious error, be neglected. This simplification has been used in obtaining the values in the last two columns of Table 1 and in designing the nomogram, Figure 19.

Workers in the field may prefer to use mixing ratio (practically equal to specific humidity) in place of

TABLE 1. Standard atmosphere with 60 per cent relative humidity.

| NACA standard atmosphere | | | | Moist standard atmosphere | | |
Altitude, meters	Temp, C	Dry air pressure, mb	Dry air index, $(n-1)10^6$	$e(mb)$ for 60% RH	Moist air index, $(n-1)10^6$	$M = (n + h/a - 1)10^6$
0	15.0	1013	278	10.2	325	325
150	14.0	995	274	9.6	318	342
300	13.0	977	270	9.0	312	359
500	11.7	955	265	9.3	304	382
1000	8.5	894	251	6.7	283	440
1500	5.2	845	240	5.3	266	501

the water vapor pressure. The relation is given by

$$e = 0.00161\, ps \quad \text{or} \quad s = \frac{621e}{p}, \qquad (17)$$

where s is in grams of water per kilogram of air.

The variation of n with temperature and relative humidity for an air pressure of 1,000 mb is illustrated in Figure 18. It is seen that the refractive index depends on humidity more critically than on tempera ture. The dependence on humidity is greater at the higher temperatures where a given relative humidity represents a larger amount of water vapor.

In practice it is customary to use the modified refractive index given by

$$M = \left(n + \frac{h}{a} - 1\right) 10^6 \cong \frac{79p}{T} + .\frac{3.8 \times 10^5 e}{T^2}$$
$$+ 0.157h \quad (h \text{ in meters})$$
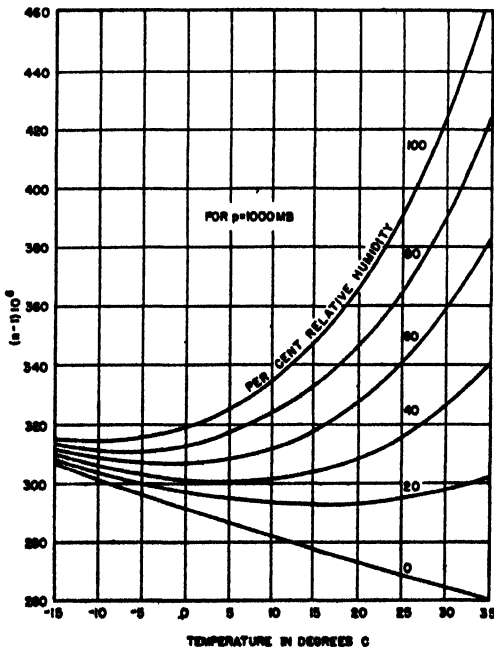
FIGURE 18. Relation of n to temperature and relative humidity.

In order to compute M directly from temperature, relative humidity, and height data, the nomogram (Figure 19) has been constructed. Detailed instructions for its use are given.

The National Advisory Committee on Aeronautics [NACA] standard atmosphere commonly used in

aeronautics assumes a sea level pressure of 1,013 mb (= 760 mm Hg) and a sea level temperature of 15 C decreasing at a rate of 6.5 C per kilometer in the lower atmosphere. The NACA standard atmosphere is not concerned with the moisture content. In the actual atmosphere the moisture may vary between extremely wide limits, but as a typical value a relative humidity of 60 per cent may be assumed as the standard condition. This corresponds to a water vapor pressure of approximately 10 mb at sea level and a rate of decrease of water vapor pressure in the lower levels of about 1 mb per 1,000 ft. At higher levels the rate of decrease of the water vapor pressure is less rapid. These conditions are represented in Table 1 for the atmosphere up to 1,500 m.

Both the dry and the moist standard atmosphere exhibit a very nearly linear increase of M with height. According to equation (12),

$$M - M_0 = \frac{h}{ka} \cdot 10^6 = 0.157\frac{h}{k}; \quad h \text{ in meters}.$$

By using this formula in conjunction with Table 1 it is easily shown that $k = \frac{4}{3}$ for the dry standard atmosphere, and $k = \frac{3}{4}$ for the standard atmosphere with a 60 per cent relative humidity. This value of k is the one commonly adopted in coverage diagrams corrected for standard refraction.

Because of the great variability of the moisture content of the atmosphere with season, geographical location, etc., a moist standard atmosphere has a limited physical significance. The standard should rather be defined in terms of a fixed linear slope of the refractive index, and for this purpose the value $k = \frac{3}{4}$ has been chosen.

The Measurement of Refractive Index

The lower atmosphere frequently is stratified by nonstandard distributions of temperature and humidity which vary rapidly and irregularly as functions of the height. The refractive index is then no longer linear but has a more complicated dependence on height, determined from equation (16). The stratification which is of particular importance in tropospheric propagation is found in the lower part of the atmosphere, that is, below about 4,000 to 5,000 ft and frequently in the lowest few hundred feet above ground.

Since the variation in the atmospheric pressure
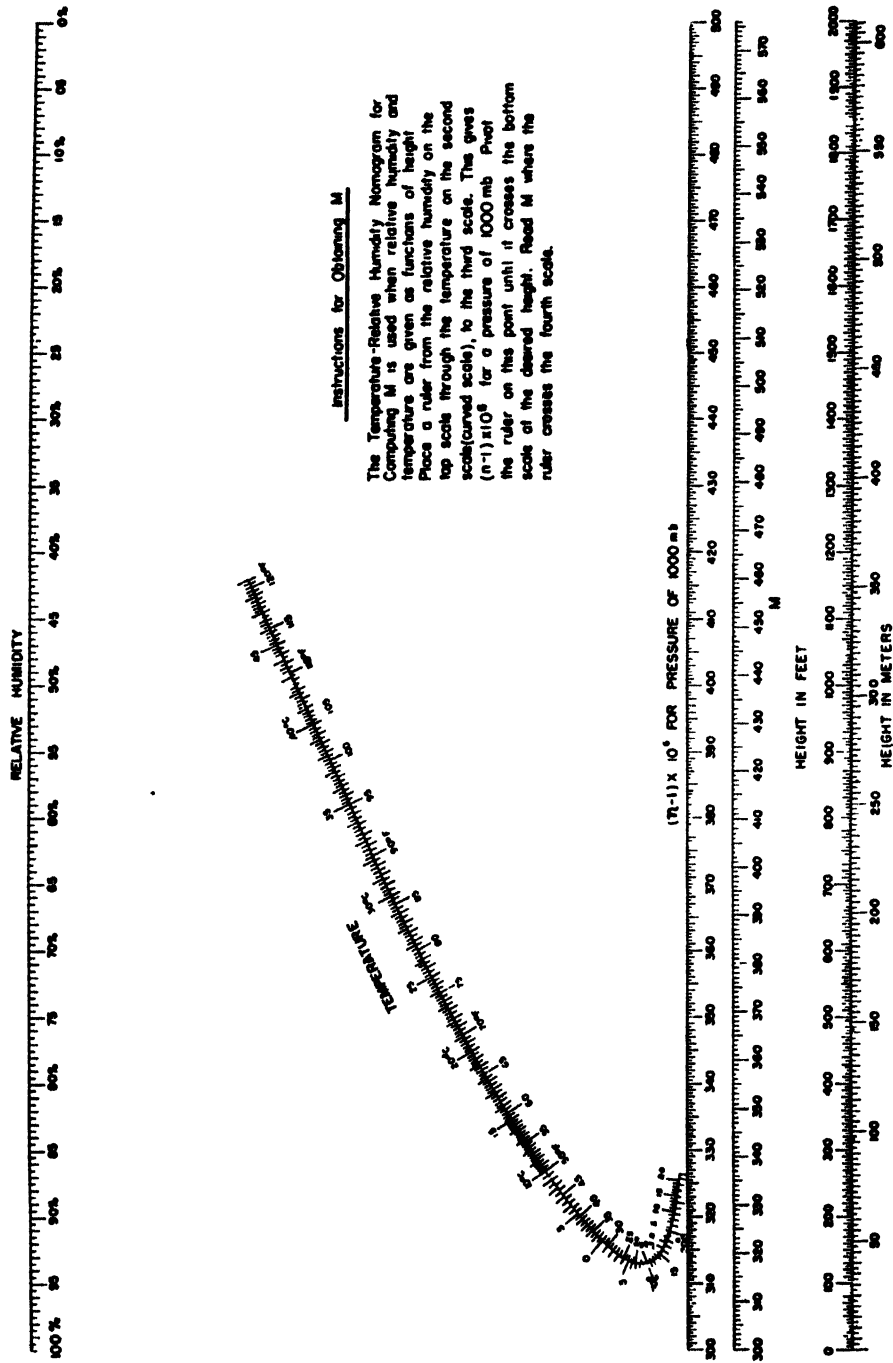
FIGURE 19. Temperature-relative humidity nomogram for computing M.

gradient is small, interest is mainly centered in the dependence of the modified refractive index M on the temperature and humidity distributions. Methods, useful in the field, have been developed for obtaining rapid determinations of temperature and humidity in the lowest levels of the atmosphere. The ordinary radiosonde (radiometeorograph) is not well adapted for this purpose since it is usually designed to give data at levels about 100 m apart, which often is not close enough to reveal the significant details of the M curve. Consequently it has proved to be necessary to develop new instruments for this purpose.

Several types of instruments have been designed which can be placed on towers, or carried by slow-flying airplanes or dirigibles or carried aloft by captive balloons or kites with wires connecting the temperature and humidity elements to measuring or recording equipment located on ground or aboard ship.

Some such measurements have been made with instruments using electrical methods in which dry and wet electrical resistance elements are connected into a circuit to give "dry bulb" and "wet bulb" temperatures. Another electrical method uses the same "dry" temperature element but, in place of the wet bulb, obtains a relative humidity measurement by using an electrolytic humidity element of the type employed in the U. S. Weather Bureau radiosonde. Hair hygrometers, are definitely not suitable for this type of work on account of their lag in adjusting themselves to changes in relative humidity (of the order of 3 to 5 min for appreciable changes in humidity).

Measurements made from airplanes have the advantage that it is possible to survey a comparatively large area within a short time. This can be of great importance along coasts where conditions in the lowest levels of the atmosphere sometimes change rather rapidly with increasing distance from the shore. In the absence of suitable special equipment an ordinary psychrometer held out of the window of a plane will give quite satisfactory results in slow-flying planes, providing care is taken to keep the wet bulb sufficiently moist. When measurements are made from an airplane the height above the ground is determined for each measurement by means of the plane's altimeter. Unless carefully done this introduces the possibility of considerable error.

In another method captive balloons, kites, ordinary radiosonde balloons, and, occasionally, barrage balloons have been used to carry the measuring elements aloft. Ordinary captive balloons will work in wind speeds up to about 8 miles per hour; in higher winds kites or, occasionally, barrage balloons are used. Kites can be flown from boats even at low wind speeds or in calm weather. With this type of equipment the electrical measuring elements aloft are connected to an indicating or recording instrument at the ground or aboard ship by means of fine insulated wires wound around the balloon cable.

Types of Modified Index Curves

A large number of meteorological soundings of the lower atmosphere have been carried out by several laboratories and Service units. From these measurements the modified index curves have been calculated as a function of height, and it has been shown that practically all these curves fall into one of the six types illustrated in Figure 20.
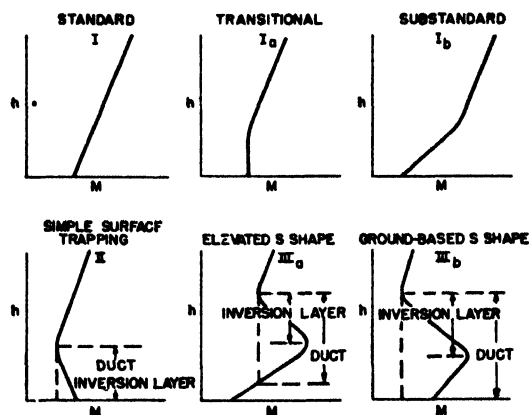
FIGURE 20. Types of M curves.

For the standard atmosphere the M curve increases with height as shown in curve I. For nonstandard atmospheres, the M curves will take one or another of the forms illustrated in curves Ia, Ib, II, IIIa, and IIIb. Of particular interest are those curves in which M decreases with height for a range of altitudes. (This decrease is the result of a sufficiently sharp decrease in n with height as illustrated in Figure 15.) In this event an inversion layer is formed in the atmosphere.

Throughout the range of altitudes of decreasing M the curvature of the rays exceeds the curvature of the earth. Nearly horizontal rays which either originate in, or penetrate into, this layer are trapped, and, if the layer extends far enough, energy may be carried to distances far beyond the geometrical horizon. However, the region in which the waves or rays are trapped may have a thickness or depth exceeding that of the inversion layer. This region is known as a duct. Its precise definition may be taken from Figure 20. It is the strip between an upper minimum of the M curve and either the ground or the point where the vertical projection from the upper minimum intersects the M curve. There are two main types of ducts, the ground-based duct, illustrated by curves II and IIIb, and the elevated duct, illustrated by curve IIIa.

The height in the atmosphere at which the variations in refractive index occur may vary from a few feet to several hundred or even a few thousand feet. These variations are likely to be found at fairly low elevations in cold climates and at the higher elevations in warm climates. The meteorological con-

ditions which yield these various M curves are described on pages 152-164

The opposite effect occurs when the M curve takes the substandard form (curve Ib in Figure 20). Here the lower portion of the M curve has a slope which is less than standard. In this event the rays in the lower atmosphere are bent downward to a lesser degree than in the standard atmosphere or may even be bent upward. Depending to some extent upon the elevation of the transmitter, the field strength in the substandard region may be reduced considerably below normal, even to the point of producing a radar and communication "blackout." If the M curve is steeper than average in the lowest layers, the transitional case arises (curve Ia). Here a slight change in the temperature and moisture distribution might lead to a curve of type II and a duct.

Rays in a Stratified Atmosphere

Nonstandard vertical variations of refractive index occur frequently in the lower atmosphere. In addition there may be gradual variations in the horizontal direction. So far, the theory of propagation has not reached a stage where such horizontal variations can be taken into account. Unless otherwise stated it is always assumed that the stratification extends horizontally as far as the coverage of the transmitter and that the variation in the M curve is entirely vertical. Weather conditions often are sufficiently homogeneous horizontally to warrant this assumption, but there are exceptions, mainly near coasts (see pages 152-164)

Only those rays are affected by the vertical variations of refractive index in the lower atmosphere which leave the transmitter at a very small angle. Both theoretically and practically it has been found that the effects of nonstandard refraction are negligible for rays that leave the transmitter at an angle with the horizontal of more than about 1.5°. Rays that leave at an angle with the horizontal of less than 1.5°, and especially those emerging at angles with the horizontal of 0.5° or less, are strongly

affected by nonstandard refraction. This part of the transmitter radiation is of paramount importance in early warning radar and in communications. For such applications of radar as gun-laying or searchlight control the effects of nonstandard propagation are usually negligible because the rays which reach the target have emerged from the transmitter at a fairly large angle with the horizontal.

The progress of a ray through the stratified atmosphere is described by Snell's law, discussed previously (p.138) When the angle α between the ray and the horizontal is small

$$\cos \alpha = 1 - \frac{\alpha^2}{2},$$

provided α is expressed in radians.

Introducing this into Snell's law for a curved earth, equation (6), noting that $n + h/a = 1 + M \cdot 10^{-6}$ and neglecting second order quantities, it is seen that

$$\tfrac{1}{2} (\alpha^2 - \alpha_0{}^2) = (M - M_0)10^{-6}. \qquad (18)$$

Since α is the angle which the ray makes with the horizontal it is equal to dh/dx, the slope of the ray. Solving equation (18) for α,

$$\alpha = \frac{dh}{dx} = \sqrt{\alpha_0{}^2 + 2(M - M_0)10^{-6}}. \qquad (19)$$

These relations apply to *any two* levels provided α and α_0 are the angles at the levels to which M and M_0 refer.

Equation (19) provides a technique for tracing the paths of rays emitted by a transmitter at various angles with the horizontal, and it indicates how their passage through the atmosphere is controlled by the variations of the modified index. Although this ray tracing method is only an approximation of the true solution of the wave equation, it can be used, subject to certain limitations, for computing quantitatively the strength of the field. The approximation breaks down when *neighboring* rays cross each other and form caustics.

The method may be illustrated by the case of standard refraction with $k = \frac{4}{3}$. As shown in Figure 21, draw the M curve with a slope $ka = 4a/3$. Let
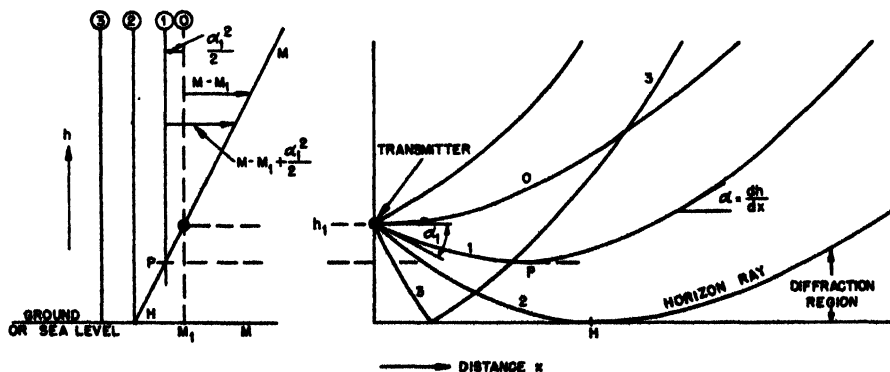
DISTANCE x

FIGURE 21. Rays in the standard atmosphere.

the subscript 1 stand for the transmitter level (of height h_1). Pass a vertical line through the corresponding point M_1 of the M curve. Lay off the distance $\alpha_1^2/2$ to the left of M_1 for a particular ray, 1, which emerges from the transmitter at angle α_1 with the horizontal. In order to make α and M comparable numerically, the factor 10^{-6} should be eliminated from equation (18) above. For this purpose α^2 should be measured in the same unit as M, that is, in 10^{-6} radian. The distance between M and 1 at any height h then is equal to $(M - M_1) + \alpha_1^2/2$, and by equation (19) the square root of twice this quantity is equal to the slope of the ray at height h. Hence, ray 1 starting downward from the transmitter is bent more and more toward the horizontal as h decreases. At point P this ray becomes horizontal and from there on increases in slope with increasing height.

Ray 1' starting upward from the transmitter at the same angle α_1 continues to curve upward more and more rapidly as the height increases. Ray 2 is the horizon ray which represents the limit to which rays can be directed by refraction. Beyond this lies the diffraction region where ray tracing cannot be used. To study the field in the diffraction region the original wave equation must be used. Ray 3 is reflected from the ground and in crossing some of the other rays produces the phenomenon of interference. In connection with Figure 21 it must be emphasized that the height scale is tremendously exaggerated and that all the rays shown come from a small group which are propagated in a nearly horizontal direction.

Sometimes it is convenient to express the path of the ray in terms of ray *curvature*. The true curvature of a ray as it appears on an undistorted (curved earth) diagram is different from the curvature exhibited by a ray on a plane earth diagram. The true curvature of a ray is given by $1/\rho$, where ρ is the radius of curvature, and it can be shown that, for nearly horizontal rays, this is related to the gradient of n by

$$\frac{1}{\rho} = -\frac{dn}{dh}.\tag{20}$$

However, the relative curvature of the earth with respect to that of a ray is $(1/a) - (1/\rho)$. Now let us set this equal to the curvature $1/ka$ of an equivalent earth. Then

$$\frac{1}{a} - \frac{1}{\rho} = \frac{1}{ka},\tag{21}$$

and, introducing equation (20),

$$k = \frac{1}{1 - \dfrac{a}{\rho}} = \frac{1}{1 + a\dfrac{dn}{dh}}.\tag{22}$$

This amounts to a definition of k which is more general than the one introduced before on page 140 but reduces to the latter when the index curve varies linearly with height.

For a plane-earth diagram, M is used in place of n. Since

$$M = \left(n + \frac{h}{a} - 1\right)10^6,$$

$$\frac{dM}{dh} = \frac{1}{a}\left(a\frac{dn}{dh} + 1\right)10^6.$$

Substituting the last equation into equation (22) gives

$$k = \frac{1}{a}\frac{dh}{dM}10^6\tag{23}$$

and shows that k, in its most general form, is proportional to the slope of the M curve. Reference to Figure 20 shows that k assumes negative values for a range of altitudes whenever a duct is formed in the atmosphere.

These relations may also be expressed in terms of m, where

$$m = \frac{\rho}{a}\tag{24}$$

is the ratio of the radius of curvature of a ray to the radius of the earth. From equation (22) it follows that

$$\frac{1}{k} + \frac{1}{m} = 1.\tag{25}$$

Both k and m vary with height except in the special circumstance that the M curve is linear. Table 2 gives a number of corresponding values of k and m and indicates their significance.

TABLE 2. Relation of k and m

k	1	$\frac{6}{5}$	$\frac{5}{4}$	$\frac{4}{3}$	2	∞	-2	-1
m	∞	6	5	4	2	1	$\frac{2}{3}$	$\frac{1}{2}$
		U.S. Brit. Standard		Moist standard		Zero relative curvature	Duct formation	

The Duct—Superrefraction

When the M curve has a negative slope, k is negative; the curvature of the rays is concave downward on a plane earth diagram, and the true curvature of the rays is greater than the curvature of the earth. Hence rays which enter the duct under sufficiently small angles are bent until they become horizontal and then are turned downwards. This particular form of refraction is called superrefraction. Such rays will be trapped in the duct, oscillating either between the ground and an upper level, or between two levels in the atmosphere. These conditions are illustrated by Figure 22 for the case of a

ground-based duct and by Figure 23 for an elevated duct.

The detailed construction of a ray diagram in the case of an elevated duct is shown in Figure 23. It is assumed, for illustration, that the transmitter is placed at the point which produces the maximum amount of trapping, and this point turns out to be located at the maximum of the bend in the M curve. The vertical line for M_1 corresponding to h_1 is drawn as shown, and again the line 1 is drawn to the left of M_1 at the distance $\alpha_1{}^2/2$, to represent ray 1 which departs from the transmitter at angle α_1 measured from the horizontal. As the ray proceeds outward and downward it is bent less and less, corresponding to the decreasing distance between the M and 1 lines. Finally it reverses and rises to the height indicated. Ray 1 must therefore oscillate between the heights determined by the crossing of the M and 1 lines. Ray 1' starting upward at the same angle α_1 oscillates between the same height limits as ray 1.

Rays 2 and 2' emerging at angle α_p are the limiting rays which are trapped in the duct between the heights h_t and h_b. Beyond the horizon ray 3 and

below the duct lies the diffraction region for this case. Ray 4 emerging at an angle greater than α_p is not trapped but after reflection passes entirely through the duct.

Ground-based ducts are likely to be found along coasts where warm, dry air from over land flows out over a colder sea. This situation, for instance, prevails in the summer months along the northeastern coast of the United States. Elevated ducts occur frequently along the southern California coast.

An illustrative series of theoretical coverage diagrams as obtained by the ray tracing method described are collected in reference 448. A few of these diagrams are reproduced in Figure 24, for a frequency of 200 mc and a transmitter elevation of $h_1 = 100$ ft, corresponding to an h_1/λ ratio of approximately 20. The height scale is exaggerated in the ratio 40/1. Transmission over sea water is assumed. The coverage range is adjusted to "define the probable low-level zone of detection of a medium bomber with fair aspect by an SC-1 or SC-2 radar at 100-ft elevation. For SK radars and higher altitude installations, the diagrams are conservative.
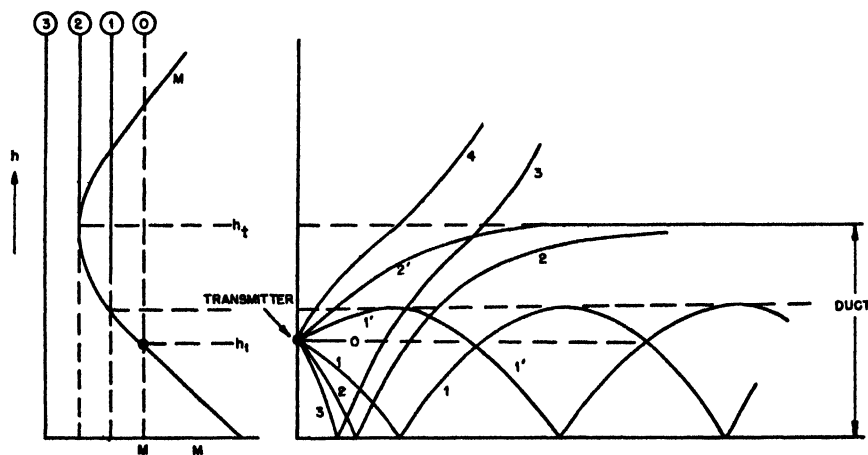
FIGURE 22. Rays with a ground-based duct.
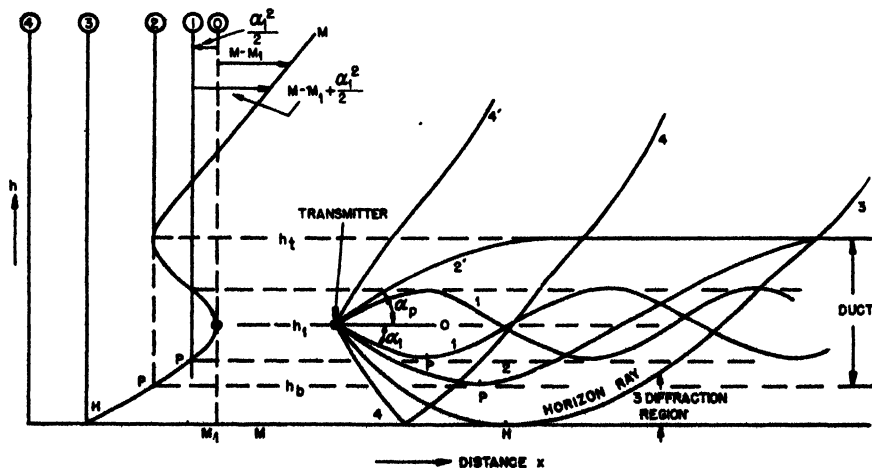
FIGURE 23. Rays with an elevated duct.

For SC and SA radars or for lower altitude installations, they are optimistic."

Figure 24A shows the lobe structure for the standard atmosphere in which M increases 36 MU per 1,000 ft. It also shows the value of $M - M_{100}$; that is, the M curve is drawn so as to pass through zero at the transmitter elevation of 100 ft. On diagrams B through E the lower portion of the standard lower lobe is indicated by a dash-dot line. The blind zones are cross-hatched, and their boundaries represent the calculated limits of detection. An interesting feature of these diagrams is the appearance, in some cases, of blind zones of considerable range and altitude along the surface. These cause "skip ranges" for ground targets that are significant in operational problem Ray diagrams were used in calculating the field strengths in Figure 24.

The relative heights of the transmitter and the duct have an important bearing on the mechanism of transmission. The duct may develop entirely below the transmitter site or entirely above, or the duct may include the transmitter. With these alternatives a variety of propagation conditions is possible.

One of the important concepts of radiation theory is contained in the principle of reciprocity. This principle states that when a transmitter is at a point in space A, and the receiver at a point B, the received intensity is the same when they are interchanged, the transmitter being at B and the receiver at A. (It is assumed in making this statement that the transmitter and receiver may be regarded as point sources.) Similarly, for radar the signal intensity remains unaltered if the positions of radar and target are interchanged. It is known that there are serious limitations to the reciprocity principle where ionospheric reflections are involved, but for shorter waves and tropospheric propagation the principle may be applied without restriction. By means of the reciprocity principle any coverage diagram may be used to obtain the field strength when the heights of the target and the radar are interchanged.

From a study of such evidence on coverage diagrams as is available, it appears that (a) the effects of superrefraction are most marked when the transmitter lies in the duct; (b) they exist to a lesser degree if the transmitter lies below the duct: in particular no excessively long ranges for targets are then found above the duct—sometimes the ranges are extended slightly, other times slightly decreased; (c) for a transmitter above the duct no excessive changes in field strength occur below the duct—this can be deduced from (b) by using the reciprocity principle; (d) there is no appreciable superrefraction when the transmitter lies appreciably above the duct.

For some time after the discovery of superrefraction it was thought that the concentration of radiative energy in the duct might result in a decrease of the
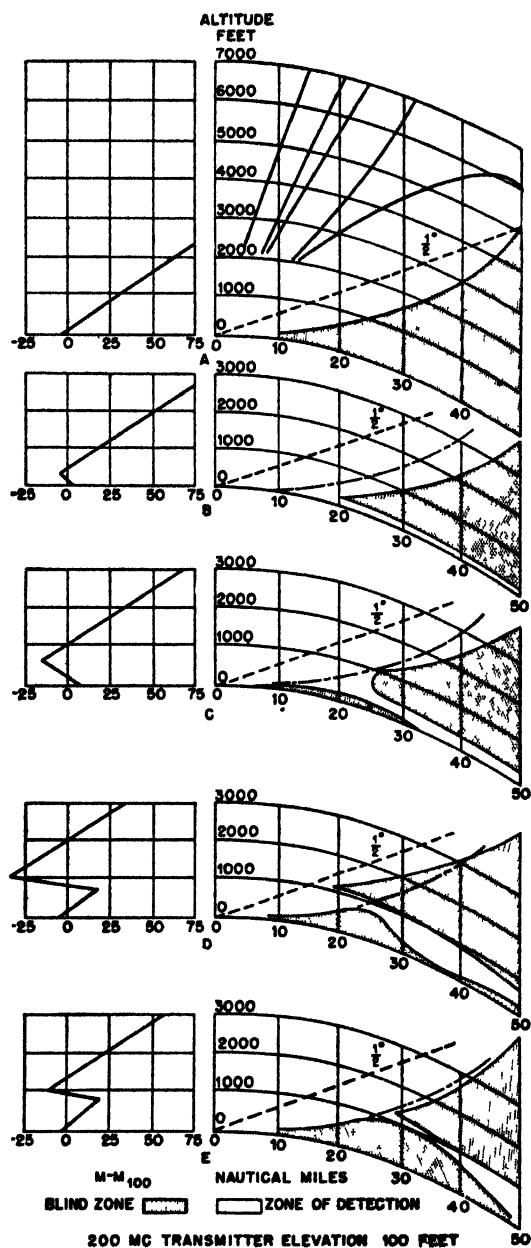
FIGURE 24. Calculated coverage diagram.

amount of radiation above the duct and hence in a reduction of coverage there. The cases illustrated in Figure 24, at least, are not in accord with this presumption. In spite of the great increase in ranges in the duct the amount of energy trapped is small compared to the total energy of the radiation field.

Wave Picture of Guided Propagation

It must be realized that while ray treatments give accurate results under certain conditions, there are features of the propagation problem which can be satisfactorily discussed only on the basis of the electromagnetic wave equations. As an aid to under-

standing the wave treatment the close analogy between the functioning of a duct and a hollow metal waveguide (or dielectric wire) may be used. In both cases the field which is being propagated may be represented as the sum of an infinite number of terms (modes). Each waveguide mode is propagated with a separate phase velocity and an exponential attenuation factor and has a field distribution over the wavefront that is independent of distance in the direction of propagation.

In a metallic waveguide a finite number of modes are propagated with very small attenuation, while the remaining modes, infinite in number, have attenuations so high that they are, practically speaking, not propagated at all. The same division of modes into those that are freely propagated and those that are highly attenuated is found for duct propagation. In the duct, however, the difference between the two types of modes is less pronounced than in a hollow metal tube.

As the frequency is decreased, the number of transmission modes decreases both for the hollow metal tube and the duct until the cutoff frequency is reached, below which neither serves as a waveguide. For simple surface trapping (discussed on page 145), the following formula gives the approximate maximum value of the wavelength for which guided propagation inside the duct can still take place:

$$\lambda_{max} = 2.5d \sqrt{\Delta M \cdot 10^{-6}}.$$

Here d is the height of the top of the duct above the ground in the same units as λ_{max}, and ΔM is the decrease in M inside the duct. This relationship is represented in Figure 25 where, it should be noted,
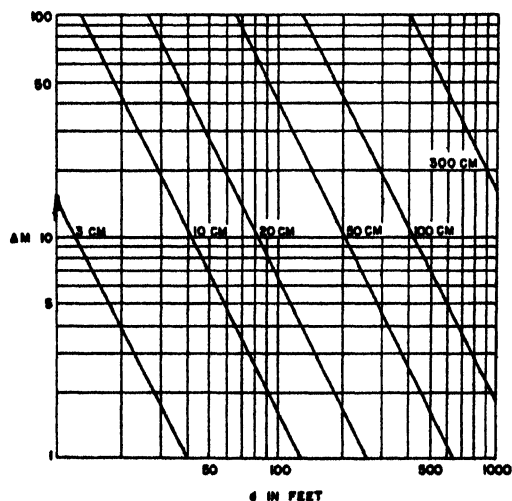
FIGURE 25. Maximum wavelength trapped in simple surface trapping. Duct width d in feet. ΔM is total decrease of M in duct.

the duct width is given in feet and the wavelength in centimeters. When the wavelength exceeds the critical value obtained from this graph, guided

propagation is no longer to be expected. M curves of different shapes will require slightly different numerical factors in the formula.

The main difference between the modes is found in the vertical distribution of field strength. The first three modes for a simple ground-based duct are illustrated in Figure 26. The lowest mode has
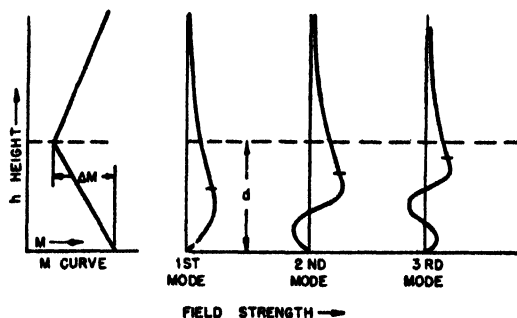
FIGURE 26. Vertical distribution of field strength for first three modes in a duct.

approximately ⅜ of a cycle of an approximate sine wave, followed by an exponential decrease. Higher modes have multiples of half cycles added to the sinusoidal part.

How these modes must be combined to give the total field strength and its vertical distribution is a question which depends on the height of transmitter, the distance out to the point where the total field strength is to be obtained, the rate of attenuation of each mode as a function of the distance, and its phase velocity. Since the attenuation and the phase velocity are different for the various modes, the vertical distribution of the total field changes with the distance from the transmitter, and the number of modes composing the total field decreases with increasing distance.

Reflection from an Elevated Layer

This phenomenon has been studied extensively at San Diego. The meteorological situation there is rather unique in that the warm and extremely dry upper air overlies a cooler and very moist lower stratum. The transition between the two layers is very sharp. This gives rise to an elevated duct of the type exhibited by the M curves of Figures 24D and 24E. Often the reversal of the M curve takes place over an even narrower interval of height than shown in these graphs. In such cases there is a reflection analogous to the reflection of waves at a true discontinuity between two media and which cannot be accounted for by the bending of rays.

At an interface between two media of different refractive indices there is partial reflection of radiation for any angle of incidence, but when the phenomenon (partial reflection and partial transmission) takes place in a layer of finite thickness,

the reflected radiation is appreciable only at angles near grazing (less than 1° under the conditions found at San Diego). Furthermore, other things being equal, the reflection coefficient increases with increasing wavelength. This feature distinguishes the reflection by a layer from the duct effects produced by this layer, as the latter generally tend to become less pronounced for longer waves. The reflection gives rise to an additional field strength near the ground, often well beyond the optical horizon.

Transmission experiments carried out at San Diego at frequencies between 50 and 500 mc gave results that are explained satisfactorily on the basis of reflections of the type just described but not on the duct theory. Thus most of the ducts caused by reversals of the M curve of the type shown in Figure 24D will be beyond cutoff for a frequency of 50 mc, as indicated on page 150. No guided propagation should therefore be expected, whereas the observed field at the receiver, located well beyond the optical horizon, was consistently very high.

At a frequency of 500 mc the reflection is found to be highly critical with respect to the angle of incidence at the reflecting layer. When meteorological conditions are such that the layer is high (3,000 to 4,000 ft), and therefore the angle of incidence large, the intensity of the reflected radiation is found to be very low; when the layer forms at a low level (a few hundred feet only) the reflected radiation becomes very strong. This behavior agrees with the predictions of electromagnetic theory.

So far, the experiment at San Diego is the only instance where a clear-cut case of reflection by an elevated layer has been found, although indications of similar effects have been observed elsewhere. Whether or not this phenomenon will occur at other places in or near the subtropical belt is not conclusively known since our knowledge of meteorological conditions in these climates is far from complete. If it does occur, it will obviously be of great operational significance.

Operational Applications

Radar

Ground radars have experienced most of the effects of propagation in nonstandard atmospheres so far observed operationally. Phenomenal ranges on ship and low-flying airplane targets have been observed, especially in the Mediterranean area, the Arabia-India area, in Australia, and the Southwest Pacific theaters. In the United States and Europe ground-based ducts over land have occasionally produced fixed echo clutter seriously interfering with the plotting of aircraft targets over land. This ground clutter interference is especially troublesome with microwave early warning sets plotting targets over land. On ground radars with high pulse repetition rates, echoes from large distances frequently return

on the second or later traces. Such echoes interfere with first sweep echoes and sometimes are misinterpreted as having ranges appropriate to the first sweep, with serious tactical consequences.

One of the most serious operational consequences of superrefraction is a secondary effect, that of misleading operators as to the overall performance of the equipment. Long-range echoes caused by superrefraction have frequently been assumed to indicate good condition of the equipment, when precisely the opposite is actually the case. The phenomenon of superrefraction does not, however, in the same degree invalidate the measurement of signal-to-noise ratio of *nearby* echoes, as a criterion of relative overall set performance. Field strengths from nearby objects well within the optical horizon are far less subject to propagation variations. Echo strengths (signal-to-noise ratio) from nearby objects are still considered a good relative index of overall performance, provided that easily recognized echoes can be measured which are not sensitive to very small changes in the radar frequency. There are other sources of echo fluctuations such as the motion of objects (trees, towers) caused by the wind (important at wind speeds above 15 miles per hour). Great care is needed in the choice of fixed echo "standards" so that they are kept free of the effects enumerated. Sometimes artificial echoing objects are constructed of flat mesh screens perpendicular to the beam in order to secure suitable echoes which are not frequency sensitive. The extreme variability of long-range fixed echoes emphasizes the operational need for reliable test equipment for making quantitative tests on the components as well as on the overall performance of the equipment aspects of radars, as distinct from propagation effects.

In addition to the direct electrical checks on set performance there are a number of ways of making sure indirectly whether any failures of detection by radar may be due to a deformation of the coverage pattern by superrefraction. In the first place, superrefraction rarely affects detection at angles of elevation above about 1.5°. Any irregularity at higher angles must be attributed to other causes. Even between 0.5° and 1.5° failures of detection are exceptional and occur only where there are very strong ducts. A clue to the probability of occurrence of such conditions can be ascertained from a study of the primary meteorological effects which cause them; and even with only a moderate amount of meteorological information it is usually possible to make an estimate of this probability. Such superrefractive conditions almost invariably show up in intensified and extended ground echoes (ground clutter on the scopes) and, in case of an overwater path, in extended ranges of ship detection. A record of meteorological data will be very helpful in deciding, after the fact, whether any specific failure of aircraft detection might have been ascribed to weather. Even if this

is probable, there are, of course, a number of other operational causes that might be responsible rather than the weather.

Experience gained in England indicates that the technique of forecasting whether or not superrefraction occurs is, on the whole, fairly successful, but there are still many occasions when the predictions are not fulfilled. It has been intimated that in England this was due, at least partly, to variations in the sensitivity of the 10-cm set used; when the set is not at peak efficiency, maximum ranges of surface targets appear shortened, and the coverage in the duct may be reduced to a value corresponding to standard conditions.

A major problem in any early warning radar system is that of heightfinding by means of maximum ranges. On this it is difficult to make general statements. The method of heightfinding usually employed in long-range radar work consists in using the boundary of the lowest lobe as a height indicator, assuming that when the target is first sighted it has just entered the lowest lobe. When superrefraction is present, the height estimated in this way can be seriously in error. It may be too high if the enemy is flying in the duct, so that he is discovered earlier than he would be normally; or it may be too low if the enemy is flying in the region above the duct and so he is discovered later than he would be under standard atmospheric conditions. Here, again, it should be possible to find out whether repeated errors in height determination are the result of superrefraction or whether they are due to faulty calibration or to other features not related to the weather. Other methods of heightfinding, such as are used in fighter control and control of antiaircraft fire, are usually carried out at angles of elevation too large to be affected by nonstandard types of atmosphere.

VHF COMMUNICATIONS AND NAVIGATIONAL AIDS

The extension of the maximum range of very high frequency [VHF] navigational aids has already been mentioned as an important consequence of superrefraction. Similar extensions of communication ranges of VHF radio sets also occur. Because VHF air-to-ground communications are relied upon only for comparatively short-range communications, this extension of the normal range by atmospheric conditions is important primarily from a security standpoint. It must always be borne in mind that transmissions on VHF may frequently be propagated hundreds of miles beyond the normal limiting range and are subject to enemy interception. Superrefraction has also been observed to cause very objectionable mutual interference between two control towers attempting to use a common VHF channel, although the distance between the airports was great enough to prevent serious mutual interference under normal conditions. Point-to-point VHF radio links are also affected by refraction, over longer paths than optical.

RADIO COUNTERMEASURES

The laws of radio propagation enter into the problem of jamming the enemy communication and. radar equipment. Since it is rarely possible to locate the jamming transmitter coincident with the enemy transmitter whose signals it is desired to mask, the efficiency of propagation of the signals from the enemy transmitter relative to those of the friendly transmitter enters into the problem. This has been worked out in detail for the standard atmosphere. When conditions are not standard, however, the effectiveness of the enemy transmitter, as determined for standard conditions, no longer applies. A case of special interest occurs when an airborne jamming transmitter is used as a countermeasure against an enemy radio communication link operating between two points on the ground. If the meteorological situation is such as to be favorable to formation of a ground-based duct the enemy signals may be propagated with small attenuation, whereas the signals from the jamming transmitter may be unaffected or even weaker than would normally be expected.

Plans for the employment of ground-based jammers against enemy radio and radar systems should take into consideration the ability of atmospheric refraction to increase, or occasionally to decrease, the signal propagated to the enemy's installation for jamming purposes. However, there has been only limited use of ground-based jamming so far. Unintentional mutual jamming has occurred between the spaced radar sets of a coastal system on the same frequency, where nonstandard propagation conditions caused strong signals to be propagated between normally noninterfering radars.

RADIO METEOROLOGY

Temperature and Moisture Gradients

This section is devoted to a survey of the meteorological conditions which produce the various types of propagation described in the preceding sections. This brief outline is not intended to replace the assistance of a professional meteorologist in analyzing short and microwave propagation problems; but by familiarizing radar or communications personnel with the fundamental physical processes of low-level weather it may open the way toward a more fruitful consultation with the meteorologist.

Duct formation is the most important phenomenon for which a detailed knowledge of the physical state of the lower atmosphere is required. Whenever a duct is formed, M decreases with height within a certain height interval. Since, according to text on pages 139 - 143 , $M = (n - 1) \cdot 10^6 + 0.157h$, the

existence of a duct presupposes that the refractive index n decreases with height over at least a limited range of altitudes at a rate more rapid than 0.157 MU per meter. Such a decrease can be produced by two different meteorological conditions.

1. A rapid increase of temperature with height. This temperature inversion must be very pronounced in order, by itself, to produce a duct. In practice, a temperature inversion contributes to duct formation when accompanied by a sufficiently strong moisture lapse.

2. A rapid decrease of humidity with height designated as a "steep moisture lapse."

When ducts are produced by only one of these causes, they may be designated as "dry ducts" and "wet ducts," respectively. In the general case a temperature inversion and a moisture lapse cooperate in producing a duct, but one of the two factors will be preponderant, thus facilitating the analysis of the meteorological problem.

Whether or not a duct occurs under given meteorological conditions and what the rate of change of M is inside the duct may be determined by means of the diagram, Figure 27. (This discussion is presented for the purpose of illustrating the importance of temperature and moisture gradients. The technique more readily usable in practice is to compute the values of M at various altitudes directly from temperature and relative humidity data with the aid of Figure 19.) The abscissa in Figure 27 is the rate of

T°C	(f)T
−30	6.390
−25	6.134
−20	5.894
−15	5.666
−10	5.452
−5	5.250
0	5.049
+5	4.878
+10	4.706
+15	4.543
+20	4.389
+25	4.241
+30	4.102
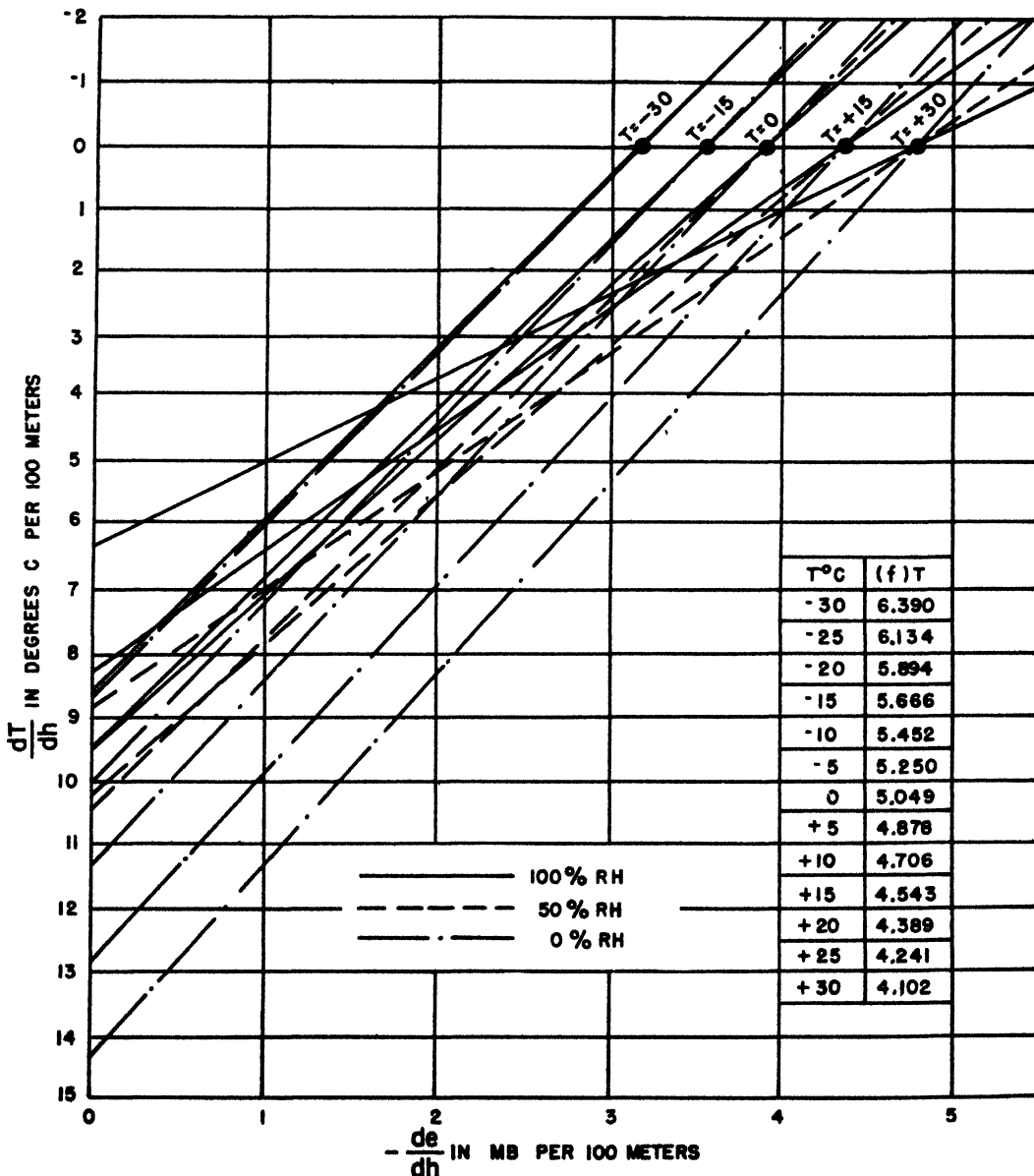
FIGURE 27. Temperature and humidity gradients.

decrease of humidity with height $(-de/dh)$, where e is the water vapor pressure in millibars. (e can be found from meteorological tables when relative humidity and temperature are known.) The ordinate is the rate of *increase* of temperature with height (dT/dh). The slanting lines represent various values of temperature and relative humidity at some particular height h. The lines passing through the same point at the upper right of the diagram correspond to the same mean temperature; lines of different slopes represent different mean relative humidities.

In order to determine the rate of change of M at a given level, find the point in the diagram corresponding to the actual rates of change of moisture and temperature. Also pick out the straight line representing the actual mean values of temperature and humidity in the layer considered. If the point is at the lower right relative to this straight line, M decreases with height in the layer chosen; that is, a duct exists. If the point is at the upper left of the straight line, M increases with height and there is no duct.

The rate of change of M, (dM/dh), may be obtained from the diagram by measuring the horizontal distance from the point to the line and multiplying by the function of the temperature $f(T)$ given in the table on Figure 27. The result is the value of dM/dh, the rate of change of M, in M units per 100 m. This quantity is negative when the point is to the right of the line and positive when the point is to the left of the line.

It is seen at once from the diagram that for small values of the moisture lapse an extremely steep temperature gradient is required in order to produce a duct (lower left part of the diagram). In cold air such as is found in the arctic the total moisture is small, and hence the moisture gradient will in general be quite small. Ducts will then only occur when a very strong temperature inversion exists.

Strong temperature inversions occur only under special meteorological conditions which will be discussed below. Ordinarily the temperature of the air decreases with height; and this will put our representative point into the upper part of Figure 27. A duct can then exist only when the moisture lapse is large enough, so that the representative point falls to the right of the appropriate slanting line. Such conditions are common in the lower atmosphere. This leads to a wet duct, which is determined almost completely by the moisture lapse.

Physical Causes
of Stratification—Turbulence

There are three basic meteorological factors which tend to modify the temperature and moisture distributions in the lowest layers of the atmosphere. These are: (1) advection, (2) nocturnal cooling (over land), and (3) subsidence.

Advection is a meteorological term used to designate the horizontal displacement of air having particular properties. Advection is of great interest in propagation problems particularly because it leads to an exchange of heat and moisture between the air and the underlying ground or sea surface and thus affects the physical structure of the lowest layers.

Nocturnal cooling over land is caused by a loss of heat from the ground by infrared (heat) radiation. The cooling of the ground is communicated to the lower layers of air and leads to the establishment of a low-level temperature inversion.

Subsidence means a slow vertical sinking of air over a very large area. It is most likely to be found in regions where barometric Highs are located. Subsidence tends to produce a temperature inversion and also produces very dry air which, spreading out over a humid surface, creates a situation which is favorable for the formation of a duct.

The processes (1) and (2) change the physical characteristics of the air through transfer of heat or moisture between the air and the underlying surface of the ground or sea. The operating factor in this exchange is turbulence. The main features of turbulence in the lower atmosphere are outlined briefly below.

Convection occurs spontaneously whenever the decrease of temperature with height exceeds a value of about 1 C per 100 m. This convective condition is usually produced as a result of the heating of the ground by the sun's rays. Even with a cloudy sky the diffuse daylight often is strong enough to produce moderate convection. On a hot summer day convection over land extends to great heights. Convection mixes the air thoroughly and thus causes a uniform distribution of moisture and a uniform decrease of temperature with height of about 1 C per 100 m. Hence even moderate convection tends to produce a smooth M curve which varies linearly with height. Standard conditions may therefore be assumed to prevail on clear summer days (and not infrequently on clear days in the cooler seasons) from the hours of late morning until late afternoon, during which time convection is most active.

Frictional turbulence occurs frequently in the lower atmosphere even in the absence of convective conditions. It is caused by the wind and requires the presence of at least light winds, but with moderate or strong winds the effect is more pronounced. In conditions of calm or with a gentle breeze, frictional turbulence is confined to the lowest strata. Moderate or strong winds develop a layer of intense turbulence, caused by friction of the air at the irregularities of the ground. This layer is usually quite well defined in height and extends to an average elevation of about 1,000 m over land. Over a relatively smooth sea where friction is small the height of the layer is much reduced. In this frictional layer the air becomes thoroughly mixed; the vertical temperature gradient

caused by convection is about -1 C per 100 m, and the moisture lapse is steady and rather small. Standard refraction will therefore prevail when winds are moderate to strong over land, and over the ocean also when the winds are sufficiently strong.

Temperature inversions occur when the temperature of the surface (sea or land) is appreciably lower than the temperature of the air. The transition from the ground temperature to the free air temperature takes the form shown in Figure 28. The heat and moisture
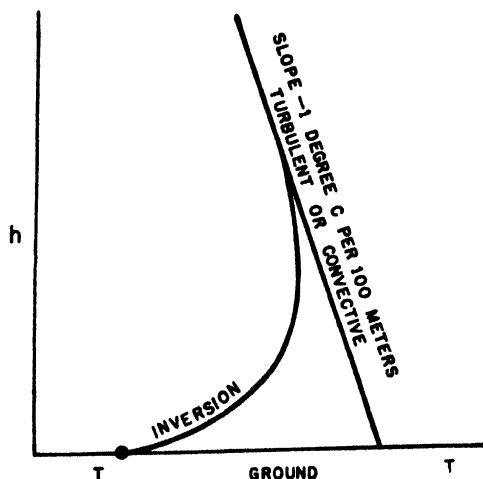
FIGURE 28. Air temperature versus height for an inversion.

transfer caused by turbulence in a temperature inversion is less simple than that in a frictional layer. The turbulent processes active in inversion regions are highly complex and are not yet very well explored. It is known, however, that the intensity of the vertical transfer of heat and moisture is greatly reduced as compared to the rate of transfer with frictional turbulence. The reduction is the more pronounced, the steeper the vertical increase of temperature; in a steep inversion the rate of transfer may be many times less than in a frictional layer. This tends to produce a vertical stabilization of the air layers in the inversion region. As soon, therefore, as a temperature inversion has begun to form, the rapid mixing in the lowest layers, usually effected by frictional turbulence, stops and is replaced by a much more gradual diffusion.

Assume now, for instance, that the rate of diffusion has become so slow that the transfer of moisture over a height of a few hundred feet takes many hours or, perhaps, a day or two. When the air in the inversion is dry to begin with and flows over ground capable of evaporation (the sea or moist land) there will be established, in such an air mass, a steep moisture lapse, since the water vapor that has been taken up by the air near the ground will only gradually diffuse into the dry air aloft. Conditions are then favorable for the formation of an evaporation duct, in addition

to whatever tendency toward duct formation may be caused by the temperature inversion itself.

Advective Ducts—Coastal Conditions

Advective formation of ducts may occur both over land and over sea, but this process is most important over the ocean near coasts. The most common illustration is that of air above a warm land surface flowing out over a cooler sea. Over the land the air will usually have acquired a convective or nearly convective temperature gradient of -1 C per 100 m. When this air flows out over the cool water surface, a temperature inversion is rapidly formed which grows in height as the process of turbulent transfer progresses. The temperature inversion does not, in itself, give rise to a pronounced duct because the effect of a temperature gradient upon the M curve is relatively small; but when the air is dry, evaporation from the sea surface takes place simultaneously with the heat transfer, and a moisture lapse rate is established in the lowest layers. The combination of temperature inversion and moisture lapse rate is most favorable for the formation of a duct off shore.

The gradual formation of this type of duct is illustrated in Figure 29. This shows M curves, corres-
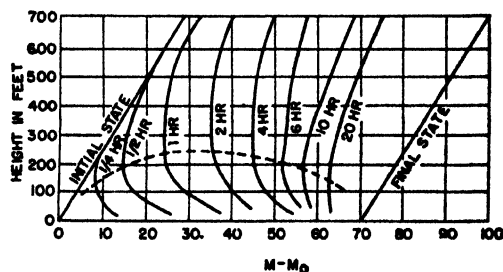
FIGURE 29. Development of duct off coast. Initial state corresponds to air at coast line. ¼ hr, ½ hr, etc., refer to time air has been over water. Initial conditions for this set of curves: unmodified air $T_0 = 32$ C, $e = 12.3$ mb; water $T_w = 22$ C, $e_w = 26.5$ mb saturation.

ponding to the simple surface type of trapping (see Figure 20, curve II) for a series of time intervals (and distances) as the air moves out over the water. The top of the duct is given by the elevation of the minimum value of the M curve. It will be noticed that the duct acquires a maximum depth some time after the air has touched the cold water surface; thereafter the depth decreases. The cause of this behavior is found in the progressive decrease in moisture and temperature differences which is the final result of the diffusion process. Thus the final stage of this transformation is an air mass whose temperature and moisture distributions are in equilibrium with the underlying water surface and no longer show a rapid variation with height.

Duct formation in such a case depends on two quantities: (1) the excess of the unmodified air temperature above that of the water and (2) the

humidity deficit, that is, the difference of the satura-
tion vapor pressure corresponding to the water tem-
perature minus the actual water vapor pressure in
the unmodified air. If these quantities are large,
especially the humidity deficit, a duct will develop.
A great variety of local conditions may, however,
be encountered in problems of this type, and empiri-
cal rules developed for one locality may not at all
apply to others.

Advective processes may also occur over land, but
the conditions required for duct formation are likely
to be found much less frequently. Evaporation over
land need by no means be small unless the land
surface is very arid (desert); in fact, evaporation over
a moist soil or a ground covered with vegetation may
be comparable to, or even larger than, evaporation
from a sea surface. A duct may therefore be formed
when dry, warm air flows over a colder ground surface
capable of evaporation. The temperature excess and
humidity deficit may again be defined as above.

Land and sea breezes often produce ducts near
coastal regions. These winds are of thermal origin
and are produced by temperature differences between
land and sea. The mechanism is illustrated in Figure
30. During the day, when the land gets warmer than
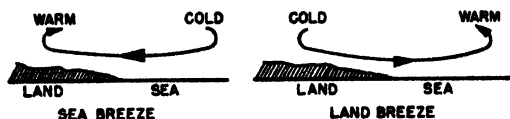
FIGURE 30. Land and sea breezes.

the sea, the air rises over the land and descends over
the sea and causes an air circulation in which the
wind blows from sea to land (sea breeze) in the lowest
levels. Vice versa, if during the night the land becomes
colder than the sea, a circulation in the opposite
direction arises. This is the land breeze. As a rule,
this type of phenomenon is extremely shallow, and
the winds do not extend above a few hundred feet
at the most. Often there is a reverse wind in the
layer above the land or sea-breeze layer. A sea breeze
may modify the advective conditions described above
in various ways, and extremely strong ducts have
been observed repeatedly under sea breeze condi-
tions. The land and sea breezes are of a strictly local
nature and in some cases will extend only a few
kilometers to both sides of the shore. Nevertheless
this region may be an important part of the trajec-
tory of radiation. These breezes develop only under
fairly calm conditions; under conditions of moder-
ately strong wind, the sea and land breeze will be
perceptible only as a slight modification of the
existing wind. Because of their limited extent, fore-
casting of these breezes requires a study of the local
wind and temperature conditions.

Advective ducts caused in the manner described
here are often quite limited horizontally. This is
especially true if a sea breeze is involved. The

assumption made throughout this report, namely
that the stratification of the air is of infinite extent
horizontally, will no longer be valid, and superrefrac-
tion may be restricted to a stretch along the coast.

Ducts over the Open Ocean

A type of duct that is somewhat similar to the
advective duct described above is found over the
open ocean where the air has had an extensive over-
water trajectory. It has been studied in experiments
carried out at the island of Antigua in the West
Indies. The subsequent description refers to this
particular location, but on the basis of experience
gained operationally and in other experiments it may
be presumed that similar conditions prevail in
numerous other regions of the world, particularly in
the trade wind regions.

At Antigua, in winter and early spring when these
tests were made, the wind is usually from the north-
east since the island is situated at the southeastern
fringe of the so-called Bermuda High, a large semi-
permanent circulation system over the North
Atlantic, extending from about 10° to 30° North
latitude. The air at Antigua has thus had an ocean
trajectory of thousands of miles. The relative hum-
idity is of the order of 60 to 80 per cent, indicating
that in spite of the long passage over the sea no
diffusion equilibrium has been established between
the sea surface and the moisture in the lower atmos-
phere. On the other hand, there is little difference
between the air and sea temperature, the latter
being rather constant at 25 C and the former varying
between 23 and 26 C. The air is, therefore, nearly
in convective thermal equilibrium with the sea sur-
face, and no appreciably "dry" duct can develop.
The duct is caused by the moisture variation in the
lowest layers.

A typical *M* curve is shown in Figure 31. It may
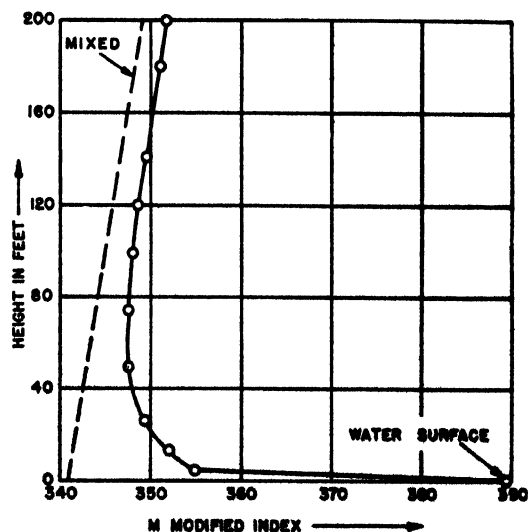
FIGURE 31. *M* curve over West Indian Ocean.

be seen that at as small a height as 0.5 m above the sea M has a value much lower than at the surface itself. As the surface value of M is obtained by the assumption that the air in immediate contact with the water is saturated with moisture, this indicates that 0.5 m above the water the moisture content of the air is still appreciably below saturation. The moisture in the lowest levels is subject to considerable variations caused partly by turbulence, partly by the waviness of the sea surface. M curves, such as Figure 31, are obtained by averaging over several measurements.

These ducts are much lower than the advective ducts discussed in the previous section; their height is about 12 to 15 m (around 40 ft). The effective decrease of M in the duct (apart from the sharp decrease in the lowest half meter) is of the order of 4 to 8 MU.

The latter figure depends somewhat on the wind speed. There is a maximum decrease of 8 MU at a wind speed of about 8 m per sec (13 miles per hour) and lower values for both lower and higher wind speed. The duct height in turn shows a very slight dependence on wind speed, increasing somewhat with increasing speed.

These ducts are so low that they are not very effective for trapping of waves even as short as S band, presumably on account of strong leakage (see pages 149-150), and signal strength is not increased when an S-band transmitter or receiver is placed inside the duct. For K band, on the other hand, the trapping effect is marked; on raising the transmitter or receiver from the ground a maximum of signal strength is observed at about 9 m, but from there on the signal begins to decrease up to about 20 m (overall decrease 5 db); at greater heights the signal gradually rises again.

These ducts appear to be a permanent feature at Antigua, at least during the season these observations were carried on. This is probably true also for many locations in the trade wind belt. The daily variation of weather phenomena and of duct characteristics at such purely maritime locations seems to be insignificant.

Nocturnal Cooling—Daily Variations

A daily variation of surface temperature occurs only over land. During the day the heating is caused by the sun's rays, and the cooling of the ground surface during the night is produced by radiation from the ground. The diurnal temperature variation of the sea is extremely small. However, shallow bodies of water sometimes have an appreciable diurnal variation.

The radiation which causes nocturnal cooling of the ground is temperature or heat radiation which is composed of waves in the infrared portion of the spectrum. It is the same kind of radiation that is given off by a hot stove or electric heater, but since the temperature of the earth is less than that of a stove the earth emits comparatively less heat radiation. Nevertheless, radiation is a very powerful agent in cooling the ground. From about sunrise until the late afternoon, the surface of the earth gains more heat from the sun and atmosphere than it loses by radiation to space; in the late afternoon and during the night, the surface loses more heat than it gains. The amount of heat radiated is very nearly independent of the physical constitution of the ground but is dependent upon its temperature and increases very rapidly with a rise in ground temperature.

The atmosphere has a "blanketing" effect upon the infrared radiation emitted by the ground. The atmosphere itself absorbs and emits infrared radiation, and the cooling of the ground may be greatly reduced by the action of the atmosphere. The blanketing effect is least with a clear sky and dry, cool air; it is somewhat stronger when, with a clear sky, the atmosphere is very warm and humid, as in the tropics. A cloud will produce a distinct blanketing effect, and with a complete overcast of low cloud the blanketing is so pronounced that the nocturnal cooling of the ground is reduced to only a small fraction of its value with clear skies.

The loss of heat from the ground is distributed by turbulence over the lowest layers of the atmosphere, thus giving rise to a temperature inversion. Inversions of this type are strongest in temperate and cold climates with a clear sky and cold, dry air overhead; they are less pronounced in the tropics with humid air and a clear sky and are practically absent with an overcast sky. A meteorologist, after some experience, can estimate the magnitude of an inversion to be expected with given local weather conditions.

Temperature inversions, by themselves, can at best produce only weak ducts, but strong ducts may result when the inversion is accompanied by a sufficient moisture lapse. This requires that the air be dry enough to allow evaporation into it from the ground. In warmer climates where the transition between night and day is rapid, evaporation may set in in the early hours of the morning before the nocturnal inversion has been completely destroyed by the action of the sun. A strong duct will then be formed for a short period. This condition seems to be frequent during certain seasons in Florida.

It is obvious that the shape of the M curve, when it deviates from the normal, may undergo rapid variations with the period of a day. One example has just been quoted; another is illustrated by the advective ducts over the North Sea produced by the mechanism described on pages 155-156. These ducts usually form in the hours before midnight and last until the early hours of the morning.

Fog

Contrary to what might perhaps be expected, the

formation of fog results, in general, in a decrease of refractive index. When fog forms, e.g., by nocturnal cooling of the ground, the total amount of water in the air remains substantially unchanged, but part of the water changes from the gaseous to the liquid state. The contribution of a given quantity of water to the refractive index is found to be far less when the water is contained in liquid drops than when it exists in the form of vapor. The formation of fog, therefore, results in a reduction of the amount of water vapor contributing to the value of M. If there is a temperature inversion in the fog layer, the saturation vapor pressure increases with height, and a substandard M curve frequently results (see Figure 20, curve Ib). This occurs with radiative fog (caused by nocturnal cooling of the ground) and also with advective fog (caused by the advection of warmer air over a cooler surface). Advective fog is very common in the Aleutian Islands and off Newfoundland.

If fog causes a substandard M curve, it is to be inferred that the rays will be bent upward, instead of downward as with superrefraction, and lead to a weakening of the field in the lowest layers, even to the point of producing a complete fade-out of radio reception. Appreciable reduction of radar ranges and interruption of microwave transmission have frequently been observed in such cases.

Fog, however, does not always produce a substandard M curve, though this is the most common case. In certain other less frequent types of fog, the temperature (and thereby the vapor pressure) may be constant or increase with height through the fog layer. In this event near-standard propagation will prevail, or a duct may develop when the temperature inversion is strong enough. An example is steam fog, formed when cold air passes over a warm sea (see also pages 160-164).

Subsidence—Dynamic Effects

The temperature inversions discussed so far owe their existence to the modification of air by contact with the ground, but subsidence inversions are produced by a mechanism of an entirely different nature. By subsidence is meant the sinking of air, that is, a vertical displacement, which must of course be accompanied by a lateral spreading (divergence) in the lower part of the subsiding column of air; otherwise there would be an accumulation of air in the lower levels. The thermodynamic analysis of this complex process shows that if the effect of subsidence is strong enough a temperature inversion will be created. Since this process does not require the presence of a ground surface, it may occur, and in fact often does occur, aloft in the atmosphere. The effects of subsidence frequently are the most pronounced at an elevation of the order of a kilometer or more.

As a general rule, subsidence occurs in regions of high barometric pressure. In fact, subsidence always does occur in such regions, but it may not always be intense enough to give rise to a strong temperature inversion. The flow of air in a barometric High is shown in Figure 32 as it appears on a weather map
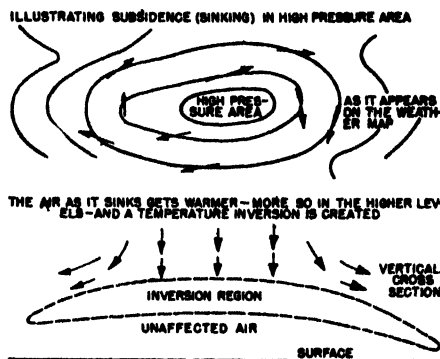
FIGURE 32. Characteristics of subsidence.

in horizontal projection, and also in a vertical cross section.

With subsidence, the air as a rule is very dry, and there is nothing in the process which can change the moisture content or produce moisture gradients. If, however, the dry air finds itself over a surface capable of evaporation, such as the sea surface, a steep moisture gradient may be established and a duct will be created. It is thus seen that subsidence in itself does not produce a duct, except in extreme cases, but it can act as an auxiliary factor and greatly enhance the formation of a duct whenever other conditions are favorable. Thus, forecasts of superrefraction based on a purely advective mechanism, or purely on radiative cooling or evaporation, may have to be modified in the presence of subsidence; an otherwise very weak duct may be converted into a strong duct by the effect of subsidence upon the lower strata.

Strong subsidence effects are of frequent occurrence on the southern California coast where they may continue with little change for days at a time. At times the duct is elevated, giving an elevated S-shaped M curve like IIIa in Figure 20. Again the duct may extend practically from the ground up with M curves similar to curves II or IIIb in Figure 20. The elevation of the top of the duct may vary from 300 to 5,000 ft, and the thickness may lie between a few feet and 1,000 ft. Coverage diagrams and the corresponding M curves for several typical situations are illustrated in Figure 24.

For a number of reasons the meteorological conditions in a barometric High are favorable for the formation of ducts. Among the favorable factors are: subsidence, creating very dry air into which evaporation from the surface can take place; again subsidence, creating temperature inversions; calm

conditions preventing mixing of the lowest layers by frictional turbulence and maintaining the thermal stratification caused by radiative cooling or local breezes; clear skies producing nocturnal cooling over land.

The conditions in a barometric Low, on the other hand, generally favor standard propagation. A lifting of the air, the opposite of subsidence, usually occurs in such regions and is accompanied by strong winds. The combined effect is to destroy any local thermal stratification and to create a deep layer of frictional turbulence. The air is therefore well mixed, and nonstandard vertical temperature and moisture gradients are wiped out in the early stages of their creation. Moreover, the sky is usually overcast in a low-pressure area and nocturnal cooling, therefore, is negligible.

To summarize, high-pressure regions, clear skies, and calm air are conducive to duct formation, while low-pressure areas, cloudy skies, and winds favor standard refraction.

Fronts in the atmosphere are possible sources of refractive effects. A front is a surface of discontinuity which separates two air masses of different temperatures. The surface slants at an angle of 1° to 2° with the horizontal, with the colder air forming a wedge under the warmer air. Fronts are a common occurrence in the atmosphere, and it might be thought that they should have a considerable influence on wave propagation. This is, however, not borne out by English radar experience, which shows very little superrefraction connected with fronts. The explanation is probably that fronts are invariably accompanied by low-pressure areas, and turbulence along a front is usually so strong that the transition from the cold air to the overlying warm air takes place continuously over a vertical distance of about a kilometer. Propagation conditions might, however, be somewhat different with fronts in sub-tropical climates, although our knowledge is still inadequate on this point. In one-way transmission frontal effects have been studied to a limited extent (pages 160-164).

Seasonal and Global Aspects of Superrefraction

Although the general picture is still incomplete, enough is now known about the geographical and seasonal aspects of superrefraction to warrant a general summary.

ATLANTIC COAST OF THE UNITED STATES

Along the northern part of this coast superrefraction is common in summer, while in the Florida region the seasonal trend is the reverse, with a maximum in the winter season.

WESTERN EUROPE

On the eastern side of the Atlantic, around the British Isles and in the North Sea, there is a pronounced maximum in the summer months. Conditions in the Irish Sea, the Channel, and East Anglia have been studied by observing the appearance or non-appearance of fixed echoes (see Figure 33). Additional
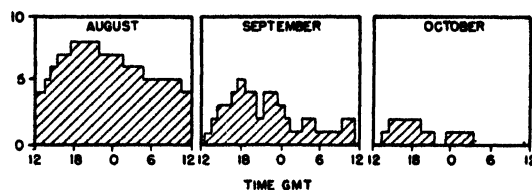
FIGURE 33. Diurnal frequency of long-range fixed echoes at North Foreland, Kent. Wavelength 10 cm.

data based on one-way communication confirmed the radar investigations.

MEDITERRANEAN REGION

The campaign in this region provided good opportunities for the study of local propagation conditions. The seasonal variation is very marked, with superrefraction more or less the rule in summer, while conditions are approximately standard in the winter. An illuminating example is provided by observations from Malta, where the island of Pantelleria was visible 90 per cent of the time during the summer months, although it lies beyond the normal radio range.

Superrefraction in the central Mediterranean area is caused by flow of warm, dry air from the south (sirocco) which moves across the ocean and thus provides an excellent opportunity for the formation of ducts. In the winter time, however, the climate in the central Mediterranean is more or less a reflection of Atlantic conditions and hence is not favorable for duct formation.

THE ARABIAN SEA

Observations covering a considerable period are available from stations in India, the inlet to the Persian Gulf, and the Gulf of Aden. The dominating meteorological factor in this region is the southwest monsoon that blows from early June to mid-September and covers the whole Arabian Sea with moist equatorial air up to considerable heights. Where this meteorological situation is fully developed, no occurrence of superrefraction is to be expected. In accordance with this expectation the stations along the west side of the Deccan all report normal conditions during the wet season (middle of June to middle of September). During the dry season, on the other hand, conditions are very different. Superrefraction then is the rule rather than the exception, and on

some occasions very long ranges, up to 1,500 miles (Oman, Somaliland), have been observed on 200-mc radar on fixed echoes.

When the southwest monsoon sets in early in June, superrefraction disappears on the Indian side of the Arabian Sea. However, along the western coasts conditions favoring superrefraction may still linger. This has been reported from the Gulf of Aden and the Strait of Hormuz, both of which lie on the outskirts of the main region dominated by the monsoon. The Strait of Hormuz is particularly interesting as the monsoon there has to contest against the shamal from the north. The Strait itself falls at the boundary between the two wind systems, forming a front, with the dry and warm shamal on top, and the colder, humid monsoon underneath. As a consequence, conditions are favorable for the formation of an extensive radio duct, which is of great importance for radar operation in the Strait.

THE BAY OF BENGAL

Such reports as are available from this region indicate that the seasonal trend is the same as in the Arabian Sea, with normal conditions occurring during the season of the southwest monsoon, while superrefraction is found during the dry season. It appears, however, that superrefraction is much less pronounced than on the northwest side of the peninsula.

THE PACIFIC OCEAN

This region appears to be the one where, up to the present, least precise knowledge is available. There seems, however, to be definite evidence for the frequent occurrence of superrefraction at some locations; e.g., Guadalcanal, the east coast of Australia, around New Guinea, and on Saipan. Along the Pacific coast of the United States observations indicate frequent occurrence of superrefraction, but no statement as to its seasonal trend seems to be available. The same holds good for the region near Australia.

In the tropics there is found a very strong and persistent seasonal temperature inversion, the so-called trade wind inversion. It has no doubt a very profound influence on the operation of radar and short-wave communication equipment in the Pacific theater.

Fluctuations in Signal Strength with Time

A number of different causes tend to produce variations of signal strength with time. These are discussed briefly in the following paragraphs.

TARGET MODULATION

Very rapid fluctuations having periods of only a small fraction of a second frequently are encountered in radar observations, especially with centimeter waves. These fluctuations arise as a consequence of the internal motions of the target and are especially noticeable for aircraft. Similar effects have been observed with reflection of microwaves from wooded hills, the fluctuations in signal probably being caused by foliage moving in the wind.

EFFECT OF WAVES ON THE SEA

A similar phenomenon is observed when the transmitter and receiver are so situated that reflection from a water surface contributes to the received signal strength. Owing to irregularities of the water surface and their rapid change with time, variations in signal strength will appear. The fluctuations arising in this way have a time scale of the order of a second, in the case of a lightly ruffled sea (see Figure 34). Evidently rays reflected from different
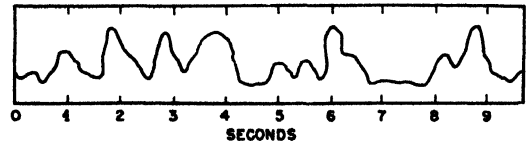
FIGURE 34. Variation in signal strength with time in radiation reflected from the sea (direct radiation cut off). $\lambda = 9$ cm.

parts of the water surface interfere, and with the changing form of the surface the interference pattern at the place of the receiver changes accordingly. The time scale of these changes must be connected with the speed, wavelength, and amplitude of the waves, but the exact relation is not known thus far.

TIDAL EFFECTS

The rise and fall of the tide produces a gradual variation in signal strength by changing the interference between the direct and the reflected rays. The path difference between these rays is $2h_1h_2/R$, where h_1, h_2 are the heights of the transmitter and receiver relative to the instantaneous water level and R is the range. The corresponding difference in phase between the two rays is equal to

$$\frac{2h_1h_2}{R} \cdot \frac{2\pi}{\lambda} = \phi , \qquad (26)$$

measured in radians. The variation in the signal strength depends upon the variation in ϕ. It is small when the change in ϕ is small and increases to a maximum for a change in ϕ of π radians. It follows from equation (26) that the tidal effect increases with the variation in the water level of the tide and with the heights h_1 and h_2 and decreases with the range and the wavelength.

SCINTILLATIONS

The really conspicuous fluctuations in propagation

conditions, however, are due to changing meteorological conditions. A characteristic type is an irregular fluctuation in signal strength on a time scale of the order of a minute and with an amplitude rarely of moderate periods (of the order of 15 min). A detailed theory of this type of fluctuation in signal strength is not available. When the duct is fully developed, there is a large-scale deviation from standard conditions with regard to mean field strength. If, in particular, both transmitter and receiver are situated inside the duct, there is a great increase in received field strength. Suppose, however, that for some reason the duct does not function according to the simple theory. The field strength at the receiver may then drop to the value corresponding to standard conditions. The observed fades exhibit just this characteristic in that they consist in sharp drops of signal strength *down* from a mean upper level. The conditions are illustrated in Figure 35, which shows three records obtained for a 22-mile path over sea. Figure 35A shows the normal record on a calm day when the only disturbances are due to scintillations. The record shown in Figure 35B, on the other hand, was obtained for a condition of simple surface trapping, with transmitter and receiver inside the duct. Figure 35A shows that the signal strength is considerably above the 95-db average .

Duct-type fades have been observed over land as well as over sea and appear to form a characteristic feature from which the presence of superrefraction may be inferred.
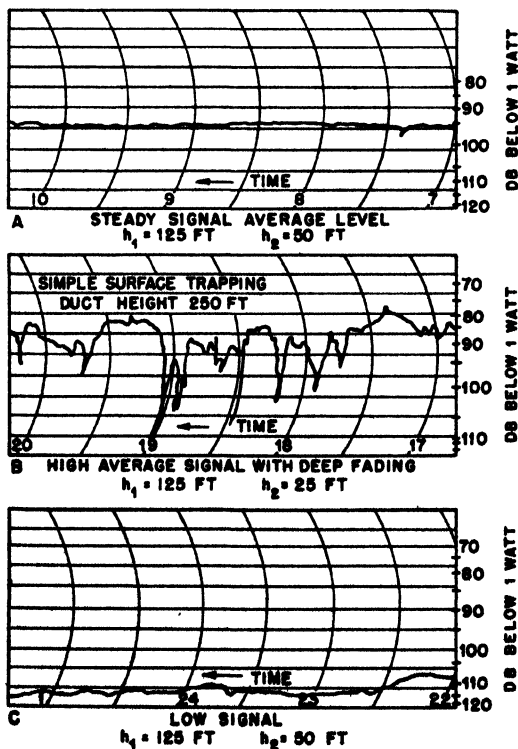
FIGURE 35. Signal strengths for λ = 10 cm over sea.

DUCT FADES

A duct is normally accompanied by fades in the signal strength of large amplitude (up to 30 db) and exceeding 2 db. It varies in intensity according to the state of turbulence in the air along the propagation path. In perfectly calm air the fluctuation is practically nonexistent but becomes quite noticeable in turbulent air. This sort of fading is analogous to the scintillation of the fixed stars or the unsteadiness of the telescopic picture of distant objects occurring especially on warm summer days. The physical explanation for the scintillations is found in the fact that the turbulent motion of the air produces irregular variations in refractive index. The consequent irregular bending of rays passing through such a medium produces a patchy distribution of intensity over the wave front. In the case of stellar scintillations the main change in refractive index is caused by fluctuations in air density, and the significant level of turbulence is at an elevation of several thousand feet. For radio waves fluctuations of water vapor density are the chief cause of the scintillations, and the active region is consequently close to the ground. For typical radio scintillations see Figure 35A.

BLACKOUT

Figure 35C shows a fade in which the signal level is far *below* average and which for this reason is called "blackout." This type is liable to occur when warm, moist air is cooled from below (see the substandard M curve Ib in Figure 20) and is often correlated with fog. The main irregularities in signal strength are again on a time scale of the order of $\frac{1}{4}$ hour; the amplitude of variation is smaller than in the preceding case and rarely exceeds 10 db.

FRONTS AND THUNDERSTORMS

On several occasions marked variations in signal strength have been observed when fronts pass between the transmitter and receiver. The passage of the front itself is marked by very rapid and deep fluctuations, followed by less violent changes on a longer time scale (see Figure 36). It appears that similar effects are likely to occur during thunderstorms.
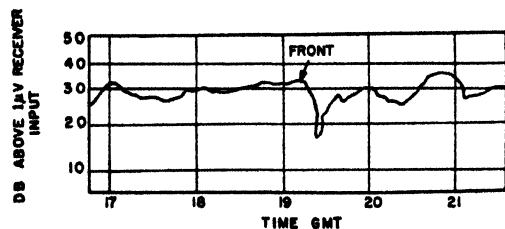
FIGURE 36. Effect of a front on signal strength (Haslemere-Wembley Link, England).

Fog

Some peculiar effects were observed by transmission through fog over an experimental overland radio link in England. The effect of a shallow layer of radiation fog in the early autumn (September-October) was to produce a nearly complete fade-out of signal strength which lasted for hours and rose to normal as the fog cleared. The explanation of this effect is probably the same as in the case of the "blackout" type fades discussed above, indicating that radiation fog produces a substandard M curve. Later in the autumn (November-December) or winter (January) it was found that the effect of fog was quite different. In this season the signal strength was increased and deep fades appeared which are reminiscent of the duct-type fades described earlier.

Fading on Different Wavelengths

Several experiments have been performed in which transmitters working on different wavelengths operate simultaneously over the same path and the received field intensities are recorded on the same chart. Figure 37 shows one such record for the 42.5-mile (optical) path from the Empire State Building, New York City, to Hauppauge, Long Island, for May 14 and 15, 1943, at frequencies of 474 mc and 2,800 mc. It will be noticed that on May 14 up to about 5:45 p.m. the two records show a close agreement. At 6:00 p.m. violent fading sets in on both frequencies, but with great diversity in detail. Not infrequently the signal on one frequency increases while on the other frequency it decreases. About 1:00

a.m. on May 16 the disturbance dies down, and the initial harmony in the two records is restored.

Experiments over the longer (nonoptical) path from the Empire State Building, New York City, to Riverhead, Long Island (range 70.1 miles), showed much greater diversity in the fading patterns for the different frequencies. On the other hand, observations over the British radio link from Guernsey to Chaldon on 60 mc and 37.5 mc (range 85 miles) showed that if there were marked variations on one frequency similar results were likely to be found on the other frequency.

Reliability of Circuits

The reader must be warned that the amount of the fading in the signal strength is not a measure of the performance of radar and communication circuits. These will operate successfully so long as the periods of low signal are relatively short. Neither the scintillations of Figure 35A nor the larger dips of Figure 35B would seriously affect operation, but a prolonged signal such as in Figure 35C would certainly interfere seriously with communication and radar performance.

Some quantitative data are available from the transmission path referred to in the previous paragraph. On the optical path, New York to Hauppauge, the range of signal fluctuations increased rapidly with increasing frequency. On 45 mc the "undisturbed" level (the observational equivalent of standard) was 21 db below free space with an amplitude of fluctuations that very rarely exceeded ±4 db. On the 474-mc circuit the undisturbed level was 3.5 db below
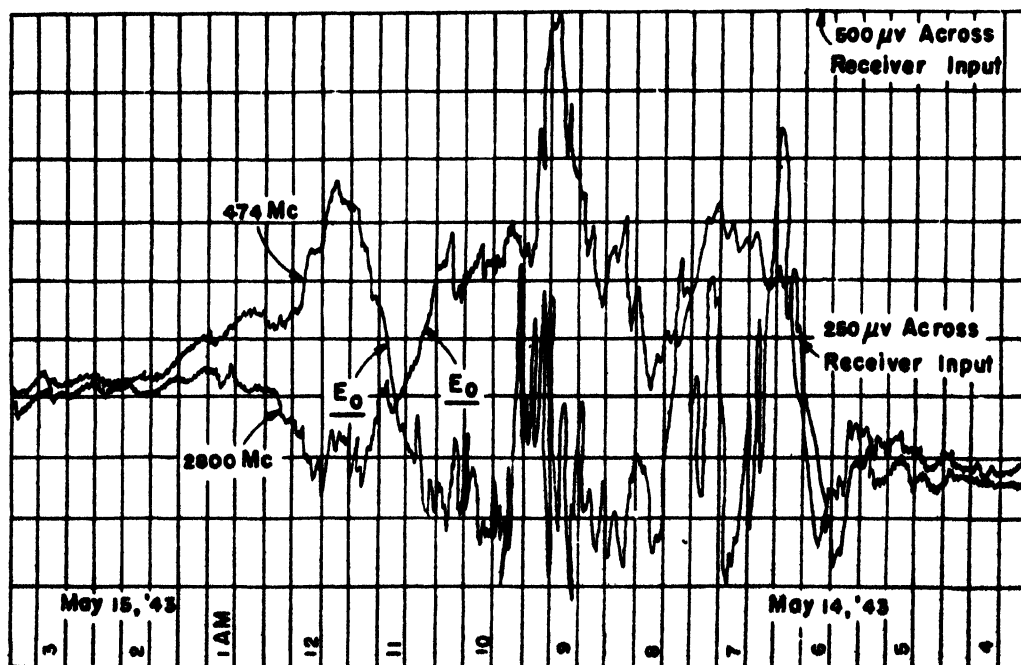
Figure 37. Simultaneous variations of signal strength with frequency. (Empire State Bldg. to Hauppauge, L. I., N. Y.)

free space while the fluctuations varied between 10.5 db above to more than 30 db below free space. The level was 5 db or more below the undisturbed value during 0.01 per cent of the time in January and during 0.4 per cent of the time in July. On the 2,800-mc circuit the undisturbed level was −2 db below free space; the maximum was 12 db above and the minimum more than 25 db below free space. During 0.15 per cent of the time the signal was 5 db or more below the undisturbed level in January; the corresponding figure for July was 3.6 per cent. The conclusion may be drawn from this and similar experiments that over optical paths transmission becomes gradu-

ally less reliable as the frequency is raised.

Over the nonoptical path, New York to Riverhead, the margin of fluctuations was much larger. On the 45-mc circuit the undisturbed value was 35 db below free space, the maximum 18 db below, and the minimum more than 50 db below free space. During 1.6 per cent of the time the signal was 5 db or more below the undisturbed level. On the 474-mc circuit the undisturbed signal was 30 to 35 db below free space, the maximum 10 db above, and the minimum 44 db below free space. During 0.47 per cent of the time the signal was 5 db or more below the undisturbed value. At 2,800 mc the undisturbed signal
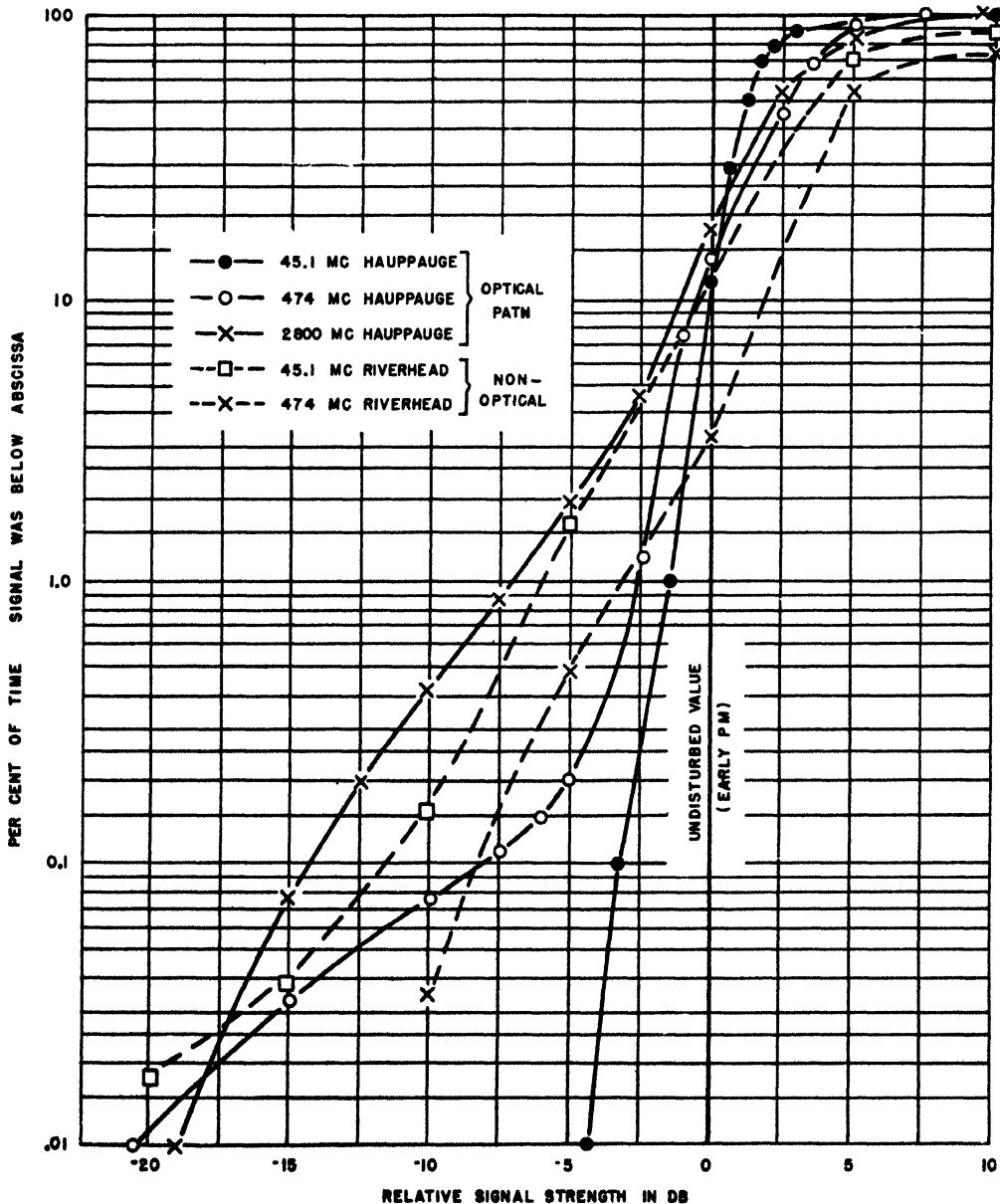
FIGURE 38. Reliability of circuit. Average of July 1943 and January 1944. (Empire State Building to Hauppauge and Riverhead, L. I., N. Y.)

was 50 to 60 db below free space near the limit of sensitivity; the observed maximum was 13 db above free space, and the minimum could not be observed. In this case the effects of superrefraction were quite pronounced. In January the signal was less than 40 db below free space during 6.5 per cent of the time; the corresponding figure for July is as high as 33 per cent.

The reliability of these transmission circuits is shown in Figure 38. Here, both for the optical and nonoptical paths, the percentage of time during which the signal strength was below specified values is plotted for the various frequencies used. The specified values of signal strength, for each frequency and path, are measured relative to the corresponding undisturbed value. The results, which give averages of the performance during July 1943 and January 1944, indicate that the reliability increases appreciably with decreasing frequency.

It must be said that the New York area where these experiments were made is not particularly affected by blackout situations, and the results are probably not typical for locations where blackouts are a frequent occurrence. The general nature of these data is confirmed by results of extensive experiments in England and in Massachusetts Bay.

Scattering and Absorption by Water Drops

As microwave sets have come into general use in recent years the "rain echoes" frequently seen on the scope have attracted attention. The possibility of using microwave radar as an aid to meteorological forecasting and for aerial navigation was early recognized and is now being put to operational use.

At first sight, ground clutter resulting from trapping of radiation in a ground-based duct and rain reflections look somewhat alike on the scope of a radar set. At closer inspection differences appear; the cloud pictures are usually more fuzzy and less sharply defined than the echoes received from ground targets. An experienced operator usually has little difficulty in distinguishing rain echoes from echoes of targets or objects at the ground, but occasional mistakes have been reported, especially from the tropics.

Rain echoes are a result of the scattering of microwaves by the raindrops. Electromagnetic theory shows that the amount of scattering increases very rapidly as the wavelength is decreased. It also increases rapidly with increasing drop diameter. On account of this sharp variation the scattering effects become appreciable only when the wavelength is below a certain maximum value and when the drops exceed a certain critical size. Rain echoes are rarely observed at longer waves than S band, but they are common at S band and become very important at the shorter microwaves.

For a time it was thought that clouds could produce microwave echoes, but more thorough investigations have now established the fact that the droplets in clouds are too small to produce appreciable scattering. Only drops that are large enough to constitute genuine rain are seen by a radar, and, especially at S band, light rains will often escape detection. The term "storm echo," invented at a time when the origin of these echoes was not yet clearly understood, should be avoided, and the terms "rain echo" or "precipitation echo" should be used instead. A rain seen by the radar is not necessarily recorded by an observer at the ground, as the rain may be confined to the free atmosphere and never reach the earth. This occurs either when the rain falls in an ascending stratum of air where the air rises more rapidly than the drops fall or when the raindrops evaporate again before reaching the ground. Both cases occur quite commonly in the atmosphere, especially under convective conditions such as are indicated by cumulus clouds and thunderstorms. Snow may also be seen on microwave scopes provided the snowfall is sufficiently heavy.

While clouds themselves do not produce microwave echoes, they may contain falling rain of one of the forms just indicated. Visual appearances are deceiving, and an imposing looking cumulus cloud might be entirely invisible on the scope, whereas a cloud that is inconspicuous to the eye but contains falling raindrops might give a pronounced echo.

The question of "shadow" cast by a storm echo is of some operational interest. A shadow is formed when the absorption that accompanies scattering by the raindrops becomes so strong that the remaining radiation no longer suffices to produce visible echoes from targets behind the rain area. This effect is pronounced on X band, and even more on K band, and is often quite conspicuous with airborne equipment where it may happen that a rain storm blanks out a sector of the sweep. On S band the absorption is usually much weaker and targets can often be seen behind a rain echo.

The usefulness of rain echoes for aerial navigation, particularly in the tropics, is now so generally known that the subject need not be discussed further.

SNELL'S LAW

The ordinary law of refraction known as Snell's law may be expressed as

$$n_0 \sin \beta_0 = n_1 \sin \beta_1 ,$$

where β_0 and β_1 are the angles which the ray makes with the perpendicular to the boundary. Here it is more convenient to take the angle α between the ray and the boundary surface. Snell's law then reads

$$n_0 \cos \alpha_0 = n_1 \cos \alpha_1 .$$

The refraction at a sharp boundary is shown in
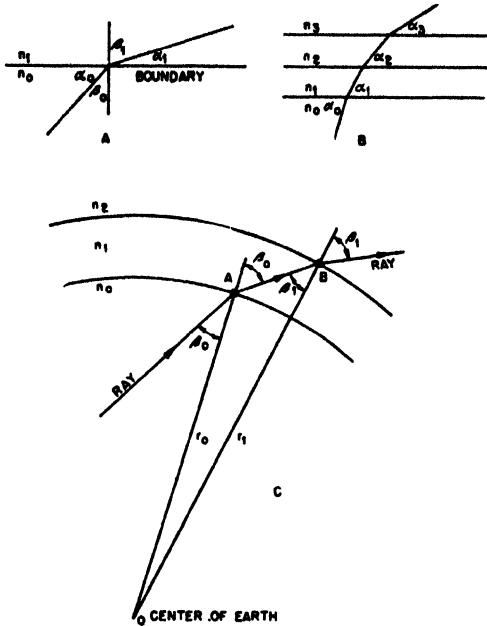
FIGURE 39. Application of Snell's law of refraction.

Figure 39A. If there are several boundaries it is readily seen that Snell's law generalizes (Figure 39B) to

$$n_0 \cos \alpha_0 = n_1 \cos \alpha_1 = n_2 \cos \alpha_2 = \cdots ,$$

and for a continuously variable layer it becomes

$$n \cos \alpha = n_0 \cos \alpha_0 ,$$

where n and α are continuous variables which are functions of the height and the index 0 designates an arbitrary reference level.

Snell's law for a curved earth may be derived from Figure 39C. For successive boundaries it is found:

$$n_0 \sin \beta_0 = n_1 \sin \beta'_0 ,$$
$$n_1 \sin \beta_1 = n_2 \sin \beta'_1 , \text{ etc.}$$

Multiply the first equation by r_0, the second by r_1, etc. Then

$$n_0 r_0 \sin \beta_0 = n_1 r_0 \sin \beta'_0 ,$$
$$n_1 r_1 \sin \beta_1 = n_2 r_1 \sin \beta'_1, \text{ etc.}$$

But from the triangle OAB

$$\frac{\sin \beta'_0}{r_1} = \frac{\sin \beta_1}{r_0} , \text{ etc. ,}$$

so that:

$$n_0 r_0 \sin \beta_0 = n_1 r_1 \sin \beta_1 = n_2 r_2 \sin \beta_2 = \cdots$$

Again introducing the angle α with the horizontal and making the transition to a continuously variable refractive index gives

$$nr \cos \alpha = n_0 r_0 \cos \alpha_0 ,$$

which is the generalization of Snell's law for a curved earth. r_0 may be chosen as any convenient height, say a for the surface of the earth or $a + h_1$ for the height of the transmitter, and n_0 is the corresponding value of n.

THEORETICAL TREATMENT OF NONSTANDARD PROPAGATION IN THE DIFFRACTION ZONE[*]

THE ASSUMPTIONS and restrictions underlying this presentation are:

1. We concern ourselves with problems of the *diffraction region* only: the field is calculated at considerable distance from the transmitter and not too great height above the ground.

2. The plane-earth model is used, in which the effect of curvature is simulated by using the modified index M instead of the index of refraction n.

3. The earth's surface is assumed smooth, and M depends on height only (horizontal stratification).

4. Simplified boundary conditions at the earth's surface are used, appropriate to the treatment of the diffraction zone at microwave frequencies. This results in a formula which refers only to a discrete spectrum of modes and makes the calculations independent of polarization.

5. The directional pattern of the transmitter need not be considered, since only the intensity at the azimuth in question and within 1 degree of the horizontal plane is of importance. The problem solved is that of a vertical dipole, electric or magnetic.

6. The field is described in terms of a single quantity Ψ, the Hertzian vector being $(0,0,\Psi)$. Then, at a point in the diffraction region,

$$\text{actual field strength} = |\Psi|^2 \cdot d^2 \cdot E_0, \quad (1)$$

with d = horizontal distance from source,
E_0 = free space field at distance d.

An expression for Ψ can then be found in the form

$$\Psi(d,z) = e^{i\omega t - i\pi/4} \sqrt{\frac{2\pi}{kd}} \sum_m e^{-\gamma_m d} U_m(h_1) U_m(z), \quad (2)$$

where h_1 = transmitter height;

z = height at which Ψ is calculated;

$$\omega = 2\pi f, \quad k = \frac{2\pi}{\lambda}.$$

γ_m and U_m are characteristic values and functions of the boundary value problem

$$\frac{d^2 U}{dz^2} + [k^2 M^2(z) + \gamma^2] U = 0, \quad (3)$$

where $\begin{cases} U e^{i\omega t} & \text{wave moving upward, } z \to \infty, \quad (4) \\ U(0) = 0. & \quad (5) \end{cases}$

The modified index of refraction M is supposed to be defined without the factor 10^6 usually included

The functions U must be normalized in a suitable

way. If we had not agreed to use simplified boundary conditions, the last equation (5) would be more complicated and would depend on the type of polarization. Also an integral would appear in addition to the discrete sum in the expression for Ψ. The actual value for Ψ, for the diffraction zone and microwave frequencies, would not be affected significantly.

The quantities γ_m are complex:

$$\gamma_m = \alpha_m + i\beta_m. \quad (6)$$

α_m and β_m are positive real quantities. It is convenient to think of the terms of the series as arranged in order of increasing α:

$$\alpha_1 < \alpha_2 < \alpha_3 < \alpha_4 \cdots.$$

These quantities determine the *horizontal attenuations* of the various modes. For large d only one or at most a few terms of the series are required to give the value of Ψ. The quantities β_m are all very nearly equal to k. The slight differences between the β_m's determine the phase relations and hence the interferences between the various modes.

It is convenient to classify the modes into two types: (1) "Gamow" modes which are strongly trapped, so that α is very small; (2) "Eckersley" modes which are incompletely trapped or untrapped. The names "Gamow" and "Eckersley" refer to the men who devised the approximate phase integral methods which apply in the two sorts of cases. For practical purposes, when working within the diffraction region, we need consider only the Gamow modes, or at most the Gamow modes and the first Eckersley mode.

In order to be able to use the formula to calculate Ψ for a given index curve $M(z)$, we must obtain the following information about the modes which are to be used:

1. The characteristic values.

2. "Raw" or unnormalized characteristic functions, which satisfy the differential equation and the boundary conditions but still require multiplication by suitable normalization factors.

3. The normalization factors.

There are three methods of attack on the problem:

1. Numerical integration of the differential equation, accomplished in practice by the use of a differential analyser.

2. Phase integral methods.

3. Use of known functions and tables, for suitably chosen M curves.

---

[*]By W. H. Furry, Radiation Laboratory, MIT.

The method of numerical integration is being used intensively in England by Booker, Hartree, and others. It encounters considerable difficulties in connection with the fitting of the boundary condition at $z \to \infty$ and also in the determination of normalization factors. These difficulties have been overcome by special and fairly elaborate procedures. In this country the feeling has been that we should direct our efforts toward the use of the other methods.

If either method (2) or method (3) is to be readily applied to a variety of cases without a prohibitive amount of labor, the M curves must have a suitable form. The form indicated turns out to be the same in both cases. It consists of portions, each of which is a straight line. If enough such portions are used, any actual M curve can be accurately represented, but it is impractical to use more than a very few. Present efforts are directed toward dealing with cases where there are just two straight-line portions and there is no prospect of going beyond the cases with three (Figure 1).
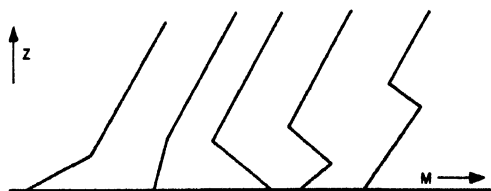
FIGURE 1. Schematic straight-line M curves.

At first sight these curves look overly artificial, but there are considerations which indicate that they are really an altogether reasonable choice. First, some actually occurring curves have very much this sort of appearance. Second, the sharp breaks in the curves have no really strong effect on the results. Third, practical considerations severely limit the number of parameters which can be used in specifying the curve, so that a meticulous reproduction of every actual curve is out of the question. Fourth, the assumption of horizontal stratification is usually not well enough justified to make highly precise results really significant.

The phase integral methods were pushed first, because the calculations are quite easy and do not require special tables of functions. Unfortunately the gaps between the regions of validity of the different phase integral approximations turn out to be extremely wide and to cover just the more interesting ranges of slope and duct height. This makes it necessary to resort to the exact solutions to determine characteristic values and normalization factors. The phase integral methods provide limiting cases which can help in guiding the exact computations. Also the phase integral formulas are usually quite adequate for the computation of the "raw" characteristic functions, once the characteristic values are known.

In order to make the exact calculation, we need tables for *complex arguments* of the solutions of the equation

$$\frac{d^2 U}{dz^2} = - z U \ .$$

These solutions can be expressed in terms of the Airy integrals, but for greater convenience the solutions have been standardized in the form

$$h_j(z) = \left(\frac{2}{3}\right)^{\frac{1}{3}} z^{\frac{1}{2}} H^{(j)}_{\frac{1}{3}}\left(\frac{2}{3} z^{\frac{3}{2}}\right) \quad (j = 1,2) \ .$$

The tabulation of these functions for $|z| \le 6$, on a square mesh 0.1 unit on a side is being done on the automatic sequence-controlled calculating machine at Harvard University. Work was begun in the latter part of August 1944, under authorization from the Bureau of Ships. Photostats of about one-fourth of the tables were obtained by November 1944.

The present objective is to produce charts from which α_1 and β_1 and the normalization factor for the first mode can be obtained for any M curve made up of two straight portions, the upper one being of standard slope. After this, similar charts for the second mode, and perhaps the third and fourth, will be undertaken. When this has been done, the approximate determination of field strengths and coverage will be possible by a definite routine procedure.

CHARACTERISTIC VALUES FOR THE FIRST MODE
FOR THE BILINEAR M CURVE[a]

THE MODEL of an M curve composed of straight-line segments suggested itself to workers at the Radiation Laboratory early in 1944 as one in which phase integral calculations could be carried out very rapidly. At about the same time Lt. Comdr. Menzel suggested the use of this model together with tables of Hankel functions to obtain exact solutions. In the fall of 1944 it became evident that phase integral methods were not of much use with this model. Tables of the required Hankel functions, essentially standard height-gain functions, for complex argument were prepared at the Harvard Computation Laboratory, and considerable effort was directed to the obtaining of exact solutions.

The units, notation, and model are given by the following formulas and illustrated in Figure 1.
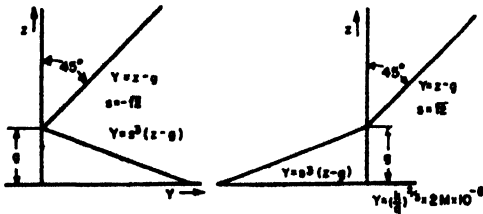
FIGURE 1. Models and units.

$$H = (k^2 q^2)^{-\frac{1}{3}} = \left(\frac{\lambda}{2\pi}\right)^{\frac{2}{3}} \cdot \left(\frac{\frac{2}{3}a}{2}\right)^{\frac{1}{3}}$$

with
$$H \text{ (feet)} = 7.24 \, [\lambda(\text{cm})]^{\frac{2}{3}} ,$$

$$L = 2(kq^2)^{-\frac{1}{3}} = 2\left(\frac{\lambda}{2\pi}\right)^{\frac{2}{3}} \cdot \left(\frac{\frac{2}{3}a}{2}\right)^{\frac{1}{3}}$$

with L(thousand yds) $= 6.69 \, [\lambda(\text{cm})]^{\frac{2}{3}} ,$

$$z = \frac{h}{H} \; ; x = \frac{d}{L} \; ; \frac{d^2 U}{dz^2} + (Y + D) U = 0 .$$

The natural units of height and distance represent two different compromises between wavelength λ and earth radius a, so that $\lambda \div H \div L \div a$ form, very roughly, a geometric progression. It is seen that for microwaves, heights and distances occurring in practice are fairly small numbers of natural units.

The M curves are plotted in terms of the height z in natural units and of a quantity Y which is simply M multiplied by a suitable wavelength dependent factor. The standard part of the curve then has slope unity. In the bilinear model the anomaly consists of a segment with slope s^3 times standard, or, in these diagrams, simply slope s^3. For negative s

[a]By W. H. Furry, Radiation Laboratory, MIT.

there is a duct; s positive but less than 1 gives transitional cases; and s greater than 1 gives substandard cases.

The essential quantity Ψ used in calculating the field is given by:

$$\Psi = (e^{i\omega t - 2\pi i \, d/\lambda - i\pi/4}) \frac{2\sqrt{\pi}}{L} x^{-\frac{1}{2}} \times$$

$$\sum_m e^{-A_m x + iB_m x} U_m(z_1) \, U_m(z_2) .$$

The power density is equal to the free space power density multiplied by $\Psi^2 d^2$. The characteristic values are complex: $D = B + iA$. For the standard case: $D_1 = -1.17 + 2.02i$. (For $\lambda = 10$ cm this corresponds to an attenuation of 1.22 db per thousand yards.) Ψ consists of three factors: one, that for a plane wave, which can ordinarily be omitted; the second, a constant factor which depends on wavelength through L, the natural unit of distance [this factor can be replaced by just $2\sqrt{\pi}$ if $x^2 (= d^2/L^2)$ instead of d^2 is written in the first line]; and finally the critical factor written in terms of natural units only and involving characteristic values and characteristic functions. The imaginary parts of the characteristic values are the coefficients of horizontal attenuation, and the characteristic functions are the height-gain functions.

It is seen that for a typical microwave frequency the horizontal attenuation of the first standard mode ($g = 0$) is rather sizable. The plot of the height-gain curve shows that if both transmitter and receiver are at about 200 ft there is a gain of 50 to 60 db.
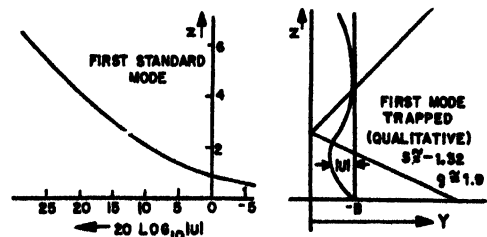
FIGURE 2. First standard and first trapped mode.

In discussing the behavior of U in relation to the Y curve, it is best to plot U or $|U|$ rather than decibels. It is also helpful to draw a vertical line at the abscissa $-B$, and this is then usually used as the axis in plotting U or $|U|$. The diagram for a trapped mode shows that $|U|$ shows exponential decay in the "barrier" region where the Y curve lies
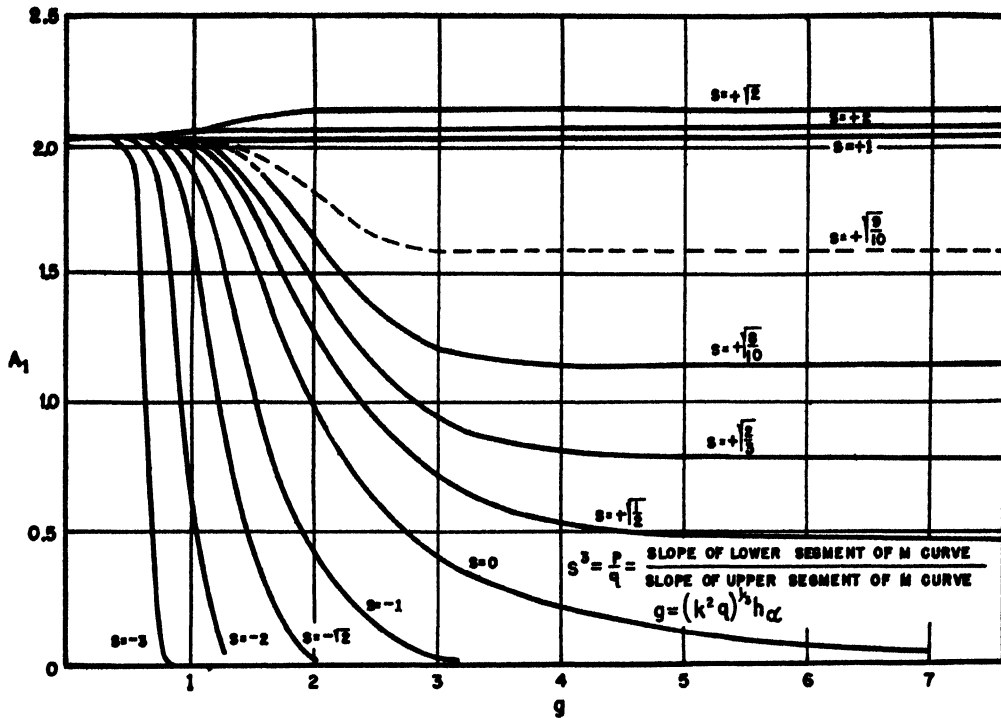
FIGURE 3. Attenuation constant versus anomaly height for bilinear M curve, first mode.

to the left of the line at $-B$. Below the barrier U shows oscillatory behavior, but with no nodes for the first mode; above the barrier U is a spiral, which shows only as a slow increase in the plot of $|U|$.

This same difference in the behavior of U for $Y >$ or $< -B$ is a useful thing to remember in more general cases. Sometimes it is not quite so clear-cut as in this case of trapping. If A is not small, the situation cannot be so completely defined in terms of B alone. It is certain, however, that $|U|$ will
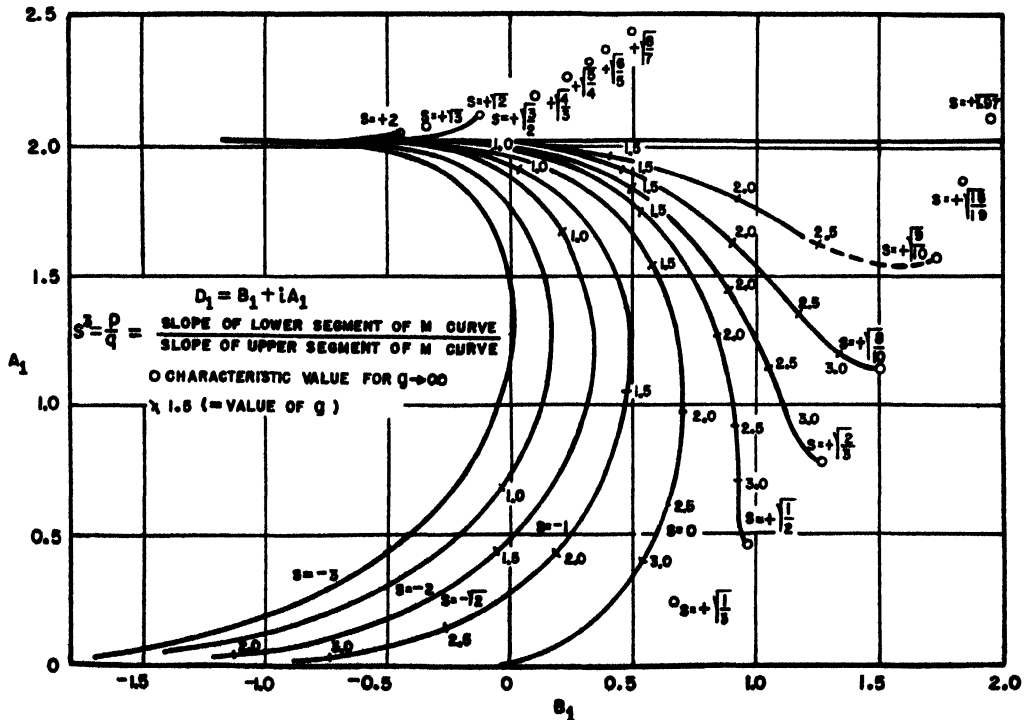
FIGURE 4. Characteristic values for the first mode.

show essentially exponential behavior in any region where the "height of the barrier," i.e., the amount by which the Y curve lies to the left of the line at $-B$, is greater than A.

This sort of general physical consideration about the U curve leads, on being put in more precise mathematical form, to the phase integral methods. Unfortunately, no phase integral method can claim validity for this model except in cases of trapping. In general, the Eckersley phase integral method for untrapped modes requires that the Y curve be an analytic function, and the bilinear curve obviously is not. Most of the values presented are, accordingly, the results of exact calculation.

Figure 3 shows that for negative s the attenuation falls rather suddenly to very small values at a certain value of g and then quickly approaches zero. This indicates the occurrence of trapping. On the other hand, for positive s, the attenuation constant approaches a finite asymptotic value. It is interesting to note that this is always definitely less than the value s^2x standard, which corresponds to a single straight line of slope s^2x standard slope.

It is also useful to know the real part B of the characteristic value. Figure 4 shows the complex D plane. For $g = 0$ the Y curve is just standard, and as g increases the value of D for each value of s traces out a curve; for *small* values of g all these curves practically coincide. For negative s the real part decreases steadily as soon as the imaginary part becomes very small. For positive s, on the other hand, the real part as well as the imaginary approaches a finite limiting value, so that each curve has an end point.

Some of the consequences of this behavior of the real part can be seen by studying Figure 5. The first row of diagrams shows the situation for fixed negative s and increasing value of g. The first diagram shows the standard curve. The next shows a curve with a small superstandard section, but $-B$ still lies in nearly the same location relative to the dotted line which marks where the origin lay for the stand ard curve; thus B has increased. The first figure o
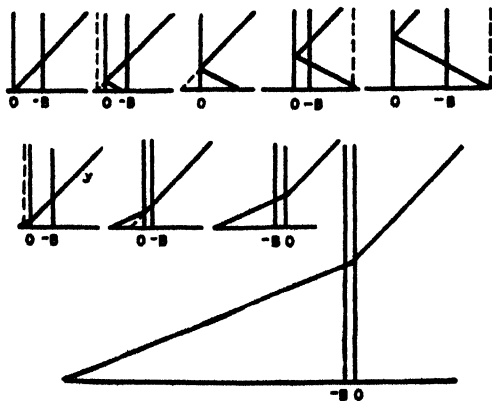
FIGURE 5. Curves for negative and positive s.

the second line shows how the same thing happens for a small substandard section. Thus for small g the first order effect is just to add the amount g to D, for all values of s.

In the third diagram of the first row we have a case in which the superstandard has a pronounced effect, but trapping has not yet set in. In such intermediate cases B may become positive, but the diagram shows a case in which it happens to be zero. In the fourth diagram trapping is definitely established; B has become negative, and the line $-B$ has taken on a definite position relative to $Y(0)$ (dotted line). This same relation is maintained for larger values of g, as in the last diagram of the top row. In the last diagram the "barrier" has become much more formidable. This means that the value of U just above the barrier is extremely small, and thus the attenuation is very small because of the small leakage.

In the second row, as has been remarked, the first diagram shows a small substandard section which has only a small perturbing effect; $-B$ lies essentially at the standard distance from the intercept of the extrapolated standard curve. The second shows an intermediate case. In the third diagram the limiting value of D has been reached, and the line at $-B$ has taken its final position relative to the joint of the Y curve. In the last, larger, diagram g has become much larger, but $-B$ has still the same position relative to the joint.

The difference between the last two diagrams is essentially the increase in the strength of the *surface barrier*. The structure of the height-gain curves near and above the joint is practically the same in the two cases. The very thick barrier in the last case causes the intensity near the earth's surface to be extremely small. This particular kind of height-gain effect can be more suggestively referred to as *depth loss*. The amount of this depth loss is very large: the first 200 ft of the substandard layer produces a loss in the product $U(z_1)U(z_2)$ of at least 200 db (at 10 cm), which is about four times the gain for a similar height in the standard case. Moreover, this loss proceeds at a rapidly accelerating rate, whereas standard height gain goes at a decreasing rate. The same situation of depth loss in thick nonstandard layers occurs in transitional cases, with s positive but less than unity.

In general the results for the first mode for positive s can be summarized as follows:

In nonstandard layers of fairly small thickness, less than 100 ft for 10-cm waves, the propagation is not markedly different from standard for the substandard case and can have attenuation strikingly less than standard for suitable thickness of a transitional layer.

For thick layers there is a strong depth-loss effect in the first mode in both sorts of cases, and the first mode cannot be expected to be the dominant term

in Ψ except at great distances. Some other mode, which does not suffer from the depth-loss effect, although it may have greater attenuation, will be the important mode at smaller distances.

The conclusions for positive s cannot be expected to apply unless the lower part of the M curve is really sensibly straight over a considerable part of its length. For negative s (trapping) this requirement is not so important.

It was mentioned that other models had been employed by various investigators in calculating field strength in the presence of a duct. The British used an index distribution given essentially by $Y = (z - z^m/m)$, where m lies between zero and unity. When $m = \frac{1}{2}$ the problem could be treated by a phase integral method, which Booker had done. The differential analyzers at Manchester and Cambridge had been used to obtain the characteristic values for other values of m. The linear variation of index had been studied by Hartree and Pearcey. In this case of linear exponential variation $Y = z + Ae^{-Bz}$, where A and B are adjustable parameters. This model offers the advantage that the index is an analytic function of z and also that the modification term approaches zero with increasing height.

An alternative method (Langer's) for joining the two parts of an otherwise bilinear M profile was brought up. This method gives a solution in terms of Bessel functions and solves the difficulty perfectly for joining two straight lines.

It was inquired whether, in case of positive s it had been ascertained that for large g there were no roots of the secular equation corresponding to a linear M curve having the slope of the lower segment. There was the possibility that the root found might be one of a possible pair and that there might be another solution of the wave equation for positive s which had not yet been discovered.

The author replied that the roots varied continuously as g varied and that the investigation had dealt with the root obtained when starting with the first standard value for $g = 0$. What happened with increasing g when the start was made from some other standard value of $g = 0$ was not known definitely, but the effects were believed to be peculiar. It is expected that there may be some values lying fairly near the s squared value for the imaginary part. They are not considered to lie close to the s squared value for the real part, as they would for the simple assumption previously mentioned—that when the joint is very high the upper segment can be forgotten and the curve can be assumed to be a single line all the way. This is believed incorrect, because when the result is derived by taking only the first terms in the asymptotic expansions, computing a small correction from the next terms in the asymptotic expansions produces terms which are infinite compared to the first terms. This means that the value s squared times D is an impossible one.

It may well be that there are results with s squared times A plus some different value of B rather than simply s squared times B, but these have not been investigated. This does not occur for the first mode, which is all that this report covers, but it may happen that some other mode goes over to that value. Any mode which does so would probably not suffer from depth-loss effect and would be the important mode close in when there was a thick layer with positive slope.

The need was pointed out for stressing the difference between "completely trapped" modes and "leaky" modes. With completely trapped modes the field decreases exponentially with height, and the power carried by each mode is finite, but with leaky modes the field increases exponentially with height, and the power carried by each mode is infinite. This means that completely trapped modes may exist separately, but leaky modes may not. The expansions of fields in terms of leaky modes are thus essentially mathematical and from physical considerations it is no longer possible to anticipate that these expansions would be convergent; the question of convergence has to be settled formally. The reactions of trapped and leaky modes to small perturbations are quite different. The former are relatively insensitive and the latter are very sensitive. In considering the field at a certain distance from the transmitter, it must be ascertained whether the relevant modes are affected by changes in the dielectric constant at heights large compared with this distance; if this is the case particular care must be taken in proving the sum to be still the same, since even a perfectly reflecting layer at such great heights can have little effect on the field in the region of interest.

It was noted that these remarks pertained to a phenomenon which had greatly puzzled the investigators for several months. The trouble occasioned by the concept that infinite energy is carried by a mode does exist. This means that the formula in terms of modes is valid only if all those modes are summed that make any appreciable contribution. It becomes extremely difficult to carry out the summation when there are numerous modes, as they begin to cancel each other more and more with progress into that region. This occurs in leaving the diffraction region to which this work is meant to apply and in approaching the optical region. The question of what a small departure from the shape of the curve at great heights does is something which was very troublesome during studies made of the first mode There is no doubt that a small departure from a smooth shape of the M curve has an enormous effect on the results if it occurs at a great height. If the departure is located high enough it need not amount to more than a millionth of an M unit to spoil the calculation completely. That is because it is a reflecting layer similar to the Heaviside layer,

and if placed high enough it not only can reflect to enormous distances but also becomes extremely effective. It was decided not to give this effect too much concern as all these calculations are made on the basis of horizontal stratification. Doubtless all sorts of small departures from a smooth curve occur at various rather large heights, but they do not occur perfectly stratified over areas of hundreds of square miles, and only such perfectly stratified departures could cause embarrassing results. Accordingly it was decided that such fluctuations as occur probably cause fading or fluctuation but do not cause the particularly troublesome effect mentioned, because they are local and not stratified over large areas.

INCIPIENT LEAKAGE IN A SURFACE DUCT

CALCULATIONS FOR THE FIRST MODE OF THE BILINEAR MODEL

A RECENT INTERCHANGE of ideas on problems of mutual interest with members of the wave propagation group of the Radiation Laboratory prompted the author to investigate the variation of the attenuation constant (or space decrement) $\alpha(h)$ of the first mode with the duct height h and negative index gradient a of a surface duct (see Figure 1).
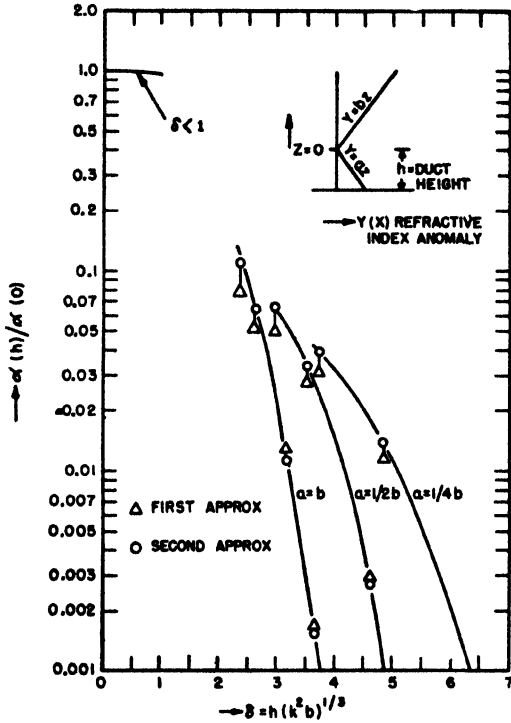
FIGURE 1. Variation of the attenuation constant with duct height.

The attenuation constant is defined as the constant α which occurs in the factor as: $(1/\sqrt{d})\,e^{-\alpha d}$, giving the variation of the amplitude with range d.

The results are shown in Figure 1. In this figure the attenuation constant $\alpha(h)$ is expressed in terms of the attenuation constant for zero duct height $\alpha(0)$. In Figure 1 the curve for $\delta < 1$ was computed from a formula developed by Freehafer and Furry of the Radiation Laboratory:

$$\frac{\alpha(h)}{\alpha(0)} = 1 - \left(1 + \frac{a}{b}\right)\frac{\delta^6}{90}$$

$$- \left(1 + \frac{a}{b}\right)\frac{\delta^6}{1,260} - \cdots \quad (1)$$

where $\delta = h(k^2 b)$

Here $h \doteq$ duct height;
$a = -dM/dz$ inside the duct;
$b = dM/dz$ above the duct;
$k = 2\pi/\lambda$.

It was felt that this equation could be used up to δ equal to about 1.3 but not beyond this value.

The curves on the right for $\delta > 2$, for which a condition of nearly complete trapping is approached, were obtained as follows. The secular equation for the proper value of $\Lambda(\alpha \sim I_m\Lambda)$, is

$$\frac{H_{\frac{1}{3}}^{(2)}(p)}{H_{\frac{1}{3}}^{(1)}(p)} - \frac{H_{\frac{1}{3}}^{(2)}(s)H_{-\frac{1}{3}}^{(2)}(q) + H_{-\frac{1}{3}}^{(2)}(s)H_{\frac{1}{3}}^{(2)}(q)}{H_{\frac{1}{3}}^{(2)}(s)H_{-\frac{1}{3}}^{(1)}(q) + H_{-\frac{1}{3}}^{(2)}(s)H_{\frac{1}{3}}^{(1)}(q)} = 0, \quad (2)$$

where

$$q = \frac{2k}{3a}\Lambda^{\frac{3}{2}},\; p = \frac{2k}{3a}(\Lambda + ah)^{\frac{3}{2}},\; s = \gamma q,\; \gamma = \frac{a}{b} \quad (3)$$

is transformed by the substitution

$$q = e^{i3\pi/2}\,x,\; p = (x^{\frac{3}{2}} + \beta)^{\frac{3}{2}}.\; \beta = ah\left(\frac{2k}{3a}\right)^{\frac{3}{2}} \quad (4)$$

into $\qquad f(p) - F(x) = 0, \quad (5)$

with

$$f(p) = \frac{H_{\frac{1}{3}}^{(2)}(p)}{H_{\frac{1}{3}}^{(1)}(p)}$$

$$F(x) = \frac{U(\gamma x)\,V(x) + V(\gamma x)\,U(x)}{e^{i\pi/3}\,V(\gamma x)\,\overline{U}(x) - U(\gamma x)\,\overline{V}(x)} \quad (6)$$

$$U(x) = I_{\frac{1}{3}}(x) + e^{-i\pi/3}I_{-\frac{1}{3}}(x),$$

$$V(x) = I_{\frac{1}{3}}(x) + e^{i\pi/3}I_{-\frac{1}{3}}(x). \quad (7)$$

Assume now that

$$p = p_0 + \Delta, \quad (8)$$

where p_0 is a constant, which is to be chosen in such a manner that Δ is small in comparison to p_0 in the region under consideration. Expanding equation (5) in a power series in Δ, one obtains as a first approximation for Δ:

$$\Delta_1 = \frac{F(x_0) - f(p_0)}{f(p_0)}, \quad (9)$$

and for a second approximation

$$\Delta_2 = \Delta_1\left[1 - \frac{\Delta_1}{2}\frac{f(p_0)}{f(p_0)} + \frac{F(x_0)\frac{dx}{dp}}{f(p_0)}\right] \quad (10)$$

These expressions can be computed with the aid of the WPA Tables (unpublished) for the I functions with *real* argument. The curves in Figure 1 were computed down to values of δ such that Δ_2 did not deviate appreciably from Δ_1.

Conclusion. From the computed attenuation for a surface duct it appears that, for the first mode, when $\delta (= hk^{\frac{1}{3}}b^{\frac{1}{3}})$ is less than 1, trapping is less than 2 per cent and that when $\delta = 3$ to 5 (depending on the negative gradient a), trapping is 98 per cent complete. There is therefore a rather narrow range of values of the parameter δ (1 to 4) within which a rapid transition takes place from a condition of negligible trapping to a condition of nearly complete trapping. This result may have a bearing on the observed fading which is associated with ducts.

CALCULATIONS FOR THE SECOND AND HIGHER MODES OF THE BILINEAR MODEL

Computations of characteristic values and height-gain functions for the second and higher modes of a bilinear model M curve was carried on by the Analysis Section of Columbia University Wave Prop-

agation Group. The first mode of the bilinear model was treated at the Radiation Laboratory MIT. The computations were carried out with the aid of tables of h functions prepared by the Harvard Computation Laboratory, under the direction of Furry. The work discussed here is mainly on surface ducts in which the slope of the low segment of the M curve is negative. Cases with positive slopes of the low segment of the M curve have been tried but were found to involve functions which are beyond the range of existing tables.
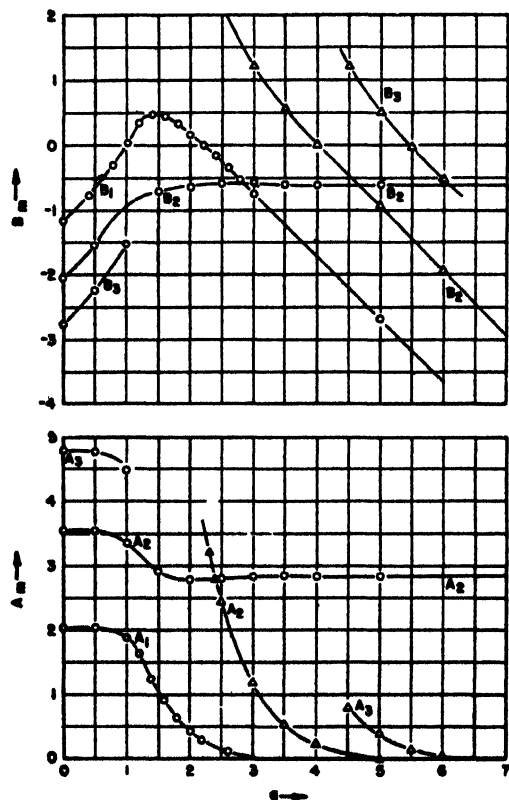
Some results on the characteristic values are shown in Figures 2 and 3 (for a definition of natural units see preceding articles). In Figure 2 the slope of the lower segment of the M curve is the negative of the standard slope, while in Figure 3 the ratio of the slope of the lower segment to the standard slope is $-\sqrt{8}$. The curves A_1 and B_1 for the first mode were computed at the Radiation Laboratory. An imaginary part A_1, which is proportional to the horizontal attenuation (decrement), starts at $g = 0$ with a value appropriate for a standard atmosphere and decreases continuously as duct height g increases. Beyond $g = 3$ the first mode is completely trapped. The curve A_2 for the second mode decreases initially too but beyond $g = 2$ is seen to level off to a constant limiting value. The real part of the characteristic value B_2 also approaches a constant limiting value for g greater than 3. These curves were obtained by solving the secular equation for D and also determining the slope dD/dg at each point. The characteristic values curves can also be computed by starting first with Gamow's values appropriate for large g and continuing backwards toward smaller values of g, being careful to determine the slope of the curves at each point. It is seen from Figures 2

FIGURE 2. Characteristic values of D_m for a bilinear model. $s = -1$. $D_m = B_m + i A_m$. $s^1 =$ ratio of slope of lower segment to standard slope $= s^1$. $g =$ height of joint in natural units.
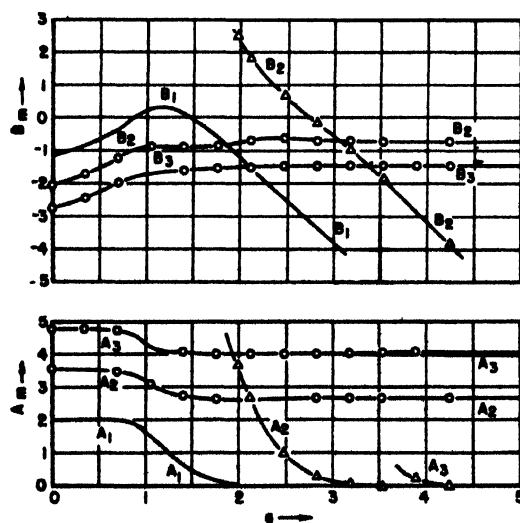
FIGURE 3. Characteristic values D_m for a bilinear M curve. $s = -\sqrt{2}$. $g =$ height of joint in natural units. $s^1 =$ ratio of slope of lower segment of M curve to the standard slope. $D_m = B_m + i A_m$.

and 3 that, in contrast to the first mode, these branches of the curves for the second and third modes do not join on smoothly to the other branches which start with standard values- at $g = 0$ and approach limiting values for large g

This duplicity of the solutions, which was doubted at first, was substantiated in two ways. The values of A_2 and B_2 at $g = 3$ and $g = 5$ in Figure 1 were computed at both branches with increasing accuracy (up to 10^{-5}), and it was found that the matching of the solutions at the duct height and the degree of vanishing of the height-gain function of the ground improved correspondingly in both branches. This proves that both solutions satisfy the boundary conditions. As a second step in testing the reality of the limiting points, an asymptotic expression was derived for the limiting values, and the values computed therefrom were found to be in fair agreement with the exact values, as is shown in Table 1.

The physical nature of the duplicity of solutions seems to be as follows. The solutions approaching a limiting characteristic value for large duct height g correspond to the case where the ground sinks to great depths; the other solution corresponds, of course, to the limiting case when the height of joint rises to infinity.

The relative importance of the two types of solution will depend on the ranges and heights considered. At sufficiently great ranges the solutions with the smaller value of A_m will predominate, but the greater
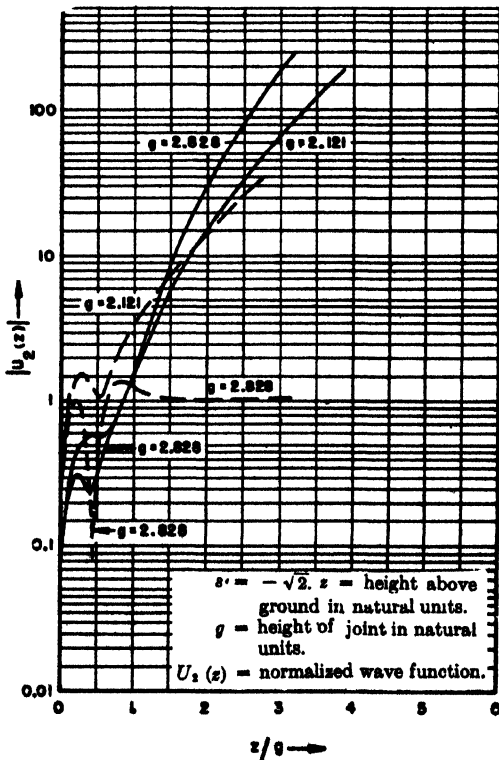
FIGURE 4. Height-gain functions of the second mode for a bilinear M curve.
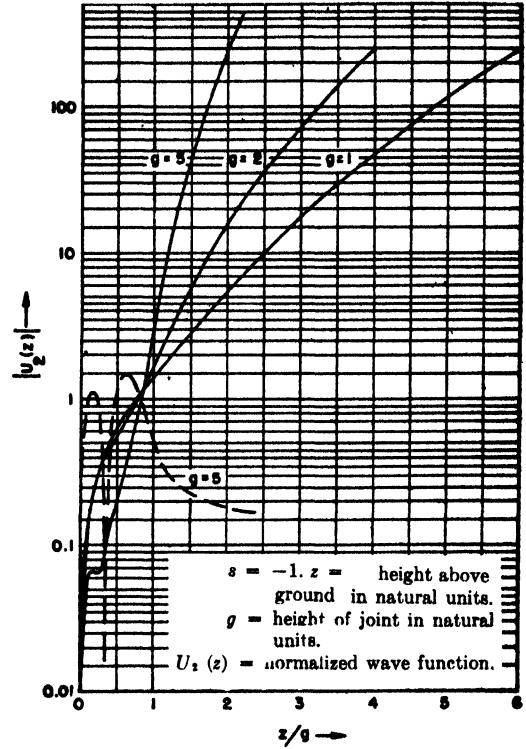
FIGURE 5. Height-gain functions of the second mode for a bilinear M curve.

the height considered the farther must one recede from the source before the initial advantage of the limiting solution due to a greater height gain is overcome by the stronger horizontal attenuation. The greater height gain of the limiting solutions at high elevations is illustrated in Figures 4 and 5. In these figures, the height-gain functions for the limiting solutions are drawn in solid lines, those for the Gamow solutions in dashed lines; and the unit of height is the duct height. It should also be pointed out that the normalization condition applied was

$$\int U_m^2(z)dz = g , \qquad (13)$$

so that, if a comparison of height-gain functions of solutions of the same class for different values of g is desired, the plotted values should be divided by $\sqrt{g}$.

TABLE 1. Comparison of exact limiting values of D with values obtained from the asymptotic formula.*

s	Second mode	Third mode	
-1	$-0.60 + 2.80i$	$-1.06 + 3.60i$	Asymptotic
	$-0.59 + 2.83i$		Exact
$-\sqrt{2}$	$-0.78 + 2.74i$	$-1.22 + 3.40i$	Asymptotic
	$-0.70 + 2.70i$	$-1.42 + 4.08i$	Exact
-2	$-1.00 + 2.60i$	$-1.36 + 3.48i$	Asymptotic
	$-0.80 + 2.44i$		Exact

$$*\exp\left(-\frac{i4}{3}D^{\frac{3}{2}}\right) - \left(1 - s^2\right)/8D^{\frac{1}{2}} = 0 .$$

Chapter 17

THE SOLUTION OF THE PROPAGATION EQUATION IN TERMS OF HANKEL FUNCTIONS[*]

THE CALCULATION of the field strength in the atmosphere depends upon finding a solution of a wave equation incorporating the propagation properties of the atmosphere and satisfying the boundary conditions at the surface of the earth and for large heights. This chapter shows how the wave equation, for certain specified conditions, may be solved in terms of Hankel functions.

Let z = height of receiver above earth's surface,

h_t = height of transmitter,

d = great circle distance between source and receiver,

λ = wavelength, $k = 2\pi/\lambda$,

f = frequency, $\omega = 2\pi f$,

M = modified index of refraction,

a = radius of the earth

Under the simplifying assumptions of horizontal stratification, slight variation of refractive index in a wavelength, smooth earth's surface, the plane earth representation, and the use of the simplified boundary condition $\Psi = 0$ for $z = 0$, which eliminates the polarization of the source, the field of a (dipole) source is described by a scalar wave equation:

$$\Delta^2 \Psi + k^2 M^2 \Psi = 0 , \qquad (1)$$

plus appropriate boundary conditions. Separation of equation (1) in cylindrical coordinates leads to the formal expansion for the field of a dipole source:

$$\Psi = e^{i\omega t} \sum_{n=1}^{\infty} - i\pi H_0^{(2)}(kd \cos \alpha_n) U_n(z) U_n(h_t) , \quad (2)$$

where Re $(\cos \alpha_n) > 0$

Here the characteristic values $\sin^2 \alpha_n$ and the (normalized) characteristic functions $U_n(z)$ satisfy the equation

$$\frac{d^2 U}{dz^2} + k^2 [\sin^2 \alpha + M^2] U = 0 , \qquad (3)$$

plus the boundary and normalization conditions:

$$U(0) = 0 \qquad (3a)$$

$e^{i\omega t} U(z)$ represents an outgoing wave for large positive z . $\qquad (3b)$

$$\lim_{(h) \to 0} \int_0^\infty U^2 dz = 1 . \qquad (3c)$$

Usually $\sin^2 \alpha$ is small, kd is large, and one has

$$\left| H_0^{(2)}(kd \cos \alpha_n) \right|$$

$$\cong \left| \left(\frac{2}{\pi kd \cos \alpha_n} \right) \right|^{\frac{1}{2}} \left| e^{-i(kd \cos \alpha_n)} \right|$$

$$\cong \left| \frac{2}{dk\pi \cos \alpha_n} \right|^{\frac{1}{2}} \left| e^{-ikd(1 - (1/2) \sin^2 \alpha_n)} \right| \qquad (4)$$

The exponential decay factor of the horizontal waves thus has the form $\exp \left[(- kd/2) I_m (\sin^2 \alpha_n) \right]$, and the $\sin^2 \alpha_n$ values evidently lie in the upper half of the complex plane.

The problem is then to find the characteristic values and characteristic functions of the system (3) for a given dependence of modified index of refraction upon height. For a ground-based duct of height h with an M curve made up of two line segments, the upper having standard slope, equation (3) becomes

$$\frac{d^2 U}{dz^2} + k^2 [\Lambda + y(z)] U = 0 , \qquad (3')$$

where $\qquad y(z) = 2a_1(z - h) , 0 \le z \le h ,$

$$y(z) = 2a_2(z - h) , z \ge h ,$$

$$\Lambda = \sin^2 \alpha + 2a_2 h ,$$

$$a_2 = \frac{1}{\frac{2}{3}a} .$$

The linear change of variable

$$x_1 = \left(\frac{k}{2} a_1 \right)^{\frac{1}{3}} [\Lambda + 2a_1(z - h)]$$

inside the duct, and

$$x_2 = \left(\frac{k}{2} a \right)^{\frac{1}{3}} [\Lambda + 2a_2(z - h)]$$

above the duct reduces equation (3') to

$$\frac{d^2 U}{dx^2} + xU = 0 , \qquad (3'')$$

whose general solution is

$$U = \begin{cases} A_1 h_1(x_1) + B_1 h_2(x_1) \\ A_2 h_1(x_2) + B_2 h_2(x_2) . \end{cases}$$

The "h_j" functions are expressible in terms of Hankel functions of order $\frac{1}{3}$:

$$h_j(x) = \left(\frac{2}{3} \right)^{\frac{1}{3}} x^{\frac{1}{2}} H_{\frac{1}{3}}^{(j)} \left(\frac{2}{3} x_{\frac{3}{2}} \right) \quad (j = 1,2) . \qquad (5)$$

Condition (3b) is satisfied by setting $A_2 = 0$. A_1 and B_1 are determined by the requirement of continuity of U and dU/dz at $z = h$.

$$A_1 = \frac{i\pi(\frac{2}{3})^{\frac{1}{3}}}{4} B_2 \left\{ h_2 \left[\left(\frac{k}{2a_2} \right)^{\frac{1}{3}} \Lambda \right] h_2' \left[\left(\frac{k}{2a_1} \right)^{\frac{1}{3}} \Lambda \right] \right.$$

$$\left. \left(\frac{a_2}{a_1} \right)^{\frac{1}{3}} h_2' \left[\left(\frac{k}{2a_2} \right)^{\frac{1}{3}} \Lambda \right] h_2 \left[\left(\frac{k}{2a_1} \right)^{\frac{1}{3}} \Lambda \right] \right\} \qquad (6)$$

$$B_1 = \frac{i\pi(\frac{2}{3})^{\frac{1}{3}}}{4} B_2 \left\{ \left(\frac{a_2}{a_1} \right)^{\frac{1}{3}} h_2' \left[\left(\frac{k}{2a_2} \right)^{\frac{1}{3}} \Lambda \right] h_1 \left[\left(\frac{k}{2a_1} \right)^{\frac{1}{3}} \Lambda \right] \right.$$

$$\left. h_2 \left[\left(\frac{k}{2a_2} \right)^{\frac{1}{3}} \Lambda \right] h_1' \left[\left(\frac{k}{2a_1} \right)^{\frac{1}{3}} \Lambda \right] \right\}$$

176

The characteristic values Λ then appear as the roots of the equation

$$U(0) = A_1 h_1 \left[\left(\frac{k}{2a_1} \right)^{\frac{1}{3}} (\Lambda - 2a_1 h) \right]$$
$$+ B_1 h_2 \left[\left(\frac{k}{2a_1} \right)^{\frac{1}{3}} (\Lambda - 2a_1 h) \right] = 0 . \quad (7)$$

The constant factor B_2 appearing throughout is determined by the normalization condition (3c), which takes a peculiarly simple form in this case, since (3″) implies the identity

$$U^2 = \frac{d}{dx} \left[xU^2 + \left(\frac{dU}{dx} \right)^2 \right] \quad (8)$$

Owing to the present lack of adequate tables of the $H_1^{(j)}$ or h_j functions for *complex* arguments and the complicated nature of equation (7), one is forced to employ asymptotic expansions to determine the Λ's so far as possible. Due care must be exercised in dealing with the branches of the multiple-valued approximations appearing, as well as with the so-called "Stokes phenomenon." Thus in deciding between the two rival asymptotic approximations

$$H_1^{(2)}(W) \cong \left(\frac{2}{\pi W} \right)^{\frac{1}{2}} e^{-i(W - 5\pi/12)} , \quad (9)$$
$$H_1^{(2)}(W) \cong \left(\frac{2}{\pi W} \right)^{\frac{1}{2}} [e^{-i(W - 5\pi/12)} + e^{i(W + 11\pi/12)}] ,$$

both formally valid in the common domain $0 < \arg W < \pi$, one employs the first when $\arg W < \pi/2$, and the second when $\arg W > \pi/2$. The ambiguity on a "Stokes line" ($\arg W = \pi/2$) apparently must be resolved by taking the mean of the two expressions when their difference is important, as it is when strongly trapped modes exist ($a_1 < 0$).

The nature of the results is shown in the important case of complete inversion ($a_1 < 0$). For simplicity

$$\rho = - \frac{\Lambda}{2a_1 h} , \quad \sigma = \left(\frac{k}{-3a_1} \right) (-2a_1 h)^{\frac{1}{2}} . \quad (10)$$

Then

$$\text{I} \quad (\rho + 1)^{\frac{1}{2}} - \left(1 - \frac{a_1}{a_2} \right)^{\frac{1}{2}} \rho^{\frac{1}{2}} = \frac{(n - \frac{1}{4})}{\sigma}$$
$$\left[\arg (\rho + 1) > \frac{\pi}{3} \right]$$

$$\text{II} \quad 1 + ie^{-2i\sigma(\rho + 1)^{\frac{1}{2}}} + e^{-2i\sigma(1 - \frac{a_1}{a_2}) \rho^{\frac{1}{2}}} = 0 , \quad (11)$$
$$\left(\frac{\pi}{3} < \arg \rho < \pi - \delta \right)$$

$$\text{III} \quad 1 + ie^{-2i\sigma(\rho + 1)^{\frac{1}{2}}} + \frac{1}{2} e^{-2i\sigma(1 - \frac{a_1}{a_2}) \rho^{\frac{1}{2}}} = 0 ,$$
$$(\arg \rho \cong \pi)$$
$$(n \text{ a positive integer})$$

The corresponding regions of validity are indicated in Figure 1, which also shows the dependence of one characteristic value on σ for a particular ratio a_2/a_1. If one numbers the characteristic values ρ_n in order of increasing imaginary part, those for which n is greater than some integer are defined by equation I. There is an infinite number of these "Eckersley"
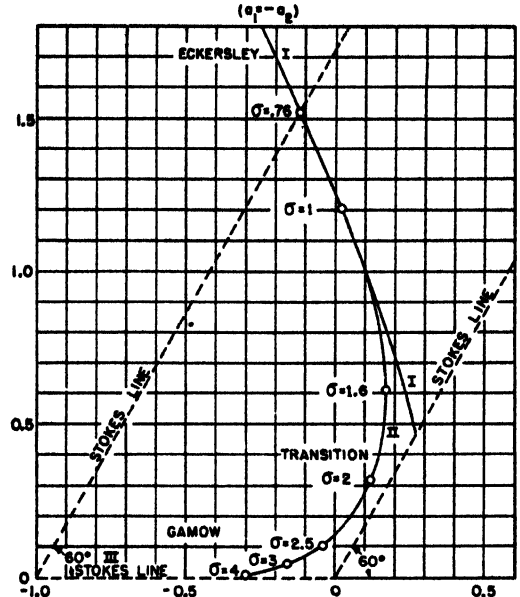
FIGURE 1. Diagram showing the locus of ρ in the complex plane of σ varies.

or leaky" modes. Equation II joins on smoothly to I and defines a finite number of "transitional" or "semileaky" modes.

Equation III defines the strongly trapped or Gamow modes for which $0 < I_m(\rho) \ll - \text{Re}(\rho) < 1$. In this case the characteristic values lie almost upon a Stokes line ($\arg \rho = \pi - \delta$). The approximations valid above the line yield II; the ones valid below yield

$$\text{IV} \quad 1 + ie^{-2i\sigma(\rho + 1)^{\frac{1}{2}}} = 0 , \text{ or}$$
$$(\rho + 1)^{\frac{1}{2}} = (n - \frac{1}{4}) \frac{\pi}{\sigma} < 1 \quad (n = 0,1,2 \cdots).$$

Thus in the Gamow case IV makes $I_m(\rho) = 0$ while II yields almost the same real part, but a very small positive imaginary part for ρ. The mean approximations effectively yield III whose roots are essentially the mean of the roots of II and IV. This averaging process checks closely with an exact calculation based on the (unpublished) WPA tables of Bessel functions of order $\frac{1}{3}$ for real and pure imaginary arguments. It is to be noted also that IV determines the number of strongly trapped modes as the largest integer n such that $(n - \frac{1}{4}) \pi/\sigma < 1$.

The characteristic value problem may be regarded as essentially solved in the cases of leaky modes (I) and strongly trapped modes (III). In doubt still is the question of the transition between III and II; this uncertainty plus the fact that actual determination of the roots of II is much more complicated than in the other cases, and that in case II the arguments of certain of the Hankel functions lie so close to the origin as to make doubtful the validity of the asymptotic procedure—all these considerations indicate that resolution of the transitional mode question awaits appearance of adequate tables of the Hankel functions for complex arguments.

Chapter 18

ATTENUATION DIAGRAMS FOR SURFACE DUCTS[*]

THE HORIZONTAL ATTENUATION (decibels per unit distance) of a signal under assumed propagation conditions not only is of intrinsic interest but is one of the simplest quantities to verify experimentally. In terms of the wave equation formulation this attenuation is proportional to the imaginary part of the characteristic value associated with the mode dominant in the region of space in question. No one mode may necessarily be dominant, and in certain regions a weakly attenuated mode may be outweighed by a mode more strongly attenuated but with a

stronger initial excitation. Well inside the shadow zone, however, the "first" or least attenuated mode
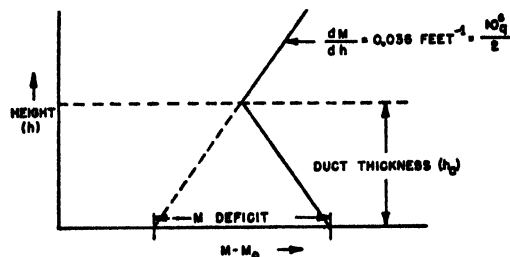
FIGURE 1. M-curve model.
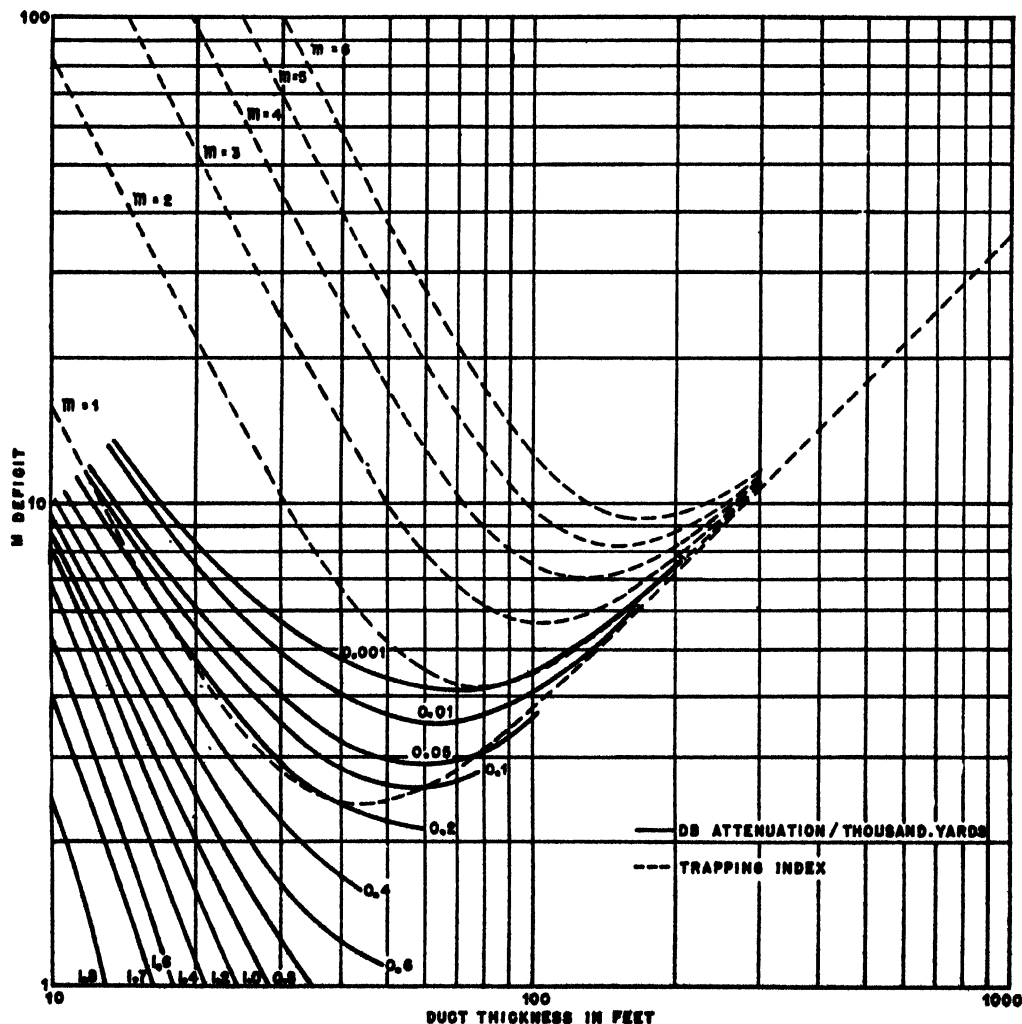
FIGURE 2. Horizontal attenuation of first mode and trapping index, 10,000 mc, standard attenuation (0 M deficit): 1.83 db per 1,000 yd.
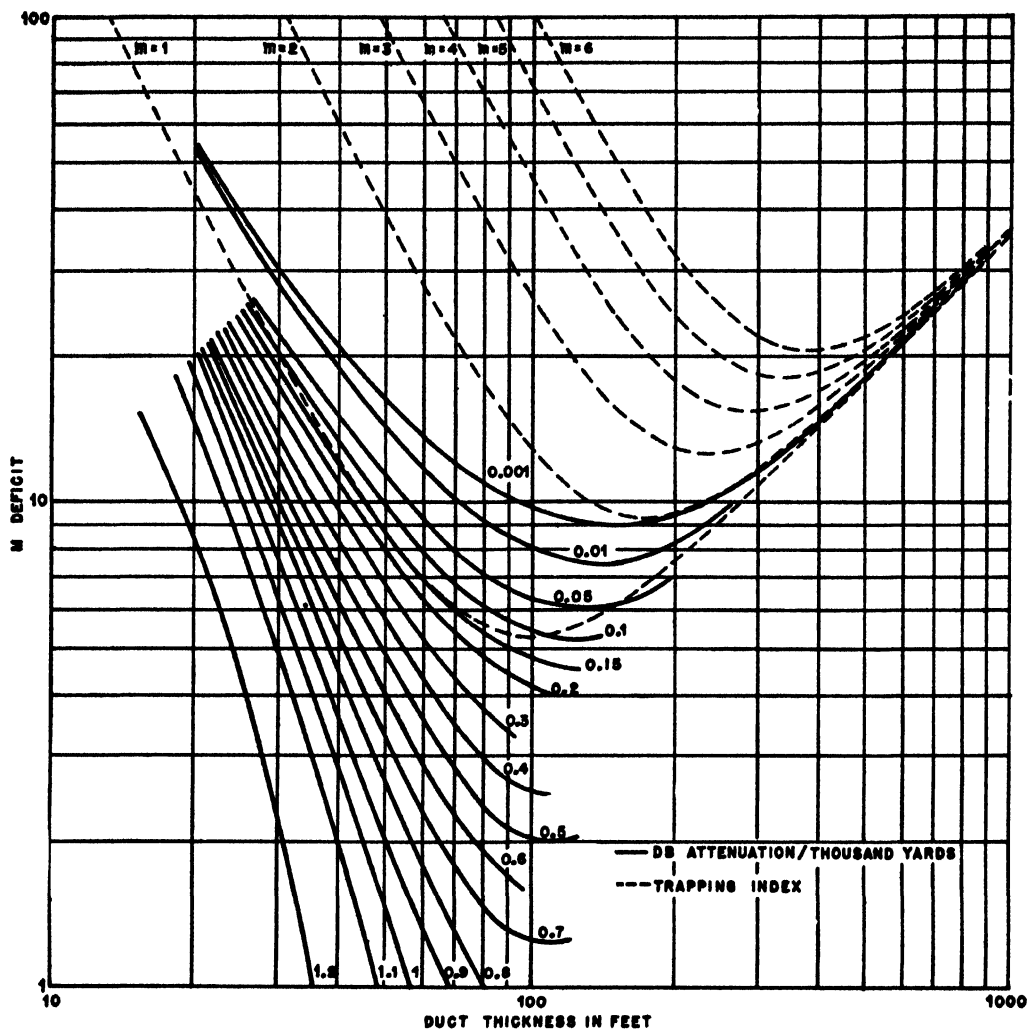
FIGURE 3. Horizontal attenuation of first mode and trapping index, 3,000 mc, standard attenuation (0 M deficit): 1.23 db per 1,000 yd.

is frequently dominant. The results presented apply primarily to this situation

The type of M curve considered is the bilinear model in which the M curve consists of two straight-line segments, the upper being assumed to possess standard slope. This model M curve is completely characterized by two parameters: duct thickness and M deficit. Figures 2, 3 and 4 refer to three frequencies (200, 3,000, and 10,000 mc) and super-standard conditions corresponding to ranges of 1 to 100 M units in M deficit and 10 to 1,000 ft in duct thickness.

The solid curves are contours of constant decibel attenuation (of the first mode) per thousand yards. One enters the diagram with given values of duct thickness and M deficit and interpolates between these contours to obtain the corresponding attenuation.

The dashed curves are contours of constant "trapping index" (number of classically trapped modes).

In terms of the standard notation their equation is

$$ M \text{ deficit} = \frac{10^6}{2}\left[qh_a + \frac{9\lambda^2}{16h_a^2}\left(m - \frac{1}{4}\right)^2\right] $$

Their significance lies in that they furnish an indication of the number of modes other than the first that must be taken into account. If, for example, the bilinear M curve in question corresponds to a point midway between the $m = 1$ and $m = 2$ contours, the first mode is strongly trapped and the second mode attenuation is reduced considerably below standard. Which mode is dominant then depends critically upon the heights of transmitter and receiver, and the simple first mode picture becomes incomplete except at great distances and small heights.

If one attempts to apply these results to simple surface ducts differing from the idealized bilinear

model one should first approximate the actual M curve by a bilinear curve and then enter the diagram with the values of M deficit · and duct thickness corresponding to the *idealized curve*. How to make the best bilinear approximation to a given M curve is an important but still open question.

Except for the 0.01- and 0.001-db contours, which were computed by an asymptotic method, the attenuation contours were cross-faired from preliminary Radiation Laboratory calculations.
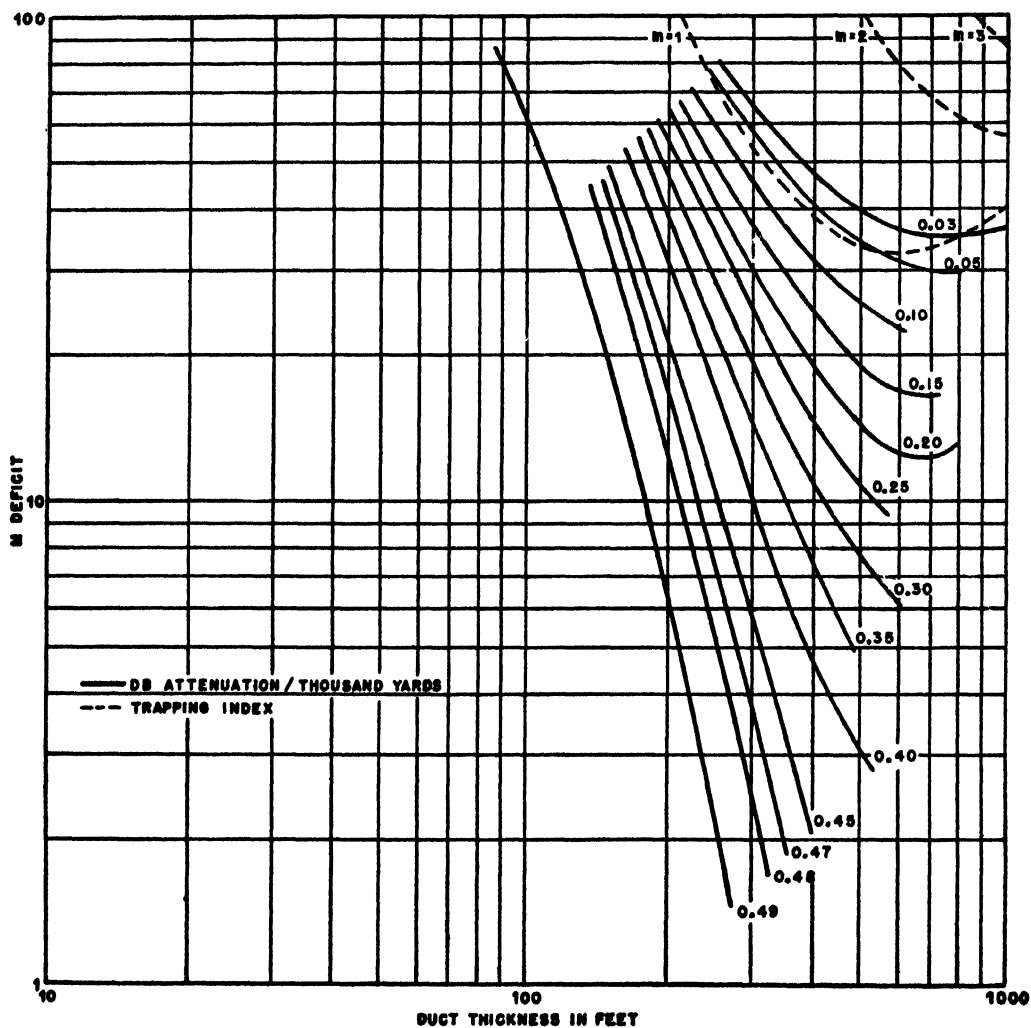
FIGURE 4. Horizontal attenuation of first mode and trapping index, 200 mc, standard attenuation (0 M deficit): 0.498 db per 1,000 yd.

APPROXIMATE ANALYSIS OF GUIDED PROPAGATION
IN A NONHOMOGENEOUS ATMOSPHERE*

THE MILITARY IMPORTANCE of guided or "anomalous" propagation in a stratified atmosphere is now well known. Unfortunately, or perhaps fortunately, the problem cannot be treated with the aid of known and tabulated functions except in some special cases because the exact field distribution with height is a function of a function, namely a function of the distribution of the modified index of refraction. For each distribution of this index with height we should have a curve for the field distribution. These curves will look similar in a general way and yet they will differ in detail; but in this particular problem we are not much concerned with details. Even if we had exact solutions we should still want some generalized way of expressing pertinent information.

An approximate analysis of field distribution in terms of master curves, depending on one, or at most, two parameters, will be discussed. For example, if we have atmospheric conditions favoring formation of a guiding layer immediately above the ground or sea level, then we can try to represent the field distribution with height with the aid of the master curve shown in Figure 1. This curve depends on only one parameter, H, so chosen that in the layer between $(\frac{1}{5}) H$ and H, the field intensity does not deviate by more than 6 db from the maximum.
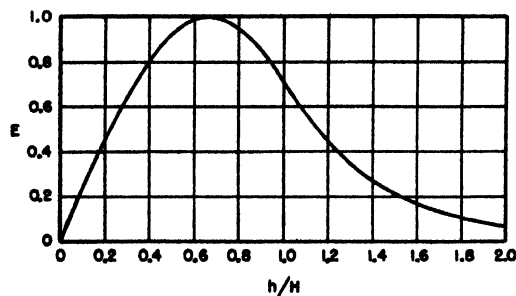
FIGURE 1. Master curve for field distribution with height inside a duct.

This particular curve is chosen for *the first transmission mode*, and it has been suggested by the exact analysis of guided waves in a homogeneous layer. In this case of sharp discontinuity in the index of refraction the field distribution curves are sinusoidal in the layer and exponential outside. The position of the maximum of the sinusoidal portion of the curve and the relative rate of decay of the exponential part depend on the ratio of the wavelength to

*By S. A. Schelkunoff, Bell Telephone Laboratories.

the thickness of the layer and on the amount of discontinuity in the index of refraction. In Figure 2, curve 1 is identical with the curve in Figure 1; curve 2 shows what happens if the wavelength is doubled;
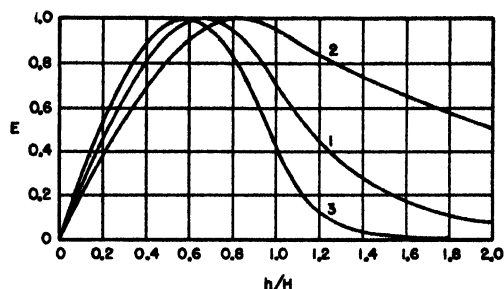
FIGURE 2. Master curves for wavelength λ (1), 2λ (2), and $\frac{1}{2} \lambda$ (3).

and curve 3 corresponds to the case in which the wavelength is halved. If the wavelength is $(3\pi\sqrt{2})/4 \cong 3.3$ times as large as the wavelength corresponding to curve 1 or larger, no guided waves are possible with the field intensity vanishing at the ground or sea level.

The situation is different if the index of refraction is allowed to vary continuously and to diminish indefinitely. Suppose, for instance, that the lapse rate of the index of refraction is constant. We don't expect any critical wavelength in this case; as the wavelength increases we expect the field to spread out more and more. In fact, we expect the shape of the field distribution curve to remain the same, namely to be determined by that solution of

$$\frac{d^2E}{dh^2} = [\hat{\beta}^2 - \omega^2\mu\epsilon\,(h)]\,E \qquad (1)$$

which vanishes at $h = 0$. In this equation

$E =$ the electric intensity;
$h =$ the height;
$\epsilon =$ the modified dielectric constant;
$\omega =$ the radian frequency;
$\hat{\beta} =$ the phase constant in the direction parallel to the stratification.

We can try to approximate this solution by a curve of the type shown in Figure 1 in which case the problem is to select a proper value for H. The question may be raised regarding our preference for this particular curve rather than for curve 2 or 3 in Figure 2. We shall return to this point later; for the present we shall merely point out that curve 1

occupies a "mean" position among other curves of this type.

There are two methods for selecting H. In one method H is defined as that value of h for which the coefficient $\hat{\beta}^2 - \omega^2\mu\epsilon(h)$ in equation (1) vanishes. This value of h separates the region in which the solution of equation (1) is "more" or less sinusoidal" from the region in which the solution is "more or less exponential." This definition leads to one equation connecting H and $\hat{\beta}$. Next, the stratified region $0 < h < H$ is replaced by a homogeneous region in which the dielectric constant is equal to the average value of $\epsilon(h)$ in the interval $(0,h)$. If we impose the requirement that curve 1 represents the exact field distribution under the new conditions, we obtain the second equation for H and $\hat{\beta}$. Eliminating $\hat{\beta}$ and expressing the result in symbols approved by the wave propagation committee, we have

$$H\int_0^H M(h)\, dh - H^2\, M(H) = \frac{9 \times 10^6}{128} \lambda^2 . \quad (2)$$

If the lapse rate of M is constant, this equation gives

$$H = 65\lambda^{\frac{2}{3}} \left(-2\frac{dM}{dh} \right)^{-\frac{1}{3}} . \quad (3)$$

If $M(h)$ is proportional to h^2, then

$$H = 18\lambda^{\frac{2}{3}} \left[\frac{-M(h)}{h^2} \right]^{-\frac{1}{3}} . \quad (4)$$

If the lapse rate of M is constant, the exact solution may be expressed in terms of Bessel functions. Figure 3 shows the exact and approximate solutions.

The second method is based on the fact that the solutions of equation (1) minimize and reduce to zero the following function:

$$I = \hat{\beta}^2 \int_0^\infty E^2\, dh - \omega^2\mu\epsilon(o) \int_0^\infty \frac{\epsilon(h)}{\epsilon(o)} E^2\, dh$$
$$+ \int_0^\infty \left(\frac{dE}{dh} \right)^2 dh . \quad (5)$$

In deriving this equation we should remember that

$$Ey = (\text{const})\ U^{\frac{1}{2}}\ [J_{\frac{1}{3}}(U) + J_{-\frac{1}{3}}(U)] \qquad Ey = \sin \rho\ \rho \leq \tfrac{3\pi}{4}$$

$$U = {}^{3\pi}/_4 \left\{ 1 - \frac{8}{3^{3/2}\pi} \right\}^{\frac{3}{2}} \qquad Ey = \frac{\sqrt{2}}{2} e^{3\pi/4} e^{-\rho}\ \rho \geq \tfrac{3\pi}{4}$$
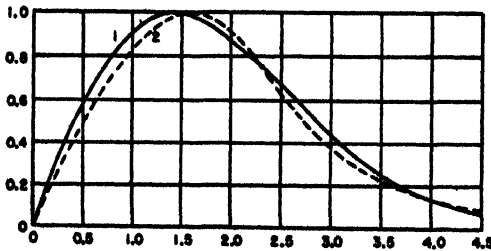
FIGURE 3. (1) Exact solution normalized to have minimum value of unity. (2) Approximation.

we are concerned with solutions which vanish at $h = 0$ and $h = \infty$. Hence, if we wish to approximate this solution by a function of one parameter H, we eliminate H from the following two equations

$$I = 0, \frac{\partial I}{\partial H} = 0 . \quad (6)$$

If, for instance, we wish to approximate the field distribution by the master curve in Figure 1, we solve

$$H^2 \frac{\partial P}{\partial H} - HP = \frac{9 \times 10^5}{128} \lambda^2 , \quad (7)$$

where

$$P = -\int_0^H M \sin^2 \frac{3\pi h}{4 H}\, dh$$
$$- 55.5 \int_H^\infty M \exp \frac{-3\pi h}{2 H}\, dh . \quad (8)$$

By this variational method the numerical coefficient in equation (3) is found to be 64 rather than 65.

The great advantage of the variational method lies in the fact that, if we wish, we can increase the number of parameters in the approximating function. For example, we can assume

$$E(h) = \sin \left(\frac{\theta h}{H} \right), 0 \leq h \leq H$$
$$= \sin \theta \exp \left[-\psi \frac{h - H}{H} \right], h > H , \quad (9)$$

without specifying that $\theta = \psi = 3\pi/4$ as we did in obtaining the curve in Figure 1. We should then calculate H, θ, and ψ from

$$I = 0, \frac{\partial I}{\partial \theta} \doteq 0, \frac{\partial I}{\partial \psi} = 0 . \quad (10)$$

However, aside from the labor of solving these equations and having to deal with more complicated results, we shall lose the advantage inherent in a description of the field in terms of only one easily understood parameter. The most we could hope for from an analysis of these equations is a somewhat better choice of the master curve for the type of atmospheric conditions which are the most likely to occur.

The obvious general conclusion from equations (7) and (8) is this: if $M(h)$ is multiplied by a constant factor, the effect on H is the same as that obtained if we divide λ by the square root of this factor. If M is proportional to h^n, then H is proportional to $\lambda^{2/(n+2)}$. Since the gain of the guided wave over a free space wave is proportional to $\lambda\rho/H^2$, where ρ is the distance from the transmitter, the gain is independent of the wavelength when $M(h)$ is proportional to h^2. For a uniform lapse rate the gain varies inversely as one-third power of the wavelength.

SOME THEORETICAL RESULTS ON NONSTANDARD PROPAGATION[a]

PROPAGATION IN THE OCEANIC SURFACE DUCT

THE ANALYSIS SECTION of Columbia University Wave Propagation Group undertook a theoretical study of propagation in case of surface ducts, which have recently been reported to be of common occurrence in oceanic areas. The M curve chosen was

$$M(h) = 346.4 + 0.036h + 43e^{-0.1h} \qquad (1)$$

where the height h is expressed in feet. This curve has an M deficit of 43 units and a duct height of 48 ft and is considered to be representative of conditions prevailing around Saipan when the wind is of the order of 10 to 20 mph.

The analysis was based on the phase integral method. The standard W.K.B. (Wentzel-Kramers-Brillouin) version of the asymptotic solutions of the wave equation[107] had to be extended in two ways. One was in the adoption of Langer's form of the asymptotic solutions,[449] which enables one to bridge the "gaps" around the turning points. The other, and more important, development was in the extension of Langer's method to handle a case with *two* turning points. This was accomplished by joining the solutions from each turning point at the duct height. The resulting solution agrees with Gamow's for completely trapped modes but deviates from it when leakage begins. For leaky modes the standard Langer solution is adequate.

Coverage diagrams were computed for the S and X bands and for transmitter heights of 16 and 46 ft. In case of the S band, it was found that the first mode was nearly trapped, while the second mode was considerably leaky with a decrement of about 3 db per nautical mile. The two modes were combined, and coverage diagrams were computed over ranges and heights such that the second mode contributed no more than 25 per cent to the total field.

In the case of the X band, it was found that the first two modes were completely trapped, the third mode nearly trapped, while the fourth mode was leaky with a decrement of over 3 db per nautical mile. In computing the coverage diagrams for the X band, the four modes were combined over such ranges and heights that the fourth mode did not contribute more than 25 per cent to the total field.

CHARACTERISTIC VALUES FOR A CONTINUOUSLY VARYING MODIFIED INDEX

In the theoretical treatment of nonstandard propagation by the method of normal modes, one is confronted with the task of solving the differential equation for the height-gain function $U(h)$ given by equation (2), which, it will be noted, is identical with equation (8) in Chapter 2b.

$$\ddot{U}_m(h) + k^2 [y(h) + \Lambda_m] U_m(h) = 0 ,$$
$$k = \frac{2\pi}{\lambda} , \qquad y(h) = 2 \times 10^{-6}M(h) , \qquad (2)$$

by asymptotic methods, the characteristic value Λ_m is determined, to a first approximation, by the condition that

$$k \int_0^{h_1} \sqrt{y(h) - y(h_1)} \, dh = v_m \cong \pi \left(m - \frac{1}{4} \right) , \quad (3)$$
$$\Lambda_m = -y(h_1) . \qquad (4)$$

In order to solve equation (3) one has to find a value h_1, which is generally complex, such that when $y(h_1)$ is substituted in the radicand and the integral

$$\int_0^{h_1} \sqrt{y(h) - y(h_1)} \, dh \equiv F(h_1) \qquad (5)$$

evaluated, the result should be purely real, and equal to v_m/k. In case of a surface duct, $F(h_1)$ is real and is a continuously increasing function of its argument for real values of h_1 ranging from zero up to the duct height h_0. In order for $F(h_1)$ to increase beyond the value $F(h_0)$ and still to remain real it is found that h_1 must be complex; i.e., the path in the complex h_1-plane along which $F(h_1)$ is real consists of the portion of real axis $0 \leq h_1 \leq h_0$ followed by a curve in the fourth quadrant.

In case of substandard refraction, $F(h_1)$ is real only for complex values of h_1, and the method of solving equation (3) to be explained presently is particularly helpful in this case.

Let

$$y(h) = y(0) + b_1 h + b_2 h^2 + \cdots + b_n h^n + \cdots ,$$
$$\dot{h} = \frac{dh}{dy} (h = 0) = \frac{1}{b_1} , \qquad \ddot{h} = \frac{-2b_2}{b_1^3} ,$$
$$\dddot{h} = \frac{(-6b_3 b_1 + 12b_2^2)}{b_1^5} ,$$
$$\ddddot{h} = \frac{(120b_1 b_2 b_3 - 24b_1^2 b_4 - 120b_2^3)}{b_1^7} , \text{ etc.}$$

and

$$\theta = e^{i\pi/3}\left(\frac{3v_m}{2\lambda h}\right)^{\frac{1}{2}}, \quad w = \Lambda_m + y(0), \qquad (6)$$

then

$$\Lambda_m = -y(h_1) = -y(0) + \theta^2 + \left(\frac{4}{15}\right)(h_2)\,\theta^4$$

$$+ \theta^6\left[\frac{4}{25}(h_2)^2 - \frac{8}{105}(h_3)\right]$$

$$+\frac{16}{27}\theta^8\left[\frac{77}{375}(h_2)^3 - \frac{33}{175}(h_2)(h_3) + \frac{1}{35}(h_4)\right]+\cdots,(7)$$

$$h_1 = -\dot{h}w + \frac{\ddot{h}}{2!}w^2 - \frac{\dddot{h}}{3!}w^3 +\cdots, \quad (8)$$

where

$$h_2 = \frac{\ddot{h}}{\dot{h}}, \quad h_3 = \frac{\dddot{h}}{\dot{h}},\cdots.$$

Equations (7) and (8) are of the nature of asymptotic formulas; they should be terminated when the individual terms begin to increase, and the error in Λ_m or h_1 is then of the order of magnitude of the last term retained.

The following examples in Table 1 illustrate the degree of accuracy obtainable from equation (7).

As a further check, we treated the case $\alpha = +20$, $\lambda = 0.6356$, for which Pearcey and Whitehead[164] give a value $\Lambda_1 = -10.21 + 1.07 \times 10^{-13}i$. Equation (7) yields $\Lambda_1 = -10.22$, while the imaginary part obtainable from Gamow's formula is $1.24 \times 10^{-13}i$.

It must be emphasized that the value obtained from equation (7) should be verified by carrying out the integration of $F(h_1) = \int_0^{h_1}\sqrt{y(h) + \Lambda_m}dh$. While doing so, one may as well compute

$$\frac{dF}{dh_1} = -\frac{1}{2}y'(h_1)\int_0^{h_1}\frac{dh}{\sqrt{y(h) - y(h_1)}}, \quad (10)$$

and then obtain a correction to h_1 by Newton's method.

The method of solving equation (3) explained above has been found especially useful in the treatment of substandard refraction, and to a lesser extent in the treatment of the trapped modes in case of a surface duct. In the latter case one can, of course, solve for Λ_m directly by computing $F(h_1)$ by numerical integration. The method is not applicable for the leaky modes in case of a surface duct.

So far the discussion has centered on the solution of equation (3), which in itself is only an approximate asymptotic formula valid for large values of k. Let the value of Λ_m which satisfies equation (3) be denoted by $\Lambda_m^{(0)}$; then an improved value for Λ_m can be obtained from

$$\Lambda_m = \Lambda_m^{(0)}$$

$$+ \frac{3e^{i\pi/3}(v_m)^{\frac{1}{2}}}{\theta'h^{7/3}}\left(\frac{3}{2}\right)^{4/3}(\dot{y})^{-1}\left[\frac{1}{35}\left(\frac{\ddot{y}}{\dot{y}}\right)^2 - \frac{2}{63}\left(\frac{\dddot{y}}{\dot{y}}\right)\right](11)$$

where

$$\theta' = \int_0^{h_1}\frac{dh}{\sqrt{y(h) + \Lambda_m^{(0)}}}, \quad \dot{y} = \frac{dy}{dh_1}, \text{ etc}, \quad (12)$$

and the derivatives of y are to be evaluated at $h = h_1$.

TABLE 1. Approximate determination of Λ_1 from equation (7) and the verification that $\int_0^{h_1}\sqrt{y(h) + \Lambda_1}\,dh = 2.383$.*

α	λ	Λ_1 from equation (7)	h_1 from $y(h_1) = -\Lambda_1$	$\int_0^{h_1}\sqrt{y(h) + \Lambda_1}\,dh$	v_1
-20	0.6356	12.360 + 9.775i	0.3997 − 0.9518i	2.370 + 0.004i	2.383
-10	0.6356	4.878 + 6.302i	0.4745 − 1.1982i	2.397 + 0.010i	2.383
-5	0.6356	1.499 + 4.257i	0.5691 − 1.4692i	2.393 + 0.000i	2.383
-2	0.6356	−0.246 + 2.902i	−0.764 − 1.787i	2.363 − 0.008i	2.383

$y(h) = h + ce^{-\lambda h}$.

PERTURBATION THEORY FOR AN EXPONENTIAL M CURVE IN NONSTANDARD PROPAGATION[a]

ABSTRACT

IN THIS chapter a perturbation method is developed for treating nonstandard propagation in the case when the deviation of the M curve from the standard (≡ the M anomaly) can be represented by a term $\alpha e^{-\lambda z}$, where z denotes height in natural units. The method is also applicable to other forms of the M anomaly which can be derived from an exponential term by differentiation with respect to λ; in fact, in its region of convergence, it is formally applicable to the most general type of M curve, including elevated ducts. The region of practical convergence of the method ranges from standard down to cases where the decrement is a small fraction of the standard value.

The procedure followed is to express the height-gain function $U_k(z)$ of the k-th mode in the nonstandard case as a linear combination of the height-gain functions $U_m{}^0(z)$ of all the modes in the standard case.

$$U_k(z) = \sum_{k=1}^{\infty} A_{km} U_m{}^0(z) . \tag{1}$$

The execution of this plan hinges on the possibility of evaluating the quantities

$$\beta_{nm}(\lambda) = \int_0^{\infty} U_n{}^0(z) \, U_m{}^0(z) \, e^{-\lambda z} dz . \tag{2}$$

It is shown that $\beta_{nm}(\lambda)$ satisfies the differential equation

$$\frac{d\beta_{nm}}{d\lambda} = \frac{1}{2\lambda} + \beta_{nm}(\lambda) \cdot$$

$$\left[-\frac{1}{2\lambda} + \frac{1}{2}(D_m{}^0 + D_n{}^0) + \frac{\lambda^2}{4} + \frac{1}{4\lambda^2}(D_m{}^0 - D_n{}^0)^2 \right], \tag{3}$$

whose solution is

$$\beta_{nm}(\lambda) = \frac{1}{2\sqrt{\lambda}} e^{\frac{\lambda}{2}(D_n{}^0 + D_m{}^0) + \frac{\lambda^3}{12} - \frac{1}{4\lambda}(D_m{}^0 - D_n{}^0)^2}$$

$$\int_0^{\lambda} \frac{dx}{\sqrt{x}} e^{-\frac{x}{2}(D_m{}^0 + D_n{}^0) - \frac{x^3}{12} + \frac{1}{4x}(D_n{}^0 - D_m{}^0)^2} . \tag{4}$$

Here $D_m{}^0$ denotes the characteristic value of the m-th mode in the standard case. For large λ the

following asymptotic formula holds

$$\beta_{nm} = $$

$$-\frac{2}{\left[\lambda^3 + 2\lambda (D_m{}^0 + D_n{}^0) - 2 + \frac{1}{\lambda}(D_m{}^0 - D_n{}^0)^2 \right]}$$

$$+ \frac{8 \left[3\lambda^2 + 2\lambda (D_m{}^0 + D_n{}^0) - \frac{1}{\lambda}(D_m{}^0 - D_n{}^0)^2 \right]}{\left[\lambda^3 + 2\lambda (D_m{}^0 + D_n{}^0) - 2 + \frac{1}{\lambda}(D_m{}^0 - D_n{}^0)^2 \right]^4} . \tag{5}$$

Having determined the $\beta_{nm}(\lambda)$ from equation (4), or by a numerical solution of equation (3), the characteristic values D_k and the coefficients A_{km} are to be solved from the infinite system of equations

$$\sum_{m=1}^{\infty} A_{km} \left[(D_k - D_m{}^0) \delta_{nm} + \alpha \beta_{nm} (\lambda) \right] = 0 ,$$

$$n = 1, 2, 3 \cdots \tag{6}[b]$$

For this purpose a simple iterative procedure has been developed, which has been found to be rapidly convergent. The A_{km} are normalized by the condition

$$\int_0^{\infty} U_k{}^2 (z) \, dz = 1 = \sum_{m=1}^{\infty} A_{km}{}^2 \tag{7}[c]$$

One can also expand D_k as a power series in α

$$D_k = D_k^0 + \alpha D_k^1 + \alpha^2 D_k^2 + \cdots ,$$

$$D_k{}^{(1)} = -\beta_{kk} ; D_k{}^{(2)} = e^{i\pi/3} \sum_m \frac{\beta_{mk}^2}{(\tau_m - \tau_k)} , m \pm k$$

An alternative expression for $D_k^{(2)}$ is given in equation (65).

INTRODUCTION

In the theoretical treatment of nonstandard propagation by the method of normal modes, one is confronted with the task of solving the equation

$$\frac{d^2 U_m}{dh^2} + k^2 \left[\eta(h) + \Lambda_m \right] U_m = 0 , \tag{8}$$

subject to the condition that $U_m(0) = 0$ and that

[b] $\delta_{nm} = 1, \quad n = m$

$\delta_{nm} = 0, \quad n \pm m.$

[c] The integral $\int_0^{\infty} U_k{}^2(z) dz$ diverges when taken along the real axis; it converges, however, and to the same limit, when the path is a radial line in the fourth quadrant of the z plane. In the sequel, whenever an integral is divergent it will be understood that the path is suitably modified.

[a] By C. L. Pekeris, Columbia University Wave Propagation Group.

at $h \rightarrow \infty$, U_m should represent an upgoing wave only. Here h denotes height in feet.

$$y(h) = N^2(h) - 1 = 2 \times 10^{-6} M(h) , k = \frac{2\pi}{\lambda} , \quad (9)$$

and Λ_m is the characteristic value which is generally complex. It is convenient to introduce natural units of height

$$z = \frac{h}{H} , H = (k^2 q)^{-\frac{1}{3}}, q = \frac{dN^2}{dh} = 2.36 \times 10^{-9} \text{ cm}^{-1} ,$$

$$D_m = \Lambda_m \left(\frac{k}{q}\right)^{\frac{2}{3}} , \quad (10)$$

whereby equation (8) is transformed into

$$\frac{d^2 U_m}{dz^2} + \left[z + f(z) + D_m \right] U_m(z) = 0 . \quad (11)$$

The term $f(z)$ in equation (11) represents the refraction anomaly and is equal to zero for a standard atmosphere. In the first instance we shall be treating the case where

$$f(z) = \alpha e^{-\lambda z} , \quad (12)^{\text{d}}$$

and we shall later generalize the treatment to deal with any M curve represented as a series of Laguerre functions. If the original M curve is represented by the expression

$$M(h) = bh + ae^{-ch} , b = 0.036 \text{ ft}^{-1} , \quad (13)$$

then α and λ are obtained as follows:

$$\alpha = 2 \times 10^{-6} \left(\frac{k}{q}\right)^{\frac{2}{3}} a , \lambda = cH . \quad (14)$$

It is to be noted that in contrast to the constants a and c in equation (13), which are independent of frequency, the constants α and λ in equation (12) are frequency dependent. For a given observed M curve the constants α and λ will therefore differ with the frequency band used, as will also the height represented by one unit of z.

FORMAL SOLUTION OF THE PROBLEM BY THE PERTURBATION METHOD

In order to solve the equation

$$\frac{d^2 U_k(z)}{dz^2} + \left[z + \alpha e^{-\lambda z} + D_k \right] U_k(z) = 0 , \quad (15)$$

we seek a solution in the form

$$U_k = \sum_{m=1}^{\infty} A_{km} U_m^0(z) , \quad (16)$$

where $U_m^0(z)$ are the height-gain functions of the m-th mode in the standard case, which satisfy the

equation

$$\frac{d^2 U_m^0(z)}{dz^2} + \left[z + D_m^0 \right] U_m^0(z) = 0 \quad (17)$$

$$\int_0^\infty \left[U_m^0(z) \right]^2 dz = 1 . \quad (18)$$

The solutions of equations (17) and (18) are:

$$U_m^0(z) = C_m u^{\frac{1}{2}} H_{\frac{1}{3}}^{(2)}(u) , u = \frac{2}{3} (z + D_m^0)^{\frac{3}{2}} , \quad (19)$$

$$C_m = \left\{ e^{i\pi/3} \frac{2}{\sqrt{3}} \left(\frac{3}{2}\right)^{\frac{1}{3}} v_m^{\frac{1}{3}} \left[J_{\frac{2}{3}}(v_m) - J_{-\frac{2}{3}}(v_m) \right] \right\}^{-1} \quad (20)$$

$$D_m^0 = \tau_m e^{i2\pi/3} . \quad \tau_m = \left(\frac{3 v_m}{2}\right)^{\frac{2}{3}} , \quad (21)$$

where

$$J_{\frac{1}{3}}(v_m) + J_{-\frac{1}{3}}(v_m) = 0 . \quad (22)$$

For small z the power series development of $U_m^0(z)$ is useful:

$$U_m^0(z) = i \sum_{k=1} A_k z^k , \quad (23)$$

$$A_k = -\frac{1}{k(k-1)} \left[D_m^0 A_{k-2} + A_{k-3} \right] , \quad (24)$$

$$U_m^0(z) = i \left[z - \left(\frac{D_m^0}{6}\right) z^3 - \frac{z^4}{12} \right.$$

$$\left. + \left(\frac{D_m^0}{120}\right)^2 z^5 + \left(\frac{D_m^0}{120}\right) z^6 + \cdots \right] , \quad (25)$$

while for large z one may use asymptotic expansion of equation (19)

$$H_{\frac{1}{3}}^{(2)}(u) \rightarrow \sqrt{\frac{2}{\pi u}} e^{i(-u + 5\pi/12)} .$$

$$\left[1 + \frac{5i}{72u} - \frac{385}{10,368 u^2} + \cdots \right] . \quad (26)$$

If now the expansion (16) be substituted into equation (15), we obtain, on making use of equation (17), the condition

$$\sum_{m=1} A_{km} \left[(D_k - D_m^0) + \alpha e^{-\lambda z} \right] U_m^0(z) = 0 . \quad (27)$$

On multiplying this equation by $U_n^0(z)$, where n is any integer, and integrating from 0 to ∞ we get a system of equations for the determination of D_k and the A_{km}:

$$\sum_{m=1}^{\infty} A_{km} \left[(D_k - D_m^0) \delta_{nm} + \alpha \beta_{nm}(\lambda) \right] = 0 ,$$

$$n = 1, 2, 3 \cdots \quad (28)$$

$$\beta_{nm}(\lambda) = \int_0^\infty U_m^0(z) U_n^0(z) e^{-\lambda z} dz . \quad (29)$$

---

^dNo confusion should arise from the use of λ in equation (12) and the standard usage of λ to denote wavelength.

The characteristic values D_k are then obtained as the roots of the infinite determinant.

$$\begin{vmatrix} D_k - D_1{}^0 + \alpha\beta_{11}, & \alpha\beta_{12}, & \alpha\beta_{13}, & \cdots \\ \alpha\beta_{21}, & D_k - D_2{}^0 + \alpha\beta_{22}, & \alpha\beta_{23}, & \cdots \\ \alpha\beta_{31}, & \alpha\beta_{32}, & D_k - D_3{}^0 + \alpha\beta_{33}, & \cdots \\ \cdots, & \cdots, \cdots, & \cdots \end{vmatrix} = 0 . \tag{30}$$

Having determined D_k from equation (30), the A_{km} are obtained by solving the system of linear equations (28).

EVALUATION OF $\beta_{nm}(\lambda)$
AS AN INDEFINITE INTEGRAL

The primary task in the perturbation method is the evaluation of the exchange integrals $\beta_{nm}(\lambda)$ defined in equation (29). We shall accomplish this by proving that $\beta_{nm}(\lambda)$, as a function of λ, satisfies a differential equation of the first order for which an explicit solution can be given. For this purpose we shall study the function

$$F(z) \equiv U_n{}^0(z) \, U_m{}^0(z) , \tag{31}$$

where

$$\ddot{U}_m{}^0(z) + [z + D_m{}^0] \, U_m{}^0(z) = 0 , \tag{32}$$

$$\ddot{U}_n{}^0(z) + [z + D_n{}^0] \, U_n{}^0(z) = 0 . \tag{33}$$

By multiplying equation (32) by $U_n{}^0(z)$, equation (33) by $U_m{}^0(z)$ and subtracting, we obtain

$$\frac{d}{dz} (\dot{U}_m{}^0 U_n{}^0 - U_m{}^0 \dot{U}_n{}^0) = - (D_m{}^0 - D_n{}^0) \, U_m{}^0 U_n{}^0 , \tag{34}$$

$$\dot{U}_m{}^0 U_n{}^0 - U_m{}^0 \dot{U}_n{}^0 = - (D_m{}^0 - D_n{}^0) \int_0^z U_m{}^0(x) \, U_n{}^0(x) \, dx . \tag{35}$$

Now it can be verified by direct substitution that

$$\dddot{F} + 2\dot{F} (D_n + D_m + 2z) + 2F$$
$$= (D_m{}^0 - D_n{}^0) (\dot{U}_m{}^0 U_n{}^0 - U_m{}^0 \dot{U}_n{}^0)$$
$$= - (D_m{}^0 - D_n{}^0)^2 \int_0^z F(x) \, dx . \tag{36}*$$

From equation (36) it follows that

$$F = \frac{d}{dz} \left[(2z + D_m{}^0 + D_n{}^0) F + \frac{1}{2} \ddot{F} \right]$$
$$+ \frac{1}{2} (D_m{}^0 - D_n{}^0)^2 \int_0^z F(x) \, dx . \tag{37}$$

We may also note that

$$\ddot{F}(0) = 2\dot{U}_m{}^0(0) \, \dot{U}_n{}^0(0) = -2 , \tag{38}$$

This is the first occasion in the author's experience where use is made of the fact that the product of two functions, each of which is a solution of a distinct second order ordinary linear differential equation, satisfies a fourth order linear differential equation.[40]

$$\int_0^\infty e^{-\lambda z} \, \ddot{F} dz = e^{-\lambda z} \, (\dot{F} + \lambda F) \Big|_0^\infty + \lambda^2 \int_0^\infty e^{-\lambda z} \, F dz$$
$$= \lambda^2 \int_0^\infty e^{-\lambda z} \, F dz . \tag{39}$$

$$\int_0^\infty e^{-\lambda z} \, dz \int_0^z F(x) \, dx = - \frac{1}{\lambda} e^{-\lambda z} \int_0^z F(x) \, dx \Big|_0^\infty$$
$$+ \frac{1}{\lambda} \int_0^\infty e^{-\lambda z} \, F(z) \, dz = \frac{1}{\lambda} \int_0^\infty e^{-\lambda z} \, F(z) \, dz . \tag{40}$$

$$\int_0^\infty e^{-\lambda z} \, F(z) \, dz = - \frac{d}{d\lambda} \int_0^\infty e^{-\lambda z} \, F(z) \, dz . \tag{41}$$

We now substitute equation (37) in the integrand of equation (29) and obtain

$$\beta_{nm} (\lambda) = \int_0^\infty F(z) \, e^{-\lambda z} \, dz = \int_0^\infty e^{-\lambda z} \, dz \times$$
$$\left\{ \frac{d}{dz} \left[(2z + D_m{}^0 + D_n{}^0) F + \frac{1}{2} \ddot{F} \right] \right.$$
$$\left. + \frac{1}{2} (D_m{}^0 - D_n{}^0)^2 \int_0^z F(x) dx \right\}$$
$$= \frac{1}{2\lambda} (D_m{}^0 - D_n{}^0)^2 \int_0^\infty e^{-\lambda z} \, F(z) \, dz$$
$$+ \left[(2z + D_n{}^0 + D_m{}^0) F + \frac{1}{2} \ddot{F} \right] e^{-\lambda z} \Big|_0^\infty$$
$$+ \lambda \int_0^\infty e^{-\lambda z} \left[(2z + D_n{}^0 + D_m{}^0) F + \frac{1}{2} \ddot{F} \right] dz$$
$$= 1 + \int_0^\infty e^{-\lambda z} \, F(z)$$

$$\left[2\lambda z + \lambda(D_m{}^0 + D_n{}^0) + \frac{1}{2} \lambda^3 + \frac{1}{2\lambda} (D_m{}^0 - D_n{}^0)^2 \right] dz$$

$$= 1 - 2\lambda \frac{d\beta_{nm} (\lambda)}{d\lambda}$$

$$+ \beta_{nm}(\lambda) \left[\lambda(D_m{}^0 + D_n{}^0) + \frac{\lambda^3}{2} + \frac{1}{2\lambda} (D_m{}^0 - D_n{}^0)^2 \right] \tag{42}$$

It follows that the exchange integral $\beta_{nm}(\lambda)$ satisfies the first order differential equation

$$\frac{d\beta_{nm} (\lambda)}{d\lambda} = \frac{1}{2\lambda} + \beta_{nm} (\lambda) \cdot$$

$$\left[-\frac{1}{2\lambda} + \frac{1}{2}(D_m{}^0 + D_n{}^0) + \frac{\lambda^2}{4} + \frac{1}{4\lambda^2} (D_m{}^0 - D_n{}^0)^2 \right] \tag{43}$$

The solution of equation (43) is

$$\beta_{nm} (\lambda) = \frac{1}{2\sqrt{\lambda}} e^{\frac{\lambda}{2} (D_m{}^0 + D_n{}^0) + \frac{\lambda^3}{12} - \frac{1}{4\lambda} (D_m{}^0 - D_n{}^0)^2}$$

$$\int_0^\lambda \frac{dx}{\sqrt{x}} e^{-\frac{x}{2} (D_m{}^0 + D_n{}^0) - \frac{x^3}{12} + \frac{1}{4x} (D_m{}^0 - D_n{}^0)^2} . \tag{44}$$

PROPERTIES OF $\beta_{nm}(\lambda)$

For small λ the solution of the differential equation (43) can be started with a power series in λ.

1. $n \pm m$

$$\beta_{nm}(\lambda) = -\frac{2\lambda e^{i2\pi/3}}{(\tau_m - \tau_n)^2} \sum_{k=0}^{\infty} C_k e^{i2\pi k/3} \lambda^k , \qquad (45)$$

$$C_0 = 1 \cdot , \; C_1 = \frac{6}{(\tau_m - \tau_n)^2} ,$$

$$C_2 = \frac{10C_1 - 2(\tau_m + \tau_n)}{(\tau_m - \tau_n)^2} ,$$

$$C_3 = \frac{14C_2 - 2C_1(\tau_m + \tau_n)}{(\tau_m - \tau_n)^2} ,$$

$$C_n = \frac{(4n+2)C_{n-1} - 2(\tau_m + \tau_n)C_{n-2} - C_{n-4}}{(\tau_m - \tau_n)^2} . \quad (46)$$

2. $n = m$

$$\beta_{nm} = 1 + B_1 \lambda + B_2 \lambda^2 + \cdots , \qquad (47)$$

$$B_1 = \frac{2}{3} D_m^0 , \; B_2 = \frac{4}{15} D_m^{2(0)} ,$$

$$B_3 = \frac{1}{14} + \frac{8}{105} D_m^{3(0)} ,$$

$$B_n = \frac{1}{(2n+1)} \left[2D_m^0 B_{n-1} + \frac{1}{2} B_{n-3} \right] \quad (48)$$

For intermediate values of λ one may either use the integral in equation (44) or integrate numerically the differential equation (43). The latter procedure was advocated by Hartree.

For large values of λ an asymptotic expansion can be obtained directly from equation (43) by writing it in the form

$$\beta_{nm}(\lambda) =$$

$$\frac{-2 + 4\lambda \dfrac{d\beta_{nm}(\lambda)}{d\lambda}}{\lambda^3 + 2\lambda(D_m^0 + D_n^0) - 2 + \dfrac{1}{\lambda}(D_m^0 - D_n^0)^2} \longrightarrow$$

$$-\frac{2}{\lambda^3 + 2\lambda(D_m^0 + D_n^0) - 2 + \dfrac{1}{\lambda}(D_m^0 - D_n^0)^2}$$

$$+\frac{8\left[3\lambda^3 + 2\lambda(D_m^0 + D_n^0) - \dfrac{1}{\lambda}(D_m^0 - D_n^0)^2\right]}{\left[\lambda^3 + 2\lambda(D_m^0 + D_n^0) - 2 + \dfrac{1}{\lambda}(D_m^0 - D_n^0)^2\right]^3} . \quad (49)$$

An alternative asymptotic expansion can be derived from equation (44) by partial integration

$$\beta_{mn} \rightarrow$$

$$-\frac{2}{\left[\lambda^3 + 2\lambda(D_m^0 + D_n^0) + \dfrac{1}{\lambda}(D_m^0 - D_n^0)^2\right]}$$

$$+\frac{4\left[5\lambda^3 + 2\lambda(D_m^0 + D_n^0) - \dfrac{3}{\lambda}(D_m^0 - D_n^0)^2\right]}{\left[\lambda^3 + 2\lambda(D_m^0 + D_n^0) + \dfrac{1}{\lambda}(D_m^0 - D_n^0)^2\right]^3} \quad (50)$$

In doing so one needs to prove that

$$\int_0^\infty \frac{dx}{\sqrt{x}} e^{-\frac{x}{2}(D_m^0 + D_n^0) - \frac{x^3}{12} + \frac{1}{4x}(D_m^0 - D_n^0)^2}$$

$$\equiv \Psi_{nm} = 0 \qquad (51)$$

We shall state here without proof that

$$\Psi_{mm} = \int_0^\infty \frac{dx}{\sqrt{x}} e^{-x D_m^0 - \frac{x^3}{12}}$$

$$= \frac{\pi\sqrt{\pi}}{2} \left(\frac{2}{3}\right)^{\frac{1}{3}} h_1(D_m^0) h_2(D_m^0) , \qquad (52)$$

where h_1 and h_2 are Furry's functions of the first and second kind defined as

$$h_1(x) = \left(\frac{2}{3}\right)^{\frac{1}{3}} \sqrt{x} H_{\frac{1}{3}}^{(1)} \left(\frac{2}{3} x^{\frac{3}{2}}\right) \qquad (53)$$

$$h_2(x) = \left(\frac{2}{3}\right)^{\frac{1}{3}} \sqrt{x} H_{\frac{1}{3}}^{(2)} \left(\frac{2}{3} x^{\frac{3}{2}}\right). \qquad (54)$$

Since by definition of D_m^0, $h_2(D_m^0) = 0$, it follows that $\Psi_{mm} = 0$. The proof of equation (51) for $n \pm m$ is left as an exercise to the interested reader.

ITERATION METHOD OF SOLVING FOR THE CHARACTERISTIC VALUES D_k AND THE COEFFICIENTS A_{km}

In solving equations (28) and (30), which are of infinite order, one proceeds by first assuming that $A_{km} = 0$ for $m > p$, where p is a convenient integer, and then evaluating D_k and A_{km}, $m = 1, 2 \cdots p$ Next, one assumes that $A_{km} = 0$ for $m > p + 1$, resolves for D_k and the A_{km}, and the accuracy of the results is judged by the agreement between the values in successive approximations. The direct solution of equations (30) and (28) is, however, a laborious process which rapidly increases in complexity as p exceeds about 4. The following iterative procedure has been found effective and of the same intrinsic simplicity for any value of p.

To begin with, the p equations in equation (28), being homogeneous, do not determine the absolute values of all the A_{km} but merely the ratios of $(p - 1)$

of them to a p-th one. The absolute values are then determined from the normalization condition

$$\int_0^\infty U_k{}^2(z)\,dz = 1 = \sum_{m=1}^\infty A_{km}{}^2 . \tag{7}$$

Let therefore

$$C_{km} = \frac{A_{km}}{A_{kk}} , \quad C_{kk} = 1 , \tag{55}$$

and the p equations in equation (24) are just sufficient to determine the $(p-1)$ constants C_{km} and D_k. We divide the equations in (28) by A_{kk} and pick the k-th equation ($n = k$) to solve for D_k, while the other equations are used to solve for the C_{km}, as is illustrated in the scheme below for the particular case of $k = 1$.

$$\frac{D_1}{\alpha} = \frac{D_1{}^0}{\alpha} - \beta_{11} - C_{12}\beta_{12} - C_{13}\beta_{13} - \cdots , \tag{56}$$

$$\left(\frac{D_1}{\alpha} - \frac{D_2{}^0}{\alpha} + \beta_{22}\right) C_{12}$$
$$= -\beta_{12} - C_{13}\beta_{23} - C_{14}\beta_{24} - \cdots , \tag{57}$$

$$\left(\frac{D_1}{\alpha} - \frac{D_3{}^0}{\alpha} + \beta_{33}\right) C_{13}$$
$$= -\beta_{13} - C_{12}\beta_{23} - C_{14}\beta_{34} - \cdots , \tag{58}$$

$$\left(\frac{D_1}{\alpha} - \frac{D_4{}^0}{\alpha} + \beta_{44}\right) C_{14}$$
$$= -\beta_{14} - C_{12}\beta_{24} - C_{13}\beta_{34} - \cdots . \tag{59}$$

As a first approximation one puts

$$\frac{D_1}{\alpha} = \frac{D_1{}^0}{\alpha} - \beta_{11} , \tag{60}$$

$$C_{12} = -\frac{\beta_{12}}{\left(\dfrac{D_1}{\alpha} - \dfrac{D_2{}^0}{\alpha} + \beta_{22}\right)} , \tag{61}$$

$$C_{13} = -\frac{\beta_{13}}{\left(\dfrac{D_1}{\alpha} - \dfrac{D_3{}^0}{\alpha} + \beta_{33}\right)} , \text{ etc. }, \tag{62}$$

where the value of D_1/α obtained from equation (60) is used in equations (61) and (62). Next, one substitutes these values of the C's in the right-hand sides of equations (56) to (59) and resolves for D_1/α and the C's. This procedure has been found to be rapidly convergent and is, furthermore, self-correcting in case of arithmetical errors.

EXPANSION OF D_k INTO A POWER SERIES IN α

When α is small, it is convenient to expand D_k

into the series

$$D_k = D_k{}^{(0)} + \alpha\,D_k{}^{(1)} + \alpha^2\,D_k{}^{(2)} + \cdots . \tag{63}$$

It is known from standard perturbation theory that

$$D_k{}^{(1)} = -{}_{\bullet}\beta_{kk} \,;\, D_k{}^{(2)} = e^{i\pi/3}\sum_m \frac{\beta_{mk}{}^2}{(\tau_m - \tau_k)} , \quad m \neq k . \tag{64}$$

It is possible also to derive an alternative expression for $D_k^{(2)}$:

$$D_k{}^{(2)}(\lambda) = \frac{1}{2}\lambda\,D_k{}^{(1)}(\lambda)^2 + \frac{1}{2\sqrt{\lambda}}\,e^{D_k{}^0\lambda + \frac{\lambda^3}{12}} \cdot$$

$$\int_0^\infty e^{-D_k{}^0 z - (z^3/12)} \cdot$$

$$\left[\left(1 + \frac{\lambda}{2x}\right) D_k{}^{(1)}(\lambda + x) + D_k{}^{(1)}(\lambda)\,D_k{}^{(1)}(x)\right]\sqrt{x}\,dx$$

$$= \lambda\,D_k{}^{(1)}(\lambda)^2 + \frac{1}{4\sqrt{\lambda}}\,e^{D_k{}^{(0)}\lambda + (\lambda^3/12)} \cdot$$

$$\int_0^\lambda\left[D_k{}^{(1)}(\lambda) + \left(2 + \frac{\lambda}{x}\right) D_k{}^{(1)}(\lambda + x)\right]\sqrt{x}\,dx . \tag{65}$$

Since the former expression is simpler for computational purposes, we shall not give here the derivation of equation (65).

APPLICABILITY OF PERTURBATION METHOD TO A MORE GENERAL CLASS OF M ANOMALIES

It is possible to apply the results obtained for the case when the M anomaly is of the form $f(z) = \alpha e^{-\lambda z}$ to more general types of M anomalies. To begin with, if

$$f(z) = \alpha e^{-\lambda z} + \gamma e^{-\mu z} , \tag{66}$$

then we merely write in equation (28) in place of $\alpha\beta_{nm}(\lambda)$, $[\alpha\beta_{nm}(\lambda) + \gamma\beta_{nm}(\mu)]$. Once the $\beta_{nm}(\lambda)$ are computed as functions of λ, there is no additional labor required to deal with an $f(z)$ which consists of a sum of any number of exponential terms. If instead of $f(z) = \alpha e^{-\lambda z}$ we had $f(z) = \alpha z e^{-\lambda z}$, then the corresponding $\beta'_{nm}(\lambda)$ would be

$$\beta'_{nm}(\lambda) = \int_0^\infty U_m{}^0(z)\,U_n{}^0(z)\,z e^{-\lambda z}\,dz = -\frac{d\beta_{nm}(\lambda)}{d\lambda} . \tag{67}$$

If $\beta_{nm}(\lambda)$ is known, $d\beta_{nm}(\lambda)/d\lambda$ can be computed directly from equation (43). When equation (43) is integrated numerically, the derivative $d\beta_{nm}(\lambda)/d\lambda$ is computed at each point in any case. Evidently, for $f(z) = \alpha z^k e^{-\lambda z}$, where k is a positive integer.

$$\beta'_{nm}(\lambda) = \int_0^\infty U_m{}^0(z)\,U_n{}^0(z)\,z^k e^{-\lambda z}\,dz$$

$$= (-)^k\,\frac{d^k\beta_{nm}(\lambda)}{d\lambda^k} . \tag{68}$$

By successive differentiation of equation (43), it is possible to express any high order derivative of $\beta_{nm}(\lambda)$ in terms of $\beta_{nm}(\lambda)$. From a purely formal point of view we can say therefore that by our method we can treat any M anomaly by expanding it into a series of Laguerre functions, since these functions involve only terms of the form $z^k e^{-\lambda z}$. It may be pointed out that a single term $z^k e^{-\lambda z}$ vanishes both at the ground and at great height and reaches a maximum at $z = k/\lambda$. Such a single term is therefore suitable to represent an elevated duct.

COMPUTATIONAL PROGRAM FOR THE EXPONENTIAL MODEL

The Analysis Section of the Columbia University Wave Propagation Group has undertaken the computation of $\beta_{nm}(\lambda)$ for $\lambda = 0(0.1)4.0$ and $n, m = 1, 2, 3, 4, 5$. With these functions tabulated, it is planned to compute the characteristic values D_k for such values of α and λ that the difference between the values of D_k obtained from the fourth order determinant and from the fifth order determinant will be only about 0.01. The program also calls for the computation of the height-gain functions from equation (2), since the coefficients A_{km} will be obtained simultaneously with the D_k when the iteration procedure is used. This will be possible only in a limited region of low altitudes, since at great heights the $U_m{}^0(z)$ increase rapidly in magnitude as m is increased. However, near the ground the $U_m{}^0(z)$ are all of the same order of magnitude ($= iz$) and

$$\frac{dU_k(0)}{dz} = i \sum_{m=1} A_{km}.$$ (69)

If this derivative of $U_k(z)$ at the ground can be obtained with sufficient accuracy, then one may use it to integrate numerically the original equation (11). It is well known that, for a given order of the determinant used, the characteristic values D_k are obtained with higher accuracy than the height-gain functions.

It may be added here that $\beta_{11}(\lambda)$ computed from equation (44) agrees up to $\lambda = 5.0$ with the values given by Pearcey and Tomlin.[106]

The perturbation method will of course become inefficient when trapping conditions are approached. For such values of α and λ, asymptotic methods may provide approximate values for the D_k, provided care is taken at each stage to estimate the order of magnitude of the error involved. It is planned to map out by a combination of these methods the real and imaginary parts of D_k in the operationally relevant region of the α, λ plane.

Symbols for Use in Theory of Nonstandard Propagation

$q =$ standard slope of N^2 curve $= 2.38 \cdot 10^{-7} \, m^{-1}$.

$p =$ slope of lower section of N^2 curve in bilinear model .

$\dfrac{p}{q} = s^2$.

$y = N^2 - 1 = 2M \cdot 10^{-6}$.

$z = (k^2 q)^{\frac{1}{3}} h = h/H$ height in natural units $(k = 2\pi/\lambda)$.

$H = (k^2 q)^{-\frac{1}{3}} = 7.24 \lambda_{cm}{}^{\frac{2}{3}}$ (feet) natural unit of height.

$x = 1/2 (kq^2)^{\frac{1}{3}} d = d/L$ distance in natural units .

$L = 2 (kq^2)^{-\frac{1}{3}} = 6.69 \lambda_{cm}{}^{\frac{1}{3}}$ (thousands of yards) $=$ natural unit of distance .

$h_a =$ anomaly height (height of joint in bilinear model) .

$g = h_a/H$ anomaly height in natural units .

$\Lambda_m =$ characteristic value (for $y = 0$ at $h = h_a$) .

$D_m = (k/q)^{\frac{1}{3}} \Lambda_m = B_m + iA_m$ characteristic value in natural units

$X = s^{-2} D$ (abbreviation for use in computing) .

$\Psi = e^{\underbrace{i\omega t - 2\pi i d/\lambda - i\pi/4}_{\text{plane wave}}} \cdot \underbrace{\dfrac{2\pi^{\frac{1}{2}}}{L}}_{\substack{\text{depends} \\ \text{on } \lambda}} \cdot$

$x^{-\frac{1}{2}} \underbrace{\sum_1^\infty e^{-A_m x + iB_m x}}_{} \cdot \underbrace{U_m(z_1) U_m(z_2)}_{}$

natural units only

$$\int_0^\infty U^2 \, dz = 1 .$$

$R =$ slant range .

$d =$ horizontal range .

FIRST ORDER ESTIMATION OF RADAR RANGES
OVER THE OPEN OCEAN*

THE MOST STRIKING nonstandard propagation conditions are for the most part associated with meteorological conditions which can exist only over those portions of the sea which are contiguous to extensive land masses. At large distances from the coasts, however, low ducts exist which, though they never produce strongly locked modes at the usual radar frequencies, nevertheless modify radar ranges. The problem of the low duct has the great advantage that conditions are sufficiently near standard that numerical solutions can be found in convenient form by an extension of the perturbation methods of wave mechanics.

At appreciable distances from land the temperature of the air is essentially that of the sea, and the air is in neutral equilibrium. Montgomery has pointed out that under these conditions there is much evidence to support a logarithmic distribution of specific humidity.

The logarithmic distribution of water vapor leads to an M curve given by

$$M - M_0 = \frac{3}{4} \cdot 10^6 \left(\frac{d}{a}\right)\left[\frac{z}{d} - \ln \frac{z}{d}\right]$$

where d is the duct thickness, z is the height coordinate, and a is the radius of the earth. If we plot the function in the brackets, we obtain the dashed curve of Figure 1.

This type of M distribution is inconvenient because (a) the logarithmic term which represents the modification does not approach zero as the height increases as a modification term should; and (b) $\ln(z/d)$ becomes infinite when $z = 0$. Accordingly it is proposed to replace the function in the brackets by the first two terms of its series expansion about the minimum. This amounts to substituting for the logarithmic curve a parabolic curve which has the same minimum point and the same radius of curvature at the minimum point as the original distribution. At twice the duct height the parabola has a standard slope, and it is continued from that point upward as a straight line of this slope (AB in Figure 1).

The modification term is now represented entirely by the departure of the parabola from the line AB, i.e.,

$$M - M_0 = \frac{3}{4}10^6\frac{d}{a}\left[1 + \frac{1}{2}\left(\frac{z}{d} - 1\right)^2\right], \quad 0 \leq \frac{z}{d} \leq 2$$

$$M - M_0 = \frac{3}{4}10^6\frac{d}{a}\frac{z}{d}, \qquad 2 \leq \frac{z}{d}.$$

*By J. E. Freehafer, Radiation Laboratory, MIT.

When the duct is low, the modes leak and are not far different from the standard ones. Thus it seems
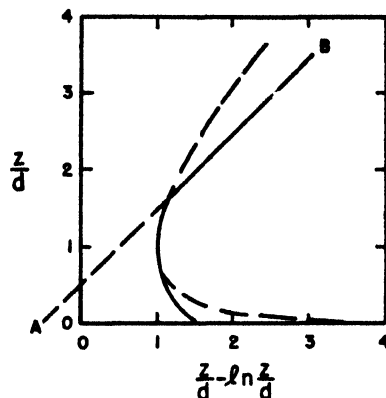
FIGURE 1. Schematic M curve for ground-based duct.

reasonable to employ the well-known methods of perturbation theory for calculating the characteristic values and functions of the parabolic atmosphere in terms of departures from standard.

If we brush aside mathematical questions of a delicate nature, it is possible to obtain an approximation for the characteristic values which leads to the following expression for the fractional change in the attenuation constant (i.e., the real part of γ_m)

$$\frac{\text{Re}(\bar{\gamma}_m) - \text{Re}(\gamma_m)}{\text{Re}(\bar{\gamma}_m)}$$

$$= \frac{-\int_0^\delta (\zeta - \delta)\,\text{Im}\,[h_2{}^2\,(\zeta + e_m)]\,d\zeta}{\delta\,[h_2{}'\,(e_m)]^2\,\text{Im}\,(e_m)} = \frac{\delta^6}{315} + .$$

Here, Re and Im designate the real and imaginary parts, and

$$\delta = \frac{2d}{L}.$$

L is an abbreviation for $(a\lambda^2/6\pi^2)^{\frac{1}{3}}$ and is equal to 33 ft for $\lambda = 10$ cm,

$\bar{\gamma}_m$ is the characteristic value for the standard case,

γ_m is the characteristic value for the parabolic case,

$h_2(z)$ is $\left(\frac{2}{3}\right)^{\frac{1}{3}} z^{\frac{1}{2}} H_{\frac{1}{3}}{}^{(2)}\left(\frac{2}{3}z^{\frac{3}{2}}\right)$,

$H_{\frac{1}{3}}{}^{(2)}$ is the Hankel function of second kind, order $\frac{1}{3}$, of the argument $\left(\frac{2}{3}z^{\frac{3}{2}}\right)$,

e_m's are roots of $h_2(\zeta) = 0$.

The expression above has been evaluated for the

first mode by summing the series for h_2 and performing the integration numerically. This curve is remarkable for the considerable interval in which the ordinate is practically zero. The attenuation constant differs by less than 1 per cent from the standard for ducts below $\delta = 1.2$. Beyond this value the effect of the duct increases rapidly, and when $\delta = 1.7$ the attenuation constant is 10 per cent different from standard, and at $\delta = 2$ it is 20 per cent different.

It seems that at least for radar purposes the condition $\delta \leq 1$ is a reasonable and convenient condition for defining a negligible duct. This is equivalent to saying that $L/2$ is the thickness below which a duct may for practical purposes be disregarded. For instance, at $\lambda = 10$ cm, $L = 33$ ft, and hence we conclude that the effect of ducts less than 16 ft in thickness on 10-cm radars may be neglected. On the other hand, if the wavelength is 3 m, $L = 300$ ft, and ducts below 150 ft in thickness are negligible.

If in the interest of simplicity we neglect the effect of small variations in the characteristic values on the characteristic functions, the fractional change in attenuation constant is also equal to the fractional change in the range against surface targets. It follows that the estimation of range can be reduced to a measurement of sea temperature and specific humidity at masthead level; for the duct thickness d under conditions of neutral equilibrium is given by

$$ d = - \frac{(q_s - q_a)\, \Gamma}{\left(\dfrac{dq}{dz}\right)_0} . $$

q_s is the saturation specific humidity at sea temperature and q_a the specific humidity at masthead. Γ is a parameter for which a representative value is 0.08, and $(dq/dz)_0$ is the gradient of specific humidity required to give zero M gradient under conditions of constant potential temperature. It is taken as $\frac{1}{2}$ g per kg.

Thus it turns out that

$$ \delta = 0.32 \frac{q_s - q_a}{L} $$

where $\dfrac{q_s - q_a}{L}$ is in grams per kg per 100 ft .

If L is given the appropriate value for $\lambda = 10$ cm

$$ \delta \cong q_s - q_a \text{ (g per kg)} . $$

For illustrative purposes, scales of $(q_s - q_a)/L$ and $q_s - q_a$ for $\lambda = 10$ cm have been added in Figure 2.
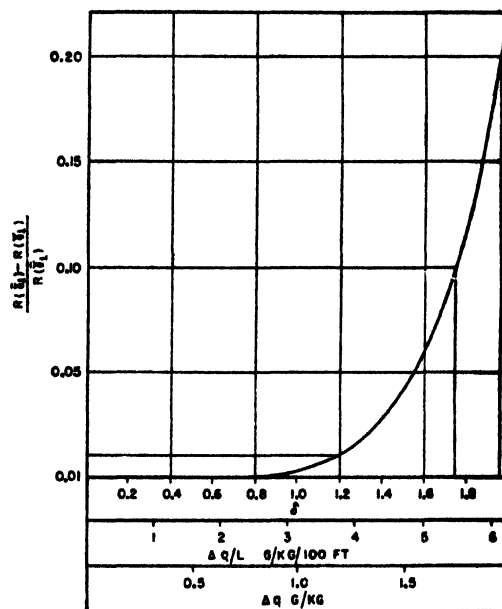
FIGURE 2. Fractional drop in attenuation constant of the first mode versus duct thickness. Bottom scale for Δq and $\Delta q/L$ corresponds to $\lambda = 10$ cm.

It is emphasized that the calculations are rough and are presented only in the belief that some sort of simple guiding principle may be more useful than a highly accurate and cumbersome formula. The results given are accurate out to variations in range of 1 per cent, and the determination of threshold thickness is completely reliable. Extension beyond $\delta = 1.2$ is a definite extrapolation. The trend indicating that the increase in range goes up at least as fast as the sixth power of the duct thickness for $\delta > 1$ is, we believe, real.

CONVERGENCE EFFECTS IN REFLECTIONS FROM TROPOSPHERIC LAYERS*

AN ELEVATED DUCT may be treated as a concave spherical mirror whose radius of curvature is a, the *effective* earth radius. This includes any layer that can act as a reflector to radiation incident at a sufficiently small angle. The problem is here considered as one of geometrical optics only. Ray tracing methods are used, and the phases are assumed to add randomly. This assumption may introduce an error as large as 3 db in the result but is necessary to simplify the solution of the problem. If the reflection' coefficient is other than unity, it must be multiplied into the general relation which will be given for $C = KLM$ the net convergence factor.

CONVERGENCE FACTOR

A bundle of rays leaving a transmitter below the reflecting layer is converged on reflection from a concave surface. The convergence factor K is the ratio of the power density at the receiving antenna after convergence to the power density at the receiver that would be expected after reflection from a plane surface (essentially free space condition). Referring to Figure 1, the convergence factor can be expressed as

$$K = \frac{(x + y)\,\delta\theta_1}{x\delta\theta_1 + y\delta\theta_2},\qquad(1)$$

or

$$K = \left(1 - \frac{2xy}{aR \sin\phi}\right)^{-1}\qquad(2)$$

where x = distance from transmitter to point of reflection,
  y = distance from receiver to point of reflection,
  $R = x + y$ = total range,
  a = *effective* earth's radius (usually 4,590 nautical miles),
  ϕ = angle of incidence of radiation at reflection,

other angles as shown on Figure 1.
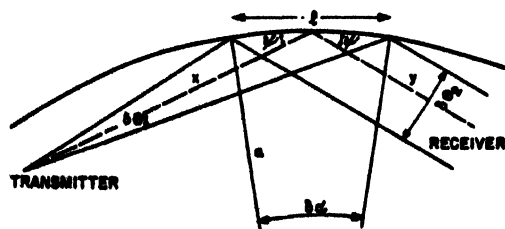
FIGURE 1. Convergence factor K.

Equation (2) can be deduced from equation (1) by remembering that

$$l = ad\alpha = \frac{x\delta\theta_1}{\sin\phi},\qquad(3)$$

and

$$\delta\theta_1 - \delta\theta_2 = 2d\alpha = \frac{2x\delta\theta_1}{a\sin\phi}.$$

The form shown in equation (2) is the more useful and is similar to the divergence factor for reflection at a convex surface that has been in use for some time. Equation (2) shows that K can grow quite large and even become infinite for certain conditions. Curve 1, Figure 2, shows a plot of the absolute value
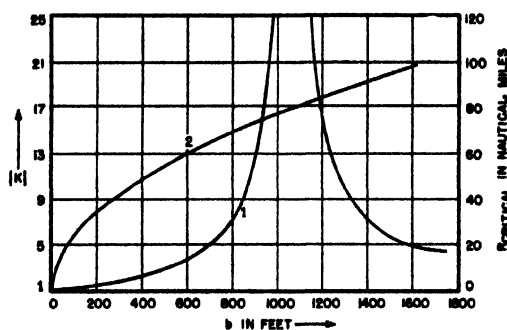
FIGURE 2. Value of K for height of layer (b in ft) versus range (nautical miles).

of K as a function of b, the height of the layer above the antennas, for a total range of 80 nautical miles. This plot also assumes $x = y = 40$ miles, which is a necessary condition for a smooth reflector. In this case, K becomes infinite for a layer 1,100 ft above the antennas. Curve 2, Figure 2, shows a plot of the layer height b necessary to give infinite convergence as a function of the range (plotted on right-hand scale).

ROUGHNESS EFFECT

The most apparent difficulty with the picture presented so far is that the layers actually are not perfectly smooth. In order to take that fact into consideration, it was assumed that the layer was composed of a large number of plates set at various small angles about the horizontal according to a Gaussian distribution. As in other parts of this

*By Ensign W. W. Carter, USNR Radio Division, Consultant Group.

problem, variations are considered only in the plane of transmission, since the effect of sideways deviation would cancel out. This reduces the problem to one of two dimensions only. Each plate is further assumed to retain its original curvature.

A beam falling on a patch of these plates would be reflected in such a way as to spread the energy at the receiver in a vertical pattern similar to the Gaussian distribution of the plates. It is only necessary to integrate this curve over the width of the antenna to find the fraction, L, of the total energy that will be useful. L will be a function of the probable value of the deviation of the plates, the range, and the antenna width.

With the rough layer assumption, there will be some plates correctly oriented at each part of the layer to reflect energy into the receiver. Therefore, a third factor, M, must be included that is the ratio of γ/β, where γ is the total angle subtended by the layer that can reflect rays to the receiver. γ would be limited by the optical horizons. β is the angle subtended by the receiving antenna when reflection is from a plane surface; i.e., essentially, free space conditions.

The net convergence factor C must be the product of these three quantities K, L, M. In this case, K must be the mean value of K averaged for various points of reflection. In order to integrate the expression for the mean value of K, it is necessary to substitute for $\sin \phi$ in equation (2).

$$\sin \phi = \left(\frac{b}{x} + \frac{x}{2a} + \frac{b}{y} + \frac{y}{2a} \right), \qquad (5)$$

which gives

$$K = \left[1 - \frac{8\,(xy)^2}{R^2\,(2ab + xy)} \right]^{-1} \qquad (6)$$

This expression is easily integrated if the product xy is used for the variable and $x_1 y_1 = x_1(R - x_1)$.

Example. The preceding developments have been applied to the one-way link of the U. S. Navy Radio and Sound Laboratory at San Diego, which has been extensively studied. High subsidence layers are common for this region. The probable value of the deviation of a reflecting plate from horizontal was taken as 0.1° as an engineering approximation. In this case, C equals 43, assuming a reflection coefficient of 1. If the reflection coefficient is not unity, its value as a function of angle of incidence must be multiplied into the equation.

Since K, L, and M can each vary through considerable limits, C can vary through a very wide range of values.

CONCLUSIONS

The statistical treatment of the roughness is not always applicable, since a finite number of plates would actually be engaged in reflecting energy. Hence, the received signal would vary almost randomly with time as the orientation of the plates changed slightly. This could produce marked fading and peaks of large amplitude. Primarily, however, it would explain signals of the magnitude of free space signals or higher.

RADIO WAVE PROPAGATION

EXPERIMENTS

VOLUME II

PART I

METEOROLOGY

Chapter 1

METEOROLOGY—THEORY[a]

MODIFICATION OF WARM AIR BY A COLD WATER SURFACE[b]

Two of the commonest types of M curves which produce nonstandard propagation are the S-shaped curve and the simple trapping curve where M decreases from the surface to 200 ft, say. The S-shaped curve occurs in regions of subsidence, for example, in the extensive subtropical anticyclones. The forecasting of this phenomenon will not be presented in this discussion which is confined to the simple trapping case.

During 1943 the question arose regarding the feasibility of forecasting the change in the temperature and vapor pressure distribution as warm air flows over a cold water surface. Through practice, considerable success had already been obtained in forecasting the M curve a few miles offshore in Boston Harbor. However, it was suggested that a general method be devised whereby the M curve could be predicted for greater distances from the shoreline and for different regions of the world. In order to solve this forecast problem the Boston Harbor soundings were investigated in the light of turbulence theory.

Two factors had to be kept in mind, namely:

1. The Boston Harbor soundings of temperature and vapor pressure were scant. A more serious difficulty was the total absence of data at distances in excess of 15 miles from the land.

2. Since forecasting techniques were the primary aim it was necessary to find a solution which was suitable for field use.

Diffusion Equation

The differential equation for turbulent mass exchange may be written

$$\frac{\partial T}{\partial t} = \frac{\partial}{\partial z}\left(K \frac{\partial T}{\partial z}\right). \tag{1}$$

If K, the coefficient of eddy diffusion, is assumed con-

stant, then

$$\frac{T' - T}{T_0 - T_w} = E\left(\frac{z}{\sqrt{4Kt}}\right) - 1, \tag{2}$$

where E = error function, that is,

$$E(\xi) = \frac{2}{\sqrt{\pi}} \int_0^\xi e^{-x^2} dx,$$

T' = temperature at a level z over the ocean,
T = initial temperature at z over the land,
T_0 = initial air temperature over land at $z = 0$,
T_w = water temperature,
t = time.

Values of K were then computed from the observational data by evaluating the ratio $(T'-T)/(T_0-T_w)$ for different evaluations and different times. These values were averaged for each level and the results shown in Table 1 were obtained. After plotting K

TABLE 1. Values of K.

Elevation in ft	20	50	100	200	300
K	0.014×10^4	0.07×10^4	0.18×10^4	0.38×10^4	0.67×10^4

against elevation, the approximate linear variation of K was extrapolated to give values of K for elevations up to 700 ft. This level of 700 ft lies well within the limit of 250 m which was indicated by Mildner[1] to be the level where K reaches its maximum.

These values of K were then used to construct Table 2, which gives $(T'-T)/(T_0-T_w)$ for all levels in terms of the time that the air has been over the water. The same values of K were obtained from the analysis of vapor pressure changes; hence the same table can be used to evaluate the ratio $(e'-e)/(e_0-e_w)$. From this table it is a simple matter to reconstruct the M curve at any distance over the ocean, provided the initial state of the air is known. An example of the changes in the M curve are given in Figure 1.

Discussion of Procedure

Summarizing the favorable aspects of this study, it can be stated that:

1. The values of K were almost identical for vapor

---

pressure and temperature changes. This suggests that the data were reliable.

2. The values of K agreed with those of Giblett[2] for wind variations from the surface to 150 ft.

3. This extrapolation method, that is, the error function extrapolation, gives reasonable values after a long period of time. A check was made by comparing Taylor's data off Newfoundland with computed values. This check was quite good.

4. The procedure is simple, and consequently the weather officer could readily calculate the M curve.

However, the entire method may be criticized because:

1. In the integration of the diffusion equation K is assumed constant while in the application of the in-

FIGURE 1. Changes in M curves resulting from modification of warm, dry air over cool, moist surface. Zero time corresponds to the coast line; ¼ hr, ½ hr, etc., refer to the time the air has been over water.

tegrated formula K was found to vary with elevation. The values of K which were used in the final analysis are therefore "effective values."

2. K has been considered to be independent of the degree of roughness (probably a justifiable assumption over the ocean), the degree of stability, and the wind velocity. These factors were neglected solely because the scant data did not allow a complete analysis of the variation of K.

These "effective values" should give some indication of the true variation of K. They suggest that K varies

linearly with elevation except for a quite rapid increase in about the first 30 ft. Consequently it seems reasonable to assume that

$$\frac{\partial T}{\partial t} = \frac{\partial}{\partial z}\left[(pz + q)\frac{\partial T}{\partial z}\right].$$

If $K = pz + q$ then, from the statement that $K(\delta u/\delta z) = $ constant (eddy stress does not vary with height), the velocity variation with elevation is given by

$$u = a\log(z + b) + C.$$

The question now arises: In the laminar layer, is the wind variation with height represented by a logarithmic law?

Previous Investigations

For many years research workers have studied the wind variation near the ground. A few of the conclusions will now be presented.

1. In 1932, Sutton[3] assumed a certain form of the coefficient of correlation between the velocities of the air particles considered at time t and at an interval of time later. This assumption implied that there was a power law for the variation of wind with height.

$$\frac{u}{u_1} = \left(\frac{z}{z_1}\right)^m \qquad m = \frac{n}{2 - n}.$$

2. In 1933, Cardington and Giblett[2] analyzed an extensive series of observations at 4 ft and 143 ft. Of course with only two points the observations could be made to fit either a power law or a logarithmic law. If a power law held, then m is a function of the degree of stability and wind velocity. If a logarithmic law held, then K is a function of these same quantities.

3. In 1934, Best[4] analyzed data which was measured at seven elevations between 2 cm and 5 m. He concluded that the velocity variation was best represented by a logarithmic function of the form

$$u \backsim \log(z - C)$$

where C is a constant.

Furthermore he found that the power law could be

TABLE 2. Values of $(T' - T)/(T_0 - T_w)$ or $(e' - e)/(e_0 - e_w)$; initially $T_0 > T_w$, $e_0 < e_w$.

Elevation in ft	Time in hours											
	¼	½	¾	1	1½	2	3	4	6	10	15	20
0	1.0	1.0	1.0	1.0	1.0	1.0	1.0	1.0	1.0	1.0	1.0	1.0
20	0.23	0.40	0.49	0.55	0.63	0.67	0.73	0.77	0.81	0.85	0.88	0.89
50	0.17	0.34	0.43	0.50	0.58	0.63	0.69	0.73	0.78	0.83	0.86	0.88
100	0.09	0.23	0.33	0.40	0.49	0.55	0.63	0.67	0.73	0.79	0.83	0.85
150	0.04	0.15	0.24	0.31	0.41	0.48	0.56	0.61	0.67	0.74	0.80	0.82
200	0.02	0.10	0.19	0.25	0.35	0.42	0.51	0.57	0.64	0.71	0.77	0.80
250	0.01	0.08	0.15	0.22	0.31	0.38	0.47	0.54	0.62	0.69	0.75	0.78
300	0.01	0.07	0.14	0.20	0.29	0.36	0.45	0.52	0.60	0.68	0.74	0.77
350	0.01	0.05	0.11	0.17	0.26	0.33	0.43	0.49	0.58	0.67	0.73	0.76
400	0.00	0.04	0.09	0.14	0.23	0.30	0.40	0.46	0.55	0.65	0.70	0.74
450	0.00	0.03	0.07	0.12	0.20	0.27	0.37	0.43	0.53	0.63	0.68	0.72
500	0.00	0.03	0.05	0.10	0.17	0.24	0.34	0.40	0.51	0.61	0.67	0.71
550	0.00	0.02	0.04	0.08	0.15	0.22	0.32	0.38	0.49	0.59	0.65	0.70
600	0.00	0.01	0.03	0.07	0.13	0.20	0.29	0.35	0.46	0.57	0.64	0.69
650	0.00	0.01	0.02	0.06	0.11	0.18	0.27	0.33	0.44	0.55	0.62	0.67
700	0.00	0.00	0.01	0.05	0.10	0.16	0.25	0.31	0.42	0.53	0.61	0.66

All values are negative.

applied only to shallow layers and even then m varies quite considerably with height, wind velocity, and vertical temperature gradient.

4. In 1936, Sutton,[5] who in 1932 suggested the power law variation, definitely favored the logarithmic variation. Furthermore he showed how one could handle the problem of varying stability. Sutton. analyzed different sets of data, ranging to 30 m in elevation, to support the logarithmic variation.

5. In 1936, Sverdrup[6] criticized Sutton's logarithmic law and favored a power law in regions of stability. As evidence he introduced Rossby and Montgomery's[7] analysis as well as his own data.

6. In 1937, Sutton[8] quite satisfactorily met Sverdrup's criticism and pointed out that all experimental evidence suggested the logarithmic variation rather than the power law variation.

This represents only a cross section of opinion and perhaps may be summarized as follows:

1. In an indifferent or unstable atmosphere the logarithmic law is generally accepted.

2. In a stable atmosphere there is more support for the logarithmic law than for the power law.

One writer summarized the situation very aptly when he said that all modern mathematical studies on atmospheric turbulence are inexact and depend on certain wide assumptions.

Conclusion

The question now arises, should one assume a power law variation, or is the true wind variation better represented by a logarithmic law? Certainly the experimental evidence tends to favor a logarithmic variation. The advantages and disadvantages of either assumption may be summarized briefly as follows:

1. Power law variation.
   a. m varies with stability, wind velocity, roughness, and elevation.
   b. The mathematical analysis is too complicated for practical use.

2. Logarithmic law variation.
   a. Agrees reasonably well with experimental data.
   b. Agrees with von Kármán's logarithmic law. von Kármán has shown that this law covers an exceedingly wide range of turbulence.
   c. K, like m, varies with stability, wind velocity, roughness, and elevation.
   d. If the logarithmic law holds, K is then a linear function of height. With this relatively simple expression for K it should be much easier to handle the diffusion equation than in the case of a power law variation.
   e. Provided the integration of the diffusion equation is not too complicated, one should be able to reconstruct the temperature and vapor pressure curves. Consequently the exact shape of the M curve can be calculated.

In conclusion it should be borne in mind that theoretical discussion is futile. At best we can only make certain assumptions and derive a result. If this result agrees with observational data then the original assumptions are justified. Furthermore, practical considerations demand that the final solution be simple enough for application in the field.

It seems certain that over a wide range of elevation, say 300 ft, the true wind variation cannot be uniquely defined by one specific logarithmic law or one specific power law. The most desirable procedure may then be an analysis of observations in as simple a manner as possible but yet flexible enough to take care of the most important changes. Consequently it is suggested that experimental data be analyzed on the assumption that K varies linearly with elevation, i.e.,

$$\frac{\partial T}{\partial t} = \frac{\partial}{\partial z}\left(K\frac{\partial T}{\partial z}\right) \quad \text{or} \quad u\frac{\partial T}{\partial x} = \frac{\partial}{\partial z}\left(K\frac{\partial T}{\partial z}\right),$$

where $K = pz + q$, and x is the distance measured horizontally. If accuracy is not seriously affected it is further suggested that approximations be introduced in order to facilitate the application of the results for field use.

DIFFICULTIES OF LOW-LEVEL DIFFUSION PROBLEMS[c]

The effect of a temperature inversion is largely a secondary one in that by reducing the coefficient of diffusion it favors the formation of large humidity gradients. The coefficient of diffusion K is calculated from the wind profile which is assumed to satisfy a power law of the form $U = Az^m$.

The difficulty arises because m is fixed once and for all before we solve the equation and thus the theory cannot take account of changes in the temperature gradients of a diurnal character in so far as they affect the humidity distribution. At the same time we believe that K is very sensitive to the temperature gradient.

Further, values of m have been used which have no meteorological support. The value $m = 0.5$, for example, implies a wind structure which is absurd if extended up to 100 m and it certainly is invalid near the ground. Chemical warfare technique measures m directly by measuring R, the ratio of the wind at 2 m to the wind at 1 m. Even in the very extreme conditions which prevail over land no value of R exceeding 1.35 is observed. This makes $m = 0.33$. Over the sea, even in a low layer, it is very unlikely that a value of m differing significantly from $\frac{1}{7}$ would be found.

The difficulty is that power laws apply only for very limited ranges of height and can be extended only by using a different power. Their only merit is that they enable the equation of diffusion to be solved; the

[c] By Lt. Comdr. F. L. Westwater, Naval Meteorological Service, Royal Navy.

power law is not a law of nature. A complete solution of the problem would involve a theory giving K as a function of temperature gradient. A start has been made on this for the case of still air which is agitated by thermal turbulence originating from heating on its lowest level. The value of K so calculated is small compared with that for a light wind. It seems likely that the effect of an inversion on K will also be small.

To sum up, radar personnel should be warned that the diffusion theory is at present in a highly unsatisfactory state; any conclusions drawn from it should be treated with the greatest reserve, and some calculations already published are based on assumptions which have no meteorological foundations.

PRELIMINARY RESULTS OF METEOROLOGICAL MEASUREMENTS IN MASSACHUSETTS BAY[d]

The modification produced in land air when it passes out over water is known to be particularly effective in producing nonstandard microwave propagation. The preliminary results of this study are covered in the present report; they are necessarily incomplete and tentative.

Modification of Air Flowing over Water

To begin with, some basic considerations will be presented. Figure 2 shows an airplane sounding in air which is warm and dry relative to the underlying water. Before leaving land the air was vertically homogeneous; that is, potential temperature and specific humidity were constant. This may be seen by comparing the observed temperature and vapor pressure with the broken straight lines drawn for

OCTOBER 19, 1944   1141-1203   C-231
5 MILES NORTH OF PROVINCETOWN, MASS
SURFACE WIND WEST 48

O FIRST ASCENT
• SECOND ASCENT
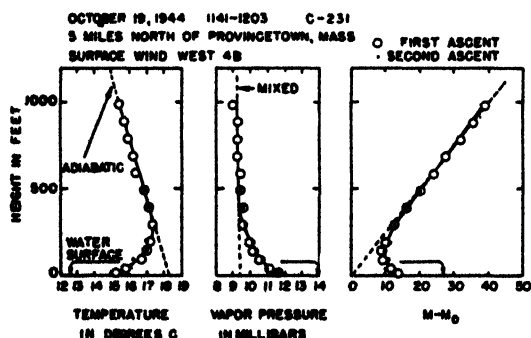
FIGURE 2. Typical airplane sounding, giving temperature and water vapor variation with height.

homogeneous air. The straight line of modified index of refraction M is constructed for homogeneous air; it is close to standard. The air is being modified by loss of heat to the water and by evaporation.

At the common boundary the temperatures of air and water are identical. The vapor pressure also is given by the water temperature; over sea water the

vapor pressure is 98 per cent of the saturation value corresponding to the water temperature. It follows that the modified index at the surface is determined by the water temperature alone.

Figure 2 illustrates in a striking manner the similarity in shape of the three curves. The ratio of the change from unmodified value at any height to the change at the surface is the same for all three quantities.

Modification of air over water is due largely to turbulent mixing, which transports heat and water vapor in exactly the same manner (the eddy diffusivity is identical for both). Next to the water boundary there is always a laminar layer, through which heat is transported to the turbulent layer by true conduction while the water vapor is transported by true diffusion; the coefficients for these two related processes happen to be nearly the same, so heat and water vapor are transported vertically to nearly the same relative degree. The temperature distribution is modified by radiation also, but for an initial period of a few hours this is unimportant compared with the processes just mentioned.

When initially homogeneous air flows over water of constant temperature, a necessary result is therefore that the curves of temperature and water vapor pressure are similar. Furthermore the M curve is similar also, because within the range of any sounding the modified index is approximately a linear function of temperature, vapor pressure, and height.

The extent of similarity revealed in Figure 2 is unusual. Often the three curves have very different shapes. In the latter case the deviation from similarity can be ascribed (1) to lack of homogeneity in the unmodified air, (2) to varying water temperature along the air's trajectory, or (3) to radiation during prolonged over-water modification.

The M Deficit

The distances on the base line from the straight broken line to the arrow are the temperature excess and humidity deficit respectively. There is obviously a corresponding quantity pertaining to index of refraction. The M deficit may be defined as the value of the modified index at the water surface less the representative surface value in the unmodified air.

Temperature excess, humidity deficit, and M deficit are related, so any two fully determine the difference between unmodified air and air at the water surface. The two of most direct significance are M deficit and temperature excess. Forecasting is simplified by their use: Temperature excess is necessary in drawing the temperature curve; similarity and M deficit then give the M curve directly. Another advantage in using M deficit is that whether it is positive, zero, or negative determines at once whether the modified air is probably characterized by an M inversion (layer where modified index of refraction decreases upward)

by standard, or by substandard M curves, respectively. For instance, the positive M deficit in Figure 2 is a condition necessary for the M inversion to occur.

Specifically, if homogeneous air blows over a water surface of constant temperature and if the M deficit is positive, there is always an M inversion at the water surface. Whether or not this extends sufficiently high to be of importance in the refraction of radio waves depends in part on the magnitude of the M deficit and on the temperature excess.

If homogeneous air blows over a water surface of constant temperature and if the M deficit is zero, the M curve necessarily remains practically standard.

In the case of a negative M deficit a substandard M curve is developed. It should be noted that in this case (as well as in the previous one) the air is losing water vapor by condensation on the water surface. This is simply the reverse of the process with dry air.

Neutral Equilibrium

For simplicity the analysis which follows is limited to cases of positive M deficit. There is then a surface M inversion, the height of which is a convenient quantity to study as a dependent variable. The independent ones are M deficit and temperature excess and, as will be seen, two others.

The first and least complicated case is the one of neutral equilibrium, which corresponds to a temperature excess close to zero, say within 1 C of zero. Since there is no appreciable temperature gradient, the M curve depends only on the moisture distribution. Furthermore this case practically requires a vapor-pressure lapse at the surface, because in the lower part of a homogeneous layer the vapor cannot be saturated (see Figure 3). Hence there is always an M inversion at the surface. Neutral equilibrium is prevalent far from shore.
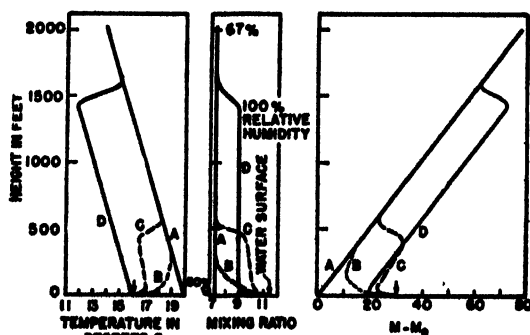
FIGURE 3. Probable course of modification of warm air over water under ideal conditions. A, initial stage. D, final stage.

With neutral equilibrium frictional turbulence is unhindered. Mixing extends to a height roughly proportional to the wind speed; a wind of 20 mph at 100 ft gives mixing up to about 2,000 ft.

The intensity of mixing increases upward rapidly

from the surface, so large vertical gradients are confined to the region of relatively little mixing close to the surface. The M inversion probably never extends above 100 ft.

It has been well established that under neutral equilibrium the eddy diffusivity is directly proportional to height within the so-called turbulent boundary layer, which forms the lower tenth of the entire frictional layer mentioned above. In this case wind speed, temperature, and vapor pressure are linear functions of the logarithm of elevation.

While the details are not presented here, it is easily shown that these logarithmic distributions demand that the height of the top of the M inversion be

$$d = \frac{4}{3} a \ \Gamma \Delta M \ 10^{-6},$$

where a is the radius of the earth, ΔM is the M deficit, and Γ is a meteorological parameter depending on wind speed alone in the case of complete neutral equilibrium. Thus the height of the M inversion is directly proportional to the M deficit with neutral equilibrium.

Published data indicate that the effect of wind speed is not great and give an average value of $\Gamma = 0.08$. This yields $d/\Delta M = 2$ ft. Data obtained during the summer's (1944) project agree with this result.

Unstable Equilibrium

The second case is the one of unstable equilibrium or negative temperature excess. This is similar to neutral equilibrium in that the M deficit is always positive and there is always a surface M inversion.

Instability adds convective mixing to the frictional mixing that would otherwise be present. This convective mixing is especially effective in the central region of the unstable layer and hence confines the large vertical gradients within a still thinner surface layer.

The logarithmic distributions are characteristic of neutral equilibrium only. Consequently, in the unstable cases the height of the M inversion is not simply proportional to M deficit but depends on M deficit in a more complicated manner. In spite of this the proportionality will be assumed as a useful approximation in studying the unstable and stable cases also.

The ratio of height of M inversion to M deficit is definitely less for unstable than for neutral equilibrium. Tentatively it may be said to range between 0.2 ft and 2 ft.

Stable Equilibrium

The last case is the one of stable equilibrium. Stability reduces the mixing with high levels, thus permitting a deeper surface layer of strong gradients to form (as shown in Figure 2). Thus the ratio of height of M inversion to M deficit may be expected to be always greater in stable equilibrium than in neutral equilibrium.

Stability reduces the mixing to such an extent that the air is progressively modified during a long over-water trajectory. It is therefore necessary to introduce a fourth independent variable, length of over-water trajectory, to supplement M deficit, temperature excess, and wind speed.

Under ideal conditions there is reason to believe that the modification would pursue the course sketched in Figure 3. The final state would be an essentially homogeneous layer capped by a temperature inversion at the level already mentioned for the top of the frictionally produced turbulence in neutral equilibrium. The temperature of the layer would follow an adiabatic lapse rate from the water surface to the top. The water vapor would be saturated at the top of the layer, specific humidity being nearly constant throughout the layer except for a strong lapse at the surface. Intermediate stages in the formation of this final state are indicated qualitatively in Figure 3.

It should be noted that the later stages have a transitional or S-shaped M curve and that qualitative theoretical considerations do not reveal which. The initial stage is, however, characterized by simple surface trapping, and it is this stage only for which data are presented below.

The soundings have been studied to determine empirically how the ratio of height of M inversion to M deficit depends on temperature excess, wind speed, and length of trajectory. To eliminate complex M curves the analysis has been limited to cases conforming closely to the following ideal conditions.

1. Initially homogeneous air.

2. Constant surface-water temperature along the air trajectory.

3. Constant wind (wind not changing with time following a parcel).

The ratio of height of M inversion to M deficit is found to increase with length of over-water trajectory quite markedly in the first 10 miles. From 10 miles to 30 miles there is not much further increase. Beyond 30 miles the preliminary analysis reveals no general information.

Figure 4 gives some tentative results based on various sources of information. This includes the cases of neutral and unstable equilibrium in addition to stable equilibrium. Within the stated range of over-water trajectory this diagram gives the height of the M inversion as a function of temperature excess, wind speed, and M deficit. A complete analysis of the observations will yield similar diagrams both more accurate and more detailed. These should prove of definite use in forecasting M curves.

In conclusion, it should be made clear that the work summarized in this report is a group undertaking. A large number of persons, some of them members of Radiation Laboratory Group 42 and other members of the U. S. Army Air Forces, took part in the
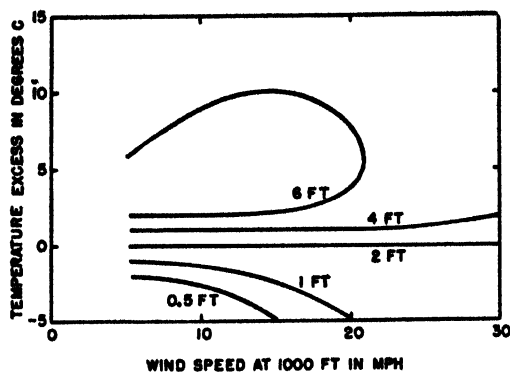
FIGURE 4. Ratio of height of M inversion to M deficit. For positive temperature excess the over-water trajectory is 10 to 30 miles.

development and construction of the instruments and in the observing.

METEOROLOGY OF THE SAN DIEGO TRANSMISSION EXPERIMENTS[*]

During the summer of 1944 a rather intensive experimental propagation program was carried on in San Diego area. The main purpose was to determine the distribution of radiated radio energy in the lower troposphere under the wide range of weather conditions prevailing during this season. A temperature inversion was present from around the first of June through October; the base of the inversion varying from the surface, on a few occasions, up to an altitude of some 4,000 ft. This inversion is characterized by dry superior air subsiding over moist maritime polar air.

Methods of Observation

The field strength data were taken in two ways. A fixed one-way link between San Pedro and San Diego gave continuous records on frequencies of 52, 100, and 547 megacycles, and vertical airplane sections taken at several different distances west of San Diego gave almost instantaneous records of the energy distribution for the same range of frequencies.

The meteorological data were obtained by the use of an airplane and wired sonde; the technique of the latter was described in detail in a previous report.[9] The captive balloon or wired sonde is a modified version of the Washington State College equipment.[10] Daily soundings were taken at the Scripps Pier at La Jolla, 11 miles north of the laboratory. Two 1-week periods of continuous shipboard soundings were made from a YP ship operating in the middle of the San Pedro to San Diego link.

The principal use of the airplane has been in taking vertical field strength sections seaward from the

_____

[*]By Lt. A. P. Stokes, U.S. Navy Radio and Sound Laboratory

laboratory. During these flights meteorological soundings were made as frequently as possible. The laboratory was fortunate in obtaining from the Washington State College group one of their original sonde units and has adapted this equipment for use in the airplane soundings. The temperature and humidity elements were mounted in an unobstructed aluminum housing approximately 1½ ft above the nose of the PBY-5A airplane.

Since the airplane served the dual purpose of obtaining both meteorological and field strength measurements, all the data were obtained on a fixed course.

Field strength sections were made in rapid descents and the meteorological data were obtained in ascents. Navigational difficulties prohibited spiraling for the meteorological data and therefore these soundings covered considerable horizontal distance. Due consideration of this was made in plotting the cross sections.

The San Diego High Inversion

In the summer season San Diego lies within the belt of the subtropical anticyclones, and, with the absence of surface frontal activity, a stagnant circula-
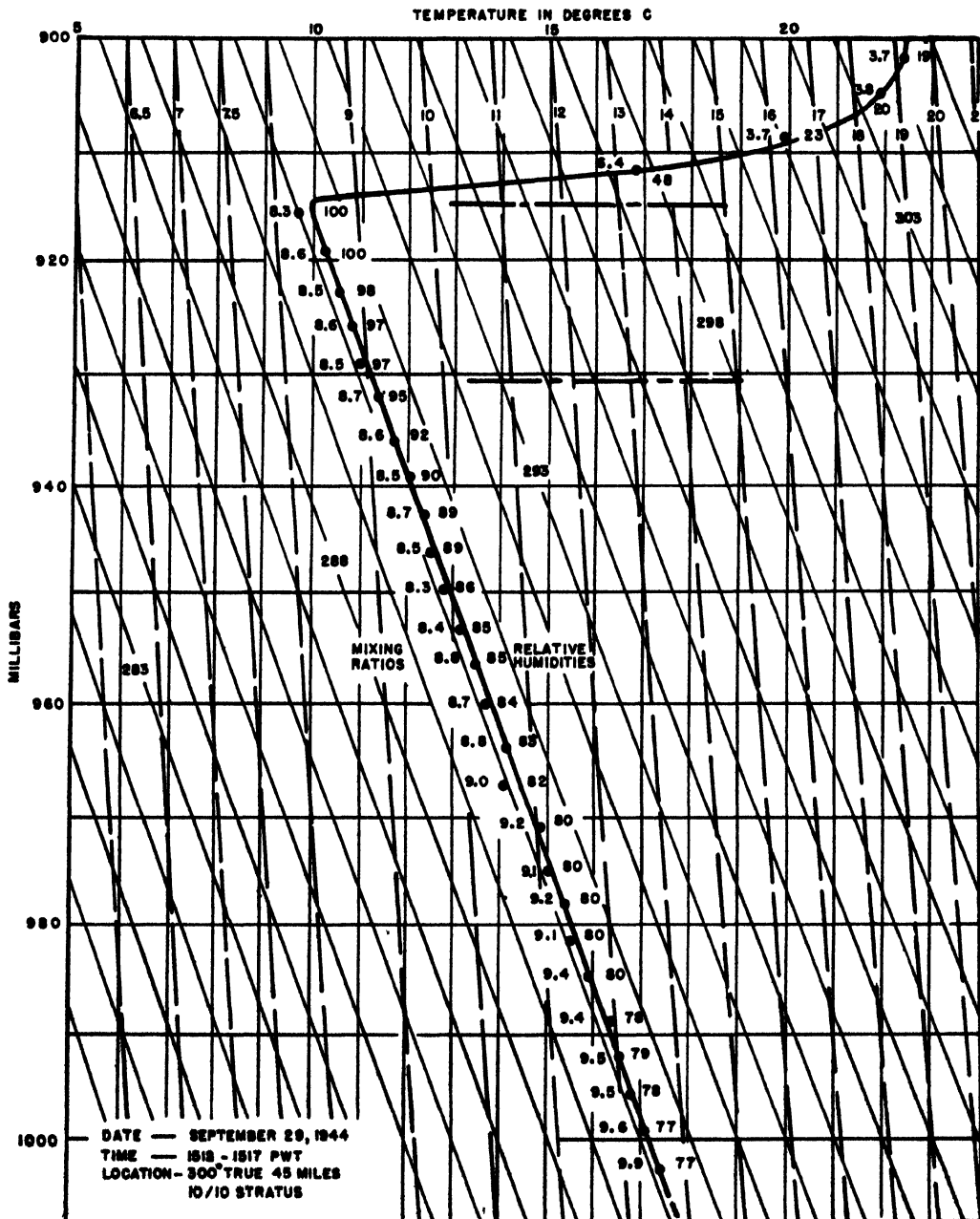
FIGURE 5. Structure of a moderately high inversion near San Diego.

tion exists. Because of the persistence of high-level anticyclonic circulation aloft, pronounced subsidence is maintained throughout this season; 1944, in particular, was characterized by very low humidity above the 2-km level. By subsidence aloft a thermal inversion exists over a large maritime area and thus forms the boundary between the lower maritime polar and the continental tropical or superior air aloft. Variation in height and magnitude of the inversion is the governing factor in daily weather phenomena. There exists a close correlation between the height of the base of the inversion, the pressure at 10,000 ft, and the lapse rate of temperature between the 5,000- and 10,000-ft levels. It is found that with the intensification of the pressure field aloft, the lapse rate of temperature approaches the dry adiabatic condition and thus, under these conditions, indicates increased subsidence. Consequently the depth of this marine structure is diminished by the lowering of the base of the inversion.

Figure 5 shows the typical structure of a moderately high inversion. Usually the lapse rate of temperature below the base approaches, and in some cases exceeds, the dry adiabatic condition. This vertical mixing insures a homogeneous air mass characterized by the constant vapor pressure in the marine stratum.

Figure 6 shows the typical elevated S type M curve for this condition.

The discontinuity surface between the two distinct air masses exists over a large area. Soundings have been confined within a 130-mile radius of the laboratory, but observations on an FC radar indicate trapping conditions existing between San Diego and Guadalupe Island 225 miles to the southwest.
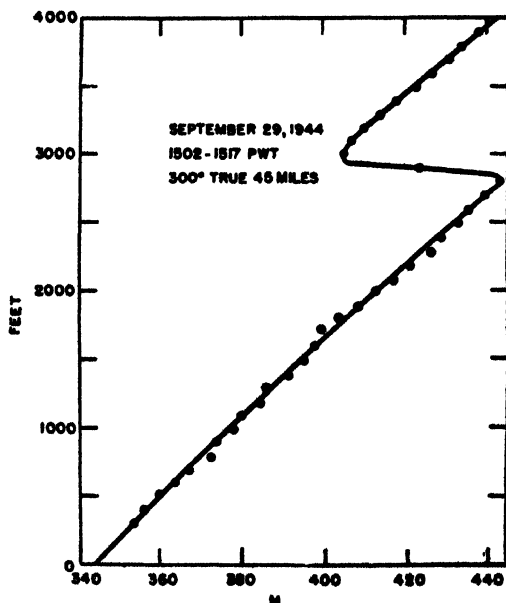
FIGURE 6. M curve corresponding to the inversion shown in Figure 5.

Shape of the Inversion Surface

Emphasis must be placed on the fact that, the discontinuity surface is not horizontal over the area but is at any time a warped surface. Figure 7 shows a series of M curves taken by airplane to the seaward of the laboratory. Both the height of the inversion and gradients in the transitional layer vary greatly
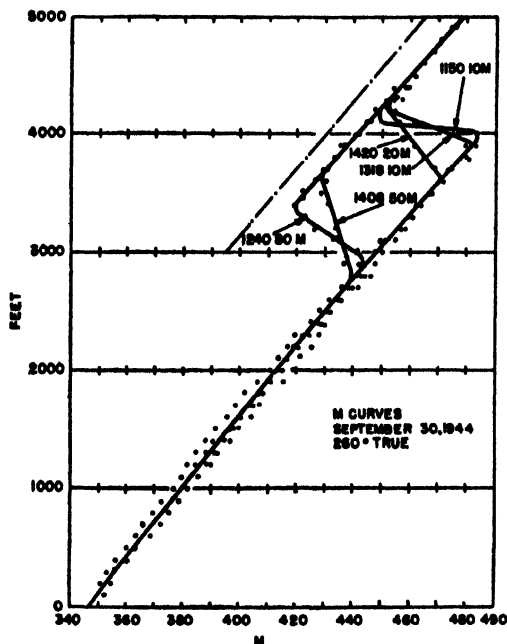
FIGURE 7. M curves at different distances and times.

with distance. Repeated soundings indicate that the apparent slope is not due to large scale lowering during the time interval between observations. The cluster of M values along the mean lapse rate of M in the upper and lower strata indicates the homogeneity of the two air masses along the vector. The possibility of the coexistence of elevated and surface gradients has been considered. No significant surface discontinuities have been detected.

There is a general tendency for the base of the inversion along the shore to have a maximum height at 0800 and a minimum at 1600. Through the exchange of meteorological data between the University of California at Los Angeles and the laboratory this fact is now fairly well established.

Figure 8 is a plot of refractive index from a series of plane soundings. The diagonal lines show the height and distance from the base at which measurements were made. Each line is marked with the time of beginning and ending the flight. The numbers at the ends of the curves are the refractive index $(n-1)$ multiplied by 10^6. The indices are independent of frequency for this range. Again it is noted that conditions vary along the vector.

Figure 9 is a plot of refractive index taken by airplane along the San Diego-San Pedro path, indicat-

FIGURE 8. Isopleths—refractive index $[(n-1)10^6]$.
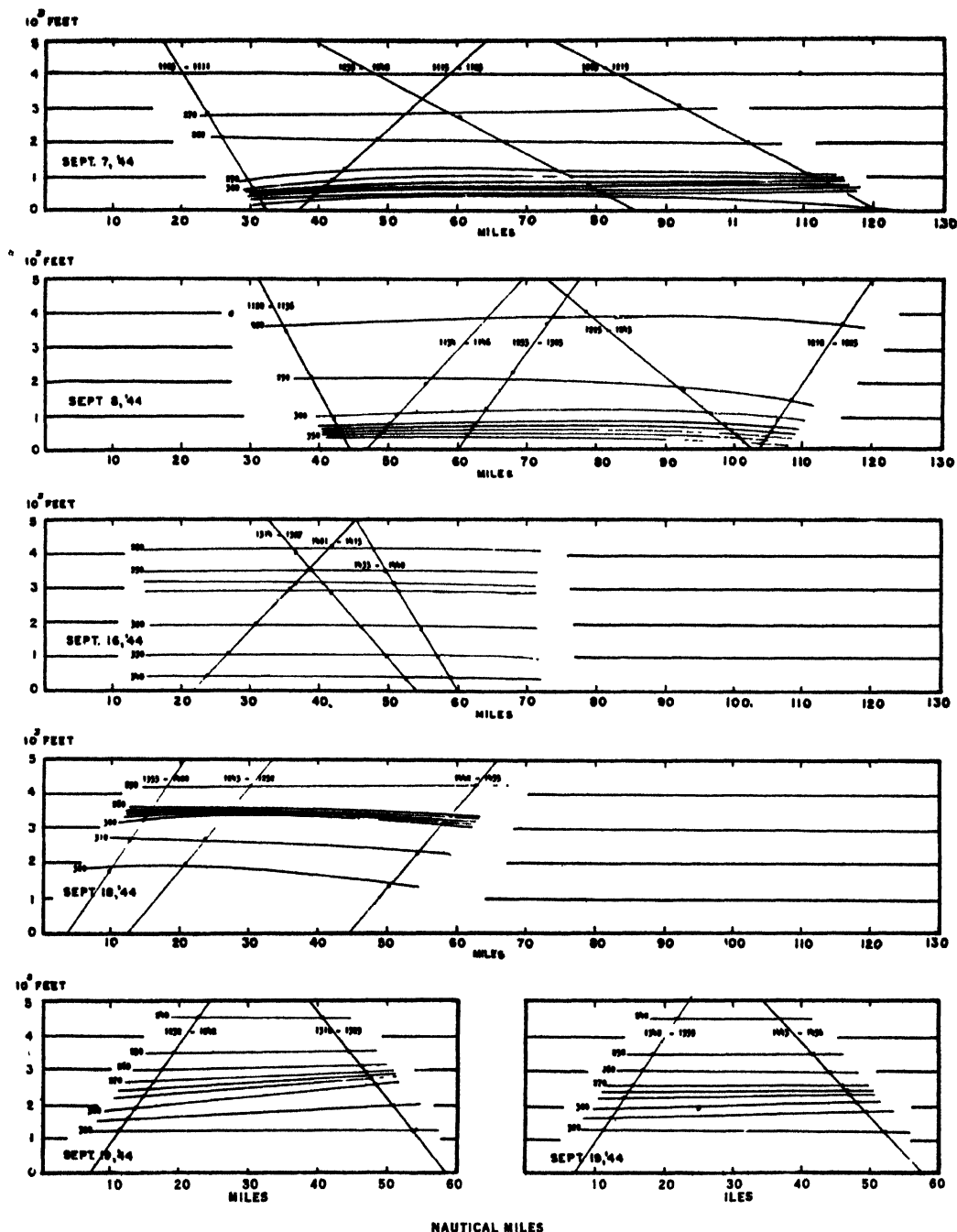
ing the magnitude and height of the strong gradients along the path. The time interval of each sounding is shown on the appropriate section.

Again it must be emphasized that the discontinuity takes the shape of a warped surface, that the gradients vary from point to point, and that the maximum air density change occurs in the region of maximum refractive index gradient. Interface waves in the density discontinuity are possibly superimposed on the already nonuniform structure. These small interface waves are evident by the undulations on the top surface of the stratus cloud deck. The top surface of the cloud deck, which is often present, marks the air mass boundary and is thus a good indicator of the base of the inversion.

It is therefore evident that meteorological observations required for a thorough study of propagation conditions must be as extensive as possible.

FEET
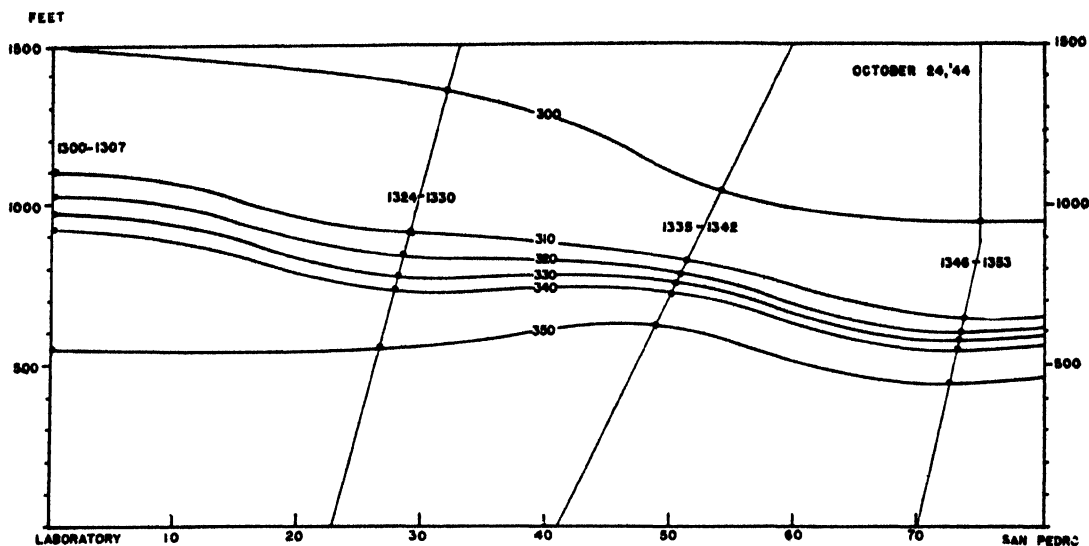
FIGURE 9. Curves of constant refractive index along the San Diego to San Pedro path.

TABLES FOR COMPUTING THE MODIFIED INDEX OF REFRACTION, M^t

Introduction

The index of refraction of the atmosphere, modified for use on a plane-earth diagram, is a quantity of great importance in the study of radio wave propagation. It is defined by

$$M = \left[(n-1) + \frac{h}{a} \right] 10^6, \qquad (1)$$

where n = ordinary index of refraction,

    h = height above sea level (not ground level),

    a = radius of the earth.

The equation for n is obtained from Debye's theory of the dielectric constant of gases. In terms of atmospheric quantities, equation (1) assumes the form

$$M = \frac{Ap}{T} - \frac{De}{T} + \frac{Be}{T^2} + Ch, \qquad (2)$$

where p = barometric pressure (in millibars)

    (1 mm Hg = 1.333 mb),

    e = water vapor pressure (mb)

    (e is of order of 1% of p),

    T = temperature in degrees Kelvin,

    $A = 79$, $B = 3.8 \times 10^5$, $C = 0.1570$, $D = 11$,

where h, the height above sea level, is measured in meters.

The constants A, B, and D have been selected to get

the best agreement with experimentally determined values of n. The constant C is 10^6 times the reciprocal of the earth's radius in meters. A more detailed explanation of this formula is given under "Constants of the Index of Refraction Formula"found on p. 219.

The formula (2) may be used to calculate M when p, T, and e are known functions of height. Nomograms have been prepared to facilitate such calculations. In this paper tables are presented which permit these calculations to be carried out quickly and accurately. M is a number of the order of 300 to 500. Physically, the important quantity is the slope of M, i.e., dM/dh. This often calls for calculating M at fairly close height intervals, 15 m or even less. The values of M at such heights may differ by only two or three M units. Hence, to obtain even two significant figures for this quantity, the M's must be computed to four significant figures, that is, to tenths of an M unit. It is with a view to this situation that tables were computed.

These tables fall into two groups, depending upon how the moisture in the atmosphere is evaluated. In the first group (Tables 3 to 7) the moisture is given in terms of relative humidity or vapor pressure; in the second (Tables 8 to 11) the mixing ratio is used.

Use of Tables

The following examples explain the mechanics of using these tables. The first two examples use the first group of tables: Tables 3 to 7 inclusive. The quantities H and G which appear in these examples are auxiliary functions which are fully explained in the appendix. Examples III and IV use Tables 8 to 11.

Example I

Relative humidity and temperature given.
$p_0'' = 1,000$ (p_0 is pressure at sea level).

h^* meters above sea level	$t°C$	RH%	$H^\dagger$	$G\Delta t^\ddagger$	$M_d^\S$	$M_w^\|$	$M_c^\P$	M^{**}
20	13	60	275.6	0.0	275.6	41.4	3.1	320.1
70	13	50	274.0	0.0	274.0	34.5	11.0	319.5
120	15	35	270.5	0.0	270.5	27.1	18.8	316.4
450	12	30	262.6	0.0	262.6	19.5	70.7	352.8
1,000	9	20	248.2	0.2	248.4	10.9	157.0	416.3
5,000	—20	20	159.0	7.0	166.0	1.2	785.0	952.2

*Columns for h (meters), $t°C$, and RH% give the experimentally determined data. (The heights are measured from sea level.)

†Column for H is read from Table 3.

‡$G\Delta t$ is obtained by multiplying values of G given in Table 4 by $\Delta t = t_0 - t$, where t_0 is the air temperature at ground level. Interpolation is unnecessary in this table. This correction may be omitted except where high accuracy is desired.

§M_d is the sum of H and $G\Delta t$. (If $p_0 \neq 1,000$ this column should be multiplied by $p_0/1,000$ to obtain the true M_d. This, however, is necessary only if p_0 differs appreciably from 1,000 mb, since only the difference of refractive index from its value at the ground is of importance and this difference is not sensitive to moderate changes of p_0.)

‖M_w is obtained from Table 5.

¶M_c is obtained from Table 7 or by multiplying the column for h by 0.1570.

**M is the sum of M_d, M_w and M_c.

††It should be noted that p_0 refers to the barometric pressure at sea level, not ground level. The difference in these quantities may be appreciable

Table 9, which gives pressure as a function of height and temperature, provides a simple method of calculating the sea level pressure from a measurement of the ground level pressure. For example, suppose the elevation of the ground above sea level is 100 m, the temperature is 15 C, and pressure at the ground is 993.0 mb. Table 9 shows for this height and temperature, $p/p_0 = 0.9882$. In this case, $p = 993.0$, and hence

$$p_0 = \frac{p}{0.9882} = \frac{993.0}{0.9882} = 1004.9.$$

Example II

Vapor pressure and temperature given.
$p_0 = 1,000$ mb at sea level.

h^* meters above sea level	t	e	$H^\dagger$	$G\Delta t^\ddagger$	$M_d^\S$	f	$M_w^\|$	$M_c^\P$	M^{**}
10	15.0	10.0	274.0	0.0	274.0	4.543	45.4	1.6	321.0
40	15.2	9.8	273.0	0.0	273.0	4.537	44.5	6.3	323.8
75	15.5	9.6	271.5	0.0	271.5	4.527	43.5	11.8	326.8
150	16.0	9.2	268.6	0.0	268.6	4.511	41.5	23.6	333.7
300	15.0	9.0	264.7	0.0	264.7	4.543	40.9	47.1	352.7
1,000	10.0	7.0	247.4	0.3	247.4	4.706	32.9	157.0	437.8

*Columns for h, t, and e are the given data. (The heights are measured from sea level.)

†Column for H is read from Table 3.

‡$G\Delta t$ is obtained by multiplying values of G given in Table 4 by $\Delta t = t_0 - t$, where $t_0 =$ temperature at ground level. Interpolation is unnecessary in this table.

§M_d is the sum of H and $G\Delta t$. [If $p_0 \neq 1,000$ this column should be multiplied by $p_0/1,000$ to obtain the true M_d. This correction may usually be omitted (see Note §, Example I).]

‖M_w is obtained by taking the product of f, given in Table 6, by e. A slide rule gives sufficiently close results here.

¶M_c is obtained from Table 7 or by multiplying the column for h by 0.1570.

**M is the sum of M_d, M_w, and M_c.

Example III

Mixing ratio w and temperature given.
$p_0 = 1,000$ mb at sea level.

h^* meters above sea level	t	w	$F^\dagger$	$p/p_0^\ddagger$	$(p/p_0)F^\S$	$M_c^\|$	$M^\P$
20	15	9	339.0	0.9976	338.2	3.1	341.3
40	16	8	330.6	0.9953	329.0	6.3	335.3
100	17	7	322.2	0.9882	318.4	15.7	334.1
150	17	7	322.2	0.9824	316.5	23.6	340.1
300	14	6	319.0	0.9650	307.8	47.1	354.9
500	11	4	307.9	0.9420	290.0	78.5	368.5

*Columns for h, t, and w are the assumed data. w is expressed in grams of water vapor per kg dry air.

†F is read directly from Table 8.

‡p is read from Table 9. In this table t means average temperature between ground and height h.

(If $p_0 \neq 1,000$ this result should be multiplied by $p_0/1,000$. This step may usually be omitted.)

§$(p/p_0)F$ is the product of the two previous columns.

‖M_c may be obtained from Table 7 or by multiplication of h by $C=0.1570$.

¶M is the sum of $(p/p_0)F$ and M_c.

Example IV

Mixing ratio and temperature given. Simplified method satisfactory for $h \leq 500$ m.**

h^* meters above sea level	t	w	$F^\dagger$	$u^\ddagger$	$\frac{h\Delta u^\S}{100}$	$(n-1)10^6\|$	$M_c^\P$	M
20	15	9	339.0	0.9	0.0	338.1	3.1	341.2
40	16	8	330.6	1.7	0.1	329.0	6.3	335.3
100	17	7	322.2	4.0	0.2	318.4	15.7	334.1
150	17	7	322.2	6.0	0.3	316.5	23.6	340.1
300	14	6	319.0	11.8	0.6	307.8	47.1	354.9
500	11	4	307.9	18.7	1.0	290.2	78.5	368.7

*Columns for h, t, and w are the assumed data. These data are the same as in Example III.

†F is read from Table 8, as before.

‡u is read from Table 10.

§Δu is read from Table 11. Δu is then to be multiplied by $h/100$ to give the column $h\Delta u/100$. t is the average centigrade temperature from ground to h.

‖The column $(n-1)10^6$ is given by $F - u + h\Delta u/100$. If the average temperature t is negative, this column is $F - u - (h\Delta u/100)$.

¶M_c is obtained, as before, from Table 7. M is the sum of $(n-1)10^6$ and M_c.

**This method is not accurate above 500 m. It will be noted, by comparing the results here with those of Example III, that there are occasional differences of 0.1 M units. This is due to rounding off and is not significant.

Procedure Used in Setting up Tables

TABLES 3 TO 7 — RELATIVE HUMIDITY AND TEMPERATURE GIVEN

Equation 2 may be written

$$M = M_d + M_w + M_c, \qquad (3)$$

where

$$M_d = \frac{Ap}{T}, \qquad (4)$$

$$M_w = fe, \qquad (5)$$

$$M_c = Ch, \qquad (6)$$

with

$$f = \frac{B}{T^2} - \frac{D}{T}. \qquad (7)$$

Tables have been prepared which give the quantities

M_d (dry term), M_w (wet term), and M_o (curvature term) separately.

Dry Term. Since equation (4) contains the pressure *p*, which is not usually measured as a function of height, it is necessary to eliminate direct consideration of *p*. For this purpose a simplification of the elaborate formula used in the Smithsonian tables for calculating height as a function of pressure is sufficient. This simplification neglects very small pressure effects caused by humidity variations and the change of the acceleration of gravity with height. This problem is discussed more fully in the section on pressure versus height, below. The pressure may then be written

$$p = p_0 e^{-ah/\bar{T}}, \qquad (8)$$

TABLE 3A.   H for t from −30 C (−22 F) to −20 C (−4 F); h to 2,000 m (6,562 ft).

p_0 = 1,000 mb at sea level

h (m)	−30	−29	−28	−27	−26	−25	−24	−23	−22	−21	−20	h (ft)
0	325.1	323.8	322.4	321.1	319.8	318.5	317.3	316.0	314.7	313.5	312.3	0.0
10	324.6	323.3	322.0	320.7	319.4	318.1	316.9	315.6	314.3	313.1	311.9	32.8
20	324.2	322.9	321.5	320.3	319.0	317.7	316.5	315.2	313.9	312.7	311.5	65.6
30	323.7	322.4	321.1	319.8	318.5	317.2	316.0	314.7	313.5	312.2	311.0	98.4
40	323.3	322.0	320.6	319.4	318.1	316.8	315.6	314.3	313.1	311.8	310.6	131.2
50	322.8	321.5	320.2	319.0	317.7	316.4	315.2	313.9	312.7	311.4	310.2	164.0
75	321.7	320.4	319.1	317.9	316.6	315.3	314.1	312.9	311.6	310.4	309.2	248.1
100	320.6	319.3	318.0	316.8	315.5	314.2	313.0	311.8	310.5	309.3	308.1	328.1
150	318.3	317.0	315.8	314.5	313.3	312.0	310.8	309.6	308.4	307.2	306.0	492.1
200	316.1	314.9	313.6	312.4	311.1	309.9	308.7	307.5	306.3	305.1	303.9	656.2
250	313.9	312.7	311.5	310.2	309.0	307.8	306.6	305.4	304.3	303.1	301.9	820.2
300	311.7	310.5	309.3	308.0	306.8	305.6	304.5	303.3	302.2	301.0	299.9	984.3
350	309.5	308.3	307.1	305.9	304.7	303.5	302.4	301.2	300.1	298.9	297.8	1,148.0
400	307.3	306.1	305.0	303.8	302.7	301.5	300.4	299.2	298.1	296.9	295.8	1,312.0
450	305.2	304.0	302.9	301.7	300.6	299.4	298.3	297.2	296.0	294.9	293.8	1,476.0
500	303.0	301.9	300.7	299.6	298.4	297.3	296.2	295.1	294.1	293.0	291.9	1,640.0
600	298.8	297.7	296.6	295.5	294.4	293.3	292.2	291.2	290.1	289.1	288.0	1,969.0
700	294.6	293.5	292.5	291.4	290.4	289.3	288.3	287.2	286.2	285.1	284.1	2,297.0
800	290.5	289.5	288.4	287.4	286.3	285.3	284.3	283.3	282.3	281.3	280.3	2,625.0
900	286.5	285.5	284.5	283.4	282.4	281.4	280.4	279.4	278.5	277.5	276.5	2,953.0
1,000	282.5	281.5	280.5	279.5	278.5	277.5	276.6	275.6	274.7	273.7	272.8	3,281.0
1,500	263.3	262.5	261.6	260.8	259.9	259.1	258.3	257.5	256.6	255.8	255.0	4,921.0
2,000	245.4	244.7	244.0	243.2	242.5	241.8	241.1	240.4	239.7	239.0	238.3	6,562.0
t F	−22.0	−20.2	−18.4	−16.6	−14.8	−13.0	−11.2	−9.40	−7.60	−5.80	−4.00	h (ft)

TABLE 3B.   H for t from −20 C (−4 F) to −10 C (+14 F); h to 2,000 m (6,562 ft).

p_0 = 1,000 mb at sea level

h (m)	−20	−19	−18	−17	−16	−15	−14	−13	−12	−11	−10	h (ft)
0	312.3	311.0	309.8	308.6	307.4	306.2	305.0	303.8	302.7	301.5	300.4	0.0
10	311.9	310.6	309.4	308.2	307.0	305.8	304.6	303.4	302.3	301.1	300.0	32.8
20	311.5	310.2	309.0	307.8	306.6	305.4	304.2	303.0	301.9	300.7	299.6	65.6
30	311.0	309.8	308.6	307.4	306.2	305.0	303.8	302.7	301.5	300.4	299.2	98.4
40	310.6	309.4	308.2	307.0	305.8	304.6	303.4	302.3	301.1	300.0	298.8	131.2
50	310.2	309.0	307.8	306.6	305.4	304.2	303.0	301.9	300.7	299.6	298.4	164.0
75	309.2	308.0	306.8	305.6	304.4	303.2	302.1	300.9	299.8	298.6	295.5	248.1
100	308.1	306.9	305.7	304.6	303.4	302.2	301.1	299.9	298.8	297.6	296.5	328.1
150	306.0	304.8	303.6	302.5	301.3	300.1	299.0	297.9	296.8	295.7	294.6	492.1
200	303.9	302.8	301.6	300.5	299.3	298.2	297.1	296.0	294.9	293.8	292.7	656.2
250	301.9	300.8	299.6	298.5	297.3	296.2	295.1	294.0	293.0	291.9	290.8	820.2
300	299.9	298.8	297.7	296.5	295.4	294.3	293.2	292.1	291.1	290.0	288.9	984.3
350	297.8	296.7	295.6	294.5	293.4	292.3	291.2	290.2	289.1	288.1	287.0	1,148.0
400	295.8	294.7	293.6	292.6	291.5	290.4	289.4	288.3	287.3	286.2	285.2	1,312.0
450	293.8	292.7	291.7	290.6	289.6	288.5	287.5	286.4	285.4	284.3	283.3	1,476.0
500	291.9	290.8	289.8	288.7	287.7	286.6	285.6	284.6	283.5	282.5	281.5	1,640.0
600	288.0	287.0	285.9	284.9	283.8	282.8	281.8	280.8	279.9	278.9	277.9	1,969.0
700	284.1	283.1	282.1	281.1	280.1	279.1	278.1	277.2	276.2	275.3	274.3	2,297.0
800	280.3	279.3	278.3	277.4	276.4	275.4	274.5	273.5	272.6	271.6	270.7	2,625.0
900	276.5	275.5	274.6	273.7	272.7	271.8	270.9	270.0	269.0	268.1	267.2	2,953.0
1,000	272.8	271.9	271.0	270.0	269.1	268.2	267.3	266.4	265.6	264.7	263.8	3,281.0
1,500	255.0	254.2	253.4	252.6	251.8	251.0	250.2	249.5	248.7	248.0	247.2	4,921.0
2,000	238.3	237.6	237.0	236.3	235.7	235.0	234.3	233.7	233.0	232.4	231.7	6,562.0
t F	−4.00	−2.20	−0.40	+1.40	+3.20	+5.00	+6.80	+8.60	+10.4	+12.2	+14.00	h (ft)

where

p_0 = barometric pressure at sea level,

ϵ = natural logarithmic base,

$\alpha = 0.034163$,

and

$$\overline{T} = \frac{1}{h}\int_0^h T(h)dh. \tag{9}$$

$\overline{T}$ is thus the average temperature from $h = 0$ to the

height h. Strictly, T should be calculated from equation (9). However, it turns out that p is rather insensitive to $\overline{T}$, and that, except perhaps where high accuracy is desired, it is sufficient to replace equation (9) with

$$\overline{T} = T + \frac{\Delta T}{2}, \tag{10}$$

where $\Delta T = T_0 - T$ and T_0 is the temperature at the surface.

TABLE 3C. H for t from −10 C (+14 F) to 0 C (32 F); h to 2,000 m (6,562 ft).

p_0 = 1,000 mb at sea level

h(m)	10	−9	−8	−7	−6	−5	−4	−3	−2	−1	±0	h (ft)
0	300.4	299.2	298.1	297.0	295.9	294.8	293.7	292.6	291.5	290.4	289.4	0.0
10	300.0	298.8	297.7	296.6	295.5	294.4	293.3	292.2	291.1	290.1	289.0	32.8
20	299.6	298.4	297.3	296.2	295.1	294.0	292.9	291.9	290.8	289.7	288.7	65.6
30	299.2	298.1	297.0	295.9	294.8	293.7	292.6	291.5	290.4	289.4	288.3	98.4
40	298.8	297.7	296.6	295.5	294.4	293.3	292.2	291.2	290.1	289.0	288.0	131.2
50	298.4	297.3	296.2	295.1	294.0	292.9	291.8	290.8	289.7	288.7	287.6	164.0
75	295.5	296.3	295.2	294.1	293.0	291.9	290.8	289.8	288.7	287.7	286.6	248.1
100	296.5	295.4	294.3	293.3	292.2	291.1	290.0	289.0	287.9	286.9	285.8	328.1
150	294.6	293.5	292.4	291.4	290.3	289.2	288.2	287.1	286.1	285.0	284.0	492.1
200	292.7	291.6	290.5	289.5	288.4	287.3	286.3	285.3	284.2	283.2	282.2	656.2
250	290.8	289.7	288.7	287.6	286.6	285.5	284.5	283.5	282.5	281.5	280.5	820.2
300	288.9	287.9	286.8	285.8	284.7	283.7	282.7	281.7	280.7	279.7	278.7	984.3
350	287.0	286.0	285.0	283.9	282.9	281.9	280.9	279.9	279.0	278.0	277.0	1,148.0
400	285.2	284.2	283.2	282.1	281.1	280.1	279.1	278.2	277.2	276.3	275.3	1,312.0
450	283.3	282.3	281.3	280.3	279.3	278.3	277.3	276.4	275.4	274.5	273.5	1,476.0
500	281.5	280.5	279.5	278.6	277.6	276.6	275.6	274.7	273.7	272.8	271.8	1,640.0
600	277.9	276.9	276.0	275.0	274.1	273.1	272.2	271.3	270.3	269.4	268.5	1,969.0
700	274.3	273.4	272.4	271.5	270.5	269.6	268.7	267.8	266.9	266.0	265.1	2,297.0
800	270.7	269.8	268.9	268.0	267.1	266.2	265.3	264.4	263.6	262.7	261.8	2,625.0
900	267.2	266.3	265.4	264.6	263.7	262.8	262.0	261.1	260.3	259.4	258.6	2,953.0
1,000	263.8	262.9	262.1	261.2	260.4	259.5	258.7	257.8	257.0	256.1	255.3	3,281.0
1,500	247.2	246.5	245.7	245.0	244.2	243.5	242.8	242.1	241.3	240.6	239.9	4,921.0
2,000	231.7	231.0	230.4	229.7	229.1	228.4	227.8	227.2	226.5	225.9	225.3	6,562.0
	14.0	15.8	17.6	19.4	21.2	23.0	24.8	26.6	28.4	30.2	32.0	h (ft)
												t F

TABLE 3D. H for t from 0 C (32 F) to 10 C (50 F); h to 2,000 m (6,562 ft).

p_0 = 1,000 mb at sea level

h(m)	±0	1	2	3	4	5	6	7	8	9	10	h (ft)
0	289.4	288.3	287.3	286.2	285.2	284.2	283.2	282.1	281.1	280.1	279.2	0.0
10	289.0	288.0	286.9	285.9	284.8	283.8	282.8	281.8	280.8	279.8	278.9	32.8
20	288.7	287.6	286.6	285.5	284.5	283.5	282.5	281.4	280.5	279.5	278.5	65.6
30	288.3	287.3	286.2	285.2	284.1	283.1	282.1	281.1	280.1	279.1	278.2	98.4
40	288.0	286.9	285.9	284.8	283.8	282.8	281.8	280.7	279.8	278.8	277.8	131.2
50	287.6	286.6	285.5	284.5	283.4	282.4	281.4	280.4	279.5	278.5	277.5	164.0
75	286.6	285.7	284.7	283.6	282.6	281.6	280.6	279.6	278.7	277.7	276.7	248.1
100	285.8	284.8	283.8	282.7	281.7	280.7	279.7	278.7	277.8	276.8	275.8	328.1
150	284.0	283.0	282.0	281.0	280.0	279.0	278.0	277.1	276.1	275.2	274.2	492.1
200	282.2	281.2	280.2	279.3	278.3	277.3	276.3	275.4	274.4	273.5	272.5	656.2
250	280.5	279.5	278.5	277.6	276.6	275.6	274.7	273.7	272.8	271.8	270.9	820.2
300	278.7	277.7	276.8	275.8	274.9	273.9	273.0	272.0	271.1	270.1	269.2	984.3
350	277.0	276.0	275.1	274.1	273.2	272.2	271.3	270.4	269.4	268.5	267.6	1,148.0
400	275.3	274.3	273.4	272.4	271.5	270.5	269.6	268.7	267.8	266.9	266.0	1,312.0
450	273.5	272.6	271.7	270.7	269.8	268.9	268.0	267.1	266.2	265.3	264.4	1,476.0
500	271.8	270.9	270.0	269.0	268.1	267.2	266.3	265.4	264.6	263.7	262.8	1,640.0
600	268.5	267.6	266.7	265.8	264.9	264.0	263.1	262.2	261.4	260.5	259.6	1,969.0
700	265.1	264.2	263.4	262.5	261.7	260.8	259.9	259.1	258.2	257.4	256.5	2,297.0
800	261.8	260.9	260.1	259.2	258.4	257.5	256.7	255.9	255.0	254.2	253.4	2,625.0
900	258.6	257.8	256.9	256.1	255.2	254.4	253.6	252.8	252.0	251.2	250.4	2,953.0
1,000	255.3	254.5	253.7	252.9	252.1	251.3	250.5	249.7	249.0	248.2	247.4	3,281.0
1,500	239.9	239.2	238.5	237.7	237.0	236.3	235.6	234.9	234.3	233.6	232.9	4,921.0
2,000	225.3	224.7	224.1	223.5	222.9	222.3	221.7	221.1	220.5	219.9	219.3	6,562.0
	32.0	33.8	35.6	37.4	39.2	41.0	42.8	44.6	46.4	48.2	50.0	h (ft)
												t F

By substituting from equations (8) and (10), equation (4) assumes the form

$$M_d = \frac{Ap_0}{T} \epsilon^{-\omega\lambda/(T+\Delta T/2)}$$

For all practical cases,

$$\frac{\Delta T}{2T} \ll 1$$

and hence,

$$M_d = \frac{Ap_0}{T} \epsilon^{-(\omega\lambda/T)[1-(\Delta T/2T)]}$$

$$= \frac{Ap_0}{T} \epsilon^{-\omega\lambda/T} \epsilon^{+(\omega\lambda\Delta T/2T^2)}$$

Even at heights as great as 10^4 m it can be seen that the second of these exponentials can be replaced by the

TABLE 3E. H for t from 10 C (50 F) to 20 C (68 F); h to 2,000 m (6,562 ft).

$p_0 = 1,000$ mb at sea level

h (m)	t C → 10	11	12	13	14	15	16	17	18	19	20	h (ft)
0	279.2	278.2	277.2	276.2	275.3	274.3	273.4	272.4	271.5	270.5	269.6	0.0
10	278.9	277.9	276.9	275.9	274.9	274.0	273.1	272.1	271.2	270.2	269.3	32.8
20	278.5	277.5	276.6	275.6	274.6	273.7	272.8	271.8	270.9	269.9	269.0	65.6
30	278.2	277.2	276.2	275.2	274.3	273.3	272.4	271.5	270.5	269.6	268.7	98.4
40	277.8	276.8	275.9	274.9	274.0	273.0	272.1	271.2	270.2	269.3	268.4	131.2
50	277.5	276.5	275.6	274.6	273.7	272.7	271.8	270.9	269.9	269.0	268.1	164.0
75	276.7	275.7	274.8	273.8	272.8	271.9	271.0	270.1	269.1	268.2	267.3	248.1
100	275.8	274.9	273.9	273.0	272.0	271.1	270.2	269.3	268.3	267.4	266.5	328.1
150	274.2	273.3	272.3	271.4	270.4	269.5	268.6	267.7	266.8	265.9	265.0	492.1
200	272.5	271.6	270.7	269.7	268.8	267.9	267.0	266.1	265.2	264.3	263.4	656.2
250	270.9	270.0	269.1	268.1	267.2	266.3	265.4	264.5	263.7	262.8	261.9	820.2
300	269.2	268.3	267.4	266.5	265.6	264.7	263.8	262.9	262.1	261.2	260.3	984.3
350	267.6	266.7	265.8	264.9	264.0	263.1	262.2	261.4	260.5	259.7	258.8	1,148.0
400	266.0	265.1	264.2	263.4	262.5	261.6	260.7	259.9	259.0	258.2	257.3	1,312.0
450	264.4	263.5	262.6	261.8	260.9	260.0	259.2	258.3	257.5	256.6	255.8	1,476.0
500	262.8	261.9	261.1	260.2	259.4	258.5	257.7	256.9	256.0	255.2	254.4	1,640.0
600	259.6	258.8	258.0	257.1	256.3	255.5	254.7	253.9	253.0	252.2	251.4	1,969.0
700	256.5	255.7	254.9	254.0	253.2	252.4	251.6	250.8	250.1	249.3	248.5	2,297.0
800	253.4	252.6	251.8	251.1	250.3	249.5	248.7	247.9	247.2	246.4	245.6	2,625.0
900	250.4	249.6	248.8	248.1	247.3	246.5	245.8	245.0	244.3	243.5	242.8	2,953.0
1,000	247.4	246.6	245.9	245.1	244.4	243.6	242.9	242.1	241.4	240.6	239.9	3,281.0
1,500	232.9	232.2	231.6	230.9	230.3	229.6	228.9	228.3	227.6	227.0	226.3	4,921.0
2,000	219.3	218.7	218.1	217.6	217.0	216.4	215.8	215.2	214.7	214.1	213.5	6,562.0
	50.0	51.8	53.6	55.4	57.2	59.0	60.8	62.6	64.4	66.2	68.0	h (ft)
												t F

TABLE 3F. H for t from 20 C (68 F) to 30 C (86 F); h to 2,000 m (6,562 ft).

$p_0 = 1,000$ mb at sea level

h (m)	t C → 20	21	22	23	24	25	26	27	28	29	30	h (ft)
0	269.6	268.7	267.8	266.9	266.0	265.1	264.2	263.3	262.5	261.6	260.7	0.0
10	269.3	268.4	267.5	266.6	265.7	264.8	263.9	263.0	262.2	261.3	260.4	32.8
20	269.0	268.1	267.2	266.3	265.4	264.5	263.6	262.7	261.9	261.0	260.1	65.6
30	268.7	267.8	266.9	266.0	265.1	264.2	263.3	262.5	261.6	260.8	259.9	98.4
40	268.4	267.5	266.6	265.7	264.8	263.9	263.0	262.2	261.3	260.5	259.6	131.2
50	268.1	267.2	266.3	265.4	264.5	263.6	262.7	261.9	261.0	260.2	259.3	164.0
75	267.3	266.4	265.5	264.7	263.8	262.9	262.0	261.2	260.3	259.5	258.6	248.1
100	266.5	265.6	264.7	263.9	263.0	262.1	261.2	260.4	259.5	258.7	257.8	328.1
150	265.0	264.1	263.2	262.4	261.5	260.6	259.7	258.9	258.0	257.2	256.3	492.1
200	263.4	262.5	261.7	260.8	260.0	259.1	258.3	257.4	256.6	255.7	254.9	656.2
250	261.9	261.0	260.2	259.3	258.5	257.6	256.8	256.0	255.1	254.3	253.5	820.2
300	260.3	259.5	258.6	257.8	256.9	256.1	255.3	254.5	253.6	252.8	252.0	984.3
350	258.8	258.0	257.2	256.3	255.5	254.7	253.9	253.1	252.2	251.4	250.6	1,148.0
400	257.3	256.5	255.7	254.8	254.0	253.2	252.4	251.6	250.8	250.0	249.2	1,312.0
450	255.8	255.0	254.2	253.4	252.6	251.8	251.0	250.2	249.4	248.6	247.8	1,476.0
500	254.4	253.6	252.8	251.9	251.1	250.3	249.5	248.7	248.0	247.2	246.4	1,640.0
600	251.4	250.6	249.8	249.1	248.3	247.5	246.7	246.0	245.2	244.5	243.7	1,969.0
700	248.5	247.7	247.0	246.2	245.5	244.7	243.9	243.2	242.4	241.7	240.9	2,297.0
800	245.6	244.9	244.1	243.4	242.6	241.9	241.2	240.5	239.7	239.0	238.3	2,625.0
900	242.8	242.1	241.3	240.6	239.8	239.1	238.4	237.7	237.0	236.3	235.6	2,953.0
1,000	239.9	239.2	238.5	237.8	237.1	236.4	235.7	235.0	234.3	233.6	232.9	3,281.0
1,500	226.3	225.7	225.1	224.4	223.8	223.2	222.6	222.0	221.4	220.8	220.2	4,921.0
2,000	213.5	213.0	212.4	211.9	211.3	210.8	210.3	209.7	209.2	208.6	208.1	6,562.0
	86.0	87.8	89.6	91.4	93.2	95.0	96.8	98.6	100.4	102.2	104.0	h (ft)
												t F

first two terms of its expansion. Therefore

$$M_d = \frac{Ap_0}{T} \epsilon^{-\alpha h/T} + \frac{Ap_0 \alpha h}{2T^3} \epsilon^{-\alpha h/T} \cdot \Delta T,$$

or

$$M_d = H(T,h) + G(T,h)\,\Delta T, \qquad (11)$$

where

$$H(T,h) = \frac{Ap_0}{T} \epsilon^{-\alpha h/T}$$

and

$$G(T,h) = \frac{Ap_0}{2T^3} \alpha h \epsilon^{-\alpha h/T} \qquad (12)$$

Table 3 gives the quantity $H(T,h)$ as a function of

h and t, where

$$t = T - 273$$

is the standard centigrade temperature. In this table, it is assumed that $p_0 = 1{,}000$ mb.

Table 4 gives $G(T,h)$. The term $G\Delta t$ in equation (11) is very small at altitudes less than 500 m and for this range of altitudes may be safely neglected.

Since it is assumed in these tables that $p_0 = 1{,}000$, the value of M_d read from the tables should be multiplied by $p_0/1{,}000$, where p_0 is the actual air pressure at sea level. This step may, however, be eliminated in most cases, particularly as the physically important

TABLE 3G. H for t from 30 C (86 F) to 40 C (104 F); h to 2,000 m (6,562 ft).

$p_0 = 1{,}000$ mb at sea level

h(m) \ tC →	30	31	32	33	34	35	36	37	38	39	40	h (ft)
↓ 0	260.7	259.9	259.0	258.2	257.5	256.5	255.7	254.8	254.0	253.2	252.4	0.0
10	260.4	259.6	258.7	257.9	257.2	256.2	255.4	254.5	253.7	252.9	252.1	32.8
20	260.1	259.3	258.4	257.6	256.9	255.9	255.1	254.3	253.4	252.6	251.8	65.6
30	259.9	259.1	258.2	257.4	256.5	255.7	254.9	254.0	253.2	252.4	251.6	98.4
40	259.6	258.8	257.9	257.1	256.2	255.4	254.6	253.8	252.9	252.1	251.3	131.2
50	259.3	258.5	257.6	256.8	255.9	255.1	254.3	253.5	252.6	251.8	251.0	164.0
75	258.6	257.7	256.9	256.0	254.2	254.4	253.6	252.8	251.9	251.1	250.3	248.1
100	257.8	257.0	256.2	255.3	254.5	253.7	252.9	252.1	251.3	250.5	249.7	328.1
150	256.3	255.5	254.7	253.9	253.1	252.3	251.5	250.7	249.9	249.1	248.3	492.1
200	254.9	254.1	253.3	252.5	251.7	250.9	250.1	249.3	248.5	247.7	246.9	656.2
250	253.5	252.7	251.9	251.1	250.3	249.5	248.7	247.9	247.2	246.4	245.6	820.2
300	252.0	251.2	250.4	249.7	248.9	248.1	247.3	246.6	245.8	245.1	244.3	984.3
350	250.6	249.8	249.0	248.3	247.5	246.7	245.9	245.2	244.4	243.7	242.9	1,148.0
400	249.2	248.4	247.7	246.9	246.2	245.4	244.6	243.9	243.1	242.4	241.6	1,312.0
450	247.8	247.0	246.3	245.5	244.8	244.0	243.3	242.5	241.8	241.0	240.3	1,476.0
500	246.4	245.6	244.9	244.1	243.4	242.6	241.9	241.2	240.4	239.7	239.0	1,640.0
600	243.7	242.9	242.2	241.4	240.7	239.9	239.2	238.5	237.8	237.1	236.4	1,969.0
700	240.9	240.2	239.5	238.7	238.0	237.3	236.6	235.9	235.2	234.5	233.8	2,297.0
800	238.3	237.6	236.9	236.1	235.4	234.7	234.0	233.3	232.7	232.0	231.3	2,625.0
900	235.6	234.9	234.2	233.5	232.8	232.1	231.4	230.8	230.1	229.5	228.8	2,953.0
1,000	232.9	232.2	231.6	230.9	230.3	229.6	228.9	228.3	227.6	227.0	226.3	3,281.0
1,500	220.2	219.6	219.0	218.4	217.8	217.2	216.6	216.0	215.5	214.9	214.3	4,921.0
2,000	208.1	207.6	207.1	206.5	206.0	205.5	205.0	204.5	203.9	203.4	202.9	6,562.0
	86.0	87.9	89.6	91.4	93.2	95.0	96.8	98.6	100.4	102.2	104.0	h (ft)

t F

TABLE 4. G for h from 50 m (164 ft) to 2,000 m (6,562 ft) and t from -30 C (-22 F) to 40 C (104 F).

h (m) \ tC →	−30	−25	−20	−15	−10	−5	±0	+5	+10	+15	+20	+25	+30	+35	+40	h (ft)
↓ 50	0.005	0.004	0.004	0.004	0.004	0.003	0.003	0.003	0.003	0.003	0.003	0.003	0.003	0.002	0.002	164.0
100	0.009	0.009	0.008	0.008	0.007	0.007	0.007	0.006	0.006	0.006	0.006	0.005	0.005	0.005	0.004	328.1
150	0.014	0.013	0.012	0.012	0.011	0.010	0.010	0.010	0.009	0.009	0.008	0.008	0.008	0.007	0.007	0.006	492.1
200	0.018	0.017	0.016	0.015	0.014	0.014	0.013	0.012	0.012	0.011	0.010	0.010	0.009	0.009	0.009	656.2
250	0.023	0.021	0.020	0.019	0.018	0.017	0.016	0.015	0.014	0.014	0.013	0.012	0.012	0.011	0.011	820.2
300	0.027	0.025	0.024	0.023	0.021	0.020	0.019	0.018	0.017	0.016	0.016	0.015	0.014	0.013	0.013	984.3
350	0.031	0.030	0.028	0.026	0.025	0.023	0.022	0.021	0.020	0.019	0.018	0.017	0.016	0.016	0.015	1,148.0
400	0.036	0.033	0.032	0.030	0.028	0.027	0.025	0.024	0.023	0.022	0.020	0.019	0.019	0.018	0.017	1,312.0
450	0.040	0.037	0.035	0.033	0.031	0.030	0.028	0.027	0.025	0.024	0.023	0.022	0.021	0.020	0.019	1,476.0
500	0.044	0.041	0.039	0.037	0.035	0.033	0.031	0.030	0.028	0.027	0.025	0.024	0.023	0.022	0.021	1,640.0
600	0.052	0.049	0.046	0.044	0.041	0.039	0.037	0.035	0.033	0.032	0.030	0.029	0.027	0.026	0.025	1,969.0
700	0.060	0.056	0.053	0.050	0.047	0.045	0.043	0.040	0.038	0.036	0.035	0.033	0.031	0.030	0.029	2,297.0
800	0.067	0.063	0.060	0.057	0.053	0.051	0.048	0.046	0.043	0.041	0.039	0.037	0.035	0.034	0.032	2,625.0
900	0.075	0.070	0.066	0.063	0.059	0.056	0.053	0.051	0.048	0.046	0.043	0.041	0.039	0.038	0.036	2,953.0
1,000	0.082	0.077	0.073	0.069	0.065	0.062	0.059	0.056	0.053	0.050	0.048	0.045	0.043	0.041	0.039	3,281.0
1,500	0.114	0.108	0.102	0.097	0.092	0.087	0.082	0.078	0.075	0.071	0.068	0.064	0.061	0.059	0.056	4,921.0
2,000	0.142	0.134	0.127	0.121	0.114	0.109	0.103	0.098	0.094	0.089	0.085	0.081	0.077	0.074	0.071	6,562.0
	−22.0	−13.0	−4.0	+5.0	14.0	23.0	32.0	41.0	50.0	59.0	68.0	77.0	86.0	95.0	104.0	t F

TABLE 5. M_o for t from −30 C (−22 F) to 40 C (104 F).

t C	\multicolumn{10}{c}{Relative humidity}	t F
	10	20	30	40	50	60	70	80	90	100	
−30	0.2	0.5	0.7	1.0	1.2	1.5	1.7	2.0	2.2	2.453	−22.0
−29	0.3	0.5	0.8	1.1	1.4	1.6	1.9	2.2	2.2	2.700	−20.2
−28	0.3	0.6	0.9	1.2	1.5	1.8	2.1	2.4	2.7	2.967	−18.4
−27	0.3	0.7	1.0	1.3	1.6	2.0	2.3	2.6	2.9	3.261	−16.6
−26	0.4	0.7	1.1	1.4	1.8	2.1	2.5	2.9	3.2	3.580	−14.8
−25	0.4	0.8	1.2	1.6	2.0	2.4	2.7	3.1	3.5	3.925	−13.0
−24	0.4	0.9	1.3	1.7	2.2	2.6	3.0	3.4	3.9	4.301	−11.2
−23	0.5	0.9	1.4	1.9	2.4	2.8	3.3	3.8	4.2	4.708	− 9.4
−22	0.5	1.0	1.5	2.1	2.6	3.1	3.6	4.1	4.6	5.155	− 7.6
−21	0.6	1.1	1.7	2.3	2.8	3.4	3.9	4.5	5.1	5.637	− 5.8
−20	0.6	1.2	1.8	2.5	3.1	3.7	4.3	4.9	5.5	6.130	− 4.0
−19	0.7	1.3	2.0	2.7	3.4	4.0	4.7	5.4	6.1	6.724	− 2.2
−18	0.7	1.5	2.2	2.9	3.7	4.4	5.1	5.8	6.6	7.300	− .4
−17	0.8	1.6	2.4	3.2	4.0	4.8	5.6	6.4	7.2	7.999	+ 1.4
−16	0.9	1.7	2.6	3.5	4.3	5.2	6.1	6.9	7.8	8.678	+ 3.2
−15	0.9	1.9	2.8	3.8	4.7	5.7	6.6	7.6	8.5	9.461	+ 5.0
−14	1.0	2.1	3.1	4.1	5.1	6.2	7.2	8.2	9.3	10.287	+ 6.8
−13	1.1	2.2	3.3	4.5	5.6	6.7	7.8	8.9	10.0	11.157	+ 8.6
−12	1.2	2.4	3.6	4.8	6.1	7.3	8.5	9.7	10.9	12.124	+10.4
−11	1.3	2.6	4.0	5.3	6.6	7.9	9.2	10.5	11.9	13.185	+12.2
−10	1.4	2.9	4.3	5.7	7.1	8.6	10.0	11.4	12.9	14.284	+14.0
− 9	1.5	3.1	4.6	6.2	7.7	9.3	10.8	12.4	13.9	15.472	+15.8
− 8	1.7	3.4	5.0	6.7	8.4	10.1	11.7	13.4	15.1	16.754	+17.6
− 7	1.8	3.6	5.4	7.2	9.1	10.9	12.7	14.5	16.3	18.117	+19.4
− 6	2.0	3.9	5.9	7.8	9.8	11.7	13.7	15.7	17.6	19.568	+21.2
− 5	2.1	4.2	6.3	8.5	10.6	12.7	14.8	16.9	19.0	21.156	+23.0
− 4	2.3	4.6	6.9	9.1	11.4	13.7	16.0	18.3	20.6	22.871	+24.8
− 3	2.5	4.9	7.4	9.9	12.3	14.8	17.3	19.7	22.2	24.670	+26.6
− 2	2.7	5.3	8.0	10.6	13.3	16.0	18.6	21.3	23.9	26.589	+28.4
− 1	2.9	5.7	8.6	11.5	14.3	17.2	20.1	22.9	25.8	28.685	+30.2
± 0	3.1	6.2	9.3	12.4	15.5	18.5	21.6	24.7	27.8	30.911	+32.0
1	3.3	6.6	9.9	13.2	16.5	19.8	23.0	26.3	29.6	32.919	+33.8
2	3.5	7.0	10.5	14.1	17.6	21.1	24.6	28.1	31.6	35.139	+35.6
3	3.8	7.5	11.3	15.0	18.8	22.5	26.3	30.0	33.8	37.509	+37.4
4	4.0	8.0	12.0	16.0	20.0	24.0	28.0	32.0	35.9	39.939	+39.2
5	4.3	8.5	12.8	17.0	21.3	25.5	29.8	34.0	38.3	42.533	+41.0
6	4.5	9.1	13.6	18.1	22.6	27.2	31.7	36.2	40.8	45.280	+42.8
7	4.8	9.6	14.5	19.3	24.1	28.9	33.7	38.5	43.3	48.175	+44.6
8	5.1	10.2	15.4	20.5	25.6	30.7	35.9	41.0	46.1	51.215	+46.4
9	5.4	10.9	16.3	21.8	27.2	32.6	38.1	43.5	49.0	54.394	+48.2
10	5.8	11.6	17.3	23.1	28.9	34.7	40.5	46.2	52.0	57.793	+50.0
11	6.1	12.3	18.4	24.5	30.6	36.8	42.9	49.0	55.1	61.270	+51.8
12	6.5	13.0	19.5	26.0	32.5	39.1	45.6	52.1	58.6	65.094	+53.6
13	6.9	13.8	20.7	27.6	34.5	41.4	48.3	55.2	62.1	69.010	+55.4
14	7.3	14.6	22.0	29.3	36.6	43.9	51.2	58.5	65.9	73.169	+57.2
15	7.8	15.5	23.3	31.0	38.8	46.5	54.3	62.0	69.8	77.505	+59.0
16	8.2	16.4	24.6	32.8	41.0	49.2	57.4	65.6	73.9	82.060	+60.8
17	8.7	17.4	26.0	34.7	43.4	52.1	60.8	69.5	78.1	86.813	+62.6
18	9.2	18.4	27.6	36.7	45.9	55.1	64.3	73.5	82.7	91.866	+64.4
19	9.7	19.4	29.1	38.9	48.6	58.3	68.0	77.7	87.4	97.127	+66.2
20	10.3	20.5	30.8	41.1	51.4	61.6	71.9	82.2	92.4	102.71	+68.0
21	10.8	21.7	32.5	43.4	54.2	65.1	75.9	86.8	97.6	108.46	+69.8
22	11.5	22.9	34.4	45.8	57.3	68.7	80.2	91.6	103.1	114.56	+71.6
23	12.1	24.2	36.3	48.3	60.4	72.5	84.6	96.7	108.8	120.87	+73.4
24	12.8	25.5	38.3	51.0	63.8	76.5	89.3	102.0	114.8	127.53	+75.2
25	13.4	26.9	40.3	53.8	67.2	80.7	94.1	107.6	121.0	134.44	+77.0
26	14.2	28.3	42.5	56.7	70.9	85.0	99.2	113.4	127.6	141.74	+78.8
27	14.9	29.9	44.8	59.8	74.7	89.6	104.6	119.5	134.5	149.39	+80.6
28	15.7	31.5	47.2	62.9	78.7	94.4	110.1	125.9	141.6	157.34	+82.4
29	16.6	33.1	49.7	66.2	82.8	99.4	115.9	132.5	149.1	165.62	+84.2
30	17.4	34.9	52.3	69.7	87.1	104.6	122.0	139.4	156.8	174.27	+86.0
31	18.3	36.7	55.0	73.3	91.7	110.0	128.3	146.7	165.0	183.32	+87.8
32	19.3	38.5	57.8	77.1	96.4	115.6	134.9	154.2	173.5	192.74	+89.6
33	20.3	40.5	60.8	81.0	101.3	121.5	141.8	162.0	182.3	202.56	+91.4
34	21.3	42.6	63.9	85.1	106.4	127.7	149.0	170.3	191.6	212.86	+93.2
35	22.4	44.7	67.1	89.4	111.8	134.1	156.5	178.8	201.2	223.50	+95.0
36	23.5	46.9	70.4	93.9	117.3	140.8	164.2	187.7	211.2	234.63	+96.8
37	24.6	49.2	73.9	96.5	123.1	147.7	172.3	197.0	221.6	246.20	+98.6
38	25.8	51.6	77.5	103.3	129.1	154.9	180.8	206.6	232.4	258.23	+100.4
39	27.1	54.2	81.2	108.3	135.4	162.5	189.6	216.6	243.7	270.80	+102.2
40	28.4	56.8	85.2	113.6	142.0	170.4	198.8	227.2	255.5	283.94	+104.0

quantity is not M but differences in M at various heights.

Wet Term. Since

$$e = (RH)e'$$

where RH = relative humidity,

e' = saturation vapor pressure,

and since e' is a function of temperature only, it is possible to prepare a table giving M_w as a function of RH and t. This is Table 5.

A table for f, defined by equation (7), is also included, so that if e is known, M_w can be obtained by simply taking the product fe as indicated by equation (5). Table 6 gives the values of f.

TABLE 6. f for t from -30 C $(-22$ F$)$ to 40 C $(104$ F$)$.

t C	f	t F	t C	f	t F	t C	f	t F
-30	6.390	-22.0	-6	5.289	$+21.2$	$+18$	4.449	$+64.4$
-29	6.338	-20.2	-5	5.250	$+23.0$	$+19$	4.419	$+66.2$
-28	6.286	-18.4	-4	5.210	$+24.8$	$+20$	4.389	$+68.0$
-27	6.233	-16.6	-3	5.172	$+26.6$	$+21$	4.359	$+69.8$
-26	6.183	-14.8	-2	5.133	$+28.4$	$+22$	4.330	$+71.6$
-25	6.134	-13.0	-1	5.095	$+30.2$	$+23$	4.300	$+73.4$
-24	6.084	-11.2	± 0	5.059	$+32.0$	$+24$	4.271	$+75.2$
-23	6.036	-9.4	$+1$	5.021	$+33.8$	$+25$	4.241	$+77.0$
-22	5.988	-7.6	$+2$	4.984	$+35.6$	$+26$	4.213	$+78.8$
-21	5.940	-5.8	$+3$	4.948	$+37.4$	$+27$	4.186	$+80.6$
-20	5.894	-4.0	$+4$	4.913	$+39.2$	$+28$	4.158	$+82.4$
-19	5.847	-2.2	$+5$	4.878	$+41.0$	$+29$	4.130	$+84.2$
-18	5.801	$-.4$	$+6$	4.843	$+42.8$	$+30$	4.102	$+86.0$
-17	5.755	$+1.4$	$+7$	4.808	$+44.6$	$+31$	4.076	$+87.8$
-16	5.710	$+3.2$	$+8$	4.773	$+46.4$	$+32$	4.049	$+89.6$
-15	5.666	$+5.0$	$+9$	4.738	$+48.2$	$+33$	4.022	$+91.4$
-14	5.622	$+6.8$	$+10$	4.706	$+50.0$	$+34$	3.997	$+93.2$
-13	5.579	$+8.6$	$+11$	4.666	$+51.8$	$+35$	3.970	$+95.0$
-12	5.537	$+10.4$	$+12$	4.640	$+53.6$	$+36$	3.944	$+96.8$
-11	5.494	$+12.2$	$+13$	4.607	$+55.4$	$+37$	3.918	$+98.6$
-10	5.452	$+14.0$	$+14$	4.576	$+57.2$	$+38$	3.893	$+100.4$
-9	5.410	$+15.8$	$+15$	4.543	$+59.0$	$+39$	3.868	$+102.2$
-8	5.370	$+17.6$	$+16$	4.511	$+60.8$	$+40$	3.844	$+104.0$
-7	5.329	$+19.4$	$+17$	4.480	$+62.6$			

Error. The discussion of this first group of tables is concluded with some observations on their order of accuracy. Theoretically any errors which arise are due to the expansions used in calculating M_d. At a height as great as 10,000 m, Δt might be, say, 70°. This would give $G\Delta T = 13.3$ for $t = 0$. If the next term had been included the correction would have been only a fraction of this amount. Since at these heights $M\sim1,800$, we are safe in saying that the relative error is less than 0.5 per cent, probably much less than this amount. At altitudes of 1,000 m or less the approximation introduces errors too small to be reflected in the fourth significant figure.

Aside from this theoretical error, there are errors in the table due to rounding off in the numerical work. An effort was made to keep this error less than 0.1 M units.

Curvature Term. Table 7 gives the values of the linear term $h/a \times 10^6$, which must be added to obtain the index of refraction modified for use on a "plane earth" diagram.

TABLE 7. M_c for h from 10 m $(32.8$ ft$)$ to $2,000$ m $(6,562$ ft$)$.

h(m)	M_c	h(ft)	h(m)	M_c	h(ft)	h(m)	M_c	h(ft)
10	1.6	32.8	280	44.0	918.6	625	98.1	2,051.0
20	3.1	65.6	290	45.5	951.4	650	102.1	2,133.0
30	4.7	98.4	300	47.1	984.3	675	106.0	2,215.0
40	6.3	131.2	310	48.7	1,017.0	700	109.9	2,297.0
50	7.9	164.0	320	50.2	1,050.0	725	113.8	2,379.0
60	9.4	196.9	330	51.8	1,083.0	750	117.8	2,461.0
70	11.0	229.7	340	53.4	1,115.0	775	121.7	2,543.0
80	12.6	262.5	350	55.0	1,148.0	800	125.6	2,625.0
90	14.1	295.3	360	56.5	1,181.0	825	129.5	2,707.0
100	15.7	328.1	370	58.1	1,214.0	850	133.5	2,789.0
110	17.3	360.9	380	59.7	1,247.0	875	137.4	2,871.0
120	18.8	393.7	390	61.2	1,280.0	900	141.3	2,953.0
130	20.4	426.5	400	62.8	1,312.0	925	145.2	3,035.0
140	22.0	459.3	410	64.4	1,345.0	950	149.2	3,117.0
150	23.6	492.1	420	65.9	1,378.0	975	153.1	3,199.0
160	25.1	524.9	430	67.5	1,411.0	1,000	157.0	3,280.0
170	26.7	557.7	440	69.1	1,444.0	1,100	172.7	3,609.0
180	28.3	590.6	450	70.7	1,476.0	1,200	188.4	3,937.0
190	29.8	623.4	460	72.2	1,509.0	1,300	204.1	4,265.0
200	31.4	656.2	470	73.8	1,542.0	1,400	219.8	4,593.0
210	33.0	689.0	480	75.4	1,575.0	1,500	235.5	4,921.0
220	34.5	721.8	490	76.9	1,608.0	1,600	251.2	5,249.0
230	36.1	754.6	500	78.5	1,640.0	1,700	266.9	5,577.0
240	37.7	787.4	525	82.4	1,722.0	1,800	282.6	5,906.0
250	39.3	820.2	550	86.4	1,804.0	1,900	298.3	6,234.0
260	40.8	853.0	575	90.3	1,886.0	2,000	314.0	6,562.0
270	42.4	885.8	600	94.2	1,969.0			

TABLES 8 TO 11 — MIXING RATIO AND TEMPERATURE GIVEN

In terms of atmospheric pressure and water vapor pressure, the mixing ratio w is given by

$$w = \frac{623e}{p - e}. \tag{13}$$

Since w involves the pressure p, the scheme used in the first group of tables must be modified. Using equation (13), equation (2) assumes the form

$$M = \frac{p}{p_0} F(T, w) + Ch, \tag{14}$$

where

$$F(T, w) = p_0 \frac{A}{T} + \frac{w}{w + 623}\left(\frac{B}{T^2} - \frac{D}{T}\right). \tag{15}$$

Table 8 gives F for the range of usable values of temperature and mixing ratio. Since F is sensitive to variations in both T and w, the tabulation is made for all integral values of both T and w to avoid laborious interpolation.

Following the procedure used in the discussion of dry term on page 208, the pressure p is calculated from equation (8). These results are given in Table 9. In view of the insensitivity of p to $\overline{T}$, the average temperature, it is unnecessary to tabulate p for all values of $\overline{T}$; it is sufficient to tabulate p at 5-degree intervals of $\overline{T}$.

The term Ch has been calculated in connection with the first group of tables and is given in Table 7.

TABLES 10 AND 11 FOR USE AT LOW ALTITUDES

An objectionable feature of the method given in the preceding section is that it involves taking the product, pF, which makes an application of the tables

rather slow. The following method circumvents this difficulty for heights less than 500 m. From equations (1), (8), and (15)

$$(n - 1) 10^6 = F\epsilon^{-ah/T}.\qquad (16)$$

For altitudes of less than 500 m it is safe to suppose that

$$\frac{ah}{\overline{T}} = \frac{ah}{273}\left(1 - \frac{\bar{t}}{273}\right),$$

where $\bar{t}$ is the average centigrade temperature, and

TABLE 8A. $F(t, w)$ for t from −30 C (−22 F) to 40 C (104 F): w from 0 to 12.

t C	w 0	1	2	3	4	5	6	7	8	9	10	11	12	t F
−30	325.1	335.1												−22.0
−29	323.8	333.9												−20.2
−28	322.4	332.4												−18.4
−27	321.1	331.0												−16.6
−26	319.8	329.7												−14.8
−25	318.5	328.3												−13.0
−24	317.3	327.0												−11.2
−23	316.0	325.6												− 9.4
−22	314.7	324.3												− 7.6
−21	313.5	323.0												− 5.8
−20	312.3	321.7												− 4.0
−19	311.0	320.3												− 2.2
−18	309.8	319.1												− 0.4
−17	308.6	317.8												+ 1.4
−16	307.4	316.5												+ 3.2
−15	306.2	315.9	324.9											+ 5.0
−14	305.0	314.0	322.8											+ 6.8
−13	303.8	312.7	321.6											+ 8.6
−12	302.7	311.6	320.4											+10.4
−11	301.5	310.3	319.0											+12.2
−10	300.4	309.1	317.8											+14.0
− 9	299.2	307.9	316.5											+15.8
− 8	298.1	306.7	315.3											+17.6
− 7	297.0	305.5	314.0	322.5										+19.4
− 6	295.9	304.4	312.8	321.2										+21.2
− 5	294.8	303.2	311.6	319.9										+23.0
− 4	293.7	302.0	310.4	318.7										+24.8
− 3	292.6	300.9	309.1	317.4										+26.6
− 2	291.5	299.7	307.9	316.1	324.2									+28.4
− 1	290.4	298.6	306.7	314.8	322.9									+30.2
± 0	289.4	297.5	305.6	313.6	321.7									+32.0
+ 1	288.3	296.4	304.4	312.4	320.4	328.3								+33.8
+ 2	287.3	295.3	303.3	311.2	319.1	327.0								+35.6
+ 3	286.2	294.1	302.0	309.9	317.8	325.6								+37.4
+ 4	285.2	293.1	300.9	308.8	316.6	324.4	332.0							+39.2
+ 5	284.2	292.0	299.8	307.6	315.4	323.1	330.7							+41.0
+ 6	283.2	291.0	298.7	306.4	314.1	321.7	329.4							+42.8
+ 7	282.1	289.8	297.5	305.2	312.8	320.3	327.9	335.5						+44.6
+ 8	281.1	288.8	296.4	304.0	311.5	319.1	326.6	334.1						+46.4
+ 9	280.1	287.7	295.3	302.8	310.3	317.8	325.3	332.8	340.2					+48.2
+10	279.2	286.8	294.3	301.8	309.2	316.7	324.1	331.6	338.8					+50.0
+11	278.2	285.7	293.2	300.5	307.9	315.3	322.7	330.1	337.3	344.6				+51.8
+12	277.2	284.7	292.1	299.4	306.8	314.1	321.5	328.8	336.0	343.3	350.5			+53.6
+13	276.2	283.6	291.0	298.2	305.6	312.9	320.2	327.4	334.0	341.8	349.0			+55.4
+14	275.3	282.7	290.0	297.2	304.5	311.7	319.0	326.2	333.3	340.5	347.6	354.7		+57.2
+15	274.3	281.6	288.9	296.0	302.3	310.5	317.7	324.9	331.9	339.0	346.1	353.1	360.2	+59.0
+16	273.4	280.7	287.9	295.0	302.2	309.3	316.4	323.5	330.6	337.6	344.7	351.7	358.6	+60.8
+17	272.4	279.6	286.8	293.8	301.0	308.1	315.1	322.2	329.2	336.1	343.2	350.2	357.0	+62.6
+18	271.5	278.7	285.7	292.8	299.9	307.0	313.9	320.9	327.9	334.8	341.8	348.7	355.6	+64.4
+19	270.5	277.6	284.6	291.7	298.7	305.5	312.6	319.6	326.6	333.4	340.3	347.1	354.0	+66.2
+20	269.6	276.7	283.6	290.6	297.6	304.5	311.5	318.4	325.2	332.1	339.0	345.7	352.6	+68.0
+21	268.7	275.7	282.6	289.6	296.5	303.4	310.3	317.2	323.9	330.8	337.5	344.3	351.1	+69.8
+22	267.8	274.8	281.6	288.5	295.5	302.2	309.1	315.9	322.7	329.5	336.2	342.9	349.7	+71.6
+23	266.9	273.8	280.6	287.5	294.4	301.1	307.9	314.7	321.4	328.2	334.8	341.5	348.1	+73.4
+24	266.0	272.9	279.6	286.5	293.3	300.0	306.8	313.4	320.2	326.9	333.5	340.1	346.7	+75.2
+25	265.1	271.9	278.6	285.4	292.2	298.9	305.6	312.2	318.9	325.4	332.1	338.7	345.2	+77.0
+26	264.2	271.0	277.7	284.4	291.0	297.7	304.4	311.0	317.6	324.2	330.8	337.3	343.8	+78.8
+27	263.3	270.0	276.7	283.4	290.0	296.6	303.3	309.8	316.4	322.9	329.5	335.9	342.4	+80.6
+28	262.5	269.2	275.8	282.4	289.0	295.6	302.2	308.7	315.3	321.7	328.2	334.6	341.1	+82.4
+29	261.6	268.3	274.8	281.4	287.9	294.5	300.9	307.5	314.0	320.4	326.9	333.3	339.7	+84.2
+30	260.7	267.3	273.8	280.4	286.8	293.4	299.8	306.3	312.7	319.1	325.5	331.9	338.2	+86.0
+31	259.9	266.5	272.9	279.5	285.9	292.4	298.7	305.2	311.5	318.0	324.3	330.6	336.9	+87.8
+32	259.0	265.5	271.9	278.4	284.8	291.3	297.6	304.0	310.3	316.7	323.0	329.3	335.5	+89.6
+33	258.2	264.7	271.1	277.5	283.8	290.3	296.5	302.9	309.2	315.5	321.7	328.0	334.2	+91.4
+34	257.3	263.8	270.1	276.5	282.8	289.2	295.4	301.7	308.0	314.2	320.4	326.7	332.8	+93.2
+35	256.5	262.9	269.2	275.6	281.8	288.1	294.4	300.7	306.8	313.0	319.2	325.3	331.6	+95.0
+36	255.7	262.1	268.3	274.6	280.9	287.2	293.3	299.5	305.7	311.8	318.0	324.1	330.3	+96.8
+37	254.8	261.1	267.3	273.5	279.8	286.0	292.2	298.3	304.5	310.6	316.7	322.8	328.8	+98.6
+38	254.0	260.8	266.5	272.6	278.8	285.0	291.1	297.2	303.4	309.4	315.5	321.5	327.5	+100.4
+39	253.2	259.4	265.6	271.7	277.9	284.0	290.1	296.2	302.3	308.8	314.3	320.3	326.3	+102.2
+40	252.4	258.5	264.7	270.8	276.9	283.0	289.1	295.1	301.2	307.1	313.1	319.1	325.1	+104.0

that

$$\epsilon^{-ah/\overline{T}} = \epsilon^{-ah/273} \cdot \epsilon + \frac{ah\overline{t}}{(273)^2} = \epsilon^{-ah/273}$$

$$+ \frac{ah\overline{t}}{(273)^2} \epsilon^{-ah/273}. \quad (17)$$

Hence

$$(n-1)10^6 = F - u + \frac{h\Delta u}{100}, \quad (18)$$

where

$$u = F(1 - \epsilon^{-ah/273}), \quad (19)$$

and

$$\Delta u = \frac{\alpha F t}{(273)^2}. \quad (20)$$

Equation (19) is evaluated in Table 10.

Equation (20) is a small correction which must be taken into account when t, the average temperature, differs appreciably from zero. Since this term contributes only 1 per cent to the refractive index in the extreme case of $h = 500$ m, $\overline{t} = 40$, it is sufficient to

TABLE 8B. $F(t, w)$ for t from 15 C (59 F) to 40 C (104 F); w from 12 to 24.

tC	w 12	13	14	15	16	17	18	19	20	21	22	23	w 24	F
15	360.2													59.0
16	358.6													60.8
17	357.0	364.0												62.6
18	355.6	362.5	360.2											64.4
19	354.0	360.9	367.6											66.2
20	352.6	359.3	366.1	372.8										68.0
21	351.1	357.8	364.5	371.1	377.9									69.8
22	349.7	356.3	363.0	369.6	376.2	382.8								71.6
23	348.1	354.8	361.5	368.0	374.6	381.1	387.7							73.4
24	346.7	353.3	359.8	366.4	372.9	379.5	385.9	329.4						75.2
25	345.2	351.8	358.3	364.8	371.3	377.7	384.2	390.6	397.0	403.4				77.0
26	343.8	350.3	356.8	363.2	369.7	376.1	382.5	388.9	295.3	401.6	407.9			78.8
27	342.4	348.8	355.3	361.7	368.1	374.5	380.9	387.2	393.5	399.8	406.0	412.3	418.5	80.6
28	341.1	347.5	353.9	360.2	366.7	372.9	379.2	385.6	391.8	398.1	404.3	410.5	416.7	82.4
29	339.7	346.0	352.3	358.7	365.0	371.3	377.6	383.9	300.0	396.2	402.5	408.6	414.7	84.2
30	338.2	344.6	350.8	357.2	363.4	369.6	375.9	382.1	388.3	394.5	400.6	406.8	412.8	86.0
31	336.9	343.2	349.5	355.8	362.0	368.1	374.4	380.5	386.7	392.8	398.9	405.0	411.1	87.8
32	335.5	341.8	348.0	354.1	360.4	366.5	372.7	378.8	384.9	391.1	397.1	403.1	409.2	89.6
33	334.2	340.4	346.6	352.7	359.0	365.0	371.1	377.3	383.3	389.3	395.4	401.4	407.3	91.4
34	332.8	339.0	345.2	351.3	357.4	363.5	369.5	375.6	381.6	387.6	393.7	399.6	405.5	93.2
35	331.6	337.6	343.8	349.8	355.9	362.0	368.0	374.0	380.0	386.0	391.9	397.9	403.8	95.0
36	330.3	336.3	342.4	348.5	354.4	360.4	366.5	372.4	378.3	384.3	390.2	396.1	402.0	96.8
37	328.8	334.9	340.9	346.9	352.9	358.8	364.8	370.8	376.6	382.5	388.5	394.3	400.1	98.6
38	327.5	333.6	339.6	345.5	351.5	357.4	363.3	369.3	375.1	380.9	386.8	392.6	398.4	100.4
39	326.3	332.3	338.2	344.1	350.1	355.9	361.8	367.9	373.5	379.3	385.1	390.9	396.7	102.2
40	325.1	330.9	336.9	342.8	348.6	354.5	360.3	366.5	371.9	377.8	383.5	389.2	394.9	104.0

TABLE 8C. $F(t, w)$ for t from 27 C (80.6 F) to 40 C (104 F); w from 24 to 36.

tC	w 24	25	26	27	28	29	30	31	32	33	34	35	36	w tF
27	418.5													80.6
28	416.7	422.9												82.4
29	414.7	421.0	427.1											84.2
30	412.8	418.9	425.2	431.1	437.1									86.0
31	411.1	417.1	423.2	429.2	435.2	441.2	447.2							87.8
32	409.2	415.2	421.2	427.2	433.2	439.2	445.0	451.0	456.8	462.6				89.6
33	407.3	413.4	419.3	425.3	431.1	437.2	443.0	448.8	454.6	460.5	466.4	472.1		91.4
34	405.5	411.5	417.4	423.3	429.2	435.1	440.9	446.7	452.5	458.4	464.1	469.9	475.6	93.2
35	403.8	409.6	415.6	421.4	427.2	433.1	439.9	444.7	450.4	456.2	461.9	467.7	473.4	95.0
36	402.0	407.9	413.7	419.5	425.4	431.1	436.9	442.6	448.3	454.1	459.8	465.5	471.1	96.8
37	400.1	405.9	411.8	417.6	423.3	429.0	434.8	440.5	446.2	451.9	457.5	463.1	468.9	98.6
38	398.4	404.1	410.0	415.7	421.4	427.1	432.9	438.5	444.2	449.8	455.4	461.0	466.7	100.4
39	396.7	402.4	408.1	413.9	419.6	425.3	430.9	436.5	442.1	447.8	453.4	458.9	464.5	102.2
40	394.9	400.7	406.4	412.1	417.7	423.4	429.0	434.6	440.2	445.7	451.3	456.8	462.4	104.0

TABLE 8D. $F(t, w)$ for t from 34 C (93.2 F) to 40 C (104 F); w from 36 to 45.

tC	w 36	37	38	39	40	41	42	43	44	45	w tF
34	475.6										93.20
35	473.4	479.1									95.00
36	471.1	476.8	482.4	488.1	493.7						96.80
37	468.9	474.5	480.1	485.6	491.2	496.7	502.2	507.7			98.60
38	466.7	472.3	477.8	483.3	488.9	494.4	499.8	505.3	510.8		100.40
39	464.5	470.0	475.5	481.0	486.6	492.1	497.5	502.9	508.4	513.8	102.20
40	462.4	467.9	473.4	478.9	484.3	489.8	495.2	500.6	506.0	·511.4	104.00

replace the exponential by its value at the middle of the height range. This approximation does not lead to an error of more than 0.1 M units at these low altitudes.

Pressure versus Height

The differential equation connecting height with pressure may be written

$$\frac{dp}{p} = -\frac{g}{R}\frac{dh}{T}, \qquad (21)$$

where g = acceleration of gravity,

   R = gas constant for air.

Table 9. p/p_0 for h from 50 m (164 ft) to 2,000 m (6,562 ft) and $\bar{t}^*$ from −30 C (−22 F) to 40 C (104 F).

h (m)	−30	−25	−20	−15	−10	− 5	±0	+5	+10	+15	+20	+25	+30	+35	+40	h (ft)
50	0.9930	0.9931	0.9933	0.9934	0.9935	0.9936	0.9938	0.9939	0.9940	0.9941	0.9942	0.9943	0.9944	0.9945	0.9946	164.0
100	0.9860	0.9863	0.9866	0.9869	0.9871	0.9874	0.9876	0.9878	0.9880	0.9882	0.9884	0.9886	0.9888	0.9890	0.9892	328.1
150	0.9791	0.9795	0.9799	0.9802	0.9807	0.9810	0.9814	0.9817	0.9821	0.9823	0.9827	0.9829	0.9832	0.9835	0.9837	492.1
200	0.9723	0.9727	0.9734	0.9738	0.9744	0.9748	0.9753	0.9757	0.9761	0.9766	0.9770	0.9774	0.9777	0.9780	0.9784	656.2
250	0.9655	0.9662	0.9668	0.9674	0.9681	0.9686	0.9692	0.9698	0.9703	0.9707	0.9713	0.9717	0.9722	0.9727	0.9730	820.2
300	0.9587	0.9595	0.9603	0.9610	0.9618	0.9625	0.9632	0.9637	0.9644	0.9650	0.9656	0.9662	0.9667	0.9672	0.9678	984.3
350	0.9519	0.9529	0.9538	0.9547	0.9556	0.9564	0.9572	0.9579	0.9586	0.9593	0.9600	0.9607	0.9613	0.9619	0.9625	1,148.0
400	0.9453	0.9464	0.9474	0.9484	0.9494	0.9503	0.9512	0.9519	0.9529	0.9537	0.9544	0.9551	0.9559	0.9566	0.9572	1,312.0
450	0.9387	0.9399	0.9410	0.9421	0.9432	0.9442	0.9452	0.9462	0.9471	0.9480	0.9489	0.9497	0.9505	0.9513	0.9520	1,476.0
500	0.9321	0.9334	0.9347	0.9359	0.9371	0.9383	0.9394	0.9404	0.9414	0.9424	0.9434	0.9443	0.9452	0.9460	0.9469	1,640.0
600	0.9191	0.9206	0.9222	0.9236	0.9250	0.9263	0.9277	0.9289	0.9301	0.9313	0.9324	0.9335	0.9346	0.9355	0.9366	1,969.0
700	0.9063	0.9081	0.9098	0.9115	0.9131	0.9146	0.9161	0.9176	0.9190	0.9203	0.9216	0.9229	0.9241	0.9253	0.9264	2,297.0
800	0.8936	0.8957	0.8976	0.8995	0.9013	0.9030	0.9047	0.9063	0.9079	0.9095	0.9109	0.9124	0.9138	0.9151	0.9164	2,625.0
900	0.8812	0.8834	0.8856	0.8876	0.8897	0.8916	0.8935	0.8953	0.8971	0.8987	0.9004	0.9019	0.9035	0.9050	0.9064	2,953.0
1,000	0.8688	0.8712	0.8737	0.8760	0.8782	0.8803	0.8824	0.8843	0.8863	0.8881	0.8899	0.8917	0.8934	0.8950	0.8966	3,281.0
1,500	0.8099	0.8133	0.8166	0.8198	0.8230	0.8260	0.8289	0.8317	0.8344	0.8370	0.8395	0.8420	0.8444	0.8467	0.8490	4,921.0
2,000	0.7549	0.7592	0.7633	0.7674	0.7712	0.7749	0.7786	0.7821	0.7855	0.7888	0.7920	0.7951	0.7981	0.8011	0.8039	6,562.0
	−22.0	−13.0	−4.0	+5.0	+14.0	+23.0	+32.0	+41.0	+50.0	+59.0	+68.0	+77.0	+86.0	+95.0	+104.0	t F

*$\bar{t}$ = temperature averaged from the ground to the height h.

Table 10A. u for h from 10 m (32.8 ft) to 150 m (492.1 ft); F from 250 to 370. Values to be subtracted from F to obtain $Fp = (n - 1)\,10^6$.

h (m)	250	260	270	280	290	300	310	320	330	340	350	360	370	h (ft)
10	0.3	0.3	0.3	0.3	0.3	0.4	0.4	0.4	0.4	0.4	0.4	0.4	0.4	32.8
20	0.6	0.7	0.7	0.7	0.7	0.8	0.8	0.8	0.8	0.9	0.9	0.9	0.9	65.6
30	0.9	1.0	1.0	1.0	1.1	1.1	1.1	1.2	1.2	1.3	1.3	1.3	1.4	98.4
40	1.3	1.3	1.4	1.4	1.5	1.5	1.6	1.6	1.7	1.7	1.8	1.8	1.9	131.2
50	1.6	1.6	1.7	1.7	1.8	1.9	1.9	2.0	2.0	2.1	2.2	2.2	2.3	164.0
60	1.9	1.9	2.0	2.1	2.1	2.2	2.3	2.4	2.4	2.5	2.6	2.7	2.7	196.9
70	2.2	2.3	2.3	2.4	2.5	2.6	2.7	2.8	2.9	3.0	3.0	3.1	3.2	229.7
80	2.5	2.6	2.7	2.8	2.9	3.0	3.1	3.2	3.3	3.4	3.5	3.6	3.7	262.5
90	2.8	2.9	3.0	3.1	3.2	3.4	3.5	3.6	3.7	3.8	3.9	4.0	4.1	295.3
100	3.1	3.2	3.3	3.5	3.6	3.7	3.8	4.0	4.1	4.2	4.3	4.5	4.6	328.1
110	3.4	3.5	3.7	3.8	3.9	4.1	4.2	4.4	4.5	4.6	4.8	4.9	5.0	360.9
120	3.7	3.9	4.0	4.2	4.3	4.5	4.6	4.8	4.9	5.1	5.2	5.4	5.5	393.7
130	4.0	4.2	4.3	4.5	4.7	4.8	5.0	5.2	5.3	5.5	5.6	5.8	6.0	426.5
140	4.4	4.5	4.7	4.9	5.0	5.2	5.4	5.6	5.7	5.9	6.1	6.3	6.4	459.3
150	4.7	4.8	5.0	5.2	5.4	5.6	5.8	6.0	6.1	6.3	6.5	6.7	6.9	492.1

Table 10B. u for h from 10 m (32.8 ft) to 150 m (492.1 ft); F from 370 to 500. Values to be subtracted from F to obtain $Fp = (n - 1)\,10^6$.

h (m)	370	380	390	400	410	420	430	440	450	460	470	480	490	500	h (ft)
10	0.4	0.5	0.5	0.5	0.5	0.5	0.5	0.5	0.5	0.6	0.6	0.6	0.6	0.6	32.8
20	0.9	1.0	1.0	1.0	1.0	1.1	1.1	1.1	1.1	1.2	1.2	1.2	1.2	1.3	65.6
30	1.4	1.4	1.4	1.5	1.5	1.6	1.6	1.6	1.7	1.7	1.7	1.8	1.8	1.9	98.4
40	1.9	1.9	2.0	2.0	2.1	2.1	2.2	2.2	2.3	2.3	2.4	2.4	2.5	2.5	131.2
50	2.3	2.4	2.4	2.5	2.5	2.6	2.7	2.7	2.8	2.9	2.9	3.0	3.0	3.1	164.0
60	2.7	2.8	2.9	3.0	3.0	3.1	3.2	3.3	3.3	3.4	3.5	3.6	3.6	3.7	196.9
70	3.2	3.3	3.4	3.5	3.6	3.7	3.7	3.8	3.9	4.0	4.1	4.2	4.3	4.4	229.7
80	3.7	3.8	3.9	4.0	4.1	4.2	4.3	4.4	4.5	4.6	4.7	4.8	4.9	5.0	262.5
90	4.1	4.3	4.4	4.5	4.6	4.7	4.8	4.9	5.0	5.2	5.3	5.4	5.5	5.6	295.3
100	4.6	4.7	4.8	5.0	5.1	5.2	5.3	5.5	5.6	5.7	5.8	6.0	6.1	6.2	328.1
110	5.0	5.2	5.3	5.4	5.6	5.7	5.8	6.0	6.1	6.3	6.4	6.5	6.7	6.8	360.9
120	5.5	5.7	5.8	6.0	6.1	6.3	6.4	6.6	6.7	6.9	7.0	7.2	7.3	7.5	393.7
130	6.0	6.1	6.3	6.4	6.6	6.8	6.9	7.1	7.2	7.4	7.6	7.7	7.9	8.1	426.5
140	6.4	6.6	6.8	7.0	7.1	7.3	7.5	7.7	7.8	8.0	8.2	8.4	8.5	8.7	459.3
150	6.9	7.1	7.3	7.4	7.6	7.8	8.0	8.2	8.4	8.6	8.7	8.9	9.1	9.3	492.1

Since g is not strictly constant (it varies slightly with height and locality) and since R, to a slight extent, is dependent on the percentage of water vapor in the air and, finally, since T may be an arbitrary function of height, this differential equation cannot be integrated exactly. However, a careful consideration of the order of magnitude of changes in the pressure brought about by the slight changes of g and R leads to the conclusion that such variations may be neglected, particularly as these changes have practically no effect on the slopes of M curves. Picking the best overall values of g and R ($g = 9.80665$ and $R = 287.05$ in the units used in this report) gives $\alpha = g/R = 0.034163$ as the value to be used in equation (8).

The variation of temperature with height cannot, however, be neglected in the integration of equation

TABLE 10C. u for h from 150 m (492.1 ft) to 500 m (1,640 ft); F from 250 to 340. Values to be subtracted from F to obtain $Fp = (n - 1) 10^6$.

h (m) \ F	250	260	270	280	290	300	310	320	330	340	h (ft)
150	4.7	4.8	5.0	5.2	5.4	5.6	5.8	6.0	6.1	6.3	492.1
175	5.4	5.6	5.9	6.1	6.3	6.5	6.7	6.9	7.2	7.4	574.1
200	6.2	6.4	6.7	6.9	7.2	7.4	7.7	7.9	8.2	8.4	656.2
225	7.0	7.2	7.5	7.8	8.1	8.3	8.6	8.9	9.2	9.5	738.2
250	7.7	8.0	8.3	8.6	8.9	9.2	9.5	9.9	10.2	10.5	820.2
275	8.5	8.8	9.1	9.5	9.8	10.1	10.5	10.8	11.1	11.5	902.2
300	9.2	9.6	9.9	10.3	10.7	11.0	11.4	11.8	12.1	12.5	984.3
325	10.0	10.3	10.7	11.1	11.5	11.9	12.3	12.7	13.1	13.5	1,066.0
350	10.7	11.1	11.6	12.0	12.4	12.8	13.3	13.7	14.1	14.6	1,148.0
375	11.5	11.9	12.4	12.8	13.3	13.7	14.2	14.7	15.1	15.6	1,230.0
400	12.2	12.6	13.2	13.7	14.2	14.6	15.1	15.6	16.1	16.6	1,312.0
425	13.0	13.5	14.0	14.5	15.0	15.5	16.1	16.6	17.1	17.6	1,394.0
450	13.7	14.2	14.8	15.3	15.9	16.4	17.0	17.5	18.1	18.6	1,476.0
475	14.4	15.0	15.6	16.2	16.7	17.3	17.9	18.5	19.0	19.6	1,558.0
500	15.2	15.8	16.4	17.0	17.6	18.2	18.8	19.4	20.0	20.6	1,640.0

TABLE 10D. u for h from 150 m (492.1 ft) to 500 m (1,640 ft); F from 340 to 420. Values to be subtracted from F to obtain $Fp = (n - 1) 10^6$.

h (m) \ F	340	350	360	370	380	390	400	410	420	h (ft)
150	6.3	6.5	6.7	6.9	7.1	7.3	7.4	7.6	7.8	492.1
175	7.4	7.6	7.8	8.0	8.2	8.5	8.7	8.9	9.1	574.1
200	8.4	8.6	8.9	9.1	9.4	9.6	9.9	10.1	10.4	656.2
225	9.5	9.7	10.0	10.3	10.6	10.8	11.1	11.4	11.7	738.2
250	10.5	10.8	11.1	11.4	11.7	12.0	12.3	12.6	12.9	820.2
275	11.5	11.8	12.2	12.5	12.8	13.2	13.5	13.9	14.2	902.2
300	12.5	12.9	13.2	13.6	14.0	14.4	14.7	15.1	15.5	984.3
325	13.5	13.9	14.3	14.7	15.1	15.5	15.9	16.3	16.7	1,066.0
350	14.6	15.0	15.4	15.8	16.3	16.7	17.1	17.5	18.0	1,148.0
375	15.6	16.0	16.5	16.9	17.4	17.9	18.3	18.8	19.2	1,230.0
400	16.6	17.1	17.6	18.1	18.5	19.0	19.5	20.0	20.5	1,312.0
425	17.6	18.1	18.6	19.2	19.7	20.2	20.7	21.2	21.8	1,394.0
450	18.6	19.2	19.7	20.3	20.8	21.4	21.9	22.5	23.0	1,476.0
475	19.6	20.2	20.8	21.3	21.9	22.5	23.1	23.7	24.2	1,558.0
500	20.6	21.2	21.8	22.4	23.0	23.6	24.2	24.8	25.5	1,640.0

TABLE 10E. u for h from 150 m (492.1 ft) to 500 m (1,640 ft); F from 420 to 500. Values to be subtracted from F to obtain $Fp = (n - 1) 10^6$.

h (m) \ F	420	430	440	450	460	470	480	490	500	h (ft)
150	7.8	8.0	8.2	8.4	8.6	8.7	8.9	9.1	9.3	492.1
175	9.1	9.3	9.5	9.8	10.0	10.2	10.4	10.6	10.9	574.1
200	10.4	10.6	10.9	11.1	11.4	11.6	11.9	12.1	12.4	656.2
225	11.7	12.0	12.2	12.5	12.8	13.1	13.3	13.6	13.9	738.2
250	12.9	13.2	13.6	13.9	14.2	14.5	14.8	15.1	15.4	820.2
275	14.2	14.5	14.9	15.2	15.5	15.9	16.2	16.6	16.9	902.2
300	15.5	15.8	16.2	16.6	16.9	17.3	17.7	18.0	18.4	984.3
325	16.7	17.1	17.5	17.9	18.3	18.7	19.1	19.5	19.9	1,066.0
350	18.0	18.4	18.8	19.3	19.7	20.1	20.5	21.0	21.4	1,148.0
375	19.2	19.7	20.2	20.6	21.1	21.5	22.0	22.4	22.9	1,230.0
400	20.5	21.0	21.5	22.0	22.4	22.9	23.4	23.9	24.4	1,312.0
425	21.8	22.3	22.8	23.3	23.8	24.3	24.9	25.4	25.9	1,394.0
450	23.0	23.6	24.1	24.7	25.2	25.8	26.3	26.9	27.4	1,476.0
475	24.2	24.8	25.4	26.0	26.5	27.1	27.7	28.3	28.9	1,558.0
500	25.5	26.1	26.7	27.3	27.9	28.5	29.1	29.7	30.3	1,640.0

(21). The integrated form of equation (21) is equation (8), where the approximation

$$\int_0^h \frac{dh}{T} = \frac{h}{T} \qquad (22)$$

has been made. $\overline{T}$ is the average temperature defined by equation (9) or, more roughly, by equation (10).

An estimate of the order of accuracy of this approximation may be obtained from an examination of the case in which T varies linearly with h. Let the reference level temperature be T_0 at $h = 0$ and the temperature at the height h_1 be T_1.

Then

$$\frac{h_1}{\overline{T}} = \frac{2h_1}{T_0 + T_1} \qquad (23)$$

and, for this linear case

$$\int_0^{h_1} \frac{dh}{T} = \frac{h_1}{T_1 - T_0} \log \frac{T_1}{T_0}$$

$$= \frac{2h_1}{T_1 - T_0}\left[\frac{T_1 - T_0}{T_1 + T_0} + \frac{1}{3}\left(\frac{T_1 - T_0}{T_1 + T_0}\right)^3 + \cdots\right] \qquad (24)$$

TABLE 11A. Δu for $\bar{t}^* \neq 0$. Values to be multiplied by $h \times 10^{-2}$ and $\begin{Bmatrix}\text{added to} \\ \text{subtracted from}\end{Bmatrix}$ u for $\begin{Bmatrix}\bar{t} < 0 \\ \bar{t} > 0\end{Bmatrix}$.

$\bar{t}$ \ F	250	260	270	280	290	300	310	320	330	340	350	360	370
±10	0.1	0.1	0.1	0.1	0.1	0.1	0.1	0.1	0.1	0.2	0.2	0.2	0.2
±20	0.2	0.2	0.2	0.3	0.3	0.3	0 3	0.3	0.3	0.3	0.3	0.3	0.3
±30	0.3	0.4	0.4	0.4	0.4	0.4	0.4	0.4	0.4	0.5	0.5	0.5	0.5
±40	0.5	0.5	0.5	0.5	0.5	0.5	0.6	0.6	0.6	0.6	0.6	0.7	0.7

$*\bar{t}$ = temperature in degrees centigrade averaged from the ground to the height h

TABLE 11B. Δu for $\bar{t}^* \neq 0$. Values to be multiplied by $h \times 10^{-2}$ and $\begin{Bmatrix}\text{added to} \\ \text{subtracted from}\end{Bmatrix}$ u for $\begin{Bmatrix}\bar{t} < 0 \\ \bar{t} > 0\end{Bmatrix}$.

$\bar{t}$ \ F	370	380	390	400	410	420	430	440	450	460	470	480	490	500
±10	0.2	0.2	0.2	0.2	0.2	0.2	0.2	0.2	0.2	0.2	0 2	0.2	0.2	0.2
±20	0.3	0.3	0.4	0.4	0.4	0.4	0.4	0.4	0.4	0.4	0.4	0.4	0.4	0.5
±30	0.5	0.5	0.5	0.5	0.6	0.6	0.6	0.6	0.6	0.6	0.6	0.7	0.7	0·7
±40	0.7	0.7	0.7	0.7	0.7	0.8	0.8	0.8	0.8	0.8	0.9	0.9	0.9	0.9

$*\bar{t}$ = temperature in degrees centigrade averaged from the ground to the height h

TABLE 11C. Δu for $\bar{t}^* \neq 0$.   Values to be multiplied by $h \times 10^{-2}$ and $\begin{Bmatrix}\text{added to} \\ \text{subtracted from}\end{Bmatrix}$ u for $\begin{Bmatrix}\bar{t} < 0 \\ \bar{t} > 0\end{Bmatrix}$.

$\bar{t}$ \ F	250	260	270	280	290	300	310	320	330	340
±10	0.1	0.1	0.1	0.1	0.1	0.1	0.1	0.1	0.1	0.1
±20	0.2	0.2	0.2	0.2	0.3	0.3	0.3	0.3	0.3	0.3
±30	0.3	0.3	0.4	0.4	0.4	0.4	0.4	0.4	0.4	0.5
±40	0.4	0.5	0.5	0.5	0.5	0.5	0.5	0.6	0.6	0.6

$*\bar{t}$ = temperature in degrees centigrade averaged from the ground to the height h

TABLE 11D. Δu for $\bar{t}^* \neq 0$.   Values to be multiplied by $h \times 10^{-2}$ and $\begin{Bmatrix}\text{added to} \\ \text{subtracted from}\end{Bmatrix}$ u for $\begin{Bmatrix}\bar{t} < 0 \\ \bar{t} > 0\end{Bmatrix}$.

$\bar{t}$ \ F	340	350	360	370	380	390	400	410	420
±10	0.1	0.2	0.2	0.2	0.2	0.2	0.2	0.2	0.2
±20	0.3	0.3	0.3	0.3	0.3	0.3	0.4	0.4	0.4
±30	0.5	0.5	0.5	0.5	0.5	0.5	0.5	0.5	0.6
±40	0.6	0.6	0.6	0.7	0.7	0.7	0.7	0.7	0.7

$*\bar{t}$ = temperature in degrees centigrade averaged from the ground to the height h.

TABLE 11E. Δu for $\bar{t}^* \neq 0$. Values to be multiplied by $h \times 10^{-2}$ and $\begin{Bmatrix}\text{added to} \\ \text{subtracted from}\end{Bmatrix}$ u for $\begin{Bmatrix}\bar{t} < 0 \\ \bar{t} > 0\end{Bmatrix}$.

$\bar{t}$ \ F	420	430	440	450	460	470	480	490	500
±10	0.2	0.2	0.2	0.2	0.2	0.2	0.2	0.2	0.2
±20	0.4	0.4	0.4	0.4	0.4	0.4	0.4	0.4	0.4
±30	0.6	0.6	0.6	0.6	0.6	0.6	0.6	0.7	0.7
±40	0.7	0.8	0.8	0.8	0.8	0.8	0.8	0.9	0.9

$*\bar{t}$ = temperature in degrees centigrade averaged from the ground to the height h.

by a well-known expansion for the natural logarithm. The first term in the series (24) gives exactly equation (23). Hence, the approximation (22) amounts to dropping the higher-order terms in equation (24). The ratio of the second term to the first is only $\frac{1}{3}[(T_1 - T_0)/(T_1 + T_0)]^2$ or about two parts in 10,000 for the first 2,000 m of the standard atmosphere. This comes out to give an error of about 0.006 mb in the pressure at this height. This is certainly negligible.

For a nonlinear atmosphere the question of the error in equation (22) is chiefly a question of the accuracy in determining T, since any such atmosphere can be broken up into a number of layers in each of which T is linear in h.

CONSTANTS OF THE INDEX OF REFRACTION FORMULA

The formula for the ordinary index of refraction, n, which has been used in calculating these tables, is

$$(n-1) 10^6 = \frac{Ap}{T} - \frac{De}{T} + \frac{Be}{T^2}, \qquad (25)$$

where $A = 79, D = 11, B = 3.8 \times 10^5$. (26)

The formula given in reference 11, in the units adopted here, is the same as (25) but with

$$A = 78.7, D = 11.2, B = 3.77 \times 10^5. \qquad (27)$$

The formula used by Bell Telephone Laboratories (Monograph B-870, 1935) is also (25) but with

$$A = 79.1, D = 10.9, B = 3.81 \times 10^5. \qquad (28)$$

The third significant figure in all these constants is questionable. Moreover, the absolute value of n (or M) is not important but only the slopes of M curves. For this purpose it is sufficient if the right form of equation and approximately correct values of the constants are chosen. Hence, in these tables, equations (25) and (26) were adopted

DIURNAL VARIATION OF THE GRADIENT OF MODIFIED M INDEX[a]

The vertical gradient of modified refractive index depends on the vapor pressure and temperature gradients according to the formula[b]

$$\frac{dM}{dz} = \frac{79}{T}\left(\frac{4800 - 0.14T}{T}\right)\frac{de}{dz} - \frac{79}{T^2} \cdot$$
$$\left(\frac{9600e}{T} + p - 0.14e\right)\frac{dT}{dz} + \left(\frac{1}{21} + \frac{79}{T} \cdot \frac{dp}{dz}\right)$$

[a]By Raymond Wexler, Camp Evans Signal Laboratory.

[b]Symbols have same meaning as in preceding section, except that h is replaced by z.

Coefficients of vapor pressure and temperature gradients are about 4.5 and 1.5 respectively. The third term gives a positive increase of 4 M units per 100 ft. In this paper[11-14] the diurnal variation of the vertical M gradient will be inferred from the diurnal variation of temperature and humidity gradients.

Temperature Lapse Rates over Land

On clear nights with light winds temperature inversions form in the lower atmosphere. The following characteristics of these inversions are to be noted.

1. The inversion begins as a shallow layer near the ground before sunset, rises sharply after sunset and then more gradually to a maximum height at about sunrise.

2. The temperature difference between two fixed levels in the first 100 ft of the ground is maximum shortly before sunset and oscillates about a slightly lower value the remainder of the night. (See Figure 10.)

Observations at Leafield, England, and Potsdam, Germany, corroborate this. This phenomenon is probably due to the more favorable humidity gradient in the early evening and to the heat of condensation released by dew formation in the later night hours.

Superadiabatic lapse rates characterize the lower atmosphere during clear days. The lapse rates increase sharply from sunrise to 3 or 4 hours after, gradually reach a maximum at about noon, and decrease sharply after the time of the maximum temperature.

Temperature Lapse Rates over the Sea

The air over the sea has a greater diurnal range than the sea itself. Over the Sunda Sea this range has been observed to increase from 0.5 C at the sur-
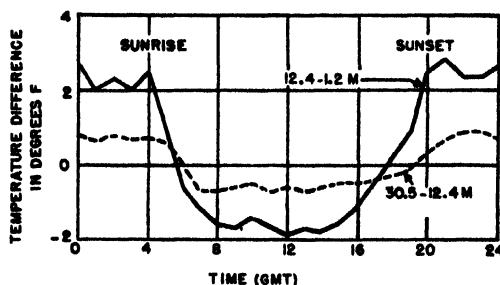
FIGURE 10. Mean temperature variation on clear June days at Leafield, England.

face to 1.5 C at 500 m. The night lapse rates over the ocean are therefore more unstable than the day lapse rates. Observations of the *Meteor* expedition in equatorial regions revealed a mean inversion of 0.2 C in the first 9 m during the early afternoon, whereas in the early morning a mean lapse of 0.6 C was observed.

Vertical Vapor Pressure Gradients

At locations where a continuous supply of moisture

on the ground is available, vapor pressure gradients follow evaporation processes and are maximum at the time of the maximum temperature at about sunrise. This diurnal course characterizes conditions over the sea, cloudy days over the land, and winter or rainy seasons over the continent.

On clear days over the continent the vertical vapor pressure gradient is minimum at about sunrise, reaches a maximum in midmorning, and lowers to a secondary minimum at the time of the maximum temperature (in desert regions this is the principal maximum shortly after sunset). Evaporation and mixing with drier air aloft govern this course. At night the soil absorbs moisture from the air causing a decrease in vapor pressure gradient.

The seasonal and diurnal variation of vapor pressure gradient is illustrated in Figure 11. Maximum vapor pressure gradients are noted during April, the hottest time of year, and minimum in January. The oceanic type is represented by the curve for July in the rainy season.

Vertical M Gradient

Over the sea both temperature and humidity gradients aid in causing a maximum of trapping during the day and a minimum during the night. The effect, however, is probably small.

Over the continent, a minimum of trapping will exist in midafternoon. Thereafter both temperature and humidity factors will cause a rise in the vertical M gradient t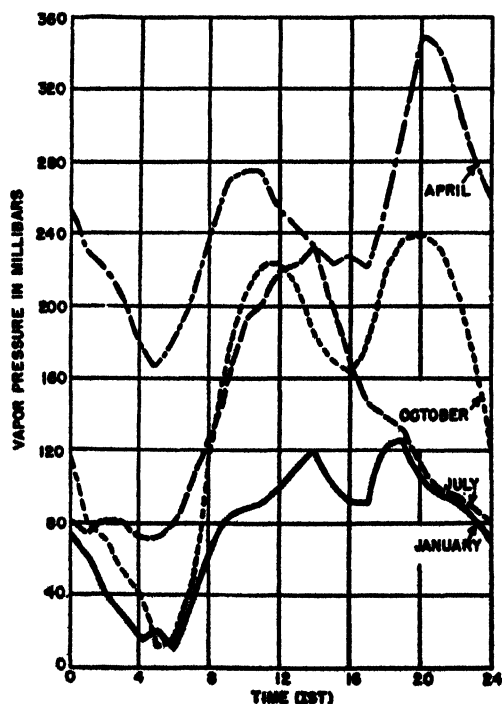o a maximum shortly after sunset. From that time to sunrise a decrease in the M gradient will occur. However, the height of the inversion continues to grow until sunrise, tending to cause an increase in the height of the duct. Whether a maximum or minimum of trapping will occur at sunrise will depend on whether the increase in the height of the inversion balances the decrease in vertical humidity gradient. It is probable that the humidity factor is the more important since the small magnitude of the temperature increase in the upper portions of the inversion will seldom be sufficient to cause a decrease in M with height. After sunrise rising humidity gradients, partially balanced by falling temperature gradients, will cause a small maximum of M gradient at midmorning. Thereafter the M gradient will decrease to the afternoon minimum.

The maximum and minimum decrease of M from 6 ft to 46 ft, based on mean temperature and humidity data at Calcutta, India, are given in Table 12.

In July the morning minimum and afternoon maximum with small amplitude illustrate the oceanic type. The other months illustrate the continental type. According to the table a maximum of trapping in India should occur in April just prior to the rainy season.

TABLE 12. Decrease of M from 6 to 46 ft (Calcutta).

Month	A.M.		P.M.	
	Min	Max	Min	Max
Jan	1	4	1	6
April	7	9	5	16
July	2	..	..	6
Oct	1	7	3	11

DETERMINING FLUCTUATIONS IN REFRACTIVE INDEX NEAR LAND OR SEA[1]

In connection with the rapid fluctuation or scintillation frequently observed in microwave reception, questions arise concerning turbulent atmospheric fluctuation at fixed points along the transmission path, particularly fluctuations in refractive index. Rapid measurement of both temperature and humidity so as to give a direct determination of fluctuation in refractive index is difficult. The purpose of this paper is to suggest that in certain cases the measurement of temperature fluctuation alone can give a good indirect estimate of fluctuation in the modified index.

The basic principle underlying this suggestion is that, if two initial kinds of air are mixed in different proportions, for all possible mixtures a fixed relation exists between any two properties conservative for adiabatic changes.

To illustrate this, consider a diagram with potential temperature and specific humidity as coordinates. Two initial kinds of air would be represented by two

FIGURE 11. Hourly vapor pressure difference, 6 to 46 ft at Calcutta.

points on this diagram, and all mixtures of the two kinds would be represented by points on the straight line drawn between the two initial points.

The practical case occurs when one point represents a large homogeneous mass of air, and the other a fixed boundary condition at the ground or water surface. The straight line then represents the mixtures that can occur in the vicinity of the boundary. For these the line shows specific humidity as a function of potential temperature. The relation between potential temperature and potential refractive index could be shown by a similar diagram.

Figure 12 shows some corroboration of this method and also how the method can be applied. This characteristic diagram has the same orientation as the Rossby diagram which is in routine meteorological use but with somewhat different coordinates.

The ordinate is temperature and the abscissa is vapor pressure. A pair of curves gives the vapor pressure over fresh water and over sea water. The family of curves gives refractive index at radio frequencies and at a total pressure of 1,000 mb, or $h = 0$.

On the diagram are plotted a few of a long series of determinations made by reading a sling psychrometer at half-minute intervals. These were recently obtained by the Woods Hole Oceanographic Institution at the masthead of a ship crossing the Gulf

Stream at a time when the air was much colder than the water. The water temperature was 70 F, fixing the boundary condition. The points lie fairly well on the straight line through the boundary value. They cover a range of 5×10^{-6} in refractive index. Probably a greater range would be indicated by a psychrometer having a more rapid response.

It is seen that, whenever the fluctuation in refractive index at a point in the atmosphere is due to turbulent mixing between a large homogeneous mass of air and air controlled by a fixed boundary condition, the fluctuation may be obtained as follows: Measure the average temperature and humidity at this point and at the boundary, thus determining the relation between refractive index and temperature. Measure the fluctuation of temperature, from which the fluctuation of refractive index may be found from the established relation.

It may be noted that the water temperature less the average air temperature gives a value for the temperature deficit. In the same way one may arrive at a humidity deficit and an M deficit (one million times the deficit of refractive index). Each of these quantities is represented on the diagram by the change from one end to the other of the line. It follows that the suggested method may be stated in terms of the relation that the ratio of temperature fluctuation
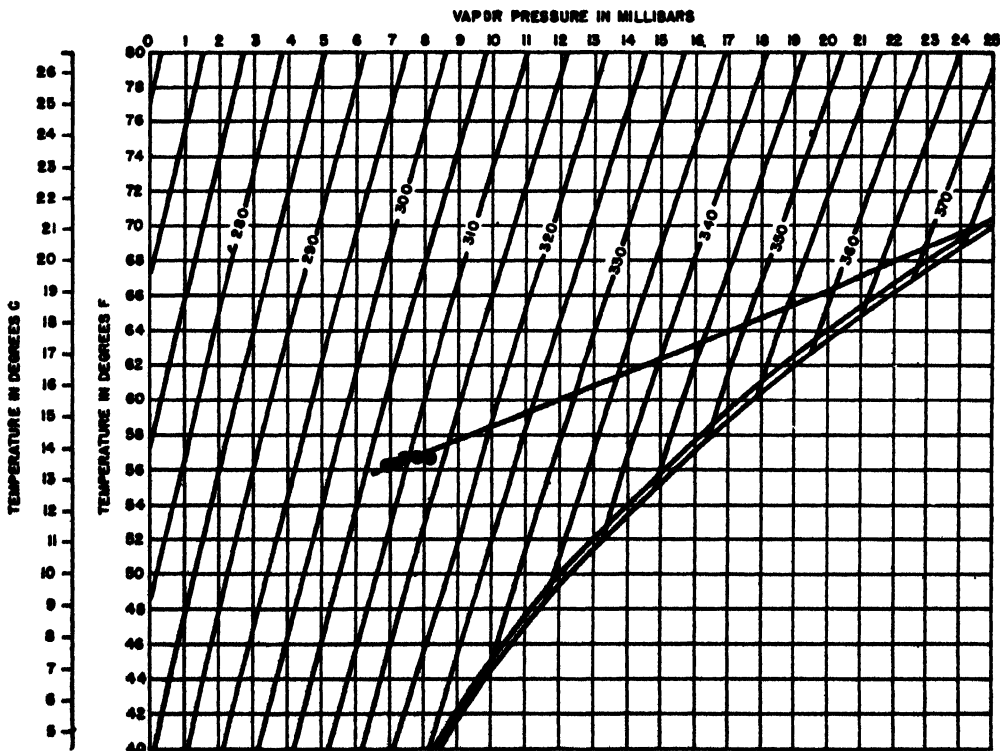

FIGURE 12. Observations on February 24, 1945 at masthead of ship in Gulf Stream, wind 14 knots. Characteristic diagram. Vapor pressure over water is shown by lower bounding curve, over salt water by upper bounding curve. The family of curves gives modified index for 1,000 mb and zero height; or $(n-1)10^6$ for microwaves at 1,000 mb, zero height, where n is refractive index at $h = 0$.

to temperature deficit is equal to the ratio of humidity fluctuation to humidity deficit and very nearly equal to the ratio of M fluctuation to M deficit.

GRAVITATIONAL WAVES AND TEMPERATURE INVERSIONS[j]

It has been noted that the guided propagation of microwaves is often accompanied by deep fades with periods of the order of a few minutes. The suggestion has been made that these fluctuations may be associated with atmospheric wave motion which could make the top of the duct an undulating surface rather than a level one.[16,17] Therefore, it seems desirable to discuss, from a meteorological point of view, the possibility of the existence of such atmospheric waves and the physical characteristics of any which might exist. The purpose of this paper is to review and summarize the meteorological information which is available concerning the subject.

A theoretical consideration of the problem indicates that atmospheric wave motion can occur at any surface in the atmosphere where there is a rapid change in wind velocity with height and a stable stratification of temperature. Such conditions are best fulfilled at temperature inversions, which, it will be noted, usually correspond to a rapid decrease with height of the index of refraction. The wind shear supplies the energy to set up the wave motion, in the same way in which waves are formed at the surface of the ocean. Gravitation acts as a stabilizing or restoring force. Hence, these waves are of a mixed shearing and gravitational type. The waves may be stable or unstable, depending on their wavelength, on the density and wind speed differences between the two media, and on the lapse rates in the two media. For any given values of the density and wind velocity differences and of the lapse rates, there is a critical wavelength below which wave motion is unstable; that is, it disappears into turbulent eddies because of the shearing effect. All wavelengths above this critical value will remain stable because of the gravitational effect. Hence one may speak of the former as "shearing waves" and of the latter as "gravitational waves." It is the stable or gravitational type with which we are concerned.

These considerations hold for wavelengths up to about 500 km. For longer wavelengths the effect of the earth's rotation must be considered. In this paper only the shorter wavelengths where this effect may be neglected will be discussed.

A mathematical analysis of wave motion and determination of the critical wavelengths involves a solution of the equations of motion and continuity and an application of certain boundary conditions. In order

[j]By Lt. R. A. Craig, AAF, Weather Division.

to derive the critical wavelengths given below, the following assumptions have been made.

1. The inversion or shearing layer may be regarded as a strict discontinuity between the air above and the air below. This assumption is sufficiently accurate provided the thickness of the layer is small compared to the wavelengths which occur.

2. The velocities associated with the wave motion are small compared with the undisturbed velocities of the air masses above and below the inversion.

3. The height of the inversion above the lower boundary (ground) is equal to or greater than 40 per cent of the wavelength which occurs.

4. There is no friction between the two fluids.

Two cases may be considered. The first is the case where the air masses are assumed to be incompressible and homogeneous. It also holds for two air masses with adiabatic lapse rates. In this case the critical wavelength is given by[18a]

$$\lambda_{crit} = \frac{2\pi}{(T'-T)g} \frac{(U'-U)^2}{T'+T} T'T$$

In the second case the air masses are compressible and isothermal. For this case the critical wavelength is given by[19]

$$\lambda_{crit} = \frac{2\pi}{g} \frac{(U'-U)^2}{4} \cdot \frac{T'+T}{\sqrt{(T'-T)^2 + 2\frac{k-1}{kR}(T'+T)\frac{(U'-U)^2}{4}}} \cdot$$

In these two formulas,

T' = temperature in the upper air,
T = temperature in the lower air,
U' = velocity in the upper air,
U = velocity in the lower air,
g = acceleration of gravity,
k = c_p/c_v = 1.405,
R = gas constant for air
    = 2.87×10^6 cm²/sec² degree.

In Table 13 the critical wavelengths in meters are tabulated for various values of wind shear and temperature difference. Values for the adiabatic case are tabulated above values for the isothermal case. For an intermediate lapse rate some intermediate value holds.

Thus, for any given inversion, stable wave motion may exist so long as the wavelength is equal to or greater than the listed values and less than about 500 km. There is no theoretical reason to believe that any particular wavelength in this wide range is more apt to occur in nature than any other.

There is, however, some observational evidence to indicate that the wavelengths which occur in the atmosphere are near the lowest possible values which can occur, namely, the critical values tabulated above. Billow clouds have been observed to occur near in-

Table 13. Critical wavelengths in meters for $T = 280°A$.

ΔT (C)	ΔU (meters per second)							
	0	2	4	6	8	10	12.	14
0	..	∞	∞	∞	∞	∞	∞	∞
	0	339	677	1016	1354	1693	2031	2370
2	0	180	718	1616	2872	4488	6463	8796
	0	159	493	860	1225	1584	1938	2287
4	0	90	359	808	1436	2244	3231	4398
	0	87	317	632	985	1351	1720	2087
6	0	60	239	539	958	1496	2155	2933
	0	59	226	479	782	1121	1478	1843
8	0	45	180	404	718	1122	1616	2199
	0	44	174	375	634	935	1264	1612
10	0	36	144	323	574	898	1293	1759
	0	36	140	308	529	793	1090	1413
12	0	30	120	269	479	748	1077	1465
	0	30	118	260	451	684	952	1247
14	0	26	103	231	410	641	923	1256
	0	26	101	225	393	600	841	1110

Upper value: incompressible, homogeneous fluids. Lower value: compressible, isothermal fluids.

versions, and there are some ten cases on record where wavelengths of the billows as well as values for the temperature and wind velocity differences have been observed. In these cases the maximum difference between observed wavelength and critical wavelength was 48 per cent. In only three cases was the difference greater than 15 per cent.[18b]

Other weather phenomena have been observed which indicate stable wave motion in the atmosphere. In 1936, quite regular fluctuations were measured in ceiling height at San Diego on two occasions. The amplitude of the fluctuations averaged 25 to 30 m in the two cases, with periods of about 15 to 20 min over time intervals of 4 or 5 hours.[20] In 1934 at the Blue Hill Observatory in Massachusetts, there occurred wave-like fluctuations in the pressure record, which were analyzed by Haurwitz.[21] In these cases upper-air data were not sufficiently accurate to compute wavelengths quantitatively by means of the critical wavelength formula, but it appeared from approximate values of wind shear and density difference that the critical wavelengths might well be occurring.

If it is desired, then, to predict what wavelengths will occur with a given inversion, the critical values would seem in the light of these observations to give a good estimate of the order of magnitude.

Assuming that these wavelengths are the ones which occur, one can discuss the velocities and periods of the wave motion. For these critical wavelengths, the velocity of the wave motion is the mean of the velocities of the air masses above and below the inversion. Hence the period can be estimated by dividing the wavelength given in the table by this value. As an example, for a mean velocity of 5 m per second, the periods vary from about 6 sec to about 8 min, depending on the wind shear and density difference.

The vertical velocity at the inversion cannot be determined, since an arbitrary constant is involved. However, it can be said that this vertical velocity will

be reduced to one-tenth its inversion value at a height d equal to 37 per cent of the wavelength above the inversion. This holds strictly only for the incompressible, homogeneous case but is approximately correct for the other case as well.

It is known, then, from theoretical considerations and some observational material, that wave motion is apt to occur at a layer in the atmosphere where there is a temperature inversion accompanied by wind shear. When such inversions are believed to be of importance in affecting the propagation of radio waves, it should be remembered that there may well be wave motion occurring and that the interface is not necessarily a level surface. It remains to be determined whether this fact will help to explain the observed very high frequency fading. An estimate of wavelength, period, and velocity of the atmospheric wave motion, as given by Table 13, may be of assistance in testing this possibility.

ANALYSIS OF DUCTS IN THE TRADE WIND REGIONS[k]

This report is an analysis of the frequency and magnitude of low-level and elevated ducts as indicated by meteorological observations over the trade wind areas of the Atlantic and Pacific Oceans. Meteorological soundings of the *Meteor* expedition,[22] taken during 1925 to 1927 over the Atlantic Ocean were utilized in analyzing elevated ducts. Climatological data of the Atlantic and Pacific Oceans were employed in study of low-level ducts. A qualitative analysis of 95 soundings of the *Meteor* expedition had previously been made in reference 23.

Elevated Ducts

TRADE WIND AND DOLDRUMS AREAS

A semipermanent high-pressure system is located over the oceans at about 30 degrees of latitude. The northeast trade winds blow from 30°N to about 5°N. Between the equator and 30°S the southeast trade winds prevail. The doldrums, a region of light winds and heavy rainfall, appears between the two wind systems.

DUCTS IN THE TRADE WIND REGION

In the trade winds a warm, dry subsiding air mass exists over a cool, moist ground layer. The transition zone between the two air masses is characterized by a temperature inversion (increase with height) and a sharp decrease of the water vapor content of the air. It is this transition layer which coincides with the duct, which in this paper is defined as a layer in which the curvature of the path of high-frequency electromagnetic waves exceeds the curvature of the

[k]By Raymond Wexler, Signal Corps Ground Signal Agency.

earth. Within these ducts these waves may be trapped, and abnormally long ranges may occur.

As the trade winds blow toward the equator over warmer ocean areas the heating from below causes the duct to rise and to become weaker until finally near the equator the duct disappears and the two air masses become thoroughly mixed.

HEIGHT OF THE DUCT BASE

The base of the inversion (or duct) increases in elevation equatorward. According to the *Meteor* soundings, taken during March and April, the average elevation of the base of the inversions rose from 700 m at latitudes 15°N to 20°N, to 1,020 m at 10°N to 15°N, and to more than 2,000 m at latitudes 5°N to 10°N. Between the equator and 5°N, no ducts existed to an elevation of 2,500 m.

The elevation of the base of the inversion also increases westward into the Atlantic from the African Coast. At latitudes 15°N to 20°N, its elevation increases from less than 300 m off the African Coast to 1,500 m in mid-Atlantic.
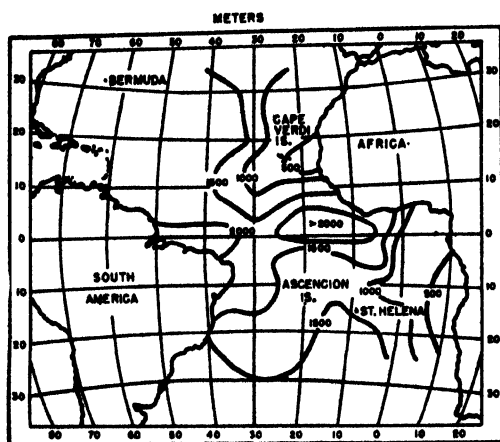

METERS

FIGURE 13. Height of the temperature inversion base over the Atlantic. (After von Ficker.)

Figure 13* depicts the height of the temperature inversion base in the Atlantic, based largely on the data from the *Meteor* expedition. South of the equator, soundings were made during the winter season (June to August), while north of the equator the soundings were made chiefly in the spring (March to May). The height of the base of the inversion has a seasonal variation, being greater in winter than in summer.

Figure 14 represents typical *M* curves computed from the soundings of the *Meteor* expedition. Curves A (sounding 182 of the *Meteor* expedition taken just off the African Coast) show a ground-based duct of elevation 140 m on the ascent curve and 90 m on the descent curve. Oceanward, the duct becomes ground-based, S-shaped, as is shown by curves B (sounding 183)
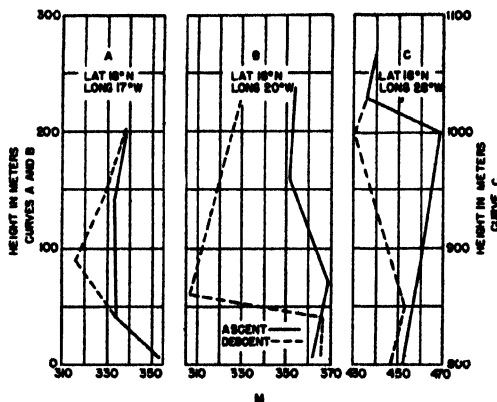

FIGURE 14. *M* curves, *Meteor* expedition, March 1927.

The descent curve[1] shows a decrease of 59 *M* units in 20 m, corresponding to a ray curvature about 20 times greater than that of the earth's surface. Westward into the Atlantic the inversion base rises to about 1,000 m. (Curve C, sounding 184.)

FREQUENCY OF DUCT OCCURRENCE

Within the trades proper a duct is practically certain to exist. In Table 14 the percentage of duct occurrence, by latitude according to *Meteor* soundings, is tabulated. The extreme curve (ascent or descent) was utilized in determining the existence of a duct.

TABLE 14. Frequency of duct occurrence by latitude over the Atlantic Ocean based on the *Meteor* soundings.

Latitude, degrees	Frequency (% of all cases)	No. of cases
20–15N	100	19
15–10N	71	19
10–5N	40	17
5–0N	0	18
0–5S	0	17
5–12S	56	16
12–18S	53	15
18–24S	73	26
24–35S	10	20
35–50S	19	21
50–63S	0	20

It is evident from Table 14 that in the vicinity of the doldrums (5°N to 5°S) the existence of ducts is rare. A maximum frequency occurs between latitudes 15° and 25°. Note that all soundings made between latitudes 15° to 20°N indicated the presence of a duct.

THICKNESS OF DUCTS

The average thickness of the duct in the trade wind inversion, according to *Meteor* data, is about 130 m. According to the theory of the dissipation of the ducts near the equator due to heating from below, the thickness should decrease toward the equa-

---

[1] The ascent and descent curves disagree largely because of the lag of the humidity element in the sounding rig. The curve showing sharper inversion is therefore probably the more accurate.

tor. No evidence of such a decrease was found from the *Meteor* soundings, probably because of the large height interval between observations. For this reason too, the figure for average thickness of 130 m is probably too large.

INTENSITY OF DUCTS

The decrease of the modified index of refraction within the duct averaged 28 *M* units between latitudes 10° to 20°N, and only 14 *M* units between latitudes 5° and 10°N, indicating a decrease in the intensity of the duct equatorward. The intensity of the duct also decreases oceanward from the coast of Africa.

Surface Ducts

The thickness of surface ducts depends on the wind speed and the magnitude of the vapor pressure difference between the ocean surface and the air at some representative level (say the ship's bridge) It is probable that the wind factor is the more important. Near the west coasts of continents the lowering of the trade wind inversion becomes the most important factor. Duct intensities over the ocean in the Northern Hemisphere, based on climatic charts of the ocean, have been computed by Montgomery and Burgoyne.[25]

WIND SPEED

According to observations taken in the Pacific north of New Guinea and northeast of Saipan, ducts were less than 10 ft in depth at wind speeds of one knot and were 40 to 60 ft at wind speeds of 10 to 20 knots.[26] According to climatic charts of the ocean (6), the average wind speed in the trade winds is maximum in summer at 15° to 20°N and in winter at 10° to 15°N. In the Southern Hemisphere maximums are at 10° to 15°S in summer (December to February) and at 5° to 10°S in winter. These latitudes in the respective seasons should also coincide with the maximum thickness of surface ducts.

VAPOR PRESSURE DIFFERENCE

As the air flows toward the equator over continually warmer water surfaces moisture is being supplied to the air by evaporation from the water surface. Nearer the equator the increased rainfall decreases the water vapor pressure difference between the ocean surface and the air above. According to climatic charts[27] the maximum vapor pressure difference between ocean

surface and the air above in the trade exists at about latitudes 20° in summer (in both hemispheres) and at latitudes 10° to 15° in winter. This effect should also contribute to the existence of a maximum duct height in the trade winds at about 20° latitude in summer, 15° in spring and fall, and 10° in winter.

SURFACE DUCTS NEAR THE WESTERN COASTS OF CONTINENTS

All soundings of the *Meteor* expedition within 300 miles of the coast of Africa showed intense ground-based ducts or S-shaped ground-based ducts. These ground-based ducts are also a common occurrence on the west coast of the United States. At San Diego the average height of the inversion base is near 1,000 ft during the summer.[28] The height of the duct base has a diurnal variation, being maximum in the morning at about 0800 local time and minimum at about 1600. The diurnal variations are governed by land and sea breeze phenomena.

Experimental Evidence

During 1944, aircraft traffic to and from Ascension Island at 8°S in the Atlantic was tracked by two 105-mc radars sited 2,500 and 1,700 ft above mean sea level. The following observed phenomena were reported verbally.

1. Ranges were greater during the dry season than during the wet season.

2. Ranges westward (270°) were greater than to the northeast (40°), and greater northeastward than to the north (10°).

The decrease in duct intensity equatorward described herein is commensurate with observation (2), in which ranges are reported to be less toward the equator than along a parallel of latitude.

Conclusions

1. Over the trade wind areas of the oceans both elevated and surface ducts often exist.

2. The elevated duct is of maximum intensity and frequency at 15° to 20° of latitude. It decreases in intensity and frequency equatorward, disappearing in the doldrums.

3. The surface duct, dependent largely on wind speed, is of maximum depth at about latitude 20° in summer, 15° in spring and fall, and 10° in winter.

4. Near the western coasts of continents the elevated duct lowers into an intense ground-based duct.

METEOROLOGICAL EQUIPMENT FOR SHORT WAVE

METEOROLOGICAL EQUIPMENT FOR PROPAGATION STUDIES[a]

Outline of Problem

EXPERIENCE GAINED during the recent years with radar, especially microwave radar, and with experimental microwave communication equipment has shown that the electromagnetic radiation field produced by a transmitter is subject to large variations depending on the weather. These variations are caused by *refraction* and so are related to variations of dielectric constant in the atmosphere. Pressure, temperature, and humidity determine the dielectric constant (refractive index).

It has been found that above a certain height variable with season and geographical location but rarely exceeding 1,500 m above ground, atmospheric refraction is reasonably constant. In the lower levels and especially in the lowest hundred meters of the atmosphere, temperature and moisture conditions strongly affect the radiation field and thereby influence the operation of radar and other short and' microwave equipment. In order to evaluate this effect in quantitative terms, the temperature and moisture distribution in the lowest layers must be determined with as high a degree of accuracy as is compatible with speed, ease of operation, and other practical limitations.

A number of methods have been tried during the recent years which range from measurements with ordinary radiosonde equipment to the use of a psychrometer on the steps of a fire ladder. Two facts have appeared rather clearly: First, hairs are not suitable for moisture measurements of this type on account of their great sluggishness (except perhaps for stationary use on towers), since the time of adaptation of a hair to appreciable changes in humidity is of the order of 3 to 5 minutes. Secondly, it has been found that ordinary radiosondes are not usually appropriate because the readings obtained from them normally are taken about 100 m apart in vertical distance and for this particular problem a more detailed knowledge of the temperature and.moisture distribution is necessary. With a clock-driven radiosonde this can be remedied by loading the sonde down by means of a ballast (water or sand) which slows down the ascent of the instrument in the lower levels. If the ballast is made to run out gradually, the full lift of the balloon may be restored at any given level. This method cannot be applied to the U. S. Weather Bureau radiosonde in which temperature and moisture data are sent out by a mechanism in which electric contacts are closed by a pressure cell at predetermined levels (see, however, pages 230-231).

On the whole it has been found more advisable to develop new or improved instruments or to adapt special instruments for a low-level sounding technique rather than to rely on the existing facilities for aerological measurements. The methods developed so far involve the use of planes and dirigibles as well as captive balloons and kites. For the lowest strata, specially built towers and ship installations have come into use.

Wet and Dry Bulb Methods

The use of humidity data for radio propagation problems involves new features in instrumental technique because the main effects of strong refraction are found under approximately calm weather conditions. Therefore, when wet and dry bulb methods for humidity measurements are used, particular care must be taken to insure satisfactory aeration of the wet bulb. As a rule, an air speed of about 3 m per second (about 6.5 mph) is considered adequate ventilation for the wet bulb. In a plane, dirigible, or kite the necessary aeration is automatically provided. But on a tower or when carried by a captive balloon, artificial aeration will frequently be necessary. It has been claimed,[b] however, that if a wet bulb electrical resistor is used in conjunction with a captive balloon adequate aeration can be provided by giving the balloon cable a few violent jerks of about 5-ft amplitude.

An ordinary sling psychrometer held out of the window of a flying plane and aerated by the slip stream has been found to give fairly reliable results, provided the wet bulb is kept properly moistened. This method has been used with good success for preliminary research work. It may be presumed that the use of a rather slow-flying plane is essential, in order to keep the dynamic temperature correction small and also in order to insure a not too excessive rate of evaporation.

Thermocouples, thermopiles, and temperature-sensitive resistors frequently are used as temperature responsive elements in place of actual wet and dry bulb thermometers. They are incorporated in specially designed electrical bridge circuits in which the temperatures are read on either indicating or recording meters.

---

[a] By W. M. Elsasser, Columbia University Wave Propagation Group.

[b] Data, courtesy of U.S. Navy Radio and Sound Laboratory, unpublished.

Temperature and Humidity Resistance Elements

TEMPERATURE

Temperature-sensitive resistors are satisfactory both with regard to accuracy and the absence of lag. The British have used platinum resistance thermometers very successfully in stationary installations. In the United States electrolytic or ceramic resistance elements are commonly used. The latter can be made to change their resistance several fold over a relatively narrow temperature interval. Their accuracy is therefore limited, not so much by the accuracy of the current measurement as by their intrinsic stability after calibration, proper radiation shielding, etc.

The electrolytic element developed for the Bureau of Standards radiosonde[1,2] has a time-lag constant (time required to attain the fraction $(1-e^{-1}) = 0.63$ of the total change) of 8 sec at an airspeed of 3 m per second, of 14 sec at an airspeed of 1 m per second, and of 40 sec in still air

Recently the ceramic Sanborn element[*] has come into use; it has about the same lag characteristics as the electrolytic element but is practically free from

[*]Manufactured by Paul H. Sanborn, 2602 Riverview Drive, Parkersburg, W. Va.

aging. The following time-lag constants have been measured:[4] 8 sec at an airspeed of 3 m per second and 12 sec at an airspeed of 1 m per second. Another source reports 20 sec at an airspeed of 5 m per second (this value seems too large in comparison with the others) and 42 sec in still air.

MOISTURE

The Bureau of Standards resistance element as well as the Gregory humidiometer (a British development) uses a dilute solution of lithium chloride.

In the Bureau of Standards element the lithium chloride film is deposited on the surface of a thin cylinder on which there is a bifilar winding of two thin wires. The stability and aging characteristics of this element are described in the literature.[1,3] An average actual accuracy of 5 per cent relative humidity is claimed for the ordinary radiosonde when used under routine conditions. Higher accuracy (1 per cent RH) is claimed, at least at temperatures above freezing, when used with captive balloon equipment,[5a] partially because the current is frequently reversed to cut down polarization effects and partially because the calibration can be more closely watched. Tests[3] show that at an airspeed of 2.5 m per second the time lag constant is 3 sec at 24 C and 11 sec at 0 C.

FIGURE 1. Wired sonde circuit.

The potentiometer P applies a constant voltage (0.36 v at low and 0.18 v at high RH) to both of the independent circuits of the sonde proper. The currents, determined by the resistances of the relative humidity and temperature elements respectively, are read on the RH meter and T meter. S_1 commutates these currents at half-second intervals; S_1 and S_2, actuated simultaneously with S_3, maintain constant polarity at the meters. The 1,000-μf condensers CC smooth the currents through the meters. $S_1 S_2 S_3$ are contained in the pile-up of a single relay which is actuated by a miniature worm-geared motor as shown. The 10,000-ohm protective resistance R is shorted out during measurement. Connections to the ground end of the cable are made through slip rings (not shown) mounted on the cable reel. All components, excepting the sonde, cable, and 6-v storage battery, are housed in a single case 20x9x7 in.

METEOROLOGICAL EQUIPMENT FOR SHORT WAVE

METEOROLOGICAL EQUIPMENT FOR PROPAGATION STUDIES[a]

Outline of Problem

EXPERIENCE GAINED during the recent years with radar, especially microwave radar, and with experimental microwave communication equipment has shown that the electromagnetic radiation field produced by a transmitter is subject to large variations depending on the weather. These variations are caused by *refraction* and so are related to variations of dielectric constant in the atmosphere. Pressure, temperature, and humidity determine the dielectric constant (refractive index).

It has been found that above a certain height variable with season and geographical location but rarely exceeding 1,500 m above ground, atmospheric refraction is reasonably constant. In the lower levels and especially in the lowest hundred meters of the atmosphere, temperature and moisture conditions strongly affect the radiation field and thereby influence the operation of radar and other short and microwave equipment. In order to evaluate this effect in quantitative terms, the temperature and moisture distribution in the lowest layers must be determined with as high a degree of accuracy as is compatible with speed, ease of operation, and other practical limitations.

A number of methods have been tried during the recent years which range from measurements with ordinary radiosonde equipment to the use of a psychrometer on the steps of a fire ladder. Two facts have appeared rather clearly: First, hairs are not suitable for moisture measurements of this type on account of their great sluggishness (except perhaps for stationary use on towers), since the time of adaptation of a hair to appreciable changes in humidity is of the order of 3 to 5 minutes. Secondly, it has been found that ordinary radiosondes are not usually appropriate because the readings obtained from them normally are taken about 100 m apart in vertical distance and for this particular problem a more detailed knowledge of the temperature and moisture distribution is necessary. With a clock-driven radiosonde this can be remedied by loading the sonde down by means of a ballast (water or sand) which slows down the ascent of the instrument in the lower levels. If the ballast is made to run out gradually, the full lift of the balloon may be restored at any given level. This method cannot be applied to the U. S. Weather Bureau radiosonde in which temperature and moisture data are sent out by a mechanism in which electric contacts are closed by a pressure cell at predetermined levels (see, however, pages 230-231).

On the whole it has been found more advisable to develop new or improved instruments or to adapt special instruments for a low-level sounding technique rather than to rely on the existing facilities for aerological measurements. The methods developed so far involve the use of planes and dirigibles as well as captive balloons and kites. For the lowest strata, specially built towers and ship installations have come into use.

Wet and Dry Bulb Methods

The use of humidity data for radio propagation problems involves new features in instrumental technique because the main effects of strong refraction are found under approximately calm weather conditions. Therefore, when wet and dry bulb methods for humidity measurements are used, particular care must be taken to insure satisfactory aeration of the wet bulb. As a rule, an air speed of about 3 m per second (about 6.5 mph) is considered adequate ventilation for the wet bulb. In a plane, dirigible, or kite the necessary aeration is automatically provided. But on a tower or when carried by a captive balloon, artificial aeration will frequently be necessary. It has been claimed,[b] however, that if a wet bulb electrical resistor is used in conjunction with a captive balloon adequate aeration can be provided by giving the balloon cable a few violent jerks of about 5-ft amplitude.

An ordinary sling psychrometer held out of the window of a flying plane and aerated by the slip stream has been found to give fairly reliable results, provided the wet bulb is kept properly moistened. This method has been used with good success for preliminary research work. It may be presumed that the use of a rather slow-flying plane is essential, in order to keep the dynamic temperature correction small and also in order to insure a not too excessive rate of evaporation.

Thermocouples, thermopiles, and temperature-sensitive resistors frequently are used as temperature responsive elements in place of actual wet and dry bulb thermometers. They are incorporated in specially designed electrical bridge circuits in which the temperatures are read on either indicating or recording meters.

---

[a] By W. M. Elsasser, Columbia University Wave Propagation Group.

[b] Data, courtesy of U.S. Navy Radio and Sound Laboratory, unpublished.

Temperature and Humidity
Resistance Elements

TEMPERATURE

Temperature-sensitive resistors are satisfactory both with regard to accuracy and the absence of lag. The British have used platinum resistance thermometers very successfully in stationary installations. In the United States electrolytic or ceramic resistance elements are commonly used. The latter can be made to change their resistance several fold over a relatively narrow temperature interval. Their accuracy is therefore limited, not so much by the accuracy of the current measurement as by their intrinsic stability after calibration, proper radiation shielding, etc.

The electrolytic element developed for the Bureau of Standards radiosonde[1,2] has a time-lag constant (time required to attain the fraction $(1-e^{-1}) = 0.63$ of the total change) of 8 sec at an airspeed of 3 m per second, of 14 sec at an airspeed of 1 m per second, and of 40 sec in still air

Recently the ceramic Sanborn element[c] has come into use; it has about the same lag characteristics as the electrolytic element but is practically free from

[c]Manufactured by Paul H. Sanborn, 2602 Riverview Drive, Parkersburg, W. Va.

aging. The following time-lag constants have been measured:[4] 8 sec at an airspeed of 3 m per second and 12 sec at an airspeed of 1 m per second. Another source reports 20 sec at an airspeed of 5 m per second (this value seems too large in comparison with the others) and 42 sec in still air.

MOISTURE

The Bureau of Standards resistance element as well as the Gregory humidiometer (a British development) uses a dilute solution of lithium chloride.

In the Bureau of Standards element the lithium chloride film is deposited on the surface of a thin cylinder on which there is a bifilar winding of two thin wires. The stability and aging characteristics of this element are described in the literature.[1,3] An average actual accuracy of 5 per cent relative humidity is claimed for the ordinary radiosonde when used under routine conditions. Higher accuracy (1 per cent RH) is claimed, at least at temperatures above freezing, when used with captive balloon equipment,[5a] partially because the current is frequently reversed to cut down polarization effects and partially because the calibration can be more closely watched. Tests[3] show that at an airspeed of 2.5 m per second the time lag constant is 3 sec at 24 C and 11 sec at 0 C.

FIGURE 1. Wired sonde circuit.

The potentiometer P applies a constant voltage (0.36 v at low and 0.18 v at high RH) to both of the independent circuits of the sonde proper. The currents, determined by the resistances of the relative humidity and temperature elements respectively, are read on the RH meter and T meter. S_1 commutates these currents at half-second intervals; S_1 and S_2, actuated simultaneously with S_3, maintain constant polarity at the meters. The 1,000-μf condensers CC smooth the currents through the meters. $S_1S_2S_3$ are contained in the pile-up of a single relay which is actuated by a miniature worm-geared motor as shown. The 10,000-ohm protective resistance R is shorted out during measurement. Connections to the ground end of the cable are made through slip rings (not shown) mounted on the cable reel. All components, excepting the sonde, cable, and 6-v storage battery, are housed in a single case 20x9x7 in.

The Gregory humidiometer[d,e] uses a lithium chloride solution soaked in a clean cotton cloth. The resistance of the element changes from over 100,000 ohms at 30 per cent RH to as little as 50 ohms at 100 per cent RH. It undergoes pronounced aging during the first several days and then remains sensibly constant for a number of weeks. The instrument is in an experimental stage and is at present being tried out at the Rye towers in Sussex (see page 229).

Circuit Design for Resistor Elements

Thermocouples or thermopiles are commonly used in a conventional bridge circuit. In connection with the electrolytic and ceramic type of resistance elements, circuits have recently been developed that include certain features novel in the technique of atmospheric measurements.

In the equipment developed by Washington State College[5a] the standard radiosonde temperature element was originally used, but in a more recent type they have combined the Sanborn temperature element and the radiosonde electrolytic humidity element. The electric equipment (Figure 1) consists of a dry cell with potentiometer supplying about ½ volt, two double-pivot microammeters, one in series with each of the elements, and a 6-volt d-c motor. The relay reverses the current through the elements at a rate of 50 cycles (100 reversals) per minute while maintain-

---

[d] Information supplied to the U. S. Propagation Mission to England.

[e] Instruments made by Negretti and Zamba, Ltd., London.

ing constant polarity at the meters. The current is smoothed by large condensers in parallel with the meters. The commutation eliminates polarization of the electrolytic elements and greatly increases their accuracy and useful life. The commutation period is so selected that it is long enough to prevent inductive and capacitive interaction between the two circuits but is short enough to allow of smoothing the currents through the meters.

The circuit illustrated in Figure 2 has been developed by the Propagation Group at the Radiation Laboratory, MIT.[4] The apparatus includes two Sanborn resistance elements, one of them surrounded by a moistened wick. The current flowing through the resistors originally was fed into an amplifier which drove a recording milliammeter. However, after a number of amplifiers had been tried, the simple scheme shown in Figure 2 was adopted and, at the time of the writing of this report, is being used for all measurements made by the Radiation Laboratory, those from planes as well as those from captive balloons which will be described later.

The dry and wet elements are placed in the circuit alternately by means of a hand-operated switch. The device can be calibrated by means of a set of fixed precision resistors and the balance of the bridge is checked before each flight. An advantage of this method is the possibility of using a commercial d-c recorder (0 to 1 ma) immediately at the plate terminals of the amplifier tube. This is particularly favorable for use in airplanes and dirigibles.
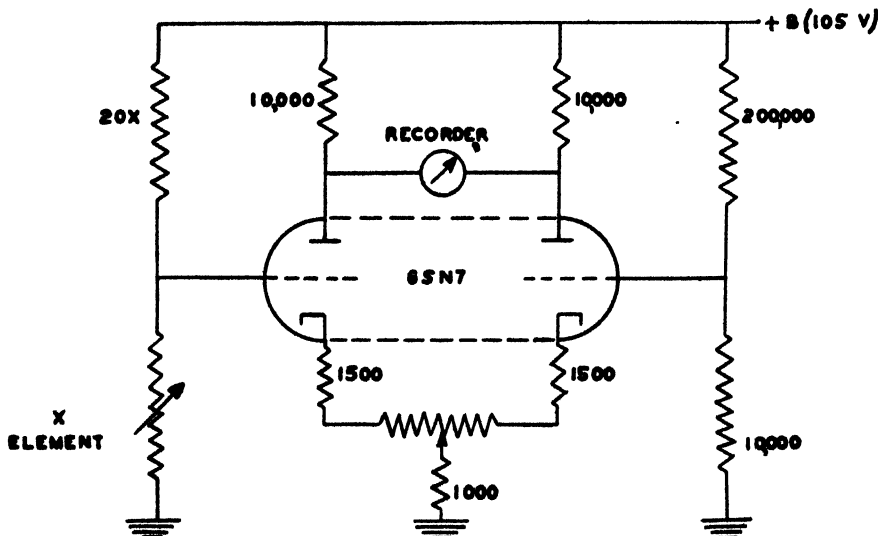
FIGURE 2. Schematic circuit of electronic amplifier.

The resistance of the thermal element, X, controls the bias of one triode of the double triode, 6SN7, which acts as a vacuum tube voltmeter to compare the resistance of the thermal element with a standard resistance. A 1-ma recording meter is placed between the two plates. The resistance in the grid circuits is so chosen as to place 10 v across the thermal element at the lowest temperature of each range. This voltage decreases as the temperature rises. The zero is set by means of a 100-ohm potentiometer in the cathode circuit. Calibration of the amplifier is obtained by switching a series of precision resistors in steps of 1,000 ohms into the circuit in place of the thermal element. A range of roughly 25 C for full scale is used, and changes of 0.25 C can be measured. Sufficient overlapping is provided so that both wet and dry bulbs can record on a single setting.

The stability is such that, with a change in line voltage between 95 and 120 v there is no readable change in the meter deflection at 0 (when the tubes are balanced) or at full scale reading. When tubes are replaced there is, at worst, a change of 1 per cent of full scale deflection tapering to no deflection at 0.

It is well known that the ordinary thermocouple is not readily adapted to recording purposes. Only at stationary installations such as towers, where multijunction thermopiles can be used, is it possible to record the indication of the sensitive galvanometer required.

Anemometers

Wind measurements are of importance in connection with off-shore winds at coasts which give rise to pronounced refraction of short and microwaves. The ordinary commercial anemometers become quite unreliable at very low wind speeds (of the order of ½ m per second) and may stop completely. A special anemometer for low wind speeds[6] has been designed by the British Chemical Warfare Service and is used as a regular piece of field equipment by its units. In the United States a highly sensitive anemometer has been developed at the California Institute of Technology.[7] This instrument records wind speeds from 0.5 to perhaps 30 mph. It has the conventional three cups rotating on a vertical axis. Each rotation is registered on a counter by magnetically operated electrical contacts. For higher wind velocities the counter may be switched to record only every hundred rotations. The apparatus is delicate and is critical in its behavior toward certain adjustments.

Semipermanent Installations

Towers

Two major installations of towers are at present in existence in England. They are the Porton towers and the Rye towers. The Porton towers on the Salisbury Plain form part of the extensive meteorological equipment of the British Chemical Warfare Service and have been in use for a considerable number of years.[8] Continuous records of dry and wet bulb temperatures at heights of 4, 23, and 56 ft above the ground are made. The elements used are platinum resistance thermometers connected into bridge circuits and are artificially aerated. The recording mechanism is located near the bottom of the tower.

A similar set has recently been installed on the Rye towers in Sussex which form part of a CH radar system. Temperature and relative humidity are recorded for heights of 4, 50, 155, and 360 ft above ground. The resistance thermometers are similar to those at Porton, but the moisture measurements are made with the Gregory humidiometer described above.

In a large research project on microwave refraction carried on in the summer of 1944 by the Propagation Group at the Radiation Laboratory, a mast was erected at one terminal of the path. Wet and dry bulb temperatures are recorded continuously with the device described in text on p. 228 at heights of 4, 16, 36, and 55 ft above the sea surface, these heights varying somewhat with the tide. The measuring elements are located in one end of a horizontal piece of tubing 3 ft

long, and in the other end, close to the pole, an aeration fan is mounted. Wind velocity records are made by means of Stewart anemometers.

Ships

The Royal Navy has detailed three yachts for atmospheric measurements on an experimental microwave transmission path over the Irish Sea. They are provided with dry and wet thermocouples at altitudes of 5, 10, 40, and 50 ft above sea level. The former two are mounted on hinged beams outboard, while the latter two are on a mast in the forward part of the ship. The thermocouples are copper-constantan, and there are two in series for the temperature measurement with the cold junctions placed in a Dewar flask filled with melting paraldehyde (maintaining a temperature of 50 F). There are two pairs of dry and wet junctions connected in series which measure the wet bulb depression. The galvanometer is in the ship's cabin. Aeration is provided by the ship's movement, and when measurements are made the ship sails into the wind to minimize the effects of the discharge from the smokestack.

In the project at the Radiation Laboratory just referred to measurements are also being made from the mast of a boat. The 48-ft mast is provided with a 6-ft cross arm and a motor-aerated housing containing the elements can be raised from the bottom of the mast to the end of the cross arm, giving continuous information over the height of its travel.

Measurements carried out on shipboard by means of captive balloons or kites will be discussed in following text.

Measurements on Board Planes and Dirigibles

As has been mentioned before, a sling psychrometer held out of the window of a flying plane will give reasonably accurate results if some elementary precautions are taken to insure proper moistening of the wick.

The two types of instruments described before on p. 228 have been adapted for use with airplanes. In the Radiation Laboratory instruments the two elements are mounted diagonally in a piece of Bakelite tubing about 1½ in. in diameter, the dry element in front of the wet element, relative to the wind stream. In the earlier airplane measurements water was blown over the moist element and a reading made when the recorder showed equilibrium to be reached. Now capillary action is used throughout, the water being supplied from a small vessel underneath the Bakelite tube. This instrument has been tested in a wind tunnel with wind speeds up to 145 mph. The dynamic pressure effect increases the reading by 0.4 C at the cruising speed of the plane (100 mph). This value was checked, both in the plane itself and in a wind tunnel.

The Washington State College [WSC] instrument has been adapted for airplane measurements and has been used on several types of planes during tests in Panama.[9b] The elements were housed in a single-walled cylinder of aluminum, about 1.75 in. in diameter, covered on the forward end with a cone. A small circular opening (⅜ in. in diameter) made by cutting off the end of the cone reduced the velocity of the air across the elements to about one twenty-second of the plane's speed. Comparison of a plane sounding and a balloon sounding in the same region at the same altitude and time gave identical results within reasonable experimental error.

With airplane measurements the determination of the plane's altitude becomes an important task. In the experimental flights at the Radiation Laboratory the altimeter of the plane itself was used. According to the experience obtained in Panama it is desirable to have an additional altimeter placed directly before the operator in order to facilitate rapid and accurate altitude determinations. The nominal accuracy of an airplane altimeter is about 20 ft. Over sea it may be possible to determine the absolute altitude of the plane with about the same degree of accuracy, but over land less accuracy is to be expected.

Measurements from a dirigible (blimp) have been carried out by Radiation Laboratory. The instrument is suspended on a cable about 100 ft below the ship.

Captive Balloon Sondes and Kites

RADIO TRANSMISSION TYPE

Two different methods have been tried in connection with balloons and kites. When first used in practice an ordinary radiosonde was attached to the balloon (kite) and the results were recorded on the ground by radio in the usual way. This method was used in an experimental investigation carried out under the auspices of the AAF Board, Orlando, Fla.[9] Although by the nature of the instrument the measurements are spaced 200 to 300 ft apart, a rough survey of the temperature and moisture distribution sufficient for some operational purposes was gained in this way. The record on the ground was taken by means of a standard U. S. Army radiosonde receiver.

It was pointed out in this report[9] that it might be advantageous to use a combination of two radiosondes in tandem, such that in one instrument the contacts are connected to the temperature device, in the other to the humidity element. It would then be possible to obtain simultaneous temperature and moisture readings at the same elevation, instead of alternating ones, as is the case when only one instrument is used. This would, however, require the use of two receivers at the ground with two slightly different carrier frequencies.

Another adaptation of the standard Weather Bureau radiosonde was made by WSC.[5a] The ground installation was similar to that used by the Weather Bureau in its full radiosonde measurements, but the standard radiosonde was modified by replacing the pressure- (altitude-) actuated switch by a clock-driven commutator. The results obtained were quite satisfactory, and the technique may be appropriate at stations where standard radiosonde equipment is available.

WIRED TRANSMISSION TYPE

The other captive balloon or kite instruments are of the wired type with galvanometers or recorders at the ground. They may be classified as light and heavy types. The light instrument merely carries temperature and humidity elements aloft which together with the radiation shield do not weigh more than a few ounces. To this is added the weight of the cable or string carrying the connecting wires. The heavy instrument carries its own aeration equipment in the form of a fan driven by a small electric motor. The fan and the heavier construction of the frame required to accommodate it increase the weight of the airborne unit to several pounds. In addition there must be at least one more lead on the cable to supply power to the fan.

The first captive balloon instrument was built in England several years ago.[10] The balloon is anchored by an electric cable and the instrument is provided with a fan. The overall weight of the instrument without cable is about 8 lb. Its main part is a piece of polythene tubing in the shape of an inverted Y with the fan placed on top of the tubing while the two legs of the Y contain the dry and wet thermopiles. The latter are four-junction copper-constantan combinations. The cold junctions are enclosed in a small Dewar flask filled with melting ice which is located about 10 in. below the Y piece.

The cable of this instrument has five leads, three for the thermocouples and two for the fan (2 to 4 volts of direct current); the instrument is suspended from the balloon proper by means of a 100-ft string which minimizes the influence of irregular motions of the balloon upon the instrument. The ground equipment consists of potentiometers and a spot galvanometer with a switch to alternate between the dry and wet couples.

The light type of balloon or kite sounding equipment was first developed by WSC.[5a,5b] The temperature and humidity elements are surrounded by a double-walled aluminum radiation shield, and the whole airborne assembly weighs only a few ounces. Originally the standard Weather Bureau temperature element was used; now they use the Sanborn element together with the Bureau of Standards humidity elements in the circuit shown in Figure 1.

The sounding procedure used with this instrument consists in letting the balloon go rapidly up to a maximum altitude chosen so high that moisture and tem-

perature variations with height are comparatively slow. The characteristic features of the atmospheric stratification lie below this level. A rough survey of this stratification is made during the ascent. The instrument is then reeled in and is stopped at a number of predetermined levels, long enough to let the elements reach equilibrium with the surrounding air. The levels chosen are spaced at height intervals small enough so that the readings taken reveal the atmosphere structure accurately. It has been found that rapid lowering of the sonde between readings will provide sufficient aeration of the elements to give quite accurate readings even in completely calm weather.

The balloon sonde of the Navy Radio and Sound Laboratory uses a dry and a wet Sanborn resistor surrounded by a double-walled aluminum radiation shield. Often wind aeration is found to be sufficient for the wet bulb element, but in calm air the instrument is aerated before readings by giving the cable a series of rapid jerks of about 5-ft amplitude. The ground equipment consists of a 0 to 50 microammeter which can be connected to the dry element, the wet element, and a standard resistor in turn by means of a double-pole triple-throw switch. Voltage is supplied by a dry cell and potentiometer.

The captive balloon sondes used by Radiation Laboratory[4] employ dry and wet Sanborn resistors mounted diagonally in a piece of Bakelite tubing surrounded by an aluminum radiation shield. The circuit and amplifier have been described in text on p 228. In the lightweight wind-aerated instrument the piece of Bakelite tubing containing the resistors is horizontal. Owing to the shape of the aluminum shield it will take up an orientation in the wind such that the air strikes the dry element before the wet element. More frequently, however, they use a heavier, fan-aerated instrument in which the Bakelite tubing is vertical and the fan is placed on top of the assembly. This instrument has been extensively used in the recent experiments at the New England coast; either it was attached to a barrage balloon (35-lb lift), or in calm weather to a large Neoprene balloon (see text on p 230). The latter type of balloon was also used to make ascents from a boat in light and moderate winds

Recently, a type of captive balloon equipment has been developed commercially[11] which uses the standard United States radiosonde recording equipment as the ground component. The airborne component consists of an audio relaxation oscillator with the measuring element connected in the grid circuit. Changes in the measured temperature or relative humidity alter the frequency developed by the oscillator. By means of a special attachment on the ground the balloon sonde is used in connection with the regular radiosonde receiving and recording equipment. The airborne component includes dry cells for the operation of the oscillator and the weight of the airborne unit is approximately 2 lb.

CABLE AND BALLOON TECHNIQUE

The cable which connects the measuring elements aloft to meters on the ground is one of the most critical parts of the wired sonde. The earliest British instrument[10] used a cable obtained by stranding together thin, insulated, flexible copper cables; the weight is about 2½ lb per 100 ft. Similar cables were used for a while by Radiation Laboratory; later on they changed to the types of cable to be described presently.

WSC developed a cable technique[5a,5b] in which the pull of the balloon or kite is taken up by a strength member such as strong linen twine. Fishline, breaking strength 64 lb, was originally used.[5a] Three No. 30 enameled copper wires are wound around the strength member with a pitch of several inches. After being made up the cable was passed under thinned airplane dope to cement it together and make it waterproof. The weight of this cable is about 1 lb per 1,000 ft.

Later developments in this cable resulted in three types that have survived accelerated tests equivalent to 1 year's exposure to salt spray without developing serious leakage.[5b]

Type A consists of a braided Fiberglas strength member (nominal strength 80 lb), three No. 30 Formex-insulated copper wires, and a braided nylon sheath impregnated with vinyl plastic.[f]

Type B has an enameled stainless steel strength member (nominal strength 40 lb) and three Formex conductors within an impregnated nylon sheath.[g]

Type C is similar to Type A but has a 180-lb test Fiberglas strength member; it is used with large kites.[f]

These cables are wound around the drum of an ordinary winch, and the conductors are connected to the ground equipment by means of slip rings mounted on the winch.

It has been found advantageous, especially for the heavier instruments, to suspend the instrument from the balloon on a 100-ft fishline; this line acts as a buffer in protecting the instruments from sudden jerks of the balloon.

Neoprene balloons[h] are recommended in preference to rubber latex balloons. They have a much longer useful life than rubber balloons and give warning before breaking by becoming misshapen. The 300-g N-4 balloon is used in connection with the WSC instrument.[5b] The N-700 balloon has been used by Radiation Laboratory for the fan-aerated instrument. Barrage balloons (lift 35 lb) were also successfully used in winds slightly in excess of those that permit the use of lighter balloons.

The light type of balloon becomes unmanageable in winds above about 6 to 8 miles per hour. A two-reel technique has been developed[5b] to extend the use of bal-

[f]Supplied by International Braid Co., Providence, R. I.
[g]Supplied by Boston Insulated Wire and Cable Co., Boston, Mass.
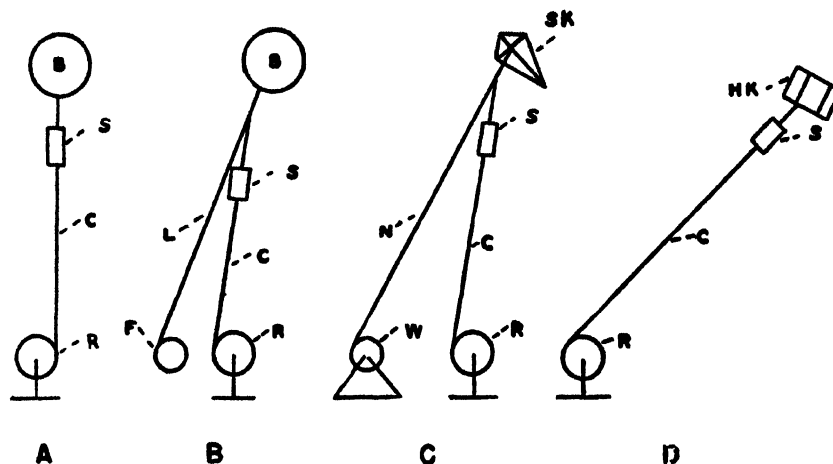[h]Supplied by the Dewey and Almy Co., Cambridge, Mass.

FIGURE 3. Sounding techniques for use at the wind speed ranges indicated. [5b]

Temperature and humidity-elements mounted within the radiation shield S are connected through the 3-conductor cable C with slip rings on the cable reel R. The meter box (not shown) is connected to the brushes of R. B 300-g Neoprene balloon L· light fishline. F: fishline reel. SK: Seyfang 7-ft kite N: nylon kite line W: kite winch HK: Hoffman single cell box kite Arrangement (D) is suitable for sounding from moving ships; its ceiling is limited to about 400 ft by the small lift of this kite

loons to somewhat higher wind speeds (from 6 to 10 mph). The pull of the balloon is taken up by a separate fishline, the reel of the fishline being placed windward relative to the reel of the cable (Figure 3).

In-wind speeds above about 8 mph kites are used in place of balloons. A small folding kite[j], standard for "Gibson Girl" emergency radio equipment, is easy to handle and requires only a light cable, but its ceiling is limited to about 400 ft. This type of kite has been used successfully for soundings from boats.

A heavier, 7-ft kite[j] is well adapted to land-based soundings. It flies at a high angle (55° to 60°) and can be put up at minimum wind speeds. At the high relative wind speeds encountered in ship-based soundings the pull of this kite is excessive and launching correspondingly difficult.

Sounding techniques are shown schematically in Figure 3. For the kite a braided, waterproof nylon line, breaking strength 150 lb. is recommended. For ship-based soundings or conditions where sudden high stresses are likely, a 300-lb test nylon line may be used.

There seems to be no difficulty in measuring the altitude of the captive balloon or kite.[5a] The length of line paid out is determined either by counting the turns of the reel or by means of markers attached to the cable at regular intervals; if the line is off the vertical, its mean inclination can be measured with sufficient accuracy by a simple hand inclinometer.

AUTOMATIC RECORDING OF METEOROLOGICAL SOUNDINGS[k]

A means has been developed for making automatic

recordings on a Leeds and Northrup Speedomax or Friez Cycloray recorder of low-level meteorological soundings of temperature and humidity. The design of the equipment has been restricted in the sense that the standard Weather Bureau-Army-Navy electrolytic hygrometer and negative resistance temperature units must be utilized; all recordings must be made on the existing automatic radiosonde recorders just named.

GENERAL DESIGN CONSIDERATIONS

The existing standardized electrolytic hygrometer strip polarizes when direct current is placed on its terminals. However, if a reversed direct current is placed on the terminals of the strip, this polarization tendency is neutralized. This would seem to indicate the desirability of placing a low-frequency alternating current on its terminals in lieu of the direct current commutation principle which generally has been used in existing low-level meteorological sounding equipment.

The frequency of the alternating current to be placed on the strip will in general be controlled by the reactance of the low-level sounding cable. In view of this limitation a frequency of approximately 10 c has been used.

The temperature resistor operates equally well on either direct or alternating current; therefore, it requires no equipment design considerations.

ELECTRICAL CHARACTERISTICS OF ELEMENTS

Present practice makes the "lock-in" for the temperature and humidity elements through a resistor in series with the elements. However, this technique introduces errors in the readings both above and below that for the lock-in point. Effectively, the slopes of the calibration curves are altered, affecting the readings on the indicators. In view of this situation, it is
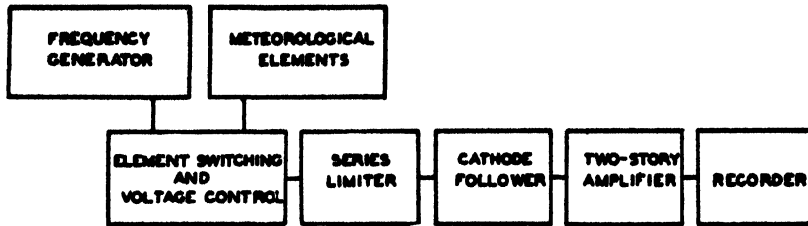
FIGURE 4. Basic components of amplifier-recorder.

fundamental that voltages should be measured across the hygrometer or temperature elements. Any lock-in device must be inherent in the equipment as remote from the voltage appearing across the elements. This principle has been incorporated in the design of the equipment.

Since the electrolytic hygrometer element can be designed so that it will not polarize under direct currents approaching 100 μa, it appears desirable to design the recording equipment for possible adaptation to this type of element. In other words, the amplifiers must be capable of handling direct currents as well as alternating currents.

CABLE ERROR

If the standard temperature and hygrometer curves are used originally for calibrating the recorder, it is important to note that the cable resistance will introduce a positive error. For average Southwest Pacific climate and sounding heights up to about 3,000 ft, the positive temperature error is roughly 1.5 F while the positive hygrometric error is about 5 per cent RH.

These errors, unfortunately, cannot be compensated without complete recorder calibration at the outset or by mathematically adjusting the standard calibration curves. Thus, since the cable is a fixed resistance, the standard curve can be recomputed to allow for any fixed cable resistance, with the result that no error will be introduced into the recorder.

In consideration of the above requirements, it will be necessary, in adapting the standard U. S. Weather Bureau electric hygrometer and temperature elements, to provide (1) a means of developing a stable low-frequency voltage across the elements, (2) to switch from one element to another in measuring the voltages across these elements, (3) to amplify such voltages,

(4) to provide a means of controlling the sensitivity and range of the recorder, and (5) to supply the output of the amplifier to a 0 to 500 microammeter automatic recorder.

ELECTRONIC AMPLIFIERS

The basic components of the amplifier-recorder are shown in Figure 4. The frequency generator operates at 10 c and is composed of three units, (1) a phase-shift oscillator, (2) a paraphase amplifier, and (3) a controllable push-pull output amplifier.

The amplifier-recorder unit is composed of (1) a series limiter, (2) a cathode follower, and (3) a two-story amplifier, as shown in Figure 5. For the sake of simplicity, the automatic switching device that changes the current from hygrometer to temperature element has been shown schematically. The switching takes place at any rate between approximately 1.0 to 0.1 c; this rate is not critical.

Since the amplifier must be able to handle either direct or alternating current, the balanced two-story amplifier has been constructed, wherein the top tube is the plate load for the lower tube of the two-story amplifier. The output of this amplifier is approximately equal to one-half the amplification factor of the tube.

As shown in Figure 5, this amplifier is fed by a cathode follower which has impressed upon it from the series limiter only the positive peaks of the a-c voltage drop across the hygrometer or temperature element. The voltage across the elements can be as low as ¼ to ½ v, depending upon the sensitivity adjustment of the amplifier. It will operate with voltages as high as 30 to 60 v across the elements.

REDUCING AMPLIFIER OUTPUT TO GROUND

The amplifier output is at one-half the positive volt-
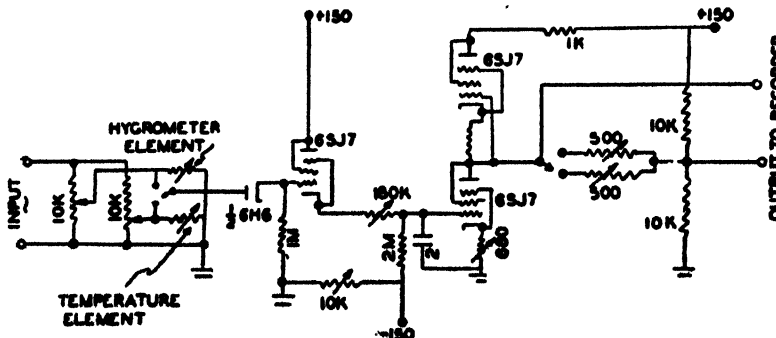
FIGURE 5. Automatic recorder circuit.

age of the plate supply above ground. However, this output can be reduced to ground by the introduction of a cathode follower or more simply by three series sections of a resistor and glow tube connected in series. The output of the two-story amplifier is fed into the junction between the first and second sections while the output is taken from the junction of the second and third sections, where the first section is connected to the positive plate supply and the third section connects to a negative potential equal to one-half the positive voltage. It is not necessary to make this addition to the present equipment.

RECORDER ACCURACY

It is possible to measure temperatures to less than ¼ of a degree Fahrenheit and humidities to less than ½ of 1 per cent. However, this accuracy is not necessarily required for low-level atmospheric soundings and construction of M curves.

CONCLUSION

Direct automatic recording of low-level temperature and hygrometer readings is suggested. The method is especially adaptable for fixed or shipboard station operation.

METEOROLOGY—FORECASTING

FORECASTING TEMPERATURE AND MOISTURE DISTRIBUTION OVER MASSACHUSETTS BAY [a]

BEFORE GOING into a description of the forecast program and results it will be profitable to describe the method used in coordinating the observations.

Meteorological Observations

Soundings were made according to two major plans. The first was in conjunction with the radio path. According to that plan, airplane soundings were made once or twice a day at two or three points along the transmission path. The boat would take either mast or balloon soundings along the path while measurements at Race Point Light (Provincetown) would continue at 2- to 4-hour intervals during most of the day and sometimes at night. The Race Point Station had the advantage of being well away from land (for all but easterly winds) and soundings there would thus represent the condition of the air over a large portion of the path. The soundings just described were made primarily for correlation with the signal strength measurements.

The second plan was to obtain soundings in successive steps in air moving off the coast as that air became more and more modified by the cool ocean surface. For this reason, days during which the air was westerly or nearly so were set aside for this type of measurement. The Duxbury soundings gave a representation of the structure of the air before it left the land. One airplane made soundings at about 2, 7, and 25 miles offshore. The times of take-off were staggered to allow the first airplane to complete its third ascent before the second plane would begin its first sounding.

The boat played a vital role in such a plan. It ran along the line of the air trajectory for as long as was practicable to take water temperature measurements and mast soundings, usually an 8- to 10-hour period.

The Race Point Meteorological Station was coordinated into this general plan by having it take continual balloon soundings at, say, 2-hour intervals both before and after the airplane ascents. The purpose of these soundings was both to fit in as an extra sounding in the general plan and also to yield some information as to amounts of change of the meteorological conditions with time. Also, in general, the

times of soundings at Race Point Station were scheduled about 1 hour later than those at the overland station to give the air sufficient time to travel from one to the other.

Forecast Program

A forecast program was begun during July and continued to October 10, 1944, in order to try out existing methods of forecasting and to help develop new techniques. A more natural step would have been to analyze the data taken during the summer and then to put that analysis into the form of forecast procedures, as was done at the end of the 1943 Boston Harbor transmission experiment. However, since speed was essential it was decided to initiate a forecast program simultaneous with the observations. The very act of forecasting tended to focus attention on the important weather factors, at the same time giving invaluable help in planning the day-to-day observations

The type of forecast made was different from the usual form. It consisted of a "space forecast" rather than the usual time forecast. That is, knowing the conditions at one point at a given time the problem was one of finding the conditions at another location at the same time. It involves the entire problem of modification of an air mass by a water surface.

The forecasts were in the form of curves of temperature and moisture, from which the modified index [*] curve was computed. A time and a location in Massachusetts Bay were selected at which it had been determined previously that a sounding would be made. Almost invariably airplane observations were chosen to use as verifications because those soundings were at sufficient altitudes so that both the modified and the unmodified air were sampled. The forecasts were made from the surface to 1,000 ft, whereas the airplane soundings started from about 20 ft and continued to 1,000 ft. For verification, the forecast and the sounding were plotted on the same graph.

Army Analysis and Forecasts

The program of the Army forecasters included the forecasting of transmission and radar ranges; the approach to this problem was empirical. The basis of the program was again the analysis of the first 6 weeks' data, this time including the signal strength measurements which have been described. Signal strengths were divided into four ranges qualitatively described

[a] By I. Katz, Radiation Laboratory, Lt. J. R. Gerhardt, Lt. W. E. Gordon, Army Air Forces, and P. W. Kenworthy, U. S. Weather Bureau, Boston, Mass.

. as low, standard, high, and very high, corresponding
to M curves of the types substandard, standard, super-
standard, and trapping. This analysis did not con-
sider variations in the M curve over the path but
rather related signal to the prevailing type of curve. On
this basis, then, a transmission forecast for a 24-hour
period involved the forecasting of prevailing M curves
over the transmission path for appropriate time in-
tervals. The length of these time intervals was deter-
mined by the rapidity with which the weather factors
affecting the M distribution were changing. Specific-
ally, a 24-hour transmission forecast involved two
M-curve forecasts plus forecasts of temperature and
dew point trends. These forecasts were supplemented
frequently with M-curve forecasts for times of mini-
mum or maximum propagation conditions. These
meteorological data could then be translated quali-
tatively into values and trends of signal strength. This
information was presented in the form of a graph of
signal strength versus time.

How the Forecast Is Made

The forecast in general involves two determinations
one, of the initial conditions of the air before it leaves
land; and two, the modifications of the air by the
water surface. A study of the synoptic situation and
the low-level circulation reveals the location of the
point where the air in question leaves the land. The
synoptic situation shows the general flow pattern
local winds from the surface to 2,000 ft indicate the
specific pattern over the area under consideration.

The initial temperature and moisture distributions
are determined by studying the local hourly teletype
sequences and radiosonde observations. The modifica-
tion of the air is determined by considering the relation
of the surface water temperature to the representa-
tive air temperature and dew point, the over-water
travel, and the rate of modification.

Time forecasts were also made by the Army fore-
casters. They involved straight meteorological fore-
casts of the initial conditions to which were applied
the space forecast technique just described.

Example. This is a forecast made by the Weather
Bureau. The synoptic weather map on the morning
of July 26 indicated a rather weak flow of modified
continental polar air moving in an easterly direction
from the mainland of eastern Massachusetts out over
the waters of Massachusetts Bay. The temperature of
this air was potentially more than 21 C and under
sunshine was developing surface temperatures near
the shore line of more than 21 C by 0800. The fore-
cast was for 1000 about 5 miles southeast of Eastern
Point, Massachusetts. The temperature over land
about a half-hour before this was expected to be about
24 C, and the air flow as indicated by winds aloft was
such as to allow the air warmed to about this figure
to be out over this position within a half-hour. The
lapse rate over land would be approaching the dry

adiabatic by this time; so, as a guide, a lapse rate
amounting to about 3 C per 1,000 ft was projected
to 1,000 ft starting from 24 C at the surface. A value
for the sea water temperature of 17 C was predicted
from recent observations made in the Bay. Using past
experience, one then assumed a water modification up
to about 300 ft, and the T curve was constructed
starting from the surface value of 17 C, showing a
sharp inversion at first and a gradual inversion until
it met the guiding line representing the air from the
land. The radio observation made at MIT about mid-
night, July 25 to 26, was considered to be a fairly
good check of the properties of the air mass involved.
A surface temperature of between 21 and 22 C was
indicated.

In forecasting the moisture curve, a value at the
surface corresponding to the water temperature was
made the base of the curve. Over-land dew points were
initially predicted to be about 13.5 C, which would
give a vapor pressure value of between 15 and 16 mb
at the top of the water modification zone. An examina-
tion of the raobs, both MIT and Portland, show mix-
ing ratios of about 10.5 g per kg between 500 and
1,000 ft, which corresponds to 15 or 16 mb. This makes
a good check on the prevailing initial dew points. The
raob at Albany indicated that air which was a little
drier was moving in from the west so that a slight
decrease in the vapor pressure was forecast between 500
and 1,000 ft. (This part of the forecast did not prove
to be correct, since, as the verification of the forecast
in the figure shows, the moisture value remained
fairly uniform from 400 up to 1,000 ft.) Another
curve was drawn similar to the T curve to connect
the surface vapor pressure value with that value at
the top of the water modification zone, and from
there to 1,000 ft a gradual decrease was forecast on
the basis of the conclusions regarding the advection
of a little dry air indicated by the midnight Albany
sounding.

The verification shown by the broken line in Fig-
ure 1 turned out rather well in this instance. The
computed and verified M curve proved to possess
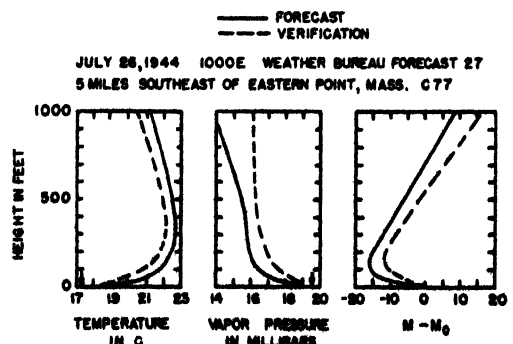almost identical slopes throughout with the top of

FIGURE 1. Space forecast of M curves.

the M inversion in both very close to 150 ft. This was one of the better forecasts. It can be seen that actual values of temperature and vapor pressure between forecast and verification might vary by several degrees, but as long as they have the same slopes at the same elevation they will produce M curves reasonably close to one another.

Conclusions. It is felt that the method of forecasting used was a marked improvement over the technique employed previously. It is potentially capable of dealing with the low-level modification problem in the case where the intial air is stratified as well as the one in which the initial air is homogeneous before it passes out to sea.

RADAR PROPAGATION FORECASTING[b]

This is a report of results obtained by an AAF board project investigating radar propagation forecasting, which was started as two distinct programs in September 1944. The first part of the project was carried out at the Radiation Laboratory with facilities used by Group 42 during over-water transmission measurements in the summer of that year. During that time, with the invaluable assistance of Group 42, a forecasting system was developed for the over-water case, the results of which are presented in previous text[c] These reports gave preliminary results of the MIT program and the recommended forecasting procedures. The second part of the propagation forecasting program was set up at Orlando, Florida, to study particularly the *over-land* forecasting phase and to investigate some of the operational uses of such forecasts.

With this in mind, AAF Board Project H3767, "The Determination of the Practicability of Forecasting Meteorological Effects on Radar Propagation," was initiated late in 1945 with the following specific objectives:

1. To determine the practicability of forecasting those low-level meteorological conditions which affect radar propagation.

2. To determine the accuracy with which radar propagation forecasts can be made from the corresponding meteorological conditions.

3. To determine the operational uses of such forecasts.

4. To determine the optimum meteorological observation site with relation to the site of the radar employing the forecasts.

5. To determine the suitability of available low-level sounding equipment.

It was originally planned to study the over-land and over-water problems simultaneously, but because of the lack of a coastal radar site until the last month of the program the project was divided into two

phases: (1) the general study of the over-land propagation variations in an attempt to devise a suitable forecasting procedure and (2) an evaluation of the results obtained from both the over-water and over-land methods, with possible tactical applications under field conditions at the site of a powerful coastal radar.

Figure 2 is a map of central Florida giving in detail specific facilities used throughout the project. Headquarters was established at the Weather Central, Orlando, where complete weather information, forecasts, and analyses were available. The meteorological data used throughout the project consisted of surface and upper air observations for the general central Florida area.

Detailed synoptic maps of Florida were drawn covering periods of 6 hours each to determine wind patterns and representative land temperatures and dew points; piballs[d] for Orlando, Sebring, and Tampa were plotted up to 2,000 ft to determine trajectories and wind speeds above surface levels, while the Orlando, Tampa, Tallahassee, and Jacksonville raobs were studied to correlate subsidence and radiation effects with radar propagation variations.

During the first phase of the project, sounding stations were established at Leesburg and New Port Richey using both the Washington State College wired sonde and the MIT psychrograph. Radar data were taken from the S-band V beam and the P-band SCR-588 at Tomato Hill, only a few miles from the Leesburg sounding site, the SCR-584 at Winter Garden, and the P-band SCR-271 at Crystal River during their operating hours. The Tarpon Springs program employed a medium early warning and an SCR-615 radar, both on S band, located on the Gulf coast, and the Crystal River SCR-271 and Winter Garden SCR-584. The sounding station was located within a half mile of the Tarpon Springs radar site. During the entire program sea surface temperatures were measured several times weekly at either the Cedar Keys or Anclote Crash Boat bases out to a distance of about 20 miles at 2- to 4-mile intervals.

Low-level soundings were made during the entire project primarily as an aid in interpreting radar performance and in determining representative air values and secondarily in an attempt to evaluate the operational suitability of the available sounding equipment. Results of the latter portion of the work will be presented later in this report. Ground-based soundings were made by means of various combinations of 350- and 700-g balloons, 7-ft Seyfang kites, and a small barrage balloon.

The sounding stations were originally located so as to be as representative as possible of interior and coastal areas, although it was found later that, without the additional mobility of airborne measurements,

[b]By Lt. J. R. Gerhardt and Lt. W. E. Gordon, AAF Board.
[c]Elaborated in references 1 to 3.

[d]A small balloon with standard rate of rise released for tracking by a theodolite for estimation of upper-air winds.
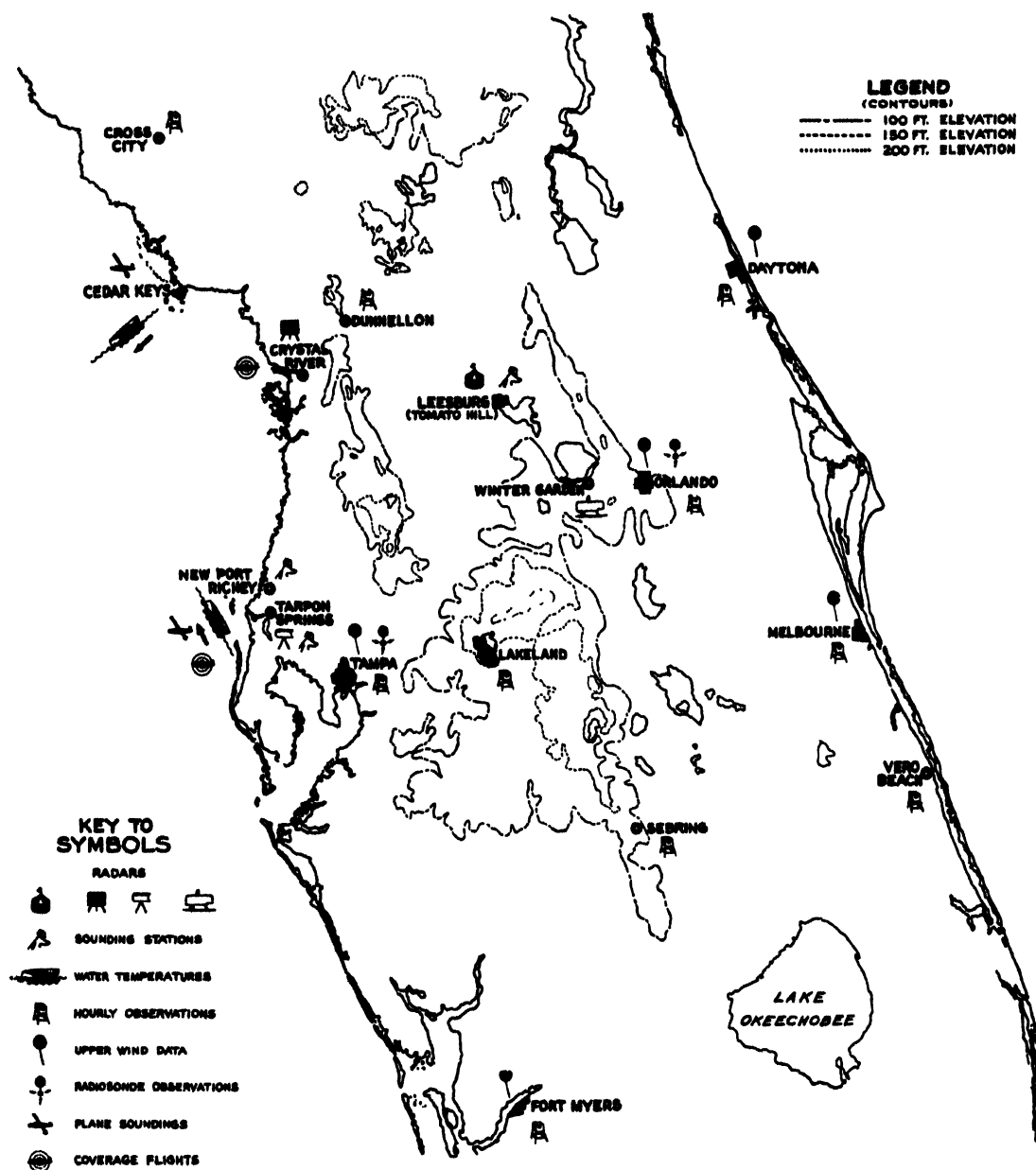
FIGURE 2. Map of central Florida with locations of weather and radar installations used in Project 3767.

individual ground-based soundings were likely to be too strongly influenced by local topographic effects to be completely reliable. Because of clearance requirements, the ground-based soundings were restricted to 600 ft, although it was determined that 1,000 ft would be a much safer limit, with occasional measurements up to 3,000 ft considered desirable. Soundings were taken before dawn at 1000 Eastern War Time, after sunset, and at 2300 EWT to obtain sufficient data on the effects of radiation and other meteorological phenomena. As far as specific sounding procedures are concerned, both the small balloons and kites gave satisfactory results, although for most of the wind

speeds encountered in this area the 7-ft kite was too small for efficient operation. No limiting surface wind speed can be given as a dividing line between kite and balloon operation, since it has been found that occasionally even in surface calms strong velocity gradients exist immediately above the surface layer. Although it is realized that a barrage balloon is not a standard item of equipment for sounding measurements, it is unreservedly recommended and whenever available should be used for simplicity and reliability of sounding procedure.

The method employed in this project for the radar verification of superrefraction was to record

plan position indicator [PPI] scope appearance of ground clutter return. The oscilloscope screen was assumed segmented into eight 45° sectors, and the maximum range on a ground target in each sector was noted hourly during periods of operation. In an attempt at correlating the radar performance with the existing meteorological conditions, a classification system was devised in which each distinguishable propagation condition was assigned a single number. After collecting observations for some time from each unit the data were examined, and an average of the normal pattern was chosen as the standard, or class 1, type of propagation. Averages of reported increased ranges in various sectors were calculated, while the azimuthal variations due to shadow effects of surrounding terrain, coast line and obstructions were

FIGURE 4A Class 3 pattern, SCR-271, Crystal River Coast line well painted in.

FIGURE 3A. Typical Class 1 pattern, P-band SCR-271, Crystal River. Grid squares are approximately 5 miles on a side
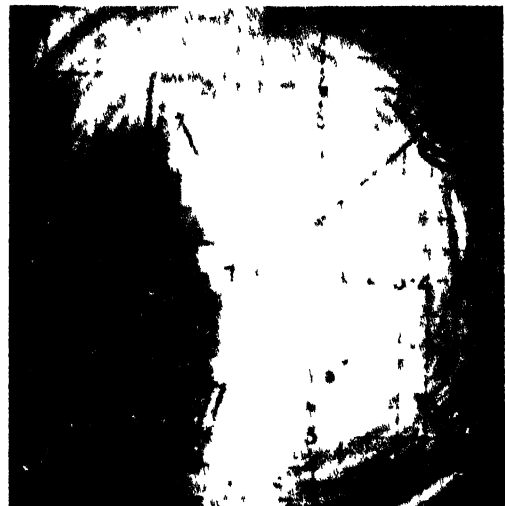
FIGURE 4B. Typical Class 4 pattern, SCR-271, Crystal River

considered. The consistency with which various increased range averages were attained determined the number of classes of propagation assumed for each unit. On the assumption that the meteorologist could forecast and correlate *M*-curve types corresponding with four types of propagation, four such propagation classes were chosen for the S-band V beam and the P-band SCR-271 at Crystal River. Figures 3 and 4 show the four classes of propagation as defined for the SCR-271 at Crystal River. The class 4 picture definitely shows the Florida coast-line detail painted in. Observations from most of the other units, however, were classed only as 1 (standard) and 2 (non-standard) propagation because of the radar shadows of certain topographical features near their sites. Due possibly to the peninsular situation of Florida, it was

FIGURE 3B. Typical Class 2 pattern, P-band SCR-271, Crystal River.

impracticable to forecast accurately four different classes of propagation, but forecasting on a basis of two classes, standard and nonstandard, can and should be done.

During the first part of the over-land program an attempt was made to forecast the specific M curves as shown by the Leesburg and New Port Richey sounding stations and to correlate these curves with the two to four propagation classes outlined for each radar unit. However, because of the wide variation of surface terrain (sand, swamps, lakes, forests) in this general area, no single sounding was necessarily representative of the entire air mass, since subsidence and radiation effects almost certainly varied considerably over the different kinds of terrain surrounding the sounding locations. On this basis, then, rather than attempting to forecast a hypothetical representative M curve, a series of correlations was made relating the general synoptic situation directly to the radar performance. Using this method, the actual over-land forecasting results showed that, while approximately 80 to 85 per cent of the total operating hours could be correctly forecast as either standard or non-standard propagation periods, only some 50 per cent of the nonstandard hours could be forecast correctly. This is only a little better than climatology, and more work remains to be done on the over-land forecasts of propagation variations.

In addition to the ground clutter verification of superrefraction, several low-level coverage flights were made from Leesburg to Crystal River and some 80 miles out into the Gulf at an altitude of 100 ft, returning at 1,000 ft to check coverage above duct levels. Only a very few flights were made during periods of extended propagation, but during these periods, while interference from extended ground clutter prevented detection of the plane over land, extended ranges were recorded for the VHF (very high frequency) air-to-ground communication contact.

In a further attempt to investigate some of the operational possibilities of trapping conditions at low and intermediate altitudes, measurements were taken of maximum ranges on the airborne X-band APQ/13 radar during routine flights. However, as the ranges observed were very erratic, no conclusions could be drawn. In this respect it should be stated that while excellent cooperation was obtained in getting various radar and aircraft observations, the project had a low priority and as a consequence could not fully investigate many of the more important operational possibilities which would have required extensive use of radar and aircraft facilities.

The over-water forecasting program at Tarpon Springs was set up to compare the results of forecasts made under field conditions of limited meteorological data with those made using all available meteorological information given in the forecasting system presented in reference 3. This system was based primarily on the over-water modification studies presented at the last conference, where duct height d was related to the wind speed at 1,000 ft, the distance of over-water travel, and the M deficit, which is the difference between the M value at some reference level, in this case the sea surface, and the M value of the unmodified air reduced to sea level. In general, no attempt was made to forecast the specific lapse rates and M curves corresponding to the current meteorological situation. With uniform weather conditions existing over water, there was assumed a 100 per cent correlation betwen the M curve and the corresponding radar performance, so that it was merely necessary to determine the representative d and ΔM of the air mass to obtain the complete propagation forecast.

As it was impracticable to establish a permanent target in the Gulf of Mexico beyond the radar horizon, the existence of superrefraction was generally assumed when there was extended appearance of coast-line clutter. It is realized that such an effect may not be representative of open water conditions because of the possibility of local sea breezes giving rise to the necessary temperature and moisture gradients for trapping. However, on this basis, 18 out of 20 forecasts correctly verified the presence or absence of extended coast-line clutter to within 1 to 2 hours of the total duration. With extended echoes existing during 55 per cent of the test days over the coastline, this accuracy is considerably greater than could be arrived at by any purely statistical procedure. It should be stated here that these forecasts proved to be particularly valuable to the radar personnel, since certain engineering tests in progress on the radars made an accurate evaluation of the effects of superrefraction on the radar set performance necessary during the calibration flights.

As an additional check on the existence of superrefraction over water, forecasts were made of the ranges for S-band radars and VHF communication on low-level coverage flights into the Gulf. Of a total of ten flights, six were made during periods of extended coast-line return, three of which were correctly forecast as giving superrefraction on S-band radar and two as giving increased ranges on VHF communication. Although this is not so accurate as the forecast of surface effects, a large error may have been introduced by the fact that the forecasted duct heights were of the same order of magnitude as the lowest levels attained by the plane in its flight over the Gulf. All the over-water flights showed normal horizon ranges at 1,000- to 3,000-ft levels on the return legs.

In another attempt to determine the vertical coverage patterns resulting from low-level nonstandard propagation, several free balloon flights were made. Standard weather service reflectors were attached to

the balloons, which were released from Army crash boats at distances of 20 and 60 miles from the coast. Possibly because of lack of radar efficiency, only the balloons released at 20 miles were picked up by the coastal radar. Although no nonstandard conditions were observed during the releases, the method seems suitable for making vertical coverage measurements.

Radar and weather data for the period January 1 to March 15 were tabulated and analyzed during the month of March. The primary data consisted of S-band radar reports from Winter Garden and Leesburg and low-level soundings from Leesburg, supplemented by the synoptic charts and radiosonde observations supplied by the 26th Weather Region.

The analysis resulted not in a system of forecasting such as that developed for over-water use but rather in a series of clues to be used as an aid to over-land forecasting in Florida. Since the clues are closely related to the topography and peninsular situation of Florida and to the season of the year, they are not directly applicable to other locations in their present form. However, they suggest that investigation of these points at other locations would quickly yield useful correlations. Some examples of these relations follow.

1. Of the 600 ft low-level sounding standard curves, 90 per cent gave standard ranges.

2. During early morning hours:

  a. Surface winds of 10 mph or more produced standard propagation always; winds of 5 to 9 mph produced superrefraction 20 per cent of the time; 2 to 4 mph showed superrefraction 60 per cent of the time; and calm winds produced superrefraction almost always.

  b. Similarly, the 1,000-ft winds of 30 mph or more produced standard, while 1,000-ft winds of 10 mph or less almost always produced superrefraction.

  c. Superrefraction occurred with clear skies except on two occasions, one with broken high clouds, the other with broken middle clouds, never with low clouds.

  d. High-pressure centers within 700 miles and with gradients of 1 mb per 100 miles or less produced superrefraction.

  e. Ground fog patches were observed during periods of class 4 propagation, with two exceptions.

3. Simple surface ducts of 70 ft and ΔM_{50} (reference level 50 ft) of 4 or more and elevated S curves with ducts above 200 ft and ΔM_{50} of 6 or more produced class 3 or 4 propagation with possibly one exception.

4. Large ΔM's observed by radiosonde between 1,000 and 3,000 ft showed no correlation with S-band propagation but did show fair correlation with superrefraction on P band. Superrefraction on both S and

0030 EWT　　　　0130 EWT

0300 EWT　　　　0400 EWT
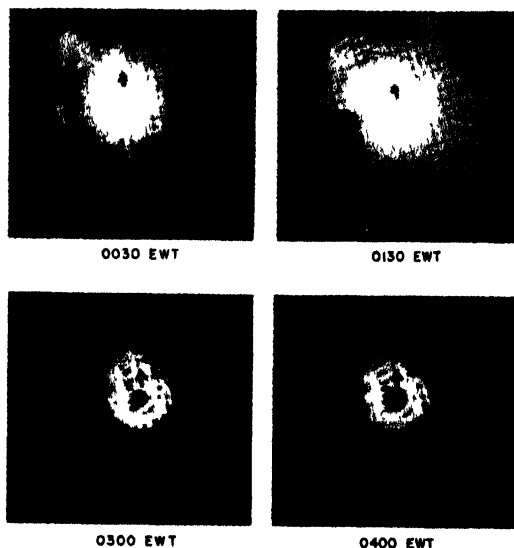
FIGURE 5. SCR-588, Leesburg, night of March 5 to 6, 1945.

P band showed good correlation with large ΔM's observed below 1,000 ft.

5. The height of the temperature inversion increased with increasing 1,000 ft wind speeds up to 10 or 12 mph, then decreased slowly with further increase in wind.

6. Substandard propagation conditions were never observed over land, either on the radar or the soundings.

A series of low-level soundings taken at hourly intervals throughout the night were related to corresponding radar ranges. The soundings were made at Leesburg; the radar data were taken at Tomato Hill (2 miles west of the sounding site) and at Winter Garden (25 miles southeast of the sounding site).

The general weather situation for the night of March 5 to 6 shows maritime tropical air pouring up over Florida around the western end of the Bermuda high, giving clear skies and southerly winds of 10 mph at 1,000 ft and 2,000 ft at 2000 EWT,[*] increasing to 20 and 25 mph respectively by midnight, and to 23 and 35 mph by 0400. Figure 5 shows the PPI scopes of the P-band SCR-588. The arrows point north; the small grid squares are 5 miles on a side. Before midnight, propagation was standard, as illustrated by the 0400 frame. The ranges built up rapidly, reaching 65 miles and decreased slowly between midnight and 0400. (Radar shadows of surrounding topographical features account for the uneven distribution of range increase.)

Figure 6 shows the progression on the S-band SCR-584. The bold line points north, the range markers are at 10,000-yd intervals. (The sounding site is roughly 315° at 45,000 yd.) From 1900 to 2200 propagation

All times to follow are Eastern War Time.

TABLE 1. Radar-weather tabulation, March 5-6.

	Time (EWT)												
	19	20	21	22	23	00	01	02	03	04	05	06	07
SCR-584 ground range* (S-band)	1	2	2	1	1	1	2	2	2	1	1	1	1
SCR-588 ground range (P-band)	..	..	1	..	..	2	2	3	2	1	1	1	1
M-curve type†	S	D	D	..	..	L	G	L	L	S	T$_a$	S	S
Duct height (ft)	..	200	200	..	..	370	350	380	400	..	450	..	..
ΔM	..	14	14	..	..	14	14	14	11	..	6	..	..
Surface wind (mph)	5	4	4	..	..	0	1	3	5	6	6	5	7

*Ground range: 1, standard; 2, 3, 4, degrees of superrefraction.

†M-curve types: S, standard; D, duct (simple surface trapping); G, ground-based S curve; L, elevated S curve; T$_a$, transitional aloft.
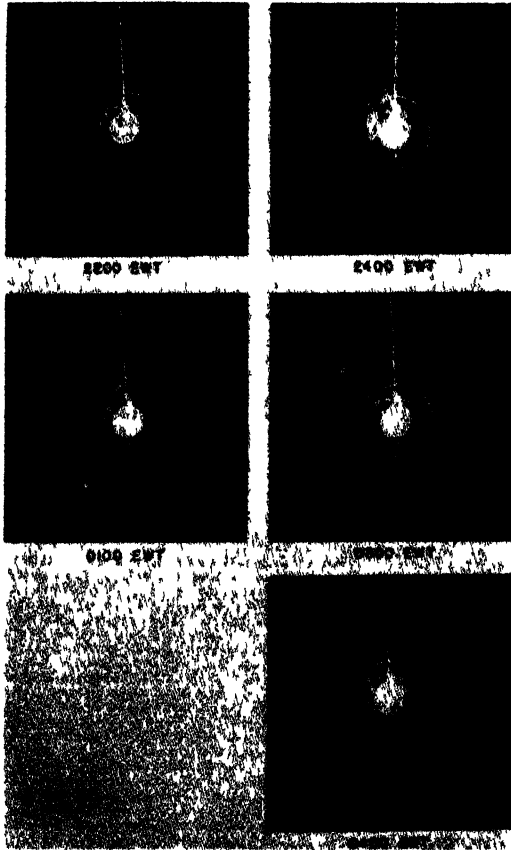
FIGURE 6. SCR-584, Winter Garden, night of March 5 to 6, 1945. Superstandard propagation occurs to the northwest at 0100 and 0300 EWT. At 0400 EWT the pattern is again standard. The line on the PPI indicates true north.

went from standard to above standard and returned to standard. After midnight ranges built up rapidly and held until after 0300, when they began a gradual return to standard, reaching that condition shortly after 0400.

The M curve measured at 1900 was standard, followed by those illustrated in Figure 7. Unfortunately, no soundings were taken between 2035 and 0008, and consequently the evolution of the elevated S from the surface duct is not shown. We know that the surface wind decreased from 4 mph at 2000 to calm at midnight, while the 1,000-ft wind increased from 10 to 20 mph. The duct height and ΔM value were approxi-

mately constant from midnight to 0200, after which the curve gradually approached standard.

Table 1 summarizes the weather and radar variations. It should be pointed out that the antenna height for the P-band SCR-588 was 140 ft above the sounding site, for the S-band SCR-584 the same height as the sounding site. Thus at 2100 we have a 200-ft surface duct trapping the SCR-584, but not trapping the SCR-588 (duct height 60 ft above the antenna), while from midnight to 0300 an elevated duct of the order of 380 ft traps both sets (duct height some 250 ft above the SCR-588 antenna). By 0400 the winds became strong enough to wipe out the stratified layers and mix the air, giving standard conditions. At 0500 a trace of a transitional condition aloft appears in the sounding but is not sufficient to extend the range.

During the months of January and February data were collected on S-band V beam at Tomato Hill during 47 days. Of these days' observations 37 per cent showed nonstandard conditions. During the same period the SCR-271 at Crystal River showed at least slight increases in ranges on 72 per cent of the days'
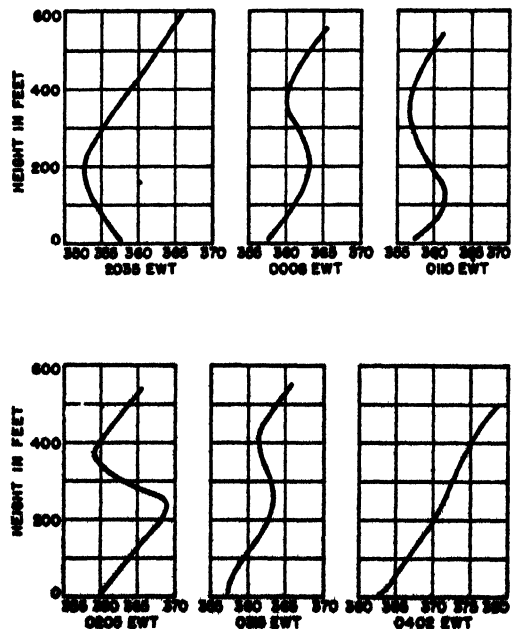
FIGURE 7. M curves for night of March 5 to 6, 1945, based on soundings at Leesburg AAF.

observations which were recorded, although only 17 per cent attained the strength of class 3.

The longest ground range observed on the S-band set at Tomato Hill was 200 miles on the morning of January 25, while the longest ground range observed on the SCR-271 at Crystal River was 140 miles on the morning of February 17. Both these ranges were the maximum permitted by the radar presentation.

During the month of April at Tarpon Springs, 65 per cent of 24 days' observations showed nonstandard conditions, with 46 per cent giving surface return at greater than 80 miles, indicating strong superrefraction. The longest range recorded was the coast-line effect out to 220 miles.

To determine suitable low-level airborne sounding equipment, the psychrometer equipment ML-313/AM, the WSC wired sonde, and sling psychrometer. ML-24A were mounted in aircraft L-4 (cruising speed 55 mph) and compared with the MIT psychrograph carried by a barrage balloon.

From considerations of the forecasting method an accuracy of ±0.2 C in wet and dry bulb temperatures and a lag coefficient less than 45 sec are desirable. The accuracy of the MIT psychrograph is ±0.2 C in temperatures, with a lag coefficient of the order of 15 sec.

These data were gathered during hours of daylight and are spread rather evenly between 0900 and 1700. The MIT psychrograph was held at a fixed point in space where a conservative estimate of the fluctuations of temperature was 0.3 C. The airborne instruments integrate the measurements for a given level, hence a spread in the data is reasonably indicated and the

statistical value of sigma may be considered representative of the accuracy of the test instrument.

The procedure for each test instrument involved making five to ten regular low-level soundings supplemented by a series of passes at a fixed level. Necessary ground checks were carefully made using forced ventilation, and standard corrections for airborne instruments were applied.

Psychrometer equipment ML-313/AM, consisting of a wet and dry bulb thermometer in a streamline housing, was mounted as far back in the cabin of the L-4 as was practical. Since the L-4 is a single engine plane it was expected that the engine heat and propellor blast would influence the readings. The data are as follows:

Dry bulb
   Number of pairs of readings: 174
   Average difference: — 0.06 C
   67% of the points agree to within   0.20 C
Wet bulb
   Number of pairs of readings: 156
   Average difference: + 0.08 C
   67% of the points agree to within   0.14 C

The ML-313 was, in addition, mounted on aircraft L-5 (single-engined, cruising speed 100 mph). The data are similar to those given above. The data indicate that, despite the expected influences of propeller blast and engine heat, the equipment is suitable for low-level soundings for propagation work.

The WSC wired sonde was mounted on the strut of the L-4 some 5 ft away from the cabin of the plane. The comparison data follow:

Dry bulb
   Number of pairs of readings: 140
   Average difference: + 0.10 C
   67% of the points agree to within   0.30 C

Vapor pressure
   Number of pairs of readings: 140
   Average difference: + 0.06 mb
   67% of the points agree to within   0.98 mb

The differences in moisture readings are rather larger than desirable.

The sling psychrometer ML-24A was tested similarly but was considered unsuitable because of lack of protection from radiation.

Of the ground-based sounding equipment used during the program, the MIT psychrograph consistently gave excellent results. The WSC wired sonde is capable of good results, but several mechanical difficulties render it unsuitable for field use by the services in its present form. It is expected that these difficulties will be ironed out in a revision of the wired sonde.

The following statements are the personal opinions of the authors and do not represent the official opinion of the Army Air Forces Board.

1. There is a military need for a propagation forecasting service. If a radar set is to be used most efficiently, its full capabilities and limitations (including
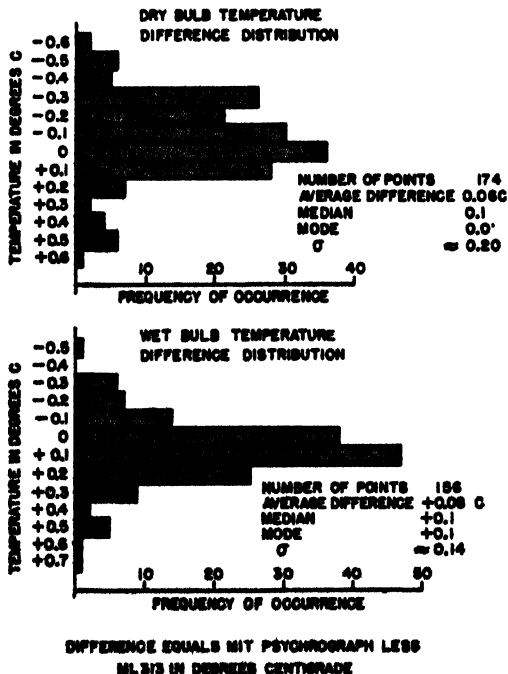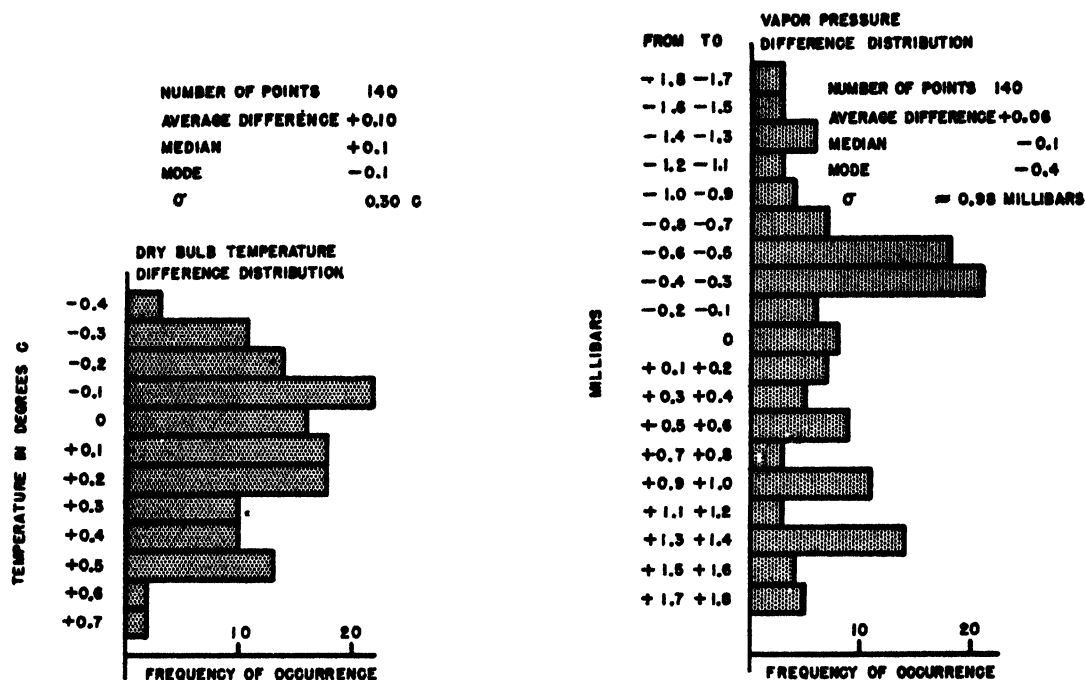

FIGURE 8. Instrument comparison. MIT psychrograph and psychrometer ML 313/AM on Aircraft L-4.

NUMBER OF POINTS   140
AVERAGE DIFFERENCE +0.10
MEDIAN   +0.1
MODE   -0.1
σ 0.30 C

DRY BULB TEMPERATURE
DIFFERENCE DISTRIBUTION

VAPOR PRESSURE
FROM TO DIFFERENCE DISTRIBUTION

NUMBER OF POINTS   140
AVERAGE DIFFERENCE +0.06
MEDIAN   -0.1
MODE   -0.4
σ = 0.98 MILLIBARS

DIFFERENCE EQUALS MIT PSYCHROGRAPH LESS WSC WIRED SONDE IN DEGREES CENTIGRADE
AND MILLIBARS OF VAPOR PRESSURE

FIGURE 9. Instrument comparison. MIT psychrograph and WSC wired sonde on Aircraft L-4.

the effects of weather) must be known.

2. Propagation forecasts over water using the method described in reference 3 are sufficiently accurate for operational purposes. It is recommended that further experimental study of long over-water propagation and vertical coverage be carried on.

3. Propagation forecasts over land are not sufficiently accurate for operation uses. Further study of the over-land forecasting problem is indicated.

4. For maximum operational employment of the forecasts, the forecaster should be located at the radar site. Communication with a class A weather station, a ground-based low-level sounding station at the radar site, and supplementary airborne soundings are required.

5. Psychrometer equipment ML-313/AM mounted on a slow, single-engined aircraft is suitable for low-level airborne soundings for propagation forecasting work.

APPLICATION OF FORECASTING TECHNIQUES AND CLIMATOLOGY[f]

MATERIAL COVERED

Radio-Meteorology. Since most of the basic information which has been obtained by various research

groups and in military and naval operations involving radar is familiar to the reader or is adequately covered in other reports,[4-7] the essential points with reference to the effect of meteorological factors have been extracted and are here presented in condensed form. The primary emphasis is on the phenomena associated with nonstandard propagation, i.e., on the conditions under which radar ranges are unusually large or unusually small. Related elements—temperature, humidity, the variation of each of these with height, *M* curves, ducts, etc.—are defined, and the role they play in the effectiveness of radar performance is discussed briefly.

Specific Relationships between Meteorological Elements and Radar Performance. Of the several investigations carried out on this subject, mostly in connection with the prediction of trapping effects and consequently of radar ranges, one which has met with as much success as any and is fairly similar in essence to some of the others is presented here. It was developed in a study of the modification that air undergoes in passing over water and is designed to predict the formation and subsequent structure of surface ducts which are formed along coast lines and over oceanic areas.

From observations of the representative surface temperature and humidity of the air, the sea temperature, and the wind direction and velocity, this method indicates whether a surface duct is to be expected and the height to which it is likely to extend. Practical

---

[f] By A. T. Waterman, Jr., and C. Harrison Dwight, Columbia University Wave Propagation Group.

application of the method can therefore be of direct assistance in anticipating radar performance for short periods in advance or for regions where detailed meteorological observations may be limited. Enough particulars, together with charts and nomograms, are given to enable one with meteorological training to apply these prediction techniques and thus facilitate daily or hourly adjustments to make optimum use of radar equipment.

Computed Climatological Information on Surface Ducts. To obtain a broad picture of the variation in radio and radar ranges likely to be encountered in the western Pacific region, average duct widths (height from the base to the top of the duct) have been computed. These computations are based on the relationships between meteorological elements and radar performance mentioned above and utilize climatological data consisting of monthly averages of air temperature, humidity and sea temperature, and monthly frequencies of winds with specified direction and speed.

The area covered·includes the Japanese islands, the coasts of Korea, Manchuria, and China, the northern Philippines, the Marianas, the Bonins, and the Ryukyu Islands—approximately 10° to 50°N latitude and 120° to 150° E longitude. The computations indicate the percentage of time surface ducts of various widths may be expected at different times of the year and at different locations within the region. This information is summarized in tabular form. The results are not intended to represent an accurately detailed picture but do give a sufficiently close approximation of average conditions influencing certain aspects of radio and radar performance so that they may be used as a guide in long-term operational planning.

Radio-Meteorology

EVIDENCES OF NONSTANDARD PROPAGATION

Since the start of the war, cases of very long radio ranges and radar coverages, together with extreme variations of these quantities, have become well known to personnel working at microwave frequencies. Such phenomena, when due to influences acting on the propagated electromagnetic waves and not to freak behavior in set performance, have been classed under the term nonstandard propagation. It has been found that nonstandard propagation (such as is illustrated by the behavior of microwaves when they are constrained to follow a path of such curvature that the rays remain close to the surface of the earth and hence reach otherwise inaccessible targets—a phenomenon frequently referred to as trapping) is directly associated with certain conditions that occur in the lower levels of the atmosphere (normally below 5,000 ft) which have been given the name of ducts. Detailed analyses of the structure of ducts have been presented

adequately in the previously mentioned reports. Hence the paragraphs immediately following give only a brief and somewhat simplified description of the meteorological elements associated with ducts.

METEOROLOGICAL CONDITIONS ASSOCIATED WITH DUCTS

Remarks on Pressure, Temperature, and Humidity. The meteorological situations in which trapping of microwaves occurs involve certain types of stratification in the lower levels of the atmosphere. The amount of stratification is dependent on the vertical distributions of pressure, temperature, and humidity.

Although the atmospheric pressure at any particular elevation and, to a lesser extent, the rate at which pressure decreases with altitude may vary from one time to another, these variations are relatively unimportant as far as their direct influence on propagation is concerned and so· may be neglected in practical considerations.

On the other hand, temperature and its change with altitude do have an immediate bearing on duct formation. Under more or less average conditions throughout the troposphere, the temperature decreases with increasing altitude and the term "temperature lapse rate" is defined as the rate of decrease of temperature with height (and consequently is usually expressed in degrees Fahrenheit per 1,000 ft or degrees centigrade per kilometer). For reference purposes a "standard" lapse rate has been taken as 3.47 F ner 1,000 ft. (Further details of the National Advisory Committee on Aeronautics standard atmosphere are given in the Appendix on page 258.) Under certain conditions the temperature throughout a layer of the atmosphere may *increase* with height, in which case a temperature inversion (Figure 10) is said to exist.
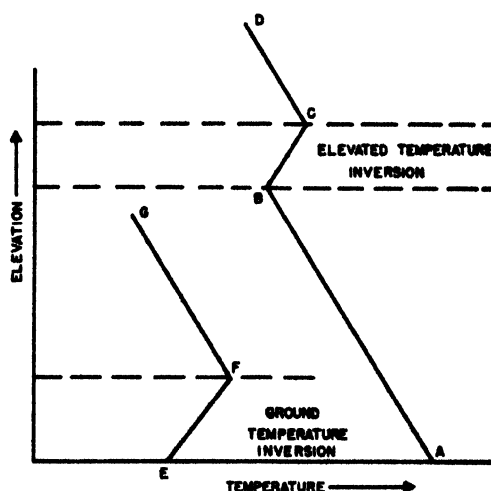

FIGURE 10. Vertical variation of temperature showing a ground inversion EF and an elevated inversion BC. The slopes of the portions FG, AB, and CD denote standard conditions, a decrease of temperature with elevation.

In general the lapse rate of temperature is important in meteorology because of its relationship to the vertical *stability* of the atmosphere, that is, to the feasibility with which vertical air currents can develop. It turns out that, except within clouds or regions of active precipitation, the stability conditions can be closely evaluated from a knowledge of the actual lapse rate relative to the "dry adiabatic" lapse rate (approximately 5.5 F per 1,000 ft). If the actual lapse rate is larger than the dry adiabatic, i.e., if the temperature decreases at a rate greater than 5.5 F per 1,000 ft in elevation, any vertical currents which develop will tend to exaggerate in intensity, and a condition of unstable equilibrium (Figure 11A) will exist. Conversely, if the actual lapse rate is less than the dry adiabatic or, especially, if a temperature inversion is present, the development of vertical currents will be hindered and the air will tend to become horizontally stratified. This is the case of stable equilibrium (Figure 11C). The in-between case, in which the actual temperature lapse rate is the same as the dry adiabatic, is that of neutral equilibrium (Figure 11B).
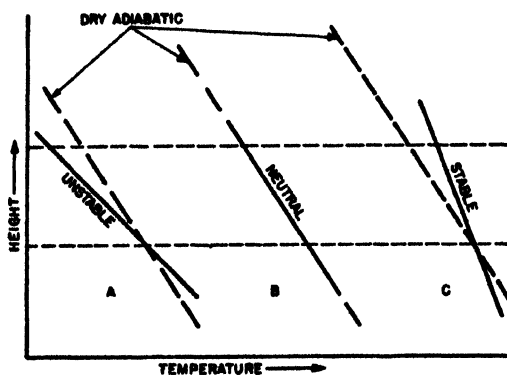

FIGURE 11. Temperature-height curves for the cases of (A) unstable air, (B) neutral air, and (C) stable air. The dry adiabatic (lapse rate) is indicated for comparison.

In addition to the direct relationship which these stability conditions bear toward the trapping of microwaves, which will be described presently, there is also an indirect relationship caused by the modification that air undergoes when it moves over a sea or land surface with properties (temperature and moisture) different from those of the air itself. For example, air moving over land, the temperature of which is *higher* than that of the air, will be heated in its lowest layers by contact with the ground and thus tend to become *unstable*. This leads to vertical currents which will carry the modifying influences to appreciable heights in the air. On the other hand, air moving over a surface cool in relation to the air will be cooled by contact with the ground, tend to develop *stable* characteristics, damp out vertical currents, and so confine the modifying influences to very low layers.

The distribution of moisture with altitude, in its direct influence on nonstandard propagation, has an even more pronounced effect than that of temperature. As a means of describing the moisture content of the air, any one of several concepts may be used: dew point, wet bulb temperature, relative humidity, absolute humidity, specific humidity, and mixing ratio, all of which are defined on pp 258-259. Except when evaporation or condensation is taking place (as in the case of clouds, rain, dew, etc.), the moisture content of the air has little effect on the temperature structure and therefore is not a major influence on stability conditions in so far as they are connected with the formation of ducts. What is of direct importance is the vertical distribution of humidity itself and the manner in which this distribution is affected by modifying influences. As an example of the latter, the case of warm and relatively dry air moving over a humid surface, such as dense vegetation or the ocean, might be mentioned. In this case, evaporation of water into the lower layers of the air leads to a greater decrease in moisture with altitude than was originally present in the air.

Other modifying influences, of course, affect both the vertical distribution of temperature and humidity and the stability conditions of the air. Some of these are subsidence (the gradual sinking of large layers of air leading to increased stability and decreased relative moisture content), radiation, and turbulent mixing. These are merely mentioned here in view of the fact that their various interactions at times may become quite complicated, hence requiring that proper interpretation be made by one trained or experienced in meteorology.

Refractive Index. The manner in which pressure, temperature, and humidity directly influence trapping depends on the phenomenon of refraction or the bending of rays as they pass through media with different dielectric properties or through a medium with variable dielectric properties. The velocity of electromagnetic waves through any particular medium such as the air depends on a quantity known as the refractive index of that medium. When the refractive index varies throughout the medium, as is usually the case in the atmosphere, the resulting variation in wave velocity leads to a bending of the rays. For example, the refractive index of the atmosphere often decreases with height, in which case rays are bent downward toward the surface of the earth, so that instead of traveling in straight lines they tend to follow to a certain extent the curvature of the earth. The amount of bending depends on the manner in which the refractive index varies with height. Under the proper conditions it is possible for rays to be bent to such a degree that they are confined to one layer of the atmosphere. This phenomenon, the trapping of radio waves, is usually associated with only the microwave frequencies and is limited to those rays which leave the

transmitter at an angle with the horizontal of less than 1 degree, and therefore to only the lowest lobe in a radar coverage diagram.

For the atmospheric refraction to be strong enough to cause trapping of microwaves it is necessary that the refractive index of the atmosphere decrease with altitude at a sufficiently rapid rate. For convenience in dealing with problems of nonstandard propagation, a quantity known as the modified refractive index has been defined and is usually denoted by the letter M. It depends on pressure, temperature, humidity, and height and can be readily calculated from the proper nomograms[8] or from tables,[9] or directly from the formula.[9]

When values of M are computed for various elevations from measurements of the pressure, temperature, and humidity at those elevations, a graph can be made of the value of M plotted against height. This M curve gives directly a graphical representation of the structure of the atmosphere with reference to the existence of ducts. A decrease of M with elevation is called an M inversion, since under standard conditions M increases with altitude, and indicates the existence of a duct. This, then, is the criterion for the meteorological conditions necessary for the trapping of radio waves. The top of the duct is taken to be that level at which M reaches a minimum (as in Figure 15) and the base of the duct the level at which a vertical projection from the value of M at the top of the duct intersects the lower portion of the M curve (as in Figure 16) or the ground (as in Figure 17). The term "duct width" is used to refer to the thickness of the duct, i.e., the vertical distance between the top and the base.

The vertical distribution (a) of temperature and (b) of humidity may each contribute to the formation of an M inversion, in the following ways.

1. A strong temperature inversion tends to lead to duct formation.

2. A rapid decrease of humidity with altitude tends to lead to duct formation.

If the first of these is predominant the duct is said to be dry, and if the latter is predominant the duct is said to be wet. Often both factors are operative together; that is, in the M inversion there is both an increase in temperature with altitude and a decrease in humidity with altitude, the duct being more sensitive to the effect of the humidity distribution than to that of the temperature distribution.

Types of M Curves. For purposes of clarification, the various types of M curves that may exist can be classified as follows:

1. *Standard type* (Figure 12). In a standard atmosphere M increases linearly with altitude at a rate of 3.6 M units per 100 ft (0.118 M unit per m). Radio and radar waves are bent slightly downward, the paths of the rays actually having a radius of curvature about four times that of the earth; but no trapping occurs.

Standard conditions, in their effect on propagation, hardly differ at all from those of neutral and unstable
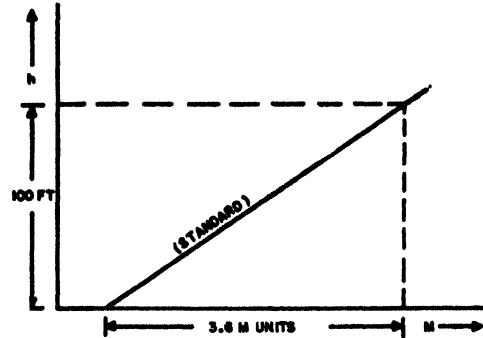
FIGURE 12. Standard type of M curve.

equilibrium (except in special cases as mentioned later) and so are frequently found in well-mixed air, as is likely to occur on sunny afternoons and in areas of turbulence.

2. *Transitional type* (Figure 13). In the lower levels M is constant with elevation. Correspondingly, rays are bent downward more than in the standard case but not so strongly as in a duct, i.e., the rays are not actually trapped. Being literally a transitional case,
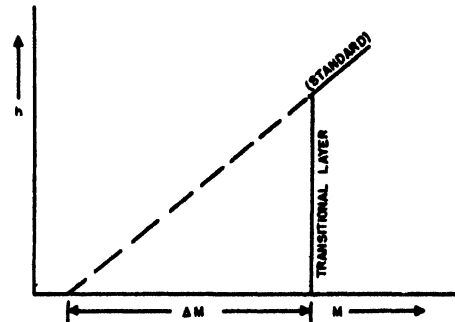
FIGURE 13. Transitional type of M curve.

this type of M curve is likely to occur during the formation or dissolution of a duct, or when the meteorological factors tending to cause a duct are incompletely operative. The M deficit (ΔM, given on pages 249-251), is indicated in the figure.

3. *Substandard type* (Figure 14). In the lower levels M increases *more than* 3.6 M units per 100 ft, which corresponds to rays being bent downward only very slightly or, in some cases, actually upward from the line of sight, thus giving shorter maximum ranges on surface and low-flying targets. There is no trapping. Depending to some extent upon the elevation of the transmitter, the field strength in the substandard region may be reduced considerably below normal, even to the point of producing radar and communication "blackout." The M deficit is negative with this type of curve. Associated meteorological conditions are usually those in which warm, moist air passes over a
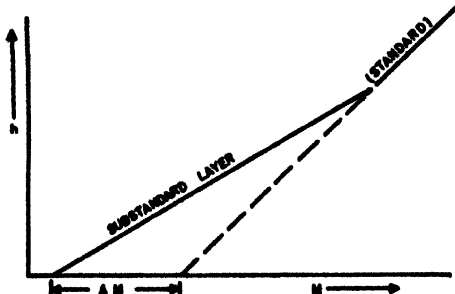
FIGURE 14. Substandard type of M curve.

relatively cool land or sea surface, quite frequently in connection with the formation of surface fog.

4. *Simple surface trapping* (Figure 15). The M curve has a negative slope in the inversion layer which comes down to the land or water surface. The duct is of the ground-based type, and its width is the height of the upper boundary of the inversion layer. Rays which are propagated at an angle of 1 degree or less with the horizontal may be trapped within the duct. As a consequence, radio and radar ranges may be exceedingly large. Simple surface trapping occurs quite frequently over the oceans—particularly where warm, dry air from over land flows out over a cooler sea surface—along coast lines with an afternoon sea breeze, and occasionally over land with radiational cooling at night.
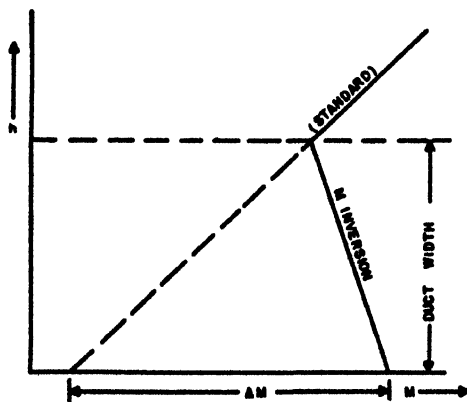
FIGURE 15. Simple surface trapping.

5. *Elevated S-shaped type* (Figure 16). The inversion layer has a width given by the difference in elevation of the end points of the negative portion of the M curve, but the width of the duct extends downward to the level where the vertical projection of the upper minimum of the M curve intersects the latter. Trapping occurs when the transmitter is at an elevation which places it within (or close to) the duct and is most pronounced when the transmitter is at the elevation of the base of the M inversion. This type of duct may be brought about by subsidence or as the result of a Föhn wind blowing off shore from mountains

paralleling a coast. Examples of elevated S-shaped M curves are observed off the southern California coast and off the east coasts of Japan and New Guinea (see page 256-258).
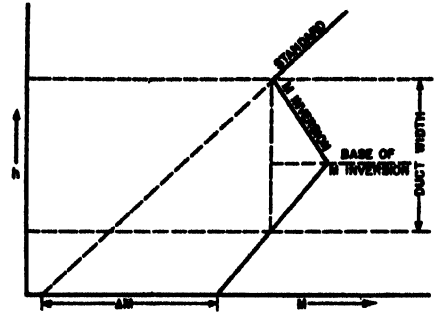
FIGURE 16. Elevated S-shaped type.

6. *Ground-based S-shaped type* (Figure 17). When the conditions which could produce type 5 (Figure 16) exist down to the surface of the earth or to the sea, this type of duct may occur. It usually has a width considerably greater than that found in the simple trapping case (type 4, Figure 15).

That it is possible for ducts of two types to occur simultaneously has been shown from observations off
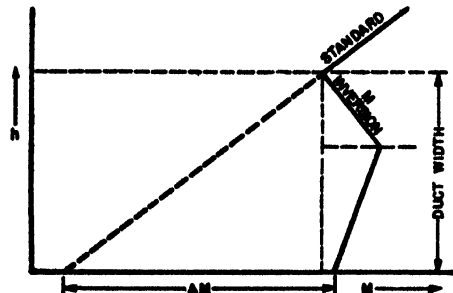
FIGURE 17. Ground-based S-shaped type.

the east coast of New Guinea when a Föhn wind flows out over a sea breeze, the latter producing simple surface trapping (Figure 18). (See pp. 256-258.)

Factors Affecting the Extent of Trapping. The principal factors which determine the extent of trapping are:
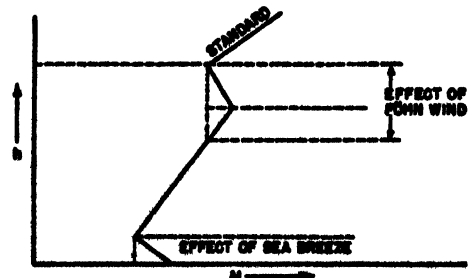
FIGURE 18. Combination of types 4 and 5. (See Figures 15 and 16.)

1. The amount by which M decreases through the M inversion.

2. The duct width, for the wider the duct the more energy will be trapped.

3. The elevation of the transmitter with respect to the duct, the trapping being most complete when the transmitter is at the base of the M inversion.

4. The angle at which the rays are propagated from the transmitter; the smaller the angle made with the top of the duct, the greater the range.

5. The frequency of the propagated waves; in general, the higher the frequency, the greater the extent of trapping.

Specific Relationships Between Meteorological Elements and Radar Performance

RESEARCH ON FORECASTING OF RADIO AND RADAR RANGES

Army Air Force Board Project. Realizing the important and direct effects of temperature and humidity distributions on microwave propagation, several projects have been undertaken in the attempt to develop a systematic method of forecasting the meteorological conditions leading to nonstandard propagation. Of these methods, one which has met with a considerable degree of success is described below. The methodology, developed by the Army Air Force Board working in conjunction with the Radiation Laboratory at MIT,[9] is designed to predict the formation of surface ducts over water. Its fundamental concepts are quite similar to those used in other methods of radio and radar forecasting.[10]

General Procedure. In essence the method consists of an analysis of the modification that air undergoes in the lower 1,000 ft as it moves from a large land mass out over the ocean. The study was carried out in the vicinity of Cape Cod, but indications are that the numerical factors entering into the procedure are much more generally applicable. In the modification of the air moving over the sea, the following assumptions are made.

1. The air initially (before moving off the land mass) is well mixed, i.e., it exhibits conditions close to neutral equilibrium (see Figure 11).

2. The stability conditions of the air as it moves out over water are determined by its initial temperature (over land) relative to that of the sea surface.

3. The modified air at the sea surface acquires the same temperature as the sea.

4. In the modified air at the sea surface the moisture content becomes that corresponding to saturation at the sea surface temperature, except for a correction owing to the salinity of the sea.

5. The resulting M curve is determined by the

quantities:

   a. Temperature excess.[s]
   b. M deficit.[s]
   c. Wind speed and direction.
   d. Distance of over-sea travel (in some cases).

Thus the method attempts to relate duct formation to a limited number of easily determined meteorological factors. It involves a simplified consideration of the upward diffusion of heat and moisture. It turns out, however, that the simplified assumptions yield results which in practical application are of sufficient accuracy to be of definite use in forecasting the existence of nonstandard conditions. It should also be mentioned that, although the method is designed primarily for situations in which air over land moves out over the sea, it can also be satisfactorily applied to situations in which the air has a purely over-sea trajectory.

The particular steps to be taken in carrying out the procedure follow.

METHOD OF DETERMINING DUCT WIDTH

Observation of Initial Conditions. The necessary meteorological measurements to be taken should be as representative as possible, i.e., uninfluenced by purely local effects. Measurements are:

1. Surface air temperature (of the unmodified air over land, in the case of air moving off a land mass);

2. Surface air humidity (also of the unmodified air which can be expressed in terms of relative humidity, specific humidity, dew point, wet bulb temperature, or vapor pressure);

3. Sea surface temperature;

4. Wind speed and direction (preferably at 1,000 ft elevation); and sometimes

5. Distance from land (of primary importance only in the case of stability conditions, when the air is warmer than the sea surface).

All these data may, of course, be profitably supplemented by aerological soundings, weather maps, and any other pertinent information available.

Modification of Air by Sea Surface. As a qualitative description of the modification that the air undergoes in moving over water, three cases may be distinguished:

1. *Neutral equilibrium* (resulting when the initial surface air temperature is the same as the sea temperature). The temperature structure of the air remains unchanged; however, since the air is usually not completely saturated, moisture is supplied to the lower layers by evaporation from the sea surface, in this way causing a greater decrease of humidity with height, which tends to establish an M distribution such that the modified refractive index is either constant or decreasing with height. In the case in which the air is initially completely saturated no modification takes place.

2. *Unstable equilibrium* (resulting when the initial surface air temperature is less than the sea surface temperature). In this case the moisture content of the air is always less than that corresponding to saturation at the sea surface temperature, so that the lower layers of air suffer an increase in humidity as well as in temperature. Owing to the greater sensitivity of M to humidity than to temperature this tends to bring about a decrease of M with height in a layer of air adjacent to the sea surface, while the unstable conditions give rise to vertical mixing which keeps the M distribution close to standard above this layer so that the duct is confined to lower levels than in the case of neutral equilibrium.

3. *Stable equilibrium* (resulting when the initial surface air temperature is greater than the sea surface temperature). If, in addition, the air is initially quite dry, i.e., has a moisture content less than that corresponding to saturation at the sea surface temperature, then the resulting rapid decrease of moisture with height plus the stable temperature distribution leads to a tendency to surface duct formation. On the other hand, if the initial moisture content of the air is relatively large, moisture may be condensed out of the surface layers of air thus tending to give rise to an increase in humidity with elevation which when sufficiently marked may counteract the effect of the stable temperature distribution and so prevent the formation of a duct or even produce substandard conditions. In either case, the stable structure of the air tends to hinder vertical mixing so that modification from the surface upward proceeds slowly and hence is highly dependent on the distance traveled by the air over the water.

Necessary Calculations. To determine quantitatively the possibilities of duct formation, the following items can be readily calculated from any particular observed set of initial conditions.

1. *Temperature excess,* which is merely the representative surface air temperature (before modification) minus the sea surface temperature.

2. *M deficit,* defined as the value of M corresponding to the sea surface temperature minus the value of M determined from the representative surface air temperature and humidity (before modification); values of M can be ascertained from nomograms,[h] tables,[i] or directly from the formula.[j] In the case of M corresponding to the sea temperature, a 98 per cent saturation is assumed; the 2 per cent vapor pressure correction is subtracted to take into account the salinity of the sea water.

3. *Ratio of duct width to M deficit,* determined from the chart in Figure 19 for a given temperature

excess and wind speed as measured at the 1,000-ft level.

4. *Duct width,* found by multiplying the above ratio (3) by the M deficit.

Applicability of the Method. Since the procedure is designed to take into account only the surface modification of air over water, its application is restricted to the prediction of the first four types of M curves described on pages 245-248: standard, substandard, simple surface trapping, and transitional. The causes of S-shaped M curves are not considered in this method. Standard conditions can be presumed to occur when the calculations indicate a duct width of zero, which is the case when the M deficit is zero. If the M deficit is *negative,* then the calculated duct width will be negative, and substandard conditions are to be inferred. A *positive* M deficit indicates duct formation (simple surface trapping), and the calculations of the duct width given an estimate of the height to which the duct extends. If this height is small, conditions may be inferred to correspond to the transitional case. Once the duct width is calculated, a complete picture of the distribution of M with height
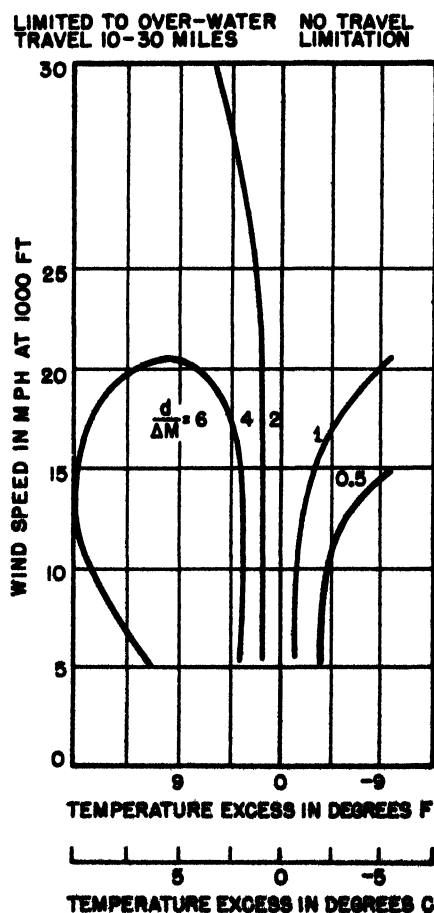
FIGURE 19. Graphs showing the value of the ratio of duct width d to the M deficit, ΔM for values of temperature excess and wind speed at the 1,000-ft level. (Typical values are given in Table 2.)

---

[h]Nomograms are included and explained on pages 256-257.

[i]Tables for computing M can be found in references 8 and 9.

[j]The formula expressing M in terms of pressure, temperature, humidity, and elevation is given on pages 256-257.

can be approximated as indicated in Figure 15 by assuming that standard conditions prevail above the duct and that the M deficit (ΔM) is the difference between the actual M value at the sea surface and the M value that would exist at the sea surface if the standard conditions were extended down to the surface.

The method is not applicable to conditions over land.

In the case of air with a purely sea trajectory, it turns out that the procedure is closely valid if, in place of the air temperature and humidity measurements made over land, these measurements are taken in the air at a slight elevation above the sea surface, for example, at bridge level on a large ship.

In practical application results will be most reliable when the assumptions listed under "General Procedure" are satisfied. However, this does not mean that the method is useless under other circumstances. Figure 19, which is the crux of the method, is largely empirical and is based on relationships·which have been observed to hold under various meteorological conditions. Consequently, reasonably accurate results are not limited to only a few idealized situations.

It should be mentioned also that use of the method in a literal manner can be improved upon if the calculated results are modified by the judgment of someone trained or experienced in meteorology. Complicating factors such as variations in the initial stability conditions, variability of the sea surface temperature, effects of convergence, divergence, and subsidence, and presence of fronts can best be taken into account by one familiar with their effects.

QUALITATIVE PREDICTION OF RADAR RANGES

The method described above gives a means of estimating surface duct formation, whereas what is needed is a knowledge of the effect of the duct on radio propagation. It is impossible to make a blanket statement giving the exact range that will be obtained with any particular duct width, since the range depends on the power of the radio or radar set (also on the character of the target, in the case of radar), as well as on the factors listed on pages 245-248. However, some numerical estimates of trapping effects can be made.

Dependence on Duct Width, Frequency, and Elevation of Site. An approximate expression relating the maximum wavelength that can be trapped by surface ducts is given by

$$\lambda_{max} = 0.076d\sqrt{\Delta M - 0.036d},$$

in which λ_{max} is the maximum wavelength in centimeters, d is the duct width in feet, and ΔM is the M deficit in M units. Table 2 is developed from this formula and indicates, for given values of ΔM and d, the wavelength above which trapping will not occur. A rough generalization can be made by stating that, when the wavelength of the radiation is around 3 cm, duct widths of 20 ft or more will be sufficient to cause

simple surface trapping, and, when the wavelength is around 10 cm, duct widths of at least 40 or 50 ft will be sufficient, provided in each case that the transmitter is located within the duct. Thus, for a particular radar frequency and location, an estimation of duct width becomes a critical factor in anticipating whether an appreciable amount of trapping will occur and consequently whether radar ranges will be appreciably larger than under standard conditions.

TABLE 2. Values of the maximum wavelength (in cm) for which waves can be trapped in a surface duct for given values of M deficit (ΔM) and duct width (d).

d(ft)	ΔM (M units)					
	2	5	10	15	20	25
10	0.97	1.63	2.36	2.90	3.36	3.78
20	1.72	3.14	4.62	5.75	6.67	7.49
30	2.19	4.52	6.80	8.50	9.93	11.1
40	2.28	5.74	8.88	11.2	13.1	14.7
50	1.69	6.80	10.9	13.8	16.2	18.3
60	..	7.65	12.8	16.3	19.2	21.8
70	..	8.35	14.5	18.8	22.2	25.2
80	..	8.82	16.2	21.2	25.2	28.6

Dependence on Extraneous Factors. Meteorological conditions other than ducts often have important effects on propagation. Surface fog frequently causes substandard conditions. Rain and clouds may attenuate the propagated energy and effectively decrease the range. Heavy rain and sometimes cumulo nimbus clouds cause radar echoes.

OPERATIONAL USE AND LIMITATIONS

The restrictions surrounding the possible utilization of this prediction technique have been covered earlier in this section, where it is indicated in what respects applicability is limited. Subject to these limitations, the method can be employed to advantage. Short-term predictions (a day or so ahead) of duct formation and radar range can aid in estimating the coverage of a particular radar set. Information of this nature should lead to the more efficient use of radar facilities.

Computed Climatological Information on Surface Ducts

PURPOSE OF THIS INFORMATION

Inasmuch as the present report is designed to aid radar and meteorological officers in the Pacific theater of war, it has been thought expedient to include climatological information on that area which gives an indication of the occurrence of surface ducts. For this purpose, computations have been carried out, using the methodology given on pages 249-150, to yield the following:

1. Estimation of the per cent of time surface ducts of certain widths are likely to occur at various times of the year and at various places in the western Pacific theater.

2. Estimation of the variation in duct width with

the time of year, geographical location, etc.

3. Estimation, from (1) and (2) above, of the amount of trapping to be expected for specified radio frequencies and specified elevations of sites.

Regions Chosen for Study

The area chosen for investigation was that bounded approximately by 10° and 50° N latitude and by 120° and 150° E longitude. These regions include the Japanese islands, the coasts of Korea, Manchuria, and China, northern Philippines, the Marianas, the Bonins, and the Ryukyu Islands. The computations were carried out for representatively selected 5x5 degree sectors or "squares." The results for several regions in this area are summarized and are given below.

Sources of Climatological Data

The charts and atlases used in compiling the data can be found in references 11 to 15.

Method of Computation

The procedures described on pp. 246-251 were applied as follows:

1. A determination of the monthly mean temperature excess was made for each 5x5 degree square for each month (1) by taking the difference between the mean temperature of the air over the sea and the mean sea surface temperature, and (2) by taking the difference between the mean temperature of the air at a land station (when the given square was near a coast) and the mean sea surface temperature.

2. A determination of the monthly mean M deficit[k] was made for each square for each month using the nomograms and taking the data for (1) the mean temperature and wet bulb depression of the air over the sea and the mean sea temperature, and (2) the mean temperature and relative humidity of the air at a land station (when the given square was near a coast) and the mean sea temperature.

3. For each square for each month note was made of the various surface wind velocity ranges that occurred with each wind direction (eight points of the compass) and the percentage of time the wind lay within each velocity range.[l]

4. In terms of the mean temperature excess and mean M deficit, the corresponding duct width was computed for each wind velocity range, and, knowing

the percentage of time that winds of each magnitude occurred, it was possible to compute the percentage of time that ducts of various widths would occur, both for each wind direction (on an eight point compass) and for the overall picture regardless of wind direction.

Results of Computations

The results were summarized by lumping individual squares showing similar characteristics into nine regions within the whole area. In each region data for the individual months were lumped together on the basis of similarity to divide the year into three or four parts (these varying according to region). Then for each group of months in each region were listed those results which were considered to be the most important, namely,

1. The range in duct widths, giving an indication of the variability at any one place at any one time of year.

2. The percentage of time that ducts characterized by widths greater than 40 ft occur and, following this, the most prevalent wind direction associated with ducts of these widths, as well as the minimum wind velocity necessary to establish them.

3. The percentage of time that ducts characterized by widths from 20 to 40 ft occur, similarly followed by the associated prevailing wind direction and the minimum required wind velocity.

4. The percentage of time that ducts do not occur or have a width less than 20 ft.

Figure 20 contains these summarized results. The numerical listings in the figure make no claim toward being exact, as is evident in view of the remarks made on pp. 249-251 on the applicability and limitations of the method, in addition to the slightly erroneous computations of the monthly mean M deficit and the use of the surface winds instead of those at 1,000 ft. (The effect of the latter two errors is mainly to cause the calculated duct widths to tend toward the conservative side.) In Figure 20, for purposes of consistency throughout the area, only the calculations based on air temperature and humidity records over the sea were used [i.e., only (1) under "Method of Computation"]. The difference between these calculations and those based on land station data is primarily that temperature excesses and M deficits are larger in the latter case (this again tends to make the tabulated results conservative).

Other deficiencies of the method which might be cited are the neglect to take into account the occurrence of fog or rain (which tends to create substandard or standard conditions) and the omission of the influence of local effects such as the topography along coast lines (see pp. 254-256). In some cases the period of record was fairly short, so that the data used in the calculations were not always completely representative. Lastly, the ranges of duct widths were calculated on the assumption that there was a varia-

---

[k] These calculations do not represent exactly the correct mean value of the M deficit, since M is not a linear function of the temperature and humidity, and so the value of M computed from mean temperature and humidity data is not quite the same as the mean of all M's computed from individual temperatures and humidities. A cursory evaluation of this error has indicated that the values computed are if anything conservative, i.e., that the actual mean M deficits are probably larger than those computed.

[l] This led to a slight error, inasmuch as the wind at 1,000 ft should have been used in place of the surface wind (data were available only for the latter). This error in most cases resulted in calculated duct widths of slightly less magnitude than would have been obtained if the 1,000-ft wind had been used.

FIGURE 20. Summarised results of climatological duct with calculations.

LEGEND
HEAVY LINES SEPARATE THE OCEANIC REGIONS.
MONTHS (DECEMBER, JANUARY AND FEBRUARY).
RANGE OF DUCT WIDTH IN FEET (5 TO 30 FEET).
PERCENTAGE OF TIME DUCTS OF WIDTH GREATER THAN 40
FEET OCCUR (0 PER CENT).
PERCENTAGE OF TIME DUCTS OF WIDTH 20 TO 40 FEET OCCUR
(30 PER CENT); PREVAILING WIND DIRECTION WITH DUCTS OF
THESE WIDTHS (NORTH). WIND VELOCITY NECESSARY TO CAUSE
DUCTS OF THESE WIDTHS (GREATER THAN 20 MPH).
PERCENTAGE OF TIME DUCTS OF WIDTH LESS THAN 20 FEET
OCCUR (70 PER CENT).

tion of wind speed only, not allowing for possible variation in temperature excess and M deficit.

In spite of these shortcomings, the calculated results show regional and seasonal trends consistent both with what might be expected on the basis of qualitative physical reasoning and also with a limited number of actual observations taken in the Pacific (see pp. 254-256). In conclusion we may safely state that the results represent to a reasonable approximation the average conditions of surface duct width and variability.

Use of Computed Results

Since the computations are based on climatological data and are limited in exactness, they do not have

what trapping conditions will be on any particular day. They serve merely to indicate in a general way the average conditions that might be expected over a period of time. For example, the percentage of time that duct widths in excess of 40 ft occur gives an estimate of the fraction of time that properly sited S- or X-band radars would be able to take advantage of extremely large ranges; the percentage of time that duct widths from 20 to 40 ft occur indicates that portion of the time in which X-band radars would be needed to benefit from surface duct conditions; the percentage of time that no ducts (or exceedingly small ducts) occur points out limitations in the utilization of simple surface trapping. Inasmuch as the transmitter should be located within the duct (if the maximum

forecasting value in the sense of indicating specifically benefit is to be received from trapping conditions), these factors indicate preferable elevations of the transmitter. In general, the information given in Figure 20 can be helpful in relatively long-range planning procedures, in deciding on the most effective type of radar set, the optimum frequency to use, and the most advantageous elevations at which to establish sites, etc., for operations to be conducted during a particular season of the year and in a particular region.

Direct Indications of Nonstandard Conditions in the Western Pacific

GENERAL CONCLUSIONS

Evidences of superrefraction have frequently been found at Guadalcanal and in the general vicinity of New Guinea and New Zealand. Data obtained on the radio-meteorology of the western Pacific in the region from New Guinea to Saipan, from soundings made there in 1944 and 1945,[16-18] indicate the following conditions in both the equatorial and trade wind belts of the Pacific.

1. Unmodified winds of long sea trajectory produce ducts which attain sufficient height and intensity to trap microwaves in the 3,000- to 10,000-mc range.

2. At the relatively low wind speeds characteristic of the equatorial belt (4 to 10 knots), the duct height increases with wind speed from about 20 to about 40 ft. X-, and possibly S-, band radars with properly placed antennas may be expected to show marked increase in range on surface craft and on aircraft flying within the duct.

3. At the higher wind speeds typical of the trade wind belt (10 to 20 knots), ducts 50 to 60 ft wide occur regularly. Properly sited S-, as well as X-, band radars may be expected to show marked and persistent increases of range on surface targets. The persistence of the duct in these regions suggests its use in microwave communications.

4. Unless modified by passage over nearby land masses, the atmosphere is approximately *standard* from 60 to 1,000 ft.

5. The results are so similar to earlier measurements taken in the Caribbean on northeast trade wind air of long sea trajectory as to warrant the conclusion that this type of duct formation is general, at least in tropical and subtropical regions, throughout the world.

6. From the experimental results around Saipan and the Marianas it is concluded that the coverage of radars operated at frequencies much lower than 3,000 mc will probably not be affected by the oceanic ducts.

7. The coverage of microwave radars (3,000 mc and higher) which are sited above 100 ft may not be affected by low-level conditions.

8. If coverage on surface craft or ultra-low-flying aircraft beyond the range of existing facilities is re-
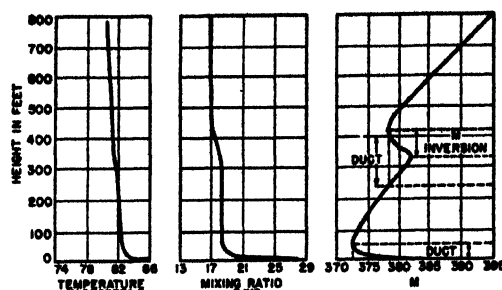
FIGURE 21. Data from Geelvink Bay, New Guinea, showing surface duct as well as elevated S-shaped duct due to Föhn effect from 10,000-ft mountains 100 to 150 miles to windward (SW).

quired and if prevailing wind speeds exceed 10 knots, S-band radars sited 10 to 30 ft above sea level may give better results than high-sited ones.

9. X-band radars sited at 10 to 20 ft should be useful down to wind speeds of the order of 6 knots.

10. In microwave communication links, the use of low-sited antennas may increase range beyond that attainable by siting at the highest available altitudes. (From the standpoint of water vapor attenuation and duct utilization, X-band frequency appears to be the optimum for this purpose.)

11. From a series of ship-based kite soundings taken northeast of Saipan in the two distinct weather regimes, (1) a typical fair weather period, with steady 10- to 20-knot trades blowing and (2) a stormy period with variable 4- to 15-knot southerly winds and frequent rain squalls, it has been found that *all* soundings yield simple surface trapping curves exclusively, the average duct widths being respectively (1) 44 ft and (2) 37 ft.

12. Although measurements were not taken under the conditions mentioned in paragraph 11 (2) above,
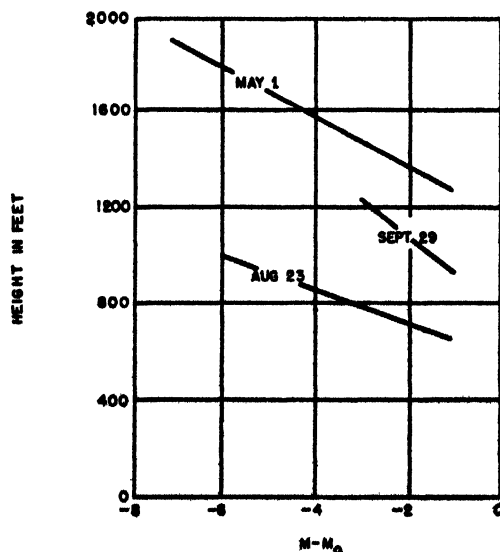
FIGURE 22. M deficits calculated from soundings made at Tateno, Honshu, 1926.
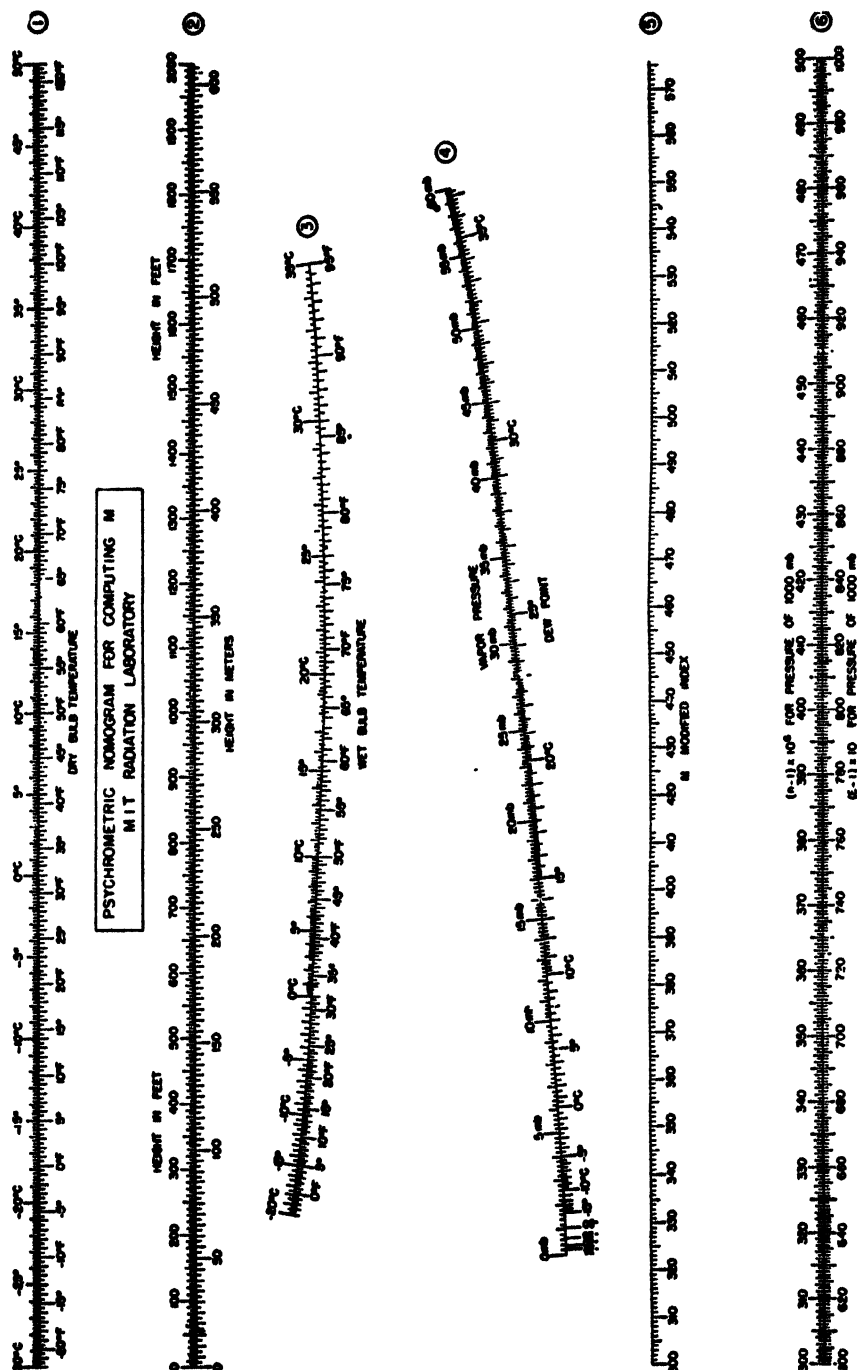
FIGURE 23. Psychrometric nomogram.

soundings immediately after the squalls showed the usual duct. (Sea surface temperatures were constant at 84 to 85 F. Close to the surface the temperature lapse rate was superadiabatic, but it was dry adiabatic above 100 ft.)

OBSERVATIONS UPON DUCTS OTHER THAN SIMPLE SURFACE TRAPPING

Although the emphasis in this report is placed upon simple surface trapping, nonstandard propagation is found under other distributions of atmospheric moisture and temperature. Elevated inversions are found up to around 5,000 ft, due to subsidence in anticyclones over the Pacific[7]; the western and the southern portions of this area usually exhibit the higher elevations. Illustrative of one of the other factors in nonstandard propagation is the Föhn wind

which often produces an elevated S-shaped duct and frequently is superimposed upon a sea breeze. Figure 21, plotted from data taken in the vicinity of the New Guinea coast,[18] indicates the occurrence of an elevated S-shaped curve, below which is found simple surface trapping or the usual trade wind surface inversion. While the existence of conditions favorable to such effects off the coasts of Japan may be assumed, on account of the lofty mountains, there are no data available on this point. The only information on trapping in the Japanese area has been obtained from a study of soundings made in 1928 at Tateno,[19] on the east coast of Honshu, some fifty miles from Tokyo. The data, plotted in Figure 22, shows three cases of an M inversion. The numerical quantities are given in Table 3.

TABLE 3. Aerological soundings at Tateno, Honshu, in 1928, together with computed duct widths and the magnitude of the M deficit.

Date	Elevation of duct top (ft)	Elevation of duct base (ft)	Duct width (ft)	Magnitude of M deficit
May 1	1,900	1,300	600	−6
August 23	1,000	650	350	−5
September 29	1,250	950	300	−2

NOTE ON ATTU AND THE ALEUTIANS[20,21]

Fixed echoes have been obtained at abnormally long ranges (100 to 150 miles). The "Battle of the Pips" was an illustration of pronounced superrefraction. The latter has been observed on at least four occasions by operators of airborne radars returning to Attu from missions over the Kuriles, when VHF radar beacons have returned signals to planes at 5,000 ft and 300 to 350 miles, or about three times the horizon line distance. Meteorological data on duct conditions during the cycle of the Aleutian seasons are needed (up to 1,000 ft).

APPENDIX

STANDARD ATMOSPHERE

Definition. The National Advisory Committee on Aeronautics [NACA] defines the "standard atmosphere" as that which exhibits:

1. A sea level pressure of 1,013 mb (= 760 mm of mercury = 29.92 in. of mercury).

2. A sea level temperature of 15 C (= 59 F) which decreases at a rate of 6.5 C per km (= 3.47 F per 1,000 ft) in the lower atmosphere; and in addition the moisture content may be specified as follows:

3. A relative humidity of 60 per cent, which corresponds to a water vapor pressure of approximately 10 mb at sea level and to a rate of decrease in the lower atmosphere of about 1 mb per 1,000 ft.

Properties. The following table for the standard atmosphere indicates the variation with height of (a) temperature, (b) pressure, (c) water vapor pressure for 60 per cent relative humidity, (d) a quantity con-

taining the index of refraction, n, and (e) the modified refractive index, M.

Altitude Meters	Feet	Temperature C	F	Pressure (mb)	Water vapor pressure for 60% RH (mb)	$(n-1) \times 10^6$	M
0	0	15.0	59.0	1,013	10.2	322	322
150	492.1	14.0	57.2	995	9.6	316	339
300	984.3	13.0	55.4	977	9.0	309	357
500	1,640.4	11.7	53.1	955	8.3	300	379
1,000	3,280.8	8.5	47.3	894	6.7	281	438
1,500	4,921.2	5.2	41.4	845	5.3	266	501

RADIO METEOROLOGY TERMS

Index of Refraction. This can be defined for any particular medium as the ratio of the velocity of electromagnetic waves in a vacuum to their velocity in the medium. The relationship indicating the amount of bending or change in direction that occurs as electromagnetic radiation crosses a boundary between two media with different refractive indices is given by Snell's law:

$$n_1 \cos \alpha_1 = n_2 \cos \alpha_2$$

in which n_1 is the refractive index of the first medium, n_2 that of the second medium, α_1 the angle which the ray in leaving the first medium makes with the boundary, and α_2 the angle which the ray in penetrating the second medium makes with the boundary. In the case of the atmosphere (one medium with a variable refractive index) this expression can be modified to relate the gradual bending of a ray to the manner in which the refractive index varies. The value of the refractive index, n, at any particular point in the atmosphere can be determined from measurements of pressure, temperature, and humidity by substitution in the formula,

$$n = 1 + \frac{79}{T}\left(p + \frac{4800e}{T}\right)10^{-6}$$

or, expressed differently,

$$(n - 1)\,10^6 = \frac{79}{T}\left(p + \frac{4800e}{T}\right),$$

in which the temperature, T, is measured in °K, and the atmospheric pressure, p, and vapor pressure, e, in millibars.

Modified Refractive Index. It is considered more convenient, in problems of radio propagation, to define a slightly different quantity M, which is related to the index of refraction by

$$M = \left(n + \frac{h}{a} - 1\right)10^6,$$

in which n is the index of refraction, a is the radius of the earth (21×10^6 ft) and h is the height above the surface of the earth (measured in the same units as a). In terms of pressure, temperature, humidity, and height, M is given by

$$M = \frac{79}{T}\left(p + \frac{4800e}{T}\right) + \frac{h}{a}\,10^6,$$

in which the units of measurement used are the same as above. The rate at which M increases with altitude is given by

$$\frac{dM}{dh} = \left(\frac{dn}{dh} + \frac{1}{a}\right) 10^6 ,$$

which in the standard atmosphere is

$$\frac{dM}{dh} = -0.039 + 0.157$$

$$= 0.118 \ M \text{ unit per meter}$$

$$= 0.036 \ M \text{ unit per foot.}$$

Psychrometric Nomogram. Radiation Laboratory (MIT) has developed a nomogram with which to compute the modified index of refraction from the necessary meteorological parameters. This chart is known as the psychrometric nomogram. (See p. 255.)

METEOROLOGICAL TERMS

Absolute Humidity. The mass of water vapor present in a unit volume of air is known as the absolute humidity of the air. It is another way of expressing the water vapor density.

Specific Humidity. The specific humidity of moist air is the ratio of the weight of water vapor mixed with the air to the weight of the.moist air. If p is the barometric pressure and e is the partial pressure of the water vapor, then the specific humidity is given by

$$q = 622 \ \frac{e}{p - 0.377e} \ \text{g per kg} .$$

Mixing Ratio. The ratio of the mass of water vapor mixed with unit mass of perfectly dry air is known as the mixing ratio and may be expressed as

$$w = 622 \ \frac{e}{p - e} \ \text{g per kg} .$$

Relative Humidity. The ratio of the actual water vapor pressure to the saturation vapor pressure at the same temperature is known as the relative humidity of moist air. If e and e_s are the respective vapor pressures, then (in per cent) the relative humidity is expressed as

$$\text{RH} = \frac{e}{e_s} \times 100 .$$

Wet Bulb Temperature. The lowest temperature to which a wetted ventilated thermometer can be brought by evaporation is called the wet bulb temperature. It is not strictly an air temperature.

Air Mass. An extensive body of air which approximates horizontal homogeneity is known as an air mass. The four principal types are illustrated by the accompanying table.

Source region	Moisture classification	Thermal classification	Name	Symbol
Land	Dry	Hot	Tropical continental	cT
		Cold	Polar continental	cP
Oceanic	Wet	Hot	Tropical maritime	mT
		Cold	Polar maritime	mP

Front. The surface of separation between dissimilar air masses is known as a frontal surface. On a surface weather map a "front" is the intersection of this surface with the surface of the earth.

Dry Adiabatic Lapse Rate. When dry air ascends so as to expand adiabatically, it is said to cool at the dry adiabatic lapse rate (5.5 F per 1,000 ft or 1 C per 100 m). There must be no condensation or evaporation of associated water vapor during the process.

Subsidence. An extensive sinking process, resulting in dynamically heated air and an increase in stability, most frequently observed in anticyclones, is known as subsidence.

INSTRUCTIONS FOR USE OF NOMOGRAM

This nomogram (Figure 23) may be used to compute M when temperature is expressed in degrees Fahrenheit or centigrade, humidity in terms of wet bulb (degrees Fahrenheit or degrees centigrade), dew point (degrees centigrade), or vapor pressure (millibars), and height in feet or meters. Place a straightedge so as to align the temperature on scale 1 with the wet bulb temperature on scale 3 (or with the dew point or vapor pressure on scale 4). The point at which the straightedge intersects scale 6 indicates the value of the modified index uncorrected for height. Pivot the straightedge at this point (on scale 6) so that it crosses scale 2 at the desired height. Then read the value of M where the straightedge crosses scale 5.

PART II

MISCELLANEOUS EXPERIMENTS

Chapter 4

REFLECTION COEFFICIENTS

REFLECTION COEFFICIENT MEASURE-MENTS AT THE RADIATION LABORATORY*

DURING THE LATTER PART of 1943 the S-band reflection coefficient measurements begun in the spring and reported at the July 1943 conference have been carried on, and work of a similar nature has been started to determine X-band values. The interference pattern was observed by recording field strength as a function of distance with both receiver and transmitter heights held constant. One end of the path was ground-based, while the other end was carried in an airplane which flew over sea toward the land station at a constant altitude and bearing. A one-way c-w path was used, the transmitters, receivers, and recorders being identical to those used previously. The time constant of the receiver and recorder was 0.3 sec, corresponding to 0.01 mile for the usual air speeds used.

When appreciable specular reflection was obtained, a regular succession of maxima and minima were observed on the record. The product of the divergence factor and reflection coefficient was found by determining the ratio of electric field strength at adjacent maxima and minima. The geometrical expression for the divergence factor was assumed correct and all variations were lumped in the experimental value of the reflection coefficient. It was required that a record give a check on the positions of maxima and minima for standard refraction and that the maxima obey the $1/R^2$ law (power) before the record would be worked up.

Flights over land made in 1943 at Orlando, Florida, Riverhead, Long Island, and Cambridge, Massachusetts, fail to show a regular interference pattern. There is a more or less erratic variation of field intensity with distance, but the magnitude of the variation is generally small, and the records obey the $1/R^2$ law. It is believed that the terrain is rough enough to scatter all incident radiation of microwaves and that specular reflection will therefore not

---

*By W. J. Fishback, Radiation Laboratory, MIT.

be observed. There is considerable evidence, however, that if a microwave transmitter is placed at a fairly low height over terrain as smooth as an airport runway, specular reflection will be observed.

Observations over sea made late in 1943 on S band with horizontal polarization have not agreed with earlier results. A correlation has been found between wind (and presumably wave) direction with respect to the path and the magnitude of the reflection coefficient. The correlation suggests that low values observed are due to back scattering. Figure 1 shows lines drawn as a means of the values observed on the 4 days when exceptionally good flights were made during the winter. On November 25, the wind was blowing across
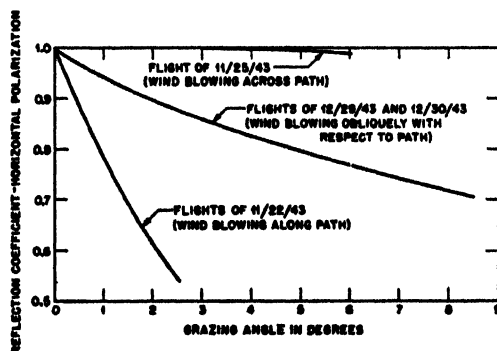
FIGURE 1. Reflection coefficient, horizontal polarization, versus grazing angle. Sea water. Wavelength—S-band.

the path, and high values of the reflection coefficient were observed. On November 22, the wind was blowing along the path, and low values were observed. On December 29 and 30, the wind was blowing obliquely with respect to the path and intermediate values were observed. While the values on any given flight lie fairly close to the lines, there is a considerable amount of scatter. This scatter is now believed to be real and supports the results obtained by the British.

Figure 2 shows the results obtained this winter on S band with vertical polarization. The values observed fall about the theoretical curve. If any corre-

259

lation with wind direction exists, it is masked by the variation within a single flight.

Equipment difficulties have just been overcome and work is getting under way to determine X-band values. One flight made on horizontal polarization shows values greater than 0.9 up to 3 degrees. On three flights made with vertical polarization the points have fallen just slightly above the theoretical curve.

It is planned to carry on simultaneous measurements of X- and S-band values to determine the values to be expected on X band and to prove or disprove the correlation suggested above.

ELECTRICAL CONSTANTS OF THE GROUND, SEA, AND FRESH WATER

To obtain reliable data on the reflection coefficient, dielectric constant, and conductivity of the ground and also of fresh and sea water, a series of radio experiments were performed[1-3] which gave results that compared fairly well with those obtained in laboratory experiments. The experimental conditions were relatively well defined and the physical characteristics of the ground or water derived from these experiments appear to be highly reliable. The wavelengths of the
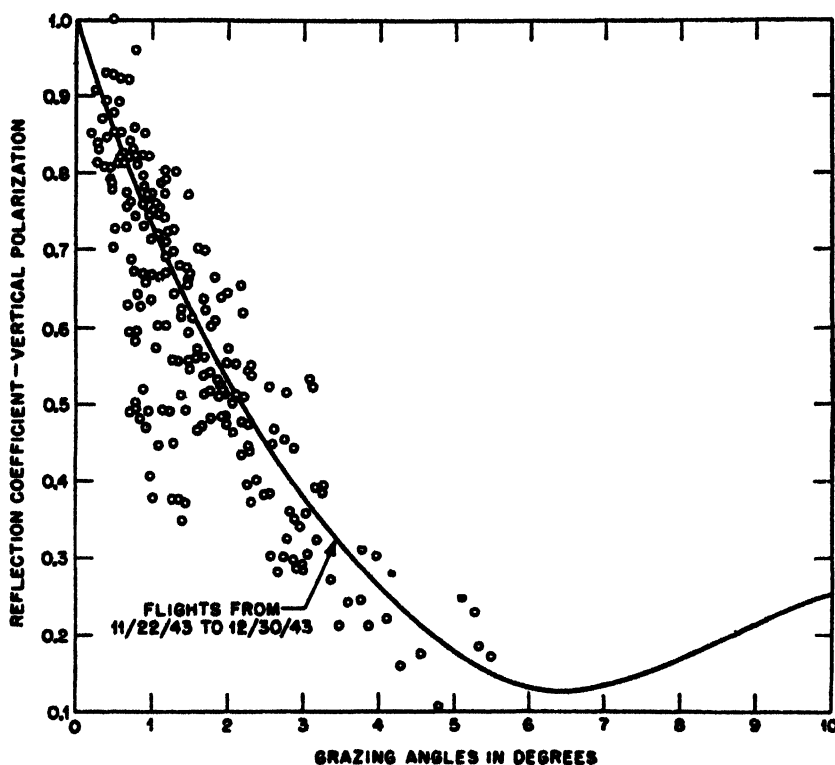
FIGURE 2. Reflection coefficient, vertical polarization, versus grazing angle. Sea water. Wavelength—S band.

EARTH CONSTANTS IN THE MICROWAVE RANGE[b]

Reflection Coefficients

In writing a summary of the latest results, it was thought that the following grouping of the data would be useful.

1. Determination of the electrical constants of the ground, sea, and fresh water.

2. Study of ground and sea reflections under conditions encountered in actual operations.

3. Irregular reflections or scattering.

[b]By L. Goldstein, Columbia University Wave Propagation Group.

radiation used in these experiments lie in the S band at 9 and 10.cm.

In the experiments with 9-cm waves,[1,2] the nature of the reflecting surface was prepared beforehand and its humidity, occasionally, well controlled. Similarly, with vegetation on the ground, the reflection could be measured with different heights of the turf which was grown on the grounds reserved for the measurements.

The conditions of the ground in the experiments with 10-cm waves were somewhat less well defined. However, the experimental setup was portable in this case, which proved to be advantageous.

It seems desirable to give first the results obtained under the best-defined conditions[1,2] (9 cm) for a variety of grounds and compare those with the re-

sults of the 10-cm waves obtained under less well-defined conditions.[3] The latter results are given always in graphical form.

The grazing angle interval (0° to about 30°) explored with the 10-cm waves was quite large, and a graphical representation of the results is well justified. At 9 cm only three or at most four angles of incidence were investigated.

The schematic representation of the experimental setup is given in Figure 3. If ρ denotes the ratio of
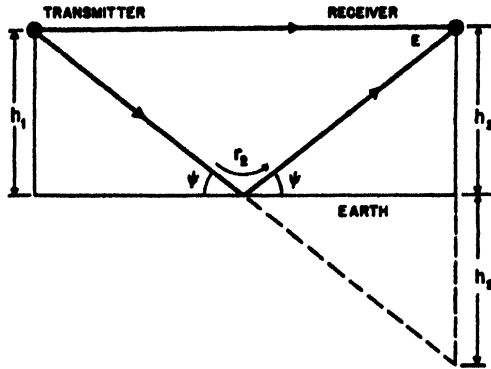
FIGURE 3. Idealised geometry of the experiment.[3]

the amplitude of the reflected wave to that of the incident wave in the vicinity of the reflecting surface, then at the position of the receiver the total field received in case of reinforcement is

$$E_{max} = E + k\rho E.$$

E is the field strength of the direct wave and k is a correction factor taking into account the directivity of the transmitter and receiver as well as the increased path length of the reflected ray as compared to that of the direct ray. In case of phase opposition

$$E_{min} = E - k\rho E.$$

These lead to

$$\rho' = k\rho = \frac{(E_{max} / E_{min}) - 1}{(E_{max} / E_{min}) + 1}.$$

Throughout the work at 10 cm this corrected reflection coefficient ($k\rho$) or ρ' has been investigated. Presumably k is nearly unity so that $\rho' = \rho$.

Very Dry Sandy Ground. Table 1, for 9 cm, refers to very dry ground. In order to obtain a precise value of the complex dielectric constant of this very dry sandy ground its absorption coefficient was measured directly. The measurement was made by interposing a filled container between transmitter and receiver.

TABLE 1. Reflection coefficients of very dry sandy ground for $\lambda = 9$ cm.[1,2]

Grazing angle degrees	Vertical polarisation Calculated	Observed	Horisontal polarisation Calculated	Observed
22	0.18	0.20	0.48	0.47
36.5	0.015	0.03	0.33	0.33
46.5	0.08	0.09	0.26	0.27

The container, a wooden trough, had ¼ in. plate glass ends, 18 in. square, one of which was movable, thus allowing a test of the absorber up to a thickness of 12 in. The most suitable values of ϵ_r (real part of the complex dielectric constant ϵ_c) and conductivity σ or $\epsilon_i = 60 \, \sigma\lambda$ (imaginary part of the complex dielectric constant) which fit the reflection and absorption coefficient data were found to be $\epsilon_r = 2$, $\sigma = 0.033$ mho per meter, $\epsilon_i = 0.18$.

It should be mentioned here that the calculated reflection coefficients were obtained by using the generalized Fresnel formulas for reflection of electromagnetic waves by plane dielectric surfaces. The incident waves travel in vacuum (or air) and fall on the plane surface of a dielectric at the grazing angle ψ.
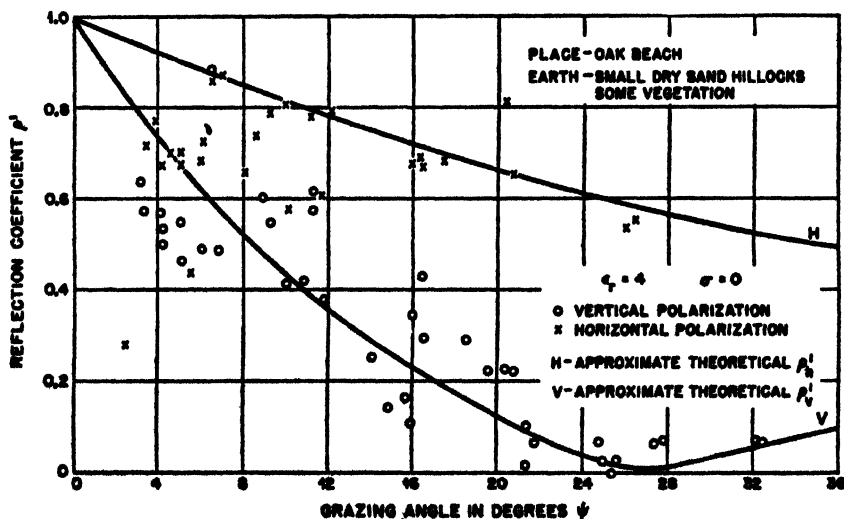
FIGURE 4. Reflection coefficient ρ' versus ψ. $\lambda = 10$ cm. $d = 225, 100, 75$ ft.

The complex dielectric constant ϵ_c is

$$\epsilon_c = \epsilon_r - j\epsilon_i,$$
$$= \epsilon_r - j60\sigma\lambda,$$

where ϵ_r is the real part of the dielectric constant and $\epsilon_i = 60\sigma\lambda$ is its imaginary part. σ is the conductivity of the dielectric medium in mhos per m, and λ is the wavelength, in vacuum, of the· incident radiation. The generalized Fresnel formulas, for horizontally and vertically polarized waves, respectively, are

$$\rho_h e^{-j\phi_h} = \frac{\sin\psi - (\epsilon_c - \cos^2\psi)^{\frac{1}{2}}}{\sin\psi + (\epsilon_c - \cos^2\psi)^{\frac{1}{2}}} \quad \text{(horizontal)}$$

$$\rho_v e^{-j\phi_v} = \frac{\epsilon_c\sin\psi - (\epsilon_c - \cos^2\psi)^{\frac{1}{2}}}{\epsilon_c\sin\psi + (\epsilon_c - \cos^2\psi)^{\frac{1}{2}}} \quad \text{(vertical)},$$

where ρ denotes the magnitude of the complex reflection coefficient and ψ is the angle of lag of the reflected component behind the incident component of the electric field.

The results at 10 cm and for dry sand are given in Figure 4. The theoretical curves given on the graph do not necessarily represent the best fit. These curves were computed for $\epsilon_r = 4$ and $\sigma = 0$ (perfect dielectric). The experimental Brewster angle turns out to be around 23° (grazing angle).

The experimental results for clay-sand soil are given in Figure 5. The theoretical curves are the same as those given in the preceding case, that is, for $\epsilon_r = 4$ and $\sigma = 0$. It will be noted that the fit with the experimental values is less satisfactory in this case. The author attributes the discrepancy between the observed and computed values of the reflection coefficient, in part, to the quality of the soil which consisted of lumps of about a half wavelength diameter. In general the roughness of the ground contributes considerably to scattering. It is rather to be expected that a theoretical curve representing specular reflection coefficients from a smooth surface should not fit well the experimental data referring to such a rough ground.

Saturated Ground. Table 2 represents the results obtained at 9 cm for the reflection coefficient of saturated ground.

The most suitable values of ϵ_r and σ or ϵ_i to fit both reflection and absorption measurements are $\epsilon_r = 24$, $\sigma = 0.66$ mhos per meter, and $\epsilon_i = 3.56$.

Tests carried out at 10 cm on ground of somewhat similar type (tidal flat and moist sand) are given in
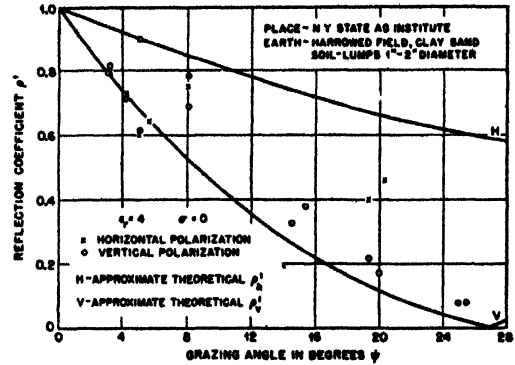
FIGURE 5. Reflection coefficient ρ' versus ψ. $\lambda = 10$ cm. $d = 100$, 300 ft.

Figures 6 and 7. The theoretical curves in Figure 6 correspond to a perfect dielectric ($\sigma = 0$) with $\epsilon_r = 10$. Since the conductivity of the soil is not zero, the true value of the reflection coefficient for vertical polarization cannot be zero at the Brewster angle. The data seem to confirm this point.

The data of Figure 7 refer to moist and very smooth beach sand. It is thought that these observations are the most reliable so far as self-consistency is concerned. Again the computed curves refer to a perfect dielectric with $\epsilon_r = 15$.

An important difference between the measurements at 9 cm at a fixed location and those made at 10 cm with the portable setup consists of the fact that at 9 cm direct absorption measurements could be performed in addition to measurements of the reflection coefficient.The electrical constants could thus be determined at 9 cm without ambiguity.
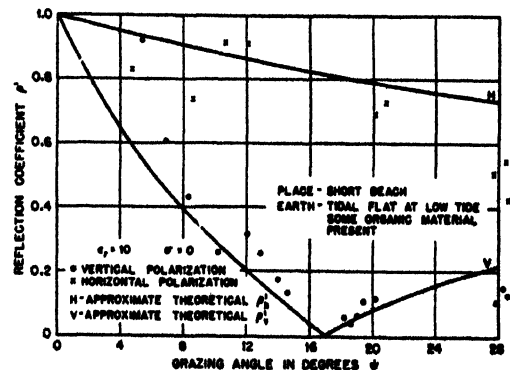
FIGURE 6. Reflection coefficient ρ' versus ψ. $\lambda = 10$ cm. $d = 90$ ft.

TABLE 2. Reflection coefficients of saturated ground. $\lambda = 9$ cm.[1,2]

Grazing angle degrees	Vertical polarization				Horizontal polarization			
	Calculated		Observed		Calculated		Observed	
	$\epsilon_r = 24$ $\sigma = 0.66$	$\epsilon_r = 25$ $\sigma = 0$	Heavy rain	Watered by hose	$\epsilon_r = 24$ $\sigma = 0.66$	$\epsilon_r = 25$ $\sigma = 0$	Heavy rain	Watered by hose
22	0.31	0.31	0.28	0.32	0.85	0.86	0.90	0.85
36.5	0.50	0.50	0.50	0.50	0.78	0.79	....	0.78
46.5	0.57	0.57	0.58	0.58	0.74	0.75	0.72	0.74
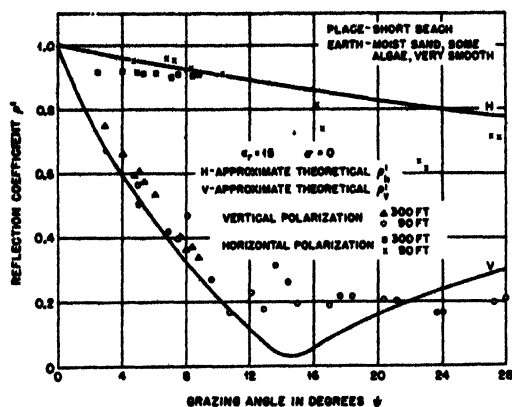
FIGURE 7. Reflection coefficient ρ' versus ψ. $\lambda = 10$ cm. d = 300, 90 ft.

Fresh Water and 4% Salt Solution (or Sea Water)
(1) *Tap water.* Table 3 gives the results on the reflection coefficients of tap water (temperature not given).

TABLE 3. Reflection coefficients of tap water. $\lambda = 9$ cm.[1,2]

Grazing angle degrees	Vertical polarization Calculated	Observed	Horizontal polarization Calculated	Observed
20	0.51	0.51	0.92	0.90
35	0.69	0.67	0.88	0.88
45.5	0.73	0.70	0.85	0.83

The values of ϵ_r and ϵ_i which best represent both the reflection and absorption data are $\epsilon_r = 80$, $\sigma = 2.2$ mhos per m, and $\epsilon_i = 11.9$.

2. *Fresh water pond.* The results on 10-cm waves are collected in Figure 8.[3] These data refer to a fresh water pond and the theoretical curve corresponds to a smooth and perfect dielectric surface with $\epsilon_r = 80$. The curves do not fit too well at the smaller grazing angles. If the conductivity were taken into account,
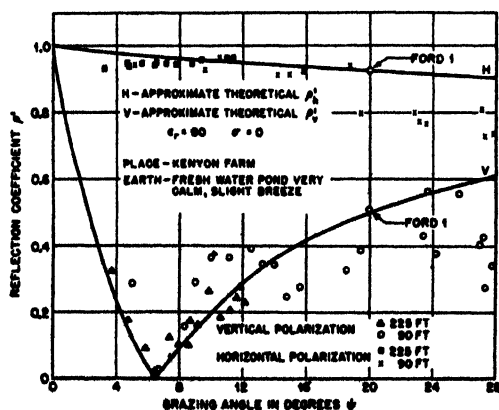
FIGURE 8. Reflection coefficient ρ' versus ψ. $\lambda = 10$ cm. d = 90, 225 ft. Fresh water pond.

presumably a better fit might be achieved. Two points, marked Ford,[1,2] taken from Table 3 were included for comparison.

3. *Salt solution.* In order to simulate sea water a 4 per cent salt solution was used for the determination of the reflection coefficient. At 9 cm the best fit was obtained with $\epsilon_r = 80$, $\sigma = 6.1$ mhos per m, and $\epsilon_i = 33$.

4. *Sea water.* Figure 9 gives the results obtained at 10 cm. The computed curves drawn to fit the data correspond to $\epsilon_r = 69$, $\sigma = 6.5$ mhos per m, $\epsilon_i = 39$. It appears that the data can be fitted with the com-
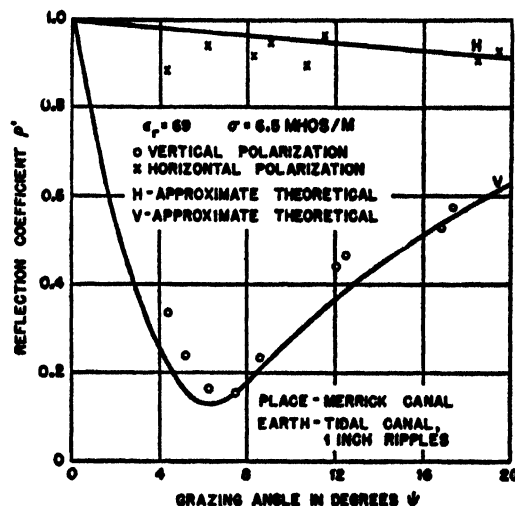
FIGURE 9. Reflection coefficient ρ' versus ψ. $\lambda = 10$ cm. d = 130 ft. Sea water (tidal canal).

puted curves as long as the ripples on the tidal canal are of small amplitude (about 1 in.).

Figure 10, which also refers to sea reflection, corresponds to ripples which had an amplitude of about 2 in., and here the observed reflection coefficients for vertical polarization fall well below the computed curve at the larger values of grazing angle. Probably the choice of the dielectric constants used in the computations may account for at least a part of the discrepancy.

Grass-Covered Ground. The following results obtained at the experimental grounds[1,2] with 9-cm waves
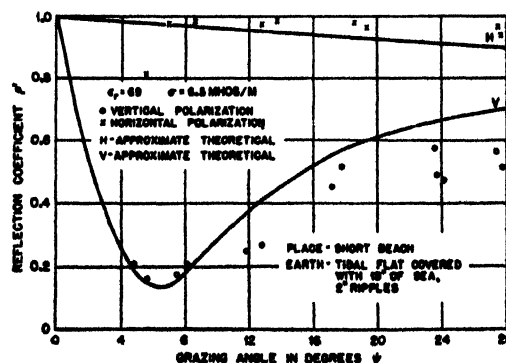
FIGURE 10. Reflection coefficient ρ' versus ψ. $\lambda = 10$ cm. d = 90 ft. Sea water.

TABLE 4. Reflection coefficient of level, grass-covered ground. λ = 9 cm. Grazing angle 10°.

Ground conditions	Vertical polarisation		Assumed constants		Horizontal polarisation	
	Calculated	Observed	ϵ_r	σ mhos/m	Calculated	Observed
Grass cut very short and rolled dry. (No rain for at least 7 days.)	0.47	0.46	3	0.055	0.79	0.79
Cut very short and rolled wet. (Several hours of rain on previous night.)	0.36	0.37	6	0.11	0.86	0.86
Grass about 1 in. high, wet. (Same day as previous test.)	0.36	0.51	6	0.11	0.86	0.83

TABLE 5. Magnitudes ρ_v and ρ_h, observed values. λ = 9 cm.[1,2]

Appearance of ground	Height of vegetation, cm	22°		Grazing angle 36.5°		56.5°	
		v	h	v	h	v	h
Bare	0	0.32	0.86	0.50	0.78	0.58	0.74
True leaves beginning to form, ground visible	3–4	0.40	0.50	0.44	0.55	0.47	0.56
Dense clumps, ground showing in places	9–12	0.18	0.65	0.23	0.58	0.33	0.49
Ground almost obscured	20–25	0.06	0.32	0.10	0.39	0.17	0.41
Ground completely obscured	35–45	0.04	0.19	0.05	0.26	0.11	0.28

refer to various types of grass-covered earth.

The results obtained with the portable 10-cm set appear on Figures 11, 12, 13, and 14. These graphs show clearly the influence of vegetation on the reflection coefficient. Consult Table 5 for corresponding results at 9 cm.
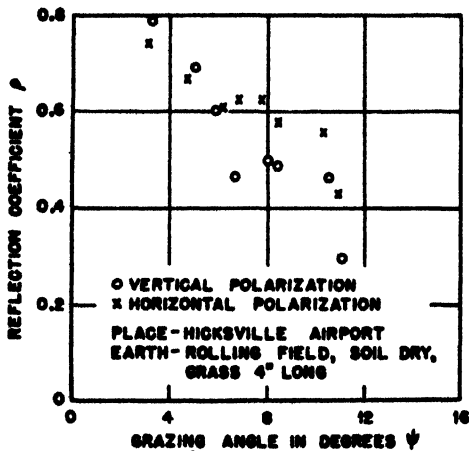
FIGURE 11. Reflection coefficient ρ versus ψ. λ = 10 cm. d = 225 ft. Grass covered ground.
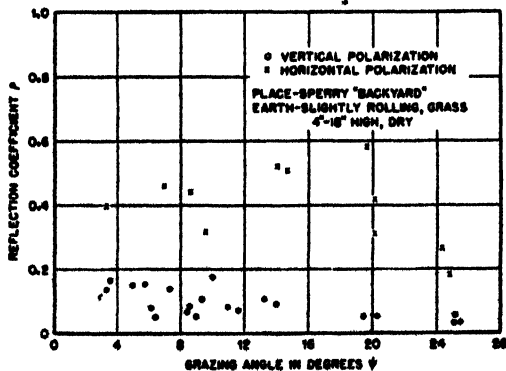
FIGURE 12. Reflection coefficient ρ versus ψ. λ = 10 cm. d = 100, 225 ft. Grass covered ground.

Since, however, the data of Table 5 refer to wet vegetation-covered ground, they cannot be compared directly with the results at 10 cm since these seem to correspond to dry vegetation.

Table 6 gives the data obtained at 9 cm for unmown meadow land having an average variation in ground level of about 7 cm. The ground was covered with a dense layer of grass about 30 cm high. The reflection coefficient of this surface was measured, then remeasured with the grass mown as short as the roughness of the ground permitted. The turf was next removed, some of the irregularities of the ground were eliminated, and the reflection coefficient of the sur-
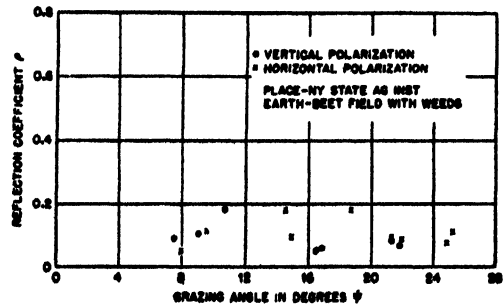
FIGURE 13. Reflection coefficient ρ versus ψ. λ = 10 cm. d = 100 ft. Beet field with weeds.
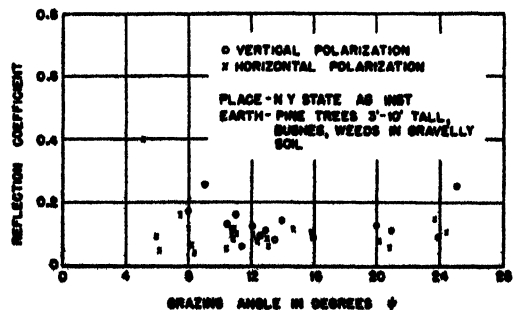
FIGURE 14. Reflection coefficient ρ versus ψ. λ = 10 cm. d = 102, 300 ft. Trees, bushes, weeds in gravelly soil.

TABLE 6. Reflection coefficient of rough ground. $\lambda = 9$ cm.[1,2]

Grazing angle, degrees	Vertical polarization				Horizontal polarization			
	Level estimated	Long grass	Short grass	Bare	Level estimated	Long grass	Short grass	Bare
22	0.20	0.08	0.20	0.23	0.82	0.12	0.74	0.81
36.5	0.40	0.06	0.17	0.27	0.73	0.12	0.43	0.50
46.5	0.48	0.06	0.16	0.26	0.68	0.03	0.36	0.46

face so prepared was measured again. The results of these measurements are to be found in Table 6. The *estimated* reflection coefficient of level ground of the same moisture content is also included here.

Finally, the results on the electrical constants of different kinds of grounds for 9-cm waves have been collected in Table 7.

TABLE 7. Electrical constants of the ground. $\lambda = 9$ cm.[1,2]

Medium	ϵ_r	σ mhos/m	ϵ_i	Attenuation factor db/m
Very dry sandy loam	2	0.033	0.178	36
Saturated sandy loam	24	0.666	3.54	220
Tap water	80	2.22	12.0	380
4% solution of coarse salt	80	6.11	33.0	1100
Dry turf	3	0.055 (est)	0.30	50 (calc)
Wet turf	6	0.11 (est)	0.60	80 (calc)

It is seen that in the previous experiments[1,2] no attempt was made at finding the phase angle shift at reflection. At 10 cm[2] such an attempt was made. How-

ever, the distances involved here could not be measured more accurately than a small fraction of a half wavelength, or 5 cm. Therefore, these experiments are not to be considered, as the author himself points out, as giving quantitative information on the phase angle shift at reflection and they will not be discussed here.

Summary of Experimental Investigations on Reflection

Here the results of certain additional reports of experiments on microwave reflection by either sea or land performed under more nearly operational conditions are summarized.[4-7]

In one series of experiments[4] performed by British workers, at 9.3 cm, the transmitter was located on the shore and could be placed at two heights, 35 and 130 ft. The receiver was placed on a ship at a constant height of about 33 ft. The field strength of the radia-

FIGURE 16. Sea reflection coefficient ρ_v versus grazing angle ψ at 10 cm. Vertical polarization.
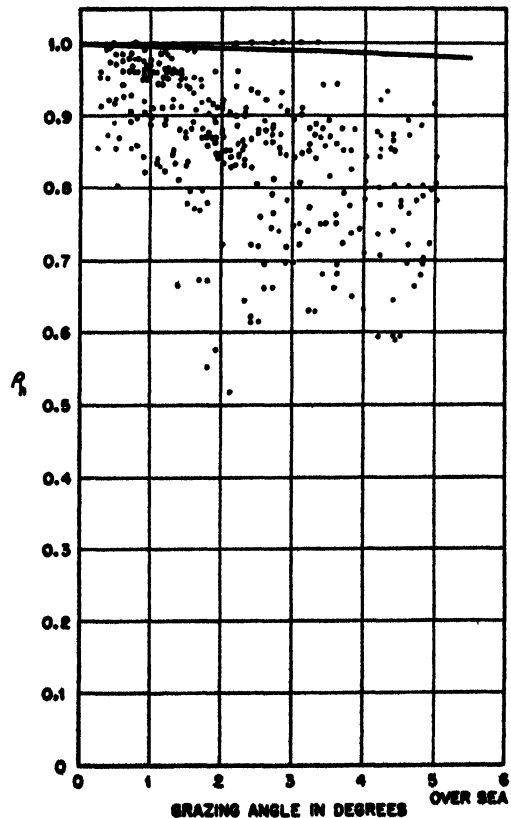
FIGURE 17. Sea reflection coefficient ρ_h versus grazing angle ψ at 10 cm. Horizontal polarization.
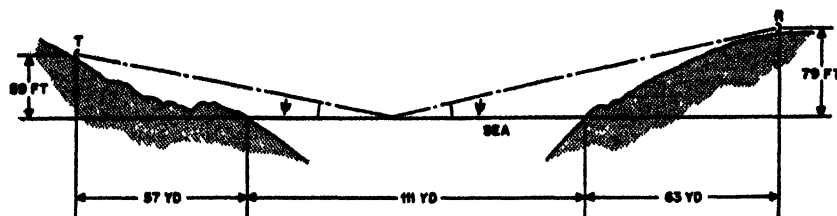
FIGURE 15. Cross section of Porth Gain Bay (Wales) in vertical plane through transmitter and receiver.

tion was measured as a function of the distance from the transmitter. This distance varied between 3,500 and 42,000 yd. The observed values of the field strengths correspond well with calculations based on electromagnetic theory.

In a second series of experiments[5] both the transmitter and receiver were stationary. The topography of the location and the experimental setup are represented schematically in Figure 15. The main conclusion drawn from these experiments was that even for a calm sea (vertical amplitude of the waves less than 8 in.) the mean amplitude of the reflected vertically polarized beam was only about half the steady amplitude of the direct wave. The amplitude of the reflected wave, however, occasionally rises to greater values than that of the direct wave, but this lasts only

for short lengths of time of the order of 0.5 sec.

In the case of the reflection of horizontally polarized radiation at the surface of a smooth sea it is known that even for grazing angles as large as 10° the amplitude of the reflected wave is very nearly equal to that of the direct wave. The irregularities of the sea, however, reduce the amplitude of the reflected wave. This reduction is due to scattering, i.e., to nonspecular reflection of the radiation by the irregularities of the sea surface. It is recalled here that the surface irregularities will play an important role as soon as they are larger than λ/ψ, λ being the wavelength and ψ the grazing angle in radians.

The Radiation Laboratory workers,[6,7] used an airplane as the carrier of the receiver flying toward the transmitter. For 10- and 3.2-cm waves the latest re-
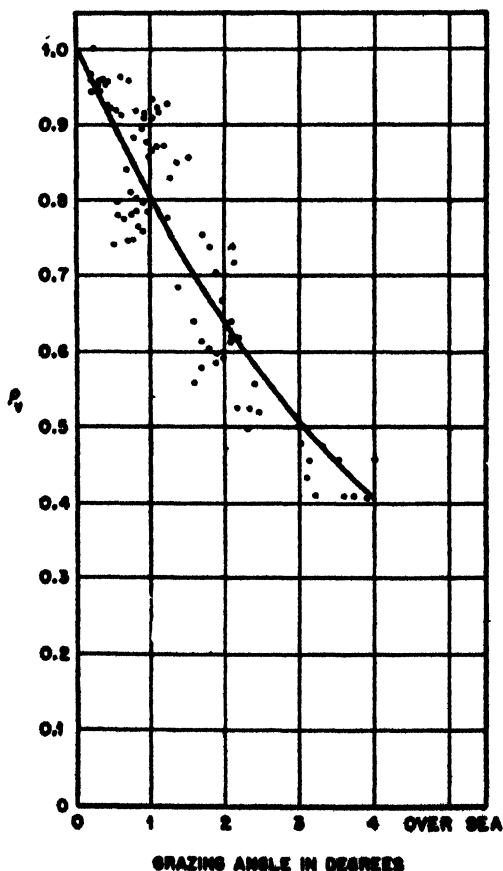
FIGURE 18. Sea reflection coefficient ρ_v versus grazing angle ψ at 3.2 cm. Vertical polarization.
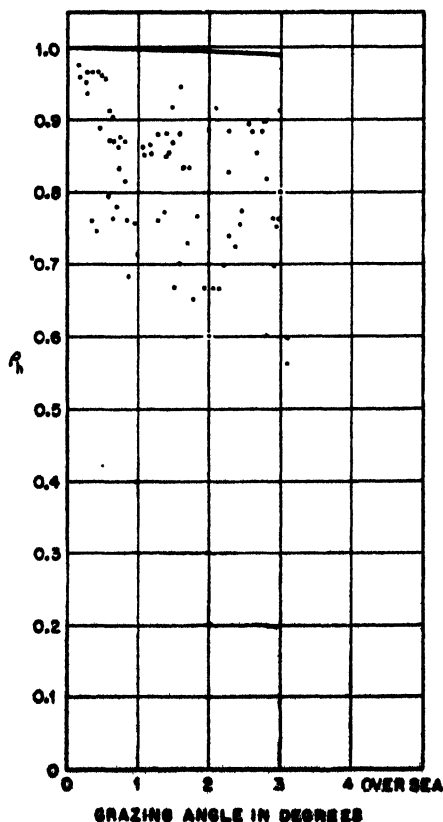
FIGURE 19. Sea reflection coefficient ρ_h versus grazing angle ψ at 3.2 cm. Horizontal polarization.

sults are given in Figures 16, 17, 18, and 19. These show that theory and experiment check satisfactorily for vertical polarization, but for horizontal polarization the experimental values of reflection coefficient generally fall well below the theoretical values based on the assumption of a smooth sea. Whereas over sea a regular interference pattern existed, over land (Orlando, Florida) no specular reflection was observed. The lobe structure was absent in the observations over land.

Another experiment[8] carried out over land was performed using X-band waves between Beer's Hill and Deal, New Jersey. The reflection coefficient of the ground is expected to change with the seasons on account of seasonal vegetation changes on the path. One series of measurements lead to reflection coefficients of 0.17 and 0.20 for horizontally and vertically polarized radiation respectively.

Specular Reflection and Scattering

Ordinarily neither the sea nor the land are ideally smooth, and one would expect always nonspecular reflections which tend to perturb the interference pattern of the direct and reflected rays from a smooth surface.

It has been pointed out[9] that the condition which has to be fulfilled for specular reflection to occur is that the grazing angle ψ be such that $\sin \psi \leqq \lambda/g$, where g is the wavelength of the sea waves. Clearly this is a kind of limiting condition and assumes the perfect regularity of the sea waves. It is seen that the above condition expresses the fact that the smaller the grazing angle, the smaller are the apparent irregularities of the sea and, if these apparent irregularities are much closer than the wavelength of the incident radiation, it is to be expected that specular reflection should predominate.

A direct consequence of this condition is that the echoes from a target, that is, a ship, will not be drowned by the clutter from the sea waves for large distances between the target and observer. Whereas at closer distances (large grazing angles) the echo from the target might be drowned by the irregular reflection, i.e., scattering from the sea. To this effect, a report is quoted in which it is stated that ships could only be detected beyond a certain distance from the shore.

It is also thought[10] that the discrepancies observed between the theoretically predicted and measured sea reflection coefficients (horizontal polarization) could be attributed to scattering. The irregular reflections have the effect of decreasing considerably the ratio of the successive maxima and minima of the interference pattern developed. The discrepancies referred to are those discussed by the Radiation Laboratory workers. In this connection, Eckersley mentions some experiments by Hoyle on sea reflections in which no correlation could be observed on the voltage registered by two aerials a few inches apart. This tends also to suggest the existence of scattering from the sea.

In another series of transmission experiments[10] it was observed that the contrast between maxima and minima was poor. Here the experiments were carried out at 200 mc over sea at a distance of 100 miles between an airplane and a ground station. The divergence of the observed from the calculated values of reflection increases as the grazing angle increases. This seems to be in agreement with the results according to which the sea surface may be considered as formed by a number of corrugations which, for small grazing angles, appear to be so close together that the reflection is mostly specular.

As to the frequency variation of scattering one would expect more and more scattering with increasing frequency.

The effect of uneven ground on the reflection coefficient was investigated by the British workers already mentioned.[1,2] The reflecting ground consisted of an artificially prepared series of uniform ridges placed along, across, and at 45° to, the direction of

TABLE 8. Reflection coefficient of ground ridged at 45° with the direction of transmission. $\lambda = 9$ cm.[1,2]

Grazing angle, degrees	Vertical polarization				Horizontal polarization			
	Level estimate	$D = 60$ cm $h = 14$ cm	$D = 120$ cm $h = 10$ cm	$D = 120$ cm $h = 5$ cm	Level estimate	$D = 60$ cm $h = 14$ cm	$D = 120$ cm $h = 10$ cm	$D = 120$ cm $h = 5$ cm
22	0.08	0.07	0.09	0.13	0.65	0.14	0.18	0.30
36.5	0.13	0.04	0.05	0.07	0.51	0.04	0.06	0.16
46.5	0.22	0.04	0.04	0.04	0.45	0.07	0.06	0.10

TABLE 9. Reflection coefficient of ground ridged along or across the direction of transmission. $\lambda = 9$ cm.

Grazing angle, degrees	Vertical polarization				Horizontal polarization			
		Along	Across			Along	Across	
	Level estimate	$D = 60$ cm $h = 14$ cm	$D = 60$ cm $h = 16$ cm	$D = 120$ cm $h = 12$ cm	Level estimate	$D = 60$ cm $h = 14$ cm	$D = 60$ cm $h = 16$ cm	$D = 120$ cm $h = 12$ cm
12	0.23	0.20	0.10	0.30	0.86	0.4	0.2	0.4
22	0.06	0.03	0.05	0.12	0.76	0.07	0.10	0.18
36.5	0.28	0.03	0.02	0.06	0.64	0.10	0.12	0.16
46.5	0.36	0.04	0.06	0.06	0.58	0.04	0.08	0.14

propagation. These ridges simulated waves, and their wavelength D lay between 0.6 and 1.2 m, whereas the double amplitude h varied between 5 and 15 cm, and the wavelength of the radiation used was 9 cm.

Tables 8 and 9 give the reflection coefficients of the uneven ground when the direction of propagation is at 45° with the ridge and along or across the ridge system. The tables also give an estimation of the reflection coefficient of level ground of the same moisture content as that under test.

The results given in these tables show how a relatively small irregularity in the ground surface is sufficient to prevent regular reflection. The reflection coefficient becomes erratic when it has fallen below a value of about 0.1. The values given for level ground refer only very approximately to the state of the ground in the ridged condition. Since the measurements extended over several days, those relative to level ground may not correspond necessarily to the same degree of moisture as those referring to the ridged ground. The level reflection coefficients in the two preceding tables differ from each other because those of Table 8 refer to drier ground than those of Table 9.

MEASUREMENTS OF THE REFLECTION COEFFICIENT OF LAND AT CENTI- METER WAVELENGTHS, CARRIED OUT AT NATIONAL PHYSICAL LABORATORY[*]

Experiments have been made on the reflection and absorption of radio waves in the S-band of wavelengths by workers in the National Physical Laboratory in England. The reflection coefficient has been measured at angles of incidence to the vertical, of 80°, 68°, 54°, and 44° on level ground, fresh water, sea water, uneven ground, ground covered with vegetation, and ground covered with ½ in. mesh wire netting. The absorption

[*]By W. Ross, British Central Scientific Office, Washington, D. C.

in soil, fresh water, sea water, and ½ in. mesh wire netting has also been measured by a laboratory method. An interim report[1] gave some of the salient results obtained on ground reflection.

The main conclusions which have been drawn from the results obtained are given below.

1. Specular reflection can be obtained only from a very level surface, with little or no vegetation on it. The electrical constants of such surfaces are given in Table 10, from which the coefficient of specular reflection can be deduced for the angle of incidence and state of polarization concerned.

2. The reflection coefficient decreases with uneven ground and is reduced to a value of about 0.2 by inequalities of level of about one wavelength. This conclusion is based mainly on a series of experiments in which the ground was raked into a series of ridges resembling waves, which could be either in, across, or at an angle to, the direction of transmission. Similar results were obtained when a large sheet of wire netting was similarly disposed in a series of waves.

3. Vegetation reduces the reflection coefficient, in general, and when about 2 ft high causes a reduction in reflection coefficient to a value of about 0.2. An interesting exception was found when level ground was covered with vegetation less than half a wavelength high (about 1½ in.) when the reflection coefficient with vertical polarization increased slightly with high angles of incidence over that obtained with level ground.

TABLE 10

Nature of surface	Dielectric constant	Conductivity mhos / m
Bare sandy loam, very dry	2	3×10^{-2}
Bare sandy loam, saturated with water	24	6×10^{-1}
Turf with grass very short (cricket wicket), dry	3	5×10^{-2}
Turf with grass very short (cricket wicket), wet	6	1×10^{-1}
Fresh water	80	2
Sea water (4% salt solution)	80	5

DIELECTRIC CONSTANT, ABSORPTION AND SCATTERING

ABSORPTION AND SCATTERING OF MICROWAVES BY THE ATMOSPHERE[a]

THE PRESENT REPORT deals with the absorption of microwaves in the 0.2- to 100-cm wavelength range, by the atmospheric gases and by floating or falling water drops like clouds, fog, and rain of maximum drop diameter 0.55 cm.

The theory of absorption and scattering of waves by spherical particles is briefly reviewed. The results are applied to water drops.

For small drops, the attenuation, which depends only upon the amount of liquid water per unit volume and is independent of the drop size, is 0.28, 0.049, and 0.0045 db per kilometer for each gram of liquid water per cubic meter of air for the K, X, and S bands, respectively. Since the concentration of liquid water in clouds does not seem to exceed 1 g per cubic meter of air, the above values represent upper limits. These values refer to water droplets at temperatures around 18 C. The attenuation increases with decreasing temperature of the water drops.

While the attenuation does not depend upon the total rate of rainfall, it is ·possible to calculate the maximum values to be expected for any precipitation rate. These are 0.16, 0.45, 0.005, 0.001, and 0.0006 db per kilometer for each millimeter precipitation per hour at 1.25, 3, 5, 8, and 10 cm, respectively. These theoretical maximum values of attenuation compare fairly well with the values observed and are for water drops at 18 C.

In the wavelength range mentioned it is shown that, with the exception of the biggest drops and shortest waves, the wave energy converted into heat inside the drops is much larger than the scattered energy.

The radar absorption coefficient, defined as the fraction of the incident power scattered backward per unit layer thickness of the echoing medium, has been computed for different rains. This allows the estimation of the power received in radar observations of storm clouds and rains. The theoretical predictions seem to be consistent here also with the results of the few recent radar studies which tend to show that echoes are due mainly to water drops of the dimensions occurring in rains.

In the introduction a résumé is given of the status of microwave absorption by atmospheric oxygen and water vapor. With the exception of the resonance region of oxygen (resonance wavelength around 0.5 cm), this absorption turns out to be of only very limited practical importance for waves longer than about 3 to 5 cm.

Introduction

The present report is intended to review the status of microwave propagation through rain, clouds, and fog. In order, however, to convey a precise idea of the total atmospheric absorption, we shall include here some of the most important numerical results recently obtained on the absorption of microwaves by atmospheric gases, like oxygen and water vapor.[1-7]

First of all, in medium- and low-altitude fair-weather clouds and fogs, with the possible exception of heavy sea fogs, the attenuation is of negligible importance for longer waves. It may become important at shorter waves. For instance, in the K band the attenuation[b] is 0.28 db per kilometer for each gram of liquid water per cubic meter of air. The X- and S-band waves are attenuated, respectively, 0.049 and 0.0045 db/km/g/m³. Since in these clouds and ordinary fogs the liquid water concentration does not seem to exceed 1 g/m³, these values are very likely upper limits. Actually, by halving these numbers one would be nearer the true values, inasmuch as liquid water contents reported in clouds[8,9] varies between 0.15 and 0.50 g/m³. An interesting and simplifying feature of cloud and fog absorption is the fact that the smallness of their water drops, as compared with the wavelength, makes the attenuation independent of the drop sizes. The cloud and fog attenuation depends linearly on the liquid water concentration of the atmosphere, and in the microwave region it decreases monotonically with increasing wavelength.

In rains or rain clouds the attenuation does not depend directly on the total rate of rainfall, a variable so familiar to meteorologists. It is, nevertheless, possible to give upper limits to the attenuation per unit precipitation rate. These are as follows: 0.16, 0.45, 0.005, 0.001, and 0.0006 db per kilometer for each millimeter per hour rate of rainfall, at 1.25-, 3-, 5-, 8-, and 10-cm wavelengths, respectively. The drops forming these rains were supposed to be at temperatures near 18 C. By increasing the preceding values by about 30 per cent one would very likely take care of raindrops at lower temperatures, since the absorption increases with decreasing temperature of the drops.

In the computation of attenuation for rains it was

---

assumed that ideal conditions prevailed throughout the rains under consideration. By this was meant that the same sample of rain falling, say, over an area of 1 sq m would be found anywhere inside the area covered by the rain. Such ideal rains seem to be rather simple theoretical models. Considerable fluctuations in the rate of rainfall over relatively short distances (1 km or less) have been reported.[10] These spatial irregularities of rains exclude any simple interpretation of the experimental data on rain attenuations. The computed values of attenuation are based on a few data on drop size distributions[11] in rains.

In Figure 1,[2] the individual oxygen and water vapor attenuation curves have been plotted in the 0.2- to 10-cm wavelength range, using the most acceptable data available on the position of line centers and line widths. Any change in the water vapor content from the one adopted for this graph (7.5 g/m³ of air or 6.2 g per kilogram of air) or the total pressure can be taken rapidly into account in computing the combined oxygen and water vapor attenuations, since the attenuation values are proportional to the partial pressures of oxygen and water vapor. For practical purposes the effect of atmospheric temperature variations can be neglected.
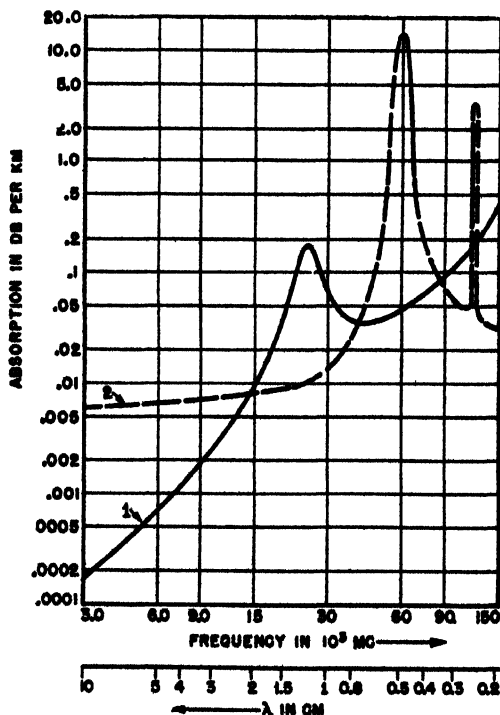
FIGURE 1. Oxygen and water vapor absorption versus wavelength. (1) Absorption due to water vapor in an atmosphere at 76-cm pressure containing 1 per cent water molecules, or 7.5 g per cu m. The water resonance line is assumed to be at 24,000 mc, and its half-width at half maximum (line breadth) is 3,000 mc. (2) Absorption due to oxygen in an atmosphere at 76-cm pressure, whose resonance band at 60·10³ mc is supposed to have a line breadth of 600 mc.
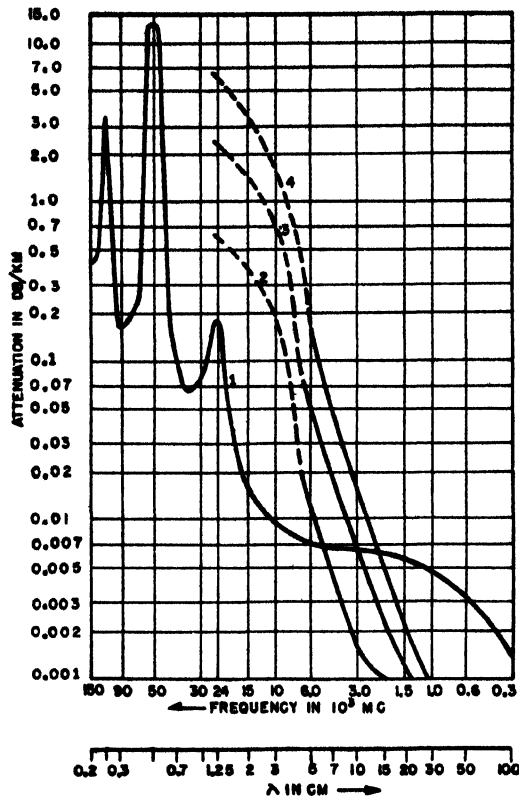
FIGURE 2. Atmospheric attenuation for one-way transmission. (1) Oxygen and water vapor (total p=76 cm Hg, t=20 C, water vapor=7.5 g per cu m). (Van Vleck). (2) Moderate rain (6 mm per hr) of known drop size distribution. (3) Heavy rain (22 mm per hr). (4) Rain of cloudburst proportion (43 mm per hr).

In Figure 2 is plotted the total (oxygen plus water vapor) attenuation (curve 1) in an atmosphere at 76-cm pressure with the same water vapor content as the water curve of Figure 1. Curves 2, 3, and 4 are rain attenuation curves computed for a moderate rain (rate of rainfall 6mm per hour), a heavy rain (22mm per hour), and an excessive rain of cloud burst proportion (43 mm per hour). The corresponding drop size distributions were given by Best.[11]

In any rain the resulting total attenuation is the sum of the gaseous (oxygen plus water vapor) and corpuscle or liquid drop attenuation values.

It is thus seen that for waves of 3 cm or shorter the rain attenuation may become prohibitive, whereas the gaseous attenuation loses its practical importance at waves longer than about 2 cm. The attenuation of rain computed in this report extends from 5 cm toward longer waves. In the region λ = 1.25 — 5 cm, only two attenuation values are available,[12] at 1.25 and 3 cm respectively. The dashed portions of the rain attenuation curves are thus extrapolations drawn through the two computed points. The shape of these extrapolated portions of the curves, in view of the decreasing trend of the computed dielectric absorption values

with the wavelength,[18] seems to suggest that the rain attenuation might level off or even decrease for waves shorter than 1 cm. However, without a closer investigation of the raindrop absorption in this wavelength region, no precise statement can be made on this subject.

As regards the normal atmospheric absorption of microwaves, it may be mentioned that the oxygen absorption is due to the paramagnetic character of this gas. It is through the interaction of the magnetic field strength with the magnetic dipole moment of the oxygen molecule that microwaves are absorbed by this gas. In the microwave region the oxygen molecule has a resonance line at $\lambda = 0.25$ cm and a band near 0.5 cm, while water vapor seems to have a resonance line around 1.25 cm and interacts with the radiation field through its electric dipole moment. The whole subject has been discussed exhaustively.[1,2]

The study of the scattering of microwaves by raindrops shows that the radar observations of rainclouds can be explained satisfactorily if the scattering is attributed to spherical particles of dimensions similar to those of raindrops, even though no rain reaches the ground. Recent experimental work[14,15] has helped considerably in clearing up the apparent inconsistency which previously existed in this subject.

On the whole, taking into consideration the irregularities of the precipitation forms in space, it may be said that theory provides a fairly good picture of microwave propagation through a cloudy, foggy, or rainy atmosphere.

The major object of the present paper is to report the theoretical and experimental work done on attenuation of microwaves by liquid or solid water particles falling through the atmosphere, as well as clouds and fog, which are water and ice particles in suspension

Theoretical work has thus far been concerned with the problem of a plane electromagnetic wave scattered and absorbed by a single spherical or spheroidal particle, first studied in detail by Mie[16] for other purposes.

The application of the results of Mie to very short radio waves propagated through rain, clouds, and fog, i.e., through a swarm of spherical water droplets, was made by Ryde.[12,17] The present report is, in part, an extension of his work using more detailed meteorological data on rains.

A compact and elegant presentation of the problem of absorption and scattering of a plane wave by a sphere is given by Stratton.[18a] The method followed by him was first used by Lord Rayleigh.[19] In the following section a brief review of this method will be given.

Scattering and Absorption of Radio Waves by Spherical Particles

Let the center of a sphere of radius a be the origin of a rectangular coordinate system and suppose a plane wave to be propagated along the positive z axis

and to fall on the sphere (Figure 3). The sphere of permeability μ_1 (henrys per meter) and complex inductive capacity ϵ_1 (farads per meter) is embedded in a medium of permeability μ_2 and inductive capacity ϵ_2. The plane wave is supposed to be polarized parallel to the x axis.
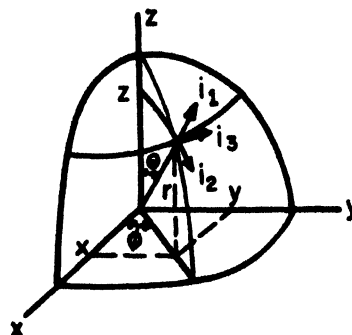
FIGURE 3. Spherical coordinates.

The electric and magnetic field strengths $\mathbf{E}_i$, $\mathbf{H}_i$ of the incident wave (subscript i) are expanded into spherical wave functions.[18a] The reason for this expansion lies in the boundary conditions and will appear clearly below.

$$\mathbf{E}_i = \mathbf{E}_x = \mathbf{a}_x E_0 e^{-jk_2 z + j\omega t},$$

$$\mathbf{H}_i = \mathbf{H}_y = \frac{1}{\eta_2} \mathbf{a}_y E_0 e^{-jk_2 z + j\omega t}, \qquad (1)$$

where

$$k = (\mu\epsilon\omega^2 - j\mu\sigma\omega)^{\frac{1}{2}} \qquad (2)$$

is the complex wave number of the medium (here $k_2 = 2\pi/\lambda$, λ being the wavelength referred to air or free space), the square root is so taken that the imaginary part is negative, and η is the intrinsic impedance of the medium, or

$$\eta = \frac{\mu\omega}{k}, \quad \eta_2 = \sqrt{\frac{\mu_2}{\epsilon_2}} = 377 \text{ ohms.} \qquad (3)$$

The conductivity σ is expressed in mhos per meter; the frequency ω, in radians per second; $\mathbf{a}_x$, $\mathbf{a}_y$, and $\mathbf{a}_z$ are unit vectors pointing in the positive x, y, and z directions, respectively.

The plane wave vectors[c] $\mathbf{a}_x e^{-jk_2 z}$ and $\mathbf{a}_y e^{-jk_2 z}$ will now be expanded into spherical wave vectors[18a] at a point of spherical polar coordinates (r,θ,ϕ). It is readily recalled that

$$x = r \sin\theta \cos\phi,$$
$$y = r \sin\theta \sin\phi,$$
$$z = r \cos\theta, \qquad (4)$$

with

$$0 \leq \theta \leq \pi \text{ and } 0 \leq \phi \leq 2\pi.$$

---

[c] Henceforth the time factor $e^{+j\omega t}$ will be omitted, as it does not play a direct role in what follows.

equation (7). Elimination of a_n^i from the first pair and that of b_n^i from the second pair of these equations leads to

$$a_n^s = -\frac{\mu_1 z_n^{(1)}(N\rho)[\rho z_n^{(1)}(\rho)]' - \mu_2 z_n^{(1)}(\rho)[N\rho z_n^{(1)}(N\rho)]'}{\mu_1 z_n^{(1)}(N\rho)[\rho z_n^{(3)}(\rho)]' - \mu_2 z_n^{(3)}(\rho)[N\rho z_n^{(1)}(N\rho)]'},$$

(14)

$$b_n^s = -\frac{\mu_1 z_n^{(1)}(\rho)[N\rho z_n^{(1)}(N\rho)]' - \mu_2 N^2 z_n^{(1)}(N\rho)[\rho z_n^{(1)}(\rho)]'}{\mu_1 z_n^{(3)}(\rho)[N\rho z_n^{(1)}(N\rho)]' - \mu_2 N^2 z_n^{(1)}(N\rho)[\rho z_n^{(3)}(\rho)]'},$$

(14)

The primes at the square brackets stand for differentiation with respect to the argument of the Bessel function inside the brackets. Similarly, eliminating a_n^s and b_n^s, respectively, one would get a_n^i and b_n^i appearing in the field strengths inside the sphere.

For the computation of either the scattered or absorbed radiation, one needs to know the field strengths at a large distance r from the center of the sphere, i.e., for $r \gg a$, or $k_2 r \gg k_2 a$. It is important to notice in this connection that the coefficients a_n and b_n become small for $n > k_2 a$, and the summation over n may then be limited to the integer $n \sim k_2 a$. At great distances r, $k_2 r > n$; in other words, the order n of the terms of importance is less than the argument $(k_2 r)$ of the spherical Bessel functions. Under these conditions the asymptotic expressions of these functions can be used. These are given by[18a]

$$z_n^{(1)}(kr) \cong \frac{1}{kr} \cos\left(kr - \frac{n+1}{2}\pi\right),$$

$$z_n^{(3)}(kr) \cong \frac{1}{kr} e^{-i\left(kr - \frac{n+1}{2}\pi\right)} \quad (15)$$

From these asymptotic expressions one sees that the radial components of the scattered field strengths can be practically neglected; they decrease with r as $1/r^2$, in contrast with the θ and ϕ components which decrease as $1/r$. This means that for large r, the field is transverse to the direction of propagation (radiation zone). Hence,

$$E_r^s = H_r^s = 0, \ r \gg a, \quad (16)$$

and with $\sigma_2 = 0$

$$E_\theta^s = \eta_2 H_\phi^s = -\left(\frac{j}{kr}\right) E_0 e^{-jkr} \sum_{n=1}^{\infty} \frac{2n+1}{n(n+1)} \cdot$$

$$\left(a_n^s \frac{P_n^1}{\sin\theta} + b_n^s \frac{dP_n^1}{d\theta}\right) \cos\phi,$$

$$E_\phi^s = -\eta_2 H_\theta^s = -\left(\frac{j}{kr}\right) E_0 e^{-jkr} \sum_{n=1}^{\infty} \frac{2n+1}{n(n+1)} \cdot \quad (17)$$

$$\left(a_n^s \frac{dP_n^1}{d\theta} + b_n^s \frac{P_n^1}{\sin\theta}\right) \sin\phi.$$

Since the resultant field at any point outside the sphere is obtained by superposition of the incident and scattered or reflected fields, one has

$$\mathbf{E} = \mathbf{E}_i + \mathbf{E}_s; \ \mathbf{H} = \mathbf{H}_i + \mathbf{H}_s. \quad (18)$$

In view of equation (16), the complex Poynting vector

associated with this resultant field is radial, so that

$$S_o = \frac{1}{2}(E_\theta H_\phi^* - E_\phi H_\theta^*), \quad (19)$$

where an asterisk denotes the complex conjugate. Using equation (18) one gets

$$S_o = \frac{1}{2}(E_\theta^i H_\phi^{i*} - E_\phi^i H_\theta^{i*}) + \frac{1}{2}(E_\theta^s H_\phi^{s*} - E_\phi^s H_\theta^{s*})$$

$$+ \frac{1}{2}(E_\theta^s H_\phi^{i*} + E_\theta^i H_\phi^{s*} - E_\phi^i H_\theta^{s*} - E_\phi^s H_\theta^{i*}). \quad (20)$$

The first term on the right-hand side is the rate of flow of energy in the incident wave and the second term is the rate of flow in the scattered wave. The total scattered power is then

$$P_s = \frac{1}{2} \text{Re} \int_0^{2\pi}\int_0^\pi (E_\theta^s H_\phi^{s*} - E_\phi^s H_\theta^{s*}) r^2 \sin\theta d\theta d\phi, \quad (21)$$

where Re denotes "Real part of ..." and the integral is extended over the surface of a large sphere of radius r. In our case, using equations (16) and (17), one gets

$$P_s = \frac{1}{2\eta_2} \text{Re} \int_0^{2\pi}\int_0^\pi (|E_\theta^s|^2 + |E_\phi^s|^2) r^2 \sin\theta d\theta d\phi. \quad (22)$$

In the case of an absorbing sphere, the net flow of energy across a closed surface around the sphere is absorbed energy flow, and it is directed inward. One may thus write that this absorbed energy, which disappears in the form of heat, is

$$P_{ab} = \text{Re} \int_0^{2\pi}\int_0^\pi (-S_o) r^2 \sin\theta d\theta d\phi. \quad (23)$$

Since the integral of the incident flow across a closed surface is zero, equation (23) in connection with equation (21) leads to the definition of the rate of flow of total energy or the power subtracted from the beam, i.e., $(P_{ab} + P_s)$, as an integral over a closed surface of the third term on the right-hand side of the radial component S_o of the Poynting vector, equation (19). Thus

$$P_t = P_{ab} + P_s = \frac{1}{2}(-\text{Re})\int_0^{2\pi}\int_0^\pi$$

$$(E_\theta^i H_\phi^{s*} + E_\theta^s H_\phi^{i*} - E_\phi^i H_\theta^{s*} - E_\phi^s H_\theta^{i*}) r^2 \sin\theta d\theta d\phi. \quad (24)$$

Substituting equations (16) and (17) into equation (24) and remembering that the ϕ integration leads one finds,

$$P_s = \frac{\pi E_0^2}{k_2^2 \eta_2} \sum_{n=1}^{\infty} (2n+1)(|a_n^s|^2 + |b_n^s|^2), \quad (25)$$

$$\int_0^\pi \left[\left(\frac{P_n^1}{\sin\theta}\right)^2 + \left(\frac{dP_n^1}{d\theta}\right)^2\right] \sin\theta d\theta$$

$$= \frac{2}{2n+1}[n(n+1)]^2,$$

to a factor π and that the integrals over products of the associated Legendre polynomials $P_n^1(x)$ are different from zero only in the following combination of these products appearing in equations (22) and (24),

and

$$P_t = \frac{\pi E_0^2}{k_2^2 \eta_2} (-\operatorname{Re}) \sum_{n=1}^{\infty} (2n+1)(a_n^s + b_n^s). \quad (26)$$

We shall also need the fraction of the power scattered backwards by the sphere, i.e., in the direction $\theta = \pi$, per unit solid angle. One thus obtains, with $d\omega = \sin\theta d\theta d\phi$,

$$\left(\frac{dP_s}{d\omega}\right)_{\theta=\pi} = \frac{E_0^2}{8k_2^2 \eta_2} \operatorname{Re} \sum_{n=1}^{\infty} \sum_{m=1}^{\infty} (-)^{n+m}(2n+1) \cdot$$
$$(2m+1)(a_n^s - b_n^s)(a_m^{s*} - b_m^{s*}), \quad (27)$$

as a simple calculation shows, starting from equation (22).

It has already been mentioned in connection with the definition of the complex wave number, equation (2), of a homogeneous and isotropic medium that its imaginary part is chosen to be negative. We shall write

$$jk = \alpha + j\beta, \quad (28)$$

where β is the phase constant and α the attenuation constant; both are real. The explicit expressions of β and α in terms of the characteristic electromagnetic properties of the medium, namely, inductive capacity ϵ, permeability μ and conductivity σ for the given frequency $\omega/2\pi$ are the following:[18a]

$$\beta = \omega \left[\frac{\mu\epsilon}{2} \left(\sqrt{1 + \frac{\sigma^2}{\epsilon^2 \omega^2}} + 1 \right) \right]^{\frac{1}{2}}, \quad (29)$$

$$\alpha = \omega \left[\frac{\mu\epsilon}{2} \left(\sqrt{1 + \frac{\sigma^2}{\epsilon^2 \omega^2}} - 1 \right) \right]^{\frac{1}{2}}. \quad (30)$$

With equation (28) the field strength, electric or magnetic, in a plane wave propagated in such a medium along, say, the z axis, is, omitting the time factor, of the form:

$$\mathbf{F} = \mathbf{F}_0 e^{-j\beta z - \alpha z},$$

$\mathbf{F}_0$ being an amplitude vector directed along either one of the two remaining coordinate axes. The attenuation factor α simply means that in this medium an advance of the wave through a distance of $1/\alpha$ meter is accompanied by a decrease in the field strengths in the ratio of $1:e = 0.368$, or the power per unit area (Poynting vector) decreases in the same ratio over half that distance or $1/2\alpha$ meter.

In the mks system, the attenuation factor is then α nepers per meter, whereas the power absorption coefficient is 20α ($\log_{10}e$) decibels per meter $= 8.686\alpha$ db per meter.

Our problem is the study of propagation in a medium which is neither homogeneous nor isotropic, inasmuch as it consists of a suspension of water droplets in the atmosphere. It can be proved that in such a medium the attenuation factor is the sum of all the different partial attenuation factors due to different physical phenomena.

The particle attenuation factor will still be denoted by α. More appropriately we might call α the average particle attenuation factor. It may be defined as

$$\alpha = \frac{1}{2} N Q_t \text{ neper per unit length,} \quad (31)$$

where N is the average number of water drops per unit volume and Q_t the total cross section of one droplet. The absorption effect of one spherical water drop is given by Q_t which is the ratio of the power P_t removed by the drop from the beam falling on it to the incident power per unit area. Provided the effect of all the drops be linearly additive, equation (31) will express their average attenuation effect. The incident power density is the complex Poynting vector of the beam

$$S_{e,s} = \frac{E_0^2}{2\eta_2}. \quad (32)$$

Therefore, with equations (3) and (26),

$$Q_t = \frac{\lambda^2}{2\pi} (-\operatorname{Re}) \sum_{n=1}^{\infty} (2n+1)(a_n^s + b_n^s), \quad (33)^d$$

where $\lambda = 2\pi/k_2$ is the wavelength of the radiation in air or free space. Similarly the cross section for scattering is, with equation (25),

$$Q_s = \frac{\lambda^2}{2\pi} \sum_{n=1}^{\infty} (2n+1)(|a_n^s|^2 + |b_n^s|^2). \quad (34)$$

The differential cross section for back scattering (or radar cross section) is then, with equations (27) and (32),

$$\left(\frac{dQ_s}{d\pi}\right)_{\theta=\pi} = \sigma(\pi)$$
$$= \left(\frac{\lambda}{4\pi}\right)^2 \operatorname{Re} \sum_{n=1}^{\infty} \sum_{m=1}^{\infty} (-)^{n+m}(2n+1)$$
$$(2m+1)[a_n^s a_m^{s*} + b_n^s b_m^{s*} - 2a_n b_m^{s*}]. \quad (35)$$

These are the formulas on which the computations of attenuation have been based. They are certainly correct in the wavelength region 1 cm to 100 cm with which the present study is mainly concerned, and they correctly take into account the linear dimensions of the scattering and absorbing particles. According to Brillouin[20] these formulas have to be modified in the limit $\lambda \ll a$, in which case for perfect reflection they lead to a scattering cross section $2\pi a^2$, double of the expected geometrical cross section. Since the modifications mentioned do not play any role for $\lambda \geq 3a/10$, which condition will always be satisfied in the present report, they will not be discussed here.

---
[d] The minus sign is missing in the presentation in reference 18a; see formulas (26) and (29) on page 569. This leads to the incorrect result, for nonabsorbing spheres, that the scattering cross section Q_s reduces in this case to the negative of the total cross section Q_t. Clearly Q_s reduces to $+Q_t$.

The Scattering Amplitudes*
a_n^s and b_n^s

The scattered fields (E_s, H_s) outside the sphere and the transmitted fields (E_t, H_t) inside are due to forced oscillations of the sphere caused by the incident field (E_i, H_i). The fields (E_s, H_s) and (E_t, H_t) given by equations (7) and (8) can be regarded as due to electric and magnetic 2^n-poles ($n = 1$ corresponds to dipoles, $n = 2$ to quadrupoles, etc.) induced in the substance of the spherical particle. In the steady state these poles oscillate with the frequency of the incident radiation field. When this frequency approaches a characteristic frequency of the free vibrations of the electric or magnetic 2^n-poles of the sphere, resonance will occur. It can, indeed, be shown that the amplitudes a_n are associated with vibrations of magnetic poles and the b_n's with vibrations of electric poles. The characteristic frequencies of the free vibrations of magnetic poles of a sphere are determined by a condition which annuls the denominator of a_n, those of electric poles by a condition which annuls the denominator of b_n, given by equation (14).[18b] The characteristic frequencies of the free vibrations are, however, complex in contrast with the real frequency of constraint of the radiation field falling on a sphere, as in the present case. The denominators of the amplitudes a_n and b_n, although reduced, can never become zero, and there are no difficulties caused by resonance.

A glance at the formulas (14) shows the complexity of the amplitudes a_n and b_n. An exact computation of these coefficients is out of the question on account of the lack of tables of Bessel and Hankel functions* of complex argument in the range needed here. They reduce to simple expressions in the limit when the parameter $\rho = 2\pi a/\lambda \ll 1$. In the present work we shall be mostly interested in the cases where $\rho < 1$ or $\rho \ll 1$. In these cases a series expansion of the amplitudes in ascending powers of the parameter ρ can be used. With the expansions of the spherical Bessel and Hankel functions

$$z_n^{(1)}(\rho) = 2^n \rho^n \sum_{m=0}^{\infty} \frac{(-)^m (n+m)!}{m!(2n+2m+1)!} \rho^{2m},$$

$$z_n^{(2)}(\rho) = 2^n \rho^n \sum_{m=0}^{\infty} \frac{(-)^m (n+m)!}{m!(2n+2m+1)!} \rho^{2m}$$
$$+ \frac{j}{2^n \rho^{n+1}} \sum_{m=0}^{n} \frac{(2n-2m)!}{m!(n-m)!} \rho^{2m}$$

used in equation (14), one is lead to the following amplitudes, keeping the first few terms of the expansions and assuming $\mu_1 = \mu_2$, i.e., the equality of the permeabilities of the medium and the sphere:

$$a_n = -j2^{2n} \left(\frac{n!}{(2n+1)!} \right)^2 \frac{N^2-1}{2n+3} \rho^{2n+3} \cdot$$

$$\left[1 + \rho^2 \left(\frac{N^2-1}{2n+1} - \frac{N^2+1}{2(2n+5)} \right) + \cdots \right], \quad (36)$$

$$b_n = -j2^{2n} \left(\frac{n!}{(2n+1)!} \right)^2$$

$$\frac{(2n+1)(n+1)(N^2-1)}{nN^2+n+1} \cdot \rho^{2n+1} \cdot \quad (37)$$

$$\left[1 + \rho^2 \frac{(2n+1)[(2n-1)N^2-n-1]}{(2n+3)(2n-1)(nN^2+n+1)} + \cdots \right.$$

$$- j2^{2n} \left(\frac{n!}{(2n+1)!} \right)^2$$

$$\left. \frac{(2n+1)(n+1)(N^2-1)}{nN^2+n+1} \cdot \rho^{2n+1} + \cdots \right]$$

From these expressions one derives at once the explicit formulas representing the induced magnetic dipole (a_1), electric dipole (b_1), and electric quadrupole (b_2) amplitudes. One has, then, neglecting powers of ρ higher than the sixth,

$$a_1 = \frac{-j}{45} (N^2 - 1)\rho^5,$$

$$b_1 = \frac{-2j}{3} \frac{N^2-1}{N^2+2} \rho^3 \left(1 - \frac{3}{5} \frac{N^2-2}{N^2+2} \rho^2 \right.$$

$$\left. - \frac{2j}{3} \frac{N^2-1}{N^2+2} \rho^3 \right), \quad (38)^t$$

and

$$b_2 = \frac{-j}{15} \frac{N^2-1}{2N^2+3} \rho^5.$$

It would appear interesting to present the relationships connecting the amplitudes of the electric and magnetic poles a_n and b_n with those appearing in the treatment of Mie which was used by Ryde.[17] The magnetic and electric amplitudes in Mie's notation are respectively p_n and a_n, and the relationships in question are the following:

$$p_n^{Mie} = (-)^n j(2n+1) a_n,$$

$$a_n^{Mie} = (-)^{n+1} j(2n+1) b_n. \quad (39)$$

Finally the formulas (38) can be transformed so

---

*Since henceforth we will deal only with the scattering coefficients a_n^s, b_n^s, we will omit the superscript s.

†Some misprints and slight errors in the expressions for these amplitudes may be noted in reference 18a. On page 571 in the formula (35) and in the denominator of the coefficient of ρ^3, read $(2n + 2)$ instead of $(2n + 1)$. In the formula (36) the minus sign on the right-hand side is missing. In reference 18a, b_1' and b_1'' have the wrong sign and the ρ^3 term in b_1'' is incomplete. It is recalled that $+i$ has been replaced throughout this report by $-j$.

as to have the real and imaginary parts of the amplitudes separated easily. The refractive index N of the spheres is connected with their complex dielectric constant by

$$\epsilon_c = N^2 = \epsilon_r - j\epsilon_i, \qquad (40)$$

or with

$$N = n\,(1 - j\chi), \qquad (41)$$

the complex index of refraction, one has

$$\epsilon_r = n^2\,(1 - \chi^2); \quad \epsilon_i = 2n^2\chi. \qquad (42)$$

Using equation (40) in the amplitudes (38) one gets

$$a_1 = \frac{1}{45}\,[-\epsilon_i - j\,(\epsilon_r - 1)\,]\,\rho^5,$$

$$\operatorname{Re} b_1 = \frac{-2\epsilon_i}{(\epsilon_r + 2)^2 + \epsilon_i^2}\,\rho^3 - \frac{2}{5}\;.$$

$$\epsilon_i\,\frac{[\,(\epsilon_r + 2)\,(7\epsilon_r - 10) + 7\epsilon_i^2\,]}{[(\epsilon_r + 2)^2 + \epsilon_i^2]^2}\,\rho^5 - \frac{4}{9}\;.$$

$$\frac{(\epsilon_r - 1)^2(\epsilon_r + 2)^2 + \epsilon_i^2[2(\epsilon_r - 1)\,(\epsilon_r + 2) - 9] + \epsilon_i^4}{[\,(\epsilon_r + 2)^2 + \epsilon_i^2\,]^2}\,\rho^5,$$

$$\operatorname{Im} b_1 = -\frac{2}{3}\,\frac{(\epsilon_r - 1)\,(\epsilon_r + 2) + \epsilon_i^2}{(\epsilon_r + 2)^2 + \epsilon_i^2}\,\rho^3 - \frac{2}{5}\;.$$

$$\frac{(\epsilon_r - 1)(\epsilon_r - 2)(\epsilon_r + 2)^2 + \epsilon_i^2[2(\epsilon_r + 1)^2 - (3\epsilon_r + 20)] + \epsilon_i^4}{[(\epsilon_r + 2)^2 + \epsilon_i^2]^2}\;.$$

$$\rho^5 + \frac{8}{3}\,\frac{\epsilon_i\,[(\epsilon_r - 1)\,(\epsilon_r + 2) + \epsilon_i^2]}{[\,(\epsilon_r + 2)^2 + \epsilon_i^2\,]^2}\,\rho^5,$$

$$b_2 = \frac{1}{3}\,\frac{-\epsilon_i - (j/5)\,[(\epsilon_r - 1)\,(2\epsilon_r + 3) + 2\epsilon_i^2]}{(2\epsilon_r + 3)^2 + 4\epsilon_i^2}\,\rho^5.$$

$$(43)$$

These amplitudes are the same as those found by Ryde.[8] They allow the computation of attenuation and back scattering with a certain approximation. The results thus obtained are the more accurate, the smaller the parameter $\rho = 2\pi a/\lambda$.

In the computation of the amplitudes a_n and b_n we have used the same values of the real and imaginary parts of the dielectric constant of water ϵ_r and ϵ_i as the ones used by Ryde. These were obtained by using the Clarendon Laboratory values for ϵ_r and ϵ_i for waves of 1.26-cm wavelength[21] and determining with them the transition wavelength λ_0 in the Debye[12] formulas

$$\epsilon_r = \epsilon_{\infty} + \frac{\epsilon_{\omega} - \epsilon_{\infty}}{1 + \left(\dfrac{\lambda_0}{\lambda}\right)^2}, \quad \epsilon_i = \frac{\lambda_0}{\lambda}\,(\epsilon_r - \epsilon_{\infty}),\quad (44)$$

$$\epsilon_{\infty} = 1.33,\ \epsilon_{\omega} = 81,\ \lambda_0 = 1.59\ \text{cm}.$$

---

[a]In his first report Ryde[17] gave incorrectly the coefficients of ρ^5 in both the real and imaginary parts of b_1. The coefficient of ρ^5 in the real part was corrected in the second report. In comparing the b_1's with the amplitudes given by Ryde, the relations (38) have to be taken into account.

λ, cm	ϵ_r	$\epsilon_i = 60\sigma\lambda$	σ mhos/m
1	24.2	35.6	5.93×10
1.26	32.5	38.6	5.11×10
1.62	43.3	39.5	4.13×10
2	50.6	38.5	3.20×10
2.5	58.2	35.9	2.39×10
3.0	63.6	32.7	1.81×10
4.0	70.3	27.2	1.13×10
5	73.8	22.7	7.56
6	76.0	19.3	5.36
8	78.0	15.1	3.15
10	79.0	12.3	2.05
15	81	8.40	9.33×10^{-1}
20	81	6.30	5.25×10^{-1}
30	81	4.20	2.33×10^{-1}
50	81	2.52	8.40×10^{-2}
75	81	1.68	3.73×10^{-2}
100	81	1.26	2.10×10^{-2}

*The computations of the attenuation and scattering effects are all based on this table and refer therefore always to temperatures of about 18 C, unless stated otherwise.

Table 2. Temperature variation of the dielectric constant of water (K band).

	Degrees C	ϵ_r	ϵ_i
Water	3	27	27
	25	35	23
	60	44	14
Ice	−15	3.3	0.011

The values of ϵ_r computed with these formulas happen to be in fair agreement with the experimental values obtained by a large group of independent workers.[17,22] There seems to be a regrettable situation concerning the values of ϵ_i, and no serious studies have been made on the temperature and frequency variation of this quantity, so fundamental for the microwave region. A beginning in this direction has been undertaken by the Radiation Laboratory.[23] In Figure 4 we have drawn the curves $\epsilon_r(\lambda)$ and $\epsilon_i(\lambda)$ in the range 1 to 11 cm, and Table 1 gives the values of the dielectric constant used in this work in the wavelength interval 1 to 100 cm.

It is interesting to consider here the temperature variation of ϵ_r. Recent measurements made in the Radiation Laboratory in the K band[23] gave the results shown in Table 2.
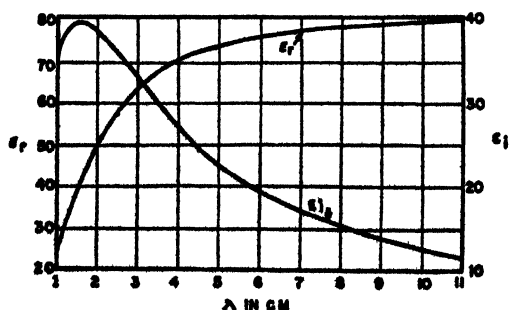
Figure 4. Dielectric constant of water $(t \sim 18\,C)$ $\epsilon_c = \epsilon_r - j\epsilon_i$.

As might have been expected, the dielectric absorption ϵ_i increases with decreasing temperature.

With the above values of ϵ_r and ϵ_i the computation of the amplitudes a_n and b_n is straightforward. The amplitudes a_n and b_n have the form

$$a_n = \sum_{l=2n+3}^{\infty} (\alpha_n^{(l)} + j\bar{\alpha}_n^{(l)}) \rho^l, \qquad (45)$$

$$b_n = \sum_{l=2n+1}^{\infty} (\beta_n^{(l)} + j\bar{\beta}_n^{(l)}) \rho^l. \qquad (46)$$

Thus we let $\alpha_1^{(5)}$ denote the real part of the coefficient of ρ^5 in a_1 and $\bar{\alpha}_1^{(5)}$ its imaginary part. Similarly, $\beta_1^{(3)}, \bar{\beta}_1^{(3)}$ are the real and imaginary parts of the coefficient of ρ^3 in b_1, etc.

As equation (43) shows $\alpha_1^{(5)}$ and $\bar{\alpha}_1^{(5)}$ are directly proportional to $(-\epsilon_i)$ and (ϵ_r-1) respectively. As the wavelength increases, $\alpha_1^{(5)}$ changes approximately from -0.9 to -0.03 after passing through a shallow minimum on account of the variation of ϵ_i. In the same interval $\bar{\alpha}_1^{(5)}$ increases from about 0.5 to 1.8.

$\beta_1^{(3)}$ turns out to be practically negligible, in comparison with $\bar{\beta}_1^{(3)}$, which is almost constant in this wavelength range. $\beta_1^{(5)}$ and $\bar{\beta}_1^{(5)}$ behave similarly. With $\beta_1^{(6)}$ and $\bar{\beta}_1^{(6)}$ the roles are inverted.

Finally $\beta_3^{(5)}$ and $\bar{\beta}_3^{(5)}$ both vary in the range under consideration.

As a rule, those coefficients of the powers of ρ ($= \pi D/\lambda$) (D = diameter of the sphere) which do not contain terms in ϵ_r and powers of ϵ_r separately in the numerator, but only the products ϵ_r ϵ_i, and powers of ϵ_i are considerably smaller than those which do contain ϵ_r and its powers separately.

The Attenuation of Radio Waves by Spherical Raindrops[h]

The knowledge of the coefficients a_n and b_n allows finally the computation of the absorption cross section for any spherical water drops of given diameter D at those temperatures where the amplitudes can be computed.

The absorption coefficient becomes, with the cross section found above, [equations (33) and (43)],

$$\alpha = 0.4343 \times 10^6 \frac{N\lambda^2}{2\pi} (-\text{Re}) \sum_{n=1}^{n=\infty} (2n+1)(a_n+b_n)$$

$$\text{db per kilometer.} \quad (47)$$

In our approximation for the amplitudes, we may write

$$\alpha = 0.4343 \times 10^6 \frac{3\pi NV}{\lambda} (c_1 + c_2\rho^2 + c_3\rho^4 + \cdots)$$

$$\text{db per kilometer} \quad (48)$$

---

where N is the number of spherical drops, each of volume V per cubic centimeter, λ is the wavelength in centimeters of the incident radiation. The parameter ρ is, as above, $\pi D/\lambda$, D being the diameter in centimeters of a drop, and the coefficients $c_1, c_2, c_3, \cdots$ are the following functions of the wavelength, the temperature of the drops being taken as a constant ($t \sim 18$ C),

$$c_1 = \frac{6\epsilon_i}{(\epsilon_r+2)^2 + \epsilon_i^2},$$

$$c_2 = \frac{\epsilon_i}{15} + \frac{5}{3} \frac{\epsilon_i}{(2\epsilon_r+3)^2 + 4\epsilon_i^2}$$

$$+ \frac{6}{5} \frac{\epsilon_i[(\epsilon_r+2)(7\epsilon_r-10)+7\epsilon_i^2]}{[(\epsilon_r+2)^2+\epsilon_i^2]^2},$$

$$c_3 = \frac{4}{3} \frac{(\epsilon_r-1)^2(\epsilon_r+2)^2+\epsilon_i^2[2(\epsilon_r-1)(\epsilon_r+2)-9]+\epsilon_i^4}{[(\epsilon_r+2)^2+\epsilon_i^2]}. \quad (49)$$

It is possible to give the attenuation formula another simple form by noticing that NV is the total volume of water per cubic centimeter in the form of drops or 10^6 NV is the total volume of water per cubic meter. Since the density of water is 1 g per cubic centimeter, numerically, the quantity 10^6 NV is the mass m of liquid water per cubic meter, in air. The transformed attenuation formula becomes finally

$$\alpha = 4.092 \frac{m}{\lambda} (c_1 + c_2\rho^2 + c_3\rho^4 + \cdots) \quad \text{db per kilometer.} \quad (50)$$

It is seen that when $\rho = \pi D/\lambda \ll 1$ so that all the terms in the expansion in equation (50) are small in comparison with c_1, the attenuation factor reduces to

$$\alpha_{\rho \ll 1} = \frac{4.092\,mc_1}{\lambda} = \frac{24.55}{\lambda} \frac{m\epsilon_i}{(\epsilon_r+2)^2+\epsilon_i^2}$$

$$\text{db per kilometer.} \quad (51)$$

Hence, when the diameter of the water drops is very small in comparison with the wavelength of the incident radiation, the attenuation does not depend on the size of the drops but only on the total mass of liquid water per unit volume contained in the air. It is interesting to find, for a given wavelength, the largest diameter for which the approximation (51) can still be used in practice. If it is practical to use (51), (as in reference 12), for

$$c_2\rho^2 \leq \frac{c_1}{10}, \quad (52)$$

then in order that (51) shall represent the attenuation factor within 10 per cent, the diameter of the spheres must (for given λ), be equal to or less than D_c with

$$D_c = \frac{\lambda}{10} \left(\frac{c_1}{c_2}\right)^{\frac{1}{2}} \text{cm.} \quad (53)$$

In Table 3 appear the values of c_1, c_2, and D_c in the

TABLE 3

λ, cm	c_1	c_2	D_e cm
1	0.109	2.53	0.0656
1.1	0.0994	2.60	0.0680
1.26	0.0862	2.69	0.0713
1.5	0.0730	2.73	0.0774
2	0.0543	2.64	0.0906
3	0.0365	2.23	0.121
4	0.0273	1.85	0.154
5	0.0217	1.54	0.187
6	0.0179	1.31	0.222
8	0.0137	1.01	0.293
10	0.0110	0.835	0.363
15	0.00724	0.570	0.534
20	0.00541	0.427	0.712
25	0.00437	0.342	0.892
30	0.00364	0.285	1.07
50	0.00219	0.171	1.78
75	0.00146	0.114	2.68
100	0.00109	0.085	3.57

wavelength range 1 to 100 cm. The values of c_2 are not included, since this coefficient turns out to be practically constant, in this range, increasing from the value of 1.224 for $\lambda = 1$ cm to 1.239 for $\lambda = 100$ cm.

It is evident that for values of ρ which are not too small, equation (48) or (50) has to be used. When ρ is sufficiently close to unity these series cease to give any good values of the absorption cross section Q_t or the attenuation factor α. In the K and X bands, Ryde and Ryde[12] have, therefore, computed the attenuation factors exactly. These computations were included (without being checked) in Tables 4 and 5, where Q_t and α have been computed for a series of drops ranging in diameter from 0.05 to 0.55 cm. For wavelengths $\lambda \geq 5$ cm, the three-term series expansion (48) was

used. It is expected that at these shorter waves, where the critical diameters are smaller than the drop diameters mentioned, the cross sections and attenuation factors given in the tables will be but fair approximations of the exact values of these quantities.

The range of values of ρ covered by these tables extends from about $\rho = 0.0016$ to $\rho = 1.4$. In Figures 5 and 6 two families of curves are drawn giving $Q_t (\lambda)_D$ and $\alpha(\lambda)_D/N$, the diameter of the drops being
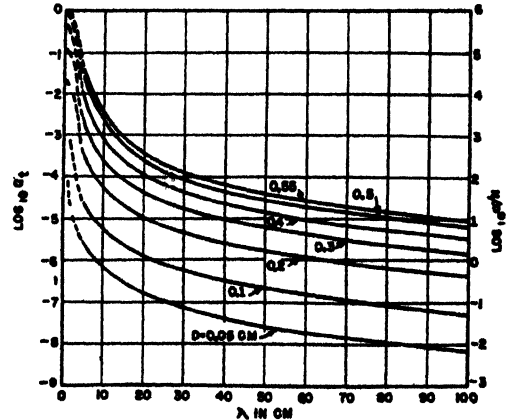
FIGURE 5. Absorption cross section, Q_t, and attenuation constant, α, of spherical water drops as a function of the wavelength. The abscissa gives the wavelength, λ, in centimeters. The right-hand ordinate scale gives $\log_{10} (\alpha/N)$, where α/N, the attenuation constant in a rain with 1 drop per cu cm, is expressed in decibels per kilometer. The numbers on the curves give the diameter, D, of the drops in centimeters. The left-hand ordinate scale gives $\log_{10} Q_t$ with Q_t being expressed in square centimeters.

TABLE 4. Absorption cross section Q_t (cm²) of water drops with diameter D (cm).

λ, cm	D, cm 0.05	0.10	0.15	0.20	0.25	0.30	0.35	0.40	0.45	0.50	0.55
1.25	$6.19 \cdot 10^{-5}$	$9.60 \cdot 10^{-4}$	$5.66 \cdot 10^{-3}$	$1.89 \cdot 10^{-2}$	$5.04 \cdot 10^{-2}$	$1.13 \cdot 10^{-1}$	$2.15 \cdot 10^{-1}$	$3.66 \cdot 10^{-1}$	$5.66 \cdot 10^{-1}$	$7.62 \cdot 10^{-1}$	1.01
3	$9.19 \cdot 10^{-6}$	$1.52 \cdot 10^{-4}$	$1.30 \cdot 10^{-3}$	$5.53 \cdot 10^{-3}$	$1.63 \cdot 10^{-2}$	$3.73 \cdot 10^{-2}$	$6.65 \cdot 10^{-2}$	$1.08 \cdot 10^{-1}$	$1.52 \cdot 10^{-1}$	$2.15 \cdot 10^{-1}$	$2.72 \cdot 10^{-1}$
5	$2.84 \cdot 10^{-6}$	$2.75 \cdot 10^{-5}$	$1.20 \cdot 10^{-4}$	$3.79 \cdot 10^{-4}$	$9.85 \cdot 10^{-4}$	$2.24 \cdot 10^{-3}$	$4.59 \cdot 10^{-3}$	$8.68 \cdot 10^{-3}$	$1.54 \cdot 10^{-2}$	$2.59 \cdot 10^{-2}$	$4.18 \cdot 10^{-2}$
8	$1.09 \cdot 10^{-6}$	$9.49 \cdot 10^{-6}$	$3.65 \cdot 10^{-5}$	$1.02 \cdot 10^{-4}$	$2.40 \cdot 10^{-4}$	$4.98 \cdot 10^{-4}$	$9.63 \cdot 10^{-4}$	$1.74 \cdot 10^{-3}$	$2.97 \cdot 10^{-3}$	$4.85 \cdot 10^{-3}$	$7.63 \cdot 10^{-3}$
10	$6.90 \cdot 10^{-7}$	$5.84 \cdot 10^{-6}$	$2.16 \cdot 10^{-5}$	$5.76 \cdot 10^{-5}$	$1.46 \cdot 10^{-4}$	$2.59 \cdot 10^{-4}$	$4.81 \cdot 10^{-4}$	$8.44 \cdot 10^{-4}$	$1.40 \cdot 10^{-3}$	$2.25 \cdot 10^{-3}$	$3.47 \cdot 10^{-3}$
15	$2.98 \cdot 10^{-7}$	$2.45 \cdot 10^{-6}$	$8.66 \cdot 10^{-6}$	$2.18 \cdot 10^{-5}$	$4.59 \cdot 10^{-5}$	$8.65 \cdot 10^{-5}$	$1.51 \cdot 10^{-4}$	$2.51 \cdot 10^{-4}$	$3.98 \cdot 10^{-4}$	$6.10 \cdot 10^{-4}$	$9.06 \cdot 10^{-4}$
20	$1.67 \cdot 10^{-7}$	$1.36 \cdot 10^{-6}$	$4.71 \cdot 10^{-6}$	$1.15 \cdot 10^{-5}$	$2.36 \cdot 10^{-5}$	$4.31 \cdot 10^{-5}$	$7.29 \cdot 10^{-5}$	$1.17 \cdot 10^{-4}$	$1.78 \cdot 10^{-4}$	$2.66 \cdot 10^{-4}$	$3.85 \cdot 10^{-4}$
30	$7.36 \cdot 10^{-8}$	$5.93 \cdot 10^{-7}$	$2.02 \cdot 10^{-6}$	$4.88 \cdot 10^{-6}$	$9.74 \cdot 10^{-6}$	$1.73 \cdot 10^{-5}$	$2.83 \cdot 10^{-5}$	$4.38 \cdot 10^{-5}$	$6.45 \cdot 10^{-5}$	$9.29 \cdot 10^{-5}$	$1.30 \cdot 10^{-4}$
50	$2.67 \cdot 10^{-8}$	$2.14 \cdot 10^{-7}$	$7.27 \cdot 10^{-7}$	$1.73 \cdot 10^{-6}$	$3.41 \cdot 10^{-6}$	$5.96 \cdot 10^{-6}$	$9.57 \cdot 10^{-6}$	$1.45 \cdot 10^{-5}$	$2.09 \cdot 10^{-5}$	$2.93 \cdot 10^{-5}$	$3.97 \cdot 10^{-5}$
75	$1.19 \cdot 10^{-8}$	$9.44 \cdot 10^{-8}$	$3.21 \cdot 10^{-7}$	$7.63 \cdot 10^{-7}$	$1.49 \cdot 10^{-6}$	$2.60 \cdot 10^{-6}$	$4.15 \cdot 10^{-6}$	$6.23 \cdot 10^{-6}$	$8.94 \cdot 10^{-6}$	$1.24 \cdot 10^{-5}$	$1.66 \cdot 10^{-5}$
100	$6.77 \cdot 10^{-9}$	$5.41 \cdot 10^{-8}$	$1.83 \cdot 10^{-7}$	$4.34 \cdot 10^{-7}$	$8.50 \cdot 10^{-7}$	$1.47 \cdot 10^{-6}$	$2.35 \cdot 10^{-6}$	$3.51 \cdot 10^{-6}$	$5.02 \cdot 10^{-6}$	$6.92 \cdot 10^{-6}$	$9.27 \cdot 10^{-6}$

TABLE 5. Attenuation α/N (db/km) in fictitious rains with a concentration of one drop per cubic centimeter of D cm diameter.

| λ, cm	D, cm 0.05	0.10	0.15	0.20	0.25	0.30	0.35	0.40	0.45	0.50	0.55
1.25	$2.69 \cdot 10$	$4.17 \cdot 10^{2}$	$2.46 \cdot 10^{3}$	$8.23 \cdot 10^{3}$	$2.19 \cdot 10^{4}$	$4.90 \cdot 10^{4}$	$9.33 \cdot 10^{4}$	$1.59 \cdot 10^{5}$	$2.46 \cdot 10^{5}$	$3.31 \cdot 10^{5}$	$4.37 \cdot 10^{5}$
3	3.99	$6.61 \cdot 10$	$5.63 \cdot 10^{2}$	$2.40 \cdot 10^{3}$	$7.08 \cdot 10^{3}$	$1.62 \cdot 10^{4}$	$2.89 \cdot 10^{4}$	$4.68 \cdot 10^{4}$	$6.61 \cdot 10^{4}$	$9.33 \cdot 10^{4}$	$1.18 \cdot 10^{5}$
5	1.23	$1.19 \cdot 10$	$5.22 \cdot 10$	$1.65 \cdot 10^{2}$	$4.28 \cdot 10^{2}$	$9.72 \cdot 10^{2}$	$1.99 \cdot 10^{3}$	$3.77 \cdot 10^{3}$	$6.69 \cdot 10^{3}$	$1.13 \cdot 10^{4}$	$1.81 \cdot 10^{4}$
8	$4.73 \cdot 10^{-1}$	4.12	$1.59 \cdot 10$	$4.43 \cdot 10$	$1.04 \cdot 10^{2}$	$2.16 \cdot 10^{2}$	$4.18 \cdot 10^{2}$	$7.54 \cdot 10^{2}$	$1.29 \cdot 10^{3}$	$2.10 \cdot 10^{3}$	$3.31 \cdot 10^{3}$
10	$2.99 \cdot 10^{-1}$	2.54	9.37	$2.5 \cdot 10$	$6.35 \cdot 10$	$1.12 \cdot 10^{2}$	$2.09 \cdot 10^{2}$	$3.66 \cdot 10^{2}$	$6.09 \cdot 10^{2}$	$9.76 \cdot 10^{2}$	$1.51 \cdot 10^{3}$
15	$1.30 \cdot 10^{-1}$	1.07	3.76	9.47	$1.93 \cdot 10$	$3.76 \cdot 10$	$6.55 \cdot 10$	$1.09 \cdot 10^{2}$	$1.73 \cdot 10^{2}$	$2.65 \cdot 10^{2}$	$3.93 \cdot 10^{2}$
20	$7.26 \cdot 10^{-2}$	$5.89 \cdot 10^{-1}$	2.04	5.02	$1.03 \cdot 10$	$1.87 \cdot 10$	$3.17 \cdot 10$	$5.07 \cdot 10$	$7.73 \cdot 10$	$1.15 \cdot 10^{2}$	$1.67 \cdot 10^{2}$
30	$3.20 \cdot 10^{-2}$	$2.57 \cdot 10^{-1}$	$8.79 \cdot 10^{-1}$	2.12	4.23	7.50	$1.23 \cdot 10$	$1.90 \cdot 10$	$2.82 \cdot 10$	$4.04 \cdot 10$	$5.63 \cdot 10$
50	$1.16 \cdot 10^{-2}$	$9.29 \cdot 10^{-2}$	$3.16 \cdot 10^{-1}$	$7.53 \cdot 10^{-1}$	1.48	2.59	4.16	6.29	9.10	$1.27 \cdot 10$	$1.72 \cdot 10$
75	$5.16 \cdot 10^{-3}$	$4.12 \cdot 10^{-2}$	$1.39 \cdot 10^{-1}$	$3.31 \cdot 10^{-1}$	$6.49 \cdot 10^{-1}$	1.13	1.80	2.70	3.88	5.37	7.21
100	$2.94 \cdot 10^{-3}$	$2.35 \cdot 10^{-2}$	$7.93 \cdot 10^{-2}$	$1.89 \cdot 10^{-1}$	$3.69 \cdot 10^{-1}$	$6.40 \cdot 10^{-1}$	1.02	1.53	2.18	3.01	4.66
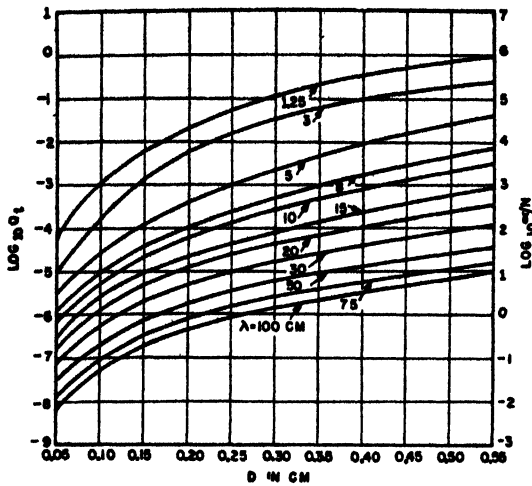
FIGURE 6. Absorption cross section, Q_t, and attenuation constant, α, of spherical water drops as a function of the drop diameter. The abscissa gives the drop diameter, D, in centimeters. The right-hand ordinate scale gives $\log_{10}(\alpha/N)$, where α/N, the attenuation constant in a rain with 1 drop per cu cm, is expressed in decibels per kilometer. The numbers on the curves give the wavelength, λ, of the incident radiation in centimeters. The left-hand ordinate scale gives $\log_{10} Q_t$, with Q_t being expressed in square centimeters.

kept constant, and $Q_t(D)_\lambda$ and $\alpha(D)_\lambda/N$, the wavelength of the radiation being kept constant. Since our computations cover the range from $\lambda = 5$ cm, we have extended our curves on Figure 5 so as to cover the K and X bands, using the values of the cross sections and attenuations given in these bands by Ryde and Ryde. Their data are represented again in the upper curves of Figure 6.

We are now prepared to apply these results to meteorological phenomena and shall, for this purpose, give a summary of typical data on clouds, fogs, and rains to be used in this work.

Typical Data on Clouds, Fogs, and Rains

To compute the attenuation due to the different forms of condensation demands a knowledge of the water drop size distributions and their volume concentration. Indeed, if such a form of condensation contains N_k droplets per cubic centimeter having a diameter of k cm, with k varying from, say, 0 to s, then the attenuation factor due to this form will be the sum of the attenuation factors associated with each of the different drop groups with diameter of $1, 2, \cdots, \cdots, \cdots, n, \cdots, s$ cm. In other words,

$$\alpha_{total} = \sum_{k=0}^{s} \alpha_k = 0.4343 \times 10^5 \sum_{k=0}^{s} N_k Q_{t,k}$$

$$\text{db per kilometer,} \quad (54)$$

according to equation (31), where N_k is the number per cubic centimeter of the drops k, and $Q_{t,k}$ is the total absorption cross section in square centimeters of one spherical water drop of diameter k cm.

It was shown above that theory allows a precise computation of the cross sections Q_t, provided the dielectric constant of water is given at the temperature of the drops. The concentration of N_k is a purely meteorological datum and must be obtained experimentally. As far as as the writer is aware, data on drop concentrations and drop size distributions are extremely scarce, and it appears that no systematic researches have as yet been undertaken for the purpose of obtaining such data.

Recently, observations were made available on drop size distributions in clouds of different types.[8,9] The main results of interest to the attenuation problem are that in clouds of different altitudes the diameter of the drops does not seem to exceed 0.02 cm. The liquid water content of the clouds examined by Mazur[9] varied between about 0.15 and 0.50 g/m³. The results of Diem[8] are, on the whole, similar.

Some data on ice clouds are included in Best's memoranda.[11]

Data on fogs are extremely meager. The diameter of fog droplets appears to be of the same order of magnitude as those of liquid water clouds.[24,25] Humphreys, in his table of precipitation values, gives 0.006 g/m³ as the liquid water content in fog.

The data on rains used in this report are those from reference 11. For additional data recently collected see reference 26.

The most important set of data which is directly usable in this work is contained in Table 6. In the last row of this table p is the precipitation rate or rate of rainfall, expressed in millimeters per hour, and results directly from the total volume of water falling per square meter per second, since $p = 36 \times 10^{-4} V$, where V is expressed in cubic millimeters per square meter per second.

Rains 1 and 2 refer, according to Best,[11] to a rain looking very ordinary, falling over a large area. Type 3 is a rain with breaks and sunshine. Type 4 corresponds to the beginning of a short rainfall like a thundershower. Type 5 refers to a sudden rain from a small cloud, associated with a calm, sultry atmosphere. Type 6 was a violent rain like a cloudburst with some hail. Types 7, 8, an 9 are for the heaviest period and the period of stopping of a continuous fall which at times took the form of a cloudburst. The preceding characteristics of the rains in Table 6 are quotations from the paper of Best.

These data on drop size distributions are the only data available to the writer. Clearly the rate of rainfall cannot be correlated from these data to any drop size distribution. A priori, it seems unlikely that a strict correlation between drop size distribution and rate of rainfall should exist. To a rain of given drop size distribution corresponds necessarily a determined rate of rainfall, but the reverse is not true, since a given rate of rainfall might be obtained with a large variety of drop size distribution.[10] In other words, the drop size distribution is the only physical charac-

TABLE 6. Drop size distributions in rains.

D, cm	Number of drops/m²/sec in nine different types of rain								
	1	2	3	4	5	6	7	8	9
0.05	1,000	1,600	129	60	...	100	514	679	7
0.10	200	120	100	280	50	1,300	423	524	233
0.15	140	60	73	160	50	500	359	347	113
0.20	140	200	100	20	150	200	138	295	46
0.25	...	...	29	20	0	0	156	205	7
0.30	...	...	57	...	200	0	138	81	0
0.35	...	...	...	...	0	0	0	28	32
0.40	...	...	...	...	50	0	0	20	39
0.45	...	...	...	...	...	200	101	...	0
0.50	...	...	...	..	. .	...	...	...	25
Total No. of drops	1,480	1,980	488	540	500	2,300	1,840	2,180	500
Total volume mm³/m²/sec	1,005	1,112	1,656	681.2	5,258	11,970	9,535	6,298	4,236
p mm/hr	3.6	4.0	6.0	2.46	18.9	43.1	34.3	22.6	15.2

teristic of a rain as far as attenuation and back scattering (echo) of radiowaves are concerned.

In any one location, even the drop size distribution of a rain is but an instantaneous characteristic of that rain. No data are available concerning the fluctuations in time of drop size distribution.

The space distribution of raindrops is another problem on which too few data are available. According to Kerr and Rado,[10] K-band rain absorption experiments over a relatively short path (~4km) have shown that the simultaneous rates of rainfall at three points of such a path were almost invariably appreciably different. The rates were measured at the location of the transmitter, the receiver, and at a point in between. Needless to say, under such circumstances the possibility of a quantitative interpretation of the experimental data on attenuation is almost excluded. It may be mentioned here that the earlier attenuation experiments on 1-cm waves by Robertson and his collaborators[37] as well as those of Mueller[2] on K/2 band were made over a shorter path (about 400 meters) and the rate of rainfall was measured only at one place, roughly in the middle of the path. Since the path length of the Oxford workers[26] was 2 km, there was ample room for possible fluctuations in the rate

of precipitation. The K-band radar transmission studies by the Bell Telephone Laboratory workers were made over longer paths,[29] and here, too, a situation somewhat similar to those reported by the Radiation Laboratory workers might have existed, as the authors duly noticed it.

The meteorological irregularities which thus seem to be inherent in precipitation data eliminate the possibility of a quantitative theory of attenuation and back scattering of radiowaves by rains or other precipitation forms. Although the data contained in Table 7 are used extensively in this report, the results thus obtained should be regarded as semiquantitative indications rather than rigorous theoretical predictions.

Given the number of raindrops of known dimensions falling over a certain area in a given time and given also the terminal velocity of the drops, the spatial concentration of raindrops can be derived at once. In Figure 7 the terminal velocity curve is drawn as a function of drop diameter. These velocities were measured at Porton and are quoted in Best's paper.[11]

From Table 6 we may obtain data for Table 7, giving raindrop concentration N_k of drops with diameter $k=D$ cm. These concentrations, as are the data in-

TABLE 7. Number of raindrops per cubic meter in rains of different precipitation rates.

D, cm	Distribution								
	A	B	C	D	E	F	G	H	I
	p, mm/hr								
	2.46	3.6	4.0	6.0	15.2	18.7	22.6	34.3	43.1
0.05	28.5	476	752	61.4	3.33	.....	323	245	47.6
0.10	71.8	512	30.8	25.6	59.7	12.8	134	108	333
0.15	31	27	11.4	14	21.5	9.52	66	68.4	95.2
0.20	3.13	22	31.2	15.6	7.2	23.4	46.1	21.6	31.2
0.25	2.76	...	...	4.0	0.96	0	28.3	21.5	0
0.30	...	...	...	7.2	0	25.3	10.2	17.6	0
0.35	...	...	...	...	3.83	0	3.35	0	0
0.40	...	...	...	...	4.48	5.75	2.2	0	0
0.45	...	...	...	...	0	...	...	11.3	22.5
0.50	...	...	...	...	2.71	...	...	...	...
Liquid water g/m³	0.130	0.439	0.217	0.242	0.521	0.673	0.990	1.25	1.55
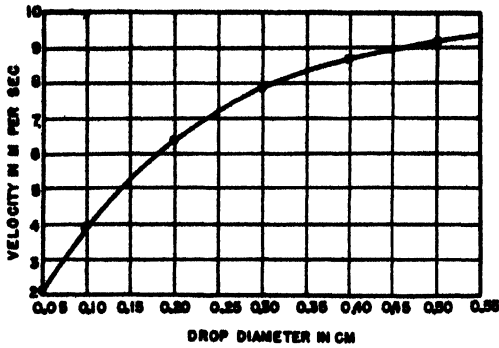
FIGURE 7. Terminal velocity of raindrops (experimental).

cluded in Table 6, may be regarded as characteristic for rains of the indicated precipitation rate, but they are not necessarily typical for those rains. Also given is the liquid water content of the atmosphere associated with the rains of Table 6 and its graphical representation in Figure 8. The curve drawn on this graph should not, however, be considered as representing any functional relationship between the liquid water concentration of the rainy atmosphere and the rate of rainfall. It can indeed easily be proved that the liquid water concentration associated with a rain depends only on the fractional precipitation rates of the different drop groups. It does not depend directly on the total rate of rainfall. Any rain of given total precipitation rate can be built up by a number of drop size distributions which determine different liquid water concentrations in the atmosphere. This means that it is *theoretically* incorrect to draw a graph entitled "Liquid Water Concentration versus Rate of Rainfall", as is frequently done. A curve so drawn can however be of considerable practical value when rough concentrations corresponding to given rates of rainfall are desired.

It can be seen that the resulting liquid water distributions are in fair agreement with those reported by Humphreys in his table of precipitation values[25]
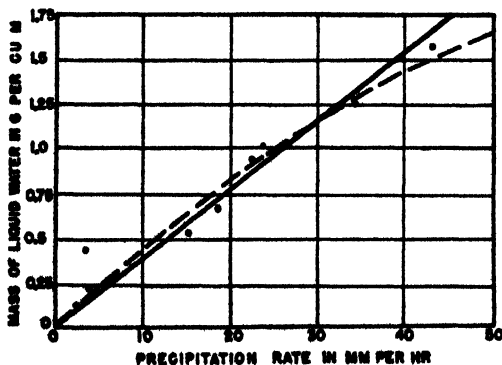
FIGURE 8. Computed liquid water distribution (cm³/m³ or g/m³) based on experimental drop size distributions in different rains. The slope of the straight line approximation is 0.088 g/m³/mm/hr.

already mentioned. It may be added here that aloft and in certain parts of rain clouds, where considerable updraft exists, the drop concentrations may be expected to be larger than those derived from Table 6.

These data will now be used in the computation of attenuation and back scattering by the different precipitation forms, assuming always ideal conditions and leaving aside the above-mentioned irregularities in space. For reasons stated above, theoretical results are significant only with regard to orders of magnitude.

Attenuation by Idealized Precipitation Forms

The data included in the preceding section show, first of all, that in clouds and fogs the attenuation can be given rigorously. Indeed, Table 3 indicates that the critical diameter even for waves of 1-cm wavelength is over 0.06 cm. Since we have seen that in clouds and fogs the drop diameters never exceed 0.02 cm, it appears that formula (51)' is applicable, and the attenuation of all waves of wavelength $\lambda \geq$ 1 cm is independent of the size of the drops. Furthermore, taking $m = 1$ g per cubic meter in formula (51) one probably obtains an upper limit for the attenuation of these waves.[1] In Figure 9 the attenuation is plotted down to $\lambda = 0.2$ cm. The dielectric constant of water has been computed in this range by using the Debye formula for wavelengths $\lambda > 1$ cm. Clearly the attenuation in fogs and clouds even in the region $\lambda \sim 1$ cm is not of great importance except for long ranges and radar observations. The attenuation becomes negligible for waves with $\lambda \geq$ 10 cm.

Table 3 also shows that the attenuation becomes practically independent of the drop size distribution for wavelengths equal to or larger than about 20 cm. In the 5- to 20-cm range the three-term formula (48) or (50) in connection with (54) will represent fairly well the attenuation in different rains, with increased accuracy at longer wavelengths. Below $\lambda = 5$ cm this formula is inapplicable, but there Ryde and Ryde's[12] exact attenuation values are available. The attenuation formula in a rain, as given by equation (54), can be transformed easily to another form. If p_k denotes the partial precipitation rate of the drops of k cm diameter in a given rain of total precipitation rate p, then clearly,

$$p = \sum_{k=0}^{s} p_k, \qquad (55)$$

s being the diameter of the largest drops in this rain. Now

$$p_k = 3.6 \times 10^6 \, V_k v_k N_k \text{ mm per hour}, \qquad (56)$$

[1] Attention may be called to the absence of data on the liquid water distributions in heavy sea fogs.
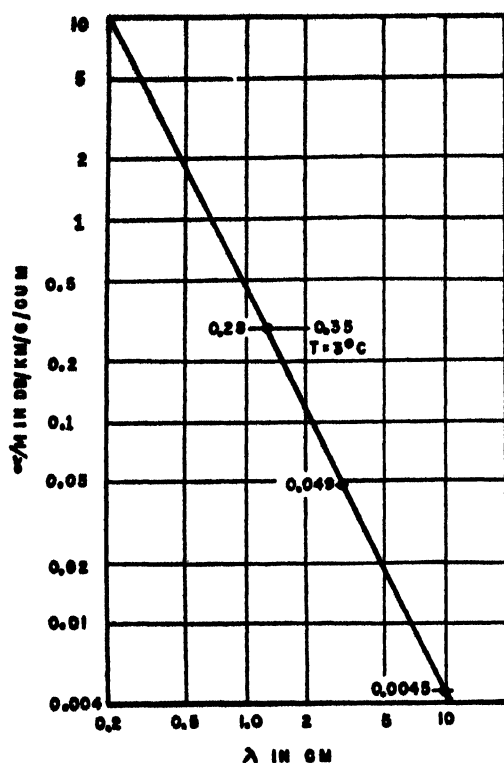
where V_k is the volume of a raindrop of k cm diameter, v_k is its terminal velocity in meters per second and N_k is their number per cubic centimeter. The attenuation of a rain of total precipitation rate p is, then, according to equation (54),

$$\alpha_{\lambda,p} = \sum_{k=0}^{s} \alpha_\lambda(p_k) = \frac{0.4343}{3.6} \sum_{k=0}^{s} \frac{p_k Q_{t,k}}{V_k v_k}$$

$$\text{db per kilometer,} \quad (57)$$

after substituting N_k from equation (56) into (54).

For a given wavelength λ, the ratio $Q_{t,k}/V_k v_k$ is a constant characteristic of drops whose diameter is k cm. This ratio will be denoted by q_k. The attenuation formula then becomes, finally,

$$\alpha_p = 0.126 \sum_{k=0}^{s} p_k q_k, \quad (58)$$

which shows that the attenuation in rains of a total

precipitation rate of p mm per hr depends linearly on the individual precipitation rates p_k of all the drop groups k which build up this rain. The attenuation does not depend directly on the total precipitation rate p. The points representing the experimental observations in the coordinate plane (α,p) should cover a certain region of this plane, but no single curve $\alpha(p)$ exists, since there is no direct relationship between α and p. A curve drawn in this plane is significant only in so far as it permits one to predict a possible attenuation value in any rain of given precipitation rate or vice versa.

It is, however, possible to draw in the (α,p) coordinate plane a straight line which, at a given wavelength, will represent the theoretical upper limit for the attenuation. Indeed, using Table 6 for the attenuation in fictitious rains with a distribution of one drop per cubic centimeter, and Table 9, giving the precipitation associated with the same fictitious rains, one may compute the ratio α_k/p_k for any such rain formed by a single group of drops of diameter k cm and the precipitation rate p_k of the same rain. This ratio for a given wavelength λ of the radiation varies with k, the diameter of the drops, and in the diameter range 0 to 0.55 cm this ratio takes on an optimum value for a certain diameter D. This, then, is the slope of the straight line in the (α,p) plane which determines the theoretical upper limit α_{max} of the attenuation in any rain of total rainfall p.

TABLE 8. Precipitation rates p/N in fictitious rains with a concentration of one drop per cubic centimeter.

Drop diameter D, cm	p/N mm/hr
0.05	4.99×10^2
0.10	7.34×10^3
0.15	3.34×10^4
0.20	9.6×10^4
0.25	2.14×10^5
0.30	4.08×10^5
0.35	6.76×10^5
0.40	1.05×10^6
0.45	1.54×10^6
0.50	2.17×10^6
0.55	2.92×10^6

The different steps taken in computing the total attenuation equation (58) in a rain of total rate of fall of p mm per hour appear in Figure 10 where the drop size distribution and the partial attenuations due to the different drop groups of a 22.6-mm per

TABLE 9. Attenuation in rains of known drop size distribution and rate of fall (db/km).

mm/hr	1.25	3	5	8	10	λ, cm 15	20	30	50	75	100	Distribution
2.45	$1.93\,10^{-1}$	$4.92\,10^{-2}$	$4.24\,10^{-3}$	$1.23\,10^{-3}$	$7.34\,10^{-4}$	$2.90\,10^{-4}$	$1.52\,10^{-4}$	$6.49\,10^{-5}$	$2.33\,10^{-5}$	$1.03\,10^{-5}$	$5.85\,10^{-6}$	A
4.0	$3.18\,10^{-1}$	$8.63\,10^{-2}$	$7.11\,10^{-3}$	$2.04\,10^{-3}$	$1.19\,10^{-3}$	$4.69\,10^{-4}$	$2.53\,10^{-4}$	$1.08\,10^{-4}$	$3.88\,10^{-5}$	$1.72\,10^{-5}$	$9.75\,10^{-6}$	C
6.0	$6.15\,10^{-1}$	$1.92\,10^{-1}$	$1.25\,10^{-2}$	$3.02\,10^{-3}$	$1.67\,10^{-3}$	$5.84\,10^{-4}$	$3.02\,10^{-4}$	$1.25\,10^{-4}$	$4.34\,10^{-5}$	$1.93\,10^{-5}$	$1.09\,10^{-5}$	D
15.2	2.12	$6.13\,10^{-1}$	$5.91\,10^{-2}$	$1.17\,10^{-2}$	$5.68\,10^{-3}$	$1.69\,10^{-3}$	$7.85\,10^{-4}$	$2.95\,10^{-4}$	$9.28\,10^{-5}$	$4.15\,10^{-5}$	$2.35\,10^{-5}$	E
18.7	2.37	$8.01\,10^{-1}$	$5.13\,10^{-2}$	$1.10\,10^{-2}$	$6.46\,10^{-3}$	$1.85\,10^{-3}$	$9.09\,10^{-4}$	$3.60\,10^{-4}$	$1.30\,10^{-4}$	$5.36\,10^{-5}$	$3.03\,10^{-5}$	F
22.6	2.40	$7.26\,10^{-1}$	$5.29\,10^{-2}$	$1.21\,10^{-2}$	$6.96\,10^{-3}$	$2.37\,10^{-3}$	$1.17\,10^{-3}$	$4.51\,10^{-4}$	$1.66\,10^{-4}$	$7.41\,10^{-5}$	$4.19\,10^{-5}$	G
34.3	4.51	1.28	$1.12\,10^{-1}$	$2.82\,10^{-2}$	$1.17\,10^{-2}$	$3.64\,10^{-3}$	$1.75\,10^{-3}$	$6.83\,10^{-4}$	$2.24\,10^{-4}$	$9.95\,10^{-5}$	$5.63\,10^{-5}$	H
43.1	6.17	1.64	$1.65\,10^{-1}$	$3.33\,10^{-2}$	$1.62\,10^{-2}$	$4.96\,10^{-3}$	$2.39\,10^{-3}$	$8.71\,10^{-4}$	$2.78\,10^{-4}$	$1.23\,10^{-4}$	$6.96\,10^{-5}$	I
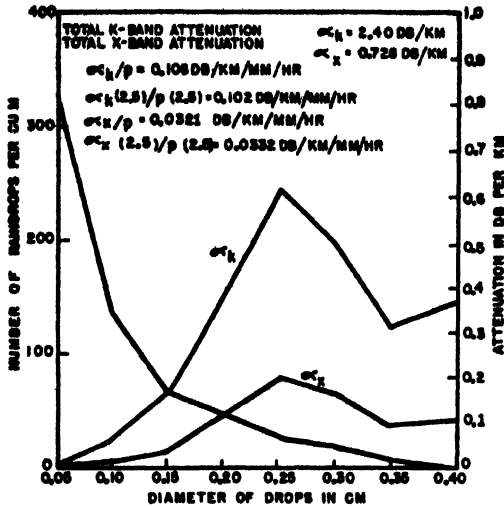
FIGURE 10. Drop size distribution and attenuation in a 22.6-mm per hr rain. Unlabeled curve represents N_k values; number of raindrops per cu m $= N_k$.

hour rain are plotted. It is seen that the numerous smaller drops hardly contribute to the attenuation, which is caused mostly by the fewer larger drops and has a maximum around the 2.5-mm drops.

In Table 9 is given the total attenuation (decibels per kilometer) in the wavelength range 1.25 to 100 cm in different rains of precipitation rates ranging from 2.46 to 43.1 mm per hour corresponding to given distributions. In Figure 11 are plotted some
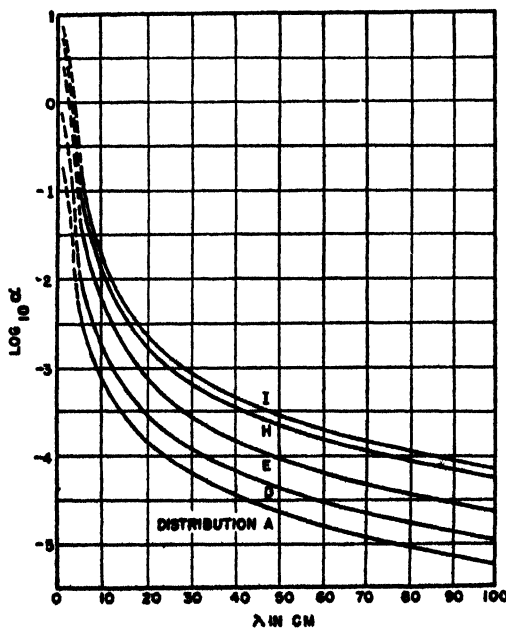
FIGURE 11. Attenuation in rains of known drop size distribution as a function of the wavelength. The abscissa gives the wavelength, λ, in centimeters. The ordinate scale gives $\log_{10} \alpha$, where the attenuation constant, α, is expressed in decibels per kilometer. The letters on the curves refer to the drop size distributions given in Table 7.
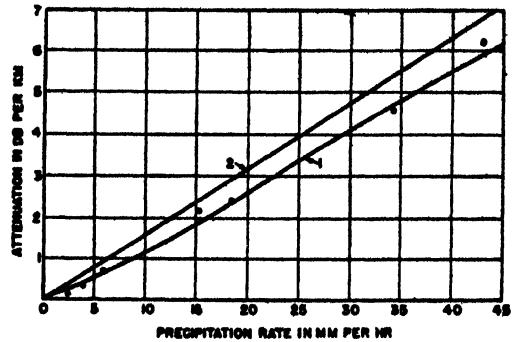
FIGURE 12. (1) Computed K-band attenuation based on experimental drop size distributions. (2) Theoretical upper limit. $\alpha/p = 0.16$ db/km/mm/hr. $t = 18$ C.

curves showing, for a few rains, the variation of the total attenuation factor as a function of the wavelength. The dashed portions of these curves join the points previously computed,[13] the calculations starting at $\lambda = 5$ cm.

Figures 12, 13, and 14 represent, at three typical wavelengths, the total attenuations in different rains. The results of the calculation are represented by the
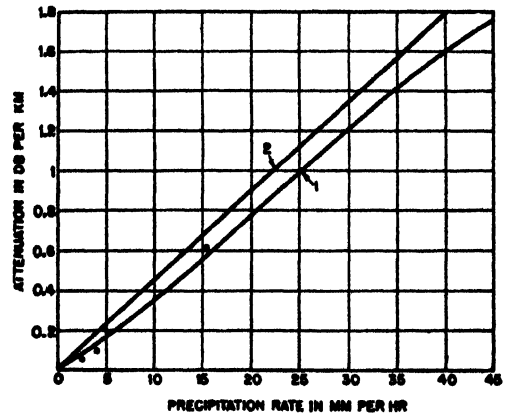
FIGURE 13. (1) Computed X-band attenuation based on experimental drop size distributions. (2) Theoretical upper limit. $\alpha/p = 0.045$ db/km/mm/hr. $t = 18$ C
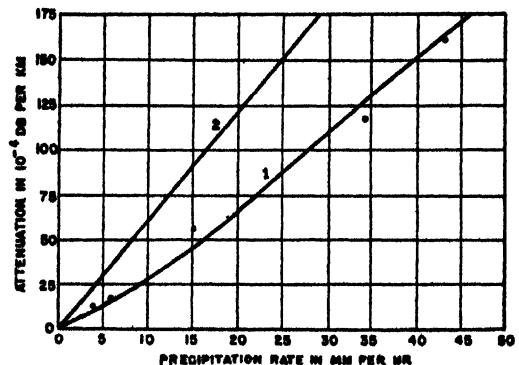
FIGURE 14. (1) Computed S-band attenuations based on experimental drop size distributions in different rains. (2) Theoretical upper limit of α/p, attenuation per unit rate of precipitation, is 6.10^{-4} db/km/mm/hr. $t = 18$ C.

points indicated on these figures, and the smooth curve passing through these points serves to illustrate the procedure usually followed by the experimental workers, as we have already mentioned. It is evident that these curves have little, if any, direct physical significance. Similarly the curves of Figure 11 associated with different rains merely indicate the trend of variation of α as a function of the wavelength, since no single curve of this type can characterize a rain of given total precipitation rate of p mm per hour.

Table 9 shows that the attenuation is of no practical importance for S band and longer waves even with the heaviest rains or cloudbursts. This result is summarized in Table 10 (the theoretical upper limits of the attenuations per unit precipitation rate).

TABLE 10.　Theoretical upper limits of attenuation per unit precipitation rate ($t \sim 18°C$).

λ, cm	$(\alpha/p)_{max}$ db/km/mm/hr
1.25	1.6×10^{-1}
3	4.5×10^{-2}
5	5.0×10^{-3}
8	1.0×10^{-3}
10	6.0×10^{-4}
15	3.0×10^{-4}
20	1.4×10^{-4}
30	6.4×10^{-5}

These values in Table 10 correspond to raindrop temperatures of about 18 C. At lower temperatures the values of (α/p) included in this table might be increased about 25 to 30 per cent.

The results of the different workers in the field are summarized in Table 11.

It will be seen that the above values of α/p compare favorably with the theoretical values.[j] The difficulties

TABLE 11.　Experimental values of the attenuation per unit precipitation rate.

λ, cm	(α/p) db/km/mm/hr	Authority
0.62	0.37	Mueller[5]
0.96	0.15	Adam et al[24]
1.089	0.2	Robertson[27]
1.25	{ 0.19	Southworth et al[29]
	{ 0.09—0.40	Rado[10]
3.2	0.032—0.042	King and Robertson[30]

in the interpretation of the experimental data as mentioned already should be kept in mind when comparing the experimental values with the theoretical predictions.

As remarked by Ryde and Ryde,[12] the attenuation by hailstones and snow should be appreciably smaller than that due to raindrops, the dielectric constant of ice being considerably smaller than that of liquid water.

A final remark may be made concerning the theoretical results given here. It has been assumed throughout the preceding discussion that the raindrops are

---

[j] The same seems to be true of S-band wavelengths where rough attenuation measurements are available in "solid" storm clouds.[31]

spherical. This is likely to be the case with practically all the drop groups existing in rains, with the exception of the biggest drops, which may undergo deformations. Presumably the effects of small deformations are not of great importance.

The Scattering of Microwaves by Spherical Raindrops

The cross section for scattering of electromagnetic waves by spherical particles is given for any direction by equation (34). Using the approximate expressions of the amplitudes as given by equations (38) and (43) and the notation $a_1^{(6)}$, $\bar{a}_1^{(6)}$, $\beta_1^{(3)}$, $\bar{\beta}_1^{(3)}$ representing the real and imaginary coefficients of ρ^5 in a_1^r, of ρ^3 in b_1^r, etc., as indicated above, we get the following expression for the total scattering cross section:

$$Q_s = \frac{\lambda^2}{2\pi} \rho^6 \left\{ 3 \mid \beta_1^{(3)} \mid^2 + 6 [\beta_1^{(3)} \beta_1^{(6)} \right.$$
$$+ \bar{\beta}_1^{(3)} \bar{\beta}_1^{(6)}] \rho^2 + 6 [\beta_1^{(3)} \beta_1^{(6)} + \bar{\beta}_1^{(3)} \bar{\beta}_1^{(6)}] \rho^6$$
$$+ \{ 3 [\mid a_1^{(6)} \mid^2 + \mid \beta_1^{(6)} \mid^2]$$
$$+ 5 \mid \beta_2^{(6)} \mid^2 \} \rho^4 + 6 [\beta_1^{(6)} \beta_1^{(6)}$$
$$+ \bar{\beta}_1^{(6)} \bar{\beta}_1^{(6)}] \rho^6 + 3 \mid \beta_1^{(6)} \mid^2 \rho^6 + \cdots \right\} \text{ cm}^2.$$
$$(59)$$

Here, for instance,

$$\mid \beta_1^{(3)} \mid = [\beta_1^{(3)}]^2 + [\bar{\beta}_1^{(3)}]^2 ; \mid a_1^{(6)} \mid^2$$
$$= (a_1^{(6)})^2 + (\bar{a}_1^{(6)})^2, \text{ etc.}$$

For values of $\rho \ll 1$ and when the terms in ρ^2 and higher powers can be neglected in the braces, the total cross section for scattering reduces, using the explicit expressions of $\beta_1^{(3)}$ and $\bar{\beta}_1^{(3)}$, to

$$Q_{s, \rho \ll 1} = \frac{128\pi^5 a^6}{3\lambda^4} \cdot$$
$$\frac{(\epsilon_r - 1)^2 (\epsilon_r + 2)^2 + \epsilon_i^2 [2(\epsilon_r - 1)(\epsilon_r + 2) + 9] + \epsilon_i^4}{[(\epsilon_r + 2)^2 + \epsilon_i^2]^2} \text{ cm}^2.$$
$$(60)$$

When the dielectric absorption vanishes, i.e., $\epsilon_i \to 0$, this reduces further to

$$Q_{s, \rho \ll 1, \epsilon_i \to 0} = \frac{128\pi^5 a^6}{3\lambda^4} \left(\frac{n^2 - 1}{n^2 + 2} \right)^2 \text{ cm}^2, \quad (61)$$

which is the well-known Rayleigh scattering cross section, since $\epsilon_r = n^2$ in this case.

In Table 12 are given the scattering cross sections computed within the range of ρ, 0.00157 to 0.576, or in the drop diameter range 0.05 to 0.55 cm and wavelength range 3 to 100 cm. Needless to say, the actual cross sections for scattering at the larger ρ values are always larger than the Rayleigh cross sections [equation (60)]. For $\rho < 0.10$ the scattering cross sections are, within a few per cent, given by the first Rayleigh term (60) of equation (59). However, in the present case of absorbing spherical drops, the parametric

TABLE 12. Total scattering cross section Q_s (cm²) of spherical water drops of D cm diameter.

λ, cm	D, cm										
	0.05	0.10	0.15	0.20	0.25	0.30	0.35	0.40	0.45	0.50	0.55
3	$3.62\,10^{-8}$	$2.35\,10^{-6}$	$2.74\,10^{-5}$	$1.58\,10^{-4}$	$6.06\,10^{-4}$	$1.98\,10^{-3}$	$5.36\,10^{-3}$	$1.31\,10^{-2}$	$2.96\,10^{-2}$	$6.36\,10^{-2}$	$1.31\,10^{-1}$
5	$4.70\,10^{-9}$	$3.04\,10^{-7}$	$3.51\,10^{-6}$	$1.97\,10^{-5}$	$7.56\,10^{-5}$	$2.32\,10^{-4}$	$5.97\,10^{-4}$	$1.36\,10^{-3}$	$2.86\,10^{-3}$	$5.61\,10^{-3}$	$1.04\,10^{-2}$
8	$7.23\,10^{-10}$	$4.64\,10^{-8}$	$5.35\,10^{-7}$	$2.98\,10^{-6}$	$1.14\,10^{-5}$	$3.44\,10^{-5}$	$8.72\,10^{-5}$	$1.96\,10^{-4}$	$4.01\,10^{-4}$	$7.65\,10^{-4}$	$1.37\,10^{-3}$
10	$2.93\,10^{-10}$	$1.88\,10^{-8}$	$2.15\,10^{-7}$	$1.21\,10^{-6}$	$4.62\,10^{-6}$	$1.38\,10^{-5}$	$3.50\,10^{-5}$	$7.85\,10^{-5}$	$1.59\,10^{-4}$	$3.01\,10^{-4}$	$5.41\,10^{-4}$
15	$5.80\,10^{-11}$	$3.75\,10^{-9}$	$4.33\,10^{-8}$	$2.43\,10^{-7}$	$9.03\,10^{-7}$	$2.70\,10^{-6}$	$6.80\,10^{-6}$	$1.52\,10^{-5}$	$3.10\,10^{-5}$	$5.87\,10^{-5}$	$1.04\,10^{-4}$
20	$1.83\,10^{-11}$	$1.17\,10^{-9}$	$1.35\,10^{-8}$	$7.51\,10^{-8}$	$2.86\,10^{-7}$	$8.53\,10^{-7}$	$2.16\,10^{-6}$	$4.81\,10^{-6}$	$9.74\,10^{-6}$	$1.83\,10^{-5}$	$3.25\,10^{-5}$
30	$3.62\,10^{-12}$	$2.32\,10^{-10}$	$2.66\,10^{-9}$	$1.49\,10^{-8}$	$5.66\,10^{-8}$	$1.69\,10^{-7}$	$4.11\,10^{-7}$	$9.51\,10^{-7}$	$1.92\,10^{-6}$	$3.62\,10^{-6}$	$6.43\,10^{-6}$
50	$4.65\,10^{-13}$	$2.99\,10^{-11}$	$3.44\,10^{-10}$	$1.91\,10^{-9}$	$7.29\,10^{-9}$	$2.18\,10^{-8}$	$5.51\,10^{-8}$	$1.22\,10^{-7}$	$2.48\,10^{-7}$	$4.65\,10^{-7}$	$8.27\,10^{-7}$
75	$9.22\,10^{-14}$	$5.91\,10^{-12}$	$6.79\,10^{-11}$	$3.78\,10^{-10}$	$1.44\,10^{-9}$	$4.31\,10^{-9}$	$1.08\,10^{-8}$	$2.42\,10^{-8}$	$4.91\,10^{-8}$	$9.22\,10^{-8}$	$1.63\,10^{-7}$
100	$2.93\,10^{-14}$	$1.88\,10^{-12}$	$2.15\,10^{-11}$	$1.20\,10^{-10}$	$4.56\,10^{-10}$	$1.37\,10^{-9}$	$3.45\,10^{-9}$	$7.64\,10^{-9}$	$1.56\,10^{-8}$	$2.93\,10^{-8}$	$5.20\,10^{-8}$

representation (59) of the cross section is not of much practical interest since some of the coefficients of the powers of ρ are strongly dependent on the wavelength. The cross section is not a unique function of $\rho = (\pi D/\lambda)$ but is a complicated function of λ and D, and the series representation is valid only in describing the dependence on the diameter D of the drops, the wavelength being kept constant. In Figures 15 and 16 two families of curves have been plotted representing Q_s as a function of the diameter D of the raindrops at constant wavelength and as a function of the wavelength at constant diameter, respectively.

The knowledge of the total scattering cross section Q_s and the total cross section Q_t allows at once the computation of the absolute probabilities $\tilde{\omega}_s$ for electromagnetic waves falling on spherical water drops to be scattered in any direction and the absolute probabilities $\tilde{\omega}_{abs}$ for being absorbed by the drops, the absorbed energy being then transformed into heat in the drops (true absorption). Indeed, this probability ω_s of the waves being scattered in any direction is equal to the ratio of the scattering cross section Q_s to the cross section Q_t which is associated with all the possible eventualities, here only two, namely, scattering and true absorption. Hence,

$$\tilde{\omega}_s = \frac{Q_s}{Q_t} \qquad (62)$$

and, consequently, the probability of true absorption is

$$\tilde{\omega}_{abs} = 1 - \tilde{\omega}_s. \qquad (63)$$
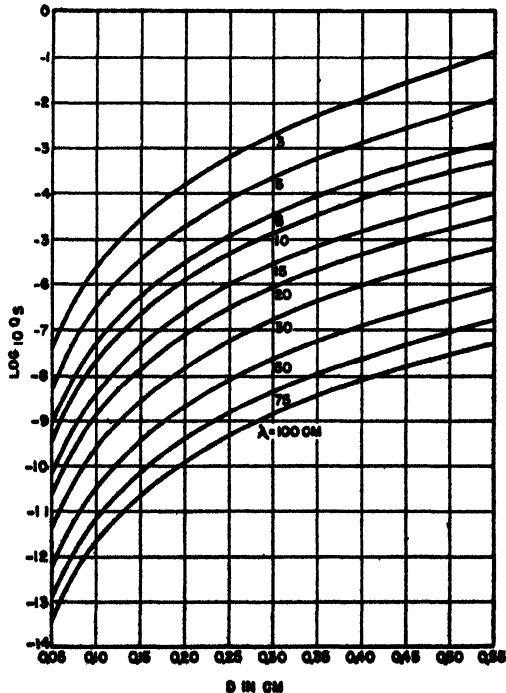
FIGURE 15. Scattering cross section, Q_s, of spherical water drops as a function of the drop diameter. The abscissa gives the drop diameter, D, in centimeters. The ordinate scale gives $\log_{10} Q_s$, the scattering cross section Q, being expressed in square centimeters. The numbers on the curves indicate the wavelength, λ, of the incident radiation in centimeters.
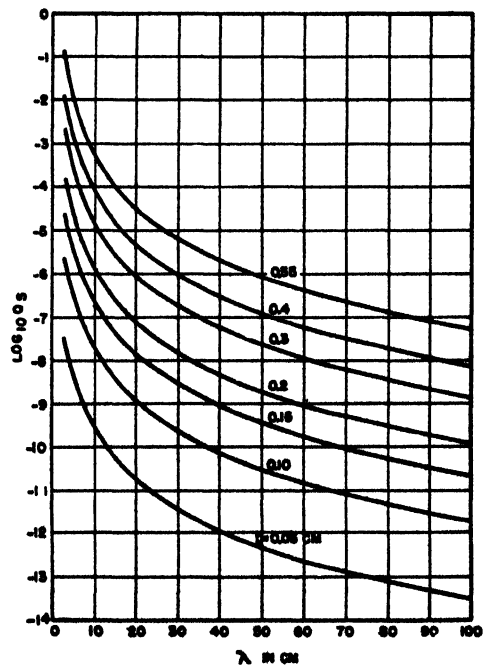
FIGURE 16. Scattering cross section, Q_s, of spherical water drops as a function of the wavelength. The abscissa gives the wavelength, λ, of the incident radiation in centimeters. The ordinate scale gives $\log_{10} Q_s$, the cross section Q, being expressed in square centimeters. The numbers of the curves indicate the drop diameter, D, in centimeters.

In Table 13 are given the probabilities $\tilde{\omega}_s$ in the drop diameter range 0.05 to 0.55 cm and wavelength range 3 to 100 cm. A glance at this table shows that with the exception of the shortest wavelengths and largest drops the probability of the waves being truly absorbed is always much larger than that of their being scattered. The smaller the drops the greater the chance of absorption, since, according to the cross-section formulas, for small drops Q_s is proportional to D^6/λ^4 (Rayleigh's law) whereas $Q_t \sim Q_{abs}$ is proportional to D^3/λ and in our case the drop diameter D is always smaller than the wavelength λ of the radiation.

$$= \left(\frac{\lambda}{2\pi}\right)^2 \mathrm{Re} \sum_{n=1}^{n=\infty} \sum_{m=1}^{m=\infty} \frac{(2n+1)(2m+1)}{n(n+1)\,m(m+1)} \cdot$$

$$\left[a_n a_m^* \left(\frac{P_n^1 P_m^1}{\sin^2 \theta} \cos^2 \phi + \frac{dP_n^1}{d\theta} \frac{dP_m^1}{d\theta} \sin^2 \phi \right) \right.$$

$$+ b_n b_m^* \left(\frac{P_n^1 P_m^1}{\sin^2 \theta} \sin^2 \phi + \frac{dP_n^1}{d\theta} \frac{dP_m^1}{d\theta} \cos^2 \phi \right)$$

$$\left. + 2a_n b_m^* \left(\frac{P_n^1}{\sin \theta} \frac{dP_m^1}{d\theta} \cos^2 \phi + \frac{P_m^1}{\sin \theta} \frac{dP_n^1}{d\theta} \sin^2 \phi \right) \right] \mathrm{cm}^2 .$$

$$(65)^k$$

TABLE 13. Probability of scattering $\tilde{\omega}_s$ by spherical water drops of D cm diameter.

D, cm	λ, cm									
	3	5	8	10	15	20	30	50	75	100
0.05	$3.94\ 10^{-3}$	$1.64\ 10^{-3}$	$6.63\ 10^{-4}$	$4.25\ 10^{-4}$	$1.94\ 10^{-4}$	$1.09\ 10^{-4}$	$4.92\ 10^{-5}$	$1.74\ 10^{-5}$	$7.74\ 10^{-6}$	$4.33\ 10^{-6}$
0.10	$1.54\ 10^{-2}$	$1.09\ 10^{-2}$	$4.89\ 10^{-3}$	$3.22\ 10^{-3}$	$1.53\ 10^{-3}$	$8.60\ 10^{-4}$	$3.91\ 10^{-4}$	$1.40\ 10^{-4}$	$6.33\ 10^{-5}$	$3.47\ 10^{-5}$
0.15	$2.11\ 10^{-2}$	$2.90\ 10^{-2}$	$1.47\ 10^{-2}$	$9.96\ 10^{-3}$	$5.00\ 10^{-3}$	$2.87\ 10^{-3}$	$1.32\ 10^{-3}$	$4.73\ 10^{-4}$	$2.11\ 10^{-4}$	$1.17\ 10^{-4}$
0.20	$2.86\ 10^{-2}$	$5.15\ 10^{-2}$	$2.91\ 10^{-2}$	$2.10\ 10^{-2}$	$1.11\ 10^{-2}$	$6.51\ 10^{-3}$	$3.05\ 10^{-3}$	$1.10\ 10^{-3}$	$3.95\ 10^{-4}$	$2.76\ 10^{-4}$
0.25	$3.72\ 10^{-2}$	$7.60\ 10^{-2}$	$4.75\ 10^{-2}$	$3.16\ 10^{-2}$	$1.97\ 10^{-2}$	$1.21\ 10^{-2}$	$5.81\ 10^{-3}$	$2.14\ 10^{-3}$	$9.66\ 10^{-4}$	$5.37\ 10^{-4}$
0.30	$5.31\ 10^{-2}$	$1.03\ 10^{-1}$	$6.91\ 10^{-2}$	$5.33\ 10^{-2}$	$3.12\ 10^{-2}$	$1.75\ 10^{-2}$	$9.77\ 10^{-3}$	$3.66\ 10^{-3}$	$1.61\ 10^{-3}$	$9.32\ 10^{-4}$
0.35	$8.06\ 10^{-2}$	$1.29\ 10^{-1}$	$9.06\ 10^{-2}$	$7.28\ 10^{-2}$	$4.50\ 10^{-2}$	$2.96\ 10^{-2}$	$1.45\ 10^{-2}$	$5.76\ 10^{-3}$	$2.60\ 10^{-3}$	$1.47\ 10^{-3}$
0.40	$1.21\ 10^{-1}$	$1.54\ 10^{-1}$	$1.13\ 10^{-1}$	$9.31\ 10^{-2}$	$6.06\ 10^{-2}$	$4.11\ 10^{-2}$	$2.17\ 10^{-2}$	$8.42\ 10^{-3}$	$3.88\ 10^{-3}$	$2.18\ 10^{-3}$
0.45	$1.95\ 10^{-1}$	$1.84\ 10^{-1}$	$1.35\ 10^{-1}$	$1.14\ 10^{-1}$	$7.79\ 10^{-2}$	$5.47\ 10^{-2}$	$2.96\ 10^{-2}$	$1.19\ 10^{-2}$	$5.50\ 10^{-3}$	$3.11\ 10^{-3}$
0.50	$2.96\ 10^{-1}$	$2.17\ 10^{-1}$	$1.58\ 10^{-1}$	$1.34\ 10^{-1}$	$9.63\ 10^{-2}$	$6.88\ 10^{-2}$	$3.90\ 10^{-2}$	$1.59\ 10^{-2}$	$7.43\ 10^{-3}$	$4.23\ 10^{-3}$
0.55	$4.82.\ 10^{-1}$	$2.49\ 10^{-1}$	$1.80\ 10^{-1}$	$1.56\ 10^{-1}$	$1.15\ 10^{-1}$	$8.44\ 10^{-2}$	$4.95\ 10^{-2}$	$2.08\ 10^{-2}$	$9.82\ 10^{-3}$	$5.61\ 10^{-3}$

Back Scattering (Echoes)

Whereas the attenuation of microwaves is of interest to both communication and radar, back scattering is of importance to radar only. The importance of the echo phenomena is twofold. On the one hand, it is of operational interest to distinguish between atmospheric echoes of the waves and their reflection from other targets in the atmosphere. On the other hand, the observation of these phenomena has led to the recognition of its meteorological value in helping to map the storm topography of the atmosphere (storm detection) around the position of the observer and at ranges limited only by the characteristics of the radar set used.[14,31-33]

The echo intensities may be computed from formula (35) for the differential cross section of drops $\sigma(\pi)$ for back scattering (scattering angle π).

According to equation (22), the power scattered by a spherical particle per unit solid angle at a point (r, θ, ϕ) is

$$\left(\frac{dP_s}{d\omega}\right)_{\theta,\phi} = \frac{1}{2\eta_2} \cdot [\,|E_\theta^s|^2 + |E_\phi^s|^2\,]\, r^2 . \quad (64)$$

Using equations (16) and (17), we obtain, remembering that the incident power per unit area is $(1/2\eta_2)\, E_0^2$, the following expression for the differential scattering cross section:

$$\left(\frac{dQ_s}{d\omega}\right)_{\theta,\phi} = \sigma(\theta,\phi)$$

Or, limiting ourselves to the approximation where only the electric dipole (b_1), electric quadrupole (b_2), and magnetic dipole (a_1) are effective, we find, using the explicit expressions of the associated Legendre polynomials,

$$\left(\frac{dQ_s}{d\omega}\right)_{\theta,\phi} = \sigma(\theta, \phi)$$

$$= \left(\frac{\lambda}{4\pi}\right)^2$$

$$\mathrm{Re}\left[9|b_1|^2 (\sin^2 \phi + \cos^2 \theta \cos^2 \phi) + 9|a_1|^2(\cos^2 \phi \right.$$
$$+ \cos^2 \theta \sin^2 \phi)$$
$$+ 25|b_2|^2 (\cos^2 \theta \sin^2 \phi + \cos^2 (2\theta)\cos^2 \phi)$$
$$+ 18 a_1 b_1^* \cos\theta + 30 b_1 b_2^* \cos\theta(\sin^2 \phi + \cos(2\theta)\cos^2\phi)$$
$$\left. + 30 a_1 b_2^*(\cos^2\theta \sin^2\phi + \cos(2\theta)\cos^2\phi) \right]\mathrm{cm}^2. \quad (66)$$

Here the first term inside the brackets represents the contribution of the electric dipole, the second is the magnetic dipole term, the third is the electric quadrupole term, and the three others correspond to interference terms between these three poles.

In the optical case it is known that the larger the parameter $\rho = \pi D/\lambda$, i.e., the nearer the wavelength is to the diameter of the scattering sphere, the more the radiation is scattered forward than backward. A study of equation (66) for water drops of 1-cm diameter shows that for spheres of this size it is only when $\lambda \geq 15$ cm or $\rho \leq 0.2$ that the back-scattered intensity

---

[k] With $\theta = \pi$ this reduces to equation (27) of the radar cross section.

is about the same as the forward-scattered intensity. For such ρ values only the dipole term in equation (66) remains of practical importance.

Suppose that we adopt a ρ value of 0.2 as a rough indication of what happens in the case of actual raindrops, the diameter of which is less than about 0.55 cm. It is then seen that for radar purposes the use of longer waves is favored, as far as the amount of backscattered power is concerned, viz., in those cases where the greatest amount of back scattering from water drops is of operational importance. This will clearly occur in radar meteorology. However, when it is desirable to limit as much as possible the back scattering from rain or rainclouds, one might make use of this forward-backward scattering dissymmetry, which is the more pronounced the shorter the wavelength as compared with the diameter of the raindrops. This dissymmetry might, however, be counterbalanced by a rapid increase in the attenuation as well as a general decrease in the intensity of scattering.

The differential cross section for back scattering results from equation (66) by taking $\theta = \pi$ there. Using the explicit expressions (43) of the amplitudes a_1, b_1, and b_2, one obtains for this back scattering (or radar cross section)

$$\sigma(\pi) = \left(\frac{\lambda}{4\pi}\right)^2 \rho^6 (A_0 + A_2\rho^2 + A_3\rho^3 + A_4\rho^4 + A_5\rho^5 + A_6\rho^6 + \cdots)\ \text{cm}^2, \quad (67)$$

with the following coefficients A^n, using the notation defined by equations (45), (46), and (59):

$$A_0 = 9|\beta_1^{(3)}|^2,$$

$$A_2 = 18\,[\beta_1^{(3)}\beta_1^{(5)}\bar{\beta}_1^{(3)}\bar{\beta}_1^{(5)} - \alpha_1^{(5)}\beta_1^{(3)} - \bar{\alpha}_1^{(5)}\bar{\beta}_1^{(3)}] - 30\,[\beta_1^{(3)}\beta_2^{(5)} + \bar{\beta}_1^{(3)}\bar{\beta}_2^{(5)}],$$

$$A_3 = 18\,[\beta_1^{(3)}\beta_1^{(6)} + \bar{\beta}_1^{(3)}\bar{\beta}_1^{(6)}], \quad (68)$$

$$A_4 = 9\,[|\alpha_1^{(5)}|^2 + |\beta_1^{(5)}|^2] - 18\,[\alpha_1^{(5)}\beta_1^{(5)} + \bar{\alpha}_1^{(5)}\bar{\beta}_1^{(5)}] - 30\,[\beta_1^{(5)}\beta_2^{(5)} + \bar{\beta}_1^{(5)}\bar{\beta}_2^{(5)} - \alpha_1^{(5)}\beta_2^{(5)} - \bar{\alpha}_1^{(5)}\bar{\beta}_2^{(5)}] + 25|\beta_2^{(5)}|^2,$$

$$A_5 = 18\,[\beta_1^{(5)}\beta_1^{(6)} + \bar{\beta}_1^{(5)}\bar{\beta}_1^{(6)} - \alpha_1^{(5)}\beta_1^{(6)} - \bar{\alpha}_1^{(5)}\bar{\beta}_1^{(6)}] - 30\,[\beta_1^{(6)}\beta_2^{(5)} + \bar{\beta}_1^{(6)}\bar{\beta}_2^{(5)}],$$

$$A_6 = 9|\beta_1^{(6)}|^2.$$

The radar cross-section formula (67) is the same as that given by Ryde.[17] Again $\sigma(\pi)$ is not a function of ρ only since the coefficients of the successive powers of ρ in the expansion (67) depend on the wavelength. The computed echo cross sections $\sigma(\pi)$ for spherical water drops with diameters in the range 0.05 to 0.55 cm and the wavelength range 3 to 100 cm are given in Table 14.[1] These cross sections reduce practically to the Rayleigh type, i.e., the series (67) reduces to its first term for the smaller drops at any wavelength and for any drops for wavelengths larger than about 15 cm. Since the Rayleigh term predominates in $\sigma(\pi)$, with the exception of the larger drops and smaller wavelengths, the trends of variation of $\sigma(\pi)$ with either the diameter, at constant wavelength, or the wavelength, at constant diameter, are similar to those of Q_s, the total scattering cross section. A graphical representation of the data of Table 14 is thus of no particular interest; they appear implicitly in Figures 15 and 16.

In order to compute the radar attenuation factor α associated with echo phenomena occurring with rain of known drop size distribution, we have but to use equation (31) and hence obtain for N_k drops of k cm diameter per cm^3,

$$\alpha_{\pi,k} = \tfrac{1}{2}N_k\,\sigma_k(\pi)\ \text{neper/cm}, \quad (69)^m$$

and for a given distribution of particles

$$\alpha_\pi = \sum_{k=0}^{s} \alpha_{\pi,k} = \frac{1}{2}\sum_{k=0}^{s} N_k\,\sigma_k(\pi)\ \text{neper/cm}. \quad (70)$$

Using the radar cross section of Table 14 and the drop size distributions in different rains as given in Table 7, we have computed α_π, the attenuation factor due to back scattering in the wavelength range 3 to 100 cm. The results of these calculations are included in Table 15 and in Figure 17. The variation of α_π is represented as a function of the wavelength of the incident radia-

---

[1] For the shorter waves and large drops the cross sections given are merely orders of magnitude, as the convergence of equation (67) is too slow in that case; in fact, it is even slower than the expression for Q_s.

[m] The coherent portion of the scattering is neglected here on account of the assumed random distribution of the scatterers. See, nevertheless, a recent note by F. Hoyle.[34]

TABLE 14. Back scattering cross section $\sigma(\pi)$ (cm^2) of spherical water drops of D cm diameter.

D, cm	λ, cm									
	3	5	8	10	15	20	30	50	75	100
0.05	$4.25\ 10^{-9}$	$5.55\ 10^{-10}$	$8.63\ 10^{-11}$	$3.50\ 10^{-11}$	$6.96\ 10^{-12}$	$2.18\ 10^{-12}$	$4.32\ 10^{-13}$	$5.60\ 10^{-14}$	$1.11\ 10^{-14}$	$3.50\ 10^{-15}$
0.10	$2.64\ 10^{-7}$	$3.52\ 10^{-8}$	$5.47\ 10^{-9}$	$2.24\ 10^{-9}$	$4.44\ 10^{-10}$	$1.40\ 10^{-10}$	$2.77\ 10^{-11}$	$3.59\ 10^{-12}$	$7.09\ 10^{-13}$	$2.24\ 10^{-13}$
0.15	$2.88\ 10^{-6}$	$3.97\ 10^{-7}$	$6.28\ 10^{-8}$	$2.54\ 10^{-8}$	$5.10\ 10^{-9}$	$1.60\ 10^{-9}$	$3.18\ 10^{-10}$	$4.12\ 10^{-11}$	$8.14\ 10^{-12}$	$2.57\ 10^{-12}$
0.20	$1.48\ 10^{-5}$	$2.15\ 10^{-6}$	$3.45\ 10^{-7}$	$1.42\ 10^{-7}$	$2.84\ 10^{-8}$	$8.94\ 10^{-9}$	$1.77\ 10^{-9}$	$2.29\ 10^{-10}$	$4.52\ 10^{-11}$	$1.43\ 10^{-11}$
0.25	$5.02\ 10^{-5}$	$7.42\ 10^{-6}$	$1.30\ 10^{-6}$	$5.34\ 10^{-7}$	$1.07\ 10^{-7}$	$3.42\ 10^{-8}$	$6.73\ 10^{-9}$	$8.72\ 10^{-10}$	$1.72\ 10^{-10}$	$5.45\ 10^{-11}$
0.30	$1.34\ 10^{-4}$	$2.25\ 10^{-5}$	$3.80\ 10^{-6}$	$1.57\ 10^{-6}$	$3.19\ 10^{-7}$	$1.20\ 10^{-7}$	$2.02\ 10^{-8}$	$2.62\ 10^{-9}$	$5.17\ 10^{-10}$	$1.64\ 10^{-10}$
0.35	$2.48\ 10^{-4}$	$5.40\ 10^{-5}$	$9.37\ 10^{-6}$	$3.91\ 10^{-6}$	$8.01\ 10^{-7}$	$2.58\ 10^{-7}$	$5.04\ 10^{-8}$	$6.53\ 10^{-9}$	$1.29\ 10^{-9}$	$4.08\ 10^{-10}$
0.40	$5.04\ 10^{-4}$	$1.12\ 10^{-4}$	$2.03\ 10^{-5}$	$8.55\ 10^{-6}$	$1.77\ 10^{-6}$	$5.75\ 10^{-7}$	$1.13\ 10^{-7}$	$1.46\ 10^{-8}$	$2.88\ 10^{-9}$	$9.13\ 10^{-10}$
0.45	$7.76\ 10^{-4}$	$2.12\ 10^{-4}$	$3.99\ 10^{-5}$	$1.70\ 10^{-5}$	$3.55\ 10^{-6}$	$1.16\ 10^{-6}$	$2.32\ 10^{-7}$	$3.00\ 10^{-8}$	$5.92\ 10^{-9}$	$1.87\ 10^{-9}$
0.50	$9.91\ 10^{-4}$	$3.65\ 10^{-4}$	$7.30\ 10^{-5}$	$3.14\ 10^{-5}$	$6.63\ 10^{-6}$	$2.18\ 10^{-6}$	$4.32\ 10^{-7}$	$5.60\ 10^{-8}$	$1.11\ 10^{-8}$	$3.50\ 10^{-9}$
0.55	$5.95\ 10^{-4}$	$5.82\ 10^{-4}$	$1.24\ 10^{-4}$	$5.44\ 10^{-5}$	$1.16\ 10^{-5}$	$3.87\ 10^{-6}$	$7.70\ 10^{-7}$	$9.98\ 10^{-8}$	$1.97\ 10^{-8}$	$6.24\ 10^{-9}$

TABLE 15. Absorption coefficient due to back scattering (echo) $2\alpha_r$ km^{-1} in rains of known drop size distribution and rate of fall.

mm/hr	3	5	8	10	15	λ, cm 20	30	50	75	100	Distribution
2.46	$2.94\ 10^{-5}$	$4.21\ 10^{-6}$	$7.01\ 10^{-7}$	$2.86\ 10^{-7}$	$5.74\ 10^{-8}$	$1.82\ 10^{-8}$	$3.60\ 10^{-9}$	$4.66\ 10^{-10}$	$9.20\ 10^{-11}$	$2.91\ 10^{-11}$	A
4.0	$5.06\ 10^{-5}$	$7.31\ 10^{-6}$	$1.17\ 10^{-6}$	$4.81\ 10^{-7}$	$9.63\ 10^{-8}$	$3.03\ 10^{-8}$	$5.99\ 10^{-9}$	$7.76\ 10^{-10}$	$1.53\ 10^{-10}$	$4.85\ 10^{-11}$	C
6.0	$1.44\ 10^{-4}$	$2.32\ 10^{-5}$	$3.90\ 10^{-6}$	$1.61\ 10^{-6}$	$3.25\ 10^{-7}$	$1.17\ 10^{-7}$	$2.31\ 10^{-8}$	$2.99\ 10^{-9}$	$5.91\ 10^{-10}$	$1.87\ 10^{-10}$	D
15.2	$6.12\ 10^{-4}$	$1.73\ 10^{-4}$	$3.30\ 10^{-5}$	$1.41\ 10^{-5}$	$2.94\ 10^{-6}$	$7.62\ 10^{-7}$	$1.50\ 10^{-7}$	$1.94\ 10^{-8}$	$3.83\ 10^{-9}$	$1.21\ 10^{-9}$	E
18.7	$6.67\ 10^{-4}$	$1.27\ 10^{-4}$	$2.22\ 10^{-5}$	$9.25\ 10^{-6}$	$1.90\ 10^{-6}$	$6.51\ 10^{-7}$	$1.28\ 10^{-7}$	$1.66\ 10^{-8}$	$3.28\ 10^{-9}$	$1.04\ 10^{-9}$	F
22.6	$5.69\ 10^{-4}$	$1.01\ 10^{-4}$	$1.74\ 10^{-5}$	$7.24\ 10^{-6}$	$1.47\ 10^{-6}$	$4.91\ 10^{-7}$	$9.70\ 10^{-8}$	$1.26\ 10^{-8}$	$2.49\ 10^{-9}$	$7.88\ 10^{-10}$	G
34.3	$1.28\ 10^{-3}$	$3.02\ 10^{-4}$	$5.58\ 10^{-5}$	$2.36\ 10^{-5}$	$4.90\ 10^{-6}$	$1.63\ 10^{-6}$	$3.22\ 10^{-7}$	$4.17\ 10^{-8}$	$8.24\ 10^{-9}$	$2.61\ 10^{-9}$	H
43.1	$1.83\ 10^{-3}$	$4.89\ 10^{-4}$	$9.16\ 10^{-5}$	$3.90\ 10^{-5}$	$8.14\ 10^{-6}$	$2.66\ 10^{-6}$	$5.26\ 10^{-7}$	$6.82\ 10^{-8}$	$1.35\ 10^{-8}$	$4.26\ 10^{-9}$	I
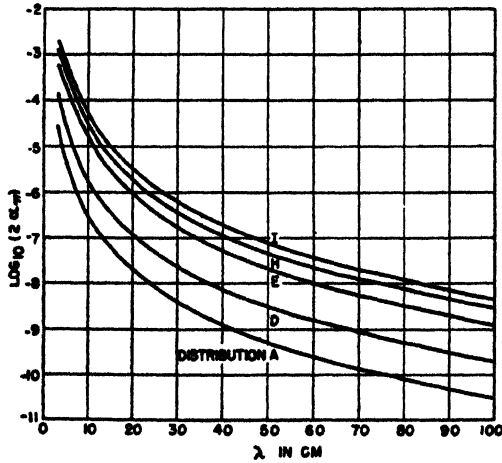
FIGURE 17. Absorption coefficient, $2\alpha_r$, due to back scattering (echo) as a function of the wavelength in different rains. The abscissa gives the wavelength, λ, in centimeters. The ordinate scale gives $\log_{10}(2\alpha_r)$, the absorption coefficient $2\alpha_r$ being expressed in km^{-1}. The letters on the curves refer to the drop size distributions listed in Table 7.

tion in different rains of given drop size distribution and precipitation rate. As already emphasized in connection with the study of the attenuation, these curves are characteristic, probably, of those rains, but they are not unique, since a given rain of known precipitation rate might very likely be built up from a variety of drop size distributions.

Since the absorption coefficient $(2\alpha_r)$ for back scattering represents also the fraction of the incident power back scattered per unit thickness of the scattering medium, Tables 14 and 15 allow the computation and estimation of the echo power to be expected in radar observations under given conditions. The difficulties which seemed to exist earlier are cleared up by assuming that in those clouds which give rise to echoes precipitation actually occurs, even though no rain reaches the ground.[12] This is substantiated to some extent by recent work[13] which succeeded in verifying Rayleigh's law by observing cloud echoes simultaneously with both S- and X-band radar sets. Further proof was added by the Canadian group,[14] whose exhaustive study in the S band clearly showed the role of raindrops in cloud echo phenomena. In fact, these workers

stated that there was no record of an echo without rain.

It is interesting to extract from Table 15 the fraction of the incident power back-scattered from different rains of 1-km depth expressed in decibels. As just mentioned, the power back-scattered by a thickness Δx is

$$\Delta P_\pi = -2\alpha_r P_i \Delta x, \qquad (71)$$

and the fraction of the incident power P_i scattered backward by a layer $\Delta x = 1$ km is then $10 \log_{10} \Delta P_\pi/P_i$ db or $(10 \log_{10} 2\alpha_r)$ db $(2\alpha_r)$ is given in Table 15. The results are included in Table 16.

With Table 16 and the known sensitivity of a radar set, the maximum free space distance from the set at which these rains are observable can be computed at

TABLE 16. Power scattered backward by a layer of 1 km of rain in different rains (decibels).

Distribution	p, mm/hr	3	5	8	λ, cm 10	15	20	30	50
A	2.46	−45	−54	−61	−65	−72	−77	−84	−93
D	6.0	−38	−46	−54	−58	−65	−69	−76	−85
E	15.2	−32	−37	−45	−48	−55	−61	−68	−77
H	34.3	−29	−35	−42	−46	−53	−58	−65	−74
I	43.1	−27	−33	−40	−44	−51	−56	−63	−71

once. The peak power received by a radar set from Volume 3, Chapters 2 and 9, is

$$P_2 = P_1 G_1 G_2 \frac{S_\pi}{4\pi d^2}\left(\frac{3\lambda}{8\pi d}\right)^2$$

where P_1 is the transmitted power (peak power),

G_1 and G_2 are respectively the transmitter and receiver antenna gains relative to a doublet,

d is the distance of the set from the echoing rain drops, and

S_π is the back scattering cross section.

The beam usually intersects the rain boundary and therefore it can be assumed that S_π is made up of the combination of all the drops included in the echoing volume. This volume may be taken as a spherical shell of thickness Δd whose base is a spherical segment of area

$$2\pi d^2(1 - \cos\theta),$$

2θ being approximately the half-power beam width of the set.

The rain echo cross section is then

$$S_\pi = 2\pi d^2 (1 - \cos \theta) \left[\Delta d \sum N_i \sigma_i(\pi) \right]$$

Here the summation extends over all the different drop groups forming the rain and $\sigma_i(\pi)$ is the differential cross section for back scattering in the direction π with the direction of propagation of the initial beam. It should be remembered that $\sigma_i(\pi)$ is the cross section per unit solid angle. Hence, the received peak power,

$$P_2 = \frac{P_1 G_1 G_2}{4} \left(\frac{3\lambda}{8\pi d}\right)^2 \theta^2 \left[\Delta d \sum N_i \sigma_i(\pi) \right]$$

for small θ (θ in radians). The quantity $[\sum N_i \sigma_i(\pi) \Delta d]$ is tabulated in Table 16 for $\Delta d = 1$ km and the different rains of Table 7. It is thus clear that the knowledge of the set characteristics permits at once the computation of the received power echoed by a rain falling at a certain distance r from the set provided the assumption is made that the echoing rain layer is 1 km thick. This is clearly arbitrary but is likely to give the right order of magnitude.

There has been discussed in a rather unorthodox way[12] the effect of the absorption on the back scattering of radiation taking into account also the finite pulse length of the radiation source.

These results seem to be consistent with the meager quantitative information available in this field. This fact would tend to classify the atmospheric radar echoes as back scattering phenomena due to water drops of precipitation size. It may further be re-emphasized that theory provides an adequate explanation for scattering and absorption of electromagnetic waves passing through different clouds or precipitation forms. The limitations imposed on the theoretical results are due essentially to irregularities inherent in the meteorological elements.

Summary

The present report gives a detailed review of the theoretical and experimental status of microwave atmospheric absorption. This absorption is due to the gases of the atmosphere, oxygen, and water vapor, on the one hand, and to the swarms of floating or falling water drops, clouds, fog, rain, and snow, on the other.

The status of the gaseous absorption of the atmosphere is reviewed briefly in Section 10.1.1. Figure 1 gives the oxygen and water vapor attenuation curves in the 0.2 to 10-cm wavelength range. The water vapor attenuation is given for a vapor content of 7.5 g/m³ of air, or 6.2 g per kilogram of air. In the equatorial belt, 15° S to 15° N, at sea level, the attenuation due to the atmospheric gases is approximately constant. It is about 0.18 and 0.008 db per kilometer for 1.25- and 3-cm waves respectively. In the tropical region the seasonal variation of these attenuations is quite large.

Figure 2 helps to give a clear picture of the atmospheric absorption due to oxygen and water vapor
simultaneously with the absorption in rains of different types. It is seen that in the wavelength range 1 to 5 cm the rain attenuation is more important than the gaseous atmospheric attenuation. The latter predominates at waves shorter than 1 cm and longer than about 5 cm, losing entirely its practical importance at these longer waves.

The theory of absorption and scattering of electromagnetic waves by dielectric spheres (see text on pp. 271-274) is briefly presented following the Rayleigh method as developed by Stratton.

The contribution of a swarm of spherical water drops of the same size, floating or falling in the atmosphere, to the average field strength attenuation factor is given by

$$\alpha = \frac{1}{2}NQ_t \text{ neper per unit length,}$$

where N is the average concentration of the drops, and Q_t their total cross section. This total cross section is the ratio of the power removed from the incident beam by one drop, through scattering and internal absorption to the power density of the incident beam. Similar definitions hold for the scattering cross section, absorption cross section and differential cross section for back scattering or radar cross section. The total cross section Q_t has the following form:

$$Q_t = \frac{\lambda^2}{2\pi} (-\text{Re}) \sum_{n=1}^{n=\infty} (2n+1) (a_n + b_n),$$

where λ denotes the wavelengths in free space of the incident radiation and a_n and b_n, ($n = 1,2,3,\ldots$) form an infinite set of scattering amplitudes or coefficients associated with magnetic and electric poles of increasing order induced in the water drop by the field strengths of the radiation. Thus a_1 is associated with a magnetic dipole, b_1 with an electric dipole, b_2 with an electric quadrupole, etc.

Pages 275-276 are devoted to study of the amplitudes a_n and b_n. These are complicated functions of the wavelength λ, diameter D, or radius a of the drops, as well as the complex refractive index N or dielectric constant ϵ_0 of water. Approximate expressions of the amplitudes can be derived by expanding them in series of ascending powers of the parameter $\rho = \pi D/\lambda$ for $\rho < 1$. Retaining only terms up to ρ^6, we found the following expressions of the first amplitudes,

$$a_1 = - \frac{j}{45} (N^2 - 1) \rho^5,$$

$$b_1 = - \frac{2j}{3} \frac{N^2-1}{N^2+2} \rho^3 \left(1 + \frac{3}{5} \frac{N^2-2}{N^2+2} \rho^2 - \frac{2j}{3} \frac{N^2-1}{N^2+2} \rho^3\right),$$

$$b_2 = - \frac{j}{15} \frac{N^2-1}{2N^2+3} \rho^5,$$

where N is the complex refractive index of water with respect to free space and $N^2 = \epsilon_0 = (\epsilon_r - j\epsilon_i)$ is its complex dielectric constant. The numerical computa-

tion of these amplitudes requires knowledge of the dielectric constant of water in the desired wavelength and temperature range. Whereas experimental data on the real part of the dielectric constant of water are relatively abundant in the microwave region and around 18 C, data on the imaginary part or the conductivity are very scarce. The Debye theory has, therefore, been used to compute the dielectric constant of water in the microwave region, and the theoretical results seem to be supported by the new experimental data (see Table 1). Recent data in the K-band on the temperature variation of the dielectric constant of water are given in Table 2. The graphical representation of both real and imaginary parts of the dielectric constant in the wavelength range 1 to 11 cm appears on Figure 4. The numerical values of a_1, b_1, and b_2 are discussed briefly at the end of this section.

The attenuation factor (see pp. 277-279) is here computed to the approximation of taking into account the amplitudes a_1, b_1, and b_2. Clearly, inasmuch as these amplitudes are expressed in the form of series in ascending powers of the parameter $\rho = \pi D/\lambda$, the attenuation factor takes on a similar form. One gets

$$\alpha = \frac{3\pi}{20} \frac{m}{\lambda} (c_1 + c_2\rho^2 + c_3\rho^3 + \cdots) \text{ neper per unit length,}$$

where m is the mass of liquid water in the form of drops per unit volume of the atmosphere, λ is the wavelength of the radiation in free space, and c_1, c_2, c_3, etc. are dimensionless coefficients depending on the wavelength implicitly through the dielectric constant of the substance of the sphere. For values of ρ small compared with unity, i.e., for waves long compared with the diameter of the drops, for which the terms in ρ^2, ρ^3, . . . can be neglected, the attenuation factor reduces to one term,

$$\alpha_{\rho \ll 1} = \frac{3\pi}{20} \frac{mc_1}{\lambda}$$

$$= \frac{9\pi}{10} \frac{m}{\lambda} \frac{\epsilon_i}{(\epsilon_r + 2)^2 + \epsilon_i^2} \text{ neper per unit length.}$$

This shows that for small drops or longer waves the attenuation factor becomes independent of the drop size and depends only on the amount of liquid water per unit volume present in the atmosphere. Table 3 contains (in the 1- to 100-cm wavelength range) the values of the coefficients c_1, c_2, c_3. It also gives the critical drop diameters below which, for a given λ, the one term attenuation formula holds within 10 per cent accuracy. A few values of D_c are the following:

λ, cm	1	1.26	3	5	10	15
D_c, cm	6.56×10⁻⁴	7.13×10⁻⁴	1.21×10⁻⁴	1.57×10⁻⁴	2.62×10⁻⁴	2.54×10⁻⁴

Table 4 gives the total cross section of spherical water drops in the diameter range 0.05 to 0.55 cm and wavelength range 1.25 to 100 cm. Table 5 gives

attenuation values in decibels per kilometer. Figures 5 and 6 represent in graphical form the variation of the absorption cross section and attenuation factor (1) at constant drop diameter, as a function of the wavelength, and (2) at constant wavelength, as a function of the drop diameter, respectively.

These results are directly applicable to any precipitation forms of which drop size distribution and average drop concentration have been determined.

Meteorological data necessary to the computation of the attenuation factor of different precipitation forms have been given on pages 279-280. Data on drop concentrations and drop size distributions are extremely scarce.

In liquid water clouds of different altitudes and in fogs, observations indicate that the drop diameters do not exceed 0.02 cm. In low and medium altitude good weather clouds the liquid water concentration varies between 0.15 and 0.50 g per cubic meter, and a concentration of 1 g/m³ is very likely an extreme upper limit. In fogs, with the possible exception of heavy sea fogs, the liquid water concentration seems to be considerably smaller.

The data on drop size distribution in rains used in this work are given in Table 6, and, in a different form, directly applicable to the computation of the attenuation factor, in Table 7. These data indicate that the precipitation rate does not determine the drop size distribution of a rain, inasmuch as a rain of given precipitation rate can be built up with different drop size distributions. It does not seem, therefore, that the precipitation rate can play the role of a true physical variable in the attenuation law of rains.

Attention is also called to observed irregularities in the precipitation rate over relatively small distances (about 1 km), which makes it difficult to interpret the experimental data on radio wave attenuations even in terms of this apparent variable of total precipitation rate. These and other meteorological irregularities seem to eliminate the possibility of a quantitative theory of attenuation or back scattering of radio waves by rain or other precipitation forms. Clearly, the experimental study of these as yet chaotic meteorological features might disclose certain trends which could be advantageously incorporated in the theory of attenuation of a stormy atmosphere.

Figure 7 gives the empirical relationship between the terminal velocity of raindrops and their diameter. The measurements cover practically the whole range of drops which reach the ground in rains, or from 0.05 to 0.55 cm. The terminal velocity of these drops varies between 2 and 9 m per second approximately. Figure 8 represents another empirical relationship between the liquid water concentration of the rainy atmosphere and the rate of rainfall. A rough linear approximation to the apparent empirical curve leads to a water content 0.038 g/m³ for each millimeter per hour precipitation rate. But, strictly speaking, there

cannot be an analytical connection between the liquid water concentration and the rate of rainfall. Inasmuch as the same rate of rainfall can be achieved by a number of different drop size distributions, therefore, to a single value of the abscissa — the precipitation rate — there may be associated a series of ordinate values or liquid water concentrations. The curves of Figure 8 are, therefore, of interest only because they are helpful in predicting very roughly liquid water concentrations in different rains.

The text on pp 281-284 discusses computation of the attenuation in different precipitation forms, no account being taken of the inherent irregularities.

Since the size of the drops in fogs and fair weather clouds are small compared with even the shortest wavelength (1.25 cm) considered in this report, the one term attenuation formula holds rigorously. Figure 9 represents the attenuation curve in decibels per kilometer in clouds and fogs for a liquid water concentration of 1 g/m³ which, as mentioned above, is an upper limit.

A few attenuation values may be given as follows:

λ, cm	1.25	3	5	10
α/m db/km/gm/m³	0.28	0.049	0.018	0.0045

Even for 1.25-cm waves the attenuation would become important only at long ranges for radar observations. For waves of length $\lambda > 3$ cm the attenuation in fair weather clouds and fogs is of no practical importance.

Table 3, on the critical diameter of water drops, shows that the attenuation becomes practically independent of the drop size distribution in rains for wavelengths longer than about 15 or 20 cm, inasmuch as raindrops whose diameter is larger than 0.55 cm or 0.6 cm do not reach low altitudes. In the 5- to 20-cm wavelength range the three-term attenuation formula will represent fairly well the attenuation in different rains. At wavelengths smaller than 5 cm exact computations of the amplitudes a_n, b_n are necessary.

It is shown that in any rain the attenuation depends linearly on the partial precipitation rates of the different drop groups making up this rain, but it does not depend directly on the total rate of rainfall.

Figure 10 purports to show the connection between the drop size distribution in a given rain and the partial or fractional attenuation values in the K and X bands of the different drop groups making up this rain. It is seen that the numerous small drops do not, for practical purposes, contribute to the attenuation, which is due mainly to the bigger drops.

Table 9 contains attenuation values of different rains of known drop size distribution and rate of rainfall. Figure 11 is a graphical representation of these results. It will be seen that at the shorter waves the attenuation may become important in heavy rains.

Figures 12, 13, and 14 are graphical representations of certain results included in Table 9 at K-, X-, and S-band wavelengths, respectively. The attenuation values corresponding to the points in these graphs have been computed for the rains of Table 9, and we have drawn a curve through the computed points. Accordingly, the plot of attenuation as a function of total precipitation is a mass plot. That is, for any given total precipitation the attenuation will have different values, depending upon the distribution of the drop size for the rain in question. Figures 12, 13, and 14 represent mass plots of the meager data available for K, X, and S bands, respectively, together with the limiting curve that would result if all the drops were of the size that gives maximum attenuation. Tables 10 and 11 contain, respectively, the theoretically predicted upper limits of attenuation for water drops around 18°C and the experimental attenuation per unit rate of precipitation. In view of the difficulties in the interpretation of the experimental data, it may be said that there is fair agreement between the observed and predicted attenuation values in rains.

The attenuation due to hailstones and snow should be considerably smaller than that caused by rain. The reason for this difference is due to the small dielectric absorption of ice as compared with the dielectric absorption of liquid water.

Pages 284-286 deal with the total scattering (in the whole solid angle) of microwaves by spherical water drops. The scattering cross-section formula is given in a series of ascending powers of $\rho = \pi D/\lambda$, the first term of the series being ρ^6. For small values of ρ, the cross section reduces to the first term of this series, which, when the dielectric absorption is negligible, reduces to the Rayleigh scattering cross section. Table 12 includes the results of the numerical computations and Figures 15 and 16 are their graphical representation.

The knowledge of the total cross section and scattering cross section allows the computation of the absolute probabilities $\tilde{\omega}_s$ for the waves to be scattered in any direction or to be absorbed internally by spherical water drops. The scattering probabilities are given in Table 13. The probabilities for internal absorption are complementary to these, i.e., they are equal to $(1 - \tilde{\omega}_s)$. It is thus seen that, with the exception of the shortest waves and the biggest raindrops, the probability of the waves being absorbed internally, the absorbed wave energy heating the drops, is much larger than the probability of their being scattered in any direction.

On pp. 286-289 the differential scattering cross section in a chosen direction is first derived rapidly and then is given explicitly so as to show clearly the contributions of the induced electric dipole, electric quadrupole, magnetic dipole, and their interference terms.

Attention is here called to the already well-known fact that in the optical spectrum region dissymmetry appears in the angular distribution of the scattered radiation. That is to say, the larger the parameter ρ or the nearer the drop diameter to the wavelength, the greater the power scattered in the direction of the propagation in comparison with that scattered backward or at 180° to the direction of propagation.

The back-scattering cross section or radar cross section of water drops is given in the form of a series in ascending powers of the parameter ρ. Table 14 contains the results of numerical computations of these radar cross sections for water drops in the diameter range 0.05 to 0.55 cm and wavelength range 3 to 100 cm.

The radar cross section allows the determination of a radar attenuation constant. The radar absorption coefficient, or the double of the attenuation constant, is the fraction of the incident power scattered backward by a layer of unit thickness of the echoing medium. Table 15 contains the numerical values of this radar absorption coefficient in different rains of known drop size distribution, and Figure 17 is its graphical representation. Table 16 is a somewhat modified form of Table 15, in so far as it gives in decibels the fraction of the incident power scattered backward by a 1-km layer of different rains. The theoretically predicted back scattering seems to be in fair agreement with the rather few experimental data on the power received in radar observations of rains or rain clouds.

In conclusion it may be stated that, in view of the scarcity of meteorological data and the irregularities inherent in meteorological phenomena, the theory provides a satisfactory picture of the propagation of microwaves through a variety of precipitation forms present in the atmosphere.

K-BAND ABSORPTION — EXPERIMENTAL[a]

Our knowledge of the attenuation of K-band radiation in the normal atmosphere is based upon the theory outlined by Van Vleck and upon a number of experiments, some of which were undertaken to obtain data needed in the theory, others of which were attempts to measure directly absorption by the atmosphere.

The width of the rotational lines of water vapor in the infrared has recently been measured in work at the University of Michigan. The width of the oxygen lines responsible for the strong absorption at 0.5 cm and the rather small effect at K band are inferred from experiments at the Radiation Laboratory. The absorption in oxygen was measured directly at sev-

eral wavelengths in the neighborhood of 0.5 to 0.6 cm. The gas was contained in a wave guide about 6 m long. This guide could be evacuated and then filled with gas to any desired pressure between zero and roughly 1,000 mm Hg. The radiation was obtained as the second harmonic generated in a crystal rectifier fed by a K-band oscillator. The source was amplitude modulated at audio frequency, and the signal was detected by a second crystal at the far end of the wave-guide path. The attenuation in the gas was determined by comparing the signal received with the guide evacuated to that received with gas present in the guide. The absorption of pure oxygen, at various pressures, as well as that of controlled mixtures of oxygen and other gases, was measured. The results confirm the predictions of the theory in a very convincing manner and suggest a value of the line width lying between 0.05 and 0.02 cm^{-1}.

Direct measurements of atmospheric absorption at K band have been made by a group at the Radiation Laboratory using a K-band radar set in an airplane. For this purpose, the set was provided with fixed attenuators which could be switched in or out of the system. Both r-f and i-f attenuators carefully calibrated were used. The experiment consisted in flying a straight level course away from a known target and determining the maximum range to which the target could be seen with and without attenuation in the system. The maximum ranges involved were of the order of 30 miles. From the results a value for the attenuation in the atmosphere can be calculated, assuming free space propagation, and this value in turn correlated with the meteorological data. The latter were obtained from radio-sonde flights at MIT.

After making allowance for the rather small oxygen effect, the results are best represented by a figure of 0.02 db per nautical mile for 1 g/m³ of water vapor. In several of the flights the target was an accurately made 4-ft corner reflector. This provides an independent upper limit to the attenuation, since all system parameters (antenna gain, S/N, etc.) were known, and one can calculate how far the corner should have been seen with any supposed amount of atmospheric attenuation. The upper limit estimated in this way is about 0.04 db per nautical mile for 1 g/m³ of water vapor.

An entirely different method for measuring attenuation in the atmosphere has been developed at Radiation Laboratory. It is possible to measure the apparent radiation temperature of any matched r-f load, including an antenna, with great precision (~ 1 C). In the case of an antenna, the temperature measured is the temperature of whatever the antenna is looking at, that is, the temperature of whatever would absorb the energy emitted from the antenna if the antenna were transmitting. When the antenna is pointed at the sky, the temperature measured is some mixture of the temperature of outer space and the temperature of the air,

---

the influence of the latter being determined in a direct and simple manner by the absorption coefficient of the air layer. From measurements of the apparent temperature of the sky at various elevation angles, the total absorption in decibels for a vertical path through the entire atmosphere can be deduced. The data which have been collected in this manner show good internal consistency; assuming that the MIT radio-sonde data give the total water vapor in the atmosphere correctly, a value of 0.04 db per nautical mile for 1 g/m^3 is obtained for the water vapor attenuation. This is larger than the other value quoted above. The reason for the discrepancy is not yet known.

ABSORPTION OF K-BAND RADIATION BY WATER VAPOR[°]

An experiment to determine the location and shape of the water vapor absorption line in the K-band region of the electromagnetic spectrum is in progress. The experiment consists in the measurement of the change in Q of a large copper box when water vapor is introduced. From this change in Q the loss by absorption in the water vapor can be determined and hence the attenuation of K-band radiation in water vapor.

The experimental setup consists of an approximately cubical (but irregular in terms of λ) copper box of 15.8 cu m volume. Energy from a pulsed magnetron is fed into this box through a wave guide which terminates in a matched horn facing a rotating copper fan placed in the roof of the box. The purpose of this fan is to stir up the standing wave pattern in the box. Throughout the interior of the box are placed strings of Chromel-constantan thermocouple junctions sealed in 707 glass tubing. Alternate junctions are coated with a mixture of polystyrene and iron powder. In all, there is a total of 220 painted or "hot" junctions in the box. Provision is made for introducing water vapor into the box and for circulating the air. The temperature is maintained at 45 C during all runs, and the pressure is atmospheric (760 ± 15 mm, depending on conditions). An aperture of area 400 sq cm which may be opened or shut by means of a sliding copper door is located in one side of the box. Radiation entering the box is absorbed by the walls, by the paraphernalia in the box, by the gas, by the apertures (if any), and by the thermocouple junctions. The coated thermocouple junctions absorb more energy than the uncoated junctions and a net emf is produced. A single junction would give an emf proportional to the value of the square of the electrical field at its position, but the reading would be very sensitive to the location of the couple and, even if this were held fixed, would be sensitive to small deformations of the walls. The large number of the couples actually used averages the value of the square of the electric field, E^2, over the entire

box, and the fan previously mentioned assists in this averaging. The Q of the box and its contents is, for constant magnetron power output, proportional to E^2 and thus to the emf of the thermocouples.

Since the couple emf is also proportional to the power output of the magnetron, changes in the output power will show up in the results in the same way as changes in Q. Original difficulties arising from this cause, which were encountered because of variation in the a-c line voltage and the modulator voltage, have been largely eliminated by the use of stabilizing transformers and a magnetron load current stabilizing circuit. Furthermore, a method of taking data was devised which only required the power output to be maintained constant for a few minutes at a time.

The Q of the water vapor, Q_V, is given by

$$\frac{1}{Q_V} = K\gamma\lambda , \qquad (72)$$

where γ is the attenuation in db per nautical mile, λ is in centimeters, and K is a constant. In order to obtain absolute values of the attenuation, it is necessary to introduce into the system a known Q in terms of which the other Q's may be evaluated. For this purpose, the aperture, which acts as a perfect absorber, is used.

Lamb has derived a formula for the Q of an aperture, Q_A, and this is

$$\frac{1}{Q_A} = \frac{\lambda A}{8\pi V} , \qquad (73)$$

where A is the area of the aperture and V is the volume of the box.

The Q of the whole ensemble may now be written down.

$$\frac{1}{Q} = \frac{1}{Q_B} + \frac{1}{Q_V} + \frac{1}{Q_A} , \qquad (74)$$

where Q_B takes account of all losses (including the losses in oxygen) other than those in the vapor and the aperture. Inserting values, and using $1/\eta$ as the proportionality constant connecting the emf, $\mathcal{E}$, and Q, one then has

$$\frac{1}{\mathcal{E}} = \eta\left(\frac{1}{Q_B} + K\gamma\lambda + \frac{\lambda A}{8\pi V}\right) . \qquad (75)$$

For constant conditions of humidity, wavelength, and magnetron power output, measurements are now made of the emf $\mathcal{E}_0$, with $A = 0$, and emf $\mathcal{E}_A$, with $A = A$. Using these measured values of emf, equation (75) can be written in the form

$$\frac{\mathcal{E}_A}{\mathcal{E}_0 - \mathcal{E}_A} = \frac{8\pi V}{\lambda A}\left(\frac{1}{Q_B} + K\gamma\lambda\right) \equiv F . \qquad (76)$$

The humidity is then changed and the measurement repeated until enough points have been obtained to provide a curve of F as a function of ρ, the water vapor density, for constant wavelength.

Since, presumably, γ is the only quantity in this equation which is a function of ρ, and since $\gamma = 0$ for $\rho = 0$, the plot of F against ρ extrapolated to zero humidity will yield a value of Q_s. Consequently, γ is determined as a function of ρ.

Examples of the γ versus ρ curves so obtained are shown in Figure 18 for the wavelengths 0.96, 1.16, 1.28, and 1.69 cm. Data were also taken at the wave-
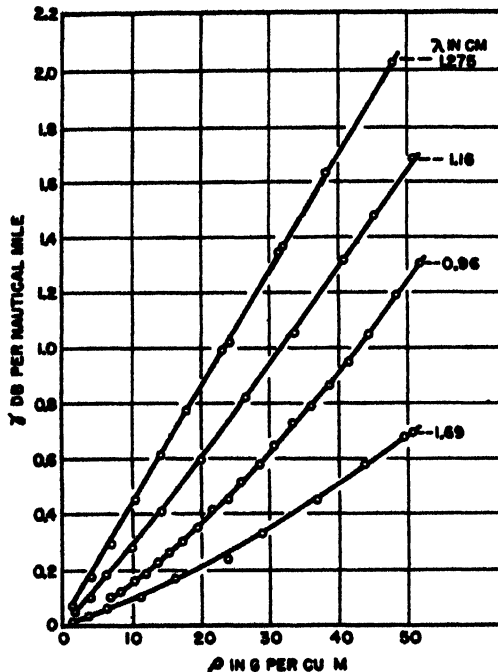
FIGURE 18. Attenuation in water vapor.

lengths 1.06, 1.31, 1.37, and 1.49 cm, These lines are all concave upward with the exception of those at 1.28, 1.31, and 1.37 cm. There is some evidence that the line at 1.31 cm is concave downward, while within experimental error the 1.28- and 1.37-cm lines are straight.

The curvature is surprising, since it was believed that γ would be proportional to ρ. The reason for the curvature is not understood, and it is possible that it arises from some systematic experimental error. However, it is difficult to conceive of a systematic error which disappears at resonance.

Because of this curvature, it is not possible to draw a single attenuation curve showing absorption as a function of wavelength for all humidities. Figure 19 shows the variation with wavelength of the attenuation coefficient γ/ρ in decibels per nautical mile per gram of water vapor per cubic meter for humidities of 10 g per cubic meter and of 50 g per cubic meter. It is to be noted that the peak of this curve, at 1.32 cm, is very close to the standard K-band wavelength.

These experimental results are in agreement with other results for the water vapor attenuation at K band. Furthermore, for all practical radar purposes,
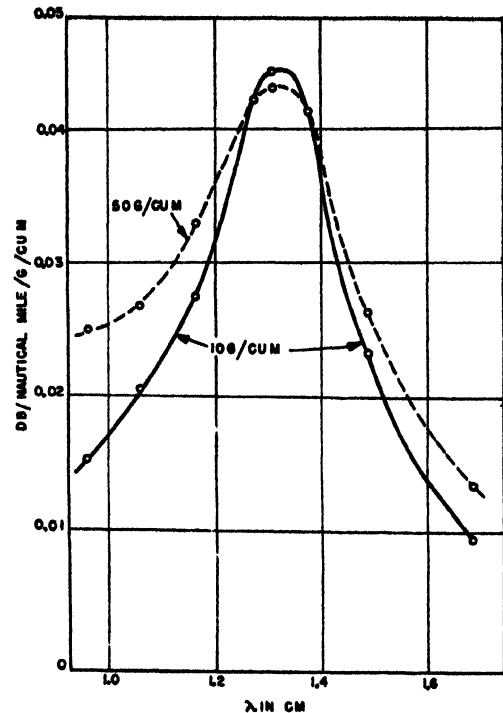
FIGURE 19. Attenuation coefficient, water vapor, 45 C.

and within the range of the measurements, they are in agreement with Van Vleck's theory of the absorption of this water vapor line.

DISCUSSION

Comments were made on the great accuracy of the experiment, pointing out that the quantity being measured was extremely small and that other experiments, particularly one made in Florida by measurement of the sky temperature, were leading to substantial agreement with the present findings. The best available data on the performance of K-band radars supported the experimental result obtained and would be of great help in choosing wavelengths for radar and other apparatus in the future.

The good agreement between theory and the experimental result achieved was stressed. Whereas in infrared absorption measurements the results had disagreed with theory by as much as 10 db or more, the discrepancy in these results amounted to a few per cent only. It was noted that from the purely physical standpoint this water vapor line and the 0.5-cm oxygen absorption line were the most carefully investigated lines in the spectrum, aside from some lines in the visible region. The explanation was given that the microwave measurements were much more instructive than the optical ones from the standpoint of the collision broadening theory because the width of the microwave absorption line was comparable to the frequency of the radiation. This results in a shape factor or line form which can be studied in detail. The reported dependence on den-

sity presents a difficult problem which is not yet well understood.

The practical importance of the curvature shown in Figure 18 was emphasized. It was pointed out that the effects of a wide range of humidities had been investigated, some very high compared to those ordinarily encountered. In practical work most of the data would be obtained from the low end of the curves of Figure 18, where little ambiguity in numerical values would obtain.

K-BAND ATTENUATION DUE TO RAINFALL[p]

Introduction

In order to determine the attenuation of 1.25-cm wavelength radiation by rain, controlled radio and meteorological measurements were undertaken in an area providing adequate climatic conditions for the study. It was apparent that the attenuation measurements should be made in an area of maximum precipitation for expediency. Furthermore, the experiment demanded periods of varying rates of rainfall with frequent "clearing" for calibration purposes. Tropical orographic (mountainous) rain seemed to offer the greatest probability of fulfilling these conditions.

A brief reconnaissance of the Hilo, Hawaii, area showed that a site near Kaumana was adequate, having a yearly fall in excess of 250 in., as compared with an annual rainfall of 10.10 in. in the San Diego area. A 1.21 statute mile link was chosen parallel to the mean trade wind vector, i.e., due east-west, and was located on a lava flow of 1881. The lava was covered with saw grass and low brush. The terrain had a gentle slope from the receiver at 2,500 ft to the transmitter at 2,800 ft above mean sea level.

Rainfall Intensity

Orographic lifting of the unstable moist tropical air caused frequent 2- to 3-day periods of precipitation having a wide range in intensity. On one occasion in-

[p]By L. J. Anderson, U. S. Navy Radio and Sound Laboratory.

tensities as high as 125 mm per hour were observed. Due to the light winds associated with orographic precipitation an essentially vertical trajectory of the raindrops was obtained; and, therefore, representative sampling of the rain falling through the radiated energy path was accomplished by placing the gauges directly in line between the transmitter and receiver.

Although the rainfall intensity varied widely both with time and in space, well-coordinated measuring techniques having sufficient coverage detected periods when the rate of fall along the path was uniform. Since such periods of uniformity seldom lasted longer than 60 sec, precise control and timing were vital. Two methods of determining the rate of precipitation were employed. Five Julien Friez tipping-bucket automatic recording rain gauges were evenly dispersed along the path and their signals were recorded on a single Esterline-Angus five-pen recorder at the receiver station. In addition, four rain shelters employing the "funnel and graduate" technique were installed between the automatic gauges as shown in Figure 20. The rain shelters were provided with field phones for
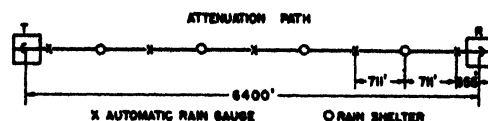
FIGURE 20. Layout of experimental path and apparatus.

receiving instructions as well as simultaneous signals for taking graduate readings and exposing drop size blotters. During operations, signals for graduate readings were given every 30 sec. Blotters for drop size measurements were simultaneously exposed on an average of every 5 min.

Radio Equipment

The equipment used for the attenuation measurements is shown in Figure 21. It was relatively simple and required little attention once the initial warm-up drifts were stabilized. The technique for a satisfactory measurement involved a comprehensive check of the "clear weather" values before and after any one rainfall.
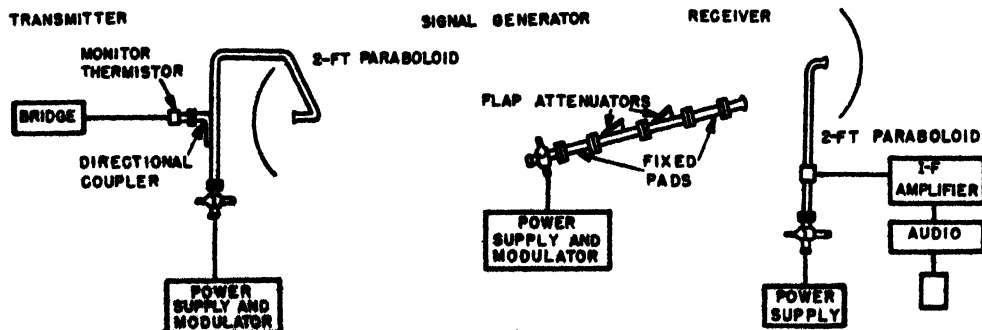
FIGURE 21. Block diagram of K-band attenuation measurement apparatus.

The transmitter was housed in a small elevated shack and the antenna and guide were protected from the rain by a back-sloping shutter flap.

A 2K33 tube, modulated with 800 c, was used as the transmitter. Wave-guide feed was employed on a 2-ft paraboloid antenna (beam width 1.7°). A thermistor with a directional coupler was used as a power monitor.

A 2-ft paraboloid collected energy at the receiving end and fed the receiver through a wave guide. A superheterodyne utilizing a 2K33 local oscillator drove a 30-mc i-f amplifier with 6-mc bandwidth. The second detector output fed an audio amplifier and recorder.

A signal generator was used to check the receiver characteristic. This generator consisted of a 2K33 tube and two flap attenuators. Fixed pads were used on either side of the flap attenuators to provide a flat line. The characteristics of the flap attenuators were checked every few hours, using a K-band thermistor. Each flap was calibrated and used over a 12-db range. Resettability was approximately ±0.1 db. A small nozzle was used to direct the output of the signal generator upon the receiving paraboloid. Calibrations were made before, during, and after rainfalls and were within ±1.0 db over the 5- and 6-hour measuring periods.

Analysis

The primary attenuation curve of Figure 22, shown with solid dots, was obtained by choosing periods when the rainfall at all stations, including the automatic gauges, was essentially uniform. Six such periods of
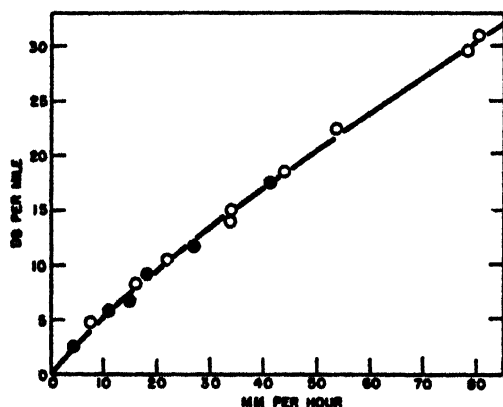
Figure 22. Primary attenuation curve of K-band radiation in rain. K-band attenuation versus rainfall intensity. (Note: Decibels per nautical mile.)

uniform fall along the path were selected covering the important range of 0 to 41 mm per hour. Figure 23 is a rainfall intensity profile of the highest uniform fall recorded. By Humphreys' classification of rain* the intensities covered by the primary curve are more

*1 mm per hour, light rain; 4 mm per hour, moderate rain; 15 mm per hour, heavy rain; 48 mm per hour, excessive rain. See reference 24.
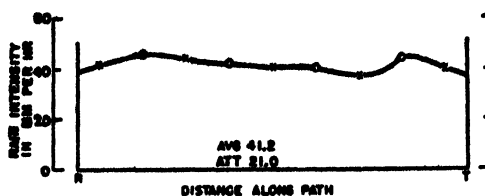
Figure 23. Profile of rain intensity along the path. Time 223645.

than adequate for normal rates of precipitation encountered in nature.

Using the primary attenuation curve thus obtained, it was possible to extend the curve for extremely high rates of fall (cloudbursts) in the following manner. Figure 24 is a rain intensity profile at an interval of
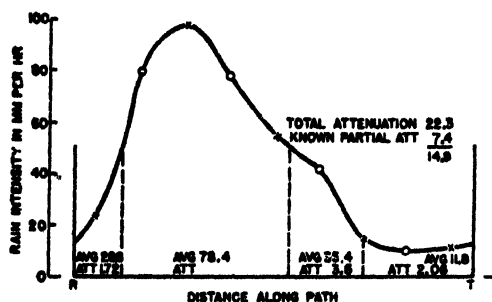
Figure 24. Intensity profile during uneven precipitation. Time 171115.

nonuniform rainfall distribution. The area under the curve is divided into sections as shown. These sections cover the portions of the path where the intensity was below 41 mm per hr. Hence with the primary attenuation curve and a planimeter it is possible to assign the contribution that each section makes to the total observed attenuation (assuming that the attenuation in decibels is linear with distance).

After subtracting out the part of the attenuation already known, the high intensity central portion is left to account for the residual attenuation. Dividing the residual attenuation by the fraction of a mile covered by this part of the path and plotting this value against the average intensity in the interval gives a point at 78 mm per hour. As a check on the method, similar profiles were worked up which gave points below 40 mm per hour. These are plotted as open circles, as shown in Figure 22. It will be seen that the open circles agree quite well with the solid ones, and hence considerable confidence in the high intensity points is justified.

Discussion

The total observation time of the experiment was roughly 3 hours, about half of this total time being represented by the figures presented with the paper. It was necessary to employ a large number of precipitation measuring stations along the path in order to obtain an accurate precipitation profile. Some inci-

dental work on drop size was also done. The spread in drop size at a given time was rather large, probably because of the orographic character of the precipitation, which was made up of drops falling on the average not much more than 1,000 ft, as compared to ordinary rain falling 5,000 to 6,000 ft. The longer period of fall in ordinary rain probably permits a greater number of drops to reach the characteristic sizes.

ABSORPTION OF MICROWAVES BY THE ATMOSPHERE, BRITISH WORK[r]

The working committee of the Ultra Short Wave Panel has presented a report in which the following questions are treated in detail:

1. The absorption of microwave radiation by oxygen and vapor.

2. The absorption of microwave radiation by water in macroscopic form, for example, rain, clouds, fog.

3. The measurement in the laboratory of dielectric constants and conductivity which have already been described (see page 268).

The work under item (1) consisted chiefly in showing that the attenuation given by Telecommunication Research Establishment radar experiments at Llandudno at a wavelength of 1.25 cm was consistent with the theoretical values given in reference 1. The experimental method consisted of comparing the echoes received on X- and K-band radars from a standard reflector at short range and from land echoes at a large range. Care was taken to insure that the reflecting targets did not reflect an amount of energy which was dependent on frequency. In this way a minimum value for the attenuation on $\lambda = 1.25$ cm was found to be 0.14 db per kilometer. New values based upon revised values of the widths of the various lines of water vapor and oxygen show that almost the whole of this attenuation must be due to absorption by water vapor and further that to obtain an absorption as high as 0.14 db per kilometer the frequency at the important water vapor line must lie close to 1.25 cm.

The work under item (2) has been carried out, in the case of rain, by assuming what seemed a plausible distribution of drop sizes and calculating on this basis the attenuation that would occur at a standard precipitation rate. Then by making a climatological survey, information can be given of the proportion of time during which the attenuation can be expected to exceed a given value for a radar or radio communication set working on a given wavelength at a given location. The calculations for a standard precipitation rate gave the following estimates for the maximum attenuation likely to occur (that is, for the most unfavorable drop size distribution that was thought likely to occur).

S band: 0.003 db per km per mm per hr.
X band: 0.06 db per km per mm per hr.
K band: 0.22 db per km per mm per hr.

The climatological part of the program involves a great deal of statistical work and is not yet complete. The following preliminary results can be given.

At Padang in Sumatra we may expect, twelve times a year, periods of 1 hr when the average attenuation on 1.25 cm will be some 6 to 12 db per kilometer; on 3.0 cm, 2 to 4 db per kilometer; and on 10 cm, 0.1 to 0.2 db per kilometer.

In England only once a year will the average attenuation over a period of one hour reach 1 to 2.5 db per kilometer on 1.25 cm; 0.3 to 0.8 per kilometer on 3.0 cm; and 0.02 to 0.04 db per kilometer on 10.0 cm.

It should be noticed that these attenuation figures are for point-to-point communication and must be doubled in the radar case.

DIELECTRIC CONSTANT AND LOSS FACTOR OF LIQUID WATER AND THE ATMOSPHERE[*]

In propagation problems the knowledge of the electric properties of the ground, sea, and fresh water, as well as those of the atmospheric gases, are of fundamental importance. Collected here are the available data on these materials. Clearly, the study of the reflection coefficients leads indirectly to the dielectric properties of these materials. Here we will be concerned more with the direct determination of their dielectric constants and loss factors.

Experimental Methods

REFLECTION-TRANSMISSION METHOD

First we should like to sketch here the basis of the different experimental methods used in the determination of the dielectric properties of materials.

One of these is the reflection-transmission method which was used by Ford[37] in his studies of the properties of the ground. This same method has also been used recently by Saxton[38,39] on water in investigating the temperature dependence of its dielectric properties at 1.25 and 1.58 cm.

If the power transmitted through two thicknesses d_1 and d_2 of the material in question are

$$P_1 = P_0 e^{-\alpha d_1},$$
$$P_2 = P_0 e^{-\alpha d_2},$$

then the absorption coefficient α is given by

$$\alpha = \frac{2.3}{d_2 - d_1} \log_{10} \frac{P_1}{P_2}, \qquad (77)$$

[r]By F. Hoyle, Ultra Short Wave Panel, Ministry of Supply, England.

[*]By L. Goldstein, Columbia University Wave Propagation Group.

where P_0 is the incident power.

The absorption index k in the complex refractive index

$$N = n - jk \quad (78)$$

is related to the absorption coefficient by

$$\alpha = \frac{4\pi k}{\lambda} \quad (79)$$

and hence

$$k = \frac{2.3\lambda}{4\pi d} \log_{10} \frac{P_1}{P_2}, \quad (80)$$

where d stands for $(d_2 - d_1)$. Also

$$N^2 = (n - jk)^2 = \epsilon_r - j\epsilon_i,$$
$$= \epsilon_r - j60\sigma\lambda. \quad (81)$$

ϵ_r is the real part of the dielectric constant, ϵ_i its imaginary part; σ is the conductivity of the substance in mhos per meter; and λ the wavelength in meters. One obtains readily from equation (81)

$$n^2 - k^2 = \epsilon_r$$
$$2nk = \epsilon_i = 60\sigma\lambda. \quad (82)$$

The absorption index k is measured directly by two galvanometer readings proportional to P_1 and P_2. The refractive index n is derived from the reflection coefficient R_N for almost perpendicular incidence, using

$$R_N^2 = \frac{n^2 + k^2 + 1 - 2n}{n^2 + k^2 + 1 + 2n}. \quad (83)$$

Then n and k determine ϵ_r and σ. Saxton claims that in this method at least one quantity, the absorption index, is measured directly while the other, the refractive index, is derived from the measurement of the reflection coefficient.

In the other methods, given later, neither of these quantities is measured directly.

STANDING WAVE RATIO METHOD

By limiting the electromagnetic field to the enclosure of a hollow pipe or coaxial line, the energy is completely confined, stray effects are eliminated, and small amounts of any dielectric can be investigated accurately.[40-42] The following gives the theoretical foundation of this "standing wave ratio" method for measuring complex dielectric constants.

1. A transmitter radiates waves of a given frequency into one end of a closed wave guide. These are reflected by the metallic boundary at the other end. Standing waves are set up in the guide, and they can be measured by a probe detector traveling along a slot in the pipe parallel to its axis. The dielectric is inserted at the closed end of the pipe, opposite the transmitter, and fills the pipe up to a height d. Above it the standing wave pattern is measured in air. The real and imaginary parts ϵ_r and ϵ_i of the dielec-

tric constant are calculated from the ratio of the field strengths in node and antinode E_{min}/E_{max}, and the distance x_0 of the first node from the surface of the dielectric.

The modulus and the argument of the reflection coefficient are obtained from

$$R = \rho e^{-j\Phi} = \frac{(Z(0)/Z_{01}) - 1}{(Z(0)/Z_{01}) + 1}, \quad (84)$$

where $Z(0)$ is the characteristic impedance of the pipe section filled with the dielectric understudy, Z_{01} is the intrinsic impedance of the air-filled portion of the pipe. By denoting

$$\frac{Z(0)}{Z_{01}} = \tanh \delta = \tanh (\delta_r + j\delta_i), \quad (85)$$

where δ_r and δ_i are, respectively, the real and imaginary part of δ, the reflection coefficient R can be written as

$$R = |R| e^{-j\Phi},$$
$$= \rho e^{-j\Phi}, \quad (86)$$

with

$$\rho = |R| = e^{-2\delta_r}; \arg R = -\pi - 2\delta_i = -\Phi. \quad (87)$$

From the expression of the reflected field strengths one finds that the distance x_0 of the first node from the surface is given by

$$x_0 = \frac{-\delta_i \lambda_1}{2\pi}, \quad (88)$$

where δ_i is connected directly to the phase shift Φ at reflection through equation (87), and λ_1 is the wavelength in air of the radiation. The measurement of x_0 thus yields δ_i. Similarly, one finds that

$$\tanh \delta_r = |E_{min} / E_{max}|. \quad (89)$$

2. *Calculation of dielectric constant and loss factor from terminating impedance.* The intrinsic impedance of the dielectric-filled portion of the guide is found to be

$$Z(0) = Z_{02} \tanh \gamma_2 d, \quad (90)$$

where

$$Z_{02} = \frac{j\omega\mu_2}{\gamma_2}. \quad (91)$$

The subscript 2 refers to the dielectric medium, μ_2 is its permeability and γ_2 is the propagation constant of dielectric-filled section of the guide; for the TE waves, Z_{02} is the impedance of the dielectric medium itself. Using equations (90) and (91), one gets

$$\frac{\tanh \gamma_2 d}{\gamma_2 d} = \frac{Z(0)}{Z_{01}} \frac{\mu_1}{d\gamma_1 \mu_2}. \quad (92)$$

The propagation constant γ_2 determines finally the complex dielectric constant ϵ_r through the funda-

mental relation

$$\gamma_2 = \left[\left(\frac{2\pi}{\lambda_o} \right)^2 - \omega^2 \mu_2 \epsilon_2 \right]^{\frac{1}{2}}, \qquad (93)$$

where the cutoff wavelength λ_o is determined by the geometry of the guide and the type of wave. In the air-filled section of the guide

$$\gamma_1 = \left[\left(\frac{2\pi}{\lambda_o} \right)^2 - \omega^2 \mu_1 \epsilon_1 \right]^{\frac{1}{2}}. \qquad (94)$$

Consequently, from equations (93) and (94), the complex dielectric constant of the material under study becomes

$$\epsilon_o = \epsilon_1 \frac{(1/\lambda_o)^2 - (\gamma_2/2\pi)^2}{(1/\lambda_o)^2 + (1/\lambda_1)^2}, \qquad (95)$$

where

$$\gamma_1 = j \frac{2\pi}{\lambda_1}. \qquad (96)$$

for free space. Finally

$$\epsilon_o = \epsilon_1 \left(\frac{\gamma_2}{\gamma_1} \right)^2. \qquad (97)$$

The solution of equation (93) can be found from charts. It is claimed that with this method materials with very low dielectric losses can be investigated satisfactorily.

THE RESONATOR Q METHOD[45]

Here the procedure consists in measuring the change of resonant frequency of a closed cylindrical resonator upon the insertion, along the axis, of a rod of the dielectric material in question. By observing the change of Q value resulting from the insertion of similarly dimensioned specimens of different materials, it is possible to obtain comparative loss tangent values. The relevant theoretical relations are summarized below.

By definition the Q value of a resonator system is given in convenient form by the relation

$$Q = 2\pi \frac{\text{energy stored}}{\text{energy loss per half cycle}}$$

Both the energy stored and the energy loss can be computed from the field distributions within the resonator, and these are given, for a TM wave, as

$$H_\phi = A J_1(\gamma\rho), \qquad (98)$$

$$E_z = \frac{A\gamma}{\sigma + j\omega\epsilon_r} J_0(\gamma\rho), \qquad (99)$$

where H_ϕ is the tangential magnetic field strength in amperes per meter. E_z is the axial electric field strength in volts per meter, ρ is the distance of the point in question from the cylinder axis, γ is the propagation constant

$$\gamma^2 = \mu\epsilon_r\omega^2 - j\omega\sigma\mu,$$

ω is the angular frequency, μ the permeability in henrys per meter, and A is a constant determined by the strength of the exciting source. In the formulas (98) and (99) it was assumed that the walls of the resonator are of infinite conductivity so that no electric intensity exists in them. This requires that

$$E_z(\rho = a) = J_0(\gamma a) = 0, \qquad (100)$$

where a denotes the radius of the resonator. This equation has an infinite number of real roots, the lowest being $\gamma a = 2.4048$, and this determines the fundamental resonant frequency and wavelength λ_0. If σ, the conductivity of the dielectric, is neglected in comparison with $\epsilon_r\omega$, the propagation constant becomes

$$\gamma = \omega \sqrt{\mu\epsilon_r} = \frac{2\pi}{\lambda}. \qquad (101)$$

ϵ_r is the dielectric constant of the material filling the resonator taken relative to air. Since λ can be measured, this dielectric constant may be derived from the relation

$$\frac{2\pi a \epsilon_r}{\lambda} = 2.4048$$

or

$$\epsilon_r = 0.146 \left(\frac{\lambda}{a} \right)^2 = \left(\frac{\lambda}{\lambda_0} \right)^2. \qquad (102)$$

No appreciable error will be committed in using the preceding results for the practical case of dielectrics with low but finite conductivity.

The Q of the filled cylindrical resonator is shown to be

$$Q = \frac{a}{d \left(1 + \frac{a}{2z_0} \right) + a \tan \delta}. \qquad (103)$$

Here d is the wave-guide skin depth, $2z_0$ is the axial length of the resonator and $\tan \delta = \epsilon_i/\epsilon_r$ is the loss factor of the dielectric. Consequently

$$\tan \delta = \frac{1}{Q} - \frac{1}{Q_0}, \qquad (104)$$

where Q_0 is the Q of the air-filled resonator.

It should be remembered in this connection that the theoretical Q_0 values, in general, are found to be considerably different from the measured ones. This tends to limit the reliability of the method.

After having thus sketched the different methods used in the determination of the complex dielectric constant of substances of importance in wave propagation, we turn now to the presentation of the data.

LIQUID WATER

Table 17 gives the results obtained recently on liquid water.[33,38,39,44]

It has been found by Saxton and Lane that the temperature variation of the dielectric constant in the range 0 to 40 C at 1.24 and 1.58 cm can be ac-

TABLE 17. Temperature variation of the dielectric properties of water. λ = 1.24 cm.[38,39]

t°C	n	k[a]	ϵ_r	ϵ_i	σ mhos/m
0	4.68	2.73	14.4	25.5	34.3
3	....	....	27[a]	27[a]	36.0[a]
5	5.24	2.89	19.1	30.3	40.7
10	5.74	2.92	24.4	33.5	45.0
15	6.17	2.88	29.8	35.5	47.8
18	....	....	32.1	39.2	51.8
20	6.53	2.77	34.9	36.2	48.6
25	6.84	2.63	35[a]	23[a]	30.6[a]
..	....	....	39.8	36.0	51.1
30	7.10	2.48	44.2	35.2	50.0
35	7.30	2.30	48.0	33.6	45.1
40	7.47	2.11	51.3	31.5	42.4
60	....	....	44[a]	14[a]	18.6[a]

[a]Data from reference 22, at λ = 1.25 cm.
[b]Data from reference 44, at λ = 1.26 cm.

TABLE 18. Temperature variation of the dielectric properties of water.[38,39] λ = 1.58 cm.

t°C	n	k	ϵ_r	ϵ_i	σ mhos/m
0	5.24	2.90	19.0	30.4	32.0
5	5.84	2.97	25.3	34.7	36.6
10	6.36	2.91	32.0	37.1	39.2
15	6.77	2.78	38.1	37.6	39.7
20	7.13	2.61	44.0	37.2	39.2
25	7.40	2.41	49.0	35.7	37.6
30	7.59	2.21	52.7	33.5	35.4
35	7.72	2.01	55.5	31.0	32.7
40	7.81	1.80	57.7	28.1	29.7

TABLE 19. Relaxation times of water at different temperatures.[38,39]

t°C	$\tau \times 10^{12}$ sec	t°C	$\tau \times 10^{12}$ sec
0	19.0	25	6.8
5	14.6	30	5.9
10	11.85	35	5.2
15	9.6	40	4.5
20	8.1		

counted for with simple theoretical formulas. At any given temperature one single characteristic constant, the "relaxation time," was sufficient to account for the frequency dependence of the complex dielectric constant of water. The formulas in question are the following:

$$2n^2 = \left(\frac{\epsilon_i^2 + \epsilon_\infty^2 x^2}{1+x^2}\right)^{\frac{1}{2}} + \frac{\epsilon_i + \epsilon_\infty x^2}{1+x^2},$$

$$2k^2 = \left(\frac{\epsilon_i^2 + \epsilon_\infty^2 x^2}{1+x^2}\right)^{\frac{1}{2}} - \frac{\epsilon_i + \epsilon_\infty x^2}{1+x^2}, \qquad (105)$$

or

$$\epsilon_r = n^2 - k^2,$$

$$= \frac{\epsilon_i + \epsilon_\infty x^2}{1+x^2}, \qquad (106)$$

and

$$\epsilon_i = 2nk.$$

Here

$$x = \omega\tau = 2\pi f\tau,$$

with τ denoting the relaxation time, ϵ_i is the static dielectric constant, ϵ_∞ the optical dielectric constant due to the sum of the electronic and atomic polarizations.

Considering τ as a parameter to be derived from the experimental data, one finds in Table 19 the relaxation times in the 0 to 40 C temperature range.

Table 20 refers to 10-cm waves for which measurements were made in the temperature range 0 to 40 C.[45,46] In one series of measurements the wavelength was 9.72 cm, but this is considered close enough to have the corresponding data included with the 10-cm waves.

The preceding table indicates that the agreement between calculated and measured values of n and k is satisfactory. It is to be noted here that the experimental results on S band were obtained by the standing wave ratio method, those at K band with the reflection-transmission method.

Using equations (105) and (106), the temperature variation of the refractive and absorption index, or real and imaginary parts of the complex dielectric constant, can be computed at any wavelength provided that the relaxation time at the temperature in question is known.

In tables on page 301 the temperature variation of the indices n and k are given. These results were computed with the aid of formulas (105) and (106).

It is thought[38,39] that until more extensive experimental results become available the computed values can be regarded as representing the best information available on the dielectric constant of water in the millimeter and centimeter range. Figure 25 represents the best available information on water at 20 C.

ICE

A certain number of measurements on the dielectric

TABLE 20. Temperature variation of the dielectric properties of water.[45,46] λ = 10 cm.

t°C	Refractive index n			Absorption index k			ϵ_r calc	ϵ_i calc	σ mhos/m
	Calc	Experimental		Calc	Experimental				
		λ = 9.72 cm	λ = 10 cm		λ = 9.72 cm	λ = 10 cm			
0	8.99	8.95	....	1.47	1.35	....	78.66	26.43	4.40
5	9.04	....	....	1.14	....	....	80.42	20.61	3.44
10	9.02	9.00	....	0.90	1.10	....	80.55	16.23	2.70
15	8.96	....	....	0.76	....	....	79.7	13.61	2.27
20	8.88	8.88	8.84	0.63	0.90	0.66	78.46	11.20	1.84
25	8.80	....	....	0.50	....	....	77.20	8.80	1.46
30	8.71	8.75	8.69	0.45	0.73	0.54	75.66	7.84	1.30
35	8.62	....	....	0.40	....	....	74.14	6.89	1.16
40	8.53	8.60	8.56	0.36	0.60	0.40	72.63	6.15	1.02

TABLE 21. Temperature variation of the dielectric properties of water.[38,39] $\lambda = 0.50$ cm.

$t°C$	n	k	ϵ_r	ϵ_i	σ mhos/m
0	3.18	1.76	7.01	11.2	37.3
5	3.50	2.03	8.13	14.2	47.3
10	3.80	2.25	9.38	17.1	57.0
15	4.10	2.41	11.0	19.7	65.6
20	4.39	2.54	12.8	22.3	74.3
25	4.67	2.62	14.9	24.4	81.3
30	4.94	2.67	17.3	26.4	88.0
35	5.21	2.69	19.9	28.0	93.3
40	5.47	2.69	22.7	29.4	98.0

TABLE 22. Temperature variation of n, k, ϵ_r, ϵ_i and σ.[38,39] $\lambda = 3.2$ cm.

$t°C$	n	k	ϵ_r	ϵ_i	σ mhos/m
0	7.10	2.89	42.0	41.1	21.4
5	7.63	2.62	51.3	40.0	20.8
10	8.00	2.33	58.6	37.3	19.4
15	8.22	2.00	63.6	32.9	17.1
20	8.33	1.72	66.4	28.7	14.9
25	8.38	1.50	68.0	25.1	13.1
30	8.39	1.31	68.7	22.0	11.4
35	8.38	1.16	68.9	19.4	10.1
40	8.35	1.02	68.7	17.0	8.85

constants of ice were made in the centimeter wavelength range. The British workers[47] used the resonator Q method at 3 and 9 cm. The latest results on both these wavelengths are collected on the accompanying graph (Figure 26). The temperature range extends from about —50 C to 0 C. The refractive index turns out to be constant in this range. It was found to be equal to 1.75 at 3.01 cm and 1.72 at 9.18 cm. The absorption index increased in this temperature range from about 0.0001 to 0.0010.
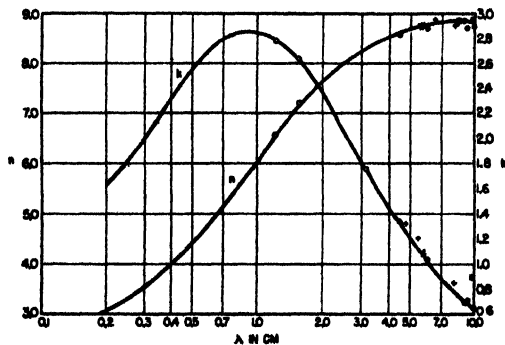
FIGURE 25. Refraction and absorption indices for water.

Younker,[28] using the standing wave ratio method at 1.25 cm, found at about —15 C

$\epsilon_r = 3.3$ and $\epsilon_i = 0.011$, or $\sigma = 0.013$ mhos/m.

These data can be compared with those obtained at 3.01 cm,[47] where

$\epsilon_r = 3.06$ and $\epsilon_i = 0.00080$, $\sigma = 0.00044$ mhos/m.

The difference at these two wavelengths between the conductivities appears much too large and further studies should clear up this discrepancy. The dielectric losses in ice in the centimeter region are, however, very small.
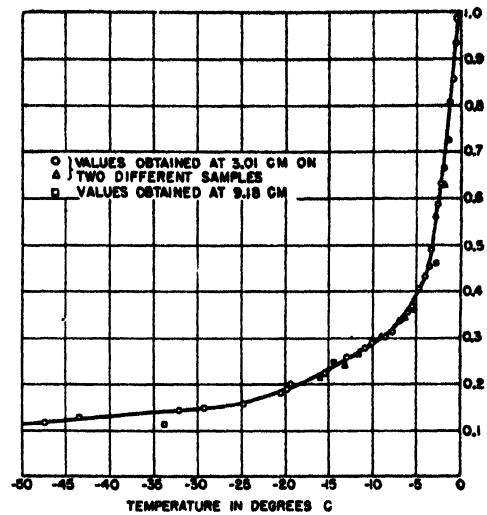
FIGURE 26. Absorption index $(k \times 10^{+3})$ versus temperature for ice.

At much lower frequencies the dielectric behavior of ice is given in Figure 27. These data refer to a temperature of —12 C.[47]

ATTENUATION DUE TO WATER VAPOR

In order to determine the attenuation due to water vapor, Saxton endeavored to measure the refractive and absorption indices of water vapor.[48] Using the resonator Q method, he found that by passing from 9 to 3.2 cm the real part of the dielectric constant changes from 1.0056 to 1.0051. According to a general relationship connecting the real and imaginary parts of the complex dielectric constant,[49] the indicated variation of $(\epsilon_r - 1)$ given by Saxton should be accompanied by a tremendous absorption by water vapor in the microwave region as pointed out by Van Vleck.[49] This is contrary to the data available and rules out the frequency variation of $(\epsilon_r - 1)$ given by Saxton.
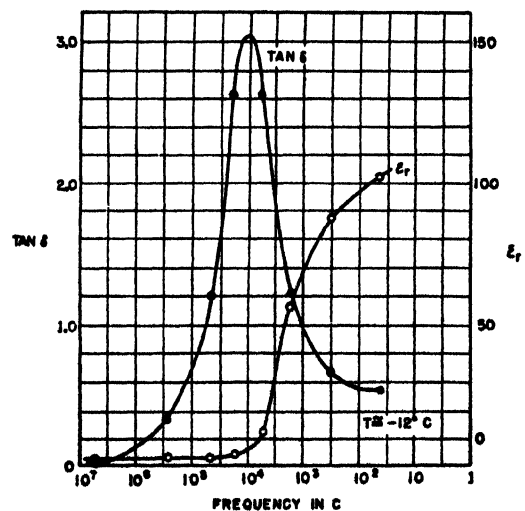
FIGURE 27. Loss factor and dielectric constant of ice.

According to Van Vleck, in the microwave region outside of any resonance region, the refraction[(n^2-1), n being the refractive index] or $(\epsilon_r - 1)$, must be appreciably constant over the microwave region to account for the absence of any large absorption coefficients.

The conclusion is similar in case of resonance which occurs for both O_2 (0.25 cm and the 0.5-cm. band) and H_2O (—1.30 cm). The refractive index of the atmosphere free of condensation should be constant throughout the microwave region. The refractive index for infinitely long waves or the static dielectric constant can be used here. In the presence of condensation, clouds, fog, and rain, the attenuation is increased considerably, and the refraction or $(\epsilon_r - 1)$ might then differ from the static value. But under standard conditions, the refraction of the atmosphere should not change by more than a few parts in a thousand in the microwave region.

LABORATORY MEASUREMENTS OF DIELECTRIC PROPERTIES[t]

The working committee of Ultra Short Wave Panel has presented a report dealing with the measurement in the laboratory of

1. The dielectric constant and loss angle in superheated steam for wavelengths in the S, X, and. K bands.

2. The dielectric constant and conductivity of bulk water for the K band.

These experiments have been carried out by Saxton. The method adopted on S and X bands in (1) was to allow superheated steam to issue freely through a resonator into the air. The pressure throughout the apparatus was accordingly the atmospheric pressure. The temperature of the steam was measured before

---

‘By F. Hoyle, Ultra Short Wave Panel, Ministry of Supply, England.

entering and after leaving the resonator. The temperature difference between these measurements was no more than 2 C, so it seems clear that no condensation of water droplets could occur within the resonator. A somewhat different technique was employed for X band in that the resonator was replaced by a wave guide. If ϵ is the dielectric constant, then the best representation of the results is obtained by plotting $(\epsilon-1)$ against $1/T$, for each wavelength where T is in degrees absolute. It was found that the results for different values of T fitted very well to a straight line as they should theoretically, but the value of $(\epsilon-1)$ for all values of T was found to be systematically about 10 per cent less than would have been expected on the basis of previous measurements of the dielectric constant of steam at much longer wavelengths. This discrepancy was found on X and K bands. The reason for the discrepancy is not yet understood. It is known, however, that the reduced value of $(\epsilon-1)$ does not arise from strong dispersion occurring in the microwave band since there is no evidence of any abnormal absorption.

The method adopted in (2) was to measure first the attenuation factor of radiation passing through water. This was done by placing a transmitting horn above a large shallow trough and a receiving horn below the trough. The attenuation factor was measured immediately by varying the depth of the water in the trough. Second, the reflection coefficient of electromagnetic waves incident normally on a plane surface of water was measured. These two observations were sufficient to determine the dielectric constant and conductivity of water. The results obtained for a wavelength of 1.58 cm were:

Dielectric constant about 40;

Conductivity about 4.10 esu.[11]

The same values were obtained for both tap water and distilled water, showing that the presence of salts in the water had little effect on the value of the conductivity.

Chapter 6

STORM DETECTION

STORM DETECTION BY RADAR[*]

THIS SUMMER (1944) a study was made of the meteorological echoes observed on a Canadian microwave S-band early warning radar set at Ottawa. These were correlated with check observations on the weather made by a large number of local observers distributed over the area covered by the set. It was found that observers inside the source area of the echo always reported rain; just outside the echo (1 to 5 miles) there was a half chance of light rain. Atmospheric electrical disturbance was present in less than half the cases checked. Echoes became less frequent at increasing distances from the set but in some cases were seen at 160 miles.

The display system that we have used is a *plan position indicator* [PPI] tube. This tube provides a map of a circular area centered on the location of the set and extending out at choice to 40 or 80 or 160 miles. The last-mentioned setting was the one used most of the time.

Procedure

During the hours of operation a 16-mm motion-picture camera was kept running, taking pictures of the PPI display and a clock alongside, exposing one frame of the film for the duration of each revolution of the array. Thus about four photographs were obtained per minute. At the same time we watched the progress of moving echoes across the screen and made telephone calls to any observers that were available, in the neighborhood of any echo. From the observer the existing state of the weather was determined; his remarks and the exact time were carefully noted.

We checked the echoes and their movement as recorded on the film against the information obtained about the weather from the observers. We also made charts of the echoes, based on the film, at 30-minute intervals.

Weather Information

Facilities of which we availed ourselves for obtaining information were, among others:

1. Ottawa meteorological stations. These stations provided us with as many as three forecasts a day and with weather information generally.

2. Distant meteorological stations. Apart from the Ottawa stations, the nearest weather station, 57 miles away, is at Canton, N. Y. Its reports are included in

the teletype sequences that come to us.

3. Unofficial observers, consulted by telephone. Since the official weather stations did not provide the close network that we required, we compiled a list of persons whose location could be closely marked on our map and whom we could consult about existing weather conditions to the extent that an untrained observer would be competent.

Correlations

Our aim was to correlate observed echoes with weather conditions. At first clouds were thought to be possible sources of echoes, and it was thought that fronts might produce some sort of echo quite independently of cloud or precipitation along the front. The earlier part of our work showed that on afternoons with heavy cumulus clouds but with no precipitation there were no weather echoes. On days with scattered showers, however, echoes were observed. Also, the passage of a front did not seem to produce any peculiar sort of echo or any echo that could not be attributed to precipitation along the front.

In analyzing our correlations, we have found it convenient to consider them in two groups. First, there are *correlations with echo*, that is, correlations when the observer was in the vicinity of an echo, although not necessarily right inside the echo. All correlations involving telephone calls to local observers were of this type, for we didn't make such a telephone call unless there was an echo in the vicinity. Second, there are *correlations with weather*, or correlations with weather stations, when we first select an occasion when precipitation is reported (by an official station) and then go looking in our records for an echo to match. Nearly all the precipitation recorded at the weather station during our hours of operation was light, and too light, as it proved, for us to detect it at the distance we were away. Thus there is only a very small number of echoes associated with correlation with weather, and so very little overlapping between this group and the group of correlations with echo.

TABLE 1. Precipitation inside and just outside echoes.

| | Observer's position relative to echo | | | |
| | Inside | | Outside (1 to 5 miles) | |
	No.	%	No.	%
Cases of no rain	0	0	19	48
Very light rain	6	13	7	17
Light rain	16	33	13	33
Moderate rain	13	27	1	2
Heavy rain	13	27	0	0
Total	48	100	40	100

Correlations with Echo

Table 1 gives a summary of the results obtained in the form of a comparison of precipitation observed inside and just outside the echoes.

Correlations with Weather Stations

Correlations with weather stations were notable chiefly for the rain we did not detect. Nearly all the precipitation observed at the station was light and apparently too light to produce echoes effective at such distances. Weather reports on the teletype from Ottawa itself were not correlated with echoes because most meteorological echoes within 10 miles were obscured by permanent echoes and distortion at the center of the PPI. The next closest weather station is at Canton, N. Y., 57 miles from our set. The rainfall for every hour was obtained from a rain gauge at Canton, and in addition some of the teletyped weather reports were received. Rain was reported from Canton on five occasions during our hours of operations. On one of these occasions we had an echo directly over Canton; on three others we had an echo within three miles of Canton; on one occasion we had no echo in the vicinity at all. The details are given in the table. It can be seen that we detected rain falling at a rate of 0.2 in. per hour and failed to detect rain falling at a rate of 0.03 in. per hour.

TABLE 2. Rain at Canton, New York (U. S. Weather Station, 57 miles from set) during analyzed hours of operation.

Case	Rainfall in./hr*	Thunder	Echo
1	0.20	Yes	Overhead
2	0.05	Yes	1 mile away
3	0.3	Yes	2 miles away
4	Trace	No	3 miles away
5	0.03	Yes	No echo

*All rates taken from gauge reading made at hourly intervals.

Résumé of Correlations

Our checks with local observers out to 60 miles from the set revealed the following: Inside the echo there is sure to be rain, with a 0.3 chance that it is moderate or heavy. Just outside (1 to 5 miles) there is never more than light rain, and a half chance of none at all. Further, the chance of an observer in the vicinity of an echo reporting thunder was 0.4. Our checks with weather stations were less relevant, because only two echoes passed over weather stations during the period studied. But from the numerous cases of light rain at these stations that we did not detect, we can say that we cannot detect light rain at 90 miles. By light rain we mean rainfall less than 0.1 in. per hour, and this can just be detected at 50 miles. Further, to judge by one storm that we detected and one we missed at Canton, we can detect 0.2 in. per hour and cannot detect 0.03 in. per hour at 57 miles.

Fraction Detected by Radar of Total Quantity of Rainfall

Starting from the proportion of hours of rain that give an echo, we have used the distribution with rate of rainfall of the hours of rain to give us a value for the minimum rate of rainfall that will give us an echo. Now using a distribution with rate of rainfall of the quantity of rainfall, we can proceed to determine the proportion of the total quantity of rain that was observed by radar. The proportion is quite high: 83 per cent close to the set, 62 per cent at 50 miles.

Comparison with Ryde's Theory

Computations of the echo strength to be expected have been made on the basis of the theory developed by J. G. Ryde of the General Electric Company (British). The experimental results are in satisfactory agreement with theory. (See page 269 ff.)

The Best Frequency for Storm Detection

The sensitivity to rain of the frequencies we have been using is such that with the power available we can obtain satisfactory performance. At higher frequencies the sensitivity, according to theory, is considerably higher, but considerations of absorption made by Ryde would keep us from going to much higher frequencies. Absorption affects us in two different ways. In the case of widespread rain, even of moderate intensity, there is enough absorption between the set and the echo source to reduce our effective range considerably. Where there is no widespread rain but the rain that we want to see is heavy and concentrated, the absorption of high-frequency radiation by heavy rain can be so great that hardly any of the radiation impinging on the storm makes its way back out to be reflected. We could actually fail to detect a storm in this way, because the storm was too intense. The frequency we are using (S-band) is safe against both these effects, but increasing it by a factor 3 would lead us well into them.

Ultimate Range—Greater Range of a Production Set

The performance of the prototype set we have used has been specified in the previous section by its range for aircraft. The performance of the same design of set, constructed and installed to the final production specification, is known to be better: the range for aircraft is approximately twice as great, and some calculations show that very roughly the range of a production set for storms will be twice that of our prototype set.

The full account of this work is published as: Summer Storm Echoes on Radar MEW, Report No. 18 of the Canadian Army Operational Research Group.
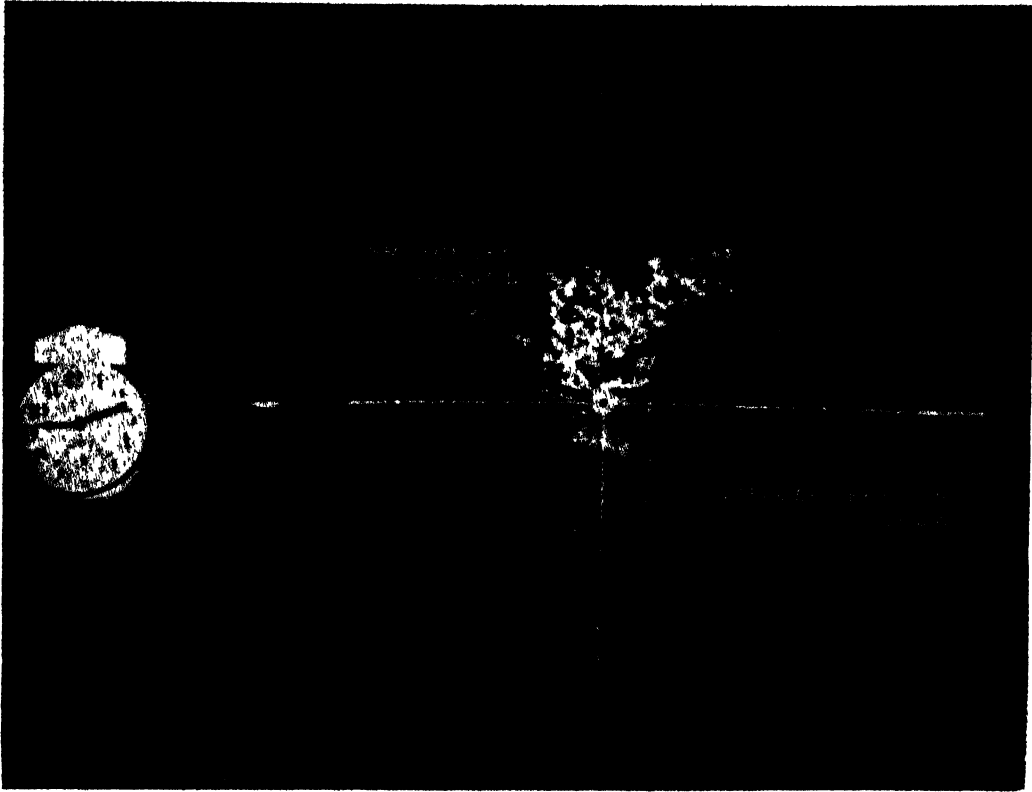
FIGURE 1. Typical S-band PPI display of snow echoes.

S-BAND RADAR ECHOES FROM SNOW[b]

Since June 1944, the Canadian Army Operational Research Group has been studying the nature and application of S-band radar echoes from storms. During the past winter we studied echoes from snow, obtained on occasions when snow was present and rain definitely was not.

Heavy snow has been detected on five occasions, with maximum ranges varying from 30 to 65 miles. One moderate snowfall which kept all aircraft grounded was not detected at all, even at the minimum range of 10 miles.

Roughly, rain and snow of the same intensity, expressed in inches of liquid water per hour, produce about the same echo and are detectable to the same range. Further, there seems to be no useful difference in pattern between echoes from the two sources. Figure 1 shows a typical PPI picture of snow echoes made during the course of the study.

Theoretically, this equality is not directly significant; in the case of snow there is a much greater bulk of lighter material, falling more slowly and reflecting less well.

Operationally, there are two reasons why radar

[b] By J. S. Marshall, Canadian Army Operational Research Group.

storm detection is less useful in winter (in Canada). A given intensity of precipitation in the form of snow, say 0.1 in. of water per hour, is much more hazardous to flying and to ground activities than the same intensity in the form of rain. Further, great intensities of precipitation such as lead to long-range echoes in summer are almost nonexistent in winter in this region; therefore, detection at great ranges is not achieved. Thus S-band radar in summer can detect important storm areas to a radius of about 100 miles; in winter it detects hardly .any weather beyond 50 miles and misses some important snow even at 10 to 20 miles.

For the greatest total contribution of radar to flying it is a good thing that echoes from snow are weak. This is important, for while the cumulo-nimbus activity detected in summer must always be avoided by aircraft because of violent air currents, flying in moderate snow can be safe with good blind-flying control. It is fortunate, therefore, that echoes from snow are probably not strong enough to interfere with any radar elements of this control.

This work has been done with the cooperation of the National Research Council of Canada, the Canadian Meteorological Service, and the Royal Canadian Air Force.

ECHOES AND TARGETS

FLUCTUATIONS OF RADAR ECHOES[a]

SINCE JUNE, 1943, the Propagation Group of the Radiation Laboratory has had a project under way to investigate the nature and origin of fluctuations from close targets. This work has been done in the microwave region using the mobile S- and X-band sets belonging to the group. Most of the work has been on S band. We have restricted ourselves to targets sufficiently close to the radar that the more usual effects of atmospheric refraction can be neglected. We have not paid much attention to moving targets such as ships or planes, as their echoes are easily accounted for by the changing aspect of the target, propeller modulation, etc.

One of the obvious sources of signal fluctuation is instability in the system. In our case system instability was chiefly due to ripple in the receiver, and sensitivity to changes in line voltage affecting the modulator, receiver, and indicator units. After considerable effort these forms of instability have been reduced but not completely eliminated. The transmitted pulse shows an average fluctuation about the mean of ± 0.1 db with a maximum deviation about 0.5 db. Pulse-to-pulse frequency changes are not greater than 0.1 or 0.2 mc, and frequency modulation inside the pulse is less than 0.2 to 0.3 mc. These figures are for the S-band set, and instability is somewhat greater on X. The r-f signal intensity is measured by comparison with a pulse from a calibrated signal generator. This pulse shows a fluctuation as large as the transmitted pulse, i.e., about ± 0.12 db. It is believed that this apparent change is not in the signal generator but rather in the receiver and indicator units.

Some radar signals show almost as little fluctuation. These are large man-made targets in isolated positions viewed over land. Some examples that we have found are the Provincetown standpipe as viewed from Race Point in Provincetown and the Winthrop standpipe in Boston viewed from Deer Island. In these cases the average pulse to pulse deviation from the mean is ± 0.14 db. Such steady signals are the rare exception. Most echoes show changes that are much larger than can be accounted for by instability in the system tests.

The Interference Concept

When this research was started, it seemed to be a common idea that changes in atmospheric refraction

in the path between the target and set could account for the observed variations. We have found little evidence for this belief. If the targets are closer than 10 miles, the effects due to the atmosphere, if there are any, must be small compared to the more important phenomena shown by the echoes. The behavior of the radar echo is determined by the fact that a radar signal is usually not the return from a single target but rather the sum of returns from all targets within the area illuminated by the set. Since the radar beam is coherent, the individual signals must be added in amplitude taking into account the relative phase of the echoes. The total signal is the result of the interference between these component echoes. In the case of the standpipes mentioned above there were intervening hills so that only the top portions of the targets were seen by the radar, but in most other cases there is more than one target present, and the interference between these targets will determine the nature of the total echo.

In the Boston region, we have found one very simple dual target consisting of two radio towers 500 ft high and 60 yd apart in range. Both constructive and destructive interference has been observed in this case.

The changes in the phase between the component signals might be due to several causes. If the index of refraction in the path between the two towers changes, then the optical path length would change. However, the deviation of the index from 1 would have to double in order to produce sufficient phase change. A change in the frequency of the transmitter could also account for the phase change. To produce the observed effect it would have to be greater than $\frac{1}{2}$ mc, which is larger than the frequency instability of the system. Finally, the towers themselves could physically move relative to each other and produce the phase change in a manner similar to that in the Michelson interferometer. To produce a phase change of π the targets need only move $\lambda/4$ relative to each other. At S band this amounts to 1 in. It does not seem unnatural that such tall structures might sway in the wind by even a greater amount. To test this conclusion the signal from these towers was measured over a period of 4 days. The amount of fluctuation was estimated visually every half hour. These results showed a definite correlation with the speed of the wind. Large fluctuations occurred only with high winds. It was calculated that if the fluctuation had indeed been independent of wind speed the odds against getting the set of readings obtained by these measurements would be 10,000,000 to 1.

Assemblies of Random Scatterers

In a more common type of radar target the entire illuminated area contains a large number of independent targets with random phases. If we represent the signal from each target by a vector showing amplitudes and phase, then the total signal is found by adding up all these vectors. If the phase of the individual vector is changed slightly (for instance, by relative motion) this vector diagram would be rearranged and the total signal changed. Some practical examples are precipitation echoes, where the individual targets are the drops; window, where the echo arises from many strips of tin foil; and sea echo, where the individual targets are probably areas of reflection from the surface of the sea.

The theory of this type of target has been extensively worked out.[1-3] One of the questions that can be answered by the theory is to determine the probability $P(I)$ that a given signal from the target will be of intensity I in range dI. Or equivalently, one can find the fraction of returned pulses having intensity I in range dI. [$P(I)$ has been called the first probability distribution.] The result is simply

$$P(I)\, dI = e^{-I/I_0} \frac{dI}{I_0},$$

where I_0 is the average intensity of the echo. The continuous curve in Figure 1 is a plot of this experimental formula.

The equation for $P(I)$ is independent of the distribution of the individual amplitudes, nor is it required that the individual amplitudes be constant with time, only that the distribution shall be stationary with time. The only other conditions that must be satisfied are that there shall be a large number of scatterers and that they shall be independent of each other with phase random both in space and time. It will be seen from the formula that the most probable signal is always zero. Furthermore the distribution is independent of the number of targets. The rapidity of the fluctuations is determined essentially by the echo changes and the relative velocity of the scatterers. The detailed relation has been worked out between the frequency spectrum of the fluctuations and the velocity distribution of the particles.[3] The frequency of fluctuations should increase linearly with r-f frequency.

In order to investigate experimentally this type of radar signal, it is necessary to get some method of measuring the intensity of the individual pulses. In our case this was obtained by photography of the single sweeps on the A scope. For this purpose a special A scope was used with a blue screen tube operated at 6 kv. Commercial 16-mm movie cameras were used in which the shutter and claw had been removed and to which a high-speed motor drive had been added.

By photographing a calibrated r-f signal generator pulse at the same receiver gain but at different r-f

levels, one can obtain a curve for the deflection in centimeters against r-f intensity. By means of this curve the measured deflections from the pulse-to-pulse films can be converted into measurements of r-f intensity. From these experimental data it is possible to compute an experimental first probability distribution.

Figure 1 is an example of such an experimental distribution obtained by measuring a thousand pulses of
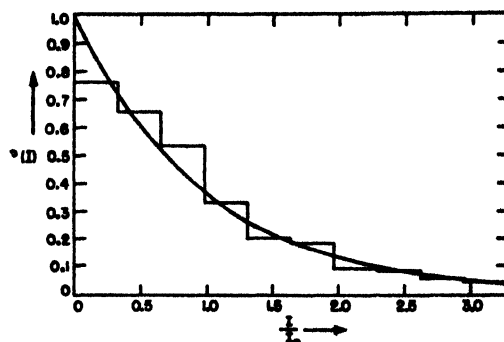
FIGURE 1. The first probability distribution, $P(I)$ of the intensity of cloud echoes. Curve: $P(I) = e^{-I/I_0}$ Histogram: experimental results. Film 90, S band, 1,000 pulses.

precipitation echo on S band. The continuous curve in that figure shows the theoretical formula given above. The agreement is good.

By what is essentially a Fourier analysis of these data, one can also determine the frequency spectrum of the video signal. Figure 2 shows such an experimentally determined frequency spectrum for sea echo on both S and X bands. The spectrum extends to 120 c on X band and about 50 c on S. The ratio between the width of the spectra is 2.4 compared to
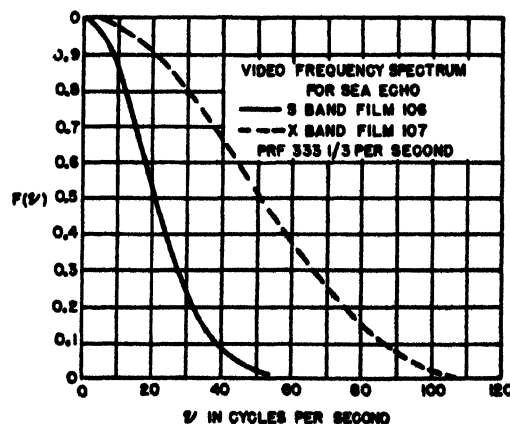
FIGURE 2. Experimentally determined frequency spectrum for sea echo.

tween the width of the spectra is 2.4 compared to 2.88 for the ratio of wavelengths. This discrepancy is probably due to the crudity of the measurements on X band.

Ground Clutter

The ordinary ground clutter consists of echoes from a variety of types of targets: earth, rocks, trees, branches, bushes, leaves, grass. Our present conception is that the fluctuation in ordinary ground clutter arises from the motion of leaves and branches in the wind, changing the phase patterns in a manner somewhat similar to that for random scatterers. There will in addition be a relatively steady signal from fixed objects such as rocks and tree trunks.

We have obtained much qualitative evidence for this picture, but it is difficult to obtain quantitative
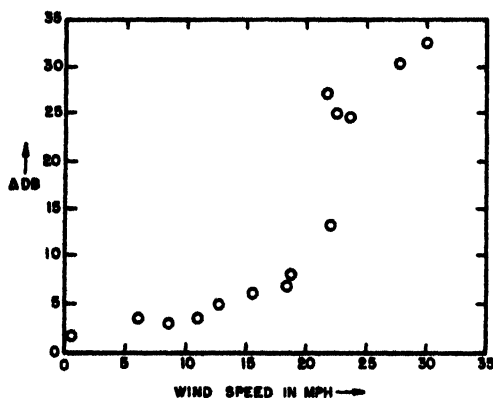
FIGURE 3. Fluctuation in signal from Blue Hills versus wind speed. S band, 10 a.m. April 24, 1944 to 11 a.m. April 25, 1944.
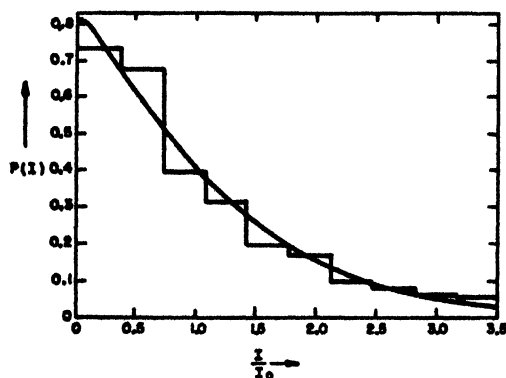
FIGURE 4. First probability distribution, Baker Hill, Maine. Wind speed 25 mph. Curve: theoretical, fixed to random signal = 1 db. I_0 = average intensity. Histogram: experimental results. Film 103, 3,000 pulses, S band.

data because the wind speed at the target is not usually known. Fortunately, in the Boston area the largest ground signal is due to the Great Blue Hills, which is the site of the Blue Hill Observatory. It is thus possible to obtain data on the wind speed at the target. We monitored the signal from Blue Hills for a 24-hr period in April of 1944. Movies were taken of the A scope at regular intervals. During the period of observation the wind speed varied between 30 mph and dead calm. To interpret the data a somewhat crude

parameter was defined as a measure of the amount of fluctuation. The change in the signal strength from one frame to the next (0.06 sec) was measured and averaged over 200 frames.
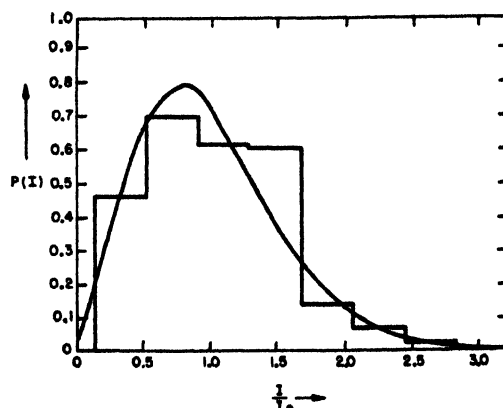
FIGURE 5. First probability distribution, Mt. Penobscot, Maine. Wind speed 10 mph. Curve: theoretical, fixed to random signal = + 7.2 db. I_0 = average intensity. Histogram: experimental results. Film 82 (16 fr per sec), 400 frames, S band.

This parameter was then plotted against the wind speed as shown in Figure 3. There is a quite good correlation between the amount of fluctuation as measured by this parameter and the speed of the wind. The fluctuation is of the order of 0.2 db at 0 mph, which is almost as good as our steadiest signals. At the other extreme the fluctuation is about 3.4 db at 30 mph. There appears to be a rather sudden jump in the fluctuation at a wind speed in the neighborhood of 20 mph. This jump has been observed at other seasons of the year and is believed to be rather general. It is significant that the wind speed at which the jump occurs is roughly that at which large branches and small trees begin to move as a whole.

The theoretical description for a simple picture of ground clutter consisting of an assembly of random scatterers (leaves, grass, etc.) plus a fixed signal (rocks, trees, trunks) is not difficult to work out. When the proportion of steady signal is small, the first probability distribution closely resembles that for purely random scatterers. For a large ratio of fixed-to-random signal the amount of fluctuation is greatly reduced, and the first probability distribution tends to a Gaussian curve about the average intensity. This is illustrated in Figures 4 and 5. Figure 4 is a plot of the experimentally determined first probability distribution for a signal from heavily wooded terrain on S band at 25-mph wind speed. This has been fitted by a theoretical curve for a ratio of fixed to random signal of —0.1 db.

Figure 5 shows the distribution for a similar type of terrain but for a wind speed of 10 mph. Here the results are fitted to a curve for a ratio of fixed to
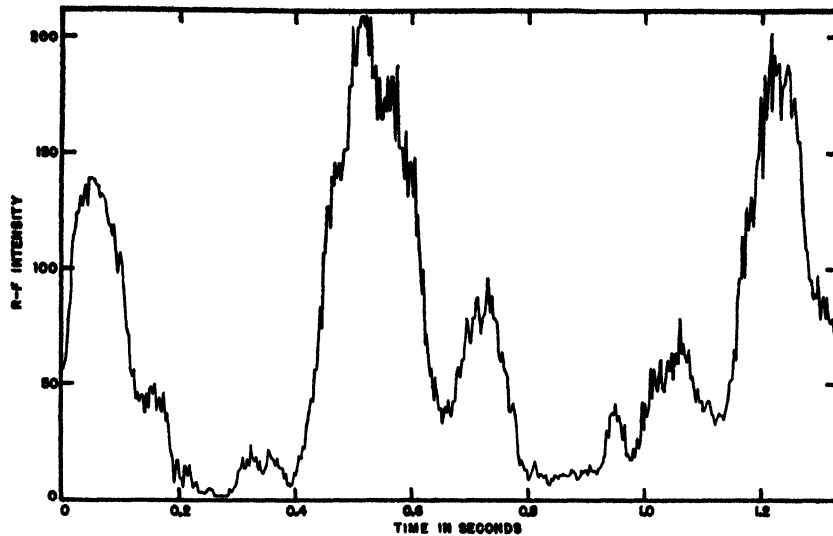
FIGURE 6. Pulse-to-pulse record of the signal from Black Woods, Bar Harbor. Film 87, July 9, 1944. S-band, prf 333½ per sec, wind speed 22 mph.
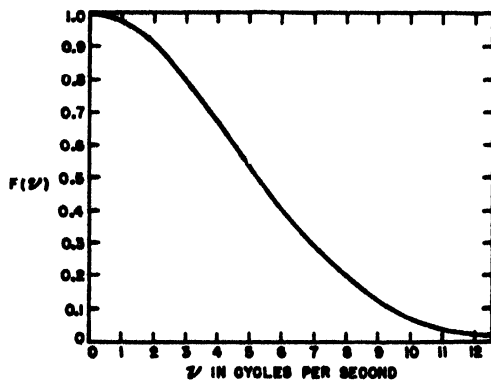
FIGURE 7. Video frequency spectrum for ground clutter, Baker Hill, Maine. Film 103, wind speed 25 mph, prf 333½ per sec, wavelength S band.
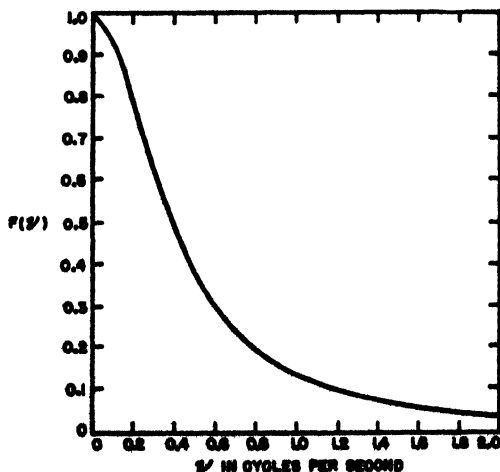
FIGURE 8. Video frequency spectrum for ground clutter. Mt. Penobscot, Mt. Desert Island. Film 82, wind speed 10 mph, wavelength S band, prf 333½.

random signal of $+$ 5 db. The most probable intensity is no longer at zero, and the amount of fluctuation is considerably reduced.

Figure 6 is a plot of the intensity of some ground clutter at high wind over a period of 1½ seconds as obtained from a pulse-to-pulse film. While the signal changes quite rapidly, it is not nearly so fast as sea return, for example (see Figure 7).

The frequency spectrum can be obtained from these data as in the previous case. Figure 7 shows the video frequency spectrum obtained under the same conditions as Figure 4 for high winds. The spectrum extends as high as 12 c. Figure 8 is a plot of the frequency spectrum obtained from the same film as in Figure 5. Here at a wind speed of 10 mph the frequency spectrum does not extend beyond 2 c.

Targets Viewed over Water

In addition to the sources of fluctuation described above, echoes from targets viewed over water will change due to the varying reflection from the surface of the sea. Some English investigations have shown that at high angles of incidence the amount of reflection can often change quite rapidly. However, there is another effect due to reflection from the sea surface which is of a much longer period, namely, tidal variations.

Some of our earliest work consisted of monitoring the signal from a number of isolated targets viewed over water over a period of many tidal cycles. It was found that quite a large number of echoes showed a definite correlation with the tide. One very striking example is the case of two standpipes on Strawberry Hill on Nantasket Peninsula, which when viewed

from Deer Island in Boston Harbor showed a 15-db variation with tide. Their range is 10,000 yd, and the targets are about 60 ft high. Under these conditions the targets subtend more than two lobes of the interference pattern at S band. Since the effect of the tidal change is to move this lobe structure up and down by 10 ft, it is difficult to believe that a change as large as 15 db could be thus produced. However, one can break up the returned signal into a number of separate signals differing as to whether they suffer two reflections on the surface of the sea or one reflection or go directly to and from the target. While the amplitude of each of these signals does not vary much with tide, their relative phases do, and the total signal can still change considerably in amplitude because of the interference. A similar set of measurements was made on a corner reflector mounted on a small island in Boston Harbor. Here the corner reflector although only 6,000 yd away acts essentially as a point target. The agreement with the theory for a point target is quite good.

Our results emphasize the extreme caution that must be employed in the use of standard targets to monitor radar performance. They are just the type of targets which are normally chosen in the field, and obviously their variations with the tide make them entirely unsuitable for the purpose. It may be possible to find targets whose echoes are sufficiently steady so that they can be used for monitoring. However, they cannot be found without the use of such test equipment as would obviate the need for standard targets.

THE FREQUENCY DEPENDENCE OF SEA ECHO[b]

As the power and frequency of radar sets continue to increase, and the size of the target to be detected decreases, the presence of sea echo becomes of ever greater operational significance. It acts as a built-in jammer, blanketing and obscuring the desired signals. Despite this growing practical importance the basic phenomena of sea echo have not yet been established. Certainly, the fundamental mechanism responsible for the signal is not yet known. Various conflicting theories have been proposed. It has been suggested that scattering from drops of spray is the cause of the echo. Another hypothesis is that of reflection or diffraction from the large surfaces of the waves themselves. Still other theories have been advanced at one time or another.

Whatever the size of the scatterers, the power received at the radar can be described by a common formula. Consider some particular scatterer, say the jth one. Then the returned signal from this particular target is

$$P_{rj} = \frac{P_t\, G^2\, \lambda^2}{(4\pi)^3\, R^4}\sigma_j,$$

[b]By H. Goldstein, Radiation Laboratory, MIT.

where σ_j is the radar cross section of the jth scatterer, P_t the power transmitted, G the gain, λ the wavelength, and R the range. σ_j differs from the customary cross section in that it incorporates the propagation factor and hence may depend on the height of target and the glancing angle of the incident ray. In considering the time average of the total power received by the radar we can take the scattering to be incoherent. Hence the average radar signal is the sum of P_{rj} over all the j scatterers lying within the area illuminated by the beam width and pulse length:

$$\bar{P}_r = \frac{P_t\, G^2\, \lambda^2}{(4\pi)^3\, R^4}\sum_j \sigma_j.$$

It is assumed that the illuminated area is sufficiently large that the sum contains many scatterers and is proportional to the size of the area. In that case this formula can be written

$$\bar{P}_r = \frac{P_t\, G^2\, \lambda^2}{(4\pi)^3}\,\phi\,\frac{\tau c}{2}\,\sigma,$$

where ϕ is the azimuthal beam width, τ the pulse length in seconds, c the speed of light, and σ is defined as the radar cross section of sea echo per unit area of the sea surface and hence is dimensionless. This quantity σ is a function of many parameters: the state of the sea, the glancing angle of the incident beam (and therefore the range), the polarization, and the wavelength. A comprehensive program is under way in the Radiation Laboratory to check the assumptions underlying this formula and to determine the cross section σ as a function of these parameters.

Uhlenbeck has pointed out that the dependence of σ on wavelength should be an especially sensitive function of the scattering mechanism assumed. For drops whose circumference is small compared to the wavelength, the scattering should be of the Rayleigh type, i.e., varying as $1/\lambda^4$. If one takes into account the lobe pattern of the incident field due to reflection on the water surface, the dependence is even faster, possibly as $1/\lambda^8$. On the other hand, if we are dealing with reflection or diffraction from large curved surfaces, then σ should be substantially independent of wavelength or even increase with λ. By measuring σ simultaneously on two or more frequencies, it should be possible to decide between these mechanisms.

Accordingly, such measurements were made in the summer of 1944 at Bar Harbor, using the calibrated S- and X-band mobile radars belonging to the Wave Propagation Group of the Radiation Laboratory. The site elevation was 1,500 ft, and the ranges about 10,000 yd, so that the incident angles were quite small. The constants in the formula for P_r were determined as accurately as possible. In addition, the power, pulse length, and beam width were made comparable in both systems. For relatively stormy sea conditions the ratio of σ on the two wavelengths was found to be:

$$\frac{\sigma_X}{\sigma_S} = +5 \pm 4 \, db$$

for both polarizations. If the Rayleigh $1/\lambda^4$ law holds, the ratio should be $+18.5$ db, which would seem to exclude spray drops as the scatterers.

One of the difficulties of this type of measurement is to determine the average level of a signal that fluctuates as rapidly as does sea echo. To remove this source of trouble, a device has been developed that reads the average power directly. It might be described as a gated noise meter. With the aid of this instrument we have again begun making measurements of σ on S and X bands, this time from Deer Island in Boston Harbor. The elevation is only 120 ft, and the ranges are correspondingly small.

The results obtained so far do not agree in all respects with the previous data obtained at Bar Harbor. When the sea is fairly calm (Beaufort 3 or less), the ratio of σ_X to σ_S is reproducibly given by:

$$\frac{\sigma_X}{\sigma_S} = +12 \pm 2 \, db \quad \text{horizontal}$$

on horizontal polarization. The scatter is much greater on vertical polarization, and the ratio is much smaller:

$$\frac{\sigma_X}{\sigma_S} \sim +4 \, db \quad \text{vertical.}$$

One set of worth-while measurements has been made with a sea that was considerably rougher (Beaufort 4-5). The ratio was significantly smaller for both polarizations:

$$\frac{\sigma_X}{\sigma_S} = +5 \pm 2 \, db \quad \text{horizontal}$$

$$\frac{\sigma_X}{\sigma_S} = +2 \, db \quad \text{vertical.}$$

At the time these data were obtained the first measurements were made with a calibrated experimental K-band set recently constructed. Only horizontal polarization was available. It was found that

$$\frac{\sigma_K}{\sigma_X} = 3 \text{ to } 5 \, db.$$

Hence under these sea conditions the increase in σ on going from S to X is about the same as when going from X to K.

An interesting by-product of these measurements was the comparison of polarizations, keeping the wavelength the same. This ratio was quite variable, ranging from

$$\frac{\sigma_V}{\sigma_H} = -9 \, db \quad \text{X band}$$

on X band under stormy conditions, to

$$\frac{\sigma_V}{\sigma_H} > +25 \, db \quad \text{S band}$$

on S band with a calm sea. In general the ratio decreases as sea becomes rougher and is almost always

less on X than on S band.

It is too early in the investigation to attempt a detailed interpretation of the results. It does seem that scattering from small spray drops is not the sole mechanism, despite the popular observation that sea echo seems to increase rapidly with the appearance of whitecaps. Other evidence also seems to confirm this. Under favorable conditions sea echo appears as discrete signals, moving with the wind, that can be tracked for 15 to 20 sec. This seems longer than one would expect from a breaking wave. On the other hand, reflection from large wave surfaces cannot be the whole story either. This is indicated by the fairly rapid increase of σ with frequency and by the complicated changes with polarization. It is probable that we are dealing with a combination of mechanisms, and it will be a difficult task to unscramble the contribution of each to the total signal.

It should be emphasized that these measurements were taken near the coast, though outside the breakers. Conditions on the high seas might conceivably be quite different.

DISCUSSION

It was stated that individual sea echoes which persist for many seconds cannot be caused either by specular reflection from an inclined water-air interface or by random (Rayleigh) scattering from individual drops of spray. Instead, an aerated surface layer created by a breaking whitecap may persist for many seconds and may be responsible for persistent echoes. Such a layer constitutes an irregular network of air-water interfaces and may give rise to considerable scatter of microwaves. The actual mechanism by which such a layer gives rise to a sea echo is likely to be different at different sea states. If a large area is covered with foam, then in the presence of strong swell the chief return should be expected from a wave crest, and the radar signal would appear to travel slowly on the radar screen as the wave crest progresses.

The author stated that so far no consideration had been given to such involved mechanisms as the one suggested, but added that data already collected might well lead to such an investigation.

It was suggested that several mechanisms, including scattering from droplets, were probably responsible for sea echo in rough weather. Experiments in Britain reported by the British Army Operational Research Group showed that echoes from shell splashes viewed on an S-band gunnery radar could be resolved into two parts. One was from the "boil," a solid wall of water with enclosed air bubbles, which could be readily distinguished from the superimposed response from the larger portion of the splash called the "plume," which is a region of isolated water droplets. Echoes from the droplets in the "plume" region were of many seconds duration, and it seemed likely

that an investigation of the frequency dependence of such scatterers would produce useful results.

THE DEPENDENCE OF SIGNAL THRESHOLD POWER ON RECEIVER PARAMETERS[a]

This paper deals with the effect on the signal threshold power of various parameters in the receiving systems of radar sets, i.e., with the minimum signal power necessary for visibility. Although this is a difficult problem and all the important factors entering it are not known, it is felt that at least qualitatively, and sometimes quantitatively, a fairly good answer can be given at present. First of all it is necessary to define some of the parameters involved in ordinary radar reception. When a signal is reflected from a target the power entering the receiving system may be written in the following form:

$$P_r = \frac{P_t G^2 \lambda^2 \sigma}{(4\pi)^3 R^4}$$

where G, λ, and σ are the antenna gain, radar wavelength, and target echoing area or cross section, respectively. P_t is the transmitted power and R the target range. This is, of course, the free space formula. The propagation conditions can be conveniently lumped into a multiplicative factor, which in the following arguments is of little concern. To determine the maximum range capability of the radar set, it is necessary to determine how large P_r must be in order to be detectable. It is then possible to calculate the maximum range capability of the radar set from the above formula, on writing it:

$$R_{max} = \left(\frac{P_t G^2 \lambda^2 \sigma}{(4\pi)^3 P_{r\,min}} \right)^{\frac{1}{4}}.$$

It has been common practice to assume that $P_{r\,min}$, or the signal threshold power, is of the order of magnitude of the noise power in the radar receiver. This is certainly true; it is of the order of magnitude of that noise power but is not generally equal to it. This paper deals with the various factors in the receiving system and display system which affect $P_{r\,min}$.

A few of the things that affect $P_{r\,min}$ are

1. The capabilities of the human observer.

2. The properties of the display system on which the signal is presented to the observer.

3. The type of interference which prevents the detection of an extremely small signal.

This interference is not always receiver noise. There are storm cloud echoes and similar interferences, but this discussion will deal only with the case in which receiver noise is the limiting factor.

It is useful to define the signal threshold power. A good deal of work has been done on this question,

[a]By J. L. Lawson, Radiation Laboratory, MIT.

both theoretical and experimental, and in the course of events a satisfactory criterion has been developed. There is not a defined minimum threshold power above which the signal is always seen and below which it is never seen. One finds experimentally that if the signal power S is plotted against the percentage of cases in which the signal is correctly identified, a "betting curve" is obtained. It takes several times as much signal power to obtain a correlation of 90 per cent as it does to obtain a correlation of 10 per cent. In this paper the signal power which permits a correlation of 90 per cent will be considered the threshold signal.

Two main types of displays are used in radar sets, the A-scope display and the *plan position indicator* [PPI] or intensity-modulated display. In the A-scope display there is presented a trace in which the apparent range of the target appears as abscissa and the amplitude of the received echo as ordinate. Along the trace the ever present receiver noise appears; where the target is there will be a larger average deflection. In experiments on the A scope an artificial echo of controlled amplitude and range was introduced into the receiving system. This artificial echo was so introduced that it could fall into any one of several fixed range positions. Usually six fixed range positions were used. The observer then attempted to call the position occupied by the signal. "Betting" curves were then drawn and S_{90} (90 per cent signal threshold power) determined. This is the signal power, usually measured in terms of noise power in the receiver. Between zero correlation and 90 per cent correlation a change in signal power of perhaps 5 db is usually required. This is quite a large spread, and it is very difficult to determine S_{90} accurately because of the statistical fluctuations. Ordinarily in running such a curve a single threshold power measurement requires 50 to 100 observations. This laborious and lengthy process of obtaining signal threshold is necessary to remove the subjective element. The results obtained in this way are remarkably constant and consistent among different observers. They do depend on other factors, however. They depend both experimentally and theoretically on the number of range positions, and it becomes necessary to indicate the type of variations which obtain. A "6 position, 90 per cent point" has already been defined for this experiment. This is taken as the standard of reference denoted by 0 db. S_{90} for a "1 position" experiment is $+0.8$ db experimentally and $+1.5$ db theoretically. S_{90} for an "N position" experiment is $+1.0$ db both experimentally and theoretically. S_{90} for the "2 position" experiment is -2 db experimentally and $-\frac{1}{2}$ db theoretically. In this last case the experimental improvement is due in part to the statistical difference and in part to the greater ease with which the observer can con-

centrate on the range positions.

In spite of these variations it is felt that any one of these definitions is representatively good. For convenience the S_{90} for the "6 position" experiment has been chosen, since it gives a sufficient number of positions so that statistical determination of S_{90} can be obtained with reasonable ease. It is possible to make the same correlation trials for the intensity-modulated PPI as for the A scope. The signal is put at any of a number of range positions which are fixed in azimuth. Scanning conditions may be included if desired. Some factors which affect the signal threshold power will now be enumerated, and the magnitude of their effects described.

The first such factor is the noise figure of the receiver. In brief, this is simply a multiplicative factor which would go with any of the other determinations made. The noise figure of the receiver specifically measures the amount by which that receiver is noisier than the best theoretical receiver. Ordinarily this noise figure runs to the order of 10 db, which means that the receiver is something like 10 times as noisy as the theoretically perfect receiver. As we are dealing with signal threshold power in terms of the receiver noise power (the latter being a universal parameter) it is only necessary to determine the noise figure of a given receiver in the field to determine what sort of input signal power is necessary.

The second factor affecting the signal threshold is the intermediate frequency or the radio frequency bandwidth B of the receiving system. B represents specifically the narrower of the two. This bandwidth will affect the signal visibility in a way which will be discussed presently. The third quantity is the video bandwidth b of the receiver. At one time it was thought that the video bandwidth and the i-f bandwidth were equivalent, but this is not at all true. Between the i-f and the video systems there is a second detector which is a nonlinear element, which causes frequency conversion to take place. This causes the video bandwidth to have an entirely different action from that of the i-f bandwidth. A third factor is the sweep speed of the scope, denoted by small s. The sweep speed has an important effect which is nearly equivalent to that of video bandwidth. Another parameter is the time interval during which the signal is actually presented to the observer. This quantity will be represented by the letter T and called the signal presentation time. In addition to these there are several other factors connected with contrast effects in the presentation and the scanning variables.

The first four variables mentioned apply to the geometry of the system, and geometrical scaling arguments can be applied to these quantities. One of these variables can thus be eliminated at the start by using not the pulse length τ, but the product $s \times \tau$ as a variable. Similarly, the other variables are $B \times \tau$, $b \times \tau$, and $N \times \tau$. These quantities have a definite physical significance. The sweep speed multiplied by the pulse length is simply the length of the signal on the scope and can be expressed in millimeters if desired. $B \times \tau$ is the i-f bandwidth times the pulse length and turns out to be a simple number. This is a number which will affect the signal visibility curves. Similarly the video bandwidth $b \times \tau$ is another number. The signal power multiplied by the pulse length is simply the energy of the signal per pulse, and so on. These variables are essentially geometrical parameters. The pulse repetition frequency and the signal presentation time are statistical parameters and must be treated in a statistical way as will be shown.

The first geometrical factor to be considered is the i-f bandwidth. The interesting factor is the behavior of signal and noise. Independently, these are known quite well. With respect to noise the power response is proportional to the bandwidth. However, the response to a signal of a particular length, once there has been obtained a bandwidth which is adequate for the transmission of the pulse, will be essentially independent of the bandwidth. When the bandwidth is very narrow the voltage of the output pulse is proportional to the bandwidth of the receiver. A curve can be drawn which is essentially the signal-to-noise power response curve, which for wide bandwidth will be proportional to the signal threshold power, while for narrow bandwidth it will be inversely proportional to the bandwidth. This is exactly the form of curve obtained experimentally. The optimum bandwidth is found to be approximately 1.2 times the reciprocal of the pulse length. The noise power in the receiver is a very poor single criterion as to how small a signal can be seen. For example, with a bandwidth of 1 mc for 1-μsec pulse a signal about 2 db below the noise can be seen. But if the i-f bandwidth is 10 mc for a 1-μsec pulse, a signal is visible 7 db below noise. If the i-f bandwidth is too small, even a signal equal to noise power is invisible. In general, therefore, signal threshold power is rated in decibels above the receiver noise power for a particular value of B (usually $B = 1/\tau$), since this provides a universal scale.

For the video bandwidth the situation is more complicated. A good deal of theoretical work can be done on this problem, but the experimental data do not confirm the theory. The reason is that the video bandwidth is already effectively narrowed by the effect of sweep speed. Video bandwidth effects can be observed when the sweep speed is very fast, where $s \times \tau$ (the pulse length on the scope) is of the order of a millimeter or so. Under these conditions video bandwidth narrowing always reduces the signal visibility and increases the signal threshold power. There is a real difference between the video bandwidth and the i-f bandwidth in the following respect. Decreasing or increasing the i-f bandwidth causes the components of

low-frequency noise in the video to change proportionally. Video narrowing, however, does not change the low-frequency video noise components. Therefore, the reduction in signal visibility with video narrowing is less pronounced than with i-f narrowing.

The human eye cannot distinguish between two objects which are closer together than about 1 minute of arc. If the light intensity contrast is limited, two objects cannot be resolved even at a much greater angular separation. When the separation approaches approximately ¼ of a degree, the best visibility will be obtained for the smallest contrast. Thus, the action of the human eye can be regarded as that of a filter which preferentially selects those frequencies having a period of the order of ¼ of a degree on the scope. At normal viewing distances this value of angular separation is of the order of 1 mm linear separation. Since the screen behaves like a linear transformation between the video signal and the light transmitted to the eye, this filter action of the eye is exactly equivalent to a video filter whose maximum pass frequency corresponds to 1 mm divided by the sweep speed s. For most presentations, where the pulse length is considerably shorter than 1 mm on the scope, this effective video narrowing action of the eye is usually much more important than the effect of video bandwidth in the receiver. It is to be noted, however, that video bandwidth effects in the receiver can be observed when the sweep speed is sufficiently fast for proper delineation of the pulse. There is now a considerable amount of experimental evidence to support this rather simple picture of the combined effect of video bandwidth and the resolution properties of the eye.

Because of this property of the eye, if the viewing distance is maintained constant, a large diameter PPI will be more sensitive in the detection of signals than a small one. A magnifying glass will produce an effective increase in sensitivity on the small scope at the expense, however, of a restricted searching area.

The focus on the PPI or A scope also acts like a video narrowing device. If the tube is defocused along the range scale, equivalent video narrowing will take place by an amount which is dependent upon the spot size. However, because of the effect on the human eye a loss in signal visibility will not occur until the defocused spot is larger than approximately 1 mm. Defocusing to this extent is certainly disadvantageous in the ultimate discrimination of two close radar targets, and for this reason good spot focus must be maintained.

In signal detection it is clearly necessary that the average signal deflection voltage be as large as the average noise fluctuation in the absence of signal. This is a purely statistical problem susceptible to theoretical analysis. Calculations show that the quantities which determine signal visibility, apart from the geometrical factors just described, are the total number of sweeps on which the signal is visible and the total number of sweeps on which only noise is visible. It is assumed that for these sweeps integration or averaging takes place. This result is confirmed experimentally with two restrictions. The total number of signal pulses is given by $T \times PRF$ (pulse repetition frequency), and the signal threshold power is found to vary inversely with both PRF and T. While this holds for all values of PRF under investigation (12.5 to 3,200 c) it holds only for a limited region in T (approximately 0.05 to 3 sec). The reason why the integration is not satisfactory outside these limits of T are related to the maximum flicker frequency detectable by the eye. For times shorter than perhaps 0.05 sec additional sweeps containing only noise will be integrated. Likewise, for T greater than 3 sec the eye and brain do not appear to integrate properly all the individual voltages. In other words, the system has incomplete memory. It has been found that the maximum system integration time (usually of the order of 6 sec) can be increased appreciably by operator practice. With a considerable amount of experience a good radar operator can effectively integrate for times as long as ½ min. It is to be noticed that because of this integration in the eye and brain of a radar operator other methods for providing integration, such as P-7 screens or photographic integration, will fail to provide substantial benefit unless their effective integration time exceeds several seconds. This conclusion is borne out experimentally.

In the radar scanning problem the same factors must be considered as have already been discussed, but, in addition, one must investigate factors peculiar to scanning. Among these are the rotation speed of the antenna, the beam width of the set, etc. It has been found, however, that the statisical problem met with in scanning is quite similar to that encountered in the absence of scanning. The complete system integration depends on two factors: the number of pulses intercepted by the radar beam during one traversal of the target, and scan-to-scan integration. If the scanning rate is sufficiently rapid (faster than 10 rpm) the signal visibility will be independent of the antenna rotation rate. Faster rotation rates intercept a smaller number of pulses for each revolution, but there are a greater number of scan-to-scan integrations which just make up for the deficit. However, below the critical speed of about 10 rpm, scan-to-scan integration will not take place, and the signal threshold power will be proportional to the square root of the antenna rotation rate. This improvement in signal visibility at slower scan rates will continue until the antenna is on the target during each revolution for approximately 6 sec, whereupon the visibility is essentially that of a "searchlighting" set. Thus the total scanning loss is given by the rather simple formula

$$\text{Loss} = \frac{1}{F_t},$$

where F_t is the fraction of time that the system is on target during the scanning procedure. Ordinarily this scanning loss amounts to approximately 10 db in an average radar system, requiring a signal perhaps 10 times as large as the necessary amount for detection while searchlighting. It is important that this formula be used only where scan-to-scan integration takes place.

DISCUSSION

While this paper has specifically been limited to noise considerations, it seemed reasonable to hope that the same general considerations could be applied in determining the visibility of signals in various types of clutter, in particular the simpler types which are echoes from rain and snow. If the mechanisms involved were more thoroughly understood, the fundamentals of the problem would be understood too and could be put together in a coherent form.

The shape of the response curve has been considered by the author and is known to have some effect, but the experimental approach to various shape factors has been rather limited. In the work presented here the response curve of the receivers involved has been that of a so-called double-tuned circuit, whose amplitude response is proportional to

$$\left[1 + \left(\frac{\omega}{\omega_0} \right)^4 \right]^{-\frac{1}{2}},$$

where ω is the frequency difference between the frequency under measurement and the center of the band. ω_0 is the ½ bandwidth. The difference between this response curve's performance and that of a multiply narrowed, synchronously tuned, intermediate amplifier, which has Gaussian response, was not observable experimentally. Theoretically also, there is little difference. It is felt that the considerations may not apply in extreme cases of sharp-edged amplifiers or in single single-tuned circuits but that in other cases the same answers do apply.

The question was raised as to the dependence of signal threshold on pulse recurrence rate. In all the other parameters the visibility of the signal is proportional to the signal energy. The author found that for a given average power the visibility is distinctly better if you concentrate more energy into each pulse and separate the pulses by longer intervals. In other words, the threshold is proportional to the energy per pulse but inversely proportional to the square root of the repetition frequency. This settles a disagreement between two groups, one of which believes visibility would be found independent of pulse repetition rate and the other that it depends on average energy. The answer lies between the two views. In this matter of visibility it is interesting to recall that the first successful radar, which was giving ranges up to 25 miles in 1936, had a receiver bandwidth of about 200 kc and a pulse length of 5 μsec. a combination which lies on the peak of the maximum visibility curve. The pulse length on the radar screen was about 3 mm. The curve for optimum visibility peaks at 1 mm and does not decline very rapidly for longer pulses, so that, too, was near the optimum value. The first production radar for use in the fleet had a pulse length of about 3 μsec and a bandwidth of about 300 kc, which is again on the peak of the visibility curve, and its visible pulse was about 2 mm long on the screen. This was of course not entirely accidental but was fortunate, nevertheless. The preproduction model of this radar was built in 1938.

The author discussed the effect of fluctuating signals in scanning as distinct from the steady signals which had been employed in the experiments described. In the case of signal fluctuation, it is necessary first to define the signal amplitude in such a way that analysis is applicable. Employing the average value as a criterion, the visibility of fluctuating signals may actually prove greater than for steady signals. If the peak value of a fluctuating signal is taken as the signal threshold power, the visibility is probably poorer than for a steady echo, but it is felt that the result would be again essentially independent of the scanning speed, as long as it is high enough to cause pulse-to-pulse and scan-to-scan integration. The limit, however, may occur at 20 rpm instead of 10 rpm.

One variable has been omitted which has proven puzzling. This is the target speed. What really constitutes a scan-to-scan integration? If the target moves the distance of one spot diameter in a scanning period, is it still integrated? It would seem to be so integrated provided the observer is able to perform as an aided tracker, i.e., can appreciate a change in linear motion. If it is not integrated, one would expect to find a difference in signal threshold depending on the target speed, probably in direct proportion to the square root of target speed. Some experiments have been made on simulated echoes of this variety, and there was some indication that targets of higher velocity are definitely harder to see, but this cannot be considered quantitatively established. Signal fluctuation, however, is important, and it is felt that, in general fluctuating targets with cross sections defined on the basis given in the following paper are harder to see by perhaps 2 db but that this estimate is not affected by any arguments about scanning.

There was another inquiry concerning the explanation of the Watson effect observed occasionally at very close ranges when the background noise was so large the normal signal could not be detected. This consisted of an inverted signal smaller in amplitude than the background noise which could be observed to a range of almost 100 yd in sets which had a direct wave extending to 3,000 to 4,000 yd. In these cases the signal, instead of appearing as a small inverted V, showed up as a small upright V, approximately ⅓ the amplitude of the initial noise. This effect had been often reported

on short-range targets. The author considered this to be a form of receiver saturation. Another group had been troubled by the same phenomenon and had attributed it to receiver saturation in which there was blocking of the i-f amplifier during a portion of the time.

RADAR SCATTERING OVER CROSS-SECTION AREA[d]

It is of great interest to determine the cross-section values of aircraft, not only in order to attempt prediction of ranges on these aircraft, but also to make possible the design of radar equipment which will utilize these factors a little better. The instantaneous pattern of reflection properties of an airplane is very complex. It depends upon the frequency, type of aircraft, and certain other factors, such as propeller rotation. The pattern has an extremely complex lobe structure which depends essentially upon the lengths of the plane's structure in terms of wavelength and upon the areas of specular reflection, that is, reflection from fairly large, flat, mirror-like surfaces found in most aircraft, such as the sides, bottoms, or wing surfaces.

It would be possible to define the instantaneous cross-section area as a function of the angle from the airplane, but this kind of thing would be purely academic, since actually the airplane is moving. In the early part of this work an attempt was made to derive a cross-section number which would apply to the actual radar performance on an airplane in flight. The scattering cross section may be calculated from the relation

$$\sigma = \frac{(4\pi)^3 P_r R^4}{P_t G^2 \lambda^2},$$

where the quantities are measured in free space. The symbols are defined on pp. 312-316. They are all easily measurable except P_r, the received power. This was measured by injecting into the system, with a signal generator, an artificial echo which was matched to the size of the airplane echo.

In pratice, σ is necessarily a function of time, and for lack of a better criterion the following procedure was adopted. The signal generator reading was continuously matched to the size of the aircraft echo and recorded for successive 3-sec intervals. The signal measured in decibels above receiver noise power was plotted against range. On a logarithmic scale such a plot should be a straight line whose variation is 40 db for a factor 10 in range. This is actually found, provided one draws a line through the average of the 3-sec interval points. From moment to moment the fluctuation is rather high, but nevertheless a good average line can be drawn.

It is now possible to define a cross section by the condition that its value is exceeded in one-half of these 3-sec intervals, and this appears to be an easy

[d]By J. L. Lawson, Radiation Laboratory, MIT.

operational way of obtaining cross sections. However, this still does not represent what could be called the *average* value for each 3-sec interval. It was found very early that it was very difficult to adjust a signal generator to the average value of the signal. It is much easier to adjust to the top value that has occurred during an interval. The reason for this is that the signal is quite often fuzzy and filled in by propeller modulation. Therefore, the figures represented here are in general the highest values that occur during the 3-sec interval. For this reason we have attempted to see how the value of σ depends upon the interval timing and whether or not it is permissible to put this value into range formulas in the usual way. A rough working model is the following: If these cross-section values are reduced to 60 per cent, they may be used in the range formula presented in the previous paper to obtain the correct operational radar range. The cross section averaged over the lobe structure in the front aspect or tail aspect of a plane would be lower than these values by probably 50 per cent.

Some representative figures are as follows: Fighter aircraft usually vary from 1 to 200 sq ft; medium bombers, B-18, Beaufighter and similar aircraft range from 4 to 600 sq ft; and heavy bombers, B-17, 800 sq ft. The larger bombers such as the B-29 have not been measured but are estimated to be of the order of 1,200 sq ft.

DISCUSSION

To a question regarding the wavelength dependence of aircraft cross sections, the reply was that such a dependence was a function of the structure of the aircraft. Outside surfaces having rounded structures such as wings, wires, and similar members have a cross section which is essentially independent of wavelength and produce random scattering, provided the frequency is high enough. As the frequency is lowered, resonances in the structure of the airplane and differences in the wings may appear. This might possibly cause differences with regard to polarization. At S-band and higher frequencies there seems to be little dependence upon frequency. These figures have been checked at S and X bands with essentially the same results. No sensible dependence on polarization was observed, indicating that at S-band or higher frequencies, this sort of cross-section value will apply.

Ohio State University is conducting an extensive program of cross-section measurements on various types of aircraft for a variety of frequencies up to 500 mc. Measurements are made for all aspects of the aircraft and for both vertical and horizontal polarization. The procedure used is to scale the aircraft down to a convenient model size and to use a correspondingly higher frequency.

The results of these measurements exhibit a confusing lobe structure. In order to give an overall description of the behavior of the cross section, a reasonable

procedure must be found for averaging the data. This has been attempted. At 100 mc, the specular reflections are not particularly marked, though the cross section does increase in directions perpendicular to the axis of the aircraft. There is still fairly strong scattering in all directions. At 500 mc the echoes are almost entirely due to specular reflection. The dependence on polarization is stronger at the lower frequencies.

The author commented that simultaneous measurements of average values for different polarizations showed them to be about the same but that instantaneous pulse-to-pulse photographs of a single target with two different polarizations showed them to be quite different at a given instant.

An inquiry was made as to whether any correlation had been made between radar cross section and type and dimensions of aircraft. A report was mentioned which attempted to show that scattering cross section was proportional to wingspread. The results of the author's group did not appear to correlate with wingspread, but the fuselage is important, and both factors must be significant. Experiments had been made with controlled flights in which the aircraft was flown straight toward or away from the radar site. It was believed that, because of normal wind conditions and such factors as yawing in flight, the results obtained represented an average over an angle of about 10° for both front and rear aspects. Some measurements at 45° aspects were made which showed a drop of about 1 or 2 db for most aircraft. Some aircraft showed a difference between average head and average tail aspect of about 1.5 to 1, and the figures previously quoted represented an average between the two aspects. When the aircraft in turning presents a broadside, specular reflection occurs, and this side flash often exceeds the ordinary signal by 100 times or more.

The comment was made that the measurements described seemed to have been made entirely with tracking radars using A-scope presentation. What would be the probable effects of such fluctuations on radars with search type presentation? The author believed that such fluctuations would affect search-type radars when scanning slowly but that no serious effect had been observed at scanning speeds as low as 2 rpm. When the cross-section figures given were used with a 2-db reduction for average values, the predicted ranges were in agreement with the observed ranges even on scanning or search type radars. This is probably not true at certain longer wavelengths for which the lobe structure is such that an aircraft can "ride" a null for an appreciable time interval. At micro wavelengths, the lobes are so close together that it becomes practically impossible for an aircraft to remain in a null for an appreciable time.

It was inquired whether drops of more than 2 db were to be expected for other aspects, such as 45 degrees. While a complete series of measurements had not yet been made by the author's group, measurements on three or four aircraft in various aspects had revealed no drops below 2 db. Although the calibration had been carried out entirely with signal generators, standard targets consisting of corner reflectors and spheres later produced results in substantial agreement with the theoretically predicted values.

ANGLE-OF-ARRIVAL MEASUREMENTS

ANGLE-OF-ARRIVAL MEASUREMENTS IN THE X BAND[*]

THE PURPOSE of this work was to observe the variation in angle of arrival of waves in the X band. No simultaneous air sounding data were taken although general weather observations were made.

The method of measuring the angle of arrival makes use of a very sharp-beamed antenna (Figure 1) mounted so that it may be mechanically tilted back
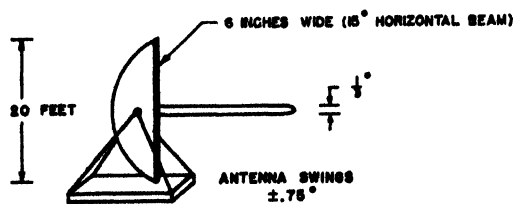
FIGURE 1. Sharp-beamed antenna used for measuring the angle of arrival.

and forth about its center thus sweeping the beam of the antenna through an arc which may be set to include the expected angle of arrival of the incoming signal.

The sharp-beamed antenna has been used to measure the angle of arrival of waves from a distant transmitter over an optical path where both a direct wave and a water-reflected wave are present. If the output
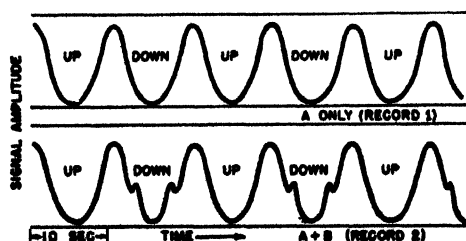
FIGURE 2. Variation in signal intensity during scan. A, direct ray only. B, direct and reflected rays superposed.

of the receiving antenna is fed to a receiver and this receiver is fitted with a recording type output meter, records of the type shown in Figure 2 will be obtained as the antenna scans. Record 1 will be obtained if only a single, direct wave is arriving at an angle corresponding to the mid-point of the antenna swing. The distances between peaks of maximum amplitude along the record will then be equal. A shift in the angle of arrival of the wave would appear on the record as a change in the spacing between the peaks. If two separate waves, direct and reflected, are arriving

[*]By W. M. Sharpless, Bell Telephone Laboratories.

simultaneously, the record will appear something like record 2.

The actual antenna used for the measurement is a section of a parabolic cylinder arranged so that its beam at the center of swing is pointed directly at the transmitter. This is also the angle at which waves arrive on a normal day. A normal day has been taken as one when the angle of arrival is the same (within the accuracy of the measurements) as that calculated from actual earth geometry and when free space field is received from the direct wave.

The physical position of the antenna may be held to approximately 1/100 degree by the use of a plum-bob line dropped from the top of the 20-ft antenna to the base. Possible errors in reading the records, however, limit the expected relative accuracy to about 1/60 degree. Slight errors in the actual building of the antennas and in the locating of the feed limit the final accuracy to what is believed to be 1/25 degree.

The horizontal angle of arrival is measured with a duplicate antenna turned 90 degrees from the vertical with its flat side toward the ground. The accuracy of measurement is the same as in the vertical plane case.

The entire equipment, including the two scanning antennas, other reference antennas, the receiving equipment, and the receiver building are located on a rotatable platform which is 25 ft in diameter. This equipment, located on top of Beer's Hill, New Jersey, may thus be pointed toward any of several transmitters and comparisons made of the angle of arrival from each transmitter.

Observations during the summer of 1944 have been made on two optical paths shown in Figure 3: (a) A 24.1-mile path partly over land and partly over water between New York City and Beer's Hill, New Jersey. The normal reflecting point for the reflected ray on this path is in the salt water of Raritan Bay; (b) a 12.6-mile path between Beer's Hill and Deal, New Jersey. This path is all over gently rolling land. The transmitters at both Deal and New York radiate waves polarized at 45 degrees so that either vertical or horizontal polarization may be used at the receivers.

Results of angle-of-arrival measurements made during the summer of 1944 indicate that on both the Deal and New York circuits the greatest variation of angle of arrival in the horizontal plane was ±1/10 degree. Times were found when the angle of arrival remained as much as 1/10 degree east for short periods on the New York circuit, but for the most part the horizontal angle of arrival normally fluctuated ±1/10 degree from the normal day direction on both the Deal and
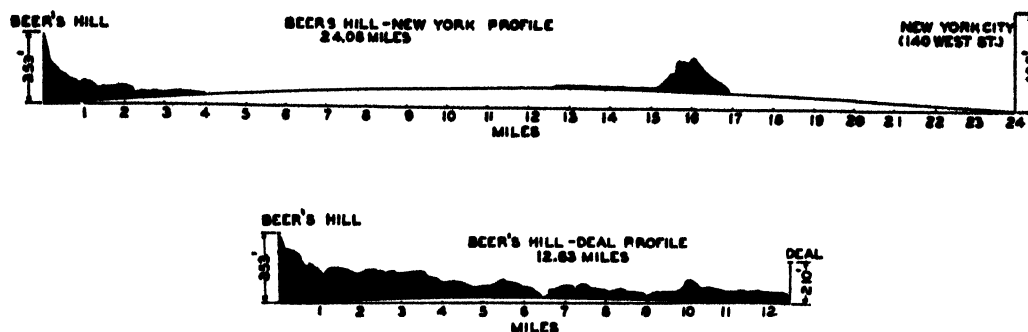
Figure 3. Propagation paths, (top) Beer's Hill to New York and (bottom) Beer's Hill to Deal.

New York circuits. The maximum variation in the vertical angle of arrival on the direct wave on the New York path has been 0.46 degree above that observed on a normal day, while the reflected wave has come in as low as 0.17 degree below the normal reflected wave. (On a normal day the reflected wave on the New York path should be, by calculations, 0.33 degree lower than the direct wave.)

There does not seem to be any correlation between the variation in angle of arrival on the direct wave and the reflected wave. These variations do not as a rule occur together. At the time when the greatest deviation in the reflected wave was present the direct wave was coming in normally. Also, when the direct wave was up 0.46 degree, it was apparently being trapped, and at that time no reflected wave was received. The greatest spread observed between the direct and reflected wave was 0.75 degree (normal 0.33 degree). At this time the direct wave was 0.35 degree above normal while the reflected wave was 0.07 degree below normal. The near proximity of Staten Island to the path normally taken by the reflected wave on the New York path has probably contributed to complexities of the results obtained on this circuit.

The vertical angle of arrival on the Deal circuit has not varied as greatly as on the New York circuit. The degree in the direct wave angle of arrival. The reflected wave is not of sufficient magnitude to be observed on the Deal circuit.

Height run experiments were conducted to obtain a value for the effective coefficient of reflection for the Deal path. An oscillator was hoisted up and down the 175-ft tower at Deal and the resulting received field recorded at Beer's Hill. The field was found to vary 3.6 db from maximum to minimum (3 maximum values and 2 minimum values) as the oscillator changed height, which indicates an effective coefficient of reflection of 0.2. This means that the received reflected wave is 5 times weaker than the direct or 14 db down. The distance above ground at which the maximum and minimum were obtained were noted on the receiver record, and from these the height of the effective reflection layer was obtained. This height was found to be approximately 100 ft above average ground level.

This experiment is to be repeated when leaves have fallen from the trees to determine if the effective reflection coefficient or the height of the reflecting layer has changed.

Rain has been found to influence the X-band circuits in a manner such as to cause a lowering of the received fields. During very heavy downpours, we have experienced as much as 0.8-db attenuation per mile of path length on both the paths. We have no way of knowing how much rain was falling over an entire path, but the figure of 0.8 db per mile represents the maximum value of rain attenuation so far recorded on our circuits.

Only part-time observations have been made on this project, and the results reported are based on such observations. It is not known, therefore, if more extreme conditions than those reported have existed at times when no observations were being made.

METEOROLOGICAL ANALYSIS OF ANGLE-OF-ARRIVAL MEASUREMENTS[b]

Purpose

Recent experiments on propagation in the X band conducted by Bell Telephone Laboratories [BTL] have indicated that the angle of arrival of microwaves may be considerably at variance with that computed on the basis of rectilinear propagation. Deviations as large as 0.46 degree from true bearing[c] were measured during the summer season over a 24-mile path, partly over land and partly over water. The deviations found experimentally exceed considerably the tolerances specified on angle of elevation, azimuth, and height determination in present military characteristics on fire-control radar equipment.

An analysis of propagation from the meteorological point of view has been undertaken to determine whether deviations from rectilinear propagation can

be explained by, and predicted from, meteorological data and whether observed extreme deviations can be realized from plausible meteorological stratification. The Bell Laboratories' experimental angle-of-arrival measurements made during the summer of 1944 have been compared with deviations evaluated from meteorological data obtained concurrently by the Signal Corps though not coordinated at the time with these experiments. The current paper is intended to report the results of this study and the procedure utilized in the analysis and, in turn, to establish a framework for interpreting further propagation experiments of this type.

Theory

The equations of propagation can be written in a form such that the angle of departure of the radiation at the transmitter (the direction of the normal to the wave front) and the angle of arrival at the receiver can be written as functions of the meteorological stratification and the constants of the installation (distance between and heights of transmitter and receiver). The solution of the equations of motion is given below by the use of an electromagnetic wave velocity profile obeying a radial power law. The relation of the exponent m in this power law to the excess modified refractive index M is then deduced. The power m in the velocity profile equation is assigned the definition of "meteorological stratification parameter," since it determines the change of modified index of refraction with height.

From Figure 4,

$$d\theta = \frac{dr}{r \tan \beta} = \frac{ds}{b}. \qquad (1)$$

Introduce the electromagnetic wave velocity profile

$$\frac{v}{v_0} = \frac{n_0}{n} = \left(\frac{r}{b}\right)^m. \qquad (2)$$

Hence,

$$s = \frac{b(\beta - \alpha)}{1 - m} \qquad (3)$$
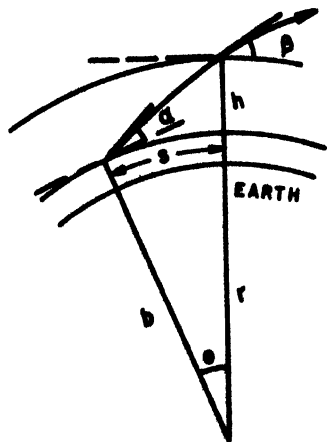
FIGURE 4. Geometry of a ray in the atmosphere.

where

$$\cos \beta = \left(\frac{r}{b}\right)^{m-1} \cos \alpha. \qquad (4)$$

Snell's law states that

$$\frac{v_0}{b \cos \alpha} = \frac{v}{r \cos \beta}. \qquad (5)$$

Then,

$$(1 - m)dr = r \tan \beta d\beta \qquad (6)$$

and

$$\frac{ds}{b} = \frac{d\beta}{1 - m}. \qquad (7)$$

Now $r = b + h,$

where $h \ll b.$ (8)

The excess modified refractive index M is given by

$$M \cdot 10^{-6} = \frac{nr}{n_0 b} - 1$$

$$= \left[1 + \left(\frac{h}{b}\right)^{1-m}\right] - 1 \simeq (1 - m)\frac{h}{b}. \qquad (9)$$

If now the relation for the distance s is solved simultaneously with the equation stating Snell's law of refraction, we have the angle of arrival α as a function of the excess modified refractive index M, uniquely relating the angular deviation from true bearing to the distribution of modified refractive index required to produce that deviation.

Analysis of the BTL New York-to-Beer's Hill Circuit

The results obtained by Bell Telephone Laboratories, Inc., on measurements of the angle of arrival of microwaves in the X band are contained in two BTL reports.[1,2] The New York-to-Beer's Hill propagation circuit proved to be the more suitable for the meteorological analysis of angle of arrival. On this path the transmitter was located on the New York Telephone building at an elevation of 492 ft above mean sea level; the receiver was erected on top of Beer's Hill at an elevation of 353 ft. The propagation path had a length of 24.08 miles and ran several degrees east of north from Beer's Hill to New York. The bearing from receiver to transmitter on this circuit on the basis of true earth geometry is 0.11 degree below zero elevation angle of Beer's Hill.

During the summer of 1944 a limited number of vertical temperature and humidity soundings were secured by personnel of Wave Propagation Studies, Evans Signal Laboratory, at a 400-ft radar tower in Oakhurst, New Jersey. The location of the tower is shown on the map in Figure 5. The tower stands on a hill 128 ft above mean sea level. The limit of observation is 375 ft above the base of the tower; hence the absolute elevation was 503 ft. It follows that soundings over the height of the tower sample the atmosphere
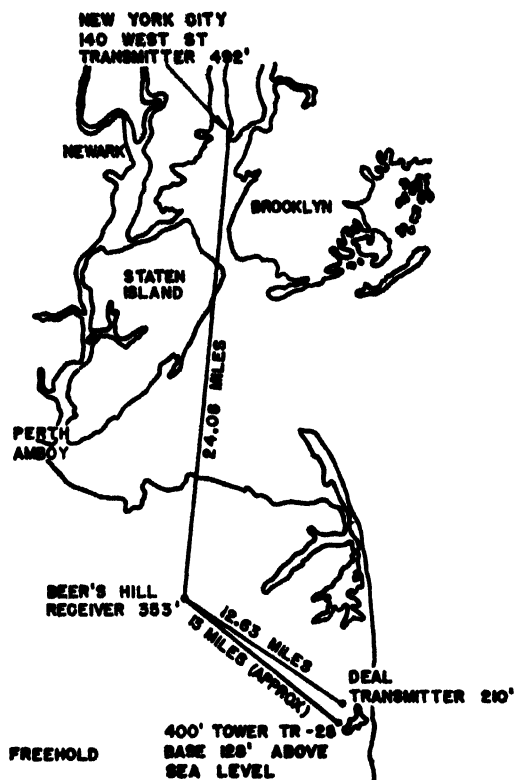
FIGURE 5. Plan view of propagation paths.

between approximately 11 ft above the transmitter and 225 ft below the receiver.

The Angle of Arrival Deduced from Type Cases of Atmospheric Stratification

When the path is confined to a layer between receiver and transmitter, there are two limiting paths, as illustrated in Figure 6A: Path A leaving the transmitter at some angle $\beta < 0$ and arriving at the receiver with $\alpha = 0$; Path B leaving the transmitter at an angle $\beta = 0$ and arriving at the receiver with $\alpha > 0$. By applying the equations deduced from theory and expressed by data in Table 1, the necessary and sufficient

TABLE 1

Path	α at receiver (degrees)	β at transmitter (degrees)	Deviation of α and β from true bearing	m
A	0	− 0.125	+ 0.111	0.64
Intervening path	+ 0.0625	− 0.0625	+ 0.1735	1.00
B	+ 0.125	0	+ 0.236	1.36

modified refractive index distributions with height in the layer can be evaluated for the limiting paths A and B and for all intervening paths. Table 2 shows the value of the stratification parameter m required. We therefore conclude that, for a path confined to the layer between transmitter and receiver, the deviation

from true bearing must be confined to the interval +0.111 to +0.236°, and the change in the modified refractive index between receiver and transmitter must be in range −2.4 to +2.4 M units. These limits hold for an approximately linear variation of index between receiver and transmitter.

Radiation along paths of type C, which penetrates the layer below the receiver height (see Figure 6B), arrives at the receiver at an angle $\alpha < 0$; therefore, M will of necessity increase by more than 2.4 units from receiver to transmitter. We consider three stratifications producing paths of this category.

1. The so-called "standard" atmosphere utilized for the purposes of representing "normal" propagation by rectilinear rays on an earth distorted to a radius 4/3 that of the true earth. The increase of M is at a rate of 3.6 units per 100 ft.

2. Adiabatic equilibrium for an unsaturated atmospheric layer, representing the condition of a completely stirred or mixed stratum of air. The increase of M is 4.0 units per 100 ft.

3. Rectilinear propagation on a true earth. For this condition there is no variation of electromagnetic velocity with height, and M increases by 4.76 units per 100 ft, equal to the rate of curvature of the earth.

The computed deviations of the angles α and β at the receiver and transmitter, respectively, are given in Table 2. It will be noted that the condition of rectilinear propagation on a true earth produces an angle
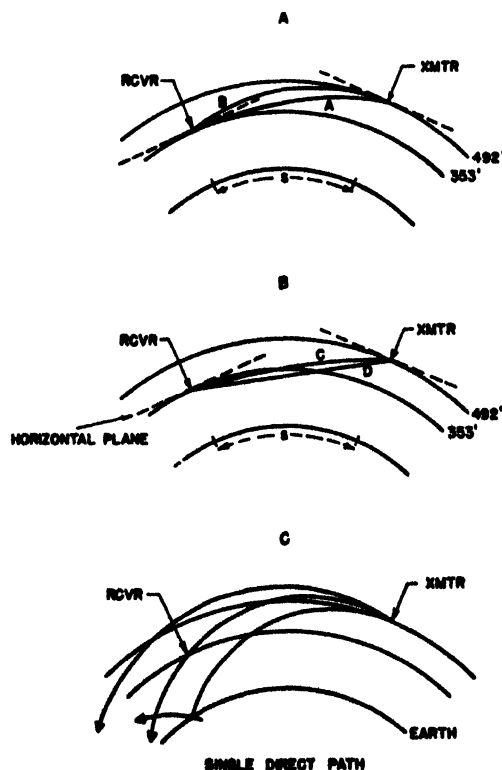
FIGURE 6. Types of vertical variation in ray paths.

TABLE 2

Type of atmospheric stratification	α at receiver (degrees)	β at transmitter (degrees)	Deviation of α and β from true bearing	m
"Standard" atmosphere	− 0.069	− 0.194	+ 0.042	2.44
Adiabatic equilibrium	− 0.083	− 0.208	+ 0.028	0.16
Rectilinear propagation on a true earth	− 0.111	− 0.236	0	0

$\alpha = -0.11°$, which is the true bearing from receiver to transmitter. From the data of Table 1 it follows that a "standard" atmosphere and an atmosphere vertically mixed so as to be in adiabatic equilibrium both provide a variation of modified refractive index with height of a magnitude such that the angle of arrival measured at the Beer's Hill receiver under these conditions is within 0.04° of true geometric bearing. In view of the fact that the instrumental accuracy of the Beer's Hill antenna system is ±0.04°, it follows further that the differences among these three meteorological stratifications will not be evident in the measurements.

Consider now a case in which the radiation path penetrates the layer above the transmitter. The occurrence of an angle of arrival at the Beer's Hill receiver in excess of 0.236° above true bearing will require a path of propagation rising to some level above the New York City transmitter. The variation of M with height within the layer immediately above the transmitter will be critical in determining the magnitude of the signal received and its angle of arrival. The analysis following is limited to one particular case of this category producing an extreme deviation from true bearing in the angle of arrival.

For the paths shown in Figure 6C, the M distribution between 353 and 492 ft above mean sea level is that computed from the observed meteorological data on the 400-ft tower at 0800 on July 7, 1944. Using only this portion of the actual sounding, the variation of modified index of refraction in the layer immediately above the transmitter has been computed as a function of the angle α at the receiver. In the case of the angle $\alpha = 0.355°$ (deviation from *true* bearing equal to +0.466°), the calculated index at the level of total refraction, which computes as 505 ft, is very closely that observed at the uppermost level of meteorological sounding (503 ft). Thus an angle of arrival deviating by as much as 0.47° from true geometric bearing is entirely possible for the meteorological situation of 0800, July 7, 1944 and for the positions of the New York transmitter and Beer's Hill receiver and could have been predicted from the observed meteorological sounding.

A second significant conclusion can be readily deduced by considering the modified refractive index

distributions required in the layer immediately above the transmitter for different values of α. It is apparent that the lapse of modified index required for any of the angles considered in this example is not substantially different among all four angles; the primary requisite for the larger α's is that the lapse continue to greater heights. Thus relatively small fluctuations in the meteorological elements can cause a time change of 0.1° in the angle of arrival measured at the Beer's Hill receiver. Furthermore, a particularly unfavorable combination of small changes in the meteorological elements in this layer may cause the signal at the receiver to fall to a very low level. A similar conclusion is not valid for the case of propagation confined to the layer between transmitter and receiver and the case of path penetration below the receiver, since another slightly different path can always be found along which energy can reach the receiver directly.

A third significant conclusion can be deduced by inspecting the computed deviations from true bearing of the angles at the receiver and the transmitter, as given in Table 3. It will be noted that the deviation from true bearing of the angle of arrival at the receiver is not the same as the deviation from true bearing of the angle of departure at the transmitter. In fact the data of Table 3 indicate that, under the meteorological situation of 0800 on July 7, 1944, the angle of arrival at the receiver would have been

TABLE 3

α at receiver (degrees)	β at transmitter (degrees)	Deviation from true bearing α	β	m
+ 0.355	+ 0.038	+ 0.466	+ 0.274	1.366
+ 0.372	+ 0.119	+ 0.483	+ 0.354	1.972
+ 0.401	+ 0.190	+ 0.512	+ 0.426	2.436
+ 0.458	+ 0.292	+ 0.569	+ 0.528	3.052
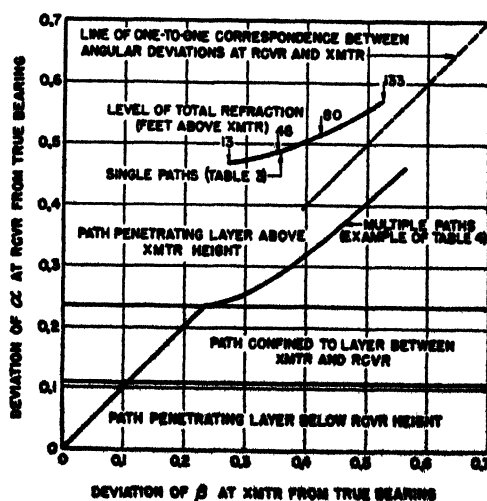
FIGURE 7. Correlation of deviations.

+0.27° above true bearing in place of +0.46°, were the receiver and transmitter interchanged at the end points of the path. On the other hand, for both cases 1 and 2 treated above, the meteorological stratification was such that the angular deviations from true bearing at both receiver and transmitter were the same. The relations of the angular deviations from true bearing at the end points of the path are summarized in Figure 7.

A fourth conclusion can be deduced by considering the curve in Figure 7 based on the computations tabulated in Table 3. It will be recalled that a fluctuation of 0.1° in angle of arrival at the receiver was concluded as possible as a result of relatively small fluctuations in the meteorological elements in the layer immediately above the transmitter. But it should now be noted that fluctuation of angle of departure at the New York transmitter is approximately 0.25° when the Beer's Hill angle of arrival varies approximately

0.1° for the particular meteorological situation of 0800 on July 7, 1944.

It therefore follows, in summary, that the deviation from true bearing measured at the position of the receiver depends not only on the range between transmitter and receiver and on the meteorological conditions but also and equally well on the relative difference in heights of transmitter and receiver and the position in height of the receiver with respect to the transmitter.

Comparison of Computed to Measured Angle of Arrival

The experimental measurements of angle of arrival secured by Bell Telephone Laboratories and the meteorological data obtained on the 400-ft tower in Oakhurst, have been analyzed to determine whether any significant correlations exist between the meas-
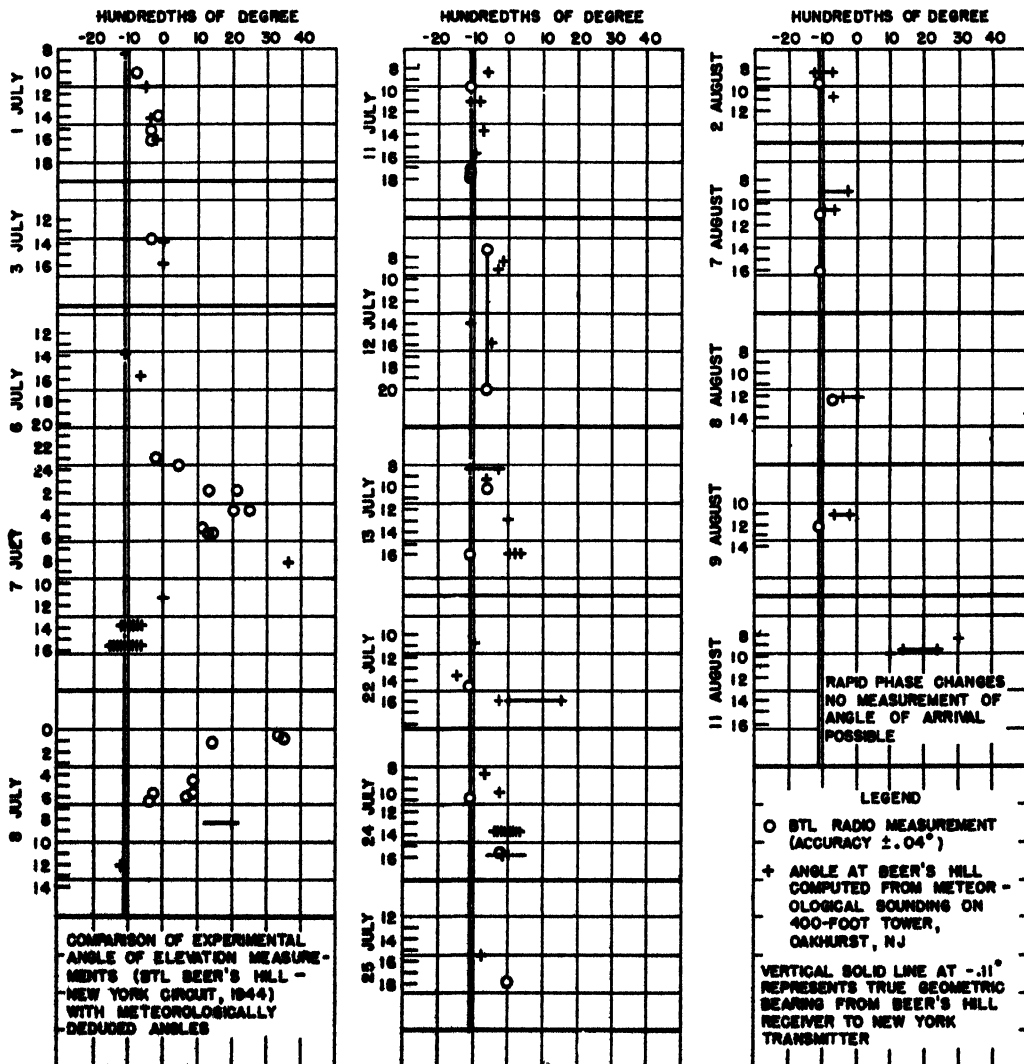
FIGURE 8. Measured versus computed angles of arrival

ured angles of arrival at the Beer's Hill receiver and the angles of arrival computed from meteorological data. A grand synthesis is presented in Figure 8 of all days for which both BTL propagation measurements and Signal Corps tower meteorological soundings were available for comparison. Since simultaneity in radio and meteorological measurements was a rare occurrence, the angle of arrival evaluations from both sources of data are plotted along a time scale (in hours) for each day of the period. The angle evaluations from radio data are represented by circles; angles calculated from the meteorological data are represented by crosses of time length equal to the duration of sampling of the layer between transmitter and receiver (including both ascent and descent of the tower). Equipment limitations set the accuracy of BTL angle of arrival measurements at $\pm 0.04°$.

It is believed that generalized, overall conclusions for the entire period of comparison can be made as follows:

1. That occasions of true bearing and "near true bearing" (say -0.11 to $0°$) could have been predicted from the meteorological data.

2. That the occurrence of extreme deviations from true bearing would have been predicted from meteorological data nearest in time to the radio measurements.

3. That the magnitude of the most extreme measured deviation ($0.46°$) from true bearing can also be calculated from observed meteorological data, though not simultaneously observed.

Conclusions

The propagation path of microwave radiation can be fairly well specified, given only a knowledge of the temperature and water vapor pressure distribution in the lower atmosphere and the positions in space of transmitter and receiver. The equations of motion of the propagation of the individual wave fronts have been written in a form such that the angles of departure from the transmitter and the angles of arrival at the receiver can be evaluated directly from the meteorological stratification. Application of the theory to certain angle-of-arrival radio propagation experiments conducted by Bell Telephone Laboratories during the summer of 1944 has resulted in the following conclusions:

1. A surprisingly good correlation exists between angles of arrival computed from meteorological and survey data only and the angles of arrival determined experimentally.

2. The extreme deviations ($0.46°$) from rectilinear propagation measured experimentally by BTL are confirmed as plausible on the basis of observed meteorological stratification.

3. The meteorological analysis indicates that deviations from rectilinear propagation and the fluctuation of the deviations about a mean value are as much a function of position of transmitter and receiver as they are a function of the existing meteorological structure.

It is strongly recommended that low-level meteorological soundings be considered an indispensable part of any experimental angle-of-arrival measurements. The good correlations secured between evaluation of angles of arrival from meteorological data and angles of arrival measured experimentally suggest that deviations from rectilinear propagation can be accounted for by measurable atmospheric conditions and that, further, these deviations can be reasonably well predicted.

THE PROPAGATION
OF RADIO WAVES THROUGH
THE STANDARD ATMOSPHERE

VOLUME III

PROPAGATION OF RADIO WAVES:
INTRODUCTION AND OBJECTIVES

FACTORS INFLUENCING PROPAGATION

THE PROPAGATION of radio waves through the atmosphere and around the curve of the earth, at frequencies above 30 mc, is influenced by so many factors that it is desirable to give first an overall survey of the problem. This chapter presents the problem of propagation in broad perspective in contrast with many of the later chapters which are devoted to detailed consideration of special phases and methods of calculation.

Our purpose has been to provide information designed for men with college training in radio, physics, or electrical engineering, which:

1. States the basic laws of propagation, ·that is, shows how the characteristics of the earth and the atmosphere control the propagation of radio waves;

2. Gives the fundamental properties of the basic types of antenna systems, particularly their directivity and gain;

3. Gives the reflecting properties of targets such as airplanes for use in detection by radar;

4. Teaches the reader how to calculate field strength or obtain the coverage diagrams, given a particular set, power, and site;

5. Gives the fundamental information required in the above calculations for application to the radar and communication sets used in operational theaters;

6. Provides illustrative material and sample calculations which show how the laws of propagation may advantageously be used in the location and operation of radar systems, communication sets, and countermeasure equipment designed to deceive the enemy and to prevent jamming of equipment by enemy action or by mutual interaction of our own sets.

FUNDAMENTAL PROBLEMS AND LIMITATIONS

Meaning of Propagation

By propagation is meant the movement of radio waves through the atmosphere, and the transfer, by a wave mechanism, of radiant energy from a transmitting antenna to a receiving antenna. The problem of propagation requires an understanding of the manner in which the wave energy is emitted and received as well as of the manner in which it flows through the atmosphere. The radio engineer must understand this general mechanism, be able to evaluate the factors which play contributory roles, and, for a given amount of power emitted from a given transmitter, be able to compute the strength of the radiation field at any point in space or to locate all the points in space where a given field strength occurs.

The problem divides naturally into two parts, (1) the one-way transmission or communication problem, and (2) the two-way transmission or radar problem. In the former the prime requisite is to calculate the amount by which the wave and its field strength are attenuated in passing from the transmitter to a receiver and yet permit a field at the receiver sufficient at least to produce the minimum detectable signal. In the latter problem the attenuation must be calculable for the two-way journey from transmitter to the target and back to the receiver, which frequently uses the same antenna as the transmitter. In this type of problem, due account must also be taken of the reflecting and reradiating properties of the target.

Knowledge of these factors is indispensable for the design, installation, and successful operation of both communication and radar systems.

Atmospheric Layers

The atmosphere from one point of view is composed of two layers, the troposphere and the stratosphere. The former is a layer adjacent to the earth which extends upward approximately 10 km, in which the temperature decreases about 6.5 C per kilometer with increasing altitude to a value, at the upper boundary, of about − 50 C. Above this is the stratosphere in which the temperature remains approximately constant at − 50 C.

The ionosphere, as its name implies, is a layer (or series of layers) composed of ions and free electrons lying at an elevation of approximately 100 km. See Figure 1. These layers play an important role in the transmission of waves at frequencies below 30 mc and are responsible for transmission over very long distances. At the higher frequencies, which are the concern of this volume, the portion of the waves which penetrate the ionosphere is not useful for transmission.

From this it follows that propagation at the higher frequencies (above 30 mc), to be useful, must occur entirely in the troposphere. This volume therefore is concerned only with tropospheric propagation.
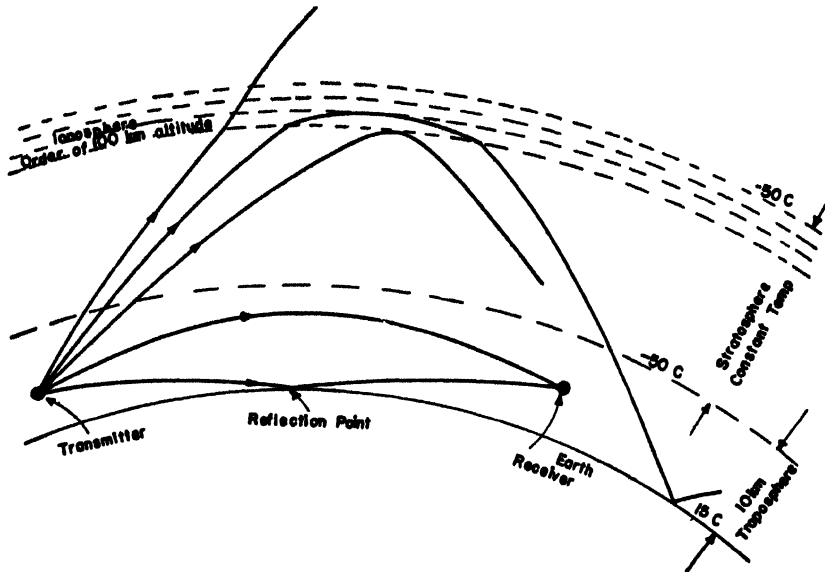
FIGURE 1. Transmission along and reflection from the ionosphere occurs primarily with frequencies below 30 mc. At higher frequencies useful transmission is primarily concerned with the nearly horizontal rays in the troposphere; higher angle radiation passes through the ionosphere and is lost.

Standard Atmosphere

Propagation of radio waves in the troposphere is materially influenced by the distributions of temperature, pressure, and water vapor. The condition most nearly approximated in the Temperate Zone has been accepted as the so-called *standard atmosphere*, and propagation under this condition has been studied and calculations made thereon.

In the standard atmosphere specified by the National Advisory Committee on Aeronautics [NACA] the temperature is assumed to decrease with altitude at the rate of 6.5 C per kilometer, starting from 15 C at sea level, with a sea level dry air pressure of 1013.2 millibars, which is equivalent to 760 mm Hg pressure (see Table 1).

To simulate the actual atmosphere of the temperate zones it is necessary further to specify a water vapor pressure. The value chosen is 10 millibars at

sea level, decreasing with altitude at the rate of 1 millibar per 1,000 ft up to 10,000 ft. With this addition the conditions for a *moist standard atmosphere* are specified in Table 1. This value of water vapor pressure yields a value of relative humidity approximating 60 per cent.

Listed also in Table 1 is the index of refraction n. The gradient of this quantity, dn/dh, controls the curvature of the rays for a wave moving in the approximately horizontal direction; n is given by the formula

$$(n - 1)10^6 = \frac{79}{T}\left(p + \frac{4800e}{T}\right), \qquad (1)$$

where T is the absolute temperature, p and e are the total pressure and moisture vapor pressure, respectively, in millibars, at height h above sea level. In the moist standard atmosphere, n decreases linearly with height h at the approximate rate of

TABLE 1. Properties of the atmosphere.

NACA standard dry atmosphere					Moist standard atmosphere			
h Altitude		t Temp C	p − e Dry air pressure millibars	Index of refraction $(n-1)10^6$	e Water vapor pressure millibars	Saturated water vapor pressure millibars	Per cent relative humidity	Index of refraction $(n-1)10^6$
Feet	Meters							
0	0	15.0	1,013.2	278	10	17.1	58.5	318
500	152	14.0	995	274	9.5	16	59.4	312.4
1,000	305	13.0	977.1	270	9	15	60.0	309
1,500	457	12.0	960	266	8.5	14	60.7	304
2,000	610	11.0	942.1	262	8	13.1	61	295.6
3,000	.915	9.1	908.1	254	7	11.6	60.3	284
4,000	1,220	7.1	875.1	247	6	10.1	59.4	273
5,000	1,525	5.1	843	240	5	8.8	57	262

0.039 × 10⁻⁶ units per meter.

There are several reasons why this book concerns propagation in the moist standard atmosphere.

1. The atmosphere in certain places (particularly the temperate zones) and over considerable periods of time is substantially standard in character.

2. Calculations based on the standard atmosphere serve as a standard against which propagation in nonstandard atmospheres may be compared.

3. A great deal of propagation information now available in the field is based on propagation calculated for standard conditions.

Propagation in the Moist Standard Atmosphere

The radiation energy emitted by a transmitter is a wave spreading out in three dimensions, which may be represented by a series of concentric spherical wave fronts or by a system of lines called rays. The velocity at any point on the wave front is given by

$$v = \frac{c}{n} = \frac{3 \times 10^8}{n} \quad \text{meters per second.} \quad (2)$$

Since n decreases with height, the upper portions of the wave front move with higher velocities than the lower portions, and the wave paths as represented by the rays are curved slightly downward, as shown in Figure 2.

The radius of curvature of the rays ρ is given by

$$\frac{1}{\rho} \cong -\frac{dn}{dh} = +0.039 \times 10^{-6} \quad \text{units per meter} \quad (3)$$

and ρ, therefore, is equal to 25.5 × 10⁶ meters, which is approximately four times the radius of the earth ($\rho = 4a$). As a result the distance to the radio horizon is some 15 per cent greater than the geometrical line-of-sight distance from the transmitter to the horizon. This curvature of the rays by the atmosphere is called *refraction*.
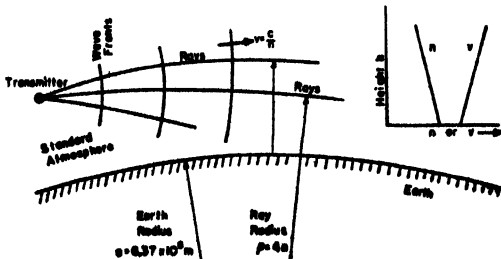
FIGURE 2. Curvature of rays in the standard atmosphere.

For the purpose of calculating wave propagation, only relative curvature of the earth and the rays is of interest. Compensation is made for the effects of refraction by replacing the actual earth with a radius a by an equivalent earth with a radius ka

and replacing the actual atmosphere (in which the index of refraction n decreases with height) by a homogeneous atmosphere (constant n) in which the rays are straight lines. Since $1/a$ is the curvature of the earth and $1/\rho$ the curvature of the rays, we may set their difference equal to $1/ka$, the curvature of the equivalent earth. Thus

$$\frac{1}{a} - \frac{1}{\rho} = \frac{1}{ka}$$

and $\quad\quad\quad\quad\quad\quad\quad\quad\quad\quad\quad\quad (4)$

$$k = \frac{1}{1-(a/\rho)} = \frac{1}{1 + a\frac{dn}{dh}}$$

Since $\rho = 4a$, $k = 4/3$, and ka, the radius of the equivalent earth, equals 8.49 × 10⁶ meters. See Figures 4 and 5 in Chapter 4.

Propagation in Nonstandard Atmospheres

Though this subject is beyond the scope of this volume it is desirable to present a brief discussion of the salient features.

Not infrequently the lower atmosphere is stratified in horizontal layers in which the variations with height of the temperature and moisture content are nonstandard. Of particular interest is a sharp rise in temperature with increasing height (temperature inversion), or a sharp decrease in water vapor content, or a combination of the two. If these variations from the standard distribution are sufficiently great, horizontal radio ducts may be formed in the atmosphere. In this event an appreciable fraction of the wave energy (only that fraction moving in the nearly horizontal direction) may be constrained to propagate along the duct to distances far beyond the horizon and the field strength may be large compared with that obtainable under standard conditions. This phenomenon produces a marked bending of the wave paths or rays and is known as super-refraction. To take fullest advantage of this phenomenon the antennas should be located in the duct.

Ducts are of various types:

1. *Overland.* These are surface ducts formed at night by the radiation cooling of the earth.

2. *Oversea.* In the trade-wind belt there appears to be a continuous duct of the order of 50 ft thick starting at sea level.

3. *Land to sea.* Warm dry air flowing from land out over cooler water often yields surface ducts 100 or more feet thick.

4. *Elevated.* Caused by subsidence of large air masses, these ducts may be found at elevations of perhaps 1,000 to 5,000 ft and may vary in thickness from a few feet to 1,000 ft. They are common in Southern California and certain areas in the Pacific.

Depending upon the strength and the thickness of the duct, there is a limiting frequency below which the duct cannot trap the wave energy. Though trapping does at times occur at 200 mc, it is more likely to occur at the higher frequencies such as 3,000 mc.

Ability to calculate performance under standard conditions is necessary if performance under non-standard conditions is to be evaluated.

Radio Gain

The basic problem to be solved is that of computing the radio gain of a transmitting-receiving system.

The radio gain of a transmitting-receiving system is defined as the ratio of received power P_2, delivered to a load matched to the receiving antenna, to power P_1, supplied to the transmitting antenna, with both antennas adjusted for maximum power transfer Thus

$$\text{Radio gain} = \frac{P_2}{P_1}, \quad (5)$$

which is equal, in the decibel scale, to

$$10 \log_{10} \frac{P_2}{P_1} = \text{radio gain in decibels} \quad (6)$$

The attenuation is the reciprocal of the gain. Since $P_2/P_1 < 1$, the gain in decibels is necessarily a negative quantity. The attenuation in decibels is a positive quantity equal in magnitude to the gain in decibels.

The radio gain can be taken as the product of physically significant factors. Among these are the gains G_1 and G_2 of the transmitting and receiving antennas respectively; and A^2 which accounts for all other influences modifying the transmission of power. A is called the gain factor.

$$\text{Radio gain} = \frac{P_2}{P_1} = G_1 G_2 A^2. \quad (7a)$$

The radar problem involves double transmission over the path as well as the reradiating properties of the target, $16\pi\sigma/9\lambda^2$.

$$\text{Radar gain} = \frac{P_2}{P_1} = G_1 G_2 A^4 \left(\frac{16\pi\sigma}{9\lambda^2}\right), \quad (7b)$$

where σ is the radar cross section of the target and λ is the wavelength.

The gain factor, A, may also be split into two factors, so that

$$A = A_0 A_\phi. \quad (8)$$

Here A_0 is the free-space gain factor for doublet antennas (see next section and pp 338, 339, 379) adjusted for maximum power transfer. $A_0 = 3\lambda/8\pi d$ where d is the distance between doublets. A_ϕ is the path gain factor which includes all additional influences modifying the transmission of power.

These factors may also be related to the field strength, E, at any point in space by

$$E = E_0 \sqrt{G_1} A_\phi \quad (9)$$

and

$$\frac{A}{A_0} = \frac{E}{E_0 \sqrt{G_1}}. \quad (10)$$

Here E_0 is the free-space field at a point in space set up by a doublet transmitter and $E_0 \sqrt{G_1}$ is the free-space field of a transmitter with antenna gain G_1.

The primary function of this book is to show how the factors A and A_ϕ may be calculated, taking into account all contributory influences which modify their magnitudes.

Radio Gain of Doublet Antennas in Free Space

This is the fundamental and simplest case of transmission of radiant energy, against which other transmitting combinations may be compared. Two doublet antennas (for which the gains, by definition, are unity) are set up in free space in a manner which insures the maximum transfer of power to the receiver circuit, i.e., the doublets are parallel to each other, have a common equatorial plane, and the receiver circuit impedance is matched to that of the receiving antenna (see Figure 3). Then for free space,

$$\text{Free-space gain} = \frac{P_2}{P_1} = A_0^2 = \left(\frac{3\lambda}{8\pi d}\right)^2, \quad (11)$$

and the free-space field strength at distance d from
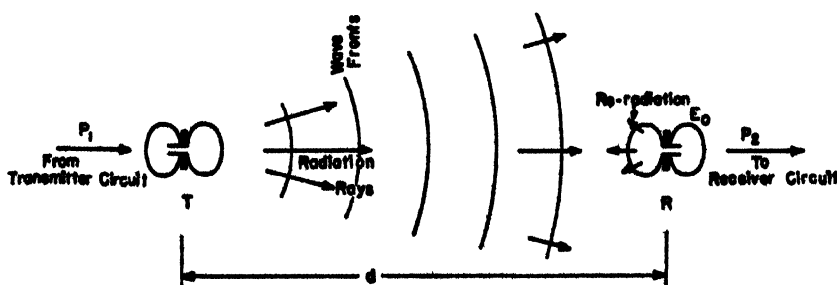
FIGURE 3.   Doublet antennas in free space.

the transmitter is

$$E_0 = \frac{3\sqrt{5}\sqrt{P_1}}{d}. \qquad (12)$$

P_1 is the power radiated by the doublet transmitting antenna (see pages 336, 337).

SURVEY OF PROPAGATION

Outline

We will first consider those factors which are instrumental in modifying the transmission or the attenuation that arises from the presence of the earth, then give typical curves of both vertical and horizontal variation of field strength, and lastly, consider the problem of coverage.

Factors Modifying Transmission

The important factors which affect the distribution of field strength are the following:

1. *Antenna characteristics.* For many applications the most important feature is the gain which is a measure of the directivity of the antenna. From a value of 1.09 for the half-wave dipole, the gain may increase to several thousand for the highly directive parabolic antennas used in the microwave range.

Antennas with high gains which concentrate the radiated energy into beams of small angles require less power to produce a detectable signal. This is particularly important in radar where the attenuation of the two-way path is pronounced.

Qualitative radiation patterns for the doublet antenna and an antenna with high directivity are illustrated in Figure 4. The radial distance to the pattern gives the relative amount of power per unit area radiated in that direction.

2. *Polarization.* The wave is said to be polarized horizontally or vertically according to whether the electric vector E is parallel to the earth's surface or is in a plane perpendicular thereto. A horizontal electric doublet (axis parallel to the earth's surface) radiates horizontally polarized waves, whereas a vertical doublet radiates vertically polarized waves.

Too many factors are involved to make it possible
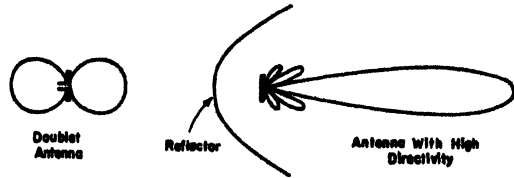
FIGURE 4. Antenna radiation patterns.

to state in general which type of polarization should be used in a particular case.

3. *Refraction.* As explained in text on page 329, refraction in the standard atmosphere can be taken into account by using an equivalent earth with a radius equal to $4/3$ that of the actual earth and a homogeneous atmosphere in which the rays traverse straight line paths.

4. *Reflection.* Well above the line of sight (see Figure 5) the field at the receiver R is, the vector sum of the fields radiated along the paths of the direct and reflected rays. The contribution from the reflected ray path depends primarily on the manner in which the earth (or sea) acts as a reflecting body.

Upon reflection, the angle of incidence ($90° - \psi$) is equal to the angle of reflection, irrespective of the polarization of the wave, but the strength of the field in the reflected ray relative to that in the incident ray depends upon (a) the grazing angle ψ, (b) the type of polarization, (c) the reflecting properties of the earth or sea, and (d) the divergence factor.

The incident beam or bundle of rays, in general, is partially absorbed by the earth, while the reflected portion is reduced in strength and suffers a phase shift relative to the incident beam. (In the case of sea water with horizontal polarization, the earth acts substantially as a perfect reflector, for which the reflection is 100 per cent complete and the phase shift is 180 degrees for all grazing angles. This is true for vertical polarization only at zero grazing angle.)

The *divergence factor* is introduced to account for the fact that an incident bundle of rays striking a spherical surface diverges upon reflection and produces a further decrease in strength of the reflected beam.

Reflection from hills, trees, and other obstacles must frequently be taken into account, particularly
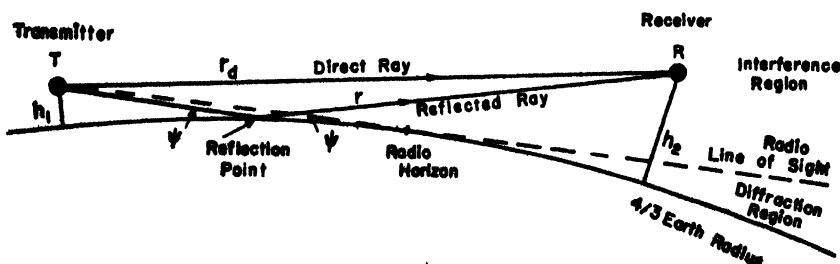
FIGURE 5. Geometrical relations for rays.

in the siting of very high frequency [VHF] communication sets.

5. *Diffraction.* The mechanism by which radio waves curve around edges and penetrate into the *shadow* region behind an opaque obstacle is called diffraction. The explanation usually given is based on Huyghens' principle. This, in effect, states that every elementary area on a wavefront (see *P* in Figure 6) is a center which radiates in all directions
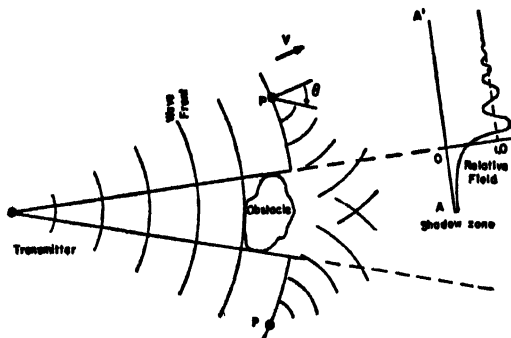
FIGURE 6. Diffraction around an obstacle.

on the forward side of the wavefront; the intensity of radiation is a maximum in the direction perpendicular to the wavefront and depends on angle θ according to the function $(1 + \cos \theta)$. The field at any point, either inside or outside the shadow zone, is obtained by summing the contributions from all the elementary areas comprising the wavefront.

As a result of these calculations, the field along the line AA' in Figure 6 varies approximately as indicated in the curve. Unity represents the field value if the obstacle were removed. It is seen that the field strength rises from a minimum at point A to 0.5 at the edge of the shadow zone and thereafter oscillates about unity. The field outside the shadow zone, therefore, at certain points is stronger and at other points is weaker than it would be if there were no obstacle. The curve, of course, varies with the position of the line AA', the size and shape of the obstacle, the wavelength of the radiation, and the type of polarization. The diffraction of radiant energy into the shadow zone increases with increasing wavelength.

Of prime importance for propagation of radio waves is the diffraction of these waves into the diffraction region below the line of sight (see Figure 5). But it should be noted that the influence of diffraction is not confined to this region but extends well above the line of sight. [In general, the influence extends upward far enough to affect the shape of the lower part of the first lobe in a coverage diagram (see Figures 25 and 26 of Chapter 5). In this region the diffraction contribution must be added to the contributions of the direct and reflected rays to give the correct value of the field strength at R in Figure 5.]

Of importance in communication problems is diffraction of waves around obstacles such as hills, trees, houses, etc. This is illustrated in Figure 6. Again diffraction is important in problems involving propagation above two different earth conditions. An especially important case is that of a radar set well inland and searching far out over the sea. Here the shore line is treated as a diffracting edge for the radiation from the image antenna.

6. *Absorption and scattering.* No account is taken in this book of the absorption and scattering of radio waves by the various constituents of the atmosphere. Oxygen, water vapor, water droplets, and rain all contribute to absorption. Their influence, however, is important only in the microwave range and in general tends to increase with frequency.

General Nature of the Radiation Field

In the last section, reference was made to the role of reflection by the earth. The resultant of the direct and indirect rays at points in the region above the line of sight gives rise to the lobes of an interference pattern (see Figures 9 to 12). The maximum number of lobes is the largest integral number of times that the quarter wavelength is contained in the transmitter height.

In the case of horizontal polarization over a smooth surface, e.g., a calm sea, the reflected and direct rays are comparable in strength, so that at certain points (on lines for which the points correspond to a path difference of a half wavelength) where the reinforcement is a maximum, the field may be as much as twice the free-space field. More exactly, the free-space field is multiplied at points of maxima by $(1 + FD)$, where D is the value of the divergence factor for the point and F gives the relative strength of the reflected and direct rays attributable to the antenna beam pattern. At points of minima (the nulls) the field is $(1 - FD)$ times the free-space field.

In general the magnitude of the reflected wave is reduced both by the increased divergence resulting from reflection from the convex surface of the earth but also because the electrical properties of the earth are such that only part of the incident energy is reflected. The magnitude of the reflection coefficient is then ρD instead of the D used in the preceding paragraph, where ρ is the magnitude of the reflection coefficient for plane waves impinging on a plane surface. The field strength, then, lies between $(1 + \rho FD)$ and $(1 - \rho FD)$. As a result of the smaller value of ρFD for vertical polarization the maxima of the interference pattern are reduced and the nulls strengthened.

At low heights (see Figure 3 of Chapter 5) the effect of diffraction is important, so that when reference is made to the optical interference region, it

should be understood that the portion of the optical region near the earth is not included. It must be considered instead as part of the diffraction region.

The diffraction region, accordingly, designates a layer in the optical region as well as the region below the line of sight (see Figure 3 in Chapter 5). Below the line of sight the field falls off exponentially. Within the diffraction region, fields are strengthened by raising the receiver or transmitter antennas.

Typical Radio Gain Curves

Three types of graphical representation of radio gain in a vertical plane through the transmitter antenna are possible, namely, (1) at a specified distance, radio gain against height; (2) at a specified height, radio gain against distance; and (3) a set of contour lines representing constant radio gain.

In Figure 7, curves of type (1) are exhibited for various frequencies. The transmission is over sea water with horizontally polarized waves. It may be observed that the higher the frequency the lower the
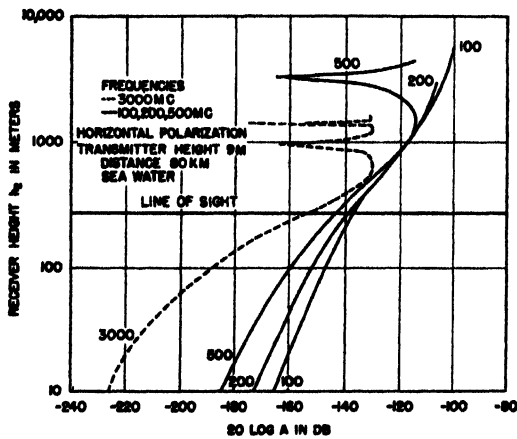
FIGURE 7. Radio gain vs receiver height for horizontal polarization.

FIGURE 8. Radio gain vs receiver height for vertical polarization.

first maximum and the narrower the lobe. Figure 8 gives similar information for vertically polarized waves. Note that the minima are not so deep with vertical polarization. Curves of type (2) exhibit similar characteristics (see Figure 6 of Chapter 5).

In Figures 9 to 12[a], vertical coverage diagrams of type (3) are given. These illustrate the effects of frequency, polarization, and transmitter height.

A comparison of Figures 9 and 10 shows the effect of frequency. As the frequency increases, the lobes become more numerous, narrower, and lower. Another effect is exhibited along the surface. For the higher frequency the corresponding decibel lines come in closer to the transmitter. This illustrates the fact that for the higher frequency the shadow effect is more pronounced along the surface of the earth.

A comparison of Figures 10 and 11 shows that for horizontal polarization the nulls are deeper but the lobes extend out farther. Along the line of sight,

[a] Figures 7 to 12 have been adapted from Radiation Laboratory Report C-6.
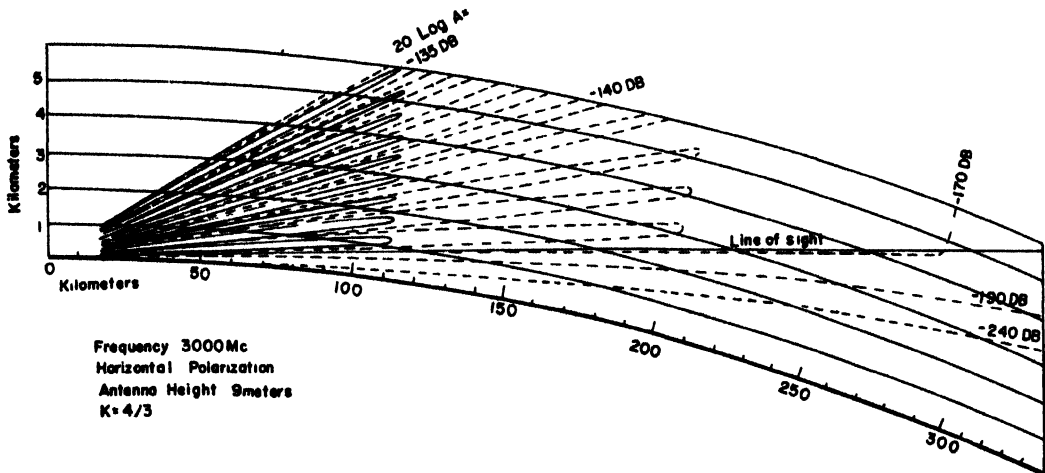
FIGURE 9. Contours of constant radio gain factor for horizontal polarization on 100 mc over sea water.

antenna height is increased, the lobes are narrower and depressed toward the horizon. The range is improved. However, there are broad nulls for the higher antenna in which detection will fail. Below the horizon, the corresponding decibel contours are pushed to the right so that point-to-point communication is improved. It should be observed that the effect of height upon the lobe structure is similar to that of frequency.

Which contour actually represents the limit of detection for a given radar depends on the power output of the transmitter, the minimum power detectable by the receiver, the antenna gains, and the radar cross section of the target. For communication sets, the same quantities, except the target cross section, apply.

UNITS AND FREQUENCY RANGES

Units

In this book the units used are those of the mks rationalized system, in which distances are expressed in meters, masses in kilograms, and time in seconds; and the formulas have been *rationalized* so that the factor 4π appears in equations involving point sources, 2π in equations involving line sources, and is generally absent from equations for uniform or unidirectional fields.

The Coulomb formula, for illustration, for point sources in classical electrostatic units,

$$f = \frac{q_1 q_2}{\epsilon r^2} \qquad (13)$$

with f in dynes, q_1 and q_2 in statcoulombs, r in centimeters and ϵ referred to unity in free space, is transformed to

$$f = \frac{q_1 q_2}{4\pi \epsilon_0 \epsilon_r r^2}. \qquad (14)$$

Here force f is given in newtons (1 newton $= 10^5$ dynes), q_1 and q_2 in coulombs, r in meters, ϵ_r is the dielectric constant relative to that of free space ϵ_0.

Similarly, the Coulomb formula for magnetic poles,

$$f = \frac{m_1 m_2}{\mu r^2}, \qquad (15)$$

with m_1 and m_2 in unit poles in the electromagnetic system and μ equal to the permeability, transforms to

$$f = \frac{m_1 m_2}{4\pi \mu_0 \mu_r r^2}, \qquad (16)$$

where m_1 and m_2 are now given in webers, μ_r is the permeability relative to that of free space μ_0.

In the mks rationalized system, the free-space values of ϵ_0 and μ_0 must carry the burden of the change of units and the inclusion of 4π, and thus take on the values

$$\epsilon_0 = 8.854 \cdot 10^{-12} \cong \frac{1}{36\pi} 10^{-9} \text{ farads per meter, (17)}$$

$$\mu_0 = 4\pi \cdot 10^{-7} \cong 1.257 \cdot 10^{-6} \text{ henries per meter. (18)}$$

With these values, c, the velocity of light in free space, is equal to

$$c = \frac{1}{\sqrt{\epsilon_0 \mu_0}} = 2.998 \cdot 10^8 \cong 3 \cdot 10^8 \text{ meters per second} \qquad (19)$$

and the impedance of free space is

$$\sqrt{\frac{\mu_0}{\epsilon_0}} = 376.7 \text{ ohms.} \qquad (20)$$

This system of units has been chosen because it is unified, free from numerical factors required in equations using arbitrary choices of units, and has been adopted by the International Electrotechnical Commission. Since the various Armed Services use differing sets of units for their operational instructions, it would have been impossible to choose any one that would have been satisfactory to all; hence the choice of using the only system which is generally recognized and scientifically sound.

Symbols for Frequency Ranges

The following symbolism has been adopted for various ranges of frequency.

TABLE 2. Symbols for frequency ranges.

Symbol	Frequency name	Frequency mc	Wavelength meters
LF	Low	0.03–0.3	10,000–1,000
MF	Medium	0.3–3	1,000–100
HF	High	3–30	100–10 short waves
VHF	Very high	30–300	10–1 } ultra-short
UHF	Ultra-high	300–3,000	1–0.1 } waves
SHF	Super-high	>3,000	<.1 microwaves

Chapter 2

FUNDAMENTAL RELATIONS

THE ELECTRIC DOUBLET IN FREE SPACE

Radiation of an Electric Doublet

IT IS CONVENIENT to present the basic relationships of radiation and reception by antennas in their simplest form, that of the radiation and reception of electric doublets in free space. The resulting formulas will later be generalized to include other types of antennas and their positions relative to the earth.

An electric doublet is a rectilinear antenna, which is symmetrical about the point or points of connection thereto and is so short that its directive properties are independent of its length. The field of such an antenna does not depend on the distribution of current along the wire, because the wire is so short
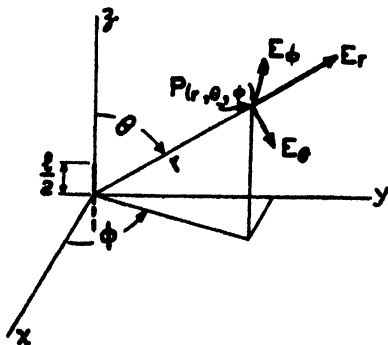
FIGURE 1. Polar coordinate system.

that there is no phase difference between waves reaching a point in space from different portions of the wire. In symbols, $l << \lambda$ where l is the length of the antenna and λ is the wavelength of the radiation.

To facilitate the analysis of the field of the doublet antenna, the spherical polar coordinate system shown in Figure 1 is introduced. The upper half of the doublet is shown in the figure. The distance from the center of the antenna to a point in space is here denoted by r. Elsewhere in this volume this quantity is written d.

Let dl be an infinitesimal portion of l, the length of the doublet, and let the current in this portion be the real part of $Ie^{j(2\pi ct/\lambda)}$. Let dE_r, dE_θ, dE_ϕ and dH_r, dH_θ, dH_ϕ be the components of the electric and magnetic field strengths at any point $P(r, \theta, \phi)$ due to the current in dl. A straightforward solution of the fundamental equations of electromagnetic theory

gives the following values for these components, valid at distances large compared with the length of the doublet:

$$dE_r = 60I\left[\frac{1}{r^2} - \frac{j\lambda}{2\pi r^3}\right] dl \cos\theta \, e^{j(2\pi/\lambda)(ct-r)}$$
$$\text{volts per meter,}$$

$$dE_\theta = 60\pi I\left[\frac{j}{\lambda r} + \frac{1}{2\pi r^2} - \frac{j\lambda}{4\pi^2 r^3}\right] dl \sin\theta \, e^{j(2\pi/\lambda)(ct-r)}$$
$$\text{volts per meter,} \quad (1)$$

$$dE_\phi = 0, \, dH_r = 0, \, dH_\theta = 0,$$

$$dH_\phi = \frac{I}{2}\left[\frac{j}{\lambda r} + \frac{1}{2\pi r^2}\right] dl \sin\theta \, e^{j(2\pi/\lambda)(ct-r)}$$
$$\text{amperes per meter,}$$

where

c = velocity of light = 3×10^8 meters per second

$j = \sqrt{-1}$,

and all distances are measured in meters. Electric field strengths are in volts per meter and magnetic field strengths are in amperes per meter. Unless otherwise explicitly stated, the mks rationalized units are used throughout this volume.

Equation (1) can be simplified at once. Since the time variation of the field is assumed sinusoidal, $e^{j(2\pi ct/\lambda)}$ may be omitted. The term $e^{-j(2\pi r/\lambda)}$ gives the phase, and it too can be omitted when only the amplitude is required. From here on, unless otherwise stated, it is understood that root-mean-square (rms) values will be used for dE_r, dE_θ, dH_ϕ, and I.

The field in the neighborhood of the doublet is called the induction field and is given by the terms in equation (1) which include the highest powers of r in the denominators. This field is important when mutual effects between closely spaced antennas, or antennas and reflectors or directors, are involved.

The radiation field, of greater interest for most of the purposes of this volume and the only important field at large distances $(r >> \lambda)$, is given by the terms in equation (1) containing r^{-1}. Thus the radiation field for the element dl of the doublet may be written:

$$dE_\theta = \frac{60\pi I dl \sin\theta}{\lambda r} \text{ volts per meter,}$$
$$(2)$$
$$dH_\phi = \frac{I dl \sin\theta}{2\lambda r} = \frac{dE_\theta}{120\pi} \text{ amperes per meter.}$$

The other components are relatively negligible except near the antenna or near ground for low antennas. The electric field dE_θ is perpendicular to the radius vector r and lies in the r, s plane, and the magnetic field dH_ϕ is perpendicular to r and to dE_θ. It will be noted that $E/H = 120\pi \cong 376.7$

ohms. This is the impedance of free space in the mks rationalized system of units, the ohms of the electrical engineer.

Equation (2) describes the radiation field of a differential element of the doublet. To get the radiation field of the whole doublet, these equations must be integrated over the length l. This gives

$$E_\theta = \frac{60\pi \sin\theta \int_{-l/2}^{l/2} I\,dl}{\lambda r} \quad \text{volts per meter}, \quad (3)$$

$H_\phi = E_\theta/120\pi$ amperes per meter.

Equation (3) may be written in exactly the form of equation (2) by introducing the *effective length*, L, of an antenna, which is defined as the length that a straight wire carrying current constant over its length would have if it produced the same field as the antenna in question. Calling the current measured at the input point I_i,

$$L = \frac{\int_{-l/2}^{l/2} I\,dl}{I_i} \quad \text{meters}, \quad (4)$$

and hence

$$E_\theta = \frac{60\pi I_i L \sin\theta}{\lambda r} \quad \text{volts per meter},$$

$$H_\phi = \frac{E_\theta}{120\pi} \quad \text{amperes per meter}, \quad (5)$$

so that equations (5) are the same as equations (2) with $I_i L$ replacing $\int I\,dl$. For a short dipole or doublet the current varies linearly from I_i at the midpoint to zero at each end so that from equation (4) $L = l/2$ for a doublet.

The power per unit area, W (that is, the power flowing through a unit area normal to the direction of propagation), is represented by Poynting's vector and is given by the product $E_\theta H_\phi$ times the sine of the angle between E_θ and H_ϕ. This angle is 90 degrees. Consequently,

$$W = EH \quad \text{watts per square meter},$$

$$W = \frac{E^2}{120\pi} \quad \text{watts per square meter}, \quad (6)$$

$$E = \sqrt{120\pi W} \quad \text{volts per meter}.$$

To find P, the power output of the doublet, W is integrated over a large sphere concentric with the source. Using equations (5),

$$P = \frac{E^2 d^2}{45} \quad \text{watts}$$

and $\qquad\qquad\qquad\qquad\qquad\qquad (7)$

$$E = \frac{3\sqrt{5}\sqrt{P}}{d},$$

where d is written in place of r. The subscripts θ and ϕ have been dropped at this point because the E and H referred to in equations (7) are the fields in the equatorial plane, where $\sin\theta = 1$.

As the antenna is part of a circuit, it is often convenient to think of the radiated power as being dissipated in a fictitious resistance called the *radiation resistance*, defined by

$$R_r = \frac{P}{I_i^2} \quad \text{ohms}, \quad (8)$$

where P is the radiated power and I_i the rms input current. For the doublet,

$$R_r = 80\pi^2 \left(\frac{L}{\lambda}\right)^2 \quad \text{ohms}, \quad (9)$$

where L is the effective length given by equation (4).

Reception by an Electric Doublet

When an electromagnetic wave falls upon an antenna, a current is induced in the antenna and power is abstracted from the wave. If the antenna is connected to a load, the power abstracted is dissipated in two ways: (1) by absorption in the load (reception), and (2) by reradiation from the antenna (scattering).

In this classification, the power dissipated by the antenna itself (due to its ohmic resistance) is ignored because this loss is likely to be negligible compared with the power dissipated through reradiation. Hereafter, power absorbed by the load will be called *received power* and power reradiated by the antenna will be called *scattered power*. The sum of these is equal to the power abstracted from the wave.

The calculation of the received and scattered power may be carried out by means of the equivalent circuit of Figure 2. In this figure, Z_a is the impedance
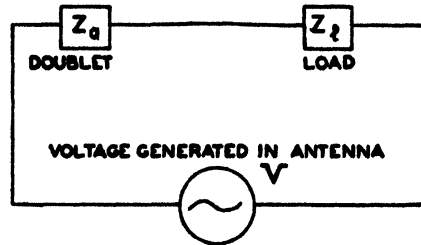
FIGURE 2. Equivalent circuit of antenna and load.

of the doublet and Z_l is the impedance of the load, that is, the impedance connected across the terminals of the antenna when it is acting as a receiver. V is the voltage generated in the antenna.

The load is supposed to be tuned, which means that the reactance part of Z_l is set equal and opposite to the reactance part of Z_a, so that $Z_a + Z_l = R_a + R_l$, that is, the total impedance is simply the sum of the resistance parts of the impedances of the antenna and the load. Hence

$$I = \frac{V}{R_a + R_l} \quad (10)$$

gives the current. But $P_r = R_l I^2$ is the power ab-

sorbed by the load and hence is equal to

$$P_r = \frac{V^2 R_l}{(R_a + R_l)^2},$$ (11)

where P_r is called the received power. In the same way

$$P_s = \frac{V^2 R_a}{(R_a + R_l)^2}$$ (12)

is the power scattered by the doublet.

It is easy to show that the maximum power is delivered to the load if $R_a = R_l$. In this, the matched load case,

$$P_r = P_s = \frac{V^2}{4R_a} = \frac{V^2}{4R_l}.$$ (13)

Now the resistance of the doublet, neglecting its low ohmic resistance, is only the radiation resistance [equation (9)] and the potential or voltage across the terminals is equal to $E_0 L$, where E_0 is the field strength of the incident plane wave and L is the effective length of the doublet. Inserting these quantities into equation (13),

$$P_r = P_s = \frac{E_0^2}{120\pi} \cdot \frac{3\lambda^2}{8\pi}.$$ (14)

In these equations it has been assumed that the line of the doublet has been oriented parallel to the electric vector of the incident wave in order to obtain maximum power absorption.

The factor $E_0^2/120\pi$ will be recognized from equation (6) as the power per unit area of the incident wave. The formula thus says that all the power crossing an area $3\lambda^2/8\pi$ is received, and that all the power crossing an equal area is scattered. The area $3\lambda^2/8\pi$ is therefore called the absorption cross section or scattering cross section of the matched doublet. Since the antenna has been placed parallel to the polarization of the incident wave, this is the

maximum absorption cross section. Moreover, this formula holds only when the doublet has been matched to its load, and consequently $3\lambda^2/8\pi$ is the maximum absorption cross section.

It will be noted, however, that $3\lambda^2/8\pi$ is not the maximum scattering cross section. This maximum is achieved by shorting out the load, that is, setting $R_l = 0$. In this case,

$$P_r = 0$$

and

$$P_s = \frac{E_0^2}{120\pi} \cdot \frac{3\lambda^2}{2\pi}.$$ (15)

Hence the scattering cross section of the shorted (dummy) doublet is four times the scattering cross section of the matched load doublet.

Transmission between Doublets in Free Space

Assume that two doublets, one to function as a transmitter and the other as a receiver, a distance $d \gg \lambda$ apart, are adjusted for maximum power transfer. This means that the axes of the doublets are parallel and lie in their common equatorial plane and that each is matched to its connected circuit. Then the power radiated by the transmitting doublet, from equation (7), is equal to

$$P_1 = \frac{E_0^2 d^2}{45} \text{ watts,}$$ (16)

and from equation (14) the power delivered to the load circuit of the receiving doublet is given by

$$P_2 = \frac{E_0^2}{120\pi} \cdot \frac{3\lambda^2}{8\pi} \text{ watts.}$$ (17)

Hence the ratio of the received power (to the load circuit) to the output power for maximum power

λ(METERS)

GAIN IN DECIBELS   20 LOG $\frac{3\lambda}{8\pi d}$ = 20 LOG A_0

d (KILOMETERS)
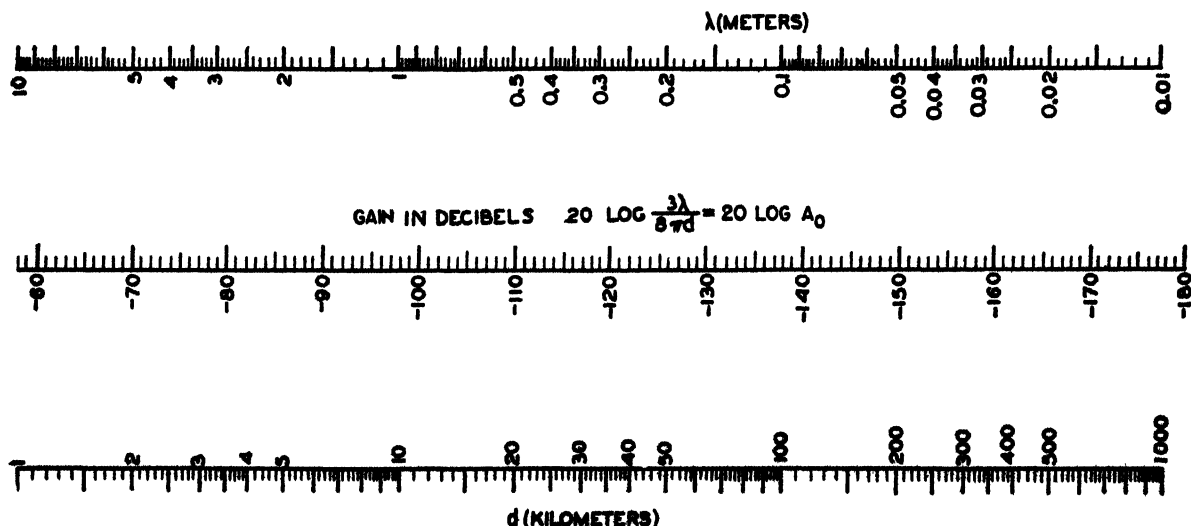
FIGURE 3.   Free-space gain for doublets $P_2/P_1 = (3\lambda/8\pi d)^2 = A^2_0$. (Adjusted for maximum power transfer.)

transfer is

$$\frac{P_2}{P_1} = \left(\frac{3\lambda}{8\pi d}\right)^2 = A_0{}^2. \qquad (18)$$

The ratio $P_2/P_1 = A_0{}^2$ (as used here) is called the free-space radio gain for matched doublets or for short the *free-space gain*, since all objects, including the earth, are supposed remote from both doublets. This free-space gain, $A_0 = 3\lambda/8\pi d$. On the decibel scale, it takes the form

$$10 \log_{10} \frac{P_2}{P_1} = 20 \log A_0$$

$$= -18.46 - 20 \log_{10} \frac{d}{\lambda} \text{ decibels. } (19)$$

The nomogram. Figure 3, gives a convenient means of calculating the *radio gain* for doublets adjusted for maximum power transfer.

POWER TRANSMISSION. RECIPROCITY

Radio Gain

Preceding formulas (16- 19) apply to doublets in free space. This section considers the modifications that must be made in the formulas when the restriction of free space is removed. In actual transmission problems, ground reflection, reflection from elevated layers of the atmosphere, diffraction by earth curvature and by obstacles, and refraction by the atmosphere must be considered. In Chapters 5, 6, and 7 special forms of gain are discussed and separate gain factors are introduced to take care of each effect. For the present a factor that will be called the *path-gain factor*, A_p, representing the product of all these special factors will be used. A_p is defined by

$$E = E_0 A_p, \qquad (20)$$

where E is the absolute value of the actual field strength and E_0 is the absolute value of the free-space field strength that would exist at the same distance d from the doublet transmitter in free space.

Replacing E_0 with $E_0 A_p$, equation (17) for the received power, becomes

$$P_2 = \frac{E_0{}^2 A_p{}^2}{120\pi} \cdot \frac{3\lambda^2}{8\pi} \qquad (21)$$

while the power output as given by equation (16) remains unchanged, so that

$$\frac{P_2}{P_1} = \left(\frac{3\lambda}{8\pi d}\right)^2 A_p{}^2 = (A_0 A_p)^2 = A^2 \qquad (22)$$

replaces equation (18) as the ratio of received power to output power for maximum power transfer between doublets. The quantity defined by (22) is the free-space gain and A is the gain factor.

The general relation between the input voltage at the receiver and the received power is $V_i = \sqrt{P_2 R_i}$, where R_i is the resistance of the receiver load circuit (which is equal to the radiation resistance for maxi-

mum power transfer) and V_i is the input voltage. Hence, using equation (14),

$$V_i = 0.0178 E_0 \lambda \sqrt{R_i} \text{ volts} \qquad (23)$$

$$= \frac{1}{8\pi\sqrt{5}} E_0 \lambda \sqrt{R_i} = \frac{E_0 L}{2}$$

Antenna Gain. Polarization

The equations given before (1-19) may be further generalized to apply to any type of antenna through the introduction of a quantity called the antenna gain. The term gain, as applied to an antenna, is a measure of the efficiency of the antenna as a radiator or receiver as compared with that of a doublet antenna, with all antennas located in free space.

Quantitatively, the gain, G_1, of a directive transmitting antenna is the ratio of the power P_1' radiated by a doublet antenna to the power P_1 radiated by the antenna in question to give the same response in a distant receiver, with both transmitting antennas adjusted for maximum transfer of power. Hence

$$G_1 = \frac{P_1'}{P_1}. \qquad (24)$$

The gain G_2 of a directive receiving antenna is the ratio of the power P_1'' radiated by a transmitting antenna, which produces a certain response in the matched load circuit of a distant doublet receiving antenna, to the power P_1 radiated by the same transmitting antenna to produce the same response in the matched load circuit of the receiving antenna in question, with both receiving antennas adjusted for maximum transfer of power. Hence

$$G_2 = \frac{P_1''}{P_1}. \qquad (25)$$

From the definitions given above it follows that for a transmitting and receiving antenna combination in free space, with gains G_1 and G_2 and adjusted for maximum power transfer, the power ratio is equal to

$$\frac{P_2}{P_1} = G_1 G_2 \left(\frac{3\lambda}{8\pi d}\right)^2 = G_1 G_2 A_0{}^2, \qquad (26)$$

where P_1, G_1 are the power output and gain of the transmitter and P_2 is the power delivered to the matched load of a receiving antenna of gain G_2.

If the antennas are not in free space, equation (26) becomes

$$\frac{P_2}{P_1} = G_1 G_2 \left(\frac{3\lambda}{8\pi d}\right)^2 A_p{}^2 = G_1 G_2 (A_0 A_p)^2, \qquad (27)$$

$$= G_1 G_2 A^2,$$

where A is the gain factor and A_p is the path-gain factor. Note that for highly directive antennas A_p may depend upon the directivity characteristic of the antennas, e.g. when the antenna discriminates between the direct and reflected waves.

Since power is proportional to the square of field

strength, equation (20), for any transmitting antenna, becomes

$$E = E_0\sqrt{G_1}A_\phi. \tag{28}$$

In defining gain, the electric doublet is selected here as the comparison antenna in place of the isotropic radiator (that is, a hypothetical antenna which radiates equally in all directions) which is sometimes used in the literature. Since the gain of an isotropic radiator relative to a doublet is $\frac{2}{3}$, the gain of any antenna referred to an isotropic radiator is 3 2 the value referred to a doublet antenna.

$$G_{(\text{isotropic})} = 1.5G_{(\text{doublet})}. \tag{29}$$

The chief objections to the isotropic radiator are that it does not occur in practice and cannot be produced experimentally, even approximately.

In experimentally measuring the gain of an antenna, a half-wave dipole is often used as a reference antenna. While the gain of a half-wave dipole relative to a doublet is approximately unity, being 1.09 for a very thin dipole, it depends somewhat on its actual dimensions so that it is better to express the experimental gain in terms of the doublet antenna even though a longer antenna is used as a reference antenna in making the measurements.

When antennas are oriented so that the directions of polarization make an angle γ with each other
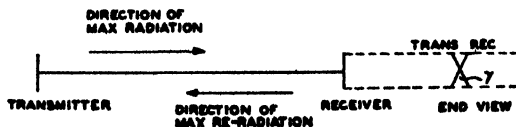
FIGURE 4. Relation of antenna axes and wave polarization.

(while the maxima of their angular patterns still point toward each other), the formulas for power transfer, equations (18), (22), and (27), are multiplied by a factor $\cos^2 \gamma$ (see Figure 4).

The Reciprocity Principle

So far in this chapter the radiation and reception of power by antennas have been treated separately. Actually, many of the properties of an antenna are the same for either reception or radiation; in particular, the current distribution, the effective length, and the gain are unchanged. The reciprocity principle, from which these propositions may be proved, may be stated as follows: If an electromotive force V, inserted in antenna 1 at a point x_1, causes a current I to flow at a point x_2 in antenna 2, then the voltage V applied at x_2 will produce the same current I at x_1.

From this principle the statement of the equivalence of current distribution, effective length, and gain follow readily.

This theorem does not hold when the propagation of a wave takes place in an ionised medium in the presence of a magnetic field (the ionosphere), but it does hold for all cases of transmission discussed in this volume.

RECEIVER SENSITIVITY

The sensitivity of a radio receiver is that characteristic which determines the minimum strength of signal input capable of causing a desired value of signal output. In high-frequency receivers the limiting factor for reception is usually set noise, that is, noise produced in the tubes or other elements, such as crystals, of the receiver itself. At frequencies below about 100 mc, atmospheric disturbances sometimes exceed the set noise in intensity, but at higher frequencies atmospheric static is negligible. Man-made noise (automobiles, etc.) may be a source of serious trouble, but such interference can often be eliminated by proper siting. Consequently, for high-frequency receivers, sensitivity may be expressed, at least approximately, in terms of set noise only.

Although set noise has an important bearing on sensitivity of radar receivers, there are other factors which must be considered for this type of equipment.

There are several types of set noise. Though all noise sources in a well-designed receiver are minimized with the exception of the thermal noise whose magnitude is independent of equipment construction, the total set noise is usually several times the purely thermal noise.

Thermal Noise

Thermal noise is generated by the random (temperature) motion of electrons in a conductor; it is, therefore, a universal property of matter and independent of the design features of the receiver. The rms thermal-noise voltage that appears across the terminals of any circuit element is a function of the frequency interval (receiver bandwidth) over which the noise is averaged; it is given by

$$V_s = \sqrt{4kT\Delta f \cdot R}, \tag{30}$$

where R is the resistance across which the noise voltage is measured, Δf the bandwidth in cycles per second, T the absolute temperature, and k, the Boltzmann constant, is equal to 1.38×10^{-23} watt-second per degree. The noise voltage is independent of the reactance components in the circuit.

Consider now, for the purpose of definition, a receiver without internal noise, that is, let all the noise be generated in the receiving antenna of resistance R_a. If R_l designates the load resistance (that is, the resistance of the receiver exclusive of its antenna), the average noise power delivered to the

receiver will be

$$P_n = \frac{V_n{}^2 R_l}{(R_a + R_l)^2}, \quad (31)$$

where V_n is the rms value of the noise generated in the antenna.

The noise power is maximum when the receiver is matched to its input; this maximum is

$$P_n = \frac{V_n{}^2}{4R_a} = kT\Delta f \quad \text{watts} \quad (32)$$

by equation (30). Assuming equivalent temperature $T = 290$ degrees absolute, and measuring Δf in megacycles,

$$P_n = 4 \times 10^{-15} \Delta f \quad \text{watt.} \quad (33)$$

This result means that in an idealized receiver, noise is the thermal noise of an antenna of equivalent temperature $T = 290$ degrees absolute, and the minimum detectable signal would be approximately equal to $4 \times 10^{-15} \Delta f$ watt.

Noise Figure

The sensitivity of a set cannot be described in terms of the thermal noise alone, because the set noise is usually several times the purely thermal noise. For this purpose another quantity called the noise figure is used. The noise figure of a system (taken here to be a receiver, for definiteness) is defined as

$$F_n = \frac{P_{no}/P_{ni}}{P_{so}/P_{si}}, \quad (34)$$

where P_{ni} = noise power ($kT\Delta f$) from the antenna which is being delivered to the receiver.

P_{no} = noise power at the output of the receiver, that is, the noise after the amplifications and additions arising in the receiver circuit.

P_{si} = signal power from the antenna which is being delivered to the receiver.

P_{so} = signal power at the output of the receiver, that is, the signal power after detection and amplification have taken place.

The ratio P_{so}/P_{si} is called the receiver gain. This quantity is called g and must not be confused with antenna gain G. Using equation (32), equation (34) may be written

$$F_n = \frac{P_{no}}{kT\Delta f} \cdot \frac{1}{g}. \quad (35)$$

The bandwidth Δf is measured by finding the area under a curve of power-gain versus frequency and equating this area to the area of a rectangle whose width is interpreted as Δf and whose height corresponds to the gain at the frequency at which the gain is a maximum.

Receiver Sensitivity

Frequently receiver sensitivity is defined by the assumption that a received signal can be discriminated when its output power is equal to the noise output power. This assumption, while true for a large class of receivers, is too rough for radar receivers. The method given here will explain the procedure used for calculating the minimum discernible power of receivers for which the assumption is true. The sensitivity of radar receivers is considered on page 342.

Referring to equation (34), the assumption that signal output power is equal to noise output power means that $P_{so} = P_{no}$. Hence

$$F_n = \frac{P_{ni}}{P_{si}}. \quad (36)$$

But P_{ni} is, on the assumption discussed above, just the minimum discernible signal power, P_{min}, at the receiver input, that is, before amplification. Hence, using equations (32) and (33),

$$P_{min} = kT\Delta f \cdot F_n \cong 4 \times 10^{-15} \Delta f \cdot F_n \text{ watt.} \quad (37)$$

Measurement of the Noise Figure

Remembering that the cases under discussion are those for which the minimum discernible signal is equal to the noise output power, equation (37) gives an estimate of the minimum detectable power from a measurement of the noise figure F_n which may be obtained as follows.

An antenna (or other signal generator) whose impedance is matched to the receiver is connected to the receiver. With the signal output reduced to zero (so that the antenna furnishes only noise power to the receiver), the receiver gain is increased until the noise gives a measurable output and the output noise power is measured with a power meter. Now a signal is impressed on the antenna and increased to a point where the receiver output power is doubled, and the input signal power is measured. Thus, referring to equation (34),

$$P_{so} = P_{no} \quad \text{and} \quad F_n = \frac{P_{si}}{P_{ni}} = \frac{P_{si}}{kT\Delta f},$$

so that the measurement of the impressed signal power indicated here gives F_n.

If the receiver consists of several elements in cascade, including attenuators, amplifiers, and converters, the overall noise figure can be compounded from the noise figures and gains of the individual components by means of the following equation:

$$F_n = F_{n1} + \frac{F_{n2}-1}{g_1} + \frac{F_{n3}-1}{g_1 g_2}, \quad (38)$$

where F_s = overall noise figure,

$\quad F_{sk}$ = noise figure of the kth element,

$\quad g_k$ = gain of the kth element.

In using this equation it is understood that the successive stages are matched.

It is clear from equation (38) that most of the noise comes from the early stages of reception; in high-frequency radar sets, it comes from the crystal mixer and the first intermediate-frequency (i-f) stage. This means of course that noise picked up at later stages is much less amplified by the system than the noise from the early stages.

In equipment specifications, the noise figure is usually expressed in the decibel scale as *decibels above thermal noise*. Actual noise figures vary from a few decibels above thermal noise in the very high-frequency [VHF] region (receivers built a few years ago often have appreciably higher noise figures) to larger values for microwave receivers.

Sensitivity of Radar Receivers

It is by no means true for radar receivers that $P_{min} = P_{so}$; as a matter of fact, $P_{min} >> P_{so}$. That is, the minimum discernible power considerably exceeds the noise level.

The largest single additional loss in radar reception is *scanning loss* which is related to the rotation of the antenna (one or several revolutions per minute). As an example, for one particular radar which has a bandwidth $\Delta f = 2$ mc, this loss is from 10 db to 12 db.

In case the antenna does not rotate, there is no scanning loss. This fact would seem to be of limited operational importance, since it would usually be necessary to locate the target (a plane, for example) by scanning.

Another loss, closely connected with scanning loss, is *sweep-speed loss*. This loss is due to the fact that practical targets, such as airplanes, reflect rapidly varying amounts of power to the radar receiver, these amounts depending on the precise orientation of the target at the moment when the radar beam sweeps over it. Consequently, sweep-speed loss will depend on the speed of rotation of the antenna, on the distance of the target from the antenna, and, to some extent, on the beamwidth and the nature of the target. The overall figure for this loss on the same radar used to illustrate scanning loss is about 4 db for targets 200 miles from the radar.

In addition to these losses, careful experiments with the radar used as an example above have indicated that there is an *operator loss* of about 4 db for even experienced operators. This might be thought of as a loss due to the difference between laboratory and field conditions.

Statistical consideration about the extent of noise fluctuation and about the fact that a target need not be seen on every sweep lead to further small losses which total, for the radar under discussion, 2 db.

Summarizing for the case of the radar of the above example, the minimum detectable power is about 34 db above $kT\Delta f$ or about 8×10^{-116} watt, not 12 db above $kT\Delta f$ or 8×10^{-138} watt, as would be indicated from the noise level alone. This amounts to 22 db or a factor of 166; that is, the actual minimum discernible power is 166 times that calculated from noise alone. It will be seen in the results of the next section that the maximum range of a radar set varies with the inverse fourth root of the minimum discernible power. Consequently, a calculation of the maximum range of the radar of the example, which assumed that the minimum discernible power was equal to the noise power, would give a range too great by a factor of $\sqrt[4]{166} = 3.59$. Since this would be a serious error, it shows the importance of a very careful consideration of radar receiver sensitivity in calculations of this type.

RADAR CROSS SECTION AND GAIN

Radar Cross Section

The total scattering of a target may be described by the use of a parameter (having the dimensions of an area) called a scattering cross section. This concept has already been presented in subject matter on page 338, where both scattering and absorption cross sections of doublets were discussed.

It should be noted in passing that the cross sections introduced here should not be confused with the radar cross section discussed before

The scattering cross section S is defined by

$$S = \frac{P_s}{W_i}, \qquad (39)$$

where P_s is the total power scattered by the target irrespective of its angular distribution and W_i is the incident power per unit area.

The scattering cross section S, which gives information about the total scattered energy, is not directly useful in radar work because in such applications one is interested only in that fraction of the total scattered power which is scattered in the direction of the radar; that is, one wants a parameter involving the scattered power per unit area at the receiver instead of the total scattered power. If the target is an isotropic scatterer,

$$W_r = \frac{P_s}{4\pi d^2},$$

where W_r is the scattered power per unit area at the

receiver, d the distance from the target to the receiver, and P_s the total scattered power. This gives, using equation (39),

$$S = 4\pi d^2 \frac{W_r}{W_i} \qquad (40)$$

as a formula for the scattering cross section of an isotropic scatterer which involves scattered power per unit area at the receiver W_r, instead of total scattered power P_s.

For targets other than isotropic scatterers, however, this procedure fails since one cannot say that $W_r = P_s/4\pi d^2$. Nevertheless, it is useful to define a parameter σ which is called the radar cross section, by

$$\sigma = 4\pi d^2 \frac{W_r}{W_i} \qquad (41)$$

in analogy with equation (40). Here W_r is the actual power per unit area at the receiver. From the preceding discussion it is apparent that σ may be thought of as the scattering cross section which the target in question would have if it scattered as much energy in all directions as it actually does scatter in the direction of the radar receiver. For a target scattering isotropically, $\sigma = S$, but for any other type of target σ does not, in general, equal S.

A radar gain formula analogous to the radio gain but applicable to two-way transmission can be developed from equation (41) by replacing W_r and W_i with the directly measurable quantities P_1 (power output) and P_2 (received power). From equation (6), $W_i = E^2/120\pi$ in which E is the field strength incident on the target. Substituting this value of E into equation (7) gives $W_i = 3P_1/8\pi d^2$ for a doublet transmitter in free space. Including the gain of any type of transmitting antenna, this takes the form

$$W_i = \frac{3P_1 G_1}{8\pi d^2} \qquad (42)$$

Further, the power received by a doublet with a matched load, equation (17), may be written

$$P_2 = \frac{3\lambda^2}{8\pi} W_r, \qquad (43)$$

if $E^2/120\pi$ is replaced by W_r, where here E is the field at the receiver. If the receiver is not a doublet, equation (43) may be replaced by

$$P_2 = \frac{3\lambda^2}{8\pi} W_r G_2 \qquad (44)$$

where G_2 is the gain of the receiver. Substituting the values for W_i and W_r, given by equations (42) and (43), into equation (41) yields

$$\frac{P_2}{P_1} = G_1 G_2 \frac{\sigma}{4\pi d^2} \left(\frac{3\lambda}{8\pi d}\right)^2. \qquad (45)$$

This is the radar gain for two-way transmission in free space. By means of it, σ may be measured, or if σ and P_2/P_1 are known, it may be used to calculate

ranges. Generalizing equation (45) we have

$$\frac{P_2}{P_1} = G_1 G_2 \frac{\sigma}{4\pi d^2} \left(\frac{3\lambda}{8\pi d}\right)^2 A_p^4, \qquad (46)$$

where A_p is the path gain factor (see page 339).

It may be observed here that some writers call σA_p^4, not σ, the radar cross section. These writers call their σ, for the case $A_p = 1$ (free space), the free-space radar cross section σ_0. Since, in this volume, the complicated terms appearing in A_p are treated separately and not as part of the cross section, this distinction is not made here.

For some simple targets, σ may be calculated. The following are a few of the values.

Targets	Condition	Radar cross section σ
Conducting sphere, radius a	$a \gg \lambda$	πa^2
Metallic plate, area $= ab$	$a \gg \lambda, b \gg \lambda$	$4\pi a^2 b^2/\lambda^2$
Cylinder, diameter $= d$, length $= l$	Axis of cylinder parallel to field and $d \gg \lambda$, $l \gg \lambda$	$\pi d l^2/\lambda$
Matched load doublet	Oriented parallel to field	$9\lambda^2/16\pi$
Shorted doublet (dummy)	Oriented parallel to field	$9\lambda^2/4\pi$

Objects of tactical interest (ships, airplanes) have very complicated radar cross sections. In particular, a strong dependence on the aspect of these unsymmetrical targets is observed. For ships the situation is still further complicated by the variability of the incident field over the target area.

Some writers on the subject of targets use a *characteristic length* L (sometimes also called a *scattering coefficient*) which is related to σ by

$$\sigma = 4\pi L^2. \qquad (47)$$

Radar Gain

It is possible to write equations for two-way transmission which bear a formal resemblance to corresponding equations for one-way transmission by introducing a quantity G_R, called the *gain* of the target. G_R is the gain of a target in the direction of the radar receiver relative to a shorted (dummy) doublet.

By writing formulas connecting the radar gain with the power per square meter incident on the target and the power per square meter scattered back to the receiver, it is possible to establish a connection between radar gain and the radar cross section defined in the last paragraph, and from this to calculate a gain formula involving G_R instead of σ.

Applying equations (15) and (6),

$$P_s = W_i \frac{3\lambda^2}{2\pi} \qquad (48)$$

for the case where the target is a shorted doublet. P_s is the total scattered power and W_i is the power per square meter incident on the target. For a target with a radar gain G_R it follows that

$$P_s = W_i \frac{3\lambda^2}{2\pi} G_R. \qquad (49)$$

In a similar way a formula for W_r, the scattered power per unit area at the receiver, can be developed. A target which scattered equally in all directions would scatter an amount

$$P_s' = 4\pi d^2 W_r. \qquad (50)$$

But

$$P_s' = \frac{3}{2} G_R P_s, \qquad (51)$$

where P_s is the amount scattered by an actual target with gain G_R. [The factor 3/2 appears because the gain of the target relative to an isotropic radiator is $(3/2)G_R$.] Hence

$$4\pi d^2 W_r = \frac{3}{2} G_R P_s. \qquad (52)$$

Eliminating P_s from equations (49) and (52),

$$\frac{W_r}{W_i} = \frac{9\lambda^2 G_R^2}{16\pi^2 d^2}. \qquad (53)$$

Putting this value of W_r/W_i in equation (41),

$$\sigma = \frac{9\lambda^2}{4\pi} G_R^2, \qquad (54)$$

which is the required general formula connecting

target gain and radar cross section. It will be noted that the factor $9\lambda^2/4\pi$ is just the radar cross section of the shorted doublet.

Inserting the value of σ given by equation (54) into equation (45),

$$\frac{P_2}{P_1} = 4G_1 G_2 G_R^2 \left(\frac{3\lambda}{8\pi d}\right)^4, \qquad (55)$$

which is the radar gain formula for free space in terms of the gain of the target relative to a dummy doublet.

The reasonableness of the factor 4 in the above equation may be made apparent by the following analogy. Compare the doublet antenna with a generator whose internal resistance corresponds to the radiation resistance of the antenna. When the generator is shorted all the power is dissipated in the internal resistance. When the doublet is shorted all the power is reradiated. The maximum power that can be extracted from either the generator or the antenna occurs when the load resistance equals the internal generator, or antenna radiation, resistance. It is ¼ the above short-circuit power. This is the 4 that occurs in the above equation.

Equation (55), in the nonfree-space case, takes the form

$$\frac{P_2}{P_1} = 4G_1 G_2 G_R^2 \left(\frac{3\lambda}{8\pi d}\right)^4 A_p^4, \qquad (56)$$

where A_p is the path gain factor defined by equation (20).

ANTENNAS

FUNDAMENTALS

Function of Antennas

A TRANSMITTING ANTENNA converts the power delivered to it into electromagnetic radiation (neglecting losses); a receiving antenna abstracts power from an incident electromagnetic wave and delivers to the receiver that part which is not re-radiated or lost in the antenna. In the short and microwave region the power conversion is effected with a very small loss so that for most practical purposes the power loss inside the antenna may be disregarded. Apparent losses caused by reflection owing to mismatch between the antenna and its input circuit are of a different nature and are not included herein.

For many purposes it is desirable to concentrate the power radiated into a beam of comparatively small angle as in this way the field strength in the preferred direction is enhanced. The gain of a directional antenna is defined by means of a comparison of the given antenna radiation pattern with that of an electric doublet.

The gain of an antenna is the ratio of power that must be supplied to a doublet to the power that must be supplied to the antenna considered in order that, at a given large distance, the electric field at the *maximum* of the antenna pattern is equal to the field at the same distance in the equatorial plane of the doublet. From the reciprocity principle it is found that the gain of a receiving antenna is equal to the gain of the same antenna used as a transmitter. A discussion of antenna gain and reciprocity is given in Chapter 2, p. 339.

Directive Antennas

Polar plots of antenna radiation patterns are of two kinds: either the relative magnitude of the Poynting vector (power per unit area) is plotted along the radius vector, or the relative magnitude of the radiation electric field strength is plotted in the same way. Usually the value of the radius vector at the maximum of the pattern is taken equal to unity. The Poynting vector plot is obtained from the field strength plot by squaring the radial distances (Figure 1).

If an antenna system is designed so that most of its power is concentrated into a comparatively small cone, the corresponding part of the radiation pattern

is called the main lobe. Commonly there are a number of secondary maxima (side lobes) much smaller than the main lobe. The width of the main lobe is measured by the angle between half-power points. Half-power points are those points in the polar diagram of the antenna pattern where the power per unit area is equal to one-half that at the maximum, the field strength being $1/\sqrt{2} = 0.707$ times that at the maximum. This angle is also referred to as the beam width. The beam width varies from a degree or less for some specialized radar antennas to very large angles such as 50 to 60 degrees, depending on the design and purpose of the antenna. The larger the beam width the smaller the gain.

It should be noted that an antenna radiation pattern may have high directivity with respect to one plane going through the antenna and little or no directivity in another plane Thus a doublet antenna (for definition see text on p. 336) is directive in a plane which contains the antenna itself but is nondirective in the equatorial plane perpendicular to the antenna (see Figure 11).

FIGURE 1. Antenna radiation patterns.

Antenna Pattern Factors in Ground Reflection

With highly directive antennas the magnitude of the direct wave may differ appreciably from that of the ground-reflected wave owing to their difference in angle of emergence from the antenna (Figure 2). This must be taken into account by using the

FIGURE 2. Antenna pattern factors.
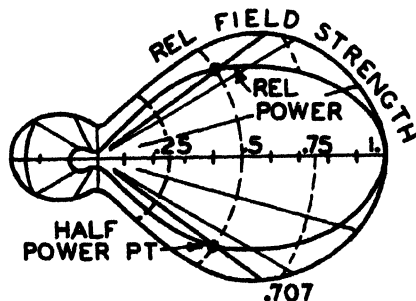
antenna pattern factors F_1 and F_2 in computing the interference pattern above the line of sight. This subject is dealt with on pages 384-385.

Standing-Wave Antennas

An important class of antennas is that in which standing waves of the currents and the voltages are set up. In a transmitting antenna of this type, for instance, a progressive or traveling wave is supplied from the connected source of power. This is reflected from the end of the antenna and the interaction of the two sets of waves moving in opposite directions results in a standing-wave system.

In this event the current amplitude is zero at the ends of the antenna and assumes differing values at the other positions on the antenna. The distribution of current amplitudes is usually assumed to vary sinusoidally with the distance from the end of the antenna. This is a good approximation where the diameter of the antenna wire is small compared with the length, but may be seriously in error for *thick-wire* antennas.

The simplest, and one of the most commonly used, standing-wave antennas is the half-wave dipole antenna, discussed on pages 347-349.

Resonant Antennas

Many antennas are operated at or near resonance, which means that the reactive component of their impedance vanishes or is very small.

Two types of resonant antenna may be distinguished: either (1) the radiating element as a whole is resonant, as in the case of the half-wave dipole, shortened the right amount; or (2) the antenna system is made resonant by adding suitable reactive components to the radiative elements. To illustrate, the center-fed half-wave dipole of exactly half-wavelength, assuming sine distribution of current, has an inductive reactance; it may be made resonant by the addition in series of a capacitive reactance. This is known as antenna loading and is common at the longer wavelengths where half-wave dipoles would be too cumbersome. Another example is that of a dipole radiator shorter than the half-wave dipole and having the form of a metallic tube; this is combined with a tunable cavity resonator inside the tube that acts as a shunt impedance, the whole system being tuned to resonance (Figure 3).
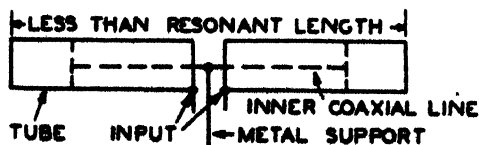
FIGURE 3. Antenna tuned to resonance by a shunt impedance.

Although the actual antenna impedance is made up in a complicated way of distributed capacitances and inductances, the input impedance of the simpler types of antennas for a limited frequency band containing the resonance frequency is essentially that of an ordinary series resonant circuit [the resistance at resonance being essentially the radiation resistance of the antenna (see text below)]. The input impedance of certain other antennas is essentially that of parallel-resonant circuits with very large shunt resistances at resonance (see text on p.347). For illustration, see Figure 6.

Traveling-Wave Antennas

In this type of antenna there is no standing-wave system set up since the progressive or traveling wave of current fed into the antenna is absorbed, without reflection, by a terminal resistance placed at the end of the antenna, which is equal to the characteristic impedance of the antenna regarded as a transmission line. Such antennas are necessarily nonresonant.

The traveling-wave antenna radiates most strongly in the general direction of the wave motion. The major lobe makes an angle $\alpha < 90$ degrees with this direction as indicated in Figure 20. Here we have a long-wire antenna with the input at the left and the characteristic impedance (resistance) at the right.

A traveling-wave V antenna uses two of these elements (see text on p 353) and a rhombic is composed of four elements (see text on p 354), with the elements arranged at angles which produce maximum directivity of the combinations.

Antennas of the nonresonant or traveling-wave types are used both for longer and for very short waves. (However, there is an intermediate frequency region extending from about 100 to 3,000 mc where the half-wave dipole is of such convenient size that standing-wave dipoles or dipole arrays are most frequently employed.)

In the microwave band where transmission is effected by wave guides it is possible to terminate a wave guide with a horn which "matches the impedance of the wave guide to that of free space" and acts as a directive antenna (see page 363). A slot or a series of slots in the side of a wave guide may also act as an antenna at these frequencies.

Radiation Resistance

The radiation resistance R_r of an antenna is the ratio P, of the total power radiated in all directions to the square of the current at the point of measurement. The power may be computed by integrating the radial component of the Poynting vector over a spherical surface surrounding the antenna. Then

if I_i is the effective value of the input current,

$$R_r = \frac{P}{I_i^2}. \qquad (1)$$

The radiation resistance of the doublet antenna is stated in equation (9) in Chapter 2 to be

$$R_r = 80\pi^2 \left(\frac{L}{\lambda}\right)^2 \text{ ohms.} \qquad (2)$$

Influence of Near-by Conducting Bodies

The impedance of an antenna is affected by the presence of conductors in the vicinity and depends upon the mutual impedances between the conductors and the antenna. The mutual impedance decreases with increasing distance so that for conducting bodies of comparable size the effect is negligible for distances greater than, perhaps, 2 to 3 wavelengths.

But for conductors set less than a wavelength apart, such as an antenna and reflector (or director) combination or as antenna arrays, the mutual effect plays an important role and modifies the input impedance of the antenna.

For an antenna set near a large conducting body, such as a large metallic sheet or the earth, the mutual effect is cared for in a different way. If the earth, for instance, is assumed plane and perfectly conducting, its effect is the same as that of the mirror image of the antenna in the ground. As shown in Figure 4,
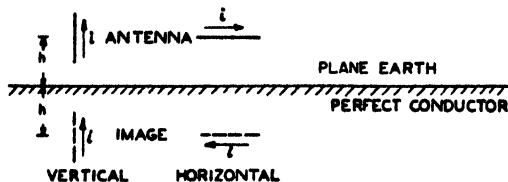
FIGURE 4. Method of images.

the image of a vertical antenna is a similar antenna with current in the same direction, while the current is reversed for a horizontal antenna. The radiation field at any point above ground is obtained by summing the radiation fields of antenna and image.

STANDING-WAVE ANTENNAS

Linear Antennas

A linear antenna is a straight thin rod supplied with alternating current. According to whether the connection to the antenna is made at the middle or at the end, center-fed and end-fed antennas are distinguished. Center-fed linear antennas are also called dipole antennas.

Typical current amplitude distributions are illustrated in Figure 5. The amplitude is always zero
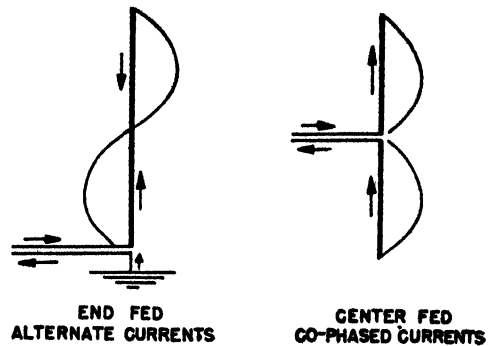
FIGURE 5. Distribution of current amplitudes with linear antennas.

at the open end while the amount at the input point depends on the position of the input connection. For thin wires, compared with the length, the distribution of amplitudes is approximately sinusoidal.

Half-Wave Antennas

Figure 6 illustrates two types of half-wave dipole or center-fed antennas and one end-fed antenna, together with their lumped-circuit analogues. The
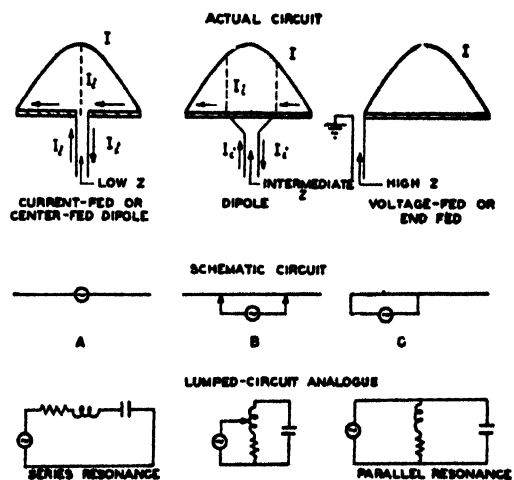
FIGURE 6. Three methods of exciting half-wave antennas and their analogues in lumped-constant resonant circuits.

input current required varies with the position of the input point. The voltage distribution in general has a maximum at the points of current zero and has a minimum where the current is maximum.

Half-Wave Dipole

The half-wave dipole, shown in A and B of Figure 6 and in Figure 7, is the type most frequently used in the 100 to 3,000 mc range. In this range the

length $\lambda/2$ lies between 1.5 and 0.05 meters. In this section it is assumed that the current distribution is sinusoidal.

1. *Radiation field.* The radiation field at point P, Figure 7, where $d >> \lambda$, is obtained by dividing the half-wave current distribution into an infinite
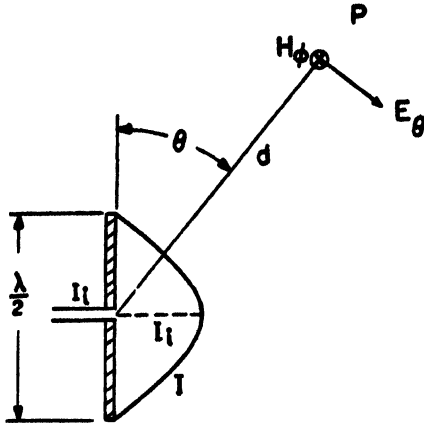
FIGURE 7. Half-wave dipole.

number of infinitesimal doublets, using equation (2) in Chapter 2 and taking into account the differences in phase at P introduced by the differences in the distances which the radiation from the various doublets must travel. The net result, using d in place of r, is

$$E_\theta = \frac{60 I_i}{d} \frac{\cos\left[(\pi/2)\cdot\cos\theta\right]}{\sin\theta} \text{ volts per meter,} \quad (3)$$

$$H_\phi = \frac{E_\theta}{120\pi} \text{ amperes per meter.} \quad (4)$$

The normal part of the field, E_θ (difference), prescribes the antenna pattern factor (measured in relative field strength) and is plotted in Figure 11. The corresponding pattern for a doublet is $E_\theta \sim \sin\theta$, which is a circle in polar coordinates. These patterns are circularly symmetric about the antenna axis. Squaring the radial lengths in the above patterns gives the pattern in terms of relative power per unit area in the same angular direction.

The radial component of radiated power per square meter (Poynting's vector) is given by

$$W_r = E_\theta H_\phi = \frac{E^2}{120\pi} = \frac{30 I_i^2}{\pi d^2}\left[\frac{\cos\left(\frac{\pi}{2}\cos\theta\right)}{\sin\theta}\right]^2 \quad (5)$$

watts per square meter.

In the equatorial plane,

$$E_\theta = \frac{60 I_i}{d}. \quad (6)$$

2. *Gain of half-wave dipole.* The gain of the dipole relative to a doublet is the ratio of the power supplied to the doublet to the power supplied to the dipole to produce the same field strength at the same distance

in the direction of maximum radiation (here the equatorial plane, $\theta = 90$ degrees).

For equal maximum fields, comparing equations (3) in Chapter 2 and (6) in this chapter,

$$\int I dl = \frac{\lambda}{\pi} I_i. \quad (7)$$

The power per unit area for the doublet, using equation (3), in Chapter 2, is

$$W_{\text{doublet}} = \frac{E^2}{120\pi} = \frac{30 I_i^2 \sin^2\theta}{\pi d^2}, \quad (8)$$

and for the dipole the power per unit area is given by equation (5).

The dipole gain is then

$$G = \frac{\int W_{\text{doublet}}\, dA}{\int W_{\text{dipole}}\, dA} = \frac{\text{Power radiated by doublet}}{\text{Power radiated by dipole}}$$

where the integration is carried out over spheres surrounding the antennas. Carrying out this operation,

$$G_{\text{dipole}} = 1.09 \quad (\text{or } 0.4 \text{ db}). \quad (9)$$

3. *Radiation Resistance.* The radiation resistance of the half-wave dipole is

$$R_r = \frac{1}{I_i^2}\int W_{\text{dipole}}\, dA = 73.1 \text{ ohms.} \quad (10)$$

4. *Impedance of an Infinitely Thin Dipole.* The formulas given here are valid only for a half-wave
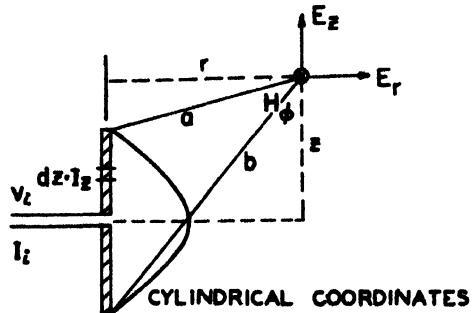
FIGURE 8. Half-wave dipole field components.

dipole composed of wire of vanishing thickness. For wire of finite dimensions, see pages 351-353.

Here (type A in Figure 6) it is necessary to calculate the voltage V_i required at the input to establish a current distribution $I_i \cos\left[(2\pi/\lambda)z\right]$, as shown in Figure 8. To do this, the *total* field of the dipole must be known, including the *induction field* which is significantly large at short distances as well as the *radiation field*. In cylindrical coordinates, the total field is given by

$$E_r = +j30 I_i\left[\frac{z-\lambda/4}{ar}e^{-j\left(\frac{2\pi a}{\lambda}\right)} + \frac{z+\lambda/4}{br}e^{-j\left(\frac{2\pi b}{\lambda}\right)}\right], \quad (11)$$

$$. E_s = - j30 I_i \left[\frac{1}{a} e^{-j\left(\frac{2\pi a}{\lambda}\right)} + \frac{1}{b} e^{-j\left(\frac{2\pi b}{\lambda}\right)} \right], \qquad (12)$$

$$H_\phi = - j \frac{I_i}{4\pi} \left[\frac{1}{r} e^{-j\left(\frac{2\pi a}{\lambda}\right)} + \frac{1}{r} e^{-j\left(\frac{2\pi b}{\lambda}\right)} \right]. \qquad (13)$$

By the reciprocity theorem a small current length $I_s dz = I_i \cos [(2\pi/\lambda)z] \cdot dz$ induces a voltage $(- dV_s)$ at the input point which is equal to the voltage $dV_s = E_s dz$ induced in dz by a small current length $I_i dz$ taken at the input point. Hence

$$\frac{E_s dz}{I_i dz} = \frac{- dV_i}{I_i \cos\left(\frac{2\pi}{\lambda} z\right) \cdot dz},$$

and the total input voltage is

$$V_i = 2 \int_{s=0}^{s=\lambda/4} - E_s \cos\left(\frac{2\pi}{\lambda} z\right) \cdot dz.$$

Carrying out the operation indicated and dividing by I_i gives the impedance of the half-wave dipole as

$$Z = 73.1 + j42.5 \text{ ohms}. \qquad (14)$$

The dipole thus has an inductive reactance of 42.5 ohms if a sine distribution of current amplitudes is assumed.

The reactance can be altered by changing the length of the wire. Increasing the length increases the inductance; decreasing the length decreases the inductance, first to zero for resonance, and then for still shorter lengths to a capacitive reactance. Changes in length of only 4 to 5 per cent will produce large changes in the reactance.

Modifications of the Half-Wave Dipole

Two modifications will be given.

1. *Quarter-wave dipole with artificial ground.* A convenient device for doubling the effective length of a dipole is to use an artificial ground plane. It usually takes the form of a number of grounded rods spreading radially from the base of the antenna (Figure 9). If the antenna is a quarter-wave dipole the effect of the artificial ground is to produce an image quarter-wave dipole; the radiation resistance and the radiation pattern of the system are those of a half-wave dipole.
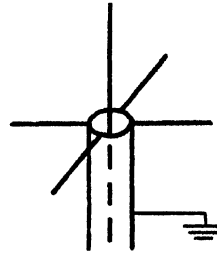
FIGURE 9. Quarter-wave dipole with artificial ground.

2. *Folded dipole.* Another variant of the dipole antenna is the *folded dipole*, shown in Figure 10. It is essentially a center-fed half-wave dipole with a parasitic counterpart "dummy" (see page 360) in its immediate neighborhood and connected to the latter at the ends of the dipole. The induced current in the dummy has the same distribution as, and is in phase with, that of the primary dipole. Hence the radiation pattern is essentially that of a simple half-wave dipole. The radiation resistance is four times that of the ordinary dipole.
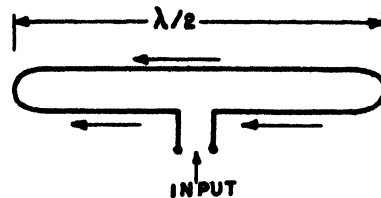
FIGURE 10. Folded dipole.
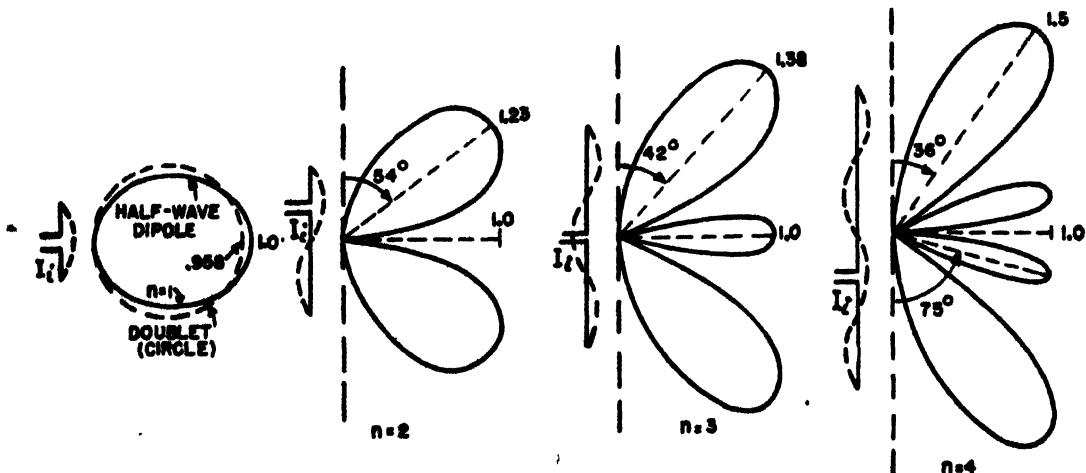
FIGURE 11. Antenna radiation patterns (relative field strength).

Multiple Half-Wave Long Antennas

For an antenna of length equal to an integral number, n, of half wavelengths, the radiation field is given by:

1. n is odd:

$$E_\theta = \frac{60 I_s}{d} \frac{\cos\left(\frac{n\pi}{2}\cos\theta\right)}{\sin\theta}. \quad (15)$$

2. n is even:

$$E_\theta = \frac{60 I_s}{d} \frac{\sin\left(\frac{n\pi}{2}\cos\theta\right)}{\sin\theta}, \quad (16)$$

where d is the radial distance to a field point and I_i is the input current at the center of one of the half-wave elements.

The radiation patterns are illustrated in Figure 11 for the doublet, $n = 1$ (the half-wave dipole), and $n = 2, 3, 4$.

The radiation resistance, both for integral and nonintegral numbers of half wavelengths, is plotted in Figure 12.
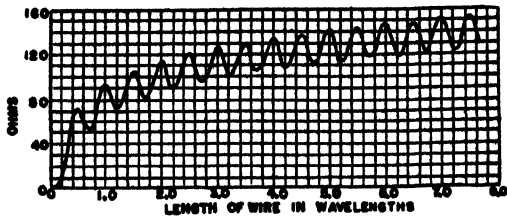
FIGURE 12. Radiation resistance for linear antennas.

In Table 1 the radiation resistances and the power gains for integral half-wavelength antennas are listed.

Cophased Half-Wave Dipoles

The directivity and gain of linear antennas may be increased considerably by the *suppression* of alternate current loops, leaving therefore only loops in which the currents are all cophased. The *suppressed* loops are contained in either (1) quarter-wave stubs

TABLE 1. Comparison of alternate and cophased half-wave dipoles.

n Half Waves	R_n Radiation resistance-ohms		$E_{m,n}$ Relative major lobe amplitudes for same current input		G_n Gain (power)	
	Alternate currents	Cophased currents	Alternate currents	Cophased currents	Alternate currents	Cophased currents
1	73.1	73.1	1.0	1	1.09	1.09
2	93	199	1.23	2	1.19	1.47
3	105	317	1.38	3	1.32	2.09
4	113	439	1.5	4	1.46	2.67
5	121	560	1.62	5	1.58	3.26

$$G_n = \frac{R_{doublet}}{R_n}\left(\frac{I_{doublet}}{I_s}\right)^2 = \frac{R_{doublet}}{R_n}\left(\frac{E_{m,n}}{E_{doublet}}\right)^2$$
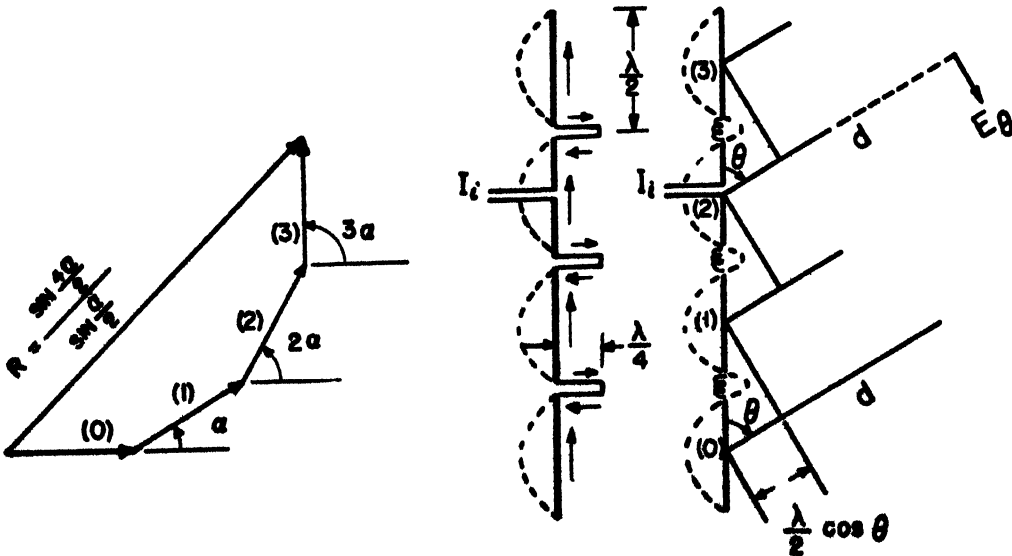
FIGURE 13. Cophased half-wave dipoles.
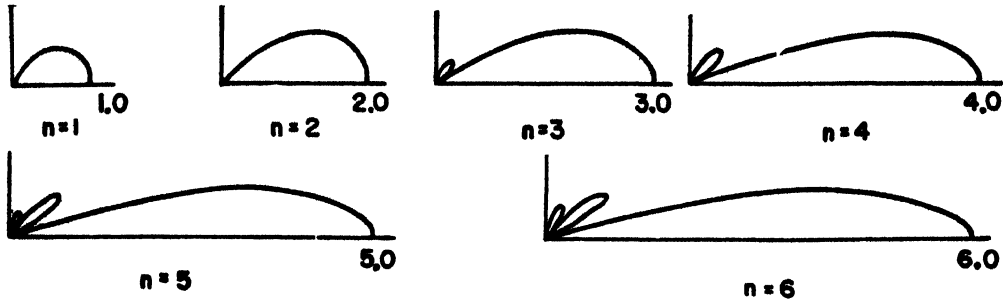
FIGURE 14. Cophased half-wave dipoles (relative fields).

or (2) short inductive elements, as indicated in Figure 13. The suppressed loops are practically nonradiative.

The radiation field at distance d is the vector sum of the fields from the n half-wave elements. The contribution from each element lags that of the next element above by an angle

$$\alpha = \frac{\lambda}{2} \cos \theta \cdot \frac{2\pi}{\lambda} = \pi \cos \theta \text{ radians,} \qquad (17)$$

determined by the extra distance $[(\lambda/2) \cos \theta]$ which it must travel. The radiation field is then equal to the radiation field of one half-wave element (as a function of angle θ) multiplied by the vector resultant for the n elements. Thus

$$E_\theta = \frac{60I_s}{d} \left[\frac{\cos\left(\frac{\pi}{2} \cos \theta\right)}{\sin \theta} \right] \times$$
$$[e^{j0} + e^{j\alpha} + e^{j2\alpha} + + + e^{j(n-1)\alpha}]$$

$$= \frac{60I_s}{d} \left[\frac{\cos\left(\frac{\pi}{2}\cos \theta\right)}{\sin \theta} \right] \left[\frac{\sin \frac{n\alpha}{2}}{\sin \frac{\alpha}{2}} \right]. \qquad (18)$$

The radiation patterns for various values of n are plotted in Figure 14. Table 1 gives the radiation resistances, relative lengths of major lobes, and the gains, with comparative figures for the doublet and the multi-half-wave antennas discussed on page 350.

Effects of Finite Diameter on Center-Fed Linear Antennas

Figure 15 shows the input reactance, and Figure 16 the input resistance of a center-fed antenna of arbitrary length. The input impedance is a series combination of the two components. The important regions of the curves correspond to antenna half-lengths near $\lambda/4$ and near $\lambda/2$. The former represents a center-fed half-wave antenna, whereas the latter represents a pair of end-fed half-wave antennas excited in phase. The half-length of the antenna was used in plotting, because in these terms the reactance curves resemble those for an open-ended transmission line.

In the regions of principal interest the reactance curves are nearly straight lines whose slopes depend on the diameter of the antennas expressed in wavelengths. The slopes of the reactance curves decrease
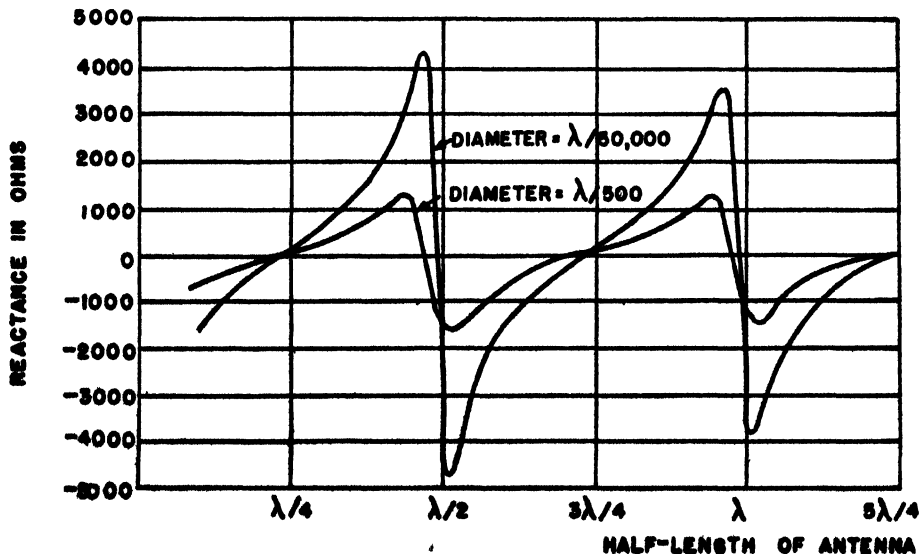
FIGURE 15. Reactance at input of a center-fed antenna of arbitrary length.
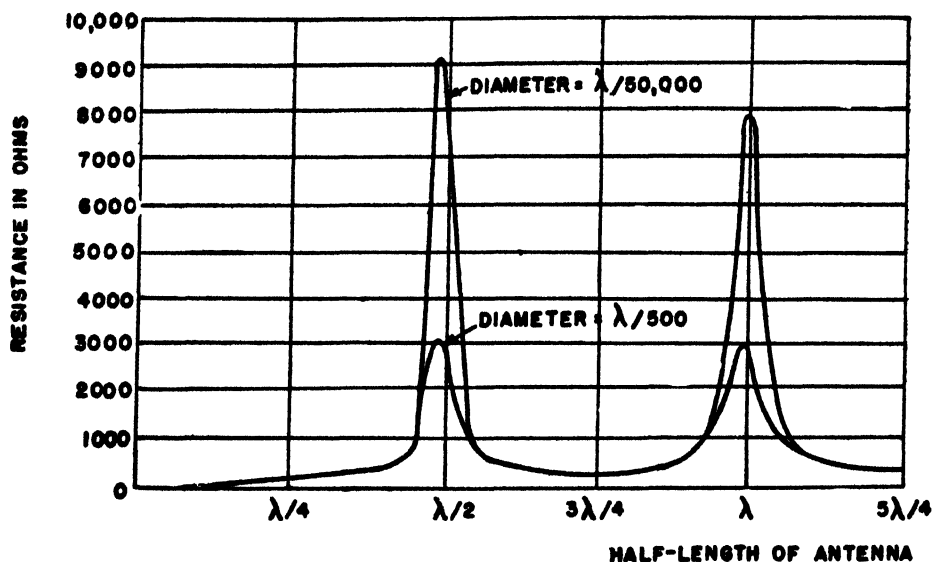
FIGURE 16   Resistance at input of a center-fed antenna of arbitrary length.

as the antenna diameter increases. This feature is important in radar antennas which need to be insensitive to small changes in frequency. The curves show that antennas of large diameter present less than a specified amount of reactance, say one ohm, over a greater range of antenna length than slender antennas do. In terms of frequency, this means that a given length of antenna has less than one-ohm reactance over a wider range of frequency when the antenna has a large diameter than when it has a small diameter. Radar antennas are commonly made of tubing and frequently have diameters in excess of $\lambda/20$.

Figure 16 shows that the input resistance also depends on antenna diameter. This dependence is more pronounced when the half-length is about $\lambda/2$ than when the half-length approximates $\lambda/4$, as it does for a single center-fed antenna. The values for an antenna whose half-length is $\lambda/4$ is not readable on the curve, but the component representing radiation ranges from 73 ohms for infinitely thin antennas, through 64 ohms for a diameter of 0.0001 λ, 55 ohms for a diameter of 0.01 λ, to less than 50 ohms for certain large-diameter radar antennas. The change is mainly due to a decrease in the resonant length of the thicker antennas.

A feature of Figure 15 which is not easily readable is that the lengths at which the reactance is zero are less than $\lambda/2$ and λ. The amount by which an antenna with zero reactance is shorter than these

lengths depends on the antenna diameter. For very slender antennas the shortening is slight, but for large-diameter antennas or for special shapes as shown in Figure 17, a resonant length may be as much as 20 per cent shorter than $\lambda/2$. Special shapes, such as the one shown in Figure 17, have the ad-

FIGURE 17.   Non-cylindrical half-wave antenna.
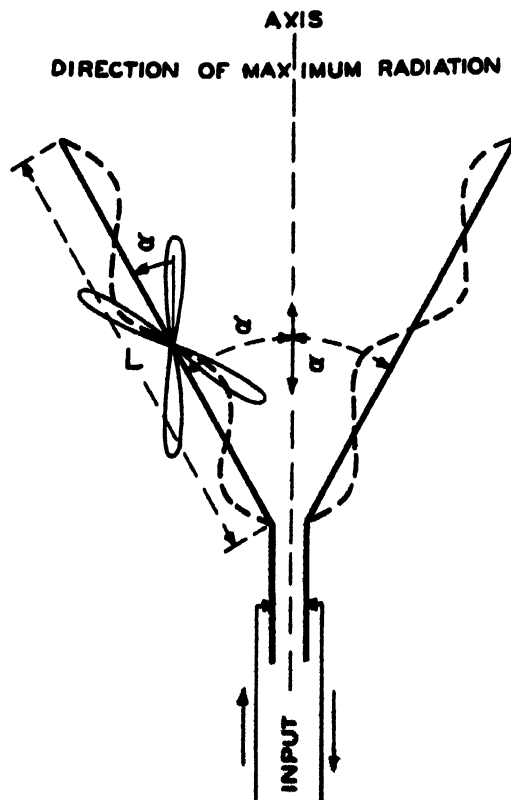
FIGURE 18.   Standing-wave V antenna ($\alpha = 36°$ for $n = 4$ half-wavelengths).

IN PLANE OF THE V
n = 16 , α = 17.5°

IN PLANE ⊥ TO V
n = 16 , α = 17.5°
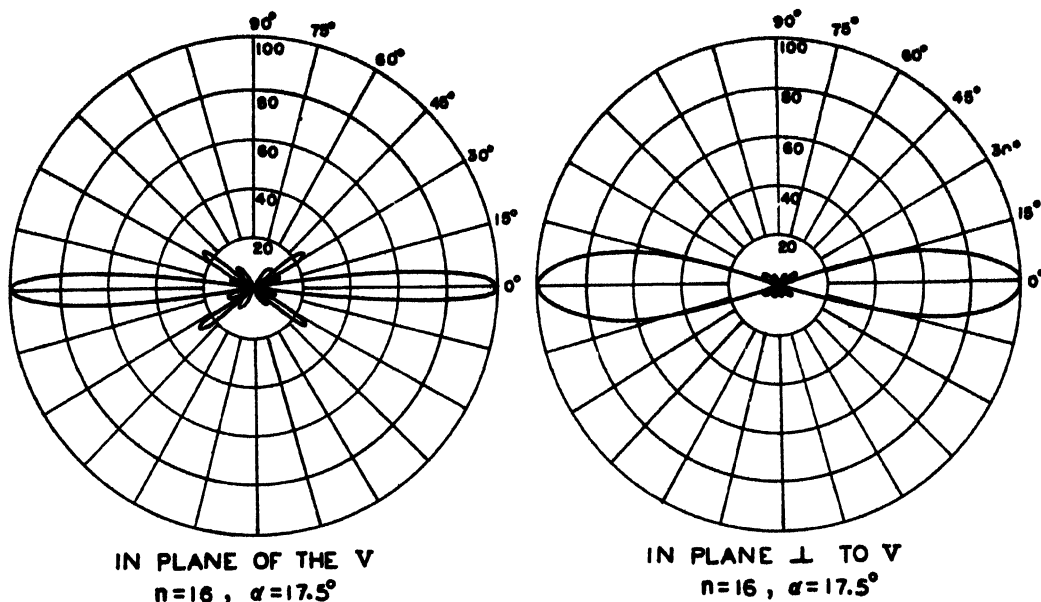
FIGURE 19. Power distribution for standing-wave V antenna. (Courtesy of IRE)

vantage of being insensitive to small changes in frequency and at the same time are not so subject to corona (breakdown of the air because of large potential gradients) as slender antennas are.

Standing-Wave V Antennas

This type of antenna (Figure 18) utilizes the directive properties of the multi-half-wave antenna. Two such elements are combined in a V arrangement so that the major lobe of each (at angle α with each element) is parallel to the axis of the V. By feeding the two halves of the V with currents 180 degrees out of phase the lobe structure is reversed to produce maxima, forward and backward, along the axial direction, while the field in the plane perpendicular to the axis is greatly reduced. The value for angle α is equal to the angle between each element and its maximum lobe (see Figure 11). Figure 19 gives the (power) radiation pattern for n = 16 half-wavelengths.

The directivity of this antenna system may be improved by adding one or more reflectors (see text on p. 358) The reflector is a V antenna of identical type. The legs of the reflector are placed parallel to those of the primary V and lie in the same plane as the original V. The reflector is set approximately λ/4 behind the primary V.

TRAVELING-WAVE ANTENNAS

Field and Pattern

A traveling-wave antenna is one in which only progressive (or traveling) waves are allowed. Reflected waves are eliminated by terminating the end

opposite the input point in the characteristic impedance. See Figure 20.

The equation of the radiation field, neglecting wire losses, is

$$E_\theta = \frac{60I}{d} \cdot \frac{\sin\theta}{1-\cos\theta} \sin\left[\frac{\pi L}{\lambda}(1-\cos\theta)\right]. \quad (19)$$

The major lobes given by this equation are plotted in Figure 21, and the major lobe angles with the wire θ_m are plotted in Figure 22. Angle θ_m, it will be noted, decreases with increasing wire length.

Traveling-Wave V Antenna

As in the case of the standing-wave antenna a pair of lines arranged at a suitable angle with each
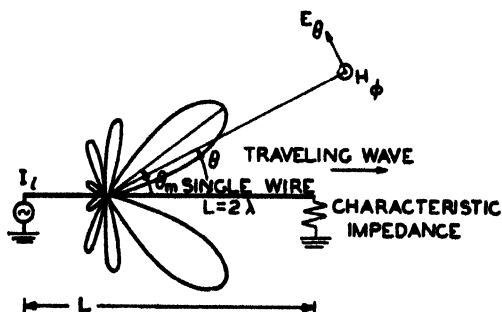
FIGURE 20. Lobe structure for L = 2λ traveling-wave antenna in free space.

other, and carrying traveling waves, can be made to produce a directional pattern with fairly high gain.

The traveling-wave V antenna can be designed so that the plane of the V is horizontal and the maximum lies in the direction of the axis of sym-
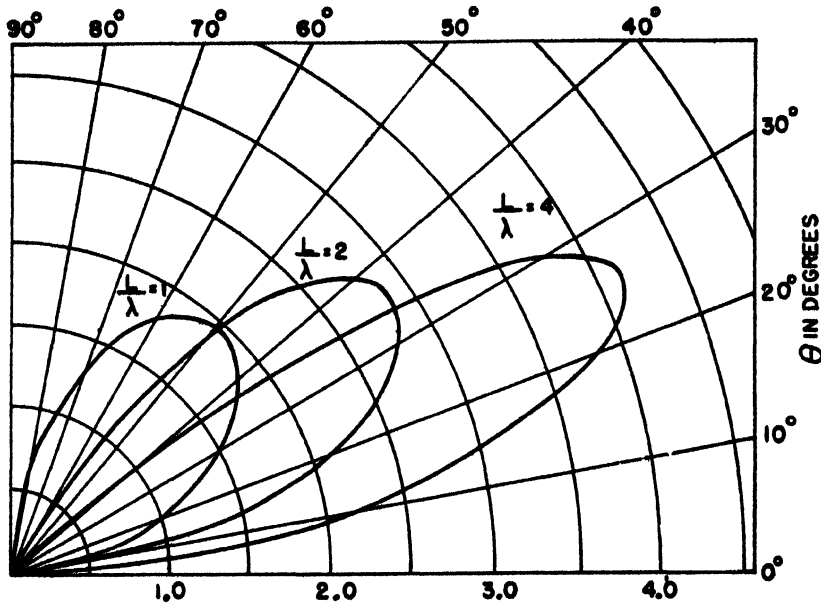
FIGURE 21. Major lobes (relative field strength) for traveling-wave antenna.

metry, as in Figure 18. In this case the radiation is horizontally polarized. It can also be used as an inverted V in a vertical plane with the point of the V directed upwards; the radiation is then vertically polarized. This antenna, also called a semi-rhombic, is represented by the upper half of Figure 20.
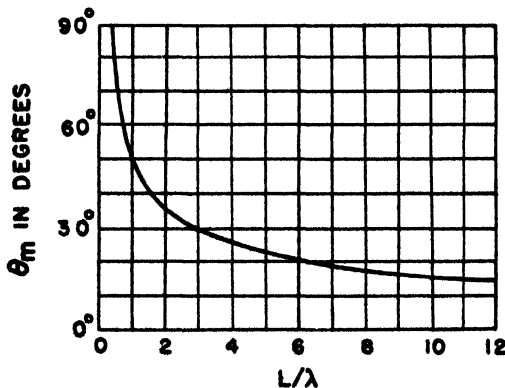
FIGURE 22. Angles for major lobes for traveling-wave antenna.

Rhombic Antenna

This type of antenna is based on the same principle as the traveling-wave V antenna. The rhombic antenna consists of four wires arranged in the form of a rhomboid or diamond (Figure 23). The reflec-
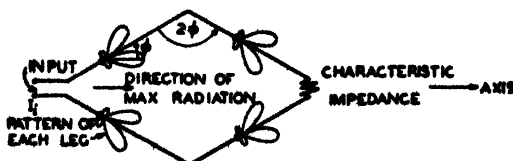
FIGURE 23. Rhombic antenna.

tionless termination of the wires is achieved by connecting the two wires at the end opposite the input to a resistance equal to their characteristic impedance.

As in the case of the V antenna, the rhombic antenna can be used both horizontally and vertically; at the longer waves the horizontal arrangement is usually more practical. The optimum tilt angle of the rhombic (angle ϕ of Figure 23) is not very critical provided the legs are not less than two wavelengths long. The radiation pattern is not very sensitive to frequency and the rhombic antenna can therefore be used over a fairly wide frequency range (of the order of 2 to 1). Rhombic antennas have appreciably higher gains than V antennas.

The field in the axial direction is equal to

$$E_{axial} = \frac{240 I_i}{d} \frac{\cos \phi}{1 - \sin \phi} \sin^2 \left[\frac{\pi L}{\lambda} (1 - \sin \phi) \right]. \quad (20)$$

Effect of Perfectly Conducting Ground. If the rhombic is placed in a horizontal plane, height H above ground, the effect of the image rhombic must also be considered. The net result is that the direction of the resultant lobe maximum is tilted up by an angle ϵ. It can be shown that, for a given angle ϵ and wavelength λ, to point the major lobe at vertical angle ϵ the following relations for H, L, and ϕ must hold:

$$H = \frac{\lambda}{4 \sin \epsilon},$$

$$L = \frac{0.371 \lambda}{\sin^2 \epsilon},$$

$$\phi = 90° - \epsilon.$$

Figure 24 illustrates the radiation·pattern (relative field strength) for a particular case.
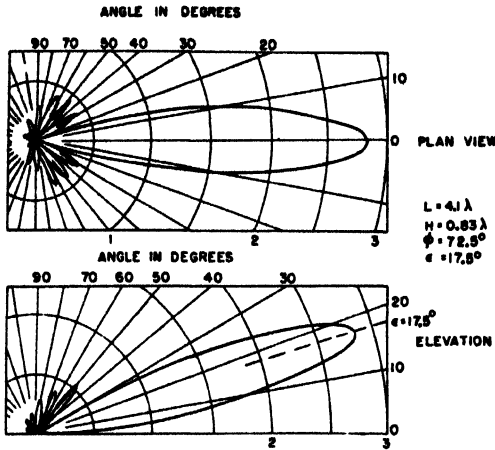
FIGURE 24. Rhombic antenna above ground (relative field strength). (Courtesy of Bell System Technical Journal.)

ANTENNA ARRAYS

Principle of Arrays

An antenna array is a combination of several antennas, usually of equal strength and equally spaced in any one given direction. One-, two-, and three-dimensional arrays may be distinguished. The spacings in different directions may be different for two- or three-dimensional arrays. The use of arrays permits great increases in the amount of power radiated, in directivity, and gain.

Although the most common array element is a half-wave dipole, the elements of an array may be radiators of any type; in particular, the elements may themselves be arrays. In this way it is possible to interpret a two-dimensional array as an *array of arrays*. A vertical curtain may be considered either as a horizontal array of elements which, themselves, are vertical, or it may be considered a vertical array of elements which, themselves, are horizontal arrays; similarly for three-dimensional arrays.

In most arrays the elements radiate very nearly equal power, but in the binomial array the elements, although identical in structure, differ in the amount of power radiated because of differing current distributions. In most arrays there is a constant phase shift (which might be zero) between adjacent elements. By suitable phasing a great variety of antenna patterns can be produced.

Basic Types of Dipole Arrays

There are three basic types of dipole arrays.

1. *Broadside array.* The centers of the elements are arranged in a line, with the axes of the elements

parallel to each and perpendicular to the line. With the currents adjusted all in phase, the maximum radiation is *broadside* to the plane of the elements.

2. *End-fire array.* The geometric ·arrangement is the same as in the broadside array, but through appropriate phasing of the currents in the elements the maximum radiation can be directed primarily along the line joining the centers.

3. *Colinear array.* Here the axes of the antenna elements are arranged along the line of centers with the currents all in phase. The radiation is a maximum in the equatorial plane perpendicular to the line of centers.

To illustrate the principles most simply, two half-wave dipole elements are considered first, and later extension is made to arrays composed of a larger number of elements.

Two-Dipole Side-by-Side Array

Two half-wave dipoles are placed side by side with spacing s and the currents I_1 and I_2 are equal but differ in phase by angle ψ (see Figure 25). If I_2 lags I_1 by time angle ψ, the field of the second element at P lags that of the first by angle α where α is
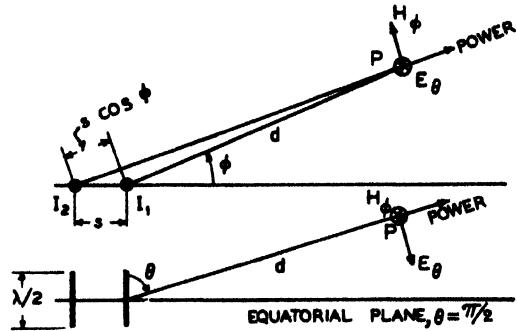
FIGURE 25. Two dipole side-by-side array.

composed of ψ and the time delay caused by the extra distance traveled, $(2\pi/\lambda)s \cos \phi \sin \theta$,

$$\alpha = \psi + (2\pi/\lambda) \ s \cos \phi \sin \theta. \qquad (21)$$

For *equal* currents, $I_1 = I_2 = I$, the field is equal to

$$E_\phi = \frac{60I}{d}\left[e^{j0} + e^{-j\alpha} \right]\left[\frac{\cos\left(\frac{\pi}{2}\cos\theta\right)}{\sin\theta} \right],$$

$$= \frac{60I}{d}\left[\frac{\sin\alpha}{\sin\frac{\alpha}{2}} \right]\left[\frac{\cos\left(\frac{\pi}{2}\cos\theta\right)}{\sin\theta} \right]. \qquad (22)$$

The first bracket gives the directional characteristic of an array of two elements, while the second bracket

gives the directional characteristic of the element itself.

BROADSIDE
$s = \lambda/2$
$\psi = 0°$

END-FIRE
$s = \lambda/2$
$\psi = 180°$

UNI-DIRECTIONAL
$s = \lambda/4$
$\psi = 90°$ (I_2 LAGS I_1)

EQUATORIAL PLANE $\theta = 90°$
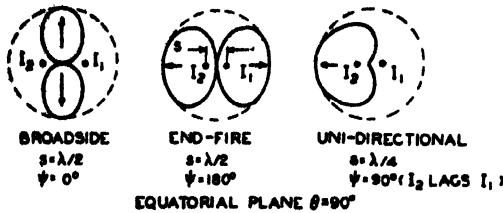
FIGURE 26.   Radiation patterns (field strength) for two dipole side-by-side array.

Three special cases are particularly to be noted. The field patterns for the equatorial plane ($\theta = 90°$) and $|I_2| = |I_1|$ are plotted in Figure 26.

1. *Broadside.* Here $s = \lambda/2$, the currents are in phase ($\psi = 0°$). The maximum field is broadside and twice that of each dipole.

2. *End-fire.* Again $s = \lambda/2$, but the currents are out of phase ($\psi = 180°$). The maximum field is found in both directions along the line of centers.

3. *Unidirectional couplet.* Here $s = \lambda/4$ and I_2 lags I_1 by $\psi = 90°$. The result of this combination is to produce a maximum field along the line of centers in the direction looking from the leading to the lagging current and zero field in the reverse direction.

Two-Dipole Colinear Array

For two equal currents in time phase (see Figure 27), the field is equal to

$$E_\theta = \frac{60I}{d}\left[\frac{\cos\left(\frac{\pi}{2}\cos\theta\right)}{\sin\theta}\right]\left[\frac{\sin\alpha}{\sin\frac{\alpha}{2}}\right], \quad (23)$$

where

$$\alpha = \frac{2\pi}{\lambda}s\cos\theta. \quad (24)$$
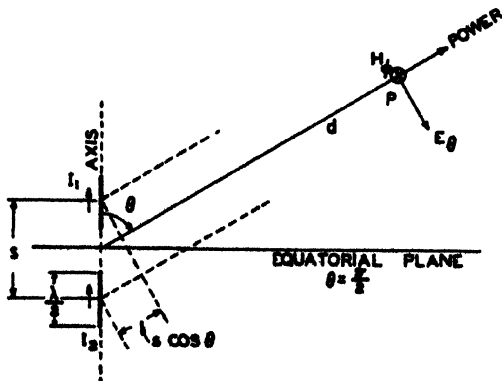
FIGURE 27.   Two half-wave dipole colinear array.

The field is circularly symmetrical about the axis. Its variation with θ is plotted in Figure 28. This is, of course, equivalent to a vertical antenna with center height at distance $s/2$ above a perfectly conducting flat earth.

$s = (1/2)\lambda$

$s = 1\lambda$

$s = (3/2)\lambda$

$s = 2\lambda$
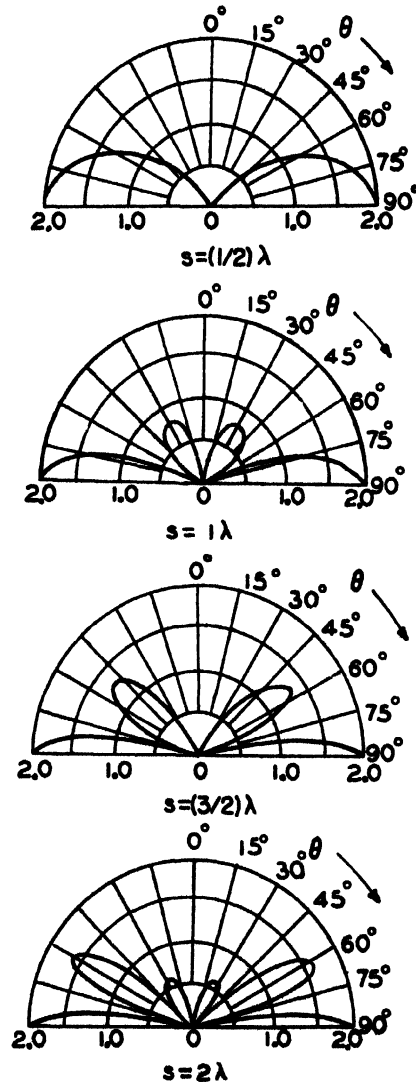
FIGURE 28.   Two half-wave dipole colinear array.

One-Dimensional Array

Two geometrical arrangements will be considered.

1. *Broadside.* Consider n elements with equal co-phased currents equally spaced (see Figure 29).

$$E_\theta = E_{el}(\theta, \phi)\frac{\sin\frac{n\alpha}{2}}{\sin\frac{\alpha}{2}}, \quad (25)$$

where

$$\alpha = \frac{2\pi}{\lambda}s\cos\phi. \quad (26)$$
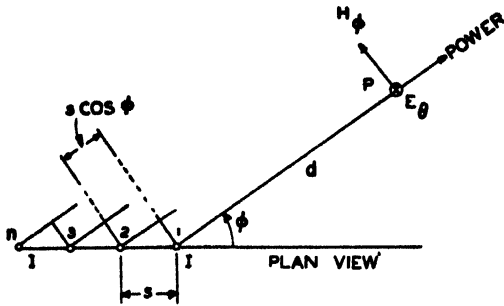
FIGURE 29. Broadside array, elements perpendicular to paper.
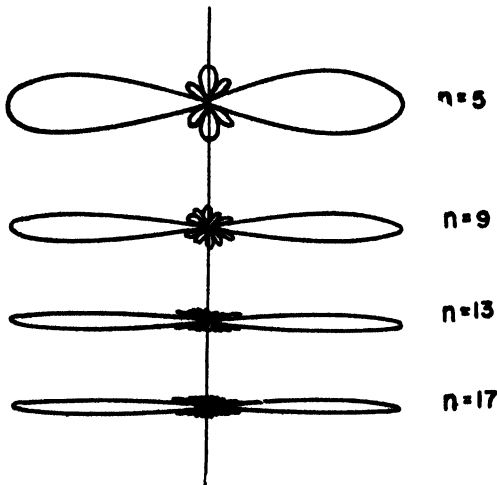
FIGURE 30A. Effect of array length for broadside with element spacing $s = \lambda/2$. (From Radio Engineers' Handbook by Terman.)

For center-fed half-wave dipoles, from equation (3)

$$E_{st} = \frac{60I}{d} \frac{\cos\left(\frac{\pi}{2} \cos\theta\right)}{\sin\theta}. \qquad (27)$$

The patterns for the equatorial plane are illustrated in Figures 30A and 30B. Figure 30A shows the increase in directivity with increasing number of elements. Figure 30B illustrates the effect of element spacing on the production of side lobes. Figure 31 gives the gain for various spacings and array lengths. From this it appears that $s = 5\lambda/8$ is approximately the optimum spacing.

2. *Broadside: pattern factor and beam width.* For illustration, suppose that the antenna consists of a vertical array of m horizontal center-fed dipoles spaced s apart with all fed in phase to give a broadside beam strongly directive in the vertical plane. For this arrangement the field strength in the horizontal plane is given by m times equation (27), that is,

$$E_{\text{horizontal}} = m\frac{60I}{d} \frac{\cos\left(\frac{\pi}{2} \cos\theta\right)}{\sin\theta} \qquad (28)$$

with angle θ measured from the dipole axis. See also equation (15) and Figure 11 (for $n = 1$).

In the vertical plane, the beam is much narrower. If ϕ is the angle from the vertical and $\beta = 90° - \phi$ is the angle from the (horizontal) broadside direction, the field in the vertical plane ($\theta = 90°$) is given
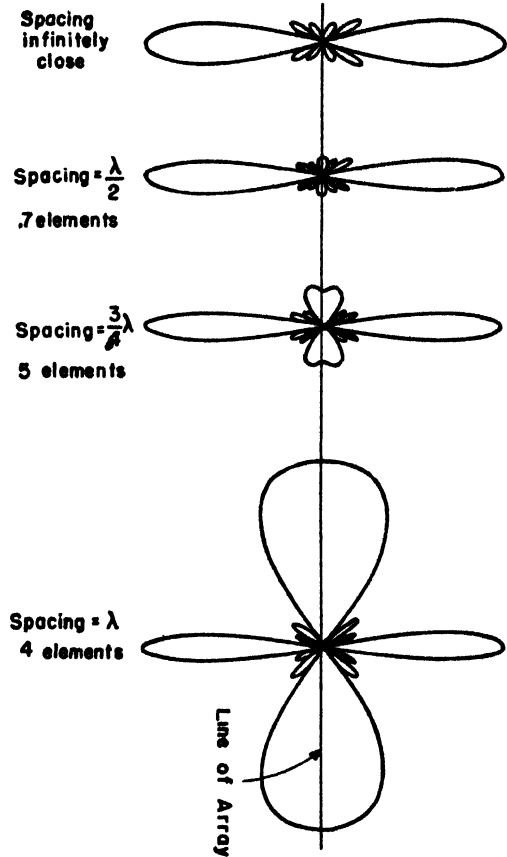
FIGURE 30B. Effect of element spacing for broadside for array length $L = 3\lambda$. (From Radio Engineers' Handbook by Terman.)
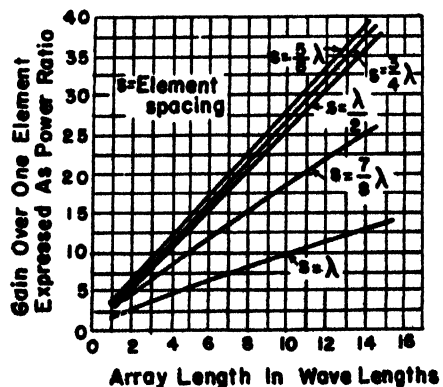
FIGURE 31. Gain for broadside array of doublets as a function of array length and spacing. (From Radio Engineers' Handbook by Terman.)

by

$$E_{\text{vertical}} = \frac{60I_s}{d} \frac{\sin \frac{m\alpha}{2}}{\sin \frac{\alpha}{2}} \tag{29}$$

with

$$\alpha = \frac{2\pi}{\lambda} s \cos \phi = \frac{2\pi}{\lambda} s \sin \beta.$$

The maximum value of equation (29), corresponding to $\theta = 90°$ and $\beta = 0°$, is equal to

$$E_{\max} = \frac{60I_s}{d} m \tag{30}$$

The relative field strength is then

$$\frac{E_{\text{vertical}}}{E_{\max}} = \frac{\sin \frac{m\alpha}{2}}{m \sin \frac{\alpha}{2}}. \tag{31}$$

The beam width in the vertical plane is determined by the angle between the half-power points, or the angle between the points where the field strength is 0.707 of the maximum. Thus, equation (31) is set equal to 0.707 and β determined. The beam width is equal to $2\beta°$.

To illustrate, let $s = \lambda/2$. For $m = 2,3,4,8;12,16$ dipoles in the array, the corresponding beam widths are 60°, 36.4°, 26.4°, 12.8°, 8.5° and 6.3°. A few field patterns are illustrated in Figure 30A and gains are shown in Figure 31.

3. *Colinear array* (see Figure 32). For n equal cophased currents, equally spaced,

$$E_\theta = E_{\text{el}}(\theta, \phi) \frac{\sin \frac{n\alpha}{2}}{\sin \frac{\alpha}{2}}, \tag{32}$$

where

$$\alpha = \frac{2\pi}{\lambda} s \cos \theta. \tag{33}$$

For center-fed half-wave dipoles, from equation (3),

$$E_{el} = \frac{60I_s}{d} \frac{\cos\left(\frac{\pi}{2}\cos\theta\right)}{\sin\theta}. \tag{34}$$

The patterns for various array lengths and spacings are given in Figure 33.

If $s = \lambda/2$, equation (32) for half-wave dipoles reduces to equation (18).
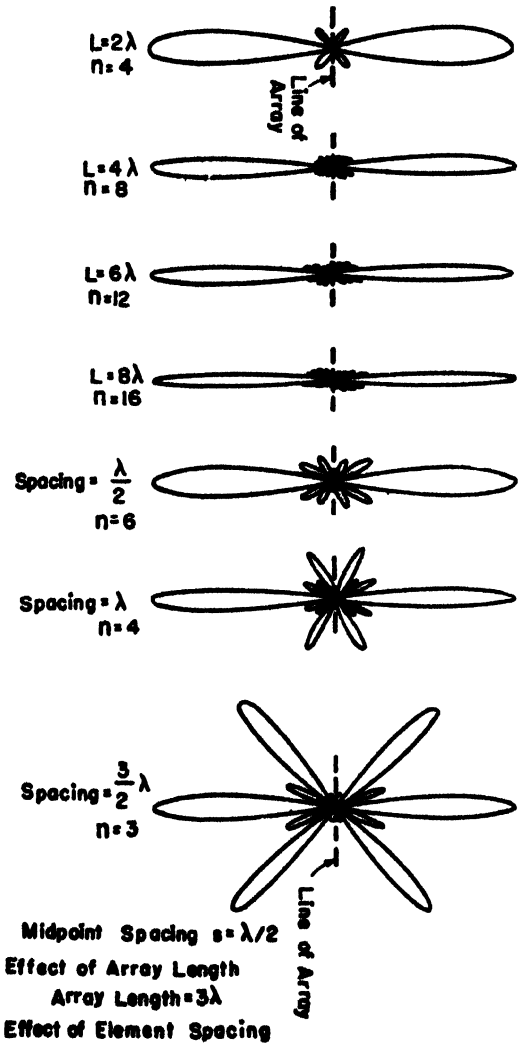
FIGURE 33   Cophased colinear half-wave dipoles. (From Radio Engineers' Handbook by Terman.)

FIGURE 32.   Cophased colinear half-wave dipoles.

Unidirectional Broadside and Colinear Arrays

If an array is backed up with a similar array, the latter may serve to concentrate the radiation in one direction, provided the currents in the arrays are properly adjusted in magnitude and phase. Patterns

for the unidirectional broadside and colinear arrays are given in Figure 34.

The broadside array is a collection of unidirectional couplets of the type illustrated in Figure 26. Increasing the number of couplets n appreciably narrows the beam width.

A similar improvement is obtained in the colinear combination.
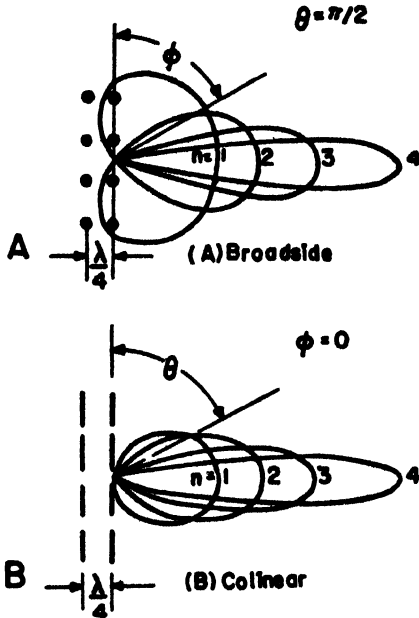
FIGURE 34. Unidirectional broadside and colinear array.

Multidimensional Arrays

Enough has already been given to show that it is not difficult to extend the principles of summation of fields from elements to cover two- and three-dimensional arrays.

Binomial Arrays

Most array patterns show, in addition to the main maximum, secondary maxima (side lobes) which are inconvenient in radar work. Side lobes are practically eliminated in the binomial array.

Consider first a two-element half-wave dipole broadside array with equal cophased currents and elements spaced a half wavelength apart. See equations (21) and (22). Then $\psi = 0$, $s = \lambda/2$, $\alpha = \pi \cos \phi$. Then with

$$E_{d} (\theta) = \frac{60I}{d} \frac{\cos\left(\frac{\pi}{2} \cos \theta\right)}{\sin \theta}, \qquad (35)$$

$$E = E_{d} (e^{j0} + e^{-j\alpha}).$$

This gives the broadside field in Figure 26 which has only two equal major lobes. There are no side lobes.

Now consider the equation

$$E = E_{d} (e^{j0} + e^{-j\alpha})^2, \qquad (36)$$

$$= E_{d} (1 + 2e^{-j\alpha} + 1e^{-j2\alpha}).$$

This represents three half-wave dipoles in broadside, spacing $s = \lambda/2$, currents in phase but with relative magnitudes $1 : 2 : 1$. The pattern has no side lobes.

Again, for five similar dipoles,

$$E = E_{d} (e^{j0} + e^{-j\alpha})^4$$
$$= E_{d} (1 + 4e^{-j\alpha} + 6e^{-j2\alpha} + 4e^{-j3\alpha} + 1e^{-j4\alpha}). \qquad (37)$$

Here the cophased current magnitudes are $1 : 4 : 6 : 4 : 1$, and there are no side lobes.

The scheme is to follow the pattern of binomial coefficients in adjusting the relative current values.

$m = 1$	1 1
2	1 2 1
3	1 3 3 1
4	1 4 6 4 1
5	1 5 10 10 5 1

Each number is the sum of the two immediately above.

Ring Arrays

A set of radiating elements can be arranged on the perimeter of a circle with equal angular distances and equal phase shift between the elements; the diameter of the ring must be properly chosen; the resulting radiation pattern can be made very nearly uniform, i.e., circular, in the plane of the ring, while the
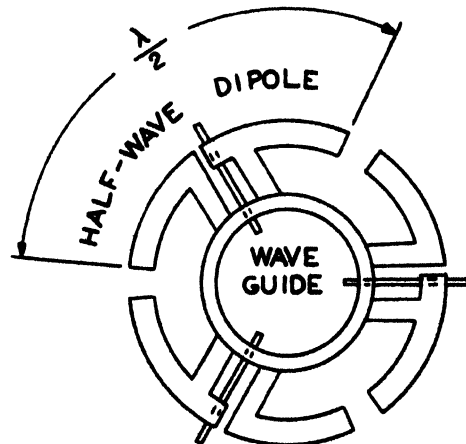
FIGURE 35. Ring array.

directivity of the pattern obtained in a plane perpendicular to that of the ring is increased compared to that of the single element.

If a number of such rings are stacked on top of each other with a common vertical axis, a linear array is formed whose elements are the rings. A radiation pattern is thus produced that has pronounced directivity in elevation while it is nearly uniform in azimuth. This is often used in microwave beacons.

The most common form of the ring antenna is the triple dipole shown in Figure 35. The elements are three half-wave dipoles spaced 120 degrees apart.

PARASITIC REFLECTORS AND DIRECTORS

Parasitic Antennas

A parasitic antenna or "dummy" is an antenna which is not connected to the antenna input terminals; if placed in the vicinity of a *driven* antenna a current is induced in the former which modifies the radiation field. Parasitic antennas provide a simple means of producing a moderate increase of directivity. Depending on the relative phase of the currents in the two antennas, the maximum of the radiation pattern either is found in the direction of the parasite and the latter is then called a *director;* or it is found in the direction of the primary element and the parasite is then called a reflector. In order to obtain good directive action the two dipoles must be close together, that is, a fraction of a wavelength.

Half-Wave Dipole and Parasite

The geometrical arrangement corresponding to the following discussion is illustrated in Figure 36. The radiation field at any point in the equatorial plane ($\theta = 90°$) is equal to

$$E_\phi = \frac{60I_0}{d}e^{j0} + \frac{60I_1}{d}e^{j[\beta - (2\pi/\lambda)s\cos\phi]}, \quad (38)$$

where I_0 is the center-fed input current to the antenna, I_1 is the center value of the current in the parasite, and β is the angle by which I_1 leads I_0. The relation between I_1 and I_0 is given by

$$I_1 = I_0\frac{|Z_{01}|}{|Z_{11}|}e^{j\beta}, \quad (39)$$

where Z_{01} is the vector mutual impedance of antenna and parasite, and Z_{11}, the vector self-impedance of the parasitic antenna, is equal to $R_{11} + jX_{11} = |Z_{11}|e^{j\delta}$. δ is the phase angle of the parasite self-impedance.

The field pattern in the equatorial plane is dependent directly on the spacing and indirectly also, since the spacing controls the mutual impedance and thus the voltage induced in the parasite. The current in the parasite is further dependent on its self-impedance, which can be changed by altering the length of the parasite. Cut to a length of just $\lambda/2$, the self-impedance is inductive, $Z_{11} = 73.1 + j42.5$ ohms; if longer, the inductive reactance is increased; if shorter, it becomes at first less inductive, then resonant with $X_{11} = 0$, and finally, capacitatively reactive. Field patterns for $s/\lambda = 0.1$ and $s/\lambda = 0.25$, and for $\delta = +22.5°$, $0°$, and $-22.5°$, are plotted in Figure 37. These illustrate that, by controlling the spacing and length of parasite, it is possible to direct the pattern maximum into either the R or D direction, so that the parasite acts primarily either as a reflector ($E_R > E_D$) or as a director ($E_D > E_R$).

1. *Parasite as a reflector.* For good reflector performance, the spacing s/λ should lie between 0.15
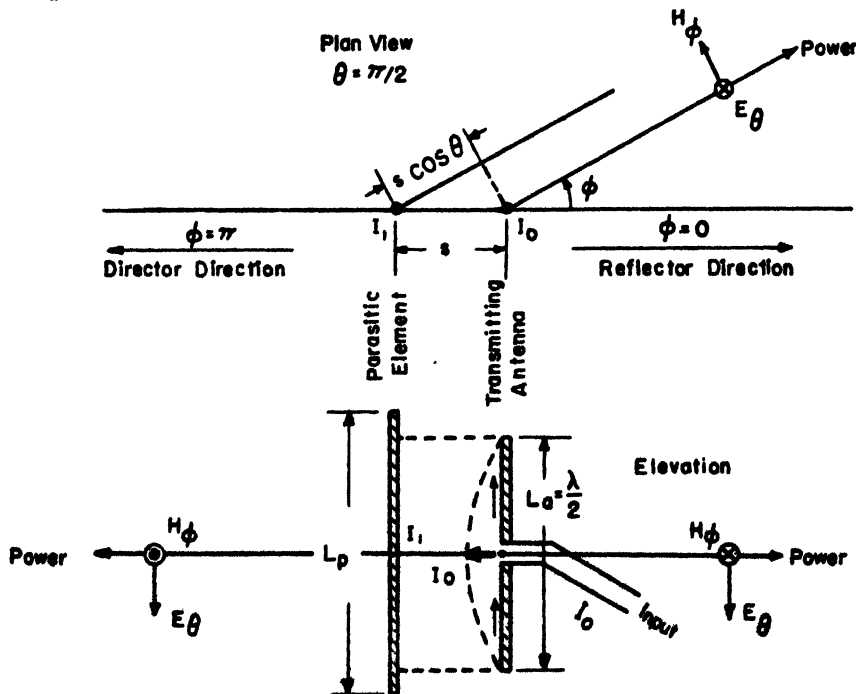
FIGURE 36. Half-wave dipole and parasite.

and 0.25 with the parasitic element made slightly longer (perhaps 5 per cent) than λ/2 in order to increase its inductive reactance. A few of the equatorial field patterns are shown in the lower row of Figure 37. To obtain the strongest field in the
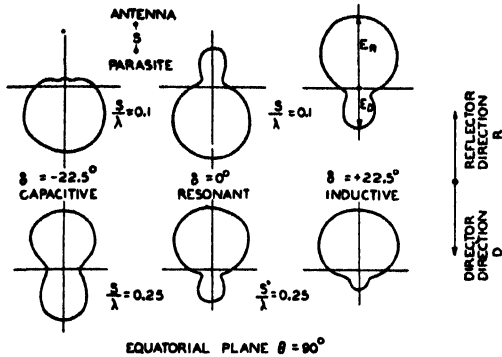
FIGURE 37. Relative field of half-wave antenna and parasite. (Courtesy of I. R. E.)

R direction, it is necessary to lengthen the parasite to a particular length (obtained by trial). If this is done, Figure 38 indicates that the field E_R is a maximum for s/λ = 0.15 and that the ratio of E_R to E for the antenna alone is 1.83; for s/λ = 0.25 it is 1.65. This does not, however, give the best *front-to-back* ratio.

2. *Parasite as a director*. Good director performance is obtained when s/λ = 0.1 and the parasitic element is cut slightly shorter (perhaps 4 per cent) than λ/2 to produce a capacitative reactance. See Figure 37, upper row, for the field patterns and Figure 38 for the best ratio of E_D to E for the antenna alone. The latter, again, does not give the best front-to-back ratio.

Multiple Parasites.
Yagi Antennas

By using several parasites, rather pronounced
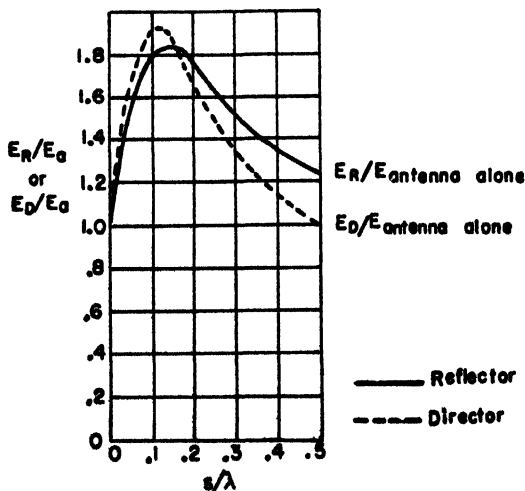
FIGURE 38. Adjustment of parasite for strongest fields E_R and E_D. (Courtesy of I. R. E.)
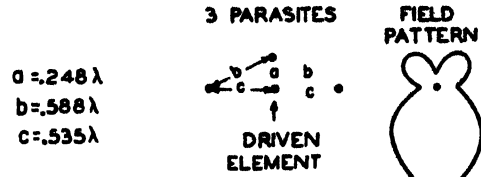
FIGURE 39. Antenna with three parasite elements. (From Radio Engineers' Handbook by Terman.)

directive effects can be achieved. Figure 39 shows a typical example. This antenna uses three parasitic dipoles arranged in a triangle or parabolic curtain. In order to obtain the most favorable pattern in such cases, careful tuning of the parasites is required.

The most commonly used of the multiparasitic arrays of half-wave dipoles is the Yagi antenna (Figure 40). It has one reflector and several (usually 2 to 5) directors. Since the voltage at the center of a dipole is always zero, it is possible to weld all the
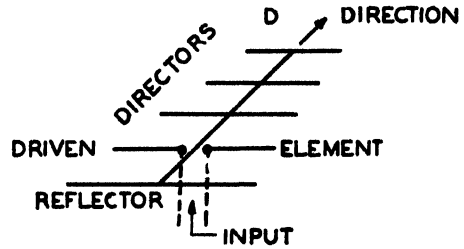
FIGURE 40. Yagi antenna with three directors.

parasites to a central sustaining rod, as shown. By increasing the number of directors, it is possible to obtain highly directive patterns.

The spacings between the elements of a Yagi array are not uniform. They are determined so that the phase difference of the currents in adjacent elements is equal to their distance expressed in wavelengths. If this condition is fulfilled, the elements are in phase with respect to radiation in the D direction. In practice, the spacing is determined experimentally rather than by calculations, which become very cumbersome when several directors are employed.

Reflecting Screens

A plane-conducting screen placed behind a radiating dipole has a similar effect in the forward direction as an image dipole whose distance s from the primary dipole is twice that of the screen and which has a phase shift of 180° from the primary dipole. Radiation in the backward direction is confined to the weak fields leaking around the edges of the screen. The pattern in the forward direction is given by the array formula of equation (22), and end-fire array with ψ = 180° and s = λ/2. Good results are achieved when the distance from the screen to the dipole is small (less than λ/4) but larger spacings are also used. The change in input impedance of the

primary element caused by the presence of the screen is appreciable.

Reflecting screens are used primarily in connection with broadside arrays (curtains) to eliminate one of the two main lobes in opposite directions. An adequate screening effect is produced by a set of wires parallel to the direction of the radiating dipole with spacings somewhat less than a tenth of a wavelength.

Corner-Reflector Antenna

A simple directional device that gives an appreciable power gain (of the order of 10 to 20) is a corner reflector, which is essentially a combination of two reflecting sheets and a dipole. In the case shown in Figure 41 where the angle subtended by

FIGURE 41. Corner reflector antenna.

the corner is 90°, the corner is equivalent to the combined radiation of three image antennas. The reflector can also be made of wires parallel to the direction of the radiating dipole. The reflecting wires do not, however, act as parasitic antennas but are taken so long that they are practically equivalent to conductors of infinite length.

These should not be confused with corner reflectors which are extensively used as targets and consist then of three mutually perpendicular conducting planes (see page 472.)

PARABOLIC ELEMENTS

Parabolic Reflectors

These reflectors are the devices most commonly used to produce highly directive radiation patterns in the microwave region. The three main types are shown in Figure 42; they are the parabolic cylinder, the paraboloid of revolution, and the truncated paraboloid, the latter being a rectangular section cut from a paraboloid of revolution. If the parabolic cylinder is relatively short and provided with flat metallic covers at the top and bottom, its shape and
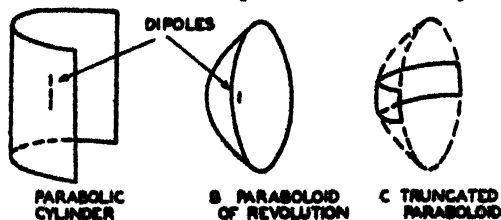
FIGURE 42. Types of parabolic reflectors.

its electrical properties resemble those of a sectoral horn (see page 363).

The directive action of the parabolic reflector depends on two geometrical properties of the parabola (Figure 43). A ray coming from the focus is reflected into a direction parallel to the axis of the parabola, and the distance from any point P on the parabola to the line called the directrix is equal to the distance from P to the focus. Consequently, the effect of the parabola in the forward direction is equivalent to that of a distribution of sources in the directrix that all oscillate in phase (but usually have varying intensities over the directrix).
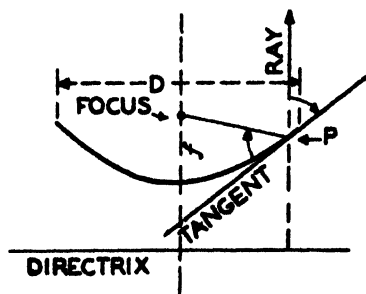
FIGURE 43. Properties of a parabola.

The parabolic cylinder produces a directive pattern only in a plane perpendicular to the generating line of the cylinder (horizontal plane in A of Figure 42). In order to concentrate the beam in a plane parallel to the generating line of the cylinder (vertical plane in Figure 42), an additional directive device must be employed. Usually this is a colinear array of dipoles, as shown; the direction of polarization is parallel to the focal axis. In microwave work this type of antenna offers advantages over the two-dimensional curtain of dipoles employed in VHF directional antennas.

For the paraboloid of revolution or the truncated paraboloid, a simple source of radiation at the focus is used. Often this is a half-wave dipole, sometimes combined with a parasitic dipole which acts as a reflector (page 360).

In other types, the energy is brought to the focal point by a wave guide and is then reflected back onto the parabolic surface.

If the wavelength is small compared with the dimensions of the parabolic reflector, the following approximate formula holds for the radiation pattern produced by a parabola:

$$E = \text{constant} \frac{\sin\left[\dfrac{\pi D}{2} \sin \dfrac{\theta}{\lambda}\right]}{\pi D \sin \theta / \lambda} (1 + \cos \theta), \quad (40)$$

where D is the aperture of the reflector and θ the angle from the axis. The half-power points correspond approximately to

$$\sin \theta \cong \theta \cong \frac{0.52\lambda}{D}. \quad (41)$$

These formulas correspond to the case of nearly uniform illumination of the reflector from the source at the focus. In practice a source that concentrates the field toward the center of the parabola is used in order to reduce the magnitude of the side lobes. The half-power angle is then more nearly equal to $\theta = 0.6\lambda/D$.

The maximum gain of a parabolic reflector is

$$G = \left(\frac{\pi D}{\lambda}\right)^2 \frac{1}{4}. \qquad (42)$$

For $D = 2$ meters and $\lambda = 0.1$ meter, the gain is approximately 1,000.

HORNS

Types of Horns

Many of the antennas previously described are used in the high-frequency [HF] and very high-frequency [VHF] bands of frequencies. Horns cannot readily be used at these frequencies because the sizes required would be excessive.

But at the microwave frequencies, the size of the horn is small and it is easy to feed energy to it through a wave guide. In this arrangement the horn acts as transition between the impedance of the wave guide and the 377 ohms impedance of free space and thus reduces to a minimum the reflection of energy backward into the guide (such as would occur if the wave guide ended in an open pipe).

Common types of horns are sectoral (discussed in next section), pyramidal, conical, biconical, etc. Only the first type is discussed in this section.

Sectoral Horn with $TE_{1,0}$ Wave

For this case the horn is flared only in width and is an extension of the wave guide of width b and depth a. For the $TE_{1,0}$ wave the electric field is parallel to the dimension a and varies in strength cosinusoidally across the wave guide and horn opening, as shown in Figure 44. The length of the horn is R and the flare angle is ϕ.
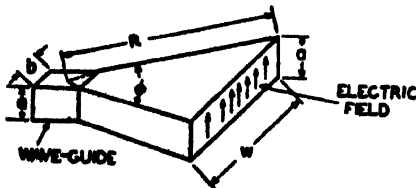
FIGURE 44. Sectoral horn.

Figure 45 illustrates the pattern shapes in the plane parallel to dimension b for various flare angles.

For this type of wave, the cutoff frequency of the wave guide is

$$f_c = \frac{3 \times 10^8}{2b}, \qquad (43)$$

with b in meters. The operating frequency should be near but not greater than twice this value.

The gain depends upon the length R and the flare angle ϕ, and is plotted in Figure 46.
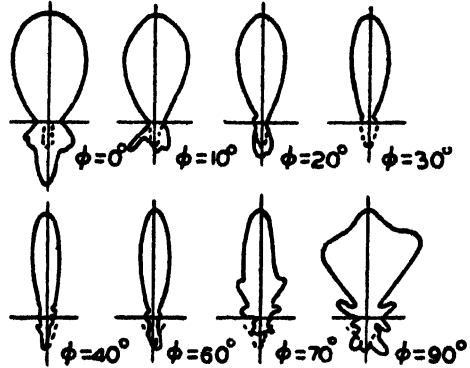
FIGURE 45. Radiation pattern for a sectoral horn having various flare angles.
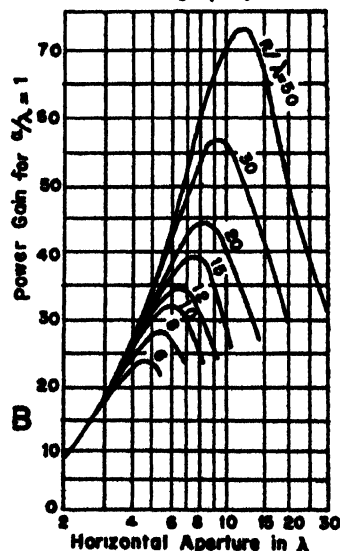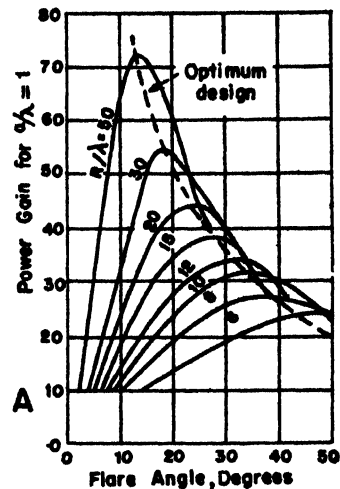
FIGURE 46. Gain of sectoral horn with $TE_{1,0}$ wave. (These curves are for a vertical aperture ratio $a/\lambda = 1$. For other ratios the gain given should be multiplied by a/λ.) (From Radio Engineers' Handbook by Terman.)

Chapter 4

FACTORS INFLUENCING TRANSMISSION

REFRACTION

Survey

REFRACTION is caused by the variation of the dielectric constant (square of refractive index) of the atmosphere. Although the atmosphere is tenuous and the variations of refractive index are small, the effect of refraction upon the field-strength distribution of waves is considerable. As will be shown, refraction under average conditions may be taken into account by using an earth with a modified radius. A representative average value of modified earth radius commonly used is ka with $k = 4/3$. Under certain conditions, especially in warmer climates, a slightly higher value of k might be preferable.

The case where a is replaced by $4a/3$ is referred to as *standard refraction*. It corresponds to a linear variation of refractive index with height in the atmosphere. In recent years, more complicated variations of refractive index in the atmosphere have received considerable attention and have proved to be of great operational interest. This volume, however, is restricted to consideration of standard atmosphere propagation.

Snell's Law

Let n_0 and n_1 denote the refractive indices of two media separated by a plane boundary. The ordinary law of refraction known as Snell's law is then usually stated (see Figure 1), as

$$n_0 \sin \beta_0 = n_1 \sin \beta_1,$$

where β_0 and β_1 are the angles which the ray makes with the perpendicular to the boundary. It is convenient to use the complementary angle α, so that
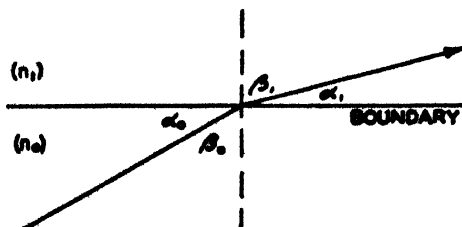
$$n_0 \cos \alpha_0 = n_1 \cos \alpha_1.$$

FIGURE 1. Refraction at boundary between two media.

For several plane-parallel boundaries, Snell's law generalizes to

$$n_0 \cos \alpha_0 = n_1 \cos \alpha_1 = n_2 \cos \alpha_2 = \cdots.$$

In the atmosphere, the refractive index is a continuous function of the height. Again, it is usually legitimate to consider the atmosphere as horizontally stratified, so that the refractive index is a function of height only. The case of a continuously variable refractive index is readily obtained by passing to the limit of an infinity of parallel boundaries infinitely close together, Snell's law remaining the same; thus

$$n(h) \cdot \cos \alpha = n_0 \cos \alpha_0,$$

where now n and α are continuous functions of the height. In place of a discontinuous change in direction, there will now occur a bending of the rays (Figure 2).
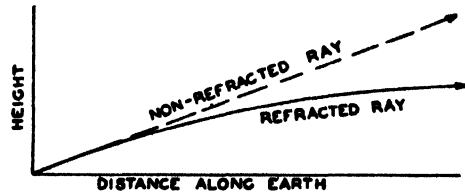
FIGURE 2. Refraction in the atmosphere with variable $n(h)$.

If the boundaries are not plane but spherical, Snell's law must be modified. Analysis shows that over a spherical earth surrounded by an atmosphere in which the refractive index n is a function of the distance r from the earth's center, the law of refraction becomes

$$n(r) \cdot r \cos \alpha = n_0 r_0 \cos \alpha_0, \qquad (1)$$

where α is the angle between a ray and the horizontal (see Figure 3).

Refraction is of practical importance *only* when the angle between the rays and the horizontal is small. In the determination of gain as given in later chapters, the effect of refraction becomes completely negligible when α is more than a few degrees.

For small angles, $\cos \alpha$ may be replaced by $1 - \alpha^2/2$. In this case equation (1) is well approximated by

$$\frac{1}{2}(\alpha^2 - \alpha_0^2) = n - n_0 + \frac{h}{a}, \qquad (2)$$

where h is the height above the ground, so that
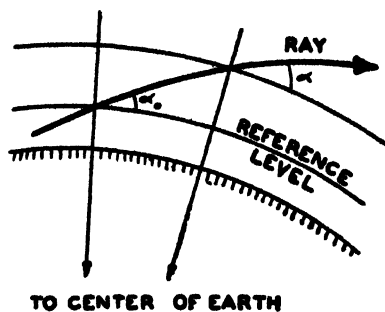
FIGURE 3. Refraction over curved earth.

$r_0 = a$ and $r = a + h$. This is the practical form of Snell's law for the atmosphere above a curved earth. The reference level (see Figure 3) is here taken at the surface of the earth where n_0 is the index of refraction.

Modified Refractive Index

In place of the sum $(n - n_0 + h/a)$ appearing in equation (2), it is customary to define and use a quantity M given by

$$M = \left[(n - 1) + \frac{h}{a}\right] 10^6. \tag{3}$$

M is called the modified refractive index. It gives a unit that is convenient for practical use. The modified index is then said to be expressed in M units, values of which commonly lie in the range of 300 to 500. Using this definition, equation (2) becomes

$$\frac{1}{2}(\alpha^2 - \alpha_0^2) = (M - M_0) \cdot 10^{-6}. \tag{4}$$

An important special case is that in which the refractive index decreases linearly with height, $n - n_0 = \text{constant} \times h$. Then equation (2) may be written in the form

$$\frac{1}{2}(\alpha^2 - \alpha_0^2) = \frac{h}{ka}, \tag{5}$$

where k is the factor mentioned in text on p. 364 which determines the modified earth's radius ka. Comparing the above expression with equation (2), and differentiating, it follows that

$$\frac{1}{ka} = \frac{dn}{dh} + \frac{1}{a}$$

or

$$k = \frac{1}{1 + a\dfrac{dn}{dh}} = \frac{1}{a} \cdot \frac{dh}{dM} \cdot 10^{+6}. \tag{6}$$

Proof of the fact that refraction is negligible unless the angle is very small may readily be deduced from the preceding formulas. Thus, on differentiating

equation (4)

$$d\alpha = dM \cdot \frac{10^{-6}}{\alpha},$$

and in the standard linear case, by equation (5),

$$d\alpha = dh/ka\alpha \sim 1.2 \cdot 10^{-7} dh/\alpha$$

for $k = 4/3$. Taking $\alpha = 0.05$ radians (3°) and $dh = 100$ meters, one finds $d\alpha = 0.00024$ radians (50 seconds of arc), a very small change in angle. This is the standard deflection which is accounted for by replacing a by ka. The deviations from this value experienced with nonstandard refraction are even smaller. The larger the angle α with the horizontal at which a ray issues from the transmitter, the less the angular deviation. In communication work and for certain radar problems, however, angles of less than one degree are of importance, and $d\alpha$ may then become comparable to α.

Graphical Representation

Figures 4 to 6 show three different ways of representing rays subject to refraction. Figure 4 gives a *true* picture apart from the exaggeration of heights. In the case of standard refraction, the curvature of the rays is always concave downwards, the center of curvature being below the surface of the earth. The middle ray shown is the horizon ray and to the lower right is the diffraction region into which rays do not penetrate. Figure 5 shows a diagram with modified earth's radius, ka, in which the rays are straight lines. Figure 6, finally, is a *plane earth* diagram; the rays are here curved upwards.

These diagrams may be considered as resulting
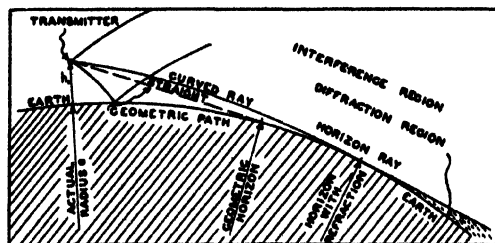
FIGURE 4. Ray curvature over earth with radius a.
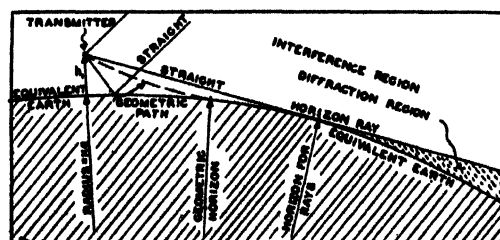
FIGURE 5. Rays in a homogeneous atmosphere (equivalent radius ka).

from each other by changing the earth's curvature by an arbitrary factor. From this viewpoint Figure 6
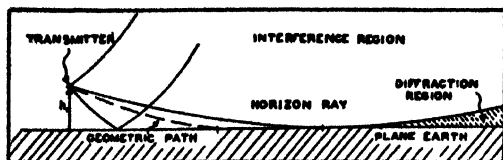
FIGURE 6. Rays in a plane earth diagram. (Radius of curvature of rays is $- ka$.)
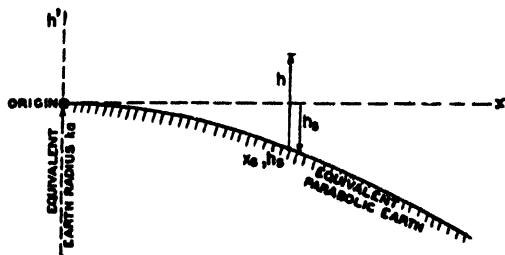
FIGURE 7. Equivalent parabolic earth diagram.

represents the limiting case of an infinite earth's radius. The plane earth diagram is widely used for problems of nonstandard propagation.

In drawing diagrams for a curved earth of equivalent radius ka, it is customary to replace the spherical earth outline by an equivalent parabola (see Figure 7). The equation for the surface reduces from the circular form,

$$x_s{}^2 + (h_s + ka)^2 = (ka)^2,$$

to the parabolic form,

$$h_s = - \frac{1}{2ka} x_s{}^2,$$

for $h_s << x_s$. The height h measured from the surface of the earth, instead of from the x axis, is given by

$$h = h' - h_s = h' + \frac{1}{2ka} x^2,$$

in which h is laid off perpendicular to the x axis and not to the earth's surface. For clarity in drawing rays or field-strength diagrams, the vertical scale is expanded by an arbitrary factor p, whence

$$h = p\left(h' + \frac{1}{2ka} x^2\right). \qquad (7)$$

This distortion of vertical distances, it can be shown, does not distort angles. The parabolic representation to be reasonably accurate must be restricted to heights in the atmosphere small compared with the extent of the horizontal scale.

Curvature Relationships

The curvature of a ray is defined as the reciprocal of the radius of curvature ρ. Let ψ be the angle between the ray and a nearly horizontal x axis. By Figure 8, $\rho = - ds/d\psi$, and since ψ is a small
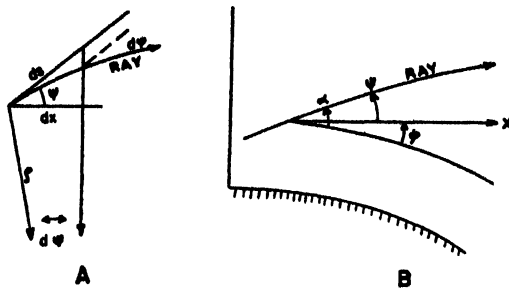
FIGURE 8. Angular relationships of rays.

angle we may, to a sufficient approximation, put $ds = dx$, so that

$$\frac{1}{\rho} = - \frac{d\psi}{dx}.$$

Here the curvature has been defined so that it is positive when the ray curves in the same direction as the earth, with this system the curvature of the earth itself is positive. Referring to Figure 8B,

$$\frac{1}{\rho} = - \frac{d\psi}{dx} = - \frac{d\alpha}{dx} + \frac{d\phi}{dx}. \qquad (8)$$

But $d\phi/dx = 1/a$, and since α is a small angle

$$\frac{d\alpha}{dx} = \frac{d\alpha}{dh} \cdot \frac{dh}{dx} = \alpha \frac{d\alpha}{dh} = \frac{1}{2} \frac{d(\alpha^2)}{dh}.$$

Consequently, by equation (2)

$$\frac{1}{\rho} = - \frac{1}{2} \frac{d(\alpha^2)}{dh} + \frac{1}{a} = - \frac{dn}{dh}. \qquad (9)$$

From this, the curvature of the ray is equal to the vertical rate of decrease of the refractive index. Notice that dn/dh is usually negative, so that the true curvature of a ray is usually concave downwards.

A simple relationship exists between $m = \rho/a$, the ratio of the radius of curvature of a ray to the radius of the earth, and k. Combining equations (6) and (9) gives

$$\frac{1}{k} + \frac{1}{m} = 1. \qquad (10)$$

Consider again the special case where $dn/dh =$ constant, so that n is a linear function of the height (standard refraction). Consider the plane earth diagram of Figure 6. The angles between corresponding curves are the same as in the true diagram, Figure 4. Hence, for the plane earth diagram, equation (8) becomes $1/\rho' = - d\alpha/dx$, where ρ' is the radius of curvature of the ray in the plane earth representation. It is readily found that

$$\frac{1}{\rho'} = \frac{1}{\rho} - \frac{1}{a} = - \frac{1}{2} \frac{d(\alpha^2)}{dh} = - \left(\frac{dn}{dh} + \frac{1}{a}\right) \qquad (11)$$

$$= - \frac{dM}{dh} \cdot 10^{-6} = - \frac{1}{ka}.$$

Since M usually increases with height, the curvature of rays is concave upwards in this diagram. Again, equation (11) shows that when the modified earth's

radius ka is introduced (Figure 5), this amount of upward curvature is just canceled and the rays appear as straight lines.

Alternate Method

Instead of taking account of refraction by changing the earth's curvature, another method is sometimes more convenient. It may be shown that the ratio of the field E to the free-space field E_0 transforms in the same way, whether (1) radius a is replaced by ka, or (2) the horizontal distance x is replaced by $xk^{-2/3}$ and at the same time all elevations h are replaced by $hk^{-1/3}$. An angle α must then be replaced by $\alpha k^{-1/3}$. Method (2) is usually less convenient than method (1) because it involves a change of horizontal distance which makes it necessary to transform the ratio E/E_0 rather than the field itself. In method (1) where only curvatures are changed, this difficulty does not appear as the distance x and hence E_0 remains unaltered.

Method (2) may be used to advantage to account for deviations of k from the standard value of $k = 4/3$. Coverage diagrams are usually drawn for this value; the deviations owing to a change in k may then be estimated by multiplying distances, heights, or angles with the appropriate powers of $k/(4/3)$.

Computation of Refractive Index

The following equation gives the dependence of the refractive index on temperature, pressure, and humidity:

$$(n - 1) \cdot 10^6 = \frac{79}{T}\left(p + \frac{4,800e}{T}\right) \quad (12)$$

where T is the absolute temperature, p is the total pressure, and e the water-vapor pressure, both the latter in millibars.

Introducing M from equation (3), the modified refractive index, for use on a plane earth diagram, is equal to

$$M = \frac{79}{T}\left(p + \frac{4,800e}{T}\right) + 0.157h, \quad (13)$$

where the height h is in meters. If h is in feet, the last term is 0.048h.

Tables have been prepared by means of which M can be computed rapidly from meteorological data, namely temperature, humidity, and pressure given as a function of height. For this purpose M is the sum of three terms which are computed independently:

$$M = M_d + M_w + M_e. \quad (14)$$

The *dry* term M_d is obtained from Table 1 as a function of temperature and height in meters above the ground. (If the pressure at the ground p_0 is substantially different from 1,000 millibars all values of M_d should be multiplied by $p_0/1,000$. In general this correction may safely be neglected unless the difference between p_0 and 1,000 is quite large, corresponding to an elevation of the ground level of several thousand feet above sea level.)

The *wet* term M_w is obtained from Table 2 as a function of temperature and relative humidity.

TABLE 1

M_d

h(m)	t(°C) −20	−18	−16	−14	−12	−10	−8	−6	−4	−2	±0	h(ft)
0	312.3	309.8	307.4	305.0	302.7	300.4	298.1	295.9	293.7	291.5	289.4	0.0
10	311.9	309.4	307.0	304.6	302.3	300.0	297.7	295.5	293.3	291.1	289.0	32.8
20	311.5	309.0	306.6	304.2	301.9	299.6	297.3	295.1	292.9	290.8	288.7	65.6
30	311.0	308.6	306.2	303.8	301.5	299.2	297.0	294.8	292.6	290.4	288.3	98.4
40	310.6	308.2	305.8	303.4	301.1	298.8	296.6	294.4	292.2	290.1	288.0	131.2
50	310.2	307.8	305.4	303.0	300.7	298.4	296.2	294.0	291.8	289.7	287.6	164.0
75	309.2	306.8	304.4	302.1	299.8	297.5	295.2	293.0	290.8	288.7	286.6	246.1
100	308.1	305.7	303.4	301.1	298.8	296.5	294.3	292.2	290.0	287.9	285.8	328.1
150	306.0	303.6	301.3	299.0	296.8	294.6	292.4	290.3	288.2	286.1	284.0	492.1
200	303.9	301.6	299.3	297.1	294.9	292.7	290.5	288.4	286.3	284.2	282.2	656.2
250	301.9	299.6	297.3	295.1	293.0	290.8	288.7	286.6	284.5	282.5	280.5	820.2
300	299.9	297.7	295.4	293.2	291.1	288.9	286.8	284.7	282.7	280.7	278.7	984.3
350	297.8	295.6	293.4	291.2	289.1	287.0	285.0	282.9	280.9	279.0	277.0	1,148.0
400	295.8	293.6	291.5	289.4	287.3	285.2	283.2	281.1	279.1	277.2	275.3	1,312.0
450	293.8	291.7	289.6	287.5	285.4	283.3	281.3	279.3	277.3	275.4	273.5	1,476.0
500	291.9	289.8	287.7	285.6	283.5	281.5	279.5	277.6	275.6	273.7	271.8	1,640.0
600	288.0	285.9	283.8	281.8	279.9	277.9	276.0	274.1	272.2	270.3	268.5	1,969.0
700	284.1	282.1	280.1	278.1	276.2	274.3	272.4	270.5	268.7	266.9	265.1	2,297.0
800	280.3	278.3	276.4	274.5	272.6	270.7	268.9	267.1	265.3	263.6	261.8	2,625.0
900	276.5	274.6	272.7	270.9	269.0	267.2	265.4	263.7	262.0	260.3	258.6	2,953.0
1,000	272.8	271.0	269.1	267.3	265.6	263.8	262.1	260.4	258.7	257.0	255.3	3,281.0
1,500	255.0	253.4	251.8	250.2	248.7	247.2	245.7	244.2	242.8	241.3	239.9	4,921.0
2,000	238.3	237.0	235.7	234.3	233.0	231.7	230.4	229.1	227.8	226.5	225.3	6,562.0
	−4.00	−0.40	+3.20	6.80	10.4	14.00	17.6	21.2	24.8	28.4	32.0	h(ft)

t(°F)

TABLE 1 (Continued)

M_d

h(m)	t(°C) ±0	2	4	6	8	10	12	14	16	18	20	h(ft)
0	289.4	287.3	285.2	283.2	281.1	279.2	277.2	275.3	273.4	271.5	269.6	0.0
10	289.0	286.9	284.8	282.8	280.8	278.9	276.9	274.9	273.1	271.2	269.3	32.8
20	288.7	286.6	284.5	282.5	280.5	278.5	276.6	274.6	272.8	270.9	269.0	65.6
30	288.3	286.2	284.1	282.1	280.1	278.2	276.2	274.3	272.4	270.5	268.7	98.4
40	288.0	285.9	283.8	281.8	279.8	277.8	275.9	274.0	272.1	270.2	268.4	131.2
50	287.6	285.5	283.4	281.4	279.5	277.5	275.6	273.7	271.8	269.9	268.1	164.0
75	286.6	284.7	282.6	280.6	278.7	276.7	274.8	272.8	271.0	269.1	267.3	248.1
100	285.8	283.8	281.7	279.7	277.8	275.8	273.9	272.0	270.2	268.3	266.5	328.1
150	284.0	282.0	280.0	278.0	276.1	274.2	272.3	270.4	268.6	266.8	265.0	492.1
200	282.2	280.2	278.3	276.3	274.4	272.5	270.7	268.8	267.0	265.2	263.4	656.2
250	280.5	278.5	276.6	274.7	272.8	270.9	269.1	267.2	265.4	263.7	261.9	820.2
300	278.7	276.8	274.9	273.0	271.1	269.2	267.4	265.6	263.8	262.1	260.3	984.3
350	277.0	275.1	273.2	271.3	269.4	267.6	265.8	264.0	262.2	260.5	258.8	1,148.0
400	275.3	273.4	271.5	269.6	267.8	266.0	264.2	262.5	260.7	259.0	257.3	1,312.0
450	273.5	271.7	269.8	268.0	266.2	264.4	262.6	260.9	259.2	257.5	255.8	1,476.0
500	271.8	270.0	268.1	266.3	264.6	262.8	261.1	259.4	257.7	256.0	254.4	1,640.0
600	268.5	266.7	264.9	263.1	261.4	259.6	258.0	256.3	254.7	253.0	251.4	1,969.0
700	265.1	263.4	261.7	259.9	258.2	256.5	254.9	253.2	251.6	250.1	248.5	2,297.0
800	261.8	260.1	258.4	256.7	255.0	253.4	251.8	250.3	248.7	247.2	245.6	2,625.0
900	258.6	256.9	255.2	253.6	252.0	250.4	248.8	247.3	245.8	244.3	242.8	2,953.0
1,000	255.3	253.7	252.1	250.5	249.0	247.4	245.9	244.4	242.9	241.4	239.9	3,281.0
1,500	239.9	238.5	237.0	235.6	234.3	232.9	231.6	230.3	228.9	227.6	226.3	4,921.0
2,000	225.3	224.1	222.9	221.7	220.5	219.3	218.1	217.0	215.8	214.7	213.5	6,562.0
	32.0	35.6	39.2	42.8	46.4	50.0	53.6	57.2	60.8	64.4	68.0	t(°F)

h(ft)

TABLE 1 (Continued)

M_d

h(m)	t(°C) 20	22	24	26	28	30	32	34	36	38	40	h(ft)
0	269.6	267.8	266.0	264.2	262.5	260.7	259.0	257.5	255.7	254.0	252.4	0.0
10	269.3	267.5	265.7	263.9	262.2	260.4	258.7	257.2	255.4	253.7	252.1	32.8
20	269.0	267.2	265.4	263.6	261.9	260.1	258.4	256.9	255.1	253.4	251.8	65.6
30	268.7	266.9	265.1	263.3	261.6	259.9	258.2	256.5	254.9	253.2	251.6	98.4
40	268.4	266.6	264.8	263.0	261.3	259.6	257.9	256.2	254.6	252.9	251.3	131.2
50	268.1	266.3	264.5	262.7	261.0	259.3	257.6	255.9	254.3	252.6	251.0	164.0
75	267.3	265.5	263.8	262.0	260.3	258.6	256.9	254.2	253.6	251.9	250.3	248.1
100	266.5	264.7	263.0	261.2	259.5	257.8	256.2	254.5	252.9	251.3	249.7	328.1
150	265.0	263.2	261.5	259.7	258.0	256.3	254.7	253.1	251.5	249.0	248.3	492.1
200	263.4	261.7	260.0	258.3	256.6	254.9	253.3	251.7	250.1	248.5	246.9	656.2
250	261.9	260.2	258.5	256.8	255.1	253.5	251.9	250.3	248.7	247.2	245.6	820.2
300	260.3	258.6	256.9	255.3	253.6	252.0	250.4	248.9	247.3	245.8	244.3	984.3
350	258.8	257.2	255.5	253.9	252.2	250.6	249.0	247.5	245.9	244.4	242.9	1,148.0
400	257.3	255.7	254.0	252.4	250.8	249.2	247.7	246.2	244.6	243.1	241.6	1,312.0
450	255.8	254.2	252.6	251.0	249.4	247.8	246.3	244.8	243.3	241.8	240.3	1,476.0
500	254.4	252.8	251.1	249.5	248.0	246.4	244.9	243.4	241.9	240.4	239.0	1,640.0
600	251.4	249.8	248.3	246.7	245.2	243.7	242.2	240.7	239.2	237.8	236.4	1,969.0
700	248.5	247.0	245.5	243.9	242.4	240.9	239.5	238.0	236.6	235.2	233.8	2,297.0
800	245.6	244.1	242.6	241.2	239.7	238.3	236.9	235.4	234.0	232.7	231.3	2,625.0
900	242.8	241.3	239.8	238.4	237.0	235.6	234.2	232.8	231.4	230.1	228.8	2,953.0
1,000	239.9	238.5	237.1	235.7	234.3	232.9	231.6	230.3	228.9	227.6	226.3	3,281.0
1,500	226.3	225.1	223.8	222.6	221.4	220.2	219.0	217.8	216.6	215.5	214.3	4,921.0
2,000	213.5	212.4	211.3	210.3	209.2	208.1	207.1	206.0	205.0	203.9	202.9	6,562.0
	86.0	89.6	93.2	96.8	100.4	104.0	89.6	93.2	96.8	100.4	104.0	t(°F)

h(ft)

Finally, $M_e = 0.157h$, if h is in meters, or $M_e = 0.048h$, if h is in feet, may readily be computed by means of a slide rule. M is then obtained by addition.

Atmospheric Stratification

Ordinary weather data give comparatively little information about the atmospheric stratification near ground level. Radiosonde data are too widely spaced (vertical distances of the order of 100 meters between successive readings) for reliable determination of the variation of M with height at low levels. Special instruments have therefore been developed in recent years for low-level soundings. Such instru-

TABLE 2

M_w

$t(°C)$	10	20	30	40	50	60	70	80	90	100	$t(°F)$
−20	0.6	1.2	1.8	2.5	3.1	3.7	4.3	4.9	5.5	6.130	− 4.0
−18	0.7	1.5	2.2	2.9	3.7	4.4	5.1	5.8	6.6	7.309	− 0.4
−16	0.9	1.7	2.6	3.5	4.3	5.2	6.1	6.9	7.8	8.678	+ 3.2
−14	1.0	2.1	3.1	4.1	5.1	6.2	7.2	8.2	9.3	10.287	+ 6.8
−12	1.2	2.4	3.6	4.8	6.1	7.3	8.5	9.7	10.9	12.124	+10.4
−10	1.4	2.9	4.3	5.7	7.1	8.6	10.0	11.4	12.9	14.284	+14.0
−8	1.7	3.4	5.0	6.7	8.4	10.1	11.7	13.4	15.1	16.754	+17.6
−6	2.0	3.9	5.9	7.8	9.8	11.7	13.7	15.7	17.6	19.568	21.2
−4	2.3	4.6	6.9	9.1	11.4	13.7	16.0	18.3	20.6	22.871	24.8
−2	2.7	5.3	8.0	10.6	13.3	16.0	18.6	21.3	23.9	26.589	28.4
→0	3.1	6.2	9.3	12.4	15.5	18.5	21.6	24.7	27.8	30.911	32.0
2	3.5	7.0	10.5	14.1	17.6	21.1	24.6	28.1	31.6	35.139	35.6
4	4.0	8.0	12.0	16.0	20.0	24.0	28.0	32.0	35.9	39.939	39.2
5	4.3	8.5	12.8	17.0	21.3	25.5	29.8	34.0	38.3	42.533	41.0
6	4.5	9.1	13.6	18.1	22.6	27.2	31.7	36.2	40.8	45.280	42.8
7	4.8	9.6	14.5	19.3	24.1	28.9	33.7	38.5	43.3	48.175	44.6
8	5.1	10.2	15.4	20.5	25.6	30.7	35.9	41.0	46.1	51.215	46.4
9	5.4	10.9	16.3	21.8	27.2	32.6	38.1	43.5	49.0	54.394	48.2
10	5.8	11.6	17.3	23.1	28.9	34.7	40.5	46.2	52.0	57.793	50.0
11	6.1	12.3	18.4	24.5	30.6	36.8	42.9	49.0	55.1	61.270	51.8
12	6.5	13.0	19.5	26.0	32.5	39.1	45.6	52.1	58.6	65.094	53.6
13	6.9	13.8	20.7	27.6	34.5	41.4	48.3	55.2	62.1	69.010	55.4
14	7.3	14.6	22.0	29.3	36.6	43.9	51.2	58.5	65.9	73.169	57.2
15	7.8	15.5	23.3	31.0	38.8	46.5	54.3	62.0	69.8	77.505	59.0
16	8.2	16.4	24.6	32.8	41.0	49.2	57.4	65.6	73.9	82.060	60.8

TABLE 2 (Continued)

M_w

$t(°C)$	10	20	30	40	50	60	70	80	90	100	$t(°F)$
16	8.2	16.4	24.6	32.8	41.0	49.2	57.4	65.6	73.9	82.060	60.8
17	8.7	17.4	26.0	34.7	43.4	52.1	60.8	69.5	78.1	86.813	62.6
18	9.2	18.4	27.6	36.7	45.9	55.1	64.3	73.5	82.7	91.866	64.4
19	9.7	19.4	29.1	38.9	48.6	58.3	68.0	77.7	87.4	97.127	66.2
20	10.3	20.5	30.8	41.1	51.4	61.6	71.9	82.2	92.4	102.71	68.0
21	10.8	21.7	32.5	43.4	54.2	65.1	75.9	86.8	97.6	108.46	69.8
22	11.5	22.9	34.4	45.8	57.3	68.7	80.2	91.6	103.1	114.56	71.6
23	12.1	24.2	36.3	48.3	60.4	72.5	84.6	96.7	108.8	120.87	73.4
24	12.8	25.5	38.3	51.0	63.8	76.5	89.3	102.0	114.8	127.53	75.2
25	13.4	26.9	40.3	53.8	67.2	80.7	94.1	107.6	121.0	134.44	77.0
26	14.2	28.3	42.5	56.7	70.9	85.0	99.2	113.4	127.6	141.74	78.8
27	14.9	29.9	44.8	59.8	74.7	89.6	104.6	119.5	134.5	149.39	80.6
28	15.7	31.5	47.2	62.9	78.7	94.4	110.1	125.9	141.6	157.34	82.4
29	16.6	33.1	49.7	66.2	82.8	99.4	115.9	132.5	149.1	165.62	84.2
30	17.4	34.9	52.3	69.7	87.1	104.6	122.0	139.4	156.8	174.27	86.0
31	18.3	36.7	55.0	73.3	91.7	110.0	128.3	146.7	165.0	183.32	87.8
32	19.3	38.5	57.8	77.1	96.4	115.6	134.9	154.2	173.5	192.74	89.6
33	20.3	40.5	60.8	81.0	101.3	121.5	141.8	162.0	182.3	202.56	91.4
34	21.3	42.6	63.9	85.1	106.4	127.7	149.0	170.3	191.6	212.86	93.2
35	22.4	44.7	67.1	89.4	111.8	134.1	156.5	178.8	201.2	223.50	95.0
36	23.5	46.9	70.4	93.9	117.3	140.8	164.2	187.7	211.2	234.63	96.8
37	24.6	49.2	73.9	98.5	123.1	147.7	172.3	197.0	221.6	246.20	98.6
38	25.8	51.6	77.5	103.3	129.1	154.9	180.8	206.6	232.4	258.23	100.4
39	27.1	54.2	81.2	108.3	135.4	162.5	189.6	216.6	243.7	270.80	102.2
40	28.4	56.8	85.2	113.6	142.0	170.4	198.8	227.2	255.5	283.94	104.0

ments contain temperature and humidity measuring elements that are relatively free of lag; they are attached to airplanes or dirigibles or they are carried aloft by means of captive balloons or kites. The above tables are for use in connection with such measurements.

Two main cases must be distinguished. First, the refractive index or M is very nearly a linear function of the height in the lower layers (at heights above about 500 to 800 meters the variation of refractive index with height will deviate from linearity only in very exceptional instances). This is the standard

case where dM/dh is independent of h, and by using equation (6), k is conveniently obtained from the slope of the $M - h$ curve. It is found that the vertical temperature gradient has a comparatively small influence on k, while fairly small variations of the humidity gradient will affect k appreciably.

The other case is that of nonstandard refraction. Here M is not a linear function of the height. The most important special case is that of superrefraction, which occurs when, in certain height intervals, M decreases with height instead of following the usual increase with elevation. Such a decrease of M in certain layers of the atmosphere is caused by a steep negative moisture gradient or steep positive temperature gradient, or even more by a combination of both influences.

With superrefraction, propagation conditions are greatly different from those encountered with standard refraction and the methods to be given later for the determination of the transmitted power do not apply. This is especially true for the field near or below the optical horizon. The discussion of nonstandard propagation is beyond the scope of this volume.

High-angle coverage is generally independent of refraction and is therefore also unaffected by the variations of M in the lowest layers of the atmosphere.

Direct Determination of k

In Figure 9 the reciprocal of k is plotted as ordinate

against the vertical gradient of relative humidity as abscissa. The values shown refer to a standard temperature gradient of -0.65 degrees Centigrade per 100 meters; unless the temperature gradient differs greatly from this value, the corresponding values of k will not be much affected. The curves given refer to 100 per cent relative humidity at ground level, and an auxiliary table is provided at the top of the graph which gives figures to be added for other values of the relative humidity. The sensitivity of k to moisture gradients in warm climates is obvious from these data.

GROUND REFLECTION

Ground Reflection and Coverage

The reinforcement of the direct ray by the ground-reflected ray is of great importance both in radar and in communication work. In favorable cases, the reflected ray may be of comparable intensity to the direct ray and thus the received intensity may be approximately doubled in places where the two rays have the same phase. This means, in many cases, the possibility of an appreciable increase in range relative to that in free space.

Complexity of Reflection Problem

In order to facilitate the discussion of the problems encountered in reflection, it is necessary to analyze the complex phenomena into simpler constituents.

(RH)	-30C	-25C	-20C	-15C	-10C	-5C	0C	+5C	+10C	+15C	+20C	+25C	+30C	+35C	+40C
10%	.009	.012	.017	.027	.039	.055	.078	.090	.118	.151	.194	.240	.301	.371	.455
20%	.008	.011	.015	.024	.034	.049	.069	.080	.105	.134	.172	.214	.267	.329	.405
30%	.007	.009	.014	.021	.030	.043	.060	.070	.092	.118	.151	.187	.234	.288	.354
40%	.006	.008	.012	.018	.026	.037	.052	.060	.079	.101	.129	.161	.200	.247	.304
50%	.005	.007	.010	.015	.021	.031	.043	.050	.066	.084	.108	.134	.167	.206	.253
60%	.004	.005	.008	.012	.017	.024	.034	.040	.052	.067	.080	.107	.134	.165	.202
70%	.003	.004	.006	.009	.013	.018	.026	.030	.039	.050	.065	.080	.100	.123	.152
80%	.002	.003	.004	.006	.009	.012	.017	.020	.026	.034	.043	.065	.067	.082	.101
90%	.001	.001	.002	.003	.004	.006	.009	.010	.013	.017	.021	.027	.033	.041	.051

FIGURE 9. Graph $1/k$ versus RH (relative humidity) gradient and temperature for 100 per cent RH at ground. Add correction tabulated to obtain $1/k$ for RH at ground less than 100 per cent.

First of all, the incident radiation field is resolved into nearly plane wave components, each forming a narrow pencil of rays striking the reflecting surface within a small area which we shall call the reflection point. There are two types of such rays depending on their state of polarization. If the electric vector is parallel to the reflecting plane, the rays are said to be horizontally polarized and if the electric vector is parallel to a vertical plane through the rays, they are said to be vertically polarized. When considering a very irregular surface, the reflected field may show extreme complexity even though the incident wave is linearly polarized. Increasing roughness may result in diffuse reflection which is ineffective in reinforcing the direct wave. The existence of diffuse reflection depends primarily on the size of the irregularities of the surface in comparison with the wavelength of the incident radiation and on the grazing angle of the incident field. This problem will be discussed in more detail later.

Plane Reflecting Surface

Consider first the simplest case, when a plane wave strikes a plane surface such as that of an absolutely calm sea. The incident ray is then split into two parts. One is the reflected ray, which is returned to the atmosphere, and the other is the refracted ray, which is absorbed by the sea. At the point of reflection, the ratio of any scalar quantity in the reflected wave to the same quantity in the incident wave is defined as the reflection coefficient of the sea for plane waves of given frequency. Thus defined, the reflection coefficient can and will be different for the various components of the field.

For simplicity, let us assume the reflecting plane to be the xy plane of a rectangular coordinate system, the xz plane to coincide with the plane of incidence, and the reflection point to be the origin of the coordinate system.
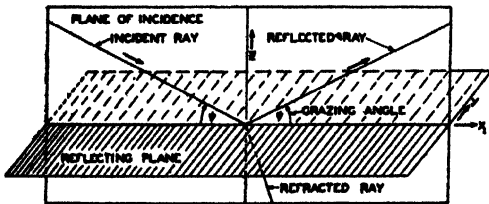
FIGURE 10. Geometry of reflection and refraction.

For horizontal polarization, the electric vector for the incident wave then is

$$E_i = E_0 e^{j2\pi f \, [t - (1/c) \, (z \cos \psi - x \sin \psi)]} \qquad (15)$$

where ψ is the grazing angle, f the frequency of the radiation and c the velocity of light in free space. The electric vector of the corresponding reflected

field is given by the similar expression

$$E_r = E_0 \rho e^{-j\phi - j2\pi f \, [t - (1/c) \, (z \cos \psi + x \sin \psi)]} \qquad (16)$$

where ρ and ϕ are real constants. The ratio of the reflected to the incident field at the reflection point ($z = x = 0$) is seen to be

$$R = \rho e^{-j\phi}. \qquad (17)$$

By definition this is the reflection coefficient for horizontally polarized waves. Thus the reflection coefficient is a complex quantity, the amplitude of which is the reflection coefficient of the wave amplitude and the phase is the lag in phase of the reflected wave with respect to the incident wave at the point of reflection.

The reflection coefficient for vertically polarized radiation is defined in the same way. It is found, however, that the expression of ρ and ϕ in terms of the grazing angle ψ and the ground constants are quite different for the two types of polarization. For an arbitrary position of the plane of polarization, the wave must be separated into its vertically and horizontally polarized components, and the proper reflection coefficient applied to each component separately.

The quantities ρ and ϕ are determined by the boundary conditions for the electric vector at the reflecting surface, namely, that the tangential components of the electric vector on the two sides of the boundary surface shall be equal. This brings in the ground constants, that is, the conductivity and dielectric constant of the reflecting body. How these boundary conditions are applied may be illustrated by the simple example of horizontally polarized rays reflected from a surface of infinite conductivity. In the surface itself, the sum of the incident and reflected field strength must always be such that the currents set up in the body just suffice to produce the reflected field. Within a reflecting body of infinite conductivity, an infinitely weak field is sufficient, and hence the boundary condition is such that the reflected field, at the reflection point, shall be equal in magnitude and opposite in phase to the incident field, so that the resultant field is zero. Hence for infinite conductivity and horizontal polarization

$$R = -1, \qquad \rho = 1, \qquad \phi = 180°. \qquad (18)$$

Fresnel's Formulas

For finite conductivity, the reflection coefficient may assume a variety of values. The general formulas, as derived from electromagnetic theory, are given in equations (19) and (20). For horizontal polarization

$$R = \frac{\sin \psi - \sqrt{\epsilon_c - \cos^2 \psi}}{\sin \psi + \sqrt{\epsilon_c - \cos^2 \psi}}, \qquad (19)$$
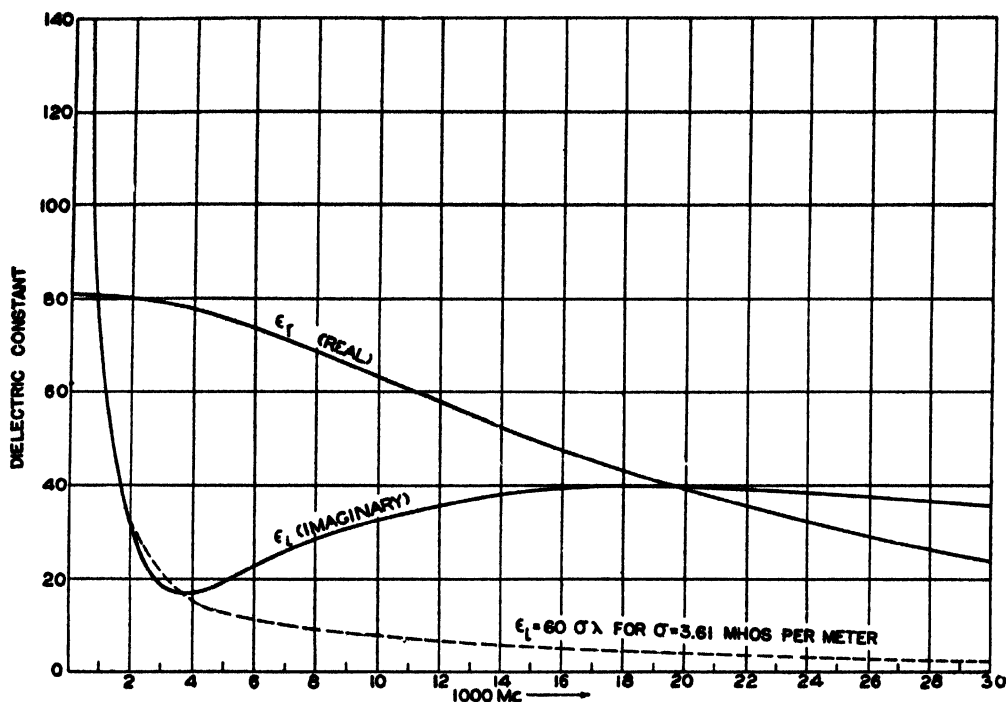
FIGURE 11.   Dielectric constant of sea water at 17 C.

and for vertical polarization

$$R = \frac{\epsilon_c \sin \psi - \sqrt{\epsilon_c - \cos^2 \psi}}{\epsilon_c \sin \psi + \sqrt{\epsilon_c - \cos^2 \psi}}, \tag{20}$$

where ϵ_c is the complex relative dielectric constant of the reflecting ground which is given by

$$\epsilon_c = \epsilon_r - j\epsilon_i. \tag{21}$$

A material that acts like a good conductor for low-frequency waves may act as an approximately pure dielectric for microwaves. The case $\epsilon_i = 0$ is therefore of considerable practical importance. When $\epsilon_i = 0$, and R consequently is real, the phase lag is 180° for horizontal polarization. For vertical polarization the phase change is 180° from $\psi = 0$ up to an angle ψ_0 determined by $\tan \psi_0 = 1/\sqrt{\epsilon_r}$. Here, the coefficient is zero. For larger angles the phase change is zero. As ϵ_r increases indefinitely, ψ_0 approaches zero and for infinite ϵ_r the phase shift is zero everywhere, except for $\psi = 0$ where it is indeterminate. The angle ψ_0 is called the Brewster angle. For $\psi = 0$ the amplitude is unity, and for $\psi = 90°$

$$\rho = \frac{\sqrt{\epsilon_r} - 1}{\sqrt{\epsilon_r} + 1} \tag{22}$$

for both cases of polarization. When ϵ_i is no longer zero, the amplitude ρ will show a deep minimum for a certain value of ψ instead of the zero found for $\epsilon_i = 0$. The angle corresponding to the minimum is

called the pseudo-Brewster angle. These various points are illustrated by examples in Figure 16.

The Complex Dielectric Constant of Water

As much of the available radar and communication equipment is either shipborne or erected along the coast, reflection from sea water is one of the principal problems to be discussed here. For microwaves the salt content in sea water makes little difference, so that it may be assumed that the dielectric constant and conductivity are the same over all oceans at the same temperature. With increasing temperature, the real part of the dielectric constant diminishes roughly by one unit per 5° C. Figure 11 gives the dielectric constant ϵ_r of ordinary sea water at 17 C as a function of frequency.

The dielectric constant also diminishes with increasing salinity, but in the UHF-SHF region, normal variations of salinity have much smaller influence than changes in temperature and frequency. The imaginary part ϵ_i of the dielectric constant is, for frequencies less than say 1,000 mc, related to the conductivity σ as follows:

$$\epsilon_i = + 60\sigma\lambda \tag{23}$$

(σ in mhos per meter and λ in meters). At 25 C the average conductivity of sea water is usually given as 4.3 mhos per meter. The temperature dependence is given by

$$\sigma = \sigma_{25}[1 + 0.02(t - 25)],$$
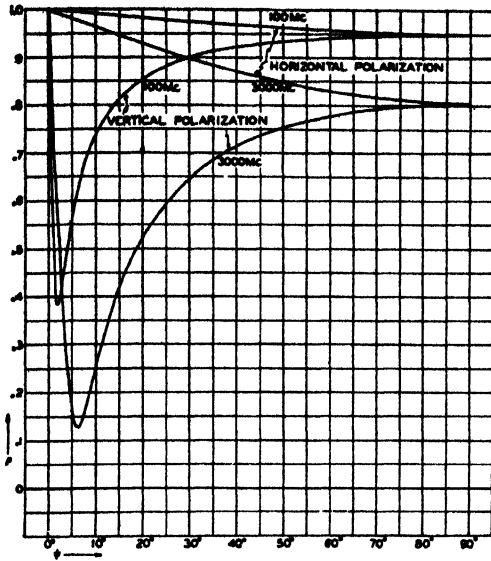
FIGURE 12. Amplitude of the reflection coefficient ρ versus angle of reflection Ψ for sea water. (From Radiation Laboratory Report C-11.)

where t is temperature in degrees centigrade.

The conductivity of fresh water is much smaller. An average for inland lakes is $\sigma = 10^{-3}$ mho per meter. For wavelengths shorter than about 10 cm, the dielectric constant is influenced by the fact that water is built up of polar molecules. The maximum effect is found for wavelengths of the order of 1 cm. For this region, there is no appreciable difference between salt and fresh water.

The probable run of ϵ_i for sea water is shown in
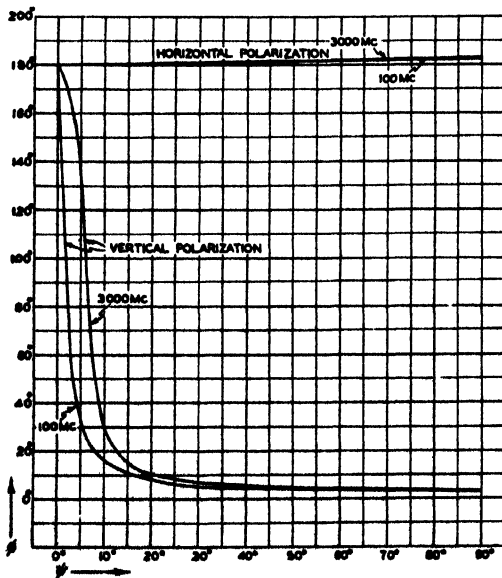
FIGURE 13. Phase of the reflection coefficient ϕ versus angle of reflection Ψ for sea water. Reflected wave E_r lags incident wave E_i by ϕ. (From Radiation Laboratory Report C-11.)
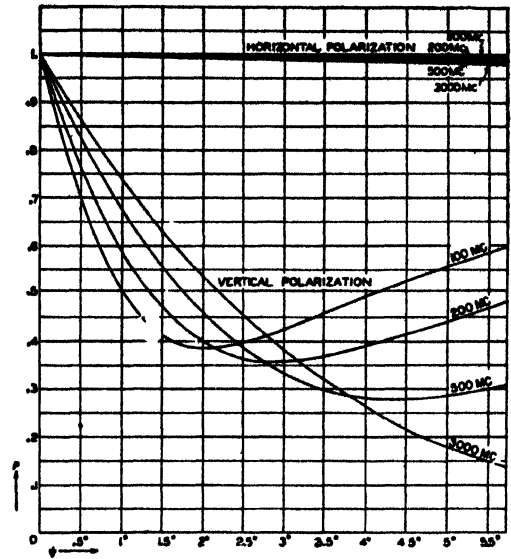
FIGURE 14. Amplitude ρ of the reflection coefficient versus reflection angle Ψ from $\Psi = 0$ to $\Psi = 5.5°$ for sea water.

Figure 11. The part of the ϵ_i curve extending from 6,000 mc to 30,000 mc corresponds essentially to results obtained at Clarendon Laboratory, Oxford. Other investigators give results which are markedly different. This curve is thus affected by considerable uncertainties and should be used with caution.

In Figures 12 to 15 are shown amplitude and phase of the reflection coefficient for a smooth sea for various frequencies. Figure 12 gives the amplitude ρ of the reflection coefficient for both kinds of polarization, for reflection angles up to 90 degrees, and for 100 and 3,000 mc. Figure 13 gives the phase ϕ under the same conditions. The next two
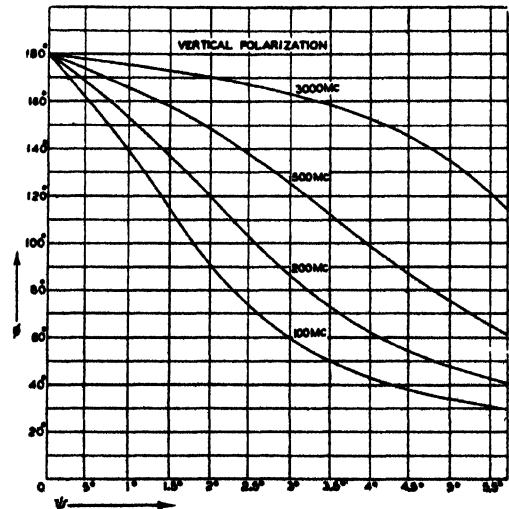
FIGURE 15. Phase ϕ of the reflection coefficient versus reflection angle Ψ from $\Psi = 0$ to $\Psi = 5.5°$ for sea water. E_r lags E_i by ϕ. (From Radiation Laboratory Report C-11.)

figures give ρ and ϕ on a greatly enlarged scale of ψ, in the interval $\psi = 0$ to $\psi = 5.5°$, which embraces all cases of practical interest.

Overland Transmission

Conditions over land are very different from those found over the sea. Land as a reflecting surface has larger irregularities and their effect is more pronounced. Therefore in selecting a radar site, it is preferable to choose a location which is surrounded by relatively smooth ground. The electrical properties of the earth vary considerably for different localities, so that it is necessary to study the ground conditions for each particular case. Experimental data concerning reflection of very short waves from ice- or snow-covered ground seem to be lacking. Precise information might be of operational interest, particularly in Arctic regions. Laboratory experiments indicate that ground covered by ice or snow will influence the propagation of short waves somewhat in the same way as very dry ground.

Conductivity of Soil

Extensive investigations have been made on the conductivity of different types of soil, particularly on low and medium frequencies. For 10 mc, the observed values range from $6 \cdot 10^{-3}$ mhos per meter for chalk to 0.13 mhos per meter for blue clay. The conductivity increases with increasing moisture
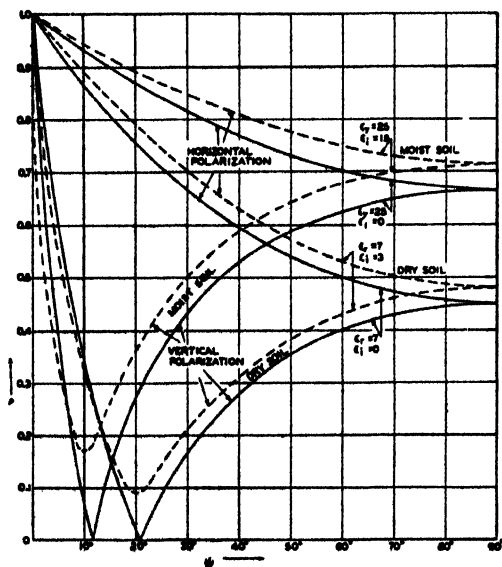
FIGURE 16. Amplitude of the reflection coefficient for moist and dry soil.

content, so that marked seasonal changes may be anticipated for a given locality. It also varies with frequency. Under field conditions it will not be possible to measure the conductivity in individual cases and one will have to assume a value of about

10^{-2} mhos per meter for poorly conducting ground like chalk or very dry soil and take a value of about 10^{-1} for good conductors like blue clay or waterbogged marshy land. Fortunately, the amplitude of the reflection coefficient is not very sensitive to minor changes in conductivity when the frequency is sufficiently high, say 200 mc or higher. Then the real part of the dielectric constant is the most important factor.

Dielectric Constant of Soil

It is not possible to give a standard table of dielectric constants of various types of soil, because the variation with the moisture content is considerable. For very dry ground ϵ_r is likely to be about 4, but this value may rise to 25 when the ground is thoroughly soaked with water. The dielectric constant of ground will normally decrease with increasing frequency.

Above 200 mc, the dielectric constant will dominate the conductivity term, and for field conditions the ground may be assumed to be a pure dielectric. This is illustrated in Figure 16 for $\epsilon_r = 7$; $\epsilon_i = 3$
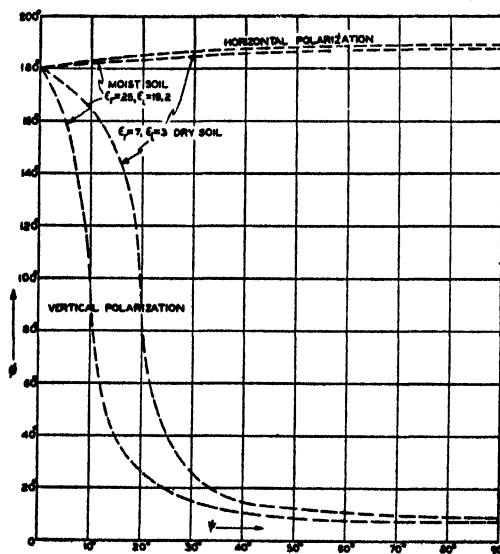
FIGURE 17. Phase of the reflection coefficient for moist and dry soil.

and $\epsilon_i = 0$; and for $\epsilon_r = 25$, $\epsilon_i = 19$ and $\epsilon_i = 0$. Except for values close to the Brewster angle, the zero conductivity curves give a usable approximation.

In Figure 17, the phase, ϕ, of the reflection coefficient corresponding to the above values of ϵ_r and ϵ_i is also given.

The Divergence Factor

The preceding considerations apply only to reflection from plane surfaces. For reflection from a
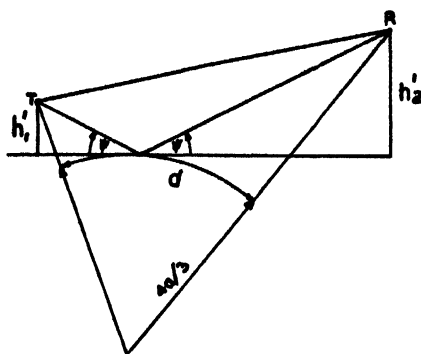
FIGURE 18. Geometry for divergence factor.

sphere like the earth, the divergence of a bundle of rays is increased when it suffers reflection, and the plane earth reflection coefficient, R, must be multiplied by a *divergence factor* denoted by D, which accounts for the earth curvature. This factor ranges from unity at close range where the earth can be considered plane to zero at points just above the tangent line. [Note: When the divergence factor approaches zero at grazing angles less than the last minimum, other components of the wave must be considered.] To a sufficient approximation D is given by the expression

$$D = \left[1 + \frac{2h_1'h_2'}{dka\tan^3\psi} \right]^{-\frac{1}{2}} \qquad (24)$$

where (see Figure 18),

h_1', h_2' = heights of transmitter and receiver above tangent plane at reflection point.

d = distance between transmitter and receiver measured along the surface of the earth.

ψ = grazing angle above tangent plane.

ka = equivalent earth radius.

Irregularity of Ground

The formulas for reflection from a plane or a spherical earth can only be applied with confidence granting a certain smoothness of the reflecting surface, depending on the wavelength. A rule of thumb for the applicability of the reflection formulas is that the vertical height of the irregularities should not exceed $\lambda/16\psi$, where λ is the wavelength and ψ the grazing angle in radians. Suppose, for instance, that the wavelength is 1 meter and the grazing angle, 1 degree. The limit of tolerance is then $56/16 = 3.5$ meters. Hence, on this wavelength one may expect specular reflection over sea in most cases. For $\lambda = 10$ cm, on the other hand, the limit is only 35 cm, and for $\lambda = 3$ cm it is 11 cm. For larger grazing angles, the limit of tolerance will be correspondingly smaller.

DIFFRACTION (GENERAL SURVEY)

Definition

The term diffraction will be understood to apply to those modifications of the field produced by material bodies outside the transmitter that cannot be described by the ray methods of geometrical optics.

With this limitation of the term diffraction, there are three main topics to be considered:

1. Diffraction by the earth's curvature.

2. Diffraction by irregular features of the terrain, such as hills, houses, etc.

3. Diffraction by objects, primarily metallic (targets) in two-way transmission (radar echoes). Also scattering by raindrops.

Diffraction by Earth's Curvature

The diffraction field in this case is the field appearing below the line of sight determined by use of the equivalent value of the earth's radius ka. The case of an idealized earth with smooth surface and given electrical properties can be treated mathematically, and the field obtained is often designated as the *standard* field (see Chapter 5). If one moves away from the transmitter horizontally, at a fixed height above the earth, the field strength decreases exponentially with distance once the line of sight is passed. Similarly the field strength decreases exponentially with height above the ground on going vertically downwards from the line of sight. In many instances, the variation in the field strength, in the diffraction region is independent of the electric properties of the ground. The main exception occurs in a comparatively shallow layer near the ground. Only for the important case of propagation over sea water and for frequencies below 100 megacycles does this layer become high enough to cover an appreciable part of the whole diffraction region.

Diffraction by Terrain

The problem of diffraction by terrain features requires special treatment. Frequently a field of appreciable magnitude is found behind hills, houses, etc. Diffraction is also important when there is a sudden change in ground properties, as for instance in a transition from land to sea. In this case the shore line acts as a diffracting edge. Only a limited number of cases lend themselves to evaluation by simple formulas. The cases are those which can be treated by the Fresnel-Kirchhoff method of optics which leads to a somewhat intricate but straightforward mathematical formula for the diffracted field strength. In spite of its apparent limitations,

the Fresnel-Kirchhoff formula is often applicable to short-wave propagation problems. It is treated in Chapter 8.

Diffraction by Targets

This problem can be dealt with theoretically by methods similar to those used in computing diffraction by terrain features, the main difference being that the angle of scattering is nearly 180 degrees
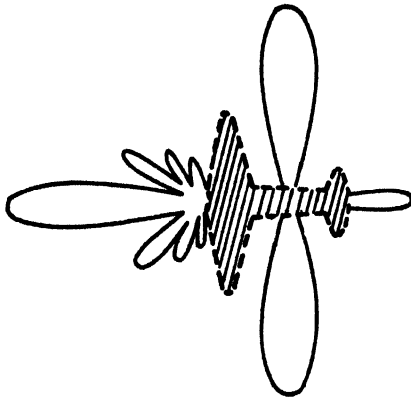
FIGURE 19. Reflecting pattern of an airplane.

instead of approximately 0 degrees.

In the case of target diffraction, theory is less useful than in many other problems of wave propagation. This is due to the fact that radar targets such as airplanes or ships have an extremely complex structure; the scattered intensity will therefore often change by many decibels as a result of only a small tilt of the target. Figure 19 shows a typical reradiating or reflecting pattern for an airplane. Numerous measurements of the average radar cross section of planes and ships have been made.

A phenomenon of great importance in the microwave region is the scattering of radiation by water drops in the atmosphere. Small droplets such as are found in fogs and most types of clouds do not give reflection visible on the scopes. Only drops large enough to produce actual precipitation give appreciable radar echoes. However, this does not necessarily mean that rain is falling at the locality indicated by the scope; frequently vertical updrafts of air will maintain drops afloat that in still air would fall to the ground; moreover, drops falling from a comparatively high cloud can evaporate before reaching the ground. Especially in tropical regions, the last-named phenomenon is more common than is ordinarily thought.

CALCULATION OF RADIO GAIN

INTRODUCTION

Objectives

THIS CHAPTER is devoted to the definition and calculation of the various factors which enter into a computation of the field strength of radio waves propagated in the standard atmosphere above the earth.

In Chapter 2, particularly in text on pp. 336-340, are given the basic definitions of path-gain factor and radio gain for transmission between doublets and other antenna types in free space. The present chapter shows how these quantities must be modified to account for the influences introduced by the curvature and electrical properties of the earth.

The methods of computation are presented in considerable detail to enable the interested reader to apply them to his particular problem, and sample calculations are given which should assist in reducing to a minimum the time required for obtaining the answers in a given case.

Definitions Relative to Radio Gain

The radio gain is defined as the ratio of received power P_2, delivered to a load matched to the receiver antenna, to transmitted power P_1, with both antennas adjusted for maximum power transfer. For doublet antennas in free space this ratio is given by $(3\lambda/8\pi d)^2$ and is denoted by A_0^2, that is,

$$\frac{P_2}{P_1} = A_0{}^2 = \left(\frac{3\lambda}{8\pi d}\right)^2 \tag{1}$$

and the free-space gain factor is given by

$$A_0 = \frac{3\lambda}{8\pi d} \tag{2}$$

in which d denotes the distance from the transmitter to the receiver measured in the same units as the wavelength λ.

When the radiation is emitted and received by directive antennas and the propagation takes place through a refracting and absorbing atmosphere, and reflection and diffraction effects of the ground are taken into account, the expression for the radio gain becomes a very complicated affair.

For the general case of one-way transmission, the radio gain is given by

$$\frac{P_2}{P_1} = G_1 G_2 A^2, \tag{3}$$

where G_1 and G_2 are the gains of the transmitting and receiving antennas, respectively, and A, the gain factor, is equal to

$$A = A_0 A_p \tag{4}$$

with A_p equal to the path-gain factor. [See equation (27) in Chapter 2.]

For radar or two-way transmission, the radar gain is decreased because the energy traverses the path both ways and is influenced by the radiating properties of the target as given by the radar cross section σ. Combining equations (46) in Chapter 2 and (2) in this chapter, the radar gain equals

$$\frac{P_2}{P_1} = G_1 G_2 \left(\frac{16\pi\sigma}{9\lambda^2}\right)[A_0{}^4 A_p{}^4] = G_1 G_2 \left(\frac{16\pi\sigma}{9\lambda^2}\right) A^4. \tag{5}$$

Comparing equations (3) and (5), it is seen that the gain factor A may be used also for two-way transmission, provided the additional term $16\pi\sigma/9\lambda^2$ is included in the formula.

Later on it will be shown how to split up A and A_p into a product of various factors, represented by graphs which make it possible to carry out computations in specific cases.

The gain factor A may also be expressed in terms of the field strength E and free-space field strength of a doublet transmitter E_0. From equation (28) in Chapter 2,

$$E = E_0 \sqrt{G_1} A_p. \tag{6}$$

Combining this equation with equation (4)

$$\frac{A}{A_0} = \frac{E}{E_0} \frac{1}{\sqrt{G_1}}, \tag{7}$$

where $E_0\sqrt{G_1}$ is the free-space field of the transmitting antenna with gain G_1.

The free-space field, in terms of the transmitted power P_1, is given by

$$\sqrt{G_1} E_0 = \frac{3\sqrt{5}\sqrt{P_1}}{d} \tag{8}$$

for a point in the direction of maximum radiation. In terms of the power P_2 delivered to the load circuit of a receiving antenna, with matched load and oriented for maximum pickup, the field at any point in space is equal, from equation (17) in Chapter 2, to

$$E = \frac{8\pi\sqrt{5}}{\lambda} \sqrt{\frac{P_2}{G_2}}. \tag{9}$$

It is sometimes convenient to express E in terms of the (radiation) field at one meter from the trans-

mitter, whence $E_0 = E_1/d$ and, from equation (6),

$$E = \frac{E_1}{d} \sqrt{G_1} A_p. \tag{10}$$

Factors Affecting Attenuation and Gain

The above definitions are quite general. In the absence of the earth, there remains only the free-space attenuation which results from the spreading out of the radiated energy as it moves away from the transmitter. At a distance which is several times larger than the wavelength, the field strength varies inversely as the distance from the antenna.

The presence of the earth affects the field through two sets of quantities. One set is geometric and includes the heights of the antennas and their distance apart, the curvature of the earth, and shape of terrain features. The other set is electromagnetic and depends on the dielectric constant and conductivity of the earth and of its atmosphere, the polarization and the wavelength of the radiation.

Simplifying Assumptions

The present chapter is mainly concerned with the computation of the field-strength distribution of a transmitter for certain idealized standard conditions, so chosen as to give a fair average picture of propagation conditions for very high-frequency radiation. The reasons for this limitation are stated in Chapter 1. In substance, the limitations are imposed by the great complexity of the general problem, which makes it necessary to proceed in successive steps. The first step is to consider propagation under standard conditions, which will be defined farther on. Successive steps take into account diffraction by terrain, that is, by trees, hills, mountain ranges, or shore lines, or by non-standard propagation effects in the atmosphere.

The fundamental importance of a knowledge of propagation under standard conditions is first of all due to the fact that in a large number of cases conditions do not differ significantly from standard. On the other hand, when they do deviate significantly, the standard solution sets up a criterion for the discovery of deviations and the evaluation of the influence of the nonstandard conditions upon propagation.

The basic assumptions which define what we have been calling standard propagation conditions will now be given.

1. *Standard atmosphere.* It is assumed that the index of refraction of the atmosphere has a uniform negative gradient with increasing elevation. As has been pointed out in Chapter 4, the influence of such an atmosphere upon propagation is equivalent to that of a homogeneous atmosphere over an earth of radius ka, where k is a constant that usually is taken

equal to 4/3.

2. *Smooth earth.* The earth is assumed to be perfectly smooth. It can be considered sufficiently smooth if Rayleigh's criterion is satisfied, that is when the height of surface irregularities times the grazing angle (in radians) is less than $\lambda/16$ (see page 375).

3. *Ground constants.* The dielectric constant and conductivity of the earth are assumed uniform. For wavelengths less than one meter this assumption is particularly valid since in this case propagation is largely independent of the ground constants. In the VHF (1 to 10 m) range, the same is true with the important exception of vertically polarized radiation over sea water. For the VHF range, the assumption of uniform earth constants is unsatisfactory for paths partly over land and partly over sea water, or over sea water with large land masses near-by (see Chapters 8 and 10).

4. *Doublet antenna and antenna gain.* For the formulas of this chapter, the radiating system is assumed to be a doublet antenna (i.e., a straight wire, short compared to the wavelength). Actual antennas have radiation patterns different from that of a doublet, usually having greater directivity. The antenna gain of a half-wave dipole is 1.09 times (or 0.4 db greater than) that of a doublet, the field maximum being the same in the two cases. This gain is insignificant in practice. For other types of antenna systems and for microwave frequencies, the gain may be many times larger.

The propagation problem, thus limited, has been solved mathematically; but the explicit mathematical formulas are far too complicated to be of much use to the practical computer. Much additional work has been done, however, to bring the solution into a form suitable for practical use. This involves reducing the computations to the use of graphs, nomograms, and tables, and it is this final stage of the problem which is the subject of subsequent parts of this chapter as well as of Chapter 6.

Curved-Earth Geometrical Relationships

Let h_1 and h_2 denote the heights of transmitter and receiver above the earth's surface, respectively, and let d denote the distance from the base of the transmitter to the base of the receiver, measured along the earth's surface. For a number of cases concerned with high-frequency radiation over the earth's surface, it is sufficient to identify the straight-line distance from transmitter to receiver with the distance d between the bases measured along the curved earth. But when path *differences* are of importance, as they are in interference problems of reflection and in diffraction, it is necessary to compute distances to a higher order of accuracy.

Throughout this chapter, the earth will be assumed

to have the equivalent radius ka, and the atmosphere to be homogeneous, and radiation to travel along straight lines.

The straight line from the transmitting antenna and tangent to the earth's surface (the so-called *line of sight*) touches the earth along a circle which constitutes the radio horizon of the transmitter. The distance measured along the earth from the transmitter to the radio horizon will be denoted by d_T; and the horizon distance of the receiver by d_R. These geometrical relations are illustrated in Figure 1.

From this figure, it follows that

$$ka + h_1 = \frac{ka}{\cos (d_T/ka)} . \tag{11}$$

Inasmuch as

$$\frac{ka}{\cos (d_T/ka)} \cong \frac{ka}{1 - \frac{1}{2}(d_T/ka)^2} \cong ka + \frac{1}{2}\frac{d_T^2}{ka},$$

equation (11) assumes the form

$$h_1 = \frac{1}{2}\frac{d_T^2}{ka}, \tag{12}$$

or

$$d_T = \sqrt{2\,kah_1} . \tag{13}$$

Similarly, the horizon distance of the receiver is

$$d_R = \sqrt{2\,kah_2} . \tag{14}$$

The sum of the two horizon distances is given by d_L, where

$$d_L = d_T + d_R. \tag{15}$$

Optical and Diffraction Regions

The points visible from the transmitting antenna (on an earth of equivalent radius ka), i.e., the points above the line of sight, constitute the optical region (Figure 1). The rest of space lies beyond the transmitter horizon and below the line of sight and is called the shadow or diffraction region.
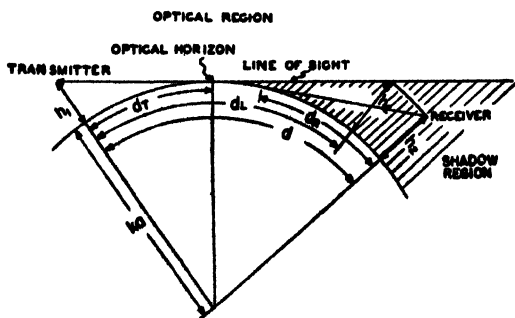
FIGURE 1. Geometry for radio wave propagation over curved earth.

It is frequently necessary to know whether a receiving antenna lies in tne optical region or the diffraction region of a given transmitter. This evidently is equivalent to knowing whether the distance d of the receiver from the transmitter is smaller or larger than the combined horizon distance d_L. By equations (13), (14), and (15), it follows that in the optical region

$$d < \sqrt{2\,ka}\,(\sqrt{h_1} + \sqrt{h_2}), \tag{16}$$

and in the shadow region

$$d > \sqrt{2\,ka}\,(\sqrt{h_1} + \sqrt{h_2}). \tag{17}$$

A graphical representation of the equation

$$d_L = \sqrt{2\,ka}\,(\sqrt{h_1} + \sqrt{h_2}) \tag{18}$$

is given in Figure 2. For $k = 4/3$, $a = 6.37 \times 10^6$ m, this takes the form

$$d_L = 4120\,(\sqrt{h_1} + \sqrt{h_2})\ \text{meters}, \tag{19}$$

where h_1, h_2 are given in meters and d_L in meters.
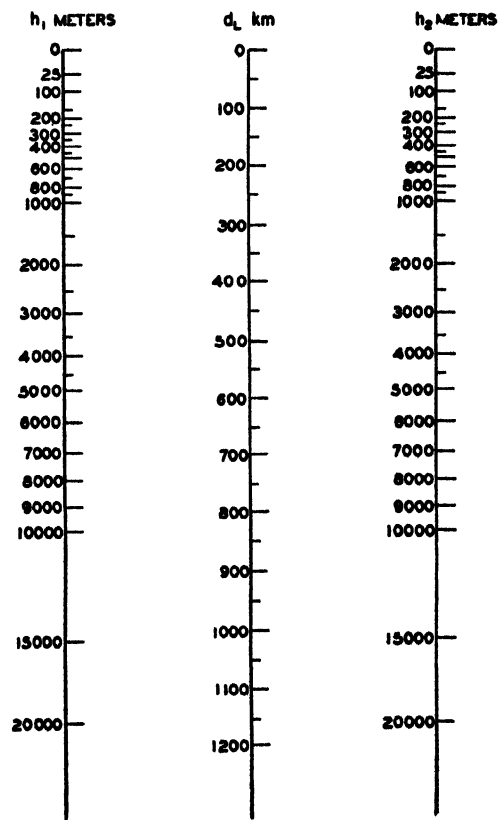
FIGURE 2. Sum of transmitter and receiver horizon distances for standard refraction. To change scale: Divide h_1 and h_2 by 100, and divide d_L by 10.

Nature of the Radiation Field in the Standard Atmosphere

The mathematical solution for the radiation field takes various forms for particular cases. The treatment for low antennas, for instance, differs from that for high antennas, and similarly the equations must be handled differently for the two types of polarization. These and related problems are discussed in general in the following.

1. *General form of field variation.* The mathematical expression for the radio gain of the radiation field of a doublet under standard conditions is given as the sum of an infinite number of complex terms or modes. (See pp. 421-428.) Disregarding the phase factor, a representative term (mode) of this series has the form

$$F(d) \cdot f_1(h_1) \cdot f_2(h_2) . \qquad (20)$$

These modes are attenuated unequally. Well within the diffraction region, the first mode contributes practically all of the field so that the effects of distance and height are separable. In this region, the problem of numerical computation is simplified, since it is possible to use separate graphs for the dependence on height and distance. As the receiver is moved toward the transmitter, the number of modes required for a good approximation increases. For low antennas, the addition of the modes is practicable and the graphical aids are useful for short distances. These conditions are illustrated in Figure 3 for horizontal polarization or ultra-short waves.

In the optical region, the methods of geometrical optics give a result equivalent to that of the rigorous solution at points which are not close to the line of sight. The field is then the sum of a direct and a reflected wave, resulting in an interference pattern.

The preceding discussion is illustrated by Figure 4 which shows the variation of field strength with distance for fixed antenna heights, for propagation over dry soil with a wavelength of 0.7 meter on vertical polarization. The numbers refer to the number of modes required for a better than 99 per cent approximation. The interference pattern is illustrated by the oscillatory nature of the curve. It will be observed that beyond the first maximum, the points found by geometric optics give a value of the field which is slightly too low. (See dots in Figure 4.) *In fact, as the line of sight is approached, the optical formula approaches zero whereas the exact solution does not.* The geometric-optical method breaks down in the optical region as the line of sight is approached. It may be noted that Figure 4 has been drawn for $k = 1$ rather than for the customary value of $k = 4/3$ corresponding to standard atmosphere conditions and is for a hypothetical isotropic radiator.

If the earth were flat and perfectly reflecting, the envelope of the maxima of the curve in Figure 4 would coincide with the line $2E_0$, twice the free-space field, corresponding to the in-phase addition of the direct and reflected waves. An envelope of the minimum points would be $E = 0$, corresponding to the destructive interference of the direct and reflected waves. The curvature of the earth, resulting in increased divergence of the waves (see text on p. 384), and the lack of perfect reflection (see text on p. 383) cause the maximal and minimal envelopes to differ from $2E_0$ and 0, respectively. In the neighborhood of the first maximum in Figure 4 (i.e., when the direct ray makes small angles with the earth), the reflection coefficient tends to be unity in magnitude for both polarizations except for the increase in divergence which results in the deviation of the maximal and minimal lines from $2E$ and 0, respectively At a smaller distance, for vertical polarization, as shown in Figure 4, the deviation is caused principally by the smaller magnitude of the reflection coefficient. The virtual meeting of the maximal and minimal lines corresponds to the minimum value of the reflection coefficient at the pseudo-Brewster angle. (For horizontal polarization at small distances, the envelope of maxima would virtually coincide with $2E_0$ and the minima would be closer to zero. As the distance is increased, the difference between the envelopes for vertical and horizontal polarization gradually decreases.)

2. *Both antennas low; $h < h_c$.* In a discussion of the height function, it is convenient to distinguish between high and low antennas. The critical height separating the two cases for horizontal polarization or ultra-short waves is given by

$$h_c = 30\lambda^{2/3} \text{ meters} \qquad (21)$$

where λ is expressed in meters. For $\lambda = 0.1$ meter, $h_c = 6.46$ meters, and for $\lambda = 10$ meters, $h_c = 139.5$ meters. If both antennas are at elevations less than h_c, the height-gain functions $f(h)$, to a first approximation, are the same for all the modes, so that the complete solution

$$f_1(h_1) \cdot f_1(h_2) \cdot F_1(d) + f_2(h_1) \cdot f_2(h_2) \cdot F_2(d) + + +$$

can be written in the form

$$f(h_1) \cdot f(h_2) \cdot (F_1 + F_2 + \cdots), \qquad (22)$$

or

$$f(h_1) \cdot f(h_2) \cdot F(d), \qquad (23)$$

where $f(h_1)$ replaces $f_1(h_1)$, $f(h_2)$ replaces $f_1(h_2)$, etc., while $F(d)$ stands for the sum $F_1 + F_2 + \cdots$.

The distance function $F(d)$ can be calculated for particular cases. This has been done for high frequencies and is represented graphically on pp. 403-432, the results being valid for low antennas for all distances in the optical as well as in the diffraction region such that $2h_1h_2 << \lambda d$ (see Figure 3). The condition $2h_1h_2 << \lambda d$ assures that the antennas are below the interference pattern.

FIGURE 3. Field regions as related to transmitter heights for horizontal polarization or ultra-short waves. Low antenna region = $\lambda d > 2h_1 h_2$; $h_1, h_2 < 30\lambda^{2/3}$.

FIGURE 4. Variation of field strength with distance for propagation on vertical polarization with a wavelength of 70 cm over dry soil. The point "due to minimum" results from minimum in reflection coefficient at the pseudo-Brewster angle.

At the ground, $f(h) = 1$, so that if both antennas are close to the ground, the distance dependence is given by $F(d)$ only.

3. *One or both antennas elevated; $h > h_c = 30\lambda^{2/3}$.* For elevated antennas, $h > h_c$ and the height-gain functions of $f(h)$ vary with the modes. Consequently, it is not possible to separate the height and distance effects as in the previous paragraph.

In the optical-interference region, it is more advantageous to use the method of combining the direct and reflected waves. This is equivalent to

the rigorous solution which is illustrated by the dots in Figure 4.

Simple graphical aids can be given for points well within the diffraction region where the first mode predominates. The range of usefulness of the first mode can be extended by plotting the field strength given by the first mode as a function of height (or distance) and plotting a similar curve by using the ray method as far as the lowest (or first) maximum (see Figure 7). Then by joining these partial curves into a smooth overall curve, a fairly good value of

the field can be obtained for intermediate points.

There is a further possibility occurring with the transmitting antenna elevated, the receiver low and lying below the interference pattern, and the distance short. In this event, none of the previous methods apply. However, the reciprocity principle (see Chapter 2) can be applied to find the radio gain at the receiver by interchanging the role of receiver and transmitter. Suppose the original transmitter height is 100 meters, the original receiver height 15 meters, and the wavelength 1 meter. Now let the transmitter height be 15 meters. If the receiver height is low ($h_2 < 30$ meters), values of the gain can be found (page 405); if the receiver height is in the interference region, the gain can be found by the ray method. Now suppose a curve be drawn for these results, giving the attenuation versus receiver height. From this graph, the value of the gain factor A at $h_2 = 100$ meters can be read. This value of A by the principle of reciprocity is the gain factor for the original heights.

4. *Ultra-short waves in the diffraction region. Dielectric earth.* For $\lambda < 10$ meters ($f > 30$ mc) and for either polarization, *land* acts as a *dielectric earth* or *absorbing earth* in contradistinction to a *conducting earth*. Propagation over a dielectric earth is practi-

cally independent of earth constants. For a given type of polarization, the chief variables affecting gain are then the heights of the antennas, their distance apart, and the wavelength. Within the diffraction region, the effect of increasing wavelength is to increase the field strength. This is illustrated by the curves in Figures 5 and 6. The dielectric earth is characterized by a value of $\delta \gg 1$. δ is given by equation (193).
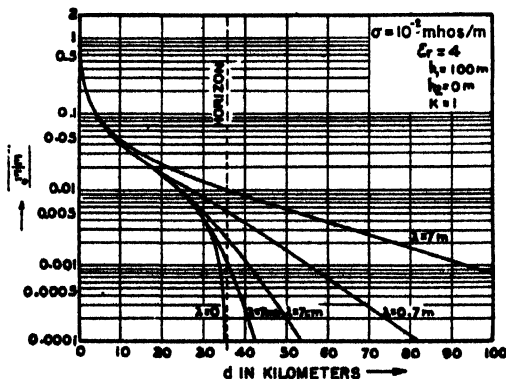
While *sea water* has a relatively high conductivity, radio wave propagation over it is the same as that over a dielectric earth in the case of horizontal polarization for $\lambda < 10$ meters, and in the case of vertical polarization for $\lambda < 1$ meter. Consequently, vertically polarized radiation of wavelength range 1 to 10 meters over sea water is given special treatment on pages 416-419.

In the same range, 1 to 10 meters, for vertically polarized radiation and for distances less than those given in Table 3, propagation conditions over land also deviate slightly from those corresponding to a dielectric earth.

5. *Optical region.* In the optical-interference region, the lobes for the shorter waves are more numerous, narrower, and lower, as can be seen from the oscillatory part of the field strength versus distance curves of Figure 6.

The dependence of reflection coefficients upon polarization, wavelength, and ground constants is discussed on pp. 370-375.

6. *Horizontal versus vertical polarization.* In the optical region, for rays at small grazing angles, there is not much difference between the two types of polarization. For larger grazing angles, the difference is more marked (see the section on reflection coefficients.

FIGURE 5. Field strength ratio versus distance for vertical polarization over dry soil for $h_1 = 100$ meters and $h_2 = 0$.

FIGURE 6. Field strength ratio versus distance for vertical polarization and heights $h_1 = h_2 = 100$ meters.
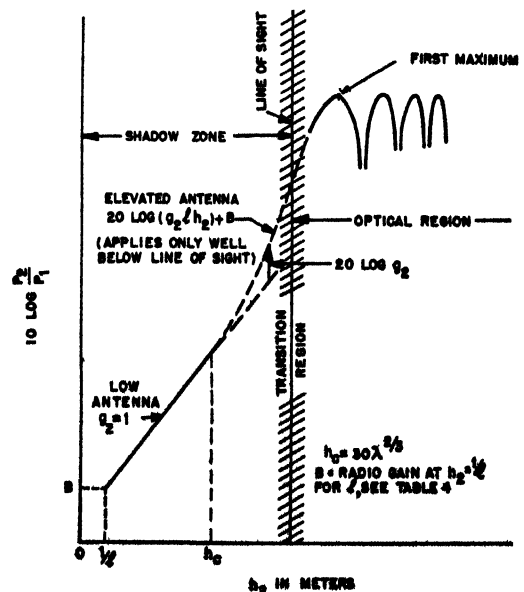
FIGURE 7. Gain versus height at distances beyond the radio horizon.

It has been pointed out in the previous paragraph that within the diffraction region for $\lambda < 10$ meters and propagation *over land*, there is practically no difference in intensity between a horizontally and a vertically polarized radiation field. For $\lambda < 1$ meter there is, similarly, no difference for propagation over *sea water*. When there is a difference, as for low antennas, horizontal polarization gives a smaller gain; but as the antennas are raised, the two cases approach equality.

PROPAGATION FACTORS IN THE INTERFERENCE REGION

Propagation Factors

The factors affecting gain in the region where the methods of geometrical optics may be applied are discussed in this and the next three sections.

Spreading Effect

From the formula of equation (1) in Chapter 2, for the field intensity components of the radiation field, it follows that for distances from the transmitter large in comparison to the wavelength, the dominant term falls off inversely as the distance from the transmitter, or

$$E = \frac{E_1}{d}, \qquad (24)$$

where E_1 is the field strength at unit distance. This means that the power per unit area in the radiation field varies inversely as the square of the distance. This spreading effect is the consequence of the fact that the energy of the wave is distributed over larger and larger areas as the wave progresses away from the transmitter.

Interference

When a wave travels over a conducting surface, constructive and destructive interference occurs between the direct wave from the transmitter and the wave reflected by the surface. This is illustrated in Figure 8, which is drawn for a plane earth. If there is no energy lost in reflection, the direct and
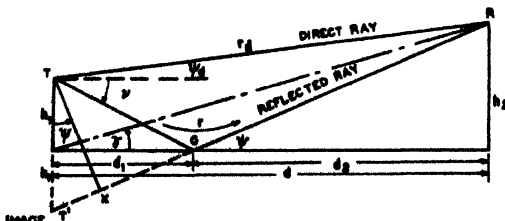
FIGURE 8. Geometry for radio propagation over a plane earth.

reflected waves are of equal intensity, and their resultant varies from zero to twice the free-space value, depending upon the phase difference between the two components. The reflected wave lags the direct wave by an angle $\delta + \phi$, where δ is the phase retardation caused by the greater path length traversed by the reflected wave and ϕ is the phase lag occurring at reflection.

Figure 9 shows the vector diagram for the case where the phase shift at reflection is $\phi = 180$ degrees.
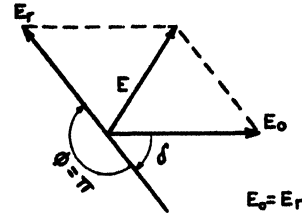
FIGURE 9. Vector diagram showing the addition of the direct and reflected waves for $\phi = 180°$ and $\rho = 1$.

This condition holds for horizontally polarized radiation of frequency above 100 megacycles, reflected from sea water at grazing angles of less than 10 degrees. The resultant electric field is equal to

$$E = \sqrt{E_0{}^2 + E_r{}^2 - 2E_0E_r \cos \delta}$$

$$= \sqrt{(E_0 - E_r)^2 + 4E_0E_r \sin^2 \frac{\delta}{2}}. \qquad (25)$$

If the reflection is complete, as from a conductor of infinite conductivity,

$$E_r = E_0, \quad E = 2E_0 \sin \frac{\delta}{2}. \qquad (26)$$

Imperfect Reflection

In general, the strength of the reflected wave E_r is less than that of the incident wave E_i, partly because of diffuse reflection and partly because some energy is refracted into the surface and absorbed. Furthermore, the phase lag usually differs from 180 degrees, depending upon the frequency and grazing angle. This is especially true for *vertical polarization* where the reflection coefficient is a *critical* function of both the grazing angle and frequency. The ratio

$$R = \frac{E_r}{E_i} = \rho e^{-j\phi} \qquad (27)$$

is a complex number and defines the reflection coefficient R, which has an absolute value ρ and a phase angle ϕ.

In equation (27), a lagging angle is considered positive. Writing $\phi = \pi + \phi'$, equation (27) may

be expressed as

$$R = \frac{E_r}{E_i} = \rho e^{-j(\pi + \phi')} = -\rho e^{-j\phi'} \qquad (28)$$

In equation (27), the lag angle ϕ is measured with respect to zero-degree phase shift at reflection. For horizontal polarization, ϕ varies from 180 degrees to 183 degrees, and from 180 degrees to 3 degrees for vertical polarization at 3,000 mc over sea water. In equation (28), lag angle ϕ' is measured with respect to a 180-degree phase shift (that is, from E_i reversed), and varies from 0 degree to 3 degrees for horizontal polarization and from 0 degree to −177 degrees for vertical polarization.

The resultant field intensity is

$$E = E_0 + \rho E_0 e^{-j(\delta + \phi)} = E_0 + \rho E_0 e^{-j(\delta + \phi' + \pi)}$$
$$= E_0(1 - \rho e^{-j\Omega}), \qquad (29)$$

where

$$\Omega = \delta + \phi' = \delta + \phi - \pi.$$

The absolute value of the received field $|E|$ is given by

or

$$|E| = E_0 \sqrt{(1 - \rho e^{+j\Omega})(1 - \rho e^{-j\Omega})}$$

$$|E| = E_0 \sqrt{1 + \rho^2 - 2\rho \cos \Omega}$$

$$= E_0 \sqrt{(1 - \rho)^2 + 4\rho \sin^2 \frac{\Omega}{2}}. \qquad (30)$$

Equation (30) shows that the received field intensity has a maximum of $2E_0$ when

$$\rho = 1,$$
$$\Omega = (2n + 1)\pi. \qquad (31)$$

The value of E is a zero when

$$\rho = 1,$$
$$\Omega = 2n\pi. \qquad (32)$$

In equations (31) and (32), n includes all integral values and zero. Equation (30) may be written as

$$E = \frac{E_1}{d} \sqrt{(1 - \rho)^2 + 4\rho \sin^2 \frac{\Omega}{2}}, \qquad (33)$$

where E is the field at distance d from the transmitter, and E_1 is the field strength at unit distance. From equation (33),

$$d = \frac{E_1}{E} \sqrt{(1 - \rho)^2 + 4\rho \sin^2 \frac{\Omega}{2}}. \qquad (34)$$

In free space where there is no reflecting earth, $\rho = 0$, and

$$d_0 = \frac{E_1}{E}, \qquad (35)$$

where d_0 is the equivalent free-space distance from the transmitter at which the field strength E would be found. Hence equation (34) may be written in

the form

$$d = d_0 \sqrt{(1 - \rho)^2 + 4\rho \sin^2 \frac{\Omega}{2}}. \qquad (36)$$

Divergence

The divergence factor D is introduced to account for the decreased gain produced by the spreading
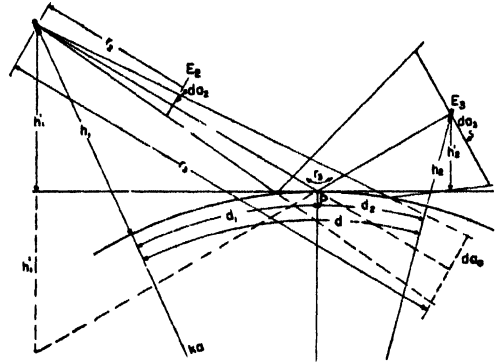
FIGURE 10. Increased divergence resulting from reflection by a sphere.

of a wave reflected from a spherical surface. Referring to Figure 10,

$$\frac{E_3}{E_2} = \sqrt{\frac{da_3}{da_3}} = \sqrt{\frac{da_2}{da_0} \frac{da_0}{da_3}} = \frac{r_2}{r_3} \sqrt{\frac{da_0}{da_3}} = \frac{r_2}{r_3} D. \qquad (37)$$

In calculating the field intensity reflected from a spherical earth, the inverse distance attenuation factor $1/r_d$ used for the direct wave must be multiplied by the divergence factor D, which is always less than unity.

As a result of this divergence the reflection coefficient for a spherical surface is less than that for a plane surface as given by

$$\rho D = \rho' \qquad (38)$$

where ρ' is the spherical earth reflection coefficient. Equations (30) and (36) may then be written as

$$|E| = E_0 \sqrt{(1 - \rho')^2 + 4\rho' \sin^2 \frac{\Omega}{2}} \qquad (39)$$

and

$$d = d_0 \sqrt{(1 - \rho')^2 + 4\rho' \sin^2 \frac{\Omega}{2}}. \qquad (40)$$

Antenna Gain and Directivity

The effects of antenna gain and directivity are expressed by means of the gain factor G, defined in text on p.339, and the antenna pattern factors F_1 and F_2, which are the fractions of the maximum radiation amplitude in the direction of the direct and reflected rays respectively. The maximum amplitude for a transmitting antenna with gain G_1 is

$E_0' = \sqrt{G_1}\,E_0$, where E_0 is the free-space field strength radiated by a doublet.

When the antenna pattern factors are taken into account, the resultant field intensity, following equation (30), is

$$E = \sqrt{G_1}\,E_0\,\sqrt{F_1{}^2 + F_2{}^2\rho^2 D^2 - 2F_1F_2\rho D \cos \Omega}. \quad (41)$$
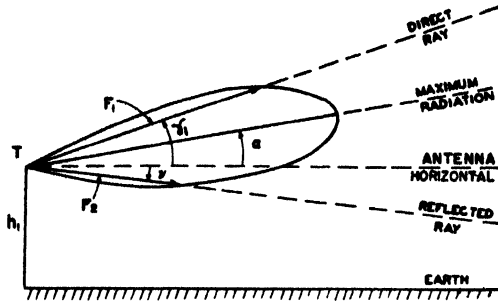
FIGURE 11   Antenna pattern factors F_1 and F_2.

The factors F_1 and F_2 are functions of the angles $\gamma_1 - \alpha$ and $\nu + \alpha$ which the direct and reflected rays make with the axis of the beam. Figure 11 is a typical antenna pattern.

GENERAL SOLUTION

Generalized Reflection Coefficient

Equation (41) may be simplified by introducing a generalized coefficient which includes the effects of reflection, divergence, and directivity. The amplitude of this coefficient will be denoted by K and is given by

$$K = \frac{F_2}{F_1}\rho D. \quad (42)$$

Substituting $F_2 = F_1 K/\rho D$ in equation (41) gives

$$E = \sqrt{G_1}F_1E_0\,\sqrt{1 + K^2 - 2K \cos \Omega} \quad (43)$$

or

$$E = \sqrt{G_1}F_1E_0\sqrt{(1 - K)^2 + 4K \sin^2 \frac{\Omega}{2}}. \quad (44)$$

If the transmitting antenna is pointed so that the direct ray lies in the direction of maximum gain, $F_1 = 1$, and

$$E = \sqrt{G_1}E_0\,\sqrt{(1 - K)^2 + 4K \sin^2 \frac{\Omega}{2}} \quad (45)$$

and

$$d = \sqrt{G_1}d_0\,\sqrt{(1 - K)^2 + 4K \sin^2 \frac{\Omega}{2}}. \quad (46)$$

Figure 12 shows

$$\sqrt{(1 - K)^2 + 4K \sin^2 \frac{\Omega}{2}}$$

as a function of K for various values of $\sin \Omega/2$ and may be used to calculate E.

The value of G_1 to be used in equation (46) may
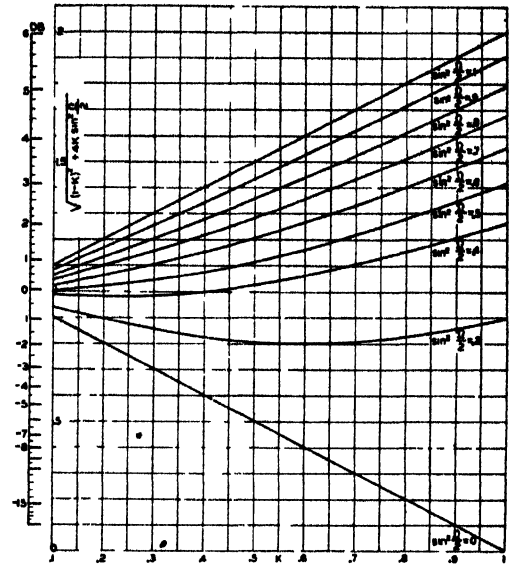
FIGURE 12. $\sqrt{(1 - K)^2 + 4K \sin^2 \frac{\Omega}{2}}$ as a function of K and Ω.

be found from the antenna specifications for a given set. The free-space field E_0 at distance d from a transmitting doublet with power output P_1 is equal to

$$E_0 = \frac{3\sqrt{5}\,\sqrt{P_1}}{d}. \quad (47)$$
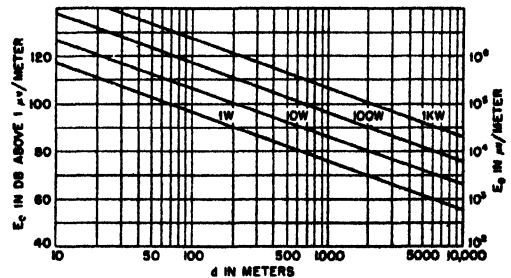
FIGURE 13.   Free-space range d as a function of field strength E_0 and transmitter power P_1.

Figure 13 shows E_0 in decibels above 1 microvolt per meter as a function of d for various values of transmitted power. The free-space field at distance of d meters expressed in decibels above 1 microvolt per meter for P_1 watts radiated is

$$\text{Decibels} = 20 \log_{10}\left[\frac{3\sqrt{5}\,\sqrt{P_1}}{10^{-6}d}\right]. \quad (48)$$

PLANE EARTH

Use of Plane Earth Formula

The following section will show that under certain conditions calculations based upon the assump-

tion of a plane earth yield satisfactory results. Calculations for propagation over a plane earth are given in this section.

Path Difference

It follows from equation (29) that when $\rho = 1$ and $\phi = 180$ degrees, the received field depends only upon the phase lag caused by path difference. Referring to Figure 8,

$$r_d = \sqrt{d^2 + (h_1 - h_2)^2} = d\sqrt{1 + \left(\frac{h_1 - h_2}{d}\right)^2}$$
$$= d\left[1 + \frac{1}{2}\left(\frac{h_1 - h_2}{d}\right)^2 - \frac{1}{8}\left(\frac{h_1 - h_2}{d}\right)^4 + \ldots\right], \quad (49)$$

$$r = \sqrt{d^2 + (h_1 + h_2)^2} = d\sqrt{1 + \left(\frac{h_1 + h_2}{d}\right)^2},$$
$$= d\left[1 + \frac{1}{2}\left(\frac{h_1 + h_2}{d}\right)^2 - \frac{1}{8}\left(\frac{h_1 + h_2}{d}\right)^4 + \ldots\right], \quad (50)$$

$$\Delta = r - r_d = d\left[\frac{2h_1h_2}{d^2} - \frac{h_1h_2(h_1^2 + h_2^2)}{d^4} + \ldots\right],$$
$$= \frac{2h_1h_2}{d}\left[1 - \frac{h_1^2 + h_2^2}{2d^2} + \ldots\right]. \quad (51)$$

If
$$\frac{h_1^2 + h_2^2}{2d^2} << 1,$$

$$\Delta \cong \frac{2h_1h_2}{d}. \quad (52)$$

The phase lag caused by the path difference Δ is equal to

$$\delta = \frac{2\pi}{\lambda}\left(\frac{2h_1h_2}{d}\right) = \frac{4\pi h_1h_2}{\lambda d}, \quad (53)$$

where λ is the wavelength of the radiation.

Field Strength Equations

When $\rho = 1$ and $\phi = 180°$, equation (26) may be used. Substituting equation (53) for δ into equation (26) gives

$$E = 2E_0 \sin\left(\frac{2\pi h_1h_2}{\lambda d}\right). \quad (54)$$

If $\delta/2 < 10°$, $\sin(\delta/2) \rightarrow \delta/2$ and

$$E = E_0 \frac{4\pi h_1h_2}{\lambda d}. \quad (55)$$

When h_1 or h_2 equals 0, equation (55) indicates that the received field intensity is equal to zero, which is contrary to fact. For this case the diffraction field must therefore be calculated and included as explained on page 380.

In the general case ($\rho < 1$), equation (44) may be applied with $K = (F_2/F_1)\rho D$. A refinement may be added to the calculation by taking into account the fact that the image source (Figure 8) of the reflected wave is at a distance $r + \Delta$ from the receiver. The reflected wave is attenuated more than the direct wave, according to the free-space attenuation ratio $(r + \Delta)/r$. If this is taken into account
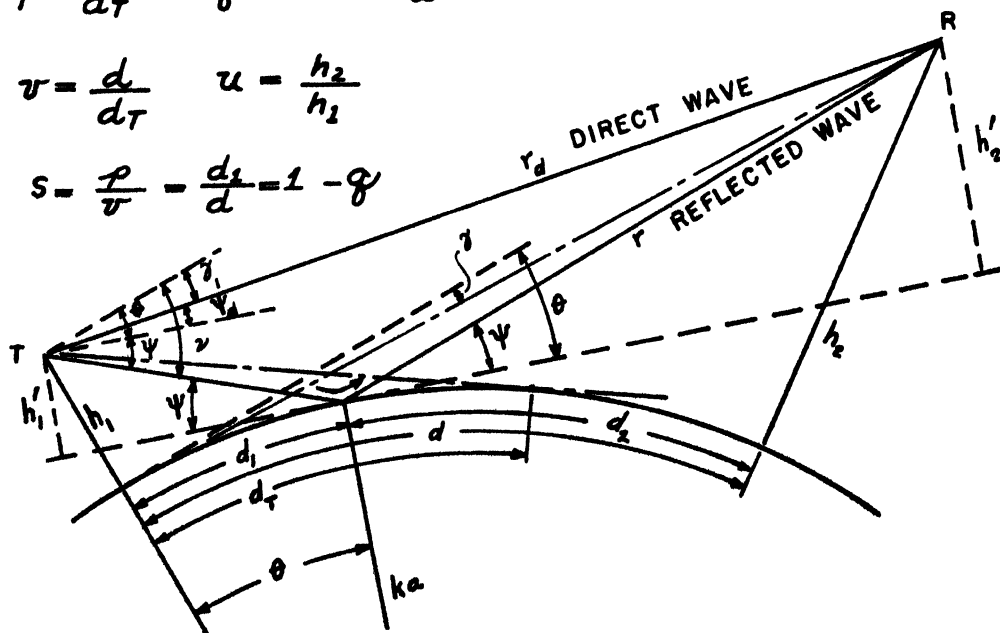
FIGURE 14. Geometry for radio wave propagation over a spherical earth. (Vertical dimensions greatly exaggerated.)

the ordinary reflection coefficient is replaced by

$$K^t = \frac{F_2}{F_1}\left(\frac{r}{r+\Delta}\right)\rho D. \qquad (56)$$

The correction is not necessary when $2h_1h_2 << d^2$ [see equation (52)].

SPHERICAL EARTH

Measurement of Distance

The difference between the slant range r_d and the distance measured along the surface of the earth and designated by d in Figure 14 is usually negligible. For a transmitter height of 1,500 meters, the error in assuming $r_d = d$ is 0.04 per cent at a distance of 161 km and height of 6,900 meters, and 1 per cent at the same distance but at a height of 22,500 meters. As the transmitter height is increased, the error is increased.

Equivalent Heights

In order to express the slant range r_d in terms of the curved distance d to a higher order of accuracy, the cosine law is applied to the triangle, transmitter-receiver-earth center. This gives the equation

$$r_d^2 = (ka + h_1)^2 + (ka + h_2)^2 - 2(ka + h_1)(ka + h_2)\cos\left(\frac{d}{ka}\right).$$

Selecting the relatively important terms of the order $d^2h_1h_2$ and $d^4(h_1 + h_2)$, as well as powers of d higher than the fourth, the above equation reduces to

$$r_d^2 = d^2 + (h_2 - h_1)^2 + \frac{d^2}{ka}\left(h_1 + h_2 - \frac{d^2}{12ka}\right). \qquad (57)$$

Solving equations (13) and (14) for h_1 and h_2 gives

$$h_1 = \frac{d_T^2}{2ka},$$

$$h_2 = \frac{d_R^2}{2ka}.$$

These results may also be expressed by saying that the distance from the surface of the earth to a plane which is tangent at a distance d_1 from the transmitter is $d_1^2/2ka$.

Hence for a transmitter of height h_1 above the ground the height above the tangent plane at the reflection point, the so-called *equivalent height* is, to a first approximation,

$$h_1' = h_1 - \frac{d_1^2}{2ka}, \qquad (58)$$

and for the receiver the equivalent height is

$$h_2' = h_2 - \frac{d_2^2}{2ka}. \qquad (59)$$

The equivalent heights are shown in Figure 14, which illustrates the geometry of the spherical earth having an effective radius of ka.

Angles

Referring to Figure 14 and remembering that the angles are greatly exaggerated in the figure, it is seen that

$$\tan\psi \cong \frac{h_1'}{d_1} = \frac{h_2'}{d_2}, \qquad (60)$$

$$\tan\gamma \cong \frac{h_2}{d} - \frac{d}{2ka}, \qquad (61)$$

$$\tan\psi_d \cong \frac{h_2 - h_1}{d} - \frac{d}{2ka}, \qquad (62)$$

$$\nu \cong \psi + \frac{d_1}{ka}. \qquad (63)$$

Angle ψ must be evaluated in order to determine the reflection coefficient. Angles ψ_d and ν determine the antenna pattern factors F_1 and F_2, which are shown in Figure 11. The angle γ is significant in coverage calculations and angular approximations.

Determination of Reflection Point (d_1)

Since several equations of the two preceding sections depend upon d_1, it is necessary to be able to determine this distance when the transmitter and receiver heights are given and the distance between them is known. Let

$$d_1 = \frac{d}{2}(1 + b), \qquad (64)$$

and

$$h_1 = \frac{(h_1 + h_2)}{2}(1 + c), \qquad (65)$$

so that

$$d_2 = \frac{d}{2}(1 - b), \qquad (66)$$

and

$$h_2 = \frac{h_1 + h_2}{2}(1 - c), \qquad (67)$$

where

$$b = \frac{d_1 - d_2}{d_1 + d_2}, \qquad (68)$$

and

$$c = \frac{h_1 - h_2}{h_1 + h_2}. \qquad (69)$$

Assume $h_1 > h_2$ and $d_1 > d_2$, so that b and c will always be positive. This is always possible because of the principle of reciprocity. From equation (60),

$$\frac{h_1'}{d_1} = \frac{h_2'}{d_2}$$

or

$$\frac{h_1}{d_1} - \frac{d_1}{2ka} = \frac{h_2}{d_2} - \frac{d_2}{2ka}. \qquad (70)$$

Substituting for d_1 and d_2 from equations (64) and (66),

$$\frac{h_1 + h_2}{d}\left(\frac{1+c}{1+b}\right) - \frac{d(1+b)}{4ka}$$

$$= \frac{h_1 + h_2}{d}\left(\frac{1-c}{1-b}\right) - \frac{d(1-b)}{4ka}.$$

Simplifying,

$$\frac{h_1 + h_2}{d} \cdot \frac{2(c-b)}{1-b^2} = \frac{bd}{2ka}.$$

Solving for c,

$$c = b + bm(1 - b^2), \qquad (71)$$

where

$$m = \frac{d^2}{4ka(h_1 + h_2)}. \qquad (72)$$

To determine d_1, equation (71) must be solved for b. This is a cubic equation, which is easily solved when m is small in comparison to unity. However, for m values comparable to unity, or larger, it is easier to plot a series of curves showing c as a function of m for assigned values of b ranging from 0 to 1. These are straight lines with a slope of $b(1 - b^2)$ and are given in Figure 15.

The procedure for calculating d_1 when h_1, h_2, and d are given is as follows:

1. Compute $c = \dfrac{h_1 - h_2}{h_1 + h_2}$.

2. Compute $m = \dfrac{d^2}{4ka(h_1 + h_2)}$.

3. Read b from Figure 15.

4. Calculate $d_1 = \dfrac{d}{2}(1 + b)$.

It should be noted that h_1 may be the height of either the transmitter or receiver. The only restrictions are that $h_1 > h_2$ and d_1 represents the distance from h_1.

Another method will now be given for calculating d_1. This method will be particularly useful when $d_1/d << 1$ and will be applied in Section 5.5.8 on generalized coordinates. Let

$$d_1 = sd, \quad s < 1. \qquad (73)$$

Hence

$$d_2 = (1 - s)d.$$

From equation (70)

$$\frac{h_1}{sd} - \frac{sd}{2ka} = \frac{h_2}{(1-s)d} - \frac{(1-s)d}{2ka}.$$
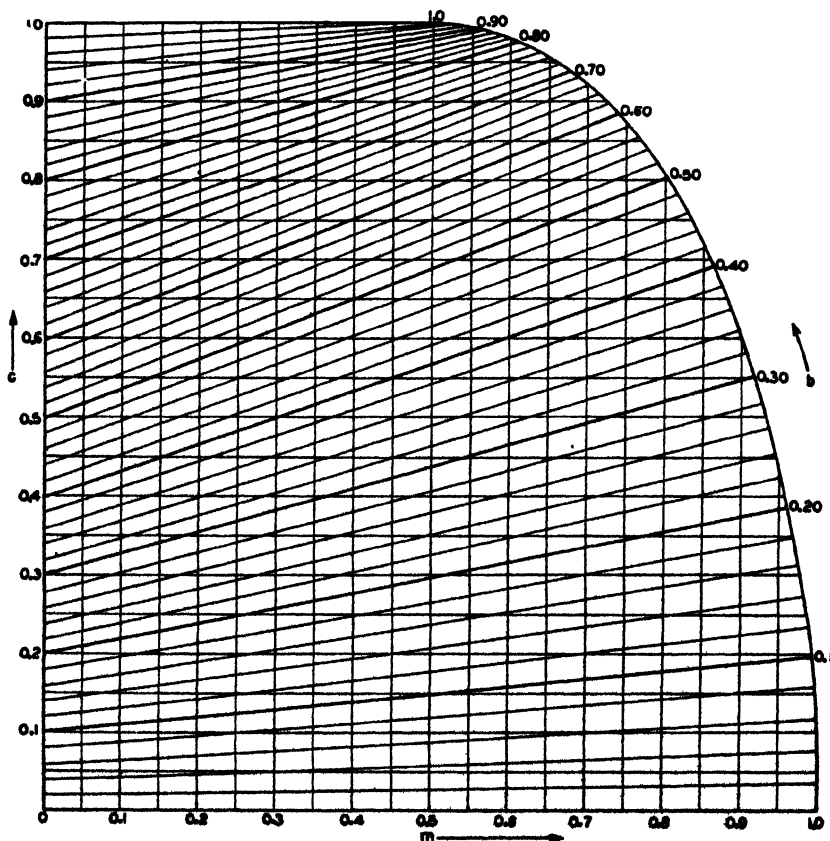
FIGURE 15.   Graph for obtaining b for given values of c and m.   (Marconi, Ltd.)

Simplifying,

$$s^3 - \frac{3}{2} s^2 - s\left[\frac{ka}{d^2}(h_1 + h_2) - \frac{1}{2}\right] + \frac{kah_1}{d^2} = 0. \quad (74)$$

If $s << 1$, the terms s^3 and s^2 may be neglected to a first approximation, and

$$s = \frac{h_1}{(h_1 + h_2) - \frac{d^2}{2ka}}. \quad (75)$$

If $d << d_L$, h_2 is well above the line of sight and s reduces to

$$s = \frac{h_1}{h_1 + h_2} = \frac{d_1}{d}. \quad (76)$$

Equation (76) is the plane earth formula.

Curves showing s as a function of h_2/h_1 and d/d_T are given in Figures 19 and 20. These may be used for the direct calculation of $d_1 = sd$ within the limits of interpolation.

Path Difference

Referring to Figure 14, the path difference Δ for a spherical earth is equal to

$$\Delta = r - r_d = \sqrt{d^2 + (h_2' + h_1')^2} \\ - \sqrt{d^2 + (h_2' - h_1')^2}. \quad (77)$$

It is usually sufficient to expand the square roots and neglect powers and products of h_1' and h_2' beyond the second. This gives

$$\Delta = r - r_d \cong \frac{2h_1' h_2'}{d}, \quad (78)$$

which is the same as the plane earth formula when h_1' and h_2' are written instead of h_1 and h_2. Equation (78) is accurate to within 1 per cent for values of γ (the angle at the base of the transmitter) less than about 8 degrees. The error is less than 10 per cent for values of γ less than about 24 degrees. When equation (78) is not sufficiently accurate, the following may be used:

$$\Delta = r - r_d = \frac{2h_1' h_2'}{\sqrt{d^2 + (h_1')^2 + (h_2')^2}}, \quad (79)$$

provided

$$\frac{1}{2} \frac{(h_1')^2 + (h_2')^2}{d^2} << 1.$$

All the above equations for the path difference depend upon the distance to the reflection point d_1. However, the calculation of d_1 may be eliminated by first computing the path difference from the plane earth formula and then subtracting the correction term $\Delta(\Delta_p)$. Thus

$$\Delta = \Delta_p - \Delta(\Delta_p), \quad (80)$$

where

$$\Delta_p = \frac{2h_1 h_2}{d},$$

and where

$$\frac{550}{h_1^{3/2}} \Delta(\Delta_p)$$

is given in Figure 16, plotted against

$$\frac{d}{d_L} = \frac{d}{\sqrt{2ka}} \cdot \frac{1}{\sqrt{h_1} + \sqrt{h_2}}.$$

If $h_2 < h_1$, interchange h_2 and h_1 on the curves and ordinate of Figure 16.

The maximum value of $\Delta(\Delta_p)$ is

$$\Delta(\Delta_p)_{max} = 5.33 \times 10^{-4} \frac{h_1 h_2}{\sqrt{h_1} + \sqrt{h_2}}. \quad (81)$$

If the plane earth correction factor is negligible for the wavelength under consideration, the plane earth formula may be used throughout the whole range within the optical region, not only for the given value of h_2/h_1 but for all lower values of h_2/h_1 with the same h_1.

When $h_2 >> h_1$, so that the reflection point is much closer to the transmitter than to the receiver, a good approximation to Δ is obtained by replacing h_1' by h_1 and h_2' by $h_2 - d^2/2ka$ in equation (78).
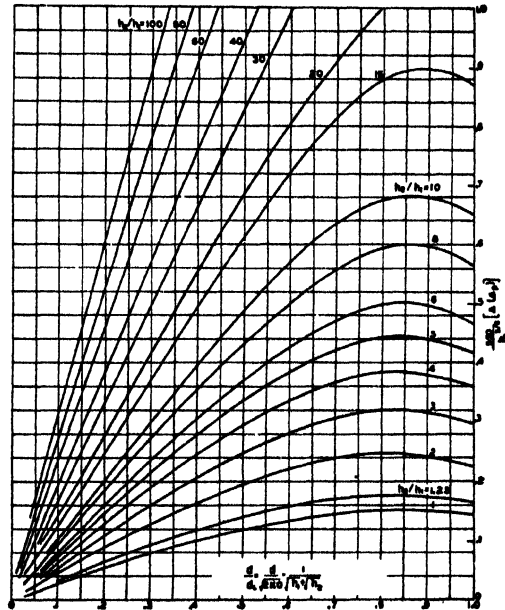
FIGURE 16. Plane earth correction factor versus $\frac{d}{d_L}$ (Radiation Laboratory.)

Then

$$\Delta \cong \frac{2h_1}{d}\left(h_2 - \frac{d^2}{2ka}\right),$$

which, to the same approximation, means that

$$\Delta \cong 2h_1 \tan \gamma. \quad (82)$$

In general, equation (82) is an improvement over the plane earth approximation except close to the transmitter and at low heights where h_2 is not much greater than h_1.

The dependence of path difference upon distance and height may be seen by considering the path difference parameter

$$R = \frac{ka\,\Delta}{h_1 d_T}. \tag{83}$$

Since $h_2' = h_1'd_2/d_1$, it follows from equations (78) and (59) that

$$\Delta = \frac{2h_1'h_2'}{d} = \frac{2(h_1')^2 d_2}{dd_1} = \frac{2d_2}{d}h_1^2\frac{\left(1 - \frac{d_1^2}{2kah_1}\right)^2}{d_1}.$$

and

$$R = \frac{d_2}{d} \times \frac{[1 - (d_1/d_T)^2]^2}{d_1/d_T}$$

Hence, using $d_T^2 = 2kah_1$,

$$\Delta = \frac{2h_1^2}{d_T}\left(\frac{d_2}{d}\right)\frac{[1 - (d_1/d_T)^2]^2}{d_1/d_T}, \tag{84}$$

$$= \left(1 - \frac{d_1/d_T}{d/d_T}\right)\frac{[1 - (d_1/d_T)^2]^2}{d_1/d_T}. \tag{85}$$

The form of this expression suggests the introduction of two new dimensionless parameters

$$p = \frac{d_1}{d_T} \text{ and } v = \frac{d}{d_T}. \tag{86}$$

In terms of these parameters, equation (85) for R assumes the form

$$R = \left(1 - \frac{p}{v}\right)\frac{(1 - p^2)^2}{p}, \tag{87}$$

and in terms of s and v

$$R = (1 - s)\frac{(1 - s^2v^2)^2}{sv}. \tag{88}$$

Divergence Factor

The reflection of a beam of radiation from the spherical earth increases the divergence of the beam and reduces the intensity of the reflected wave by spreading, as explained in preceding text. This is taken into account by introducing a divergence factor D, less than unity, which appears in the formulas as a multiplier of the plane earth reflection coefficient. Expressions for D are

$$D = \frac{1}{\sqrt{1 + 2h_1'h_2'/kad\tan^2\psi}}. \tag{89}$$

Using equation (60), D becomes

$$D = \frac{1}{\sqrt{1 + 2d_1^2 d_2/kah_1'd}}. \tag{90}$$

If $d_2 \to d$,

$$D = \frac{1}{\sqrt{1 + 2h_1'/ka\tan^2\psi}} \quad (\gamma < 3°) \tag{91}$$

and if ψ is small, so that $\tan\psi \to \psi$,

$$D = \frac{1}{\sqrt{1 + 2h_1'/ka\psi^2}}. \tag{92}$$

Parameters p and q

Useful expressions for the divergence factor, path difference, and receiver height may be obtained by use of the dimensionless parameters,

$$p = \frac{d_1}{\sqrt{2kah_1}} = \frac{d_1}{d_T} \tag{93}$$

and

$$q = \frac{d_2}{d} \tag{94}$$

or

$$d_1 = (1 - q)d = sd. \tag{95}$$

The divergence factor may be expressed directly in terms of p and q by modifying equation (90) as follows:

$$D = \frac{1}{\sqrt{1 + 2d_1^2 d_2/kah_1'd}}$$

$$= \frac{1}{\sqrt{1 + \frac{4(d_2/d)\,(d_1^2/2kah_1)}{1 - (d_1^2/2kah_1)}}},$$

where h_1' has been replaced by its equivalent expression, given in equation (58). The above form of D shows that it can be expressed in terms of p and q only:

$$D = \frac{1}{\sqrt{1 + 4p^2q/(1 - p^2)}}. \tag{96}$$

Figure 17 shows contours of constant D as a function of p and q.

The path difference Δ may be written in terms of p and q by substituting into equation (78):

$$\Delta = \frac{2h_1'h_2'}{d} = \frac{2(h_1')^2 d_2}{dd_1} = \frac{2d_2}{d}h_1^2\frac{(1 - d_1^2/2kah_1)^2}{d_1}.$$

Hence, on using equations (93), (94), and (95),

$$\Delta = \frac{2h_1^2}{d_T}q\frac{(1 - p^2)^2}{p}. \tag{97}$$

Figure 18 shows $(1 - p^2)^2/p$ as a function of p.

The receiver height h_2 may also be expressed in terms of h_1, p, and q. This will be found useful in drawing coverage diagrams in which both h_2 and d are unknowns. From equation (60)

$$\frac{h_1'}{d_1} = \frac{h_2'}{d_2}$$

or

$$h_2 - \frac{d_2^2}{2ka} = \frac{d_2}{d_1}\left(h_1 - \frac{d_1^2}{2ka}\right).$$
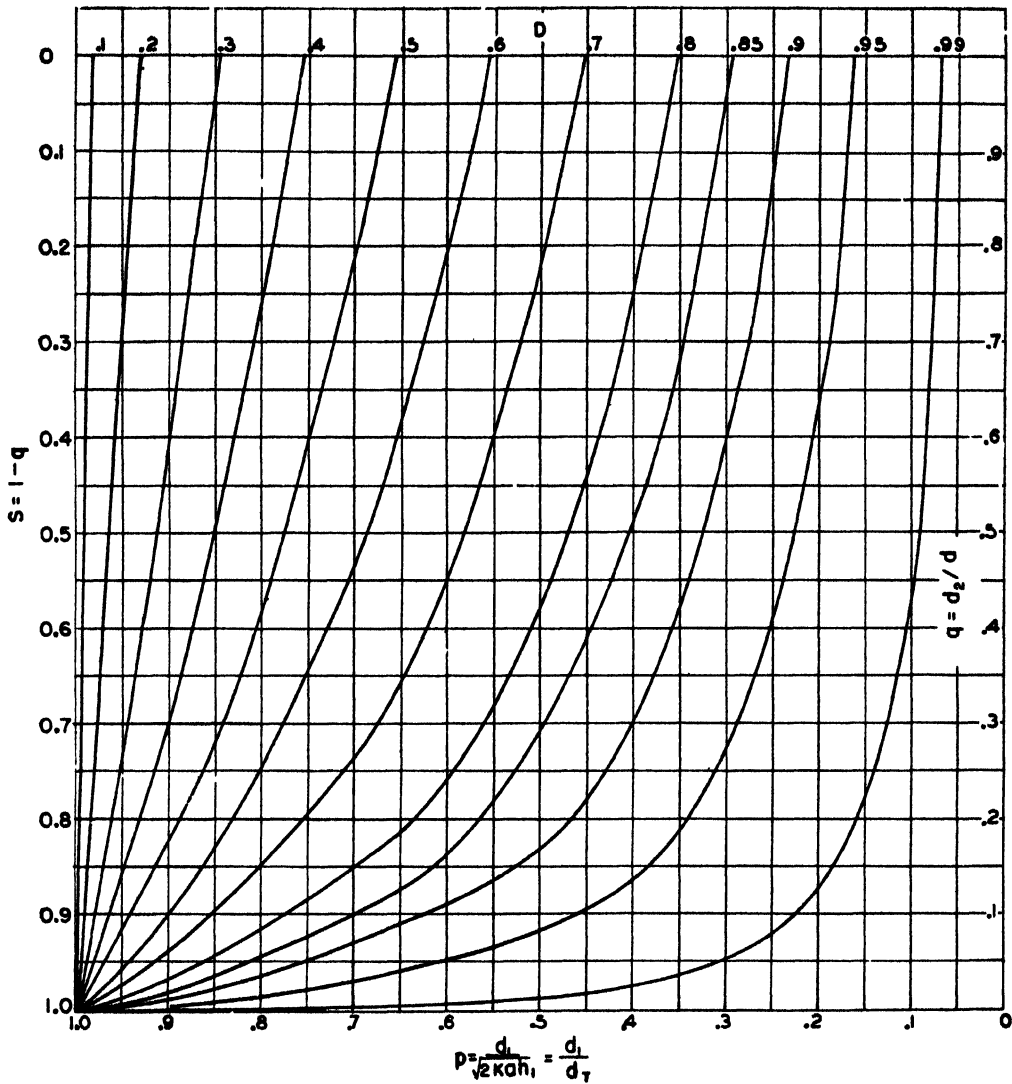
FIGURE 17. Divergence factor D as a function of p and q or p and s. (Radiation Laboratory.) ($p = 1$ is the line of sight where $D = 0$.) *Note:* $S = 1 - q = d_1/d$.
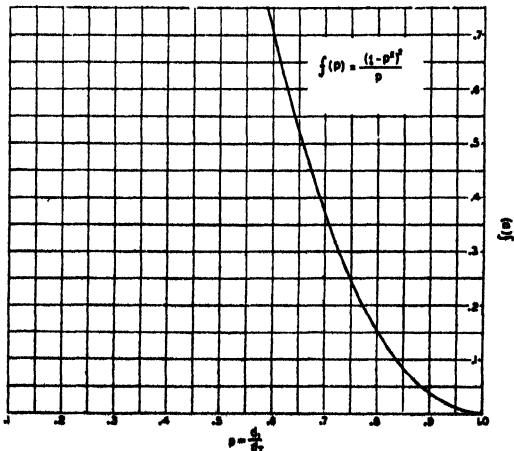
FIGURE 18. $(1 - p^2)^2/p$ as a function of p. (Radiation Laboratory.)

Hence it follows that

$$h_2 = h_1\left[\left(1 - \frac{d_1{}^2}{2kah_1}\right)\frac{d_2}{d_1} + \frac{d_2{}^2}{2kah_1}\right].$$

Since

$$\frac{d_2}{d_1} = \frac{d_2}{(1 - q)d} = \frac{q}{1 - q},$$

$$h_2 = h_1\left(\frac{q}{1 - q}\right)\left(1 - p^2 + \frac{qp^2}{1 - q}\right). \quad (98)$$

Generalized Coordinates

The distance from the transmitter to the reflection point d_1 and the ratio p may be eliminated by using the dimensionless coordinates

$$u = \frac{h_2}{h_1}, \quad (99)$$
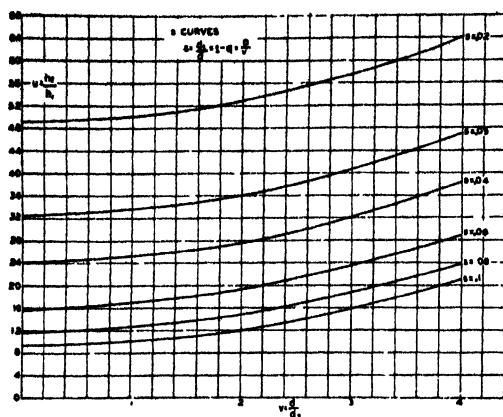
FIGURE 19. s as a function of u and v. (See Figure 14 for definition of lengths.)

FIGURE 20. s is a function of u and v. (See Figure 14 for definition of lengths.)

$$v = \frac{d}{d_T}. \qquad (100)$$

The advantage of this substitution lies in the fact that the coefficients of $s = d_1/d$ in the cubic equation (74) may be expressed as functions of u and v only. Thus,

$$s^3 - \frac{3}{2}s^2 - s\left[\frac{ka}{d^2}(h_1 + h_2) - \frac{1}{2}\right] + ka\frac{h_1}{d^2} = 0,$$

or

$$s^3 - \frac{3}{2}s^2 - \frac{1}{2}s\left[\frac{(1 + h_2/h_1)}{d^2/(2kah_1)} - 1\right] + \frac{1}{2d^2/(2kah_1)} = 0.$$
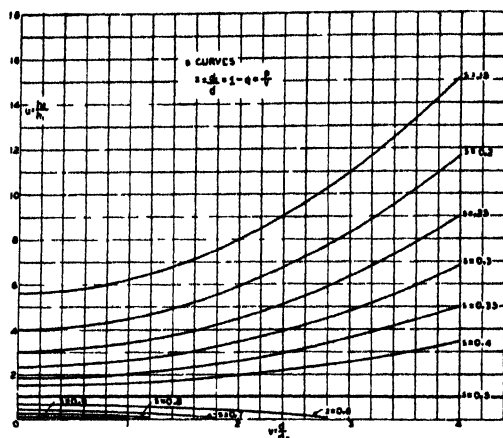
In terms of u and v,

$$s^3 - \frac{3}{2}s^2 - \frac{s}{2}\left(\frac{1 + u}{v^2} - 1\right) + \frac{1}{2v^2} = 0. \qquad (101)$$

Figures 19 and 20 show contours of constant s plotted in u, v coordinates. The curves are parabolas.

The divergence factor D is given by

$$D = \frac{1}{\sqrt{1 + 4p^2q/(1 - p^2)}}, \qquad (102)$$

where

$$p = sv$$
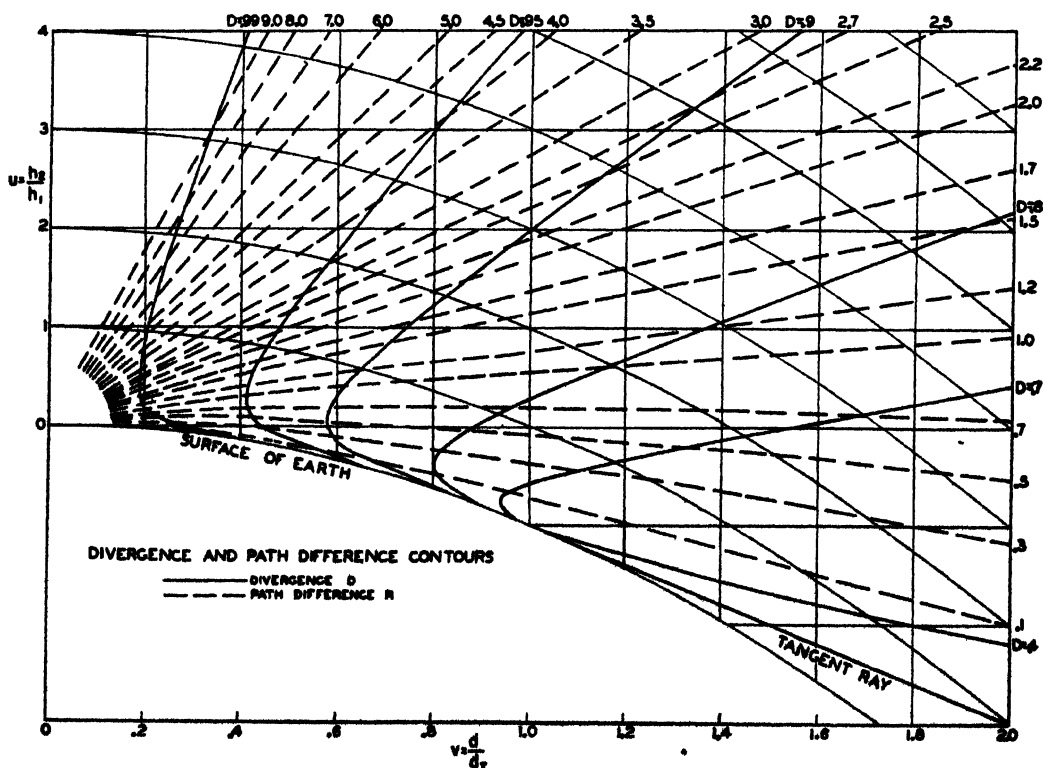
FIGURE 21.   Contours of constant divergence factor D and path difference variable R. (Radiation Laboratory.)
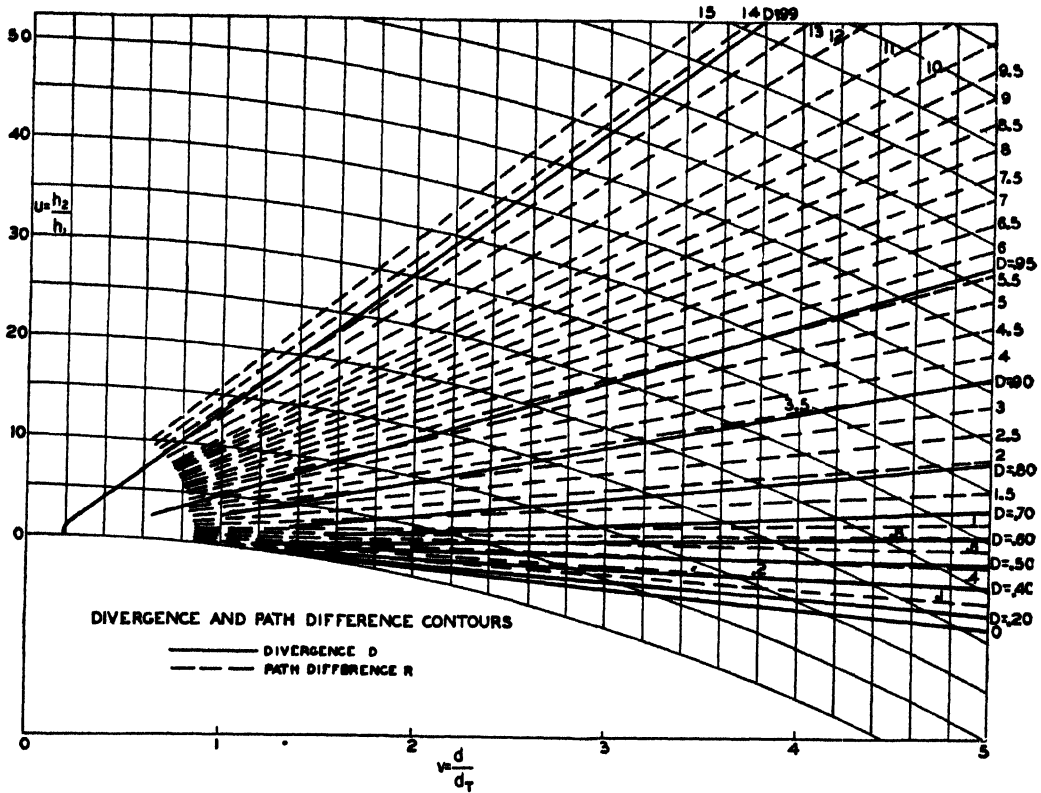
FIGURE 22. Contours of constant divergence factor D and path difference variable R. (Radiation Laboratory.)
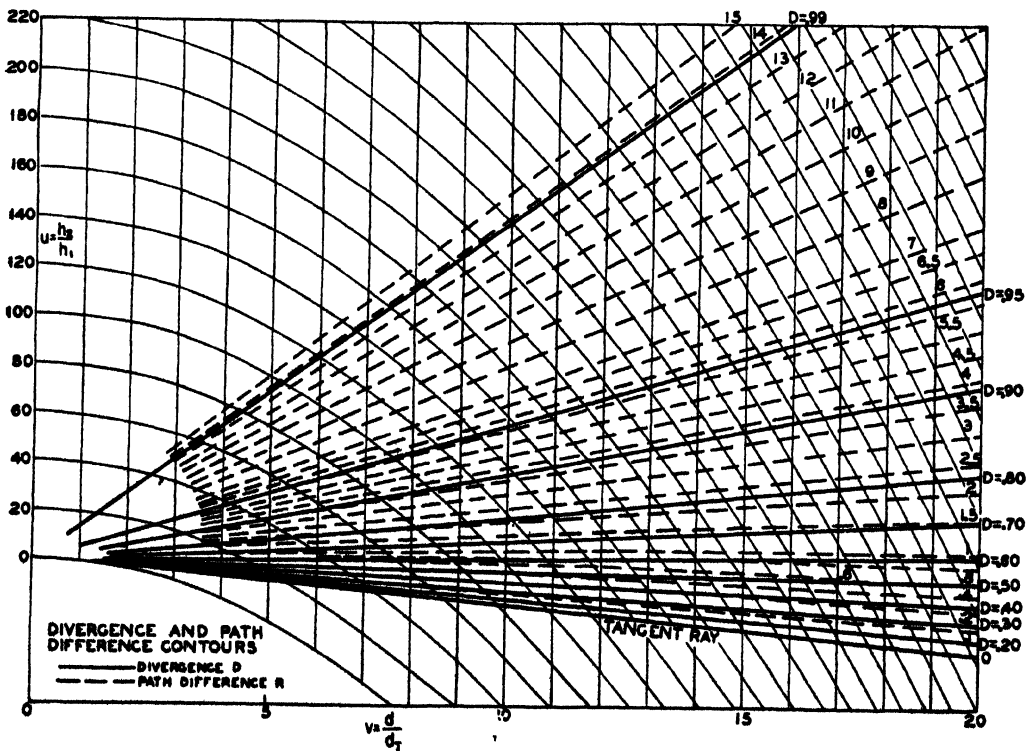
FIGURE 23. Contours of constant divergence factor D and path difference variable R. (Radiation Laboratory.)

and

$$q = \frac{d_2}{d} = \frac{d - d_1}{d} = 1 - \frac{d_1}{d} = 1 - s. \quad (103)$$

Since s is a function of u and v only, it follows that D may be plotted in u, v coordinates. This may be accomplished by solving equation (96) with respect to q, which gives

$$q = \frac{(1 - p^2)(1 - D^2)}{4p^2D^2}. \quad (104)$$

Equation (103) gives $s = 1 - q$; $v = p/s$, and u may be read from Figure 19 or 20. Contours of constant D are shown in Figures 21, 22, and 23.

The grazing angle ψ is important in calculations for vertical polarization since it determines the magnitude and phase of the reflection coefficient for a particular frequency and reflecting surface. The grazing angle ψ may be expressed in terms of s, u, and v, as follows. From equation (60),

$$\tan \psi \cong \frac{h_1'}{d_1} = \frac{h_1}{d_1}\left(1 - \frac{d_1^2}{2kah_1}\right). \quad (105)$$

Hence

$$\tan \psi = \frac{h_1}{d_T(sd/d_T)}(1 - s^2v^2) = \frac{h_1}{d_T}\left(\frac{1}{sv} - sv\right)$$

or

$$\frac{\tan \psi}{\sqrt{h_1}} = \frac{1}{\sqrt{2ka}}\left(\frac{1}{sv} - sv\right), \quad (106)$$

and for $k = 4/3$,

$$\frac{\tan \psi}{\sqrt{h_1}} = 2.4 \times 10^{-4}\left(\frac{1}{sv} - sv\right). \quad (107)$$

From Figure 24, ψ may be obtained for given values of h_1 and $sv = p$.

The generalized coordinates described in this section will be found highly useful both in field strength and coverage calculations.

ILLUSTRATIVE CALCULATIONS FOR THE OPTICAL-INTERFERENCE REGION

Introduction

The general expression for the gain factor A in the interference region is obtained by combining equations (44) and (7). Then

$$A = A_0F_1\sqrt{(1 - K)^2 + 4K \sin^2 \frac{\Omega}{2}}. \quad (108)$$

The value of the radio gain is then given by equation (3) and the value of radar gain is given by equation (5). The value of the radical which defines the interference pattern has a range of values between 0 and 2. The extreme values can occur only when $K = 1$ ($p = 1$, $D = 1$, $F_2/F_1 = 1$); the value 0 (nulls) is then given by $\sin^2(\Omega/2) = 0$ and the value 2 (maxima) is given by $\sin^2(\Omega/2) = 1$.

In general, the value of A lies between the two extremes

$$A = A_0F_1(1 \pm K),$$

the positive sign giving a maximum and the negative giving a minimum. At any other point, the value lies between these two extremes. For range calculations (which involve maxima), the variation in A is from 1 to 2 times the free-space value, according to the value of K, so that in practice a quick rule of thumb for range may be devised. Assume $(1 + K)$ equal to 1.9 for favorable conditions (sea water, horizontal polarization, or, in the case of vertical polarization, small grazing angles) down to $(1 + K) = 1$ or $K = 0$ for propagation over rough terrain. The problem of finding the range is thus reduced to a problem for free space. In range calculations, P_2/P_1 is given by the ratio of minimum detectable power to power output. A is then determined by equations (3) or (5), and the range is given by finding d from the relation (writing $A_0 = 3\lambda/8\pi d$)

$$A = \left(\frac{3\lambda}{8\pi d}\right)(1 + K). \quad (109)$$

More detailed calculations are presented in this section. However, the assumption is made generally that the reflection coefficient is equal to -1 (i.e., $\rho = 1$ and $\phi = 180$ degrees) and that the direct and reflected rays do not differ appreciably on account of the shape of the antenna beam pattern ($F_2 = F_1$). For large distances over sea water, these assumptions are approximately realized. For most of the calculations it offers no inherent difficulty to consider the effect of directivity or of a reflection coefficient different from -1 but may require considerable additional calculation.

For convenience, the formulas required in the calculations are recapitulated here. Putting $p = F_1 = F_2 = 1$, equation (108) takes the form

$$A = A_0\sqrt{(1 - D)^2 + 4D \sin^2 \frac{\Omega}{2}} \quad (110)$$

or, in decibels,

$$20 \log A = 20 \log A_0 + 10 \log\left[(1 - D)^2 + 4D \sin^2 \frac{\Omega}{2}\right].$$

The reflection point variable

$$p = \frac{d_1}{d_T} = \frac{d_1}{\sqrt{2kah_1}} \quad (111)$$

$$= \frac{d_1}{(4120\sqrt{h_1})} \quad \text{(when } k = 4/3\text{)}$$

will be used extensively. It has been found that the interference pattern is very sensitive to slight changes in p, so that an accuracy to the fourth significant figure is generally required.

The path difference variable R is related to $p = d_1/d_T$
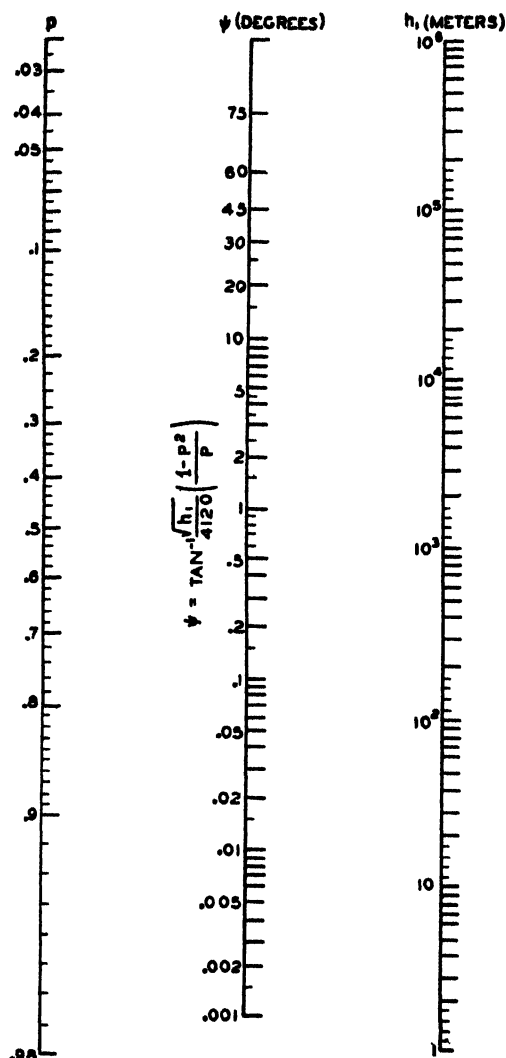
FIGURE 24. ψ as a function of h_1 and $p = sv = d_1/d_T$. [See equation (107).] (See Figure 14 for definition of lengths.)

and $v = d/d_T$ by the equation

$$R = \left(\frac{1}{p} - \frac{1}{v}\right)(1 - p^2)^2. \qquad (112)$$

Resolved with respect to $1/v$, this equation assumes the form

$$\frac{1}{v} = \frac{1}{p}\left(1 - \frac{Rp}{(1 - p^2)^2}\right) = \frac{1 - q}{p} \qquad (113)$$

Another convenient expression for R is obtained by replacing, in equation (83), the path difference Δ by $n\lambda/2$, where n (see below) may assume any positive value. Substituting $\sqrt{2kah_1}$ for d_T, equation (83) assumes the form

$$R = nr, \qquad (114)$$

where

$$r = \frac{1}{2}\sqrt{\frac{ka}{2}}\frac{\lambda}{h_1^{3/2}} \qquad (115)$$

or $\qquad r = 1030 \dfrac{\lambda}{h_1^{3/2}}$ (for $k = 4/3$).

A graphical representation of r is given in Figure 15 in Chapter 6.

Then for a reflection coefficient of $\rho = 1$, $\phi = 180$ degrees (i.e., $\phi' = 0$), equation (29) gives

$$\Omega = \delta = \frac{2\pi}{\lambda}\Delta = n\pi. \qquad (116)$$

If r is fixed, a complete pattern of contour lines (along which A is constant) is determined. Take as independent variables p and n (rather than u and v). A given choice of p and n determines R by equation (114), Ω by equation (116), v by equation (113), s by equation (118), u by equation (121), D by equation (117), and finally $20 \log A$ by equation (110). By varying r, new patterns are obtained. Accordingly, r may be called a pattern or chart parameter (see page (446)..3).

The lobes on the charts depend on n, in accordance with equation (116). Accordingly, for $\rho = 1$, $\phi = 180$ degrees, n is the lobe variable. For the first (lowest) lobe, $n = 0$ gives the first null, $n = 1$ gives the first maximum and $n = 2$ the second null. For the second lobe, n varies from 2 to 4, with a maximum at $n = 3$, and so on. It should be remembered that if $n < 1$, corresponding to the lower side of the lowest lobe, the value of the field (or of A) given by the optical formula is too low. A more accurate value can be obtained by joining the curves found in the optical and diffraction regions into a smooth overall curve.

Combining equations (102), (103), and (113) gives the divergence factor D,

$$D = \left[1 + \frac{4Rp^3}{(1 - p^2)^3}\right]^{-1/2} = \left[1 + \frac{4Rp^2}{1 - p^2}\cdot\frac{d_2}{d}\right]^{-1/2} \qquad (117)$$

The variable $s = d_1/d$ is

$$s = p/v, \qquad (118)$$

and, repeating equation (101),

$$s^3 - \frac{3}{2}s^2 - \frac{s}{2}\left(\frac{1 + u}{v^2} - 1\right) + \frac{1}{2v^2} = 0. \qquad (119)$$

In terms of p, equation (119) becomes

$$2p^3 - 3p^2v + p(v^2 - u - 1) + v = 0. \qquad (120)$$

Equation (120), resolved for v and u, gives

$$v = \frac{1}{2}\left[3p - \frac{1}{p} + \sqrt{\left(\frac{1}{p} - p\right)^2 + 4u}\right],$$

$$u = 2p^2 - 3pv + \frac{v}{p} - 1 + v^2. \qquad (121)$$

Some useful approximations:

For v large, $q \to 1$ and $R = \dfrac{q}{p}(1 - p^2)^2$ approaches the value

$$R \sim \frac{1}{p} - 2p, \qquad (122)$$

which, solved for p, becomes

$$p \sim \frac{-R + \sqrt{R^2 + 8}}{4}.$$ (123)

If $R > 2$,

$$p \sim \frac{1}{R}.$$ (124)

If $R < 2$,

$$p \sim \frac{3 - R}{4}.$$ (125)

For $R > 3$,

$$D \sim 1.$$ (126)

The calculations will be divided into four types.

Type I. The direct calculation of the radio gain (or field) when the heights and distance apart of the antennas and the wavelength are given.

Type II. The calculation of the radio gain as a function of the receiver height h_2 when the transmitter antenna height h_1, distance d, and wavelength λ are given.

Type III. The calculation of the radio gain as a function of the distance d when the transmitter antenna height h_1, receiver height h_2, and wavelength are given.

Type IV. The calculation of the possible positions of the receiver in space (h_2,d) when the radio gain will have the given value for given values of the gain factor A, the transmitter antenna height h_1, and the wavelength λ. Special cases, such as the receiver antenna height, h_2 for given d, or d for given h_2, can be solved by use of the curves in Type II and Type III.

This type of problem is of importance in estimating the range of a set when the minimum detectable power of the receiver and power output of the transmitter are known.

Problem of Type I. Radio Gain for Fixed Heights and Distance

The radio gain at a given receiver is to be found, their heights, as well as the wavelength being given.

The polarization is assumed horizontal, the effective earth's radius $4a/3$.

The following data are assumed.

Transmitter height: $h_1 = 50$ meters
Receiver height: $\quad h_2 = 1{,}500$ meters
Distance apart: $\quad d = 100$ kilometers
Wavelength: $\quad \lambda = 1$ meter $(f = 300$ mc$)$
Gains (over doublet): $G_1 = G_2 = 100$ (20 db)

ONE-WAY TRANSMISSION

1. $d_L = 188$ kilometers (Figure 2). $d < d_L$, so that the receiver is in the optical region.

2. The u,v coordinates of the receiver are

$$u = \frac{h_2}{h_1} = \frac{1{,}500}{50} = 30,$$

$$d_T = \sqrt{2kah_1} = 29{,}100 \text{ meters}$$

$$v = \frac{d}{d_T} = \frac{100}{29.1} = 3.43.$$

3. Referring to Figure 19, s ($= p/v$) is estimated to be 0.05. Since the result is very sensitive to slight changes in s, it is desirable to improve the value of s. In Newton's method, the next approximation, using equations (101) or (119), is

$$s' = s - \frac{f(s)}{f'(s)} = \frac{2s^3 - \frac{3}{2}s^2 - \frac{1}{2v^2}}{3s^2 - 3s - \frac{1}{2}\left[\frac{1+u}{v^2} - 1\right]}, \quad (127)$$

$$s' = 0.04794.$$

The next approximation gives the same result.

4. Using the above value of s' and the relation $p = sv$ ($v = 3.43$), p is equal to

$$p = 0.1645.$$

With the value of $p = 0.1645$, equation (117) and Figure 22 give the value

$$D = 0.95.$$

5. The path difference variable R is obtained from equation (112) or Figures 21, 22, 23, as

$$R = 5.477.$$

6. The number r, from equation (115), is 2.91, so that the lobe number n is

$$n = \frac{R}{r} = 1.88.$$

Hence the receiver is on the upper part of the first lobe close to a null.

7. $\quad \Omega = n\pi = 5.9$ [see equation (116)],

$$\frac{\Omega}{2} = 2.95,$$

$$\sin^2 \frac{\Omega}{2} = 0.0353.$$

8. To use equation (110), the value of the free-space gain factor A_0 is needed. Figure 3 in Chapter 2 gives

$$20 \log A_0 = -118.$$

Substituting in equation (110),

$$20 \log A = 20 \log A_0 + 10 \log (0.0025 + 0.1342)$$
$$= -118 - 8.64 \cong -127$$

By equation (3), using gains of 20 db,

$$10 \log \frac{P_2}{P_1} = -127 + 40 = -87.$$

Accordingly the radio gain is -87 db and the received power is given by

$$P_2 = P_1 10^{-8.7}.$$

Suppose the receiver has a minimum detectable power of 10^{-10} watt, then the required minimum

power output under the given conditions would be

$$P_1 = P_2 \times 10^{8.7}$$
$$= 10^{-10} \times 10^{8.7} = 10^{-1.3} \text{ watts.}$$

RADAR

Suppose that, instead of a receiver, there is a target at the same position with a radar cross section of $\sigma = 50$ square meters. The value of P_2/P_1 at the radar receiver can be found from equation (5) using the value of A found above and the given values of σ and λ. If the radar uses the same antenna for transmitting and receiving, $G_1 = G_2$, which in this case is 100 or 20 db, and the radar gain

$$10 \log \frac{P_2}{P_1} = 20 \log G_1 + 10 \log \frac{16\pi}{9} + 10 \log \sigma$$
$$+ 40 \log A - 20 \log \lambda,$$
$$= 40 + 7.5 + 17 - 254 - 0,$$
$$= -189.5 \text{ db}$$

This gives $P_1 = 10^{8.9}$ watts, which obviously is unattainable.

EFFECT OF VERTICAL POLARIZATION

The general value for K in equation (108), when the reflection coefficient ρ differs from -1 and $F_2/F_1 = 1$ is

$$K = \rho D. \qquad (128)$$

Ω in equation (108) is no longer given by equation (116) but is the sum of two phase shifts, one caused by path difference, $(R/r)\pi = n\pi$, while the other is $\phi' = \phi - \pi$, the difference between the phase of the reflection coefficient and that for perfect reflection. Hence

$$\Omega = \frac{R}{r} \pi + \phi - \pi. \qquad (129)$$

The lobe variable (for imperfect reflection) is now N, defined by

$$\Omega = N\pi \qquad (130)$$

rather than $n = R/r$. The relation between N and n is derivable from equation (129), giving

$$N = n - \frac{\pi - \phi}{\pi}. \qquad (131)$$

The propagation is assumed to take place over sea water. The angle between the reflected wave and the earth is given by equation (107) or Figure 24, and is

$$\Psi = 0.582°.$$

From Figures 14 and 15 in Chapter 4,

$$\phi = 168°, \ \rho = 0.76.$$

The lobe variable N, in terms of the old lobe variable (for $\rho = 1, \phi = 180°$), by equation (131), is

$$N = 1.88 - \frac{12}{180} = 1.81,$$

$$\frac{\Omega}{2} = 163°,$$

$$\sin^2 \frac{\Omega}{2} = 0.085.$$

The fact that $N < n$ signifies that the lobe for vertical polarization (other things being equal) has a greater angle of elevation than the lobe for horizontal polarization.

$$K = \rho D = 0.76 \times 0.95 = 0.722$$

The value of $10 \log \left[(1 - K)^2 + 4K \sin^2 \frac{\Omega}{2} \right]$
$$= 10 \log 0.322 = -5.$$

Therefore, for vertical polarization,

$$20 \log A = -118 - 5 = -123,$$

which may be compared with the value $20 \log A = -127$, obtained for horizontal polarization with $\rho = 1$.

Type II. Radio Gain Versus Receiver Height for Given Distance

Radio gain versus receiver antenna height are to be found, while transmitter antenna height, wavelength, and distance are given.

Suppose that a radar set has an antenna height of 30 meters, and an antenna gain of 13.5 db. Polarization is horizontal and the wavelength is 1.5 meters. Assume also a receiver with a gain of $G_2 = 1$ (or 0 db) at a distance of 100 km.

The following calculations are made:

1. The variation of the radio gain P_2/P_1, with receiver antenna height h_2 is to be found.

2. Instead of a receiver assume a target with cross section of 50 square meters. The value of the radar gain P_2/P_1 at the radar receiver is to be found as a function of target height h_2.

The diffraction part of the calculation is given on pp. 413-416; the optical part in this section. The results are represented in Figure 25, the two partial curves for one-way transmission having been combined into a smooth overall curve which makes possible the estimation of $10 \log P_2/P_1$ in the transition region near the line of sight. The radar gain varies as $40 \log A$ [equation (5)] rather than as $20 \log A$ and contains a constant shift $10 \log [G_1^2(16\pi\sigma/9\lambda^2)]$ rather than $10 \log G_1 G_2$.

RADIO GAIN: ONE-WAY TRANSMISSION

The calculation is most readily performed by using $p = d_1/d_T$ as the independent variable and then finding the corresponding values of h_2, the receiver height, and A.

1. From Figure 15 in Chapter 6 or equation (115),

$$r = 9.403.$$

For $n = 1$, corresponding to the first maximum, p is approximately $1/r$, since $R = nr > 2$. Accordingly, we begin with $p = 0.1$.

2. $d_T = 22.5$ km (from Figure 2), and
$$v = \frac{d}{d_T} = \frac{100}{22.5} = 4.45.$$

3. From equation (112),
$$R = 9.58.$$

4. From equation (121),
$$u = \frac{h_2}{h_1} = 62.028$$

and hence
$$h_2 = 1,861 \text{ meters.}$$

5. At $d = 100$ km, the free-space attenuation (Figure 3 in Chapter 2) is
$$20 \log A_0 = -115.$$

FIGURE 25. Radio gain in decibels versus height h_2. Horizontal polarization.

6. Compute the factor
$$\sqrt{(1 - D)^2 + 4D \sin^2 \frac{\Omega}{2}}.$$

From equation (117)
$$D = 0.980,$$
$$n = \frac{R}{r} = 1.019,$$
$$\Omega = n\pi = (1.019) \cdot (3.1416) = 3.19 \text{ radians,}$$
$$\frac{\Omega}{2} = 1.60 \text{ radians,}$$
$$\sin^2 \frac{\Omega}{2} = 0.9992.$$

From Figure 12,
$$20 \log \sqrt{(1 - D)^2 + 4D \sin^2 \frac{\Omega}{2}} = 6 \text{ db.}$$

Hence
$$20 \log A = -115 \text{ db} + 6 \text{ db} = -109 \text{ db, and}$$
$$10 \log \frac{P_2}{P_1} = -109 \text{ db} + 10 \log G_1 G_2 = -95.5 \text{ db.}$$

7. The foregoing values, together with results obtained with other values of p, are listed in Table 1. The value of P_2/P_1 [equation (3)] is represented graphically in Figure 25.

RADAR GAIN: TWO-WAY TRANSMISSION

Knowing the values of $20 \log A$, the corresponding values of P_2/P_1 are given by equation (5). Taking $G_1 = G_2 = 13.5$ db, $16\pi/9 = 5.58$, $\lambda = 1.5$,
$$10 \log \frac{P_2}{P_1} = 27 + 7.5 + 17 + 40 \log A - 20 \log 1.5,$$
$$= +40 \log A + 48.$$

Type III. Radio Gain Versus Distance for Given Antenna Heights

A radar used over the sea has a wavelength of 1.5 meters. The transmitter is 30 meters above sea level and the target is at an altitude of 1,000 meters above the sea. The power gain of the transmitting antenna is 13.5 db, the polarization horizontal. The one-way radio gain is to be found as a function of distance. Also, the radar gain at the

p	R	s	h_2	n	$\frac{\Omega}{2}$	D	†	Radio Gain $10 \log \frac{P_2}{P_1}$	Radar Gain $10 \log \frac{P_2}{P_1}$
0.15	6.16	0.0337	1,396	0.655	1.03	0.96	5	−96.5	−172
0.1	9.58	0.0225	1,861	1.019	1.60	0.98	6	−95.5	−170
0.05	19.68	0.0112	3,216	2.09	3.29	0.995	−11	−112.5	−204
0.04	24.70	0.00896	3,885	2.63	4.13	0.997	4	−97.5	−174
0.03	33.05	0.0067	5,005	3.51	5.52	0.998	3	−98.5	−176
0.02	49.74	0.0045	7,285	5.29	8.31	0.999	5	−96.5	−172
0.01	99.76	0.0022	13,917	10.61	16.67	1.000	4	−97.5	−174

* See also Table 5.

† $20 \log \sqrt{(1-D)^2 + 4D \sin^2 (\Omega/2)}$.
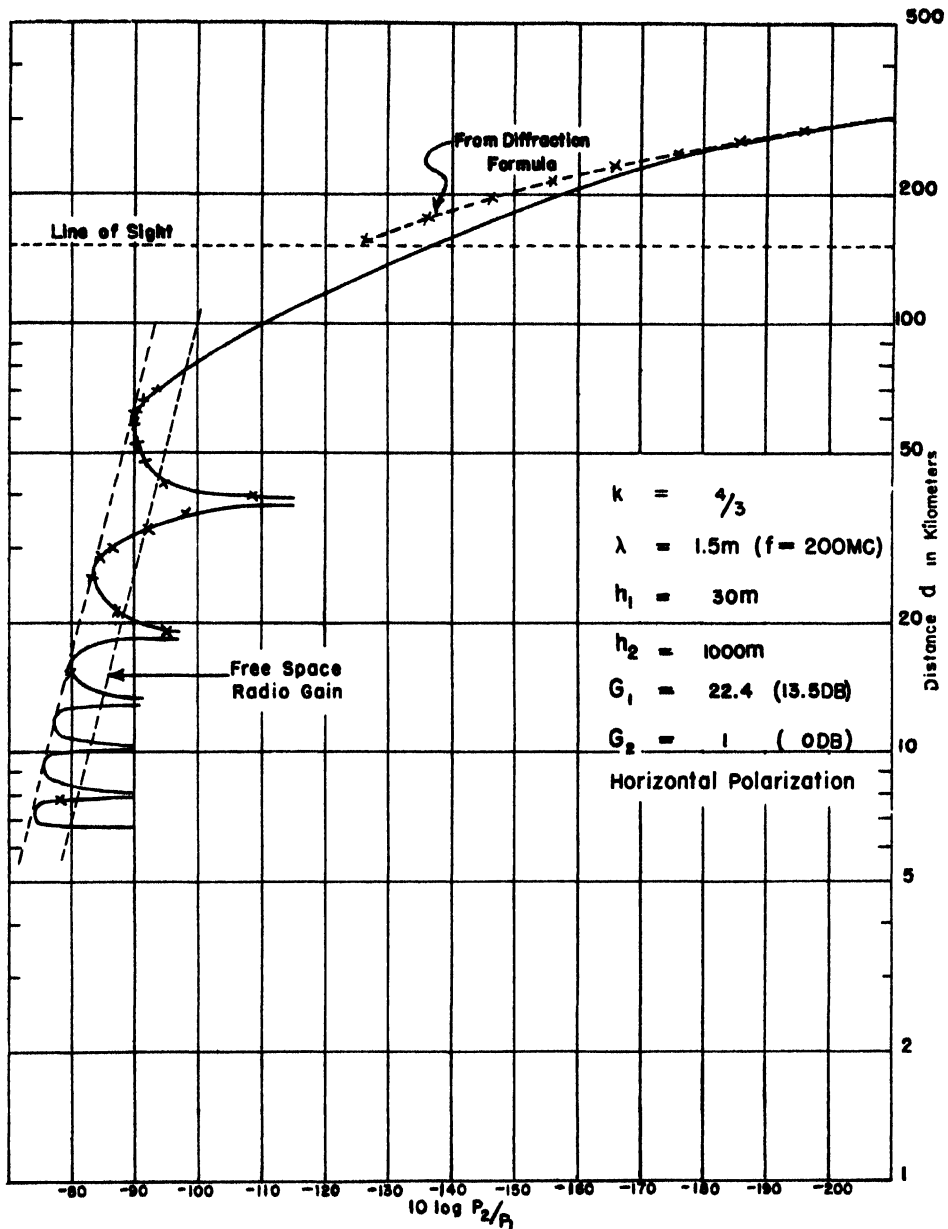
FIGURE 26.   Radio gain (in db) versus distance.

radar set by echo from the target of cross section $\sigma = 10$ square meters is to be calculated.

RADIO GAIN: ONE-WAY TRANSMISSION (see Figure 26).

1. The number r from Figure 15 in Chapter 6 or equation (115) is found to be 9.403.

2. $u = h_2/h_1 = 33.3$.

3. For $r > 2$ and $n = 1$, p is approximately equal to $1/r$. Hence we start with $p = 0.1$.

4. Equation (121), with $p = 0.1$ and $u = 33.3$, gives $v = 2.76$.

5. From equation (112), $R = 9.445$.

6. $n = R/r = 1.005$. Hence the target is on the first (i.e., lowest) lobe. Moving in the direction of increasing distance, the target soon approaches the first maximum. To get points beyond, i.e., $n < 1$, we need greater values of p but it is not necessary or desirable to go below about $n = 0.8$, since the curve beyond $n = 0.8$ is generally in the transition region in which the curve is more easily and more accurately obtained by joining the optical and diffractive curves. The diffractive part of the calculation is given on pp. 404–432. Accordingly, in Table 2, the values of p are taken only slightly above $p = 0.1$ (corresponding to $n = 1$) and are diminished to find points at the nearer distances.

TABLE 2. 10 log G_1 = 13.5 db; 10 log G_2=0.0 db; λ = 1.5 meters; h_1 = 30 meters; h_2 = 1,000 meters; σ=10 m².

p	v	d(km)	R	n	D	$\frac{\Omega}{2}$	*	20 log A_0	20 log A	Radio Gain 10 log $\frac{P_2}{P_1}$	Radar Gain 10 log $\frac{P_2}{P_1}$
0.12	3.098	70.49	7.78	0.83	0.97	1.30	5.6	−112	−106.4	−98	−172
0.11	2.934	66.75	8.54	0.91	0.98	1.43	6	−111	−105	−92.5	−170
0.10	2.755	62.68	9.45	1.005	0.98	1.58	6	−110	−104	−91.5	−169
0.09	2.561	58.25	10.55	1.22	0.98	1.76	6	−110	−104	−91.5	−169
0.08	2.349	53.45	11.92	1.27	0.99	1.99	5.2	−109	−104	−90	−167
0.07	2.119	48.21	13.68	1.45	0.99	2.29	3.5	−109	−105.5	−92	−170
0.06	1.870	42.54	16.02	1.70	0.99	2.68	−1	−107	−108	−94.5	−175
0.055	1.738	39.22	17.50	1.86	0.99	2.92	−7.5	−106	−113.5	−100	−186
0.05	1.600	36.4	19.28	2.05	1.00	3.22	−16	−106	−122	−108.5	−203
0.045	1.457	32.89	21.45	2.28	1.00	3.58	−1.5	−105	−106.5	−93	−172
0.04	1.311	29.59	24.16	2.57	1.00	4.04	+3.8	−104	−100	−87	−159
0.035	1.158	26.14	27.64	2.94	1.00	4.62	6	−103	− 97	−79.5	−153
0.03	1.002	22.62	32.28	3.43	1.00	5.39	+2	−102	−100	−86.5	−159
0.025	0.841	18.98	38.67	4.12	1.00	6.48	−8	−100	−-108	−94.5	−165
0.02	0.678	15.30	48.49	5.16	1.00	8.10	5.7	− 98	−104	−91.5	−167
0.01	0.345	7.79	97.08	10.33	1.00	16.22	0	− 92	− 92	−78.5	−143

* Lobe pattern factor = 20 log $\sqrt{(1-D)^2 + 4D \sin^2 (\Omega/2)}$.

7. To find A, we need first the free-space value A_0, which is given in Figure 3 in Chapter 2 as a function of d. Since d_T = 4.12 $\sqrt{30}$ = 22.6 km, the value of d corresponding to v = 2.76 is $d = vd_T$ = 62.3 km, and 20 log A_0 = − 111.

8. To find the value of

$$10 \log \sqrt{(1-D)^2 + 4D \sin^2 \frac{\Omega}{2}},$$

we need D. Since n is practically unity, corresponding to the first maximum, $\sin^2 (\Omega/2)$ may be taken as unity. Hence the radical reduces to $1 + D$. Calculation using equation (103) and Figure 17 gives D = 0.98, and hence

$$1 + D = 1.98,$$
$$20 \log (1 + D) = 6.$$

Since the transmitting antenna gain G_1 is 13.5 db, and assuming the receiving antenna gain to be 0 db, 10 log (P_2/P_1) has the value 20 log A + 13.5 or

$$10 \log \frac{P_2}{P_1}$$

$$= \underbrace{A_0^2}_{- \text{ 111 db}} \underbrace{\sqrt{(1-D)^2 + 4D \sin^2 \frac{\Omega}{2}}}_{+ \text{ 6·db}} \underbrace{G_1 G_2}_{+ \text{ 13.5 db}} + 0.0 \text{ db}$$

$$= - 105 + 13.5 = - 91.5 \text{ db}.$$

Repeating the process for other values of p, a table of 10 log (P_2/P_1) versus d is obtained. These points have been plotted in Figure 26, together with the points in the diffraction region obtained with the data given on pp. 413 - 416 . For sketching in the optical part, the value of n is kept in mind, since this indicates on which lobe and where on the lobe the point lies.

RADAR GAIN: TWO-WAY TRANSMISSION

To change from 20 log A = − 105 to 10 log (P_2/P_1) at the radar receiver, using equation (5) and G_1 = G_2 = 13.5 db,

$$10 \log (P_2/P_1) = 27 + 7.5 + 10 \log \sigma - 20 \log 1.5 + 40 \log A,$$

$$= 27 + 7.5 + 10 - 3.5 + 40 \log A,$$

$$= 41 + 40 \log A = - 169 \text{ db}.$$

Type IV. Determination of Contours Along which the Gain Factor A Has a Given Value, the Transmitter Height and Wavelength Being Given

This is the so-called coverage problem which is treated in greater detail in Chapter 6. While the usual coverage diagram is derived on the basis of one-way or communication formulas, the diagram is still useful for radar since a target will return more or less energy to the receiver according to its position on the coverage diagram. The contour gain factor A is readily converted to P_2/P_1 for either one-way or radar by means of equations (3) and (5).

The method described here is more accurate than the graphical methods given in Chapter 6. It is best suited for finding maximum lobe ranges corresponding to a given radar gain. If A is given, and h_2 for a given distance d is wanted, a curve can be drawn as that for Type II and then h_2 found for the given value of A.

PROBLEMS

A radar set operating over the sea has a transmitter with antenna height of 30 meters and a wavelength of 1.5 meters. As in the previous problems, a receiver with an antenna of 0 db gain is assumed in place of a target and the gain of the transmitter is again assumed as 13.5 db. The polarization is horizontal. The gain factor A, for illustration, is chosen as −130 db. Positions of the receiver are to be found at which the gain factor takes that value.

In Chapter 6, purely graphical methods of determining the contours (lobes) are given. Here we are concerned with finding individual points on the contour. Thus, for example, $n = 1$ if the tip of the lowest contour is wanted (as in range determination). Points near the tip require values of n near 1, such as $n = 1.2$ or $n = 0.9$. For the next higher lobe, the tip of the lobe corresponds to $n = 3$ and so on. The nulls are at $n = 0, 2, 4, \ldots$. However, while the optical formula gives a null at $n = 0$, that is, near the line of sight, the true value of the field, or of A, is greater. To obtain the correct result, the contours for the diffraction field (pp 413 - 416) and those obtained for the optical region should be merged into smooth overall curves.

For values of $r > 3, R = nr > 3$, the tip and upper part of the lowest lobe, and the higher lobes, by equation (126), have a value of D close to 1. Consequently, equation (110) reduces to

$$A = 2A_0 \sin \frac{\Omega}{2}. \tag{132}$$

If n is given, $\sin \Omega/2$ is determined and the calculation can be performed as a free-space calculation. In terms of d, the equivalent free-space distance d_0, corresponding to A is given by Figure 3 in Chapter 2 and is equal to

$$d = 2d_0 \sin \frac{\Omega}{2}. \tag{133}$$

In the stated problem $r > 3$, so that the free-space calculation suffices. This is given in paragraph (1). In paragraph (2), the method including the divergence is given.

1. *Free space.* In the given problem, $r = 9.4$, so that the simplified calculations should be sufficient. The value of d_0 corresponding to $20 \log A = -130$ is found from Figure 3 in Chapter 2 to be 566 km. Hence by equation (133) for $n = 1$, the true distance d for complete reinforcement by the reflected wave is twice as much and

$$d = 2 \cdot (566) = 1,132 \text{ km.}$$

For $n = 1.2, \Omega/2 = 0.6\pi$ [from equation (116)], giving

$$d = 2 \cdot (566) \sin (0.6\pi),$$
$$= 1,076 \text{ km.}$$

To find the corresponding height h_2, a curve of the type on page 397 is needed for $-20 \log A$ versus height. From this, the height corresponding to $20 \log A = -130$ can be read. Alternatively, the calculation given later in (2) will determine both d and h_2.

If instead of A, either the radio gain or radar gain is given, A is first found from equations (3) or (5).

2. *Calculation including divergence, $n = 1$.* As in the previous problem, $r = 9.4$ (from Figure 15 in Chapter 6). A convenient value of p, approximately equal to $1/r$, is selected. In this case, we take $p = 0.1$. This value is then improved by applying

Newton's method $p_1 = p - \dfrac{f(p)}{f'(p)}$ to the equation

$$f(p) = \frac{1}{v_0} - \frac{1}{v} \sqrt{(1 - D)^2 + 4D \sin^2 \frac{\Omega}{2}}, \quad (134)$$

remembering that D is a function of p as given in equation (117), where v_0 is the value of v which corresponds to the distance d_0 at which the given value of A would occur in free space.

If $n = 1$, equation (134) reduces to

$$\frac{1}{v_0} = \frac{1}{v}(1 + D). \tag{135}$$

The correction formula corresponding to equation (134), denoting by p_1 the improved value of p, is

$$p_1 = p - \frac{v - v_0 \sqrt{(1 - D)^2 + 4D \sin^2 (\Omega/2)}}{\dfrac{v^2}{p^2 D^2} + \dfrac{3(1 - D^2)}{4pD}\left[(1 - D^2) v_0^2 + v^2\right]\left(\dfrac{1 + p^2}{1 - p^2}\right)}. \tag{136}$$

The correction formula corresponding to equation (135) $(n = 1)$ is

$$p_1 = p - \frac{\dfrac{1}{v_0} - \dfrac{(1 + D)}{v}}{\dfrac{1 + D}{p^2 D^2} + \dfrac{3D}{2pv}\left(\dfrac{1 + p^2}{1 - p^2}\right)(1 - D^2)}. \tag{137}$$

Taking $n = 1$, d_0 from $A = 3\lambda/8\pi d_0$ (or Figure 3 in Chapter 2) is 566 km, and

$$v_0 = \frac{566}{d_T} = \frac{566}{22.5} = 25.1.$$

Taking $p = 0.1$ as an initial value as explained above, then D is found to be 0.9788 [equation (117)]. Using $R = nr = 9.4$ and equation (113),

$$v = 165.6.$$

Substituting these values in equation (135) gives
$$p_1 = 0.10385.$$

Repetition of this procedure requires no change in these five figures. Accordingly, for $n = 1$ and $A = -130$ db, $p = 0.10385$. The corresponding values of D and v are

$$D = 0.9789$$
$$v = 49.38, d = 1,110 \text{ km.}$$

In (1) d was found to be 1,132 km. Now $s = p/v = 0.0021$. From equation (121),

$$u = \frac{h_2}{h_1} = 2,898$$

$$h_2 = 86,940 \text{ meters.}$$

For $n = 1.2$, the calculation proceeds as for $n = 1$ except that equation (134) rather than equation (135) is used:

$$R = 11.283.$$

The value of p by successive approximations in
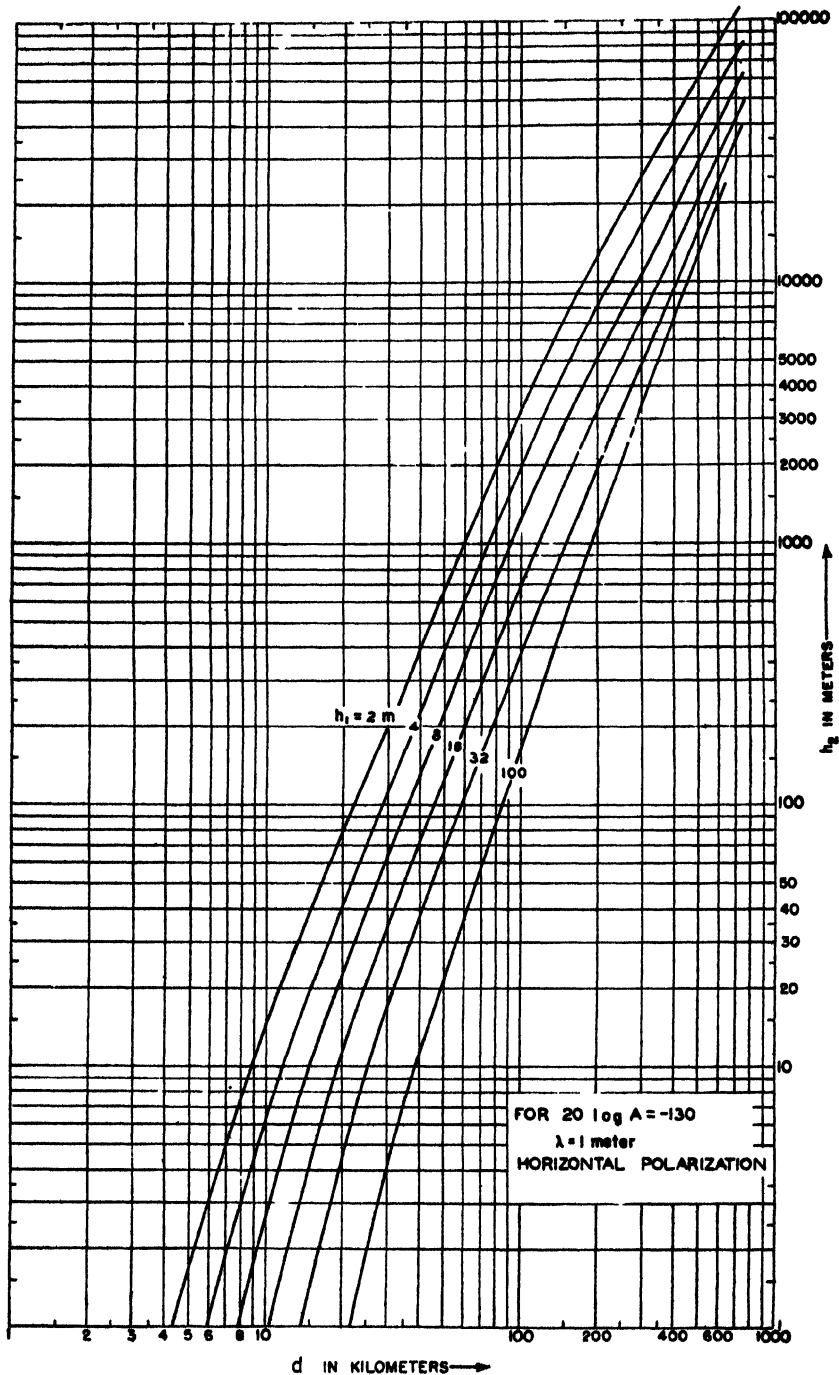
FIGURE 27.   Maximum range versus receiver height h_2 for given values of transmitter height h_1.

equation (136) is found to be

$$p = 0.08127$$
$$v = 47.35, d = 1,065 \text{ km}$$
$$D = 0.9851$$
$$s = 0.00184$$
$$\frac{h_2}{h_1} = 2,772$$
$$h_2 = 83,160 \text{ meters}$$

3. *Vertical polarization*, $\rho \neq 1$, $\phi \neq 180°$ (*sea water*). The procedure given here is first to find the position of the point for a given n assuming the reflection coefficient to equal -1 and then find the shift caused by the change in the reflection coefficient. For the most important case, $n = 1$, the new maximum distance is given by

$$d = d_0 (1 + \rho D), \tag{138}$$

where d_0 is the free-space distance corresponding to the given value of A. ρ is found from the value of ψ, the grazing angle at the reflection point given by p found above in the calculation for $\rho = 1$ and $\phi = 180°$. For the new contour tip p changes, but the angle ψ does not change sharply, so that ρ and ϕ as found for the p obtained by the simplified calculation is a close approximation.

For $\rho \neq 1$, $\phi \neq 180°$, $\Omega = \delta + \phi - \pi$ [see equation (29)] consists of two parts. $\delta = \pi R/r = (\Delta/\lambda) 2\pi = n\pi$ and $\phi' = \phi - \pi$. Writing $\Omega = N\pi$, N the lobe number for the case $\rho \neq 1$, $\phi \neq 180°$, the requirement for the new lobe tip is $N = 1$; for the first maximum $\Omega = \pi = R\pi/r + \phi - \pi$ where R is the path difference variable at the new lobe tip. Hence the value of R at the new tip is given by

$$R = r (2 - \phi/\pi). \qquad (139)$$

Using the results in (2),
$$p = 0.10385,$$
$$D = 0.9788,$$
$$r = 9.4,$$
$$d_0 = 566,$$

we find from Figure 24 or equation (107), $\psi = 0.725°$; from Figures 14 and 15 in Chapter 4, $\rho = 0.76$, $\phi = 170°$. Substituting in equation (138),

$$d = 566 (1.744) = 987 \text{ km}.$$

From equation (139),

$$R = (9.4) (1.056) = 9.92.$$

Also

$$v = \frac{d}{d_T} = \frac{987}{22.5} = 43.9.$$

The above value of p can now be improved by substitution in equation (137) with D replaced by ρD which gives

$$p = 0.0985.$$

In the calculation just made, ρ has been assumed constant. This can be checked by finding ψ as determined by the new value of p. The result is $\psi = 0.766°$ and the corresponding values are $\rho = 0.74$ (as against 0.76 previously) and $\phi = 169°$ (as against 170°), which is good enough. We now find

$$s = \frac{p}{v} = \frac{0.0985}{43.9} = 0.00224$$

$$\frac{h_2}{h_1} = 2,359$$

$$h_2 = 70,770 \text{ meters}.$$

Hence the new maximum point of the lobe is at a distance of 987 km and at an elevation of 70,700 meters, as compared with a distance of 1,110 km and height 86,900 meters for perfect reflection.

Maximum Range Versus Receiver (or Target) Height

If the value of A has been determined by using the minimum detectable power in equation (3)

or (5), the corresponding contour is a curve of maximum range versus receiver height for communication or maximum range versus target height for radar. Generally, the lower part of the lowest curve ($n < 1$) is of greatest interest. If A is sufficiently small (i.e., 20 log A numerically large and negative), the complete contour has points below the line of sight. If the transmitter antenna is low ($h_1 < 30\lambda^{2/3}$ meters), the lower points are likewise given by the diffraction formula, discussed in text on pages 380-413. Several such curves, the lower part of the lowest lobe corresponding to various transmitter heights for $\lambda = 1$ meter and 20 log $A = -130$, are given in Figure 27.

Consider, for example, the curve for $h_1 = 2$ meters. The uppermost points of the curve correspond to the tip of the lowest lobe and were found by the procedure used on pp. 400-402, putting $n = 1$. The lowest points were found from the diffraction formula by the method presented before, with the aid of Figures 31 to 36. It has been pointed out that for $n < 1$, the optical interference formula is inadequate.

To locate a point between the upper extreme ($n = 1$) and the diffraction points, a curve of A versus h_2 for some distance is constructed. In Figure 28, a set of such curves is given for the distance 100 km and for various transmitter heights. By taking the intersection of 20 log A equal to -130 with the curve $h_1 = 2$, a value of h_2 is obtained. This value $h_2 = 3,300$ and $d = 100$ km represent the coordinates of a point on the contour $h_1 = 2$ in Figure 27.

It is of some interest to observe the shortening of the lobe for $h_1 = 100$ meters on account of the divergence which is close to unity at the tips of the lobes corresponding to the low transmitter heights but drops to 0.65 at the tip of the lobe for $h_1 = 100$. Since for $h_1 = 100$, the formula for both antennas low ($h < 30\lambda^{2/3}$) is not applicable, the lowest points on the curve $h_1 = 100$ in Figure 27 were obtained by applying the reciprocity principle to the curves
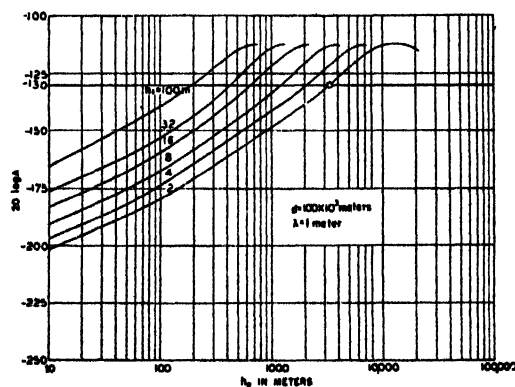
FIGURE 28. Radio gain versus receiver height h_2, for given values of transmitter height h_1.

already obtained. The distance at which $h_2 = 100$ on the $h_1 = 2$ curve is the same as that at which $h_2 = 2$ on the $h_1 = 100$ curve.

BELOW THE INTERFERENCE REGION

Analysis of the First Mode

Except for the numerical constants involved, the discussion for one mode applies to all the other modes. Each mode is of the form $\Phi(d) \cdot f(h_1) \cdot f(h_2)$, i.e., the product of a distance function Φ by two antenna height-gain functions f.

DISTANCE

$\Phi_1(d)$, the distance function of the first mode, can be represented as the product of two physically significant factors, one for free space and one for the earth effect. The latter may be divided into a plane earth factor and a shadow factor.

1. *Free space.* It has been shown in equation (18) in Chapter 2 that for doublet antennas, with matched load at the receiver and adjusted for maximum power transfer, the free-space gain factor A_0 is given by

$$A_0 = \sqrt{\frac{P_2}{P_1}} = \frac{3\lambda}{8\pi d}.$$

For other types of antennas in free space, this takes the form

$$A_0 \sqrt{G_1} \sqrt{G_2} = \sqrt{\frac{P_2}{P_1}} = \frac{3\lambda}{8\pi d} \sqrt{G_1} \sqrt{G_2}. \quad (140)$$

Under actual conditions when earth and atmospheric effects are of importance, each mode will be considered to have A_0 as one factor.

It may also be recalled that for given power P_2 delivered to the load, the corresponding electric-field strength, under matched conditions, is given by

$$E = \frac{8\pi\sqrt{5}}{\lambda} \sqrt{\frac{P_2}{G_2}}. \quad (141)$$

Combining equations (140) and (141) gives the free-space value of the electric field strength E, in terms of transmitted power

$$E = \frac{3\sqrt{5}}{d} \sqrt{P_1}\sqrt{G_1}, \quad (142)$$

which is the same as equation (7) in Chapter 2 with the addition of the transmitter gain G_1.

2. *Plane earth.* The earth modifies the field by absorbing and reflecting radiation. If the earth were plane and perfectly conducting, the value of the gain factor would be $2A_0$ and the electric field $2E_0$ for vertical antennas several wavelengths above the ground and at distances sufficiently large. The imperfect conductivity of the earth produces a change in the gain. Representing this effect by the

factor A_1 (where $A_1 < 1$),

$$A = 2A_0 A_1. \quad (143)$$

The plane earth factor A_1 depends on distance and on the electrical properties of the earth. Fortunately the earth constants enter the problem in an intrinsically simple way, as the main effect is taken into account by multiplying the distance d by a certain factor which we shall denote by p', so that A_1 is, mainly a function of $p'd$. The new parameter p' is different for the two states of polarization. For vertically polarized radiation,

$$p' = \frac{2\pi}{\lambda} \frac{|\epsilon_c - 1|}{|\epsilon_c|^2},$$

where ϵ_c is the complex dielectric constant $\epsilon_r - j60\sigma\lambda$,

or
$$p' = \frac{2\pi}{\lambda} \frac{\sqrt{(\epsilon_r - 1)^2 + (60\sigma\lambda)^2}}{\epsilon_r^2 + (60\sigma\lambda)^2}. \quad (144)$$

For horizontal polarization,

$$p' = \frac{2\pi}{\lambda} |\epsilon_c - 1| = \frac{2\pi}{\lambda} \sqrt{(\epsilon_r - 1)^2 + (60\sigma\lambda)^2}. \quad (145)$$

A_1 depends also on the phase of the complex dielectric constant. The phase is determined by the parameter

$$Q = \frac{\epsilon_r}{60\sigma\lambda}. \quad (146)$$

For ultra-short waves, with the exception of vertically polarized waves over sea water at distances less than $50/p'$ (see text p. 416 and Figure 45) and a wavelength greater than 1 meter, A_1 is independent of Q and, to a sufficient approximation, is given by

$$A_1 = \frac{1}{p'd}. \quad (147)$$

A_1 as a function of $p'd$ is plotted in Figure 56.

In the case excepted above, A_1 deviates substantially from $1/p'd$ (see Figure 45) for distances less than $50/p'$. Table 3 gives $50/p'$ as a function of λ. It appears that the deviations are immaterial for practical purposes as long as the wavelength is smaller than 3 meters, since we are usually concerned with ranges larger than 7 km. It should further be mentioned that, in the above case, A_1 depends to a small degree on Q. However, the variations are less than 1 db and may be neglected for wavelengths less than 10 meters.

The condition that the earth may be considered plane is that the shadow factor F_s [see equations (149) and (207)] shall be approximately unity. For $F_s = 0.9$, which is approximately 1 db below unity,

TABLE 3. Sea water (vertical polarization).

λ	1	2	3	4	5	6	7	8	9	10	meters
$\frac{50}{p'}$	2	4	7	12	17	24	30	50	71	200	km

$\eta = \zeta f(\delta) = 0.4$ from Figure 58; $f(\delta)$ in Figure 57 is approximately unity, so that $\zeta = sd \cong 0.4$. Since s, from equation (150) for $k = 4/3$, is given by $4.43 \times 10^{-5}\lambda^{-1/3}$, it follows that d, for the plane-earth approximation to hold, must be less than $10^4\lambda^{1/3}$,

$$d < 10^4\lambda^{1/3} \quad \text{(plane earth)}. \quad (147a)$$

3. *Curved earth.* The screening effect of the earth curvature results in a further decrease in gain. Well within the diffraction region, the shadow effect produces an exponential drop in field strength with distance, which is much greater for higher modes than it is for the first mode.

Denoting the screening or shadow factor by F_s and the distance gain factor by Φ_1, we have

$$\Phi_1 = 2A_0A_1F_s. \quad (148)$$

For the dielectric case $\delta >> 1$ and for distances greater than $1.5/s$, the shadow factor is

$$F_s = 2.507(sd)^{3/2}\,e^{-1.607\,(sd)}, \quad (149)$$

where

$$s = \left[\frac{2\pi}{\lambda}\frac{1}{(ka)^2}\right]^{1/3},$$
$$= 4.43 \cdot 10^{-5}\lambda^{-1/3}\left(\frac{4}{3k}\right)^{+2/3} \quad (150)$$

Equation (149) gives the value of the shadow factor for the first mode only. In Figure 32, the curve marked "dielectric earth" is a plot of the shadow factor evaluated by using all terms or modes. However for $sd > 1.5$ only the first mode is important. Consequently, equation (149) represents this curve accurately for all values of sd larger than 1.5.

HEIGHT-GAIN

For antennas at zero height, the height-gain functions f are equal to unity, so that equation (148) represents the actual value of the first mode ·for both antennas at zero height.

When the antennas are raised above the ground, it is convenient to distinguish between low and high antennas, the division between the two cases being given by the critical height $h_c = 30\lambda^{2/3}$.

1. *Low antenna; $h < h_c = 30\lambda^{2/3}$.* For a low antenna, f is a function of lh and of Q, where l is a quantity that depends on the complex dielectric constant and is given by

$$l = \sqrt{\frac{2\pi p'}{\lambda}}, \quad (151)$$

in which p' is the distance coefficient given by equations (144) and (145). Let the value of f for a low antenna be denoted by H_L.

The magnitude of H_L is given by

$$H_L = \sqrt{1 + \frac{2lh}{4Q^2 + 1} + l^2h^2}. \quad (152)$$

and is plotted in Figure 47.

For height h larger than $4/l$, the two first terms under the square root may be neglected in comparison to the third term, and H_L becomes approximately

$$H_L \cong lh. \quad (153)$$

In order to show more clearly when this approximation is justified, Table 4 gives values of $4/l$ for different wavelengths and vertical polarization. For horizontal polarization, $4/l$ is quite small.
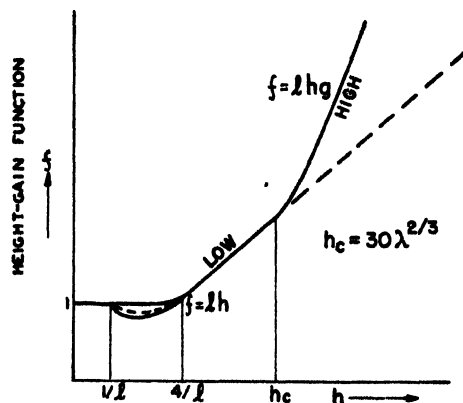
FIGURE 29. Height-gain as a function of height. (See Figures 7, 25, and 47.)

Inspection of Table 4 shows that, except for the case of sea water at wavelengths above 1 meter, the approximate equation (153) is good for heights above about 50 meters.

TABLE 4. Values of $4/l$ for different wavelengths (vertical polarization).

λ in meters	0.1	1	2	3	4	5	6	7	8	9	10
Sea water	0.06	10	28	50	80	115	133	160	235	285	300
Fresh water		6	11	17	22	30	33	40	44	53	57
Moist soil		3	7	11	15	18	21	25	28	33	36
Fertile ground		3	5	8	10	13	16	17	20	25	27
Very dry ground		2	3	4	6	8	9	10	12	15	16

To a first approximation, the value of f for low antennas is the same for all modes, so that the height-gain functions may be factored out, as was pointed out in text on p.380. The gain factor for the case when both antennas are low can then be represented by

$$A = 2A_0A_1F_s\,(H_L)_1(H_L)_2, \quad (154)$$

where F_s is sum of the shadow factors of all the modes. F_s has been plotted in Figure 32. Equation (154) is also valid in the optical region, provided

$$d >> \frac{2h_1h_2}{\lambda}. \quad (155)$$

This condition is added to insure that the point is well below the center of the lowest lobe.

2. *Elevated antenna; $h > 30\lambda^{2/3}$.* In this case the height-gain function f increases exponentially. Rep-
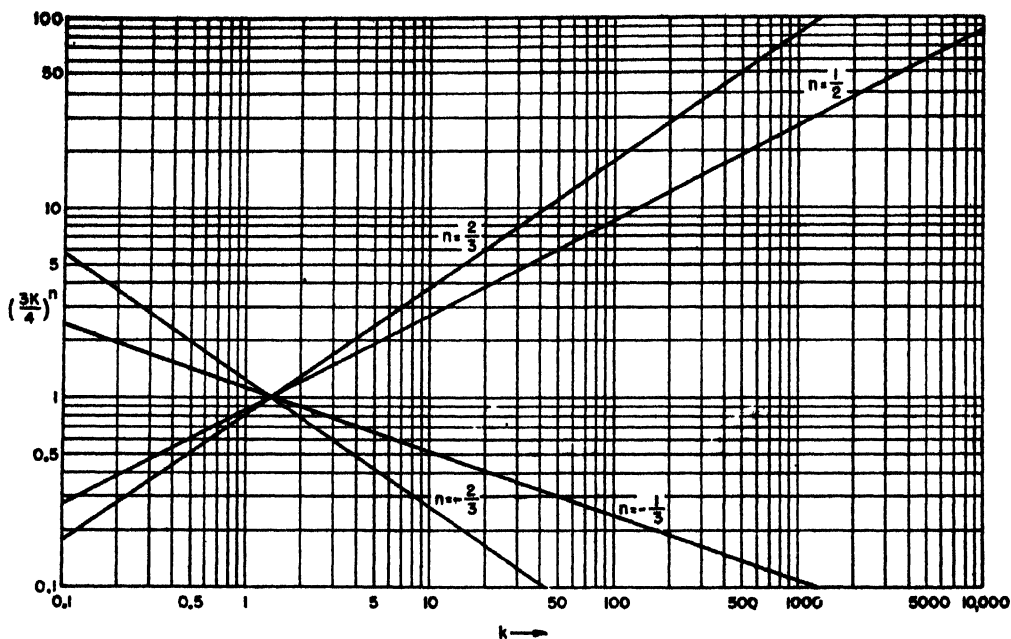
FIGURE 30   Values of $(3 k/4)^n$.

resenting the increase over lh by g, we have

$$f = glh. \tag{156}$$

For the dielectric case $\delta \gg 1$, refer to equation (193) to define δ.

$$g = 0.1356 \,(eh)^{-0.904} \, 10^{0.948 \sqrt{e\lambda}} \tag{157}$$

where

$$e = \left(\frac{4\pi^2}{\lambda^2 ka}\right)^{1/3}, \tag{158}$$

$$= \frac{1}{60}\lambda^{-2/3}\left(\frac{4}{3k}\right)^{1/3}. \tag{159}$$

See Figures 35 and 36.
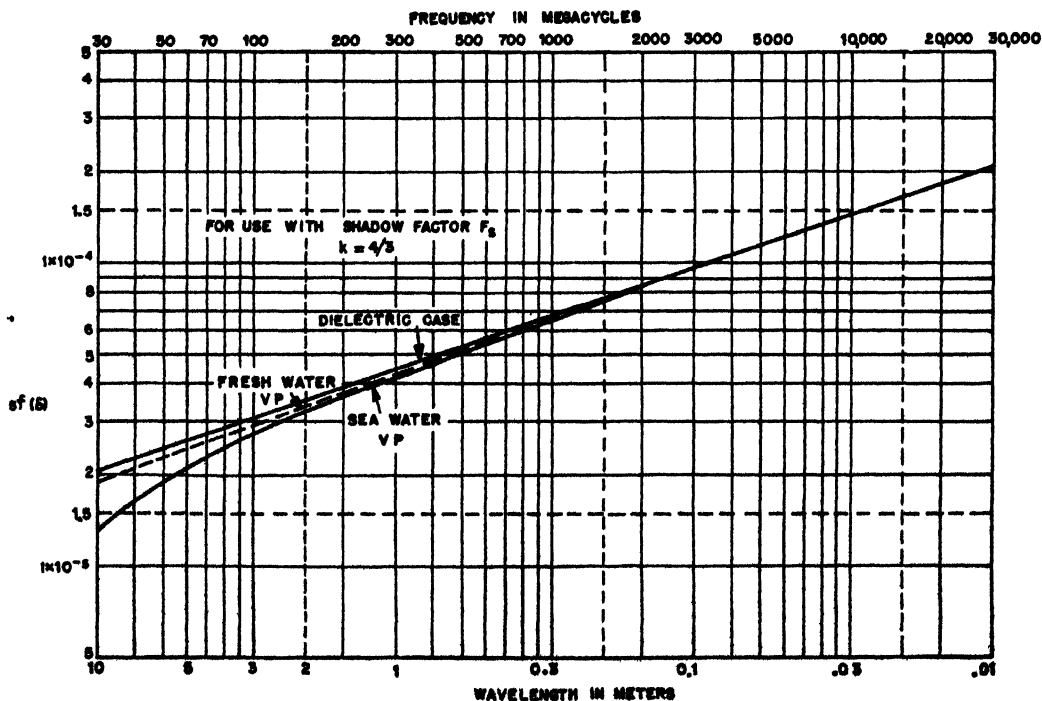
FIGURE 31. $\epsilon f(\delta)$ versus wavelength and frequency. For dielectric earth and $k = 4/3$, $f(\delta) = 1$, and $\epsilon = 4.43 \times 10^{-5}\lambda^{-1/3}$. (See Figure 57 for $f(\delta)$.)
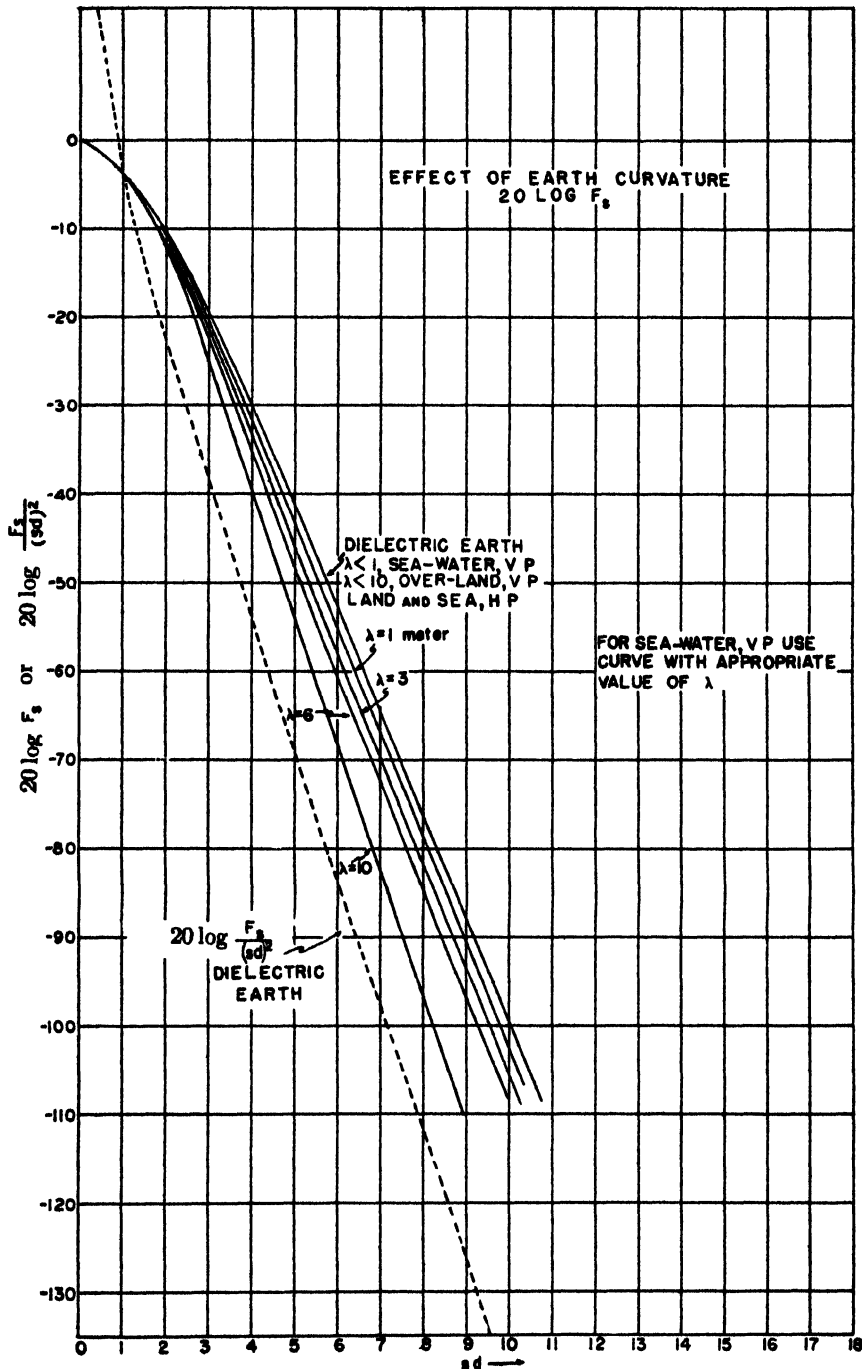
FIGURE 32. Shadow factor F_s, 20 log F_s (evaluating all modes), or 20 log $F_s/(sd)^2$ versus sd. Curve for dielectric earth, 20 log F_s, is the same as curve O in Figure 58.

For the case of sea water, vertical polarisation and wavelength in the VHF (1 to 10 meters) range, g requires a correction factor g' which depends on λ. A table of g' is given with the graph of g in Figure 36.

The change of f with height h is represented schematically in Figure 29 (also Figures 7, 25, 47).

FORMULA FOR THE DIELECTRIC EARTH.
$\delta >> 1$.

The first mode has the form $\Phi_1(d) \cdot f(h_1) \cdot f(h_2)$. If the value of the gain is given substantially by the first mode, and substitution from equation (148) is
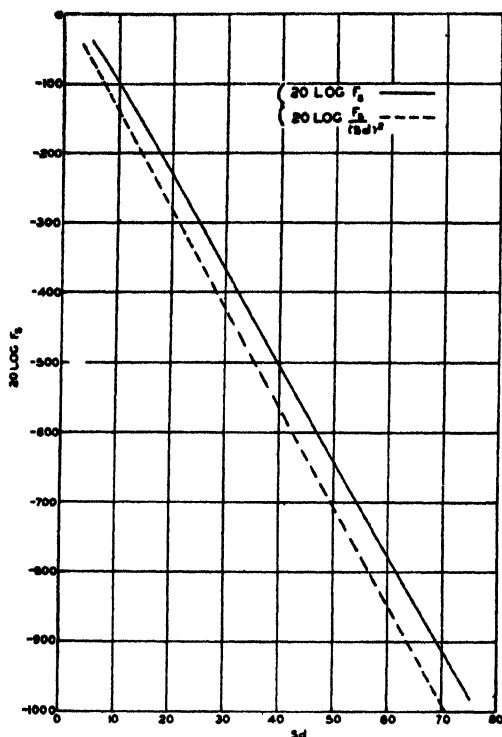
FIGURE 33. Shadow factor for dielectric earth.

made, it is found that

$$A = [2A_0 A_1 F_{s1}] f(h_1) \cdot f(h_2). \qquad (160)$$

For the dielectric case equation (160), using equations (140), (147), (151), and (156), becomes

$$A = \frac{3}{2} \frac{F_{s1}}{d^2} (gh)_1 \, (gh)_2. \qquad (161)$$

The same formula holds for sea water, vertical polarization, wavelengths in VHF range, $d > 50/p'$, and $h > 4/l$, as described above, except that F_s or F_{s1} is represented by various curves in Figure 32,

according to the value of λ, and g is modified slightly by a correction factor g'.

FORMULA FOR SEA WATER. VERTICAL POLARIZATION. VHF.

Equation (160), the general formula for the first mode, in the VHF (1 to 10 meters) range, becomes

$$A = [2A_0 A_1 F_{s1}](H_L gg')_1 (H_L gg')_2, \qquad (162)$$

where H_L is the low antenna height-gain function whose formula is given by equation (152), and $gg' = 1$ for low antennas. As pointed out above, if $h > 4/l$ and $d > 50/p'$, equation (162) reduces to equation (161). g', the correction factor for g, is given in Figure 36. For a more extended discussion, see page 416.

Effect of Changing the Value of k

In the optical region, the effect of a linear gradient of refractive index has been shown to be equivalent to replacing the radius of the earth a by an effective radius ka and then treating the atmosphere as homogeneous (see Chapter 4).

In view of the equivalence of the sum of modes to the optical formula in the optical region, it follows that the modes should be changed in the same way in the optical region, i.e., a should be replaced by ka. These same modes supply the solution of the wave equation in the diffraction region, so that in both regions the substitution of ka for a will take care of an atmosphere with a linear variation of refractive index with height for all values of k.

For given transmitter and receiver antenna heights, h_1 and h_2, the first maximum of the field-strength versus distance curve (see Figure 4) will frequently represent the limit of detection. The first maximum occurs not far from the line of sight which, for a
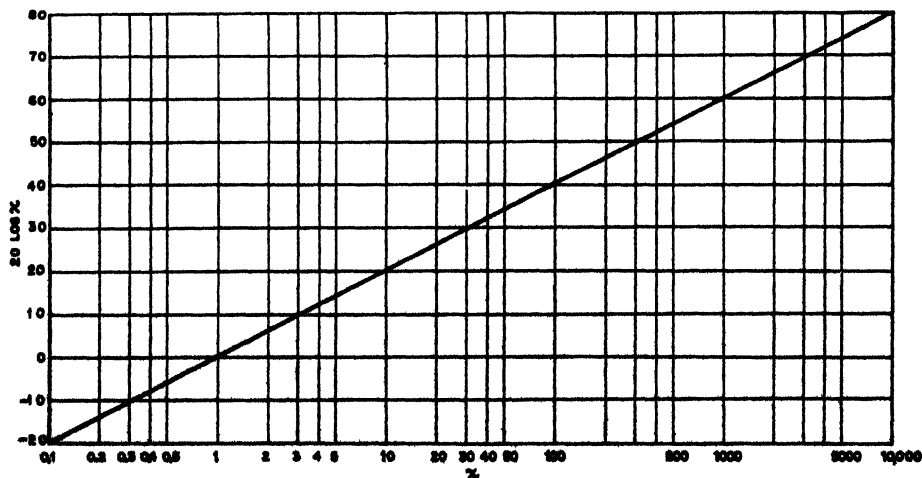
FIGURE 34. 20 log x versus x.
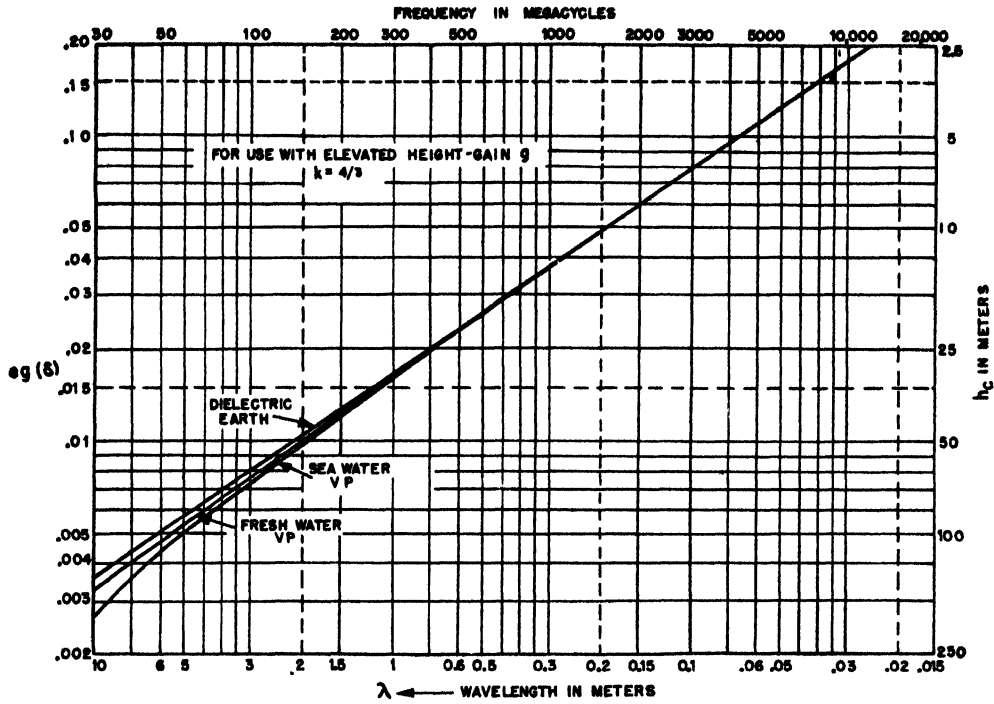
FIGURE 35 $eg(\delta)$ versus wavelength or frequency   For dielectric earth $e = \frac{1}{2}h_c$ and $g(\delta) = 1$
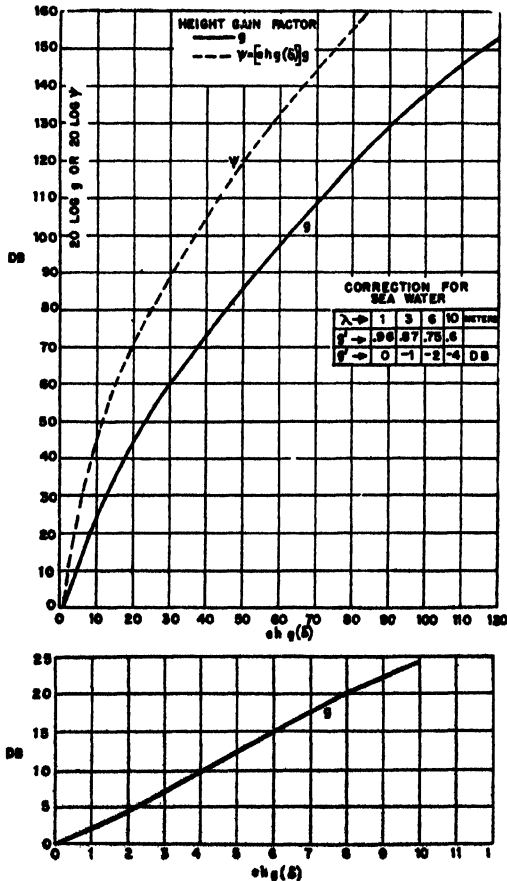
standard atmosphere ($k = 4/3$), is given by

$$d_L = \sqrt{2\left(\frac{4}{3}\right)a}\,(\sqrt{h_1} + \sqrt{h_2}). \quad (163)$$

If $4/3$ is changed to k, the more general form is

$$d_{L'} = \sqrt{2ka}\,(\sqrt{h_1} + \sqrt{h_2}). \quad (164)$$

The first maximum will now be near

$$d_{L'} = \sqrt{\frac{3k}{4}}\,d_L.$$

Suppose next that the point at distance $d_{L'}$ for the given heights was originally well within the diffractive region. The exponential part of the gain due to change of k from $4/3$ is equal to

$$\epsilon^{-1.607s\,(d_{L'}-d_L)}$$

or

$$e^{-1.607\,(\sqrt{3k/4}\,-\,1)sd_L}.$$

The above formula is obtained by combining equation (149) for F_s, and s is obtained from Figure 31 ($k = 4/3$). This corresponding gain in decibels is

$$20 \log_{10} e^{-1.607\,(\sqrt{3k/4}\,-\,1)sd\,L}$$

$$= 20\left[-1.607 \times .434\left(\sqrt{\frac{3k}{4}} - 1\right)sd_L\right],$$

$$= -14\,sd_L\left(\sqrt{\frac{3k}{4}} - 1\right) \text{ db},$$

below the free-space value. Since a maximum is now near $d_{L'}$ as a result of changing $4/3$ to k, i.e., the field has a value of 6 db above the free-space value,

FIGURE 36. g and ψ versus $ehg(\delta)$.
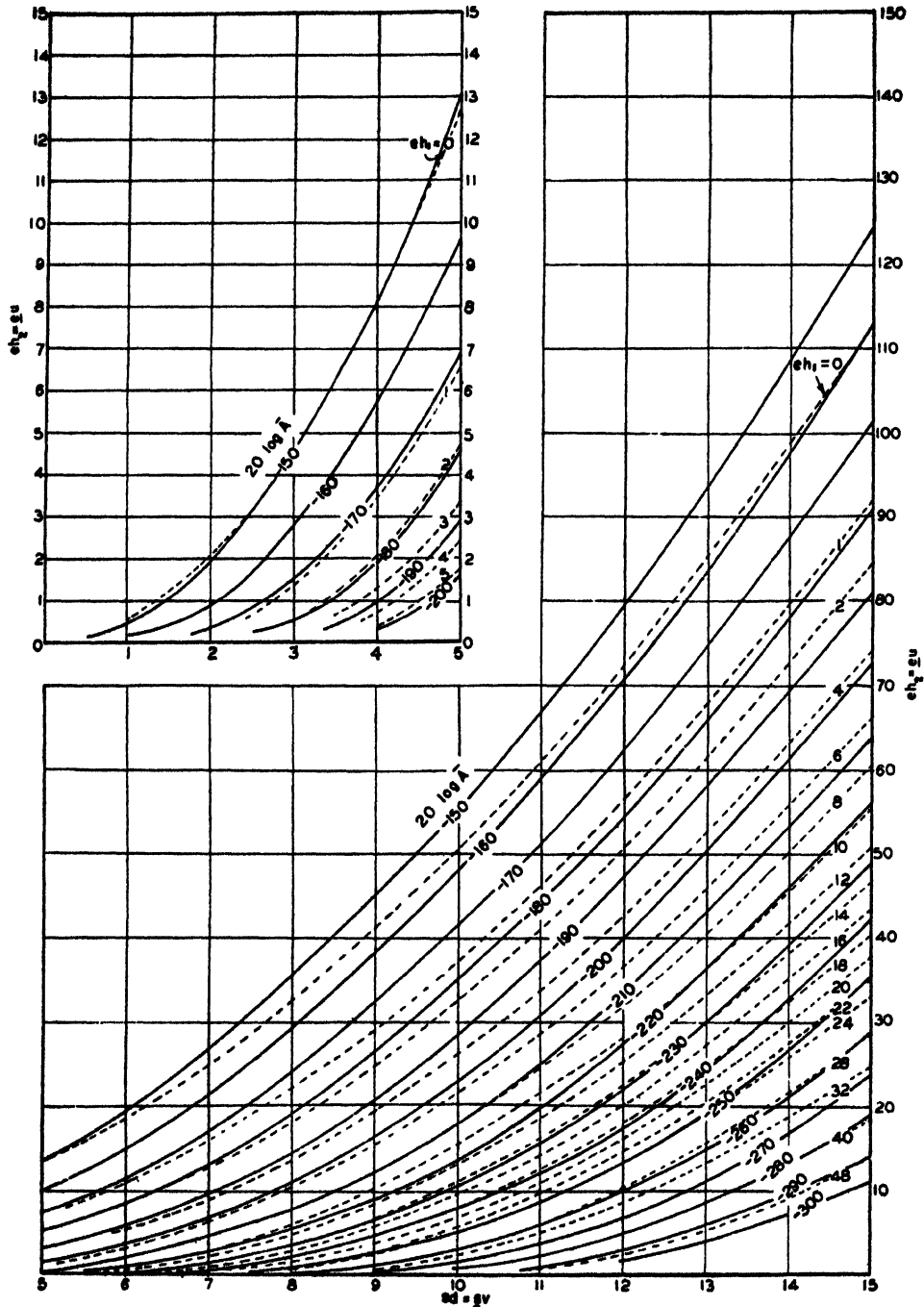
FIGURE 37. $eh_1 = gu$ versus $ed = gv$. Points $eh, ed,$ lying to right of dotted line corresponding to $eh,$ for a given transmitter indicate that the points lie in the diffraction region of the transmitter, or $d > d_L$. Diffraction region dielectric earth — curve parameter: $20 \log \overline{A} = 20 \log A - 20 \log h_1 - 20 \log g_1$.

the gain is approximately the exponential value

$$- 14\, ed_L \left(\sqrt{\frac{3k}{4}} - 1 \right),$$

as a consequence of refraction giving a value k greater than 4/3. For $k = 12$, and $ed_L = 5$, the gain would be about 140 db at some point near $d_L' = 3d_L$,

at heights h_1 and h_2 such that

$$d_{L}' = \sqrt{2ka}\, (\sqrt{h_1} + \sqrt{h_2})$$

and such that h_2 is well within the diffraction region.

For given transmitter height h_1 and distance d, the effect of increasing k is to lower the lowest lobe roughly by the amount by which the line-of-sight
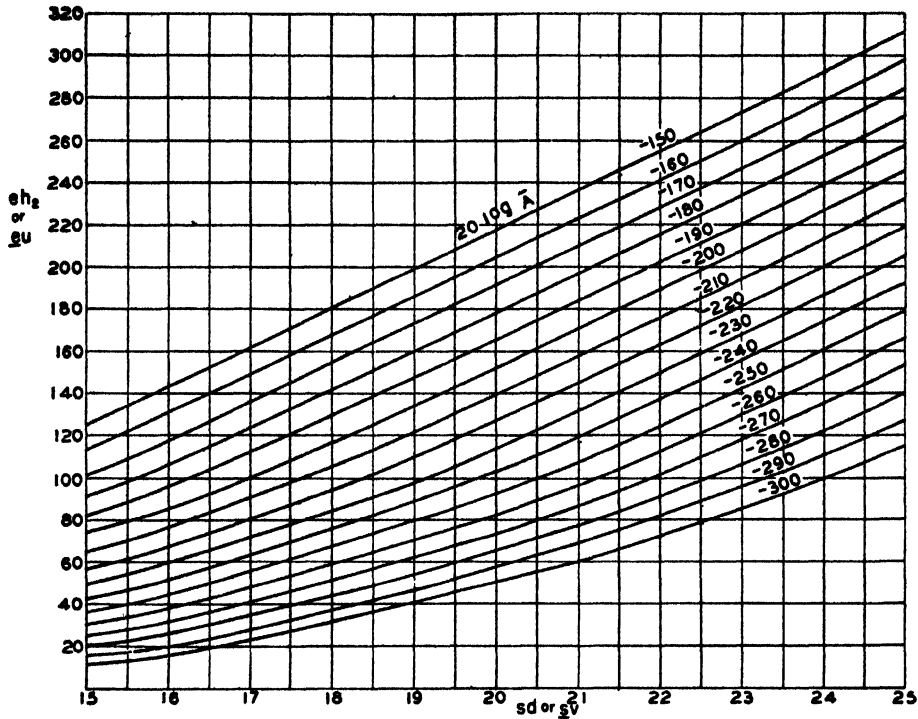
FIGURE 38. $eh_2 = eu$ versus $sd = sv$.
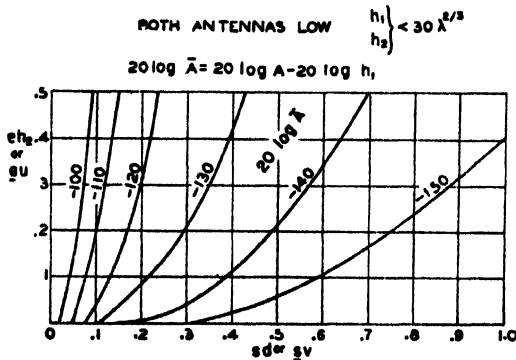
FIGURE 39. $eh_2 = eu$ versus $sd = sv$.

elevation at the distance d is lowered in changing from $4a/3$ to ka. At this distance the height of the line of sight is h_L, and

$$\sqrt{h_L} = \frac{d}{\sqrt{8\frac{a}{3}}} - \sqrt{h_1} \quad \text{(for } k = 4/3\text{)} \quad (165)$$

becomes

$$\sqrt{h_L'} = \frac{d}{\sqrt{2ka}} - \sqrt{h_1}, \quad (166)$$

so that there is a downward shift of approximately

$$h_L - h_L' = \frac{3d^2}{8a}\left(1 - \frac{4}{3k}\right) - 2\sqrt{h_1}\sqrt{\frac{3}{8a}}d\left(1 - \sqrt{\frac{4}{3k}}\right). \quad (167)$$

If h_1 is small compared with h_L and h_L', the result is approximately

$$h_L - h_L' = h_L\left(-\frac{4}{3k} + 1\right). \quad (168)$$

Receivers situated between h_L and h_L' were formerly below the line of sight but are now above it (assuming $k > 4/3$), with a consequent substantial gain in signal strength at some points and loss at others. The chances of detection in the region, however, have improved.

If both antennas are low, a change of $4a/3$ to ka gives a field strength change such that the field which was formerly at a point d well within the diffraction region will now be found at a distance of approximately

$$d\left(\frac{3k}{4}\right)^{2/3}$$

except for the decrease in free-space gain $(20/3) \log 3k/4$, occasioned by the increase in distance. If, for instance, $k = 12$, the free-space gain is equal approximately to -7 db, and the ratio of the new distance to the old is equal to $(3k/4)^{2/3} \cong 9^{2/3} \cong 4$.

More generally, if A/A_0 is known at a point (h_2,d) for a transmitter height h_1 and for $k = 4/3$, the same value of A/A_0 will be found at h_1', h_2', d where

$$h'_{1,2} = h_{1,2}\left(\frac{3k}{4}\right)^{-1/3}, \quad (169)$$

$$d' = d\left(\frac{3k}{4}\right)^{-2/3}, \quad (170)$$

The d and sd scales may be multiplied by any suitable power of 10 to accommodate values of d greater than 10 km
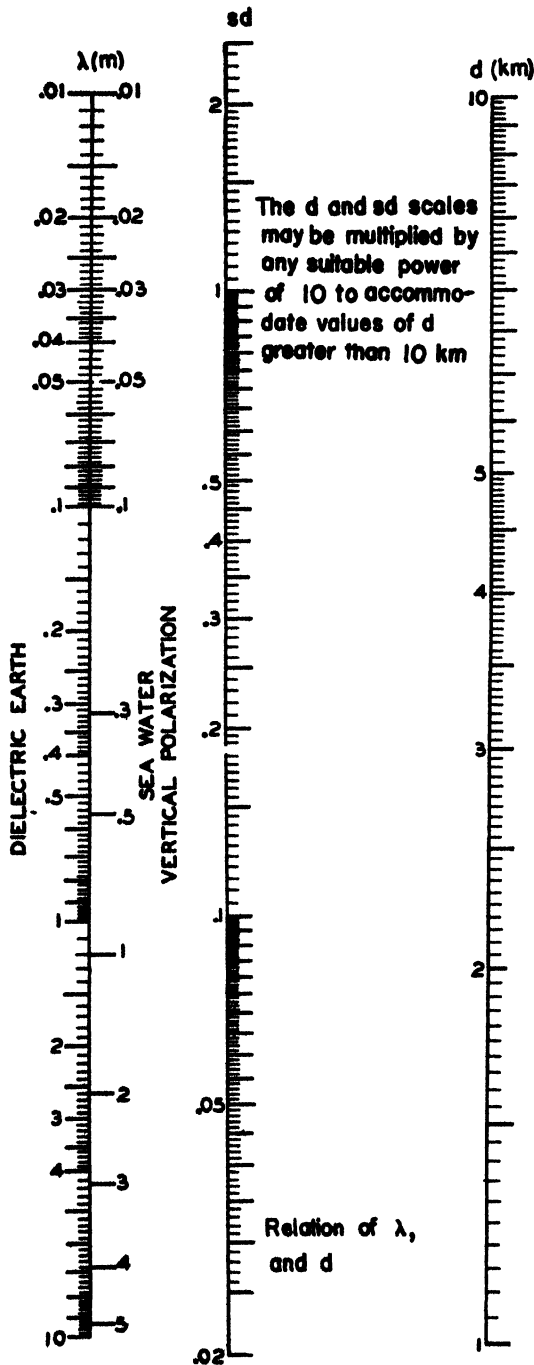
Relation of λ, and d

FIGURE 40. Relation of λ, sd [representing sdf(δ)], and d. See Figure 31. f(δ) = 1 for δ >> 1.

FIGURE 41. eh [representing ehg(δ)], 20 log g versus λ. See Figures 35 and 42.

where k may now have any value. A itself will change to A' where

$$A' = A \left(\frac{3k}{4}\right)^{2/3} \qquad (171)$$

Figure 30 illustrates the values of $(3k/4)^a$ for various

values of k and n used in equations (169), (170), and (171). Figure 43 gives the same information in nomographic form.

Hence if a coverage diagram is known for k = 4/3, then the same diagram can be used for k ≠ 4/3 if the diagram is interpreted in terms of h', d', and A'.

Graphs for the Case of the Dielectric Earth ($\delta \gg 1$)

1. *Fundamental formula for gain factor.* This formula is

$$A = \frac{3}{2}\frac{F_s}{d^2}(gh)_1 (gh)_2, \qquad (172)$$

where $g = 1$ when $h < 30\lambda^{2/3}$.

For the dielectric earth, $\delta \gg 1$. See equation (193)
If both antennas are low ($h < 30\lambda^{2/3}$) equation (172) and the accompanying figures (Figures 31 to 41) are valid for all distances d such that

$$d \gg \frac{2h_1 h_2}{\lambda}. \qquad (173)$$

If one or both antennas are elevated, equation (172) is valid only well within the diffraction region of the transmitter, i.e., for

$$d \gg d_L. \qquad (174)$$

The following quantities required to find $20 \log A$ are given in Figures 31 to 41:

s as a function of λ is given in Figure 31.
$20 \log F_s$ versus sd in Figures 32 and 33.
$20 \log d$ can be found by using Figure 34.
e as a function of λ by Figure 35.
$20 \log g$ versus eh is given by Figures 36 and 41.

When one antenna is low, $h < 30\lambda^{2/3}$, and the *other quite elevated,* $h > 1,200\lambda^{2/3}$, a result valid for h_2 near the line of sight can be found from the formula and graphs on page 419, obtained by summing several modes.

A more general method of finding the gain near the line of sight is to use equation (172) well below the line of sight to obtain a curve of A versus h_2 and by constructing a similar curve for the optical region
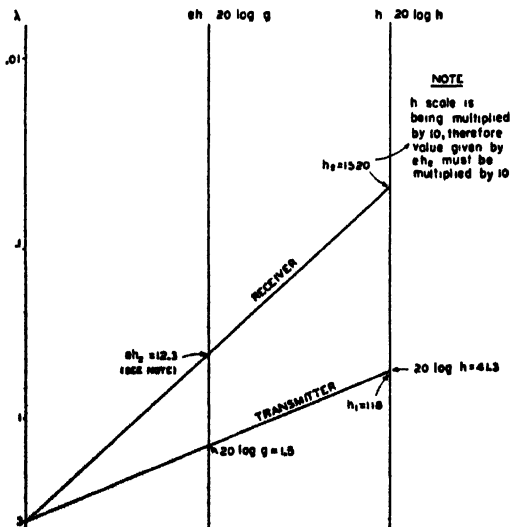
FIGURE 42. Illustrating use of Figure 41. Note: (eh represents $ehg(\delta)$); [$eh_2 = 12.3$] represents [$eh_2g(\delta) = 12.3$].

by the method of Chapter 6, "Coverage Diagrams." By joining the two curves into a smooth overall curve, it is possible to estimate A in the transition region near the line of sight.

For the case of short distances and receiver below the interference region, see page 380.

2. *For $h < 4/l$. Vertical polarization.* A more accurate result can be obtained by replacing the height-gain (gh) by H_L/l or in decibels by $20 \log H_L - 20 \log l$. H_L is given by Figure 47 and l by Figure 46 (see Table 3).

3. *Graphical aids (continued).*

A. *Definition of $\bar{A}$.* Figures 31 to 36 can be combined into a form more convenient for numerical computation. In Figure 37, a curve parameter $\bar{A}$ is introduced, defined by

$$\bar{A} = \frac{A}{h_1 g_1}, \qquad (175)$$

where g_1 is a function of eh_1. This may also be expressed in the form

$$20 \log \bar{A} = 20 \log A - 20 \log h_1 g_1. \qquad (176)$$

(For $h_1 < 4/l$, $20 \log \bar{A} = 20 \log A - 20 \log H_L + 20 \log l$.)

Equation (172) can be written as

$$\bar{A} = 1.77 \times 10^{-7} \frac{F_s}{(sd)^2}\psi \qquad (177)$$

or

$$20 \log \bar{A} = -135 + 20 \log \frac{F_s}{(sd)^2} + 20 \log \psi, \qquad (177a)$$

where

$$\psi = (eh_2)g_2,$$

with g_2 a function of eh_2. Note that $F_s/(sd)^2$ is a function of sd only and is independent of height. While h_1 usually represents the transmitter antenna height and h_2 that of the receiver, the role of h_1 and h_2 in equations (176) and (177) may be interchanged.

To facilitate the use of Figure 37, three nomograms have been added (Figure 40 gives sd when λ and d are given. Figure 41 gives eh_1, $20 \log h$ and $20 \log g$ when λ and h are known. Figure 43 gives the modified height h' and distance d' for given h, d, and k.) To find sd for a value of d which is not on the nomogram, say 120 km, find sd corresponding to a distance 100 times smaller (i.e., 1.2 km) and multiply resulting sd by 100. Proceed similarly for eh.

B. *Both antennas low.* In the case of both antennas low, h_1 and $h_2 < 30\lambda^{2/3}$, the contours $20 \log \bar{A}$ are given by Figure 39. If both antennas are so low, say, h_1 and $h_2 < 4/l$ (see Table 4) that it is desired to use H_L for greater accuracy for vertical polarization (Figure 47), then for $20 \log \bar{A}$ we take $20 \log A + 20 \log l - 20 \log H_L$ (see text above) and instead of eh_2 in Figure 39, we use as ordinate eH_{L2}/l. Then for given sd, Figure 39 would give the value of eH_{L2}/l. If the frequency is given, e/l is known

(Figures 35 and 46), and we must find the value of lh_2 which corresponds to a known value of H_{L2} (Figure 47) for the appropriate value of $Q = \epsilon_r/60\sigma\lambda$. From lh_2, h_2 is found by dividing by l.

If only one antenna height is less than $4/l$, then define $20 \log \bar{A}$ as $20 \log A + 20 \log l - 20 \log H_L$ for that antenna and h_2 then refers to the other antenna.

C. *Non-standard atmosphere.* $k \neq 4/3$. The preceding graphs are all based on $k = 4/3$. If $k \neq 4/3$, h_1, h_2, d, and A should be replaced by h_1', h_2', d', and A', where

$$h' = h \left(\frac{3k}{4}\right)^{-1/3},$$

$$d' = d \left(\frac{3k}{4}\right)^{-2/3},$$

$$A' = A \left(\frac{3k}{4}\right)^{2/3},$$

or

$$20 \log A' = 20 \log A + 20 \log \left(\frac{3k}{4}\right)^{2/3} \quad (178)$$

The change of h, d, A to the primed values can be made with the aid of Figure 43, i.e., if h, d are known, change to h', d', then Figure 37 will give $\bar{A}'$, which in turn will give A', and this with the aid of Figure 43 will give A.

D. *Change to dimensionless coordinates.* In the optical region, convenient coordinates are (see Section 6.5)

$$v = \frac{d}{\sqrt{2kah_1}} = \frac{d}{d_T}$$

$$u = \frac{h_2}{h_1}.$$

For these coordinates, equation (175) becomes

$$\bar{A} = \frac{A}{h_1 g(e)}. \quad (179)$$

Writing

$$\underline{e} = eh_1,$$
$$s = s\sqrt{2kah_1}, \quad (180)$$

it follows that

$$eh_2 = \underline{e}u,$$
$$\underline{e}v = sd,$$

and, using equations (150) and (159),

$$\underline{s}^2 = 2\underline{e}.$$

Consequently, Figure 37 can be used with $\underline{s}v$ replacing sd, $\underline{e}u$ replacing eh_2, and $\bar{A}$ is defined in equation (179).

Caution: In using the graphs, care must be exercised when one or both antennas are elevated to see that the receiver antenna is well within the diffraction region, i.e.,

$$d >> d_L. \quad (181)$$
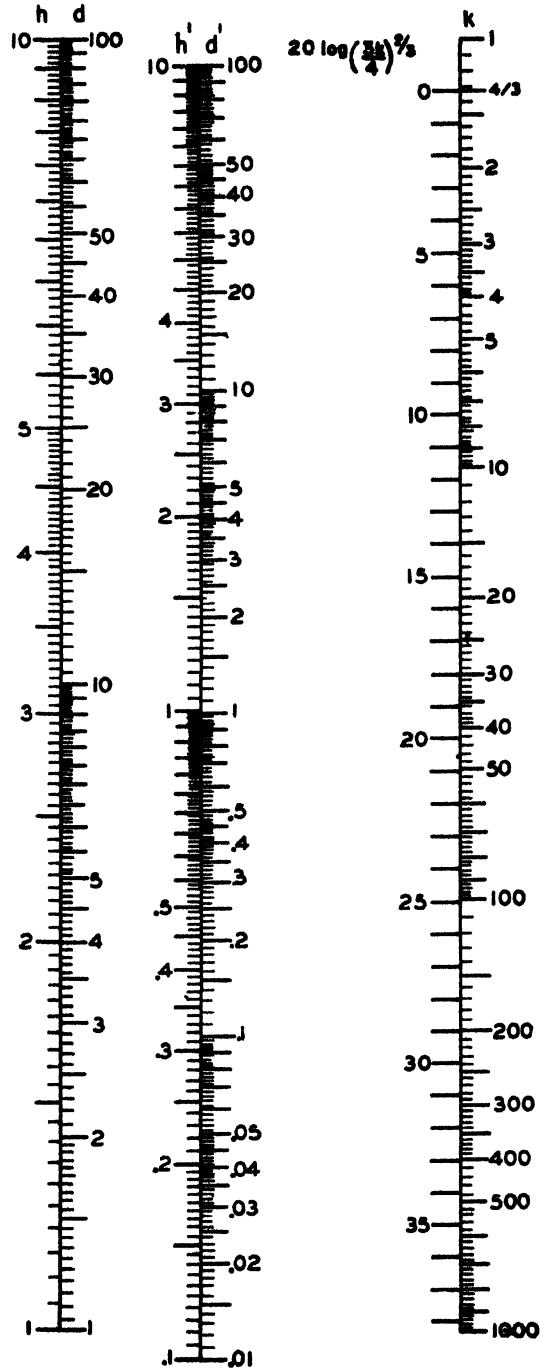
FIGURE 43. Relation of h, d to h', d' as a function of k.

E. *Illustrative problems; diffraction formula; dielectric earth.* Previously, four types of problems were considered for the optical-interference region. The same four types are given here, for a receiver below the optical-interference region. A dielectric earth is assumed so that the figures on pp. 413 - 416 are applicable. These require supplementing by equations (3) and (5).

For one-way transmission the radio gain is

$$10 \log \frac{P_2}{P_1} = 20 \log A + 10 \log (G_1 G_2). \quad (182)$$

For two-way transmission the radar gain is

$$10 \log \frac{P_2}{P_1} = 40 \log A + 10 \log (G_1 G_2) \\ + 7.5 + 10 \log \sigma - 20 \log \lambda. \quad (183)$$

Type I The heights and distance apart of the transmitter and receiver antennas and the wavelength are known. The radio gain is to be found.

An early-warning set has a horizontal antenna, located 118 meters above sea level. A receiver is located in an airplane 1,520 meters above sea level, at a distance of 300 km. The wavelength is 3 meters. The gain of the radar antenna is 96 db and its power output 100 kw. (a) The power received by the airplane receiver, assuming a gain of 10 db, is to be found. (b) The power returned to the radar by the airplane, assuming that the airplane has a radar cross section σ of 40 square meters, is to be found.

One-way: From Figure 2, $d_L = 205$ km. Hence the receiver may be assumed well within the diffraction region.

From Figure 40, $sd = 9.3$, with $f(\delta) = 1$.

From Figure 41, $eh_2 = 12.3$, with $g(\delta) = 1$.

From Figure 37, $20 \log \bar{A} = -213$.

To convert $20 \log \bar{A}$ to $20 \log A$ by equation (175), we need $20 \log h_1$ and $20 \log g_1$, which are given by Figure 41:

$$20 \log h_1 = 41.3,$$
$$20 \log g_1 = 1.5.$$

Hence

$$20 \log A = -170,$$

and by equation (182)

$$10 \log \frac{P_2}{P_1} = -170 + 96 + 10 = -64.$$

Since P_1 is 10^5 watts,

$$P_2 = 10^5 \times 10^{-6.4} = 10^{-1.4} \text{ w}.$$

Radar: Substituting in equation (183), the radar gain is given by

$$10 \log (P_2/P_1) = -340 + 2(96) + 7.5 + 16 - 9.5,$$
$$= -134 \text{ db}$$

or

$$P_2 = P_1 \times 10^{-13.4}.$$

The power output P_1 is 10^5 watts, so that the maximum received power

$$P_2 = 10^{-8.4} \text{ w}.$$

The minimum detectable power of the set is given as $1.6 \times 10^{-8} = 10^{-7.9}$ watt, so that under the given conditions the power returned by the target would be slightly below the threshold of detection.

Type II. Gain versus receiver (or target) height is to be found for given distance, given wavelength, and given transmitter height: A radar has an antenna height of $h_1 = 30$ meters, a wavelength of $\lambda = 1.5$ meters and a distance from a receiver (or target) of $d = 100$ km. Assuming a receiver antenna gain $G_2 = 1$, the variation of P_2/P_1 at the receiver with receiver height is to be found. Also, assuming a target of cross section $\sigma = 50$ sq meters, the variation of P_2/P_1 at the radar receiver with target height is to be found. The radar antenna has a gain of 13.5 db.

One-way:

$$sd = 3.9 \text{ (from Figure 40)}.$$

From Figure 37, for the fixed value of $sd = 3.9$, we find a correspondence between values of $20 \log \bar{A}$ and eh_2, listed in Table 5 below. By means of Figure 41 or equation (159), eh_2 is changed to h_2 and by means of equation (176), $\bar{A}$ to A. From Figure 41, it is seen that $20 \log h_1 = 29.5$ and $20 \log g_1 = 0$. To change A to P_2/P_1, the transmitter gain of 13.5 db and the receiver gain of 0 db must be taken into account, according to equation (182). The result is given in Table 5. The values of $10 \log (P_2/P_1)$ are plotted in Figure 25, together with the results found with the same data in text on p 397 for the optical-interference region.

TABLE 5*

h_2 Meters	eh_2	$20 \log \bar{A}$	$20 \log A$	Radio Gain in db	Radar Gain in db
63	0.8	−190	−160.5	−147	−273
142	1.8	−180	−150.5	−137	−253
259	3.3	−170	−140.5	−127	−233
417	5.3	−160	−124.5	−117	−208

* See also Table 1 and Figure 25.

Radar:

$$10 \log \frac{P_2}{P_1} = 40 \log A + 27 + 7.5 + 10 \log \sigma \\ - 20 \log 1.5,$$

$$= 40 \log A + 27 + 7.5 + 17 - 3.5,$$
$$= 40 \log A + 48.$$

Type III. Gain versus distance is to be found, with antenna heights and wavelength given: Using the same data given in text on p.398, the gain as a function of distance in the diffraction region is to be found. The result has been plotted in Figure 26. The polarization is horizontal.

$h_1 = 30$ meters $G_1 = 22.4$ (13.5 db)

$h_2 = 1000$ meters G_2 (one-way) $= 1$ (0 db)

$\lambda = 1.5$ meters G_2 (radar) $= 22.4$ (13.5 db)

$\sigma = 10$ square meters

From Figure 41,

$$eh_2 = 12.5.$$

Referring to Figure 37, we find a correspondence between $\bar{A}$ and sd. Values of $\bar{A}$ are to be assumed. To change sd to d, use Figure 40. To change $\bar{A}$ to A, use equation (176). From Figure 41,

$$20 \log 30 = 29.5,$$
$$20 \log g_1 = 0,$$
$$20 \log A = 20 \log \bar{A} + 29.5 + 0.$$

The radio gain is then given by:

One-way:

$$10 \log \frac{P_2}{P_1} = 20 \log A + 13.5 + 0;$$

The radar gain is then given by:

Radar:

$$10 \log \frac{P_2}{P_1} = 40 \log A + 7.5 + 27 + 10 - 3.5$$

$$= 40 \log A + 41.$$

These equations are evaluated in Table 6 and the one-way values are plotted in Figure 26.

TABLE 6

$20 \log \bar{A}$	sd	d	$20 \log A$	Radio Gain in db	Radar Gain in db
−170	6.2	159	−140	−127	−239
−180	6.9	177	−150	−137	−259
−190	7.6	193	−160	−147	−279
−200	8.3	213	−170	−157	−299
−210	9.0	231	−180	−167	−319
−220	9.7	249	−190	−177	−339
−230	10.3	263	−200	−187	−359
−240	11.0	282	−210	−197	−379
−250	11.8	305	−220	−207	−399
−260	12.5	320	−230	−217	−419
−270	13.2	340	−240	−227	−439
−280	13.8	357	−250	−237	−459

Type IV. The determination of contours along which the radio gain (or A) is constant (the coverage problem): A radar has a wavelength of 0.107 meter and a power output of 750 kw. Assume a receiver in space with a minimum detectable power of 10^{-10} watt. The maximum possible distance between the radar transmitter whose elevation is 100 meters and the receiver for varying heights of the receiver is to be found. The gain of the radar antenna is 10,000 (or 40 decibels), the gain of the receiver will be assumed to be 30 decibels.

For the radar problem, a target of radar cross section $\sigma = 50$ square meters is assumed to take the place of the receiver. The minimum detectable power of the radar is taken as 10^{-10} watt; the range of the set for varying altitudes of the target will be calculated.

One-way: The radio gain sought is the ratio of the minimum detectable power to the power output, or

$$\frac{P_2}{P_1} = \frac{10^{-10}}{750 \times 10^3} = \frac{4}{3} \times 10^{-16},$$

or

$$10 \log (P_2/P_1) = -160 + 1 = -159 \text{ db}.$$

From equation (3),

$$20 \log A = -159 - 40 - 30,$$

$$= -229 \text{ db}.$$

From Figure 41,

$$20 \log g_1 = 18.5,$$

$$20 \log h_1 = 40.$$

Therefore

$$20 \log \bar{A} = -229 - 40 - 18.5,$$

$$= -287.5 \text{ db}.$$

Referring to Figure 37, the pairs of values of sd and eh_2 along the contour $20 \log \bar{A} = -287$ are given in Table 7. By means of Figures 40 and 41, sd and eh_2 are changed to d and h_2. The points found are to the right of the curve for $eh_1 = 7.3$, so that they correspond to points in the diffraction region.

TABLE 7

d_{km}	sd	eh_2	h_2 meters
118	11	1.3	18
129	12	3.5	48
140	13	7.0	96
151	14	11.5	158
161	15	16.5	226

Radar: The value of $10 \log (P_2/P_1)$ is the same as for the one-way calculation, -159 db. This must be changed to $20 \log A$ by equation (5),

$$20 \log A = -141 \text{ db},$$

and, as above,

$$20 \log \bar{A} = -141 - 40 - 18.5,$$

$$= -199.5 \text{ db}.$$

Referring to Figure 37, we see that the contour $20 \log \bar{A} = -199.5$ is to the left of $eh_1 = 7.3$ [see caution in equation (181)]. Therefore it is not possible to get the necessary power return P_2 from the given target so long as it is below the line of sight. The desired contour would lie above the line of sight. The determination of the contour is discussed on page 400.

Sea Water, VHF, Vertical Polarization

1. *Graphical Aids.* Graphical aids are given in this section, which, as in text on p.413, are valid for all practical distances when both antennas are low $[h < h_e$ (see Figure 35)] and $2h_1h_2 << \lambda d$. If one or both antennas are elevated, they will give the value of the radio gain for the first mode, which is a good approximation for the result found by summing all the modes when the receiver is well within the diffraction region, i.e., when $d > d_L$. [If one antenna is low ($h < h_e$) and one *well* elevated ($h > 40h_e$), the result found by using several modes is given in

Referring to equation (162) and Section 5.7.1,

$$A = 2A_0 A_1 F_0 (H_{L}gg')_1 (H_{L}gg')_2, \tag{184}$$

with $gg' = 1$ for $h < h_e$.

h_c is given by Figure 35,

20 log gg' is given by Figure 36,

20 log A_0 is given by Figure 3 in Chapter 2,

F_s is given by Figures 31, 32, and 33.

2. *Plane earth factor* A_1. This has been discussed in Section 5.7.1. A_1 is a function of $p'd$; p' is given in Figure 44 and 20 log A_1 in Figure 45. The curve shift of A_1 with λ in the VHF band is less than 1 db. When $p'd > 50$, $A_1 = 1/p'd$, as in the dielectric case.

3. *The low height-gain* H_L is a function of lh (see text on p.404). l is given by Figure 46, H_L or 20 log H_L by Figure 47. H_L depends on the curve parameter $Q = \epsilon_r/60\sigma\lambda$ which for sea water is $1/3\lambda$. Since $H_L \rightarrow lh$ for $lh > 4$, 20 log H_L can be found from Figure 34.

4. h_1, $h_2 > 4/l$ *and* $d > 50/p'$. As in text on p.405 [noting especially equations (151) and (153)], equation (184) reduces, when $h > 4/l$ and $d > 50/p'$, to

$$A = \frac{3}{2} \frac{F_s}{d^2} (gg'h)_1 (gg'h)_2 \qquad (185)$$

Equation (185) may be used generally, provided $(gg'h)$ is replaced by H_L/l when $h < 4/l$, and the right-hand member is multiplied by $A_1 p'd$ or, in decibels, 20 log $A_1 +$ 20 log $p'd$ are added, when $d < 50/p'$. In this formula $d < 50/p'$ is given in meters.

5. *Horizontal versus vertical polarization.* It is of interest to compare the gain of vertically and hori-
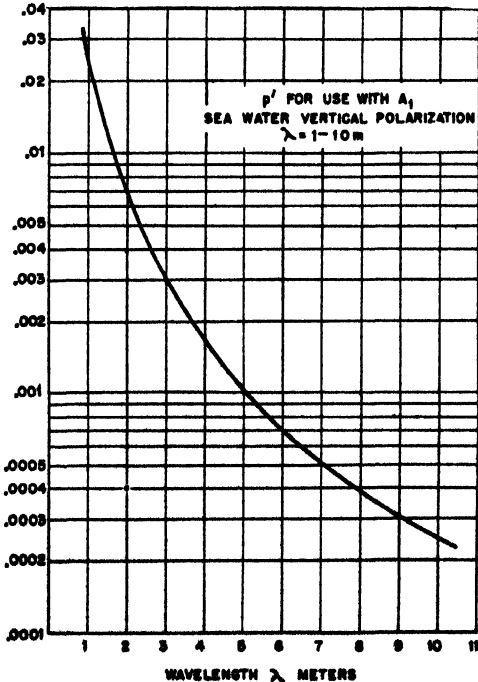
FIGURE 44. p' versus λ for sea water, vertical polarization.

TABLE 8. Values of $4/l$ and $50/p'$ for various wavelengths.

λ	1	2	3	4	5	6	7	8	9	10	m
$\dfrac{4}{l}$	3	27	50	80	110	143	174	222	267	308	m
$\dfrac{50}{p'}$	2	17	17	30	50	71	100	125	175	200	km

zontally polarized waves over sea water at VHF. (It has been pointed out earlier that there is no marked difference in attenuation between horizontally and vertically polarized waves for wavelengths less than one meter.) Equation (184) is valid for horizontally polarized waves also by using the appropriate F_s curve and putting $g' = 1$ and can be made the basis of a comparison between vertical and horizontal polarization. See, for comparison, equation (160).

For antennas at, or very close to, zero height, the gain-factor ratio depends on A_1F_s. While F_s gives greater attenuation (lower gain) for horizontal than for vertical polarization, the difference between the two lies principally in the values of A_1. For $\lambda = 1$ meter, the ratio is 64,000 to 1 in favor of vertical polarization. For $\lambda = 10$ meters, the ratio is about 8.6×10^6.

However, as the antennas are raised above the ground, the strength of a horizontally polarized field increases much more rapidly than does the corresponding vertically polarized field, for a given wavelength up to a certain height above which the field is substantially independent of polarization. For example, above a height of 3 meters for $\lambda = 1$ meter, and above 77 meters for $\lambda = 10$ meters, the two fields are practically equal.

6. *Parameter* $\bar{A}$. As on pp. 413-416, curves can be drawn in terms of the parameter $\bar{A}$ where

$$\bar{A} = \begin{cases} \dfrac{A}{(hgg')_1} & \text{for } h_1 > 4/l, \\[2ex] \dfrac{Al}{H_L} & \text{for } h_1 < 4/l. \end{cases} \qquad (186)$$
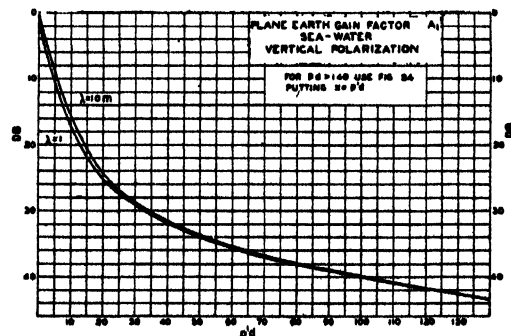
FIGURE 45. Plane earth factor A_1, for sea water, vertical polarization. *Note:* All db values are negative.
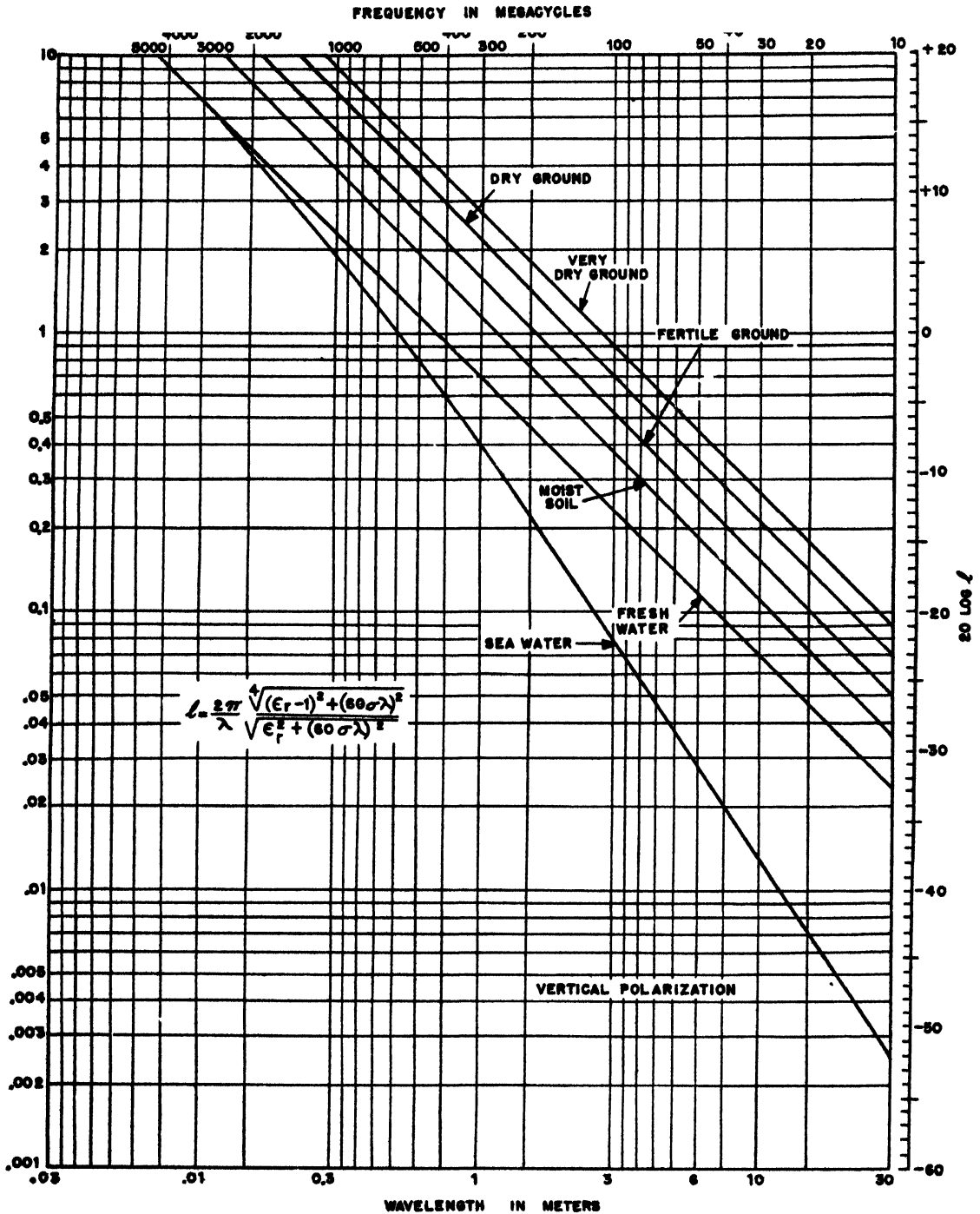
FIGURE 46.   Parameter l versus frequency for vertical polarization. See Table 10.

Equation (185), including the correction for $d < 50/p'$, becomes

$$A = \frac{3}{2}\frac{F_e}{d^2}(A_1 p'd)\,(gg'h)_1(gg'h)_2,\qquad (187)$$

which can be written

$$\bar{A} = 1.77 \times 10^{-7}\left[\frac{F_e}{(sd)^2}\right]A_1 p'd\,\psi\qquad (188)$$

or

$$20\log\bar{A} = -135 + 20\log\frac{F_e}{(sd)^2} + 20\log A$$
$$+ 20\log p'd + 20\log\psi.\qquad (189)$$

Since F_e has a graphical representation which depends on the wavelength, it is necessary to assume a particular value of λ; equation (188) then becomes
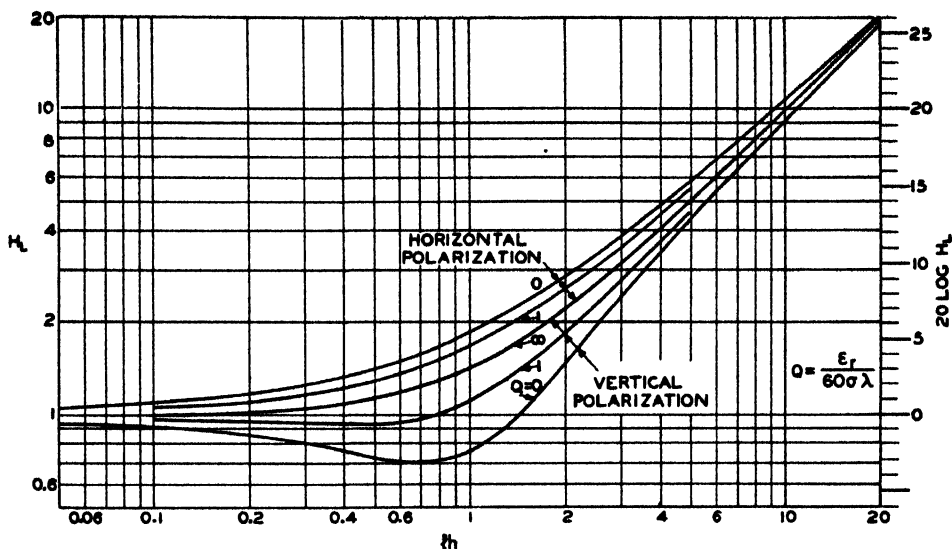
FIGURE 47. Height-gain function H_L versus lh, for low antenna heights [See equation (152)]

a relation between $\bar{A}$, d_1, and h_2, and Figures 48, 49, and 50 for $\lambda = 1, 3, 6$ meters are in terms of these coordinates. The height-gain function of the transmitter g_1 can be found from Figure 41.

7. *Illustrative example: Communication.* A communication set used in ship-to-ship work has a wavelength of 1 meter, a receiver sensitivity of 10 microvolts with a resistance of 50 ohms across the input terminals and a transmitter power output of 100 watts. The transmitter and receiver antennas are vertical half-wave dipoles at an elevation of 30 meters. The range is to be found.

To produce a voltage of 10 microvolts across 50 ohms, a power of

$$P_2 = \frac{V^2}{R} = \frac{100 \times 10^{-12}}{50} \text{ watt} = 2 \times 10^{-12} \text{ watt,}$$

so that this is the minimum detectable power. The value of P_2/P_1 for the given power output of 100 watts is

$$\frac{2 \times 10^{-12}}{100} = 2 \times 10^{-14},$$

and

$$10 \log \frac{P_2}{P_1} = 3 + (-140) = -137.$$

This is to be changed to $20 \log A$ by equation (3). The gain of a half-wave dipole over a doublet is 1.09 so that $G_1 = G_2 = 1.09$, or 0.4 db,

$$20 \log A = -137 - 0.8 \cong -138 \text{ db.}$$

In changing from $20 \log A$ to $20 \log \bar{A}$ it must be determined which of the relations in equation (186) is required by comparing the transmitter height of 30 meters with $4/l$. The value of l as given by

Figure 46 is 0.4. Hence the value of $4/l$ is 10, which is less than 30. Then

$$20 \log \bar{A} = 20 \log A - 20 \log 30 - 20 \log gg',$$
$$= -138 - 30 - 0,$$
$$= -168.$$

Referring to the chart for $\lambda = 1$, Figure 48, we find that for $h_2 = 30$ meters and $20 \log \bar{A} = -168$, the distance d is 53 kilometers. This then is the maximum theoretical range between the two sets.

Radio Gain Near the Line of Sight

For d much greater than d_L, the first mode is sufficient, as given in the last two sections. For d nearly equal to d_L, i.e., the receiver near the line of sight, a formula [equation (190)] can be given which takes into account several modes and still permits the use of graphical aids. This formula is valid only when the elevated antenna is very high, i.e., $h > 1,200\lambda^{2/3}$ and the other antenna is low, i.e., $h < 30\lambda^{2/3}$. (Otherwise the transition curve near the line of sight must be sketched in graphically, as indicated by the broken portion in Figure 7.)

Denoting by H_{L1} the height-gain of the low antenna at height h_1,

$$A = 2A_0 H_{L1} M(\delta) \left[\frac{(sd)^2}{2eh_2} \right]^{1/4} F_2(\Delta) \qquad (190)$$

where h_2 and $F_2(\Delta)$ refer to the elevated antenna.

1. sd and eh are given in Figures 40 and 41. δ is given on page 422.

2. $\Delta = \sqrt{g(\delta)} \left(sd - \sqrt{2eh_2} \right)$.

3. $g(\delta) = 1$, except for the VHF range, vertical polarization, over sea water. The values are given in Table 9.
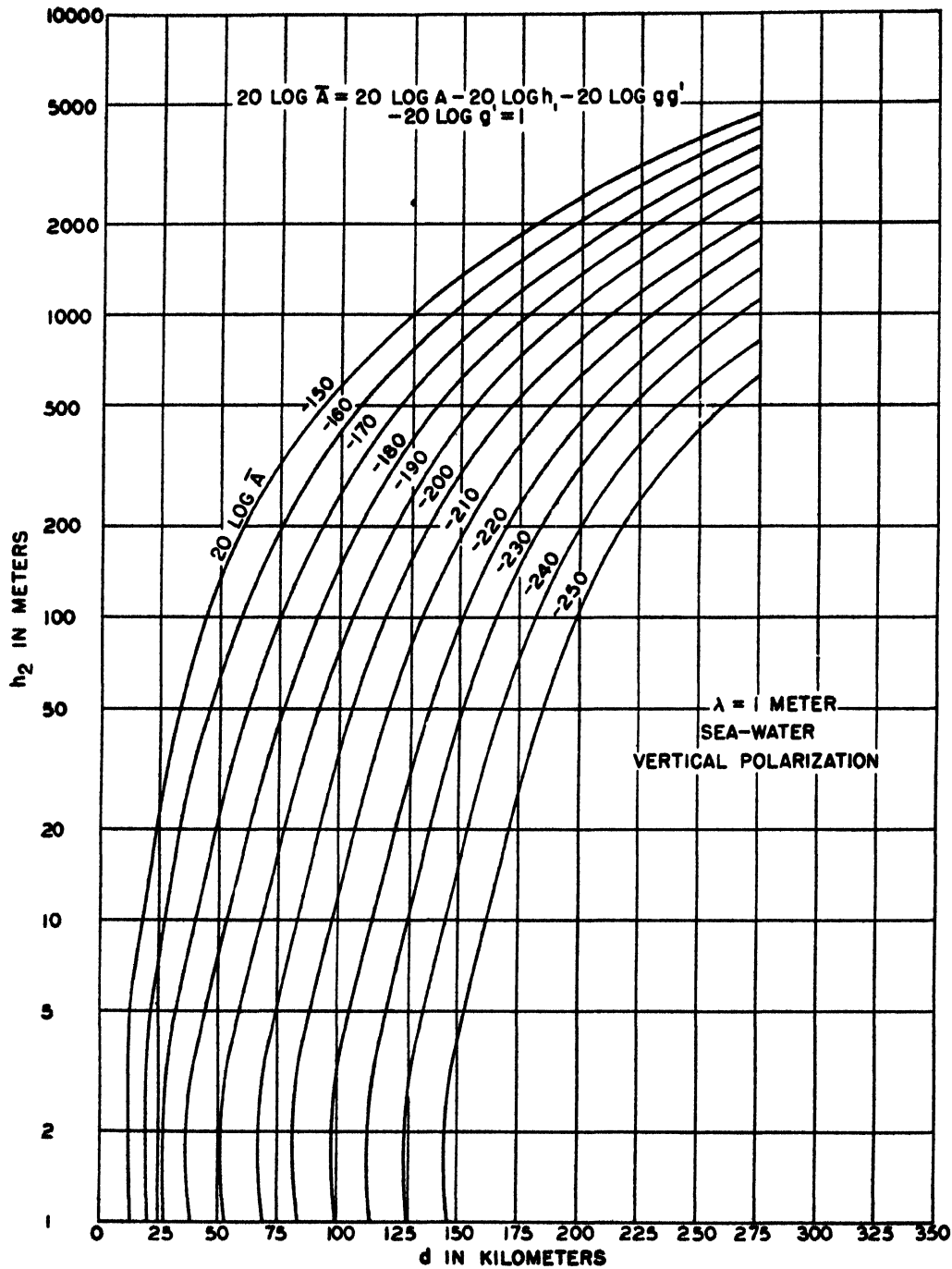
FIGURE 48. Maximum range for $\lambda = 1$ meter, vertical polarization. [See equation (186).]

TABLE 9. Values of $\sqrt{g(\delta)}$ for VHF (sea water).

λ	1	2	3	4	5	6	7	8	9	10 meters
$\sqrt{g(\delta)}$	0.98	0.97	0.95	0.94	0.93	0.91	0.90	0.88	0.86	0.84

4. $F_2(\Delta)$ is given by Figure 51.

5. $M(\delta)$ for vertical polarization is given by Figure 52 as a function of δ which can be found from Figures 53 and 54.

For horizontal polarization

$$M(\delta) = \frac{1}{\sqrt{|\delta|}} = \left(\frac{\lambda}{2\pi ka}\right)^{1/3} \frac{1}{\sqrt{|\epsilon_c - 1|}}$$

$$= \left(\frac{\lambda}{2\pi ka}\right)^{1/3} \frac{1}{\sqrt[4]{(\epsilon_r - 1)^2 + (60\sigma\lambda)^2}}. \quad (191)$$
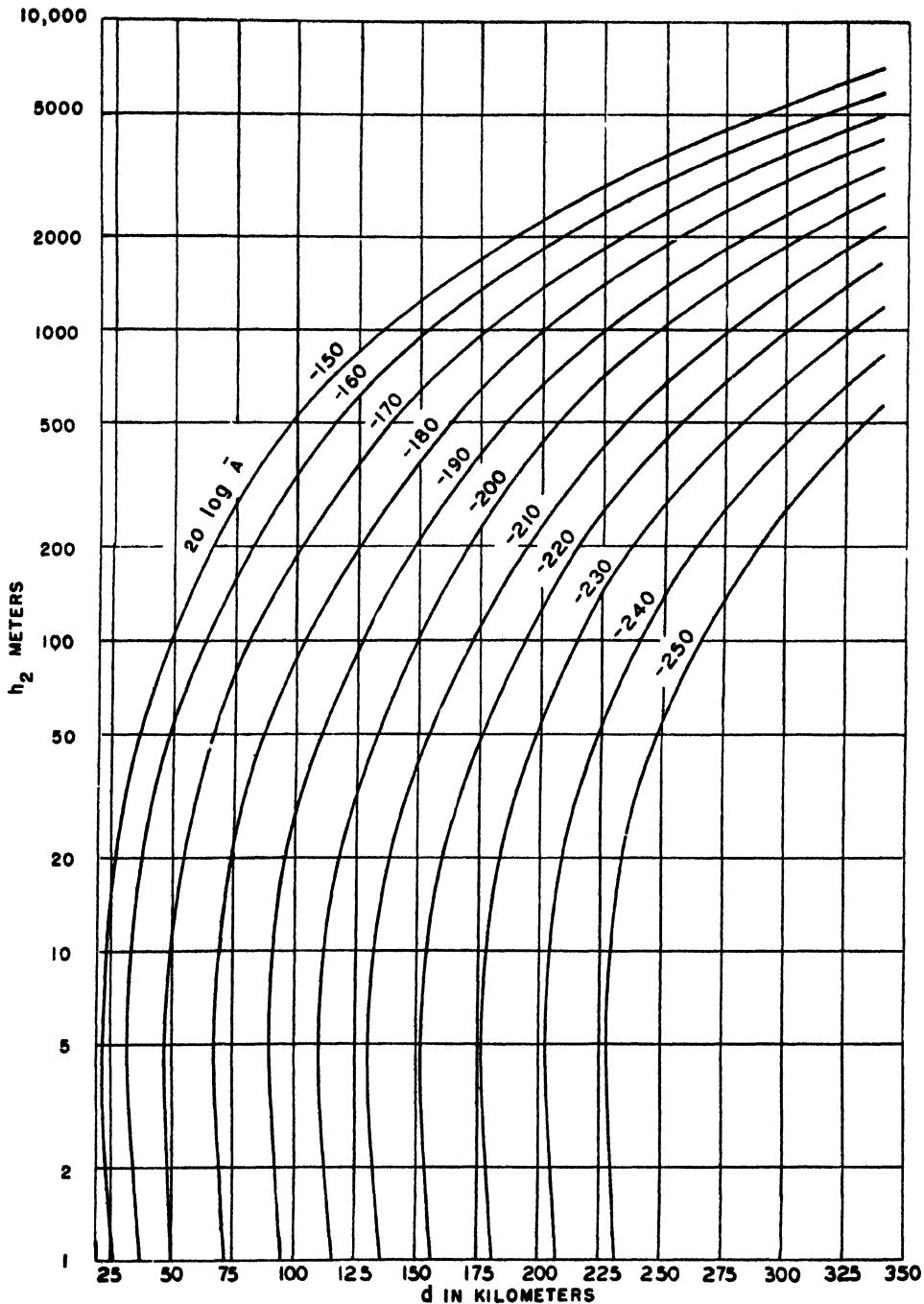
FIGURE 49. Maximum range for $\lambda = 3$ meters (sea water vertical polarization $- 20 \log g' = 1$). See equation (186).

General Solution for Vertical (or Horizontal) Dipole Over a Smooth Sphere

1. *Field strength of dipole.* The vertical component of the electrical field of a vertical dipole radiating in a homogeneous atmosphere over a sphere of radius ka (or horizontal component in the case of a horizontal dipole) is given by equation (192). The solution is valid provided the distance between receiver and transmitter and the radius of the sphere are much greater than a wavelength, conditions which are fulfilled in any practical application of short waves.

$$E = 2E_0(2\pi\zeta)^{1/2}\left|\sum_{n=1}^{\infty}\frac{e^{-j\tau_n\zeta}}{\delta + 2\tau_n}f_n(h_1)\cdot f_n(h_2)\right|. \quad (192)$$
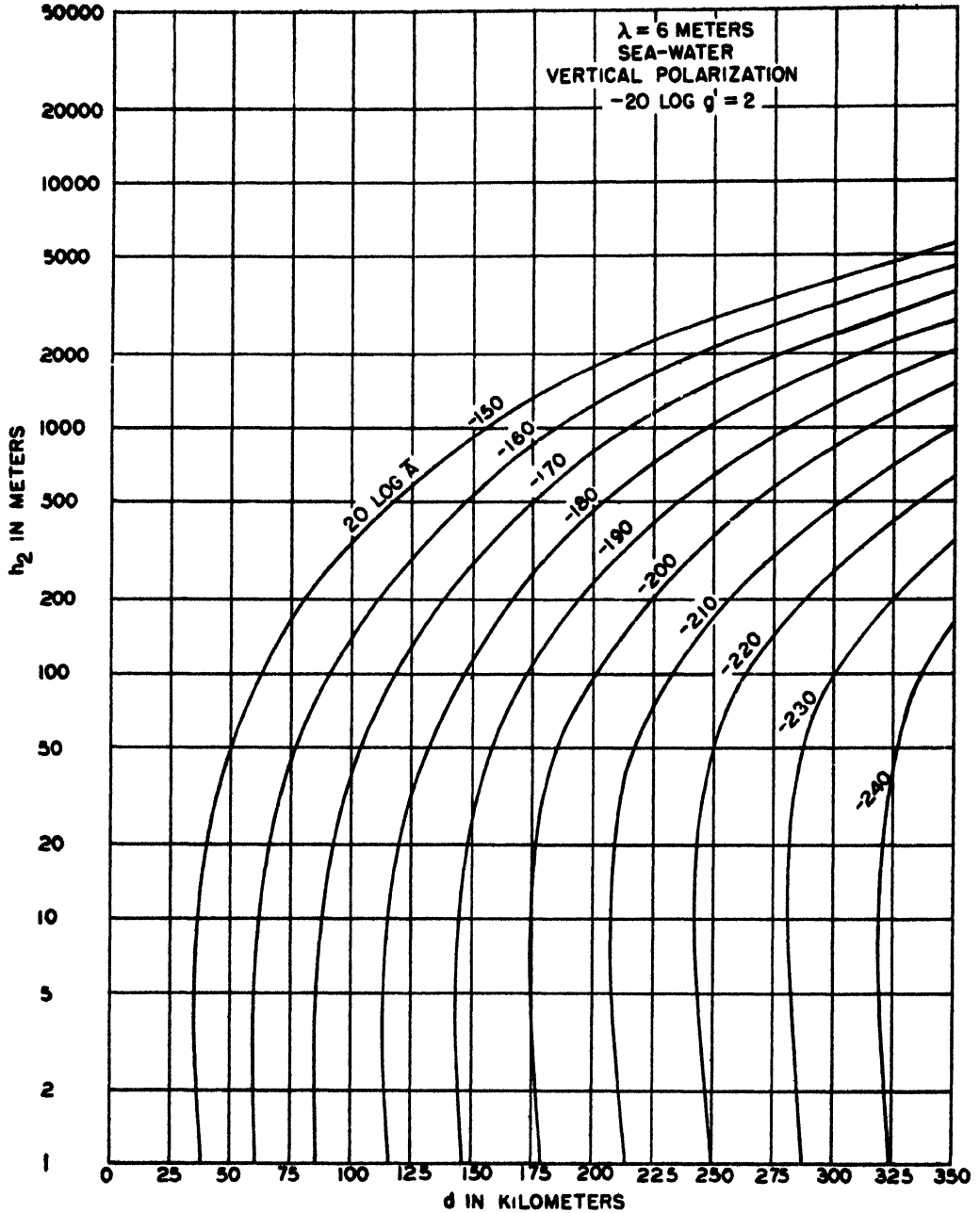
FIGURE 50. Maximum range for $\lambda = 6$ meters, vertical polarization. See equation (186).

a. h_1 and h_2 are antenna heights,

b. E_0 is the value of E for a doublet in free space,

c. δ is the ground parameter which depends on the complex dielectric constant $\epsilon_c = \epsilon_r - j60\sigma\lambda$.

For vertical polarization,

$$\delta = \left(\frac{2\pi ka}{\lambda}\right)^{2/3} \frac{\epsilon_c - 1}{\epsilon_c^2} = \frac{14.2 \times 10^4}{\lambda^{2/3}} \frac{\epsilon_c - 1}{\epsilon_c^2}$$

$$\text{for } k = \frac{4}{3}. \tag{193}$$

For horizontal polarization,

$$\delta = \left(\frac{2\pi ka}{\lambda}\right)^{2/3} (\epsilon_c - 1) = \frac{14.2 \times 10^4}{\lambda^{2/3}} (\epsilon_c - 1)$$

$$\text{for } k = \frac{4}{3}.$$

d. $\zeta = sd,$

where

$$s = \left(\frac{2\pi}{\lambda k^2 a^2}\right)^{1/3}$$

$$\Delta = \sqrt{g(\delta)}\,(sd-\sqrt{2\,s h_e})$$
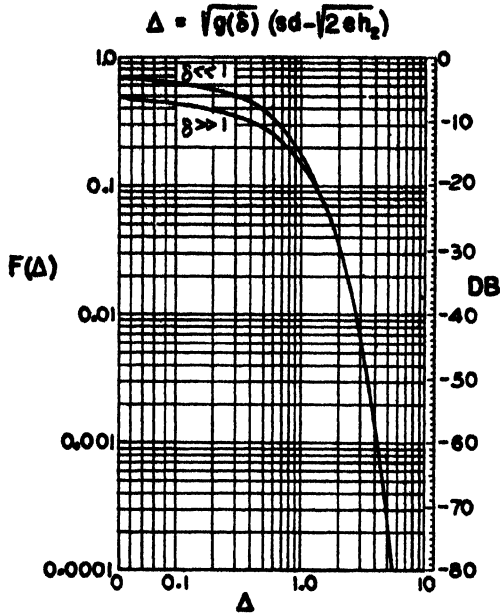
FIGURE 51. $F(\Delta)$ [representing $F_s(\Delta)$] versus Δ for use in equation (190).

or

$$s = 4.43 \times 10^{-5}\lambda^{-1/3}\left(\frac{4}{3k}\right)^{2/3} \qquad (194)$$

e. τ_n are complex numbers which characterize the individual terms (modes) in equation (192). They are a function of δ.

f. $f_n(h_1)$ and $f_n(h_2)$ are height-gain functions for the nth mode.

2. *The complex ground parameter δ.* δ depends on the wavelength and the electrical constants of the ground. (The dielectric constant is referred to air

as unity.) δ is large for horizontally polarized waves, but for vertically polarized waves it may vary considerably, as may be seen from Figure 53. In Figure 54, the phase of δ is given. For wavelengths less than 10 meters $|\,\delta\,|$, as given by Figure 53 for vertical polarization, is large except in the VHF range over sea water, $\epsilon_r = 80$, $\sigma = 4$.

The ground constants ϵ_r and σ for water and various types of earth are given in Table 10. For $\lambda < \lambda_c$ the ground material is a dielectric earth.

TABLE 10. Ground constants.

Type of ground			$\lambda_c = \frac{\epsilon_r}{60\sigma}$
Sea water	$\epsilon_r = 80$	$\sigma = 4$ mhos per meter	0.33 m
Fresh water	$\epsilon_r = 80$	$\sigma = 5 \times 10^{-3}$	267
Moist soil	$\epsilon_r = 30$	$\sigma = 0.02$	25
Fertile ground	$\epsilon_r = 15$	$\sigma = 5 \times 10^{-3}$	50
Rocky ground	$\epsilon_r = 7$	$\sigma = 10^{-3}$	117
Dry soil	$\epsilon_r = 4$	$\sigma = 10^{-2}$	6.7
Very dry soil	$\epsilon_r = 4$	$\sigma = 10^{-3}$	66.7

3. *The mode numbers* τ_n. These numbers are given below for the two limiting values for $\delta = 0$ (infinite conductivity or $\lambda \to \infty$), and for $\delta = \infty$, i.e., the dielectric earth.

Mode No.	$\delta = 0$	$\delta = \infty$
1	$\tau_{1,0} = 0.885\,e^{-j\pi/3}$	$\tau_{1,\infty} = 1.856\,e^{-j\pi/3}$
2	$\tau_{2,0} = 2.577\,e^{-j\pi/3}$	$\tau_{2,\infty} = 3.245\,e^{-j\pi/3}$
3	$\tau_{3,0} = 3.824\,e^{-j\pi/3}$	$\tau_{3,\infty} = 4.882\,e^{-j\pi/3}$
≥ 4	If $n \geq 4$, $\tau_{n,0} = \frac{1}{2}[3\pi(n+\frac{3}{4})]^{2/3}e^{-j\pi/3}$	If $n \geq 4$, $\tau_{n,\infty} = \frac{1}{2}[3\pi(n+\frac{1}{4})]^{2/3}e^{-j\pi/3}$
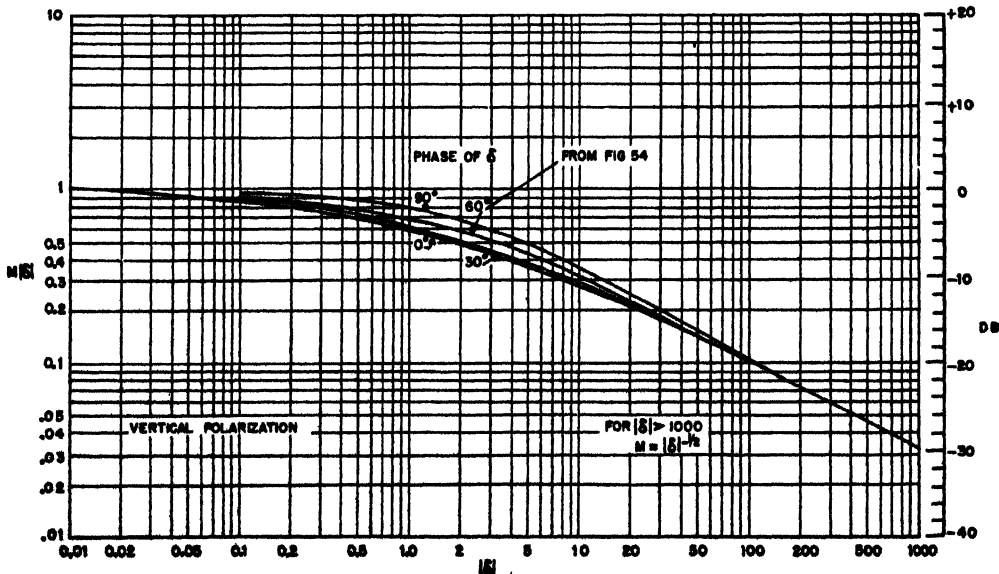
FIGURE 52. $M(\delta)$ versus $|\,\delta\,|$ for use in equation (190), vertical polarization.
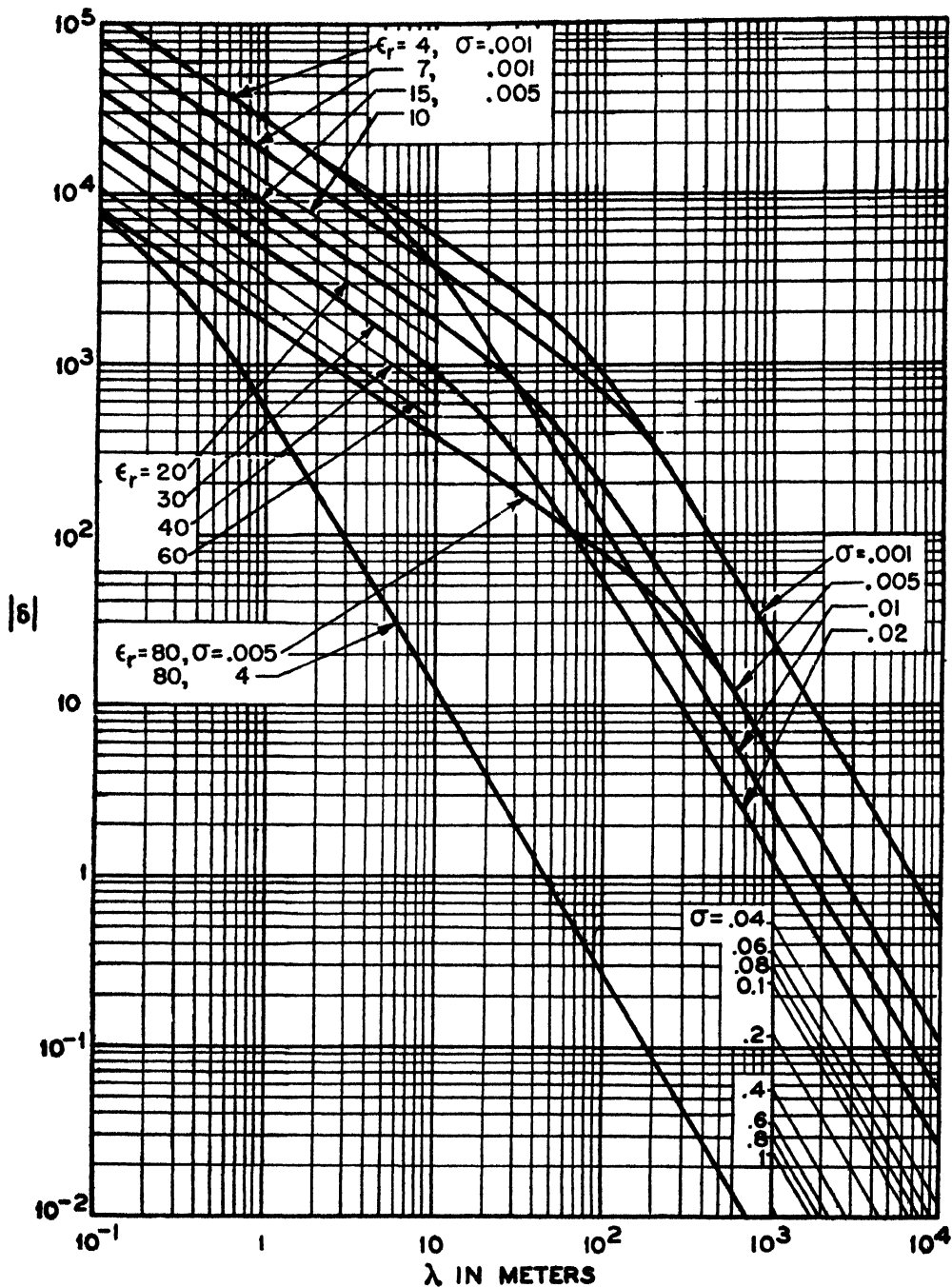
FIGURE 53. $|\delta|$ versus λ for vertical polarization (see Table 10). Dielectric earth, $\delta \rightarrow \infty$; perfect conductor, $\delta \rightarrow 0$. Phase of δ is 45° for intersection of two asymptotes for any particular ground.

From these limiting values of τ the value of τ in general for any given δ can be found from the following two series, of which only the first is of interest in short-wave work.

δ large,

$$\tau_n = \tau_{n,\infty} - \delta^{-1/2} - \frac{2}{3}\tau_{n,\infty}\delta^{-3/2} + \frac{1}{2}\delta^{-3} - \frac{4}{5}\tau_{n,\infty}^2\delta^{-3/2}$$

$$+ \cdots . \qquad (195)$$

δ small,

$$\tau_n = \tau_{n0} - \frac{\delta^{1/2}}{2\tau_{n,0}} = \frac{\delta}{8\tau_{n,0}^3}$$

$$- \frac{1}{12\tau_{n,0}^2}\left(1 + \frac{3}{4\tau_{n,0}^3}\right)\delta^{3/2} + \cdots .$$

4. The height-gain functions $f(h)$.

(a) *For low antennas* ($h < 30\lambda^{2/3}$), the height-gain
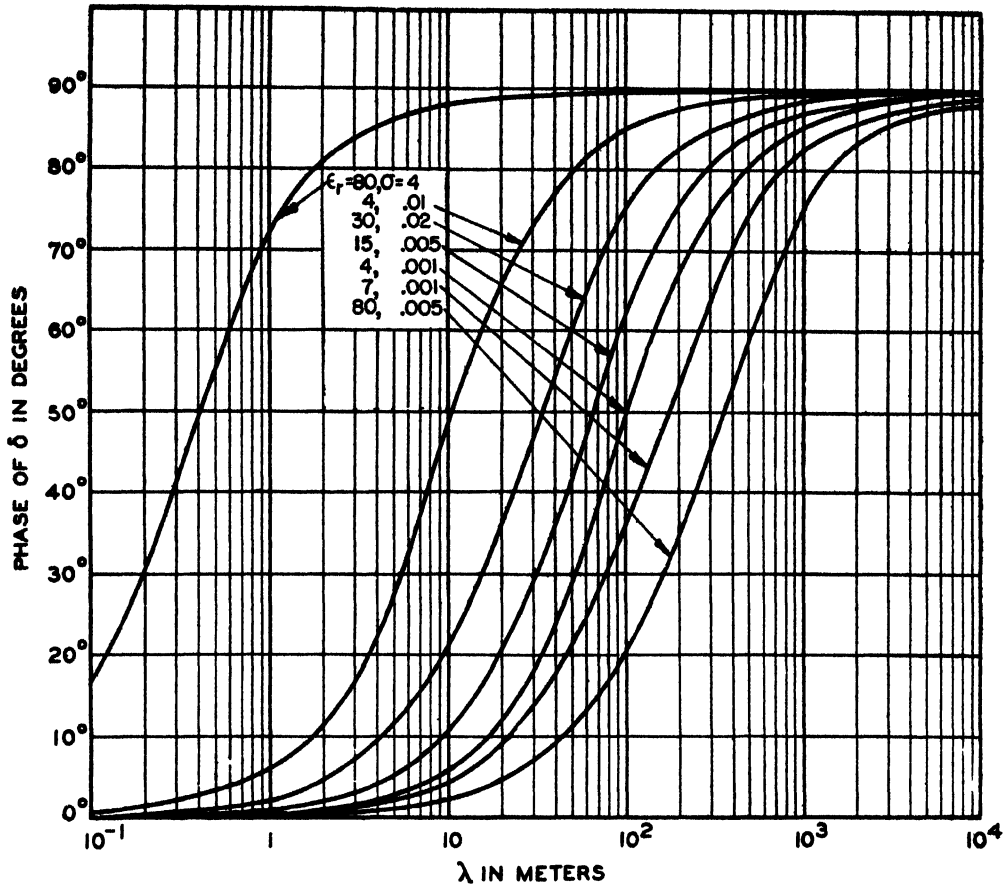
FIGURE 54 Phase of δ for vertical polarization. See Table 10.

$$\beta = \text{imaginary part of } \tau_{1,\infty}$$
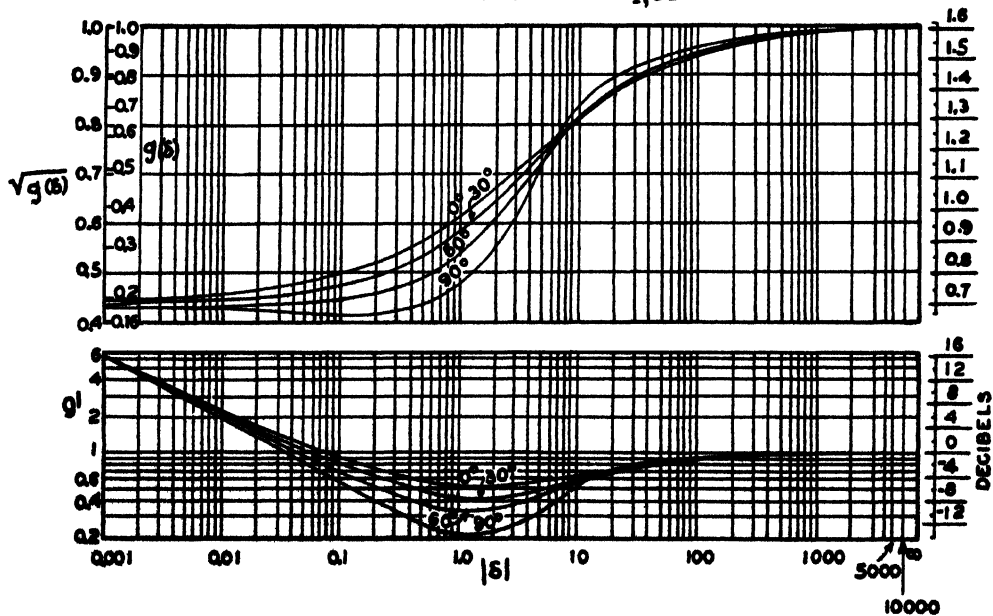
FIGURE 55. $\sqrt{g(\delta)}$ and g' as functions of magnitude and phase.

$$p'd = \frac{2\pi d/\lambda}{\sqrt{\epsilon_r^2 + (60\,\sigma\lambda)^2}}\sqrt{\frac{(\epsilon_r-1)^2 + (60\,\sigma\lambda)^2}{\epsilon_r^2 + (60\,\sigma\lambda)^2}}\quad \text{FOR VERTICAL POLARIZATION}\qquad p'd = (2\pi d/\lambda)\sqrt{(\epsilon_r-1)^2 + (60\,\sigma\lambda)^2}\quad \text{FOR HORIZONTAL POLARIZATION}$$
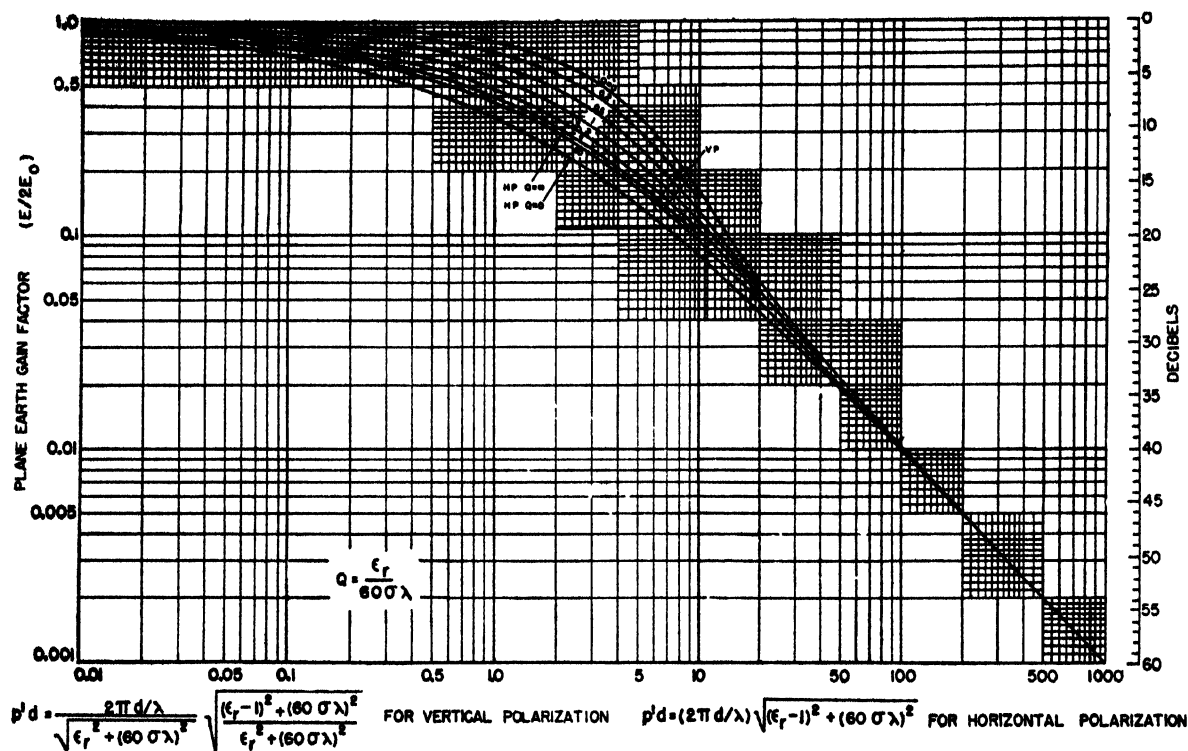
FIGURE 56. Plane earth gain factor A_1 versus $p'd$. $A_1 = 1/(p'd)$ for $p'd > 50$.

functions, to the first approximation, are independent of n.

$$f(h) = 1 + j\left[\frac{2\pi h}{\lambda}\frac{\sqrt{\epsilon_c-1}}{\epsilon_c}\right] \text{for vertical polarization,}$$

$$(196)$$

$$f(h) = 1 + j\left[\frac{2\pi h}{\lambda}\sqrt{\epsilon_c-1}\right] \text{for horizontal polarization}$$

Note that the magnitudes of the bracketed quantities are equal to lh. The magnitude of f has been denoted by H_L and is represented in Figure 47 as a function of lh. The phase of the bracketed quantities in equation (196) is taken into account by using different curves with the parameter $Q = \epsilon_r/60\sigma\lambda$. For large values of lh, $H_L \rightarrow lh$

(b) *For elevated antennas* ($h \gg 30\lambda^{2/3}$). The
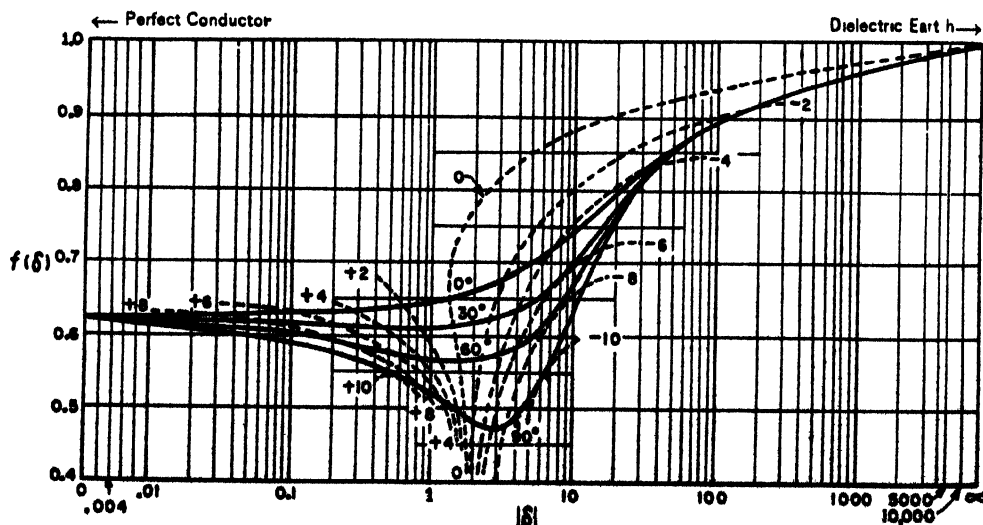
FIGURE 57. $f(\delta)$ versus δ. Solid lines correspond to phase of δ. Dotted lines indicate curve in Figure 58. For horizontal polarization $f(\delta) = 1$.
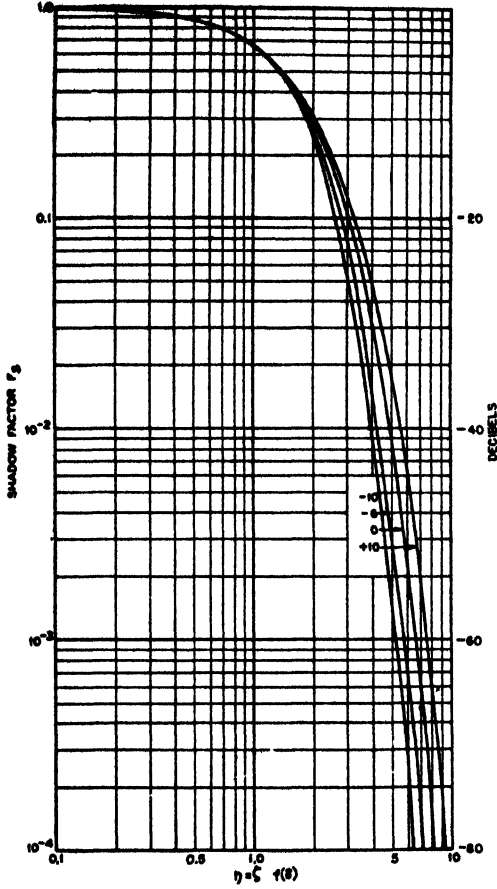
FIGURE 58. Shadow factor F_s versus $\eta = \zeta f(\delta) = s d f(\delta)$. See Figures 32, 33, and 57. Curve +10 corresponds to a perfect conductor.

function f_n can be represented by

$$f_n = \frac{3}{\sqrt{2\pi}} \frac{1}{(2eh)^{1/4}} \frac{\exp\left\{+j\frac{\pi}{4} - j\frac{1}{3}\left[(eh) - 2\tau_n\right]^{3/2}\right\}}{J_{1/3}(x) + J_{-1/3}(x)},$$

(197)

where, from equation (159),

$$e = \frac{(4\pi^2)^{1/3}}{(\lambda^2 ka)^{1/3}} = \frac{\lambda^{-2/3}}{60}\left(\frac{4}{3k}\right)^{1/3}$$

(198)

and where the argument of the two Bessel functions is

$$x = \tfrac{1}{3}(-2\tau_n)^{3/2} e^{-j\pi}$$

For the nth mode, if $(eh) \gg 2\tau_n$, the magnitude of f_n can be written

$$\left| \frac{3}{\sqrt{2\pi}} \frac{1}{(2eh)^{1/4}} \frac{\exp(j\tau_n\sqrt{2eh})}{J_{1/3}(x) + J_{-1/3}(x)} \right|.$$

(199)

For large δ, using the first two terms of equation (195), and writing x_∞ for x when τ_n is replaced by $\tau_{n,\infty}$,

$$x = x_\infty - \left(\frac{-2\tau_\infty}{\delta}\right)^{1/2}$$

Substituting this in $J_{1/3}(x) + J_{-1/3}(x)$, writing down

the first two terms of the Taylor expansion, making use of the fact that the $\tau_{n,\infty}$ are roots of $J_{1/3}(x) + J_{-1/3}(x) = 0$ and of the relation given by a property of the Bessel function,

$$J_{1/3}'(x) + J_{-1/3}'(x) = -1/(3x)\left[J_{1/3}(x) + J_{-1/3}(x)\right] + J_{-2/3}(x) - J_{2/3}(x),$$

we have

$$J_{1/3}(x) + J_{-1/3}(x)$$
$$\cong -\left(-\frac{2\tau_\infty}{\delta}\right)^{1/2}\left[J_{-2/3}(x_\infty) - J_{2/3}(x_\infty)\right].$$

(200)

If these results are substituted into equation (192) for both antennas, the factor $(\delta + 2\tau_n)$ becomes $1 + 2\tau_{n,\infty}/\delta$, which approaches unity for large δ. This means that *if both antennas are sufficiently elevated, short-wave propagation is practically independent of ground constants.*

The value of f given by equation (199) can be written as glh so that g represents the gain over lh, the value approached by H_L, when $lh > 4$. The value of g for $\delta \to \infty$ is represented in Figure 36.

If δ is not very great, as in the case of vertically polarized VHF over sea water, the effect of δ can be taken into acocunt by changing e to $eg(\delta)$ and g to gg'. The functions $g(\delta)$ and g' are given by Figure 55.

5. *Plane earth gain factor and shadow factor.* The field near the ground over a plane earth with infinite conductivity is equal to $2E_0$, twice the free-space field. For an imperfectly conducting ground, the field for antennas at zero height over a plane earth may be written

$$E = 2E_0A_1.$$

(201)

A_1 is represented in Figure 56 as a function of $p'd$, where

$$p' = \frac{2\pi}{\lambda}\frac{|\epsilon_c - 1|}{|\epsilon_c|^2} = \frac{2\pi}{\lambda}\frac{\sqrt{(\epsilon_r - 1)^2 + (60\sigma\lambda)^2}}{\epsilon_r^2 + (60\sigma\lambda)^2}$$

(202)

for vertical polarization. For horizontal polarization.

$$p' = \frac{2\pi}{\lambda}|\epsilon_c - 1| = \frac{2\pi}{\lambda}\sqrt{(\epsilon_r - 1)^2 + (60\sigma\lambda)^2}.$$

(203)

The curve parameter is $Q = \epsilon_r/60\sigma\lambda$.

Comparing equations (202) and (203) with equations (193) and (194), we find that

$$p'd = |\delta|\zeta.$$

(204)

Hence, equation (192) may be written as

$$E = 2E_0(2\pi)^{1/2}\frac{\zeta^{3/2}}{p'd}\left|\sum \frac{e^{-j\tau_n\zeta}}{1 + 2\tau_n/\delta}f_n(h_1)f_n(h_2)\right|$$

(205)

If $p'd$ is large, we see from Figure 56 that

$$A_1 \cong \frac{1}{p'd},$$

(206)

so that the physical significance of $1/p'd$ in equation (205) becomes apparent.

The factor

$$F_s = (2\pi)^{1/2} \zeta^{3/2} \left| \sum \frac{e^{-j\tau_n \zeta}}{1 + 2\tau_n/\delta} \right| \qquad (207)$$

represents the effect of earth curvature in increasing the attenuation over that of a plane earth at zero height [i.e., $f(0) = 1$] and equation (205) is now of the form

$$E = 2E_0 A_1 F_s \qquad (208)$$

If δ is large (e.g., λ small), $2\tau_n/\delta$ in equation (207) may be neglected and τ_n replaced by $\tau_{n,\infty}$ so that the shadow factor is practically independent of ground constants. The shadow factor is represented graphically in Figures 32 and 58. Where the factor $2\tau_n/\delta$ cannot be neglected, as in the VHF range, vertical polarization over sea water, the dependence of F_s on δ is accommodated by changing the abscissa from $\zeta = sd$ to $\eta = s'd$ where $s' = sf(\delta)$, and by representing F_s by a family of curves in Figure 58, whose parameter is given by dotted lines in Figure 57. $f(\delta)$ is represented also in Figure 57. For $\eta < 0.4$, F_s is less than 1 db below unity. This corresponds to a distance over which the earth may be considered plane, i.e., $d < 10^4 \lambda^{1/3}$, as given in text on p. 405. The greater the wavelength, the smaller the effect of the earth's curvature.

If the antennas are elevated, F_s can still be used for the first mode for great distances where the first mode gives most of the field.

Sample Calculation for Very Dry Soil

The general solution given in text on p. 421 is here illustrated for the case of doublet antennas, either horizontally or vertically polarized, placed at various heights over an earth assumed to be *very dry soil* for which the constants are $\epsilon_r = 4$, and $\sigma = 0.001$ mho/meter. The following graphs cover, in decimal steps, the frequency range of 30,000 to 0.03 mc or wavelengths $\lambda = 0.01$ to 10,000 meters.

Figure 59 gives the free space radio gain A_0 and the radio gain A decibels over very dry soil, as a function of distance d for doublets at zero height. Figure 60 gives the first mode height-gain factors for transmitter and receiver heights, h_1 and h_2, respectively.

To obtain the radio gain under different conditions it is merely necessary to add the decibel gains of the transmitter and receiver antennas, the radio gain for zero height (Figure 59), the height-gain factor (Figure 60) for the transmitter, and a similar figure

FIGURE 59. Free-space radio gain A_0 (— — —) and radio gain A, in decibels, for propagation over very dry soil with doublet antennas on the ground (——— for horizontal polarization and — — for vertical polarization). Numbers on the curves give the wavelength λ. *Note:* Radio gain is independent of the radiated power.

FIGURE 60. First mode height-gain factors for transmitter and receiver.

TABLE 11. Quantities independent of polarization.

Earth, Very Dry Soil.

$\epsilon_r = 4$; $\sigma = 0.001$ mhos/meter; $\epsilon_c = 4 - j0.06\lambda = 4(1 - j0.015\lambda)$; $\epsilon_c - 1 = 3 - j0.06\lambda = 3(1 - j0.02\lambda)$.

f mc	λ m	$\lambda^{\frac{1}{3}}$	$\lambda^{\frac{2}{3}}$	$h_c = 30\lambda^{\frac{1}{3}}$	$Q = \dfrac{\epsilon_r}{60\sigma\lambda}$ $= \dfrac{66.67}{\lambda}$
30,000.	0.01	0.2154	0.0465	1.4	6667.
3,000.	0.1	0.465	0.2145	6.45	666.7
300.	1.	1.	1.	30.	66.67
30.	10.	2.154	4.65	140.	6.667
3.	100.	4.65	21.54	645.	0.667
0.3	1,000.	10.	100.	3,000.	0.0667
0.03	10,000.	21.54	465.	14,000	0.00667

f mc	$d_c =$ $10^4\lambda^{\frac{1}{3}}$	$s = \dfrac{0.443}{d_c}$	$\epsilon_c - 1$	$|\epsilon_c - 1|$	$\sqrt{|\epsilon_c - 1|}$	$|\epsilon_c|^2$
30,000.	2154.	2.05×10^{-4}	$3(1 - j0.0002)$	3.	1.732	16.
3,000.	4650.	0.954×10^{-4}	$3(1 - j0.002)$	3.	1.732	16.
300.	10^4	0.443×10^{-4}	$3(1 - j0.02)$	3.0006	1.733	16.004
30.	2.15×10^4	0.205×10^{-4}	$3(1 - j0.2)$	3.06	1.75	16.36
3.	4.65×10^4	0.954×10^{-5}	$3(1 - j2.)$	6.71	2.59	52.
0.3	10^5	0.443×10^{-5}	$3(1 - j20)$	60.072	7.77	3,616.
0.03	2.15×10^5	0.205×10^{-5}	$3(1 - j200)$	600.015	24.5	360,016.

TABLE 12. Quantities dependent on polarization.

Earth, Very Dry Soil.

		HORIZONTAL POLARIZATION				
f mc	λ m	$\lvert\delta\rvert = \left(\dfrac{2\pi ka}{\lambda}\right)^{\frac{2}{3}}\lvert\epsilon_c - 1\rvert$ $= \dfrac{14.2 \times 10^4}{\lambda^{\frac{2}{3}}}\lvert\epsilon_c - 1\rvert$	Phase of δ degrees	l $= \dfrac{2\pi}{\lambda}\sqrt{\lvert\epsilon_c - 1\rvert}$	$p' = \dfrac{l^2\lambda}{2\pi}$ $= \dfrac{2\pi}{\lambda}\lvert\epsilon_c - 1\rvert$	$f(\delta)$ Fig. 57
30,000.	0.01	0.916×10^7	(Dielectric Earth)	$-$ .0114	1086.	1885.	1
3,000.	0.1	1.98×10^6		$-$ .1145	108.6	188.5	1
300.	1.	0.426×10^6		$-$ 1.145	10.86	18.85	1
30.	10.	6.933×10^5		$-$ 11.3	1.1	1.92	1
3.	100.	0.444×10^5		$-$ 63.5	0.163	0.421	1
0.3	1,000.	0.854×10^5		$-$ 87 1	0.0487	0.377	1
0.03	10,000.	1.835×10^5		$-$ 89.7	0.0154	0.377	1

		VERTICAL POLARIZATION				
f mc	λ m	$\lvert\delta\rvert = \left(\dfrac{2\pi ka}{\lambda}\right)^{\frac{2}{3}}\dfrac{\lvert\epsilon_c - 1\rvert}{\lvert\epsilon_c\rvert^2}$ $= \dfrac{14.2 \times 10^4}{\lambda^{\frac{2}{3}}}\dfrac{\lvert\epsilon_c - 1\rvert}{\lvert\epsilon_c\rvert^2}$ Fig. 53	Phase of δ degrees Fig. 54	l $= \dfrac{2\pi}{\lambda}\cdot\dfrac{\sqrt{\lvert\epsilon_c - 1\rvert}}{\lvert\epsilon_c\rvert}$	$p' = \dfrac{l^2\lambda}{2\pi}$ $= \dfrac{2\pi}{\lambda}\dfrac{\lvert\epsilon_c - 1\rvert}{\lvert\epsilon_c\rvert^2}$	$f(\delta)$ Fig. 57
30.000.	0.01	5.72×10^5	(Dielectric Earth)	0.	272.	118.	1 (0)
3.000.	0.1	1.2×10^5		0.	27.2	11.8	1 (0)
300.	1.	2.6×10^4		0.	2.72	1.18	1 (0)
30.	10.	5.7×10^3		$+$ 5.5	0.272	0.118	0.99 (0)
3.	100.	850.	(Conducting Earth)	$+$ 50.	0.0272	0.81×10^{-2}	0.96 ($-$ 1)
0.3	1,000.	23.		$+$ 85.	0.00272	1.044×10^{-4}	0.77 ($-$ 5)
00.3	10,000.	0.52		$+$ 90.	0.000272	1.047×10^{-6}	0.55 ($+$10)

for the receiver (Figure 60). This process, however, is subject to the restriction mentioned in the next paragraphs.

The addition of the factors given in the preceding paragraph is valid all the way up to the maximum of the first lobe, where the field is given by the sum of the direct and reflected rays, provided that the antennas have comparable heights.

The radio gain can therefore never be more than 6 db greater than the free-space gain with the same antennas.

If, however, one antenna is low, $h < h_o$, and the other is very high, $h > 40h_o$, the method discussed fails since the height-gain factors are based on the first mode only. In this event, either the methods outlined on pp. 419-420 must be employed or the radio gain at low elevations must be connected *graphically* with the value obtained in the optical region for the first maximum.

As an aid to the computer in checking his results, four tables of computations are given. Table 11 gives the values of certain quantities, for a wide range of frequencies and for very dry soil, which are independent of polarization. Those quantities which are dependent on polarization are given in Table 12. Table 13 gives detailed calculations for ground level radio gain for doublets for a wavelength of $\lambda = 1.0$ meter, while Table 14 gives the first mode height-gain factors for the same wavelength.

Similar charts and tables may be prepared easily for transmission over other types of earth for a similar range of frequencies.

TABLE 13. Ground level radio gain for doublets.

Earth, Very Dry Soil. $\lambda = 1.0$ m; $Q = 66.67$; $f(\delta) = 1$ (Fig. 57); $s = 0.443 \times 10^{-4}$.
Ground level radio gain for doublets, $h_1 = h_2 = 0$; $G_1 = G_2 = 1$; $P_1 = 1$ watt radiated.

d m	Polar-ization	$p'd$	A_1 Fig. 56	$\zeta = sd$	$\eta = \zeta f(\delta)$	F_s Fig. 32, 33, 58	$A_0 = \frac{3\lambda}{8\pi d}$	A_0 in db $20 \log A_0$
500	H	0.942×10^4	1.06×10^{-4}	0.02215	0.02215	1.	2.39×10^{-4}	-72.4
	V	0.059×10^4	1.695×10^{-3}	0.02215	0.02215	1.	2.39×10^{-4}	-72.4
1,000	H	1.885×10^4	0.53×10^{-4}	0.0443	0.0443	1.	1.195×10^{-4}	-78.5
	V	0.118×10^4	0.847×10^{-3}	0.0443	0.0443	1.	1.195×10^{-4}	-78.5
2,000	H	3.77×10^4	0.265×10^{-4}	0.0886	0.0886	1.	0.597×10^{-4}	-84.5
	V	0.236×10^4	0.423×10^{-3}	0.0886	0.0886	1.	0.597×10^{-1}	-84.5
5,000	H	0.942×10^5	1.06×10^{-5}	0.2215	0.2215	0.97	2.39×10^{-5}	-92.4
	V	0.059×10^5	1.695×10^{-4}	0.2215	0.2215	0.97	2.39×10^{-5}	-92.4
10,000	H	1.885×10^5	0.53×10^{-5}	0.443	0.443	0.9	1.195×10^{-5}	-98.5
	V	0.118×10^5	0.847×10^{-4}	0.443	0.443	0.9	1.195×10^{-5}	-98.5
20,000	H	3.77×10^5	0.265×10^{-5}	0.886	0.886	0.71	0.597×10^{-5}	-104.5
	V	0.236×10^5	0.423×10^{-4}	0.886	0.886	0.71	0.597×10^{-5}	-104.5
50,000	H	0.942×10^6	1.06×10^{-6}	2.215	2.215	0.25	2.39×10^{-6}	-112.5
	V	0.059×10^6	1.695×10^{-5}	2.215	2.215	0.25	2.39×10^{-6}	-112.5
100,000	H	1.885×10^6	0.53×10^{-6}	4.43	4.43	0.02	1.195×10^{-6}	-118.5
	V	0.118×10^6	0.847×10^{-5}	4.43	4.43	0.02	1.195×10^{-6}	-118.5
200,000	H	3.77×10^6	0.265×10^{-6}	8.86	8.86	5×10^{-5}	0.597×10^{-6}	-124.5
	V	0.236×10^6	0.423×10^{-5}	8.86	8.86	5×10^{-5}	0.597×10^{-6}	-124.5

d m	Polar-ization	$A = 2A_0 \cdot l_1 F_s$	A in db $20 \log A$	$\dfrac{A_V}{A_H}$	$\dfrac{A}{A_0} = 2A_1F_s = \dfrac{E}{\sqrt{G_1}E_0} = A_p$	$E_0 = \dfrac{3\sqrt{5}\sqrt{P_1 G_1}}{d}$ $\mu v/m$ for 1 watt radiated	E $\mu v/m$ for 1 watt radiated	$20 \log E =$ db above 1 $\mu v/m$ for 1 watt radiated
500	H	5.07×10^{-8}	-146	16	2.12×10^{-4}	13,420	2.84	9.1
	V	8.11×10^{-7}	-122		3.39×10^{-3}	13,420	45.5	33.1
1,000	H	1.268×10^{-8}	-158	16	1.06×10^{-4}	6,710	0.711	-2.9
	V	2.025×10^{-7}	-134		1.69×10^{-3}	6,710	11.38	21.1
2,000	H	0.316×10^{-8}	-170	16	0.53×10^{-4}	3,355	0.178	$-15.$
	V	0.505×10^{-7}	-146		0.846×10^{-3}	3,355	2.84	9.1
5,000	H	4.93×10^{-10}	-186	16	2.06×10^{-5}	1,342	0.0276	-31.1
	V	7.86×10^{-9}	-162		3.29×10^{-4}	1,342	0.441	-7.1
10,000	H	1.14×10^{-10}	-199	16	0.955×10^{-5}	671	0.0064	-43.8
	V	1.82×10^{-9}	-175		1.525×10^{-4}	671	0.1023	-19.8
20,000	H	0.224×10^{-10}	-213	16	0.376×10^{-5}	335.5	0.126×10^{-1}	$-58.$
	V	0.358×10^{-9}	-189		0.6×10^{-4}	335.5	0.0201	-33.9
50,000	H	1.267×10^{-12}	-238	16	0.53×10^{-6}	134.2	0.711×10^{-4}	$-83.$
	V	2.02×10^{-11}	-214		0.847×10^{-5}	134.2	1.137×10^{-3}	$-59.$
100,000	H	0.253×10^{-13}	-272	16	0.212×10^{-7}	67.1	0.1422×10^{-5}	$-117.$
	V	0.405×10^{-12}	-248		0.339×10^{-6}	67.1	0.227×10^{-4}	$-93.$
200,000	H	0.158×10^{-16}	-336	16	0.265×10^{-10}	33.55	0.887×10^{-9}	$-181.$
	V	0.253×10^{-15}	-312		0.423×10^{-9}	33.55	0.142×10^{-7}	$-157.$

TABLE 14. Height-gain factors (first mode).

Earth, Very Dry Soil. $\lambda = 1.0$ m; $\delta_H = 0.426 \times 10^4$ ($-1.1°$); $\delta_V = 2.6 \times 10^4$ ($0°$); $l_H = 10.86$; $l_V = 2.72$.

First mode height-gain factors, $h_c = 30.$ m; $\epsilon = \dfrac{1}{2h_c} = 0.01667$; $Q = 66.67$.

h m	Polar- ization	lh	H_L Fig. 47	eh	$g(\delta)$ Fig. 55	$ehg(\delta)$	g Eq. (157) Fig. 36	g' Fig. 55	$H_L gg'$	$20 \log(H_L gg')$
0.01	H	.1086	1.				1	1	1	0
	V	.0272	1.				1	1	1	0
0.1	H	1.086	1.5				1	1	1.5	3.5
	V	.272	1.				1	1	1	0
0.25	H	2.725	3.				1	1	2.73	8.68
	V	.68	1.25				1	1	1.25	1.9
0.5	H	5.43	5.5				1	1	5.5	14.8
	V	1.36	1.7				1	1	1.7	4.6
1.	H	10.86	10.86				1	1	10.86	20.7
	V	2.72	2.8				1	1	2.8	8.9
3	H	32.58	32.58				1	1	32.58	30.3
	V	8.16	8.16				1	1	8.16	18.2
10.	H	108.6	108.6				1	1	108.6	40.7
	V	27.2	27.2				1	1	27.2	28.7
30.	H	325.8	325.8	0.5	1	0.5	1	1	325.8	50.3
	V	81.6	81.6		1	0.5	1	1	81.6	38.3
100.	H	1,086.	1,086.	1.667	1	1.667	1.5	1	1,630	64.2
	V	272.	272.		1	1.667	1.5	1	408	52.2
300.	H	3,258.	3,258.	5.	1	5.	4.3	1	14,000	82.9
	V	816.	816.		1	5.	4.3	1	3,510	70.9
1,000.	H	10,860.	10,860.	16.67	1	16.67	100.	1	1.086×10^8	120.7
	V	2,720.	2,720.		1	16.67	100.	1	0.272×10^8	108.7
2,000.	H	21,720.	21,720.	33.33	1	33.33	1,585.	1	3.44×10^7	151.
	V	5,440.	5,440.		1	33.33	1,585.	1	0.863×10^7	139.
5,000.	H	54,300.	54,300.	83.33	1	83.33	1.497×10^6	1	8.13×10^{10}	218.
	V	13,600.	13,600.		1	83.33	1.497×10^6	1	2.035×10^{10}	206.

Chapter 6

COVERAGE DIAGRAMS

DEFINITIONS

THE LOCUS of points in space having a constant field strength is called a coverage diagram. In the optical region this is also called a lobe diagram. The construction of these diagrams is an important part of the predetermination of the performance of radar and communication sets. The basic concepts and formulas will be developed first for the case of the plane earth and then applied with necessary modifications to propagation over a spherical earth.

The method outlined in this chapter is applicable only to the lobe structure lying above the tip of the first lobe. In this region the field is given almost entirely by the vector sum of the direct and reflected waves. The lower portion of the first lobe is distorted from the regular lobe structure because, in this region, the field strength is determined in part by contributions from the diffraction terms as well as by the contributions of the direct and reflected waves.

PLANE EARTH

Field Strength

For horizontal polarization and a reflection coefficient equal to -1 (i.e., $\rho = 1$, $\phi = 180°$), the received field intensity oscillates from zero to twice the free-space value, depending on the position of the point in space, as shown in Figure 1. The position in space determines the path difference Δ,
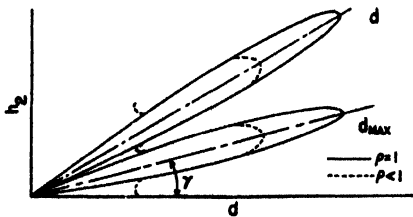
FIGURE 1. Coverage diagram for plane earth (heights h_2 are exaggerated relative to distance d). $n = 1,3,5$ .... for the first, second, third .... lobes. $d = d_{max}$ $\sin (\pi n/2)$ and $d_{max} = 2d_0$.

which in turn determines the phase retardation, δ_{lag}, due to path difference. The angle $\Omega/2$ used in calculating E by equation (29) in Chapter 5 is a function of δ_{lag} and ϕ, since $\Omega = \delta_{lag} + \phi'$. The effect of a reflection coefficient ρ less than unity is to reduce the length of the lobe maxima to values less than $2d_0$ and to increase the minima above zero as indicated by the dotted lines of Figure 1. The angles

at which the maxima and minima occur depend upon the phase shift at reflection, as will be explained in the following section.

Angles of Lobe Maxima (Horizontal Polarization)

Lobe maxima occur whenever the sum of the phase shifts caused by reflection and path difference equals an even multiple of π radians, while lobe minima (nulls) occur when the total phase shift is an odd multiple of π radians. If $\rho = 1$, the nulls are equal to zero.

It follows that for horizontal polarization ($\phi \cong \pi$), maxima occur when δ equals π, 3π, 5π, etc., and minima when $\delta = 0$, 2π, 4π, etc. This means that a path difference equal to an odd multiple of $\lambda/2$ gives a lobe maximum while a path difference equal to an even multiple of $\lambda/2$ gives a null. This holds only for horizontal polarization ($\phi = \pi$). Applying equation (52) in Chapter 5 to the case when $d_1 << d_2$ (i.e., $d_2 \cong d$),

$$\Delta = \frac{2h_1h_2}{d} = 2h_1 \tan \psi \cong 2h_1 \tan \gamma \cong 2h_1\gamma, \quad (1)$$

where γ is the angle in radians between the horizontal and the line joining the receiver or target to the base of the transmitter (see Figure 8 in Chapter 5). For equation (1) to hold, ψ must be less than 0.2. Hence for maxima,

$$2h_1\gamma = \frac{n\lambda}{2}, \quad n = \text{odd integer,}$$

and for minima, \hfill (2)

$$2h_1\gamma = \frac{n\lambda}{2}, \quad n = \text{even integer,}$$

or

$$\gamma = \frac{n\lambda}{4h_1},$$

and n has a range of 0 to 2 for the first lobe, 2 to 4 for the second lobe, etc.

The limitations of equation (2) may be summarized as follows:

1. The phase shift at reflection is π radians. This assumes horizontal polarization, or $\psi \cong 0$ for vertical polarization.

2. The reflection point is (relatively) close to the transmitter.

3. The grazing angles corresponding to lobe maxima are less than 0.2 radians. In connection with limitation (2), it should be noted that the angles for

TABLE 1

Antenna height, h_1, (meters)	γ Minimum (degrees)	$n\lambda$ Minimum (meters)	Minimum n at $\lambda = 3$ meters
120	1.44	12.9	4.3
60	1.1	4.5	1.5
30	0.78	1.6	0.53
15	0.56	0.6	0.2
9	0.4	0.25	0.08

which the approximation $\gamma = \psi$ holds depend upon the wavelength and transmitter height. The following table shows the minimum angle for various transmitter heights and wavelengths at which the error in the path difference Δ introduced by this assumption is less than 1 per cent. To satisfy equation (2), and have an error less than 1 per cent, γ should lie between the minimum value and 0.2 radians. Table 1 shows, for increasing transmitter antenna height, how the angle for which equation (2) is valid within 1 per cent also increases.

If n is set equal to $2m - 1$, integral values of m correspond to lobe maxima and half-odd integers to lobe minima. The advantage of this notation is that the value of m is the number of the maxima or lobe number. Thus for the fifth lobe, $m = 5$. The general expression for the grazing angles corresponding to lobe maxima, for a plane earth and for horizontal polarization, is

$$\gamma = \frac{(2m - 1)}{4h_1}\lambda, \qquad (3)$$

where integral values of m give maxima and half-odd integers give minima.

Angles of Lobe Maxima (Vertical Polarization)

With vertically polarized radiation the reflection phase shift ϕ [equation (27) in Chapter 5] is less than π radians (i. e., $\phi' = \phi - \pi$ is negative). It follows that the path difference for lobe maxima must be greater than $\lambda/2$ and greater than λ for the nulls. In other words, the value of n in equation (2) must be increased by $(\Delta + n)$ to compensate for the decreased phase shift of reflection, so that

$$(\Delta n)\left(\frac{\lambda}{2}\right)\left(\frac{2\pi}{\lambda}\right) - (\pi - \phi) = 0. \qquad (4)$$

Hence

$$(\Delta n) = \frac{\phi}{\pi} - 1 = +\frac{\phi'}{\pi}. \qquad (5)$$

For vertical polarization, equation (2) becomes

$$\gamma = \frac{n + (\Delta n)}{4h_1}. \qquad (6)$$

Lobe Equation

When $\rho = 1$, and $\phi = \pi$, $\phi' = 0$, and $\Omega = \delta$,

equation (46) in Chapter 5 may be written as

$$d = 2\sqrt{G_1}d_0 \sin\frac{\Omega}{2} = 2\sqrt{G_1}d_0 \sin\frac{\delta}{2}. \qquad (7)$$

Substituting

$$\delta = \frac{2h_1h_2}{d}\left(\frac{2\pi}{\lambda}\right)$$

gives

$$d = 2\sqrt{G_1}d_0 \sin\left(\frac{2\pi h_1 h_2}{\lambda d}\right), \qquad (8)$$

where d_0 is the free-space range which may be computed from the gain corresponding to the given coverage diagram by use of the nomogram given in Figure 3 in Chapter 2. Equation (8) may be written as

$$d = 2\sqrt{G_1}d_0 \sin\left(2\pi\frac{h_1}{\lambda} \cdot \sin\gamma\right). \qquad (9)$$

Equation (9) shows that for fixed values of free-space range d_0, transmitter height h_1, and wavelength, the coverage lobe may be represented by a polar sine function of the angle γ at the base of the antenna. This assumes that the slant range measured to any point on the lobe may be considered equal to the distance d measured along the surface of the earth.

If n in equation (2) is allowed to assume all fractional and integral values from 0 to 2, $\sin\gamma \rightarrow \gamma$ may be expressed as

$$\sin\gamma = \gamma = \frac{n\lambda}{4h_1}. \qquad (10)$$

Substituting this value into equation (9) gives

$$d = 2\sqrt{G_1}d_0 \sin\left(\frac{n\pi}{2}\right) = 2\sqrt{G_1}d_0 \sin(90°n). \qquad (11)$$

Equation (11) is useful in sketching the lobe contour. It holds only when the reflection coefficient equals -1 (i. e., $\rho = +1$) and the angle γ is small enough so that equation (10) is valid.

SPHERICAL EARTH

Lobe Characteristics

Figures 2 and 3 are typical vertical coverage diagrams for a smooth spherical earth. They illustrate two important points.

The first is the dependence of the number of lobes on the ratio of transmitter height to wavelength. Figures 2 and 3 show that for h_1 equal to 75.4 wavelengths, the lobes are much more closely spaced than for a transmitter height of 32.3 wavelengths.

When the number of lobes is large, there is little possibility for a target to escape detection in the small null areas. The shape of the contour is, therefore, less important and it is sufficient to find the maximum and minimum ranges and then to sketch
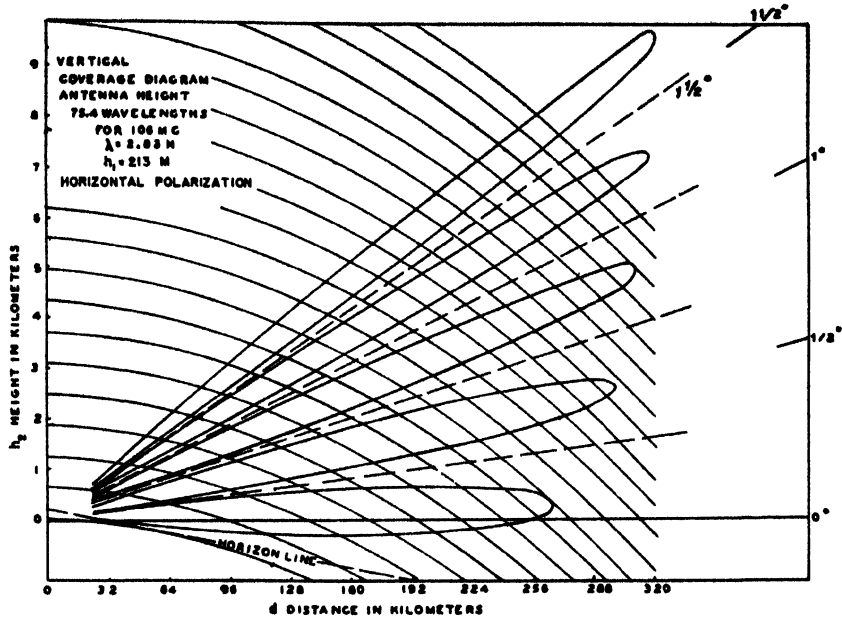
FIGURE 2. Vertical coverage diagram.

the lobe from the polar sine formula [equation (11)]. On the other hand, the shape of the contour is of great importance when there are few lobes and the null area is large. This is illustrated in Figure 3, where there are only two complete lobes in the region of interest.

The second point to be noted is the varying effect of divergence on the lobe number and angle. It may be seen from equation (89) in Chapter 5 that the divergence factor approaches unity as tan ψ

increases (see also Figure 11). The divergence factor is low for small angles and then approaches unity rapidly. This accounts for the reduced range of the first three lobes of Figure 2. For the larger angles, the maximum range is approximately equal to twice the free-space range. When the ratio h_1/λ is small, the angle at the first lobe maxima is large, since $\gamma = n\lambda/4h_1$. In this case, the effects of divergence will be negligible except for the lower part of the first lobe, and the polar sine function derived for the
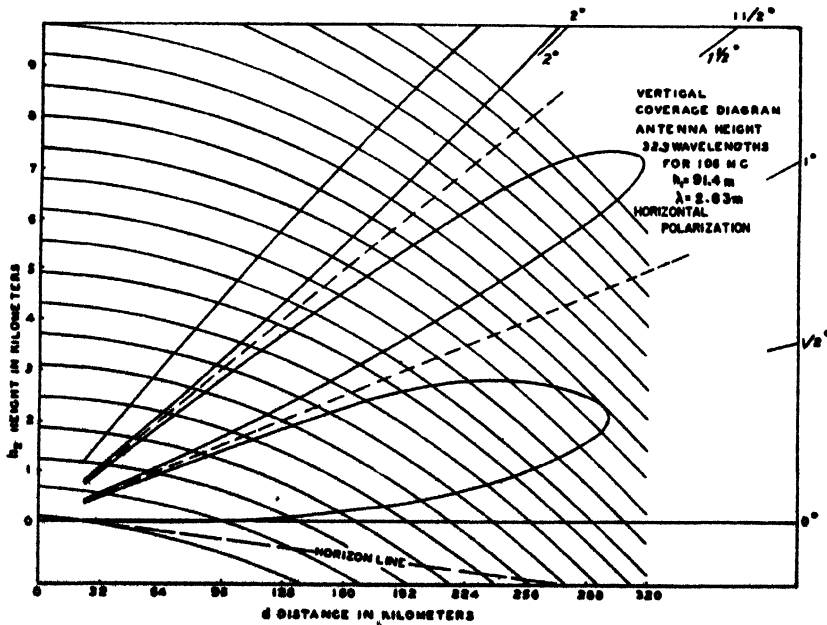
FIGURE 3. Vertical coverage diagram.

plane earth may be used.

There exists also the intermediate case where the effects of divergence may not be neglected and an accurate knowledge of the lobe shape is required. Three different solutions of this problem are given in following sections. They are

1. The *p-q method for horizontal polarization only*.

2. The *u-v method*, which may be used for both horizontal and vertical polarization.

3. *Lobe-angle method* which has the advantage of determining the lobe angles directly and is used for either polarization.

THE *p-q* METHOD (HORIZONTAL POLARIZATION)

Outline of Method

This method consists in plotting the locus of points having a constant range d and locating those points on this curve which are at such a distance from the transmitter that the phase shift caused by path difference corresponds to the required range. The range corresponding to a total phase shift Ω is given by

$$d = \sqrt{G_1} d_0 \sqrt{(1 - D)^2 + 4D \sin^2 \frac{\Omega}{2}}, \quad (12)$$

where D replaces K in equation (46) in Chapter 5, since for horizontal polarization $\rho = 1$ and since we are neglecting any effect due to the antenna radiation pattern. For this expression, D and Ω are certain functions of the antenna heights h_1 and h_2 as well as d which were considered earlier in the text of the last chapter). For a given transmitter, h_1, G_1, d_0, and λ are given, so that for a given gain contour the only variables in equation (12) are d and h_2. The difficulty of the problem consists in the fact that equation (12) provides an extremely complicated relation between h_2 and d which cannot be solved explicitly for either coordinate.

Under such circumstances, the natural procedure is to introduce new coordinates which make the handling of equation (12) easier. The method described in the following makes use of the variables

$$p = \frac{d_1}{d_T} \quad \text{and} \quad q = \frac{d_2}{d}$$

discussed on pages 389 and 390, and the procedure will be called the *p-q* method.

It may be recalled that expressed in coordinates p and q

$$d = \frac{p}{1 - q} \cdot d_T, \quad (13)$$

$$D = \left[1 + \frac{4p^2q}{(1 - p^2)} \right]^{-1/2}, \quad (14)$$

and the total phase shift, by equations (97) and (29) in Chapter 5, is

$$\Omega = \frac{4\pi}{\lambda} \frac{h_1^2}{d_T} \frac{q(1 - p^2)^2}{p} + \phi'. \quad (15)$$

For horizontal polarization, $\phi \to 0$, so that for this case (which is the one under consideration) all variable quantities in equation (12) have been expressed in terms of p and q.

Construction of Range Loci

Suppose to start with that we want to compute the position of the extreme range of a lobe. We may then proceed in the following manner. To a fair approximation, we may assume the extreme range of the lobes to correspond to $\sin^2(\Omega/2) = 1$, so that by equation (12) the corresponding distance d_{max} is given by

$$d_{max} = \sqrt{G_1} d_0 (1 + D). \quad (16)$$

Expressing d_{max} and D by p and q, the above equation determines the envelope of all lobe maxima. The practical way of doing this is to use a graphical representation of D in p and q coordinates (Figure 17 in Chapter 5) and to start by selecting a particular value of D, say $D = D_1$. Inserting this in equation (16) gives a corresponding value of d_{max}, and inserting this value of d_{max} for d in equation (13) determines a straight line in the p,q plane, since $d_T = \sqrt{2kah_1}$ is known. Whatever is the value of d_{max}, this line passes through the point $q = 1$, $p = 0$. In order to determine the position of the line, only one more point is needed. A convenient point to choose is to take $q = 0.9$ and compute the corresponding p from $p = 0.1 d_{max}/d_T$. The point of intersection of this line with the selected D_1-contour then gives the desired p,q combination that corresponds to the given values of d_{max} and D_1.

From this pair of values (p,q), the corresponding receiver height h_2 may be calculated by the relation [equation (98) in Chapter 5]

$$h_2 = h_1 \frac{q}{1 - q} \left[1 - p^2 + \frac{p^2q}{1 - q} \right].$$

Now both coordinates of the desired point are known, and the point may be plotted. Plotting a series of different points by the same method yields a smooth curve, which is the envelope of all lobe maxima.

The locus of minima may similarly be plotted by using $\sin^2 \frac{\Omega}{2} = 0$ and

$$d_{min} = \sqrt{G_1} d_0 (1 - D) \quad (17)$$

instead of equation (16). Intermediate range curves are found by assigning nonintegral values to m in the equation $\Omega = m\pi$ and substituting in equation (12).
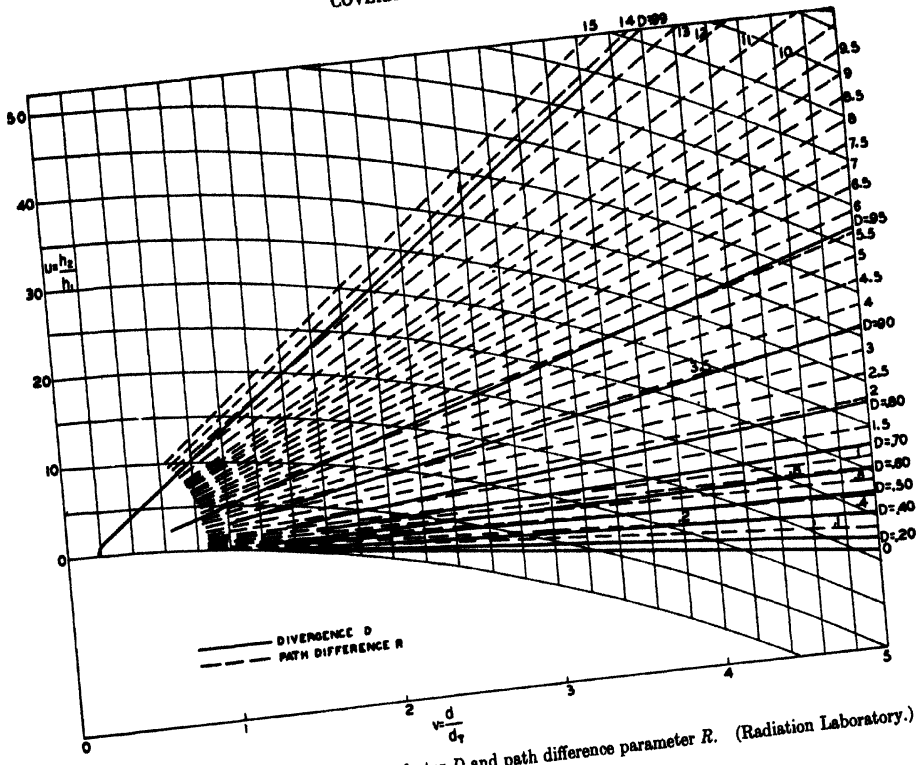
FIGURE 4. Curves of constant-divergence factor D and path difference parameter R. (Radiation Laboratory.)
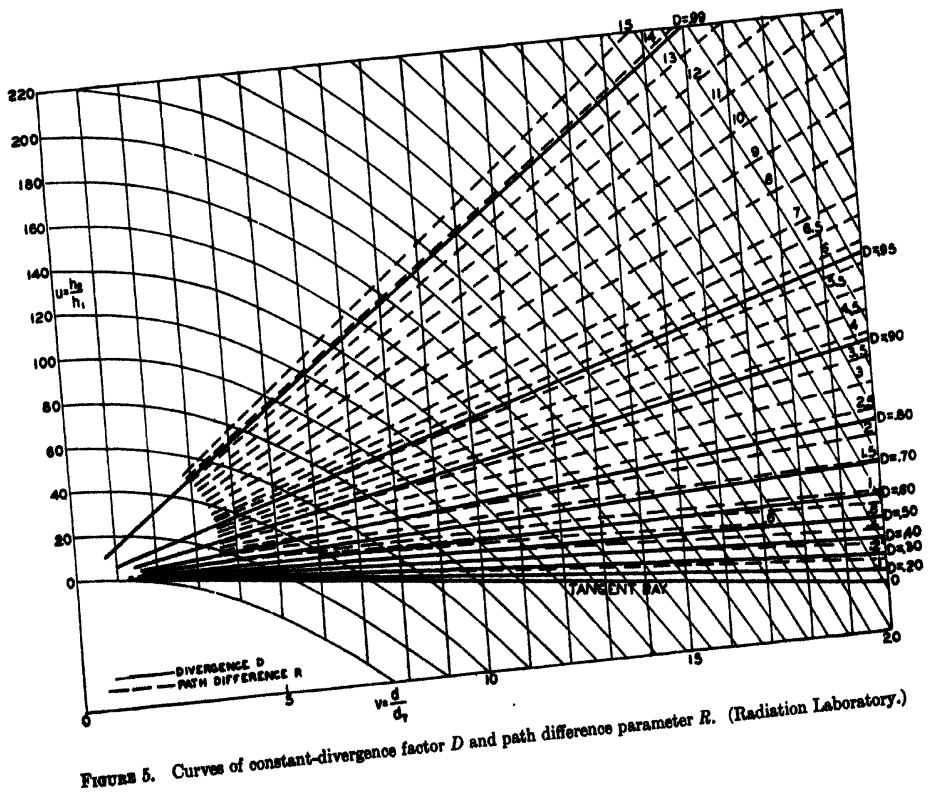
FIGURE 5. Curves of constant-divergence factor D and path difference parameter R. (Radiation Laboratory.)
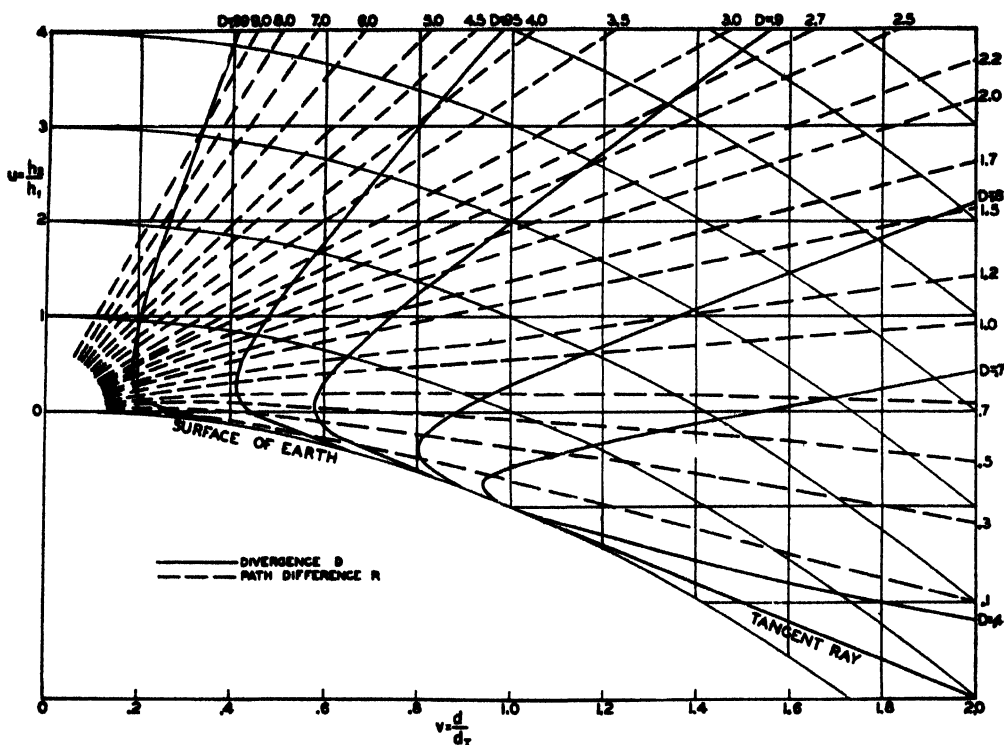
FIGURE 6. Curves of constant-divergence factor D and path difference parameter R. (Radiation Laboratory.)

Construction of Path-Difference Loci

An assumed value of Ω in equation (12) determines δ, the phase shift caused by the path difference, as

$$\delta = \Omega + 2\pi n, \tag{18}$$

where n assumes all integral values and zero. This value of δ determines the path difference $\Delta = r - r_d$,

$$\Delta = \frac{\lambda \delta}{2\pi}. \tag{19}$$

But from equation (97) in Chapter 5

$$\Delta = \frac{2h_1^2}{d_T} q \frac{(1 - p^2)^2}{p} = \frac{2h_1^2}{d_T} q f(p) \tag{20}$$

where $f(p)$ is given in Figure 18 in Chapter 5.

In this calculation, q may be taken as the independent variable. The assumed values of q together with Δ from equation (19) determine $f(p)$ in equation (20). For given values of $f(p)$, the corresponding values of p may be read from Figure 18 in Chapter 5. The coordinates h_2 and d on the path-difference loci are found from equation (98) in Chapter 5 and equation (13) in Chapter 6, giving

$$h_2 = \frac{h_1 q}{1 - q}\left(1 - p^2 + \frac{p^2 q}{1 - q}\right)$$

and

$$d = d_T\left(\frac{p}{1 - q}\right).$$

Intersections of the path-difference loci with the range curves determine points on the lobes.

THE u-v METHOD

Outline of Method

This method makes use of the generalized coordinates $u = h_2/h_1$ and $v = d/d_T$ described in text on p.391. The curves of constant-divergence factor D and path-difference parameter R are plotted on the same sheet in Figures 4, 5, and 6. The divergence lines are shown in full and the path-difference curves are dotted. Envelopes of constant $\sin^2(\Omega/2)$ [equation (46) in Chapter 5] are constructed and their intersections with path-difference contours corresponding to the assumed values of $\Omega/2$ determine points on the lobes.

Construction of Lobes (Horizontal Polarization)

In this method, the divergence factor D is considered to be the independent variable. Dividing both sides of equation (46) in Chapter 5 by d_T gives

$$\frac{d}{d_T} = \sqrt{G_1}\,\frac{d_0}{d_T}\sqrt{(1 - K)^2 + 4K \sin^2\frac{\Omega}{2}}$$

$$= \sqrt{G_1}\,d_0\sqrt{(1 - K)^2 + 4K \sin^2\frac{\Omega}{2}}, \tag{21}$$

where

$$d_0 = \frac{d_0}{d_T}.$$

If $\rho = 1$, and the effect of antenna directivity is neglected, $K = D$, and

$$v = \frac{d}{d_T} = \sqrt{G_1}\,d_0\,\sqrt{(1 - D)^2 + 4D \sin^2 \frac{\Omega}{2}}. \quad (22)$$

The following discussion illustrates how one contour of a coverage diagram, corresponding to a particular value of radio gain, may be plotted on Figure 4 or its equivalent, Figure 7. The result is a curve similar to Figure 2, but plotted in u,v coordinates instead of h_2 and d. See also Figures 16 to 39.

For illustration, let the transmitter gain, $G_1 = 1$ and let the radio gain be such a value that $d_0 = d_0/d_T = 2$. Further, let $\lambda = 0.1$ meter and $h_1 = 20$ meters. From Figure 15 it is seen that $r = 1,030\lambda/h_1^{3/2} = 1.2$. Select one of the curves for $\sin^2 (\Omega/2)$ in Figure 12, Chapter 5, say $\sin^2 (\Omega/2) = 1$, for which $\Omega = \pi, 3\pi, 5\pi$, etc. These values correspond to tips of the lobes for which $n = 1, 3, 5$, etc., since, for perfect reflection, $\Omega = n\pi$ by equation (116) in Chapter 5.

Next select values of $K = D$ and note the corresponding value of the radical

$$\sqrt{(1 - K)^2 + 4K \sin^2 \frac{\Omega}{2}}$$

given by Figure 12 in Chapter 5. Equation (22) then gives the value of v. These quantities together with $R = nr$ may conveniently be tabulated, as in Table 2. Corresponding values of D and v are plotted as crosses on Figure 7. The line drawn through these points is the locus of the tips of the lobes. The

Table 2. Values of v and R for $\sin^2(\Omega/2) = 1$, $d_0 = 2$.

D	$\sqrt{(1 - D)^2 + 4D \sin^2 \frac{\Omega}{2}}$ (Figure 12, Chapter 5)	v [equation (22)]	($r = 1.2$)		
			n	$R = nr$	Lobe maxima
0.2	1.2	2.4	1	1.2	1st lobe
0.3	1.3	2.6			
0.4	1.4	2.8	3	3.6	2d lobe
0.5	1.5	3.0			
0.6	1.6	3.2	5	6.0	3d lobe
0.7	1.7	3.4			
0.8	1.8	3.6	7	8.4	4th lobe
0.9	1.9	3.8			
0.95	1.95	3.9			
1.0	2.0	4.0			

actual position of each lobe tip is then marked with a circle where the corresponding value of R crosses the locus in Figure 7.

Additional lobe points are located by choosing some other value of $\sin^2 (\Omega/2)$, say $\sin^2 (\Omega/2) = 0.7$. Each value of $\sin^2 (\Omega/2)$ now gives two points on each lobe, one on the upper branch and the other on the lower. Again choose values of $K = D$, obtain the corresponding values of the radical

$$\sqrt{(1 - K)^2 + 4K \sin^2 \frac{\Omega}{2}}$$

from Figure 12 in Chapter 5, and calculate new values for v. The D–v values are plotted as crosses on Figure 7 and the line through them is the locus of points for which $\sin^2 (\Omega/2) = 0.7$ (see Table 3).

For $\sin^2 (\Omega/2) = 0.7$, $\sin (\Omega/2) = \pm 0.836$, $\Omega/2 = 0.315\pi$ or 0.685π. Then $\Omega = n\pi = 0.63\pi + 2k\pi$
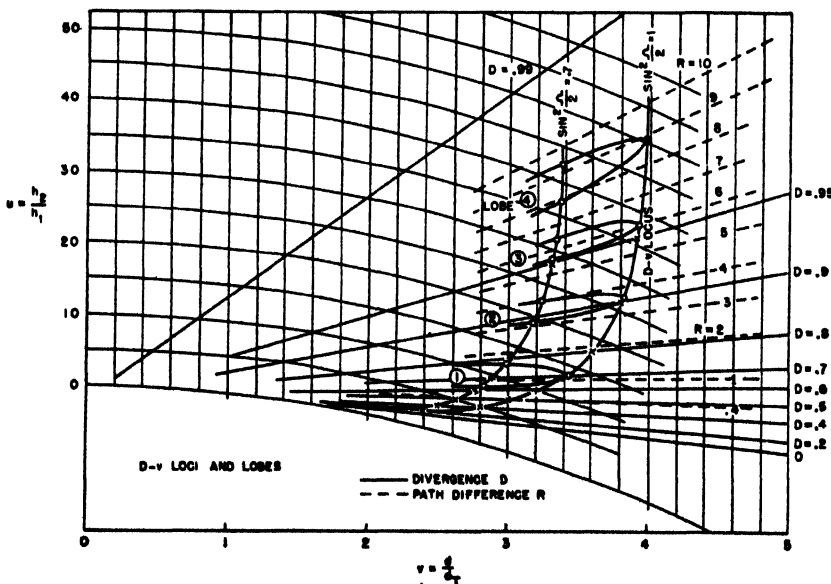
FIGURE 7. D–v loci and lobes.

TABLE 3. Values of v and R for $\sin^2 (\Omega/2) = 0.7$, $\underline{d_2} = 2$.

D	$\sqrt{(1-D)^2 + 4D \sin^2\frac{\Omega}{2}}$ (Figure 12, Chapter 5)	v	$(r = 1.2)$			
			K	n	$R = nr$	Lobe
0.2	1.1	2.2	0	0.63	0.756	1
0.3	1.15	2.3	0	1.37	1.644	1
0.4	1.22	2.44	1	2.63	3.16	2
0.5	1.28	2.56	1	3 37	4.04	2
0.6	1 36	2.72	2	4.63	5.56	3
0.7	1.43	2.86	2	5.37	6.44	3
0.8	1.52	3.04	3	6.63	7.96	4
0.9	1.6	3.2	3	7.37	8.84	4
0.95	1.64	3.28				
1.0	1.68	3.36				

and $1.37\pi + 2k\pi$, in which k is an integer. Then $n = 0.63 + 2k$ and $1.37 + 2k$, and $R = nr$. Values of n and R are listed in Table 3. The intersections of the R values and the locus for $\sin^2 (\Omega/2) = 0.7$ are plotted as circles on Figure 7.

The entire lobe structure for one contour may be drawn by choosing additional values of $\sin^2 (\Omega/2)$. A large number of contours have been calculated by the Radiation Laboratory and are plotted in Figures 16 to 39.

In order to construct one contour of a coverage diagram, it remains to find the intersection between the curves giving values of u for constant $\sin^2 (\Omega/2)$ and the corresponding path-difference contours. The equations relating R to $\Omega/2$ are given below. From equation (18)

$$\delta = \Omega + 2\pi n \quad (\phi = 180°, \phi' = 0), \qquad (23)$$

and from equation (19)

$$\Delta = \frac{\lambda}{\pi}\left(\frac{\delta}{2}\right).$$

From equation (83) in Chapter 5

$$R = \frac{ka\Delta}{h_1 d_T}.$$

An assigned value of Ω fixes two values of δ for each lobe, as explained in the previous paragraph. All values of $\sin^2 (\Omega/2)$ other than 1 or 0 determine two intersections with the lobe. When $\sin^2 (\Omega/2) = 1$, the envelope of maxima is obtained, while $\sin^2 (\Omega/2) = 0$ corresponds to the envelope of minima.

By selecting several values of $\sin^2 (\Omega/2)$ in Figure 12, Chapter 5, and following the method outlined above, a coverage diagram may be constructed in generalized (u,v) coordinates. The actual values of h_2 and d are

$$h_2 = h_1 u, \qquad (24)$$

$$d = d_T v. \qquad (25)$$

Construction of Lobes (Vertical Polarization)

Problems involving vertical polarization or cases

where the ratio of the antenna-pattern factors F_2/F_1 cannot be neglected, may be solved by successive approximation.

As a first approximation the method on pp. 438-440 is applied to determine points (h_2, d) on the lobe. The corresponding values of u and v determine s in Figure 19 or Figure 20, in Chapter 5, and $\tan\psi$ may be found from Figure 24 in Chapter 5 for the given transmitter height h_1. An alternate method is to calculate $\tan\psi$ from equations (73), (58), and (60) in Chapter 5, which are

$$d_1 = sd,$$

$$h_1' = h_1 - \frac{d_1^2}{2ka},$$

$$\tan\psi = \frac{h_1'}{d_1}.$$

The angles ψ_d and ν required to calculate the antenna pattern factors F_1 and F_2 are found from equations (62) and (63) in Chapter 5,

$$\tan\psi_d = \frac{h_2 - h_1}{d} - \frac{d}{2ka}$$

$$\nu \cong \psi + \frac{d_1}{ka}$$

The values of ρ, ϕ (or ϕ') may now be read from the reflection curves in Chapter 4.

Equation (46) in Chapter 5 may now be applied with $K = (F_2/F_1)\rho D$ where D assumes the same values as in the approximate solution. Equation (21) determines the value of d from which $u = d/d_T$ may be calculated. This value of $u = d/d_T$ is laid off on the original divergence contour in Figures 4, 5, or 6. This determines v. The assumption underlying this procedure is that the divergence factor is not appreciably affected by the change in coordinates caused by imperfect reflection and an unsymmetrical antenna pattern. The corrected phase difference δ' is found from

$$\delta' = \Omega - \phi' \qquad (26)$$

and the path difference Δ' and parameter R' from

$$\Delta' = \frac{\lambda}{\pi}\left(\frac{\delta'}{2}\right) \qquad (27)$$

$$R' = \frac{ka\Delta'}{h_1 d_T}. \qquad (28)$$
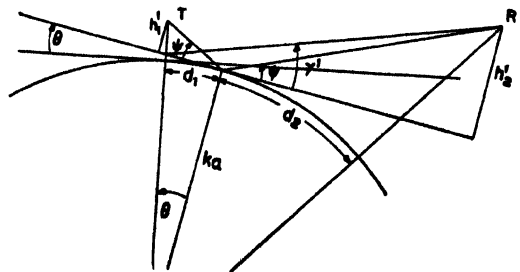
FIGURE 8. Lobe angles corrected for earth curvature.

The intersections between the path-difference contours and the distance envelope determine points on the coverage diagram.

The above method should be applied even for horizontal polarization when the directivity of the antenna is such that $F_2/F_1 \neq 1$. This follows from the concept of generalized reflection coefficients on page 385.

LOBE-ANGLE METHOD
(HORIZONTAL POLARIZATION)

Outline of Method

In this method the angles of lobe maxima are determined by modifying the plane earth formula, equation (2). In this equation, h_1 is replaced by h_1', which is the equivalent height above a plane tangent to the earth's surface at the reflection point, as shown in Figure 8.

The value of h_1' is given in equations (58) and (60) in Chapter 5. The maximum and minimum distances from the transmitter base to a point on the lobe are calculated by equation (46) in Chapter 5, using a modified divergence factor to be described in this section .

Basic Relations

Referring to Figure 8 and assuming $d_1 \ll d_2$, $\gamma' < 10°$ and $\psi \cong \gamma'$, the following relations hold.

$$\tan \gamma' \to \gamma' = \frac{n\lambda}{4h_1'} \tag{29}$$

$$\tan \gamma' \to \gamma' \cong \frac{h_1'}{d_1} . \tag{30}$$

Hence

$$\frac{h_1'}{d_1} = \frac{n\lambda}{4h_1'}$$

and

$$d_1 = \frac{(2h_1')^2}{n\lambda} , \tag{31}$$

where, from equation (58) in Chapter 5,

$$h_1' = h_1 - \frac{d_1^2}{2ka} .$$

The basic equations of the lobe-angle method are

$$\gamma' = \frac{n\lambda}{4h_1'} = \frac{n\lambda}{4\left(h_1 - \dfrac{d_1^2}{2ka}\right)} \tag{32}$$

and

$$d_1 = \frac{4\left(h_1 - \dfrac{d_1^2}{2ka}\right)^2}{n\lambda} . \tag{33}$$

Reflection-Point Curves

The elimination of d_1 from equations (32) and (33)

is most conveniently accomplished by graphical aids, which may be used in the following way.

1. From equation (33), a curve may be plotted showing d_1 as abscissa and n as ordinate for a given transmitter height and wavelength. This is illustrated in Figure 9 for two stations A and B with heights equal to 146.5 meters and 302 meters and
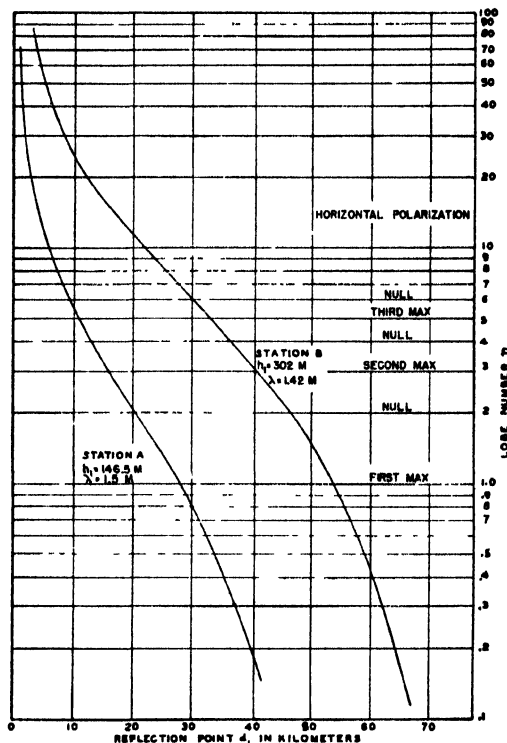
FIGURE 9. Location of reflection point d_1 as a function of lobe number n.

TABLE 4. Data for station A of Figure 9.*

n	d_1 (km)	h_1' (meters)	γ' (rad)	θ (rad)	$\gamma = \gamma' - \theta$ (rad)	D	Max. range d (km)
0	50.1	0	0	0.00789	− 0.00789		0
1	28.0	99.6	0.00362	0.00440	− 0.00078	0.502	150.2
2	20.2	122.5	0.00590	0.00317	0.00270	0.740	26.0
3	15.9	131.7	0.00827	0.00250	0.00575	0.817	181.7
4	12.8	137.0	0.01058	0.00200	0.00858	0.864	13.6
5	10.9	139.7	0.01300	0.00170	0.00130	0.910	191.0
6	9.35	141.4	0.01540	0.00145	0.01395	0.930	7.0
7	8.05	143.0	0.01760	0.00128	0.01632	0.943	194.3
8	7.25	143.6	0.02000	0.00112	0.01888	0.960	4.0
9	6.45	144.0	0.02260	0.00100	0.02160	0.964	196.4
10	5.80	144.2	0.02510	0.00090	0.0242	0.970	3.0
11	5.32	144.7	0.0275	0.00083	0.02667	0.973	197.3
12	4.98	145.0	0.03000	0.00078	0.03022	0.980	2.0
13	4.51	145.2	0.03240	0.00071	0.03169	0.982	198.2
14	4.19	145.7	0.03480	0.00066	0.03414	0.986	1.4
15	3.87	145.7	0.03730	0.00061	0.03669	0.989	198.9
16	3.70	145.7	0.04000	0.00058	0.03942	0.990	1.0
17	3.48	146	0.04220	0.00053	0.04167	0.991	199.1
18	3.22	146	0.04450	0.00050	0.04400	0.993	0.7
19	3.06	146.2	0.04700	0.00048	0.04652	0.994	199.4
20	2.90	146.2	0.04960	0.00045	0.04915	0.995	0.5

* Antenna gain and directivity factors have been omitted from the above calculations.
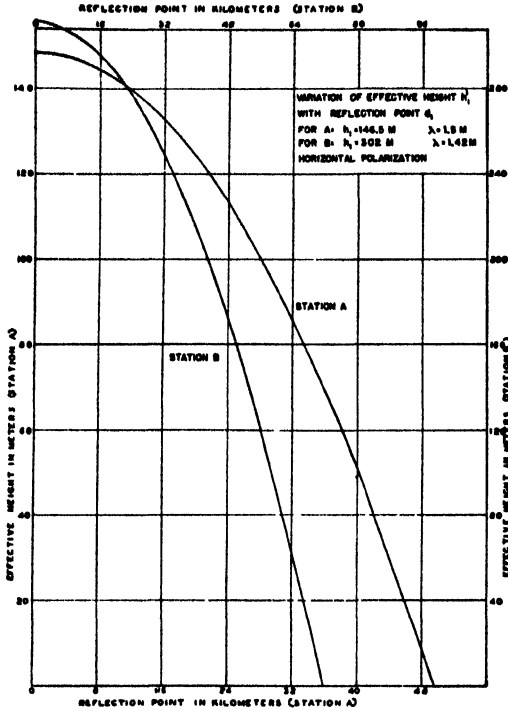
FIGURE 10. Variation in effective height h_1' with reflection point d_1.

wavelengths $\lambda = 1.50$ meters and $\lambda = 1.42$ meters respectively.

2. From equation (58) in Chapter 5, a second curve may be plotted with d_1 as abscissa and the equivalent height h_1' as ordinate as shown in Figure 10. To illustrate, computed data for station A are given in Table 4, for a free-space range of $d_0 = 100$ km. d is calculated from equations (16) and (17).

3. For any n, including integral and fractional values, d_1 may be found from Figure 9 and the corresponding h_1' from Figure 10. The angles γ' corresponding to lobe maxima may then be calculated from equation (32).

Lobe Angles with Horizontal

The angle γ' given by equation (32) is measured with respect to the tangent plane through the reflection point shown in Figure 8. This plane is inclined at an angle θ with the horizontal at the base of the transmitter. The true angle γ which the lobe-center line makes with the horizontal is

$$\gamma = \gamma' - \theta, \tag{34}$$

where

$$\theta = \frac{d_1}{ka}. \tag{35}$$

Hence by equation (32)

$$\gamma = \frac{n\lambda}{4\left(h_1 - \frac{d_1^2}{2ka}\right)} - \frac{d_1}{ka}, \tag{36}$$

where odd values of n give maxima and even values minima, provided the reflection phase shift is π radians. The angle may be either positive or negative, as shown by equation (36).

Use of Modified Divergence Factor

The value of the divergence factor must be determined in order to calculate the maximum and minimum lobe lengths by equation (46) in Chapter 5. A convenient formula for the divergence factor at the angles of lobe maxima is obtained by substituting γ' for ψ in equation (92) in Chapter 5. The errors involved in this assumption have been given previously. Substitution of $\gamma' = \psi$ in equation (92) in Chapter 5 yields

$$D = \frac{1}{\sqrt{1 + \frac{2h_1'}{ka(\gamma')^2}}}. \tag{37}$$

For lobe maxima

$$h_1' = \frac{n\lambda}{4\gamma'}. \tag{38}$$

Hence

$$D = \frac{1}{\sqrt{1 + \frac{n\lambda}{2ka(\gamma')^3}}}. \tag{39}$$

Contours of constant γ' are shown in Figures 11 and 12 where γ' is a function of D and $n\lambda$.

Construction of Lobes

For horizontal polarization, the distance d_{max} from the base of the transmitter to the lobe maximum is calculated from equation (46) in Chapter 5 by substituting $K = (F_2/F_1)\rho D$ and $\sin^2(\Omega/2) = 1$. For horizontal polarization $\rho = 1$. Thus,

$$d_{max} = \sqrt{G_1}d_0 \sqrt{\left[1 - \frac{F_2}{F_1}D\right]^2 + 4\frac{F_2}{F_1}D} \tag{40}$$

or

$$d_{max} = \sqrt{G_1}d_0\left[1 + \frac{F_2}{F_1}D\right]. \tag{41}$$

Here F_2 and F_1 are computed from the angles ψ_d and ν given by equations (62) and (63) in Chapter 5. The distance d_{min} from the transmitter base to the minimum point is obtained by substituting $\sin^2(\Omega/2) = 0$ and $K = (F_2/F_1)D$ in equation (46) in Chapter 5. Thus
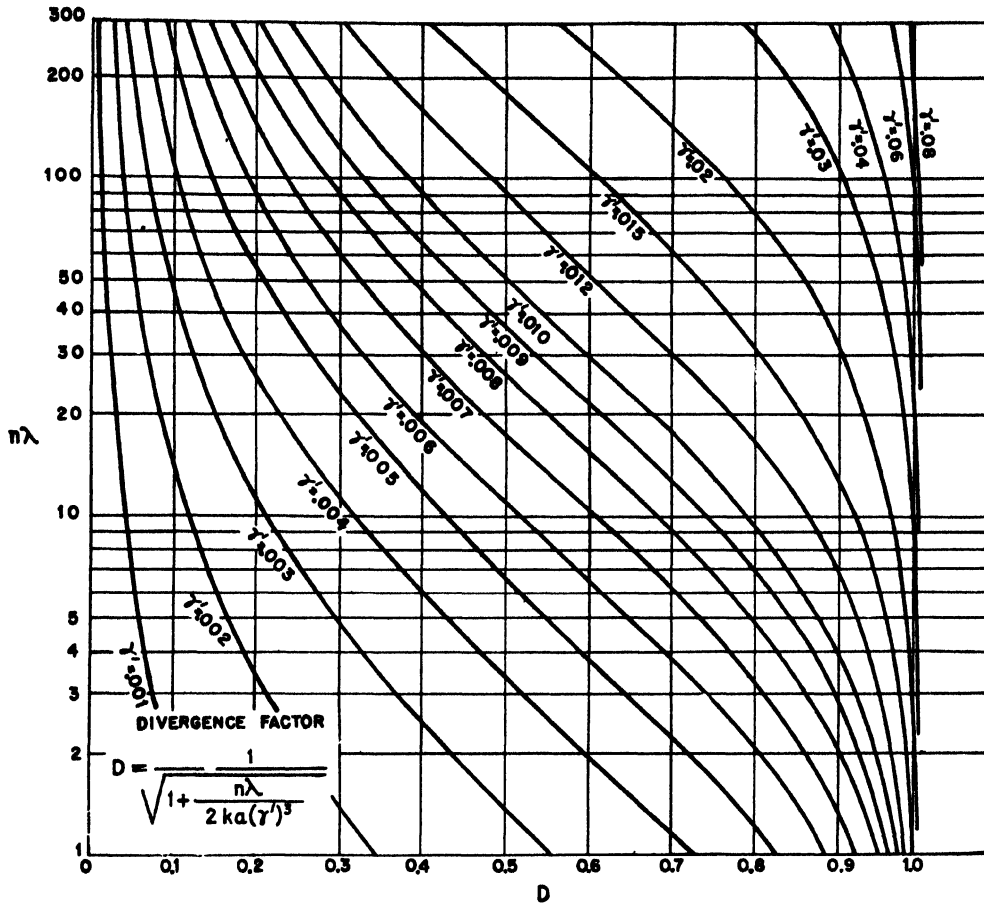
FIGURE 11. Contours of γ' as a function of D and $n\lambda$.
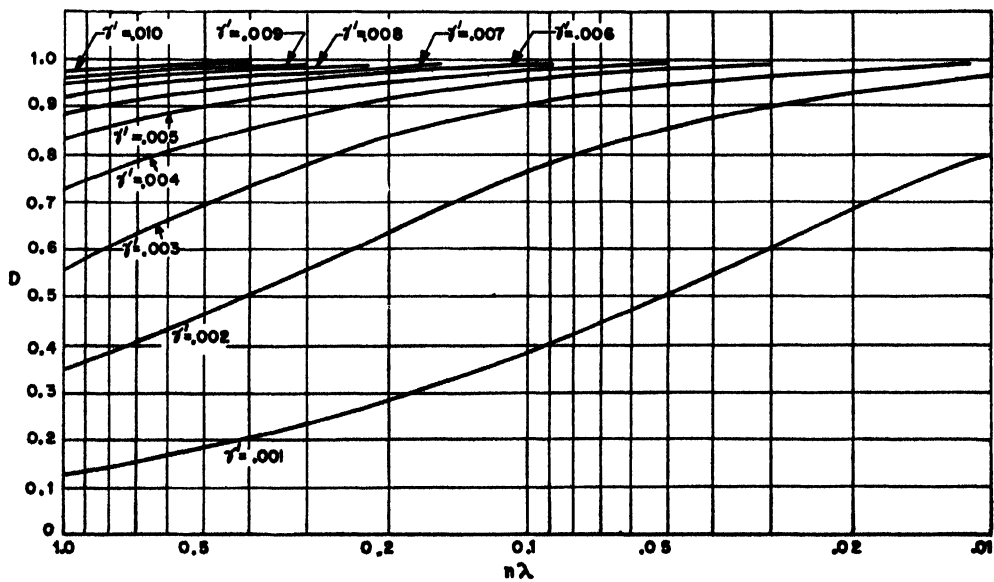
FIGURE 12. Contours of γ' as a function of D and $n\lambda$.

$$d_{\min} = \sqrt{G_1} d_0 \left[1 - \frac{F_2}{F_1} D \right]. \quad (42)$$

The values of D to be used in equations (40), (41), and (42) may be read directly from Figure 11 or Figure 12, or calculated by equation (39).

Intermediate points in the lobe may be formed by assigning fractional values to n. The corresponding path-difference angle δ may be calculated in the following manner. Suppose it is desired to find intermediate points on the fourth lobe. The values of n for this lobe range from $n = 6$ to $n = 8$, with the maximum at $n = 7$. It follows that a change of 2 in n corresponds to a change of 2π in δ. Thus if $n = 6.5$, $\delta = (0.5/2)(2\pi) = \pi/2 = 90°$. For horizontal polarization Ω ($= \delta + \phi'$) reduces to δ, since $\phi' \cong 0$. The distance from the transmitter base to this intermediate point in the lobe is equal to

$$d = \sqrt{G_1} d_0 \sqrt{(1 - K)^2 + 4K \sin^2 \left(\frac{\Omega}{2} \right)}, \quad (43)$$

as given in equation (46) in Chapter 5, in which $K = (F_2/F_1)\rho D$ and $\rho = 1$. The value of D may be read from Figures 11 and 12, using the assigned value of $n\lambda$ and the relation $\gamma' = n\lambda/4h_1'$. The proper value of d_1 to be used in equation (63) in Chapter 5 to determine the antenna-pattern angle ν may be read from Figure 9.

Correction for Low Angles

The method outlined in the last five sections depends upon the assumption that $\gamma' \to \psi$ or $d_1 \to 0$. This assumption gives good results when n is a large number but serious errors are involved for small values of n. The method described in this paragraph is designed to avoid this difficulty. The procedure consists in plotting point by point the lobe-center lines and angles of lobe maxima. The points will be located by polar coordinates with the pole at the transmitter. The coordinates are shown in Figure 13 as r_d and γ_1.

Referring to Figure 13, the following relations
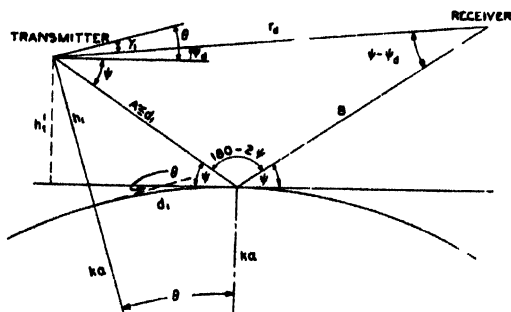
FIGURE 13. Geometry for radio propagation over spherical earth. See Figure 14 in Chapter 5.

hold when the angle ψ is less than 10 degrees:

(a) $$\psi = \frac{h_1'}{A} = \frac{h_1'}{d_1}$$

(b) $$\theta = \frac{d_1}{ka} = \frac{A}{ka}$$

(c) $$\gamma_1 = \psi_d - \theta$$

(d) $$h_1' = h_1 - \frac{d_1^2}{2ka} \quad (44)$$

(e) $$r_d \to A + B = d_1 + B$$

(f) $$\psi_d = \left(\frac{B - d_1}{r_d} \right) \psi$$

(g) $$B = \frac{(n\lambda/2)d_1}{2d_1\psi'^2 - n\lambda/2}$$

Equations [(44a to e)] are obtained by inspection of Figure 13. Equations (44f) and (44g) are derived as follows:

$$\frac{\sin 2\psi}{\sin (\psi + \psi_d)} = \frac{r_d}{B} \to \frac{2\psi}{\psi + \psi_d},$$

$$\psi + \psi_d = \frac{2\psi B}{r_d},$$

$$\psi_d = \psi \left(\frac{2B - r_d}{r_d} \right) = \psi \left(\frac{B - d_1}{r_d} \right).$$

The path difference Δ is given by

$$\Delta = A + B - r_d = \frac{n\lambda}{2} \quad (\phi = 180°).$$

Hence

$$A + B - \sqrt{A^2 + B^2 + 2AB \cos 2\psi} = \frac{n\lambda}{2}.$$

Squaring,

$$B(2A - n\lambda - 2A \cos 2\psi) = n\lambda A - \left(\frac{n\lambda}{2} \right)^2.$$

Therefore,

$$B = \frac{n\lambda A}{2} - \frac{1}{2} \left(\frac{n\lambda}{2} \right)^2}{A(1 - \cos 2\psi) - \frac{n\lambda}{2}}.$$

For small angles,

$$\cos 2\psi = 1 - \frac{(2\psi)^2}{2} = 1 - 2\psi^2.$$

Hence

$$B = \frac{\frac{n\lambda A}{2} - \frac{1}{2} \left(\frac{n\lambda}{2} \right)^2}{2\psi^2 A - \frac{n\lambda}{2}} = \frac{n\lambda}{2} \frac{A - \frac{n\lambda}{4}}{2A\psi^2 - \frac{n\lambda}{2}}.$$

Since the angle ψ is of the order of a few degrees only, it is permissible to write $A = d_1$ in the above equation.

Neglecting further the term $n\lambda/4$ in comparison with d_1, which is permissible for short waves and small values of n, the above expression for B reduces to equation (44g).

The method of determining the locus of points having a path difference of $\lambda/2$ (i.e., $n = 1$) is as follows. Assume a value of d_1 and calculate the corresponding values of

> h_1' by equation (44d),
> ψ by equation (44a),
> B by equation (44g),
> r_d by equation (44e),
> ψ_d by equation (44f),
> θ by equation (44b),
> γ_1 by equation (44c).

The assumed values of d_1 are limited to those which will give positive values of B in equation (44g). Select as many values of d_1 as are necessary to plot a smooth path-difference locus. Repeat for $n = 3$, etc.

This method of determining the angles of lobe maxima is of particular value in constructing the first few lobes, since the approximations in text on pp.441- 444 may cause considerable error for low angles. These path-difference loci will intersect a vertical line drawn from the antenna to the ground below at heights equal to $n\lambda/4$. For short waves, this height is negligible for the lower lobes.

LOBE-ANGLE METHOD (VERTICAL POLARIZATION)

Angles of Lobe Maxima

The values of n corresponding to the angles of lobe maxima are determined exactly as in text on p.434 for the case of a plane earth. The values of n in the expression $\gamma' = n\lambda/4h_1'$ are increased above those for horizontal polarization by an amount (Δn) to compensate for the reduced phase shift on reflection. In other words, the path difference must be greater than integral multiples of $\lambda/2$ to compensate for the reduced phase shift. The expression for this compensation, from equation (5), is

$$\Delta n = \frac{\phi'}{\pi} \qquad (45)$$

Hence

$$\gamma' = (n + \Delta n)\frac{\lambda}{4h_1'} . \qquad (46)$$

[See Figure 8 and equation (32).]

Construction of Lobes

As a first approximation, the angles of lobe maxima are calculated on the basis of horizontal polarization.

A table is constructed giving values of n and γ' for maxima and minima. The next approximation is to let $\psi = \gamma'$. This assumes that $d_1 < < d_2$. The values of ϕ' and ρ may then be found from reflection curves, and (Δn) calculated from equation (45). The corrected values of γ' may be determined from equation (46). It is simpler to find γ' by interpolating between integral values of n in the n versus γ' table previously constructed. The values of d_{max} and d_{min} are

$$d_{max} = \sqrt{G_1}d_0(1 + K), \qquad (47)$$
$$d_{min} = \sqrt{G_1}d_0(1 - K), \qquad (48)$$

where $K = (F_2/F_1)\rho D$. The divergence factor may be found directly from Figure 11 for the corrected values of n and γ'. It will be found that for the higher lobes, the effect of (Δn) upon the value of the divergence factor is negligible.

Table 5 shows calculations of the corrected values of n and γ when the radiation from antenna A of p.441 and Table 4 is vertically polarized. Transmission over sea water is assumed. Tables 6 and 7 illustrate the effects of vertical polarization on reducing the maxima and increasing the minima.

TABLE 5

n	$_*\phi$ (in degrees)	ϕ'^* (in degrees)	Δn	$\Delta\gamma'$ (rad)	γ' (rad)	$\gamma = \gamma' - \theta$ (rad)
0	180.0	0	0	0	0	− 0.00788
1	175.0	5.0	0.0278	0.000064	0.00369	− 0.00071
2	171.5	8.5	0.0472	0.000112	0.00602	0.00284
3	168.0	12.0	0.0664	0.000155	0.00843	0.00593
4	164.7	15.3	0.085	0.00204	0.01080	0.00878
5	160.6	19.4	0.108	0.000250	0.01325	0.01153
6	157.3	22.7	0.126	0.000290	0.01569	0.01423
7	153	27.0	0.15	0.000374	0.01807	0.01681
8	149	31.0	0.172	0.000413	0.02061	0.01947
9	144.5	35.5	0.197	0.000491	0.02309	0.02208
10	140.0	40.0	0.222	0.000532	0.02563	0.02472
11	135.2	44.8	0.249	0.000623	0.02812	0.02735
12	130.5	49.5	0.274	0.000685	0.03068	0.02991
13	125.8	54.2	0.301	0.000722	0.03312	0.03241
14	120.8	59.2	0.329	0.000790	0.03559	0.03493
15	116.0	64.0	0.355	0.000886	0.03819	0.03778
16	110.2	68.8	0.388	0.000968	0.04077	0.04019
17	105.3	74.7	0.415	0.000995	0.04320	0.04177
18	101.1	78.9	0.437	0.001091	0.04569	0.04519
19	96.1	83.9	0.466	0.001130	0.04823	0.04775
20	91.8	88.2	0.490	0.001224	0.05082	0.05037

$^*\phi$ corresponds to γ' in Table 4. $\phi' = \pi - \phi$.

TABLE 6

n	K	d_{max} (HP) (km)	d_{max} (VP) (km)	$\dfrac{d_{max} (VP)}{d_{max} (HP)}$
1	0.904	150.2	145.5	0.968
3	0.765	181.7	162.5	0.895
5	0.670	191.0	161.0	0.844
7	0.585	194.3	155.2	0.80
9	0.516	196.4	149.8	0.762
11	0.458	197.3	144.6	0.733
13	0.415	198.2	140.8	0.710
15	0.385	198.9	138.0	0.695
17	0.362	199.1	135.7	0.681
19	0.360	199.4	135.8	0.680

TABLE 7

n	K	d_{min} (HP) (km)	d_{min} (VP) (km)	$\dfrac{d_{min} \text{ (VP)}}{d_{min} \text{ (HP)}}$
2	0.835	26.0	38.2	1.47
4	0.725	13.6	37.4	2.75
6	0.625	7.0	41.9	5.98
8	0.548	4.0	44.8	11.2
10	0.486	3.0	52.9	17.6
12	0.436	2.0	57.3	28.6
14	0.40	1.40	60.6	43.3
16	0.375	1.0	62.9	62.9
18	0.360	0.70	64.3	91.9
20	0.355	0.50	64.7	129.4

Tables 6 and 7 show the effect of a reflection coefficient which is less than unity upon the maximum and minimum ranges of station A in the last section. The first table gives odd values of n and maximum ranges; the second table gives even values of n and minimum ranges The free-space range is 100 km.

GENERALIZED COVERAGE DIAGRAMS (HORIZONTAL POLARIZATION)

Basic Parameters

The u-v method applied to generalized coordinates which was given in previous text may be extended to all transmitter heights and wavelengths. In this method, points on the lobe are located by the intersection of the path-difference locus with the normalized distance envelope. The basic parameters are d_0 and R.

In constructing a coverage diagram for a doublet transmitter, the transmitter height, the wavelength and the radio gain are known. It will be shown in later text that the normalized free-space distance, $\underline{d_0} = d_0/d_T$, is related to the gain factor A by

$$\frac{1}{\underline{d_0}} = \frac{8\pi}{3\lambda} d_T A. \qquad (49)$$

The path-difference parameter R has been expressed in equation (114) in Chapter 5 in terms of a height-wavelength factor r which is defined by

$$R = nr, \qquad (50)$$

where

$$r = \frac{1}{2}\sqrt{\frac{ka}{2}} \frac{\lambda}{h_1^{3/2}}. \qquad (51)$$

The first maximum, which for horizontal polarization occurs when $\Delta = \lambda/2$, corresponds to $n = 1$, the second minimum to $n = 2$, etc. Recalling the discussion on pp. 438 ff., it follows that it is possible to construct coverage diagrams in generalized coordinates with r the pattern or chart parameter and $\underline{d_0}$ the curve parameter on a chart for which r is fixed.

Determination of $\underline{d_0}$

It is possible to express $\underline{d_0} = d_0/d_T$ in terms of E/E_1, the ratio of the field strength E corresponding to the lobe, to the free-space field E_1 at unit distance from the transmitter. Since

$$d_0 = \frac{E_1}{E},$$

it follows that

$$\underline{d_0} = \frac{d_0}{d_T} = \frac{1}{d_T}\frac{E_1}{E}. \qquad (52)$$

The ratio E_1/E may be expressed in terms of the gain factor A through the following relationships. By equation (16) in Chapter 2

$$P_1 = \frac{E^2 d^2}{45}.$$

When $d = 1$, this gives

$$P_1 = \frac{E_1^2}{45}. \qquad (53)$$

For a doublet receiver with matched load and adjusted for maximum power transfer, equation (17) in Chapter 2 gives

$$P_2 = \frac{E^2}{120\pi} \cdot \frac{3\lambda^2}{8\pi}.$$

Hence

$$\frac{E_1}{E} = \frac{3\lambda}{8\pi}\sqrt{\frac{P_1}{P_2}} = \frac{3\lambda}{8\pi A}. \qquad (54)$$

Substituting the value of E_1/E from equation (54) into equation (52):

$$\underline{d_0} = \frac{1}{d_T}\left(\frac{3\lambda}{8\pi A}\right), \qquad (55)$$

and

$$\frac{1}{\underline{d_0}} = d_T\left(\frac{8\pi}{3}\right)\frac{\lambda}{A} = \sqrt{2ka}\left(\frac{8\pi}{3}\right)\frac{\lambda}{A}\sqrt{h_1}. \qquad (56)$$

Equation (56) shows that if $\log h_1$ is plotted against $\log A$ for fixed values of $\underline{d_0}$ and λ, a straight line results. These straight lines are shown in Figure 14. If h_1 and E/E_1 or h_1, λ, and A are known, $\underline{d_0}$ may be calculated from equations (52) or (55). The value of $\underline{d_0}$ determines the range of the lobe for specified values of r. In Figure 14, the various values of $\underline{d_0}$ used in constructing the charts are specified as $A, B, C, \cdots, M, N$, and are shown as functions of h_1 as ordinate and $20 \log A - 20 \log \lambda$ as abscissa.

Determination of r

Figure 15 shows r for various values of transmitter height h_1 and wavelength λ where

$$\frac{1}{r} = \frac{2h_1 d_T}{\lambda ka} = \frac{h_1^{3/2}\sqrt{2ka}}{\lambda ka} = \frac{2h_1^{3/2}}{\lambda}\sqrt{\frac{2}{ka}}. \qquad (57)$$

The values of r determine how the path-difference curves intersect the envelopes corresponding to assigned values of $\sin^2(\Omega/2)$ in the equation

$$r = \frac{d}{d_T} = \underline{d_0}\sqrt{G_1}\sqrt{(1-D)^2 + 4D\sin^2\frac{\Omega}{2}}. \qquad (58)$$

The generalized coverage charts are designated as
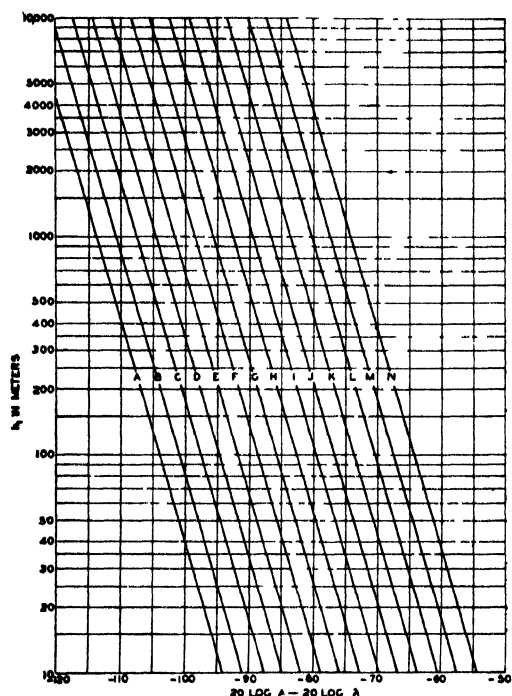
FIGURE 14. Values of d_0 as functions of h_1 and 20 log A —20 log λ. (See equation 56. The letters refer to coverage diagrams plotted in Figures 16 to 39.)

1, 2, · · · , 11, 12 in Figures 16 to 39, with the chart number being given by Figure 15

Use of Charts

The charts given in Figures 16 to 39 may be used for drawing coverage diagrams where the reflection coefficient is assumed equal to −1 and when the directivity factor F_2/F_1 is equal to unity. Each chart may be used for values of r near that for which the chart is drawn. For intermediate values, interpolation between charts is necessary. Errors inherent in interpolation limit the accuracy attained

On each chart are complete lobes or lobe outlines labeled A, B, C, · · · , M, N. In the follow

ing description these letters are referred to as lobe letters and the numbers 1 to 12 as chart numbers. Each chart is plotted to two scales.

The problem of constructing coverage diagrams resolves itself into finding the chart number and lobe letter corresponding to given values of gain factor A, transmitter height h_1, and wavelength λ. As stated in previous text the basic parameters of the generalized coverage diagrams are R and $\underline{d}_0$ or r and $\underline{d}_0$. The value of r is given in Figure 15 as a function of λ and h_1. Figure 15 was constructed from equation (51) which, after the substitution of numerical values, becomes:

$$r = \frac{1030\lambda}{h_1^{3/2}} \left(\text{for } k = \frac{4}{3}\right). \qquad (59)$$

The value of r determines the chart number. The lobe letter is found from the $\underline{d}_0$ corresponding to the given gain factor, transmitter height, and frequency. Figure 14 gives the lobe letters A, B, C, · · ·, M, N as functions of 20 log A − 20 log λ and the transmitter height. The relationship for plotting these lines is given by equation (56).

As an illustration of the use of the generalized coverage diagrams, assume 20 log A = −83, h_1 = 33 meters, and f = 200 mc (λ = 1.5 meters). If a straight line is drawn connecting h_1 = 33 and λ = 1.5 in Figure 15, it will intersect the r scale at r = 8. Thus the chart number is 5. Now the lobe letter to be used in chart 5 must be found. For this case, 20 log A − 20 log λ = −86.48. The coordinates 20 log A − 20 log λ = −86.48, and h_1 = 33, determine the lobe letter to be E in Figure 14. Figure 24 shows lobe E on chart 5. The first lobe is shown completely, together with the lower half of the second lobe. It must be noted that the coordinates of these charts, $v = d/d_T$ and $u = h_2/h_1$, are dimensionless. To convert to height h_2 and range d, the vertical distances must be multiplied by h_1 and the horizontal distances by d_T. In this case h_1 = 33 meters and $d_T = \sqrt{2kah_1}$ = 23.6 km. The actual coordinates of the position of maximum range are h_2 = 375 × 33 = 12.4 km and d = 15.4 × 23.6 = 365 km
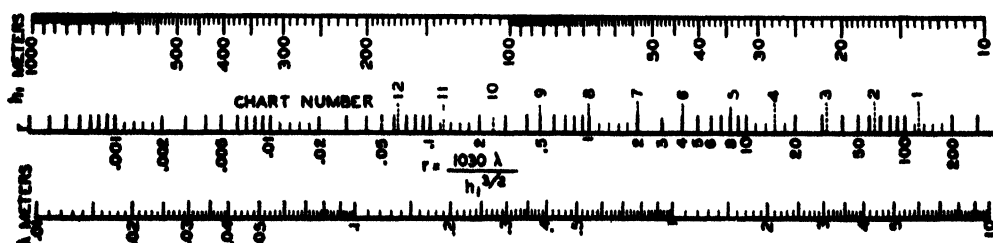
FIGURE 15. Chart number and r as a function of λ and h_1. (See Figures 16 to 39.)
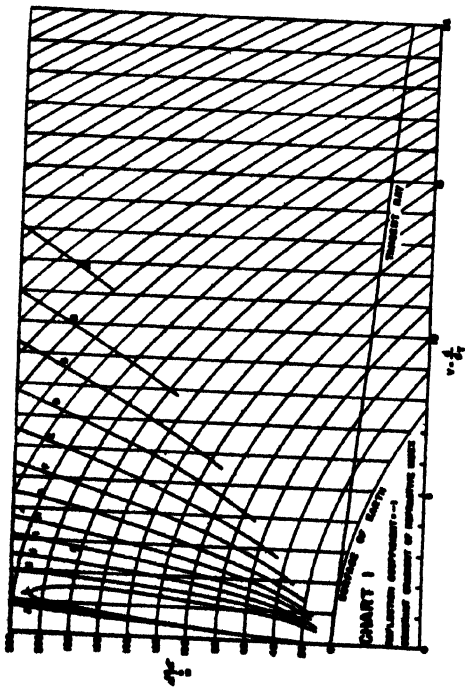
FIGURE 16. Generalized coverage diagram for $r = 128$. (See Figure 15.)
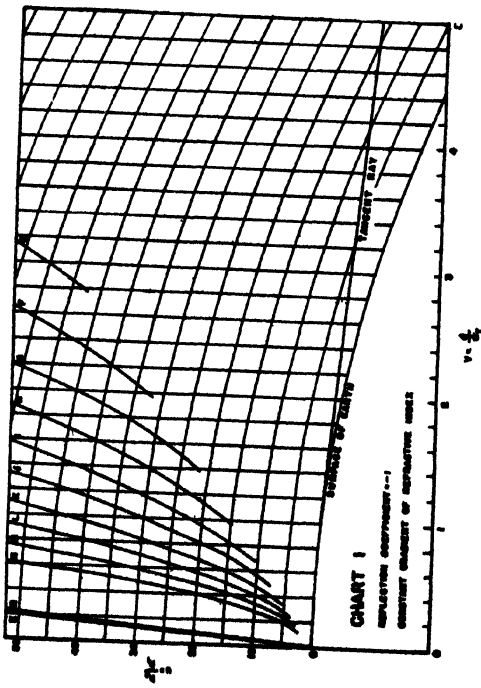
FIGURE 17. Generalized coverage diagram for $r = 128$. (See Figure 15.)
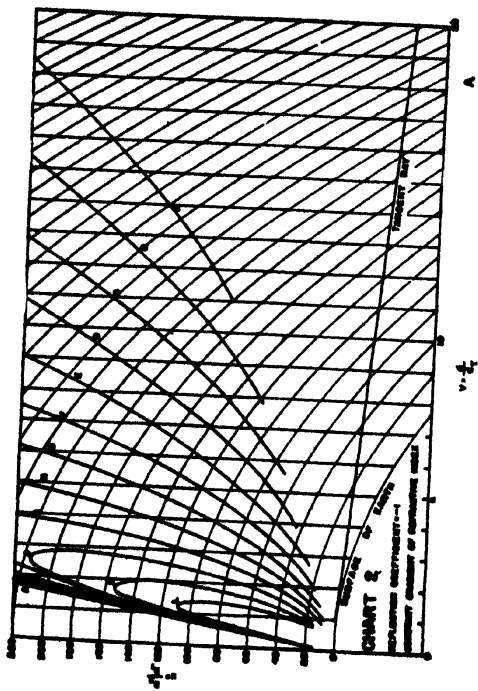
FIGURE 18. Generalized coverage diagram for $r = 64$. (See Figure 15.)
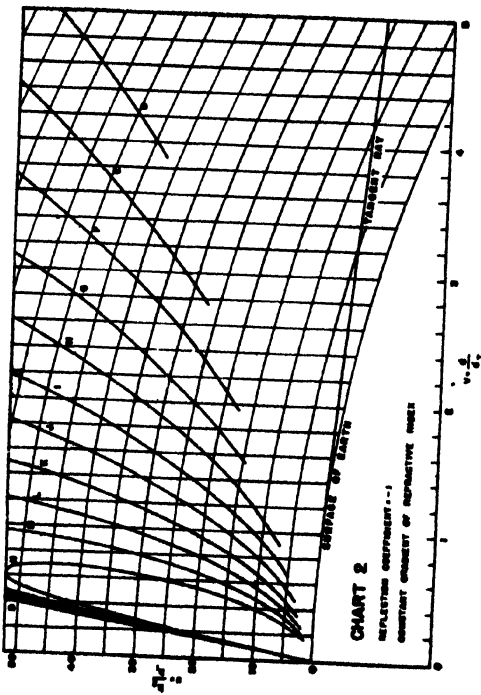
FIGURE 19. Generalized coverage diagram for $r = 64$. (See Figure 15.)

FIGURE 22.   Generalized coverage diagram for $r = 16$.   (See Figure 15.)
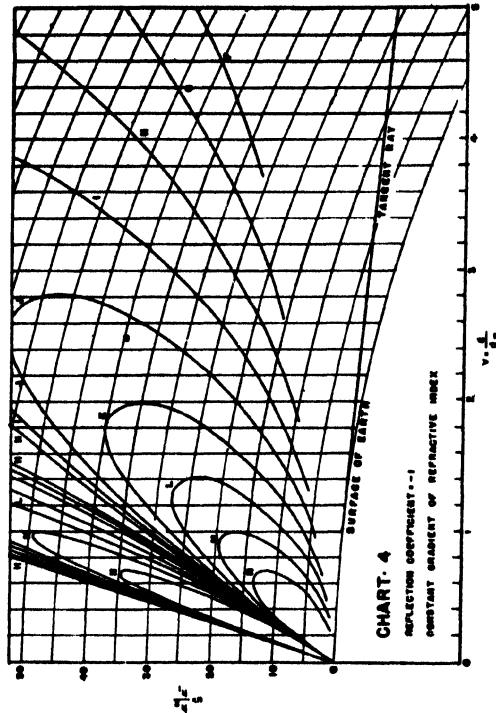
FIGURE 23.   Generalized coverage diagram for $r = 16$.   (See Figure 15.)

FIGURE 20.   Generalized coverage diagram for $r = 32$.   (See Figure 15.)

FIGURE 21.   Generalized coverage diagram for $r = 32$.   (See Figure 15.)
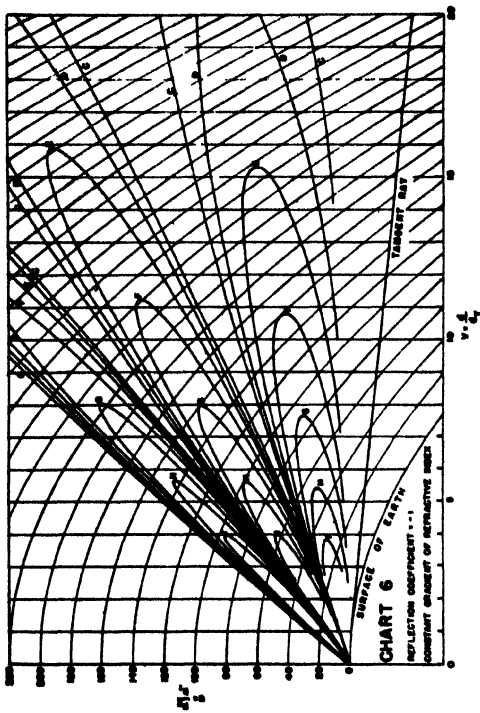
FIGURE 26. Generalized coverage diagram for r = 4. (See Figure 15.)
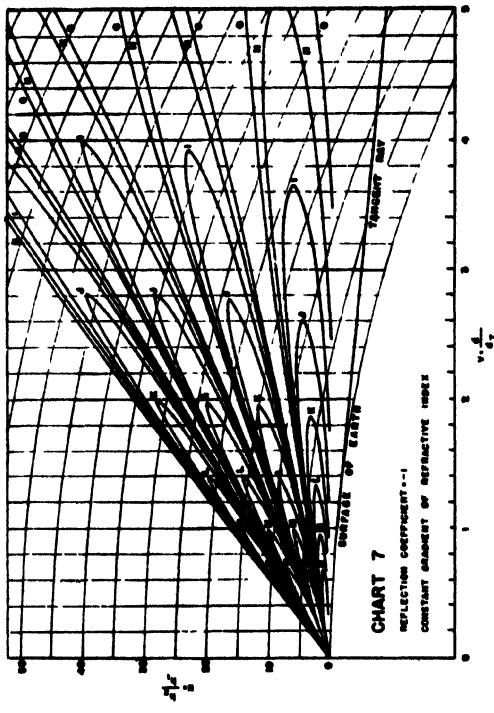
FIGURE 27. Generalized coverage diagram for r = 4. (See Figure 15.)
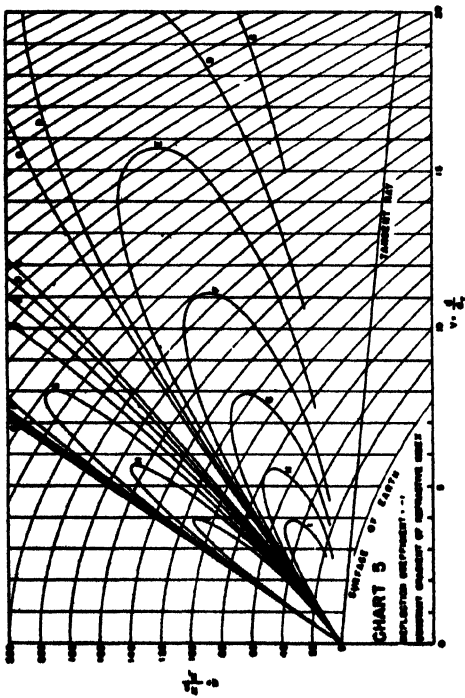
FIGURE 24. Generalized coverage diagram for r = 8. (See Figure 15.)
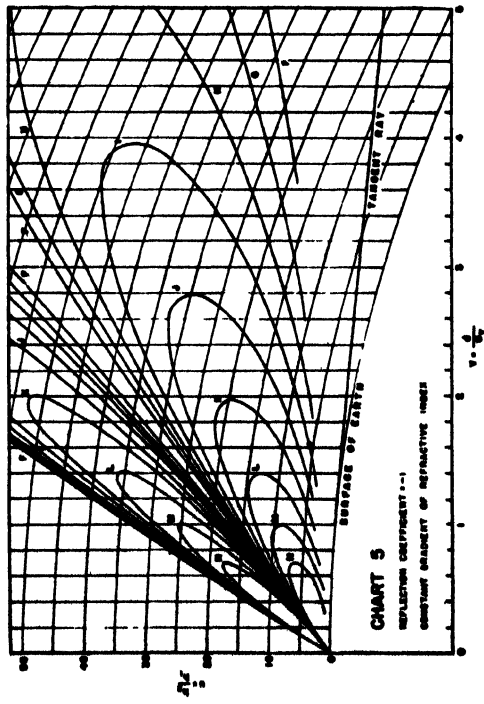
FIGURE 25. Generalized coverage diagram for r = 8. (See Figure 15.)
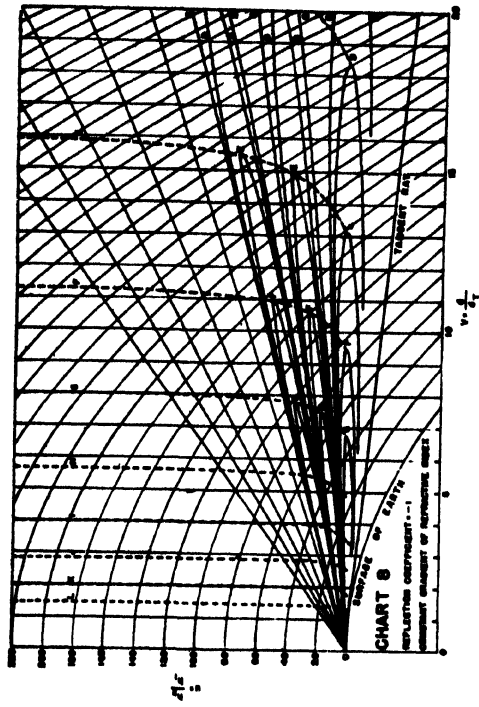
FIGURE 30. Generalized coverage diagram for $r = 1$. (See Figure 15.)
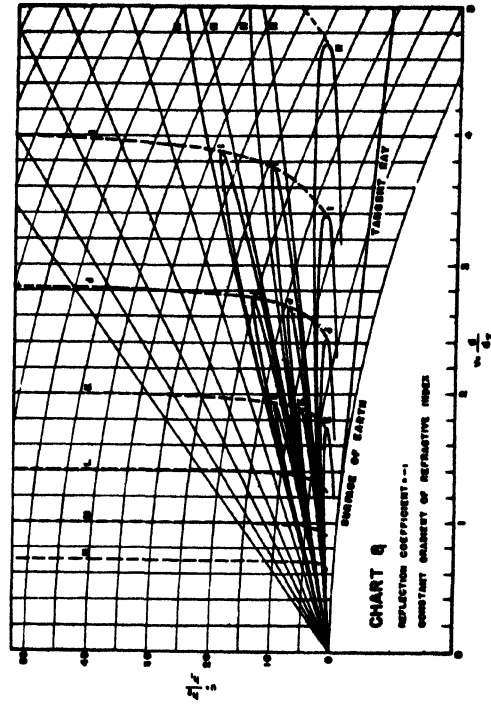
FIGURE 31. Generalized coverage diagram for $r = 1$. (See Figure 15.)
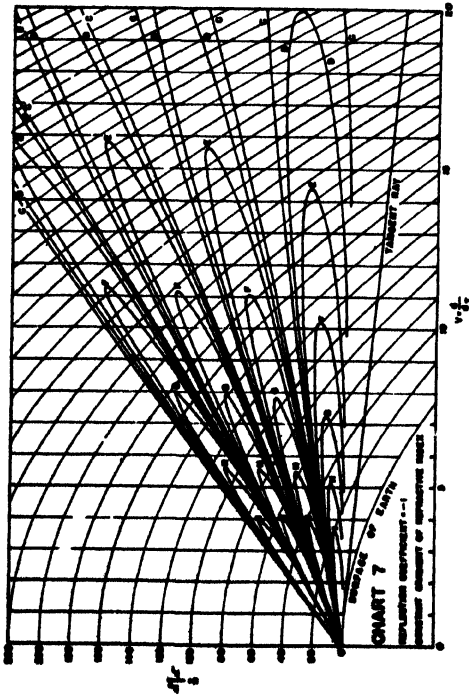
FIGURE 28. Generalized coverage diagram for $r = 2$. (See Figure 15.)
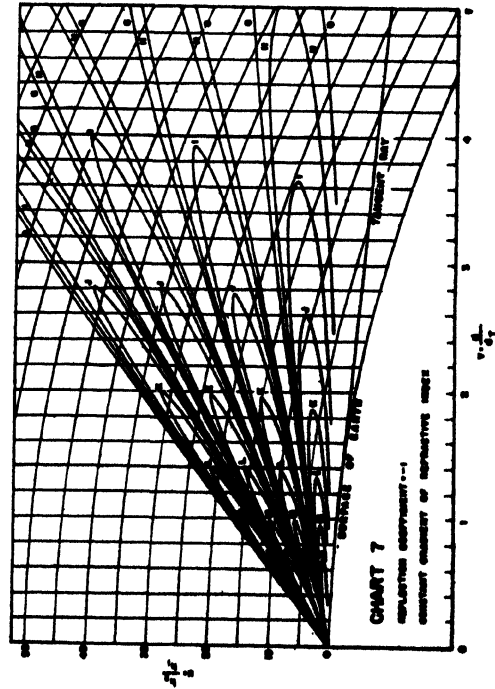
FIGURE 29. Generalized coverage diagram for $r = 2$. (See Figure 15.)

FIGURE 34. Generalized coverage diagram for $r = \frac{1}{4}$. (See Figure 15.)

FIGURE 35. Generalized coverage diagram for $r = \frac{1}{4}$. (See Figure 15.)
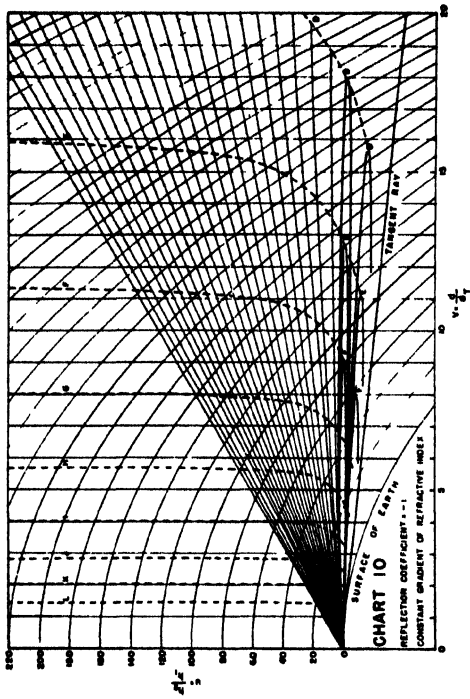
FIGURE 32. Generalized coverage diagram for $r = \frac{1}{2}$. (See Figure 15.)
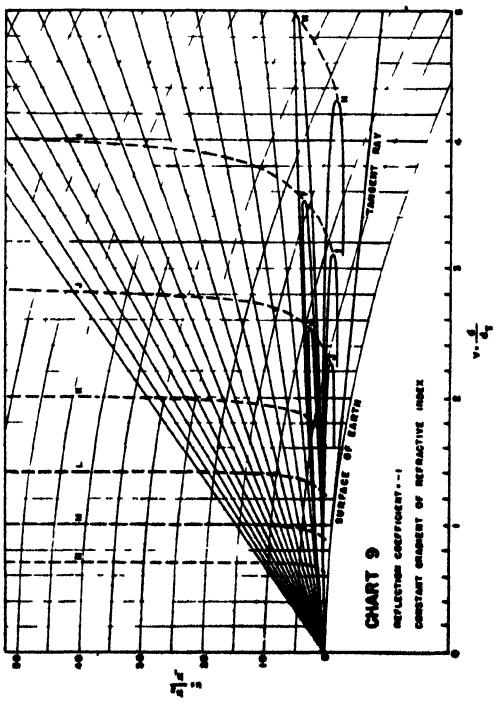
FIGURE 33. Generalized coverage diagram for $r = \frac{1}{2}$. (See Figure 15.)

FIGURE 38. Generalized coverage diagram for $r = \frac{1}{16}$. (See Figure 15.)
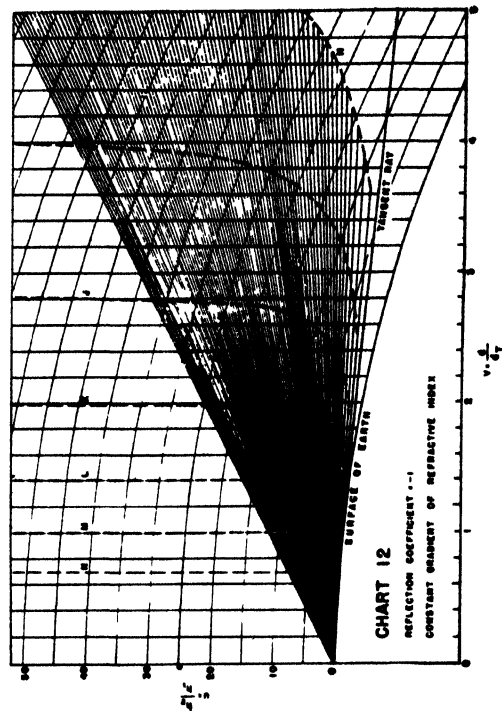
FIGURE 39. Generalized coverage diagram for $r = \frac{1}{16}$. (See Figure 15.)

FIGURE 36. Generalized coverage diagram for $r = \frac{1}{8}$. (See Figure 15.)

FIGURE 37. Generalized coverage diagram for $r = \frac{1}{8}$. (See Figure 15.)

Chapter 7

PROPAGATION ASPECTS OF EQUIPMENT OPERATION

GENERAL PROBLEM

Introduction

FOR A STANDARD atmosphere and with the basic assumptions set forth in Chapter 5 , the relation between the factors affecting the power of a set and the gain factor A is given in equations (3) and (5) in Chapter 5. The problem of computing A depends on the set in the sense that some sets are designed to operate in free space, others with the aid of reflection from the sea, as in low-angle and surface coverage.

The characteristics of a set as given in the manufacturer's description or in Tables 3, 4, and 5 at the end of this chapter may not represent the true values for a set in field use. Expected set performance, such as maximum range and coverage, can be calculated on the basis of the set's rated characteristics. Such performance can be termed "normal." If a set is behaving abnormally, it may be that it is not functioning most efficiently. Unfortunately, the problem is complicated by the possible presence of atmospheric ducts and by the variability and difficulty of finding accurately the radar cross sections of aircraft and ships.

Ducts are especially important for low antennas in surface search. In the case of communication sets, the most important item of information from a propagation standpoint is the maximum range. In the case of radar, not only is knowledge of maximum range wanted but also the ability to estimate the size and type of the target.

The Performance Figure and Efficiency

The maximum range of a set depends on the peak power output P_p of the transmitter, the minimum detectable power P_{min} (see discussion in Chapter 2) of the receiver, and the antenna gains G_1 and G_2. These can be grouped to give a performance figure. For communication, this figure is $(P_p/P_{min})G_1G_2$. For radar, the gains G_1 and G_2 are generally equal. The performance figure is then $(P_p/P_{min})G^2$. The ratio of the actual performance figure to the maximum possible value, or the difference in decibels, gives the efficiency of the set. In field use, it is generally impossible to measure the working performance figure with any precision and methods for obtaining a rough measure must be employed.

Effect of Reflection

It has been pointed out in Chapters 5 and 6 that reflection may increase the maximum range of a radar up to twice the free-space value. This aids
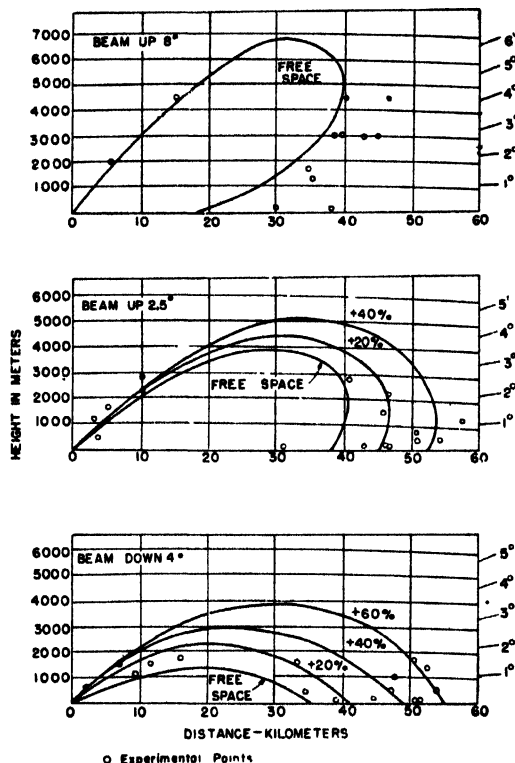

FIGURE 1. Effect of beam tilt on coverage for a radar.

the early detection of aircraft at low angles. However, the minima which occur in the resulting interference pattern prevent the continuous tracking of an airship coming in

This effect can be counteracted in several ways. One way is to employ microwaves whose interference lobes are narrow and close together. Vertical polarization is another means of filling in the nulls while gaining in maximum range at low angles. Another device is to tilt the antenna beam upward so that some radiation (but substantially less than half) falls upon the sea. The result is a gain in low-angle coverage while the high-angle coverage is that of free space, without minima.

The effect of various percentages of specular reflection in comparison with the free-space pattern is shown in Figure 1 for various beam tilts of a radar with a comparatively narrow beamwidth (11 degrees between half-power points). The experimen-

tal data, shown by small circles, illustrate the increase in detection range at 0 degree while at 5 degrees elevation angle there is little gain over free space.

The roll of a ship, by varying the beam tilt, results in a shift in coverage, as can be seen from Figure 1.

Signal-to-Noise Ratio

The visibility of a signal on a scope depends on its relation to the noise. In early work with radar, the maximum range was defined by a ratio of signal voltage S to noise voltage N of unity, i.e.,

$$\frac{S}{N} = 1. \tag{1}$$

However, as pointed out in Chapter 2 , the minimum detectable signal is greater than N. Since the pip on a scope includes noise, equation (1) is equivalent to

$$\frac{S + N}{N} = 2. \tag{2}$$

The relation of receiver power, P_2, to noise power, NP, and the signal-to-noise ratio, S/N, is given by

$$10 \log \frac{P_2}{NP} = 20 \log \frac{S}{N}. \tag{3}$$

On an A scope, this relation signifies that the height of the signal is twice that of the noise *grass*.

Since the visual signal in a set functioning properly varies linearly with the signal voltage, the size of targets can be estimated by means of the size of the visual signal. The ratio S/N gives a means of measuring a signal in terms of the noise. To change $(S + N)/N$ to S/N, the value of $(S + N)/N$ is expressed with unity as denominator. For example, if $(S + N)/N$ is estimated to be 8/2 from the scope, the equivalent fraction is 4/1. The value of S/N is $(4 - 1)/1 = 3/1$.

Calibration of an A Scope

On an A scope, the ratio $(S + N)/N$ can be estimated roughly by eye. To improve upon this, a calibration is employed. One method is to mark the A scope to facilitate the reading of heights. Another method goes beyond this and calibrates the gain control. A turn of 5 db is equivalent to a raito of 1.8/1. A datum line 1 cm above the time line and another at 1.8 cm are drawn on the A scope. The noise is brought up to the datum line by means of the gain control. The position is marked 0 on the gain control (see Figure 2). A steady signal is found (permanent echo, large boat, or signal generator) which produces a signal height of 1.8 cm above the time line. The gain control is then turned until the signal is reduced to the datum line. The position on the gain control is marked 5 db (see dotted lines in Figure 3).

Keeping the 5-db position on the gain control, another signal is obtained which comes up to 1.8-cm line. The gain control is turned until the signal is brought down to the datum line. The new setting is marked 10 db. This is repeated until markings up to about 70 db are obtained.

This calibration of $(S + N)/N$ must be corrected to S/N (Figure 3) which can be done by means of Table 1. For 25 db and above, the values of $(S + N)/N$ can be taken as equal to S/N. Any signal voltage can then be measured in decibels above the noise voltage (N) by turning the gain control until the signal height is 1 cm. By equation (3) this is also the signal power received, in decibels, above the noise power which is discussed in Chapter 2.

TABLE 1.   Correction of $(S + N)/N$ to S/N.

Corrected $\left(\frac{S}{N}\right)$ db	Uncorrected $\left(\frac{S + N}{N}\right)$ db
0	6
5	9
10	12.5
15	16.5
20	21

In the calibration just described, the pip on the scope is supposed to be proportional to the received signal strength. In a set functioning normally, this is justified, but occasionally defects in the set may destroy the linearity. The existence of a linear relation can be tested by means of a signal generator.
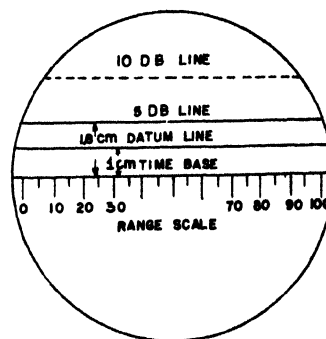
FIGURE 2.   Method of calibrating an A scope.
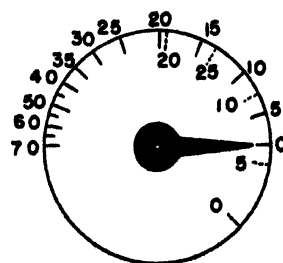
FIGURE 3.   Calibration of gain control of an A scope. (Dotted lines are uncorrected calibration.)

FREE SPACE — HIGH-ANGLE COVERAGE

Maximum Range Formulas

In free space, the gain factor A has the value $3\lambda/8\pi d$ (for maximum power transfer between doublets). Equations (3) and (5) in Chapter 5 then take the simple forms:

One-way, radio gain: $\dfrac{P_2}{P_1} = G_1 G_2 \left(\dfrac{3\lambda}{8\pi d}\right)^2 ;$ (4)

Two-way, radar gain: $\dfrac{P_2}{P_1} = G^2 \cdot \dfrac{16\pi\sigma}{9\lambda^2} \cdot \left(\dfrac{3\lambda}{8\pi d}\right)^4.$ (5)

If P_2 is replaced by the minimum detectable power of the receiver, P_{min}, and P_1 by the peak power P_p of the transmitter, the maximum range is given by:

One-way, $d_{max} = \dfrac{3}{8\pi} \sqrt{\dfrac{P_p}{P_{min}} G_1 G_2 \lambda^2} ,$ (6)

Two-way, $d_{max} = \sqrt[4]{\dfrac{P_p}{P_{min}} G^2 \lambda^2 \dfrac{9\sigma}{256\pi^3}} .$ (7)
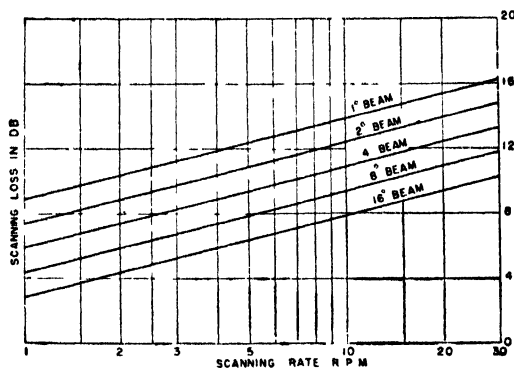
FIGURE 4. Scanning loss as a function of scanning speed and beamwidth.

Deviation from Maximum of Beam

For an antenna whose direction is fixed, the equations reported above apply only to points on the axis of the beam. Denoting by $f(\tau)$ the ratio of gain in a direction at an angle τ from the axis of the beam to the gain at the axis and by $2\tau_0$ the beam width between half-power points, then

$$f(\tau) = \exp - 0.692(\tau/\tau_0)^2. \quad (8)$$

Accordingly, for points off the axis, G must be multiplied by $f(\tau)$ before substitution in the formulas mentioned

Performance Figure

Equations (6) and (7) for d_{max} depend on the performance figure defined in the last section. The quantities which appear in the performance figure can be measured. The one which offers most difficulty is P_{min}, the minimum detectable power, which

has been discussed in Chapter 2. In Tables 3 and 4 at the end of this chapter, noise figures and bandwidths of various sets are given. An important correction to $P_{mi.}$ as determined from the noise figure and bandwidth is the scanning loss. This loss for various scanning speeds and beamwidths is represented in Figure 4. Another source of loss is deviation of the product of bandwidth B (mc) and the pulse width t (microseconds) from the optimum value of 1.2. The losses for various values of the product are tabulated in Table 2.

TABLE 2. Loss resulting from band- and pulse widths.

Bt *	Loss (db)
0.1	5.0
0.3	1.5
0.7	0.5
1.2	0.0
2.5	0.8
-5.0	3.0
10.0	5.0
20.0	8.0

*B = i-f bandwidth (mc); t = pulse width (microseconds)

A field measure of the performance figure of a radar can be determined by the use of a target of known radar cross section, such as a silvered balloon and equation (7). A check on variability of performance can be made by finding the maximum range on a plane (using a constant aspect, such as nose or tail).

Radar Cross Section

An important but troublesome factor in calculating d_{max} of a radar from a knowledge of the performance figure is σ, the radar cross section (see Chapter 2 and Chapter 9). The value of σ can be found by:

1. Laboratory measurement of the factors which constitute the performance figure and field determination of the maximum range d_{max}. The value of σ is then given by equation (7).

2. Measuring the signal returned by the target at a convenient distance on a calibrated A scope or by direct comparison with a pulsed signal generator. In this method neither P_{min} nor d_{max} enter.

The equations involving σ assume a point target. Since an airplane intercepts a small solid angle over which the beam strength varies little, the assumption of a point target is adequate for aircraft.

LOW-ANGLE AND SURFACE COVERAGE

Maximum Range

Since the gain factor A for this case is more complicated than for free space, the relation between d_{max} and the performance figure cannot be given in general by a simple expression, as can be seen from equations (172) and (184) in Chapter 5. For ranges such that the shadow factor $F_s \sim 1$, i.e.,

distances d less than $10^4\lambda^{1/3}$, λ, and d in meters, and both antennas low, or antenna and target low ($h_1, h_2 < 30\lambda^{2/3}$), the form of A is simplified so that a simple relation can be given for d_{max}. Otherwise, the methods of Chapter 5 must be employed.

Ducts and Set Performance

It has been found from field tests that atmospheric ducts are likely to be found close to the surface of the sea. The consequent increase in range may mask subnormal set performance. If the antenna is tilted upward so that no radiation reaches the earth, then the free-space discussion of this Chapter applies to the field determination or check of the performance figure. Otherwise field testing, when conditions are normal, can be accomplished by the use of permanent echoes or the use of a ship of known target cross section.

Low Heights and Plane Earth Ranges

For these conditions, the following relations must hold:
$$(h_{1,2} < 30\lambda^{2\ 3}, d < 10^4\lambda^{1\ 3}),$$
where h, d and λ are in meters.

In the dielectric case (see Chapter 5), generally applicable to radar, the value of A [equation (172) in Chapter 5] for $F_s = 1$ and $g = 1$, becomes

$$A = \frac{3}{2}\frac{h_1 h_2}{d^2}. \tag{9}$$

Since $A = A_0 A_p$ and $A_0 = 3\lambda/8\pi d$, the preceding equation is equivalent to a path-gain factor value of

$$A_p = 4\pi\frac{h_1 h_2}{\lambda d}. \tag{10}$$

[See equation (55) in Chapter 5.] Instead of equations (4) and (5), we now have [from equations (3) and (5) in Chapter 5] for a dielectric earth,

One-way, radio gain: $\quad\dfrac{P_2}{P_1} = \dfrac{9}{4}G_1 G_2 \dfrac{h_1^2 h_2^2}{d^4}.$ $\quad$ (11)

Two-way, radar gain: $\quad\dfrac{P_2}{P_1} = 9\pi G^2 \dfrac{h_1^4 h_2^4 \sigma}{\lambda^2 d^8}.$ $\quad$ (12)

Hence for maximum range, replacing P_1 by P_p, and P_2 by P_{min},

One-way, $\quad d_{max} = \sqrt[4]{\dfrac{9}{4}h_1^2 h_2^2 \left(\dfrac{P_p}{P_{min}}G_1 G_2\right)}.$ $\quad$ (13)

Two-way, $\quad d_{max} = \sqrt[8]{\dfrac{9\pi\sigma h_1^4 h_2^4}{\lambda^2}\left(\dfrac{P_p G^2}{P_{min}}\right)}.$ $\quad$ (14)

The maximum range now depends on the antenna heights and on the target height.

Radar Cross Section of Surface Craft

Effective Height of Targets. Since the field varies considerably with height for a low target, the

scattering by even simple geometrical objects requires integration. The formulas for radar in the last section apply to a point target with radar cross section σ at an effective height h_{eff}.

In the case of a cylinder of radius a and length H, the radar cross section in a uniform field is $\sigma = 2\pi a H^2/\lambda$. Under operating conditions the field is not uniform but a feasible approximation may be obtained by using the preceding value of σ and a value of h_2 equal to the average value of the target height.

Maximum Range Vs Height Curves

By the method reported in Chapter 5 and also in Chapter 6 , the maximum range versus height curves can be constructed for various values of A. These are of importance chiefly for low-angle aircraft coverage. If the performance figure, $(P_p/P_{min})G^2$, is known, equation (5), in Chapter 5, defines the relation between σ and A so that σ can be taken as the curve parameter instead of A. Equation (5), Chapter 5, can be written

$$20\log A = -5\log\frac{P_p}{P_{min}}G^2 - 5\log\sigma - 5\log\frac{16\pi}{9\lambda^2}. \tag{15}$$

A set of curves for a 10-cm radar is given in Figure 5 for a transmitter height of 30 meters. The curve corresponding to $\sigma = 31$ square meters is indicated. The corresponding value of $20\log A = -130$ was found from equation (15), using the value of

FIGURE 5. Maximum range versus height curves for various targets.

218.4 db as the performance figure.

For a ship with an effective height of 18 meters, Figure 5 gives the value of 20 log A at various distances. With the aid of equation (5), in Chapter 5, the power P_2 returned to the radar by the ship at these distances can be found, using the following data: $P_1 = P_t = 60$ kw, $G = 22.5$ db, and $\sigma = 7,440$ square meters.

In Figure 6, the maximum range versus distance curves for a set are presented. This set has a beamwidth of 60 degrees so that it is effective for tracking aircraft coming in toward the set (increasing angle of elevation). The near coverage then approximates the free-space coverage which is dependent on the angle of inclination of the antenna.

In Figure 7, curves are presented for a 3-cm set.

Estimating Ship Size

The fact that the strength of a signal received from a target depends on the size of the target can be utilized to estimate ship size. If signal strength versus distance curves are obtained for surface craft of various sizes, then by plotting readings from an unknown vessel, its size may be estimated. A field procedure for obtaining these curves is to use a number of surface craft of assorted sizes and follow them on a radar with a calibrated A scope, recording signal strength versus distance. If a number of such runs are taken during periods judged to be standard and the results averaged, a fairly reliable chart should result.

The curves can be obtained by calculation using measured power output and antenna gain and empirically determined values of σ in equation (5) in Chapter 5. The shape of such a curve for a "point" target is given in Figure 26 in Chapter 5. The radar curve can be obtained from this curve by changing the ordinate back to 20 log A [equation (3) in Chapter 5] and then using equation (5) in Chapter 5.

Since an actual surface target is generally large and at short distances intercepts a considerable part of the energy, the oscillatory part of the point curve of Figure 26 in Chapter 5 is smoothed out. The value of A for short distances is sometimes taken as $6A_0$, or 15 db above the free-space value.

In Figure 8, an example is given of curves computed for various ship sizes. Most of the plotted points fall in the 200- to 600-ton region. However, the precaution of a performance check is necessary in order to use this method most effectively (see next section). Since shape plays an important part in radar cross section, a ship of unusual shape may give a signal outside its class.

Performance Check

Since the performance of a set varies, before a chart such as has been described is used to detect unknown ships, it should be checked to determine
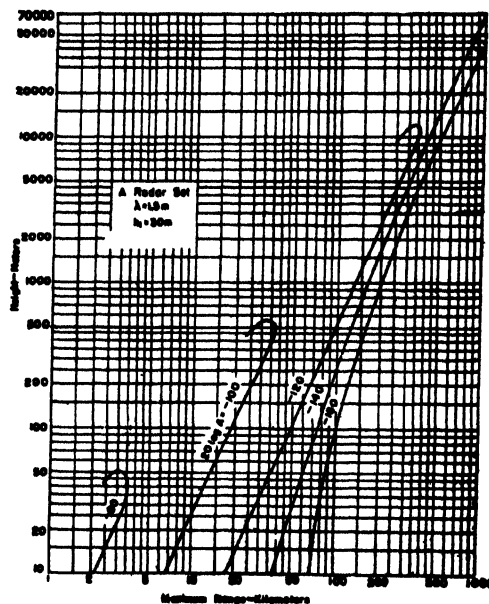
FIGURE 6. Maximum range versus height curves for various targets.
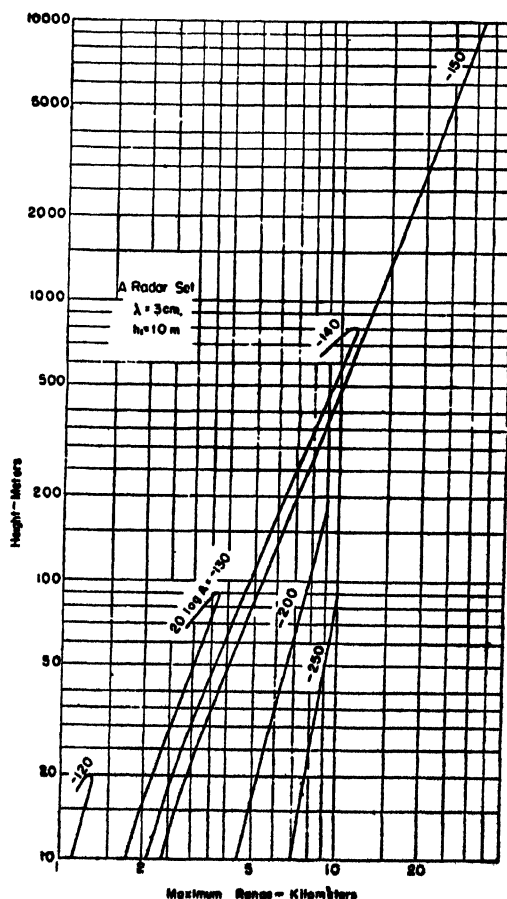
FIGURE 7. Maximum range versus height curves for various targets.
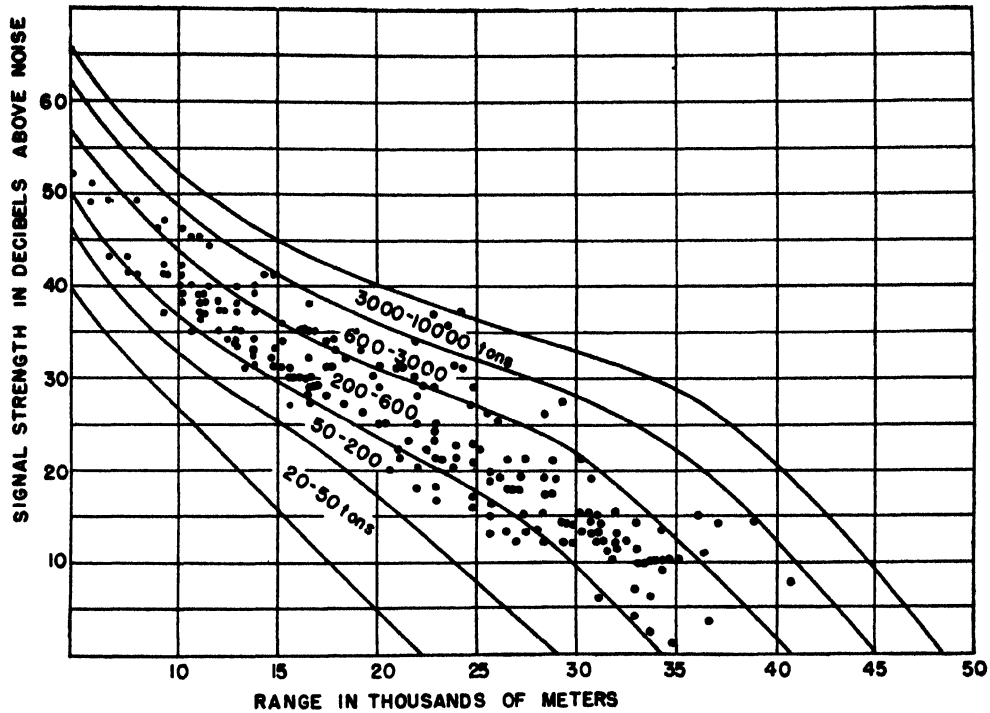
FIGURE 8. Estimation of ship sizes. (From Coast Artillery Experimental Establishment, England.)
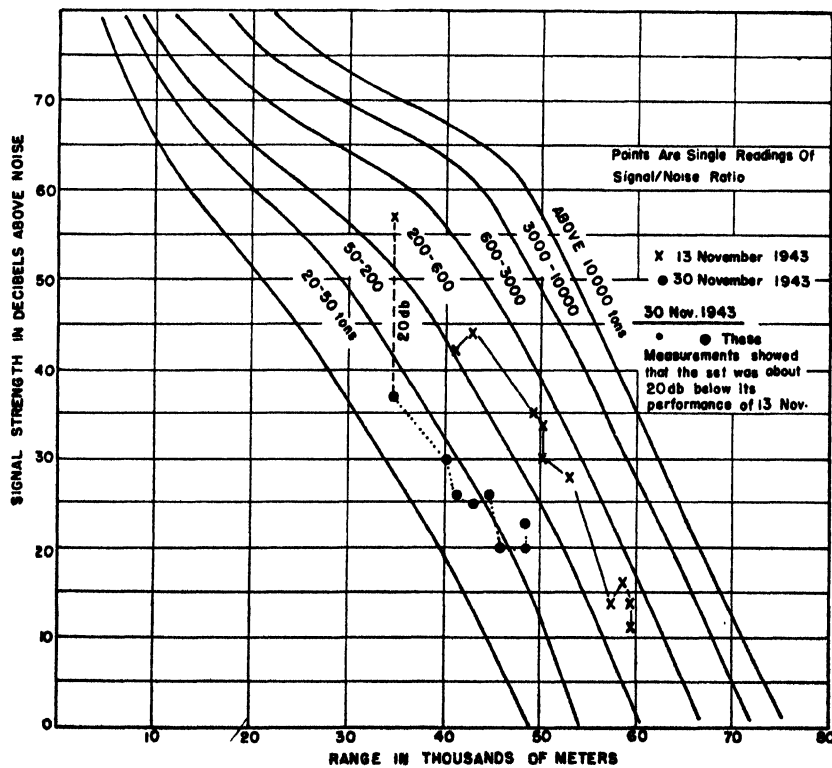
FIGURE 9. Range in thousands of meters. (From Coast Artillery Experimental Establishment, England.)

whether set performance is normal. The curves can be used for this check by using a known ship. Such·a check is shown in Figure 9 for two different days. On one day, the points for the ship fell in the correct region. On the other day, they fell too low by about 20 db. Accordingly, on the latter day the curves should have been used with an ordinate correction of −20 db.

Other types of performance check may be used, such as permanent echoes, free-space range of air-craft, or a signal generator.

DATA ON EQUIPMENT

The tables given in this section are not intended to be exhaustive. These are the best available data but should be used with caution, since specification changes may change rated characteristics of sets.

TABLE 3. Communication equipment.

Communication equipment	Frequency (mc)	Power output (watts)	Receiver sensitivity	Antenna Polarization	Gain (db)	Beamwidth Horizontal	Vertical
SCR-608	30	25	0.2 μv	V		Whip	
SCR-300	44	0.5	2.5 μv	V		Whip	
AN/TRC-1	70–100	50	25 μv (4 channel)	H	6		
SCR-522	125	6	4 μv	V		Whip	
AN/TRC-8	240	12	30 μv (4 channel)	H	7		
AN/TRC-5	1,400	400	NF* 12 db	H	14		
AN/TRC-6	4,600	2	NF* 19 db	H	33		
TBS	70	50	5 μv	V	1		
AN/ARC-1	125	10	5 μv	V		Whip	

* Noise figure.

TABLE 4. Radars.

Radars	Frequency (mc)	Power output (kw)	Receiver sensitivity Noise figure (db)	Bandwidth (mc)	Antenna Polarization	Gain (db)	Beamwidth Horizontal	Vertical
SCR-271DA	106	100	6	1	H	19.8	11°	12°
AN/TPS-3	600	200	11	1.8	H	23.4	12°	11°
SCR-584	3,000	300	15	1.7	H	30.8	7°	7°
AN/MPG-1	10,000	60	17	10		40.8	0.6°	3°
SC-4	200	200	6	0.5	H	13.5	20°	60°
SQ	2,500	1	13	2	V	20	8°	15°
SG-1	3,000	50	18	1	H	28	6°	15°
ASB	515	10	15	1.4	H	30	60°	

TABLE 5. IFF or beacons.

IFF or beacons	Frequency (mc)	Power output	Receiver sensitivity	Antenna Polarization	Gain (db)
AN/TPX-4	170	0.5 kw	15 μv	V	6
AN/UPN-1,2	3,000	50 kw	0.05 μv	H	6
AN/UPN-3,4	9,320	300 kw	0.02 μv	H	12

DIFFRACTION BY TERRAIN

OUTLINE OF THEORY

Introduction

THE EFFECTS of diffraction around natural obstacles of complicated shape are difficult to analyze. Theory offers two lines of approach to diffraction problems, both based on the substitution of contours of simple shape in place of the natural obstacle.

The first and oldest method, known as the Fresnel-Kirchhoff method, is an approximate procedure for calculating the diffraction by a flat screen. It yields comparatively simple formulas for the diffracted field; the present chapter is concerned with a presentation of this method.

The second method is based on the fact that the wave equation can be solved for obstacles of very simple geometrical shape, especially cylinders and spheres. If the curvature of a hill is fairly constant, so that its shape can be approximated by a cylinder or sphere, the field behind the hill can be obtained by the use of this method.

Observations on diffraction by obstacles in the short wave and microwave region are very sparse. It is, therefore, not possible to present a consistent body of results that could be utilized in radio practice. It seems, however, rather certain from the observations that when the shape of the obstacle approaches one of the special shapes dealt with by the theory,. the latter gives a fair account of the facts. Such cases will not be found too frequently in practice. The hope is nevertheless justified that the right order of magnitude is obtained by a judicious application of the theory. The main application is in the lower frequency band (30 to 200 mc); for higher frequencies, the diffracted field is relatively unimportant.

The Fresnel Diffraction Theory

The Fresnel-Kirchhoff approximate theory was originally developed to account for the diffraction of beams of light when cut off by diaphragms, slits, and similar optical devices. In applying this theory to the propagation of radio waves over the earth, only one basic problem is usually encountered, namely that of diffraction around a straight edge. In the present section, the general method of handling this problem and obtaining numerical results is given. On applying the method to actual cases certain

accessory problems arise which will be dealt with in following sections. . The most important of these complications is caused by ground reflection.
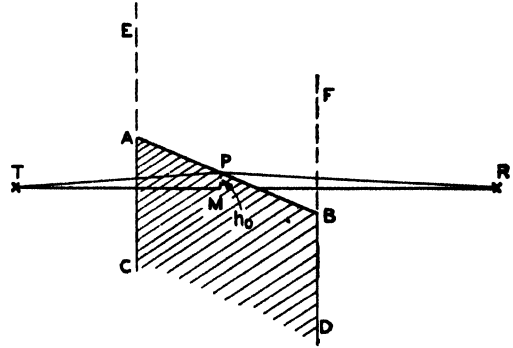
FIGURE 1. Diffraction around straight edge.

In Figure 1, the area $CAPBD$ forms an opaque screen bounded by a straight edge BPA. The width AB of the screen is assumed infinite in the mathematical theory, but is here shown finite for simplicity. The line connecting the transmitter T to the receiver R intersects the plane of the opaque screen in the point M whose distance from the edge is $PM = h_0$. The shortest unobstructed path of the radiation is TPR.

In a purely geometrical theory, the point R would be in the shadow of the screen and would receive no radiation. If the wave nature of radiation is taken into account, it is found that an electromagnetic field is generated in the shadow of the screen; the waves are *bent* around the obstacle.

The mathematical derivation of the diffraction formulas will not be given here as it is rather intricate; however, the problem is discussed in following text. The discussion here is limited to a qualitative visualization of the mechanics of diffraction in the text below; the final formulas used for computations will then be written down at once.

Mechanism of Diffraction

The physical idea underlying the Fresnel-Kirchhoff diffraction theory may be presented as follows. At points visible from T the field, to a first approximation, is equal to the free-space field E_0. This applies in particular to all points of the plane $ECDF$ containing the screen. The receiver R receives radiation from the *open* part $EAPBF$ of the plane,

while there is no radiation incident upon R from the opaque surface $CAPBD$. In order to compute the field at R, it is assumed that in the open part of the plane the field is E_0 while on the opaque screen the field vanishes. Such a field distribution may be realized physically by assuming that there is a conducting sheet in the open region $EAPBF$ with suitably chosen oscillating charges or currents such that the field E_0 is produced on the side of the sheet facing the receiver. The total radiation received at R from such a current-sheet will be equivalent to the radiation from T bent around the diffracting screen. The fictitious sheet $EAPBF$ forms a system of *secondary* sources of radiation whose effect is equivalent to that of the primary source for all points on the *far* side of the plane $ECDF$ (side of the receiver), but not on the *near* side (side of the transmitter).

It is evident that most of the radiation received at R comes from the area near the point P above the line APB. The relative importance of contributions of areas more or less removed from P is discussed in following text.

When the primary source at T is replaced by a distribution of secondary sources in the plane of the screen, an essential approximation is made. It is assumed that there are no secondary sources in the opaque region $CAPBD$. In reality, the screen is a physical body and, whether it is a conductor or a dielectric, there is an electromagnetic field in its surface layers, especially near the edge APB, and this field makes a contribution to the radiation received at R. In the approximate theory, it is assumed that the field on the surface of the opaque screen is negligible. In the terminology of optics, this implies that the screen is *black*; in radio terminology, it means that the surface of the screen is *rough*

The Straight Edge Formula

The physical picture just described can be put into mathematical language. When the rather intricate derivations are carried through, a relatively simple formula results.

The symbols and designations used are illustrated in Figure 2. In accordance with practice it is assumed that the line TR is nearly horizontal. The trace of the opaque screen on a vertical plane through T and R is assumed perpendicular to the line TR (upper part of Figure 2). The trace of the screen on a horizontal plane may, however, make an angle ϕ with the line TR (lower part of Figure 2).

In view of the approximate nature of the theory explained in the preceding paragraph, the following conditions *must* be fulfilled in order to obtain reliable results:

$$d_1, d_2 >> h_0 >> \lambda. \qquad (1)$$
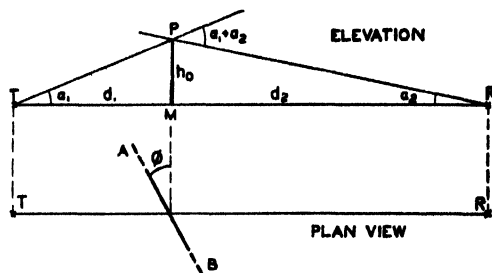
FIGURE 2.   Diffraction around straight edge.

That is, the distances from the transmitter and receiver to the obstacle must be large compared to the height of the latter above the line TR, and this height must be large compared to the wavelength. The second of these conditions is likely to be fulfilled in the short-wave and microwave bands, and the first will be fulfilled when the angles of elevation α_1 and α_2 of the rays, drawn from the transmitter and receiver to the edge, are small.

A second condition for the validity of the diffraction formula refers to the horizontal extension of the screen. The formulas are derived for a screen of infinite horizontal extent, but in practice it will usually suffice if the horizontal extension of the screen is large compared to the height h_0.

If these conditions are fulfilled, the field at the receiver is given by

$$E = E_0 \frac{e^{j\pi/4}}{\sqrt{2}} \int_{-\infty}^{v} e^{-j\pi v^2/2} \, dv, \qquad (2)$$

where E_0 is the free-space field at the receiver in absence of the screen and

$$v = \pm h_0 \sqrt{\frac{2}{\lambda}\left(\frac{1}{d_1} + \frac{1}{d_2}\right)} = \pm \sqrt{\frac{2h_0}{\lambda}(\alpha_1 + \alpha_2)}. \qquad (3)$$

In the last formula, use is made of the fact that α_1 and α_2 are small angles so that approximately $\alpha_1 = h_0/d_1$ and $\alpha_2 = h_0/d_2$.

The Fresnel Integrals

An integral of the type appearing in equation (2) is known as Fresnel's integral; its properties will now be briefly discussed and numerical data given. The standard Fresnel integral is usually defined as

$$C(v) - jS(v) = \int_0^v e^{-j\pi/2 \, v^2} dv, \qquad (4)$$

where

$$C(v) = \int_0^v \cos\left(\frac{\pi}{2} v^2\right) dv,$$

$$S(v) = \int_0^v \sin\left(\frac{\pi}{2} v^2\right) dv.$$

If this function is plotted in the complex plane, with C and S as abscissa and ordinate, respectively, for all values of v, a curve is obtained that is known as Cornu's spiral (Figure 3). $C - jS$ is represented,
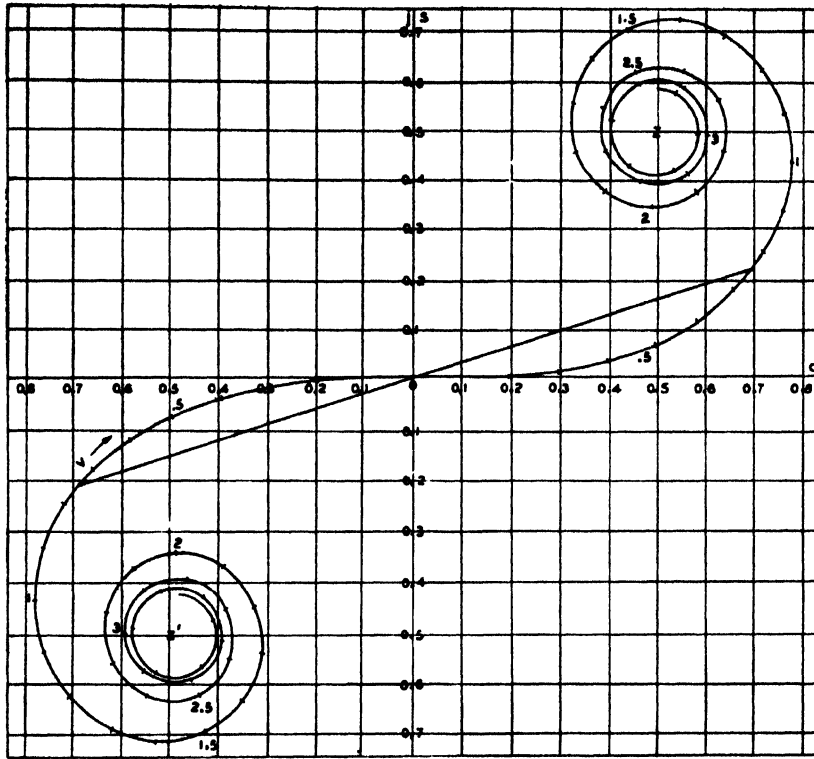
FIGURE 3. Cornu spiral.

in magnitude and phase, by a vector from the origin to a point on this spiral.

It may be shown that the length of arc along the spiral, measured from the origin, is equal to v. In the graph, values of v, counted positive in the first quadrant and negative in the third quadrant, are indicated along the spiral. As v approaches infinity, the spiral winds an infinity of times around two points lying at the distance $1/\sqrt{2}$ from the origin on a 45-degree line. C and S for the end points are

$$C(\pm\infty) = \pm\frac{1}{2}, \quad S(\pm\infty) = \pm\frac{1}{2} \quad (5)$$

Application to Straight Edge

Since

$$\frac{e^{j\pi/4}}{\sqrt{2}} = \frac{1+j}{2},$$

equation (2) may be rewritten, on using equations (4) and (5), as

$$E = E_0\frac{1+j}{2}\left[\frac{1}{2} + C(v) - \frac{j}{2} - jS(v)\right]. \quad (6)$$

It will be noticed that the quantities

$$\frac{1}{2} + C, \; j\left(\frac{1}{2} + S\right)$$

have a simple geometrical meaning. They are the real and imaginary components, respectively, of a

vector drawn from the lower point of convergence (point $-1/2$, $-j/2$) of the Cornu spiral to a point on this spiral. The bracket in equation (6) is equal to this vector in magnitude but with opposite phase.

The Fresnel formulas and Cornu spiral as given above will assist the reader in establishing the relations of our equations with the *classical* theory of diffraction as found in all textbooks on the subject. For practical purposes the field behind a diffracting straight edge given by equation (6) will be denoted by

$$\frac{E}{E_0} = ze^{-j\zeta}. \quad (7)$$

In Figure 4, the modulus z is plotted as a function of v. In Figure 5, the phase lag ζ is plotted in a similar way. (With the above choice of the sign, ζ is positive in the shadow.)

The variable v is given by equation (3). On account of the square root, there is an ambiguity in sign. Closer inspection shows that v *must be taken positive when the receiver is in the illuminated region*, above the line of sight; v *must be taken negative when the receiver is in the shadow zone.*

When v tends to $-\infty$, the line APB (Figure 1) moves far upwards relative to the line TR; the receiver lies deep in the shadow and E approaches zero by equation (6). When v tends to $+\infty$, the line APB moves far downward, and the screen ceases to form an obstruction, E approaches E_0. At the line of sight (when the point P in Figure 1 coincides

with M), $v = F(v) = 0$ and $E = E_0/2$. Clearly, the effects of diffraction are not confined to the shadow region but extend considerably into the illuminated zone. If the receiver is sufficiently deep in the shadow, about $v > -1$, the following approximate formula holds:

$$ z = \left|\frac{E}{E_0}\right| = \frac{0.225}{v}. $$
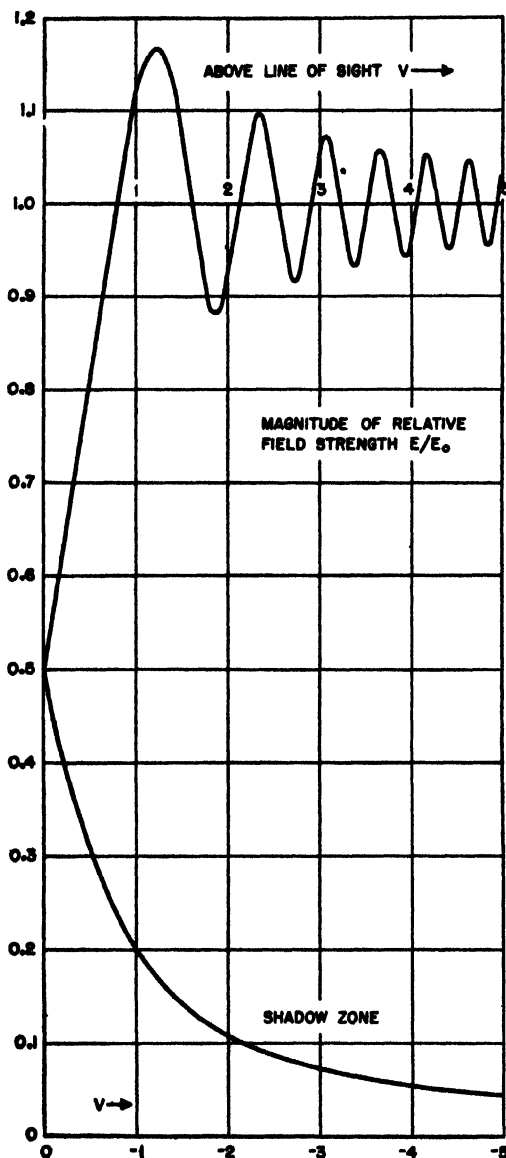
FIGURE 4. Magnitude of relative field strength E/E_0 versus v.

Polarization. Large Angles

It may be noticed that in the preceding equations no reference is made to the state of polarization of the diffraction field. The results of the approximate Fresnel-Kirchhoff theory are independent of the state of polarization in agreement with observation. If the angles of diffraction (α_1 and α_2, Figure 2) become large, larger than a few degrees, for instance, the approximate theory no longer applies. The deviations from the Fresnel formulas then go in opposite directions for the two states of polarization. If the electric vector is parallel to the diffracting edge, the field in the shadow at large angles is slightly diminished as compared with that given by the Fresnel formulas; if the electric field is perpendicular to the diffracting edge, the diffracted field in the shadow at large angles can become appreciably larger than the calculated one and, in the case of very large angles, the excess may reach the magnitude of, say, 6 to 15 db. In the region above the line of sight, the sign of the polarization effect is reversed (slight increase for polarization parallel to the edge, appreciable decrease for polarization perpendicular to the edge).

These effects are entirely analogous to those that are observed when the currents induced in the surface of the obstacle cannot be neglected and they have the same physical origin.
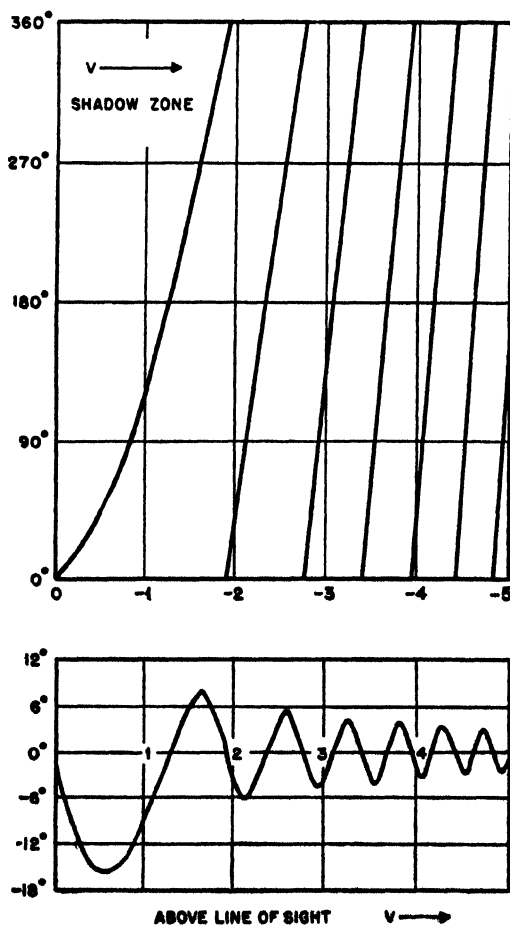
FIGURE 5. Phase lag (ordinate) of relative field strength (E/E_0) versus v (abscissa).

DIGRESSION ON FRESNEL'S THEORY

Fresnel Zones

The concept of the Fresnel zone has played an important role in the development of diffraction theory. As it is frequently referred to in papers on the subject, it may be useful to digress briefly on it. Fresnel's original construction is based on the conception that any small element of space in the path of a wave may be considered as the source of a secondary wavelet, and that the radiation field can
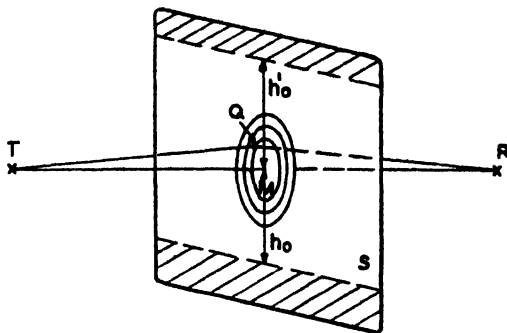
FIGURE 6. Relations of Fresnel zones and diffracting slots.

be built up by the superposition of all these wavelets (Huyghens' principle). In particular, consider the field produced by the transmitter in the *open* part of the plane containing the diffracting screen (*EAPBF* in Figure 1) and let each element of this plane be the source of a secondary wavelet. This may be achieved by distributing a suitable fictitious system of oscillating currents (or a system of elementary doublets of proper strength) over the surface of the plane. The field at the receiver is then the superposition of all the fields produced by the wavelets.

Now let (Figure 6) S be a plane perpendicular to the line TR and let M be the point in which the line TR intersects the plane S. Let Q be a point on the plane S such that the difference in path between TQR and TMR is just $\lambda/2$. The locus of these points is a circle about M. Similarly we can construct other circles so that the corresponding path differences are integral multiples of $\lambda/2$. The area within the first circle is called the first Fresnel zone, the subsequent ring-shaped areas are called the second, third, etc., Fresnel zones. The secondary wavelets originating in the first, third, fifth, etc., Fresnel zones are in phase with each other and reinforce each other by constructive interference at R, while the secondary wavelets originating in the second, fourth, etc., zones are in phase with each other but out of phase with the former group and tend to cancel the field produced by this group.

Hence if the plane S is opaque except for a round hole centered on M, the intensity of the radiation

field at R will depend on the number of Fresnel zones that fall inside the hole. If we start out with a very small hole and progressively increase its size, there will be a maximum of intensity at R (nearly twice the free-space field E_0) when the hole just comprises the first Fresnel zone. If the size of the hole is further increased, the destructive interference of the second zone comes into play, decreasing the intensity, and a minimum (very nearly zero) is reached when the hole contains just the first two zones. On continued increase of the hole size, further maxima and minima appear. The amplitude of these oscillations decreases very gradually until eventually the field at R approaches the free-space value.

Diffraction by a Slot

The preceding considerations indicate that only a comparatively small area of an opening, of the order of one Fresnel zone, is required to produce an illumination that is comparable in order of magnitude to the free-space field. It is also seen that the simple geometrical construction of the Fresnel zones is more suitable when dealing with the diffraction by round openings than with screens bounded by straightedges. Qualitatively, however, the conditions are similar.

As an example, consider the case of a slot bounded by parallel edges at distances h_0 and h_0' from the point of intersection M between the plane of the slot and the direction from the observer to the distant light source (see Figure 6). The diffracted field E will obviously be equal to the free-space field E_0 if the slot is infinitely wide on both sides of M, which corresponds to a vector joining the two foci of the Cornu spiral. However, there is an infinite number of other finite openings of the slot which also will give the free-space field. Suppose, for instance, that $h_0 = h_0'$ in Figure 6 and that the slot width is gradually increased from zero. A glance at the Cornu spiral (Figure 3) shows that when $v = 0.75$ and $v' = -0.75$, the vector representing the diffraction field is approximately equal to the free-space field. This width represents, for a slot, the analogue of the first Fresnel zone for a circular opening.

DIFFRACTION BY HILLS

Introduction

The formula for diffraction by a straight edge may be applied in radio practice to determine the diffraction field behind a ridge. The ridge need not be perpendicular to the transmission path, but the condition given in equation (1) must be approximately fulfilled. The distance from transmitter and receiver to the ridge should be large compared

to the height of the latter above the straight line
TR; and that height should be large compared to
the wavelength.

Moreover, as discussed in the first section , the
diffraction formula applies in principle only to the
case where the effect of the currents induced on the
surface of the ridge upon the field at the receiver
can be neglected. This is the case (1) when the ridge
has the shape of a steep and narrow knife-edge
protruding from the surrounding countryside; or
(2) when the surface of the ridge is *rough* (see sec-
tion below). Experience shows that so long as the
profile of the ridge is reasonably compact and its
surface reasonably rough, the diffraction formula
will give the magnitude of the field behind the ridge
to within a few decibels.

If the ground near the transmitter or receiver is
smooth, however, it becomes necessary to take
ground reflection into account. This may be done
by introducing an image transmitter and receiver.
The field is then the sum of four components whose
relative phase must be calculated (see Figure 11).

Earth curvature will be neglected throughout the
present section.

Criterion for Roughness

It is difficult to establish a quantitative criterion
for the roughness of a surface. From the viewpoint
of radiation theory, the effect of a rough surface is
to scatter incident radiation diffusely in all directions
with no preference for the direction of regular reflec-
tion, whereas a smooth surface will reflect the inci-
dent radiation according to Snell's law. In radio
work, the effect of diffuse reflection is to weaken the
radiation scattered in the direction of the receiver
so much that its intensity may be neglected com-
pared to the direct ray. A moderately rough surface
will give a coefficient of reflection intermediate
between zero and unity. A surface will be optically
smoother as the incident radiation approaches
grazing, and even surfaces that are comparatively
rough geometrically may then give partial reflection.

A rule taken from optics and known there as
Rayleigh's criterion has been used successfully in
radio practice. Assume that the roughness is pro-
duced by numerous small elevations above a level
surface and let H be the typical height of such an
elevation. The difference in path between a ray
reflected from the ground and a ray from the top
of the elevation is $2AB$ in Figure 7, which is equal
to $2H \sin \psi$ or $2H\psi$ approximately for small angles ψ.
The difference in phase between the two rays is
$2H\psi(2\pi/\lambda)$. The criterion now requires that the
surface be considered as rough when this phase
difference exceeds 45 degrees, or $\pi/4$ radians.

Hence the critical value of H is given by

$$\frac{4\pi H\psi}{\lambda} = \frac{\pi}{4}, \text{ or } H = \frac{\lambda}{16\psi}, \qquad (8)$$
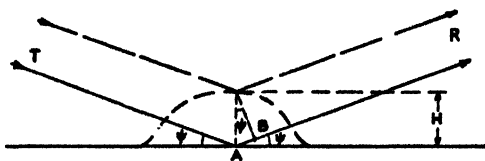
FIGURE 7. Geometry for Rayleigh's criterion for
rough ground.

with ψ in radians and

$$H = \frac{3.6\lambda}{\psi}, \qquad (9)$$

with ψ in degrees. The surface is considered smooth
or rough according to whether H is smaller or larger
than this value.

Sometimes it is convenient to refer to the field
pattern that would be present over a reflecting
surface. This is done by introducing a new variable,
the *lobe number*

$$n = \frac{4h_1\psi}{\lambda} \qquad (10)$$

(h_1 transmitter height above the ground), where
$n = 1, 3, 5$, etc., correspond to the angle of the first,
second, etc., maxima in the lobe pattern and $n = 0$,
2, 4, etc., to the nulls of the lobe pattern. Introduc-
ing n into equation (8), the criterion assumes the
form

$$H = \frac{h_1}{4n}. \qquad (11)$$

Although the criterion is approximate and gives no
more than an order of magnitude estimate, it is rather
surprisingly well fulfilled in radio practice. Experi-
ence has shown that when the differences in level
which constitute roughness are of the order indicated
by these equations, the reflection coefficient is
reduced to a small fraction (about one-fifth) of the
value calculated for an ideal surface.

Diffraction by a Straight Ridge

Assume that the ground intervening between the
transmitter and receiver is everywhere rough, so
that all ground reflection may be neglected. For
the sake of computation, the ridge is replaced by a
vertical screen of height h_0 above the line *TR*. The
top of the ridge forms the diffracting edge (P in
Figure 8). If the profile of the ridge is somewhat
more complicated, the *effective diffracting edge* might
be a purely mathematical line, as shown in the lower
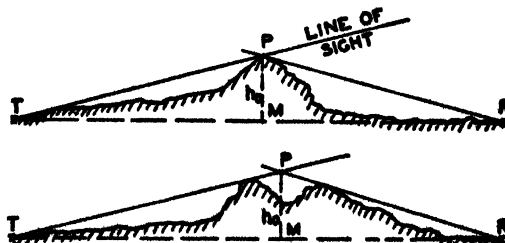
FIGURE 8.   Diffraction by a straight ridge.

part of the figure. The height h_0 is conveniently determined from a profile of the transmission path obtained from a topographic map. If the heights h_1, h_2, and h of transmitter, receiver, and obstacle, respectively, above a given reference level such as sea level are given, we have

$$h_0 = \frac{d_1 h_2 + d_2 h_1}{d_1 + d_2} - h, \qquad (12)$$

where the signs have been chosen so that h_0 is negative when the receiver is in the shadow of the ridge and positive when it is in the illuminated region. Now, by equation (3),

$$v = h_0 \sqrt{\frac{2}{\lambda}\left(\frac{1}{d_1} + \frac{1}{d}\right)} = \sqrt{\frac{2h_0}{\lambda}(\alpha_1 + \alpha_2)}. \qquad (13)$$

In these equations, give the angles α_1 and α_2 the same sign as h_0 and give v the same sign that h_0 has in equation (12).

The ratio of the field to the free-space field at the receiver is now given by $|E/E_0| = z(v)$, defined by equation (7) and plotted in Figure 4. In Figure 9, this ratio is given in decibels as a function of the quantity $\dot{x} = -h_0/\sqrt{\lambda d}$ (all lengths in meters). The successive curves in Figure 9 correspond to different values of the ratio d_1/d_2 or d_2/d_1 (choose whichever one is the smaller). Only the field below the line of sight is shown.
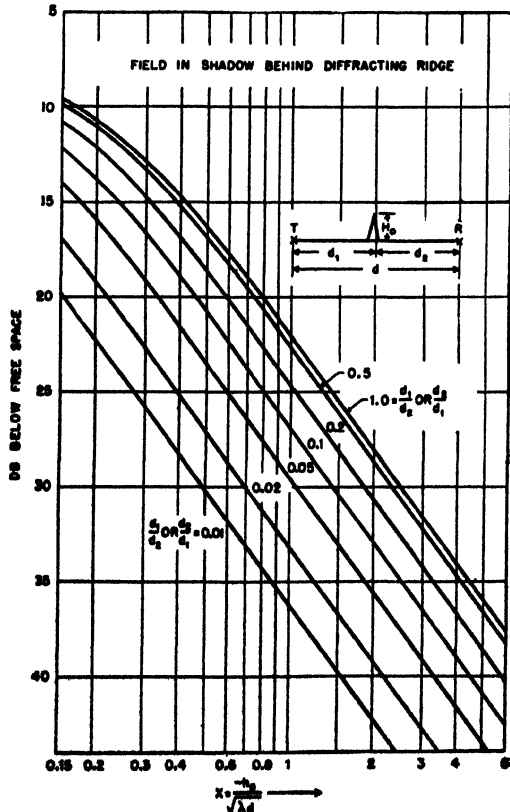
FIGURE 9. Field in shadow behind a diffracting ridge.
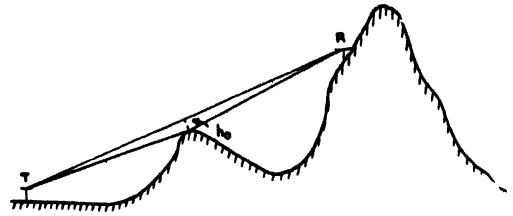
FIGURE 10. Diffraction field above the diffracting edge.

Field Near the Line of Sight

The fact that just above the line of sight the field increases above its free-space value may sometimes be used to obtain a favorable site (Figure 10). The maximum value of the field is about 1.17 times the free-space value (Figure 4), equivalent to 1.36 db. On the other hand, there are advantages in avoiding a line TR that is too close to grazing the top of an intervening obstacle, as this will substantially reduce the signal. At the line of sight, the signal is 6 db below free space. In order to get approximately the free-space value of the field, the crest of the obstacle should be sufficiently below the line TR so that $v > 0.8$ where v is given by equation (13), h_0 being the clearance between the line TR and the obstacle. In cases where the heights and distances are not quite certain, it is therefore preferable to select a higher and definitely unobstructed site rather than to try to utilize the small gain that might possibly be had from the diffraction field.

Diffraction with Reflecting Ground

When the ground near the transmitter or receiver is smooth and reflecting, the diffraction problem becomes very complicated. It can be solved by the method of images on assuming that the radiation reflected on the transmitter side of the obstacle issues from an image transmitter and that the radiation reflected on the receiver side is incident upon

FIGURE 11. Diffraction of direct and reflected rays.

an image receiver (Figure 11). The total field at the receiver may be written

$$E = E_1 - E_2 - E_3 + E_4,$$

where each term on the right-hand side is of the form of equation (6), E_1 corresponding to the direct radiation, E_2 to the radiation from the image transmitter to the receiver, E_3 to the radiation from the transmitter to the image receiver, and E_4 to the radiation from one image to the other. These four terms differ in the value of v assigned to each of them; the effective height h_0 computed by equation

(12) and the path lengths being different in each case. From Figure 9, the diffracted field is found to be 14 db below the free-space field at the same distance.

Example

Assume that from a topographic map the profile shown in Figure 12 has been drawn. The horizontal scale is in kilometers and the vertical scale in meters above sea level. From this profile, combined with inspection of the terrain, it has been found that the ground is so rough that the reflected rays may be
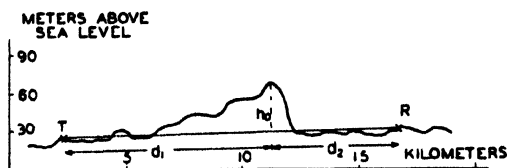
FIGURE 12.   Assumed profile.

disregarded. The heights above sea level of transmitter, receiver, and obstacle, are respectively $h_1 = 24$ meters, $h_2 = 33$ meters, $h = 69$ meters. Since $d_1 = 9,000$ meters, $d_2 = 5,400$ meters, $d = 14,400$ meters, we find from equation (12) that $h_0 = -39$ meters. Assume a wavelength of 1 meter:

$$x = \frac{-h_0}{\sqrt{\lambda d}} = 0.325 \text{ with } \frac{d_2}{d_1} = 0.6.$$

DIFFRACTION BY COASTS

Introduction

Diffraction occurring at coast lines is significant for coverage problems of coastal radars. It becomes particularly important when the sets are used for height-finding purposes where an accurate knowledge of the lobe angle and possible deformation of the lobes is required.

The diffraction might be due either to the fact that the radar is sited on a cliff or to the sudden change in surface properties. Reflection from rough ground is diffuse, so that there is no interference between direct and reflected rays when the reflection point lies on this type of terrain, but interference does occur when the reflection point lies on the sea surface from which regular reflection is obtained. A situation commonly occurring is that of a search radar sited on rough terrain a few miles inland from the coast. Here coastal diffraction may result in an appreciable deformation (shortening or lengthening) of the lobes.

More generally, diffraction occurs with level ground whenever there is a change, especially a sudden change, of ground properties along the transmission path. The formulas developed for coast-line diffraction may equally be applied to the case where rough ground suddenly changes into smooth,

reflecting ground. Similarly, the effect of patches of smooth ground in rough surroundings, such as a lake in wooded country and, vice versa, rough patches in smooth terrain, may be treated by means of the Fresnel-Kirchhoff theory. Here, attention will be confined to the case of a straight boundary, applying the diffraction theory developed in the first section of this Chapter .

Level Site Near Coast

Assume a transmitter sited on rough ground near a coast. If diffraction were disregarded, the coverage pattern would appear as follows. When the reflection point is on the land, the reflected ray is diffusely scattered and its field at the receiver is negligible. Again, if the reflection point falls on the sea, the reflected ray will be present and will interfere with the direct ray with its full or nearly its full intensity. The ray leaving the transmitter at an angle ψ_0 (Figure 13), such that its reflected counterpart undergoes reflection right at the shore line, divides the coverage diagram into two parts. For angles of
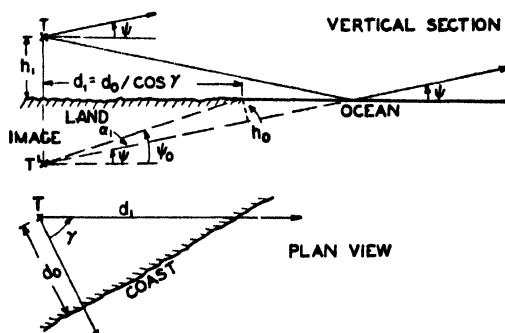
FIGURE 13.   Diffraction by a coast line.

elevation larger than $\psi = \psi_0$ the field will be essentially the free-space field; for angles of elevation less than $\psi = \psi_0$ the familiar lobe pattern, for complete reflection, will appear with maxima equal to twice the free-space field. When diffraction by the coast line is taken into account, the discontinuity expressed by this rough picture is replaced by a smooth transition of the field from one region to the other.

The land surface may be considered as an opaque screen for the image transmitter from which the reflected rays seem to come (Figure 13). This problem is somewhat different from the diffraction problem treated previously since the trace of the screen in the vertical plane through T' and R is no longer perpendicular to the line $T'R$ as it was, for instance, in Figure 2, upper part. In the present case, the effective height h_0 of the diffracting edge for any given ray is the perpendicular projection from the coast line upon this ray, as shown in Figure 13. The slant distance of the coast from the transmitter is d_1. Assuming that the receiver (target) is far distant, a condition usually fulfilled in radar

practice, $d_2 >> d_1$ and the angle ψ between the direct ray and the horizontal will be equal to the angle between the image ray and the horizontal. Then approximately, since the angles are small,

$$h_0 = d_1\alpha_1 = d_1(\psi_0 - \psi), \qquad (14)$$

where d_1 and α_1 have the significance given them on page 4 6 2. There the signs have again been chosen so that h_0 is negative when the receiver (target) is in the shadow of the screen with regard to the image transmitter.

The distance from the transmitter to the diffracting coast depends on the azimuth (Figure 13). Therefore, with the designations of the figure,

$$d_1 = \frac{d_0}{\cos \gamma}. \qquad (15)$$

Equation for Field Strength

The expression for the diffracted field of the image transmitter is given by the straightedge formula, equation (6), with v given by equation (3). Since $1/d_2$ is assumed negligibly small compared to $1/d_1$, we find, on using equation (14),

$$v = (\psi_0 - \psi)\sqrt{\frac{2d_1}{\lambda}}. \qquad (16)$$

This may be further simplified by introducing a new variable, the *lobe number*

$$n = \frac{4h_1\psi}{\lambda}. \qquad (17)$$

(h_1 = transmitter height). This quantity is equal to $1, 3, 5 \cdots$ at the interference maxima and equal to $0, 2, 4, \cdots$ at the interference minima but is here taken as a continuous variable, defined for any value of ψ. In particular for $\psi = \psi_0$ we put $n = n_0$. Since $\psi_0 = h_1/d_1$, we have by equation (15)

$$n_0 = \frac{4h_1\psi_0}{\lambda} = \frac{4h_1^2 \cos \gamma}{\lambda d_0}. \qquad (18)$$

Equation (16) may now be written

$$v = \frac{n_0 - n}{\sqrt{2n_0}}. \qquad (19)$$

The diffraction formula will again be written, in the form of equation (7), as

$$\frac{E}{E_0} = ze^{-j\zeta},$$

where z and ζ are the functions of v shown in Figures 4 and 5.

The total field obtained by the interference of the direct and reflected ray is

$$E = E_0(1 - ze^{-j\pi n - j\zeta}), \qquad (20)$$

where the negative sign in front of the second term in parentheses accounts for the 180-degree phase shift at reflection, and the phase lag πn corresponds to the path difference between the reflected and direct rays.

The absolute value of the field is

$$\left|\frac{E}{E_0}\right| = \sqrt{(1 - z)^2 + 4z \sin \tfrac{1}{2}(\pi n + \zeta)}. \qquad (21)$$

Figure 12 in Chapter 5 may be used for the numerical evaluation of this equation.

The formula can readily be generalized to the case where the reflected ray is weakened by (1) a reflection coefficient, R, different from unity, and (2) the effect of the earth's curvature expressed by the divergence factor, D, (Chapter 5). If, moreover, the phase lag at reflection is not π but $\pi + \phi'$, the equation becomes

$$\left|\frac{E}{E_0}\right| = \sqrt{(1 - zRD)^2 + 4zRD \sin^2 \tfrac{1}{2}(\pi n + \phi' + \zeta)}. \qquad (22)$$

Example

Assume the following conditions. A radar set of 200 mc (λ = 1.5 meters) is sited at a height h_1 = 15.3 meters (about 50 feet) and at a distance to a straight shore line of d_0 = 195 meters (about 0.12 mile). The ground between the radar and the seashore is level but can be considered as rough for practically any angle of elevation, on applying the criterion of data discussed . The coverage diagram will first be determined in the azimuth perpendicular to the coast line, where $d_1 = d_0$, or $\cos \gamma = 1$. Then by equation (18), n_0 = 3.20. With this value of n_0 the variable v is determined by equation (19). We shall confine ourselves to integral values of n, that is, to those angles which, in the presence of simple reflecting ground, correspond to lobe minima and maxima. Having obtained v, one then determines z and ζ from Figures 4 and 5. The field in terms of the free-space field is then obtained from equation (21), either by direct computation or by means of Figure 12 in Chapter 5. The numerical data for the first five lobes are summarized in Table 1. The last column of this table contains the values of E/E_0 which would be obtained if the magnitude of the reflection coefficient were assumed to be zero over land and unity over the sea and if diffractions were neglected.

The same calculations are carried out for an

TABLE 1. ($\gamma = 0°$).

n	v	z	ζ (degrees)	$|E/E_0|$ with diffraction	$|E/E_0|$ without diffraction
0	1.27	1.17	0	0.17	0
1	0.87	1.05	− 12	2.05	2
2	0.48	0.80	− 15	0.75	0
3	0.08	0.54	− 4	1.54	2
4	− 0.32	0.36	24	0.69	1
5	− 0.71	0.26	11	1.26	1
6	− 1.11	0.19	145	1.16	1
7	− 1.51	0.14	242	0.94	1
8	− 1.90	0.12	5	0.88	1
9	− 2.30	0.10	158	0.92	1
10	− 2.70	0.08	339	0.94	1

TABLE 2. ($\gamma = 45°$).

n	v	s	ζ (degrees)	$|E/E_0|$ with diffraction	$|E/E_0|$ without diffraction
0	1.50	1.07	6	0.10	0
1	1.17	1.17	− 3	2.17	2
2	0.83	1.03	− 13	0.21	0
3	0.50	0.82	− 15	1.80	2
4	0.17	0.59	− 8	0.42	0
5	− 0.17	0.42	11	1.42	1
6	− 0.50	0.31	42	0.80	1
7	− 0.83	0.23	90	0.91	1
8	− 1.17	0.18	157	0.88	1
9	− 1.50	0.14	240	0.99	1
10	− 1.83	0.12	338	1.12	1

azimuth inclined by an angle $\gamma = 45°$ with respect to the coast line. Then, from equation (18), $n_0 = 4.5$. The results are given in Table 2.

In the problem considered here, the angles of elevation are comparatively large (for $n = 1$, $\psi = 1° 24'$). If the effects of diffraction occur at lower angles, the divergence factor D must be taken into account (see Chapter 5). This is done by computing D for the angles desired and replacing z by zD in equation (21).

Cliff Site

If the radar is sited on a cliff and if the land intervening between the radar and the reflecting plane (ocean) is rough, the equations given on page 469 apply. We shall now consider the case where the radar is sited at some distance from the cliff edge and where the ground between the radar site and the cliff edge is reflecting. There are then two reflecting planes, the lower of which might be the ocean, or might be a reflecting land surface. In Figure 15, this surface has been designated as ocean. The upper coverage pattern corresponding to Table 1 is shown graphically in Figure 14.
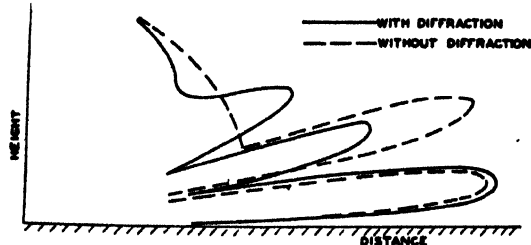
FIGURE 14. Coverage diagram (relative field strength). (Heights exaggerated 3.5 to 1.)

It is seen from these data that the lobes near the critical ray (ray whose reflection point is at the coast line) undergo very considerable deformation. The
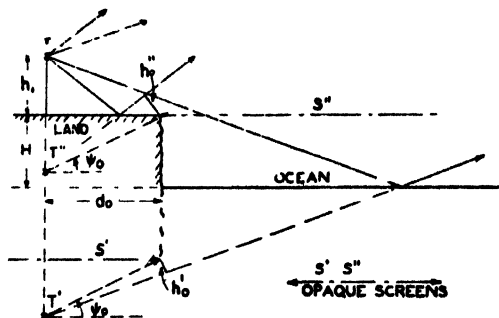
FIGURE 15. Diffraction from a cliff site.

plane is at a height H above the lower plane and the transmitter at a height h_1 above the upper plane. Assume that the azimuth chosen is perpendicular to the direction of the cliff edge; the distance of the radar to the cliff edge is d_0. For any other azimuth (angle γ in Figure 13), replace d_0 by $d_0/\cos \gamma$ in the following equations.

Two images are shown in Figure 15 and two fictitious opaque screens, one corresponding to each image. The corresponding variables are distinguished by single and double primes. The lobe numbers are given by

$$n'' = \frac{4h_1\psi}{\lambda}$$

$$n' = \frac{4(H + h_1)\psi}{\lambda} = \frac{n''(H + h_1)}{h_1}.$$

The critical angle, $\psi_0 = h_1/d_0$, is the same for both image transmitters. Thus

$$n_0'' = \frac{4h_1^2}{\lambda d_0},$$

$$n_0' = \frac{4(H + h_1)h_1}{\lambda d_0} = \frac{n_0''(H + h_1)}{h_1}$$

Further

$$v' = \frac{n_0' - n'}{\sqrt{2n_0'}},$$

$$v'' = \frac{n'' - n_0''}{\sqrt{2n_0''}} = - v' \frac{1}{1 + H/h_1}.$$

Again, the field is given by

$$E = E_0(1 - s'e^{-j\pi n' - j\zeta'} - s''e^{-j\pi n'' - j\zeta''}). \tag{23}$$

The expression for the field strength [equation (23)] is in a form where all the quantities involved may be evaluated for any given height of transmitter, height of the cliff, and any wavelength by using graphs and tables given in earlier paragraphs.

TARGETS

SCATTERING PARAMETERS

Radar Cross Section

$\mathbf{I}$N DETERMINING the coverage to be expected of radar systems, it is important to know what fraction of the power incident upon a target will be returned to the receiver. A parameter involving the dimensions and orientation of the target, and usually also the wavelength, and which measures the proportion of power returned, is called a *scattering parameter*.

The most generally used of these parameters is the radar cross section introduced in Chapter 2. It is denoted by σ and is defined by

$$\sigma = 4\pi d^2 \frac{W_r}{W_i}, \tag{1}$$

where W_r is the scattered power per unit area at the receiver and W_i is the incident power per unit area at the target. In terms of σ, the radar gain is

$$\frac{P_2}{P_1} = G_1 G_2 \frac{\sigma}{4\pi d^2} \left(\frac{3\lambda}{8\pi d}\right)^2 A_p{}^4. \tag{2}$$

This equation may also be written in the form

$$\frac{P_2}{P_1} = G_1 G_2 \cdot \frac{16\pi\sigma}{9\lambda^2} A^4,$$

where

$$A = \left(\frac{3\lambda}{8\pi d}\right) A_p = A_0 A_p$$

is the gain factor introduced earlier (see Chapter 5), A_0 is the free-space gain factor and A_p is the path-gain factor.

Target Gain

Another scattering parameter is G_R, the *target gain*, discussed in Chapter 2. It is the gain of the target in the direction of the receiver relative to a shorted (dummy) doublet antenna. The target gain is connected with σ by the relation

$$G_R = \frac{\sqrt{4\pi\sigma}}{3\lambda}. \tag{3}$$

The corresponding radar gain is

$$\frac{P_2}{P_1} = 4 G_1 G_2 G_R{}^2 A^4. \tag{4}$$

The factor 4 is due to the calculation of G_R relative to a shorted doublet rather than to a matched load doublet. If the calculation of G_R were made relative

to the matched load doublet, the factor 4 would be replaced by 1.

Echo Constant

The *echo constant*, denoted by K, is defined by

$$K = \frac{W_r}{W_i}\left(\frac{d}{\lambda}\right)^2 \tag{5}$$

and is related to σ by

$$K = \frac{\sigma}{4\pi\lambda^2}. \tag{6}$$

The corresponding power ratio is

$$\frac{P_2}{P_1} = K G_1 G_2 \left(\frac{8\pi}{3}\right)^2 A^4. \tag{7}$$

Except for the factor $\frac{1}{4}\pi$, K is just σ measured in square wavelengths.

Equivalent Plate Area

A plate of area S placed normal to the direction of propagation has a radar cross section given by

$$\sigma = 4\pi \frac{S^2}{\lambda^2}, \tag{8}$$

provided the linear dimensions of the plate are large compared with λ. Any target may be supposed to scatter (in the direction of the radar) an amount of energy equal to the amount that a plate of area S would scatter in this direction. This area S is called the *equivalent plate area* of the target. The corresponding radar gain is

$$\frac{P_2}{P_1} = G_1 G_2 \left(\frac{8\pi S}{3\lambda^2}\right)^2 A^4. \tag{9}$$

Scattering Coefficient or Characteristic Length

This parameter has also been called the *radar length* of the target. The definition is

$$L = d \frac{E_r}{E_i}, \tag{10}$$

where E_r = field strength at the receiver,
   E_i = field strength incident on target.
It is evident that

$$L^2 = \frac{\sigma}{4\pi} \tag{11}$$

connects L with radar cross section. The radar gain

becomes

$$\frac{P_2}{P_1} = G_1 G_2 \left(\frac{8\pi L}{3\lambda}\right)^2 A^4. \qquad (12)$$

RADAR CROSS SECTION
OF SIMPLE FORMS

Spheres

The radar cross section of any large curved conducting surface having principal radii of curvature ρ_1 and ρ_2 at the reflection point is given by

$$\sigma = \pi \rho_1 \rho_2. \qquad (13)$$

This formula applies if the surface is sufficiently large and sufficiently curved to contain many Fresnel zones. For a sphere of radius a, where $a >> \lambda$,

$$\sigma = \pi a^2. \qquad (14)$$

Thus, in the case of a large conducting sphere, the radar cross section is equal to the geometrical cross section and is independent of wavelength.

The result for small spheres ($a << \lambda$) is

$$\sigma = 144\pi^5 \frac{a^6}{\lambda^4}. \qquad (15)$$

There is no simple formula for the radar cross section in the region $a \sim \lambda$.

Cylinders

The radar cross section of a cylinder whose length is large compared with the wavelength is

$$\sigma = \frac{2\pi a L^2}{\lambda}, \qquad (16)$$

This formula assumes that the direction of incidence is normal to the cylindrical surface. If the cylinder is tilted so that there is a small angle θ between the normal to the cylinder and the direction of incidence, the result is

$$\sigma = \frac{2\pi a L^2}{\lambda} \cdot \left[\frac{\sin \frac{2\pi L \theta}{\lambda}}{\frac{2\pi L \theta}{\lambda}}\right]^2. \qquad (17)$$

This result holds for small angles of tilt θ such that

$$\sin \theta \cong \theta.$$

where $a = $ radius,
             $L = $ length. ($L >> \lambda$).

Plates

A flat plate of area S with all dimensions large compared with λ and oriented so that the normal to the plate is in the direction of incidence, has a radar cross section given by

$$\sigma = 4\pi \frac{S^2}{\lambda^2}, \qquad (18)$$

regardless of shape.

For a circular plate (a disk) of radius a, whose normal is at an angle θ with the direction of incidence,

$$\sigma = \pi a^2 \left[\cot \theta \cdot J_1\left(\frac{4\pi a}{\lambda}\sin\theta\right)\right]^2, \qquad (19)$$

where J_1 is the first-order Bessel function. The maximum value is at $\theta = 0$, where

$$\sigma = \frac{4\pi^3 a^4}{\lambda^2}. \qquad (20)$$

This agrees with equation (18), since at normal incidence $S = \pi a^2$.

The peculiar feature of equation (19) is that the maximum at $\theta = 0$ is very sharp. For example, if $\lambda/a = 1/10$, σ is only $1/10$ of its maximum value when $\theta = 1.25°$.

The average value of σ over all orientations is

$$\sigma = \frac{1}{2}\pi a^2. \qquad (21)$$

This result is independent of wavelength and suggests that a large number of flat plates oriented at random will have a cross section independent of λ. or that a few surfaces of rapidly changing orientation may have this property.

The results for a rectangular plate are practically the same as for a disk. If the dimensions of the plate are b and c, πa^2 is replaced by bc in equation (20) and equation (21); equation (19) is replaced by

$$\sigma = \frac{4\pi b^2 c^2}{\lambda^2}\left[\cos\theta \frac{\sin\left(\frac{2\pi b}{\lambda}\sin\theta\cdot\cos\phi\right)}{\frac{2\pi b}{\lambda}\sin\theta\cdot\cos\phi}\right.$$
$$\left.\cdot \frac{\sin\left(\frac{2\pi c}{\lambda}\sin\theta\cdot\sin\phi\right)}{\frac{2\pi c}{\lambda}\sin\theta\cdot\cos\phi}\right]^2 \qquad (22)$$

where the sides b and c are parallel to the x and y axes, and $\sin\theta\cos\phi$, $\sin\theta\sin\phi$, and $\cos\theta$ are the direction cosines of the direction of incidence relative to the plate normal.

These results hold when the linear dimensions of the target are large compared with the wavelength. If the linear dimensions are small compared with the wavelength, a plate of area S, oriented so that the normal to the plate is in the direction of incidence, has a radar cross section given by

$$\sigma = \frac{32\pi^3}{3}\frac{S^3}{\lambda^4}. \qquad (23)$$

Corner Reflectors

The corner formed by three mutually perpendicular conducting planes forms what is called a corner reflector. The faces may be triangular or square or have other shapes, depending on how the planes are bounded. A line drawn to the corner making equal angles with the three edges is called the axis of symmetry.

Reflection from a corner reflector may be analysed by the methods of geometrical optics, provided the linear dimensions of the reflector are large compared

with the wavelength. A ray which is reflected from all three surfaces is said to be triply reflected. Triply reflected rays always return to the radar and make the only large contribution to the radar cross section which in a corner reflector is

$$\sigma = \frac{4\pi S^2}{\lambda^2}, \qquad (24)$$

where S is the cross section of the triply reflected beam. S is a function of the shape of the faces of the corner reflector and of the angle of incidence of the radiation.

For a triangular corner reflector, σ is given approximately by

$$\sigma = \frac{4\pi L^4}{3\lambda^2}(1 - 0.00076\,\theta^2), \qquad (25)$$

where L = length of edge of reflector,

θ = angle between direction of incidence and the axis of symmetry in degrees ($\theta < 26°$).

As a function of θ, σ has a broad, flat maximum. Consequently, the return to the radar receiver from such a target is not sensitive to the precise orientation of the axis of symmetry.

AIRCRAFT

Variation with Aspect

Diagrams showing the dependence of σ on orientation indicate very large and irregular fluctuations. Radar cross section σ can change from values of nearly 1,000 square meters to a few square meters as a result of a change of aspect of a few degrees. These instantaneous values of the radar cross section are dependent on wavelength, polarization, details of plane design, areas of specular reflection, propeller rotation, etc. Reflection patterns have been measured for a few simplified models by laboratory means (see Figure 1 as an example). It would be difficult to calculate instantaneous values of σ by theoretical methods.

In practice, however, an airplane is in motion and is affected by air currents. These factors cause the airplane, in a short interval of time, to present many widely different instantaneous values of σ to the radar, so that the signal actually seen on the scope by the observer is in effect a time average, where the most violent fluctuations of instantaneous values of σ have been smoothed out.

Measurement of σ

The radar equation for free space, equation (45), in Chapter 2, may be used for the computation of average values of σ from observed instantaneous values, provided conditions are such that ground

reflections are unimportant. The received power P_2 is determined by matching the signal from the plane with the measured signal from a signal generator.

The procedure followed in work at the Radiation Laboratory is to measure the maximum value of P_2 for each of a series of 3-second intervals. A plot is made of P_2 against range d on log log coordinates. As might have been anticipated from equation (45), in Chapter 2, it is found that a line with a constant slope of -4 passes through the average of the 3-second interval maximum points, although the individual points fluctuate widely. The value of σ corresponding to this line is calculated.

The resulting value of σ still cannot be called an average value because the maximum value of σ has been used for each point. Consequently these values of σ, substituted into equation (45) in Chapter 2, cannot be expected to give the average value of P_2, or to give observed maximum ranges. However, it is found that if the values of σ thus computed are reduced 40 per cent, they give correct results.

These empirical cross sections are relatively independent of wavelength. This result may be interpreted to mean that a plane in motion behaves more or less like a collection of specularly reflecting surfaces oriented at random, as equation (21) indicates.

Attempts have been made to develop formulas giving operational cross sections as a function of some large feature of plane design, such as wing span or length of fuselage, but these attempts have not been successful.
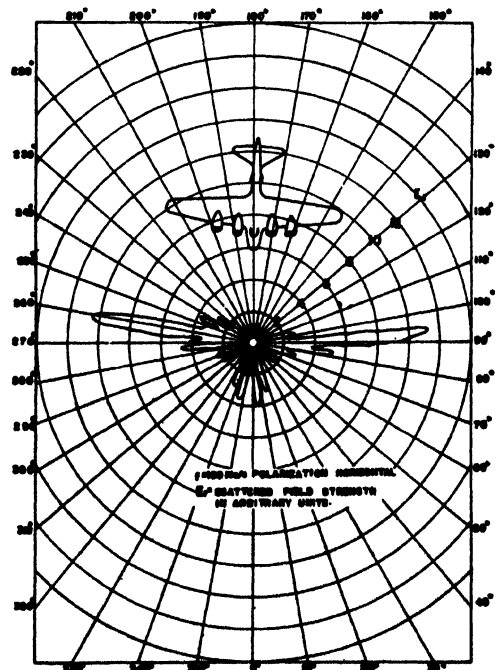
FIGURE 1.   Aspect diagrams of B-17E, 5 degrees above horizon.

Chapter 10

SITING

GENERAL

SITING REFERS to the selection and utilization of local terrain features which affect propagation and the performance of equipment. From a preliminary analysis, the general location, type of equipment, and height may be determined. The specific sites available may, however, profoundly alter performance in several ways. Careful analysis and tests may then be necessary to determine the best use of the facilities at hand and for an understanding of the limitations due to the terrain.

Siting Requirements

With communication equipment, the siting problems are principally concerned with visibility and, in wooded areas, absorption by vegetation. When siting direction-finding equipment, it is important to realize that reflections from mountains or other irregularities may cause serious angular errors which should be avoided by proper choice of the location. Both direction-finding and radar equipment require orientation.

Radar siting requirements are rather different and depend on whether ground reflection is of importance or not. The siting of radars operating mainly on the direct ray is relatively easy and is principally concerned with permanent echoes and visibility. The most exacting site requirements are presented by the VHF early warning and height-finding radars, which to a large extent depend on ground reflection for successful operation. The siting problem then requires the consideration of terrain effects such as limited reflection areas, cliff edges, obstacles, etc., which involve diffraction problems of considerable complexity. Recommendations for specific sets are given in instruction manuals furnished with the equipment.

TOPOGRAPHY OF SITING

Profiles

Radar and direction-finding systems, which may cover a large area and involve many services, use a grid for plotting purposes. The grid location, height, and orientation of each station must be known with reasonable accuracy. Topographic maps of a scale of one or two miles to the inch and contour intervals of not more than 100 feet, preferably 20 feet, should be secured. These may be supplemented by aerial photographs and surveys.

In a complicated terrain, it is usually necessary to have profiles on several azimuths to determine the effective height above the reflecting surface. The accuracy required decreases with the distance from the transmitter. In most cases sufficient detail is not available on maps, so that a personal inspection of the terrain should be made to become familiar with the nature of the soil and degree of roughness. Special attention should be given to ridges, flat areas, bodies of water, distance to the shore, hills to the rear, obstacles in the operating area and at the boundaries.

Where long distances and directive beams are involved, fairly accurate orientation of the order of one-half degree is required. Care must be taken when using compasses because of local attractions or inadequate information on declinations. Observations on Polaris give the greatest precision but this star is not always visible and it is often inconvenient to use a transit at night. Caution must be used in aligning on permanent echoes, as they may be difficult to identify. In general, several methods should be used to obtain independent checks.

Solar azimuths, correct to the nearest quarter of a degree, may be determined from the date time to the nearest minute, and the latitude and longitude to the nearest degree. Two methods will be given for obtaining the azimuth of the sun: (1) by calculation, (2) from tables.

The azimuth of the sun may be calculated from the formula,

$$\tan \beta = - \frac{\sin (\text{HA})}{\cos \phi \tan \delta - \sin \phi \cos (\text{HA})}, \qquad (1)$$

where β = bearing of the sun. The bearing is east or west of south when $\phi - \delta$ is positive. The bearing is east or west of north when $\phi - \delta$ is negative. The bearing is east in the morning (β will be negative) and west in the afternoon (β will be positive).

HA = hour angle of the sun. During the morning hours when the hour angle is greater than 12 hours, its value should be subtracted from 24 hours for use in the formula.

ϕ = latitude of the place of observation.

δ = declination of the sun at the time of observation. The signs of ϕ and δ are important and each is positive when north of the equator and negative when south.

FIGURE 1. Calculation of solar azimuth.

The hour angle HA is the local apparent time (LAT) minus 12 hours. To convert the observed time into LAT, the civil time at Greenwich (GCT) must be found and combined with the equation of time to correct for the apparent irregular motion of the sun. This gives Greenwich apparent time GAT, which is converted to LAT, by allowing for the longitude. The equation of time and the declination of the sun are plotted for 1945 in Figure 1. The annual change is small and these curves may be used for most orientations without regard to the year. Standard time meridians are given every 15 degrees east or west of Greenwich, each zone corresponding to one hour. Care should be used to take daylight saving or other changes from standard into account correctly.

The calculations may be illustrated from the following data: date, 16 March; time, 1345 hours PWT; latitude, 40° north; longitude, 118° west. The HA is computed first.

Observed time (PWT)	13 hr	45 min
Zone difference	+ 7 hr	
Greenwich civil time	20 hr	45 min
Equation of time (Figure 1)		− 9 min
Greenwich apparent time	20 hr	36 min
Longitude difference (for 118° W)	− 7 hr	52 min
Local apparent time (LAT)	12 hr	44 min
LAT −12 hours = HA	− 12 hr	
Hour angle of sun	+ 0 hr	44 min
HA in arc	+11°	
Latitude ϕ	+40°	
Declination of sun δ (Figure 1)	− 2°	

Substituting in equation (1),

$$\tan \beta = -\frac{\sin 11°}{\cos 40° \cdot \tan (-2°) - \sin 40° \cdot \cos 11°}$$

$$\beta = 16° 10'$$

Since $\phi - \delta$ is positive, β is the bearing from the
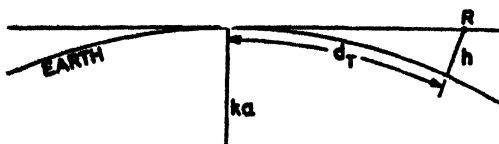
FIGURE 2. Geometry for horizon distance for zero height transmitter.
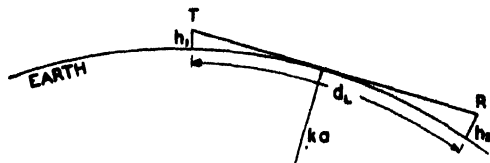
FIGURE 3. Geometry for horizon distance with elevated transmitter.

south. The bearing is west of south, since HA is positive (p.m.). The azimuth of the sun is $180° + 16° 10' = 196° 10'$.[a]

The equal altitude method is less convenient but requires no calculation. This method consists in measuring the horizontal angles between the sun and a mark taken when the sun is at the same altitude on both sides of the meridian of the observer. The bisector of the horizontal angle between the two equal altitude positions of the sun during the observations is very close to true south, and the azimuth of the mark may be determined.

GEOMETRICAL LIMITS OF VISIBILITY

Horizon Formula

It is assumed throughout that the earth radius is ka (see Chapter 4). Whenever numerical examples are given, the standard value, $k = 4/3$, is used. The alternate method of accounting for refraction given in Chapter 4 may also be used in connection with the following equations if $k \neq 4/3$.

When a horizontal ray, tangential to the earth, is drawn, the earth slopes away (Figure 2) at the rate of

$$h = \frac{d^2}{2ka}. \qquad (2)$$

Hence the horizon distance d_T for a transmitter at a height h above level ground is equal to

$$d_T = \sqrt{2kah}. \qquad (3)$$

Numerically, when all the lengths are in meters

$$d_T = 4,120 \sqrt{h} \quad \text{for } k = \frac{4}{3}. \qquad (4)$$

With h in feet and d_T in statute miles, by a curious numerical coincidence,

$$d_T = \sqrt{2h} \quad \text{for } k = \frac{4}{3}. \qquad (5)$$

When both terminals of a path are elevated above the ground (Figure 3), the horizon distance is

$$d_L = \sqrt{2ka} \left(\sqrt{h_1} + \sqrt{h_2} \right), \qquad (6)$$

where again $\sqrt{2ka} = 4,120$ in the metric system.

[a] This result could have been obtained directly from *Azimuths of the Sun*, HO71, U.S. Naval Department, Hydrographic Office. The equation of time may be obtained from a current copy of *The American Nautical Almanac*, U.S. Naval Observatory, Washington, D.C.

If d is in statute miles and h in feet,

$$d_L = \sqrt{2h_1} + \sqrt{2h_2} \quad \text{for } k = \frac{4}{3}. \quad (7)$$

The relation between h_1, h_2 and d_L is graphically presented in Chapter 5, Figure 2 as a nomogram.

Height of Obstacle

As a first case, consider a smooth earth and two terminals at the ground. The earth itself forms an obstacle which reaches its maximum height h_m in the middle of the path (Figure 4). By equation (2)

$$h_m = \frac{\left(\frac{d}{2}\right)^2}{2ka} = \frac{d^2}{8ka}. \quad (8)$$

A point P on the ground at distances d' and d'' from the two terminals (see Figure 4) has an elevation
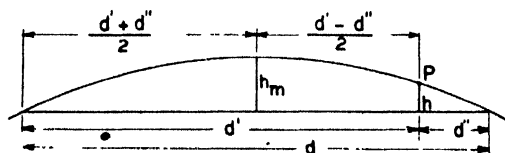
FIGURE 4. Height of earth as an obstacle.

above the straight line connecting the terminals given by

$$h = \frac{\left(\frac{d' + d''}{2}\right)^2}{2ka} - \frac{\left(\frac{d' - d''}{2}\right)^2}{.2ka}. \quad (9)$$

or, after a simple reduction,

$$h - \frac{d'd''}{2ka} = 5.9 \cdot 10^{-8} d'd'', \quad (10)$$

where h, d', and d'' are given in meters. If h is in feet and d' in statute miles,

$$h = \frac{d'd''}{2} \quad \text{for } k = 4/3. \quad (11)$$

Secondly, assume that the terminals are elevated (Figure 5). The elevation of the straight line connecting the terminals, for a flat earth, is equal to

$$h = \frac{d'h_2 - d''h_1}{d' - d''}, \quad (12)$$

where d', d'' are again the distances to the terminals, and h_1, h_2 are the corresponding elevations.

In order to account for the effect of the earth's curvature, Figure 5 may be considered as a *plane earth* diagram on which a ray will appear curved, the deviation from a straight line being downward and given by equation (10). See dashed line in Figure 5.
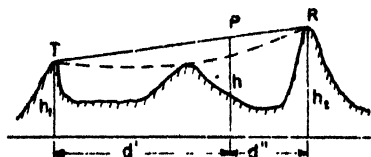
FIGURE 5. Height for elevated terminals.

Hence, the total height above the theoretical ground is

$$h = \frac{d'h_2 - d''h_1}{d' - d''} - \frac{d'd''}{2ka}. \quad (13)$$

When the heights are expressed in feet and the distances in miles, the first term remains unaltered, while the second term again becomes $d'd''/2$ for $k = 4/3$.

Equation (13) is used to decide whether and by how much an obstacle such as a hill will obstruct a given transmission path.

Extended Obstacle

When the obstacle is of appreciable horizontal extension, it may not possess a single peak to which equation (13) can be applied without ambiguity. The case of twin mountains is shown in Figure 6 for straight rays (earth's radius ka).
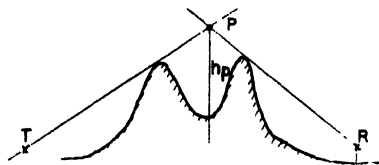
FIGURE 6. Height of equivalent diffracting edge.

The *optical peak P* of the obstacle for radio or radar transmission is the point from which both terminals are just visible. For a given profile, the limiting rays to the terminals may be found by trial and error by applying equation (13) to those points of the profile which are most likely to represent limiting elevations. In the theory of diffraction (Chapter 8) P marks the position of the equivalent diffracting edge.

Degree of Shielding

As a measure of the degree of shielding, the angle between the two limiting rays drawn from the terminals to the (actual or equivalent) peak of the obstacle of height h_p may be used.

Since all angles considered are small, the sine or tangent of the angle may be replaced by the angle in radians. Consider first the ray going from the first terminal to P (Figure 7). The angle of the ray with the horizontal at the terminal is

$$\alpha_1 = \frac{h_p - h_1}{d'} - \frac{d'}{2ka} \quad (14)$$

and its angle with the horizontal at P is

$$\beta_1 = \alpha_1 + \frac{d'}{ka} = \frac{h_p - h_1}{d'} + \frac{d'}{2ka}. \quad (15)$$

The angle of the ray going from the second terminal to P is determined correspondingly.

The angle between the two rays is then equal to

$$\beta_1 + \beta_2 = d\left(\frac{1}{2ka} + \frac{h_p}{d'd''} - \frac{h_1}{d'} - \frac{h_2}{d''}\right), \quad (16)$$

where $d = d' + d''$, and $(ka)^{-1} = 1.18 \cdot 10^{-7} \text{(meter)}^{-1}$.
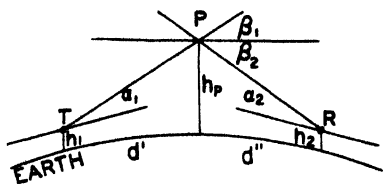
FIGURE 7. Shielding between transmitter and receiver.

When d is measured in miles and h in feet, equation (16) becomes

$$\beta_1 + \beta_2 = 1.89 \cdot 10^{-4} d \left[\frac{h_p}{d'd''} + 1 - \frac{h_1}{d'} - \frac{h_2}{d''} \right]. \quad (17)$$

PERMANENT ECHOES

Permanent echoes are caused by reflections from terrain features such as mountains or even smooth surfaces near the antenna (ground clutter). With radars, the indicator is obscured by the strong echoes from hills and the minimum detection range is increased by ground clutter. With direction finders, erroneous indications are caused by the spurious reflections. Permanent echoes are among the principal problems involved in siting, as many otherwise excellent sites are rendered worthless by excessive fixed echoes. Several methods are available for determining the suitability of sites in this regard without actual field tests.

A number of factors combine to make permanent echoes more troublesome than might be expected.

1. Hills and land surfaces are so much greater in extent than the target which the equipment is designed to detect that strong echoes may be obtained from distances where an ordinary target would give an echo far below normal detection levels.

2. The low elevation of the land surfaces places them in regions most subject to nonstandard propagation effects where extreme ranges and large responses are frequently obtained.

3. Side lobes of the horizontal pattern of the antenna cause permanent echoes to appear at several other azimuths in addition to that of the main lobe.

4. Strong permanent echoes from mountains to the rear may be caused by back radiation from the antenna. The low intensity of the back radiation may be compensated by the size of the mountains. Such echoes are especially harmful as they obscure the operating sector.

5. Objects appear wider because of the antenna beamwidth and of greater extent in range as a result of the pulse width.

6. Diffraction over intervening ridges may be sufficient to nullify their screening action so that objects behind a ridge are visible.

7. The use of a permanent echo as a standard target may be very misleading. A decrease in performance that seriously affects echoes from small targets may not have any noticeable effect on the response from large targets. An echo used for a standard target should be weak and near by.

Permanent Echo Diagrams

The permanent echoes associated with a radar station may be plotted on a polar chart and their extent, location, and strength represented. Such diagrams should be prepared for each unit of a radar system, using a standard procedure for taking and presenting the data.

Permanent echo data should be taken under average conditions with the gain set at some standard level. At intervals of azimuth such as 5 degrees, the ranges of the permanent echoes are recorded. These data are then plotted on a polar chart and the points are connected to indicate obscured areas. The skill and judgment of the operator are important factors. In most cases the amplitudes of the echoes are so far above that of ordinary target echoes that the actual amplitudes need not be noted.

In Figure 8 is shown an observed permanent echo diagram for a VHF radar. This was selected for purposes of illustration rather than as an example of a good site. The mountains to the north are unshielded and cause extensive echoes. The large echo at 200 degrees is due to a mountainous island 260 miles away and appears only during times when propagation is nonstandard.

Care must be exercised in identifying the cause of an echo. Antenna side lobes cause spurious echoes and distant echoes may come in on the second or third sweep on the scope after the main pulse. These latter echoes may be checked by changing the pulse repetition rate and observing the shift of the echo.

Permanent echo diagrams are useful for:

1. Indicating blind areas in a station's coverage.

2. Assigning the operating area of a station.

3. Checking the range and azimuth accuracy.

4. Checking the performance.

5. Estimating nonstandard propagation

6. Planning test flights.

Shielding

The principal device in the field for the control of permanent echoes is shielding. This means that the antenna must be sited in such a way that distant hills are screened by a local obstruction. This local echo at, say, three miles, is combined with the main pulse or ground return and the distant echo is weakened or eliminated entirely.

Shielding causes a loss of coverage, which in operating regions may be more serious than the permanent echoes. Rear areas which are not scanned should be well shielded so that back and side echoes do not interfere with targets in important tactical regions. Operation over such shielded sectors would be limited to high targets.
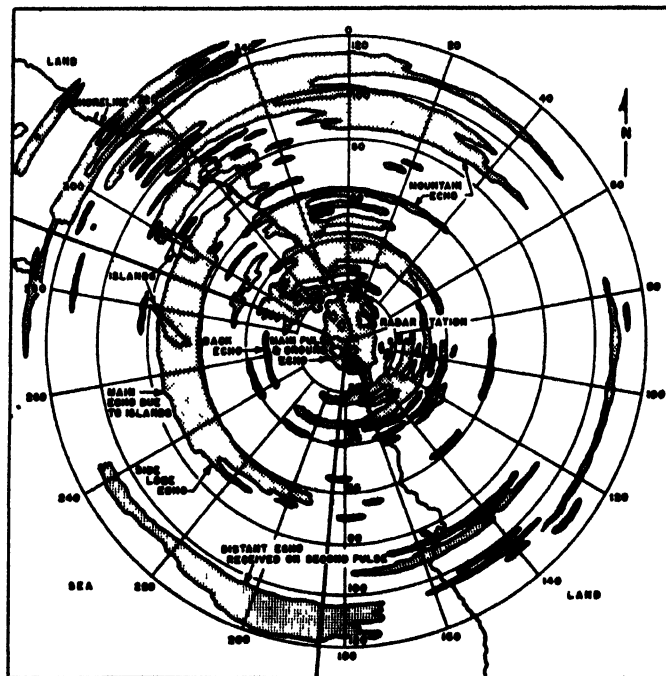
FIGURE 8. A typical permanent echo diagram for a VHF radar

Prediction of Permanent Echoes

Permanent echoes may be determined by several methods: (1) tests with the radar at the site; (2) radar planning device [RPD]; (3) supersonic method; and (4) profile method.

The feasibility of moving the radar to the site to determine the permanent echoes is dependent on the portability, accessibility, etc. Echoes obtained with one type of equipment may be very different from those of another type of radar with a different antenna directivity, frequency, and range.

The RPD technique requires construction of a relief model of the terrain considered. A small light source is used to simulate the radar transmitter and the echoes are plotted as a result of a study of the areas illuminated. This method is useful for short ranges and microwaves where the diffraction and side and back lobe radiation are small. Construction of a fairly difficult relief model may take a crew of specially trained men several days to a week, as the model should be accurate. Once completed, all possible sites or aspects from a plane or ship may be readily examined. Photographic and darkroom facilities are required and also kits containing a light source, supports, etc.

The supersonic method uses a relief model under water. Supersonic gear is used to send out pulses which are reflected like radar pulses and an echo is picked up and presented on a *plan position indicator* [PPI] scope. Photos may be taken of the scope or it may be used directly to train operators

and for briefing. Considerable equipment is required, but the construction of the models is comparatively simple.

The profile method involves a study of topographical maps and plotting of the echoes according to their visibility and the amount of diffraction. A fairly difficult site may be handled in perhaps eight man-hours. This method is adapted to long-range, low-frequency radars where diffraction and side and back lobe radiation are important. On microwave equipment, prediction of permanent echoes is simpler and the profile method may be worked out in a few hours.

Prediction by the Profile Method

The discussion here refers chiefly to VHF (1 to 10 m) radars in a mountainous terrain, but the methods have general application. The principal requirements are topographic maps of the surrounding area with a scale of one or two miles to the inch and a contour interval of 20 feet, although intervals up to 100 feet may be used. Regional aeronautical maps with a
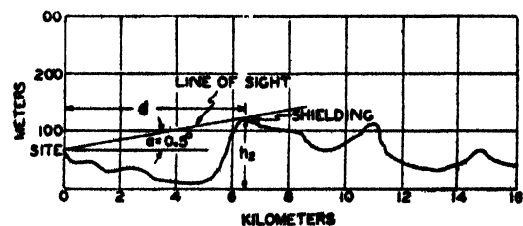
FIGURE 9 Typical profile.

scale of about 1 inch to 16 miles and 1,000-ft contours are suitable for checking distant echoes.

From the maps, profiles are prepared for various azimuths about the radar station. The first mile or so should be plotted accurately; at greater distances, the critical points, such as hills and breaks, should receive the most attention. On each profile is drawn the tangent line from the center of the antenna to the point on the profile which determines the shielding, as in Figure 9. The angular elevation α of this line of sight is marked on the diagram. If α is negative, the profile should be checked out to the radar horizon to obtain the correct shielding angle. On a plane earth diagram, the line of sight is actually curved, but for distances up to 10 miles it may be taken as straight with small error. The height difference, with α in radians, is then equal to

$$h_2 - h_1 = d \tan \alpha. \qquad (18)$$

When the distance is larger so that earth curvature has to be taken into account, to the above expression for the height difference $h_2 - h_1$ must then be added the amount by which the earth is sloping away over the distance d. This amount is $d^2/2ka$, and the complete expression for $h_2 - h_1$ becomes

$$h_2 - h_1 = d \tan \alpha + \frac{d^2}{2ka}. \qquad (19)$$

For easier handling of this equation, a set of curves may be drawn where $h_2 - h_1$ is plotted against d for various constant values of α. These curves may then be used to determine the height of the shielded region at any range. Thus all other moun-

tains along the profile in Figure 9 might be checked for visibility by comparing the height of the mountain with the value of $h_2 - h_1$ read from the curve $\alpha = 0.5°$. Any desired allowance for diffraction may be made by using a different curve such as $\alpha = 0$. When the shield consists of several ridges close together, an equivalent shield should be used. This is derived by enclosing the ridges in a triangle, whose apex is taken as the shield (see Figure 6).

The general procedure to be followed in preparing a prediction of permanent echoes will now be outlined. From an examination of the map, the azimuths at which profiles should be prepared are determined. This will normally be about every 10 degrees. Where the shielding is obviously good, the interval may be 20 degrees, but where the terrain is questionable, such as in a region of low hills, the profiles should be taken at 5-degree intervals.

An overlay of the region is then prepared, showing important geographical features and a polar-grid system. On this chart is drawn the coverage contour lines (broken lines in Figure 10). These lines represent the limits of the heights of the shielded regions. Targets or mountains below and beyond the coverage contours will not be visible except by diffraction. These contours may be drawn for several heights. Where they are close together, the shielding is good but the coverage is poor. Where the lines are widely separated, as toward the sea, there is little or no shielding except that due to earth curvature. With the coverage contour diagram superimposed on a
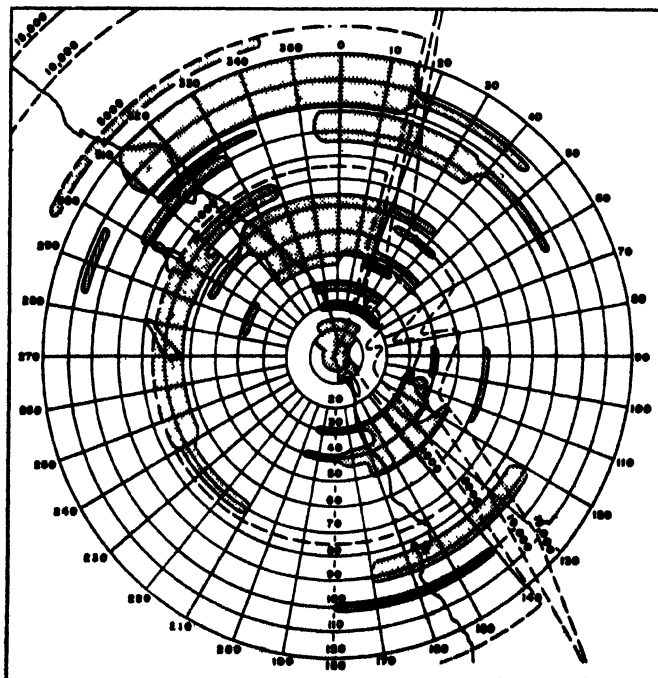
FIGURE 10. Theoretical permanent echo diagram

map, the peaks exposed to radiation may be noted.

The extent of the echoes due to these peaks depends, besides the size of the peak, on the horizontal radiation pattern, the pulse width, and the power and sensitivity of the radar. It should be noted that the half-power beamwidth is only a rough measure of the width of an echo and some greater angle between the half-power points and the nulls will usually be obtained for the echoes.

The extension of the echo in range will be at least as great as the pulse width in miles as represented on the scope. This is about 0.1 mile per microsecond of pulse width. Actual echoes are thicker than this, since all the exposed hill sends back echoes.

After a careful inspection of the profiles, taking into account the various factors mentioned above, the echoes are sketched in on the chart. In doing this the following rules may be used as a guide.

1. Shade in a circle for the main pulse several miles wide, depending on the pulse width and local return.

2. Check each profile in turn and for each peak or hillside in front of the shielding ridge or mountain plot an echo for the main and all side lobes of the antenna.

3. A series of sharp hills within the shielding part of the terrain should be plotted as a single large echo.

4. The inner edge of an echo should be at the same range as the hill.

5. Peaks beyond the shield may be in the diffraction region and the relative strength of the echo may be estimated from a diffraction curve.

6. In general, the echo strength varies as the inverse square of the distance and is roughly proportional to the target area.

7. Where there is any doubt, plot the echo.

Experience is an essential factor in permanent echo prediction, regardless of the method used. The methods described here have been used successfully in many areas and are capable of accuracy adequate for most purposes.

EFFECT OF TREES, JUNGLE, ETC.

The Effect of Trees

Trees form very effective obstacles for high-frequency radio waves. A single tree may cause a drop in signal strength of several decibels. The attenuation is less for horizontal polarization than for vertical polarization for frequencies below 300 to 500 megacycles. For higher frequencies, the polarization is not an important factor. With the transmitting antenna sited in a moderately wooded area, representative values for the losses are given in Table 1. When both antennas are in the woods these losses should be doubled. Measurements at 200 mc for transmission through a grove of trees 100 feet wide show losses of 21 db for vertical polarization and 6 db for horizontal polarization.

TABLE 1. Decrease in gain for transmitting antenna situated in a moderately wooded area.

Frequency	Horizontal polarization	Vertical polarization
30 mc	Negligible	2– 3 db
100 mc	1–2 db	5–10 db

When the antennas are in clearings, so that each is more than 200 or 300 feet from the edge of the woods, the decrease in gain is small. With vertical polarization, there may be large and rapid variations of field intensity within a small area, due to reflections from near-by trees.

The Effect of Jungles

In jungles or heavy undergrowth, an exponential absorption is to be expected. Tests made of transmission through heavy jungles show that the limit of transmission for ordinary field sets is 1 mile. An increase of power of several hundred fold is needed for a range of 2 miles. The decreases in gain encountered are of the order of 50 to 60 db per mile.

If the antennas are elevated above the jungle or located in clearings, the effect of the jungle may be minimized. Antennas should be 10 or more feet away from trees to avoid a change in antenna impedance.

The best solution is sky-wave transmission even for distances as short as 1 mile. Due consideration should be given to the selection of optimum frequencies based on ionosphere predictions. For distances up to 100 or 200 miles, a half-wave horizontal wire antenna should be used and the frequency range is about 2 to 8 mc. The decrease in gain for the short path up through the trees is negligible at these frequencies.

Effect on Microwaves

At 10 cm, the absorption is so great with most objects that the diffracted energy is the principal portion transmitted. Only windows, light wooden walls, or branches of leafless trees show less than 10 db loss. Opaque objects include:

1. Rows of trees in leaf if more than two in depth.

2. Screens of leafless trees if so dense that the skyline is invisible through them.

3. Trunks of trees.

4. Walls of masonry.

5. Any but the lightest wooden buildings, especially if there are partitions.

Losses of a brick wall may be increased from 12 db to 46 db by wetting. In computing diffraction over treetops, the diffracting edge may be taken to be 5 feet or so less in height. In a 1.25-cm test, the transmission loss through two medium-sized bare trees increased 18 db after leaves appeared.

MASSACHUSETTS BAY

MICROWAVE TRANSMISSION IN 1944
GENERAL DESCRIPTION*

THIS PAPER describes the general features of the work on atmospheric refraction undertaken during the summer and fall of 1944; other papers by members of this group will describe specific phases. The results described must be considered strictly tentative. They are the outcome of a hasty survey of a large amount of experimental data which ceased to accumulate only a short time before this report was prepared. Consequently, it has not been possible to do more than abstract the most obvious information.

The principal objectives of the present program were:

1. To study the modification of continental air by the ocean surface and from this study to improve the technique of forecasting modified index curves at low altitudes over water. The reason for the detailed meteorological study is that when beginning this work we believed that the existing ideas of the physical phenomena involved in producing low-level modification were not on a sufficiently sound basis to allow a direct analytical approach.

2. To study experimentally one-way and radar transmission through the range of refraction conditions varying from substandard to trapping. Particular emphasis was to be placed on wavelength dependence, and, when possible, information was to be obtained on vertical coverage patterns under these various refraction conditions.

Radio Program

The radio part of the project employed a combination of one-way and radar apparatus operating over Massachusetts Bay. Two paths were chosen for one-way transmission; one was the 22-mile path[1] from Deer Island (Boston Harbor) to Eastern Point (Gloucester) and the second a 41-mile path farther from the shore line (Eastern Point, Gloucester, to Race Point, Cape Cod; see Figure 1). Over the 22-mile path, transmission was on S band, while on the 41-mile path one-way transmission was on 117 mc and on S, X, and K bands. Radar sets on S and X bands were placed at the transmitter site for the latter path.

On the short path the terminals were placed so as to give approximately grazing incidence, but on the long path the terminals were well below the horizon. At the transmitting terminal of the one-way circuit were two radar sets on X and S bands; from this location they could scan the New England coast line to measure signal strength from fixed targets. Note that the short path is close to the coast line, while the longer path is considerably farther away and is so located that approximately westerly winds undergo appreciable modification by the time they have reached the transmission path.

Transmitters

The transmitter for the short path was located at Deer Island about 120 ft above mean sea level and supplied approximately 1 w to a paraboloidal antenna 30 in. in diameter.

The transmitter site for the other transmission path and the trucks housing the two radar sets were at Race Point (Provincetown). The radar sets operate on the S and X bands and are approximately 50 ft above mean sea level. They both have antenna diam-

* Figures and tables on pp. 493 to 511.

*By D. E. Kerr, Radiation Laboratory, MIT.

eters of 4 ft and a ratio of transmitted power to minimum detectable power of approximately 167 db. These sets were operated from August 1st through October 20th. The measurements consisted of hourly determination of the strength of echo from four specially selected targets and of recording maximum detection range on fixed targets over water looking up the coast line; in addition, plan position indicator [PPI] photographs were taken at hourly intervals. The performance of the radar sets was carefully monitored by appropriate means for determination of transmitted power and minimum detectable received power. All echo signal strengths were measured in absolute values with a signal generator coupled to the system. The records of signal strength from the four selected targets and those of maximum detection range were plotted and returned to the laboratory on a weekly basis.

The tower carrying the one-way transmitting equipment consisted of the bottom half of a 100-ft SCR-271 tower. The house at the foot of the tower served as operations headquarters, while the top house contained the transmitters. The 117-mc antenna was a five-element Yagi array projecting horizontally from the forward corner of the top of the house. The X- and S-band antennas were paraboloids 4 ft in diameter, made of close-spaced grid work designed to reduce wind resistance. The feed for each of these antennas was a dummy-dipole array excited from the open end of a wave guide projecting through the vertex of the paraboloid. The K-band antenna was a paraboloid 2 ft in diameter, illuminated by a small horn. Polarization was horizontal for practically the entire period of the program.

All the microwave antennas were provided with a scheme for rendering them independent of rain. A blast of air from inside the house was injected into the wave guide at the transmitter by means of a blower. This stream of air effectively prevented accumulation of a film of water on the inside of the guide feed.

The transmitter used on 117 mc was one from an SCR-624 VHF (very high frequency) communication set. Its frequency was quartz-crystal controlled, and it delivered approximately 10 w of c-w power into a balanced line connected to the Yagi antenna. The output power of the transmitter was monitored continuously on an Esterline-Angus recording milliammeter.

The S- and X-band transmitters employed pulsed magnetrons operating at a pulse recurrence frequency of 700 c with a pulse length of 1.5 μ sec and a peak power output of approximately 10 kw. The output pulse from the modulator was continually checked by the synchroscopes, and a check was made of the transmitted radio frequency spectrum of the pulses by means of the spectrum analyzer.

Both S- and X-band transmitters were provided with continuously recording monitors operating Esterline-Angus recording milliammeters. Several types of monitor circuits were employed during the course of the program, but the one which proved most satisfactory employed a thermistor bridge coupled by means of wave selector, or directional coupler, to the wave guide between transmitter and antenna. Daily calibrations of the recording thermistor bridge circuits were made, providing a constant check of power output in absolute values. In addition to recording of average power output by frequent checking of spectrum and high-voltage pulse, the cathode current of the magnetrons was also recorded.

The K-band transmitting equipment differed from the S- and X-band equipment only in matters of unessential detail.

Receivers

The receiving terminal of the one-way transmission circuit is located at Eastern Point, Gloucester; the receivers were mounted in a 100-ft tower similar to the one at Provincetown. There were two sets of receivers, one approximately 136 ft above mean sea level in a house at the top of the tower and the other approximately 30 ft above in a house at the bottom of the tower. The receiving antennas are identical with those for the transmitters.

The K-band receiver was a superheterodyne specially constructed for this purpose and put into operation late in the experiment. It had a bandwidth of 14 mc but no automatic frequency control [AFC], with the consequence that it required constant attendance to produce a satisfactory record. The receiver for the Deer Island circuit was a narrow-band c-w receiver of the type used in last year's experiments and described in reference 1.

The X- and S-band receivers deserve mention because of their special characteristics, which were developed to meet the requirements of this work. They are provided with AFC circuits arranged to search for a lost signal automatically. Having found the signal, the circuit locks the receiver in tune and continues recording. These receivers have specially designed automatic gain control circuits providing essentially logarithmic response of 70- to 80-db range well spread across the recorder scale. The minimum detectable power for these receivers is approximately 110 db below 1 w for both S band and X band, and the minimum signal required for satisfactory operation of the AFC is approximately 105 db below 1 w. The latter figures are important for this particular setup, since they determine the usefulness of the receivers in studying signal strength near or below that encountered under standard refraction conditions.

The receivers were calibrated daily by means of signal generators coupled permanently to the wave guide between the antenna and the receiver through wave selectors with known fixed coupling losses. Very close check on performance was maintained so that the receivers at all times gave an accurate indication of the absolute value of received signal strength.

The arrangement of S- and K-band receivers in the house on top of the tower was similar to that in the lower house, but the K-band receiver was of a less sensitive type requiring no tuning. There was a 117-mc receiver in the top house but not in the bottom house, and there was no receiver for the Deer Island circuit in the top house.

The outputs of all eight receivers were wired directly into an Esterline-Angus recording milliammeter. With this arrangement one operator was able to keep continuous watch on the performance of all receivers and was required to climb the tower only when major adjustments of the top receivers were necessary.

The Gloucester station was the control station for the radio network formed by all the stations involved in the project. The transmitter station at Provincetown, each of the radar trucks, the fixed meteorological stations, the boat, and one of the airplanes were all equipped to operate radiotelephone on 3.5 mc, thus allowing rapid and efficient exchange of information essential to the operation of all units involved in the program.

Meterological Program

The meteorological phase of our program consisted of two main parts: (1) meteorological meas-

urements, and (2) forecasting and analysis.

All meteorological measurements were made with varying versions of the psychrograph, earlier models of which are completely described in reference 2. This instrument measures wet and dry bulb temperatures as a function of height, using the electrical resistance thermometer principle. From these measurements the M curve is constructed.

The meteorological soundings were made in the Massachusetts Bay area with psychrographs carried by two aircraft, by captive balloons operating from a boat and from two fixed land stations. The boat operated in the Bay and out to about 100 miles off-shore, while the aircraft operated as far as 170 miles offshore. It should be mentioned that aircraft soundings of this type are rather hazardous, since they involve descending to altitudes of approximately 20 ft at large distances from land.

The fixed meteorological stations were located at Duxbury and Race Point. The Duxbury location was chosen to place the sounding station near enough to the shore to obtain a representative sample of the air just leaving the land.

The Race Point meteorological station was located at a position to allow soundings at the water's edge on the westernmost extremity of the top of Cape Cod. The primary purpose of this station was to measure the characteristics of the air after it had been subjected to the influence of the ocean surface between the mainland and the station. This location allowed measurements over a range of wind directions of approximately 180°, but no relevant soundings could be made when the wind had an easterly component, since the air would have had a land trajectory for at least a short period. It was necessary to take all soundings very close to the water's edge to prevent solar heating of the beach from influencing the bottom of the measured M curve. At both Duxbury and Provincetown soundings were taken on a prearranged schedule which, when possible, involved both day and night operation. Soundings, surface wind velocities and hourly observations of sky conditions, etc., were made at both Duxbury and Race Point. The water temperature was also measured at the Provincetown station.

A 60-ft pole was erected at Race Point carrying four anemometers, four psychrographs, and a wind direction indicator. The original scheme involved continuous recording of temperature, humidity, and wind speed at four levels by means of the instruments on the pole, but unfortunately a large sand bar formed in front of the pole soon after it was erected and caused sufficient disturbance of the air in the lowest levels that such measurements were not feasible. The psychrograph, anemometer, and wind direction indicator at the top of the pole continued to be useful, however, and provided the continuous information recorded by the station.

A 50-ft boat, the *Wanderer*, was used for making measurements in Massachusetts Bay. The psychrograph used for measurements from 2- to 48-ft elevation is attached to a cable running between a boom extending outward from the side of the ship and an extension to the top of the mast. A similar psychrograph was used for soundings to higher levels, operating from the winch at the rear of the boat. Further essential meteorological information was provided by the boat in frequent measurements of surface water temperatures in Massachusetts Bay. A direction-finding loop was used to determine position at great distances off shore

RADIO AND RADAR TRANSMISSION MEASUREMENTS[b]

The purpose of this paper is to describe the results of a rough preliminary analysis of the transmission experiment. A thorough analysis must await the completion of the meteorological study, since the trans-

[b] By Pearl Rubenstein, Radiation Laboratory, MIT.

mission depends directly upon the meteorological conditions over the path of the radiation. The emphasis here will therefore be mainly on the strictly radio data with only qualitative reference to the meteorological information.

One-Way Transmission

The values of the transmitted powers, antenna gains, and receiver characteristics were chosen so as to make the standard signal level, as computed for the receivers at the top of the tower, well above the minimum detectable level and the minimum level at which the automatic frequency control [AFC] and AFC search are effective. Sufficient compression was used to give a range of about 60 db for useful reception, which had been expected to be enough for the variations due to atmospheric conditions. It turned out, however, that additional range was needed, especially in the direction of greater signal strengths; to accommodate additional received power, attenuators were inserted in the lines. Thus the actual range of values observed is at least 90 db at the microwave frequencies and 40 db at 117 mc.

SIGNAL TYPES

Figure 2 shows that the types of signal observed at the microwave frequencies (S and X) are not essentially different from those observed in previous tests on a shorter path. The first type is high signal on the average, well above the standard level, with roller fades which may go down to the minimum detectable level and with periods of 2 minutes to an hour or so. These periods are generally shorter at any time on X than on S band. When this type of signal is present on S band it is almost invariably present on X band also and on both paths. It always occurs simultaneously on the high and low receivers at any frequency.

The second type is high and steady. Its level may be anywhere from 5 to about 30 db above the standard, generally higher on X band than on S band. Most of the time this type of signal occurred simultaneously on S and X, but there were some occasions when the S-band signal was of the high and steady type while the X-band signal became of the first type, high with roller fades.

The third kind of signal is about standard and fairly steady. (This may be a limiting case of the high and steady variety.) It does not necessarily occur on both frequencies and on both high and low receivers at the same time.

The fourth type is standard on the average, with scintillation of more than 10 db. The preliminary analysis has not revealed the reasons, or any correlations, for the difference between this and the preceding type; it is certainly nothing obvious, such as wind speed, for example; and it may occur on either frequency when the other is steady.

The fifth type is the "blackout," below standard and variable. This signal type is strongly scintillating. It occurs simultaneously on both frequencies, both paths, and on high and low receivers (except possibly for low X. where the difficulty mentioned above of determining an average value of something very low on the scale is important).

Figure 3 shows the signal types observed at 256 cm. These are distinct from those observed at the microwave frequencies not only in appearance but also in times of occurrence. In general no relation has been found to exist between the types at the two frequencies although on rare occasions such a relation is indicated; indeed the type may remain constant on one and change on either of the others. Steady signal is most frequent at 256 cm, but the other types shown also occur fairly often. Variations of 30 to 40 db overall take place, and the variations may be fast or slow.

STATISTICS

A fairly detailed statistical study has been made of the S and X signals at the top level. These were

chosen because they were available for the longest periods, and because they gave the most reliable results (because of the receiver characteristics the relation of the standard to the minimum detectable level was most suitable). The other microwave records gave similar results. As for the 256-cm transmission, the most important result was that the signal level was above the minimum detectable very nearly 100 per cent of the time, although fades to this level were fairly frequent. If a choice had to be made of the most reliable frequency for transmission over the circuit, there would be no question in the choice of the longer wavelength.

The statistics available on K band are very similar to those on X band as far as can be determined. Signal levels less than about 20 db above standard cannot be detected on the K band.

The study was made of the average signal level on a weekly basis; it showed marked differences from week to week, depending upon the specific weather situation. For purposes of the statistics a range of values around the standard was included in the standard signal (allowance for scintillation, tides, etc.). This range was taken as ± 5 db on S band and ± 10 db on X band, values determined by inspection of the entire record and thought to give comparable results.

The most interesting result of this analysis was the discovery that standard signal occurs extremely rarely over this path. High signal is most frequent; depending upon the wavelength and the season of the year, substandard and standard signal occur less frequently. In the summer no significant frequency dependence was observed in the statistics. Some typical weeks gave the figures shown in Table 1.

As the season progressed to the fall, however, several related trends became apparent: (a) the increasing incidence of standard signal, especially on S band; (b) the increasing incidence of high, steady signal, especially on X band, with the level higher above the standard on X than on S; (c) the frequency effect on the incidence of above-standard signal indicated in (b); and (d) the decreasing occurrence of substandard signal. These trends are illustrated in Table 2.

No diurnal effect was found in the signal except under some very special circumstances. Not only was no such trend apparent upon visual inspection, but also an analysis of the material by 6-hour intervals confirmed appearances.

CORRELATIONS

In addition to the statistical study, another type of analysis has been made to look for correlations between the variations of signal strength with frequency at a given location or with height at a given frequency. Figures 4 to 6 show some typical graphs of such correlations, each point representing average hourly values, for 1 week. Figure 4 shows the variation of the high S- and X-band signal strengths. It is clear that in most cases the two wavelengths change together. This was the predominant behavior throughout the summer. The notable exceptions are those points where X is high and S nearly standard; this is the frequency effect remarked in the discussion of the high and steady signal which became common in the fall. As will be seen later, this occurs with very low modified index inversions, less than 20 ft high.

Figure 5 shows the relation between S-band signal strengths for high and low receivers; the correlation is excellent in practically every case. A similar correlation exists for the high and low X-band signal, except for the case of very low signal where the apparent average value of the signal strength on the low receiver is always relatively high. Whether this is caused by the lack of receiver sensitivity or is a real transmission phenomenon cannot be conclusively decided on the basis of the present information.

Figure 6 shows the relation of signal strengths at 117 mc and S band; the difference between this figure

and the preceding two speaks for itself. From the preliminary analysis no consistent correlation has been found between the behavior of the low- and high-frequency transmission.

The variations on the two paths are generally in good agreement although changes in signal type rarely occurred exactly simultaneously; the changes on the short path are always less in magnitude than on the other, as would be expected.

As far as can be determined from the available data the K-band signal correlates quite well in general with that on S and X bands. Only high signal can be observed, of course, with the present equipment.

RELATION OF RADIO RESULTS TO MODIFIED INDEX CURVES

Detailed conclusions must await the full analysis of the data. At present certain qualitative conclusions can be drawn:

1. When the surface modified index inversions are present, the microwave signal level is high on the average, and usually the signal has roller-type fades.

2. When the M curve is substandard the signal is low and scintillating. The M curves which are standard all the way down to the surface of the water appear to be very rare, even when the air is colder than the water. The previous results on the short path had tended to discount the importance of the low M inversions which exist over water most of the time, especially with cold air flowing out from the land. The increased sensitivity of the present setup to variations in the M curve, the additional path length, and finally the inclusion of the X-band transmission on the circuit have shown definitely that such low M inversions are far from negligible but will affect S-band communications (or one-way transmission) and both one-way and radar transmission on X band. The signal occurring with these M inversions less than 20 ft high is usually the high, steady type. It is generally not quite so high in average level as that characterized by roller fades found with larger M inversions.

3. The high, steady signal occurring with very low M inversions reveals the only clear-cut cases of frequency diversity between S and X bands. In this case a variety of combinations has been found: nearly standard signal on S band with X-band signal from 10 to 30 db above standard; S band 10 to 15 db above standard with X band 30 or so db above standard; and finally S band about 20 or more db above standard and steady while X band changes to the first signal type: high with fades.

4. One of the most interesting features of the transmission is the fact that at any given location, for a fixed frequency, the increase in field strength is limited; that is, no matter how much the M inversion increases in height or in strength beyond a certain value (which is as yet unspecified) the average value of the signal strength does not continue to increase but rather remains the same within about 10 db. This "saturation" level is of the order of the free space value. (Maximum level goes up to 12 to 15 db above free space but only infrequently.) Consequently, the level reached on a given path appears to be independent of the receiver height (within the height range covered in these measurements), the height-gain effect which exists under standard conditions being essentially eliminated when shore trapping takes place. Under some conditions, especially when the signal is high with fading but has not yet reached the saturation level, the lower of the two receivers has been observed to receive higher signal than the higher one. With stronger signal the values on the two become nearly identical, as has been stated.

These results agree with unpublished calculations made for several values of duct height and M deficit for S band, of the first transmission mode alone, which indicate that the height-gain effect should disappear and the signal approach a certain saturation level. Thereafter, calculations show, the contribution of the first mode decreases, but the observations suggest that perhaps the other modes continue to cause the average level to reach approximately the same value, as duct height and M deficit continue to increase.

It has been found that, with an M inversion over only a portion of the path and a standard curve on at least a small part of it, the signal type may be high with roller fades and the average level high, so that the record is indistinguishable from that which occurs with more uniform conditions.

Radar Transmission

From Race Point, targets were available over water at ranges of 20 to several hundred miles along the coast of Massachusetts and Maine, plus some additional targets inland and whatever shipping was in the vicinity. Of the coastal targets four were chosen for regular observation. These were fairly isolated fixed targets, the echoes from which appeared to be relatively steady in several days' observations, at ranges of 22, 41, 35 and 73 statute miles. Absolute power measurements of the returns of each of these targets (whenever visible) were made hourly by comparison with a signal generator. Each measurement represents the *maximum* value of the signal during a period of 1 to 3 minutes. This differs rather essentially from the hourly averages of the one-way data.

In addition to signal strength measurements, hourly observations were also made of the maximum ranges obtained on surface targets, and *plan position indicator* [PPI] photographs were made which reveal at a glance many interesting features of the radar coverage which are hard to describe briefly in words. The maximum sweep length available on the PPI was 140 miles for the S-band set and 115 miles at X band. Additional range was available on the delayed A-scope sweeps, so that the maximum was 180 miles for most of the period of observations. This was extended to 280 miles for the last week of the test.

In addition a portable K-band radar set was set up near Race Point Light only 17 ft above mean sea level and regular observations of range were made and shipping tracked.

TARGET SIGNAL STRENGTHS

The strength of the echoes from the four targets, including the nearest one which is ordinarily visible both optically and by radar, varied from below minimum detectable to at least 60 db above for the two nearer targets and about 35 db above for the two more distant targets, at both frequencies. In general the values of the signal strength were higher for the nearer targets, but there were some interesting cases when the more distant targets were visible while the nearer ones were either not seen or were very weak. This may occur at times when the M curve varies markedly with direction, as happens occasionally when the air trajectory is S or SW or at times of skip distance.

MAXIMUM RANGES

Large variations in the maximum ranges have also been observed at both frequencies, with the upper limit apparently being set only by the length of the sweep: 280 miles on S band and 200 miles on X band. (Note that these radar sets were far from the high-power class.) Lack of fixed targets at ranges between 10 and 25 miles made it impossible to follow in detail the way in which substandard conditions reduced detection range, but there was no question as to the general trend toward reduction of range. The maximum range of the *high sited K-band receiver* [HBK] from its location at the Race Point Light was 46 miles on a land target and about 30 miles on shipping.

It should be borne in mind that our project deals with propagation near and roughly parallel to the coast line. Thus these results are not necessarily applicable to operations perpendicular to the coast with off-shore winds, where the surface M inversions become "washed out."

STATISTICS

The radar observations include about 1,200 hours of operation. Of these, overall, the X-band ranges were better than "normal" 59 per cent of the time (normal = 29 miles*) and the S-band ranges 48 per cent of the time. At both frequencies ranges were below normal 20 per cent of the time. The variations from week to week were great, the maximum values being 95 per cent above normal on X and 75 per cent above normal on S, with about 45 per cent below normal as the lowest value at both frequencies.

CORRELATIONS WITH ONE-WAY RESULTS

A visual comparison of the radar and one-way data suggests fairly good agreement in general between the two. To get a more quantitative evaluation of this agreement, however, correlation diagrams have been drawn.

Figure 7 shows such a diagram relating the signal strength of the target at Eastern Point as observed on the X-band system with the signal strength of the high X-band receiver on the one-way path. As in the previous diagrams, a week has been chosen as the time interval and hourly values are plotted. In this we neglect the difference between the single observation of the radar and the average of an hour's continuous record in the other case. Note also that all radar measurements which give values *equal to or below* the minimum detectable level are plotted *at* the minimum detectable level; thus if a more sensitive receiver had been used, many of these points would have fallen lower in the diagram. The diagram reveals the nature of the relation: the one-way signal strength must rise considerably above the standard value before the target becomes visible. Thereafter, small changes in the one-way signal correspond to much larger changes in the radar echo. As a matter of interest, which may or may not be significant, the radar ranges at times fall close to the square law, as they should if the target-reflecting properties remain constant as the tmospheric conditions change.

Figure 8 shows the relation between maximum radar ranges on surface targets and the one-way transmission results. In this case the effects of both substandard and better than standard conditions are noticeable. When the one-way signal strength is below standard, the radar ranges are mainly less than normal; exceptions occur in cases of strong directional effects and S-shaped M curves. As the one-way signal strength rises above the standard level no appreciable increase in radar range occurs at first. Only when the one-way signal strength has become fairly high do the radar ranges begin to increase. Then the entire gamut of long radar ranges, from about 40 to 280 miles, takes place while the one-way signal strength changes only slightly. This is another manifestation of the saturation of the signal at a high value.

SUMMARY

Two major conclusions may be drawn from this preliminary survey:

1. Standard signal is the exception rather than the rule for microwave radiation on this over-water path during the summer and fall. With the high M inversions, which occur with warm, dry air over water, signal strengths 30 to 45 db above the standard occur about equally often on both, the upper limit being approximately the free space value, and radar ranges on surface targets are extended to five to ten times their normal values. On the other hand, with the low M inversions (less than 20 ft, say) which occur with air colder than the water, X band is affected more than S. Both may experience increases in signal level of 10 to 30 db above the standard, but the X-band signal

*Unfortunately, in the radar case it is impossible to establish a precise definition of a "standard" range analogous to standard signal in one-way transmission unless detailed information is available on the radar target. In this case we have attempted to determine the detection range on hills available as coast line targets, at times when the curve is standard or very nearly so.

is high more often than the S and at any given time usually reaches a higher level. Radar ranges on surface targets are extended by as much as 20 to 25 per cent above normal, and again X band experiences more effect. These increases in signal strength can be of great importance for communications, beacons, or any other application involving one-way transmission of microwaves, such as countermeasure. It should also be remembered whenever secrecy is required.

2. Substandard conditions may be present for several days at a time if the air is warm and moist. The reduction in signal strengths and radar ranges on surface targets which accompanies substandard conditions does not seem to be markedly frequency sensitive. It should be stressed that variations in one-way signal strength of at least 90 db have been observed. The radar ranges have also varied from roughly 10 or 15 miles up to at least 280 miles. These changes are not rare occurrences; deviations from the standard account for the major percentage of the time, especially during warm weather, and at the higher frequencies even during the fall

TRANSMISSION CHARACTERISTICS OF AN OVER-WATER PATH[d]

Results were previously reported of some preliminary analyses of one-way radio transmission on a 41-mile over-water path from Provincetown to Gloucester, with terminals well below the horizon. S- and X-band radiations were transmitted over the double paths indicated in Figure 9 to both "high" and "low" receivers, and 117-mc radiation over only the high path. Numerous meteorological surface measurements and low-level soundings were made, and essentially through repeated comparisons with these measurements the following correlations for microwave transmission and surface M curves were obtained.

With positive M deficits, or M inversions, two cases were found.

1. Low ducts, less than 50 ft thick, resulted in a very steady signal at levels well above standard. The increase in signal level took place although the terminals were as much as 100 ft above the top of the M inversion. Such low ducts caused greater increases in the signal level on X band than on S band.

2. High ducts, 100 ft thick or more, resulted in very high signal levels on the average, but with deep fading. The signal level did not continue to increase with increasing duct height but instead "saturated" near the free space level. No frequency diversity between S and X bands was found in this case.

With negative M deficits, or substandard M curves, the signal was always below standard.

In November 1944 no correlations with M curves had been obtained for the 117-mc signal, and a clear lack of correlation with the microwaves had been noted.

A detailed analysis has since been undertaken which is as yet far from complete. This paper describes the method in use and presents some additional results.

In studying the fundamental phenomena of propagation the method employed was to tie the complete representative M curve to the observed transmission results by means of the wave theory. A threefold attack was used:

1. The meteorologists studied each situation in detail to determine a representative M curve and its changes with position and time.

2. Theoretical field strengths were found by putting the representative M curve, or a close approximation to it, back into the wave equation. These theoretical values were then compared with the observations.

3. Empirical correlations were then made between the M curves and the transmission results. This was done because the theory is applicable only to the simplest M curves and to uniform conditions.

This approach was employed in an effort to find parameters in terms of which predictions of range o field strength can be made for operational use. It is not considered a suitable method in itself for use in the field.

The meteorological part of the program has not in general received sufficient attention. Spot measurements at a given time and place do not necessarily give an adequate description of prevailing conditions. A thorough meteorological analysis of the entire period of transmission is therefore under way. For each case the synoptic situation is studied to find the trajectory of the air over the path at the time in question. Radiosondes, surface measurements, winds aloft, measured water temperatures, and all available low-level soundings are studied and the characteristics of the air over the water determined. Then representative low-level soundings are constructed. Such so-called synthetic soundings for the path midpoint are being drawn for 6-hour intervals for each day of operation. In addition, estimates are made of the departures from uniformity over the path and of the times of occurrence of marked changes.

All the radio analysis has been based upon these synthetic soundings and the accompanying discussion. The meteorological analysis is at first made completely independent of the radio data, with minor revisions when necessary after consideration of the transmission data. It is believed that full use of transmission data can be made only through such close cooperation of the persons engaged in both the meteorological and the radio work, not only in the measurements but also in the analysis.

Perhaps the most striking information which has so far resulted from the detailed analysis is the empirical correlation of the 117-mc performance with M curves. Increases in signal level above the standard are found to result from either large surface ducts (200 ft or more thick) or elevated superstandard layers which do not necessarily show overhanging M curves. Such layers occur frequently over Massachusetts Bay, mainly as a result of nocturnal cooling over land. Those which affect the 117-mc transmission occur below about 1,500 ft. Their strength is usually doubtful in view of the lack of accurate information on conditions over land in radiation inversions.

Figure 10 shows the correlation diagrams obtained when, first, all points are included, and second, all cases of elevated superstandard M layers are omitted. (Standard values are —120 db for 117 mc and —80 db for S band.) The first diagram obviously shows no correlation and is the sort of diagram obtained last fall. The second, however, is just what should be expected for the correlation with surface phenomena. The S-band signal rises to the free space value as the duct height goes up to about 100 ft and then "saturates" for higher ducts. The 117-mc signal, however, is affected only by ducts considerably more than 100 ft high. Similarly, only a thin substandard layer is required to affect the S-band signal, but not until the layer is rather thick is the low frequency affected by it.

In the period so far studied (960 hours total) the signal level was above standard 49 per cent of the time, standard 38 per cent of the time, and substandard 13 per cent of the time. Of the superstandard period 46 per cent has been correlated with elevated superstandard M layers, 36 per cent with thick surface ducts, and 4 per cent with situations in which elevated layers and thick surface ducts coexisted. Only 14 per cent of the time remains in doubt, and this includes many periods of exceedingly complex meteorological situations for which the analysis was inconclusive. In addition to correlation of field strengths with M curves, comparisons have been made between measured and theoretical values of field strengths. The theoretical values were calculated on the assumption of bilinear modified index curves, that is, curves made up of two straight-line segments. The M curve is taken to be standard above the joint, and two parameters are used: the height of the joint, or duct thickness, g, and

the ratio s of the slope. The straight lines are drawn not in terms of M deficits but to give the best possible fit to the actual M curve. For the range of values of these parameters for which the contribution of the first mode only is of importance the curves of field strength shown in the following two figures are representative.

Figure 11 shows the effect of changing duct height, 0 to 500 ft, on the 117-mc field strength for various values of the slope of the lower segment. The field strength is measured relative to free space value and —33 db is standard. (s = —3 corresponds to a value of dM/dh about —100/100 ft; s = —2 is —30 per 100 ft, etc.) Note that for the bilinear model, unless the slope of the bottom portion be extreme, the duct height must be of order 300 ft or higher before there is any appreciable effect at this frequency.

Figure 12 is a similar theoretical diagram for the high S-band path. The scale in this case is 0 to 100 ft. At X band the corresponding changes occur over a height range of only about 30 ft. For the low paths at any given frequency the curves are similar, but the increases in field strength occur more rapidly, so that the free space value is reached at essentially the same duct height for both high and low paths.

In a few special cases for S and X bands contributions of a number of modes (as many as 18 in one case) have been added in phase. In no case did the calculated field strength reach a value more than 15 db above the free space value, and in most cases it was between —5 and +10 db.

The calculations check well with observations in a qualitative way in spite of the fact that the bilinear curve is not in general a good approximation to the true M curve and that the assumption of a uniform M curve along the entire transmission path is an extreme idealization. They show the order of magnitude of duct heights at which appreciable increases in field strength first occur at a given frequency. They demonstrate also the important fact that the field strength is increased even at considerable heights above the duct. This is so because with a leaky mode the height-gain function does not decrease with height above the duct but instead becomes practically constant over an appreciable range. This is illustrated in Figure 13, where the normalized height-gain function for a leaky case is compared with the standard. The decrease in absolute value of the height gain is compensated by the reduction in the attenuation. It is thus clearly not necessary to put a transmitter inside the low duct in order to take advantage of it; nor does the first mode need to be actually trapped as indicated by ray tracing, but merely less attenuated than the standard

As to character of the signal, the theory suggests that steady signal is obtained with low ducts because only a single mode is important. With large ducts fading may be caused by interference among many modes which change rapidly in amplitude and phase with small changes in refraction. Even with very large ducts, for terminals well above the duct, steady signal might again be expected because the field strength there would probably again result from a single leaky mode, in this case not the first mode.

Finally, the calculations agree with observations in showing that even when many modes are strongly trapped, the field strength at a fixed point does not reach the high value one might expect on the basis of an attenuation proportional to 1/R but rather remains near the ordinary free space value. This results from the fact that coincident with the reduction in attenuation which occurs with trapping, there is also an appreciable reduction in the height-gain function within the duct, as shown in Figure 14. The balance of the two countereffects prevents extreme increases in field strengths at all ranges of practical interest for microwaves.

To sum up, the 117-mc transmission is noticeably affected both by thick surface ducts or substandard layers and by elevated superstandard layers up to 1,500 ft altitude, which need not necessarily overhang. The wave theory for elevated layers is not yet sufficiently

advanced to permit drawing definite conclusions. As for surface phenomena, an excellent qualitative agreement has been obtained between theoretical and observed results. There has been no indication of a need to revise the formula used for computing the modified index of refraction.

Following presentation of this paper the following data were presented on a similar experiment[3] made on an over-water path between San Pedro and San Diego, California. Transmitting and receiving antennas were at 100-ft elevation, with continuous wave transmission conducted from the San Pedro end of the link simultaneously on 52, 100, and 550 mc. The typical nonstandard condition in this area is produced by dry air aloft subsiding over moist air near the sea surface. This gives rise to a sharp discontinuity in the index of refraction distribution with altitude at some elevation above the earth.

In analyzing the data from this experiment, the index of refraction modified for $4a/3$, instead of the modified index M, was used. The new modified refractive index, B, thus obtained is shown in Figure 15. The pertinent factors for reflection considerations are as follows: h, the height of the layer above the earth; ΔB, the total change in index through the layer; and D, the thickness of the layer. For moderately high layers, D is much less than h.

Maximum field strength measured during the hour in which a meteorological sounding was taken is plotted against height of the layer above the ocean. The data are segregated into groups for different ranges of change in index of refraction through the layer. Figure 16 shows the data for changes in ΔB between 30 and 40 by means of crosses· for ΔB of 40 to 50 with dots; and for ΔB of 50 to 60 with circles.

If reflections are assumed to take place midway between the transmitters and ..ceivers, the field strength may vary roughly as shown in Figure 16. The height-gain function holds the lower frequency fields down when the layer is low, whereas the added advantage in the reflection coefficient produces relatively stronger fields for the lower frequencies when the layer is high. A complete report will be made soon on the experimental data and its relationship with this consideration.

It was further pointed out.that maximum observed field strength need not always coincide with complete trapping. The experimental evidence that for a given frequency the signal strength over a low fixed path first increases as the height of the base of the M inversion increases and then decreases does not necessarily contradict the wave guide theory. When the base is low, transmission is by means of well-excited modes with low attenuation. As the base height increases, the attenuation of some of the modes decreases and the field strength therefore increases. Further increase in base height results in well-locked modes which are more and more difficult to excite. It is then that the most effective mode is one which leaks sufficiently to be excited by a transmitter outside the duct and yet does not leak sufficiently to be strongly attenuated before reaching the receiver. As the height continues to increase, modes which can be excited are all strongly attenuated, and the ones which are only slightly attenuated cannot be excited. Thus signal strength ultimately decreases with increasing height.

NEAR SAN DIEGO

ONE-WAY TRANSMISSION EXPERIMENTS OVER THE SEA BETWEEN LOS ANGELES AND SAN DIEGO[a]

ONE-WAY TRANSMISSION tests have been made by two methods: over a fixed path and by means of an airplane to sample vertical distribution of field strength. The fixed path is a nonoptical over-water

path, 80 nautical miles in length ırom San Diego to San Pedro near Los Angeles Harbor. No intervening landscape is present at either end of the path. The c-w transmitters are located at the San Pedro end of the path at 100-ft elevation and operate on frequencies of 52, 100, 547, and 3,200 mc. The latter frequency has just recently been added, and insufficient data have been obtained to include in this report. The transmitters are quite conventional, the 52 mc being crystal controlled and the other two being self-excited units in which adequate frequency stability has been obtained by use of high-Q circuits. Monitors, which are read periodically, are provided on each transmitter. The receiver location, at 100-ft elevation, is located on Point Loma, San Diego, near the laboratory. The receivers are of standard construction incorporating a balanced d-c amplifier and Esterline-Angus recorder in the output circuit. Filament and plate voltages are regulated. Detuning effects due to temperature changes are minimized by temperature regulation in the receiver house. Receivers are calibrated at least once each week.

Four receivers have been installed in a PBY-5A plane which is used to sample vertical sections of field strength distribution at various distances up to 130 miles from the transmitters at 100-ft elevation. The frequencies used are 63, 170, 524, and 3,250 mc. Certain precautions were found necessary to insure correct orientation of transmitting antennas on the ground and receiving antennas on the plane. Receiving antennas on the plane are fixed in position, and measurements are taken only with the plane flying toward the transmitters. The plane's orientation is controlled, and the distance from transmitters determined, by utilizing the plane's Type ASE (Admiralty Signal Establishment) radar to home on a beacon located near the transmitters. All four transmitters and transmitting antennas are installed on a single rotating mount. A direction finder system also installed on the rotating assembly and operating on the plane's radar frequency is used to check the plane's bearing during flight and keep the transmitting antennas pointed at the plane. Bearing checks have been consistently obtained at ranges up to 130 miles. The d-f bearings agree quite well with those obtained by use of a type FC fire control radar.

One-Way Fixed Link Data

RAY THEORY — GEOMETRIC OPTICS

On the basis of ray theory, when it is assumed implicitly that the energy follows the rays, the modified index criterion for trapping should be expected to agree with experience. Ray tracing theory states that when the modified index attains a value equal to or less than its value at the transmitter height trapping can occur.

As a preliminary check on this criterion the maximum field strength observed during the hour in which the meteorological sounding was taken is plotted against ΔM in Figure 1. When the minimum value of M in the refracting stratum is less than its value at the transmitter elevation, ΔM is negative, and the trapping condition is fulfilled. The 52-, 100-, and 547-mc links all show strong fields for large positive ΔM. These data are not compatible with the assumption that the energy follows the rays. The diffracted field is below detection for all the frequencies used on the 80-mile over-water link. This has been confirmed experimentally. On November 5, 1944 a front passed accompanied by heavy rain which dissipated all low-level inversions, and a standard condition resulted. During this period all the signals decreased below detection.

Figure 2 shows the above field strength data plotted against the height of the base of the temperature inversion. (The curves appearing in this figure will be explained later.) Although both the thickness of the inversion layer and the strength of the inversion vary considerably, the correlation of signal strength with the height of the base of the inversion is quite remark-

able. The 547-mc signal decreases below detection as the layer heights increase above 3,000 ft; whereas the 100- and 52-mc signals are still relatively strong when the inversion base is above this altitude. These lower frequencies do show a decreasing trend as the layer continues to rise, going completely out, as stated above, when the low-level inversion is washed out.

Figure 3 shows a condensed log of the field strength data taken on the one-way link. Maximum and minimum field strengths during successive 2-hour intervals are plotted, thus showing the general level and fading range for each frequency during a 6-week period. The corresponding elevation of the base of the temperature inversion is shown by the discrete points in the upper part of Figure 3. It is at once apparent that the signal level is higher for all frequencies when the layer is low and also that the fading range is smaller under these conditions. For a given elevation of the layer the fading range is greater for the higher frequencies.

Figure 4 shows the character of the signal received on the one-way link when the inversion was low and trapping was definitely indicated by the modified index curve. Figure 5 shows the signals under the condition of a high inversion. The time scale is shown along the horizontal at the top of 547-mc tape and at the bottom of the 52-mc record. For the condition of a low layer and strong trapping the level of all the signals is high and the lower frequencies are quite steady. As the elevation of the layer increases the 547-mc signal decreases below detection, the lower frequencies become less steady and the maximum level decreases. Figure 5 in contrast with Figure 4 clearly demonstrates this situation.

WAVE GUIDE THEORY

According to the simple wave guide theory, using the modified index, trapping can occur only when $\Delta M \leq 0$; and then only when the wavelength is sufficiently small compared with the height of the reflecting layer above the earth. The degree of trapping depends upon the number of modes, or eigenvalues, allowed under the given boundary conditions.

The San Pedro to San Diego continuous transmission link yields data which can be compared with the simple wave guide theory. The 52-mc data are of particular interest, since for this frequency no meteorological data have been taken which would indicate any modes allowed. Yet the field strength has varied over a range of some 30 db, and the strongest fields occurring at times of high fields on the 547- and 100-mc links.

Figure 6 shows the variation of the maximum field strength of the 547- and 100-mc frequencies versus the number of modes allowed as calculated from the meteorological data. There is no apparent correlation at either frequency.

REFLECTION THEORY

It has been shown theoretically[1] that reflection from a nonhomogeneous stratum may occur, even when both the index of refraction and its gradient are continuous functions through the layer. The controlling factor, for a given incident angle, is the ratio of the stratum thickness to wavelength, D/λ. At normal incidence the reflection coefficient is small, even for $D/\lambda \sim 0$; however, such reflections have been observed experimentally.[2] At oblique incidence, for the cases where the index of refraction varies monotonically through the layer, the reflection ratio increases as $D/\lambda \sim 0$. For the modified index type the reflection ratio increases as D/λ decreases, passing through a maximum after which it again decreases.[4]

Figure 7 shows the reflection ratio as a function of D/λ for various angles of incidence, where here the index of refraction is a monotonically decreasing function of height through the layer. The total change in n through the layer is taken to be 60×10^{-6} which is the order of magnitude of the changes noted in this area during the summer season. For a given stratum thickness and height above the earth such that the radiation will be incident upon the layer at angles

slightly less than the critical angle, the lower frequencies will be reflected more strongly from the layer. In addition, any deviation of the layer from the horizontal plane will affect the higher frequency radiation more than the lower frequencies. This is manifested by the greater fading range of the 547-mc signal as shown in Figure 3.

Consider the case where the layer is 330 ft thick. Since the angle at which the radiation will be incident upon the layer will depend upon its elevation, it is possible to compare the experimental data with theoretically calculated reflection ratios. In Figure 2, the curves indicate the theoretically predicted variation of field strength as the layer rises. The absolute decibel scale does not apply to the theoretical curves; only the slope is significant. The actual layer thickness and the effective change of the index of refraction through the layer varied around the values used, and so an exact correspondence between theory and experiment should not be expected. However, the agreement is fair. In addition, at any given time the reflecting stratum is a warped surface which changes shape with time. This condition complicates any theoretical treatment of the problem.

The analysis thus far indicates that the variation in actual index of refraction through the layer has to be used to explain the magnitude of the fields observed on the one-way link. When the layer is thin the longer wave radiation might be expected to leak more readily through the stratum and thus show less trapping at the greater distances. Actually, the vertical sections of field strength taken in the plane (Figures 8 and 9) show rather large fields above the layer at the longer ranges. This might be interpreted in favor of the modified index over the measured index of refraction. However, on the other hand it could be diffraction due to the low elevation of the layer, or a storage field when the actual index of refraction is used. A study of the attenuation along the path should clear up this last point.

Vertical Field Strength Sections

Two typical sets of field strength data are shown in Figure 8 and in Figure 9. Figure 8 illustrates a case for which there was definite trapping predicted by the modified index criterion. It will be noted that the 63-mc radiation shows little variation in field strength with altitude. In most cases, it shows even less variation with time at a given altitude. The higher frequencies show more variation of signal with altitude, and the field strength distribution varies more with time. This variation with time is in complete agreement with the data taken on the San Pedro to San Diego one-way link. The minimum field above the minimum point of the M curve, as predicted by ray theory, is certainly missing at the lower frequencies and rather uncertain at the higher frequencies.

Figure 9 in the following paper shows field strength sections for a day when the reflecting layer was at an elevation of around 3,000 ft. Here the solid line represents the first run and the dotted line the repeat section. The time interval between sections was from an hour to an hour and a half. The sections at about 75 miles from the laboratory show results compatible with the one-way link data. At low elevations the lower frequencies show stronger fields than the higher frequencies. This again is in agreement with reflection theory.

SUMMARY

The modified index of refraction, in conjunction with ray theory, is a poor criterion for trapping. Strong fields are observed well below the horizon when the observed modified index would indicate that no trapping would be taking place. The vertical distribution of field strength for the lower frequencies appears to have little in common with the fields predicted by ray tracing methods where the energy is assumed to follow the rays.

There is no apparent correlation between the experimental data and the simple wave guide analysis.

Treating the elevated refracting stratum as a plane reflecting layer seems to agree in general with experience, for the following reasons. (1) The observed frequency sensitivity of the reflecting layer is predicted. (2) The observed fading characteristics of the different frequencies is again in the right direction, the higher the frequency the greater the fading. (3) Strong fields well below the horizon under conditions of high layers cannot be explained on the basis of refraction alone.

THE CORRELATION OF CALCULATED AND MEASURED FIELD STRENGTHS[b]

Since the time of issue of reference 3, the importance of further experimental check against the calculated patterns has been fully realised.

The field strength cross sections recently obtained by airplane-borne receivers have made possible such a check.

For anything more than a rough qualitative correlation it was soon apparent that quantitative field strength analyses were needed for the actual observed meteorological conditions.

Because of the clearly apparent influence of high level inversion layers on the observed radiation fields, this type of condition was selected. Consider, for example, the M curve at 50-mile range obtained on September 29 reduced to three linear segments as shown in Figure 9.[c] It is clear that the M curves at 10 and 100 miles are not seriously different.

We thus have a condition in which $M - M_0$ decreases by 50 units in a 200-ft interval of altitude attaining the minimum value of $+50$ at 3,000-ft elevation.

Figure 10 shows the ray diagram constructed for the analysis. The diagonal lines below 4,000 ft represent the positions at which field strengths were measured and calculated.

The actual size of the ray diagrams is 27x40 in. Rays in the region of standard refraction have a 58-in. radius. Through the transition layer the radius is 4 in. The above radii are determined by the vertical and horizontal scaling factors and are approximately one ten millionth of the curvature as given by dM/dh. Note that the downward curvature of the earth and upward curvature of rays in the standard propagation regions are made equal, thus reducing the slopes of the rays and resulting errors inherent with deformed scale graphical methods.

Since the tangent ray (shown with short dashes) intercepts only a small part of the fourth and none of the fifth section of measurements, the analysis methods employed in radar coverage diagrams had to be extended. Specifically, the coverage diagram analysis at NRSL has applied to fields between 85 and 100 db below that at a distance of one meter from the transmitter. This largely excludes consideration of any but interference and trapping zones.

The measurements with which correlation was desired extended to about 30-db weaker fields so that partial reflection and diffraction fields were involved.

Proceeding with the ray tracing analysis, the interference field was calculated at points of intersection of the direct and sea-reflected rays. Path differences were determined using a map measure and a planimeter as explained in reference 4. Ray densities were measured for the direct and reflected components, and the associated fields were added with respect to the phase. The diffraction field below the tangent ray was calculated by Norton's method.

Reflected rays from the layer were introduced as originating at the center of the layer. The reflection coefficients for the angles of incidence were calculated as described in reference 5 for the case of a monotonic transition layer in which the refractive index decreases by 50×10^{-6}. In the terms of field intensity

[b]By F. R. Abbott, U. S. Navy Radio and Sound Laboratory, San Diego, California.

[c]See discussion of Figure 9.

the reflection coefficient values ranged from 0.2 to 0.1 at 63 mc and from 0.01 to 0.003 at 524 mc.

In Figure 9 the calculated normal interference and diffraction fields are shown dotted beside the measured values except at 3,250 mc on which the 30- and 45-mile sections have been displaced for clarity. At 63 mc there is an apparent displacement of about 3 db which is probably associated with the reduction in measurements to the decibels below the field at a distance of 1 m from the transmitter. Note that at 60 miles the interference pattern of the diffraction and partial reflection fields as calculated appears with a phase displacement of about 180 degrees from the observed field. The phase relationship depends, of course, on an assumed value of 90 degree change of phase on reflection.

At 170 mc there is a displacement of about 10 db due to difficulty of reduction in measurements. Introducing a 10-db correction, all values at 170 mc agree closely, including the field at 130 miles, due solely to partial reflection. No attempt was made to calculate the detailed variation with altitude.

The agreement between calculated and observed fields at 524 mc is excellent above, but poor below, the tangent ray. At 130 miles 20- to 30-db difference appears. Note that the measured field is about 20 db greater than the 170-mc field at that range. This contradicts the trend of the calculated reflection coefficients which should decrease exponentially with relative thickness of the layer measured in wavelengths. The observed 524-mc fields at 130 miles on some other days of pronounced high-level inversions were well below the 170-mc fields and thus in qualitative agreement with theory. At 3,250 mc there is again good agreement above the tangent ray, but again, in the region below, the observed fields were high though the calculated values became very small.

Thus a preliminary check of analysis versus measurements indicates:

1. Discrepancy of absolute values except where the field at the maximum of a lobe was measured.

2. Excellent agreement as to variation with range and altitude above the geometric tangent as well as in the diffraction-partial reflection zone, except that at 524 mc and 395 mc strong fields were observed below 4,000 ft to 130 miles in contradiction with theory.

ARIZONA

ATMOSPHERIC REFRACTION UNDER CONDITIONS OF A RADIATION INVERSION[d]

AN INVESTIGATION of propagation of high-frequency radio waves under conditions of a nocturnal temperature inversion was made in Arizona over a short period in December 1944. Climatic conditions in this region permitted testing the dependency of refractive index in the lower troposphere on the temperature lapse rate, since the water vapor content was expected to remain relatively constant.

During the day in this area the soil heats rapidly, producing vertical instability and convection mixing near the ground and hence a temperature lapse rate in the lower atmosphere approaching the dry adiabatic rate. After sunset the soil temperature drops rapidly, cooling the layer of air adjacent to the surface and producing a low-level radiation inversion during the night.

It was thought that the progression of this low-level inversion would at times cause the lapse rate of refractive index to vary between slightly positive and zero, which would be the case of greatest interest. If during such a variation of lapse rate field strength observations are made with a receiving antenna which under standard conditions is in the earth shadow re-

[d]By J. B. Smyth, U. S. Navy Radio and Sound Laboratory.

gion, a test can be made of Hoyle's hypothesis[1] that temperature lapse rate is of greater significance than is now believed. If, for example, the field strength during one-way transmission reaches the value calculated for a flat earth while the modified refractive index lapse rate is still positive, then something must be wrong with either the modified index concept or the method of calculating refractive index from meteorological data.

When the modified index lapse rate is relatively constant with altitude, a fairly simple transformation makes the atmosphere nonrefracting and the effective earth radius greater or smaller than the actual radius, and ray tracing should then be valid in the interference field. If no rays reach the receiver, the diffracted field must supply all the energy received.

The propagation path extended from Datelan to Gila Bend, Arizona, a distance of 47 miles over desert terrain. A 3,200-mc transmitter was located on a tower at a height of 53 ft above ground at Datelan, with the receiver 35 ft above the ground in the control tower at the Gila Bend airfield. There is a gentle rise of ground from Datelan to Gila Bend with a total rise in elevation of 402 ft, or about 8.5 ft per mile The intervening terrain is remarkably uniform, without trees or large irregularities, and there are no buildings except in the immediate vicinity of the transmitter and receiver locations.

Figure 1 shows the diurnal variation of surface air temperature at Ajo, Gila Bend, and Phoenix for December 16 and 17, 1944. These typical data show the uniformity of conditions over that region and the effect of radiation cooling on the air mass near the surface.

Figure 2 shows the variation of the soil temperature with time at Datelan for the same period, as well as temperature changes at 25, 50, 100, and 500 ft above the earth.

The general topography around Gila Bend in conjunction with the diurnal variation in the prevailing surface wind vector shows an interesting condition. Hourly wind vector observations during November and December 1944 showed that by 1900 the prevailing wind was downslope toward the lower elevations. This flow of cold air into the area of the link may be responsible for the overall cooling of the air up to several hundred feet during the night. At present it is not clear how much of this effect should be attributed to radiation and eddy diffusion of heat toward the earth, although on nights with wind speeds from calm to a gentle variable breeze it is difficult to attribute the entire transport of heat to the latter processes.

Some pertinent data are tabulated in Table 1 showing the time at which the signal was first detected and completely lost and the general atmospheric and ground conditions nearest these times. On the afternoon of December 14, the sky was overcast, and the signal was detected about an hour earlier than on the other evenings.

Figure 3 shows the field strength data for a typical day plotted in decibels below free space. The maximum and minimum for half-hour intervals are shown so that the fading range is apparent. The meteorological data for the period are given in the form of modified refractive index curves relative to a fictitious earth radius of 4a/3, the time of the sounding being given on each curve.

The diurnal variation in field strength is quite pronounced and regular. The maximum range of fields measured was around 46 db, the maximum field generally occurring at times when the inversion layer was thickest. There is no significant correlation between strong fields and the amount that M decreases at some elevation above the antennas. In fact, at times such as 0900 on December 17 the field strength is quite high and yet M shows little indication of trapping. In most cases strong fields occur at times when the 4a/3 modification of the index of refraction gradient is near zero or varying slowly with altitude.

The general results of this experiment may be summarized in the following way. Over the desert location a ground-based temperature inversion was found each night due to radiation cooling of the underlying surface. This temperature inversion produced a strong index of refraction gradient in the first few hundred feet above the earth.

The 10-cm nonoptical link showed a marked diurnal variation in field strength in close correlation with the building up and intensification of the temperature inversion. The strongest fields generally accompanied modified index gradients approaching zero in the first few hundred feet above the earth's surface.

The trapping criterion most widely accepted heretofore specifies that, at some elevation above the transmitter and receiver antennas, M should be less than at the antennas. The data herein reported seem to indicate that this criterion is neither necessary nor sufficient to insure strong fields below the optical horizon. The strongest fields observed at 10 cm approached the flat earth value, assuming a reflection value of unity for the earth.

ANTIGUA, WEST INDIES

PROPAGATION IN S AND X BANDS IN LOW-LEVEL OCEAN DUCTS

General Description[a]

THE EXISTENCE of low-lying ducts over the seas of the world, particularly in the trade wind belt, has been known for the past 2 years. Measurements made by the British and by Washington State College and the Naval Research Laboratory have consistently indicated the presence of ducts ranging in thickness from 20 to 50 ft in regions where the trade wind followed a long over-water trajectory. These ducts are known to vary in intensity and thickness with wind velocity during the trade wind season. It was considered advisable to investigate the possibility that such ducts would permit greatly extended ranges on surface craft and very low-flying aircraft by properly sited radar installations.

Discussion by representatives of the Chief of Naval Operations, NDRC, and the Naval Research Laboratory resulted in organization of a project to make an experimental investigation of meteorological and propagational conditions in an area of the Caribbean theater where such ducts are persistent, with a view to determining their operational usefulness. It was decided that a one-way ship-to-shore transmission path over water would provide the most direct data for analysis, and such a system was set up, using transmitting and receiving equipment provided by the Radiation Laboratory. The transmitters were installed in a patrol craft assigned for the project, there being no larger vessel available, with transmitting antenna heights of 16 and 46 ft.

The site chosen for the receivers at the land-based end of the link was at Judge Bay on the island of Antigua in the Leeward Island group of the British West Indies. Antennas were installed on a tower 50 ft from the water's edge, at heights of 14, 24, 54, and 94 ft, for both S- and X-band receivers.

Antennas for both S- and X-band transmitters were installed on the patrol craft at heights of 16 and 46 ft. These consisted of parabolic reflectors arranged to permit transmission forward or astern, so that transmissions could be made on both the outward and inward legs of the runs. The S-band transmitter peak power output was 43 kw, and its antenna provided a measured gain of 27 db. Output on X band was 31 kw, the antenna providing a measured gain of 29 db. Later in the experiment an S-band antenna was installed at a height above the water of 8 ft. Tests were made with this antenna on two runs. Ad-

adequate switching arrangements to permit tests with the different antennas were provided, and power outputs were measured by means of directional couplers and thermistor bridges.

Meteorological measurements from the ship consisted of detailed temperature and relative humidity readings taken on a rigging running from a boom extending out over the water amidship to the yard-arm about 46 ft above the water. Low-level sounding equipment of Washington State College design was used for all meteorological measurements. Balloon ascents to heights of 600 ft from the stern of the ship were also made when conditions permitted. Hourly observations of sea temperature, wind, and sling psychrometer readings from the bridge were made. It was impossible to obtain satisfactory soundings on the rigging or by use of balloons and kites when running away from the tower into the wind because of the large amount of water taken over the bow and the resulting salt spray. Shipboard observations during outward runs were therefore confined to the hourly wind velocity, sea temperature, and sling psychrometer readings. On return runs with the wind, balloon and rigging soundings were made. It was necessary to estimate the height above the surface for readings taken below 10 ft because of the severe pitching and rolling motion of this type of ship, and therefore very few such readings were made.

At the receiving end of the radio path, the antennas for S band were 48-in. parabolic dishes with a gain of about 30 db. The X-band antennas were 48-in. dishes cut to 2 ft in the horizontal dimension to broaden the horizontal acceptance angle. This was done to eliminate the effects of minor deviations of the ship from a radial course. These antennas had a measured gain of 35 db. Midway in the experiment an X-band antenna was mounted at the base of the tower at a height of 6 ft, since results up to that time indicated the lowest available antenna height on X band gave the strongest signals. All antennas were mounted on swivels to allow alignment on any course over a 40-degree arc and were connected by wave guide and stub-supported coaxial cable.

Two S-band and two X-band receivers feeding Esterline-Angus recording milliammeters were kindly furnished by the Radiation Laboratory. The S-band receivers had a minimum sensitivity of 110 db below 1 w, while the X-band receivers had a minimum sensitivity of 105 db below 1 w. It was necessary to use automatic frequency control on the X-band receivers, but manual tuning was employed on the S-band receivers because of the greater frequency stability of the S-band magnetron. The receivers were calibrated with standard test sets before every run and checked upon the completion of each test. Individual calibration curves were then used in plotting the results of each run. Since only two receivers on each band were available, an r-f switching arrangement similar to that used on the ship was employed.

Two-way voice communication between the ship and shore station was maintained at all times for coordination of operations. The facilities of an Army radio direction-finding station on the island were available to obtain bearings on the ship.

Meteorological measurements were made at the shore station during operations by means of kite flights and a guy rigging running from the water's edge to 10 ft above the top of the tower. Detailed soundings in the first 100 ft were then taken by sliding the measuring instruments up and down the rigging. Since the duct conditions important in this investigation were always below 100 ft, only occasional kite soundings (two to three a day) were made to check the higher levels. Most of the data accumulated were taken on the tower rigging where detailed soundings could be made. Wind speeds at the surface and 100 ft levels were recorded hourly. Hygrothermographs were placed at the antenna levels and continuous records taken to determine the diurnal variation of temperature and relative humidity, if any.

[a] By Lt. R. W. Bauchman U. S. Naval Research Laboratory.

A typical procedure was to align the ship at a point about 6 miles off shore (closer ranges were impossible because of reefs lying off the northeastern coast of the island) and commence a run on a prescribed bearing away from the tower. This bearing was predetermined by ship observations of the current wind and sea direction. The receiving antennas were aligned to maximum signal strengths recorded by the receivers and secured in this position by clamping to the deck. The ship operating speed was usually around 10 knots, depending on the current sea conditions. While the ship was moving on the course, antenna changes on the receivers were made every 15 minutes for some runs, while antenna heights on the transmitting end were changed every 2 hours. After making several runs using this procedure, results showed that there was no discernible diurnal variation of signal strength. Therefore, later runs were made using antenna changes on the transmitting end only at the conclusion of the run out. Periodic changes of the receiving antenna heights were made in order to obtain a complete record of all possible antenna combinations during each run.

One of the main difficulties encountered in this type of operation was keeping the ship on the scheduled course. Deviations from this course were detected by means of sudden drops in signal strength on the X-band receivers. When this occurred, one of the X-band antennas was realigned to give maximum signal return and the change in ship's bearing noted by use of a bearing marker attached to the antenna. This change was then applied to the remaining antennas and the ship's course changed accordingly. Additional checks on the ship's course were obtained by means of the radio direction-finding station. By using this information, it was possible to detect deviations in the ship's course without losing any part of the record. The ranges of these runs extended up to a maximum of 190 miles. Signals were usually detected out to this range on the lowest X-band combination and the highest S-band combination of transmitting and receiving heights.

Figures 1, 2, 3, and 4 show the plots for one complete run. It is apparent that the lower antenna combinations on X band produced the highest signal level. Signal strengths from higher antenna combinations declined proportionately with height. On S band the reverse appeared to be true, the 46- to 94-ft antenna combination giving the highest average signal level.

Figure 5 shows a composite presentation of 16-ft transmitting antenna to 14-ft receiving antenna. The average received signal with this antenna combination is 5 to 10 db below the 8- to 6-ft X-band antenna combination.

Figure 6 is a record of all the runs on the 46-ft transmitting and 94-ft receiving antenna combination. This clearly shows that the highest combination available with this setup produced the best results. It can also be seen that the signal level is considerably further below the free space value than is the X-band signal for these ranges.

In order to determine the effect on the signal strength of moving the antenna inland, a mobile unit consisting of an X-band receiver, test set, recorder, and 18-in. parabolic dish were mounted in a truck and operated from a gasoline-driven generator. Measurements during several runs were recorded ¼, ½, and 1 mile inland from the water. The antenna heights above the sea surface were 25, 50, and 100 ft, respectively. In one instance, the unit was placed behind a hill with the antenna several feet below the top to see if transmission over the hill was possible. There was a noticeable decrease in signal strength, approximately 13 db, but some signal was still recorded.

Meteorological measurements were taken simultaneously with the inland radio measurements. Kite soundings at several points at increasing distances inland from the water's edge were made, and detailed soundings on a 50-ft windmill tower about ½ mile inland were recorded over a 12-hr period.

Additional meteorological measurements from the ship on the leeward side of the island were made to determine if duct conditions existed in this area. Measurements taken from 2 miles out to approximately 20 miles off shore showed that duct conditions similar to those found on the windward side of the island existed.

During the final phases of the project, an X-band radar was installed at the base of the tower with an antenna height of 6 ft. Measurements of echo strength versus range were made on the PC boat to evaluate the effect of the duct on X-band radar. Antenna heights of the radar were varied from 6 ft to approximately 90 ft by placing the installation on the truck in much the same manner as was done with the receiver in the one-way experiment. This was then set up on sites overlooking the coastline to sea. The heights at which signal strength versus range measurements were made were 6, 15, 50, and 90 ft. The variation in the range of sea clutter for these heights was also observed. Measurements on the leeward side of the island were also made with this radar with approximate antenna heights of 6, 10, and 75 ft above sea level.

The maximum range obtained using the PC boat as a target with a broadside aspect was 47 miles. This range was observed with the radar antenna at the 6-ft level. The maximum range obtained on the ship from the 90-ft level was 26 miles. Sea clutter was found to vary with the antenna height and wind speed. Maximum return of 15 miles on sea clutter was observed at the 6-ft level with wind speeds of 20 to 30 knots. The maximum range at which sea return was obtained varied proportionately with height up to the 90-ft level. This range was decreased 50 per cent with lower wind speeds of 10 to 15 knots. The most significant radar datum obtained to leeward of the island was the detection of a ship at 45 miles from a 75-ft site.

Meteorological Measurements[b]

The description of the meteorological measurements in connection with the experiment at Antigua is divided into three parts, as follows: first, a brief general description of the West Indian climate; second, a survey of the low-level soundings; and third, a necessarily hurried analysis of the data, with certain tentative conclusions.

The most noteworthy feature of the climate at Antigua during the late winter is the persistence of one type of weather. This weather condition is determined largely by the position and strength of the Bermuda high, a large semipermanent high-pressure area covering much of the Atlantic from 10 to 30 degrees north latitude. The northeast trades blow around and out of the high's southern rim. With a few exceptions during the period of the experiment, the wind direction at Antigua was east-northeast. Once, for a period of 3 days, it went around to north-northeast and on two separate occasions blew from the east. Average daily surface wind speed was 16 knots, with occasional variations between 8 and 27 knots. Representative air temperatures varied between 74 and 78 F, relative humidities between 60 and 80 per cent. The sea water temperature was reasonably constant at 77.5 F, with occasional variations between 76.5 and 78. No significant horizontal gradients of sea temperature were found. Precipitation was wholly in the form of showers with a maximum frequency of occurrence around sunrise. Periods of relatively dry weather followed by periods of relatively showery weather and accompanying transitions were experienced. It is felt that these variations were caused by fluctuations in the intensity and position of the Bermuda high or by the trough effects ahead of dissipating cold fronts.

During the entire period of observations, a simple surface duct was found to exist over the water. From the second week in February through the third week

[b] By L. W. Blumian, U. S. Naval Research Laboratory.

in March, and again in the first week of April, duct conditions were essentially constant. This condition, which is called herein the normal condition, is shown in five figures.

Figure 7 shows the average temperature and mixing ratio values for a 2-day period plotted against height. Curves of daytime and nighttime conditions are shown. Soundings were taken every 2 hours. The water surface values are derived from measurements made on the ship. Considerable difficulty was found in obtaining accurate soundings in the daytime due to radiation from the warm land in the case of the tower soundings and the warm ship in the case of ship soundings. As mentioned in Section 4.1, soundings were possible on the ship only when running with the wind. Thus, radiation effects of the ship were maximized, especially in the daytime. However, valuable psychrometer measurements were made on the outbound runs which showed the air to be consistently cooler than the water. On this basis, absolute values of temperature in the daytime tower soundings have been arbitrarily adjusted.

Figure 8 is the M curve computed from the temperature and mixing ratio curves just given. The surface duct and the small diurnal change in its properties are readily seen. An interesting point is the existence of a rather sharp discontinuity at the 1-ft level. Careful independent measurements were made using a number of locations and techniques. All these tests confirmed the failure of the sea surface values to fit to the smooth curve. It appeared possible that propagation results might be more dependent on the M deficit as computed using the 1-ft value than on that computed from the sea temperature. The terms "effective surface values" of temperature, mixing ratio, and M were therefore established, these being defined as the values of these quantities at 1 ft above the water surface. Correspondingly, the *effective* value of M deficit is the difference between the value of M at 1 ft above the sea surface and the lowest value of M for a given sounding, and this effective value should not be confused with the total M deficit, which may be considerably different. This concept will be employed later in the paper.

Another significant feature of the normal sounding is the fact that, although the minimum value of M is at a height of about 40 ft, the curve does not quite reach the slope corresponding to mixed air in the first 100 ft. Due to the roughness of the few higher soundings obtained, it has been impossible to determine the exact height at which the air becomes mixed. It appears to be between 100 and 200 ft.

The next four soundings show what happened to the duct under abnormal synoptic conditions. The major variations were (a) relatively low winds, (b) relatively high winds, (c) relatively dry air, and (d) relatively moist air.

The figures which follow are mean or representative sample soundings made during each of the conditions described above. All were made on the tower and are chosen as best illustrating the effect on the M curve.

Figure 9 is a mean curve for low winds. It shows a lowering of the top of the duct and a change in slope of that portion of the curve lying between 1 ft and the top of the duct. No marked change is found in the total M deficit.

With wind speeds greater than normal, the duct thickness increased, the effective M deficit decreased, and the total M deficit also decreased slightly. The average of 4 days' soundings during a windy period is shown in Figure 10.

At one time there was an influx of exceptionally dry air with winds of normal speed. Figure 11 shows the effect on the M curve. The major change is an increase in the total M deficit.

Figure 12 is a sample sounding made during a period when the air was relatively moist. The significant deviation from the normal soundings is the decrease in the total M deficit and the lack of any change in the effective M deficit or in the duct height.

In addition to the shore soundings made at the water's edge, a few soundings were obtained inland, in an effort to determine how far in over the land the duct extended. Unfortunately, most of the data are sparse and not too reliable. A few good soundings were obtained about 1 mile inland, an example of which is shown in Figure 13. The data were taken during the day and show clearly that no low duct existed at that time. This slide is a composite between a sounding made on a 50-ft windmill and a kite sounding made nearby. The kite was flown to 600 ft and the M curve continued at the slope representing mixed air from 60 ft on up to 600 ft. No night measurements were made.

It was possible to make a few shipboard soundings to leeward of the island, beginning at a distance of 2½ miles and continuing on out to 20 miles. A preliminary study of the results shows no appreciable change over the course and no difference between conditions to leeward and to windward of the island, indicating that the duct is restored very close to shore.

Some plots of certain correlations between wind speed, duct thickness and M deficit follow. The graphs in many cases are composed of very few points and due to the short time available are based on average soundings which have necessarily been smoothed. Figures 14, 15, 16, and 17 are based on the mean tower soundings and mean winds for each run, these being the only smooth data readily available for quick analysis.

Figure 14 shows effective M deficit plotted against wind speed. This portion of the curve seems sensitive to wind speed variation.

Figure 15 shows the effective slope (height of minimum M divided by effective M deficit) plotted against wind speed. Some connection between the two quantities is indicated.

In Figure 16 the height at which M is a minimum is plotted against wind speed. The isopleths of effective M deficit have been sketched in. A few of the points were thrown out in drawing the isopleths. For constant duct height, the effective M deficit apparently first increases with increasing wind speed and then decreases. Unfortunately there are only two points in the low wind region to establish this behavior. It is quite possible that the lines should be more nearly horizontal at low wind speeds and then should slope off in the manner shown for winds above 15 knots.

An attempt to plot sea temperature minus air temperature against wind speed showed no correlation. Plotting mixing ratio based on saturation at sea temperature minus mixing ratio computed from dry and wet bulb temperatures against wind speed also failed to show any correlation.

Figure 17 is a plot of total M deficit versus wind speed, with isopleths of total slope, that is, the duct height divided by the total M deficit. Again, the exact pattern of the isopleths is not definitely determined. With the inclusion of more data in the form of smoothed individual soundings, this chart and the previous ones may prove to be more conclusive. If this is the case, it may then be possible to estimate the values of duct height and effective M deficit simply from single observations of air temperature, air humidity, sea temperature, and wind. Psychrometric observations taken at a height of from 30 to 60 ft above the water would provide the value of M at the top of the duct to ±1 or 2 M units at the most. An observation of sea temperature leads directly to the sea surface value of M, and the wind speed can be obtained from the ship's anemometer. Thus with the aid of the charts three important points on the M curve can be obtained, namely, the values of M at the sea surface and at 1 ft and the minimum value of M and its height.

These preliminary results may be summarized as follows:

1. A surface duct between 40 and 50 ft high with a slightly transitional-type layer extending above the duct to between 100 and 150 ft exists most of the time over the water in this area.

2. The duct is destroyed over land in the daytime within about ½ mile of the shore.

3. Islands comparable in size to Antigua have little effect on the duct on the leeward side at a distance greater than 2½ miles off shore.

4. The higher the wind speed the thicker the duct becomes and the less the *effective* M deficit becomes.

5. Changes in wind speed have little effect on the total M deficit, which is determined essentially by the temperature and humidity of the air mass as a whole in relation to the surface water temperature.

6. These conditions probably prevail over ocean areas having comparable climates.

Preliminary Results of Radio and Radar Measurements[*]

The main purpose of the experiment was to establish what operational use could be made of low-lying ducts and to confirm observation of the effects of such ducts on radio and radar propagation made in various parts of the world. The data accumulated have been available for study only 2 weeks, and there has been insufficient time for a complete analysis. As a consequence only the highlights of the agreement between experiment and theory have been determined.

Ducts were present all the time, and trapping on both X and S bands, which increased the signals to levels considerably above standard propagation values, was found to exist all the time. The general conclusion regarding the effect on the two bands was that on S band antennas as high as the experiment would allow gave the highest signal strengths. On X band, on the other hand, the lowest antenna heights which were available usually gave the strongest signals.

Figure 18 is an S-band run made on March 15. It is a composite run containing the results of both the outward and the inward runs. Several of the curves have been omitted for clarity. The highest curve is for a combination of a 46-ft transmitting antenna and 94-ft receiving antenna. The lowest curve is for the two lowest heights, 16 and 14 ft. The slopes of the curves are rather steep for the first 80 miles or so, the signal declining considerably less rapidly thereafter. Also, the variation of the signal with height is shown here to be in the order in the extremes between 25 and 30 db. This interval from 80 to 50 db shows a difference between the two extremes of 30 db. To translate that into a radar situation, double that difference to get a difference of 60 db, showing that on S band the higher antenna combinations would provide considerably better coverage for targets in the order of 100 ft high and with transmitters at the height of about 50 ft. Stated another way, the highest antenna combination would provide coverage beyond that obtainable with the lowest in the order of 30 miles.

There is as yet no reasonable explanation for the extremely slow decrease in signal beyond 80 miles. This feature is very distinctive in the S-band curves. For the X band, it is generally not discernible except on a few runs toward the extreme range portion. The rate of decrease of signal with range in the region inside 80 miles would be exponential if there were a straight line on this figure. Considering it to be so, averaging over a number of runs gives roughly 0.8 db per nautical mile. That decrease is the total amount, the 1/R variation not having been extracted from it. Attempts to do so show that the resulting curve does not, in a plot of this sort, fit a straight line as well as the original values themselves, but if the 1/R value is taken out of the power relation the average attenuation is then roughly between 0.5 and 0.6 db per nautical mile. In this region (beyond 80 miles), on the other hand, the decrease of signal with range is considerably less, being between 0.15 and 0.2 db per nautical mile. No satisfactory explanation for this behavior has yet been derived.

Figure 19 shows the X-band results for the same period. Antenna heights of 16-ft transmitting and

[*]By M. Katzin, U. S. Naval Research Laboratory.

6-ft receiving produced the highest curve, the lowest curve being obtained on a 46-ft to 94-ft combination. Note that succeedingly higher antenna combinations produced successively lower signal strengths. There is some variation, but when the curves are smoothed to a straight line the attenuation is on the order of 0.33 to 0.5 db per nautical mile. Removing 1/R reduces the attenuation to roughly 0.2 db per nautical mile. There is no sharp bend in the curve at about 80 miles, as was the case on the S band. The lowest (16-ft to 6-ft) antenna combination showed more than 35 db greater signal strength than the highest (46-ft to 94-ft) combination. Considering again the radar case, it is found that the higher antenna provides relatively poor coverage compared to the lower. In terms of range for a given signal threshold, the difference in favor of the lower antenna is about 80 miles.

Figure 20 shows an X-band curve obtained during April 10 and 11, when a transmitting antenna height of 8 ft was available. Received signal powers for 6-, 14-, 24-, 54-, and 94-ft receiving antennas are shown. The curves are somewhat scrambled, but the general result is that the lowest antenna again produces the greatest signal, with increasing antenna height producing progressively smaller signals. This was not the case without exception, as can be seen in Figure 4, where the 6- and 14-ft antennas exhibit comparable behavior. In that case the maximum range was obtained on the 14-ft antenna. The average slope in Figure 20 is somewhat less than that shown in Figure 19. Exact averages of all the runs have not yet been worked up.

Figure 21 shows a plot of received signal versus range, made on a 3-cm radar, using a PC boat as a target. The highest curve was obtained with a 6-ft antenna height, using a 48-in. dish to obtain greater gain and range. The other run with 6-ft antenna was made using the regular 29-in. dish. There is a considerable spread in the values of received signal due to the difficulty of measurement. However, the significant thing is that the maximum ranges obtained are in accord with the indications given by the one-way transmission results. Striking an average slope shows the decrease of signal with range to be about 1.0 db for each 1.5 nautical miles.

The important conclusions can be summarized as follows:

1. The surface duct is very persistent.

2. The duct is very effective in extending the ranges obtainable on both S and X bands, for either one-way or two-way transmission.

3. On S band, the highest combination of transmitting and receiving antennas produces the strongest signal and the greatest range.

4. On X band, the lowest combination of transmitting and receiving antennas produces the strongest signal and the greatest range.

5. Surface ducts in the trade wind regions can be used for communication purposes to a conservative range of 100 miles. Greater ranges are probable but will require further investigation.

6. Rain in the form of squalls does not appreciably affect the received signal.

ENGLAND

BRITISH TRANSMISSION EXPERIMENTS[a]

Introduction

THE BROAD OBJECT of the studies carried out in Great Britain during the past few years has been to establish the characteristic facts of the propagation of centimeter waves (more recently of meter waves also) and especially to determine the relationship between radio performance and meteorological conditions in the lower atmosphere, with forecasting as the ultimate aim.

[a]By E. C. S. Megaw, Ultra Short Wave Panel, Ministry of Supply, England.

Although propagation of 10-cm waves to distances much beyond the optical range had been observed under favorable conditions nearly a decade earlier, it was the striking increases in range of decimeter and centimeter wave coastal radars in southern England, observed in the summers of 1940 and 1941 respectively, which led to a concentrated attack on the long-range aspects of the problem. About the same time a need arose for more accurate knowledge of both 'the short-range "interference" field and the long-range "diffraction" field for certain communication projects, and the radio equipment developed to meet this need formed a nucleus round which the later and more ambitious experiments grew. The reviews of various experimental and theoretical aspects of this work are listed in references 1 through 15.

Continuous observations have been carried out over a range of optical and nonoptical paths across the Irish Sea on S and X bands and over a single 38-mile land path on S band. These are discussed below. In addition to this work several investigations of more specific propagation problems have been carried out during the summer of 1944.

1. Measurements on two wavelengths in S band, over a 70-mile sea path between a site in South Wales and the summit of Snowdon (3,500 ft). This optical path was studied to obtain data on the probability of missing aircraft on S-band radars under conditions favorable to trapping at low levels over sea.

2. Measurements on a wavelength of about 3½ m over a 90-mile sea path, with heights such that the path length was about twice optical range, to provide quantitative data on the importance of refraction in this waveband.

3. Radar measurements from Llandudno, North Wales, with the Isle of Man and the Irish Coast as the main targets, on S, X, and K bands. The object was to obtain practical data on the relative performance of K band under a variety of meteorological conditions which were studied simultaneously with the radar observations by ship, balloon, and aircraft measurements. Some further reference to the results of (1) and (2) appears below; an interim report on (3) has been circulated.[12]

Irish Sea Measurements

The first plant for simultaneous measurements within and much beyond the optical range on wavelengths of about 9, 6, and 3 cm, using heights of about 100 and 500 ft each site, was made in the latter part of 1941.

The work was planned on an inter-service basis, with equipment provided by Admiralty (developed under Admiralty contract by General Electric Company Research Laboratories from that used in the early communication studies mentioned above) and stations provided and operated by Signals Research and Development Establishment, Ministry of Supply. Arrangements were made for analysis of the data by the National Physical Laboratory, which has also more recently undertaken the development of monitoring equipment. The collaboration of the Meteorological Office was received at an early date, but it was only when the study of the subject had made further progress that the need for detailed low-level meteorological measurements was realized; these have been undertaken by the Naval Meteorological Service, soundings being made in ships and by means of shipborne balloons. Additional arrangements have recently been made with the Meteorological Office for regular aircraft soundings over the path.

Some difficulties were encountered early in 1942 in finding sites for the stations which were acceptable from all points of view, and the field work done in that year consisted of several short-period trials over a rather wide variety of land and sea paths. In spite of many limitations, in particular as regards detailed meteorological data, the general conclusions reached in these trials[9] have been largely substantiated by later measurements. Table 1 gives details of the sites finally adopted.

The path length from South Wales (A and B) to North Wales (C and D) is 57 statute miles and that to Scotland (E and F) is 200 statute miles. The path lengths in terms of geometrical optical range for the eight possible paths are shown in Table 2.

In the original scheme all the paths were to be collinear, but this could not be realized with the sites finally adopted; the South Wales to Scotland paths differ by about 17° in bearing from the South Wales to North Wales paths, the bearing of the former being within a fraction of a degree of true north. A scheme for recording data over all paths (though necessarily not continuously) was evolved; each transmitter beam was aimed for half the time along each of the two bearings 17° apart (a 7½-minute period was found the most satisfactory, and a small change in frequency (5 to 10 mc) was made automatically when the beams switched over.

At each frequency the transmitted signal consisted of square pulses, at equal on/off ratio, with a repetition frequency of 1000 c. The "standard" power output in the "on" period was 0.6, 0.3, and 0.15 w for 9, 6, and 3 cm, respectively; the signal records were corrected for any significant departure from these powers. Paraboloid mirrors 48 in. in diameter were used for all transmitters and receivers; these were mounted inside the stations behind large canvas-covered "windows." The increase in mirror gain with frequency more than made up for the reduction in transmitter power, in spite of the less effective utilization of the mirror area. In the receivers the 1,000-c component of the modulation was rectified to operate the recording milliammeters. Provision had been made for monitoring the field radiated from the transmitters and the sensitivity of the receivers, in terms of a standard radiated field. This scheme was brought into operation as the National Physical Laboratory equipment became available; other less complete methods of monitoring the transmitters and checking the receivers had been in operation from the start. (Data for the 5-cm equipment are included here although, as will be noted, it was not used.)

Radiotelephone communication between the North Wales and South Wales stations has been maintained satisfactorily for two periods of several months each using first S- and later X-band equipment, essentially the same as that used for the signal measurements, arranged for duplex operation. A meter-wave system (which gives more continuous service over long nonoptical paths) is now being installed by Admiralty Signal Establishment to link all the stations; it is already operating satisfactorily over the 57-mile path, and a relay link from North Wales to Scotland is being provided.

On S band, operation on all four links across the 57-mile path commenced in November 1943, although the two from Station A (high site) had been running since July. During the preliminary period, up to the beginning of 1944, in which a number of practical difficulties had to be overcome, the radio results were subject to rather more uncertainty than was the case in the earlier measurements where a concentration of experienced personnel was possible for the short periods involved, and detailed analysis of these results has not yet been attempted. One S-band receiver was in operation in Scotland (Station F, low site, 200 miles) from the end of August 1943, but apart from one brief period during September, no signals were received until March 1944, just before the second S-band receiver (Station E, high site) was installed.

On X band all the stations were in operation by July 1944, operation on the 200-mile links having started a month earlier.

After a few months of operation of all 16 links it was realized that the available effort would not be sufficient to cope adequately with the tasks of editing and examining the signal records. Consequently a

rather drastic reduction of the centimeter wave program was agreed to for a trial period of 6 months, starting October 1, 1944. For this period the following links were operated continuously (without beam switching) : on S band, A to C and D (57 miles) and B to E (200 miles) ; on X band, A to C and B to D (both 57 miles). (The possibility of a link from B to D on S band with separate equipment was also envisaged.)

It was agreed to postpone operation on 6 cm, but at least one 3½-m link over each of the two path lengths would be added; preliminary measurements on this longer wavelength were already being made. In addition, K-band equipment for at least the optical 57-mile path was to be installed at an early date.

Figure 1 shows a general view of the equipment in one of the stations (D). The X- and S-band receivers are in the center of the picture, with the mirrors and canvas-covered windows behind. The S-band signal generator and monitoring equipment are on the small table beside the S-band receiver. The recorders are mounted on a temporary table (now replaced by the central control desk), extreme right. The empty bay, extreme left, was designed to house the K-band equipment. The meter-wave equipment was mounted in an adjoining room.

In addition to the radio measurements, some study was made of the behavior of a light beam over the 57-mile path during the summer of 1944 in the hope that this might provide useful information on the refraction produced (nearly) by temperature gradient alone. Measurable changes in elevation were sometimes observed by means of a theodolite, but the incidence of adequate visibility was small, and little quantitative information was obtained.

A detailed study of the S-band signal records and meteorological data obtained from February 1944 is being made at the National Physical Laboratory, particularly for the 57-mile paths AD and BD.[8] Similar study of the S band and 3½-meter data will follow.

Figure 2 shows a plot of hourly mean signal level for the S-band signal over the links AD and BD for June 1944, with a record of some meteorological factors—fronts, precipitation, and fog—with which comparison has been made.

It should be emphasized that analysis of the data obtained during this period has not yet been completed, but the following general conclusions may be drawn:

1. There is general agreement between signal variations for the two paths, though the short-period variations often differ.

2. Signals are obtained over the 200-mile path only when signals over 57-mile path BD exceed about 30 db above 1 μv. But if the latter condition is fulfilled the former does not always follow.

3. There is a marked diurnal variation, when the general level is low or moderate, with high signal in the late afternoon or evening and low level in the early morning.

4. There is evidence for an appreciable seasonal variation with high level for a greater fraction of the time in summer than in winter or spring.

5. Low level occurs commonly in conditions of fog or low visibility (e.g., low level on 174 occasions out of 233 on which fog was recorded between February and June 1944).

6. Low level is usually observed at the passage of fronts (e.g., on 78 occasions out of 106 on which fronts were recorded). ...

7. While periods of high level are sometimes characterized by large gradients of water vapor (soundings usually made for the first 200 ft, at one point near the center of the path), no satisfactory correlation has been found between the character of the M curve and the major variations in signal level for the periods which have been studied. In general, as is common experience for similar paths, high levels tend to occur in anticyclonic periods.

The general character of the S-band signal varia-

tions for the four 57-mile paths is illustrated by the plots of hourly mean levels for 5 days in August 1944 shown in Figure 3. The range of variation in level increases with the excess of path length over optical range, and there is an obvious similarity between the three nonoptical paths as regards the larger changes in level. This similarity does not extend to the optical path AC, which shows signs of an *inverse* correlation with the major variations of the nonoptical paths. For a standard atmosphere (⁴⁄₃ earth radius) the receiver on the AC path is near the record maximum of the interference field. For fairly small departures from standard (curvature corresponding to, say, 1.0 to 1.7 times earth radius) the range of variation caused by interference is quite small, about +4 to —7 db relative to free space field; the smallness of the variation is due to the appreciable effect of divergence of the reflected ray in this case.

While other factors beside interference with the reflected ray are almost certainly operative in producing variations over the optical path, slow fading with a range of the order of 10 db is quite common; and a slightly substandard index gradient, which would produce a marked decrease in level for the nonoptical paths, would leave the AC path in the neighborhood of the first interference maximum.

The free space levels (48 db above 1 μv from A, 44 db from B; difference due to different radiated powers at this period; 1½ db estimated atmospheric absorption allowed for) are marked on the plots of Figure 3. For all four paths the highest levels reached are in the neighborhood of the free space value; levels several decibels above free space are occasionally reached during good periods, but they are only rarely maintained for as much as a few hours (e.g., path BD, May 12, 13 and August 5, 6). The long-time average level for path AC should be close to free space level, probably about 2 db above. It is actually about 5 db below for the first half of August 1944 and about 3 db below over a period of several months. While some of this discrepancy may be due to residual experimental error, the fact that it appears to be least during periods of poor transmission between the low stations (e.g., August 10 in Figure 3) may be significant.

For the nonoptical paths BC, AD, and BD the standard level is 20, 37, and 79 db below free space level, respectively, for S band. The corresponding figures for X band are 28, 53, and 113 db. The standard level is shown in Figure 2, and in Figure 3 for paths BC and AD; for path BD it is over 30 db below the receiver threshold. While it is rare, during the summer months, for the level to remain near standard for a large fraction of the time (in February, however, the AD level was within 2 db of standard for about 25 per cent of the time), the minima of the major signal variations usually lie within about ±5 db of the standard level except (1) during runs of particularly good weather and (2) during foggy conditions which are likely to be associated with a substandard index gradient. Striking examples of the latter occurred on June 4, 5 (Figure 2) and August 10, 11 (Figure 3). On the last occasion the BC level went about 20 db below standard.

The X-band results for the 57-mile paths are generally similar to those for S band as regards the major variations, but the range of variation is noticeably larger, particularly on paths BC and AD, which are not much longer than optical range; the increase in range of variation for these paths is of the same order as the difference in standard level for the two wavelengths. In general, short-period variations are larger and more rapid for the shorter wavelength.

Figure 4 shows the results for both S and X bands over the 200-mile paths AE (high stations) and BF (low stations) for part of the same period as shown in Figure 3. After allowing for the estimated atmospheric absorption (6 db for S, 16 db for X) the free space levels are similar for the two wavelengths, experimental uncertainty being appreciably greater at

"general" level, which is in fact that obtained under "well-mixed" meteorological conditions.

Further details of the path and a discussion of the results in relation to general meteorological conditions over the path have been given in two National Physical Laboratory reports,[16,17] which cover the first year's operation. A further report is in preparation. The aim here is limited to a general description of the type of results obtained, with examples of some characteristic signal records.

Figure 5 gives a plot of hourly mean level for March 1944 which clearly shows the two main characteristics of the signal: the reasonably constant general level and the regular diurnal cycle which occurs with radiation nights. The period March 21 to 26 is typical of an undisturbed run of clear nights; note the period of marked substandard signal in the early morning of March 27, indicating that condensation near the ground has reduced the water vapor content there sufficiently to make the lapse rate negative. Intermittent rain in bad weather periods usually gives a more variable level than cloudy weather with no precipitation; a small rise in level is often observed with continuous rain (direct effects of rain on the equipment have been carefully guarded against and may be assumed negligible) and a more marked rise with clear skies in daylight following rain. These effects are readily explicable in terms of changes in water vapor distribution.

The work of the past 6 months (Summer 1944) has shown a definite correlation of high level at night with temperature inversion whether with clear or with variable skies; on the other hand, clear or variable skies with no temperature inversion (e.g., with incoming cold air) show no night peak of signal. In general the increase of level on an initially clear night is arrested by the development of low cloud or of fog. Double maxima are often observed in the night peaks (e.g., March 15 in Figure 5).

The magnitude of the peaks on radiation nights is usually 5 to 10 db; it can occasionally reach 15 to 20 db particularly in summer. It seems very probable from the geometry of the path that earth-reflected rays play little part, at least for moderate degrees of bending. It is therefore reasonable to seek to explain the larger variations as resulting from increasing ray curvature. In terms of the rough estimate mentioned above, a change from standard to "flat earth" conditions would give an increase in level of the order of 10 db, which is a typical figure for the observed rise on an undisturbed radiation night. It is of interest to note that free space level is never reached on this path; the highest instantaneous level reached is 10 to 12 db below free space. In other words complete, or nearly complete, reflection regions do not exist at heights of the order of 1,000 ft or more (required to "clear" the barrier) over this path. This is in line with the observed lack of any effect of high inversion on the signal level.

Overland Measurements: Whitwell Hatch to Wembley

A single S-band link has been in continuous operation over this 38-mile path since March 1943. Its terminals, with the transmitter in one of the Admiralty Signal Establishment buildings and the receiver at General Electric Company Research Laboratories, were chosen for operating convenience rather than to meet any special requirements for the path, as an important subsidiary purpose was to provide for controlled long-period tests on equipment developed for use in the less readily accessible stations of the Irish Sea program. Apart from routine checks the equipment normally operates unattended; automatic frequency control at the receiver has been in operation since June 1943. But the receiver is provided with a relay-operated alarm which can be set to operate on an abnormal change of received level in either direction (normally downwards) and this has proved valuable

in calling attention to both faults and unusual propagation conditions.

The transmitter is on a hill 725 ft above sea level and the path runs northwards across the Thames valley and the western outskirts of London to the receiver, which is only 170 ft above sea level, in low, undulating, built-up country. For standard conditions the path is clear except for the last mile where trees and houses form a barrier elevated about ½ degree above the ray path. This introduces a local diffraction loss at the receiver which has been estimated roughly at about 30 db. This estimate is necessarily an uncertain one, both because of the complexity of the real barrier (which is approximated as one or more opaque straight edges) and because of possible seasonal variations.

Seasonal variations in general signal level have been observed with a maximum in late summer of the order of 10 to 15 db higher than the single winter minimum recorded so far. An attempt to explain this variation in terms of changes in the horizontal plane diffraction pattern of part of the barrier with varying opacity of the tree background does not appear to be supported by the results of the past few months (Summer 1944). The mean level for the whole period is, however, close to 30 db below free space (52 db above 1 μv receiver input) and is thus at least of the same order of magnitude as the estimated standard level. The unfortunate effect of this uncertainty regarding standard level is mitigated to a considerable extent by the fact that a land path of this kind gives an easily definable X band as regards absolute values. The standard levels are, of course, far below the receiver threshold, actually about 275 db for path AF on S and 490 db for path BF on X.

The most striking characteristic of the results is perhaps the similarity in magnitude of the signals both for the two paths and for the two wavelengths. In general, signals are measurable for a greater fraction of the time on the longer wavelength and for the higher sites. (The difference of about 5 db in receiver threshold sensitivity between S and X has only a slight effect on this.) At the peak of good periods the lower sites and shorter wavelengths sometimes reach rather higher levels, as in the case of the 57-mile paths the maximum signal level is frequently comparable with free space; rather rarely it exceeds free space level by something of the order of 10 db. For the 200-mile path the possible error in the estimate of atmospheric absorption is rather more serious, particularly for X band, but it seems improbable that this could alter the general character of the results.

Comparison with the results for the 57-mile BD path in the bottom record of Figure 3 is interesting and is reasonably typical of the extent to which the performance of the long path can be predicted from the performance of the shorter one. It should be emphasized that this was a period of good summer weather apart from the break on August 10–11.

Figures 6, 7, and 8 show photographs of sections of the original signal records illustrating the main types of signal which are observed. The type of weather involved is shown on the record in each case, also the signal calibration. Figure 9 shows a good example of an effect which is quite often observed, particularly in the latter part of radiation nights. It consists in a regular variation showing the characteristic rounded maxima and sharp minima of interference fading. This is in some cases superimposed on a nearly steady high signal (as in Figure 9). In other cases, as in some fog fades, it is superimposed on variations of a different type. It often starts and stops suddenly, completely changing the character of the record while it lasts, and that time ranges from one or two fading cycles to many cycles. This sort of effect has also been observed on other paths, over sea as well as land.

The striking thing about patterns of this sort is that they often correspond to reflection coefficients for the interfering ray which approach unity. In Figure 9 the reflection coefficient calculated from the pattern

is about 0.8 at the start, about 0.4 in the middle, and over 0.9 at the end. It is suggested that reflection at small glancing angles from a sharp inversion top provides a possible explanation and that the first part of the pattern in Figure 9 corresponds to an increase in height (the first deep minimum occurring when the inversion top is just above the transmitter) and the latter part to a decrease in height at a different rate. The rates of climb and fall turn out to be about 200 ft per hour and 300 ft per hour respectively. No local soundings are available to check this hypothesis, but the calculated rates of change of height are quite possible.

The general meteorological data for the night (illustrated in Figure 9) are as follows: cloudless, following a fine day; temperature inversion of about 6 F in (approximately) the first 500 ft at 0600 GMT; ground mist about dawn. It is clearly desirable to obtain adequate soundings at periods when this type of effect is observed, especially on account of the widely held view that the index changes which occur at heights of the order involved (about 500 ft above ground level) are inadequate to account for reflection coefficients of the size implied by the pattern observed here.

Difficulties of Existing Theory

In this section a few general characteristics of the radio observations which appear to be at variance with previous theoretical conclusions will be summarized.

1. The most obvious point as far as the Irish Sea data are concerned is the failure of the soundings to provide an adequate guide to the signal variations. The fault may lie in the limited nature of the soundings or in the method of interpreting them, but it is clear that the problem is by no means as simple as was supposed when the soundings were started.

2. The minimum levels obtained (where they are high enough to be measured) usually agree tolerably well with the expected values. For the Irish Sea paths, as well as in other measurements, the maximum level rarely goes above that calculated for flat-earth conditions; this level is practically the same as that for free space conditions for all the Irish Sea centimeter links except for paths BF on S band (only) where there is a difference of about 10 db. If complete guiding were a common phenomenon over paths of the lengths actually used, it would appear that levels above free space should occur much oftener and more continuously than is observed. It appears to be a useful working assumption that the level obtained under favorable conditions over nonoptical paths is nearly that calculated for rays with the same curvature as the earth.

3. The fact that the Irish Sea results show that (for centimeter waves) the advantage lies only rarely with the smaller heights and shorter wavelengths suggests that the importance of complete guiding as a criterion for siting stations may have been overemphasized.

4. The good correlation obtained in a number of cases between land-sea temperature difference and signal level suggests that the importance of temperature may be greater than is indicated by existing theory.

5. It appears very difficult to account for the maximum levels reached on the basis of existing theory.

6. The interference patterns of the type discussed still await an adequate explanation.

PROPAGATION WORK AT THE NATIONAL PHYSICAL LABORATORY[b]

Analysis and Study of Centimeter and Meter Wave Propagation over Sea (Irish Sea Experiment)

This project utilizes the results of radio transmissions being conducted between two sending stations

[b] By W. Ross, British Central Scientific Office.

in South Wales and receiving stations in North Wales and Scotland, jointly by the Admiralty, Ministry of Supply and Air Ministry.

The contribution of the National Physical Laboratory to the installations being used for this investigation has been chiefly connected with the monitoring equipment used at both sending and receiving stations to insure that the radiation from the former and the sensitivity of the latter are maintained constant, so that any variations on the field strength records are known to be due to transmission effects in the atmosphere. The instruments required for the S band are in an advanced state of production, while for the X band the necessary field strength meter for the transmitters has been developed, but some development work is still required on the standard radiator for the receiver calibration. In accordance with a recent agreement as to the limitation of the scope of the investigation, all work on instruments for other wavelength bands has been put in abeyance.

Study of Centimeter Wave Propagation over Land (Whitwell Hatch to Wembley)

A transmitter operating on a wavelength in the S band has been installed at the Admiralty Signal Establishment, Whitwell Hatch, and a continuous recording is being made of the field intensity of the radiation received at the Research Laboratories of the General Electric Company, Wembley, over a land path of 38 miles. Except for some houses and trees within about 5 miles of the receiver, the path is a clear optical one; originally the transmitter was also partially obscured by some trees, removal of the tops of which produced a rise in received field of 10 db. Field strength recording has been in progress over this link since March 1943, and during the intervening 18 months there has been a seasonal variation, with the average daily value in November and December at least 10 db below the value in July and August. Two reports[16][17] have already been issued on the results obtained from an analysis of the records, and a third will be prepared shortly.

Among the main conclusions so far reached are the following. Cloudy weather, either by day or night, tends to produce a signal steady to within about 2 db, while on days of clear and variable skies, the signal exhibits slow (period 5 to 10 minutes) fluctuations of the order of 3 or 4 db, with sharper and more rapid fluctuations superposed. These rapid fluctuations are accentuated by the presence of strong wind. On nights of clear or variable skies with temperature inversions near the ground, the field intensity is from 5 to 10 db above the daytime level and is usually accompanied by variations in the absence of wind. On clear radiation nights, when the wind is too strong to permit the development of a temperature inversion, the peak of signal intensity does not occur. Fog affects the field strength differently according to its depth. A shallow autumn fog causes a sharp decrease in signal strength, while the widespread and more established type of fog experienced in winter may sometimes cause marked interference type of fading with unusually high peak values and at other times may have no apparent effect on the field strength.

The sending and receiving stations on this link are now being equipped with field strength monitoring arrangements to improve the overall accuracy of the radio recording, and a daily statement of the meteorological conditions over the path is being supplied to supplement the ground station records already available. It is contemplated that this link should remain in operation for a further period of 6 to 12 months.

FADING IN A LINE-OF-SIGHT EXPERIMENT IN ENGLAND[c]

This experiment was carried out between Aberporth, South Wales, and the summit of Mt. Snowdon (3,600

[c] By F. Hoyle, Ultra Short Wave Panel, Ministry of Supply, England.

ft). The transmitters were mounted at a height of 120 ft above sea level at Aberporth, the receivers being on Mt. Snowdon. The length of path was about 60 miles as compared with 85 miles optical range.

Two separate radio circuits were used, one on a wavelength of 9 cm and the other on 10 cm. For a standard atmosphere the phase difference between the ray reflected from the sea and the direct ray was about 4.5 radians on 10 cm and about 5 radians on 9 cm, while under "flat earth" conditions the corresponding phase differences were about 12 radians and 13 radians respectively. As the atmospheric conditions varied, an interference pattern was obtained arising from variations in the phase difference. The chief characteristic of the interference pattern was that in a plot of radio signal strength against time the peaks are broad and flat and the minima are sharp and deep. The provision of the two circuits insured that the variations due to alterations in the phase difference could easily be distinguished from variations due to other causes (described below). The reason for this is that the interference minima on one circuit tend to occur at times when the signal strength is high on the other circuit.

The length of time required for the radio signal strength to complete a cycle of the interference pattern was usually about 2 hours. The receivers and transmitters were very carefully calibrated in order to show that the received field strength at interference maximum was equal to twice the free space field. This result was established to within an accuracy of ±2 db.

For about 20 per cent of the time (June 1, 1944 to September 30, 1944) the normal interference pattern was replaced by an entirely different form of signal fading. The period of the fading was about 5 minutes, the field strength at maximum was usually between 10 and 12 db above the free space signal, and the peaks of signal were sharp and the minima broad. The latter characteristic is entirely different from interference fading between two rays which must lead to broad peaks and narrow minima; it is more akin to receiver noise or the form of the signal echo received from "window" on radar sets. Thus it would seem plausible to suppose that the signal was the result of a large number of contributions with uncorrelated phases.

The type of fading described in the previous paragraph is especially interesting in view of the very high signal maxima. It was shown that the occurrence of these variations was not associated with the reflection at the surface of the sea. It would appear therefore that atmospheric conditions can exercise a very important effect on the propagation of radio waves over a completely optical path.

TEMPERATURE EFFECTS ON NONSTANDARD RANGES[d]

Experimental work carried out in the Irish Sea has shown the following three characteristics, all of which are in disagreement with existing theory.

1. It is well known that the present theory requires the contribution of the temperature gradient to be in general small compared with the contribution of the water vapor gradient. In fact if we write

$$\frac{d\mu}{dh} = a\frac{de}{dh} - b\frac{dT}{dh}, \qquad (1)$$

where μ = refractive index,

e = partial pressure of water vapor,

T = temperature in degrees absolute,

h = height coordinate,

a, b are positive constants,

then except in rare cases the present theory requires the $(a)(de/dh)$ term to be large compared with the $(b)(dT/dh)$ term. Thus, since the radio propagation

[d] By F. Hoyle, Ultra Short Wave Panel, Ministry of Supply, England.

conditions depend on $d\mu/dh$, it is to be expected that a better correlation will exist between the radio signal and the measured value of $(a)(de/dh)$ than between the radio signal strength and the measured value of $(-b)(dT/dh)$. The reverse has, however, been found to be the case; the correlation between the radio signal strength and the measured value of $(a)(de/dh)$ is poor, while the correlation with the measured value of $(-b)(dT/dh)$ is good.

2. A situation similar to that mentioned in (1) has been encountered in attempting to forecast 12 hours ahead for operational radar sets. Table 1 summarizes the results obtained.

The continuity method of forecasting consists in predicting that tomorrow's conditions will be the same as those observed today. Forecasting from the (dT/dh)

term was empirical, it being assumed that a temperature inversion of 1.5 C per 100 ft would give very good propagation conditions, an inversion of 0.75 C per 100 ft would give good conditions, and a temperature lapse would correspond to standard or natural conditions.

3. The value of $d\mu/dh$ calculated from equation (1) using the measured values of de/dh and dT/dh are too small to explain the large signals frequently observed on a wavelength of about 80 mc.

These experimental results enable the following conclusions to be drawn so far as the meteorological conditions around the British Isles are concerned.

1. The radio signal strengths computed from the observed M curve do not agree with observation. The method of observing the temperature and water vapor

gradients to obtain an M curve is therefore unsatisfactory.

2. A reasonably satisfactory forecasting system can be obtained on the basis of temperature gradient alone. This system is empirical and does not depend on complicated mathematical computations. Accordingly the system may be suitable under operational conditions.*

* Since November 1944 the Group at San Diego has found a good correlation between the radio data and a simple meteorological parameter based on temperature excess. In the British Isles the temperature excess has to be taken between a height of about 200 ft and sea level, whereas at San Diego the temperature excess has to be taken between a height of about 5,000 ft and sea level. It has also been reported that in the Pacific Area temperature excess is by far the best index for predicting radio propagation conditions. There is some hope, therefore, that it may be possible to work out a method of fairly universal application on the basis of temperature excess.

TABLES AND ILLUSTRATIONS IN APPENDIX

MASSACHUSETTS BAY
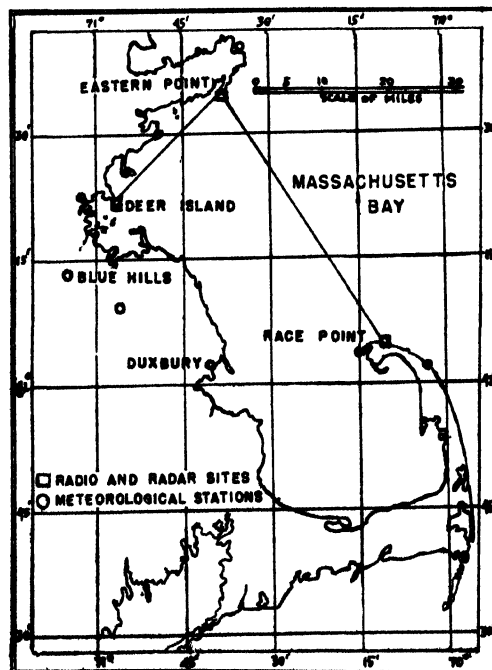
FIGURE 1. Map of transmission paths.

TABLE 1. Statistics of S- and X-band transmission in summer.

Date	Per cent of time above standard	Per cent of time below standard	Per cent of time standard
July 10–16	63	36	1
Aug. 21–27	97	3	0
Aug. 28–Sept. 3	80	15	5

TABLE 2. Statistics of S- and X-band transmission in the fall.

Date		Per cent of time above standard	Per cent of time below standard	Per cent of time standard*
Sept. 25–Oct. 1	S	58	15	27
	X	80	10	10
Oct. 16–22	S	76	2	22
	X	92	0	8

*By this term is to be understood the percentage time in which the signal is ± 2.5 db of standard on S band and ± 5 db on X band
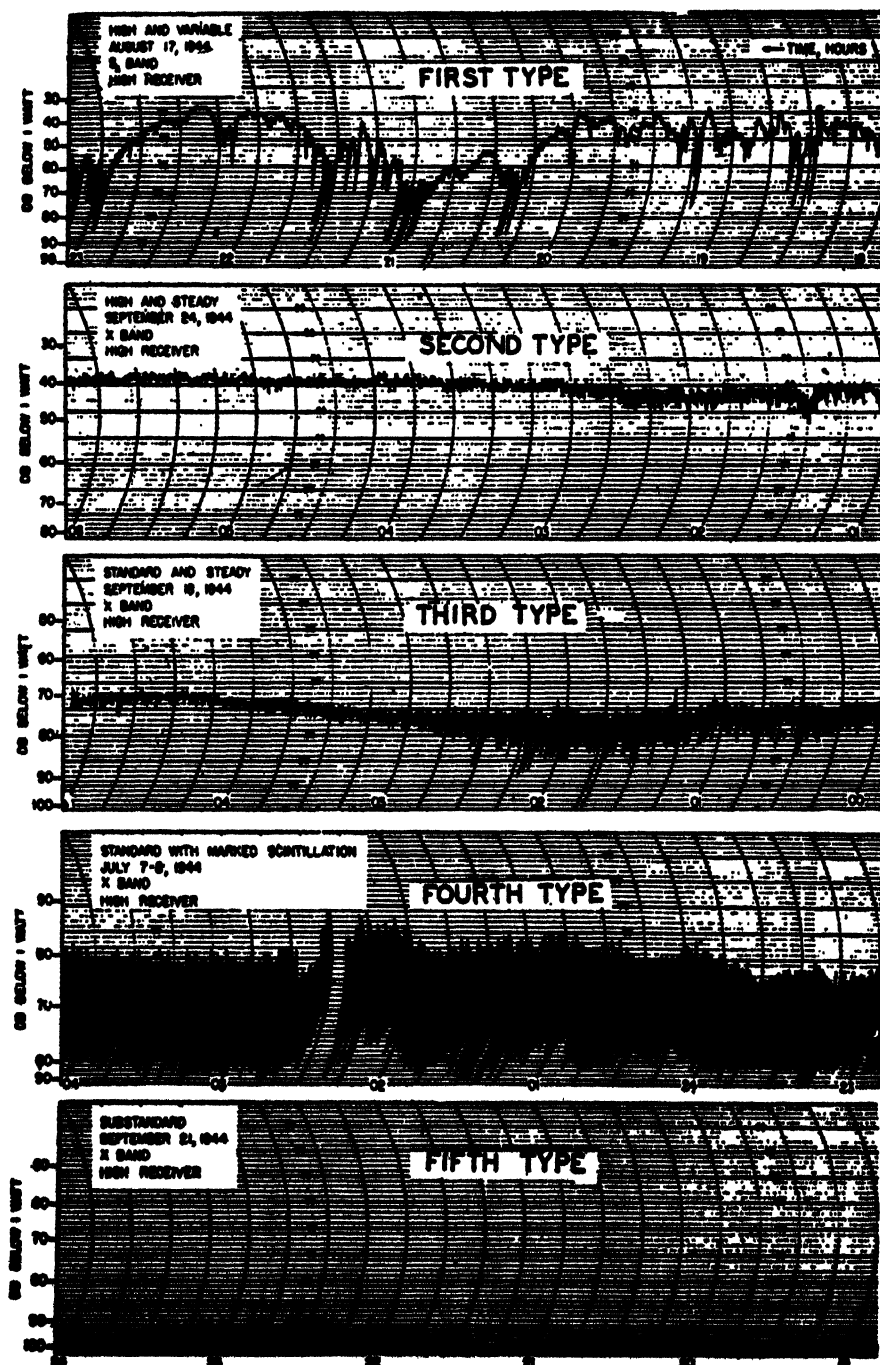
FIGURE 2. Microwave signal types
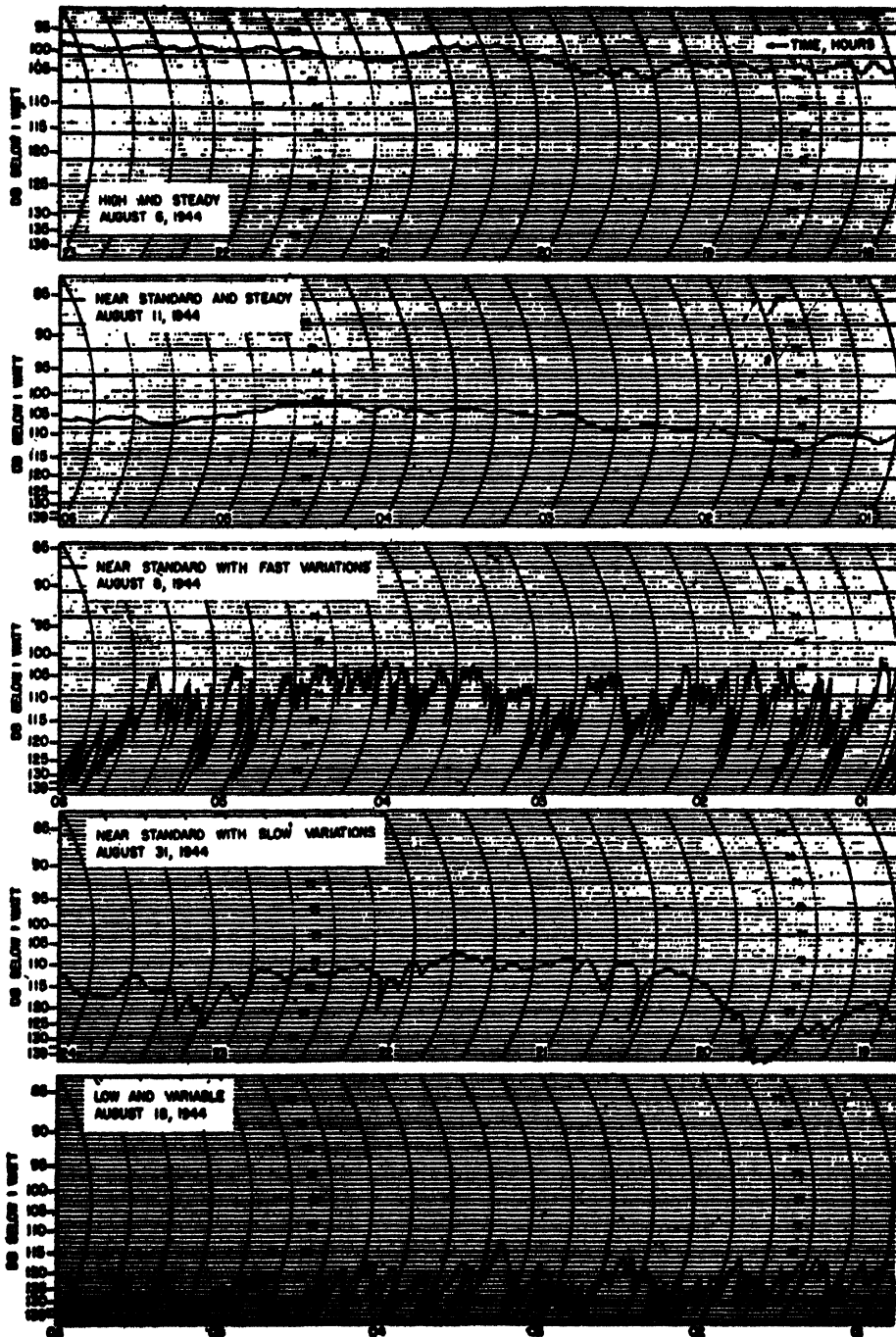
FIGURE 3. Signal types at 256 cm (117 mc).
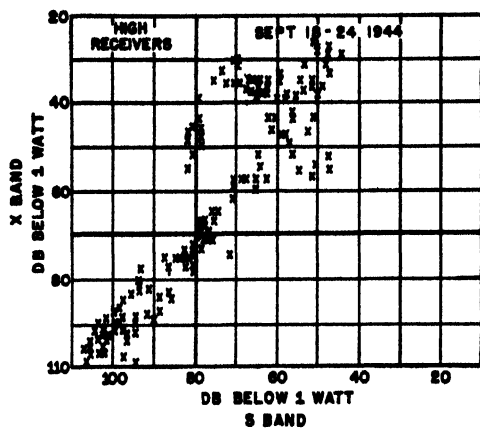
FIGURE 4. Relation between S- and X-band signal strengths.
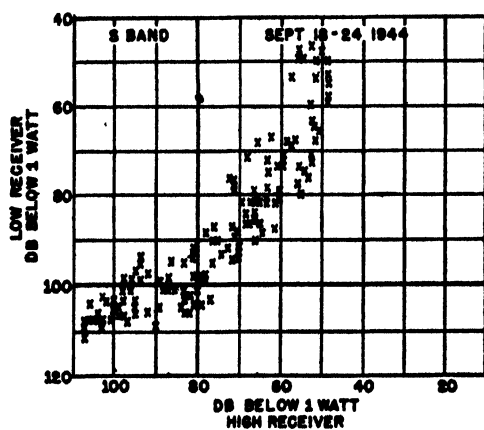
FIGURE 5. Relation between signal strengths at high and low receivers.
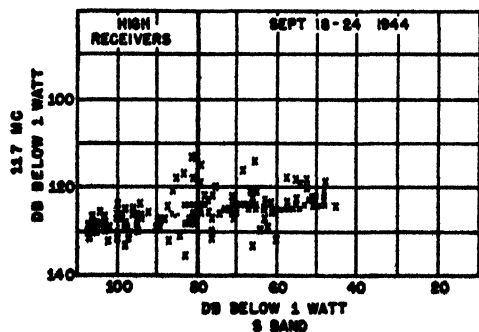
FIGURE 6. Relation between 117-mc and S-band signal strengths.
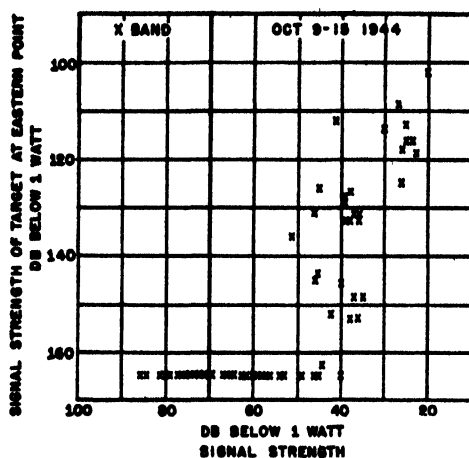
FIGURE 7. Relation between one-way and radar transmission, Race Point to Eastern Point.
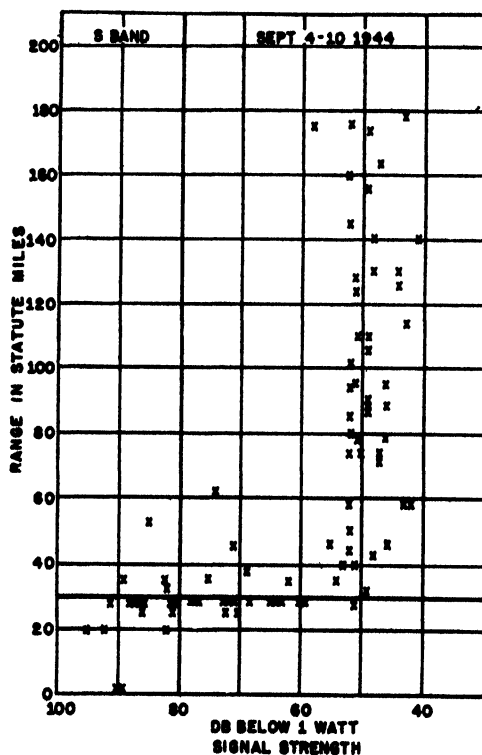
FIGURE 8. Relation between maximum radar ranges and one-way transmission.
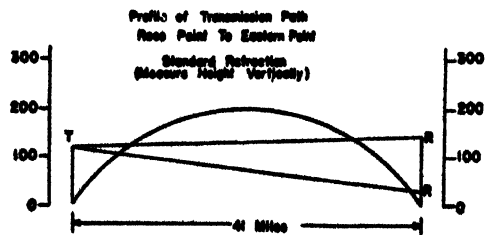
FIGURE 9. Transmission path profiles. (Heights in feet.)
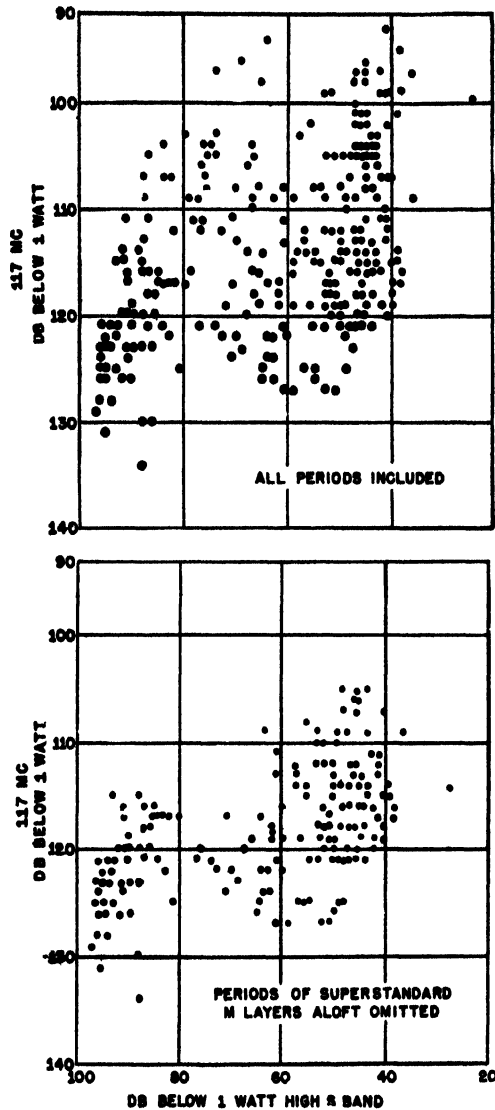
FIGURE 10. Field strengths: 117 mc and S band, July 31 to August 17, 1944.
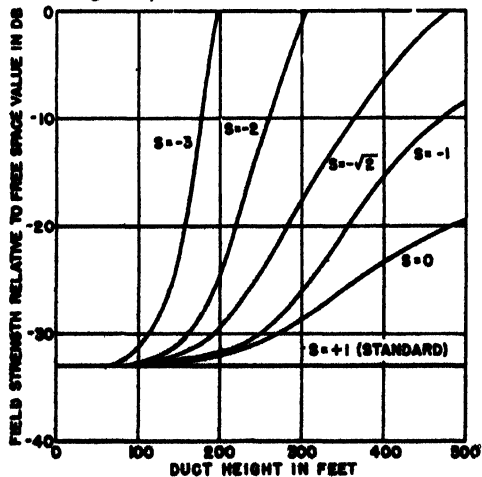
FIGURE 11. Theoretical field strength versus duct height, bilinear index, first mode, 117 mc.
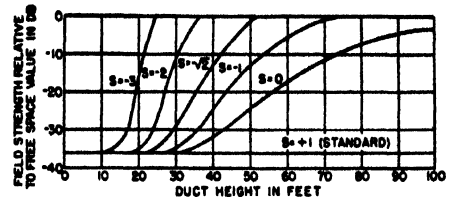
FIGURE 12. Theoretical field strength versus duct height, bilinear index, first mode, high S band.
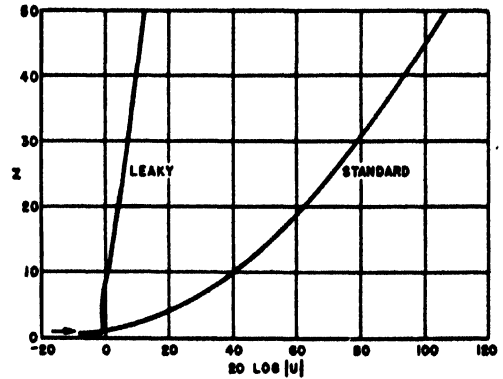
FIGURE 13. Height-gain functions, standard and leaky first modes. (Ordinate: height. Abscissa: gain.)
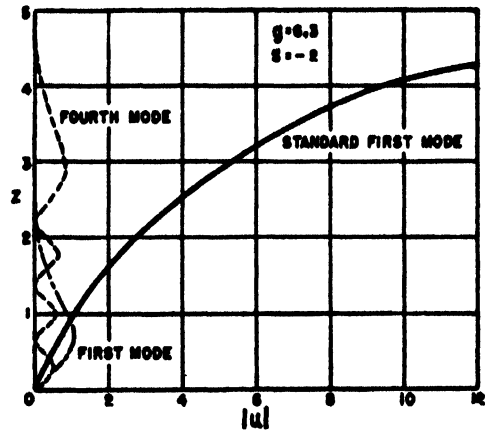
FIGURE 14. Height-gain functions within a duct compared with standard first mode. (Ordinate: height. Abscissa: gain.)
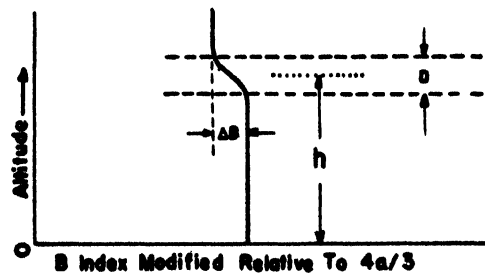
FIGURE 15. Modified index B.
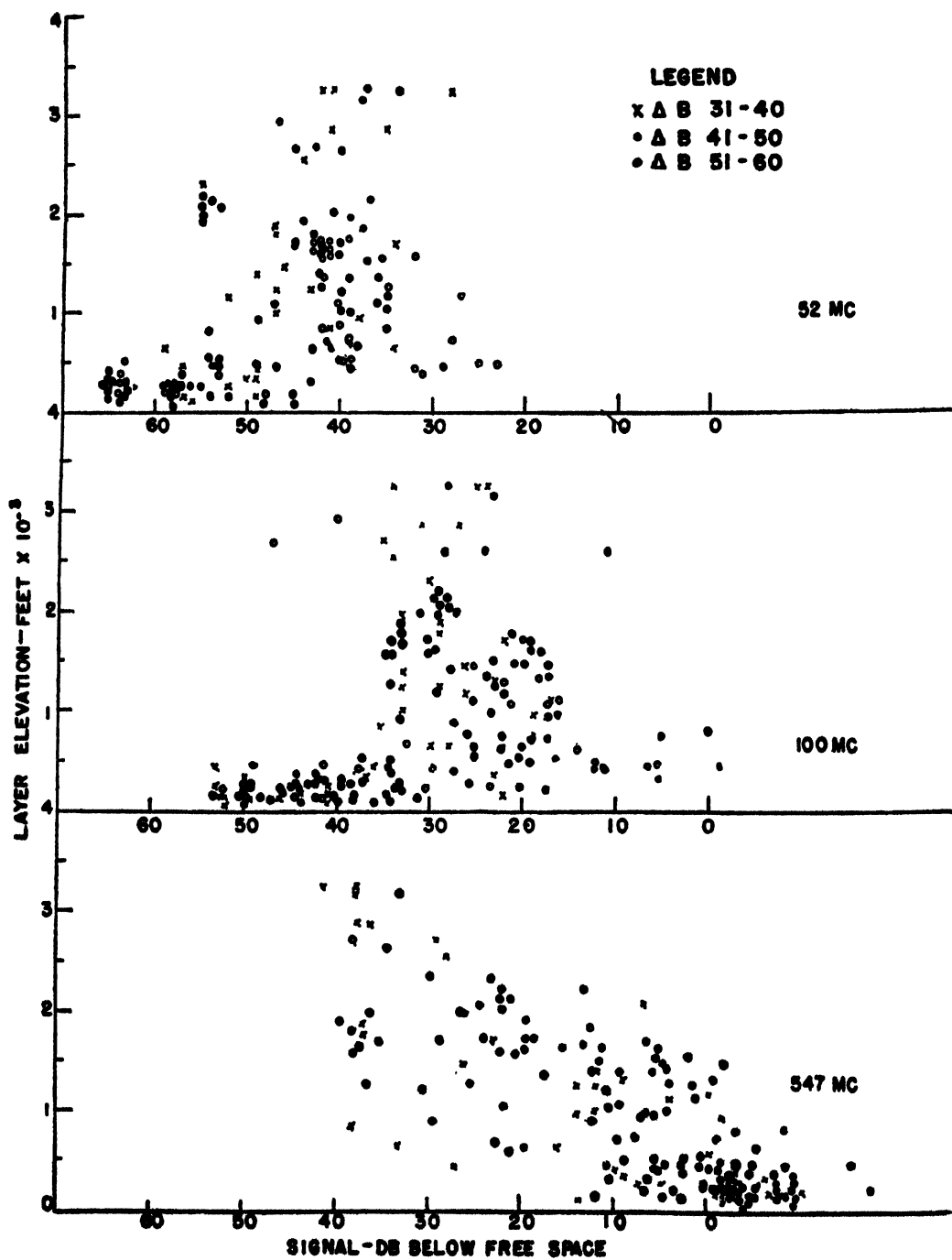
FIGURE 16. Signal versus layer elevation.

NEAR SAN DIEGO

FIGURE 1.   Maximum received signal versus atmospheric refraction.

FIGURE 2.   Maximum received signal versus altitude of base of temperature inversion.

FIGURE 3.   Maximum signal and fading range related to height of base of temperature inversion.
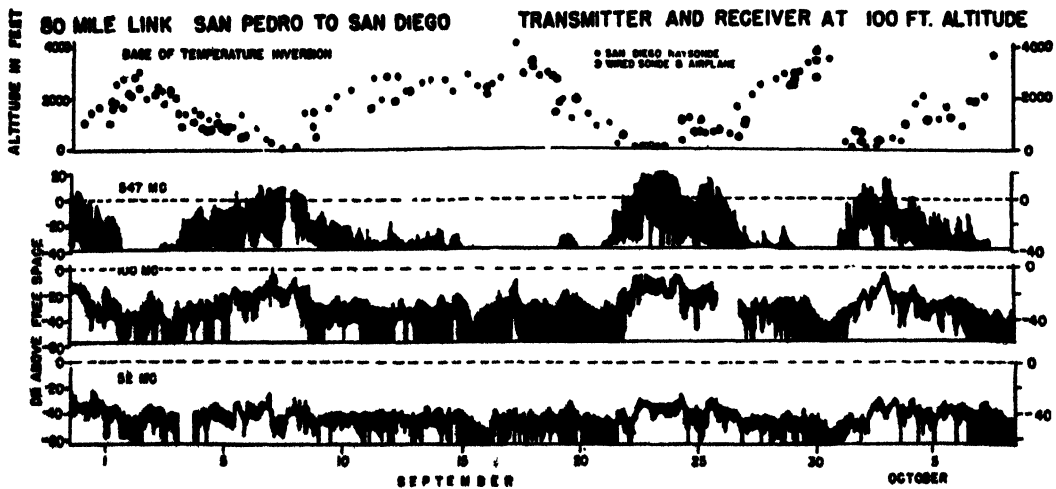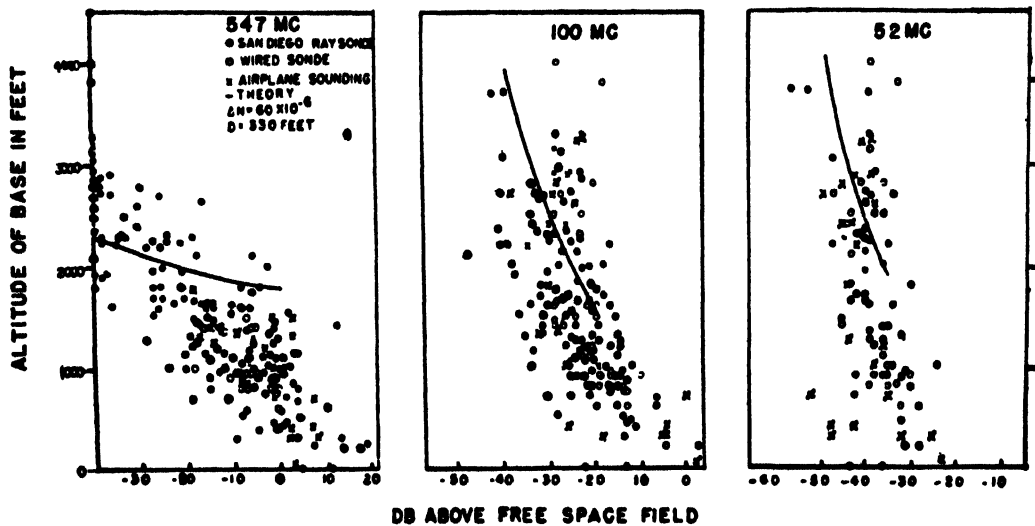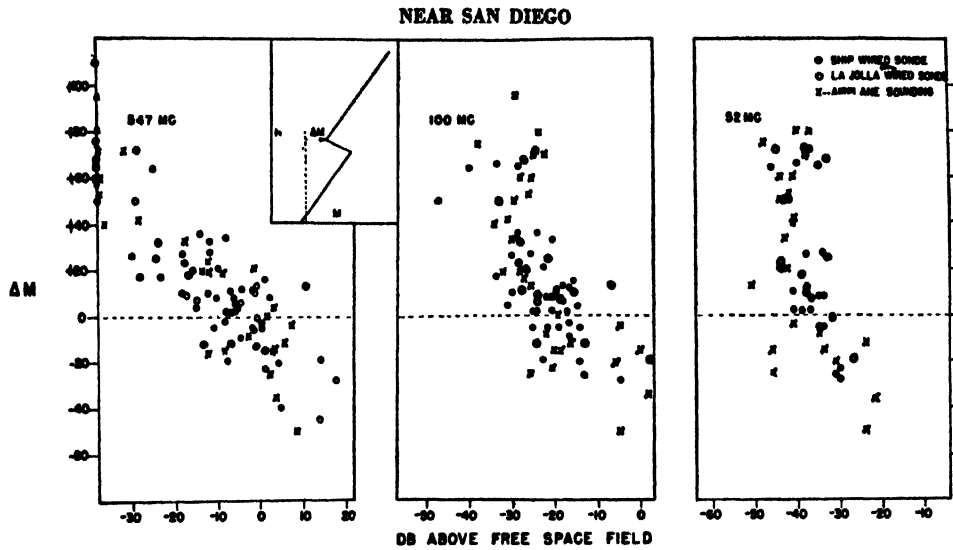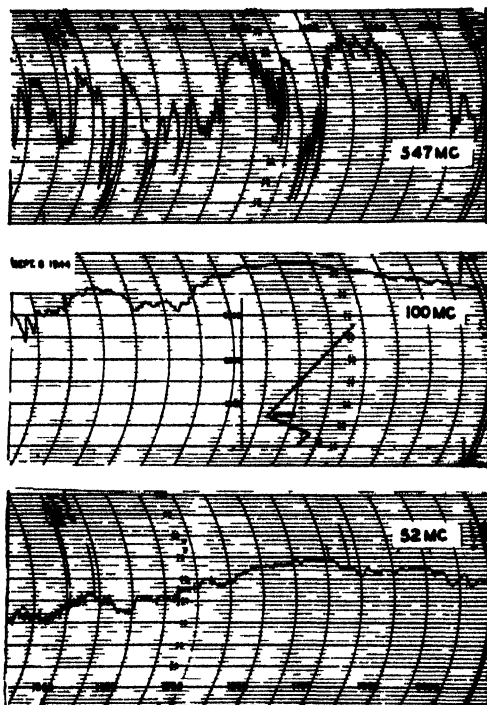
FIGURE 4   Signal types on one-way link for low inversion (trapping)

FIGURE 6   Number of modes trapped

FIGURE 5.   Signal types for high inversion   Note the low level of the 547-mc signal.
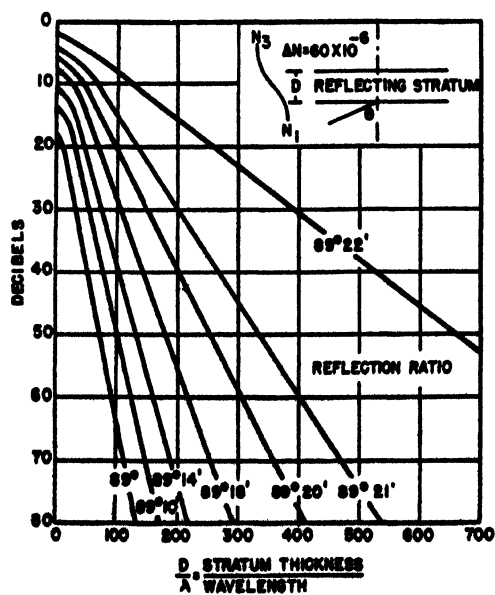
FIGURE 7   Reflection ratio.
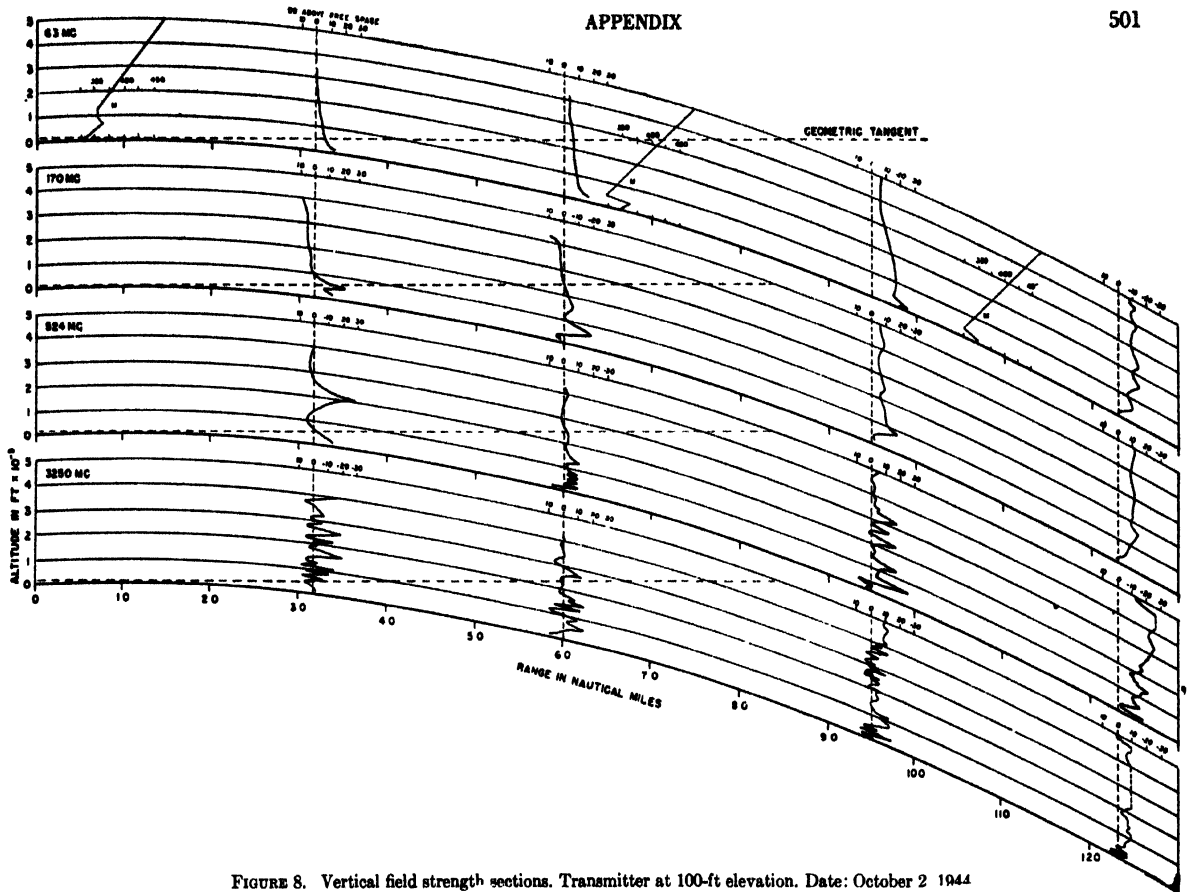
FIGURE 8. Vertical field strength sections. Transmitter at 100-ft elevation. Date: October 2 1944
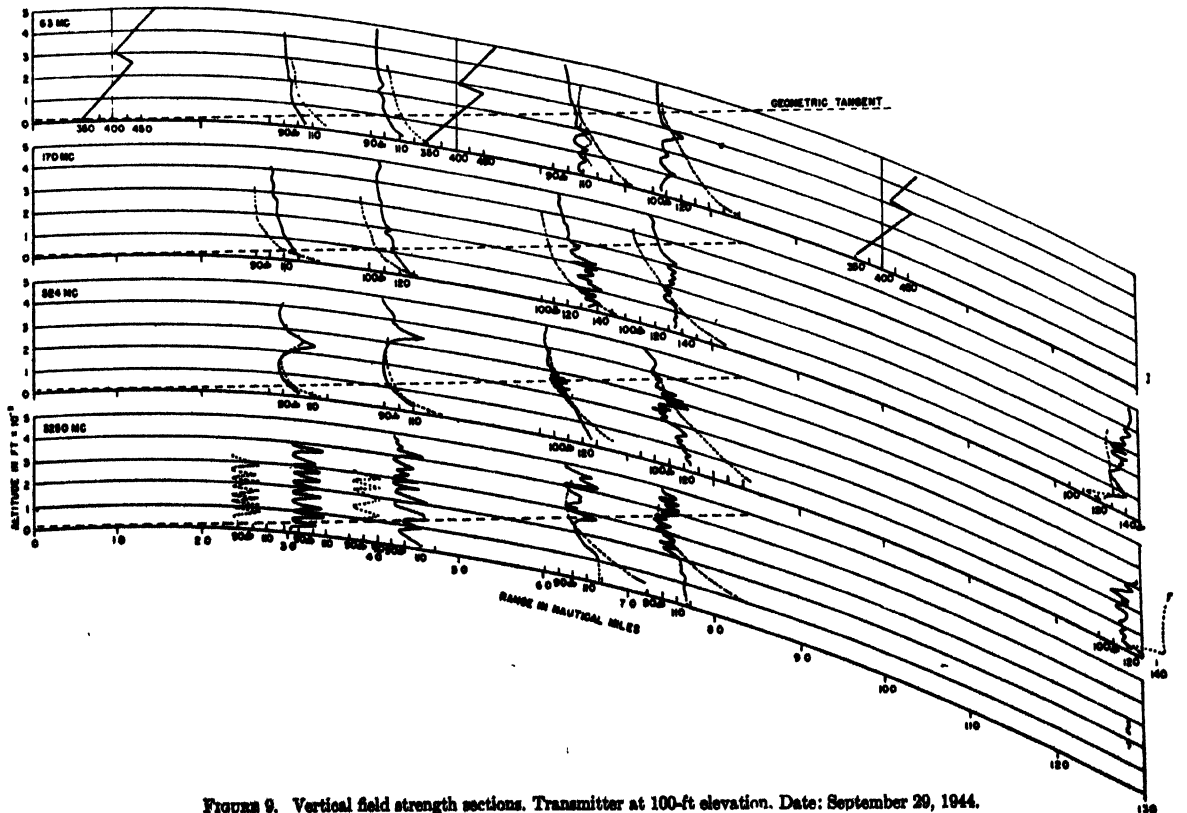
FIGURE 9. Vertical field strength sections. Transmitter at 100-ft elevation. Date: September 29, 1944.
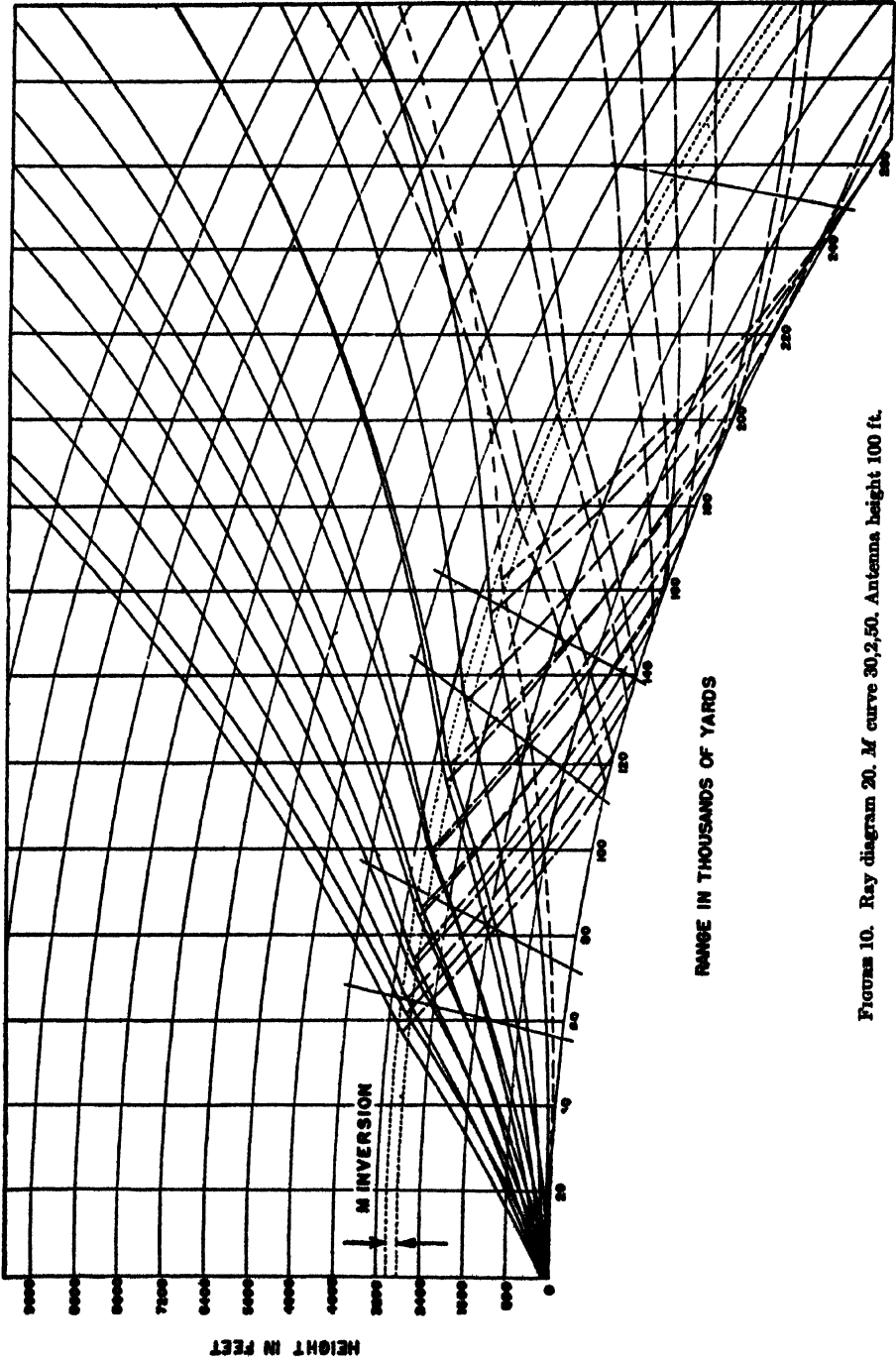
FIGURE 10. Ray diagram 20. M curve 30,2,50. Antenna height 100 ft.

ARIZONA
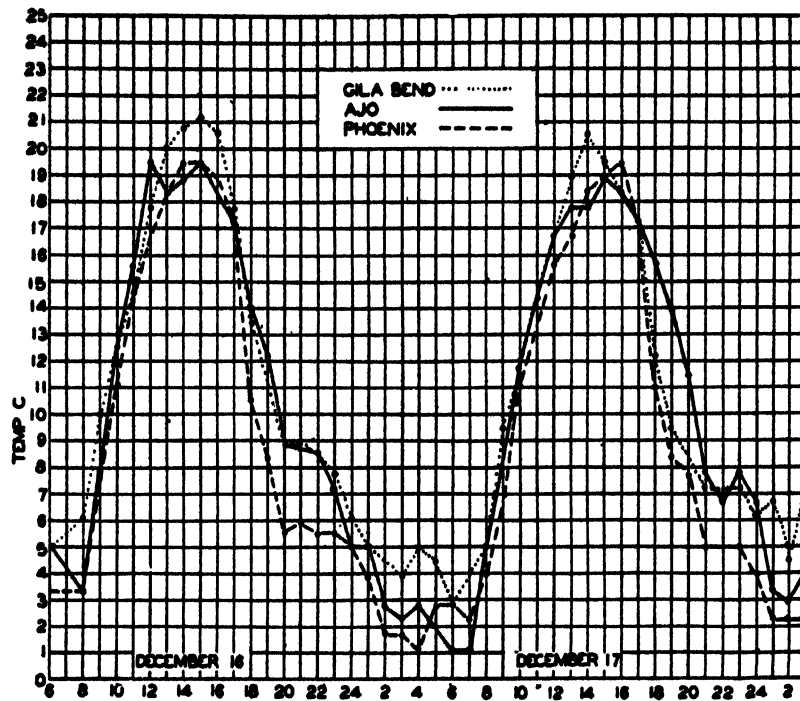
FIGURE 1. Surface air temperatures at Ajo, Gila Bend, and Phoenix, December 16 to 17, 1944.
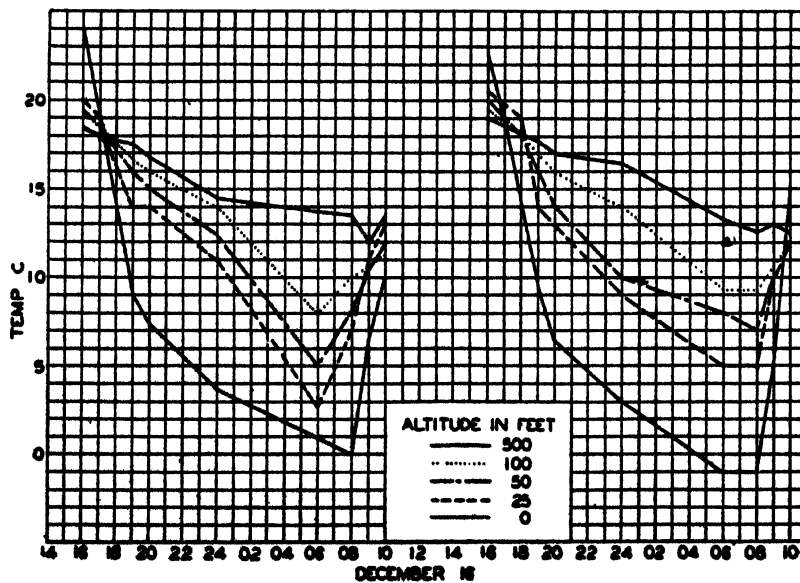
FIGURE 2. Soil and air temperatures at Datelan, December 16 to 17, 1944.

APPENDIX

TABLE 1

Date	Time of sunrise	Signal below detection, time	Cloud condition	Soil temperature	Time of sunset	Signal first detected, time	Cloud condition	Soil temperature
12/13	0653				1655		Few cirrus	1800 13C
12/14	0654	0845	0800 Clear	0800 3.1C	1656	1615	1730 Overcast Altostratus Cirrostratus	2000 9.0C
12/15	0655	0945	0800 Scattered low clouds Scattered middle clouds Scattered altostratus	0800 2.0C	1656	1715	1600 Scattered cirrus	1700 19.4C
12/16	0655	0925	0800 Overcast High cirrus	0900 6.4C	1656	1725	1700 Scattered cirrus	1700 19.3C
12/17	0656	0940	0900 Scattered cirrus	0900 5.3C	1656	1730	Few cirrus	1700 17.9C
12/18	0656	0950	0900 Clear	0900 6.0C	1657	1738	1700 Scattered cirrus and altostratus	2000 8.5C
12/19	0657	0923	0900 Clear	0900 8.8C	1657	1628	1700 Scattered cirrus	1630 20.8C
12/20	1658	0910	0900 Clear	0900 8.7C	1658			

FIGURE 3. Typical field strength and modified index curves, December 16 to 17, 1944.

ANTIGUA, WEST INDIES

Figure 3.

Figure 6.

Figure 2.

Figure 5

Figure 1.

Figure 4.

FIGURE 7. Mean temperature and mixing ratio curves.
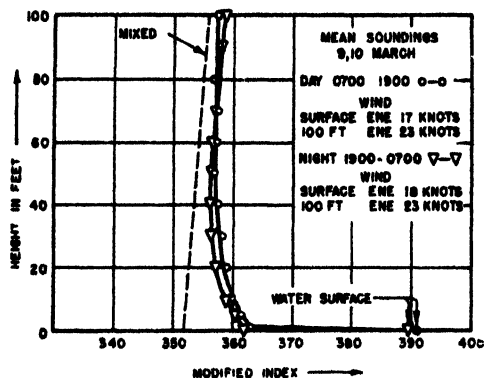
FIGURE 8. Mean modified index curves
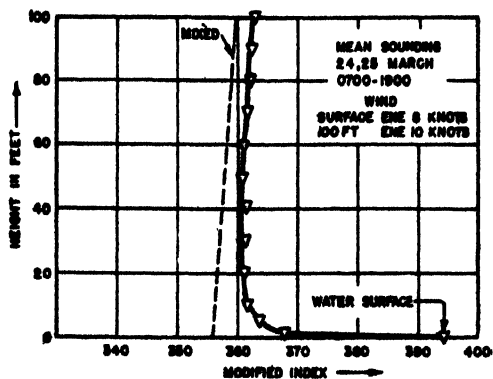
FIGURE 9. Mean sounding during low winds.
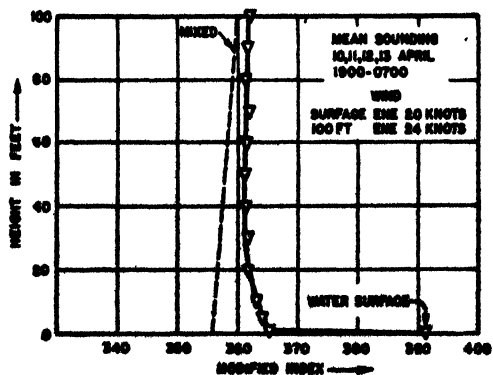
FIGURE 10. Mean sounding during high winds.
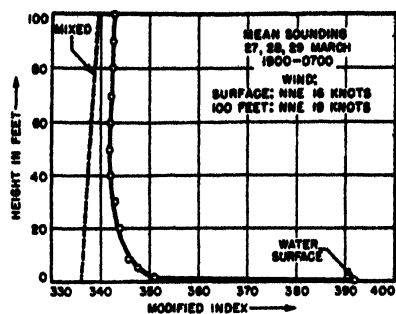
FIGURE 11. Mean soundings during an influx of dry air.
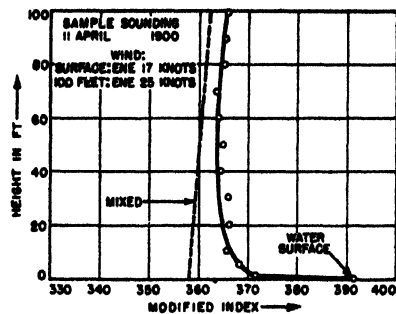
FIGURE 12. Mean soundings during an influx of moist air.
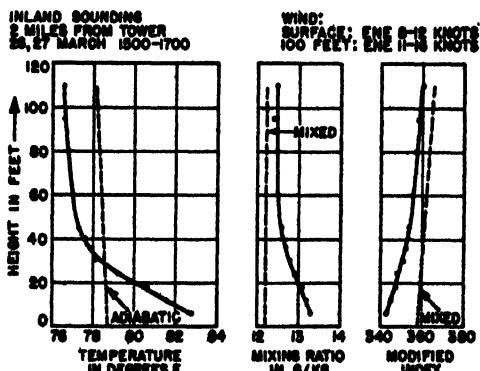
FIGURE 13. Inland soundings.
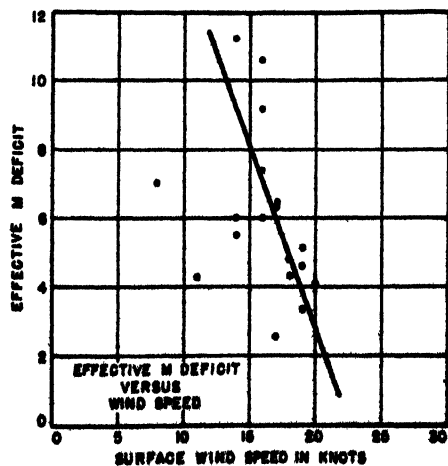
FIGURE 14. M deficit versus wind speed.
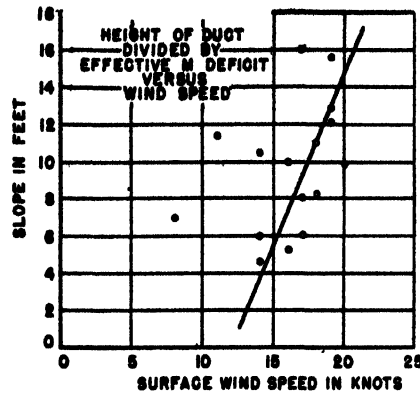
FIGURE 15. Effective M-curve slope versus wind speed.
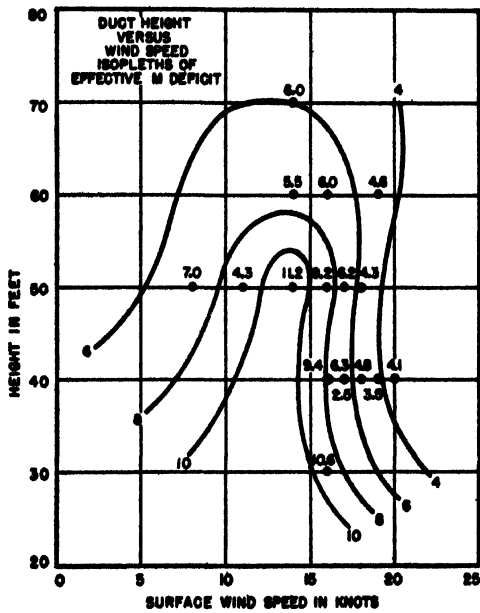
FIGURE 16. Height of M deficit versus wind speed.

FIGURE 18. Composite S-band run field strengths.

FIGURE 17. Total M deficit versus wind speed.
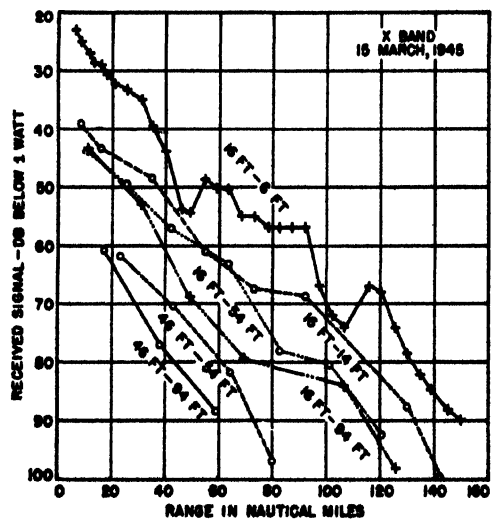
FIGURE 19. Composite X-band run field strengths.

FIGURE 20. Composite X-band run field strengths.

FIGURE 21. Radar echo strength versus range for various antenna heights.

ENGLAND

FIGURE 1 General view of the equipment in Aberdaron, North Wales.

TABLE 1

Station	Height, ft
S. Wales (transmitters)	
A. Garn-Fawr	540
B. Strumble Head	90
N. Wales (receivers)	
C. Rhiw	825
D. Aberdaron	95
Scotland (receivers)	
E. Knockharnahan	375
F. Portpatrick	95
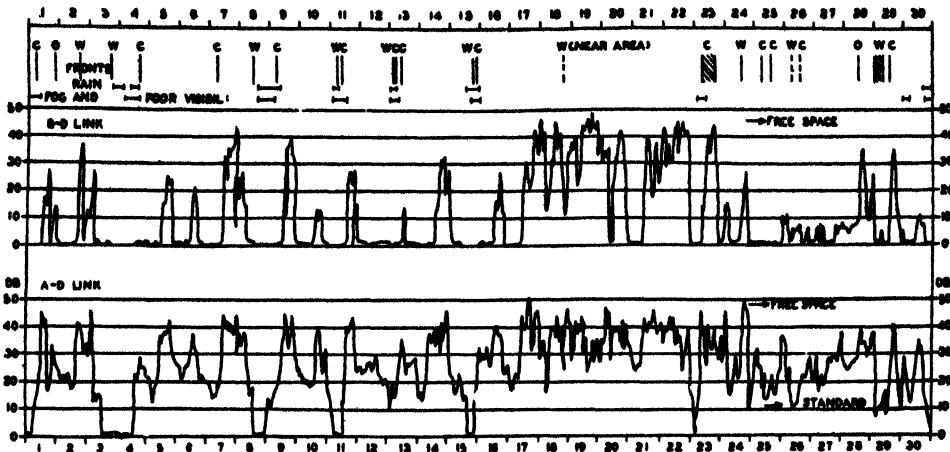
FIGURE 2. Signal strength in decibels above 1 μv receiver input, June 1944, drawn from hourly mean values.
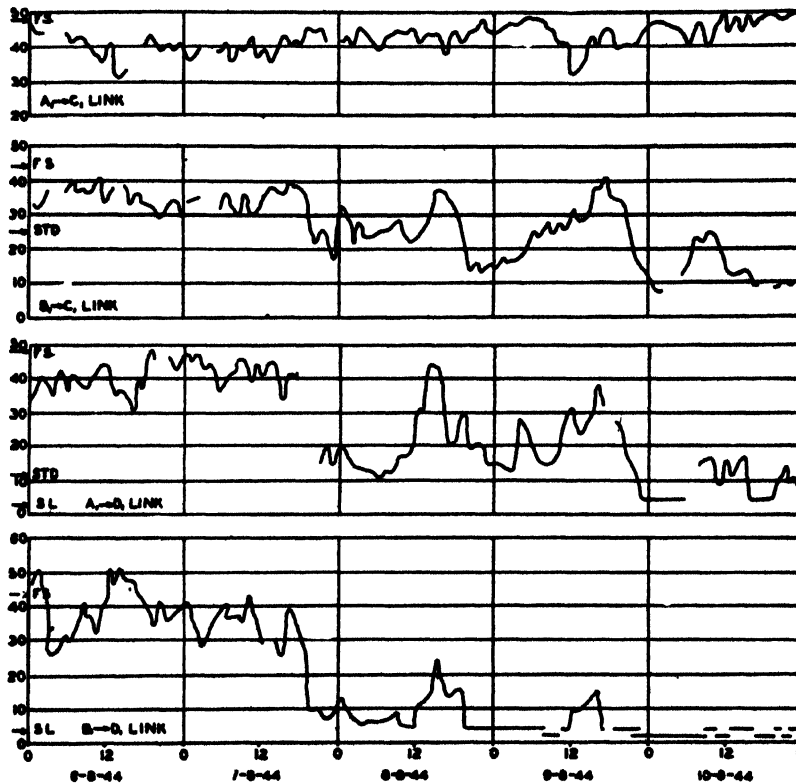
FIGURE 3. Signal strength in decibels above 1 μv receiver input. FS: Free space signal. STD: Standard signal. SL: Sensitivity limit.
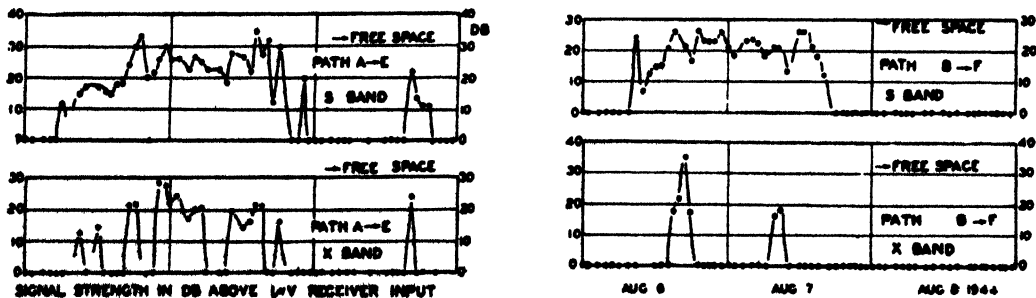
FIGURE 4. Hourly mean values of signal strength on S and X band.

FIGURE 7. Signal records. (C) June 20 to 21, 1944. Strong NE winds, little cloudy. (D) August 28. Cloudy in the early morning changing into continuous rain, then clearing with freshening SW wind. (E) Shown passage of a warm front on May 4, 1944, at 5.30 p.m. followed by a cold front 1 hr later.

TABLE 2. Transmission path lengths.

Path	AC	BC	AD	BD	AE	AF	BE	BF
Distance in units of optical range	0.90	1.21	1.40	2.40	3.82	4.92	5.63	8.45
Distance (miles)		57				200		
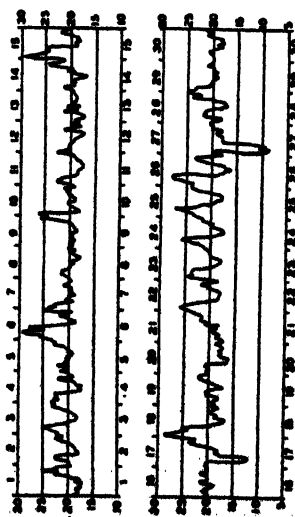
FIGURE 5. Whitwell Hatch to Wembley path, March 1944 S-band hourly mean intensities in decibels above 1 μv receiver input.

TIME IN HOURS GMT →
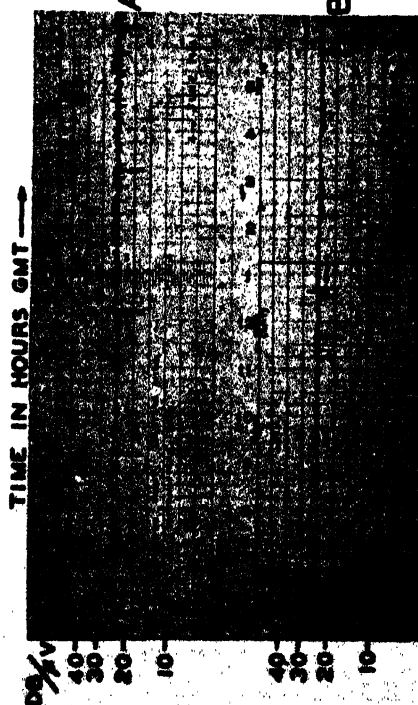
FIGURE 6. Signal records. (A) June 4, 1944 from midnight till noon. Weather cloudy, light W wind, intermittent rain (B) June 11, 1944, 6 a.m. to 6 p.m. Weather clear in the morning, later cloudy; light W wind, intermittent rain.

FIGURE 8. Signal records. (F) August 25, 1944, dip in record coincides with low mist (G) August 14, 1944, shows effect of low fog. (H) January 15, 1944, typical for widespread, thick fog.

TIME IN HOURS GMT→
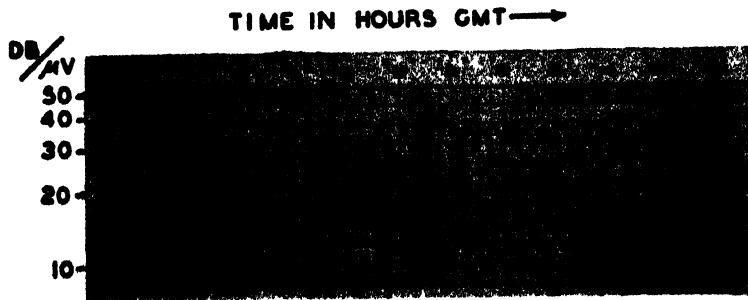
FIGURE 9. Signal record. August 26 to 27, 1944, showing examples of interference fading in radiation nights.

TABLE 1

Forecasting system	No. of cases examined	% of correct forecasts
$(de/d\lambda)$ term	600	56
Continuity method	600	57
$(dT/d\lambda)$ term	150	75

GLOSSARY

$a.$ 1) Radius of the earth
  2) Radius of scattering plate, sphere, or cylinder

$A.$ Gain factor $= A_\phi A \rho$

$A_\phi.$ Gain factor for doublet antennas in free space, adjusted for maximum transfer of power $= 3\lambda/8\pi d$

$A_1.$ Plane-earth factor

$A_P.$ Path-gain factor

$\bar{A}.$ Gain-factor curve parameter

$b.$ $b = \dfrac{d_1 - d_2}{d_1 + d_2}$

$B.$ Bandwidth

$c.$ 1) Velocity of light in free space
  2) $c = \dfrac{h_1 - h_2}{h_1 + h_2}$

$C, C(v).$ Real part of Fresnel's integral

$d.$ Distance from center of transmitting antenna to a point in space measured along earth surface

$d_\phi.$ Free-space distance for field of strength E

$d_\bullet.$ Normalized free-space distance $= \dfrac{d_0}{d_T}$

$d_1, d_2.$ Distance from transmitter, receiver to reflecting point measured along the earth's surface

$d_T, d_R.$ Distance from transmitter, receiver to the radio horizon measured along the earth's surface

$d_L.$ Line of sight distance measured along the earth's surface $= d_T + d_R$

$d_{max}.$ Maximum radar range

$D.$ 1) Divergence factor for spherical earth
  2) Aperture of reflector

$e.$ 1) Water-vapor pressure
  2) Coefficient for height-gain function

$E.$ Electric-field strength

$E_\phi.$ Maximum free-space field strength of a doublet transmitter at distance d

$E_1.$ Radiation field strength at one meter from transmitter

$f.$ 1) Frequency
  2) Focal length of paraboloid reflector

$f_c.$ Cutoff frequency of a wave guide

$f(h).$ Height-gain function

$f_n.$ Height-gain function for the nth mode

$F_1, F_2.$ Fraction of maximum radiation field strength in the direction of direct, reflected rays

$F_n.$ Noise figure

$F_s.$ Shadow factor for all modes

$g.$ 1) Receiver gain
  2) Exponential factor of height-gain function for elevated antennas

$g'.$ Correction to $g(2)$

$G_t.$ Transmitting antenna gain

$G_s.$ Receiving antenna gain

$G_R.$ Radar gain of a target

$h.$ Height above ground

$h_1, h_2.$ Height of transmitter, receiver above ground

$h_1', h_2'.$ Height of transmitter, receiver above tangent plane at point of reflection

$h_\phi.$ Critical height distinguishing high and low antennas located in diffraction region $= 30\lambda^{2/3}$

$h_s.$ Virtual height of obstructing screen

$H.$ 1) Magnetic field strength
  2) Height of a reflecting or diffracting obstruction

$H_L.$ Height-gain function for low antennas

$HA.$ Hour angle of the sun

$I.$ RMS current

$I_i.$ Input current to antenna or circuit

$j.$ $\sqrt{-1}$

$k.$ 1) Boltzmann's constant
  2) Factor multiplying earth's radius to account for atmospheric refraction

$K.$ 1) Amplitude of generalized reflection coefficient
  2) *Echo constant* of a target

$l.$ 1) Length of a doublet
  2) Height coefficient to include effect of earth's constants and wavelength

$L.$ 1) Effective length of a doublet
  2) Characteristic length or scattering coefficient of a target
  3) Radar length of a target

$m.$ 1) Ratio of radius of curvature of a ray to the radius of the earth $= \rho_\cdot'a$
  2) $m = \dfrac{d^2}{4ka(h_1 + h_2)}$

$M.$ Modified index of refraction

$n.$ 1) Index of refraction
  2) Number of elements in an antenna array

n', n'' Lobe numbers

$N.$ Lobe variable for imperfect reflection

$NF.$ Noise figure

$p.$ 1) Total pressure of the atmosphere
  2) Dimensionless parameter $= d_1/d_T$

$p'.$ Distance coefficient to include earth constants

$P.$ Power

$P_1.$ Power output of a transmitting doublet

$P_2.$ Power delivered by a receiving doublet to a matched load

$P_{min}.$ Minimum power detectable by a receiver

$P_n.$ Noise power

$P_r.$ Power received by load circuit of receiving antenna

$P_s.$ Scattered power

$q.$ Dimensionless parameter $= d_2/d$

$Q.$ Parameter determining phase of beam reflected by the earth $= \dfrac{\epsilon_r}{60\sigma\lambda}$

$r.$ 1) Distance from center of antenna to a point in space (usually replaced by d in applications)
  2) Height wavelength factor
  3) Pattern or chart parameter
  4) Path length of reflected ray

$r_d.$ Path length of direct ray

$R.$ 1) Resistance
  2) Plane-earth reflection coefficient $= \rho e^{-j\phi}$
  3) Path-difference parameter $= (ka\Delta)/(h_1 d_T)$

$R_a.$ Resistive component of antenna impedance

$RH.$ Relative humidity in per cent

$R_l.$ Resistive component of load impedance

$R_r.$ Radiation resistance of an antenna

$s.$ 1) Spacing between dipoles in an antenna array
  2) Coefficient of distance for shadow factor
  3) Dimensionless coordinate $= d_1/d$

$S.$ 1) Scattering cross section
  2) Area

$S, S(v).$ Imaginary part of Fresnel's integral

$t.$ 1) Time
  2) Pulse width
  3) Degrees centigrade

$T.$ Absolute temperature

$u.$ Dimensionless coordinate $= h_2/h_1$

$v.$ 1) Velocity of wav · propagation $= c/n$
2) Argument of Fresnel's integral
3) Dimensionless parameter $= d/d_T$

$V.$ Voltage

$V_n.$ Noise voltage

$W.$ Power per unit area

$W_i.$ Incident power per unit area

$W_r.$ Scattered power per unit area at the receiver

$z.$ Amplitude of ratio of diffracted field to free-space field

$Z.$ Impedance

$Z_a.$ Antenna impedance

$Z_l.$ Load impedance

$\alpha.$ 1) Attenuation constant, real part of propagation constant γ
2) Angle made by ray with the horizontal

$\alpha_1, \alpha_2.$ Angle of elevation of diffracting edge as seen from transmitter, receiver

$\beta.$ 1) Bearing of the sun
2) Phase constant, imaginary part of propagation constant γ

$\beta_1, \beta_2.$ Angle between ray from transmitter, receiver, and horizontal at diffracting edge

$\gamma.$ 1) Propagation constant $= \alpha + j\beta$
2) Angle between horizontal at base of transmitter and line joining transmitter base to receiver

$\gamma_1.$ Angle between the direct ray and the horizontal at the transmitter

$\delta.$ 1) Declination of the sun
2) Angle of phase retardation due to path-length difference between direct and reflected rays
3) Ground parameter depending on complex dielectric constant

$\Delta.$ Path-length difference between direct and reflected rays $= r - r_d$

$\Delta_\rho.$ $= (2h_1 h_2)/d$

$\Delta(\Delta_\rho).$ Correction factor for Δ_ρ

$\Delta f.$ Bandwidth

$\eta.$ Variable used in diffraction region

$\epsilon_0.$ Dielectric constant of free space
$= 8.854 \times 10^{-12} \cong \dfrac{1}{36\pi} 10^{-9}$

$\epsilon_c.$ Complex dielectric constant $= \epsilon_r - j\epsilon_i$

$\epsilon_i.$ Imaginary part of dielectric constant $= 60\sigma\lambda$

$\epsilon_r.$ Real part of dielectric constant

$\zeta.$ 1) Phase-angle lag due to diffraction
2) Dimensionless distance variable for curved-earth diffraction

$\theta.$ 1) Angle between horizontal at transmitter base and horizontal at point of reflection
2) Angle of tilt of scattering cylinder

$\lambda.$ Wavelength

$\mu_0.$ Permeability of free space $= 4\pi 10^{-7}$

$\mu_r.$ Permeability relative to free space

$\nu.$ Angle between reflected ray and horizontal at transmitter

$\rho.$ 1) Radius of curvature
2) Amplitude of reflection coefficient

$\sigma.$ 1) Conductivity
2) Radar cross section

$\tau.$ 1) Complex mode numbers
2) Half beam-width angle

$\phi.$ 1) Phase angle of reflection coefficient
2) Latitude

ϕ' $= \phi - \pi =$ phase angle of reflection coefficient relative to a perfect reflector

Φ_1 Distance function for the first mode

$\psi.$ 1) Phase-angle difference between currents in dipole-antenna array
2) Angle between direct or reflected ray and the horizontal at the reflection point
3) Height variable in the diffraction region

$\psi_d.$ Angle between direct ray and horizontal at reflection point

$\omega.$ Angular velocity $= 2\pi f$

$\Omega.$ Total phase lag between direct and reflected rays $= \phi' + \delta = \phi - \pi + \delta$

MASSACHUSETTS BAY

1. *Microwave Transmission over Water and Land under Various Meteorological Conditions*, Pearl J. Rubenstein, I. Katz, L. J. Neelands, and R. M. Mitchell, OEMsr-262, Division 14 Report 547, RL, June 13, 1944. CP-311-M4

2. *Meteorological Equipment for Short Wave Propagation Studies*, Walter M. Elsasser, Report WPG-3, CUDWR, August 1944.

3. *Atmospheric Refraction, A Qualitative Investigation*, Lloyd J. Anderson, F. P. Dane, J. P. Day, R. F. Hopkins, L. G. Trolese, and A. P. D. Stokes, BuShips Problem X4-49CD, Report WP-17, NRSL, Dec. 28, 1944.   CP-222-M9

NEAR SAN DIEGO

1. *Transmission of Plane Waves Through a Single Stratum Separating Two Media* (Part II), John B. Smyth, BuShips Problem X4-49CD, Report WP-13, NRSL, June 23, 1944.
CP-221-M9

2. *Proceedings of the Institute of Radio Engineers*, R. C. Colwell, **27**, October 1939, pp. 626-634.

3. *Procedure and Charts for Estimating the Low Level Coverage of Shipborne 200-Mc Radars under Conditions of Pronounced Refraction*, F. R. Abbott, Lloyd J. Anderson, F. P. Dane, J. P. Day, R. U. F. Hopkins, John B. Smyth, L. G. Trolese, and A. P. D. Stokes, BuShips Problem X4-49CD, Revised Report WP-11, NRSL, Revised May 10, 1944.   CP-202.32-M1

4. *The Mechanical Determination of the Path Difference of Rays Subject to Discontinuities in the Vertical Gradient of Refractive Index*, F. R. Abbott, BuShips Problem X4-49CD, Report WP-10, NRSL, Mar. 10, 1944.
CP-222.1-M3

5. *Calibration and Standardization of Land Based Radars by the Use of Small Plane Targets*, F. R. Abbott, BuShips Problem X4-49CD, Report WP-12, NRSL, June 10, 1944.
CP-612.5-M1

ARIZONA

1. *New Theoretical Consideration on the Dielectric Properties of the Atmosphere*, F. Hoyle, Third Conference on Propagation, Washington, D. C. on November 16-18, 1944, NDRC CUDWR-WPG, 1945, pp. 26-30.   CP-100-M4

ENGLAND

1. *Reviews of Progress of Ultra Short Wave Propagation Work, Part I, The Evaluation of Solutions of the Wave Equation for a Stratified Medium*, D. R. Hartree, OSRD WA-2961-2, Report AC-7017, USWP, Sept. 26, 1944.   CP-110-M2

2. *Reviews of Progress of Ultra Short Wave Propagation Work, Part II, Statement of Work in Progress Relevant to Investigations of the Propagation of Radio Waves Through the Troposphere.* R. L. Smith-Rose, OSRD WA-3005-2, Report AC-7018, NPL Report, USWP, Sept. 25, 1944.
CP-110-M3

3. *Reviews of Progress of Ultra Short Wave Propagation Work, Part III, Microwave Propagation Research at the Signals Research and Development Establishment*, OSRD 3156-7, Report AC-7019, USWP, Sept. 26, 1944.   CP-110-M4

4. *Reviews of Progress of Ultra Short Wave Propagation Work, Part IV, Correlation of Radar Operational Data with Meteorological Conditions*, OSRD WA-3156-8, Report AC-7020, AORG Report, USWP, Sept. 28, 1944.
CP-110-M5

5. *Reviews of Progress of Ultra Short Wave Propagation Work, Part V, Progress Report on Forecasting of Radar Conditions*, OSRD 3156-9, Report AC-7021, DMO-USWP, Oct. 2, 1944.   CP-110-M6

6. *Reviews of Progress of Ultra Short Wave Propagation Work, Part VI, Vertical,Temperature and Humidity Gradients at Rye*, OSRD WA-3156-10, Report AC-7022, DMO-USWP, Oct. 2, 1944.   CP-110-M7

7. *Reviews of Progress of Ultra Short Wave Propagation Work, Part VII, The Use of Radar for the Detection of Storms*, OSRD WA-3156-11, Report AC-7023, DMO-USWP, Oct. 2, 1944.   CP-110-M8

8. *Reviews of Progress of Ultra Short Wave Propagation Work, Part VIII, Present States of Theoretical Study of Radio Propagation Through the Troposphere by the Mathematics Group, Telecommunications Research Establishment*, OSRD WA-3156-12, Report AC-7024, Oct. 2, 1944. CP-110-M9

9. *Reviews of Progress of Ultra Short Wave Propagation Work, Part IX, Review of Short-Period Experimental Studies of Centimeter Wave Propagation, Carried Out Jointly by Admiralty Signal Establishment, Signals Research and Development Establishment, and General Electric Company*, E. C. S. Megaw, OSRD WA-3156-13, Report AC-7025, USWP, Oct. 16, 1944.   CP-110-M10

10. *Reviews of Progress of Ultra Short Wave Propagation Work, Part X, Study of Centimeter Wave Propagation over Cardigan Bay to Mount Snowden*, F. Hoyle, OSRD WA-3157-1, Report AC-7026, USWP, Oct. 14, 1944.
CP-110-M11

11. *Reviews of Progress of Ultra Short Wave Propagation Work, Part XI, Study of Reflection Coefficient of the Sea at Centimeter Wavelengths*, F. Hoyle, OSRD WA-3157-2, Report AC-7027, USWP, Oct. 14, 1944.   CP-110-M12

12. *Reviews of Progress of Ultra Short Wave Propagation Work, Part XII, Some K-, X-, and S-Band (Llandudno) Trials, General Summary of the Experimental Results Obtained which are Concerned with the Dependence of Radio Propagation on Meteorological Conditions*, OSRD WA-3157-3, Report AC-7028, TRE and RRDE Report, USWP, Oct. 14, 1944.   CP-110-M13

13. *Reviews of Progress of Ultra Short Wave Propagation Work, Part XIII, Progress Report on 369 Trials by DNMS*, OSRD WA-3156-1, Report AC-7029, USWP, Oct. 14, 1944.   CP-110-M14

14. *Reviews of Progress of Ultra Short Wave Propagation Work, Part XIV, Survey of Progress in the United Kingdom on the Electromagnetic Theory of Tropospheric Propagation*, OSRD WA-3157-4, Report AC-7030, RRDE-USWP, Oct. 16, 1944.   CP-110-M15

15. *Reviews of Progress of Ultra Short Wave Propagation Work, Part XV, Study of Meteorological Factors Responsible for the Refractive Structure of the Troposphere*, OSRD WA-3157-5, Report AC-7031, RRDE-USWP, Oct. 16, 1944.
CP-110-M16

16. *Centimeter Wave Propagation over Land, Preliminary Study of the Field Strength Records Between March and Sept., 1943*, R. L. Smith-Rose and A. C. Stickland, OSRD WA-1514-6, Report RRB/S-13, DSIR, Nov. 15, 1943. CP-333-M1

17. *Centimeter Propagation over Land, A Study of the Field Strength Records Obtained During the Year 1943-1944*, Report RRB/S-18, NPL-MO DSIR, May 11, 1944.
CP-224-M11

BIBLIOGRAPHY

VOLUME 1

Inquiries concerning the availability of microfilmed[a] and other reference material should be addressed to the War Department Library, Room 1A-522. The Pentagon, Washington 25, D. C., or to the Office of Naval Research, Navy Department, Attention: Reports and Documents Section, Washington 25, D. C.

1. *Notes on Microwave Propagation Conference at MIT,* *Radiation Laboratory,* Division 14 Report 42, RL, Sept. 24, 1943.　　　　　　　　　CP-100-M1

2. *International Radio Propagation Conference* [held at Inter-service Radio Propagation Laboratory, from April 17 to May 5, 1944], Report IRPL-C61, National Bureau of Standards, June 1944.　　　　　CP-100-M3

3. *Report of Second Propagation Conference, February 10 to 11, 1944 at the Empire State Building, New York,* OEMsr-1207, NDRC CUDWR-WPG, February 1944.
　　　　　　　　　　　　　　　　CP-100-M2

4. *Scientific Investigations on Propagation Problems in the Southwest Pacific Area,* F.W.G. White, OSRD II-5-6124(S), ATP [Australian Radio Propagation Committee], July 24, 1944.　　　CP-110-M1

5. *The Air Defense System of the Near Islands,* Thomas J. Carroll, Report OAD-55, U.S. Army Air Forces, Eleventh Air Force, OCSO, Operational Analysis Division, Aug. 30, 1944.　　　　　　　　　CP-202.1-M5

6. *Reviews of Progress of Ultra Short Wave Propagation Work,* [USWP]:

　6a. [Part] *I, The Evaluation of Solutions of the Wave Equation for a Stratified Medium,* D. R. Hartree, OSRD WA-2961-2, JEIA 5934, RDF 239, Report AC-7017, Sept. 26, 1944.　　　　　　　CP-110-M2

　6b. [Part] *II, Statement of Work in Progress Relevant to Investigations of the Propagation of Radio Waves Through the Troposphere,* R. L. Smith-Rose, OSRD WA-3005-2, Report AC-7018, NPL, Sept. 25, 1944.　　CP-110-M3

　6c. [Part] *III, Microwave Propagation Research at the Signals Research and Development Establishment,* OSRD WA-3156-7, JEIA 6464, Report AC-7019, SRDE, Sept. 26, 1944.　　　　　　　CP-110-M4

　6d. [Part] *IV, Correlation of Radar Operational Data with Meteorological Conditions,* OSRD WA-3156-8, JEIA 6463, Report AC-7020, AORG, Sept. 28, 1944.　CP-110-M5

　6e. [Part] *V, Progress Report on Forecasting of Radar Conditions,* OSRD WA-3156-9, JEIA 6462, Report AC-7021, DMO, Oct. 2, 1944.　　CP-110-M6

　6f. [Part] *VI, Vertical Temperature and Humidity Gradients at Rye,* OSRD WA-3156-10, JEIA 6461, Report AC-7022, DMO, Oct. 2, 1944.　　CP-110-M7

　6g. [Part] *VII, The Use of Radar for the Detection of Storms,* OSRD WA-3156-11, JEIA 6460, Report AC-7023, DMO, Oct. 2, 1944.　　　CP-110-M8

　6h. [Part] *VIII, Present States of Theoretical Study of Radio Propagation, Through the Troposphere by the Mathematics Group, TRE,* OSRD WA-3156-12, JEIA 6459, Report AC-7024, TRE, Oct. 2, 1944.　CP-110-M9

　6i. [Part] *IX, Review of Short-Period Experimental Studies of Centimetre Wave Propagation, Carried Out Jointly by ASE, SRDE, and GEC,* E. C. S. Megaw, OSRD WA-3156-13, JEIA 6458, Report AC-7025, Oct. 16, 1944.
　　　　　　　　　　　　　　　　CP-110-M10

　6j. [Part] *X, Study of Centimètre Wave Propagation over Cardigan Bay to Mount Snowdon,* F. Hoyle, OSRD WA-3157-1, Report AC-7026, Oct. 14, 1944.　CP-110-M11

　6k. [Part] *XI, Study of Reflection Coefficient of the Sea at Centimetre Wavelengths,* F. Hoyle, OSRD WA-3157-2, Report AC-7027, Oct. 14, 1944.　CP-110-M12

　6l. [Part] *XII, Some K-, X-, and S-Band (Llandudno) Trials, General Summary of the Experimental Results Obtained which are Concerned with the Dependence of Radio Propagation on Meteorological Conditions,* OSRD WA-3157-3, Report AC-7028, TRE and RRDE, Oct. 14, 1944.
　　　　　　　　　　　　　　　　CP-110-M13

　6m. [Part] *XIII, Progress Report on 369 Trials by Director, Naval Meteorological Service,* OSRD WA-3156-1, JEIA 6466, RDF 240, Report AC-7029, Oct. 14, 1944.
　　　　　　　　　　　　　　　　CP-110-M14

　6n. [Part] *XIV, Survey of Progress in the United Kingdom on the Electromagnetic Theory of Tropospheric Propagation,* OSRD WA-3157-4, Report AC-7030, RRDE, Oct. 16, 1944.　　　　　　　CP-110-M15

　6o. [Part] *XV, Study of Meteorological Factors Responsible for the Refractive Structure of the Troposphere,* OSRD WA-3157-5, Report AC-7031, RRDE, Oct. 16, 1944.
　　　　　　　　　　　　　　　　CP-110-M16

7. *Report No. 1 of Project SWP-3.2 of the Office of Field Service,* Paul A. Anderson and P. Squires, OEMsr-728, Research Project PDRC-647, Washington State College, Nov. 2, 1944.　　　　　CP-335-M3

8. *Data on Super Refraction Supplied by Australian Radar Stations,* J. W. Reed, Report RP-229/1, CSIR-RL, Dec. 6, 1944.　　　　　　　　CP-223-M11

9. *Report No. 2 of Project SWP-3.2 of the Office of Field Service,* Paul A. Anderson and P. Squires, OEMsr-728, Research Project PDRC-647, Washington State College, Jan. 7, 1945.　　　　　CP-335-M3

10. *Third Conference on Propagation, Washington, D. C.* [on] *November 16 to 18, 1944,* NDRC CUDWR-WPG, 1945.
　　　　　　　　　　　　　　　　CP-100-M4

11. *Survey of Field of Radio Propagation and Noise with Special Reference to Australia,* F. J. Kerr, OSRD II-5-6572(S), JEIA 8641, Report RP-231, CSIR, Nov. 27, 1944.　　　　　　　　　CP-110-M17

12. *Fourth Conference on Propagation, Washington, D. C.* [on] *May 7* [to] *8, 1945,* NDRC CUDWR-WPG, 1945.

13. *Notes on Microwaves based upon a Series of Lectures by* W. W. Hansen, Samuel Seely and Ernest C. Pollard, Division 14 Report T-2, RL, Oct. 20, 1941. CP-201.1-M1

14. *An Introduction to Microwave Propagation,* Donald E. Kerr and Pearl J. Rubenstein, Division 14 Report 406, RL, Sept. 16, 1943.　　　　CP-201.1-M2

15. *Electrical Communication Systems Engineering, General Information,* Technical Manual TM-11-486, U. S. War Department, Feb. 25, 1944.　　　CP-204-M1
Superseded by TM-11-486, Apr. 25, 1945 and *Electrical Communication Systems Equipment,* TM-11-487, Oct. 2, 1944.

16. *Anomalous Propagation and the Army,* Thomas J. Carroll, Report ORB-P-18-1, OCSO, Mar. 4, 1944. CP-221-M12

17. *Principles of Radar,* Staff of MIT Radar School, June 15, 1944.　　　　　　　　　　CP-202-M1

18. *Radar Performance Testing Manual,* Manual 28, USAAF, Second Edition, July 1944.　　　CP-202.31-M1

19. *Effects of Site Conditions on Operation of Ground Radar Installations on Aerodromes,* J. L. Putnam, OSRD WA-4172-12, Report T-1305, TRE.　CP-202.31-M2

20. "The Diffraction of Electro-magnetic Waves from an Electrical Point Source Round a Finitely Conducting

[a] Numbers such as CP-100-M1 indicate that the document has been microfilmed

Sphere, with Applications to Radiotelegraphy and the Theory of the Rainbow," H. Bremmer and Balth.· Van Der Pol, *The London, Edinburgh, and Dublin Philosophical Magazine and Journal of Science*, **24**, July 1937, Part I, pp. 141-176; Supplement, **24**, November 1937, Part II, pp. 825-864; **25**, June 1938, Part III, pp. 817-837; **27**, March 1939, Part IV, pp. 261-275.

21. *Ultra Short Wave Propagation Curves, 0.1 to 10 Meters*, OSRD WA-1502-1a, Marconi Handbook, Marconi, Ltd., Mar. 28, 1940.   CP-211-M1

22. *Report on Signal Strength Curves Within the Visual Range*, OSRD WA-1463-1, Pamphlet RD-456, Marconi, Ltd., November 1940.   CP-211-M2

23. "The Effect of the Earth's Curvature on Ground-Wave Propagation," Chas. R. Burrows and Marion C. Gray, *Proceedings of the Institute of Radio Engineers*, **29**, January 1941, pp. 16-24.   CP-231.12-M5

24. "Ultra Short Wave Propagation," I. C. Schelling, Chas. R. Burrows, and E. B. Ferrell, *Proceedings of the Institute of Radio Engineers*, **21**, March 1933, pp. 427-463. (See reference 447.)

25. *Propagation Curves for Wavelengths of 13 Meters, Supplement to U. S. W. Propagation Curves RD-456*, Appendix RD-456A, Marconi, Ltd., November 1941. (See reference 22.)

26. "The Calculation of Ground-Wave Field Intensity over a Finitely Conducting Spherical Earth," K. A. Norton, *Proceedings of the Institute of Radio Engineers*, **29**, December 1941, pp. 623-639.

27. *Siting of Stations for Maximum Range*, H. G. Booker, OSRD II-5-1183, Report M/36, TRE, Feb. 9, 1942.   CP-231.11-M2

28. *Microwave Interference Patterns*, J. A. Stratton, Division 14 Report C-1, RL, Mar. 7, 1942.   CP-232.1-M1

29. *Theoretical Field Strength of Ten-Centimeter Equipment over a Spherical Earth*, H. G. Booker, OSRD WA-210-3j, Report M/45/HGB, TRE, July 1, 1942. CP-231.12-M1

30. *Atmospheric Refraction and Height Determination by RDF*, E. Eastwood, OSRD II-5-6511, JEIA 7773, Calibration Memorandum 54, RAF, July 6, 1942. (See reference 63.)   CP-211-M3

31. *Dependence of Range of Submarine Radar Equipment on Wave Length, Case 20564*, Chas. R. Burrows, Technical Memorandum MM-42-160-70, BTL, July 9, 1942.
                                                 CP-212-M1

32. *Transmission on 3000 Mc. over Sea Water*, J. A. Stratton, Division 14 Report C-2, RL, July 14, 1942. CP-232.1-M2

33. *Transmission on 100 Mc. over Sea Water*, J. A. Stratton, Division 14 Report C-3, RL, July 14, 1942.
                                                 CP-232.1-M3

34. *Transmission on 200 Mc. over Sea Water*, J. A. Stratton, Division 14 Report C-4, RL, July 14, 1942.
                                                 CP-232.1-M4

35. *Transmission on 500 Mc. over Sea Water*, J. A. Stratton, Division 14 Report C-5, RL, July 14, 1942.
                                                 CP-232.1-M5

36. *Interim Report on Propagation Within and Beyond the Optical Range*, C. Domb and M. H. L. Pryce, Report M-448, ASE, September 1942.

37. *Theoretical Ground Ray Field Strengths and Height Gain Curves for Wavelengths of 2 to 2000 Megacycles*, OSRD II-5-5274, Technical Report 883, Section E, BRL, September 1942.   CP-211-M4

38. *Siting for Long Range Aircraft Detection*, Thomas J. Carroll, Technical Report T-13, CESL, Revised Oct. 17, 1942.   CP-202.11-M1

39. *V.H.F. Field Strength Curves for Propagation within the Line of Sight*, G. J. Camfield, OSRD WA-570-3, Report Radio/279, Radio/s.2111/OPE 16, RAE, October 1942.
                                                 CP-211-M5

40. *Relation of Radar Range to Frequency and Polarization*, J. A. Stratton and Richard A. Hutner, Division 14 Report C-6, RL, Nov. 3, 1942.   CP-212-M2

41. *Propagation Curves [of] 1 to 10 Cm*, G. Millington, OSRD WA-1502-1c, Report TR-460, Marconi, Ltd., January 1943.   CP-211-M6

42. *Properties of the Diffracted Wave Field Intensity*, Richard A. Hutner and Elizabeth M. Lyman, Division 14 Report C-8, RL, Feb. 12, 1943.   CP-233-M7

43. *The Effect of Earth Curvature on the Performance Diagram of an RDF Station*, Report 29/R102/LGHH, TRE, Feb. 25, 1943.

44. *Radar Height Finding*, Richard A. Hutner, Helen Dodson, Jocelyn Gill, Bernard Howard, Francis Parker, and J. A. Stratton, Division 14 Report C-9, RL, Apr. 6, 1943.
                                                 CP-202.311-M1

45. *Technical Requirements of Ground Communications Interceptor Search Systems, Technical Requirements for Early Warning Radar Systems*, L. J. Chu and N. H. Frank, Division 14 Report TCAW-1 and -2, RL, May 10, 1943.
                                                 CP-202.1-M1

46. *Low-Angle Coverage of Early Warning Radar Systems*, N. H. Frank, Division 14 Report TCAW-3, RL, July 26, 1943.   CP-202.1-M2

47. *Factors Relating to the Design of an RDF Air Warning Set*, F. J. Kerr, OSRD II-5-5721, Report RP-187, CSIR-RL, Aug. 11, 1943.   CP-202.1-M3

48. *A Graphical Method of Computing the Bending of Radio Beams by the Effective Earth Radius Method*, Harry Raymond, Technical Report T-14, CESL, Aug. 27, 1943.
                                                 CP-231.12-M2

49. *Transmission at Low Altitudes over Sea Water*, Richard A. Hutner, Francis Parker, Bernard Howard, Helen Dodson, and Jocelyn Gill, Division 14 Report C-10, RL, Sept. 1, 1943.   CP-232.1-M6

50. *Radio-Frequency Propagation Above the Earth's Surface*, Paul F. Godley, Jr., OEMsr-895, Division 15 Report 895-5, RCA, Sept. 11, 1943.   CP-231.12-M3

51. *Field Intensity Formulas*, Richard A. Hutner, Helen Dodson, Jocelyn Gill, Francis Parker, and Bernard Howard, Division 14 Report C-11, RL, Sept. 28, 1943.
                                                 Div. 14-111-M8

52. *Note on Field Intensity Computations for Elevated Antennas, Case 20878*, Marion C. Gray, OSRD WA-1463-23 Technical Memorandum MM-43-110-28, BTL, Oct. 9, 1943.   CP-211-M7

53. *The Calculation of Expected Vertical Coverage Diagrams by Max Sherman, February 19, 1943*, revised by Walter S. McAfee, Technical Report T-17, CESL, Oct. 15, 1943.
                                                 CP-211-M8

54. *Charts for Use in Field Intensity Computations*, K. Bullington, OEMsr-1018, Research Project C-79, NDRC Division 13 Preliminary Report 3460-KB-NF, Western Electric Company, Inc., Nov. 2, 1943.   CP-211-M9

55. *Notes on Visibility Problems, Taking Account of the Curvature of the Earth*, OSRD WA-1368-19, Report 152, AORG, Dec. 1, 1943.   CP-231.12-M4

56. *Simplified Methods of Field Intensity Calculations in the Interference Region*, William T. Fishback, Division 14 Report 461, RL, Dec. 8, 1943.   CP-211-M10

57. *Field Strength Near and Beyond the Horizon for Wavelengths of Ten and Thirty Cms.*, M/Report 53/WW, TRE, Dec. 24, 1943.

58. *Theoretical Field Strength Near and Beyond Horizon for Orthodox Propagation of Fifty Centimeter Waves*, OSRD WA-1976-5, Report T-1635/WW, TRE, Feb. 24, 1944.
                                                 CP-211-M11

59. *The Propagation Functions for an Atmosphere with Uniform Lapse-Rate of Refractive Index,* T. Pearcey, OSRD WA-2985-1, Research Report 256, RRDE, Sept. 1, 1944. CP-211-M12

60. *Propagation Curves* (third edition), NDRC Division 15 Report 966-6C, October 1944. CP-211-M13

61. *Field Strength Calculator for Vertical Coverage Patterns and Propagation Curves,* Clarence R. White, Technical Memorandum 154-E, CESL, Dec. 20, 1944. CP-211-M14

62. *Theory of the Vertical Field Patterns for RDF Stations,* J. C. Jaeger, OSRD II-5-4297, Report RP-174, CSIR-RL, Mar. 17, 1943. CP-213-M1

63. *Height, Range* [and] *Alpha Tables, Tables Relating to the Height, Range and Angle of Elevation of an Aircraft,* OSRD II-5-6512, JEIA 7766, Radar Memorandum 50, ORS-ADGB, Aug. 10, 1944. (See reference 30.) CP-213-M2

64. *The Calculation of Field Strength for Vertical Polarization over Land and Sea on 20 to 80 Megacycles per Second,* A. M. Woodward, OSRD WA-4395-11, Report T-1704, TRE. CP-211-M15

65. *Field Intensity Contours in Generalized Coordinates,* Helen Dodson, Jocelyn Gill, and Bernard Howard, OEMsr-262, Division 14 Report 702, RL, May 2, 1945. CP-211-M16

66. *The Limiting Ranges of RDF Sets over the Sea,* F. Hoyle and M. H. L. Pryce, OSRD WA-1514-17, Report M-395, ASE, 1943. CP-232.2-M2

67. *The Theory of Anomalous Propagation in the Troposphere and Its Relation to Waveguides and Diffraction,* H. G. Booker, OSRD WA-599-10, Report T-1447, M/60/HGB, TRE, Apr. 12, 1943. CP-221-M2

68. *The Tracing of Rays in the Refracting Atmosphere,* T. Pearcey, OSRD WA-645-42, Report AC-3878, ADRDE-USW, Apr. 21, 1943. CP-222-M2

69. *Graphical Construction of a Radar Radiation Pattern in a Stratified Atmosphere,* Lloyd J. Anderson and F. R. Abbott, BuShips Problem X4-49CD, Report WP-4 [for the period from] March 1, 1943 to May 1, 1943, NRSL, May 1, 1943. CP-232.2-M3

70. *Improved Tropospheric Propagation, Curves Embracing Anomalous Propagation,* H. G. Booker, OSRD II-5-4950, *Report T-1482,* M/65/HGB, TRE, July 6, 1943. CP-221-M3

71. *Radiation Patterns under Cases of Anomalous Propagation,* T. Pearcey, OSRD WA-830-8, Report R-35/TP, ADRDE, July 19, 1943. CP-221-M5

72. *Effect of Humidity Gradients in the Atmosphere on Propagation at RDF Frequencies,* Operational Research Report 22, AORG, July 28, 1943. CP-222.1-M2

73. *The Calculation of Field Strength Near the Surface of the Earth under Particular Conditions of Anomalous Propagation,* T. Pearcey, OSRD WA-931-6, Research Report 203, ADRDE, Oct. 28, 1943. CP-221-M6

74. *Anomalous Propagation over the Earth, Case 25703,* S. A. Schelkunoff, OSRD WA-1463-50, Report MM-43-110-33, BTL, Oct. 30, 1943. CP-221-M7

75. *The Effect of Atmospheric Refraction on Short Radio Waves,* John E. Freehafer, Division 14 Report 447, RL, Nov. 29, 1943. CP-222-M5

76. *Radar Ray Patterns Associated with Normal and Anomalous Propagation Conditions,* F. P. Dane, R. U. F. Hopkins, and Lloyd J. Anderson, BuShips Problem X4-49CD Report WP-6 [for the period from] November 1 to December 6, 1943, NRSL, Dec. 10, 1943. CP-221-M8

77. *Transmission of Plane Waves Through a Single Stratum Separating Two Media,* John B. Smyth, BuShips Problem X4-49CD, Report WP-9, NRSL, Dec. 22, 1943. CP-221-M9

78. *Notes on Theoretical Coverage Diagrams for Anomalous Propagation,* Donald E. Kerr, OSRD WA-1464-9, TM/Memorandum/14/AMW, TRE, Jan. 1, 1944. CP-221-M11

79. *The Dependence of Microwave Propagation over Sea on the Structure of the Atmosphere,* J. M. C. Scott and T. Pearcey, OSRD WA-1591-9, Memorandum 40, ADRDE, Feb. 4, 1944. CP-232.2 M8

80. *Improved Tropospheric Propagation, Curves Embracing Superrefraction* (revised edition), OSRD WA-1666-27, Report T-1625/WW, TRE, Feb. 18, 1944. CP-223-M1

81. *TRE Requirements for Propagation, Curves Embracing Superrefraction,* OSRD WA-1666-26, Report M/Memo-16/HAB, TRE, Feb. 25, 1944. CP-223-M2

82. *The Mechanical Determination of the Path Difference of Rays Subject to Discontinuities in the Vertical Gradient of Refractive Index,* F. R. Abbott, BuShips Problem X4-49CD, Report WP-10, NRSL, Mar. 10, 1944. CP-222.1-M3

83. *Improved Tropospheric Propagation, Curves Embracing Superrefraction,* OSRD WA-2026-2, Report T-1626/WW, TRE, Mar. 28, 1944. CP-223-M3

84. *Interservice Propagation, Curves Embracing Superrefraction, Dependence of Mathematical Parameter L on Physical Entities,* Report M/Memo-18/WW, TRE, Apr. 3, 1944. CP-223-M4

85. *Theoretical Coverage-Diagrams for 10 Cm. Radars Embracing Superrefraction,* JEIA 3229, Report T-1634, TRE, Apr. 14, 1944. CP-223-M5

86. *Theoretical Coverage-Diagrams for 50 Cm. Radars Embracing Superrefraction,* OSRD WA-1992-4, JEIA 3230, Report T-1659, TRE, Apr. 14, 1944. CP-223-M6

87. *Theoretical Coverage of Navigational Aids Embracing Superrefraction,* OSRD WA-1992-6A, Report T-1660, TRE, Apr. 14, 1944. CP-223-M7

88. *The Theory of Propagation of Radio Waves in an Inhomogeneous Atmosphere (Part I),* T. Pearcey, OSRD WA-2251-5, Research Report 245, ADRDE, April 1944. CP-221-M10

89. *Reflection Coefficient of Layers of Varying Refractive Index,* G. Millington, OSRD WA-2562-13, JEIA 4644, Report TR-483, BRL, April 1944. CP-222.1-M4

90. *Evaluation of the Solution of the Wave Equation for a Stratified Medium,* D. R. Hartree, P. Nicholson, N. Eyres, J. Howlett, and T. Pearcey, OSRD WA-2341-4, Memorandum 47, ADRDE, May 24, 1944. (See reference 108.) CP-221-M13

91. *Transmission of Plane Waves Through a Single Stratum Separating Two Media (Part II),* John B. Smyth, BuShips Problem X4-49CD, Report WP-13, NRSL, June 23, 1944. CP-221-M9

92. *Waves Guided by Dielectric Layers,* S. A. Schelkunoff, Report MM-44-110-52, BTL, July 5, 1944. CP-221-M14

93. *Microwave Transmission in Nonhomogeneous Atmosphere,* S. A. Schelkunoff, Report MM-44-110-53, BTL, July 5, 1944. CP-221-M15

94. *Contour Diagrams of the Radiated Field of a Dipole under Various Conditions of Anomalous Propagation,* T. Pearcey and F. Whitehead, OSRD WA-2985-2, Research Report 257, RRDE, July 15, 1944. (See reference 110.) CP-221-M16

95. *Theoretical Coverage-Diagrams for 1½-Meter Radars Embracing Super-refraction,* A. Woodward, OSRD WA-2854-2, Report T-1708, TRE, July 23, 1944. CP-223-M9

96. *Propagation Curves Embracing Super-refraction: SS Duct, Profile-Index 0.2* (Preliminary Edition), H. G. Booker, M/Memo-23/WW, TRE, Sept. 7, 1944. CP-223-M10

97. *A Note on the Reflection Coefficient of an Isotropic Layer of Varying Refractive Index,* G. Millington, OSRD WA-3172-1, JEIA 6481, Report TR-497, BRL, Oct. 5, 1944. CP-222.1-M5

98. *Predicted Low Level Coverage of S-Band Shipborne Radars as Affected by Weather*, F. R. Abbott, L. L. Whittemore, L. W. Cross, and E. J. Wyrostek, BuShips Problem X4-49CD, Report WP-14, NRSL, Nov. 1, 1944.
CP-232.2-M9

99. *Predicted Low Level Coverage of 200 MCS Band Shipborne Radars as Affected by Weather*, F. R. Abbott, L. L. Whittemore, L. W. Cross, and E. J. Wyrostek, BuShips Problem X4-49CD, Report WP-15, NRSL, Nov. 4, 1944.
CP-232.2-M10

100. *Variational Method for Determining Eigenvalues of Wave Equation of Anomalous Propagation*, G. G. Macfarlane, Report T-1756, TRE, Nov. 13, 1944.

101. *Wave Propagation Analysis with the Aid of Non-Euclidian Spaces*, Benjamin Liebowitz, OEMsr-1207, Report WPG-7, CUDWR, December 1944. CP-221-M18

102. *Atmospheric Waves, Fluctuations in High Frequency Radio Waves*, L. G. Trolese and John B. Smyth, BuShips Problem X4-49CD, Report WP-18, NRSL, Feb. 1, 1945.
CP-225-M1

103. *The Relation Between the Wave Equation and the Non-Linear First Order Equation of the Riccati Type*, T. L. Eckersley, OSRD WA-4223-7, JEIA 9104, Report TR-501, BRL, January 1945. (See ref. 111.) CP-221.1-M1

104. *A Report on Transmission of Waves over the Earth*, T. L. Eckersley, OSRD WA-4002-13, Report TR-504, BRL, January 1945. CP-221.1-M2

105. *New Convergent Integrals*, T. L. Eckersley, OSRD, WA-4002-11, Report TR-509, BRL, February 1945.
CP-221.1-M3

106. *The Effect of a Subrefracting Layer of Atmosphere upon the Propagation of Radio Waves*, T. Pearcey and M. Tomlin, OSRD WA-4016-28, JEIA 8371, Memorandum 83, RRDE, Feb. 12, 1945. CP-223-M13

107. *Theory of Characteristic Functions in Problems of Anomalous Propagation*, W. H. Furry, OEMsr-262, Division 14 Report 680, RL, Feb. 28, 1945. CP-221-M19

108. *The Evaluation of the Solution of the Wave Equation for a Stratified Medium* ([Part] *II*), D. R. Hartree, OSRD WA-4424-11, Research Report 279, RRDE, Mar. 12, 1945. (See reference 90.) CP-221-M20

109. *Theoretical Coverage Diagrams for 3-Meter Radars Embracing Super-refraction*, W. Walkinshaw and R. Hensman, OSRD WA-4320-7, JEIA 9198, Report T-1815, TRE, Mar. 18, 1945. CP-223-M12

110. *The Radiation Field of a Dipole under Various Conditions of Anomalous Propagation*, T. Pearcey, M. Tomlin, and F. Whitehead, OSRD WA-4392-7, Research Report 275, RRDE, Apr. 13, 1945. (See reference 94.) CP-221-M21

111. *Notes on the Solution of a Non-Linear First Order Equation of the Riccati Type*, T. L. Eckersley, OSRD WA-4428-7, JEIA 9725, Report TR-502, BRL, May 1945. (See reference 103.) CP-222.1-M6

112. *Perturbation Theory for an Exponential M-Curve in Non-Standard Propagation*, C. L. Pekeris, OEMsr-1207, Report WPG-12, CUDWR, July 1945. CP-221.1-M4

113. *Graphs for Computing the Diffraction Field with Standard and Superstandard Refraction*, Pearl J. Rubenstein and William T. Fishback, OEMsr-262, Division 14, Report 799, RL, Aug. 13, 1945. CP-222-M11

114. *Radio Interpretation of Meteorological Observations in the First Two Meters of Atmosphere Above Grass at Harlington, Middlesex, January to June, 1940*, OSRD WA-861-3, Report T-1471, M/63, TRE, June 1940. CP-222.1-M1

115. *Anomalous Echoes Observed with 10 Cm C.D. Set*, A. E Kempton, OSRD II-5-564, Research Report 119 ADRDE, Oct. 8, 1941. CP-623-M1

116. *Centimeter Wave Propagation over Sea Between High Sites just within Optical Range*, F. Hoyle and E. C. S. Megaw, OSRD WA-171-12, ASE-GEC, June 12, 1942.
CP-232.2-M1

117. *Centimeter Wave Propagation over Land (Part II), Measurements within and beyond Optical Range*, G. W. N. Cobbold, H. Archer-Thomson, and E. C. S. Megaw, Report AC-2917, Com. 136, SRDE-GEC, Oct. 16, 1942.

118. *Radar Wave Propagation*, Lloyd J. Anderson, John B. Smyth, F. R. Abbott, and R. Revelle, BuShips Problem X4-49CD, Report WP-2, NRSL, Nov. 30, 1942.
CP-623-M2

119. *Very Short Wave Interception and D.F.*, T. L. Eckersley, OSRD II-5-5276, Report TR-438, BRL, 1943.
CP-224-M2

120. *Anomalous Propagation of 10 Cm R.D.F. Waves over the Sea* (February 6, 1943); *First Supplement to Report 87* (July 26, 1943), OSRD WA-909-21, Report 87, AORG, July 26, 1943. CP-232.2-M5

121. *Investigation of Propagation Characteristics of A.W. Stations*, Report 17, AORG, Mar. 9, 1943. CP-332-M1

122. "A Study of Propagation over the Ultra-Short-Wave Radio Link between Guernsey and England on Wavelengths of 5 and 8 Meters (60 and 37.5 Mc/s)," R. L. Smith-Rose and A. C. Stickland, *The Journal of the Institution of Electrical Engineers*, OSRD WA-1463-31, NPL, Vol. 90, No. 9, March 1943, Part III. CP-224-M3

123. *The Effect of Atmospheric Refraction on the Propagation of Radio Waves*, A. C. Stickland, OSRD WA-623-19, Report RRB/S-10, NPL-RRB, Mar. 20, 1943. CP-222-M1

124. *Propagation of Ultra-Short Waves*, H. C. Webster, OSRD II-5-4575(S), Report 354, Australia, Apr. 17, 1943.
CP-224-M4

125. *Report on Radar Wave Propagation, Atmospheric Refraction, A Qualitative Investigation*, Lloyd J. Anderson and John B. Smyth, BuShips Problem X4-49CD, Report WP-5, NRSL, May 7, 1943. CP-222-M4

126. *Radio Interpretation of Meteorological Observations in the First 400 Feet Above Cardington, 1942*, OSRD WA-861-1, Report T-1413, M/61, TRE, May 14, 1943. CP-321-M1

127. *Centimeter Wave Propagation over Sea (Part II), Measurements from Shore Sites Near and Beyond Optical Range*, G. W. N. Cobbold, A. J. Jones, H. A. Bonnett, E. C. S. Megaw, H. Archer-Thomson, and E. M. Hickin, OSRD WA-792-10, Report 8180, GEC, May 27, 1943.
CP-232.2-M4

128. *Preliminary Observations on Radio Propagation at 6 Centimeters Between Beer's Hill, New Jersey, and New York, Case 37003-4, File 36691-1*, G. W. Gilman, Report MM-43-160-87, BTL, June 12, 1943. CP-224-M6

129. *Some Observations of Anomalous Propagation*, Report T-1483, M/64, TRE, July 6, 1943.

130. *Application of Anomalous Propagation to Operational Problems at Home and Abroad*, H. G. Booker, JMRP 3, Report T-1484, M/66/HGB, TRE, July 7, 1943.
CP-221-M4

131. *Propagation of Signals on 45.1, 474 and 2800 Mc from Empire State Building to Hauppauge and Riverhead, L.I., New York*. G. S. Wickizer and A. M. Braaten, OEMsr-691, NDRC Research Project 423, Division 14 Report 179, Report 1, RCA, July 20, 1943. CP-631-M1

132. *Propagation of Ultra Short Waves*, T. L. Eckersley, OSRD WA-1463-3, Report TR/476, Marconi, Ltd., August 1943. CP-224-M7

133. *The "K" Effect in Anomalous Propagation of Ultra-Short Waves*, F. Syer (RAAF), JMRP 11, Australian Paper 266, Report AC-4496, Australia, Aug. 10, 1943.
CP-224-M15

134. *The Propagation of 10 Cm Waves over Land Paths of 14, 52, and 112 Miles*, Paul A. Anderson, C. L. Barker, K. E. Fitzsimmons, and S. T. Stephenson, OEMsr-728, Research Project PDRC-647, Division 14 Report 202, Report 4, Washington State College, Oct. 26, 1943.
CP-224-M8

135. *The Propagation of 1-Cm Waves over the Sea as Deduced from Meteorological Measurements,* J. M. C. Scott and T. Pearcey, OSRD WA-1339-6, JMRP 4, Research Report 227, ADRDE, Nov. 11, 1943. CP-232.2-M6

136. *Centimeter Wave Propagation over Land, A Preliminary Study of the Field Strength Records between March and September 1943,* R. L. Smith-Rose and A. C. Stickland, OSRD WA-1514-6, JMRP 10, Paper RRB/S-13, DSIR-NPL, Nov. 15, 1943. CP-333-M1

137. *The Propagation of 10 Cm Waves over an Inland Lake, Correlation with Meteorological Soundings,* Paul A. Anderson, K. E. Fitzsimmons, and S. T. Stephenson, OEMsr-728, Research Project PDRC-647, Division 14 Report 212, Report 5, Washington State College, Nov. 12, 1943. CP-232.2-M7

138. *Measurements of Radar Wave Refraction and Associated Meteorological Conditions,* Lloyd J. Anderson and L. G. Trolese, Report WP-7, NRSL, Dec. 10, 1943. CP-222-M6

139. *Anomalous Propagation in India, Preliminary Report on Overland Transmission in Bengal,* H. G. Booker, OSRD II-5-6555(S), Report S-5, ORS-SEA, Dec. 30, 1943. CP-334-M1

140. *Atmospheric Physics, Summary of Investigations on Anomalous Propagation of Radar Signals Carried Out by the Australian Operational Research Group During 1942-43,* D. F Martyn, AORG, 1943. CP-221-M1

141. *The Cause of Short Period Fluctuations in Centimeter Wave Communication,* J. M. C. Scott, OSRD WA-1962-7 Memorandum 42, ADRDE, Mar. 8, 1944. CP-224-M10

142. *Anomalous Propagation in the Persian Gulf,* Naval Officer in Charge, Hormuz, OSRD WA-2146-23, Report AC-5975, USW, Received Mar. 20, 1944. CP-331-M4

143. *Effect of Super-refraction on Surface Coverage on Enemy 50-Cm and 80-Cm Radar Sets,* OSRD WA-2284-3, Report M/Memo-19 GGM, TRE, April 1944. CP-223-M8

144. *K-X-S Experiments, News Letter No. 1,* T. Gold, MK. 12201, ASE, May 3, 1944. CP-333.2-M1

145. *Abnormal Radar Propagation in the South Pacific, An Investigation into Conditions in New Zealand and Norfolk Island on 200 Mc/s. with Notes on Fiji, New Caledonia and Solomon Islands,* Air Department Wellington, File 135/14/10, Report 119, ORS-RNZAF, May 4, 1944. CP-335-M1

146. *Procedure and Charts for Estimating the Low Level Coverage of Shipborne 200-Mc Radars under Conditions of Pronounced Refraction,* F. R. Abbott, Lloyd J. Anderson, F. P. Dane, J. P. Day, R. U. F. Hopkins, John B. Smyth. L. G. Trolese, and A. P. D. Stokes, BuShips Problem, X4-49CD, Report WP-11, NRSL, Revised May 10, 1944. CP-202.32-M1

147. *Centimeter Propagation over Land, A Study of the Field Strength Records Obtained During the Year 1943-1944,* A. C. Stickland and R. W. Hatcher, JEIA 4789, Report RRB/S-18, NPL-MO, DSIR, May 11, 1944. CP-224-M11

148. *K-X-S Experiments, News Letter No. 2,* T. Gold, MK. 12201, ASE, May 13, 1944. CP-333.2-M1

149. *Atmospheric Propagation Effects and Relay Equipment,* Thomas J. Carroll, Report ORB-PP-12-1, OCSO, May 18, 1944. CP-311-M2

150. *Low-Level Coverage of Radars as Affected by Weather, Procedures and Charts,* Report IRPL-T2a, NRSL, May 25, 1944. (Reference 146 reprinted.)

151. *Variations in Radar Coverage,* Report JANP-101, Joint Communications Board, June 1, 1944. CP-202.4-M4 Earlier edition: IRPL T-1, CUDWR-WPG, May, 1944. CP-202.5-M1

152. *Effect of Atmospheric Refraction on Range Measurements,* G. G. Macfarlane, OSRD I-A-320, Report T-1688, TRE, June 12, 1944. CP-222-M7

153. *Microwave Transmission over Water and Land under Various Meteorological Conditions,* Pearl J. Rubenstein, I. Katz, L. J. Neelands, and R. M. Mitchell, OEMsr-262, Division 14 Report 547, RL, June 13, 1944. CP-311-M4

154. *Abnormal Propagation in W. A. C. for May and June, 1944.* Report 10, Canadian ORS-WAC, July 27, 1944.

155. *Propagation of Signals on 45.1, 474 and 2800 Mc from Empire State Building, N.Y.C. to Hauppauge and Riverhead, L.I., N.Y.,* G. S. Wickizer and A. M. Braaten, OEMsr-691, NDRC, Research Project 423, Division 14 Report 298, Report 2, RCA, July 31, 1944. CP-631-M1

156. *The Structure of the Electromagnetic Field During Conditions of Anomalous Propagation,* T. Pearcey and F. Whitehead, OSRD WA-3070-1, Research Report 258, RRDE, Sept. 19, 1944. CP-221-M17

157. *Tropospheric Propagation and Radio-Meteorology,* Report WPG-5, CUDWR-WPG, September 1944.

158. "Some Factors Causing Super-refraction on Ultra High Frequencies on South West Pacific," (Daily Report on Abnormal Echoes, RAAF Form 146 included in ATP 821), D. F. Martyn and P. Squires, Australian Ionosphere Bulletin, October 1944, Section 1.2. CP-224-M14

159. *Atmospheric Refraction, A Preliminary Qualitative Investigation,* Lloyd J. Anderson, F. P. Dane, J. P. Day, R. U. F. Hopkins, L. G. Trolese, and A. P. D. Stokes, BuShips Problem X4-49CD, Report WP-17, NRSL, Dec. 28, 1944. CP-222-M9

160. *Anomalous Propagation with High and Low Sited 3 Cm Ship Watching Radar Sets,* G. C. Varley, OSRD WA-4238-2, Report 250, AORG, Mar. 20, 1945. CP-232.2-M12

161. *Anomalous Propagation at English Coastal Radar Stations, March to September, 1944,* D. Lack, OSRD WA-4491-12, JEIA 9946, Report 258, AORG, May 30, 1945. (See also reference 6d.) CP-232.2-M13

162. *Lebanon-Beer's Hill Transmission on Wavelengths of 2.0 Meters, and 30 Centimeters, Case 20564,* A. B. Crawford, Report MM-39-326-98, BTL, Dec. 5, 1939. CP-224-M1

163. *Centimeter Wave Propagation over Land; Preliminary Trials,* G. W. N. Cobbold, H. A. Bonnett, A. J. Jones, E. C. S. Megaw, H. Archer-Thomson, A. S. Gladwin, and E. M. Hickin, Report 8045, GEC, Aug. 21, 1942.

164. *The Propagation of 10-Cm Waves on a 52-Mile Optical Path over Land, The Correlation of Signal Patterns and Radiosonde Data,* Paul A. Anderson, C. L. Barker, S. T. Stephenson, and K. E. Fitzsimmons, OEMsr-728, NDRC Research Project PDRC-647, Division 14 Report 151, Report 1, Washington State College, June 10, 1943. CP-224-M5

165. *Centimeter Wave Propagation over Sea Within and Beyond the Optical Range,* E. C. S. Megaw, H. Archer-Thomson, E. M. Hickin, and F. Hoyle, Report M-532, ASE, July 1943.

166. *Aden-Berbera V.H.F. Experiments, Final Report on Propagation Aspects,* E. W. Walker and S. R. Bickerdike, OSRD WA-2187-14, Report MS-4, SRDE, December 1942 and July 1943. CP-331-M1

167. *[Ultra Short Wave Communication], Investigation No. 369, Irish Sea Experiment,* OSRD WA-2146-18, -19, -20, -21, and -22; WA-2379-2, WA-2797-36, WA-3158-13; WA-3822-30; and -31. Or, as identified in Progress Reports AC-5970 Sept. 1, 1943, AC-5971 Dec. 14, 1943, AC-5972 Jan. 15, 1944, AC-5973 Feb. 9, 1944, AC-5974 Mar. 20, 1944, AC-6334 May 14, 1944, AC-6828 Aug. 12, 1944, AC-7206 Oct. 19, 1944, AC-7465 Nov. 10, 1944, and AC-7668 Jan. 4, 1945, British Ministry of Supply. CP-224-M9

168. *Experience with Space and Frequency Diversity Fading on New York-Neshanic Microwave Circuit, Case 37003-4,* G. W. Gilman and F. H. Willis, Report MM-43-160-

152, BTL, Sept. 18, 1943. CP-240-M1

169. *Investigation of Changes in Direction of Transmission during Periods of Fading in the Microwave Range, Case 37003-4, File 36691-1*, A. C. Peterson, Report MM-43-160-183, BTL, Oct. 30, 1943. CP-240-M2

170. *Radar Calibration Report, New York Region*, R. C. L. Timpson, Mitchell Field, N.Y., Nov. 30, 1943. CP-202.1-M4

171. *Aden-Berbera VHF Experiments, Meteorological Conditions and Possible Correlations*, E. W. Walker, OSRD WA-1614-1, JMRP 14, Report AC-5493, USW-SRDE, Dec. 20, 1943. CP-331-M3

172. *Propagation over Short Paths and Rough Terrain at 200 Mc/s*, A. B. Vane and D. G. Wilson, OEMsr-262, Division 14 Report 468, RL, Jan. 18, 1944. CP-231.2-M1

173. *Propagation and Reflection Characteristics of Radio Waves as Affecting Radar*, William G. Michels and William C. Pomeroy, Service Project (M-3) 11a, U.S. Army Air Forces Board, Jan. 31, 1944. CP-531-M1

174. *Microwave Propagation Measurements (Conference of February, 1944)*, F. H. Willis, Report MM-44-160-55, BTL, Mar. 10, 1944. (See reference 3.)

175. *An Estimation of the Incidence of Anomalous Propagation in the Cook Strait Area of New Zealand from January 1943 to January 1944*, F. E. S. Alexander, OSRD II-5-5849(S), Report RD-1/373, RDL-DSIR, NZ, May 2, 1944. CP-332-M2

176. *K-Band Radar Transmission, A Preliminary Report of Tests Made Near Atlantic Highlands, N.J. between December 1943 and April 1944*, G. C. Southworth, A. P. King, and S. D. Robertson, Report MM-44-160-115, BTL, May 19, 1944. CP-202.2-M1

177. *Report on Cross Channel Propagation of British No. 10 Set*, K. R. Spangenberg, Report OAB-2, OCSO, Aug. 26, 1944. CP-224-M12

178. *Radar Range and Signal Strength*, L. Jofey and A. C. Cossor, Report MR-142, Research Department, Myra Works, London E10, August 1944.

179. *Results of Microwave Propagation, Tests on the New York-Neshanic Path, Case 37003-4, File 36691-1*, A. L. Durkee, Report MM-44-160-190, BTL, Aug. 28, 1944. CP-224-M13

180. *Height-Gain Tests in the Troposphere*, G. A. Isted, JEIA 5560, JMRP 36, Report TR-488, BRL, September, 1944. CP-312-M1

181. *Interim Report on Investigation of 120 Mc/s and 50-Cm Propagation Across the English Channel*, W. R. Piggott, OSRD WA-3157-6, Report AC-7081, USW, Oct. 4, 1944. CP-333-M5

182. *Measurements of the Angle of Arrival of Microwaves in the X-Band, Case 20564*, W. M. Sharpless, Report MM-44-160-249, BTL, Nov. 7, 1944.

183. *Overwater Transmission Measurements, 1944-Part I Preliminary Analysis of Radio and Radar Measurements*, Pearl J. Rubenstein, OEMsr-262, Division 14 Report 649, RL, Dec. 15, 1944. CP-222-M8

184. *The Vertical Distribution of Field Strength over the Sea Under Conditions of Normal and Anomalous Propagation*, J A Ramsay and P. B. Blow, OSRD WA-3870-1, Research Report 267, CAEE-RRDE, Jan. 5, 1945. CP-232-M1

185. *Centimetre Wave Propagation over Sea, A Study of Signal Strength Records Taken in Cardigan Bay, Wales Between February and September, 1944*, R. L. Smith-Rose and A. C. Stickland, OSRD WA-4297-9, JMRP 50, Paper RRB/C-114, NPL-DSIR, Feb. 28, 1945. CP-333-M2

186. *Over-Water Tests of S-Band Early Warning for Ships, Vertical Coverage of the CXHR (SCI) Search System,*

Walter O. Gordey, Donald T. Drake, and M. Kessler, OEMsr-262, Service Project NS-194, Division 14 Report 703, RL, Mar. 5, 1945. CP-232.2-M11

187. *Preliminary Report on S- and X- Band Propagation in Low Ducts Formed in Oceanic Air*, Martin Katzin, Problem S411.2R-S, Report R-2493, NRL, Mar. 24, 1945. CP-222.2-M2

188. *Atmospheric Refraction under Conditions of a Radiation Inversion*, Lloyd J. Anderson, J. P. Day, C. H. Freres, R. U. F. Hopkins, John B. Smyth, and A. P. D. Stokes, BuShips Problem X4-49CD, Report WP-19, NRSL, Apr. 21, 1945. CP-222-M10

189. *Radio-Meteorological Relationships*, E. C. S. Megaw and F. L. Westwater, OSRD WA-4594-15, Report AC-8140, USW-138, May 4, 1945. CP-222.2-M3

190. *Calculated Relationship Between Signal Level and Uniform Gradient of Refractive Index for the Irish Sea Paths*, E. C. S. Megaw, OSRD WA-4594-13, GEC Report 8656, AC-8225, USW-141, GEC-USW, Apr. 19, 1945. CP-222.1-M8

191. *Radio-Meteorological Relationships, General Summary of Papers AC-8140/USW.138 and AC-8225/USW.141*, E. C. S. Megaw and F. L. Westwater, OSRD WA-4618-1, Report AC-8336, USW-149, USW, 1945. (See references 189 and 190.) CP-222.2-M4

192. *General Summary Covering the Work of the KXS Inter-Service Trials, Llandudno, 1944*, J. R. Atkinson, JMRP 64, Report T-1770, TRE, May 1945. CP-333.2-M2

193. *X-Band Trials at Rosehearty*, J. R. Atkinson, OSRD WA-4596-11, JEIA 10401, Report AC-8228, USW-142, May 28, 1945. CP-222.3-M1

194. *S- and X- Band Propagation in Low Ocean Ducts* (Fourth Conference), R. W. Bauchman and W. Binnian, Report R-2565, NRL, July 5, 1945. (See reference 12 and 187.)

195. *KXS Llandudno Interservice Trials, Summer 1944*, JMRP 68, Report T-1865, TRE, 1944.

196. *Survey of Radio Meteorological Information Available at TRE*, JMRP 67, Report M/98 (T-1888)/JWH, TRE, August 1945.

197. *The Diffusive Properties of the Lower Atmosphere*, O. G. Sutton, OSRD WA-670-9a, Report MRP-59, Chemical Defense Experimental Station, Air Ministry Meteorological Research Committee, Dec. 29, 1942. CP-323-M1

198. *A Study of the Effect of the Meteorology on the Refraction of Radio Beams*, H. Raymond, Technical Report T-2, CESL, May 4, 1943. CP-222-M9

199. *The Rapid Reduction of Meteorological Data to Index of Refraction*, Lloyd J. Anderson and F. R. Abbott, Report WP-8, NRSL, Dec. 10, 1943.

200. *Application of Diffusion Theory to Radio Refraction Caused by Advection*, P. M. Woodward, OSRD, WA-2047-4, Report T-1647, TRE, Apr. 6, 1944. CP-323-M2

201. *Qualitative Survey of Meteorological Factors Affecting Microwave Propagation*, I. Katz and J. M. Austin, OEMsr-262, Division 14 Report 488, RL, June 1, 1944. CP-311-M3

202. *The Influence of Ground Contour on Air Flow* (Translation), P. Queney, Translated by Walter M. Elsasser, OEMsr-1207, Report WPG-4, CUDWR, September 1944. CP-322-M1

203. *Radio-Meteorological Tables*, P. M. Woodward and J. W. Head, OSRD WA-3401-1, JMRP 30, Report T-1724, TRE. CP-232.1-M9

204. *Modified Index Distribution Close to the Ocean Surface*, R. B. Montgomery and Robert H. Burgoyne, OEMsr-262, Division 14 Report 651, RL, Feb. 16, 1945. CP-222.2-M1

205. *Tables for Computing the Modified Index of Refraction M*, E. R. Wicher, Report WPG-8, CUDWR, March 1945

206. *Nomograms for Computation of Modified Index of Refraction*, Robert H. Burgoyne, OEMsr-262, Division 14 Report 551, RL, Apr. 6, 1945. CP-222.1-M7

207. *Meteorological Report in Connection with V.H.F. Wireless Experiment Between Aden and Berbera, 1943*, Ronald Frith, OSRD WA-1746-2, JMRP 13, Report AC-5492, USW, Oct. 30, 1943. CP-331-M2

208. *Meteorological Measurements, Irish Sea Experiments Meteorological Observations* [taken] on [Board] *the Ship Glen Strathallan in the Irish Sea for the Period November 1, 1943 to October 23, 1944*, OSRD WA-1759-14, WA-1935-1, WA-1951-1, WA-2131-5, WA-2131-C5, WA-2152-13, WA-2131-5A, WA-3180-1, WA-2242-4, WA-2315-1, WA-2364-13, WA-2587-5, WA-2623-13, WA-2843-13, WA-4079-1, WA-2905-4, WA-3029-2, WA-3180-1A, WA-3180-1D, WA-3322-1, and WA-3584-3, NMS.
CP-333.1-M1
Meteorological Observations [taken] on [Board] *the Ship Coila in the Irish Sea for the Period December 15, 1943 to October 26, 1944*, OSRD WA-2131-5B, WA-2843-11, WA-2743-12, WA-4079-2, WA-3305-5, WA-3322-2, and WA-3584-2, NMS. CP-333.1-M2
Meteorological Measurements [taken] on [Board] *the Ship St. Dominica in the Irish Sea for the Period May 19, 1944 to August 29, 1944*, OSRD WA-2587-6, WA-2645-4, WA-3143-2, WA-3991-2, WA-3180-1B, and WA-3180-1C, Inter-Service Cm. Wave Prop. Research NMS.
CP-333.1-M3

209. *Tables of Temperature and Humidity Observations at Rye*, OSRD WA-1463-13A, Report JMRP-5, MO, November 1943. CP-333.3-M1

210. *Low Altitude Measurements in New England to Determine Refractive Index, 1943*, Robert H. Burgoyne and I. Katz, Division 14 Report 42, RL, Feb. 22, 1944. CP-336.2-M1

211. *Climate in Relation to Microwave Radar Propagation in Panama*, Arthur E. Bent, Division 14, Report 476, RL, Feb. 25, 1944. CP-336.1-M1

212. *The Vertical Distribution of Temperature and Humidity at Rye on the Night of January 14-15, 1944*, JEIA 10318, Report JMRP 6, MO, Feb. 26, 1944. CP-333.3-M2

213. *Analysis of Temperature and Humidity Records at Rye*, JEIA 10319, Report JMRP-7, MO, February 1944.
CP-333.3-M3

214. *Radio Climatology of the Persian Gulf and Gulf of Oman with Radar Confirmation*, H. G. Booker, Report T-1642, TRE, Mar. 15, 1944. CP-331-M5

215. *Stations in the Western Hemisphere with Conditions in the Lower Layers of the Atmosphere Similar to Those at Selected Stations in the Eastern Hemisphere*, Report 729, U.S. Army Air Forces, Weather Division, March 1944.
CP-337-M1

216. *Some Values of the Refractive Index of the Atmosphere at Rye*, S.100958, JEIA 10322, Report JMRP 23, MO 8, June 1-6, 1944.

217. *Low-Level Meteorological Soundings and Radar Correlation for the Panama Canal Zone*, K. E. Fitzsimmons, S. T. Stephenson, and Robert W. Bauchman, OEMsr-728, NDRC Research Project PDRC-647, Report 6, Washington State College, June 12, 1944. CP-336.1-M2

218. *Wave Propagation Report No. 3*, Report 413.44/R113, Naval Research Group, Intel. Br. OCSO Canal Zone, July 1, 1944.

219. *Preliminary Analysis of Height-Gain Tests in the Troposphere*, R. F. C. McDowell, OSRD WA-2930-2, JEIA 5777, Report TR-494, BRL, September 1944.
CP-333-M2

220. *Diurnal Variation of Temperature and Humidity at Various Heights at Rye*, S.100958, JEIA 10323, Report JMRP 26, MO 8, Oct. 21, 1944. CP-333.3-M4

221. *Report on General Climatic and Meteorological Conditions in Banda Sea, 4°-7° S., 126°-131° E.*, Report List 2, Section II, Series 7, No. 18, RAAF, Directorate of Meteorological Services, November 1944. CP-335-M2

222. *Hourly Values of Modified Refractive Index M for Meteorological Office* [at] *Rye, May, 1944*, JEIA 10325, Report JMRP-31, MO, Dec. 28, 1944. CP-333.3-M5

223. *Temperature and Humidity Measurements Made with the Washington State College Wired Sonde Equipment at Kaikoura, New Zealand, Between Sept. 22, 1944 and Oct. 19, 1944*, F. E. S. Alexander, Report RD-1/482, RDL-DSIR, NZ, Jan. 15, 1945. CP-332-M3

224. *Highlights of the December, 1944 Typhoon Including Photographic Radar Observations (Part I), A Distant Observation of a Warm Front Including a Photograph of Cloud Forms and Slope of Front (Part II)*, George F. Kosco, Fleet Weather Central Paper 10, U.S. Navy, Third Fleet, Feb. 10, 1944. CP-336.3-M1

225. *Results of Low Level Atmospheric Soundings in the Southwest and Central Pacific Oceanic Areas*, Paul A. Anderson, K. E. Fitzsimmons, G. M. Grover, and S. T. Stephenson, OEMsr-728, NDRC Research Project PDRC-647, Report 9, Washington State College, Feb. 27, 1945.
CP-335-M4

226. *Centimeter Wave Propagation over Sea, Correlation of Radio Field Strength Transmitted Across Cardigan Bay, Wales with Gradient of Refractive Index Obtained from Aircraft Observations*, R. L. Smith-Rose and A. C. Stickland, OSRD WA-4459-9, JEIA 9813, Paper RRB/C-121, DSIR, May 10, 1945. CP-333-M4

227. *Balloon Psychrometer for the Measurement of the Relative Humidity of the Atmosphere at Various Heights* (and Addendum), S. M. Doble and S. Inglefield, OSRD II-5-5079(S) and OSRD II-5-5080(S), ICI, Apr. 1, 1943; Addendum Sept. 25, 1943. CP-344-M1

228. *The Captive Radiosonde and Wired Sonde Techniques for Detailed Low-Level Meteorological Sounding*, Paul A. Anderson, C. L. Barker, K. E. Fitzsimmons, and S. T. Stephenson, OEMsr-728, NDRC Research Project PDRC-647, Division 14 Report 192, Report 3, Washington State College, Oct. 4, 1943. CP-341-M1

229. *Instruments and Methods for Measuring Temperature and Humidity in the Lower Atmosphere*, I. Katz, OEMsr-262, Service Project SC-8, Division 14 Report 487, RL, Apr. 12, 1944. CP-344-M2

230. *Anomalous Propagation, Adaptation of Model RAU-2 Radio Sonde Receiving and Recording Equipment for Use as Low Level Sounding Device*, Navy Dev. Project Unit 1, Friez Instrument Division, Bendix Aviation Corporation, May 31, 1944. CP-342-M1

231. *Meteorological Investigation at Rye, Instrumental Layout for Recording Gradients of Temperature and Relative Humidity (Part I)*, Report JMRP-17, Instruments Branch, MO 4, May 1944. CP-344-M3

232. *Notes on Operational Use of Low-Level Meteorological Sounding Equipment*, K. E. Fitzsimmons, S. T. Stephenson, and Robert W. Bauchman, OEMsr-728, NDRC Research Project PDRC-647, Report 7, Washington State College, June 15, 1944. CP-342-M2

233. *Microwave Propagation Studies, Detection of Troposphere Stratification by Means of Sound Echoes, Preliminary Trial, Case 37003*, H. B. Coxhead and F. H. Willis, Report MM-44-160-143, BTL, June 21, 1944.
CP-344-M4

234. *Operating Instructions for the WSC Low-Level Atmospheric Sounding Equipment*, Paul A. Anderson, OEMsr-728, NDRC Research Project PDRC-647, Report 8, Washington State College, July 10, 1944. CP-342-M3

235. *Meteorological Equipment for Short Wave Propagation Studies*, Walter M. Elsasser, Report WPG-3, CUDWR August 1944.

236. *Wired Sonde Equipment for High Altitude Soundings*, Lloyd J. Anderson, BuShips Problem X4-49CD, Report WP-16, NRSL, Nov. 17, 1944. (See reference 238.) CP-341-M2

237. *A Note on the Resistance of Electric Hygrometer Elements*, Lloyd J. Anderson and S. T. Stephenson, Report AERO-1, NRSL, May 8, 1945. CP-343-M1

238. *Improvements in USNRSL Meteorological Sounding Equipment*, Lloyd J. Anderson, S. T. Stephenson, and A. P. D. Stokes, BuShips Problem X4-49CD, Report WP-21, NRSL, July 3, 1945. (See reference 236.) CP-341-M3

239. *Forecasting of R. D. F. Conditions*, JMRP 2, Memorandum 103, AORG, May 31, 1943. CP-410-M1

240. *The Meteorological Aspects of Anomalous Propagation, Short Wave Radio*, R. W. Hatcher, Report JMRP 1, [Great Britain] June 1943. CP-410-M2

241. *Oboe Propagation, August–October, 1943*, H. G. Booker, OSRD WA-1464-5, Report T-1605, TRE, 1943. CP-422-M1

242. *"Naviprop" Forecasts*, E. Gold, OSRD WA-2255-1Q, Report SIS 45, MO, Nov. 8, 1943. CP-422-M2

243. *Issue of Anoprop Forecasts, Synoptic Instruction Special No. 39*, OSRD WA-2255-1R, Report SIS 39, MO, Feb. 11, 1944. CP-422-M3

244. *Elements of Radio Meteorological Forecasting*, H. G. Booker, Report T-1621, Mathematics Group, TRE, Malvern, Feb. 14, 1944. CP-410-M3

245. *Preliminary Instruction Manual, Weather Forecasting for Radar Operations*, Report 614, U. S. Army Air Forces, Weather Division, March 1944. CP-410-M4

246. *Tropospheric Weather Factors Likely to Affect Superrefraction of VHF-SHF Radio Propagation as Applied to the Tropical West Pacific*, E. Dillon Smith and R. D. Fletcher, Report RP-1, U. S. Department of Commerce, Weather Bureau, July 1, 1944. CP-424-M1

247. *Preliminary Instruction Manual of Weather Forecasting for Radar Operations in South West Pacific Area*, D. F. Martyn and P. Squires, Report RP-220, CSIR-RL, Sept. 4, 1944. CP-424-M2

248. *Outline of Radio Climatology in India and Vicinity*, H. G. Booker, JEIA 6061, Report JMRP-25, Report T-1727 (M/85), TRE, Sept. 12, 1944. CP-423-M1

249. *Notes on TRE Report T-1727, JMRP No. 25, Radio Climatology in India and Vicinity*, C. S. Durst, JEIA 10324, Report JMRP-27, MO, Nov. 7, 1944. (See reference 248.) CP-423-M2

250. *A Rough Sketch of World Radio Climatology over Sea*, H. G. Booker, Report T-1730, TRE, Oct. 31, 1944. CP-424-M3

251. *American Continents Meteorological Counterparts of Western Pacific and Indian Ocean Areas as Applied to Tropospheric Radio Propagation*, J. H. Brown, J. L. Paulhus, and E. Dillon Smith, Report RP-2, U. S. Weather Bureau, Nov. 15, 1944.

252. *The Possibility of Investigating the Föhn Wind and Sea Breeze Phenomena in N. Z. with a View to Elucidating Certain Problems of Radio-Meteorological Forecasting in Other Parts of the World*, M. A. F. Barnett and F. E. S. Alexander, JEIA 7469, Report RD-1/471, RDL-DSIR-NZ, Dec. 1, 1944. CP-421-M1

253. *Determination of a Suitable Method of Forecasting Radar Propagation Variations over Water, Tests Conducted by 26th Weather Region, Orlando, Florida*, J. R. Gerhardt and William E. Gordon, Service Project 4252R000.77, U. S. Army Air Forces, Mar. 10, 1945. CP-425-M1

254. *A Qualitative Outline of the Radio Climatology of Australasia*, H. G. Booker, JMRP-53, Report T-1820 (M/95), TRE, Apr. 19, 1945. CP-421-M2

255. *Determination of the Practicability of Forecasting Meteorological Effects on Radar Propagation, Tests Conducted by AAF Tactical Center, Orlando, Florida*, John R. Gerhardt and William E. Gordon, Service Project 3767B000.93, U. S. Army Air Forces, June 13, 1945. CP-425-M2

256. *Absorption of 1-Cm Radiation by Rain*, M. G. Adam, R. A. Hull, and C. Hurst, Misc. Report 3, CVD-CL.

257. *The Absorption of Ultra-Short Wireless Waves in the Water Vapour of the Earth's Atmosphere*, J.˙A. Saxton, OSRD II-5-210, Paper RRB/C-18, NPL, Feb. 14, 1941. CP-510-M1

258. *Echo Intensities and Attenuation Due to Clouds, Rain, Hail, Sand and Duststorms at Centimeter Wavelengths*, J. W. Ryde, OSRD WA-81-25, Report 7831, GEC, Oct. 13, 1941. CP-511-M1

259. *The Atmospheric Absorption of Microwaves* (in Third Conference Report of CP), J. H. Van Vleck, Report 175 (43-2), RL, Apr. 27, 1942. (See reference 10.) Div. 14-121.1-M4

260. *The Effect of Rain Upon the Propagation of 1-Cm Electro-Magnetic Waves, Case 22098*, S. D. Robertson, Report MM-42-160-87, BTL, Aug. 1, 1942. CP-511-M2

261. *The Effect of Rain on the Propagation of Microwaves, Case 22098*, A. P. King and S. D. Robertson, Report MM-42-160-93, BTL. Aug. 26, 1942. CP-511-M3

262. *Comparison of Theoretical and Experimental Values for the Attenuation of 1-Centimeter Waves in Rain, Case 22098*, S. D. Robertson, Report MM-43-160-2, BTL, Jan. 5, 1943. CP-511-M4

263. *An Investigation on the Number and Size Distribution of Water Particles in Nature*, Josef Mazur, F/Lt. Polish Air Force, OSRD II-5-6306(S), Report MRP-109, Meteorological Research Committee, Great Britain, June 1943. CP-511-M5

264. *Report on the Absorption and Refraction of Electro-Magnetic Waves by the Liquid Water, Water Vapour and Fog or Rain*, N. F. Mott, OSRD II-5-4936, Reference 43/2881, CRB, Sept. 2, 1943. CP-510-M2

265. *Report on the Absorption of Electromagnetic Waves in the Wavelength Range 1-100 Cm by Water in the Atmosphere*, N. F. Mott, OSRD II-5-4937, Reference 43/2882, CRB, Sept. 2, 1943. CP-510-M3

266. *Verification of Mie Theory, Calculations and Measurements of Light Scattering by Dielectric Spherical Particles* (Progress Report), Victor K. LaMer, OSRD 1857, OEMsr-148, Service Project CWS-1, Division 10, NDRC, Columbia University, Sept. 29, 1943. CP-512-M1

267. *The Absorption of Centimetric Radiation by Atmospheric Gases*, J. M. Hough, ADRDE, USWP-WC, Apr. 27, 1944. CP-510-M4

268. *Attenuation Due to Water Drops in the Atmosphere*, J. M. Hough, ADRDE, USWP-WC, Apr. 28, 1944. CP-511-M6

269. *Propagation of K/2 Band Waves*, G. E. Mueller, Report MM-44-160-150, BTL, July 3, 1944. CP-511-M7

270. *Preliminary Note on Secure Communications on Millimetre Waves*, OSRD WA-2868-3, JEIA 5597, Report L/M40/WBL, TRE, Sept. 11, 1944. CP-510-M5

271. *Rotational Line Width in the Absorption Spectrum of Atmospheric Water Vapor and Supplement*, Arthur Adel, OEMsr-1361, NDRC Division 14 Report 320, University of Michigan, Oct. 10, 1944; Supplement Feb. 1, 1945. CP-510-M6

272. *The Absorption of One-Half Centimeter Electromagnetic Waves in Oxygen*, E. R. Beringer, OEMsr-262, Service Project AN-25, Division 14 Report 684, RL, Jan. 26, 1945. CP-510-M7

273. *The Effect of Rain on Radar Performance*, S. C. Hight,

Report MM-44-170-50, BTL, Oct. 17, 1944. CP-511-M8

274. *Measurements of Wave Propagation*, G. E. Mueller, Report MM-45-160-17, BTL, Feb.' 5, 1945. CP-511-M9

275. *Further Theoretical Investigations on the Atmospheric Absorption of Microwaves*, John H. Van Vleck, OEMsr-262, Service Project AN-25, Division 14 Report 664, RL, Mar. 1, 1945. CP-510-M8

276. *Measurements of the Attenuation of K-Band Waves by Rain*, G. T. Rado, OEMsr-262, Service Project AN-25, Division 14 Report 603, RL, Mar. 7, 1945.
CP-511-M10

277. *Attenuation of Centimetre and Millimetre Waves by Rain, Hail, Fogs, and Clouds* (Draft), J. W. Ryde and D. Ryde, OSRD WA-5181-10, Report 8670, GEC, May 18, 1945.
CP-511-M11

278. *The Relation Between Absorption and the Frequency Dependence of Refraction* (Fourth Conference), John H. Van Vleck, OEMsr-262, Division 14 Report 735, RL, May 28, 1945. (See reference 12.) Div. 14-122.24-M4

279. *Absorption and Scattering of Microwaves by the Atmosphere* (Fourth Conference), Louis Goldstein, Report WPG-11, CUDWR, May 1945. (See reference 12.)

280. *C.V.D. Progress Report for May, 1945. The Absorption of K-Band Radiation in Gaseous Ammonia* (Part I), Progress Report, CVD-CL, May 1945.

281. *K-Band Attenuation Due to Rainfall*, Lloyd J. Anderson, J. P. Day, C. H. Freres, John B. Smyth, A. P. D. Stokes and L. G. Trolese, Report WP-20, NRSL, June 8, 1945.
CP-511-M12

282. *A New Method for Measuring Dielectric Constant and Loss in the Range of Centimeter Waves*, S. Roberts and Arthur R. von Hippel; *Wave Guides with Dielectric Sections*, L. J. Chu, Report 102, MIT, March 1941. CP-521-M1

283. *The Electrical Properties of Ice*, T. A. Taylor and Willis Jackson, OSRD W-126-42, Report AC-1516, RDF 110, Com. 78, RDF, Dec. 22, 1941. CP-522.13-M1

284. *The Dielectric Constant and Loss Factor of Water Vapor at a Wavelength of 9·Cm, Frequency 3330 Mc/s*, J. A. Saxton, OSRD W-203-2, Paper RRB/S-1, NPL-DSIR Mar. 31, 1942. CP-522.12-M1

285. *The Dielectric Constant of Water Vapour and its Effect upon the Propagation of Very Short Waves*, A. C. Stickland, OSRD WA-175-7, Paper RRB/S-2, NPL-DSIR, May 11, 1942. CP-522.12-M2

286. *Progress Report on Ultrahigh Frequency Dielectrics*, Arthur R. von Hippel, OEMsr-191, Division 14 Report 121, MIT, Laboratory for Insulation Research, January 1943.
CP-521-M2

287. *Conductivities of Sea, Tap and Distilled Water at λ = 10 Cm.*, L. B. Turner, OSRD WA-649-1, Report M-496, ASE, April 1943. CP-522.11-M1

288. *The Measurement of Dielectric Constant and Loss with Standing Waves in Coaxial Wave Guides*, Arthur R. von Hippel, D. G. Jelatis, and W. B. Westphal, OEMsr-191, Division 14, Report 142, MIT, Laboratory for Insulation Research, April 1943. CP-521-M4

289. *The Dielectric Constant and Absorption Coefficient of Water Vapour for Wavelengths of 9 Cm and 3.2 Cm, Frequencies 3,330 and 9,350 Mc/s.*, J. A. Saxton, Paper RRB/S-11, NPL-DSIR, June 14, 1943. CP-522.12-M3

290. "Electrical Measurements on Soil with Alternating Currents," R. L. Smith-Rose, *Journal of the Institution of Electrical Engineers* (London), NPL, Vol. 75, August 1943, pp. 221-237. CP-522.3-M1

291. *Memorandum on an Electrical Method of Measuring the Dielectric Constant of Atmospheric Air, and Recording it Continuously*, OSRD WA-1464-7, Report JMRP-8, Report M/Memo-15/PEC, TRE, Jan. 6, 1944.
CP-522.2-M1

292. *The Dielectric Constant and Absorption Coefficient of Water Vapour for Radiation of Wavelength 1.6 Cm, Frequency 18,800 Mc/s.*, J. A. Saxton, Paper RRB/S.17, NPL-DSIR, Apr. 22, 1944.

293. *The Dielectric Constant of Water and Ice at Centimetre Wavelengths* (Working Committee), J. M. Hough, ADRDE. USWP-WC. Apr. 28, 1944. CP-522.1-M1

294. *Preliminary Report on the Dielectric Properties of Water in the K-Band*, C. H. Collie, Report CL Misc. 25, CVD, May 1944.

295. *Recent Dielectric Constant and Loss Tangent Measurements on X-Band* (Radome Bulletin No. 5), Elizabeth M. Everhart, OEMsr-262, Division 14 Report 483-5, RL, July 14, 1944. CP-522.4-M1
Div. 14-234.5-M5

296. *Dielectric Properties of Water and Ice at K-Band*, E. L. Younker, OEMsr-262, Service Project AN-25, Division 14 Report 644, RL, Dec. 4, 1944. CP-522.1-M2

297. *The Interaction Between Electromagnetic Fields and Dielectric Materials*, Arthur R. von Hippel and R. G. Breckenridge, OEMsr-191 Division 14 Report 122, MIT, Laboratory for Insulation Research, January, 1943. CP-521-M3

298. *The Dielectric Properties of Water at Wavelengths from 2 Cm to 10 Cm and over the Temperature Range 0° to 40° C*, J. A. Saxton, OSRD WA-4340-5, Paper RRB/C-115, NPL-DSIR, Mar. 20, 1945. CP-522.11-M2

299. *The Dielectric Properties of Water in the Temperature Range 0° C to 40° C for Wavelengths of 1.24 Cm and 1.58 Cm*, J. A. Saxton and J. A. Lane, JEIA 9811, Paper RRB/C.116, NPL-DSIR, Mar. 7, 1945.

300. *The Anomalous Dispersion of Water at Very High Radio Frequencies in the Temperature Range 0° to 40° C*, J. A. Saxton, OSRD WA-4459-8, JEIA 9812, Paper RRB/C-118, NPL-DSIR, Apr. 6, 1945. CP-522.11-M3

301. *Centimeter Wave Propagation over Sea Within the Optical Range*, H. Archer-Thomson, J. C. Dix, F. Hoyle, E. C. S. Megaw, and M. H. L. Pryce, OSRD W-157-16, Report M-398, ASE, January 1942. CP-532.2-M1

302. *Preliminary Report on the Reflection of 9-Cm Radiation at the Surface of the Sea*, H. Archer-Thomson, N. Brooke, T. Gold, and F. Hoyle, OSRD WA-1131-2, Report M-542, ASE, September 1943. CP-532.2-M2

303. *Comment on the Reflection of Microwaves from the Surface of the Ocean* (Part II), S. O. Rice, Report MM-43-210-6, BTL, Oct. 13, 1943. CP-532.2-M3

304. *S-Band Measurements of Reflection Coefficients for Various Types of Earth*, E. M. Sherwood, Report 5220.129, Sperry Gyroscope Company, Oct. 29, 1943. CP-532.1-M1

305. *Special Report on the Determination of the Coefficient of Reflection of Radio Waves at 'the Ground by Means of Radar Observations*, W. Sterling Ament, Report RA-3A-212A, NRL, Nov. 10, 1943. CP-532.1-M2

306. *Scattering*, T. L. Eckersley, OSRD WA-2255-1F, JEIA 3904, Report TR-481, BRL, November 1943.
CP-512-M3

307. *Preliminary Measurements of 10 Cm Reflection Coefficients of Land and Sea at Small Grazing Angles*, Pearl J. Rubenstein and William T. Fishback, Division 14 Report 478, RL, Dec. 11, 1943. CP-532-M1

308. *Further Measurements of 3- and 10-Cm Reflection Coefficients of Sea Water at Small Grazing Angles*, William T. Fishback and Pearl J. Rubenstein, OEMsr-262, Division 14 Report 568, RL, May 17, 1944. CP-532.2-M4

309. *Microwave Propagation Studies, The Reflection of Sound Signals in the Atmosphere*, Case 37003, File 36691-1, F. H. Willis, Report MM-44-160-156, BTL, July 3 1944.

310. *Interim Report on Experiments on Ground Reflection at a Wavelength of 9 Cm*, L. H. Ford, JEIA 4899, Paper

RRB/C.101, DSIR, July 7, 1944.

311. *An Experimental Investigation of the Reflection and Absorption of Radiation of 9-Cm Wavelength*, L. H. Ford and R. Oliver, OSRD WA-3386-2, Paper RRB/C-107, DSIR, Oct. 27, 1944.   CP-532-M2

312. *The Measurement of High Reflections at Low Power (Radome Bulletin No. 7)*, Raymond M. Redheffer, OEMsr-262, Division 14 Report RL-483-7, RL, Nov. 20, 1944.   CP-531-M3

313. *Ground Reflection Coefficient Experiments on X-Band, Case 20564*, W. M. Sharpless, Report MM-44-160-250, BTL, Dec. 15, 1944.   CP-532.1-M3

314. *The Reflection Coefficient of a Linearly Graded Layer*, OSRD WA-3438-5, Report TR-492, BRL, December 1942.   CP-531-M2

315. *Reflection and Scattering*, T. L. Eckersley, OSRD WA-4002-12, Report TR-506, BRL, January 1945.
                      CP-532.2-M5

316. *Reflection from an Inversion*, L. E. Beglian and F. J. Northover, OSRD WA-4494-14, JEIA 9997, Report AC-8210, USW-140, USW, May 24, 1945.   CP-531-M5

317. *Notes on the Comparison of Vertical and Horizontal Polarization in Ground Wave Propagation*, G. Millington, OSRD WA-1463-5, Report TR/442, BRL, January 1940.   CP-540-M1

318. *Horizontal and Vertical Polarization*, T. L. Eckersley, OSRD II-5-5280, Report TR-441, BRL, July 1942.
                      CP-540-M2

319. *The Investigation of Horizontally and Vertically Polarized Direction Finding on Frequencies of the Order of 20 to 70 Megacycles per Second*, T. L. Eckersley, OSRD II-5-5284, Report TR-451, BRL, September 1942.
                      CP-540-M3

320. *Polarization Effects and Aerial System Geometry at Centimeter Wavelengths*, E. C. S. Megaw, H. Archer-Thomson, and E. M. Hickin, Report 8101, GEC, Nov. 26, 1942.

321. *Change of Polarization as a Means of Gap Filling*, Richard A. Hutner, Francis Parker, Bernard Howard, and Jocelyn Gill, Division 14 Report C-7, RL, Dec. 28, 1942.   ·
                      CP-540-M4

322. *Vertical Polarization vs Horizontal Polarization*, Ralph C. Loring, Tentative Technical Report T-1, CESL, Oct. 22, 1943.   CP-540-M5

323. *The Depolarization of Microwaves*, M. Kessler, C. E. Mandeville and E. L. Hudspeth, Division 14 Report 458, RL, Nov. 1, 1943.   CP-540-M6

324. *Polarization Studies at S and X Frequencies*, O. J. Baltzer, W. M. Fairbank, and J. D. Fairbank, OEMsr-262, Division 14 Report 536, RL, Mar. 14, 1944. CP-540-M7

325. *Screening by Hills*, H. G. Booker, OSRD WA-1105-3C, Report T-1015, TRE, May 1941.   CP-231.222-M1

326. *Diffraction Round a Sphere or Cylinder*, G. Millington, OSRD II-5-5703, Report TR-433, BRL, March 1942.
                      CP-231.21-M1

327. *Centimeter Wave Transmission Measurements from an Urban Site*, H. Archer-Thomson, E. M. Hickin, and E. C. S. Megaw, Report 8034, GEC, July 28, 1942.

328. *Report on an Investigation of the Propagation of Centimeter Waves over Ridges and Through Trees*, R. L. Smith-Rose, OSRD WA-772-19, Report AC-4345, Com. 181, NPL, June 2, 1943.   CP-231.22-M1

329. *A Note on the Propagation of K-Band Waves Through Trees, Case 29093*, S. D. Robertson, Report MM-43-160-129, BTL, Aug. 13, 1943.   CP-231.221-M1

330. *Report on Further Experiments on the Propagation of Centimeter Waves Through Trees in Leaf and over Level Ground*, OSRD WA-1337-3, Report AC-5069, Com. 197, NPL, Sept. 6, 1943.   CP-231.221-M2

331. *Centimeter Wave Propagation, Notes on the Effect of Obstruction by a Single Tree*, R. E. Jennings, E. C. S. Megaw, H. Archer-Thomson, and E. M. Hickin, OSRD WA-1356-6, Report M-565, ASE, October 1943.
                      CP-231.221-M3

332. *An Experimental Investigation on the Propagation of Radio Waves over Bare Ridges in the Wavelength Range 10 Centimetres to 10 Metres, Frequencies 30 to 3000 Mc/s*, J. S. McPetrie and L. H. Ford, OSRD WA-1463-17, Paper RRB/S-12, NPL-DSIR, Oct. 1, 1943.
                      CP-231.222-M2

333. *Some Observed Effects of Trees upon Microwave Propagation, Case 37003, File 36691-1*, A. C. Peterson, Report MM-43-160-150, Sept. 17, 1943, Revised Oct. 15, 1943.
                      CP-231.221-M4

334. *Effect of Hills and Trees as Obstructions to Radio Propagation*, Delmer C. Ports, OSRD 3070, OEMsr-1010, Jansky and Bailey, November 1943.   CP-231.22-M2

335. *Report on Some Further Experiments on the Effect of Obstacles on the Propagation of Centimetre Waves*, L. H. Ford, A. C. Grace, and J. A. Lane, JEIA 3157, Report AC-5876, NPL-RD, USW, Jan. 20, 1944.
Addendum, R. L. Smith-Rose, OSRD WA-3822-12, Report AC-5876a, NPL, Jan. 1, 1945.   CP-231.223-M1

336. *The Propagation of Ultra Short Waves Round Hills and Other Obstacles*, T. L. Eckersley, OSRD WA-2884-3, JEIA 5674, Report TR-479, BRL, May 1944.
                      CP-231.222-M3

337. *Scattering of Radio Waves by Metal Wires and Sheets*, F. Horner, JEIA 7793, Paper RRB/C-110, DSIR, Jan. 1, 1945.

338. *Some Experiments on the Propagation over Land of Radiation of 9.2-Cm Wavelength*, L. H. Ford, OSRD WA-4297-8, Paper RRB/C-113, NPL-DSIR, Feb. 15, 1945.
                      CP-231.22-M3

339. *A Preliminary Study of Ground Reflection and Diffraction Effects with Centimetric Radar Equipment*, J. S. Hey, F. Jackson, and S. J. Parsons, OSRD WA-5062-2, Report 274, AORG, June 28, 1945.   CP-231.21-M2

340. *Diffraction at Coast Line, Sloping Site*, H. G. Booker, OSRD WA-986-6c, Report 10, TRE, May 1, 1941.
                      CP-233-M2

341. *Mixed Land and Sea Transmissions*, T. L. Eckersley, OSRD II-5-5515, Report E-16, BRL, October 1941.
                      CP-233-M3

342. *Diffraction at Coast Line, Further Numerical Examples*, H. G. Booker, OSRD WA-92-5d, Report M-35, TRE, Feb. 5, 1942.   CP-233-M4

343. *Coastal Refraction*, OSRD II-5-5281, Report TR-436, BRL, May 1942.   CP-233-M5

344. *Propagation of Wireless Waves over Ground of Varying Earth Constants (Part Land and Part Sea)*, G. Millington, OSRD II-5-5277, Report TR-440, BRL-Marconi, Ltd., July 1942.   CP-233-M6

345. *Transmission over Ground of Varying Earth Constants*, OSRD II-5-5457, Report TR-473, BRL, July 1943.
                      CP-233-M8

346. *Diffraction at Coast Line* (Appendix to Report on Siting of RDF Stations), H. G. Booker, OSRD WA-986-6b, Report 6, TRE, Jan. 27, 1944.   CP-233-M1

347. *Siting and Coverage of Ground Radars*, E. J. Emmerling, OEMsr-1207, Report WPG-10, CUDWR, May 1945. (See reference 12.)   CP-202.4-M6

348. *Scattering and Spurious Echoes*, T. L. Eckersley, OSRD II-5-5275, Report TR-427, BRL, April 1942.
                      CP-521.7-M1

349. *Reflection of 10-Cm Radiation by Model Aircraft*, A. F. Phillips, Christchurch Report 174, ADRDE, Sept. 8, 1942.

350. *Elementary Survey of Scattering and Echoing by Elevated Targets*, H. G. Booker, Report M/48/HGB, TRE, December 1942.

351. *The Resolution of Composite Echoes with Centimeter Wave R.D.F.*, J. R. Benson, J. A. Ramsay, and P. B. Blow, OSRD WA-1789-2, Report 4070/C/104, CAEE, Feb. 10, 1943. CP-623-M3

352. *Microwave Radar Reflection*, J. F. Carlson and S. A. Goudsmit, Division 14 Report 43-23, RL, Feb. 20, 1943. CP-623-M4

353. *Reflection of Radar Waves from Targets of Simple Geometric Form*, Lloyd J. Anderson, John B. Smyth, and F. R. Abbott, BuShips Problem X4-49CD, Report WP-3, NRSL, Feb. 24, 1943. CP-612.4-M1

354. *Radar Echoes from Periscopes*, John E. Freehafer, Division 14 Report 42-1, RL, Mar. 1, 1943. CP-622.1-M1

355. *Radar Echoes from Atmospheric Phenomena*, Arthur E. Bent, Division 14 Report 42-2, RL, Mar. 13, 1943. CP-621.1-M1

356. *Echoes Produced by Perfectly Conducting Objects of Certain Simple Shapes in Free Space*, R. E. B. Makinson OSRD II-5-5691, Report RP-173, CSIR, Mar. 25, 1943. CP-622.5-M1

357. *Gratings and Screens as Microwave Reflectors*, Division 14 Report 54-20, RL, Apr. 1, 1943. CP-611-M1

358. *Report on an Investigation into the Nature of Sea Echoes*, OSRD WA-1142-3, Report T-1497, TRE, May 12, 1943. CP-621.6-M1

359. *The Application of Corner Reflectors to Radar (Theoretical)*, R. D. O'Neil, F. S. Holt, and Prescott D. Crout, Division 14 Report 43-31, RL, May 14, 1943. CP-611.1-M1

360. *The Application of Corner Reflectors to Radar (Experimental)*, R. D. O'Neil, Division 14 Report 55-4, RL, July 1, 1943. CP-611.1-M2

361. *Measurement of the Effective Echoing Areas of Various Aircraft*, Ross Bateman, Report ORG-P-8-1, OCSO, July 2, 1943. CP-622.3-M1

362. *Overwater Observations at X and S Frequencies on Surface Targets*, O. J. Baltzer, V. A. Counter, W. M. Fairbank, W. O. Gordy, and E. L. Hudspeth, Division 14 Report 401, RL, July 26, 1943. CP-612.3-M1

363. *Towed Radar Targets*, G. A. Armstrong and G. H. Beeching, OSRD WA-1012-2, Research Report 212, ADRDE, Aug. 6, 1943. CP-612.2-M1

364. *Corner Reflector Tests at Langley Field*, C. M. Gilbert, Division 14 Report 402, RL, Aug. 6, 1943. CP-611.1-M3

365. *Properties of Corner Reflectors, Case 22098*, S. D. Robertson, Report MM-43-160-130, BTL, Aug. 12, 1943. CP-611.1-M4

366. *Use of Corner Reflectors as IFF on Ships*, OSRD II-5-5680, Operational Research Report 24, Australian ORS and CSIR-RL, Aug. 30, 1943. CP-611.1-M5

367. *An Investigation into the Nature of Sea Echoes*, A. C. Cossor, Ltd., JEIA 1221, Report MR-109, Research Department Myra Works, London E10, Sept. 8, 1943.

368. *The Scattering of Radiation from Rectangular Planes, Half-Cylinders, Hemispheres, and Airplanes*, Contract W-2279sc-551, Item 3, Moore School of Engineering, University of Pennsylvania, Oct. 12, 1943. CP-512-M2

369. *On the Appearance of the A-Scope when the Pulse Travels Through a Homogeneous Distribution of Scatterers*, A. J. F. Siegert, Division 14, Report 466, RL, Nov. 9, 1943. Div. 14-124.2-M2

370. *On the Fluctuations in Signals Returned by Many Independently Moving Scatterers*, A. J. F. Siegert, Division 14 Report 465, RL, Nov. 12, 1943. Div. 14-122.113-M7

371. *The Use of Permanent Echo Amplitudes for Monitoring S-Band Radar Equipment*, F. J. Kerr and J. F. McConnell, OSRD II-5-5750, Report RP-177/2, CSIR-RL, Dec. 7, 1943. CP-623-M5

372. *The Range Calculator*, S. J. Mason, Division 14 Report 497, RL, Dec. 20, 1943. CP-202.4-M2

373. *The Performance of 10-Cm Radar on Surface Craft*, B. F. Schonland, OSRD WA-1570-39, Report 155, AORG, Jan. 3, 1944. CP-202.312-M1

374. *Special Report on Radar Cross Section of Ship Targets*, Martin Katzin, Report RA-3A-213A, NRL, Jan. 24, 1944. CP-612.1-M1

375. *Observations of Life Rafts Equipped with Corner Reflectors*, Emmett L. Hudspeth and John P. Nash, Division 14 Report 533, RL, Feb. 15, 1944. CP-611.1-M6

376. *Radar Cross Section of Ship Targets (Part II)*, W. Sterling Ament, Martin Katzin, and F. C. MacDonald, Report R-2232, NRL, Feb. 18, 1944. CP-612.1-M1

377. *Optical Theory of the Corner Reflector*, R. C. Spencer, OEMsr-262, Division 14 Report 433, RL, Mar. 2, 1944. CP-611.1-M7

378. *Observations on Signal Stability at S and X Frequencies*, Otto J. Baltzer, Jr., William M. Fairbank, and J. D. Fairbank, OEMsr-262, Division 14 Report 537, RL, Mar. 14, 1944. CP-632-M1

379. *Interim Report on the Recognition of Radar Echoes*, F. E. S. Alexander, OSRD II-5-5796(S), JEIA 3401, Report RD-1/353, RDL-DSIR, NZ, Mar. 20, 1944. CP-623-M6

380. *Screened and Unscreened Radar Coverage for Surface Targets*, W. Walkinshaw and J. E. Curran, OSRD WA-2284-2, Report T-1666, TRE, Mar. 1944. CP-612.3-M2

381. *The Performance of Naval Radar Systems Against Aircraft*, F. Hoyle, OSRD WA-2255-1o, Report JEIA-3902, ASE, Apr. 3, 1944. CP-202.11-M2

382. *Preliminary Report on the Fluctuations of Radar Signals*, H. Goldstein and Paul D. Bales, OEMsr-262, Division 14 Report 569, RL, May 16, 1944. CP-632-M2

383. *Radar Ranging on Land Targets*, OSRD II-5-6178(S), Memorandum 101/G-36/ALH, TRE, May 18, 1944. CP-202.4-M3

384. *The Radar Echoing Power of Conducting Spheres*, T. Pearcey, and J. M. C. Scott, OSRD WA-2334-6, Report CR-228, ADRDE, May 24, 1944. CP-623-M7

385. *Use of Corner Reflectors in Beaconry*, F. J. Kerr, OSRD II-5-6145(S), JEIA 5180, Report RP-200, CSIR-RL, June 8, 1944. CP-611.1-M8

386. *Calibration and Standardization of Land Based Radars by the Use of Small Plane Targets*, F. R. Abbott, BuShips Problem X4-49CD, Report WP-12, NRSL, June 10, 1944. CP-612.5-M1

387. *Test of the Pre-Production Model Corner Reflector, Final Report of Project E-44-37*, Alvin E. Hebert and C. B. Overacker, AAF Board Project (M-3) 69-Eglin Field, Fla., Report 413.44/R387.1, Intel. Br. OCSO-USA, June 17, 1944. CP-611.1-M9

388. *Radar Cross Section of Ship Targets (Part III)*, W. Sterling Ament, Martin Katzin, and F. C. MacDonald, Report R-2295, NRL, June 27, 1944. CP-612.1-M1

389. *Notes on Echoes and Atmospherics from Lightning Flashes on P Band*, J. L. Pawsey, OSRD II-5-6144(S), JEIA 5177, Report RP-49-2, CSIR-RL, July 11, 1944. CP-621.3-M1

390. *Theory of Ship Echoes as Applied to Naval RCM Operations*, T. S. Kuhn and Peter J. Sutro, OEMsr-411, Research Project RP-186, Report 411-93, Harvard University, RRL, July 14, 1944. Div. 15-221.11-M2

391. *Radar Echoes from the Nearby Atmosphere, Case 37003-4*, Millard W. Baldwin, Jr., Report MM-44-150-2, BTL, July 18, 1944. CP-621-M1

392. *Radar Cross Section of Ship Targets (Part IV)*, W. Sterling Ament, Martin Katzin, and F. C. MacDonald, Report R-2332, NRL, July 21, 1944. CP-612.1-M1

393. *Radar Echoes from the Nearby Atmosphere, Second Report, Case 37003-4*, Millard W. Baldwin, Jr., Report MM-44-150-3, BTL, July 31, 1944.   CP-621-M1

394. *Reflecting Properties of Metal Gratings*, J. S. Gooden, OSRD II-5-6230(S), Report RP-215, CSIR-RL, July 31, 1944.   CP-611-M2

395. *Theory of the Performance of Radar on Ship Targets* (ADRDE and CAEE Joint Report), M. V. Wilkes, J. A. Ramsay, and P. B. Blow, OSRD WA-2843-10, ADRDE Reference R04/2/CR252, CAEE Reference 69/C/149, July 1944.   CP-612.1-M2

396. *Corner Reflectors for Life Rafts*, Emmett L. Hudspeth and John P. Nash, OEMsr-262, Division 14 Report 608, RL, Aug. 1, 1944.   CP-611.1-M10

397. *The Characteristics of S-Band Aircraft Echoes with Particular Reference to Radar A.A. No. 3 MK. II.* G. H. Beeching and N. Corcoran, OSRD WA-2812-13, Research Report 253, ADRDE, Aug. 4, 1944.   CP-622.3-M2

398. *Radar Echoes from the Nearby Atmosphere, Third Report, Case 37003-4*, Millard W. Baldwin, Jr., Report MM-44-150-4, BTL, Aug. 11, 1944.   CP-621-M1

399. *Considerations Concerning Radar Coverage Diagrams*, J. L. Pawsey, OSRD II-5-6229(S), Report RP-217, CSIR-RL, Aug. 14, 1944.   CP-202.4-M5

400. *RDF Echoes to be Expected from Objects of Various Shapes*, OSRD WA-6-21, Extra Mural Res. F.72/80, Report 26, Ministry of Supply, DSR.   CP-622.5-M2

401. *Radar Echoes from Shells Bursts at 4 Meters and 50-Cm Wavelengths*, S. M. Taylor and F. E. W. Bugler, Research Report 260, RRDE, Oct. 9, 1944.   CP-622.4-M1

402. *Summer Storm Echoes on Radar MEW*, J. S. Marshall, R. C. Langille, William M. Palmer, R. A. Rodgers, G. P. Adamson, and F. F. Knowles, Report 18, CAORG, Nov. 27, 1944.   CP-621.1-M2

403. *The Cancellation of Permanent Echoes by the Use of Coherent Pulses* (Interim Report), H. Grayson, OSRD WA-3482-7C, Technical Note RAD-253, RAE, November 1944.   CP-623-M8

404. *The Fading of S-Band Echoes from Ships in the Optical Zone*, R. I. B. Cooper, OSRD WA-3677-8, Research Report 265, Dec. 12, 1944.   CP-622.2-M3

405. *Rotating Corner-Reflectors for Ship Identification*, Julian M. Sturtevant, OEMsr-262, Division 14 Report 654, RL, Jan. 1, 1945.   CP-611.1-M11

406. *Reflection from Smooth Curved Surfaces*, R. C. Spencer, OEMsr-262, Division 14, Report 661, RL, Jan. 26, 1945.   CP-531-M4

407. *Analysis of Over-Water Tracking*, Elizabeth J. Campbell, OEMsr-262, Service Project NO-166, Division 14 Report 695, RL, Feb. 12, 1945.   CP-202.12-M1

408. *Technical Report on the Maximum Range of Detection of the German Early Warning Radar Equipment, Especially when Viewing Large, Tight Formations of Bomber Aircraft*, W. E. Bales and K. A. Norton, Report OAD-13, ORS, VIII Bomber Command OCSO, Sept. 13, 1943.   CP-202.4-M1

409. *Performance Checks and Estimation of Vessel Size on Short-Based 10-Cm Radar Sets*, D. Lack, OSRD WA-1992-3, JEIA 3124, AORG, Mar. 30, 1944.   CP-622.2-M1

410. *Report of Trials to Determine the Variations of the Apparent Reflecting Point of Plain 10-Cm Waves from a Destroyer*, J. F. Coales and M. Hopkins, OSRD WA-3702-1, Report M-627, ASE, July 1944.   CP-622.2-M2

411. *The Reflection of Electromagnetic Waves by Long Wires and Non-Resonant Cylindrical Conductors*, J. M. C. Scott and T. Pearcey, JEIA 7286, Research Report 259, RRDE, Nov. 13, 1944.   CP-622.2-M2

412. *Theory of Radar Return from the Schnorkel*, P. M. Marcus,

413. *Sea Returns and the Detection of Schnorkel*, G. G. Macfarlane, OSRD WA-4196-8, JEIA 8643, Report T-1787, TRE, Feb. 13, 1945. (See reference 418.)   CP-622.1-M3

414. *Interservice KXS-Band Radar Trials; Over Water Performance Against Surface Targets*, J. A. Ramsay, P. B. Blow, and H. J. Worsdall, JEIA 8820, Report M-688, ASE, February 1945.   CP-612.3-M3

415. *An Observation of Diffuse Cloud-Like Echoes*, J. L. Pawsey and F. J. Kerr, OSRD II-5-7007(S), Report RP-246, CSIR-RL, Mar. 6, 1945.   CP-621.4-M1

416. *The So-Called Standard Target*, A. H. Brown, OEMsr-262, Division 14 Report S-43, RL, Mar. 10, 1945.   CP-612.6-M1

417. *Radar Cross Section of Ship Targets* (Part V), F. C. MacDonald, Report R-2466, NRL, Mar. 12, 1945.   CP-612.1-M1

418. *Radar Results Against Schnorkels: A Commentary on TRE T-1787, Sea Returns and the Detection of Schnorkel*, OSRD WA-4276-5, JEIA 9111, Report 338, ORS/CC, Mar. 16, 1945. (See reference 413.)   CP-622.1-M4

419. *Radar Echoes from Clouds of Water Droplets*, F. Hoyle, Report AC-7930, Report 128, USW, Mar. 16, 1945.

420. *Comments on Radar Echoes from Water Droplets*, (Paper AC-7930, USW Report 128), R. G. Ross, OSRD WA-4149-10, Paper AC-7931, Report 129, USW, Mar. 16, 1945.   CP-621.2-M1

421. *Radar Cross Section of Ship Targets* (Part VI) W. J. Barr, Report R-2467, NRL, Apr. 10, 1945.   CP-612.1-M1

422. *S-Band Radar Echoes from Snow*, R. C. Langille, J. S. Marshall, William M. Palmer, and L. G. Tibbles, Report 26, CAORG, June 14, 1945.   CP-621.5-M1

423. *Surface Coverage of Some Shipborne Radar Sets on S, X, and K Bands*, J. D. Fairbank and W. M. Fairbank, OEMsr-262, Service Projects NS-234 and NS-175, Division 14 Report 720, RL, June 15, 1945.   CP-202.4-M7

424. *Echoes from Tropical Rain on X-Band Airborne Radar*, Arthur E. Bent, OEMsr-262, Division 14 Report 728, RL, June 15, 1945.   CP-621.2-M2

425. *Analysis of Storm Echoes in Height Using MHF*, J. S. Marshall, L. G. Eon, and L. G. Tibbles, Report 30, CAORG, June 25, 1945.   CP-621.1-M3
See also: *Radar Camouflage*, Division 14 Report 766, RL, July 16, 1945.   CP-633-M1

426. *3000-Megacycle Communication*, H. H. Beverage, OEMsr-32, NDRC Projects SC-13 and PDRC-90, RCA, Mar. 10, 1942.   CP-203.1-M1

427. *Microwave Telephone, Part I Omnidirectional, Part II, Directional*, OEMsr-442, NDRC Projects C-42 and SC-13, RCA, Mar. 22, 1943.   CP-203.1-M2

428. *Factors Determining the Range of Radio Communications in the Various Theaters of Operation*, Jack W. Herbstreit, Report ORG-P-14-1, OCSO, June 3, 1943.   CP-732-M1

429. *Radiotelephone Communication on 3000 Megacycles*, Paul A. Anderson, K. E. Fitzsimmons, C. L. Barker, and S. T. Stephenson, OEMsr-728, NDRC Research Project PDRC-647, Division 14 Report 152, Report 2, Washington State College, June 12, 1943.   CP-203.1-M3

430. *An Analysis of the Effect of Frequency on Short Distance Radio Communications*, Ross Bateman and William Q. Crichlow, Report ORB-P-15-1, OCSO, Aug. 18, 1943.   CP-732.1-M1

431. *Use of the 25- to 50-Mc/s Band for Short Range Wireless Communication*, OSRD WA-1022-3, Report 130, AORG, Aug. 27, 1943.   CP-732.1-M2

432. *Trials with a 250-Watt Frequency-Modulated VHF Sender Across a Sea Water Path Beyond the Optical Range*, G. W. Higgins and W. H. Hill, OSRD WA-1352-5, Report 878, SRDE, September 1943.   CP-712-M1

OEMsr-262, Division 14 Report 671, RL, Jan. 15, 1945.   CP-622.1-M2

433. *Radio Communication in Jungles*, Arthur C. Omberg, Report ORG-2-1, OCSO, Sept. 1, 1943. CP-711-M1

434. *Measurement of Factors Affecting Jungle Radio Communication*, Jack W. Herbstreit and William Q. Crichlow, Report ORB-2-3, OCSO, Nov. 10, 1943. CP-711-M2

435. *Methods for Improving the Effectiveness of Jungle Radio Communication*, Technical Bulletin Sig. 4, U.S. War Department, Jan. 14, 1944. CP-711-M3

436. *Survey of Existing Information and Data on Atmospheric Noise Level over the Frequency Range 1-30 Mc/s*, H. A. Thomas and R. E. Burgess, OSRD WA-3201-2, JEIA 2815, Paper RRB/C-90, DSIR, Feb. 21, 1944. CP-732-M2

437. *Methods of Reducing Radar Interference to Communication*, Arthur C. Omberg, Joseph B. Epperson, and William Q. Crichlow, Report ORB-E-27-2, OCSO, Apr. 19, 1944. CP-731-M1

438. *The Application of Passive Repeaters to Point to Point Communication at VHF and UHF*, Ross Bateman, Report ORB-P-20-1, OCSO, Apr. 29, 1944. CP-721-M1

439a. *Summary of Radio Propagation Problems in Southwest Pacific Area*, W. C. Babcock, JEIA 6298, Report US/413.44/R113, Intel. Br. OCSO, Sept. 6, 1944. CP-713-M1

439b. *Point to Point Communication in MF and Via Ground Wave Propagation*, W. C. Babcock, JEIA 6770, Report 413.44/R423.4, Intel. Br. OCSO-SWPA, Aug. 15, 1944.

440. *Measurements of Factors Affecting Radio Communication & Loran Navigation in SWPA*, Ross Bateman, Jack W. Herbstreit, and Robert B. Zechiel, Report ORB-2-4, OCSO, Dec. 16, 1944. CP-713-M2

441. *Field Trials of Ultra Short Wave Frequency and Amplitude Modulated Multichannel Radio Telephone Systems*, A. W. Pearson, W. J. Bray, J. H. H. Merriman, R. W. White, J. G. Hobbs, C. H. Gibbs, and H. Prain, Radio Report 1115, POED, Mar. 27, 1944.

442. *Physics of the Air*, W. J. Humphreys, McGraw-Hill Book Co., 1940, p. 457.

443. *Ergebnisse der Exakten Naturwissenshaften*, H. Plendl and G. Eckart, Berlin, 17, 1938, p. 334.

444. "Reflection of Waves in an Inhomogeneous Absorbing Medium," P. S. Epstein, *Proceedings of the National Academy of Sciences*, 16, 1930, p. 627.

445. "Penetration of a Potential Barrier by Electrons," Carl Eckart, *The Physical Review*, 35, 1930, p. 1303.

446. "The Relation of Drop Size to Intensity," J. O. Laws and D. A. Parsons, *Transactions of the American Geophysical Union*, 1943, p. 452.

447. "Ultra Short Wave Propagation," I. C. Schelleng, Chas. R. Burrows, and E. B. Ferrell, *Bell System Technical Journal*, April 1933. (See reference 24.)

448. Report JANP 102, Joint Communications Board.

449. "On the Connection Formulas and the Solutions of the Wave Equation," R. E. Langer, *The Physical Review*, 51, 1937, p. 670.

450. *Treatise on Theory of Bessel Functions*, George Neville Watson, Cambridge University Press, Second Edition, 1944.

VOLUME 2

Chapter 1

1. *Beitraege zur Physik der Freien Atmosphere*, P. Mildner, 1932, p. 51.

2. *Geophysical Memoirs*, Giblett and others, No. 54.

3. *Proceedings of the Royal Society of London*, O. G. Sutton, 1932, p. 143.

4. *Geophysical Memoirs*, No. 65.

5. *Quarterly Journal of the Royal Meteorological Society*, O. G. Sutton, 1936, p. 125.

6. *Quarterly Journal of the Royal Meteorological Society*, H. V. Sverdrup, 1936, p. 461.

7. *MIT Papers*, Rossby and Montgomery, 1934.

8. *Quarterly Journal of the Royal Meteorological Society*, O. G. Sutton, 1937, p. 105.

9. *Wired Sonde Equipment for High Altitude Soundings*, Lloyd J. Anderson, BuShips Problem X4-49CD, Report WP-16, NRSL, Nov. 17, 1944. CP-341-M2

10. *The Captive Radiosonde and Wired Sonde Techniques for Detailed Low-Level Meteorological Sounding*, Paul A. Anderson, C. L. Barker, K. E. Fitzsimmons, and S. T. Stephenson, OEMsr-728, Research Project PDRC-647, Division 14 Report 192, Report 3, Washington State College, Oct. 4, 1943. CP-341-M1

11. *The Dielectric Constant of Water Vapour and its Effect upon the Propagation of Very Short Waves*, A. C. Stickland, OSRD WA-175-7, Paper RRB/S-2, NPL-DSIR, May 11, 1942. CP-522.12-M2

12. *Lehrbuch der Meteorologie, Fünfte Auflage*, J. Hann and R. Suring, 1939.

13. "On Temperature and Humidity Observations Made at Allahabad," S. A. Hill, *Indian Meteorological Memoirs*, 4, Part 6, 1889.

14. "Ein Beitrag zur Kenntnis der Temperatur und Feuchtigkeitsverhaltnisse in Verschiedener Höhe über dem Erdboden," K. Knoch, *Veröffentlichungen des Königlichen Preussischen, Meteorologischen Institute, Abhandlungen*, 3, No. 2, 1909.

15. "An Investigation of the Lapse Rate of Temperature in the Lowest Hundred Meters of the Atmosphere," N. K. Johnson and G. S. P. Heywood, *Geophysical Memoirs*, No. 77, 1938.

16. Walter M. Elsasser, NDRC Propagation Memorandum.

17. *Atmospheric Waves, Fluctuations in High Frequency Radio Waves*, L. G. Trolese and John B. Smyth, BuShips Problem X4-49CD, Report WP-18, NRSL, Feb. 1, 1945. CP-225-M1

18. *Dynamic Meteorology*, Bernhard Haurwitz, McGraw-Hill Book Co., 1941.

18a. *Ibid.*, p. 286.

18b. *Ibid.*, p. 288.

19. *Meteorologische Zeitschrift*, Bernhard Haurwitz, 1931.

20. *Monthly Weather Review*, W. C. Jacobs, 65, No. 9, 1947.

21. "Microbarometric Oscillations at Blue Hill," Bernhard Haurwitz, R. Stone, and C. F. Brooks, *Bulletin of the American Meteorological Society*, 16, Nos. 6-7, 1935, pp. 153-159.

22. *Wissenschaftliche Ergebnisse der Deutschen Atlantischen Expedition auf dem Forschungs-und Vermessungsschiff, Meteor*, 1925-1927, 15, Berlin Leipsig, 1933.

23. *Qualitative Survey of Meteorological Factors Affecting Microwave Propagation*, I. Katz and J. M. Austin, OEMsr-262, Division 14 Report 488, RL, June 1, 1944. CP-311-M3

24. "Die Passatinversion," von Ficker, *Veröffentlichungen des Meteorologischen Institute der Universität, Berlin*, 1, No. 3, 1936.

25. *Modified Index Distribution Close to the Ocean Surface*, R. B. Montgomery and Robert H. Burgoyne, OEMsr-262, Division 14 Report 651, RL, Feb. 16, 1945. CP-222.2-M1

26. *Results of Low Level Atmospheric Soundings in the South-*

west and Central Pacific Ocean Areas, Paul A. Anderson, K. E. Fitzsimmons, G. M. Grover, and S. T. Stephenson, OEMsr-728, Research Project PDRC-647, NDRC Report 9, Washington State College, Feb. 27, 1945. CP-335-M4

27. *Atlas of Climatic Charts of the Oceans*, W. F. McDonald, U. S. Dept. of Agriculture, Weather Bureau, 1938.

28. *Atmospheric Refraction, A Preliminary Qualitative Investigation*, Lloyd J. Anderson, F. P. Dane, J. P. Day, R. F. Hopkins, L. G. Trolese, and A. P. D. Stokes, BuShips Problem X4-49CD, Report WP-17, NRSL, Dec. 28, 1944.
CP-222-M9

Chapter 2

1. *Bureau of Standards Journal of Research*, Diamond, Hinman, F. W. Dunmore, and Lapham. 25, 1940, p. 328.

2. *Bureau of Standards Journal of Research*, D. N. Craig, 21, 1938, p. 225.

3. *Bureau of Standards Journal of Research*, F. W. Dunmore, 23, 1939, p. 702.

4. *Instruments and Methods for Measuring Temperature and Humidity in the Lower Atmosphere*, I. Katz, OEMsr-262, Service Project SC-8, Division 14 Report 487, RL, Apr. 12, 1944. CP-344-M2

5. *The Captive Radiosonde and Wired Sonde Techniques for Detailed Low-Level Meteorological Sounding*, Paul A. Anderson, C. L. Barker, K. E. Fitzsimmons, and S. T. Stephenson, OEMsr-728, Research Project PDRC-647, Division 14 Report 192, Report 3, Washington State College, Oct. 4, 1943. CP-341-M1

5a. *Report of Second Propagation Conference, February 10 to 11, 1944 at the Empire State Building, New York*, OEMsr-1207, CUDWR-WPG, February 1944, p. 38. CP-100-M2

5b. *Notes on Operational Use of Low-Level Meteorological Sounding Equipment*, K. E. Fitzsimmons, S. T. Stephenson, and Robert W. Bauchman, OEMsr-728, Research Project PDRC-647, Report 7, Washington State College, June 15, 1944. CP-342-M2
Operating Instructions for the WSC Low-Level Atmospheric Sounding Equipment, Paul A. Anderson, OEMsr-728, Research Project PDRC-647, Report 8, Washington State College, July 10, 1944. CP-342-M3

6. *Journal of Scientific Instruments*, P. A. Sheppard, 17, 1940, p. 218.

7. *A Remote Indicating Cup Anemometer with Magnetic Coupling*, Roscoe G. Dickinson and Douglas L. Kraus, OSRD 3714, NDCrc-137 and OEMsr-861, Service Project CWS-26, NDRC Division 10, CIT, Apr. 10, 1944.
Div. 10-301.1-M2

8. *Geophysical Memoirs*, N. K. Johnson, No. 46, 1929.

9. *Propagation and Reflection Characteristics of Radio Waves as Affecting Radar*, W. G. Michels and W. C. Pomeroy, Service Project (M-3) 11a, U.S. Army Air Forces Board, Orlando, Fla., Jan. 31, 1944. CP-531-M1

10. *Balloon Psychrometer for the Measurement of the Relative Humidity of the Atmosphere at Various Heights* (and Addendum), S. M. Doble and S. Inglefield, OSRD II-5-5079(S) and OSRD II-5-5080(S), ICI, Apr. 1, 1943; Addendum Sept. 25, 1943. CP-344-M1

11. *Report of Fries Instrument Division Bendix Aviation Corp.*, to the Bureau of Ships, May 1944. CP-342-M1

Chapter 3

1. *K-Band Rain and Water-Vapor Attenuation over Tokyo*, Arthur E. Bent and E. M. Purcell, Division 14 Report, RL.

2. *Modified Index Distribution Close to the Ocean Surface*, R. B. Montgomery and Robert H. Burgoyne, OEMsr-262, Division 14 Report 651, RL, Feb. 16, 1945.
CP-222.2-M1

3. *Determination of a Suitable Method of Forecasting Radar Propagation Variations over Water, Tests Conducted by 26th Weather Region, Orlando, Florida*, J. R. Gerhardt and William E. Gordon, Service Project 4252R060.77, U. S. Army Air Forces, Mar. 10, 1945. CP-425-M1

4. *Tropospheric Propagation and Radio Meteorology*, Report WPG-5, CUDWR-WPG, September 1944.

5. *Preliminary Instruction Manual, Weather Forecasting for Radar Operations*, Report 614, U. S. Army Air Forces, Weather Division, March 1944. CP-410-M4

6. *Variations in Radar Coverage*, Report JANP-101, Joint Communications Board June 1, 1944. CP-202.4-M4
Earlier edition: IRPL T-1, CUDWR-WPG, May 1944.
CP-202.5-M1

7. *Tropospheric Weather Factors Likely to Affect Super-refraction of VHF-SHF Radio Propagation as Applied to the Tropical West Pacific*, E. Dillon Smith and R. D. Fletcher, Report RP-1, U. S. Department of Commerce, Weather Bureau, July 1, 1944. CP-424-M1

8. *Nomograms for Computation of Modified Index of Refraction*, Robert H. Burgoyne, OEMsr-262, Division 14 Report 551, RL, Apr. 6, 1945. CP-222.1-M7

9. *Tables for Computing the Modified Index of Refraction M*, E. R. Wicher, Report WPG-8, CUDWR, March 1945.

10. *Elements of Radio Meteorological Forecasting*, H. G. Booker, Report T-1621, Mathematics Group, TRE, Malvern, Feb. 14, 1944. CP-410-M3

11. *World Atlas of Sea Surface Temperatures, Hydrographic Office*, No. 225, 1944.

12. *Atlas of Climatic Charts of the Oceans*, P. W. Kenworthy, U. S. Weather Bureau, 1938.

13. *Monthly Meteorological Charts of the Western Pacific Ocean*, Marine Branch of the Meteorological Office, British Air Ministry, London, England.

14. *Climatic Atlas of Japan and Her Neighboring Countries*, United States Navy Reprint, 1943.

15. *Climatic Atlas for Alaska*, Report 444, Weather Bureau Information Branch, Headquarters Army Air Forces.

16. *Third Conference on Propagation, Washington, D. C.* [on] *November 16 to 18, 1944*, NDRC CUDWR-WPG, 1945, pp. 5-6. CP-100-M4

17. *Effect of Meteorological Conditions at Saipan upon Radar Coverage*, JEIA Survey Report 8868, Dec. 5, 1944.

18. *Results of Low Level Atmospheric Soundings in the Southwest and Central Pacific Oceanic Areas*, Paul A. Anderson, K. E. Fitzsimmons, G. M. Grover, and S. T. Stephenson, OEMsr-728, Research Project PDRC-647, Report 9, Washington State College, Feb. 27, 1945. CP-335-M4

19. *Preliminary Instruction Manual of Weather Forecasting for Radar Operations in South West Pacific Areas*, D. F. Martyn and P. Squires, Report RP-220, CSIR-RL, Sept. 4, 1944, p. 46. CP-424-M2

20. *The Air Defense System of the Near Islands*, Thomas J. Carroll, Report OAD-55, U. S. Army Air Forces, Eleventh Air Force, OCSO, Operational Analysis Division, Aug. 30, 1944. CP-202.1-M5

21. *The Coincidence of Temperature Inversions and Non-Standard Radar Propagation and Reflection*, Report JEIA 8366.

Chapter 4

1. *Interim Report on Experiments on Ground Reflection at a Wavelength of 9 Cm*, L. H. Ford, RRB/C-101 or JEIA 4899, DSIR, July 7, 1944.

2. *An Experimental Investigation of the Reflection and Absorption of Radiation of 9-Cm Wavelength*, L. H. Ford and R. Oliver, OSRD WA-3386-2, Report RRB/C-107, DSIR, Oct. 27, 1944. CP-532-M2

3. *S-Band Measurements of Reflection Coefficients for Various Types of Earth*, E. M. Sherwood, Report 5220.129, Sperry Gyroscope Company, Oct. 29, 1943. CP-532.1-M1

4. *Centimeter Wave Propagation over Sea within the Optical Range*, H. Archer-Thomson, J. C. Dix, F. Hoyle, E. C. S. Megaw, and M. H. L. Pryce, OSRD W-157-16, Report M-398, ASE, January 1942. CP-532.2-M1

5. *Preliminary Report on the Reflection of 9-Cm Radiation at the Surface of the Sea*, H. Archer-Thomson, N. Brooks,

T. Gold, and F. Hoyle, OSRD WA-1131-2, Report M-532, ASE, September 1943. CP-532.2-M2

6. *Preliminary Measurements of 10-Cm Reflection Coefficients of Land and Sea at Small Grazing Angles*, Pearl J. Rubenstein and William T. Fishback, Division 14 Report 478, RL, Dec. 11, 1943. CP-532-M1

7. *Further Measurements of 3- and 10-Cm Reflection Coefficients of Sea Water at Small Grazing Angles*, William T. Fishback and Pearl J. Rubenstein, OEMsr-262, Division 14 Report 568, RL, May 17, 1944. CP-532.2-M4

8. *Ground Reflection Coefficient Experiments on X-Band, Case 20564*, W. M. Sharpless, Report MM-44-160-250, BTL, Dec. 15, 1944. CP-532.1-M3

9. *Scattering*, R. L. Eckersley, OSRD WA-2255-1f, JEIA 3904, Report TR-481, BRL, November 1943. CP-512-M3

10. *Reflection and Scattering*, T. L. Eckersley, OSRD WA-4002-12, Report TR-506, BRL, January 1945. CP-532.2-M5

Chapter 5

1. *The Atmospheric Absorption of Microwaves* (in Third Conference Report of CP), J. H. Van Vleck, Report 175 (43-2), RL, Apr. 27, 1942. Div. 14-121.1-M4 See also Third Conference, Nov. 16-18, 1944. CP-100-M4

2. *Further Theoretical Investigations on the Atmospheric Absorption of Microwaves*, J. H. Van Vleck, OEMsr-262, Service Project AN-25, Division 14 Report 664, RL, Mar. 1, 1945. CP-510-M8

3. *Propagation of K/2 Band Waves*, G. E. Mueller, Report MM-44-160-150, BTL, July 3, 1944. CP-511-M7

4. *The Absorption of One-Half Centimeter Electromagnetic Waves in Oxygen*, E. R. Beringer, OEMsr-262, Service Project AN-25, Division 14 Report 684, RL, Jan. 26, 1945. CP-510-M7

5. *The Absorption of Atmospheric Water-Vapor in the K-Band Region*, R. H. Dicke, R. L. Kyhl, A. B. Vane, and E. R. Beringer, Division 14 Report 1002, RL, Jan. 15, 1946. Div. 14-122.13-M5

6. *An Aerial Investigation of K-Band Radar Performance under Tropical Atmospheric Conditions*, R. S. Bender, A. E. Bent, and J. W. Miller, Division 14 Report 729, RL, Oct. 1, 1945. Div. 14-122.23-M6

7. *Rotational Line Width in the Absorption Spectrum of Atmospheric Water Vapor and Supplement*, Arthur Adel, OEMsr-1361, NDRC Division 14 Report 320, University of Michigan, Oct. 10, 1944; Supplement Feb. 1, 1945. (see also reference 2) CP-510-M6

8. *Annalen der Hydrographie*, M. Diem, Berlin, 70, 1942, pp. 142-150.

9. *An Investigation on the Number and Size Distribution of Water Particles in Nature*, Josef Masur, F/Lt. Polish Air Force, OSRD II-5-6306(8), Report MRP-109, Meteorological Research Committee, Great Britain, June 10, 1943. CP-511-M5

10n. *Provincetown Path*, private communication from Donald E. Kerr and G. T. Rado of RL.

10b. *Measurements of the Attenuation of K-Band Waves by Rain*, G. T. Rado, OEMsr-262, Service Project AN-25, Division 14 Report 603, RL, Mar. 7, 1945. CP-511-M10

11. *Interim Report of the U. S. W. Panel Working Committee, Part I, Water in the Atmosphere*, A. C. Best, JEIA 7607, Report AC-7375, MO-USW, Aug. 14, 1944.

12. *Interim Report of the U. S. W. Panel Working Committee, Part III, Attenuation of Centimeter Waves by Rain, Hail, and Clouds*, J. W. Ryde and D. Ryde, JEIA 7607, Report AC-7375, USWP, Report 8516, GEC, Aug. 3, 1944.

13. *Polar Molecules*, P. Debye, The Chemical Catalogue Co., New York, 1929.

14. *Summer Storm Echoes on Radar MEW*, J. S. Marshall, R. C. Langille, William M. Palmer, R. A. Rodgers, G. P. Adamson, and F. F. Knowles, Report 18, CAORG, Nov. 27, 1944. CP-621.1-M2

15. *The Effect of Clutter Fluctuations on MTI*, H. Goldstein, Division 14 Report 700, RL, Dec. 27, 1945. Div. 14-263.1-M4

16. *Annalen der Physik*, G. Mie, 25, 1908, p.377.

17. *Echo Intensities and Attenuation Due to Clouds, Rain, Hail, Sand, and Duststorms at Centimeter Wavelengths*, J. W. Ryde, OSRD WA-81-25, Report 7831, GEC, Oct. 13, 1941. CP-511-M1

18. *Electromagnetic Theory*, J. A. Stratton, McGraw-Hill Book Co., 1941.

18a. *Ibid.*, pp. 563-573.

18b. *Ibid.*, pp. 554-560.

19. *The Theory of Sound*, Lord Rayleigh, McMillan and Co., Ltd., London, 1940.

20. *On Light Scattering by Spheres, Parts I and II*, Leon Brillouin, OEMsr-1007, AMG-C 100 and 132, AMP 87.1 and 87.2, December 1943 and April 1944. AMP-202-M2, M3

21. *Preliminary Report on the Dielectric Properties of Water in the K-Band*, C. H Collie, CL Misc. 25, CVD Report, May 1944.

22. *Properties of Ordinary Water-Substance*, N. E. Dorsey, American Chemical Society Monograph Series, Reinhold Publishing Corp., New York, pp. 350-373.

23. *Dielectric Properties of Water and Ice at K-Band*, E. L. Younker, OEMsr-262, Service Project AN-25, Division 14 Report 644, RL, Dec. 4, 1944. CP-522.1-M2

24. H. G. Houghton's data reproduced in: *Aeronautical Meteorology*, G. F. Taylor, Pitman Publishing Corp., New York-Chicago, 1943.

25. *Physics of the Air*, W. J. Humphreys, McGraw-Hill Book Co., 1940.

26a. *Third Conference on Propagation, Washington, D. C. [on] November 16 to 18, 1944*, E. Dillon Smith, NDRC CUDWR-WPG, 1945. CP-100-M4

26b. J. O. Laws and D. O. Parsons, National Research Council, *Transactions of the American Geophysical Union*, Part II 1943, p. 452.

27. *The Effect of Rain upon the Propagation of 1-Cm Electro-Magnetic Waves, Case 22098*, S. D. Robertson, Report MM-42-160-87, BTL, Aug. 1, 1942. CP-511-M2

28. *Absorption of 1-Cm Radiation by Rain*, M. G. Adam, R. A. Hull, and C. Hurst, Misc. Report 3, CVD-CL.

29. *K-Band Radar Transmission, A Preliminary Report of Tests Made Near Atlantic Highlands, N. J. between December 1943 and April 1944*, G. C. Southworth, A. P. King, and S. D. Robertson, Report MM-44-160-115, BTL, May 19, 1944. CP-202.2-M1

30. *The Effect of Rain on the Propagation of Microwaves, Case 22098*, A. P. King and S. D. Robertson, Report MM-42-160-93, BTL, Aug. 26, 1942. CP-511-M3

31. *Calibration and Operational Tests of AN/CPS-1 (MEW)*, Army Air Forces Board Project (M-3)-9, Mar. 30, 1944.

32. *Radar Echoes from Atmospheric Phenomena*, A. E. Bent, Division 14 Report 173(42-2), RL, Mar. 13, 1943. CP-621.1-M1

33. A. E. Bent, RL, unpublished report, Feb. 29, 1944.

34. *Radar Echoes from Clouds of Water Droplets*, F. Hoyle, Report AC-7930, USW 128, Mar. 16, 1945.

35. A. J. F. Siegert, RL unpublished, 1943.

36. *Interim Report of the U.S.W. Panel Working Committee, Part II, The Attenuation of Centimeter Waves by Atmospheric Gases*, J. M. Hough, JEIA 7607, Report AC-7375, USW, July, 1944.

37. *Interim Report on Experiments on Ground Reflection at a Wavelength of 9 Cm*, L. H. Ford, JEIA 4899, Report RRB/C-101, DSIR, July 7, 1944.

38. *The Dielectric Properties of Water in the Temperature Range 0° C to 40° C for Wavelengths of 1.24 Cm and 1.58 Cm*, J. A. Saxton and J. A. Lane, JEIA 9811, Report RRB/C-116, DSIR, Mar. 7, 1945.

39. *The Anomalous Dispersion of Water at Very High Radio Frequencies in the Temperature Range 0° C to 40° C*,

J. A. Saxton, JEIA 9812, Report RRB/C-118, NPL-DSIR, Apr. 6, 1945.   CP-522.11-M3

40. *A New Method for Measuring Dielectric Constant and Loss in the Range of Centimeter Waves*, S. Roberts and Arthur R. von Hippel; *Wave Guides with Dielectric Sections*, L. J. Chu, Report 102, MIT, March 1941.   CP-521-M1

41. *The Measurement of Dielectric Constant and Loss with Standing Waves in Coaxial Wave Guides*, Arthur R. von Hippel, D. G. Jelatis, and W. B. Westphal, OEMsr-191, NDRC Division 14 Report 142, Laboratory for Insulation Research, MIT, April 1943.   CP-521-M4

42. *Auxiliary Equipment for the MIT Coax Instrument and Its Use*, Arthur R. von Hippel, D. G. Jelatis, W. B. Westphal, M. G. Haugen, and R. B. Charles, OEMsr-191, NDRC Division 14 Report 210, Laboratory for Insulation Research, MIT, Nov. 1, 1943.   Div. 14-131.2-M1

43. T. A. Taylor and Willis Jackson, Ministry of Supply, CPR Report 30.

44. "The Dielectric Dispersion and Absorption of Water and Some Organic Liquids," W. P. Connor and C. P. Smyth, *Journal American Chemical Society*, 65, 1943, pp. 382-389.

45. *Progress Report on Ultra High Frequency Dielectrics*, Arthur R. von Hippel, OEMsr-191, NDRC Division 14 Report 121, Laboratory for Insulation Research, MIT, January 1943.   CP-521-M2

46. R. Dunsmuir and J. Lamb, Ministry of Supply, 287/Gen/35, DSR Report 61, Department of Scientific Research, Mar. 5, 1945.

47a. *The Dielectric Constant and Absorption Coefficient of Water Vapour for Wavelengths of 9 Cm and 3.2 Cm, Frequencies*

3,330 and 9,350 Mc/s, J. A. Saxton, Paper RRB/S-11, NPL-DSIR, June 14, 1943.   CP-522.12-M3

47b. *The Dielectric Constant and Absorption Coefficient of Water Vapour for Radiation of Wavelength 1.6 Cm, Frequency 18,800 Mc/s*, J. A. Saxton, Report RRB/S-17, NPL-DSIR, Apr. 22, 1944.

48. *The Relation between Absorption and the Frequency Dependence of Refraction* (Fourth Conference), J. H. Van Vleck, Division 14 Report 735, RL, May 26, 1945.   Div. 14-122.24-M4

Chapter 7

1. *Possible Measurement of Radar Echoes by Use of Model Targets*, S. A. Goudsmit and P. R. Weiss, Division 14 Report 196 (43-24), RL, Mar. 4, 1943.   Div. 14-122.113-M5

2. *The Theory of Random Processes*, G. E. Uhlenbeck, Division 14 Report 454, RL, Oct. 15, 1943. Div. 14-125-M7

3. *On the Fluctuations in Signals Returned by Many Independently Moving Scatterers*, A. J. F. Siegert, Division 14 Report 465, RL, Nov. 12, 1943.   Div. 14-122.113-M7

Chapter 8

1. *Measurements of the Angle of Arrival of Microwaves in the X-Band, Case 20564*, W. M. Sharpless, Report MM-44-160-249, BTL, Nov. 7, 1944.

2. *Ground Reflection Coefficient Experiments on X-Band, Case 20564*, W. M. Sharpless, Report MM-44-160-250, BTL, Dec. 15, 1944.   CP-532.1-M3

GENERAL BIBLIOGRAPHY OF REPORTS ON TROPOSPHERIC PROPAGATION

REPORT WPG-14

This Bibliography is a comprehensive tabulation of the body of scientific reports pertaining to wave propagation through the troposphere, compiled by the Columbia University Wave Propagation Group to about October 31, 1945. For convenience and clarity it has been divided into twenty sections, each dealing with a particular phase of propagation phenomena. The various headings are self-explanatory, and the list of sources and their abbreviated designations, which precede the Bibliography proper will be found helpful.

In preparing the Bibliography, about 560 papers were considered. Of these, 115 were excluded as obsolete, or because their contents were included in other reports retained. An additional 46 papers dealing with doppler effect and the transmission of sound in water were also excluded as not directly relevant. It is believed that the approximately 400 titles included form a fairly exhaustive compilation of present knowledge of electromagnetic wave propagation through the troposphere.

The reports are grouped and a Bibliography number has been assigned to each report. The letter to the right of the Bibliography number designates the present United States security classification.

Requests for copies of the reports listed herein may be made by Bibliography number referring to this edition, but should be made through the proper channels. The Central Radio Bureau is the distributing agent for American reports in Great Britain and for propagation reports originating in Great Baddow, Chelmsford, England. All other British reports may be obtained from the British government department controlling the sources.

The OSRD Liaison Office will, upon request, supply readers in the United States who are not in the Armed Services with all reports originating outside of the United States. They will supply Army and Navy units with all except JEIA-numbered reports. Requests for the latter should be directed to the Joint Electronics Information Agency, Munitions Building, Washington, D.C.

In general, application should be made to the NDRC Chairman's Office for reports written by NDRC Divisions, Committees, or contractors, NDRC Section 6.1 being the present exception; to the Bureau of Ships for reports from Naval Research Laboratory, Navy Radio and Sound Laboratory, and all reports appearing in Section 20 of the Bibliography (Under-Water Sound Propagation); to the Office of the Chief Signal Officer for Signal Corps reports; to Inter-Service Radio Propagation Laboratory, Bureau of Standards for IRPL reports. Requests for case-numbered BTL reports should be sent to the Director of Research, Bell Telephone Laboratories, 463 West Street, New York, N. Y.

CLASSIFICATION OF REPORTS

1.000 Conferences and Progress Reports
2.000 General Discussions
3.000 Standard Atmosphere Propagation
4.000 Non-Standard Atmosphere Propagation
5.000 Non-Standard Atmosphere Propagation
6.000 Propagation Experiments
7.000 Meteorological Theory
8.000 Meteorological Experiments
9.000 Meteorological Equipment
10.000 Radar Forecasting
11.000 Atmospheric Absorption and Scattering
12.000 Dielectric Constant and Loss Factor
13.000 Reflection Coefficient
14.000 Horizontal and Vertical Polarization
15.000 Effect of Hills, Trees, Obstacles, etc.
16.000 Transmission over Part Land-Part Sea
17.000 Targets and Echoes
18.000 Doppler Effect
19.000 Communication (Tropospheric)
20.000 Under-Water Sound Propagation

LIST OF ABBREVIATIONS

AMERICAN

AMG-C.	Applied Mathematics Group, Columbia University
BTL.	Bell Telephone Laboratories
CBS.	Columbia Broadcasting System
CESL.	Camp Evans Signal Laboratory
CP.	Committee on Propagation
CUDWR.	Columbia University, Division of War Research
IRPL.	Inter Service Radio Propagation Laboratory; National Bureau of Standards
JEIA.	Joint Electronics Information Agency
MIT.	Massachusetts Institute of Technology
NATC.	Naval Air Training Center, Corpus Christi, Texas
NDRC.	National Defense Research Committee
NRL.	Naval Research Laboratory
NRSL.	Navy Radio and Sound Laboratory
OCSO.	Office of the Chief Signal Officer
OFS.	Office of Field Service
ORB.	Operational Research Branch; Office of the Chief Signal Officer
ORG.	Operational Research Group; Office of the Chief Signal Officer
RCA.	Radio Corporation of America
RL.	Radiation Laboratory, M.I.T.
RRL.	Radio Research Laboratory, Harvard University
SWP.	South West Pacific
TCAW.	Technical Committee on Air Warning, Office of the Sec'y of War; Reports distributed by Radiation Laboratory
UCDWR.	University of California, Division of War Research
WD., HQAAF.	Weather Division, Headquarters Army Air Forces
WPG	Wave Propagation Group

AUSTRALIAN

AORG.	Australian Operational Research Group
ATP.	Australian Technical Paper
CSIR-RL.	Council for Scientific and Industrial Research, Radiophysics Laboratory
RAAF.	Royal Australian Air Force

BRITISH

A& AEE.	Aircraft and Armament Experimental Establishment
AC.	Advisory Council on Scientific Research and Technical Development
ADRDE.	Air Defense Research and Development Establishment
AORG.	Army Operational Research Group
ASE.	Admiralty Signal Establishment
BAD.	British Admiralty Delegation
BCSO.	British Central Scientific Office
BRL.	Baddow Research Laboratory
CAEE.	Coast Artillery Experimental Establishment
CRB.	Central Radio Bureau
CVD-CL.	Coordination of Valve Development Committee, Clarendon Laboratory
DMO.	Director of Meteorological Office
DSIR.	Department of Scientific and Industrial Research
GEC.	General Electric Company
ICI.	Imperial Chemical Industries
JIEE.	Journal of the Institution of Electrical Engineers
JMRP.	Joint Meteorological Radio Propagation Sub-Committee
MAP.	Ministry of Aircraft Production
MO.	Meteorological Office, Air Ministry
MetResCom.	Meteorological Research Committee
NMS.	Naval Meteorological Service
NPL.	National Physical Laboratory
ORS-ADGB.	Operational Research Section, Air Defense of Great Britain
POED.	Post Office Engineering Department
RAE.	Royal Aircraft Establishment
RRB.	Radio Research Board
RRDE.	Radar Research and Development Establishment
SDTM.	Synoptic Divisions Technical Memorandum
SRDE.	Signal Research and Development Establishment
TRE.	Telecommunications Research Establishment
USWP.	Ultra Short Wave Propagation Panel of the RDF Application Committee
USWP-WC.	Ultra Short Wave Propagation Panel, Working Committee

CANADIAN

ORS-WAC.	Operational Research Section, Western Air Command, Royal Canadian Air Force
CAORG.	Canadian Army Operational Research Group

NEW ZEALAND

ORS-RNZAF.	Operational Research Station, Royal N.Z. Air Force
RDL-DSIR-NZ.	Radio Development Laboratory, Department of Scientific and Industrial Research—New Zealand

SOUTH EAST ASIA

ORS-SEA.	Operational Research Section, South East Asia

Bib. No.	Title Author or Source	Number	Date
	1.000 CONFERENCES AND PROGRESS REPORTS		
1.001 S	The Effect of the Atmosphere on the Propagation of Radio Waves. First Report on American Investigations.	BC80 No. 201	June 16 1943
1.002 S	The Effect of the Atmosphere on the Propagation of Radio Waves. Second Report on American Investigations.	BC80 No. 218	Aug. 6 1943
1.003 C	Notes on Microwave Propagation Conference at MIT Radiation Laboratory.	RL 42-	Sept. 24 1943
1.004 S	Report on K-Band Work in U.S.A.	RL 475	Oct. 20 1943
1.005 S	Monthly Progress Report for the Month of March, 1944 (New Zealand). RDI-DSIR NZ	RD 1/363	Apr. 14 1944
1.006 C	Report of International Radio Propagation Conference.	IRPL-C81	June 1944
1.007 C	Conference on Propagation—February 10-11, 1944—Empire State Building, New York. CUDWR WPG	CP NDRC	1944
1.008 S	TRE Progress Report for the Period 16th June to 15th July, 1944. TRE	MAP File Ref. No. SB 30917	June-July 1944
1.009 S	Progress Report, Radio Development Laboratory, DSIR, New Zealand for Months of June and July, 1944. RDI-DSIR NZ	RD 1/439 or JEIA 5491	June-July 1944
1.010 S	Scientific Investigations on Propagation Problems in the South West Pacific Area.	Australia	July 25 1944
1.011 S	The Air Defense System of the Near Islands.	OC80 OAD-55	Aug. 30 1944
1.012 S	Reviews of Progress of USW Propagation Work, I The Evaluation of Solutions of the Wave Equation for a Stratified Medium. USWP	AC 7017/ RDF 239 or JEIA 5634	Sept. 26 1944
	II Statement of Work in Progress Relevant to Investigations of the Propagation of Radio Waves Through the Troposphere. (NPL)	AC 7018/ USW	Sept. 25 1944
	III Microwave Propagation Research at Signal Research & Development Establishment. SRDE	AC 7019/ USW or JEIA 6464	Sept. 26 1944
	IV Correlation of Radar Operational Data with Meteorological Conditions. AORG	AC 7020/ USW	Sept. 28 1944
	V Progress Report on Forecasting of Radar Conditions. DMO	AC 7021/ USW or JEIA 6462	Oct. 2 1944
	VI Vertical Temperature and Humidity Gradients at Eye. DMO	AC 7022/ USW or JEIA 6461	Oct. 2 1944

Bib. No.	Title Author or Source	Number	Date
	VII The Use of Radar for the Detection of Storms. DMO	AC 7023/ USW or JEIA 6460	Oct. 2 1944
	VIII Present States of Theoretical Study of Radio Propagation Through the Troposphere by the Mathematics Group. TRE	AC 7024/ USW	Oct. 2 1944
	IX Review of Short-Period Experimental Studies of Centimetre Wave Propagation, Carried out Jointly by ASE, SRDE and GEC.	AC 7025/ USW or JEIA 6459	Oct. 16 1944
	X Study of Cm. Wave Propagation over Cardigan Bay to Mount Snowden.	AC 7026/ USW or JEIA 6458	Oct. 14 1944
	XI Study of Reflection Coefficient of the Sea at Centimetre Wavelengths.	AC 7027/ USW	Oct. 14 1944
	XII K, X, and S (LLANDUDNO) Trials—General Summary of the Experimental Results Obtained which are Concerned with the Dependence of Radio Propagation on Meteorological Conditions. TRE & RRDE	AC 7028/ USW	Oct. 14 1944
	XIII Progress Report on 369 Trials by DNMS.	AC 7029/ RDF 240 USW or JEIA 6466	Oct. 14 1944
	XIV Survey of Progress in the United Kingdom on the Electromagnetic Theory of Tropospheric Propagation. RRDE	AC 7030/ USW	Oct. 16 1944
1.013 S	XV Study of Meteorological Factors Responsible for the Refractive Structure of the Troposphere. RRDE	AC 7031/ USW	Oct. 16 1944
	Report No. 1 of Project SWP—3.2 of the OFS.	Washington State Coll.	Nov. 2 1944
1.014 C	Data on Super Refraction Supplied by Australian Radar Stations. (Progress Report on Analysis of Data from 200 Mc/s. Radar Stations Mar.-Aug., 1944).	CSIR-RL RP 229/1	Dec. 6 1944
1.015 S	Report No. 2 of Project SWP—3.2 of the OFS.	Washington State Coll.	Jan. 7 1945
1.016 S	Third Conference on Propagation—Washington, D.C.—Nov. 16-18, 1944 CUDWR-WPG	CP NDRC	1945
1.017 R	Survey of Field of Radio Propagation and Noise with Special Reference to Australia.	CSIR RP 231 or JEIA 8641	Nov. 27 1944
	2.000 GENERAL DISCUSSIONS		
2.001 S	Considerations Affecting Choice of Wavelength.	RL- V-78	Sept. 24 1941
2.002 S	Notes on Microwaves.	RL- T-2	Oct. 20 1941
2.003 S	Fundamentals of Early Warning Radar. ORG	OC80 ORG-E-5-1	Mar. 5 1943

2.000 (continued)

No.	Title	Source	Date
2.004 S	RDF Propagation at Centimeter Wavelengths.	Australia No. 284 RP 177	Apr. 27 1943
2.005 C	Notes on Ultra Short Wave Propagation in the United States.	TRE S 4457	Aug. 9 1943
2.006 C	An Introduction to Microwave Propagation.	RL 406	Sept. 16 1943
2.007 R	Electrical Communication Systems Engineering. War Dept.	TM 11-486a	Feb. 25 1944 2nd Edition
2.008 C	Anomalous Propagation and the Army. T. J. Carroll	OCSO Rep. No. ORB-P-18-1	Apr. 25 1945 Mar. 4 1944
2.009 C	Radar System Fundamentals War Dept.	TM 11-467	Apr. 28 1944
2.010 B	Radio Fundamentals. War Dept.	TM 11-455	May 22 1944
2.011 R	Radar Electronic Fundamentals. War Dept.	TM 11-466	June 29 1944
2.012 C	Principles of Radar. Staff of MIT Radar School		1944
2.013 C	Fundamentals of Radar. Staff of Radar Fund. Sec.-NATC	NAVAER 08-58-108	Nov. 10 1944
2.014	General Lecture Series on Radar Components.RL	RL T-18	Dec. 1, 1944
2.015 C	Radar Performance Testing Manual. HQ, AAF	Air Forces Manual No. 28	July 1944 2nd Edition
2.016 B	Effects of Site Conditions on Operation of Ground Radar Installation on Aerodromes. See also 10.007.	TRE T 1805	

3.000 STANDARD ATMOSPHERE PROPAGATION

No.	Title	Source	Date
3.001	The Diffraction of Electro-magnetic Waves from an Electrical Point Source Round a Finitely Conducting Sphere, with Applications to Radiotelegraphy and the Theory of the Rainbow. Part I	Phil. Mag. Vol. 24 pp 141-176	July 1937
	The Diffraction of Electro-magnetic Waves from an Electrical Point Source Round a Finitely Conducting Sphere, with Applications to Radiotelegraphy and the Theory of the Rainbow. Part II	Phil. Mag. Vol. 24 pp 825-864	Supp. Nov. 1937
	The Propagation of Radio Waves over a Finitely Conducting Spherical Earth. Part III	Phil. Mag. Vol. 25 pp.817-837	June 1938
	Further Note on the Propagation of Radio Waves over a Finitely Conducting Spherical Earth. Part IV	Phil. Mag. Vol. 27 pp 261-275	March 1939
3.002	Ultra Short Wave Propagation Curves (0.1 to 10 Meters).	Marconi Handbook	March 28 1940
3.003	Report on Signal Strength Curves Within the Visual Range.	Marconi RD 455	Nov. 1940
5.004	The Effect of the Earth's Curvature on Ground-Wave Propagation.	Proc. IRE Vol. 29 pp 16-24	Jan. 1941
3.005 C	The Siting of RDF Stations. Appendix: Screening of RDF Sets from Fixed Echoes.	TRE T 1430	July 19 1941
3.006 R	Propagation Curves for Wavelengths of 13 Meters. Supplement to USW Propagation Curves RD 455.	Marconi Appendix RD 455A	Nov. 1941
3.007	The Calculation of Ground-Wave Field Intensity over a Finitely Conducting Spherical Earth.	Proc. IRE Vol. 29 pp 623-639	Dec. 1941
3.008 S	Siting of Stations for Maximum Range.	TRE M/36	Feb. 9 1942
3.009 S	Microwave Interference Patterns.	RL-C-1	Mar. 7 1942
3.010 S	Dependence of Range of Radar Equipment on Wavelength for ASV—Case 28815 and 23817.	BTL MM-42-160-54	June 1 1942
3.011 S	Theoretical Field Strength of Ten Centimeter Equipment over a Spherical Earth.	TRE; M/45/HGB	July 1 1942
3.012 C	Atmospheric Refraction and Height Determination by RDF. (Details and Results of a Numerical Method of First Order Correction.) F/O (RAF) (See 3.050)	Calibration Memo No. 54 or JEIA 7773	July 6 1942
3.013 S	Dependence of Range of Submarine Radar Equipment on Wavelength—Case 20564.	BTL MM-42-160-70	July 9 1942
3.014 S	Transmission on 3000 Mc. over Sea Water.	RL-C-2	July 14 1942
3.015 S	Transmission on 100 Mc. over Sea Water.	RL-C-3	July 14 1942
3.016 S	Transmission on 200 Mc. over Sea Water.	RL-C-4	July 14 1942
3.017 S	Transmission on 500 Mc. over Sea Water.	RL-C-5	July 14 1942
3.018 C	Interim Report on Propagation Within and Beyond the Optical Range.	ASE M 448	Sept. 1942
3.019 C	Theoretical Ground Ray Field Strengths and Height Gain Curves for Wavelengths of 2—2000 M.	BRL Section E Tech. Rep. 383	Sept 1942
3.020 C	Siting for Long Range Aircraft Detection.	CESL No. T-13	10 17 '42 (Rev.)
3.021 C	VHF Field Strength Curves for Propagation within the Line of Sight. RAE	Radio/279 RAE Ref: Radio/s. 2111/ OPE 16	Oct. 1942

Bib. No.	Title	Number	Date
3.041 S	Theoretical Field Strength Near and Beyond Horizon for Orthodox Propagation of Fifty Centimeter Waves.	TRE T 1635	Feb. 24 1944
3.042 C	Location of Signal Strength Maxima, Nulls, and Reflection Areas for Standard U.S. Early Warning Radar Equipment.	First Air Force	Apr. 7 1944
3.043 S	Cover by German Coastal Radar on Low Flying Aircraft.	OCSO OAD-25	Apr. 15 1944
3.044 C	The Propagation Functions for an Atmosphere with Uniform Lapse-Rate of Refractive Index.	RRDE Research Rep. No. 256	Sept. 1 1944
3.045 S	Ideal Field Intensity Distribution in the Vertical Plane for Transmitting or Receiving Antennas when Each has the Same Pattern.	OCSO ORG-PP-5	1944
3.046 R	Propagation Curves. BTL (Issue 3—Replacing Previous Issues.)	NDRC Div. 15-Report 966-6C	Oct. 1944
3.047 C	Field Strength Calculator for Vertical Coverage Patterns and Propagation Curves.	CESL Tech. Memo No. 154-E	Dec. 20 1944
3.048 C	"Theoretische Resultaten over de Voorplanting Van Radiogolven.	Natuurkundig Laboratorium N. V. Philips Gloeilampen Fabrieken, Eindhoven, Holland	Aug. 1941 Trans.
3.049 S	Theory of the Vertical Field Patterns for RDF Stations.	CSIR-RL RP 174	Mar. 17 1943
3.050	Height/Range/Alpha Tables (Tables Relating to the Height, Range and Angle of Elevation of an Aircraft.) ADGB (See 3.012.)	ORS(ADGB) Radar Memo No. 50 or JEIA-7766	Aug. 10 1944
3.051 R	The Calculation of Field Strength for Vertical Polarisation over Land and Sea on 20 to 80 Megacycles per Second.	TRE T 1704	
3.052 C	Field Intensity Contours in Generalized Coordinates.	RL 702	May 2 1945
4.000	NON-STANDARD ATMOSPHERE PROPAGATION —PURE THEORY		
4.001 S	The Limiting Ranges of RDF Sets over the Sea.	ASE M 395	1943
4.002 S	The Theory of Anomalous Propagation in the Troposphere and Its Relation to Waveguides and Diffraction.	TRE M/60/HGB or T 1447	Apr. 12 1943
4.003 C	The Tracing of Rays in the Refracting Atmosphere.	ADRDE AC 3878 USW	Apr. 21 1943

Bib. No.	Title	Number	Date
	3.000 (continued)		
3.023 S	Relation of Radar Range to Frequency and Polarization.	RL-C-6	Nov. 3 1942
3.023	1 to 10 Cm. Propagation Curves.	Marconi TR 460	Jan. 1943
3.024 S	Properties of the Diffracted Wave Field Intensity.	RL-C-8	Feb. 12 1943
3.025 S	The Effect of Earth Curvature on the Performance Diagram of an RDF Station.	TRE 29/R102/LGHH	Feb. 25 1943
3.026 S	Radar Height Finding.	RL-C-9	Apr. 6 1943
3.027 S	Technical Requirements for GCI Search Systems Technical Requirements for Early Warning Radar Systems. RL	TCAW 1 and 2	May 10 1943
3.028 S	Low-Angle Coverage of Early Warning Radar Systems.	TCAW-3	July 26 1943
3.029 S	Factors Relating to the Design of an RDF Air Warning Set.	CSIR-RL RP 187	Aug. 11 1943
3.030 C	A Graphical Method of Computing the Bending of Radio Beams by the Effective Earth Radius Method.	CESL No. T-14	Aug. 27 1943
3.031 S	Transmission at Low Altitudes over Sea Water.	RL C-10	Sept. 1 1943
3.032 S	Radio-Frequency Propagation Above the Earth's Surface.	RCA Lab. Rep. No. 895-5 Div. 15 OEMsr-805	Sept. 11 1943
3.033 S	Field Intensity Formulae.	RL-C-11	Sept 28 1943
3.034 R	Propagation Curves. BTL (See 3.046)	NDRC Div. 15 966-6A	Oct. 5 1943
3.035	Note on Field Intensity Computations for Elevated Antennas. Case 20878.	BTL MM-43-110-28	Oct. 9 1943
3.036 C	The Calculation of Expected Vertical Coverage Diagrams.	CESL T-17	2/19/43 Revision 10/15/43
3.037 R	Charts for Use in Field Intensity Computations.	NDRC Proj C-79	Nov. 2 1943
3.038 S	Notes on Visibility Problems, Taking Account of the Curvature of the Earth.	AORG No. 152	Dec. 1 1943
3.039 C	Simplified Methods of Field Intensity Calculations in the Interference Region.	RL 461	Dec. 8 1943
3.040 C	Field Strength Near and Beyond the Horizon for Wavelengths of Ten and Thirty Cms.	TRE-M/Rep. 53/WW	Dec. 24 1943

4.000 (continued)

No.	Title	Source	Date
4.004 C	Graphical Construction of a Radar Radiation Pattern in a Stratified Atmosphere.	NRSL WP-4	May 1 1943
4.005 S	Improved Tropospheric Propagation—Curves Embracing Anomalous Propagation.	TRE	July 6 1943
4.006 C	Radiation Patterns under Cases of Anomalous Propagation.	M/65/HGB	July 19 1943
4.007 S	Effect of Humidity Gradients in the Atmosphere on Propagation at RDF Frequencies.	ADRDE R 35 Oper. Res. Rep. No. 22	July 28 1943
4.008 C	The Calculation of Field Strength Near the Surface of the Earth under Particular Conditions of Anomalous Propagation.	ADRDE Research Rep. No. 203	Oct. 28 1943
4.009 C	Anomalous Propagation over the Earth, Case 23703.	BTL MM-43-110 33	Oct. 30 1943
4.010 C	The Effect of Atmospheric Refraction on Short Radio Waves.	RL 447	Nov. 29 1943
4.011 C	Radar Ray Patterns Associated with Normal and Anomalous Propagation Conditions.	NRSL WP-6	Dec. 10 1943
4.012 C	Transmission of Plane Waves Through a Single Stratum Separating Two Media.	NRSL WP-9	Dec. 22 1943
4.013 S	Notes on Theoretical Coverage Diagrams for Anomalous Propagation.	TRE TM/Memo/14/AMW	Jan. 1 1944
4.014 C	The Dependence of Microwave Propagation over Sea on the Structure of the Atmosphere.	ADRDE Memo No. 40	Feb. 4 1944
4.015 S	Improved Tropospheric Propagation—Curves Embracing Superrefraction.	TRE T 1625	Feb. 18 1944
4.016 S	TRE Requirements for Propagation—Curves Embracing Superrefraction.	TRE	Feb. 25 1944
4.017 C	The Mechanical Determination of the Path Difference of Rays Subject to Discontinuities in the Vertical Gradient of Refractive Index. NRSL	M/Memo 16/HAB Rep. No. WP-10	Mar. 10 1944
4.018 S	Improved Tropospheric Propagation—Curves Embracing Superrefraction.	TRE T 1626	Mar. 28 1944
4.019 S	Interservice Propagation—Curves Embracing Superrefraction. Dependence of Mathematical Parameter L on Physical Entities.	TRE M/Memo 18/WW	Apr. 3 1944
4.020 S	Theoretical Coverage-Diagrams for 10 Cm. Radars Embracing Superrefraction.	TRE T 1634 or JEIA 3229	Apr. 14 1944
4.021 S	Theoretical Coverage-Diagrams for 50 Cm. Radars Embracing Superrefraction.	TRE T 1659 or JEIA 3230	Apr. 14 1944
4.022 S	Theoretical Coverage of Navigational Aids Embracing Superrefraction.	TRE T 1660	Apr. 14 1944
4.023 C	The Theory of Propagation of Radio Waves in an Inhomogeneous Atmosphere (I).	ADRDE Research Rep. No. 245	April 1944
4.024 C	Reflection Coefficient of Layers of Varying Refractive Index.	BRL TR 483 or JEIA 4644	April 1944
4.025	Evaluation of the Solution of the Wave Equation for a Stratified Medium. (See 4.043)	ADRDE MR 47	May 24 1944
4.026 C	Transmission of Plane Waves Through a Single Stratum Separating Two Media (II).	NRSL WP-13	June 22 1944
4.027	Waves Guided by Dielectric Layers.	BTL MM-44 110-52	July 5 1944
4.028 C	Microwave Transmission in Nonhomogeneous Atmosphere.	BTL MM-44-110-53	July 5 1944
4.029 C	Contour Diagrams of the Radiated Field of a Dipole under Various Conditions of Anomalous Propagation. (See 4.045)	RRDE Research Report No. 257	July 15 1944
4.030 R	Theoretical Coverage-Diagrams for 1½ Metre Radars Embracing Superrefraction.	TRE T 1708	July 23 1944
4.031 R	Propagation Curves Embracing Superrefraction: SS Duct, Profile-Index 0.2 (Preliminary Edition).	TRE M/Memo 23/WW	Sept. 7 1944
4.032 C	A Note on the Reflection Coefficient of an Isotropic Layer of Varying Refractive Index.	BRL TR 497 or JEIA 6481	Oct. 5 1944
4.033 R	Predicted Low Level Coverage of S-Band Shipborne Radars as Affected by Weather. (Horizontal Polarisation—Antenna Height 100 Ft.)	NRSL WP-14	Nov. 1 1944
4.034 R	Predicted Low Level Coverage of 200 Mcs Band Shipborne Radars as Affected by Weather. (Horizontal Polarisation—Antenna Height 100 Feet.)	NRSL WP-15	Nov. 4 1944
4.035 R	Variational Method for Determining Eigenvalues of Wave Equation of Anomalous Propagation.	TRE T 1756	Nov. 13 1944
4.036 C	Wave Propagation Analysis with the Aid of Non-Euclidian Spaces.	CUDWR WPG-7	Dec. 1944
4.037 C	Atmospheric Waves—Fluctuations in High Frequency Radio Waves.	NRSL WP-18	Feb. 1 1945
4.038 C	The Relation Between the Wave Equation and the Non-Linear First Order Equation of the Riccati Type.	BRL TR-501 or JEIA 9104	Jan. 1945
4.039 C	A Report on Transmission of Waves over the Earth.	BRL TR 504	Jan. 1945
4.040 C	New Convergent Integrals.	BRL TR 509	Feb. 1945
4.041 C	The Effect of a Subrefracting Layer of Atmosphere upon the Propagation of Radio Waves.	RRDE Memo No. 83 or JEIA-8871	Feb. 12 1945
4.042 C	Theory of Characteristic Functions in Problems of Anomalous Propagation.	RL 680	Feb. 28 1945
4.043 C	The Evaluation of the Solution of the Wave Equation for a Stratified Medium (II) (See 4.025)	RRDE Res. Rep. No. 279	Mar. 12 1945
4.044 R	Theoretical Coverage Diagrams for 3 Metre Radars Embracing Superrefraction.	TRE T 1815 or JEIA 9198	Mar. 18 1945

4.0(continued)

Bib. No.	Title	Number	Date
4.045 C	The Radiation Field of a Dipole under Various Conditions of Anomalous Propagation. (See 4.029.)	RRDE Res. Rep. No. 275	Apr. 13 1945
4.046 S	Notes on the Solution of a Non-Linear First Order Equation of the Riccati Type. (See 4.088.)	BRL TR 502 or JEIA-9725	May 1945
4.047 C	Perturbation Theory for an Exponential M-curve in Non-Standard Propagation.	CUDWR WPG-12	July 1945
4.048 C	Graphs for Computing the Diffraction Field with Standard and Superstandard Refraction.	RL 799	Aug. 13 1945

5.000   NON-STANDARD ATMOSPHERE PROPAGATION—EXPERIMENT AND THEORY

Bib. No.	Title	Number	Date
5.001 C	Radio Interpretation of Meteorological Observations in the First Two Meters of Atmosphere Above Grass at Harlington, Middlesex, January to June, 1940.	T 1471 TRE M/63	1940
5.002 S	Anomalous Echoes Observed with 10 Cms. CD Set.	ADRDE Research Rep. No. 119	Oct. 8 1941
5.003 C	Centimeter Wave Propagation over Sea Between High Sites just within Optical Range.	ASE GEC	June 12 1942
5.004 C	Centimeter Wave Propagation over Land, II. Measurements within and beyond Optical Range.	SRDE GEC AC 2917/ Com. 126	Oct. 16 1942
5.005 C	Radar Wave Propagation.	NRSL WP-2	Nov. 30 1942
5.006 C	Very Short Wave Interception and DF	BRL TR 438	1943
5.007 C	Anomalous Propagation of 10 Cm. RDF Waves over the Sea. Also: First Supplement.	AORG No. 87 Supplement	2/6/43 7/26/43
5.008 S	Investigation of Propagation Characteristics of AW Stations. ORG	Oper. Res. Rep. No. 17	Mar. 9 1943
5.009	A Study of Propagation over the Ultra-Short-Wave Radio Link between Guernsey and England on Wavelengths of 5 and 8 Meters (60 and 37.5 Mc/s.). NPL	JIEE 90	Mar. 1943
5.010 C	The Effect of Atmospheric Refraction on the Propagation of Radio Waves. NPL	RRB /8 10	Mar. 20 1943
5.011 S	Propagation of Ultra-Short Waves.	Australia Rep. No. 354	Apr. 17 1943
5.012 C	Report on Radar Wave Propagation. Atmospheric Refraction—A Qualitative Investigation.	NRSL WP-5	May 7 1943
5.013 C	Radio Interpretation of Meteorological Observations in the First 400 Feet Above Cardington, 1942.	TRE M/61 or T 1413	May 14 1943
5.014 S	Centimeter Wave Propagation over Sea, II. Measurements from Shore Sites Near and Beyond Optical Range.	GEC No. 8180	May 27 1943

Bib. No.	Title	Number	Date
5.015 S	Preliminary Observations on Radio Propagation at 6 Centimeters Between Beer's Hill, New Jersey, and New York—Case 27008-4, File 26091-1.	BTL MM-43-160-57	June 12 1943
5.016 C	Some Observations of Anomalous Propagation.	TRE M/64 or T 1483	July 6 1943
5.017 S	Application of Anomalous Propagation to Operational Problems at Home and Abroad.	TRE M/66/HGB or T 1484 or JMRP No. 3	July 7 1943
5.018 C	Propagation of Signals on 45.1, 474 and 2800 Mc. from Empire State Building to Hauppauge and Riverhead, L.I., New York. RCA	NDRC Proj. 423 Rep. No. 1	July 20 1943
5.019	Propagation of Ultra Short Waves.	Marconi TR/476	Aug. 1 1943
5.020 S	The "K" Effect in Anomalous Propagation of Ultra-Short Waves. RAAF	Australia No. 266 or JMRP No. 11	Aug. 10 1943
5.021 C	The Propagation of 10 Cm. Waves over Land Paths of 14, 52, and 112 Miles.	Wash. State Coll. Rep. No. 4 NDRC PDRC-647	Oct. 26 1943
5.022 S	The Propagation of 1-Cm. Waves over the Sea as Deduced from Meteorological Measurements.	ADRDE Res. Rep. 227 or JMRP No. 4	Nov. 11 1943
5.023 S	Centimeter Wave Propagation over Land. A Preliminary Study of the Field Strength Records between March and Sept. 1943. NPL	DSIR RRB/8 13 or JMRP No. 10	Nov. 15 1943
5.024 C	The Propagation of 10 Cm. Waves over an Inland Lake. Correlation with Meteorological Soundings.	Wash. State Coll. Rep. No. 5 NDRC PDRC-647	Nov. 16 1943
5.025 C	Measurements of Radar Wave Refraction and Associated Meteorological Conditions.	NRSL WP-7	Dec. 10 1943
5.026 C	Anomalous Propagation in India—Preliminary Report on Overland Transmission in Bengal.	OBS-SEA Rep. No. 8 5	Dec. 30 1943
5.027 S	Atmospheric Physics—Summary of Investigations on Anomalous Propagation of Radar Signals Carried out by the Australian Operational Research Group During 1942-43.	Aust. Oper. Research Group	1942-1943 Sum.
5.028 S	The Cause of Short Period Fluctuations in Centimetre Wave Communication.	ADRDE Memo 42	Mar. 8 1944
5.029 S	Anomalous Propagation in the Persian Gulf.	AC 5975/ USW	Rec'd Mar. 20 1944
5.030 S	Effect of Super-refraction on Surface Coverage on Enemy 50 Cm. and 80 Cm. Radar Sets.	TRE M/Memo 19	April 1944
5.031 S	K-X-S Experiments, News Letter No. 1. ASE	MK 12201	5/3/44

5.000 (continued)

5.052 S Abnormal Radar Propagation in the South Pacific. An Investigation into Conditions in New Zealand and Norfolk Island on 200 Mc/s, with Notes on Fiji, New Caledonia and Solomon Islands. — RNAZAF Rep. No. 119 — May 4 1944

5.053 C Procedure and Charts for Estimating the Low Level Coverage of Shipborne 200 Mcs. Radars under Conditions of Pronounced Refraction. — NRSL WP-11 (Rev.) BuShips Prob. No. X4-49CD — May 10 1944 Revised

5.054 S Centimeter Propagation over Land. A Study of the Field Strength Records Obtained During the Year 1943-1944. — DSIR RRB/ S 18 or JEIA 4789 — May 11 1944

5.055 S K-X-3 Experiments, News Letter No. 2. ASE — MK 12201 — May 13 1944

5.056 C Atmospheric Propagation Effects and Relay Equipment. OCSO — ORB-PP-12-1 — May 18 1944

5.057 C Low-Level Coverage of Radars as Affected by Weather. Procedures and Charts. (5.053 Reprinted.)NRSL — IRPL T2a — May 25 1944

5.058 R Variations in Radar Coverage. Joint Communications Board — JANP 101 — June 1 1944

Earlier Editions have Appeared As:

R Radar Operation and Weather. CUDWR-WPG — IRPL T-1 — May 1944

C Weather Influences in Radar Wave Propagation. CUDWR-WPG — NAVAER 50-IT-16 — May 1944

5.039 S Effect of Atmospheric Refraction on Range Measurements. — TRE T 1688 — June 12 1944

5.040 C Microwave Transmission over Water and Land under Various Meteorological Conditions. — RL 547 — June 13 1944

5.041 R Abnormal Propagation in WAC for May and June, 1944. — ORS-WAC Rep. 10 — July 27 1944

5.042 C Propagation of Signals on 45.1, 474 and 2800 Mc. From Empire State Building, N. Y. C. to Hauppauge and Riverhead, L. I., N. Y. (RCA) — NDRC Proj. 423 Rep. No. 2 — July 31 1944

5.043 C The Structure of the Electromagnetic Field During Conditions of Anomalous Propagation. — RRDE Res. Rep. 258 — Sept. 19 1944

5.044 C Tropospheric Propagation and Radio-Meteorology. — CUDWR WPG-5 — Sept. 1944

5.045 C Some Factors Causing "Superrefraction" on Ultra High Frequencies in South West Pacific. (Daily Report on Abnormal Echoes—RAAF. Form No. 146 Included in ATP 821.) — Australian Ionosphere Bul. Sect. 1.2 or ATP 821 — Oct. 1944

5.046 Aeroplane Tests. — JMRP No. 35 or BRL TR 488-A — Dec. 21 1944

5.047 C Atmospheric Refraction—A Preliminary Qualitative Investigation. — NRSL WP-17 — Dec. 28 1944

5.048 S Anomalous Propagation with High and Low Sited 3 cm. Ship Watching Radar Sets. — AORG Rep. No. 250 — Mar. 20 1945

5.049 S Anomalous Propagation at English Coastal Radar Stations, March-September, 1944. — AORG Rep. No. 258 or JEIA 9946 — May 30 1945

6.000   PROPAGATION EXPERIMENTS

6.001 Lebanon-Beer's Hill Transmission on Wavelengths of 2.0 Meters and 30 Centimeters—Case 20564. — BTL MM-39-326-06 — Dec. 5 1939

6.002 C Centimeter Wave Propagation over Land: Preliminary Trials. — GEC No. 8045 — Aug. 21 1942

6.003 C The Propagation of 10 Cm. Waves on a 52-Mile Optical Path over Land. The Correlation of Signal Patterns and Radiosonde Data. — Washington State Coll Rep. No. 1 — June 10 1943

6.004 C Centimeter Wave Propagation over Sea Within and Beyond the Optical Range. — ASE M 552 — July 1943

6.005 S Aden-Berbera VHF Experiments—Final Report on Propagation Aspects. — SRDE — Dec. '43

6.006 S Investigation No. 399 (Irish Sea Experiment). British Min. of Supply —
AC 5070 — 9/1/43
AC 5071 — 12/14/43
AC 5072 — 1/15/44
AC 5073 — 2/9/44
AC 5074 — 3/20/44
AC 6534 — 5/14/44
AC 6625 — 8/12/44
AC 7206 — 10/19/44
AC 7465 — 11/10/44
AC 7066 — 1/4/45

6.007 S Experience with Space and Frequency Diversity Fading on New York-Neshanic Microwave Circuit—Case 37003-4. — BTL MM-43-160-152 — Sept. 18 1943

6.008 C Investigation of Changes in Direction of Transmission during Periods of Fading in the Microwave Range—Case 37003-4, File 30691-1. — BTL MM-43-160-183 — Oct. 30 1943

6.009 C Radar Calibration Report—New York Region. — Mitchel Field, N. Y. — Nov. 30 1943

6.010 S Aden-Berbera VHF Experiments—Meteorological Conditions and Possible Correlation. — SRDE AC 5493/USW or JMRP No. 14 — Dec. 20 1943

6.011 S Propagation Measurements on Polo Pony R/T Equipment. — TRE T 1609 — Dec. 21 1943

6.012 C Propagation over Short Paths and Rough Terrain at 200 Mc/s. — RL 408 — Jan. 18 1944

6.000 (continued)

Bib. No.	Title	Number	Date
6.013 S	Propagation and Reflection Characteristics of Radio Waves as Affecting Radar.	Army Air Forces Board Proj. No. (M-3) 11a	Jan. 31 1944
6.014 S	Microwave Propagation Measurements—Report Presented at NDRC Conference of Feb. 10-11, 1944.	BTL MM-44-160-55	Mar. 10 1944
6.015 S	Army Air Force Cold Weather Tests, Fairbanks, Alaska, Winter 1943-1944.	Western Elec. Co.	Apr. 20 1944
6.016 S	An Ultra-Short-Wave Field, Array Polar Diagram, and DF Survey (North Devon and Cornwall—Sept.-Oct., 1943).	POED RR No. 1141	Apr. 29 1944
6.017 C	An Estimation of the Incidence of Anomalous Propagation in the Cook Strait Area of New Zealand from Jan., 1943 to Jan., 1944.	RDL-DSIR NZ RD 1/373	May 2 1944
6.018 S	K-Band Radar Transmission—A Preliminary Report of Tests Made Near Atlantic Highlands, N. J., between December, 1943 and April, 1944.	BTL MM-44-160-115	May 19 1944
6.019 S	Effect of Pulse Length on System Performance and Operation.	RL 571	May 30 1944
6.020 S	Report on Cross Channel Propagation of British No. 10 Set.	OCSO OAB-2	Aug. 26 1944
6.021 C	Radar Range and Signal Strength.	MR 142	Aug. 1944
6.022 C	Results of Microwave Propagation Tests on the New York-Neshanic Path—Case 37009-4, File 36691-1.	BTL MM-44-160-190	Aug. 28 1944
6.023 C	Height-Gain Tests in the Troposphere	BRL TR 488 or JEIA 5560 or JMRP No. 36	Sept. 1944
6.024 S	Interim Report on Investigation of 120 Mc/s. and 50 cm Propagation Across the English Channel	AC 7081/ USW	Oct. 4 1944
6.025 C	Measurements of the Angle of Arrival of Microwaves in the X-Band (Case 20504).	BTL-MM-44-160-249	Nov. 7 1944
6.026 C	Over-Water Transmission Measurements, 1944—Part I: Preliminary Analysis of Radio and Radar Measurements.	RL 649	Dec. 15 1944
6.027 S	The Vertical Distribution of Field Strength over the Sea Under Conditions of Normal and Anomalous Propagation. CAEE & RRDE	RRDE Res. Rep. No. 267	Jan. 5 1945
6.028 C	Centimetre Wave Propagation over Sea. A Study of Signal Strength Records Taken in Cardigan Bay, Wales, between February and September, 1944-NPL,	DSIR RRB/ C 114 or JMRP No. 50	Feb. 28 1945
6.029 S	Over-Water Tests on S-Band Early Warning for Ships. Vertical Coverage of the CXHR (SCI) Search System.	RL 703	Mar. 5 1945
6.030 S	Preliminary Report on S- and X-Band Propagation in Low Ducts Formed in Oceanic Air.	NRL R-2493	Mar. 24 1945
6.031 C	Atmospheric Refraction under Conditions of a Radiation Inversion.	NRSL WP-19	Apr. 21 1945
6.032 R	Radio-Meteorological Relationships.	AC 8140/ USW138	May 4 1945
6.033 S	Calculated Relationship Between Signal Level and Uniform Gradient of Refractive Index for the Irish Sea Paths.	GEC No. 8656 AC 8225/ USW 141	Apr. 19 1945
6.034 R	Radio-Meteorological Relationships. General Summary of Papers AC 8140/USW 138 and AC 8225/ USW 141.	AC 8336/ USW 149	1945
6.035 C	General Summary Covering the Work of Inter-Service Trials, LLANDUDNO, 1944.	KXS	May 1945
6.036 S	X-Band Trials at Rosehearty.	TRE T1770 JMRP No. 64 AC 8228/ USW 142	May 28 1945
6.037 C	"S- and X-Band Propagation in Low Ocean Ducts. (See 6.030.)	JEIA 10401 NRL R-2565	July 5 1945

7.000 METEOROLOGICAL THEORY

Bib. No.	Title	Number	Date
7.001 C	The Diffusive Properties of the Lower Atmosphere.	MRP 59 Air Min. Met. Res. Com.	Dec. 29 1942
7.002	Meteorology for Pilots. U.S. Dept. Commerce	Civil aero. Bul. No. 25	Jan. 1943
7.003 R	A Study of the Effect of the Meteorology on the Refraction of Radio Beams.	CRSL T-2	May 4 1943
7.004 R	The Rapid Reduction of Meteorological Data to Index of Refraction.	NRSL WP-8	Dec. 10 1943
7.005 S	Application of Diffusion Theory to Radio Refraction Caused by Advection.	TRE T 1647	Apr. 6 1944
7.006 C	Qualitative Survey of Meteorological Factors Affecting Microwave Propagation.	RL 488	June 1 1944
7.007	Suggested Programme of Observational Investigation into Profiles in the Lower Atmosphere (HQ Air Command, SE Asia, New Delhi).	TRE S No. 9831	July 29 1944
7.008 R	Analysis of Meteorological Ascents off New England. TRE	Prelim M/ Memo 22/ RAF Revised T 1774 or JMRP No. 54	Sept. 7 1944 1945

7.000 (continued)

No.	Title	Reference	Date
7.009 C	The Influence of Ground Contour on Air Flow (Translation).	CUDWR WPG-4	Sept. 1944
7.010 R	Radio-Meteorological Tables.	TRE T 1724 or JMRP No. 30	
7.011 C	Modified Index Distribution Close to the Ocean Surface.	RL 651	Feb. 16 1945
7.012 R	Report of an Investigation of Subsidence in the Free Atmosphere.	SDTM 94 or JMRP 49	Sept. 29 1944
7.013 R	The Influence of Atmospheric Stability on Air Flow	AC 7892/ USW 126 or JMRP No. 57 or JEIA 10895	Mar. 7 1945
7.014	The Slopes of Isopycnic Surfaces in the Lower Atmosphere.	JMRP No. 48	Mar. 29 1945
7.015 C	Tables for Computing the Modified Index of Refraction M.	CUDWR WPG-8	March 1945
7.016 R	Nomograms for Computation of Modified Index of Refraction.	NDRC Div. 14 RL 551	Apr. 6 1945
7.017	Note on Errors in Measurement of the Refractive Index of the Air for High Frequency Radio Waves Consequent upon Errors in Meteorological Measurements.	JMRP No. 51	April 1945
	Addendum: Note on Errors in Evaluation of Refractive Index of the Air for Ultra-Short Radio Waves from the Data Obtained on the Rye Tower.	Addendum JMRP No. 51	

8.000 METEOROLOGICAL EXPERIMENTS

No.	Title	Reference	Date
8.001	Weather in the Indian Ocean to Latitude 30° S. and Longitude 95° E. including the Red Sea and Persian Gulf.	MO 451b (7)	1940
8.002	Weather on the Australia Station.	RAAF Pub. 252 Vol. II Reprinted	July '42
8.003 S	Note on the Hydrolapse in the First 1000 Ft. of the Atmosphere.	MO SDTM No. 52	Sept. '43 July 12 1943
8.004 S	Meteorological Report in Connection with VHF Wireless Experiment Between Aden and Berbera (1943)	AC 5492 USW or JMRP No. 13	Oct. 30 1943
8.005	Meteorological Measurements (Irish Sea Experiments). NMS Ship Glen Strathallan.	S JEIA-2778	11/1-5/43
8.006	Tables of Temperature and Humidity Observations at Rye. MO	JMRP No. 5	Nov. 1943
8.007S	Meteorological Information from Radar Stations being Circular Issued to RDF Stations and Fighter Sectors.	Australia No. 405 or JMRP No. 12	Dec. 7 1943
8.008R	Low Altitude Measurements in New England to Determine Refractive Index—1943.	RL Rep. 42-2/22/44	Feb. 22 1944
8.009S	Climate in Relation to Microwave Radar Propagation in Panama.	RL 475	Feb. 25 1944
8.010S	The Vertical Distribution of Temperature and Humidity at Rye on the Night of January 14-15, 1944.	JMRP No. 6 or JEIA 10318	Feb. 26 1944
8.011S	Analysis of Temperature and Humidity Records at Rye. MO	JMRP No. 7 or JEIA 10319	Feb. 1944
8.012S	Radio Climatology of the Persian Gulf and Gulf of Oman with Radar Confirmation.	TRE T 1642	Mar. 15 1944

Reference	Note	Date
S HM 3/44		1/14-17/44
S JEIA-3059		3/5-8/44
C JEIA-3522		3/14-16/44
C JEIA-3520		3/17-18/44
S JEIA-3007		3/22-25/44
C JEIA-3523		3/27-29/44
S HM 3/44		4/3-4/44
S JEIA-3864		4/10-13/44
C JEIA-4123		4/21-23/44
C JEIA-4284		4/27-30/44
C JEIA-4729		5/6-10/44
C JEIA-5533		5/28-31/44
C HM 3/44		6/21-7/7/44
C JEIA-6185		7/17-22/44
C HM 3/44		7/24-28/44
C HM 3/44		8/10-13/44
C HM 3/44		8/26-30/44
C JEIA-6575		10/6-10/44
C JEIA-7309		10/22-23/44
C JEIA-8522	Ship Coila.	7/11-14/44
C JEIA-3521		12/15/43
C JEIA-5207		6/17-20/44
C JEIA-5525		6/9-27/44
C JEIA-6850		7/11-20/44
C JEIA-6874		10/10-11/44
C JEIA-7307		10/25-26/44
C*JEIA-8521		7/3-6/44
C JEIA-4730		5/19-30/44
C JEIA-4915	Ship St. Dominica.	6/1-5/44
C JEIA-6438		7/24-27/44
C HM 3/44		8/19-21/44
C HM 3/44		8/26-29/44
C*JEIA-8257		7/30-8/2/44

8.000 (continued)

Bib. No.	Title	Number	Date
8.013 R	Stations in the Western Hemisphere with Conditions in the Lower Layers of the Atmosphere Similar to Those at Stations in the Eastern Hemisphere. AAF	Rep. No. 729	March 1944
8.014 C	Rain Cloud Weather Reports Associated with the Frontal Passage of 17-20 December, 1943. AC	6th Weather Region Res. Section APO No. 825	April 1944
8.015	Some Extracts from Rye Records during April-May, 1944 MO	JMRP No. 20 or JEIA 10321	Apr.-May 1944
8.016	Extract from Rye Records of Temperature and Humidity Gradients during Selected Radiation Nights, March, 1944. MO	JMRP No. 18 or JEIA 10820	May 4 1944
8.017	Some Values of the Refractive Index of the Atmosphere at Rye.	JMRP No. 23 or JEIA 10322	June 1-6 1944
8.018 C	Low-Level Meteorological Soundings and Radar Correlation for the Panama Canal Zone.	Wash. State Coll. Rep. No. 6 NDRC PDRC-647	June 12 1944
8.019 C	Wave Propagation Report No. 3.	Intel. Br. OCSO Canal Zone 413.44/R113	July 1 1944
8.020 S	KX8 Inter-Service Trials at LLANDUDNO Report of Colloquium held on June 27 & 28 at ADRDE, LLANDUDNO to Discuss the Results of the Trials up till that Date and to Define the Future Programme.	Part I	Aug. 31 1944
	Minutes of a Meeting of the Radar Section of an Inter-Service Conference held at LLANDUDNO on June 28, 1944—Appendix with Figures. Appendix I, II, III, ADRDE	Part II	Aug. 31 1944
	Minutes of a Meeting of the Meteorological Section of an Inter-Service Conference held at ADRDE, LLANDUDNO, June 28, 1944.	Part III	July 10 1944
8.021 C	Preliminary Analysis of Height-Gain Tests in the Troposphere.	BRL TR 494 or JEIA 5777	Sept. 1944
8.022	Diurnal Variation of Temperature and Humidity at Various Heights at Rye. MO 8	S 100958 or JMRP No. 26 or JEIA 10823	Oct. 21 1944
8.023 C	Report on General Climatic & Meteorological Conditions in Banda Sea. (4°-7° S, 126°-181° E.)	RAAF Met. Res. No. 2 Sect. II Series 7 No. 18	Nov. 1944

Bib. No.	Title	Number	Date
8.024	Hourly Values of Modified Refractive Index (M) for Meteorological Office, Rye, May, 1944. MO	JMRP No. 31 or JEIA 10325	Dec. 28 1944
8.025 C	Temperature and Humidity Measurements Made with the Washington State College Wired Sonde Equipment at Kaikoura, New Zealand, Between Sept. 22, 1944 and Oct. 19, 1944.	RDL-DSIR NZ RD 1/482	Jan. 15 1945
8.026 C	Fleet Weather Central Paper No. 10. Part I: Highlights of the December, 1944 Typhoon Including Photographic Radar Observations. Part II: A Distant Observation of a Warm Front Including a Photograph of Cloud Forms and Slope of Front.	Fleet Weather Central Paper No. 10	Feb. 10 1944
8.027 C	Results of Low Level Atmospheric Soundings in the Southwest and Central Pacific Oceanic Areas.	Wash. State Coll. Rep. No. 9 NDRC PDRC-647	Feb. 27 1945
8.028 C	Centimetre Wave Propagation over Sea. Correlation of Radio Field Strength Transmitted Across Cardigan Bay, Wales with Gradient of Refractive Index Obtained from Aircraft Observations.	DSIR RRB/ C121 or JEIA 9813	May 10 1945

9.000   METEOROLOGICAL EQUIPMENT

Bib. No.	Title	Number	Date
9.001	Brief Comparison of Air Temperature Thermometers Used and Tested at A & AEE For Meteorological Work.	A & AEE MRP 117	Jan. 3 1943
9.002 C	Project for Making Gee Meteorological Observations on Certain CH Towers.	TRE M/Memo/2	
9.003 S	Balloon Psychrometer for the Measurement of the Relative Humidity of the Atmosphere at Various Heights. Also Addendum.	ICI	Apr. 1 1943
		Addendum	Sept. 25 1943
9.004	A Distant Reading Electrical Air Temperature Thermometer Employing a Balanced Bridge Suitable for Use in Aircraft.	MO	June 21 1943
9.005	The Cambridge Aircraft Electrical Resistance Thermometer—Notes on Its Use.	MRP 112	
9.006,S	Measurement of Atmospheric Humidity in Aircraft by Dew-Point Hygrometer.	MO MRP 113	June 21 1943
9.007 C	The Captive Radiosonde and Wired Sonde Techniques for Detailed Low-Level Meteorological Sounding.	MO MRP 126	Aug. 12 1943
		Washington State Coll. Rep. No. 3	Oct. 4 1943
9.008 C	A Comparison of Three Types of Cup Anemometer at Low Velocities.	NDRC-PDRC-647 NDRC-Div. 10	Oct. 26 1943
9.009 C	A Remote Indicating Cup Anemometer with Magnetic Coupling.	Inf Rep. 103.A-38 NDRC-Div. 10 OSRD Rep.3714	Apr. 10 1944

9.000 (continued)

	Report No.	Date
9.010 C An Apparatus for Temperature Profile Measurement.	NDRC Div. 10 Inf Rep. 0.3A-45	Apr. 11 1944
9.011 R Instruments and Methods for Measuring Temperature and Humidity in the Lower Atmosphere.	RL 457	Apr. 12 1944
9.012 C Anomalous Propagation—Adaptation of Model RAU-2 Radio Sonde Receiving and Recording Equipment for Use as Low Level Sounding Device.	Navy Dev. Project Unit No. 1	May 31 1944
9.013 R Meteorological Investigation at Rye—Part I—Instrumental Layout for Recording Gradients of Temperature and Relative Humidity. MO 4	JMRP No. 17	May 1944
9.014 C Notes on Operational Use of Low-Level Meteorological Sounding Equipment.	Washington State Coll. Rep. No. 7 NDRC-PDRC-647	June 15 1944
9.015 C Microwave Propagation Studies—Detection of Tropospheric Stratification by Means of Sound Echoes—Preliminary Trial—Case 37003.	BTL MM-44-160-143	June 21 1944
9.016 C Operating Instructions for the WSC Low-Level Atmospheric Sounding Equipment.	Washington State Coll. Rep. No. 8 NDRC-PDRC-647	July 10 1944
9.017 C Meteorological Equipment for Short Wave Propagation Studies.	CUDWR WPG-3	August 1944
9.018 R Wired Sonde Equipment for High Altitude Sounding.	NRSL WP-16	Nov. 17 1944
9.019 C Airborne Radiosonde Recorder.	Intel. Br. OCSO USA 413.6	Mar. 10 1945
9.020 KX8 Trials—LLANDUDNO June to Sept., 1944. Lower Atmosphere Radio-Meteorological Flight Technique.	JMRP No. 55	
9.021 R A Note on the Resistance of Electric Hygrometer Elements.	NRSL AERO-1	May 8 1945
9.022 F Improvements in USNRSL Meteorological Sounding Equipment. See 9.018.	NRSL WP-21	July 3 1945

10.000 RADAR FORECASTING

	Report No.	Date
10.001 S Forecasting of RDF Conditions.	AORG Memo No. 103 or JMRP No. 2	May 31 1943
10.002 The Meteorological Aspects of Anomalous Propagation—Short Wave Radio.	JMRP No. 1	June 1943
10.003 S Oboe Propagation, Aug.- Oct., 1943.	TRE T1605	July 1943
10.004 "Naviprop" Forecasts. MO	SIS No. 45	Nov. 8 1943
10.005 S Issue of ANOPROP Forecasts—Synoptic Instruction Special No. 39. MO	SIS No. 39	Feb. 11 1944
10.006 S Elements of Radio Meteorological Forecasting (Mathematics Group, TRE, Malvern).	TRE T 1621	Feb. 14 1944
10.007 C Preliminary Instruction Manual—Weather Forecasting for Radar Operations.	Rep. No. 614	March 1944
10.008 R Tropospheric Weather Factors Likely to Affect Superrefraction of VHF-SHF Radio Propagation as Applied to the Tropical West Pacific.	U.S. Weather Bureau RP-1	July 1 1944
10.009 C Preliminary Instruction Manual of Weather Forecasting for Radar Operations in South West Pacific Area.	CSIR-RL RP 220	Sept. 4 1944
10.010 C Outline of Radio Climatology in India and Vicinity.	TRE T1727 or JEIA 6061	Sept. 12 1944
10.011 Notes on TRE Report T.1727—JMRP No. 25 (Radio Climatology in India and Vicinity).MO	or JMRP No. 25 JMRP No. 27	Nov. 7 1944
10.012 A Note on the Forecasting of AP (Provisional Draft).	JEIA 10324	Sept. 44
10.013 R A Rough Sketch of World Radio Climatology over Sea.	TRE T1730	Oct. 31 1944
10.014 C American Continents Meteorological Counterparts of Western Pacific and Indian Ocean Areas as Applied to Tropospheric Radio Propagation.	U.S. Weather Bureau RP-2	Nov. 15 1944
10.015 R The Possibility of Investigating the Föhn Wind and Sea Breeze Phenomena in N.Z. with a View to Elucidating Certain Problems of Radio-Meteorological Forecasting in Other Parts of the World.	RDI-DSIR-NZ RD 1/471 or JEIA 7469	Dec. 1 1944
10.016 C Determination of a Suitable Method of Forecasting Radar Propagation Variations over Water.	AAF Bd. Proj. #4252R000.77	Mar. 10 1945
10.017 C A Qualitative Outline of the Radio Climatology of Australasia.	TRE T1820 or JMRP No. 53	Apr. 19 1945
10.018 C Determination of the Practicability of Forecasting Meteorological Effects on Radar Propagation.	AAF Bd. Proj. 3767B000.93	June 13 1945

11.000 ATMOSPHERIC ABSORPTION AND SCATTERING

	Report No.	Date
11.001 S Absorption of 1 Cm. Radiation by Rain.	CVD-CL Misc. 3	
11.002 C The Absorption of Ultra-Short Wireless Waves in the Water Vapour of the Earth's Atmosphere.(NPL)	RRB/ C 18	Feb. 14 1941
11.003 S Echo Intensities and Attenuation Due to Clouds, Rain, Hail, Sand and Duststorms at Centimeter Wavelengths.(GEC)	GEC No. 7831	Oct. 13 1941
11.004 C The Atmospheric Absorption of Microwaves.	RL 43-2	Apr. 27 1942
11.005 S The Effect of Rain upon the Propagation of 1 Cm. Electro-magnetic Waves—Case 22098. (BTL)	MM-42-160-57	Aug. 1 1942
11.006 S The Effect of Rain on the Propagation of Microwaves —Case 22098.	MM-42-160-93	Aug. 26 1942
11.007 S Comparison of Theoretical and Experimental Values for the Attenuation of 1 Centimeter Waves in Rain—Case 22098.(BTL)	MM-43-160-2	Jan. 5 1943

11.000 (continued)

Bib. No.	Title	Number	Date
11.008 S	An Investigation on the Number and Size Distribution of Water Particles in Nature	Met. Res. Com. MRP 109	June 1943
11.009	Report on the Absorption and Refraction of Electromagnetic Waves by the Liquid Water, Water Vapour and Fog or Rain.	CRB 43/2881	Sept. 2 1943
11.010	Report on the Absorption of Electromagnetic Waves in the Wavelength Range 1-100 Cm. by Water in the Atmosphere.	CRB 43/2882	Sept. 2 1943
11.011 C	Progress Report on "Verification of Mie Theory Calculations and Measurements of Light Scattering by Dielectric Spherical Particles.	OSRD 1857 Div. 10 NDRC	Sept. 29 1943
11.012 S	The Absorption of Centimetric Radiation by Atmospheric Gases. (ADRDE)	USWP WC	Apr. 27 1944
11.013 S	Attenuation Due to Water Drops in the Atmosphere. (ADRDE)	USWP WC	Apr. 28 1944
11.014 S	Propagation of K/2 Band Waves. BTL	MM-44-160-150	July 3 1944
11.015 S	Interim Report of the USW Panel Working Committee.	AC 7375/USW or JEIA-7607	Aug. 14 1944
	Part I Water in the Atmosphere. MO		July 18 1944
	Part II The Attenuation of Centimetre Waves by Atmospheric Gases. RRDE		July 1944
	Part III Attenuation of Centimetre Waves by Rain, Hail and Clouds.	GEC 8516	Aug. 3 1944
	Part IV The Attenuation of Centimetre Waves by Rain. RRDE		Aug. 1944
11.016 S	Preliminary Note on Secure Communications on Millimetre Waves. TRE	L/M40/WBL or JEIA 5597	Sept. 11 1944
11.017 C	Rotational Line Width in the Absorption Spectrum of Atmospheric Water Vapor and Supplement.	NDRC Div. 14 No. 320 Univ. of Michigan Supp.	Oct. 10 1944
11.018 C	The Absorption of One-Half Centimetre Electromagnetic Waves in Oxygen.	RL 684	Feb. 1 1945
11.019 S	The Effect of Rain on Radar Performance.	BTL MM-44-170-50	Jan. 26 1945
11.020 S	Measurements of Wave Propagation.	BTL MM-45-160-17	Oct. 17 1944
11.021 C	Further Theoretical Investigations on the Atmospheric Absorption of Microwaves.	RL 664	Feb. 5 1945
11.022 S	Measurements of the Attenuation of K-Band Waves by Rain.	RL 603	Mar. 7 1945

Bib. No.	Title	Number	Date
11.023 S	Attenuation of Centimetre and Millimetre Waves by Rain, Hail, Fogs and Clouds. (Draft.)	GEC 9670	May 18 1945
11.024 C	The Relation Between Absorption and the Frequency Dependence of Refraction.	RL 735	May 28 1945
11.025 S	Absorption and Scattering of Microwaves by the Atmosphere.	CUDWR WPG-f1	May 1945
11.026 S	CVD Progress Report for May, 1945. Part I The Absorption of K-Band Radiation in Gaseous Ammonia.	CVD CL Prog. Rep. 5/45	May 1945
11.027 S	'K-Band Attenuation Due to Rainfall.	NRSL WP-20	June 8 1945

12.000   DIELECTRIC CONSTANT AND LOSS FACTOR

Bib. No.	Title	Number	Date
12.001 R	A New Method for Measuring Dielectric Constant and Loss in the Range of Centimeter Waves.	MIT 102	March 1941
12.002 C	The Electrical Properties of Ice.	AC 1516/ RDF 110 Com. 78	Dec. 22 1941
12.003 C	The Dielectric Constant and Loss Factor of Water Vapour at a Wavelength of 9 Cms. (Frequency— 3330 Mc/s.) (NPL)	DSIR RRB/S.1	Mar. 31 1942
12.004 C	The Dielectric Constant of Water Vapour and its Effect upon the Propagation of Very Short Waves.	DSIR RRB/S.2	May 11 1942
12.005 C	Progress Report on Ultrahigh Frequency Dielectrics.	NDRC Rep. 121 Div. 14	January 1943
12.006 S	Conductivities of Sea, Tap and Distilled Water at $\lambda=10$ cm.	ASE M.496	April 1943
12.007 C	The Measurement of Dielectric Constant and Loss with Standing Waves in Coaxial Wave Guides.	Div. 14	April 1943
12.008 S	The Dielectric Constant and Absorption Coefficient of Water Vapour for Wavelengths of 9 cm. and 3.2 cm. (Frequencies 3,330 and 9,350 Mc/s.) (NPL)	DSIR RRB/S.11	June 14 1943
12.009	Electrical Measurements on Soil with Alternating Currents.	JIEE (London) 75, 221-287	Aug. 1943
12.010 C	Auxiliary Equipment for the MIT CO-AX Instrument and Its Use.	NDRC Rep. 142 Div. 14	Nov. 1943
12.011 S	Memorandum on an Electrical Method of Measuring the Dielectric Constant of Atmospheric Air, and Recording it Continuously.	NDRC Rep. 210 TRE M/Memo 15/ PEC or JMRP No. 8	Jan. 6 1944
12.012 S	The Dielectric Constant and Absorption Coefficient of Water Vapour for Radiation of Wavelength 1.6 cm. (Frequency 18,800 Mc/s.) (NPL)	DSIR RRB/S.17	Apr. 22 1944
12.013 S	The Dielectric Constant of Water and Ice at Centimetre Wavelengths (Working Committee). ADRDE	USWP WC	Apr. 28 1944

12.000 (continued)

No.		Title	Report	Date
12.014	S	Preliminary Report on the Dielectric Properties of Water in the K-Band.	CVD Rep. CL Misc. 25	May 1944
12.015	C	Transmission and Reflection of Single Plane Sheets. (Radome Bulletin No. 4.)	RL- 483-4	July 12 1944
12.016	C	Recent Dielectric Constant and Loss Tangent Measurements (on X-Band). (Radome Bulletin No. 5.)	RL- 483-5	July 14 1944
12.017	S	Dielectric Properties of Water and Ice at K-Band.	RL 644	Dec. 4 1944
12.018	R	The Interaction Between Electromagnetic Fields and Dielectric Materials.	Div. 14 NDRC Rep. 122	Jan. 1943
12.019	C	The Dielectric Properties of Water at Wavelengths from 2 mm. to 10 cm. and over the Temperature Range 0° to 40° C. (NPL)	DSIR RRB/C115	Mar. 20 1945
12.020	C	The Dielectric Properties of Water in the Temperature Range 0° C. to 40° C. for Wavelengths of 1.24 cm. and 1.58 cm. (NLP)	DSIR RRB/ C.116 or JEIA 9811	Mar. 7 1945
12.021		The Anomalous Dispersion of Water at Very High Radio Frequencies in the Temperature Range 0° to 40° C. (NPL)	DSIR RRB/ C.118 or JEIA 9812	Apr. 6 1945

13.000 REFLECTION COEFFICIENT

No.		Title	Report	Date
13.001	C	Centimeter Wave Propagation over Sea Within the Optical Range.	ASE M398	January 1942
13.002	S	Preliminary Report on the Reflection of 9 Cm. Radiation at the Surface of the Sea.	ASE M542	Sept. 1943
13.003	C	Comment on the Reflection of Microwaves from the Surface of the Ocean—II.	BTL MM-43- 210-6	Oct. 13 1943
13.004	S	S-Band Measurements of Reflection Coefficients for Various Types of Earth.	MM-43- 5220.129	Oct. 29 1943
13.005	C	Special Report on the Determination of the Coefficient of Reflection of Radio Waves at the Ground by Means of Radar Observations.	NRL RA 3A 212A	Nov. 10 1943
13.006		Scattering. BRL	JEIA 3904	Nov. 1943
13.007	C	Preliminary Measurements of 10-Cm. Reflection Coefficients of Land and Sea at Small Grazing Angles.	RL- 478	Dec. 11 1943
13.008	C	Further Measurements of 3 and 10-Cm. Reflection Coefficients of Sea Water at Small Grazing Angles.	RL- 568	May 17 1944
13.009	C	Microwave Propagation Studies—The Reflection of Sound Signals in the Atmosphere—Case 37003—File 36691-1.	BTL MM-44- 160-156	July 3 1944
13.010	C	Interim Report on Experiments on Ground Reflection at Wavelength of 9 cms.	DSIR RRB/C101 or JEIA 4899	July 7 1944
13.011	C	An Experimental Investigation of the Reflection and Absorption of Radiation of 9 cm. Wavelength.	DSIR RRB/C.107	Oct. 27 1944
13.012	R	The Measurement of High Reflections at Low Power (Radome Bulletin No. 7.)	RL- 483-7	Nov. 20 1944
13.013	C	Ground Reflection Coefficient Experiments on X-Band. (Case 20564.)	BTL MM-44-160-250	Dec. 15 1944
13.014	C	The Reflection Coefficient of a Linearly Graded Layer.	BRI TR 492	Dec. 1942
13.015	C	Reflection and Scattering.	BRL TR 506	Jan. 1945
13.016	S	Reflection from an Inversion.	AC 8210/ USW 140 or JEIA 9997	May 24 1945

14.000 HORIZONTAL AND VERTICAL POLARIZATION

No.		Title	Report	Date
14.001		Notes on the Comparison of Vertical and Horizontal Polarization in Ground Wave Propagation.	BRL TR/442	January 1940
14.002	C	Horizontal and Vertical Polarization.	BRL TR/441	July 1942
14.003	S	The Investigation of Horizontally and Vertically Polarized Direction Finding on Frequencies of the Order of 20 to 70 Megacycles per Second.	BRL TR/451	Sept. 1942
14.004	S	Polarization Effects and Aerial System Geometry at Centimeter Wavelengths.	GEC No. 8101	Nov. 26 1942
14.005	S	Change of Polarization as a Means of Gap Filling.	RL- C-7	Dec. 28 1942
14.006	S	Photographic Polarization Tests.	RL- 93-3	May 7 1943
14.007	R	Vertical Polarization vs Horizontal Polarization (Tentative Report).	CESL No. T-1	Oct. 22 1943
14.008	S	The Depolarization of Microwaves.	RL 458	Nov. 1 1943
14.009	S·	Polarization Studies at S and X Frequencies.	RL 536	Mar. 14 1944
14.010	S	Alexandria Palace Tests.	BRL TR/498	October 1944

15.000 EFFECT OF HILLS, TREES, OBSTACLES, ETC.

No.		Title	Report	Date
15.001	C	Screening by Hills.	TRE T1015	May 1941
15.002		Diffraction Round a Sphere or Cylinder. BRL	TR/433	March 1942
15.003	C	Centimeter Wave Transmission Measurements from an Urban Site.	GEC No. 8034	July 28 1942
15.004	C	Report on an Investigation of the Propagation of NPL Centimeter Waves over Ridges and Through Trees.	AC 4345/Com.181	June 2 1943

15.000 (continued)

Bib. No.	Title	Number	Date
15.006 S	A Note on the Propagation of K Band Waves Through Trees. Case 20368.	BTL, MM-43-160-129	Aug. 18 1943
15.008 S	Report on Further Experiments on the Propagation of Centimeter Waves Through Trees in Leaf and over Level Ground.	NPL	Sept. 6 1943
15.007 S	Centimeter Wave Propagation. Notes on the Effect of Obstruction by a Single Tree.	ASE M.565	Oct. 1943
15.008 S	An Experimental Investigation on the Propagation of Radio Waves over Bare Ridges in the Wavelength Range 10 Centimetres to 10 Metres (Frequencies 30 to 3000 Mc/s). NPL	DSIR RRB/ 8.12	Oct. 1 1943
15.009 S	Some Observed Effects of Trees upon Microwave Propagation—Case 37003—File 200001-1.	BTL MM-43-160-150	9/17/43 Revised 10/15/43
15.010 R	Effect of Hills and Trees as Obstructions to Radio Propagation.	Cont. OEMsr-1010: OSRD Rep. 3070	Nov. 1943
15.011 C	On Light Scattering by Spheres I.	AMG-C No. 100 NDRC-AMP No. 87.1	December 1943
15.012	Report on Some Further Experiments on the Effect of Obstacles on the Propagation of Centimetre Waves. (NPL-RD)	AC 5875/ Com. 213 USW or JEIA 3157	Jan. 20 1944
	Addendum to Paper dated 20th January, 1944 entitled, "Report on Some Further Experiments on the Effect of Obstacles on the Propagation of Centimetre Waves." (NPL-RD)	AC 5876a/ Com. 213a USWa or JEIA 7911	Jan. 1 1945
15.013 C	On Light Scattering by Spheres II.	AMG-C No. 122 NDRC-AMP No. 87.2	April 1944
15.014 C	The Propagation of Ultra Short Waves Round Hills and Other Obstacles.	BRL TR.479 or JEIA-5674	May 1944
15.015 R	Scattering of Radio Waves by Metal Wires and Sheet.	DSIR RRB/ C.110 or JEIA 7793	Jan. 1 1945
15.016 R	Some Experiments on the Propagation over Land of Radiation of 9.2 cm. Wavelength. NPL	DSIR RRB/ C.113	Feb. 15 1945
15.017 C	A Method of Calculating the Polar Diagram of a Radio Equipment Standing on Flat Ground Looking over a Screen.	RRDE Res. Rep. No. 280 or JEIA-9113	Mar. 21 1945

Bib. No.	Title	Number	Date
15.018 C	A Preliminary Study of Ground Reflection and Diffraction Effects with Centimetric Radar Equipment.	AORG No. 274	June 28 1945

16.000 TRANSMISSION OVER PART LAND–PART SEA

Bib. No.	Title	Number	Date
16.001 C	Diffraction at Coast Line: Sloping Site.	TRE Rep. No. 10	May 1 1941
16.002	Mixed Land and Sea Transmissions.	BRL E.16	October 1941
16.003 S	Diffraction at Coast Line: Further Numerical Examples.	TRE Rep. M/35	Feb. 5 1942
16.004 C	Coastal Refraction.	BRL TR/136	May 1942
16.005 C	Propagation of Wireless Waves over Ground of Varying Earth Constants (Part Land and Part Sea).	BRL Marconi TR/440	July 1942
16.006	Transmission over Ground of Varying Earth Constants.	BRL TR/473	July 1943
16.007 C	Diffraction at Coast Line. (Appendix to Report on Siting of RDF Stations).	TRE Rep. No. 6	Jan. 27 1944
16.008 C	Siting and Coverage of Ground Radars.	CUDWR WPG-10	May 1945

17.000 TARGETS AND ECHOES

Bib. No.	Title	Number	Date
17.001 C	Scattering and Spurious Echoes.	BRL TR 437	April 1942
17.002 C	Reflection of 10 Cm. Radiation by Model Aircraft.	ADRDE Christchurch Rep. No. 174	Sept. 8 1942
17.003 S	Elementary Survey of Scattering and Echoing by Elevated Targets.	TRE M/48/HGB	Dec. 1942
17.004 S	The Resolution of Composite Echoes with Centimeter Wave RDF. (CAEE)	CAEE 4070/ C/104	Feb. 10 1943
17.005 C	Microwave Radar Reflection.	RL- 43-23	Feb. 20 1943
17.006 C	Reflection of Radar Waves from Targets of Simple Geometric Form.	NRSL WP-3	Feb. 24 1943
17.007 S	Radar Echoes from Periscopes.	RL- 12-1	Mar. 1 1943
17.008 S	Possible Measurement of Radar Echoes by Use of Model Targets.	RL- 43-24	Mar. 4 1943
17.009 S	Radar Echoes from Atmospheric Phenomena.	RL- 12-2	Mar. 18 1943
17.010 S	Echoes Produced by Perfectly Conducting Objects of Certain Simple Shapes in Free Space.	DSIR RL 173	Mar. 26 1943
17.011 S	Gratings and Screens as Microwave Reflections.	RL- 54-20	Apr. 1 1943

17.000 (continued)

No.	Title	Source	Date
17.012 S	Optimum Wavelength for Long Range CW Radar Systems.	Sperry Gyroscope Co., Inc. Rep. 5220–126	May 1 1943
17.013 S	Report on an Investigation into the Nature of Sea Echoes.	TRE T.1407	May 12 1943
17.014 S	The Application of Corner Reflectors to Radar (Theoretical).	RL-43-31	May 14 1943
17.015 S	The Application of Corner Reflectors to Radar (Experimental).	RL-55-4	July 1 1943
17.016 C	Measurement of the "Effective Echoing Areas" of Various Aircraft.	OCSO ORG-P-8-1	July 2 1943
17.017 S	Overwater Observations at X and S Frequencies on Surface Targets.	RL-401	July 26 1943
17.018 C	Towed Radar Targets.	ADRDE Res. Rep. 212	Aug. 6 1943
17.019 C	Corner Reflector Tests at Langley Field.	RL 402	Aug. 6 1943
17.020 S	Properties of Corner Reflectors—Case 22098.	BTL MM-43-160-130	Aug. 12 1943
17.021 S	Use of Corner Reflectors as IFF on Ships. Australian ORS & CSIR-RL.	Oper. Res. Rep. No. 24	Aug. 30 1943
17.022 C	An Investigation into the Nature of Sea Echoes.	MR 109 or JEIA 1221	Sept. 8 1943
17.023 S	Bearing Markers for CA No. 1 Sets Provisional Instruction.	CAEE 70/C/157 or JEIA 2771	Sept. 24 1943
17.024 S	Probability of Detection of Aircraft by RDF.	CSIR-RL MUM.2 or JEIA 3954	Sept. 30 1943
17.025 S	The Scattering of Radiation from Rectangular Planes, Half-Cylinders, Hemispheres, and Airplanes.	Contract W-2270 sc-551 Item 3	Oct. 12 1943
17.026 R	The Theory of Random Processes.	RL 464	Oct. 15 1943
17.027 C	On the Appearance of the A-Scope when the Pulse Travels Through a Homogeneous Distribution of Scatterers.	RL-466	Nov. 9 1943
17.028 C	On the Fluctuations in Signals Returned by Many Independently Moving Scatterers.	RL-465	Nov. 12 1943
17.029 S	The Use of Permanent Echo Amplitudes for Monitoring S Band Radar Equipment.	CSIR-RL fRP 177/2	Dec. 7 1943
17.030 C	The Range Calculator.	RL-497	Dec. 20 1943
17.031 S	The Performance of 10 Cm. Radar on Surface Craft.	AORG Rep. No. 155	Jan. 3 1944
17.032 S	Special Report on Radar Cross Section of Ship Targets.	NRL RA 3A 213A	Jan. 24 1944
17.033 S	Observations of Life Rafts Equipped with Corner Reflectors.	RL 533	Feb. 15 1944
17.034 S	Radar Cross Section of Ship Targets, II.	NRL Rep. R-2232	Feb. 18 1944
17.035 S	Optical Theory of the Corner Reflector.	RL-433	Mar. 2 1944
17.036 C	Observations on Signal Stability at S and X Frequencies.	RL-537	Mar. 14 1944
17.037 C	Interim report on the Recognition of Radar Echoes.	RDL-DSIR NZ RD 1/353 or JEIA 3401	Mar. 20 1944
17.038 S	Screened and Unscreened Radar Coverage for Surface Targets.	TRE T.1666	March 1944
17.039 S	The Performance of Naval Radar Systems Against Aircraft.	JEIA 3902	Apr. 3 1944
17.040 S	Preliminary Report on the Fluctuations of Radar Signals.	RL-569	May 16 1944
17.041 S	Radar Ranging on Land Targets.	TRE Memo 101/G 36/ALH	May 18 1944
17.042 R	The Radar Echoing Power or Conducting Spheres.	ADRDE CR 228	May 24 1944
17.043 S	Use of Corner Reflectors in Beaconry.	CSIR-RL No. RP.200 or JEIA 5180	June 8 1944
17.044 C	Calibration and Standardization of Land Based Radars by the Use of Small Plane Targets.	NRSL WP-12	June 10 1944
17.045 S	Test of the Pre-Production Model Corner Reflector Final Report Project No. E-44-37 AAF Board Project No. (M-3) 69, Eglin Field, Florida.	Intel. Br. OCSO USA	June 17 1944
17.046 S	Radar Cross Section of Ship Targets, III.	413.44/R387.1 NRL, Rep. No. R-2295	June 27 1944
17.047 S	Notes on Echoes and Atmospherics From Lightning Flashes on P-Band.	CSIR-RL No. RP 49.2 or JEIA 5177	July 11 1944
17.048 S	Theory of Ship Echoes as Applied to Naval RCM Operations.	RRL 411-93	July 14 1944
17.049 S	Radar Echoes from the Nearby Atmosphere. Case No. 37003-4.	BTL MM-44-150-2	July 18 1944
17.050 S	Radar Cross Section of Ship Targets IV.	NRL Rep. No. R-2332	July 21 1944
17.051 S	Radar Echoes from the Nearby Atmosphere—Second Report. Case No. 37003-4.	BTL MM-44-150-3	July 31 1944

17.000 (continued)

Bib. No.	Title	Number	Date
17.052 C	Reflecting Properties of Metal Gratings.	CSIR RL No. RP 215	July 31 1944
17.053 S	Theory of the Performance of Radar on Ship Targets (ADRDE & CAEE Joint Report).	ADRDE Ref. R04/2/CR252 or CAEE Ref. 69/C/149	July 1944
17.054 C	Corner Reflectors for Life Rafts.	RL-608	Aug. 1 1944
17.055 C	The Characteristics of S-Band Aircraft Echoes with Particular Reference to Radar AA No. 3 MK II.	ADRDE Res. Rep. 253	Aug. 4 1944
17.056 S	Radar Echoes from the Nearby Atmosphere—Third Report, Case No. 37003-1.	BTL MM-44-150-4	Aug. 11 1944
17.057 C	Considerations Concerning Radar Coverage Diagrams.	CSIR RL RP-217	Aug. 14 1944
17.058 C	RDF Echoes to be Expected from Objects of Various Shapes. DSR	Extra Mural Res. F.72/80	
17.059 S	Radar Echoes from Shell Bursts at 4 Meters and 50 cm. Wavelengths.	RRDE Res. Rep. No. 26	Oct. 9 1944
17.060 S	Summer Storm Echoes on Radar MEW	CAORG Rep. No. 18	Nov. 27 1944
17.061 S	The Cancellation of Permanent Echoes by the Use of Coherent Pulses (Interim Report).	RAE Tech. Note No. RAD 253	Nov. 1944
17.062 C	The Fading of S-Band Echoes from Ships in the Optical Zone.	RRDE Res. Rep. No. 265	Dec. 12 1944
17.063 S	Rotating Corner-Reflectors for Ship Identification.	RL 654 NDRC Div. 14 OEMsr-262	Jan. 1 1945
17.064 R	Reflection from Smooth Curved Surfaces.	RL 661	Jan. 26 1945
17.065 S	Analysis of Over-Water Tracking.	RL 695	Feb. 12 1945
17.066 S	Technical Report on the Maximum Range of Detection of the German Early Warning Radar Equipment, Especially when Viewing Large, Tight Formations of Bomber Aircraft.	ORS VIII Bomber Comm. OCSO OAD-13	Sept. 13 1943
17.067 S	Performance Checks and Estimation of Vessel Size on Shore Based 10 cm. Radar Sets. AORG	JEIA No. 3124	Mar. 30 1944

Bib. No.	Title	Number	Date
17.069 S	Report of Trials to Determine the Variations of the ASE Apparent Reflecting Point of Plain 10 Cm. Waves M 627 from a Destroyer.	ASE M 627	July 1944
17.070 C	The Reflection of Electromagnetic Waves by Long Wires and Non-Resonant Cylindrical Conductors.	RRDE Res. Rep. 259 or JEIA 7296	Nov. 13 1944
17.071 C	Theory of Radar Return from the Schnorkel.	RL 671	Jan. 15 1945
17.072 S	Sea Returns and the Detection of Schnorkel. (See 17.077.)	TRE T 1787 or JEIA 8643	Feb. 13 1945
17.073 S	Interservice KXS Band Radar Trials. Over Water Performance Against Surface Targets. CAEE	ASE M 688 or JEIA 8820	February 1945
17.074 C	An Observation of Diffuse Cloud-Like Echoes.	CSIR RL RP 246	Mar. 6 1945
17.075 C	The So-Called Standard Target.	RL S-43	Mar. 10 1945
17.076 S	Radar Cross Section of Ship Targets V	NRL R-2466	Mar. 12 1945
17.077 S	Radar Results Against Schnorkels: A Commentary on TRE T.1787, "Sea Returns and the Detection of Schnorkel." (See 17.072.)	ORS/CC Rep. No. 338 JEIA 9111	Mar. 16 1945
17.078 C	Radar Echoes from Clouds of Water Droplets.	AC 7930/ USW 128	Mar. 16 1945
17.079 C	Comments on "Radar Echoes from Water Droplets." (Paper AC 7930) USW 128	AC 7931/ USW 129	Mar. 16 1945
17.080 S	Radar Cross Section of Ship Targets VI.	NRL R-2467	Apr. 10 1945
17.081 C	S-Band Radar Echoes From Snow.	CAORG Rep. No. 26	June 14 1945
17.082 S	Surface Coverage of Some Shipborne Radar Sets or S, X, and K Bands.	RL 720	June 15 1945
17.083 C	Echoes from Tropical Rain on X-Band Airborne Radar.	RL 728	June 15 1945
17.084 S	Analysis of Storm Echoes in Height Using MHF.	CAORG Rep. No. 30	June 25 1945
17.085 S	[1]Radar Camouflage.	RL 706	July 16 1945

18.000 DOPPLER EFFECT

Bib. No.	Title	Number	Date
18.001 S	Flutter. Method of Rapidly and Accurately Obtaining Velocity of A Ship or Aircraft by RDF Using Doppler's Principle.	Australia No. 296 Oper. Res. Rep. 21	

18.000 (continued)

No.	Title	Reference	Date
18.002 S	"S" Band Doppler Experiment—Case 20564.	BTL MM-43- 160-173	Oct. 20 1943
18.003 S	The Detection of Moving Targets Among Ground Clutter by Coherent Pulse Methods.	RL 480	Dec. 14 1943
18.004 S	The Elimination of Ground Clutter.	RL 526	Mar. 13 1944
18.005 Q	Pulse Doppler with Reference to Ground Speed Indication.	RL 63- 3/20/44	Mar. 20 1944
18.006 S	Pulse Doppler for Detection of Moving Ground Targets.	RL 553	Apr. 21 1944
18.007 S	Anti-Clutter in North America (Report on A Visit to U.S. and Canada).	Intel. Br. GB 413.44/R170	August 1944
18.008 S	Tests on the Doppler B-scope Presentation of Moving Targets.	RRDE Memo 82 or JEIA 8250	Feb. 12 1945

19.000   COMMUNICATION (TROPOSPHERIC)

No.	Title	Reference	Date
19.001	Data on Wave Propagation (10 Kilocycles to 60 Megacycles).	NRL Rep. No. R-1300	Aug. 20 1936
19.002 S	Study of Field Strength Records Obtained on the Post Office Ultra-Short-Wave Radio Telephone Link Between Guernsey and England. (Wavelength 5 m and 8 m).	DSIR RRB/C.39	Sept. 1 1941
19.003 C	3000 Megacycle Communication. RCA	NDRC-PDRC-90	Mar. 10 1942
19.004 C	Microwave Telephone. Part I: Omnidirectional. Part II: Directional. RCA	NDRC-SC-13	Mar. 22 1943
19.005 S	Trials of WS No. X 20. A.	AC 4139/ Com. 176	June 2 1943
19.006 R	Factors Determining the Range of Radio Communications in the Various Theaters of Operation.	OCSO ORG-P-14-1	June 3 1943
19.007 C	Radiotelephone Communication on 3000 Megacycles.	Wash. State Coll. Rep. 2 NDRC-PDRC 647	June 12 1943
19.008 S	An Analysis of the Effect of Frequency on Short Distance Radio Communications.	OCSO ORB-P-15-1	Aug. 18 1943
19.009 C	Use of the 25 to 50 Mc/s Band for Short Range Wireless Communication.	AORG No. 130	Aug. 27 1943
19.010 S	Trials with a 250-Watt Frequency-Modulated VHF Sender Across a Sea Water Path Beyond the Optical Range.	SRDE No. 878	Sept. 1943
19.011 S	Radio Communication in Jungles.	OCSO ORG-2-1	Sept. 1 1943
19.012 C	Measurement of Factors Affecting Jungle Radio Communication	OCSO ORB-2-3	Nov. 10 1943
19.013 R	Methods for Improving the Effectiveness of Jungle Radio Communication.	War Dept. TB Sig 4	Jan. 14 1944
19.014 R	Survey of Existing Information and Data on Atmospheric Noise Level over the Frequency Range 1-30 Mc/s NPL.	DSIR RRB/C.90 or JEIA 2815	Feb. 21 1944
19.015 S	Proposals for Provision and Application of Propagation Data for Operational & Field Use with Wireless Equipment in the Centimetre Band.	SRDE No. 908	Feb.-Mar. 1944
19.016 C	Methods of Reducing Radar Interference to Communication.	OCSO ORB-E-27-2	Apr. 19 1944
19.017 C	The Application of Passive Repeaters to Point to Point Communication at VHF and UHF.	OCSO ORB-P-20-1	Apr. 29 1944
19.018 R	Point to Point Communication in VHF Band Via Ground Wave Propagation. (Southwest Pacific Area.)	JEIA 6768 or Intel. Br. OCSO SWPA 413.44/R423.5	July 24 1944
19.019 R	Ground Wave Radio Propagation Report. (Southwest Pacific Area.)	JEIA 6769 or Intel. Br. OCSO SWPA 413.44/R113	Aug. 15 1944
19.020 S	Summary of Radio Propagation Problems in Southwest Pacific Area.	JEIA 6298 or Intel. Br. OCSO US/413.44/R113	Sept. 6 1944
	And Point to Point Communication in MF Band Via Ground Wave Propagation.	JEIA 6770 or Intel. Br OCSO SWPA 413.44/R423.4	Aug. 15 1944
19.021 C	Measurements of Factors Affecting Radio Communication & Loran Navigation in SWPA.	OCSO ORB-24	Dec. 16 1944
19.022 S	Field Trials of Ultra Short-Wave Frequency and Amplitude Modulated Multichannel Radio Telephone Systems.	POED Radio Rep. 1115	Mar. 27 1944

20.000   UNDER-WATER SOUND PROPAGATION

Included in this Bibliography because of the similarity of problems

No.	Title	Reference	Date
20.001 R	Sound Transmission in Sea Water. (A Preliminary Report.) Woods Hole Oceanographic Institution	NDRC	Feb. 1 1941
20.002 C	Some Characteristics of the Sound Field in the Sea. Oceanographic Division. U.C. for NDRC	NDRC C4-sr30-083	Mar. 13 1942
20.003 C	Theoretical Discussion of Reverberation. Columbia Univ.	NDRC C4-sr20-097	May 29 1942
20.004 C	Sound Ranges under the Sea. Columbia Univ.	NDRC C4-sr20-100	June 5 1942
20.005 C	Reverberation in Echo Ranging, Part I, General Principles. Columbia Univ.	NDRC C4-sr20-140	July 28 1942

20.000 (continued)

Bib. No.	Title	Number	Date
20.006 C	Attenuation of Underwater Sound.	UCDWR-NDRC C4-sr30-494	2/16/42 Revised 7/30/42
20.007 C	Reverberation Studies at 24 KC.	UCDWR-U7 NDRC-6.1sr30-401	Nov. 23 1942
20.008 C	Transmission of Explosive Impulses in the Sea.	UCDWR-U8 NDBC C4-sr30-408	Dec. 2 1942
20.009 C	Variation of the Sound Field Near the Surface in Deep Water.	UCDWR-U49 NDRC- 6.1 sr30	Mar. 16 1943
20.010 C	Reverberation in Echo Ranging, Part II. Reverberation Found in Practice.	CUDWR NDRC-6.1sr20-840	Apr. 14 1943
20.011 C	Theory of Diffraction of Sound in the Shadow Zone.	CUDWR NDRC-6.1sr30-846	May 5 1943
20.012 C	Reflection of Sound in the Ocean from Temperature Changes.	UCDWR-U74 NDRC- 6.1sr30-060	May 17 1943
20.013 C	The Discrimination of Transducers Against Reverberation.	UCDWR-U75 NDRC 6.1sr30-068	May 31 1943
20.014 C	The Propagation of Sound in Shallow Water.	BuShips Rep. 65	June 3 1943
20.015 C	Some General Ideas Concerning the Transmission of Sound in the Deep Sea.	UCDWR No. M108 NDRC Sec. 6.1-sr30	Sept. 28 1943
20.016 C	Interim Report on the Sound Field of Echo-Ranging Gear. NRSL & U. of Calif.	UCDWR No. U113 NDRC Sec. 6.1- sr30-1205	Oct. 1 1943
20.017 C	Conclusions Derived from the Analysis of Transmission Data Obtained During Harbor Surveys (Preliminary Draft, Part I).	UCDWR No. U110 NDRC Sec. 6.1-sr30	Oct. 2 1943
20.018 C	Lloyd Mirror Effect in a Variable Velocity Medium.	UCDWR M 140 NDRC Sec. 6.1-sr30	Oct. 23 1943
20.019 C	A Survey of the Problem of Maximum Echo Ranges (Preliminary Draft).	UCDWR-U130 NDRC6.1sr30-1815	Nov 20 1943
20.020 Q	Use of Submarine Bathythermograph Observations (Revision of Rules for Predicing Maximum Sound Ranges).	NAVSHIPS 943-F	1944
20.021 C	Maximum Echo Ranges—Their Prediction and Use	UCDWR-NDRC 6.1-sr30-1460	January 1944
20.022 C	Sound Transmission Through Discover Water.	UCDWR-M189 NDRC 6.1-sr30	Mar. 8 1944
20.023 C	Some Experiments on the Transmission of Continuous Sound in 100-Fathom to 600-Fathom Water	UCDWR-M193 NDRC 6.1- sr30	Mar. 15 1944

20.000 (continued)

Bib. No.	Title	Number	Date
20.024 C	Effect of the Thermocline on the Propagation of Sound.	UCDWR Rep. No. 5	Mar. 19 1944
20.025 C	Prediction of Sound Ranges from Bathythermograph Observations. (Rules for Preparing Sonar Messages.)	NAVSHIPS 943-C2	March 1944
20.026 C	Preliminary Report on the Sonic Ray Plotter.	UCDWR M 207	Apr. 21 1944
20.027 C	Current Methods for Prediction of Maximum Sound Ranges.	CUDWR Tech. Memo No.	May 1 1944
20.028 C	The Attenuation of Sound in the Sea.	UCDWR-U236 NDRC Sec. 6.1-sr30-1532	July 6 1944
20.029 C	The Sonic Ray Plotter.	UCDWR-U246 6.1- sr30-1741	Aug. 8 1944
20.030 C	Sound Ranges under the Sea. (Revision of Report dated June 5, 1942.)	CUDWR NDRC 6.1-sr11-31-1880	November 1944
20.031 C	Prediction of Sonic and Supersonic Listening Ranges.	CUDWR NDRC 6.1- sr1131-1894	December 1944
20.032 C	Relation Between Scattering & Absorption of Sound	CUDWR Memo for File SAS-8	Dec. 11 1944
20.033 C	Coherence of CW Reverberations.	CUDWR Memo for File SAS-11	Dec. 20 1944
20.034 C	Distribution of Amplitude if Two Rays with Random Phase and Given Amplitude Distributions Interfere.	CUDWR Memo for File SAS-13	Jan. 4 1945
20.035 C	Fluctuations of Transmitted Sound in the Ocean.	CUDWR Tech. Memo No. 6	Jan. 17 1945
20.036 C	Lloyd Mirror Effect in the Presence of a ? temperature Gradient.	CUDWR Memo for File SAS-17	Jan. 22 1945
20.037 C	Change of Average Peak Echo Intensity with Changing Ping Length.	CUDWR Memo for File SAS-30	Mar. 22 1945
20.038 C	The Wave Equation with Gravitational Terms.	CUDWR Memo for File SAS-37	June 18 1945

[a] TM 11-496 (Apr. 25, 1945) together with TM 11-487—"Electrical Communication Systems Equipment" (Oct. 2, 1944) supersedes TM 11-496 (Feb. 25, 1944).
[b] See also 1.012 Part I.
[c] See also 1.012 Parts I, VIII, and XIV.
[d] See also 1.012 Part IV.
[e] See also 1.012 Parts III and IX, 5.049, 15.016, and 17.073.
[f] See also 1.012 Part XII and XIII, 6.028, 6.031, and 6.047.
[g] See also 1.012 Part VI and 6.035.
[h] See also 1.012 Parts V, VII, XII, and XV, 1.014 and 8.028.
[i] See also 1.012 Part II, 17.061 and 17.081.
[j] See also 12.012.
[k] See also 6.085 and 11.008.

For Reference
Only.